This expanded new, full-colour edition of the classic *Applied Radiological Anatomy* is an exhaustive yet practical imaging resource of every organ system using all diagnostic modalities.

Every illustration has been replaced, providing the most accurate and up-to-date radiographic scans available.

Features of the second edition:

- Completely new radiographic images throughout, giving the best possible anatomic examples currently available
- Both normal anatomy and normal variants shown
- Numerous colour line illustrations of key anatomy to aid interpretation of scans
- Concise text and numerous bullet lists enhance the images and enable quick assimilation of key anatomic features
- Every imaging modality included

Edited and written by a team of radiologists with a wealth of diagnostic experience and teaching expertise, and lavishly illustrated with over 1000 completely new, state-of-the-art images, *Applied Radiological Anatomy, Second Edition* is an essential purchase for radiologists at any stage of their career.


**Paul Butler** is Consultant Neuroradiologist at The Royal London Hospital, London, UK.

**Adam W.M. Mitchell** is a Consultant Radiologist at Chelsea and Westminster Hospital, London, and Honorary Senior Lecturer at Imperial College, London, UK.

**Jeremiah C. Healy** is a Consultant Radiologist at Chelsea and Westminster Hospital, London, and Honorary Senior Lecturer at Imperial College London, UK.


**Reviews of the first edition**

'This book is first class in achieving its aim and although primarily intended for trainees in radiology, will be of value to many surgical trainees.'
*British Journal of Surgery*

'... a comprehensive, abundantly illustrated, up-to-date review of normal radiological anatomy ... a helpful guide to radiology residents and a useful reference book for both residents and practising radiologists."
*American Journal of Radiology*


Cover designed by Zoe Naylor





CAMBRIDGE
UNIVERSITY PRESS
www.cambridge.org

ISBN 978-0-521-76666-1



Butler, Mitchell and Healy

Applied Radiological Anatomy

Second Edition

CAMBRIDGE


# Applied Radiological Anatomy

EDITED BY **Paul Butler, Adam W. M. Mitchell and Jeremiah C. Healy**

**Second Edition**

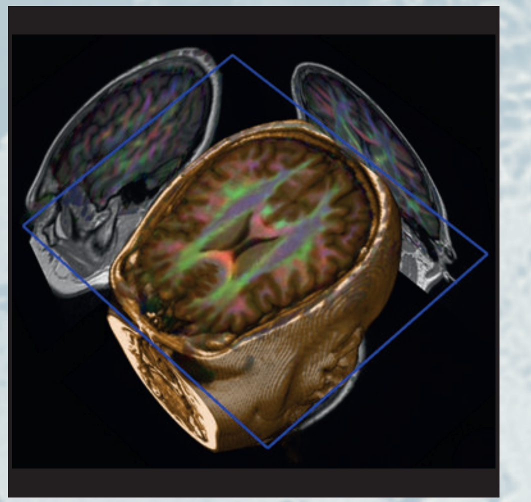

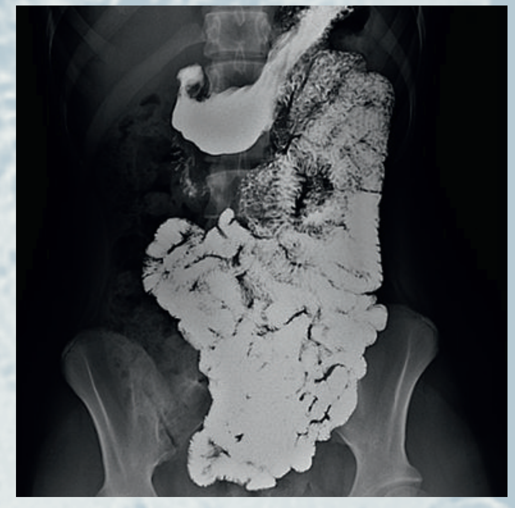

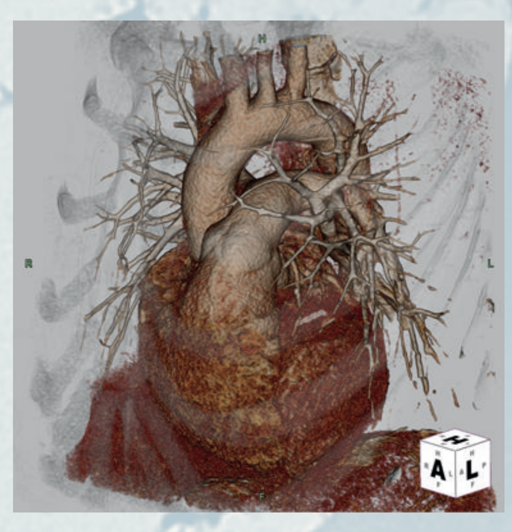


CAMBRIDGE

**Medicine**

# Applied Radiological Anatomy

Second Edition

# Applied Radiological Anatomy

Second Edition

Edited by:

**Paul Butler**
Consultant Neuroradiologist, The Royal London Hospital, London, UK

**Adam W. M. Mitchell**
Consultant Radiologist, Chelsea and Westminster Hospital, London;
Honorary Senior Lecturer at Imperial College London, UK

**Jeremiah C. Healy**
Consultant Radiologist, Chelsea and Westminster Hospital, London;
Honorary Senior Lecturer at Imperial College London, UK

CAMBRIDGE
UNIVERSITY PRESS

CAMBRIDGE UNIVERSITY PRESS
Cambridge, New York, Melbourne, Madrid, Cape Town,
Singapore, São Paulo, Delhi, Tokyo, Mexico City

Cambridge University Press
The Edinburgh Building, Cambridge CB2 8RU, UK

Published in the United States of America by
Cambridge University Press, New York

www.cambridge.org
Information on this title: www.cambridge.org/9780521766661



First edition published 1999
Second edition published 2012

Printed in the United Kingdom at the University Press, Cambridge

*A catalogue record for this publication is available from the British Library*

*Library of Congress Cataloguing in Publication data*
Applied radiological anatomy / edited by Paul Butler, Adam Mitchell,
Jeremiah C. Healy. – 2nd ed.
p. cm.
Includes bibliographical references and index.
ISBN 978-0-521-76666-1 (hardback)
1. Radiography, Medical. 2. Human anatomy. 3. Human
anatomy–Atlases. I. Butler, Paul, 1954 June 4– II. Mitchell,
Adam W. M. III. Ellis, Harold, 1926– IV. Title.
RC78.A675 2011
616.07'572–dc22 2011007348

ISBN 978-0-521-76666-1 Hardback

# Contents

# Contributors

**Steven D. Allen, BSc, MBBS, MRCS, FRCR**
Consultant Radiologist,
Royal Marsden Hospital,
Sutton, Surrey, UK

**Gonzalo Ansede**
Specialist Registrar in Radiology,
Royal Brompton Hospital,
London, UK

**Tim Beale**
Consultant Radiologist,
University College London Hospitals and
Royal National Throat, Nose and Ear Hospital,
London, UK

**Nishat Bharwani, BSc, MBBS, MRCP, FRCR**
Consultant Radiologist,
Imperial College Healthcare NHS Trust, London, UK

**Paul Butler, MRCP, FRCR**
Consultant Neuroradiologist,
The Royal London Hospital, London, UK

**Indran Davagnanam, MB, BCh, BAO, BMedSci, FRCR**
Neuroradiology Specialist Registrar,
National Hospital for Neurology and Neurosurgery,
Queen Square, London, UK

**Catriona L. Davies, MBBS, MRCP, FRCR**
Consultant Radiologist,
Chelsea and Westminster Hospital, London, UK

**Michael Gonsalves**
Radiology Registrar,
St George's Hospital, London, UK

**Jonathan L. Hart, MA (Oxon), BMBCh, MRCS, FRCR**
Specialist Registrar, Neuroradiology,
National Hospital for Neurology and Neurosurgery,
Queen Square, London, UK

**Jeremiah C. Healy**
Consultant Radiologist, Chelsea and Westminster
Hospital, London;
Honorary Senior Lecturer, at Imperial College London, UK

**Kieran M. Hogarth, BSC, MBBS, FRCR**
Consultant Neuroradiologist,
John Radcliffe Hospital, Oxford, UK

**Josef Jarosz**
Consultant Neuroradiologist,
King's College Hospital, London, UK

**Narayan Karunanithy, MRCS, FRCR**
Consultant Radiologist,
Guy's and St Thomas' NHS Foundation Trust, and Honorary
Clinical Lecturer King's College, London, UK

**Nasir Khan, MBBS, MRCP, FRCR**
Consultant Radiologist,
Chelsea and Westminster Hospital, London, UK

**Justin Lee**
Consultant Radiologist,
Chelsea and Westminster Hospital,
London, UK

**Adam W. M. Mitchel**
Consultant Radiologist,
Chelsea, and Westminster Hospital, London; Honorary Senior
Lecturer, at Imperial College London, UK

**Simon Morley**
Consultant Radiologist,
University College London Hospitals,
London, UK

**Simon Padley, BSc, MBBS, FRCP, FRCR**
Consultant Radiologist,
Chelsea and Westminster and
Royal Brompton Hospitals and
Honorary Senior Lecturer,
Imperial College London, UK

**Uday Patel**
Consultant Radiologist,
St George's Hospital, London, UK

**Gajan Rajeswaran, FRCR**
Consultant Radiologist,
Chelsea and Westminster Hospital, London, UK

**Navin Ramachandran, BSc, MBBS, MRCP, FRCR**
Consultant Radiologist,
University College London Hospitals,
London, UK

**Sheila Rankin**
Radiology Department,
Guy's Hospital, London, UK

**Rodney H. Rezrek, MA, FRANZCR (hon), FFR RCSI (hon), FRCP, FRCR**
Emeritus Professor of Diagnostic Imaging,
St. Bartholomew's Cancer Institute,
St. Bartholomew's and the London School of Medicine and Dentistry, Queen Mary University of London, UK

**Asif Saifuddin**
Consultant Musculoskeletal Radiologist,
The Royal National Orthopaedic Hospital NHS Trust,
Stanmore, Middlesex, UK

**Aslam Sohaib, MRCP, FRCR**
Consultant Radiologist,
Royal Marsden Hospital,
London, UK

**Ian Suchet**
Department of Medical Imaging,
University of Saskatchewan, Saskatoon,
Saskatchewan, Canada

**Hema Verma, MRCP, FRCR**
Specialist Registrar in Radiology,
St George's Hospital,
London, UK

**Nevin T. Wijesekera**
Specialist Registrar in Radiology,
Royal Brompton Hospital,
London, UK

Chapter 1

# The skull and brain

Kieran M. Hogarth, Jozef Jarosz and Paul Butler

## Introduction and imaging methods

Computed tomography (CT) and magnetic resonance imaging (MRI) are the mainstays of cerebral imaging. Skull radiography now plays very little part in diagnosis, being largely replaced by multislice CT.

Non- or minimally invasive angiography performed using CT (CT angiography) or MRI (magnetic resonance angiography) has resulted in invasive catheter angiography being reserved for a few special diagnostic indications or as part of an interventional, (therapeutic), procedure.

Anatomical detail is far better displayed by MRI than by CT, although both are valuable in clinical practice.

With T1-weighted (T1W) MR images, grey matter is of lower signal intensity (darker) than white matter (Fig. 1.1). On T2-weighted (T2W) images, including T2-FLAIR sequences, the reverse is true (Fig. 1.2).

With CT, somewhat paradoxically, white matter is depicted as darker grey than grey matter (Fig. 1.3). The explanation is that CT is an X-ray investigation. White matter contains lipid as part of myelin, which is relatively radiolucent.

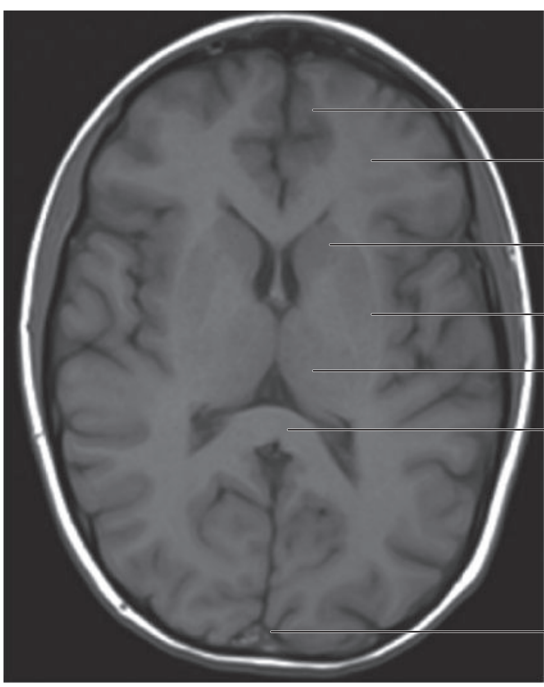


**Fig. 1.1** T1W MRI. 'Mid-axial' section of the brain.

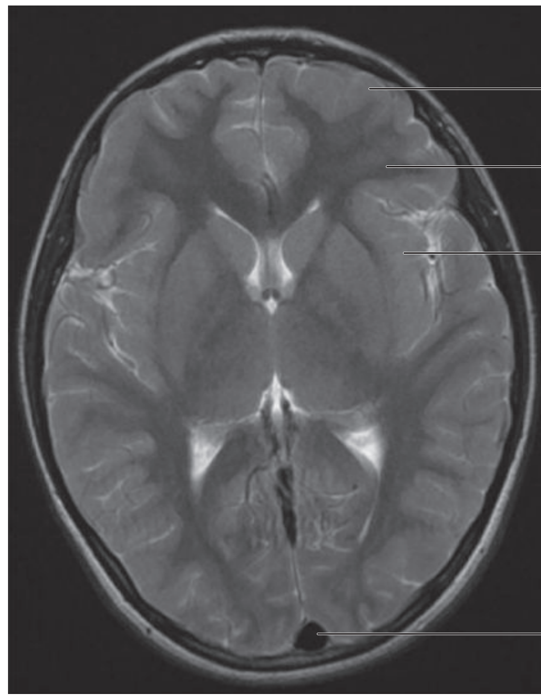


**Fig. 1.2** T2W MRI. 'Mid-axial' section of the brain. Note the signal void due to blood flowing rapidly.

The appearance of myelinated tracts on MRI is rather more variable and will be influenced by the pulse sequence used. In perhaps its simplest form, the lipid in subcutaneous fat is typically high signal (white) on both T1 and T2 MR sequences.

Conversely, lipid is extremely radiolucent and appears black on CT.

Dense bone contains few free protons on which MRI is based and therefore appears as a signal void (black) on MR.

On CT, bone, which is radio-opaque, appears white.

Air in the paranasal sinuses appears black on both CT and MRI.

Besides compact bone and air, hypointensity on MRI occurs also with iron deposition in the globus pallidus and substantia nigra and as a feature of rapid blood or CSF flow (see below).

*Applied Radiological Anatomy, 2nd Edition* ed. Paul Butler, Adam W.M. Mitchell and Jeremiah C. Healy. Published by Cambridge University Press.

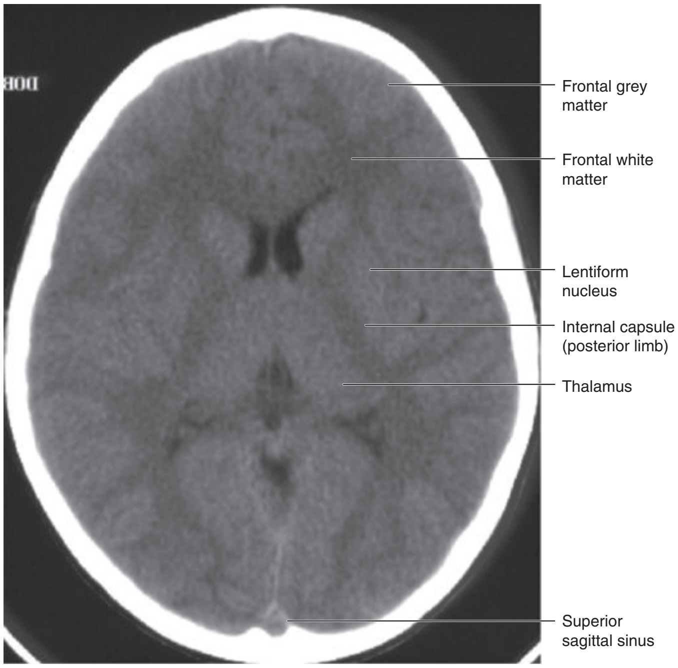


**Fig. 1.3** Cranial CT. 'Mid-axial' section of the brain.

The intravenous contrast agents used in CT and MRI do not cause significant cerebral parenchymal enhancement, when the blood–brain barrier is intact.

Iodinated contrast agents administered intravenously for CT enhance blood within the cranial arteries and veins and dural venous sinuses (Fig. 1.4).

Enhancement is seen also in the highly vascular choroid plexuses and in those structures outside the blood–brain barrier such as the pituitary gland and infundibulum.

With MRI the mechanism of contrast enhancement with intravenous gadolinium DTPA is quite different from CT, but nevertheless, on T1W images, those structures which enhance become hyperintense (whiter) in much the same way as with CT.

One notable difference, however, is in the depiction of rapidly flowing blood with MRI, which appears as a 'signal void' (black) and does not enhance (Fig. 1.2). This principle applies also to CSF, which can flow rapidly through the cerebral aqueduct, causing a signal void seen particularly on T2W axial images.

## Osteology of the skull

The brain is supported by the skull base and enclosed in the vault or calvarium. The skull base develops in cartilage, the vault in membrane. The central skull base consists of the occipital, sphenoid and temporal bones. The frontal and ethmoidal bones complete the five bones of the skull base. Skull sutures are located between bones formed by membranous ossification and consist of dense connective tissue. In the neonate they are smooth, but through childhood interdigitations develop, followed by perisutural sclerosis, prior to fusion in the third or fourth decades or even later (Fig. 1.5). The anterior fontanelle or bregma is located between frontal and parietal bones at the junction of sagittal and coronal sutures. It closes in the second year.

The posterior fontanelle or lambda is closed by the second month after birth.

The skull vault consists of inner and outer tables or diploe separated by a diploic space. This space contains marrow and large valveless, thin-walled diploic veins, which contribute to a rich cranial-cerebral anastomosis to provide both a route for the spread of infection across the vault and collateral pathways in the event of venous sinus occlusion.

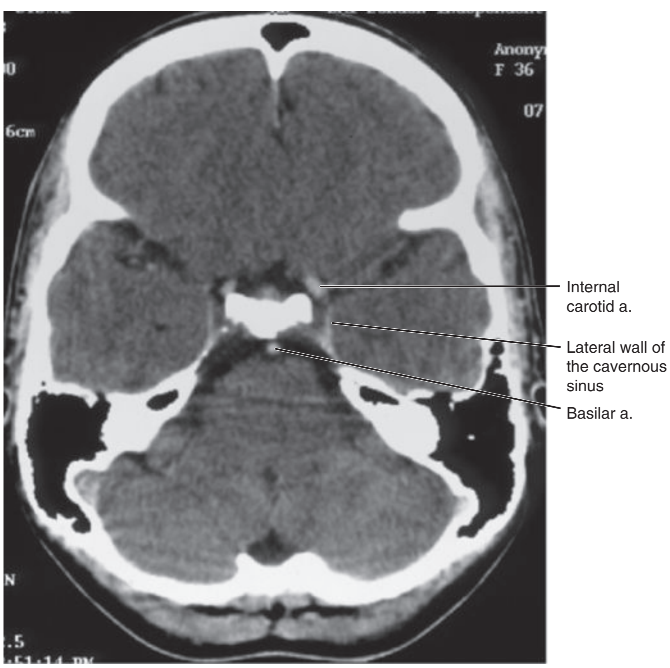


**Fig. 1.4** Contrast-enhanced cranial CT.

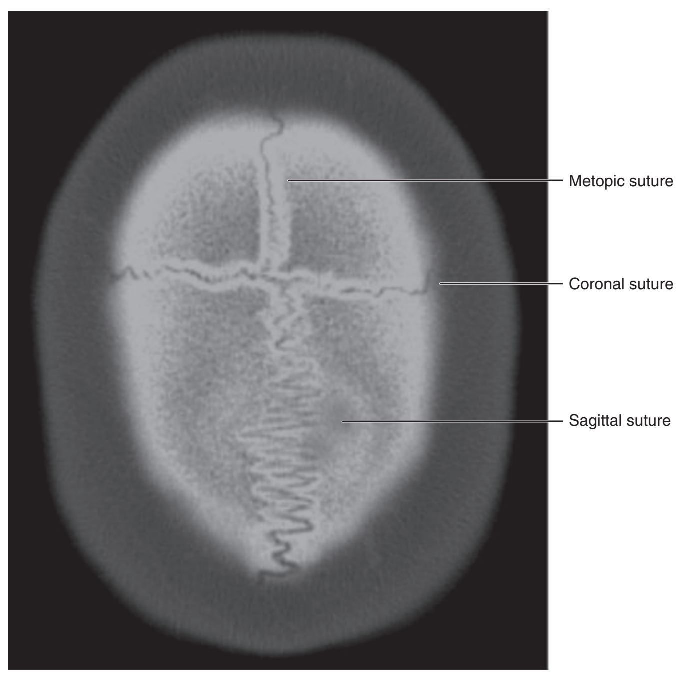


**Fig. 1.5** Cranial CT, bone algorithm. The cranial sutures at the vertex of the skull. There is a persistent metopic suture. Note the interdigitation and perisutural sclerosis of the sagittal suture.

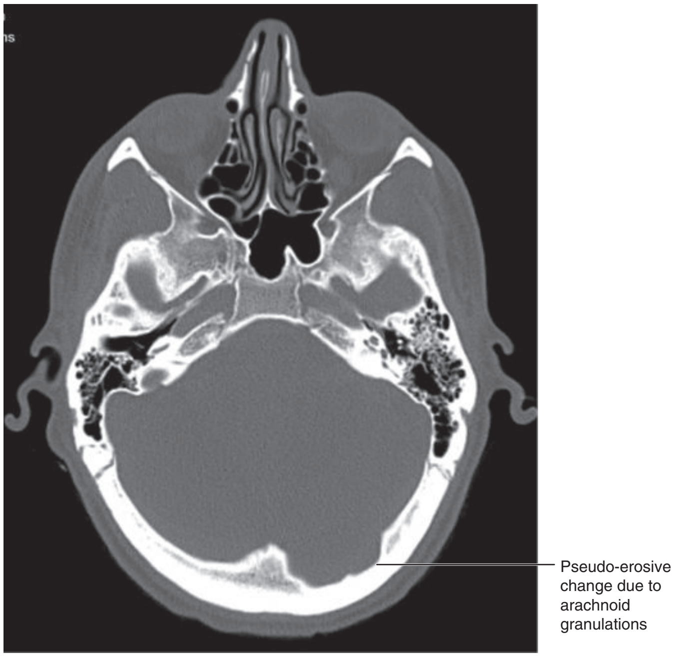


**Fig. 1.6** Cranial CT, bone algorithm. Pseudo-erosive changes due to the arachnoid granulations.

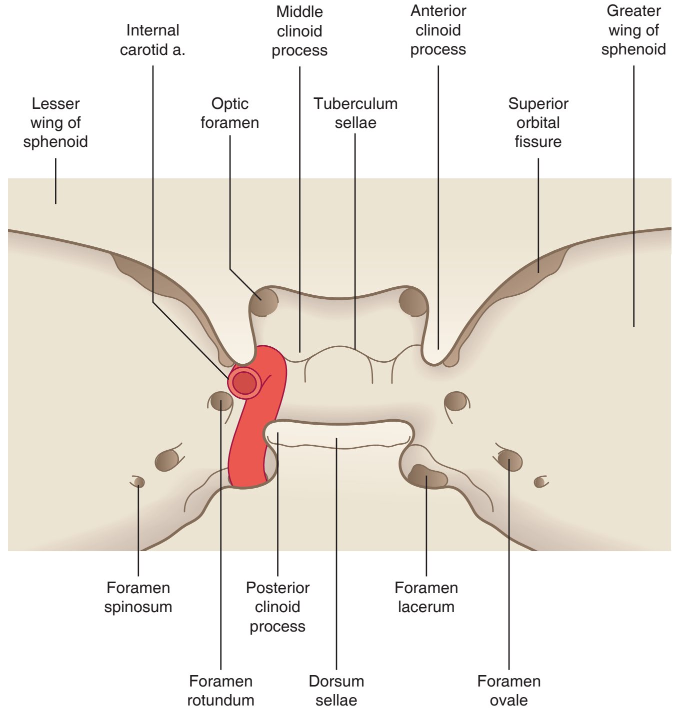


**Fig. 1.7** The bony anatomy of the sellar region.

Venous lacunae are found mainly in the parietal bone, near to the midline adjacent to the superior sagittal sinus. They receive some of the cerebral venous return and are invaginated by arachnoid granulations, which are the sites of reabsorption of cerebral spinal fluid into the venous system. Lacunae cause localized thinning of the inner table (Fig. 1.6).

The frontal bone forms in two halves, which normally fuse at five years. The intervening suture is known as the metopic suture.

Occasionally, the halves remain separate and the suture may persist wholly or in part into adult life in 5–10% of individuals (Fig. 1.5).

The orbital plates of the frontal bone contribute most of the anterior fossa floor with a cribriform plate of the ethmoid bone interposed between them in the midline. The crista galli, to which the falx is attached, ascends vertically from the cribriform plate and may appear hyperintense on T1W images due to contained fatty marrow.

The two parietal bones are separated from each other by the sagittal suture and from the frontal bone by the coronal suture (Fig. 1.5). Posteriorly, each parietal bone articulates with the occipital bone. Anteriorly, it articulates with the frontal bone and the greater wing of the sphenoid bone and inferiorly with the temporal bone. The frontal, sphenoid parietal and temporal bones meet at the pterion, which normally closes at 3–4 months.

The sphenoid bone consists of a body, greater and lesser wings and the pterygoid plates. The body encloses the sphenoid air sinuses, which are paired and usually asymmetrical. The pituitary fossa and posterior clinoid processes are borne on the superior surface. The planum sphenoidale articulates with the cribriform plate. The anterior clinoid processes are part of the lesser wing and the tuberculum sellae dips anteriorly between them into the optic groove.

The lesser wing forms the posterior part of the floor of the anterior cranial fossa and its posterior border constitutes the sphenoid ridge.

Meningiomas of the skull base may arise from any of these sphenoid locations, hence the detail given (Fig. 1.7).

The greater wing of the sphenoid bone forms the floor of the middle cranial fossa, which extends posteriorly to the petrous ridge and dorsum sellae. The dorsum sella is the posterior boundary of the pituitary fossa and merges laterally with posterior clinoid processes. The greater wing also separates the temporal lobe of the brain from the infratemporal fossa below. The medial and lateral pterygoid plates of the sphenoid bone pass inferiorly behind the maxilla.

The foramina ovale rotundum and spinosa are within the greater wing of the sphenoid bone (Fig. 1.8). The foramina ovale and spinosum are often asymmetrical, the foramen rotundum rarely so.

The foramen rotundum travels from Meckel's cave to the pterygopalatine fossa and transmits the maxillary division of the trigeminal nerve. On coronal CT the foramina are demonstrated inferior to the anterior clinoid processes.

The foramen ovale transmits the mandibular division of the trigeminal nerve and the accessory meningeal arteries. It runs anterolaterally from Meckel's cave to emerge near to the lateral pterygoid plate. The foramina may be identified on coronal CT scan inferolateral to the posterior clinoid processes.

The foramen spinosum is situated posterolateral to the larger foramen ovale and transmits the middle meningeal artery and vein between the infratemporal and middle cranial fossae.

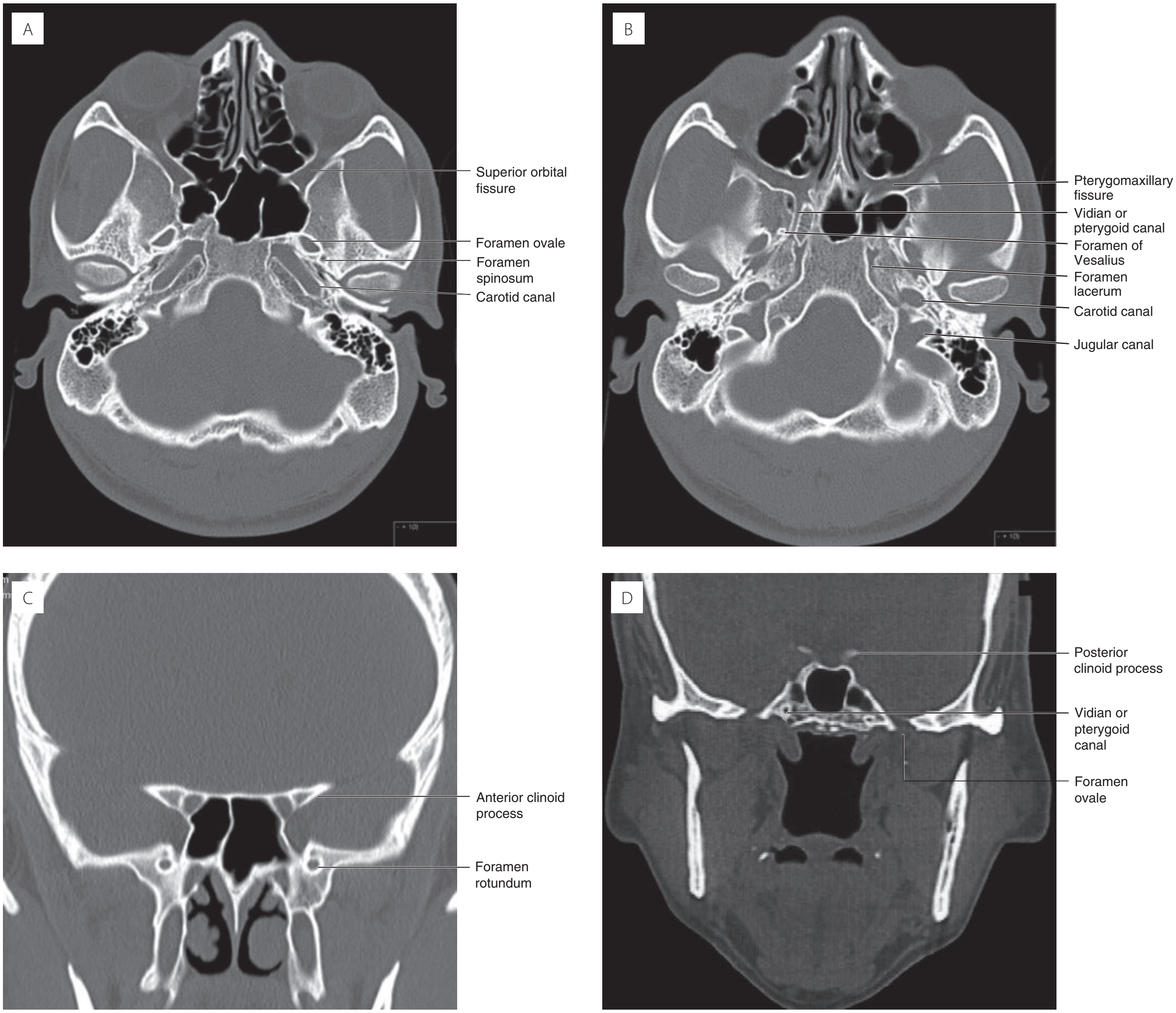


**Fig. 1.8** Cranial CT, bone algorithm. The skull base. Axial, (A) superior to (B). Coronal, (C) anterior to (D).

The foramen lacerum contains cartilage and is traversed only by small veins and nerves. It separates the petrous apex, the body of the sphenoid and the basiocciput and is crossed by the internal carotid artery. Smaller, inconstant foramina are sometimes encountered. The Vidian or pterygoid canal is found medial to the foramen rotundum. The foramen of Vesalius transmits an emissary vein and is medial to the foramen ovale.

The temporal bone has four parts. The squamous part forms the lateral wall of the middle cranial fossa and is separated from the parietal bone by the squamosal suture. Its zygomatic process contributes to the zygomatic arch and the squamosal portion also bears the mandibular condylar fossa.

The petromastoid portion forms part of the middle and posterior fossa floors. The styloid process passes inferiorly from the base of the petrous bone and the stylomastoid

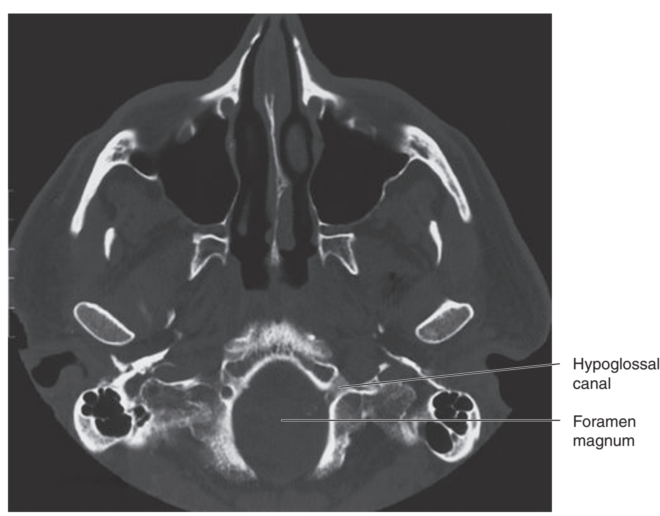


**Fig. 1.9** Cranial CT, bone algorithm. The hypoglossal canal.

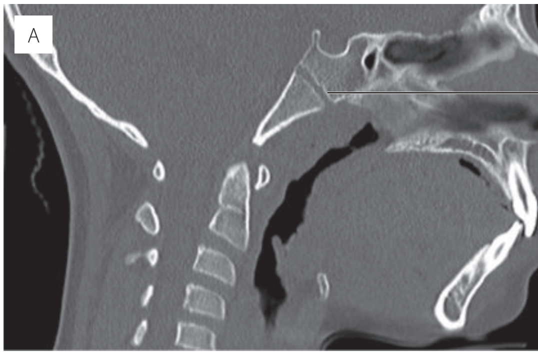



**Fig. 1.10** (A) Cranial CT. Sagittal reformat bone algorithm. (B) Cranial MR. Midline sagittal section of the brain. Spheno-occipital synchondrosis.

foramen lies behind the styloid process transmitting the facial (VIIth) cranial nerve.

The occipital bone forms most of the posterior cranial fossa walls. This is the largest of the three cranial fossae. It also gives rise to the occipital condyles which articulate with the atlas and the anterior condylar canals which transmit the hypoglossal (XIIth) cranial nerve (Fig. 1.9). Also inferiorly but more anteriorly, the occipital bone articulates with the sphenoid to form the clivus. The articulation is visible in children as the basisphenoid synchondrosis (Fig. 1.10).

In the adult the clivus is hyperintense on T1W MR images due to replacement of red marrow with fat. The transition from hypointensity occurs at around 7 years. Immature red marrow in children can enhance with intravenous gadolinium.

The occipital bone is often devoid of a diploic space inferiorly. This accounts for the sparing of the occipital bone in thalassaemia major, where the response to chronic haemolysis causes reactive change ('hair on end' appearance) elsewhere in the skull vault.

## The skull radiograph (Fig. 1.11)

Skull radiography is performed much less frequently now because of the versatility and reliability of cranial CT. The plain film images are complex with multiple overlapping lines and interfaces and of course give very limited and indirect evidence of cerebral pathology.

When interpreting a skull radiograph perhaps the most important requirement is to distinguish a normal lucency from a fracture. Convolutional markings are absent at birth, most prominent at between 2 and 5 years and absent after about 12 years.

Vascular markings similarly do not develop until the postnatal period but then persist throughout life. They are less radiolucent than fractures, with indistinct margins and often branch. Diploic veins are responsible for the majority of impressions, although the dural venous sinuses (superior sagittal, lateral and sigmoid) cause depressions on the inner table, visible on plain radiographs.

There is a vein running along the coronal suture large enough to be labelled the sphenobregmatic sinus, which gives rise to a prominent vascular impression.

Venous impressions are larger than those due to arteries and vary in calibre. Arterial impressions have parallel walls and reduce in calibre only after branching.

Normal vault lucencies and calcifications are listed in Table 1.1

**Table 1.1** Lucencies and calcifications seen on normal skull radiography

| |
|---|
| **Lucencies** |
| Sutures |
| Vascular impressions |
| Normal vault thinning, e.g. temporal bone |
| Arachnoid granulations |
| Pneumatization |
| **Calcifications** (Fig. 1.12) |
| Pineal gland |
| Habenular commissure |
| Choroid plexus |
| Dural calcification including petroclinoid and interclinoid 'ligaments' |

## The cerebral envelope

### See Fig. 1.13

The meninges invest the brain and spinal cord. The three constituent parts are the outer, fibrous dura mater, the avascular, lattice-like arachnoid mater and the inner, vascular layer, the pia mater.

Although the dura and arachnoid are applied closely, there is a potential space, known as the subdural space, between them into which haemorrhage may occur or pus form. Its existence in the normal individual is controversial. The subarachnoid space contains cerebral spinal fluid, which surrounds the cerebral arteries and veins. It is situated between the arachnoid and the pia, which is closely applied to the cerebral surface. The cranial dura has two layers, which separate to enclose the dural venous sinuses.

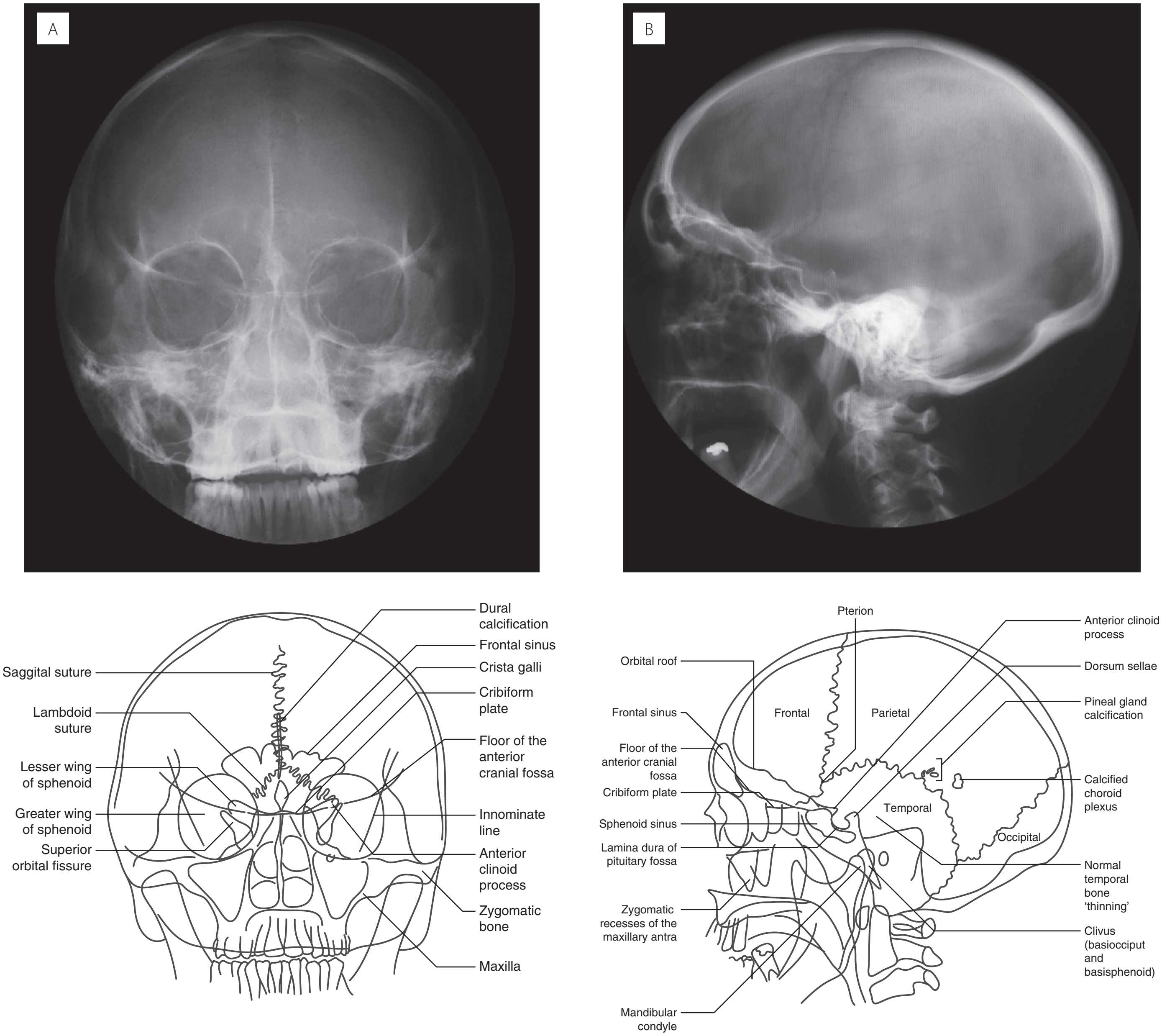


**Fig. 1.11** Frontal (A) and lateral (B) skull radiographs.

The outer layer is the periosteum of the inner table of the skull (the endosteum). The inner layer covers the brain and gives rise to the falx and tentorium. Dura is hyperdense on CT images and relatively hypointense on MRI. It shows contrast enhancement on both modalities and since the falx may calcify or ossify, MRI may demonstrate focal regions of signal void due to calcification or of hyperintensity due to fat within marrow.

The falx is a sickle-shaped fold of dura, comprising two layers, which forms an incomplete partition between the cerebral hemispheres. It extends from the crista galli to the internal occipital protuberance, where it joins the tentorium and is thinner anteriorly. The falx is demonstrated as a midline linear density on axial CT scan near to the vertex, but inferiorly and posteriorly assumes a triangular shape conforming to the superior sagittal sinus in cross-section. The tentorium cerebelli, another double dural fold, is attached from the posterior clinoid processes along the petrous ridges to the internal occipital protuberance. Its upper, free, medial border surrounds the midbrain. This passes anteriorly through the opening, known as the tentorial hiatus or incisura.

The uncus of the hippocampus and the posterior cerebral arteries lie above the free edge of the tentorium and both are at risk of compression against the tentorial edge when there is raised intracranial pressure in the supratentorial compartment ('coning'). The free border anteriorly encloses the cavernous sinus on each side of the pituitary fossa before attaching to the anterior clinoid processes.

For diagnostic purposes it is important to identify in which intracranial compartment a lesion is situated. On axial CT, structures medial to the line of the tentorial edge are in the infratentorial compartment; those lateral to that line are in the supratentorial compartment (Fig. 1.14).

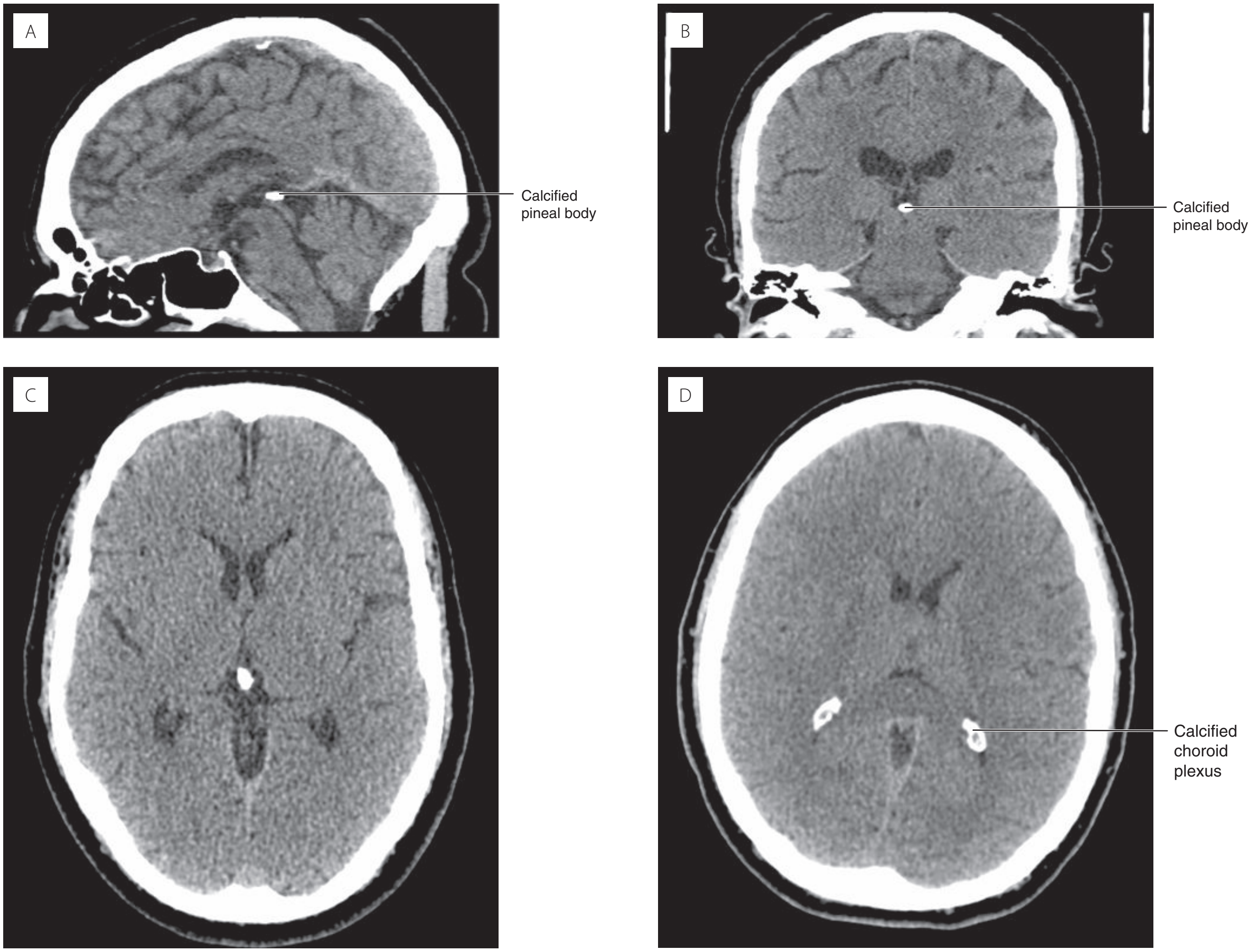


**Fig. 1.12** CT scans showing calcified pineal body in sagittal section (A), coronal section (B) and axial section (C), and choroid calcification in axial section (D).

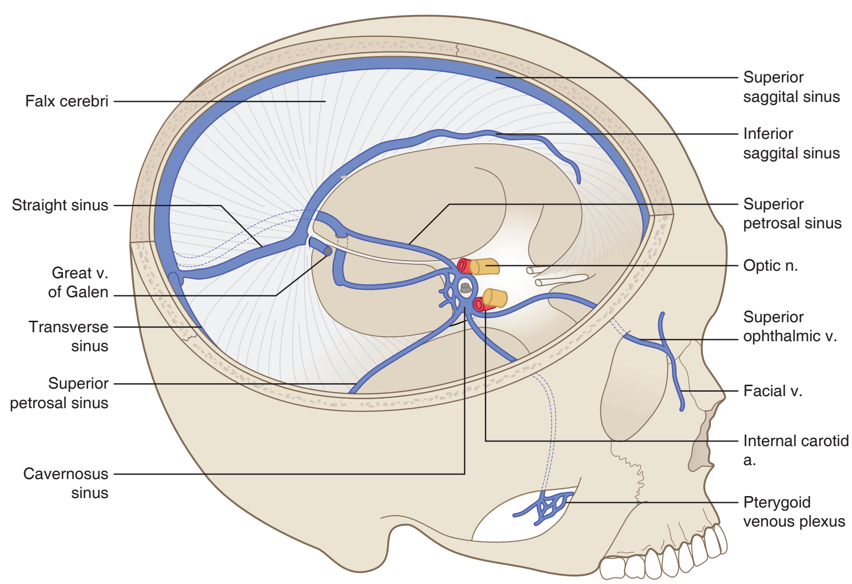


**Fig. 1.13** The cranial dura.

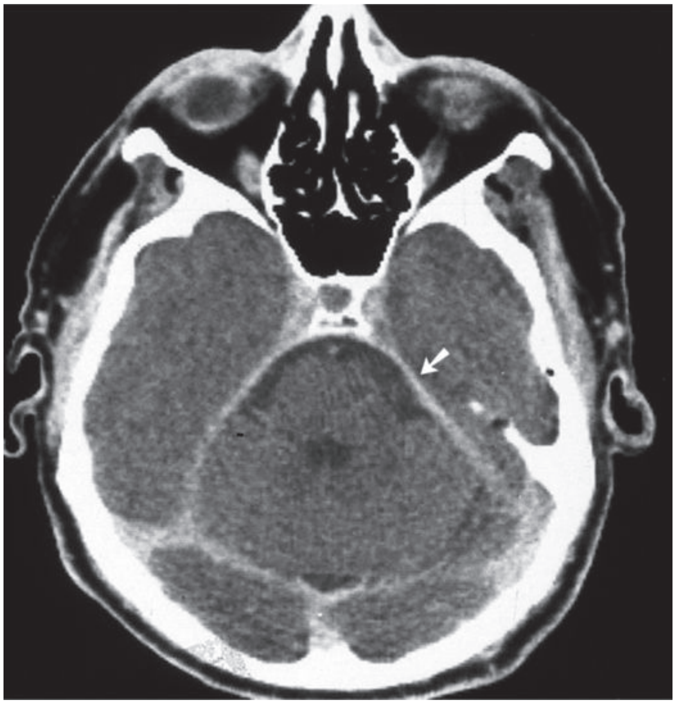

**Fig. 1.14** Axial CT with intravenous contrast showing the tentorial margins (arrow). Note that the dura continues anteriorly to form the lateral wall of the cavernous sinus.

The falx cerebelli is a small fold of dura attached superiorly to the posterior part of the tentorium in the midsagittal plane, which encloses the occipital sinus posteriorly. It terminates just above the foramen magnum and its free anterior border projects into the cerebellar notch. The diaphragma sellae is an incomplete roof over the pituitary gland and is pierced by the pituitary stalk. There is no subarachnoid space in the sella since the meningeal layers fuse. On both CT and MRI meningeal enhancement following intravenous contrast is a normal feature.

## Meningeal blood supply and innervation

The middle meningeal artery is the main arterial supply to the meninges (Fig. 1.15), but there are contributions from the cavernous carotid, the ophthalmic and vertebral arteries. There is also an accessory meningeal artery, which arises either from the maxillary or middle meningeal arteries and enters the skull through the foramen ovale. The middle meningeal artery is extradural and both it and the middle meningeal veins groove the inner table of the skull. Branches of the external carotid artery may often supply the lower cranial nerves. The middle meningeal arteries supply branches to both the trigeminal and the facial ganglia. The occipital artery gives branches which pass via the jugular foramen and condylar canal to supply the glossopharyngeal (IXth), vagal (Xth), accessory (XIth) and hypoglossal (XIIth) cranial nerves. Innervation of the dura is primarily from the trigeminal nerve, but also from the lower cranial nerves and the first three cervical segments. This may account for cervical pain in cranial subarachnoid haemorrhage.

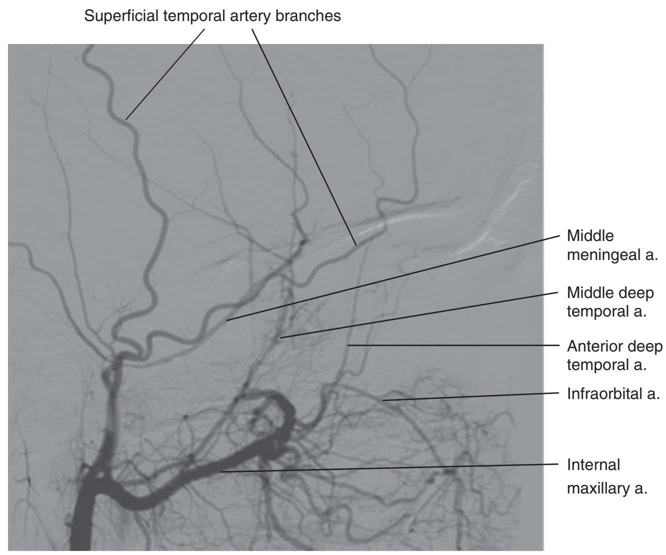


**Fig. 1.15** External carotid angiogram, lateral projection.

## The subarachnoid cisterns (Fig. 1.16)

Where the brain and skull are not closely applied, a number of subarachnoid cisterns are defined. They are situated at the base of the brain and around the brainstem, the free edge of the tentorium and the major arteries. The subarachnoid cisterns connect relatively freely with one another and their patency is essential for the normal circulation of cerebral spinal fluid. Although there are arachnoid membranes within the cisterns causing partial compartmentalization, the definition of a particular cistern is a result of the arbitrary division of what is effectively a single space.

The cisterna magna lies between the medulla and the posteroinferior surface of the cerebellum and is triangular in sagittal section. It continues below the spinal subarachnoid space and receives cerebral spinal fluid from the fourth ventricle. It is sometimes punctured percutaneously in the midline to obtain cerebral spinal fluid for examination.

The vertebral and posterior inferior cerebellar arteries travel through the lateral parts of the cisterna magna, which also contains the glossopharyngeal, vagus and spinal accessory nerves. In some, otherwise normal, individuals the system is very large and described as a mega-cisterna magna.

The pontine cistern is anterior to both the pons and medulla and contains the basilar artery and cranial nerves V to XII. It is continuous around the brainstem, with the quadrigeminal plate cistern posteriorly and the interpeduncular cistern superiorly.

The chiasmatic or suprasellar cistern extends from the infundibulum to the posterior surface of the frontal lobes and lies between the uncus on either side. It includes the proximal parts of the Sylvian fissures and contains the circle of Willis. Since the majority of berry aneurysms are borne on the circle of Willis, it can be appreciated that their rupture results in subarachnoid haemorrhage in the first instance.

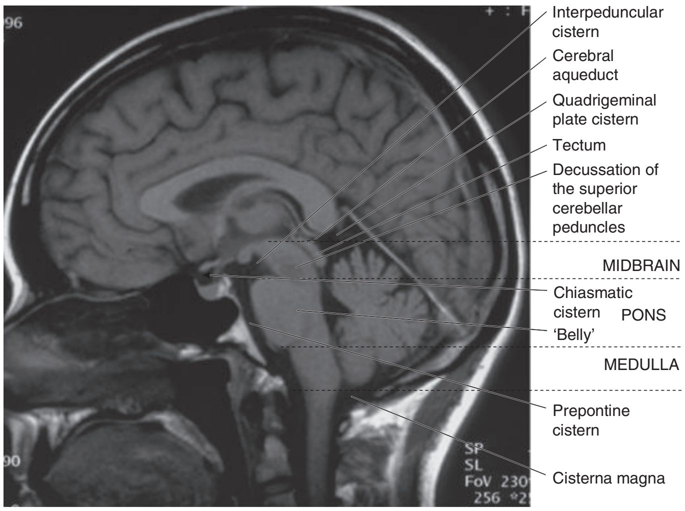


**Fig. 1.16** Cranial MR. Midline sagittal section of the brain. The subarachnoid cisterns.

The chiasmatic cistern leads posteriorly to the interpeduncular or intercrural cistern, which contains the terminal basilar artery and its branches and the oculomotor (IIIrd cranial) nerves. Blood within this cistern may be the only evidence of subarachnoid haemorrhage.

The ambient cistern surrounds the midbrain and transmits the posterior cerebral and superior cerebellar arteries, the basal veins of Rosenthal and the trochlear nerves. The 'wings' of the ambient cistern are its lateral extensions posterior to the thalami.

The quadrigeminal cistern (cistern of the great cerebral vein of Galen) lies adjacent to the superior service of the cerebellum and extends superiorly around the splenium of the corpus callosum. It contains the posterior cerebral, posterior choroidal and superior cerebellar arteries, and the trochlear (IVth cranial) nerves. It is also the location of the venous confluence where the vein of Galen joins the inferior sagittal and straight dural venous sinuses.

The cistern of the lamina terminalis is superior to the chiasmatic cistern. It contains the anterior communicating artery and leads into the callosal cistern, through which the pericallosal artery travels.

## The brainstem and cranial nerves

**See Fig. 1.17**

The brainstem consists of the midbrain, pons and medulla (Fig. 1.16). Even high field strength MRI shows little internal detail under normal scanning conditions. To demonstrate the exiting cranial nerves, high-resolution, heavily T2-weighted

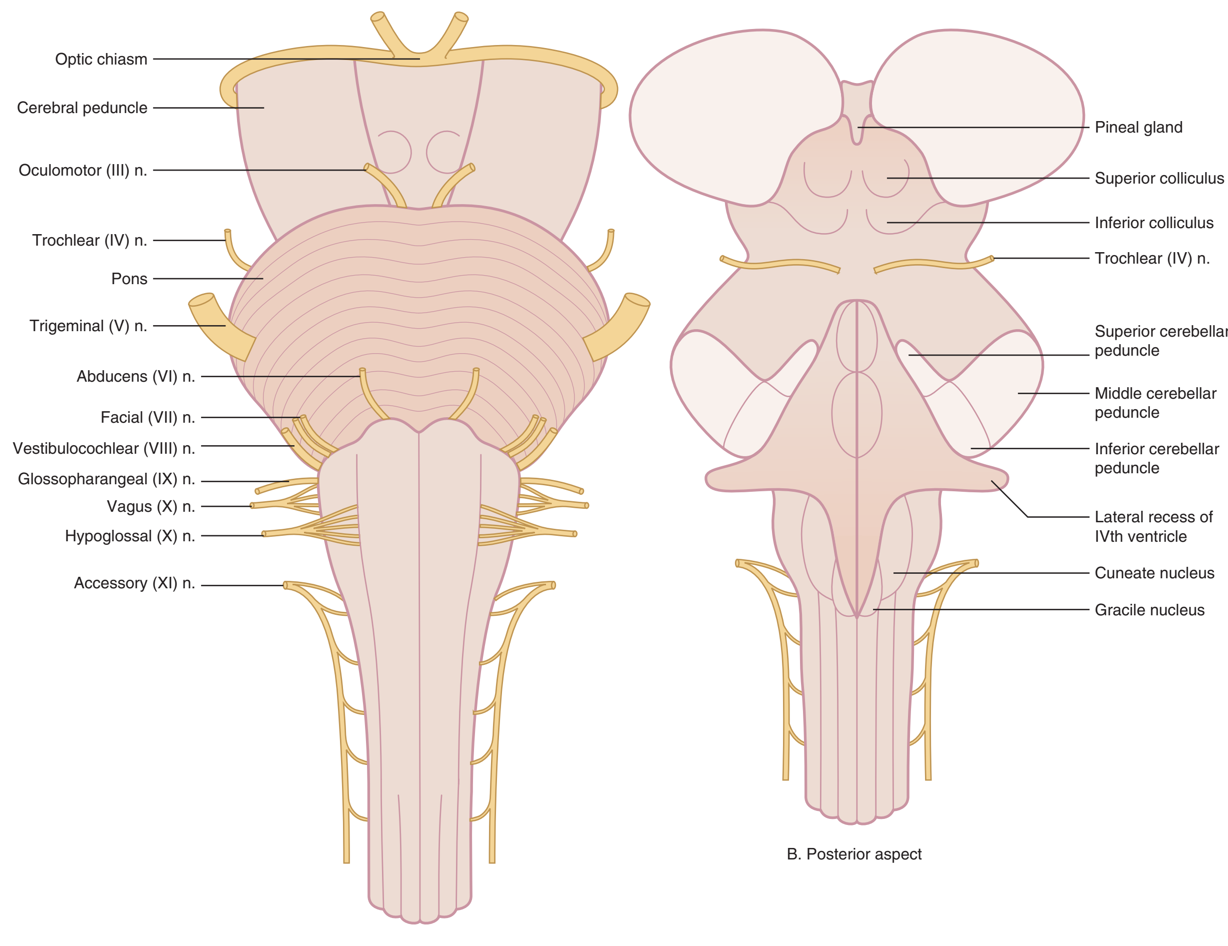


**Fig. 1.17** The brainstem. A. Anterior aspect B. Posterior

thin-section axial and coronal scans are required. These provide contour images of the nerves and brainstem against hyperintense (white) CSF. Even then the demonstration of the smaller nerves is inconstant.

## The midbrain

The midbrain has two prominent cerebral peduncles anteriorly and a dorsal tectum. Within the substance of the midbrain the red nuclei and the substantia nigra can be identified (Fig. 1.18).

The red nuclei are hypointense on T2W images due to their vascularity and the substantia nigra due to their iron content.

As with the pons the appearance of the midbrain is very different from its axial appearance. In a midline section only the central tegmentum and dorsal tectum are seen, separated by the cerebral aqueduct.

The tectum consists of four colliculi ('hillocks') or quadrigeminal bodies, which are involved in visual and auditory reflexes (Figs. 1.16, 1.28).

Cranial nerves arising in the midbrain are the oculomotor (IIIrd) and the trochlear (IVth). Both have their nuclei in the periaqueductal grey matter.

The oculomotor (IIIrd) arises from the anterior midbrain, on the medial side of the cerebral peduncle (Fig. 1.19), and passes between the superior cerebellar and posterior communicating arteries. Aneurysms arising at the origins of either of these two arteries can cause a IIIrd nerve palsy, although posterior communicating artery aneurysms are much more common.

The nerve then passes inferior to the posterior communicating artery, close to the free edge of the tentorium, into the cavernous sinus. Its cisternal portion is particularly well shown on axial FLAIR MR images.

The trochlear (IVth) nerve is the smallest in calibre, has the longest intracranial course and is the only cranial nerve arising from the dorsal aspect of the brainstem (Fig. 1.20).

## The pons

The pons has a bulbous anterior portion (the 'belly'), seen prominently on sagittal images, and a dorsal tegmentum (Fig.1.16).

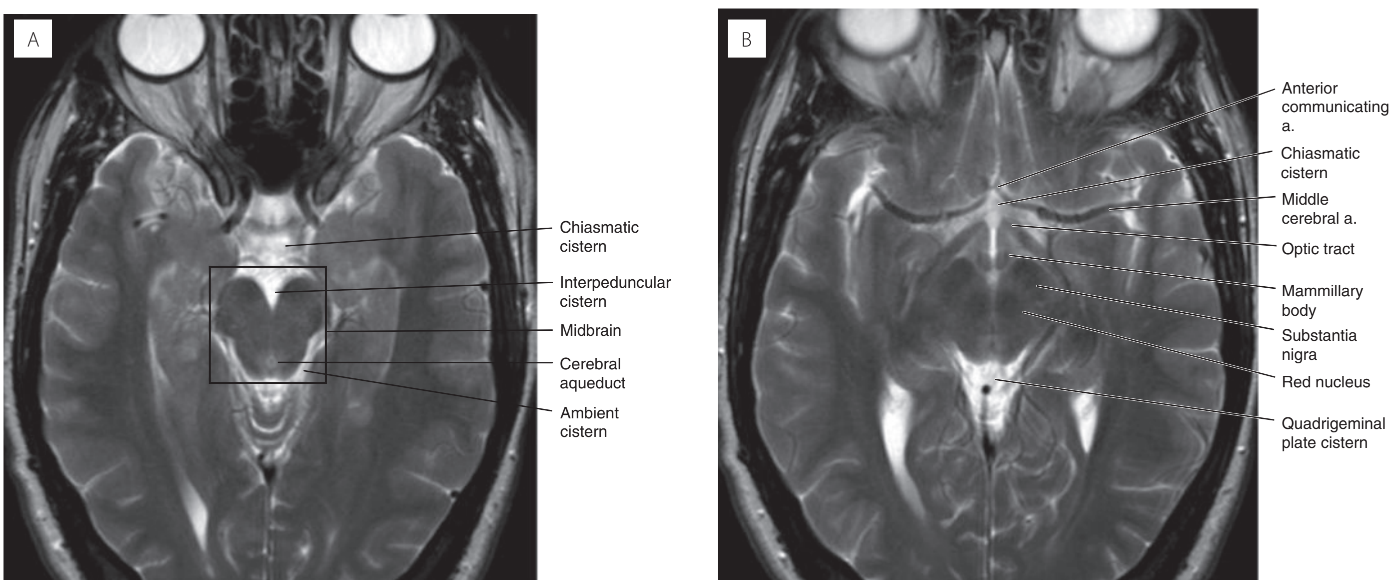


**Fig. 1.18** T2W axial MRI. The midbrain: (B) is cranial to (A).

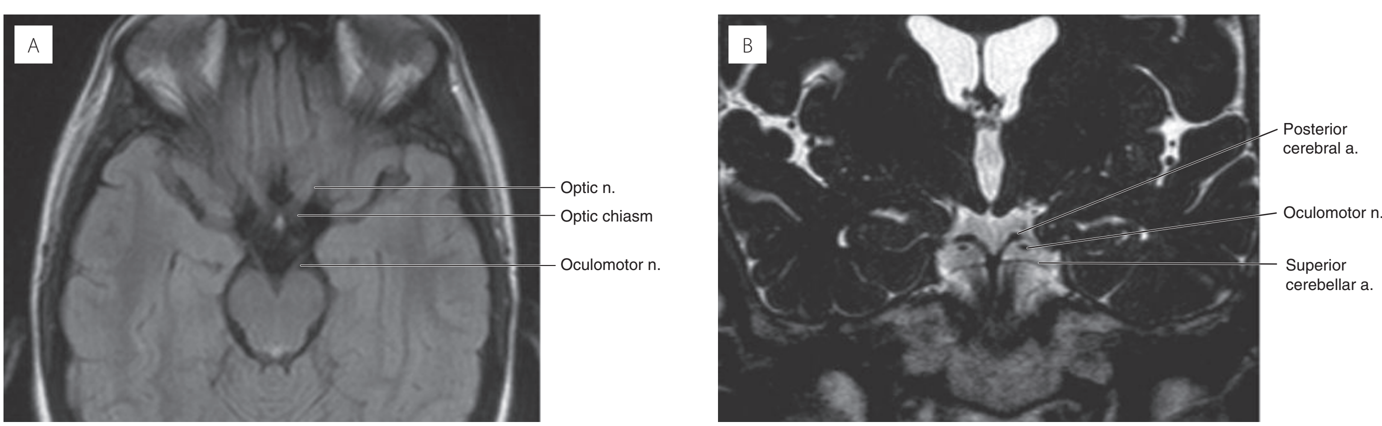


**Fig. 1.19** FLAIR axial MRI (A); T2W coronal MRI (B). The oculomotor (IIIrd cranial) nerve.

In axial section the lower pons is dominated by the posterolaterally directed middle cerebellar peduncles, giving it its descriptive bridge-like shape (Fig. 1.21).

Cranial nerves arising from the pons are, from above down, the trigeminal (Vth), the abducent (VIth), the facial (VIIth) and the vestibulocochlear (VIIIth).

The trigeminal (Vth) is the largest of the true cranial nerves and arises at the junction of pons and middle cerebellar peduncle, the two combined motor and sensory roots passing directly forwards to Meckel's cave (Fig. 1.22).

The abducent (VIth) has a relatively long intracranial course, passing in an anterolateral direction through Dorello's canal into the cavernous sinus. It loops over the petrous apex and has its own bony sulcus (Fig. 1.23).

The 'Michelin-man' appearance of the brainstem seen in Fig. 1.24 denotes the pontomedullary junction ('head' basilar artery, 'arms' middle and 'legs' inferior cerebellar peduncles).

## The medulla

The lower part of the medulla encloses a central canal continuous with the spinal cord below, and the contours of the two are similar (Fig. 1.25). It becomes 'open' superiorly where it is related to the lower part of the fourth ventricle and takes on a more complex, square-like shape.

The pyramidal and olivary eminences can be defined, separated by a sulcus.

Pyramidal (motor) tracts are anteriorly situated through the brainstem.

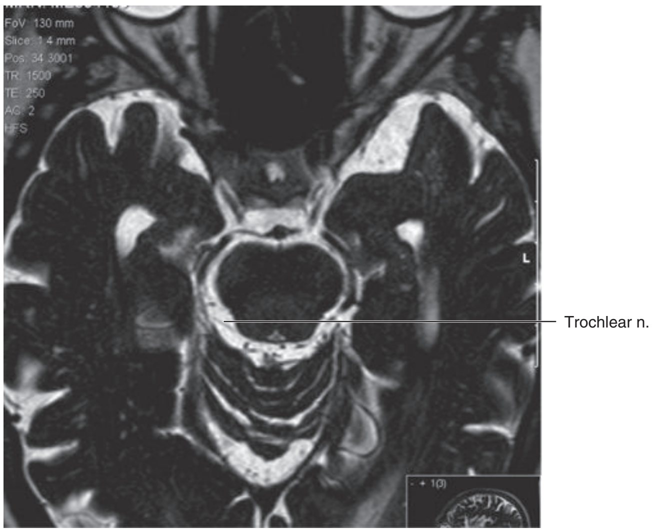


**Fig. 1.20** T2W axial MRI. The trochlear (IVth cranial) nerve.

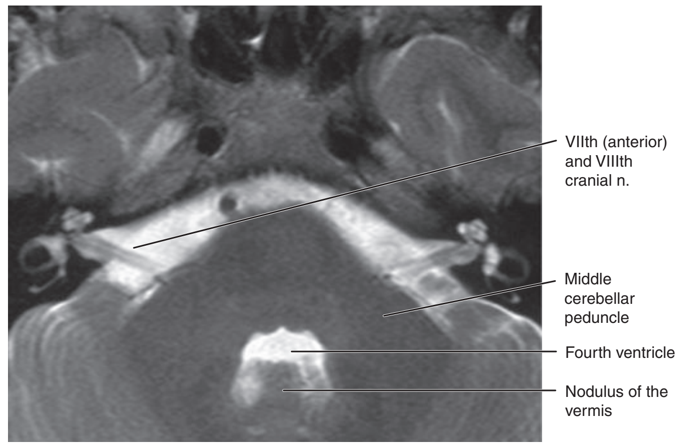


**Fig. 1.21** T2W axial MRI. The pons.

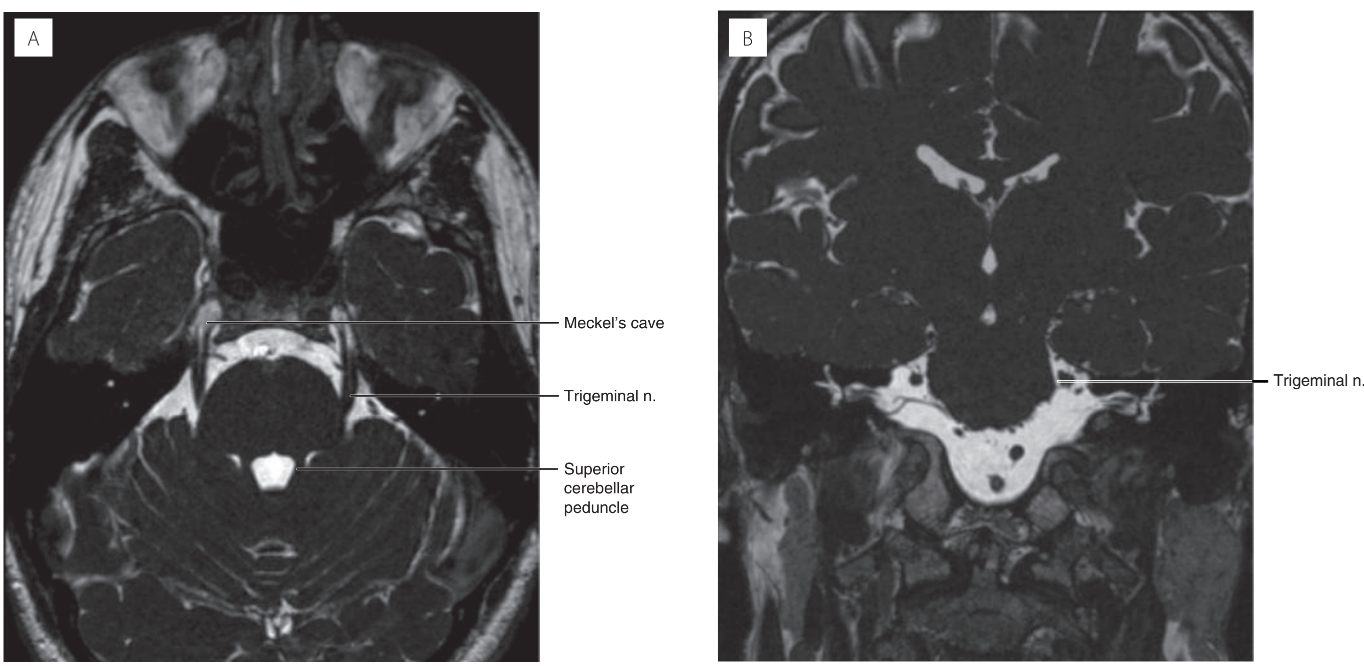


**Fig. 1.22** T2W axial MRI (A); T2W coronal MRI (B). The trigeminal (Vth cranial) nerve.

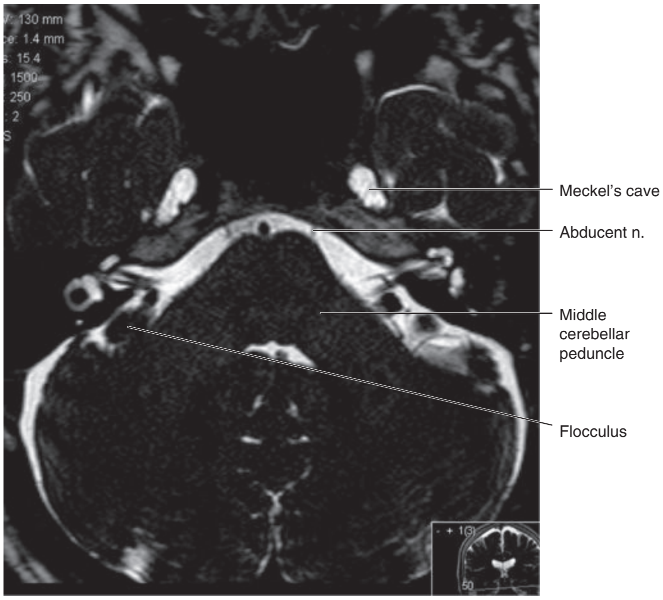


**Fig. 1.23** T2W axial MRI. The abducent (VIth cranial) nerve.

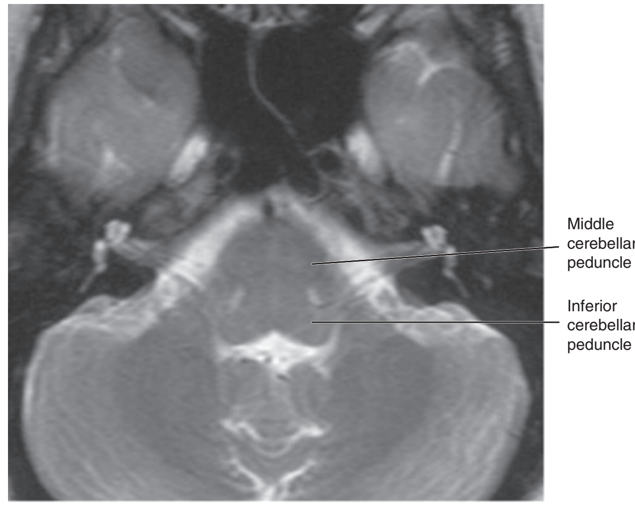


**Fig. 1.24** T2W axial MRI. The pontomedullary junction.

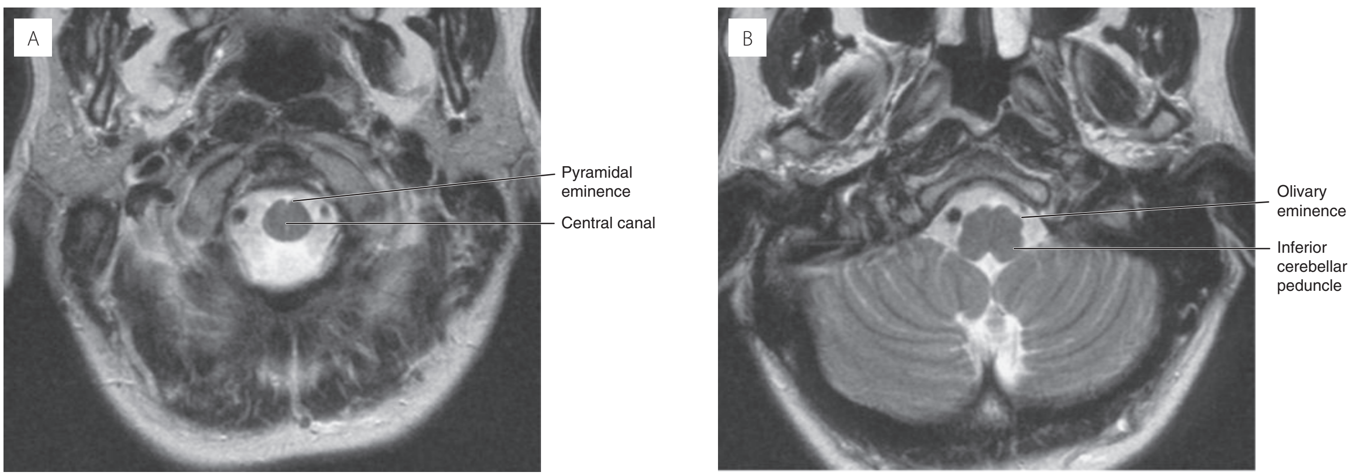


**Fig. 1.25** T2W axial MRI. The closed medulla (A). The open medulla (B).

Cranial nerves arising from the medulla are, from above down, the glossopharyngeal (IXth), the vagus (Xth), the spinal accessory (XIth) and the hypoglossal (XIIth).

The glossopharyngeal (IXth) and the vagus (Xth) cranial nerves arise from a sulcus posterolateral to the olive.

Imaging usually fails to separate completely the IXth, Xth and XIth cranial nerves and they pass as a bundle to the jugular foramen.

The hypoglossal (XIIth) nerve arises from the pre-olivary sulcus (Fig. 1.26).

## The cerebellum

The cerebellum lies posterior to the brainstem, to which it is connected by the cerebellar peduncles. The cortical mantle overlies the white matter core as in the cerebral hemispheres but the cerebellar cortical ridges, known as the folia, and the intervening sulci are approximately parallel to one another (Fig. 1.27).

The cerebellum consists of a narrow midline vermis and two hemispheres.

The flocculus is largely separate from the rest of the cerebellum and extends laterally just inferior to the vestibulocochlear (VIIIth) cranial nerve (Fig. 1.23).

The normal flocculus appears to enhance more than the rest of the cerebellum on CT after intravenous contrast because of its proximity to the choroid plexus and anterior inferior cerebellar artery. It might therefore be mistaken for an acoustic Schwannoma, although the flocculus lies posterior to the porus acousticus.

The nodule is the most ventral structure on the inferior vermian surface and is identified on axial scans indenting the fourth ventricle.

On the inferior surface of the cerebellar hemispheres are the tonsils. Posterior and lateral to the tonsils are the biventral lobules.

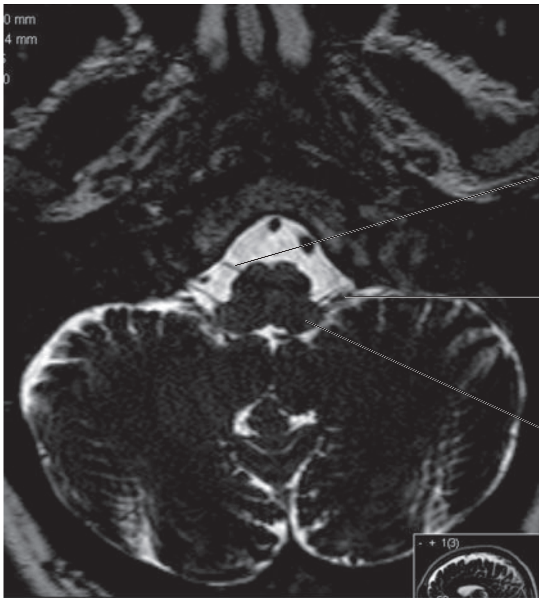


**Fig. 1.26** T2W axial MRI. The glossopharyngeal (IXth cranial), vagus (Xth cranial), accessory (XIth cranial) nerve bundle. The hypoglossal nerve.

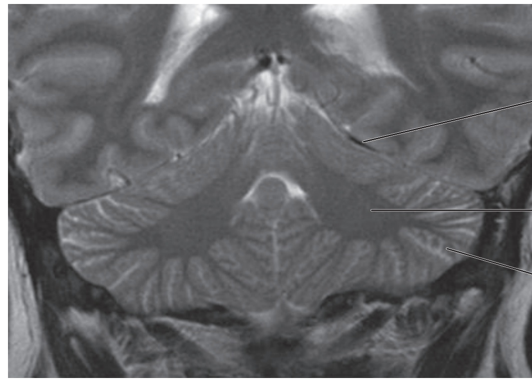


**Fig. 1.27** T2W coronal MRI. The cerebellum.

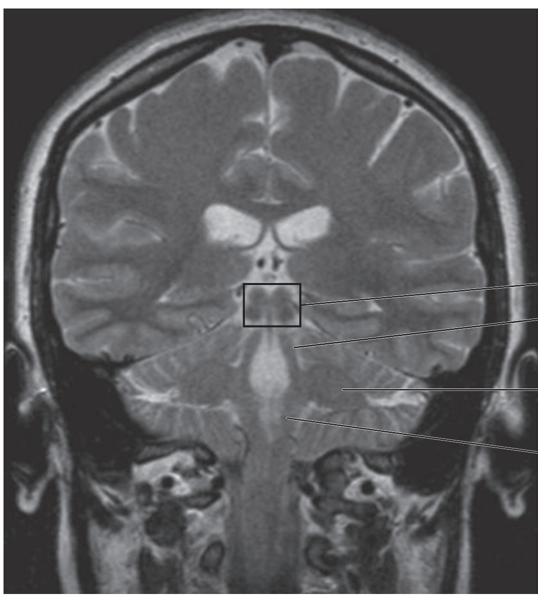


**Fig. 1.28** T2W coronal MRI. The cerebellar peduncles.

There are three cerebellar peduncles arising from the white matter core of the cerebellum on each side. The inferior cerebellar peduncle joins the medulla, the middle cerebellar peduncle (the largest) the pons and the superior, the midbrain.

Their relationship is best seen on coronal MRI (Fig. 1.28).

## The intracranial circulation

The brain is supplied by four arteries, the paired internal carotid and vertebral arteries (Fig. 1.29).

### Internal carotid artery (ICA)

The internal carotid artery arises at the carotid bifurcation at approximately the level of the third cervical vertebra.

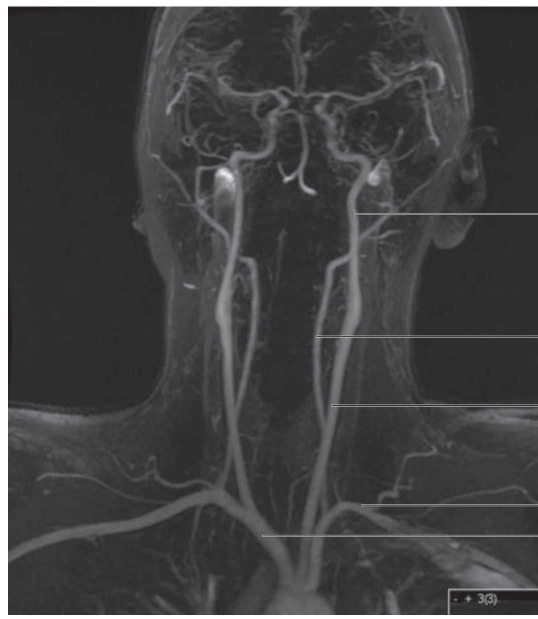


**Fig. 1.29** Time-of-flight (non-contrast) MR angiogram, frontal view. The great vessels.

It is divided into seven segments, C1–C7 (Fig. 1.30).

No constant branches arise from its cervical (C1) segment and the artery enters the cranial cavity through the carotid canal in the petrous bone, running first vertically then horizontally (C2 segment) (Fig. 1.31a).

The short C3 segment runs vertically and medially between the petrous apex and the cavernous sinus above the foramen lacerum. The artery here is closely related to the trigeminal ganglion within Meckel's cave (Fig. 1.31b).

C4 is the cavernous segment (Fig. 1.31c). The artery turns forwards in the cavernous sinus then upwards to form the clinoid (C5) segment.

The artery then enters the subarachnoid space.

The next segment is the ophthalmic (C6) segment, which extends just proximal to the posterior communicating artery. The distal segment (C7) extends to the terminal bifurcation.

C4, C5 and C6 segments form the U-shaped carotid siphon, part of which is therefore intracavernous, part in the subarachnoid space.

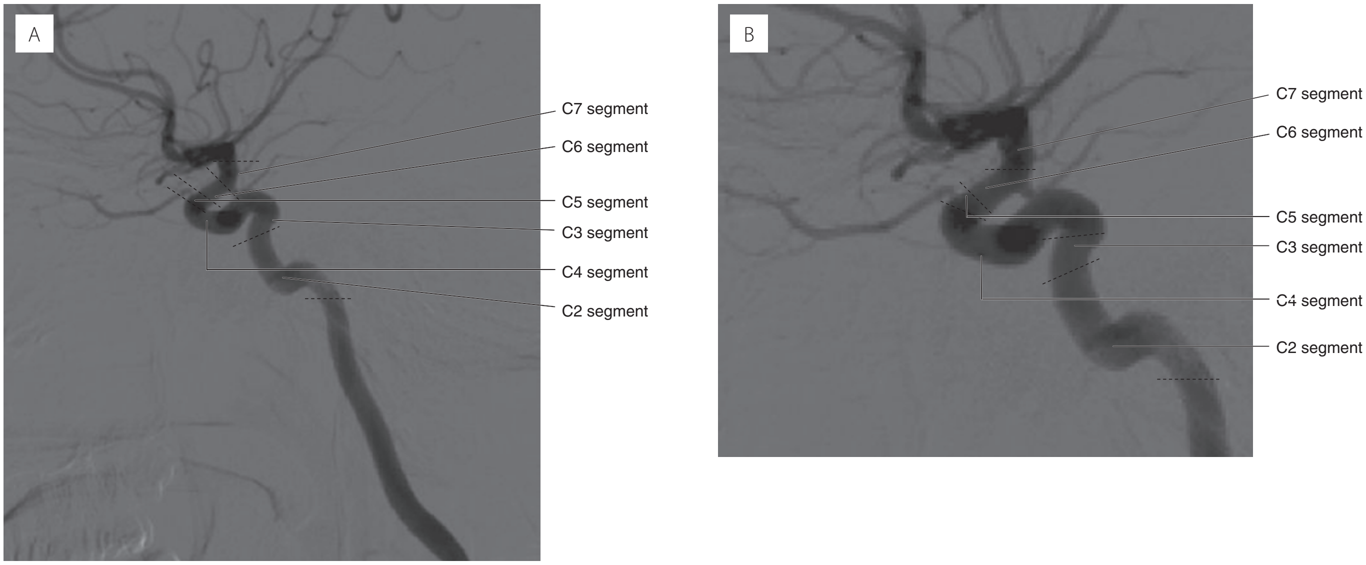


**Fig. 1.30** (A) Internal carotid angiogram; (B) lateral projections. The arterial segments.

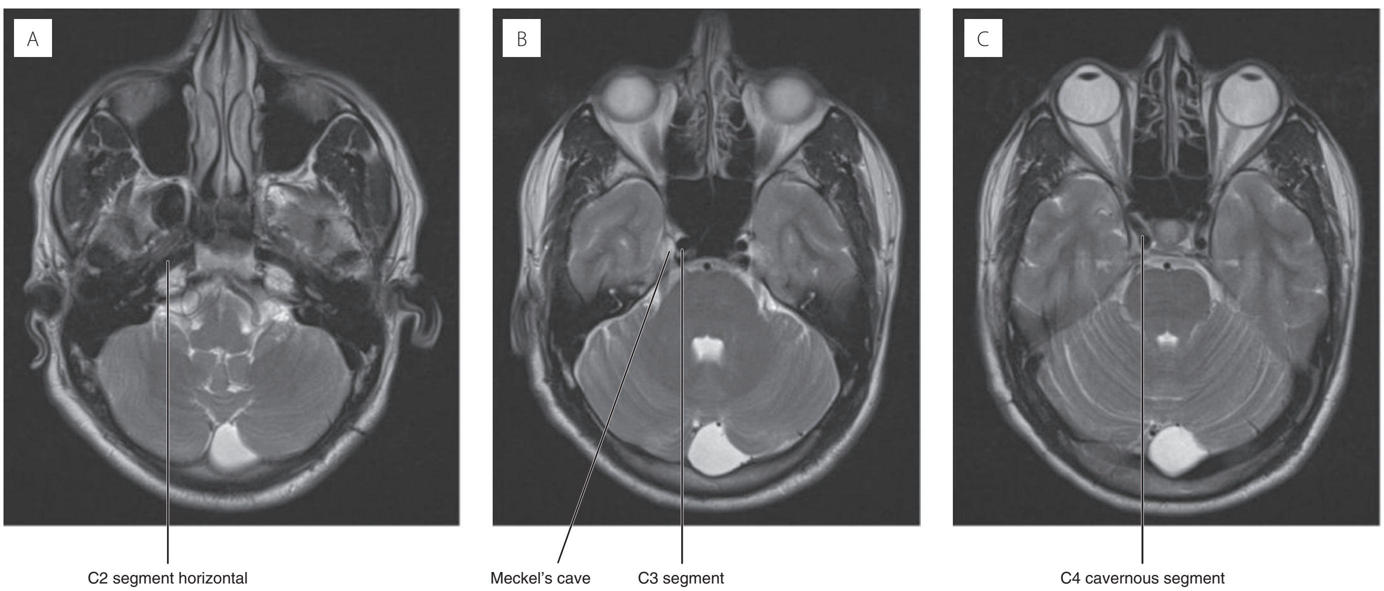


**Fig. 1.31** T2W axial MRI. The internal carotid artery at the skull base; (A)–(C), inferior to superior.

It should be noted that there are no angiographic indicators of the precise limits of the intracavernous portion of the internal carotid artery. Although there may be anatomical variation, lesions arising at, or distal to, the ophthalmic artery origin are taken to be within the subarachnoid space.

## Branches of the ICA (Fig. 1.32)

The ophthalmic artery is the first supraclinoid branch of the ICA recognizable on normal angiography. It arises in the subarachnoid space and runs forward through the optic canal within the optic nerve sheath (see Chapter 2).

The posterior communicating artery is the second intracranial branch of the ICA and connects it to the posterior cerebral artery, just distal to the origin of the latter (see 'Posterior cerebral artery' below). The oculomotor (IIIrd) cranial nerve passes between the posterior communicating artery above and the superior cerebellar artery below (Fig. 1.19).

The anterior choroidal artery arises from the posteromedial aspect of the ICA just distal to the posterior communicating artery and is well seen on the lateral angiogram. Its first or cisternal part lies between the uncus and optic tract. It then enters into the temporal horn of the lateral ventricle through the choroidal fissure into the choroid plexus. On the lateral angiogram there is an upwards 'kink', the plexal point, where the artery passes through the choroidal fissure (Fig. 1.32a).

The ICA divides, terminally, into the anterior and middle cerebral arteries. This T-shaped bifurcation is not normally in

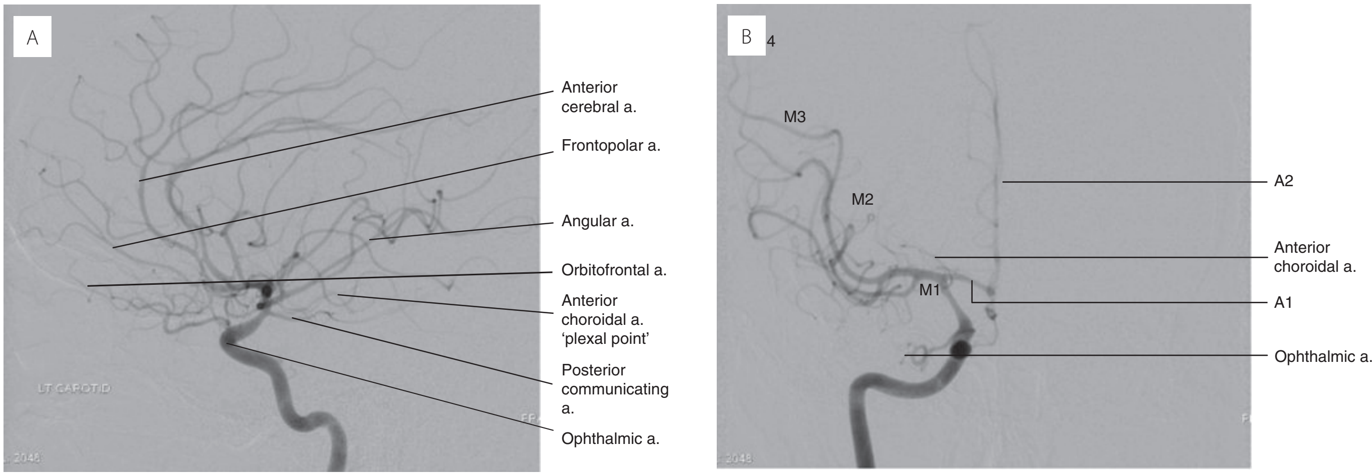


**Fig. 1.32** Internal carotid angiogram, lateral (A) and frontal (B) projections. Major named arteries.

the true coronal plane since the MCA is directed posterolaterally. This requires an oblique angiographic projection to display the anterior and middle cerebral arteries en face.

## The circle of Willis (Figs. 1.33, 1.34)

Branches of the internal carotid and basilar arteries form an anastomotic ring on the ventral surface of the brain, known as the circle of Willis. This affords some protection against cerebral infarction in the event of arterial occlusion.

The participating arteries are the terminal ICAs, the first part of the anterior cerebral arteries (A1 segments), the anterior communicating artery, the posterior communicating arteries, the first parts of the posterior cerebral arteries (P1 segments) and the basilar artery. Small perforating arteries arise from the communicating arteries.

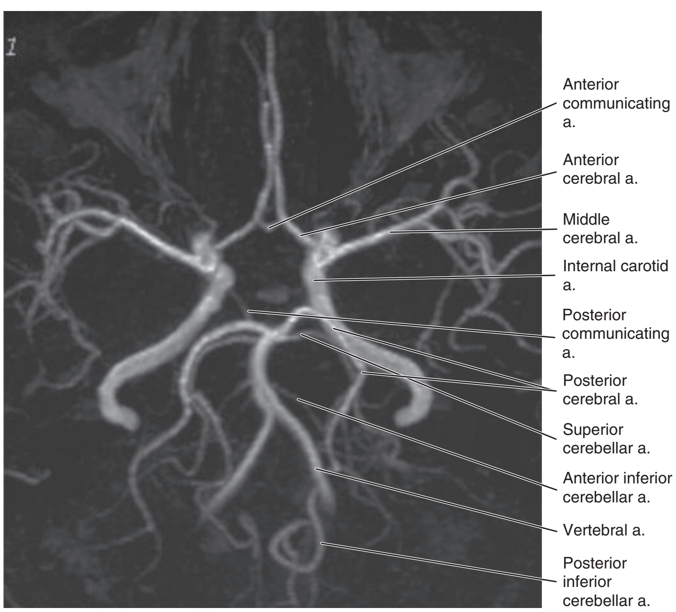


**Fig. 1.33** Time-of-flight (non-contrast) MR angiogram, axial view. The circle of Willis.

In the axial plane the 'circle' has a polygonal configuration within the suprasellar cistern.

Hypoplasia or aplasia of its component parts is common and the circle is complete in only a minority of individuals.

# Extra- and intracranial arterial connections

The circle of Willis is the 'central' anastomotic network linking the intracranial carotid circulations on each side and the vertebrobasilar circulation. There are also cortical connections between branches of the anterior, middle and posterior cerebral arteries.

Numerous anastomotic paths exist between internal and external carotid arteries and between the external carotid and vertebral arteries.

There may be persistent segmental connections between the internal carotid and basilar arteries, the commonest of which is the trigeminal artery arising from the lower part of the cavernous carotid.

## The anterior cerebral artery (ACA) (Figs. 1.32, 1.33, 1.34)

The anterior cerebral artery is the smaller terminal branch of the internal carotid artery and it runs anteromedially towards the midline, where it is seen above the optic nerve. This is the pre-communicating, horizontal or A1 segment. Both anterior cerebral arteries come to lie in close proximity at the base of the interhemispheric fissure, where they are usually linked by a short bridging vessel, the anterior communicating artery, within the cistern of the lamina terminalis.

The A2 segment of the anterior cerebral artery extends from the anterior communicating artery to the origin of the frontopolar artery. Thereafter the A3 segment travels around the genu of the corpus callosum to the origin of the callosomarginal artery.

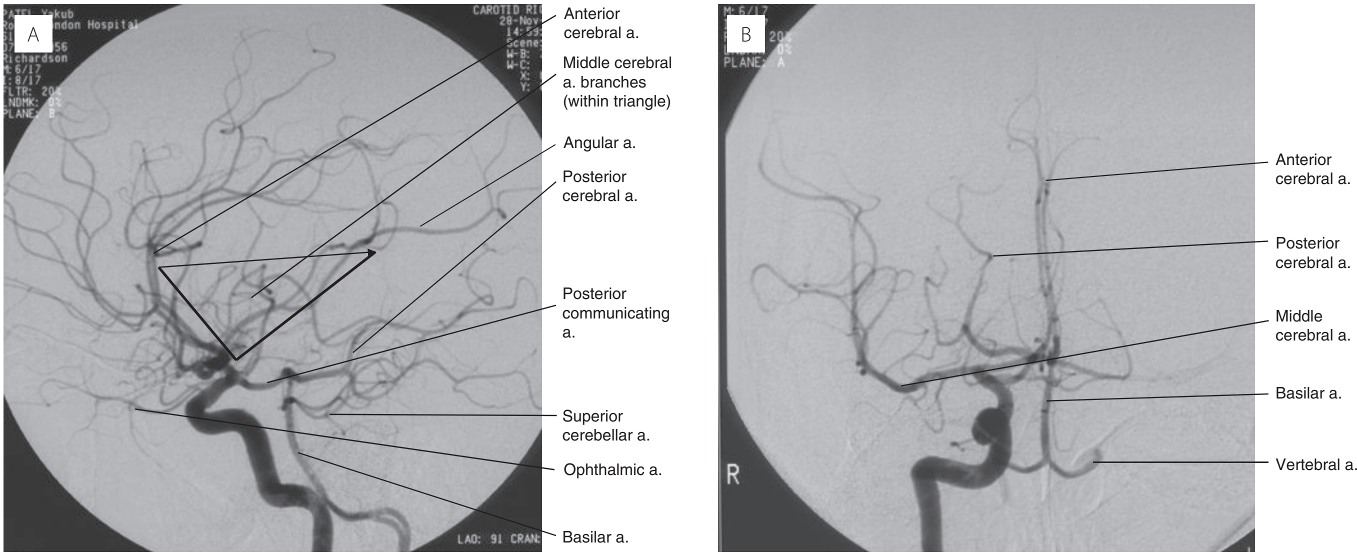


**Fig. 1.34** Internal carotid angiogram, lateral (A) and frontal (B) projections. The major named branches in a patient with a complete circle of Willis permitting opacification of the contralateral intracranial carotid circulation and the vertebrobasilar system.

## ACA branches

Heubner's recurrent artery is the largest of the perforating medial lenticulostriate branches which course posterosuperiorly. The lenticulostriate arteries supply a number of important structures of the anterobasal brain. They are also 'end' arteries.

Heubner's artery can arise from the proximal A2 segment or A1 segments along with the majority of the medial lenticulostriate branches.

The anterior communicating artery, although short, gives rise to several branches which course superiorly to supply the optic chiasm and other anterior midline structures.

The orbitofrontal artery is usually the first cortical branch of the A2 segment, arising from the subcallosal segment to supply the inferior and inferomedial surfaces of the frontal lobe including the gyri recti.

The frontopolar artery runs from the genu of the corpus callosum to the frontal pole and supplies the orbital gyri, olfactory bulb and tract and the anterior part of the superior frontal gyrus.

The callosomarginal artery is present in approximately half of all cases. It runs through the cingulate sulcus above the cingulate gyrus and gives rise to anterior, middle and posterior internal frontal branches. These supply the superior frontal gyrus.

The pericallosal artery is the continuation of the anterior cerebral artery beyond the origin of the callosomarginal artery. It arches posteriorly over the genu of the corpus callosum to lie on its superior surface as far as the splenium and below the cingulate gyrus.

The anterior cerebral arteries are sometimes fused proximally to form a single trunk or azygos artery, which arises between the hemispheres before dividing near the genu of the corpus callosum.

## The middle cerebral artery (MCA) (Figs. 1.32, 1.33, 1.34)

This is the larger terminal branch of the internal carotid artery. Its proximal portion, the M1 segment, runs laterally to the horizontal limb of the Sylvian fissure between the frontal and temporal lobes. At the anteroinferior aspects of the insula the middle cerebral artery turns upwards, forming its genu (the distal limit of the M1 segment) and its branches (the M2 segment), then runs over the surface of the insula in the depths of the Sylvian fissure.

At the superior limit of the insula they turn inferiorly and then laterally under the frontoparietal operculum (M3 segment) to emerge from the lateral aspect of the Sylvian fissure and spread out over cortical surfaces of the frontal, parietal, occipital and temporal lobes (M4 segments).

### MCA branches

A variable number of lateral lenticulostriate branches arise from the M1 segment, which supply the basal ganglia, internal capsule and caudate nucleus.

The anterior temporal arteries usually arise from the M1 segment and course over the anterior pole of the temporal lobe.

The terminal arterial division of M1 is termed the MCA trifurcation but more properly comprises two sequential bifurcations. A number of variable cortical branches extend over the surface of the hemispheres, the largest and most posterior of which is the angular artery.

## Posterior cerebral artery (see p. 22)

Figure 1.35 illustrates the territories supplied by the various arteries.

There is some individual variation.

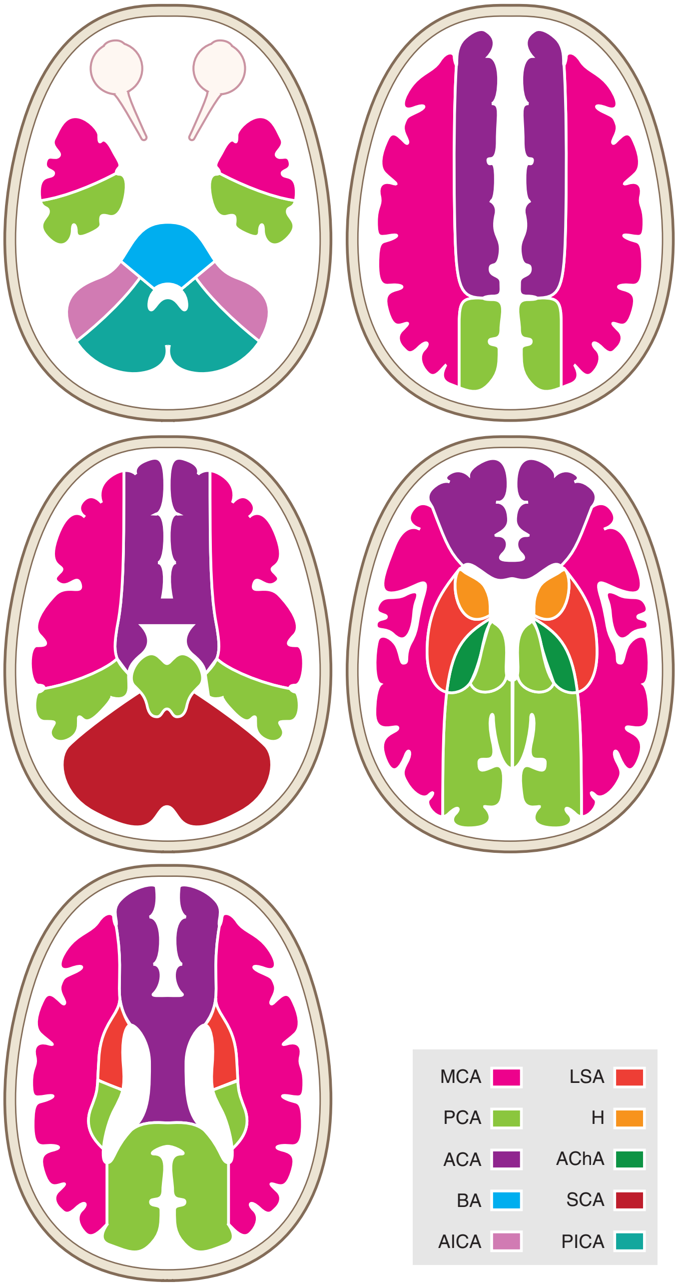


**Fig. 1.35** The vascular territories. Brain arterial distributions. ACA = anterior cerebral artery, H = recurrent artery of Heubner, MCA = middle cerebral artery, LSA = lenticulostriate artery, AChA = anterior choroidal artery, PCA = posterior cerebral artery, BA = basilar artery, SCA = superior cerebellar artery, AICA = anterior inferior cerebellar artery, PICA = posterior inferior cerebellar artery.

## The dural venous sinuses (Fig. 1.36)

The dural sinuses are valveless trabeculated venous channels and may conveniently be divided into a superior group related to the vault and the basal group found at the skull base. The sagittal, transverse and straight sinuses are the main components of the superior group. The basal group comprises the cavernous, petrosal and sphenoparietal sinuses.

The superior sagittal sinus, which is triangular in cross-section, increases in size from back to front and usually begins near the crista galli, although it may not develop anterior to the coronal suture. In the majority of individuals, most of its flow is directed to the right transverse sinus with the straight sinus draining to the left transverse sinus. Cortical veins enter perpendicular to the superior sagittal sinus anteriorly but the angle becomes shallower more posteriorly with the veins entering against the direction of flow. As with venous systems elsewhere, normal anatomical variants are common. The superior sagittal sinus may bifurcate well above its normal termination at the internal occipital protuberance ('torcular'). This early separation may lead to an erroneous diagnosis of sagittal sinus thrombosis on CT, if the intervening space is mistaken for non-enhancing thrombus (a false positive empty triangle or empty delta sign).

The inferior sagittal sinus is the marker for its inferior margin of the falx. It is not uncommon to identify it at catheter angiography and on gadolinium-enhanced T1-weighted MRI in the midsagittal plane (Fig. 1.37).

The transverse sinuses commence at the torcular and lie within the outer margins of the tentorium (Figs. 1.36, 1.38). The right is usually dominant and larger than that on the left and receives almost the entire output of the superior sagittal sinus. The sinus on one side can be poorly developed or even absent. In order to distinguish such a variant from sinus occlusion, it is often helpful to examine with CT the bony depressions in the vault in which the sinus runs to the jugular foramen, both of which will be correspondingly underdeveloped in the congenital variant.

The transverse sinuses become the sigmoid sinuses at the posterior petrous edge continuing towards the jugular bulb. The transverse and sigmoid sinuses are together known as the lateral sinus. Occasionally one encounters intraluminal filling defects in the transverse sinus due to prominent arachnoid granulations. Where the sigmoid sinus is adjacent to the petrous bone, there can be pseudo-erosive changes in the bone margin. Normal petromastoid aeration is a useful guide to this variant.

The straight sinus lies at the junction of the falx and the tentorium and the torcular is where the straight, transverse and superior sagittal sinuses meet (venous confluence 1). The vein of Galen (the great cerebral vein) joins the inferior sagittal and straight sinuses at the venous confluence within the quadrigeminal plate system (venous confluence 2) (Fig. 1.36a).

Although functionally a single unit, the paired cavernous sinuses are situated on either side of the pituitary fossa and receive the superior and inferior ophthalmic veins and the sphenoparietal sinuses (Figs. 1.36, 1.39). They connect with each other through the intercavernous sinuses and posteriorly they communicate with the transverse sinuses, by the superior petrosal sinus on each side. Each is a trabeculated, extradural venous channel lying on the body of the sphenoid bone. The internal carotid artery pursues an S-shaped course through the sinus before piercing its dural roof, medial to the anterior

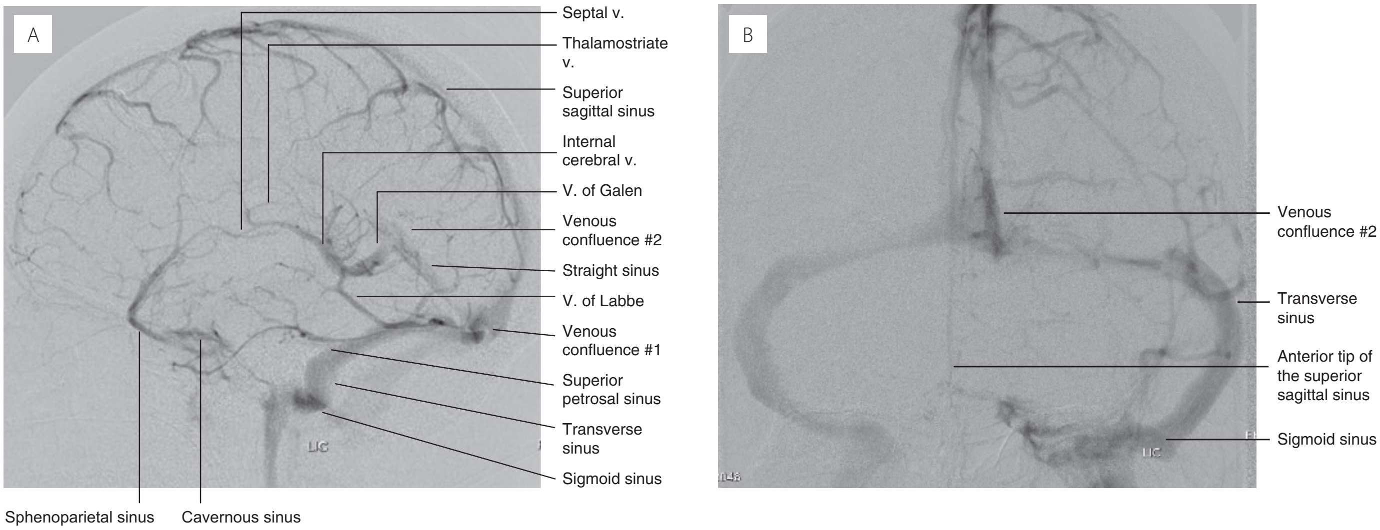


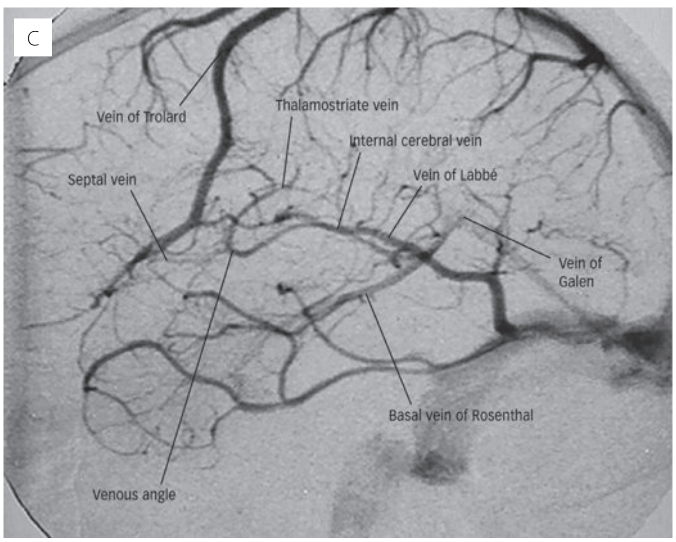


**Fig. 1.36** Internal carotid angiogram, venous (late) phase, lateral (A) and frontal (B) projections. Panel (C) is from a different patient illustrating individual variation. Note that there are two 'venous confluences'. The first is in the quadrigeminal cistern involving the great vein of Galen, the straight sinus and the inferior sagittal sinus. The second is at the torcular and involves the superior sagittal sinus, the straight sinus and the transverse sinuses.

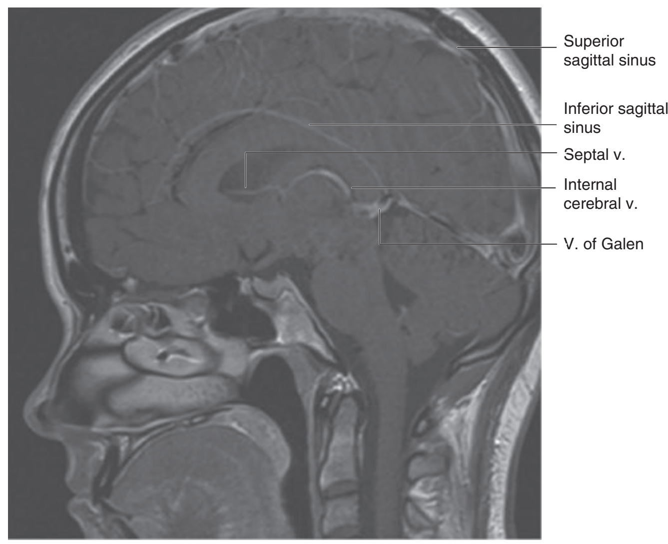


**Fig. 1.37** Contrast-enhanced T1W cranial MR. Midline sagittal section of the brain. The cerebral venous system.

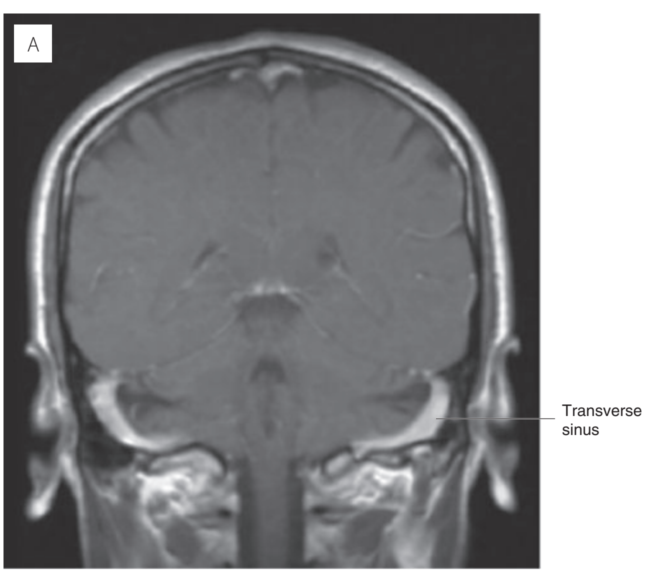


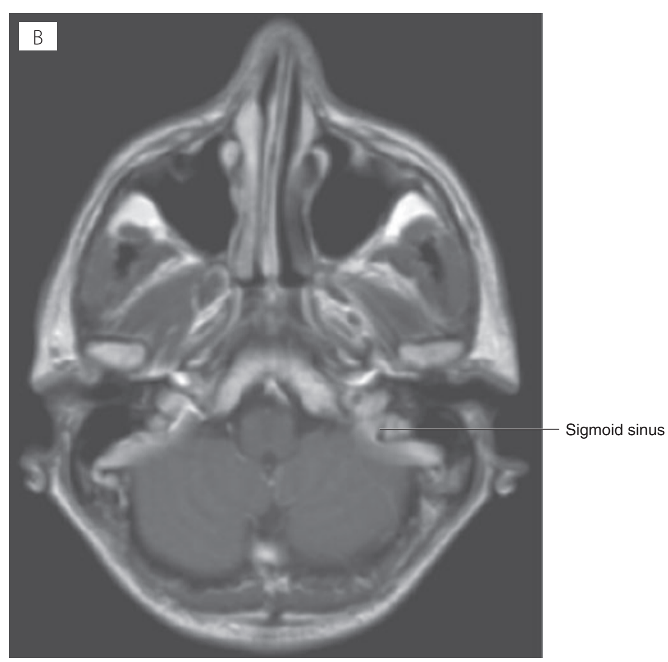


**Fig. 1.38** Contrast-enhanced T1W MRI: (A) coronal, (B) axial scans. Transverse and sigmoid sinuses.


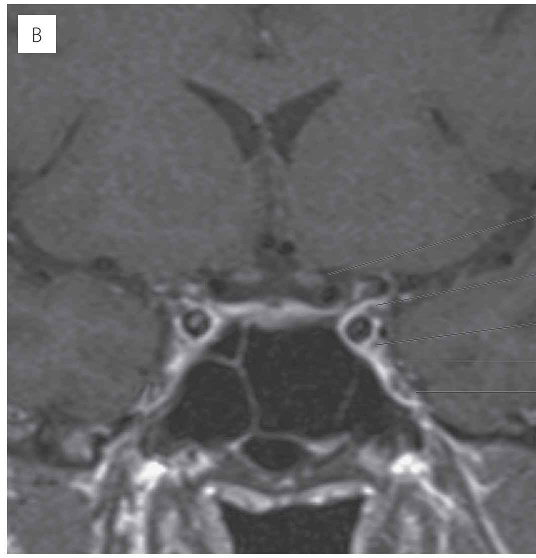



**Fig. 1.39** Contrast-enhanced T1W cranial MR: axial scan (A): coronal scans; (B) is anterior to (C). The cavernous sinuses.

clinoid process. The abducent nerve lies free within the sinus applied to the lateral wall of the artery. From above down, the oculomotor, trochlear, ophthalmic and maxillary nerves run in a common dural tunnel in the lateral wall of the sinus to reach the superior orbital fissure (Fig. 1.39).

The cavernous sinuses enhance with intravenous contrast on both CT and MRI. Fat deposits can occur normally within the sinus and are demonstrated by CT as hypodense foci. The normal sinus has a concave lateral wall and the two sinuses should be symmetrical. Inferiorly the ophthalmic division of the trigeminal nerve, also embedded in the lateral wall, courses towards the trigeminal ganglion.

The trigeminal ganglion contains the cell bodies of the sensory root of the trigeminal nerve. It is crescentic in shape and occupies a dural recess in the medial wall of the middle fossa at the petrous apex posterior to the cavernous sinus. This recess, known as Meckel's cave, is in continuity with the prepontine system and is of cerebral spinal fluid density and signal intensity on CT and MRI, respectively. It will also be opacified during CT cisternography.

The petrosal and sphenoparietal sinuses drain the cavernous sinuses on each side. The superior petrosal sinuses are situated at the junction of the tentorium and the petrous bone. They drain to the transverse sinuses. The inferior petrosal sinuses lie between the clivus and petrous apex and run medial to the superior sinus to the jugular bulb. The sphenoparietal sinus is a medial extension of the sylvian vein and courses around the greater sphenoid wing.

## The supratentorial venous system

### See Fig. 1.36

Blood within the superficial cerebral veins flows in a centrifugal direction, radially towards the dural venous sinuses or adjacent lacunae. The veins are valveless.

Almost all of the superficial veins are unnamed and inconstant, with three exceptions. The superficial middle cerebral (sylvian) vein forms along the surface of the Sylvian fissure and is convex anteriorly on a lateral projection. It is continuous with the sphenoparietal sinus.

The anastomostic veins of Trolard, superiorly, and Labbe, inferiorly, connect the superficial middle cerebral vein with superior sagittal and transverse sinuses, respectively. It is uncommon for both anastomotic veins to be well developed in an individual. Blood in the deep cerebral veins flows centripetally (i.e. centrally). Medullary veins drain to subependymal veins along the walls of the lateral ventricles. The thalamostriate vein is a member of the subependymal group and runs across the floor of the lateral ventricle over the thalamus to enter the internal cerebral vein behind the foramen of Monro.

The septal vein, another subependymal vein, passes around the head of the caudate nucleus and travels posteriorly in the septum pellucidum. It too enters the internal cerebral vein behind the foramen of Monro. The venous angle, at the confluence of the thalamostriate and septal veins, denotes the posterior margin of the foramen on the lateral angiogram.

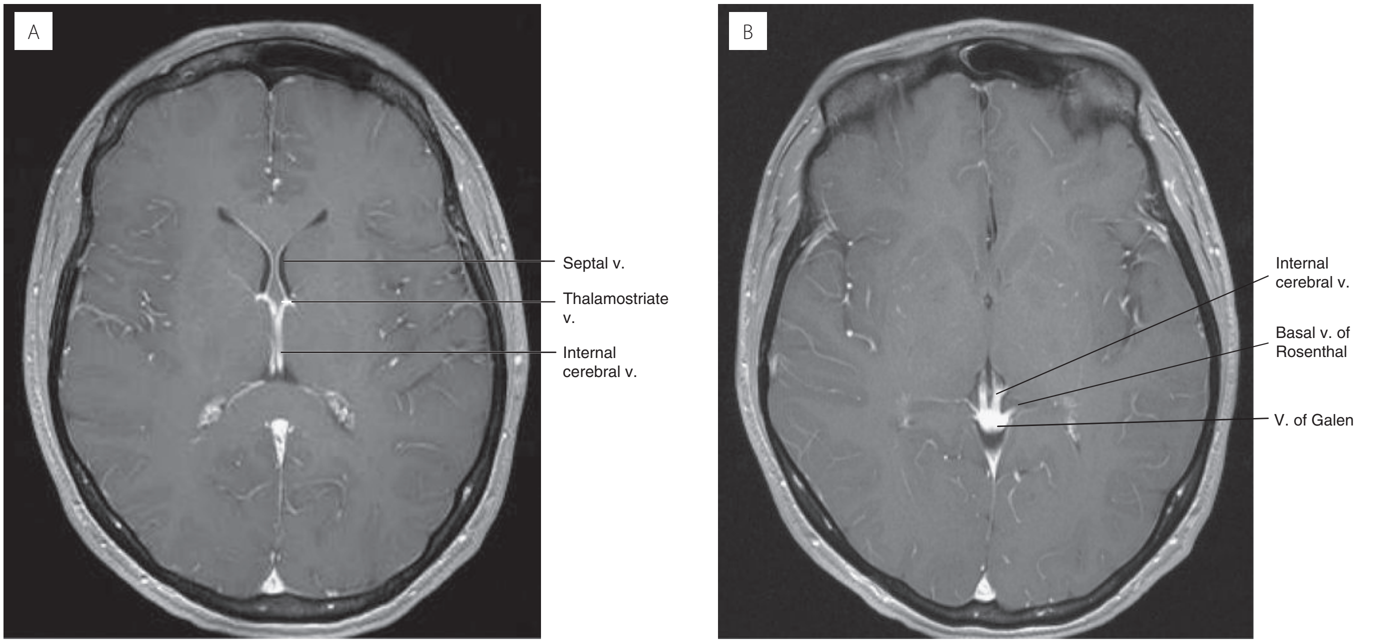


**Fig. 1.40** Contrast-enhanced T1W cranial MR, axial scans. The deep cerebral veins: (A) is superior to (B).

The basal vein of Rosenthal forms in the Sylvian fissure and travels in the ambient cistern around the midbrain to enter the vein of Galen, along with the internal cerebral vein. Both the basal vein and internal cerebral vein are paired structures, the latter running along the roof of the third ventricle, from the foramen of Monro in the cistern of the velum interpositum. The vein of Galen is a short (1–2 cm) single midline vessel and originates under the splenium of the corpus callosum, curving posteriorly and superiorly towards the straight sinus. Elements of the deep cerebral venous system can be identified on intravenous contrast-enhanced CT and MRI (Fig. 1.40).

## The vertebrobasilar arterial system

There are four vertebral artery segments. The first, extraosseous segment (V1) extends from the subclavian artery origin to the C6 foramen transversarium. Then the osseous V2 segment passes through foramina transversaria of the cervical column to C1. The arterial course here is vertical to C2. Then it turns laterally and once again vertically to the C1 foramen transversarium. V3 is the extraspinal segment directed superomedially to the foramen magnum. V4 is the intracranial segment, within the subarachnoid space (Figs. 1.41, 1.42).

The normal anatomy of the intracranial vertebrobasilar arterial is subject to some individual variation in the origins, course and distribution of the component arteries (Fig. 1.43). There is also a well-developed network of anastomoses between these arteries.

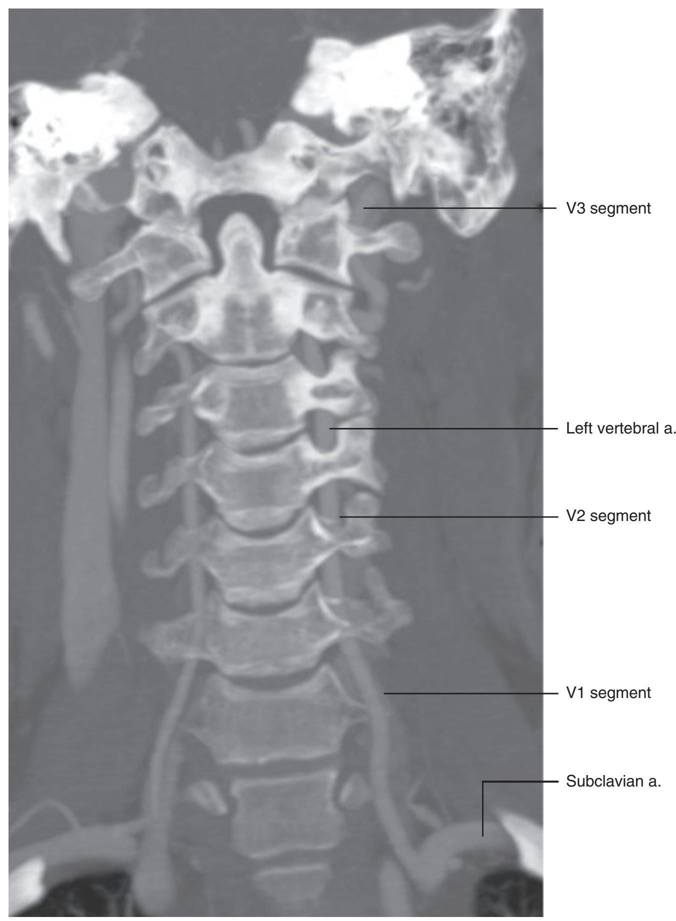


**Fig. 1.41** CT angiogram, frontal (coronal) reconstruction. The vertebral arteries. The vertebral artery segments.

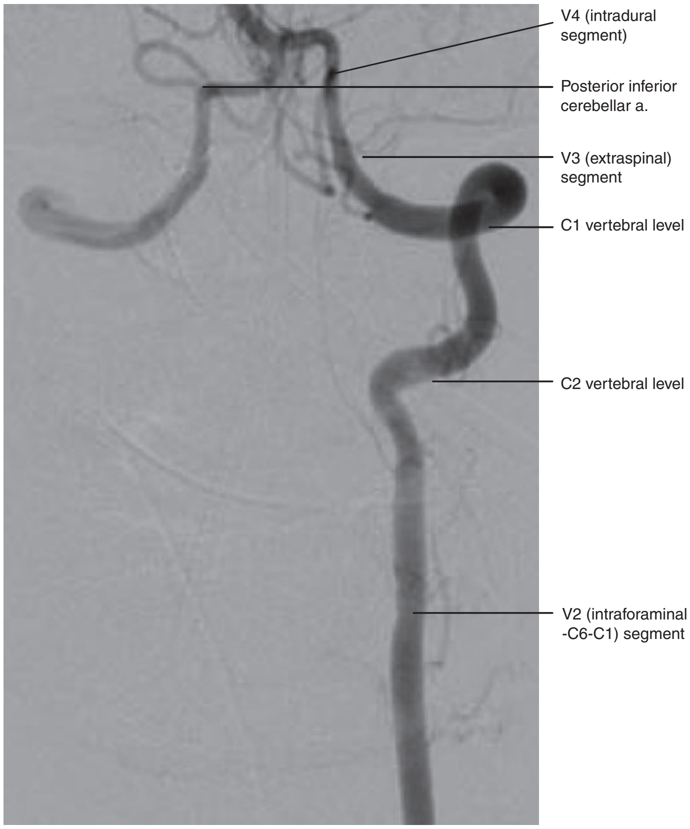


**Fig. 1.42** Left vertebral catheter angiogram, frontal projection. The vertebral artery segments.

## The posterior inferior cerebellar artery (PICA)

PICA arises from the vertebral artery as its largest and most distal branch. It usually rises well above the foramen magnum but may arise below it. There is a reciprocal arrangement with the anterior inferior cerebellar artery such that if one is hypoplastic then the other will be well-developed. In a small proportion of cases, one, usually hypoplastic, vertebral artery terminates as the PICA.

The PICA first winds around the olive of the medulla and comes near to the biventral lobule of the cerebellum. This is the anterior medullary segment (Fig. 1.43b(1)). The vessel then courses around the brainstem as the lateral medullary segment, which corresponds to the caudal loop seen on the lateral projection at angiography(2).

This curves around the inferior margin of the cerebellar tonsil. The posterior medullary segment ascends to the superior part of the tonsil and, at the apex of the cranial loop, gives off branches which supply the choroid plexus of the fourth ventricle(3). The PICA then proceeds to supply the undersurface of the cerebellar hemisphere. Meningeal branches may also arise from it.

## Basilar artery

The basilar artery forms from the confluence of the vertebral arteries at the pontomedullary junction. It ascends approximately in the midline in the pontine system and grooves the surface of the anterior pons. Superiorly it courses a little posteriorly before dividing into the posterior cerebral arteries. Throughout the length of the basilar artery, small penetrating branches pass posteriorly into the brainstem, which are at risk during vascular interventional procedures.

## The anterior inferior cerebellar artery (AICA)

AICA passes laterally from the basilar artery, closely related to the abducent nerve. It traverses the cerebellar pontine angle system, usually anterior and medial to the neural bundle. A lateral branch then courses around the flocculus and a medial branch supplies the biventral lobule and cerebellar hemisphere.

A labyrinthine artery supplies the inner ear.

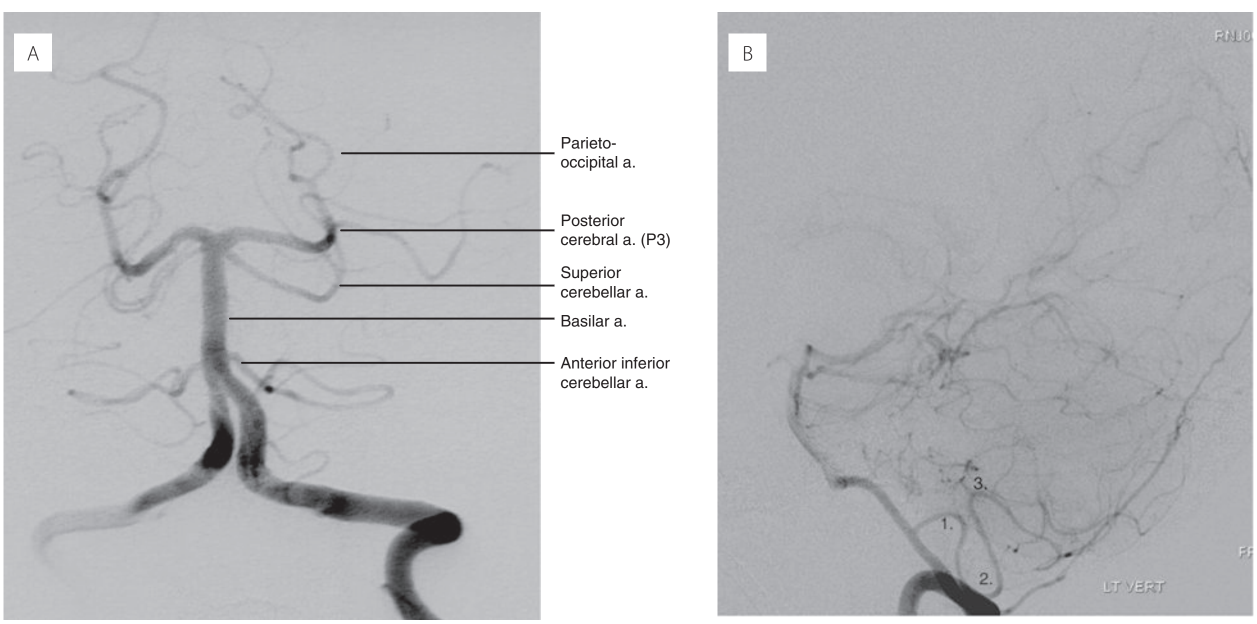


**Fig. 1.43** Left vertebral catheter angiogram: (A) frontal, (B) lateral projections. The vertebrobasilar arterial system. Posterior inferior cerebellar artery. (1) anterior medullary segment, (2) lateral medullary segment, (3) supratonsillar segment.

## The superior cerebellar artery

The superior cerebellar artery arises from the basilar artery near to its terminal division. It runs laterally around the brainstem and comes to lie inferior to the oculomotor nerve, which separates it from the posterior cerebral artery. At the lateral border of the pons it turns posteriorly over the middle cerebellar peduncle as the ambient segment and the tentorium may come into contact with the artery. The ambient segment parallels the course of the trochlear nerves, and it is notable that the basal vein, the posterior cerebral artery and the free edge of the tentorium are also in this plane. In the quadrigeminal cistern both superior cerebellar arteries approach the midline. They supply the cerebellar hemispheres and superior vermis.

## The posterior cerebral artery

Each posterior cerebral artery can be divided into a number of segments (Fig. 1.44). The P1 or pre-communicating segment extends from the basilar bifurcation to the origin of the posterior communicating artery. It lies within the interpeduncular fossa and thalamoperforating arteries rise from both this P1 segment and from the posterior communicating artery. These branches have an extensive distribution to the thalamus, hypothalamus, the oculomotor and trochlear nerves and to the internal capsule.

The P2 or ambient segment runs around the brainstem in the ambient cistern, parallel to the basal vein. It courses around the cerebral peduncles to lie above the tentorium.

The P2 segment may be compressed against the tentorial edge when there is uncal pressure on the midbrain in the presence of raised intracranial pressure. Infarction of the occipital lobe is thus a recognized consequence. The P2 segment usually gives rise to the inferior temporal artery and a single medial and multiple lateral posterior choroidal arteries.

The P3 segment extends from the quadrigeminal plate cistern to the calcarine fissure. The two major terminal branches of the posterior cerebral artery are the parieto-occipital and calcarine arteries. The smaller calcarine artery is seen angiographically to pursue a straight course, running between the parieto-occipital branch posteriorly and the posterior temporal branch inferiorly on the lateral projection. The posterior pericallosal arteries arch over the splenium and arise from either the posterior cerebral or parieto-occipital arteries. There is some variation between individuals as to the origin of the posterior cerebral artery branches. It is not uncommon to encounter the so-called fetal origin of the posterior cerebral artery. In this case the precommunicating (P1) segment is undeveloped, and the posterior cerebral artery fills exclusively from the internal carotid artery, and not from the basilar artery.

## Diencephalon

The diencephalon comprises a large aggregate of grey matter, which lies between the cerebral hemispheres and brainstem and which borders the third ventricle.

The thalamus is the largest structure in the diencephalon and is made up of a number of functionally important nuclei. The most dorsal nucleus is called the pulvinar (Fig. 1.45). The two thalami are apposed (not in continuity) in the midline at the interthalamic adhesion or massa intermedia.

The hypothalamus forms the roof of the interpeduncular fossa and the floor of the third ventricle.

The pineal gland (or body) hangs by a stalk joined to the posterior aspect of the diencephalon and third ventricle. It lies in the midline above the superior colliculi (Fig. 1.46). In adults, it is almost invariably calcified, when seen on CT (Fig. 1.12). It is not protected by the blood–brain barrier and consequently enhances avidly with contrast.

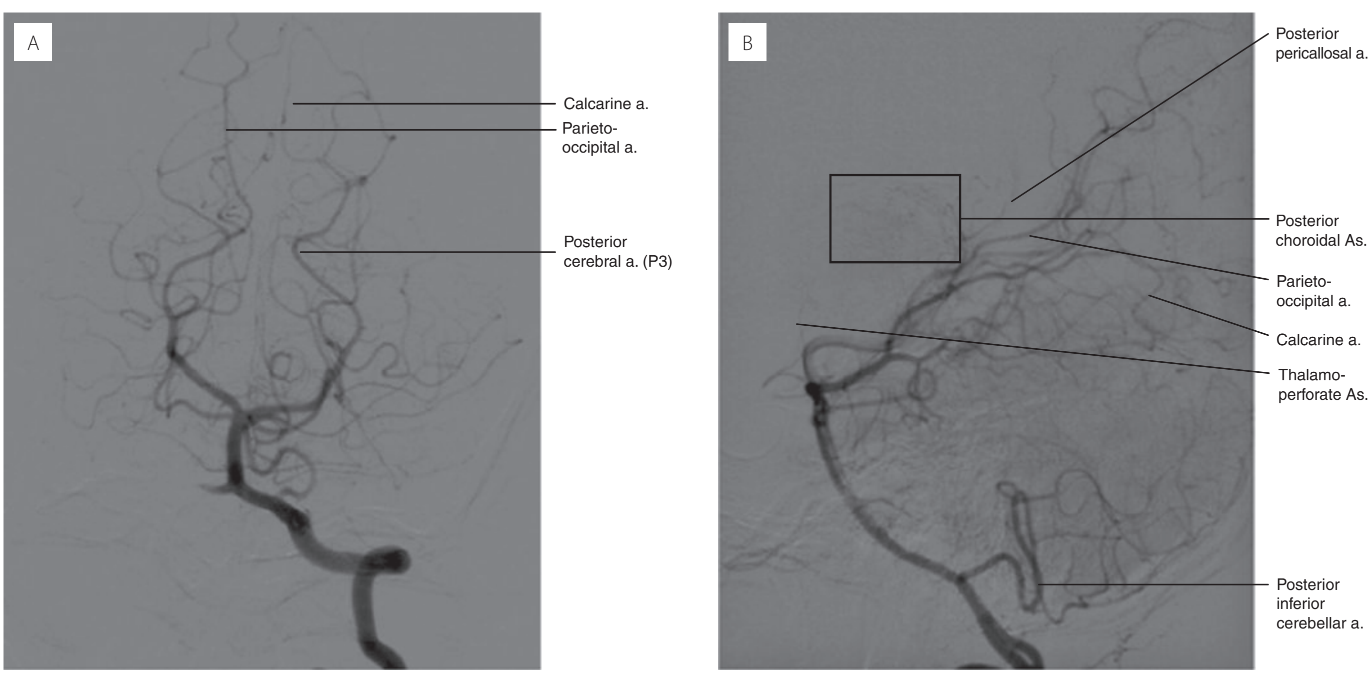


**Fig. 1.44** Left vertebral catheter angiogram: (A) frontal, (B) lateral projections. The posterior cerebral arteries.

The pineal stalk consists of two laminae, forming the habenular commissure superiorly and the posterior commissure inferiorly.

The habenular commissure can calcify and forms a C shape, the open part of the C directed posteriorly.

## The pituitary gland

The pituitary gland occupies the pituitary fossa in the body of the sphenoid bone, situated in the midline above the sphenoid sinus in between the cavernous sinuses (Fig. 1.47). It is suspended from the pituitary stalk, or infundibulum, which arises from a hollow eminence of grey matter called the tuber cinereum, the inferior part of the hypothalamus. The tuber cinereum lies posterior to the optic chiasm and anterior to the mamillary bodies.

Like the pineal gland, the pituitary gland, the infundibulum and the tuber cinereum enhance normally with contrast due to the absence of a blood–brain barrier.

The anterior lobe (adenohypophysis) can be distinguished from the posterior lobe (neurohypophysis) on sagittal MRI scans. The neurohypophysis often has a conspicuous appearance on T1W images due to the presence of vasopressin/oxytocin – the so-called pituitary 'bright spot' (Fig. 1.47a).

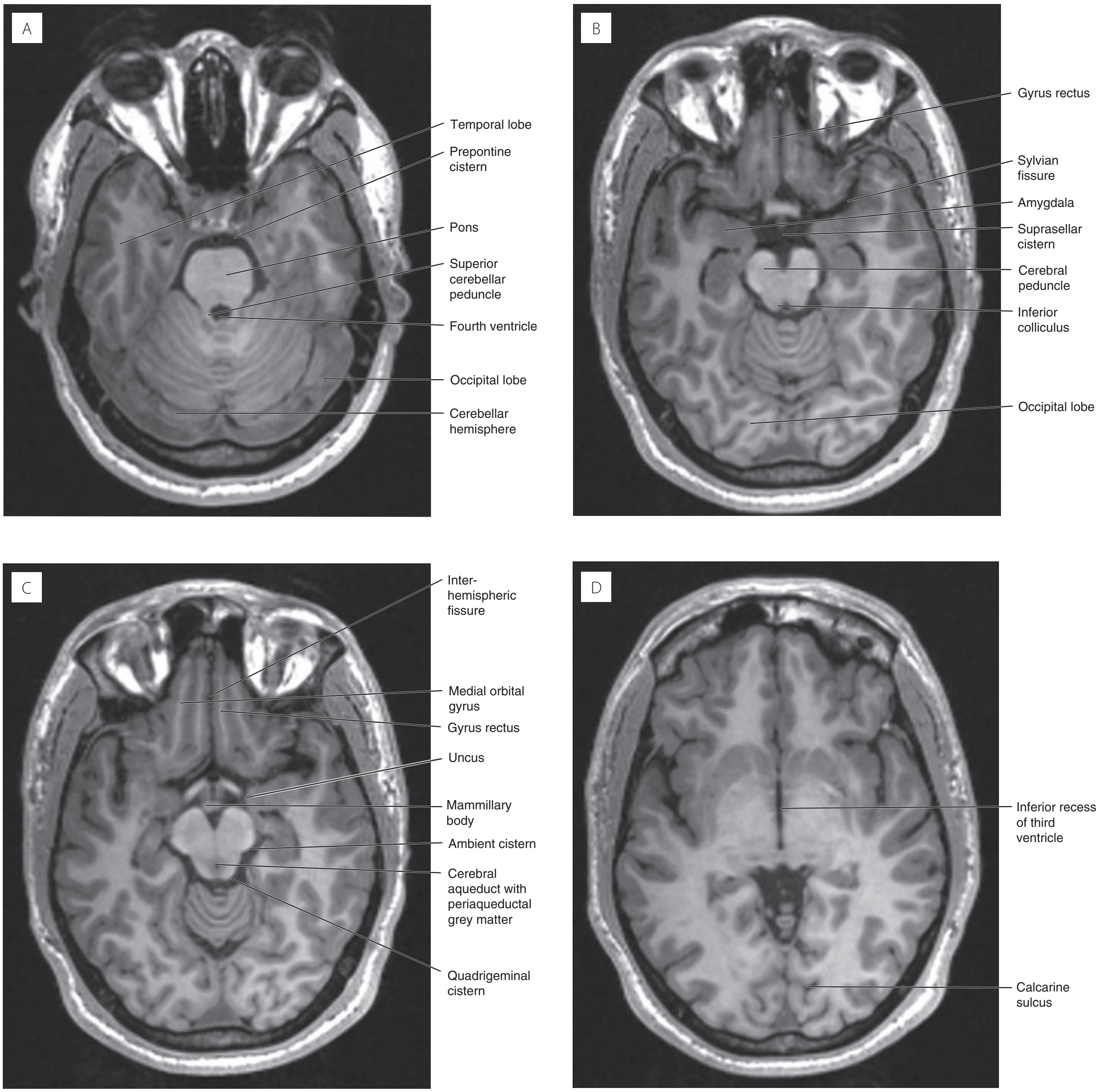


**Fig. 1.45** Axial T1-weighted images through the brain: (A)–(K), inferior to superior.

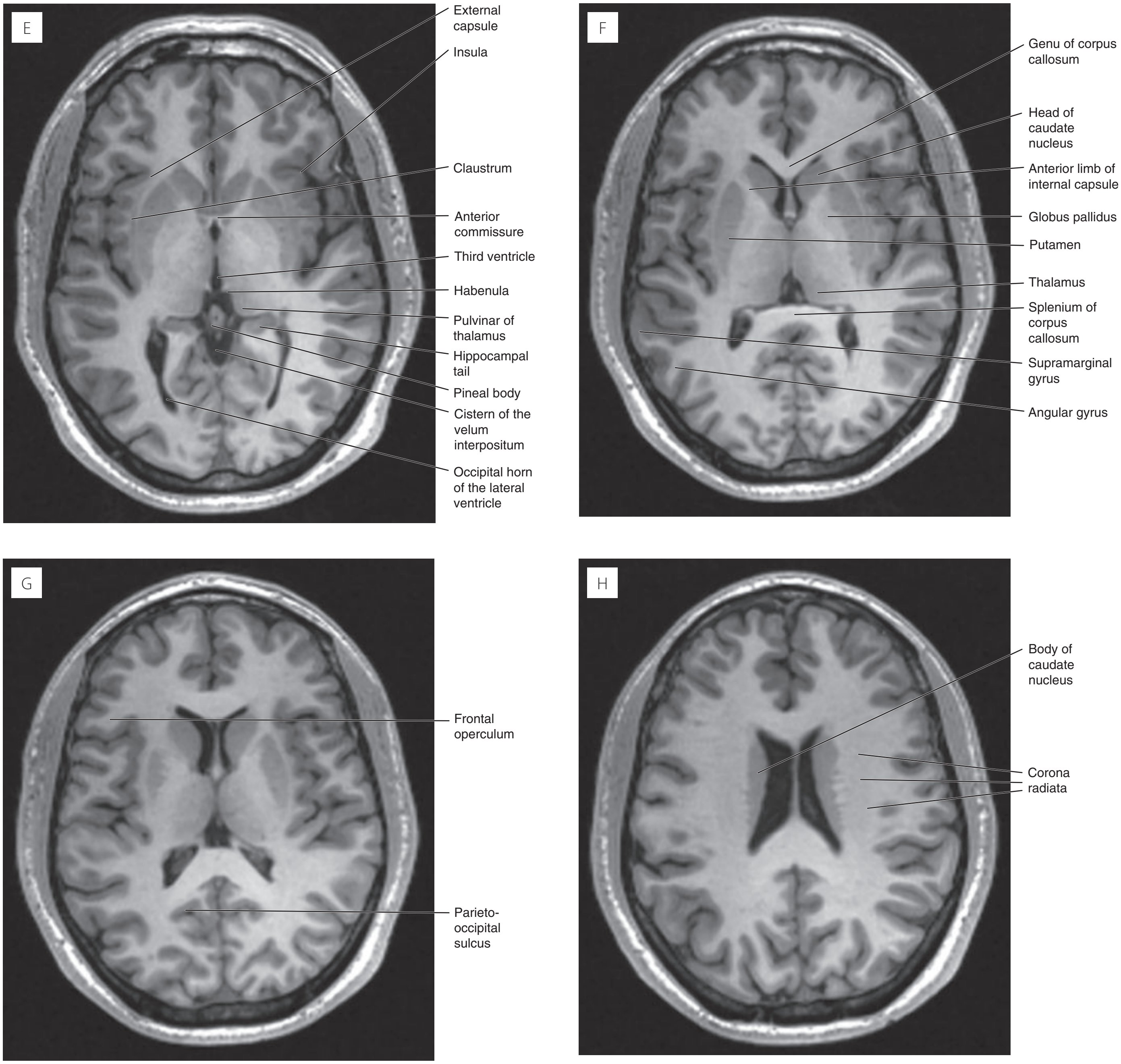


**Fig. 1.45** *(cont.)*

The presence of the bright spot is variable both between individuals and in the same individual scanned at different times.

Normal sizes (measured from superior to inferior) of the gland are:

- 6 mm or less in children
- 8 mm in males
- 10 mm in females
- 12 mm in pregnant/lactating females.

The superior margin of the gland is normally concave but can be convex in the neonate and in females of reproductive age.

## The basal ganglia

The basal ganglia comprise several deep grey matter nuclei within the forebrain, midbrain and diencephalon (Figs. 1.18b, 1.48, 1.49, 1.50):

- caudate nucleus
- putamen
- globus pallidus (also referred to as the pallidum)
- subthalamic nucleus
- substantia nigra.

Knowledge of the rather complex three-dimensional anatomy of these nuclei is invaluable when interpreting CT or MR images. The head of the caudate nucleus indents the frontal

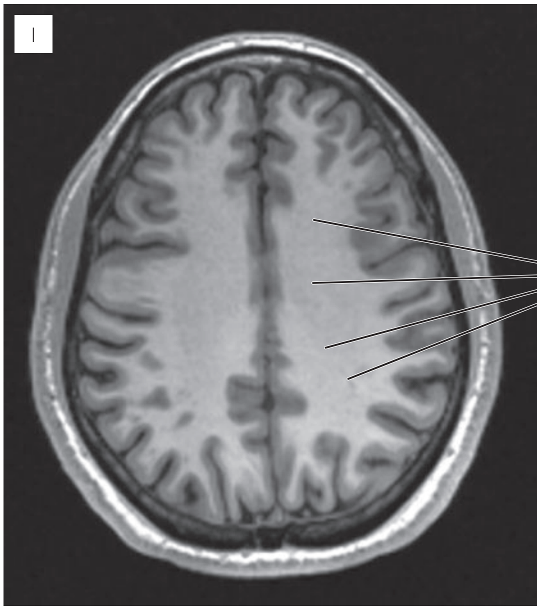


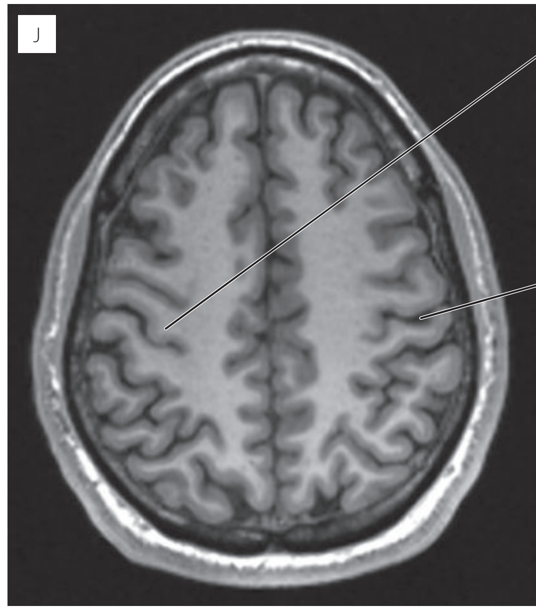


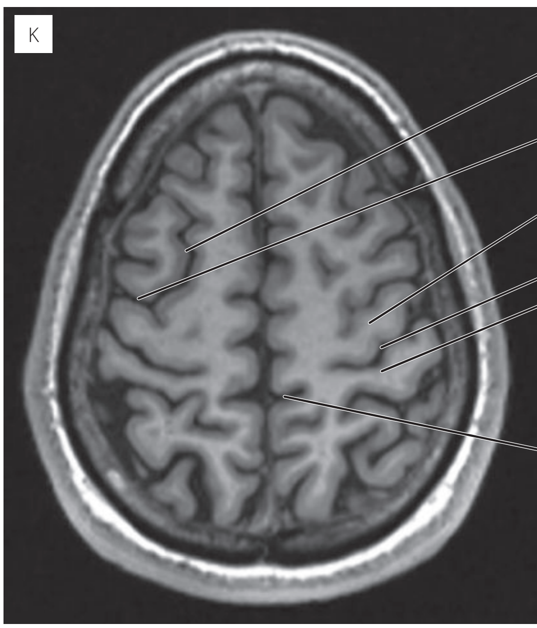


**Fig. 1.45** (*cont.*)

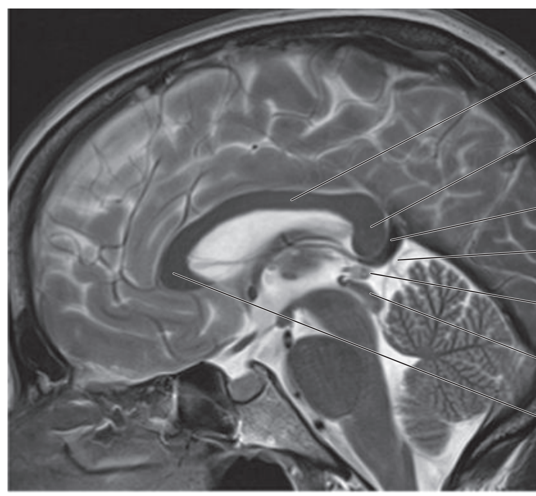


**Fig. 1.46** T2 sagittal MRI. Pineal gland.

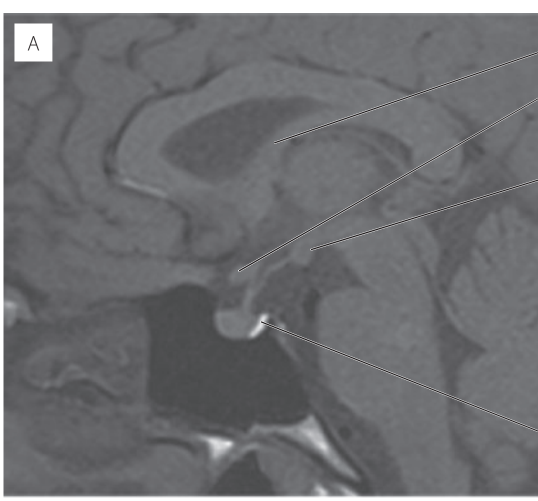


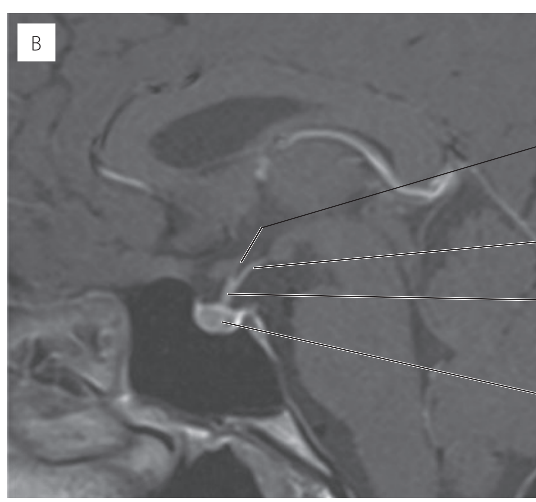


**Fig. 1.47** T1 sagittal MRI. Pituitary gland: (A) pre, (B) post contrast.

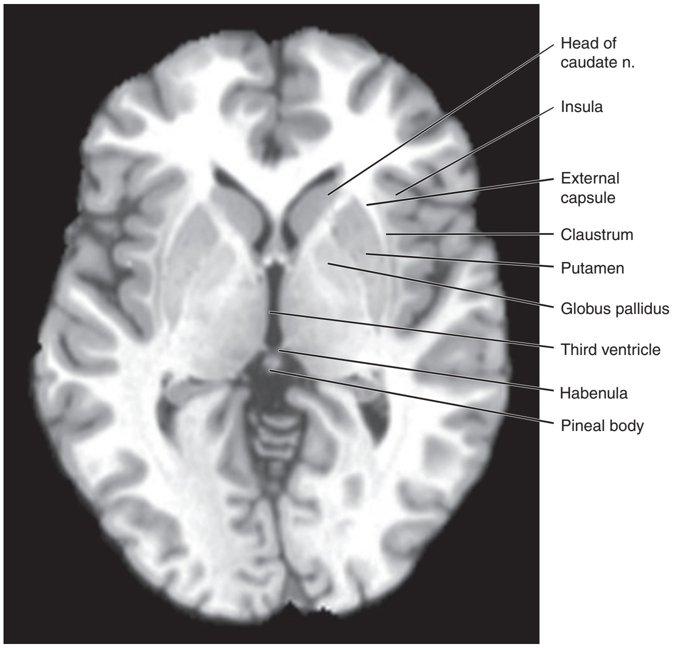


**Fig. 1.48** Skull-stripped axial T1-weighted image. The basal ganglia.

horn of the lateral ventricle. Its body curves upwards and posteriorly from the head, following the contour of the body of the lateral ventricle before continuing in an arch to its thinnest part, the tail, which comes to lie immediately superior to the temporal horn of the lateral ventricle

The subthalamic nucleus is an ovoid aggregation of grey matter that lies medial to the internal capsule, lateral to the hypothalamus and superolateral to the red nucleus (Fig. 1. 51). It establishes connections with both internal and external segments of the globus pallidus and with the thalamus. Damage to this nucleus results in contralateral hemiballismus – uncontrolled jerks of the limbs.

## The limbic system

The limbic system is a complex arrangement of interrelated cortical and subcortical structures that play a major role in memory, olfaction and emotion. The following is a list of its core components:

- hippocampal formation
- parahippocampal gyrus
- amygdala
- hypothalamus.

The limbic lobe refers to the cortical parts of the limbic system. It forms a border (limbus) around the diencephalon and midbrain, which is composed of three C-shaped arches one inside the other, viewed from a lateral perspective (Fig. 1.52).

Outer arch:

- parahippocampal gyrus
- cingulate gyrus
- subcallosal gyrus

Middle arch:

- hippocampus proper (cornu ammonis)
- dentate gyrus
- indusium griseum (supracallosal gyrus)
- paraterminal gyrus

Inner arch:

- fornix and fimbria.

The hippocampus incorporates several structures, which together may be called the hippocampal formation. During development, this area of cortex becomes rolled up into an S-shape, which forms at the medial (also called mesial) aspect of the temporal lobe (Figs. 1.53, 1.54). It comprises the hippocampus proper (also called the cornu ammonis), the dentate gyrus and the subiculum. The subiculum lies inferior to the hippocampus proper and blends into the

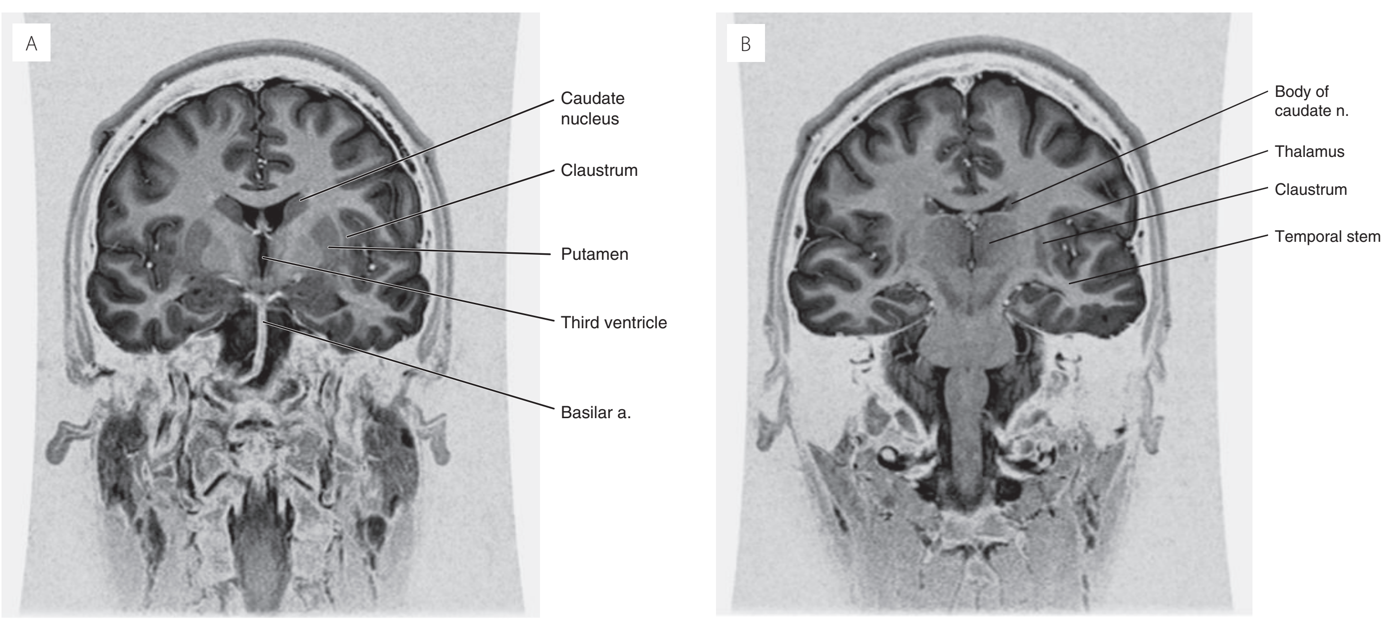


**Fig. 1.49** Coronal inversion recovery MR image (3T): (A) is anterior to (B).

adjacent parahippocampal gyrus. The hippocampi are closely scrutinized by the neuroradiologist for mesial temporal sclerosis in the context of temporal lobe epilepsy. The hippocampus can be recognized in the coronal plane as a protrusion into the medial temporal horn of the lateral ventricle. The border between the parahippocampal gyrus (medially) and the occipitotemporal gyrus (also known as the fusiform gyrus) is demarcated by the collateral sulcus (also identifiable in the coronal plane).

The uncus is the most medial portion of the temporal lobe and is continuous with the parahippocampal gyrus posteriorly (Fig. 1.45). The amygdala is just lateral to the uncus and situated anterior to the temporal horn of the lateral ventricle. The amygdala is thus anterior and superior to the hippocampus.

The fimbria of the hippocampal formation continues as the crus of the fornix, a fibre bundle that sweeps backwards, upwards and medially around the posterior aspect of the thalamus (Figs. 1.47a, 1.50). The two crura then pass forwards and converge in the midline, forming the body, where they are attached to the septum pellucidum. The body continues forwards before separating, just above the foramen of Monro, into the columns of the fornices. The fibres terminate in septal nuclei and the mammillary bodies of the hypothalamus. Only the hippocampus proper and the subicular region project fibres into the fornix.

The hippocampal tail tapers into a thin neuronal lamina, the indusium griseum, which arches around the corpus callosum along the inner border of the cingulate gyrus,

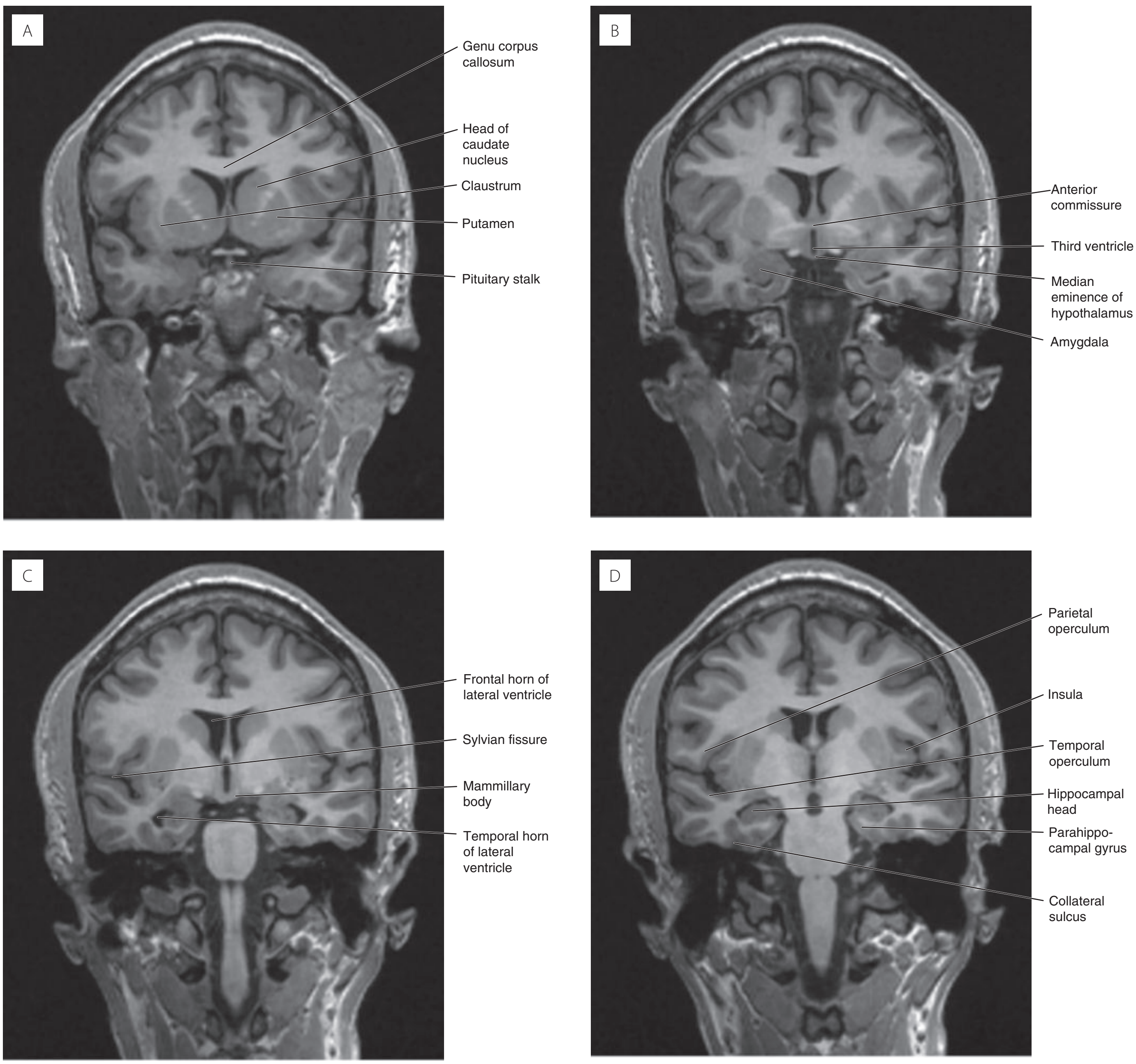


**Fig. 1.50** Coronal T1-weighted images through the brain: (A)–(G), anterior to posterior.

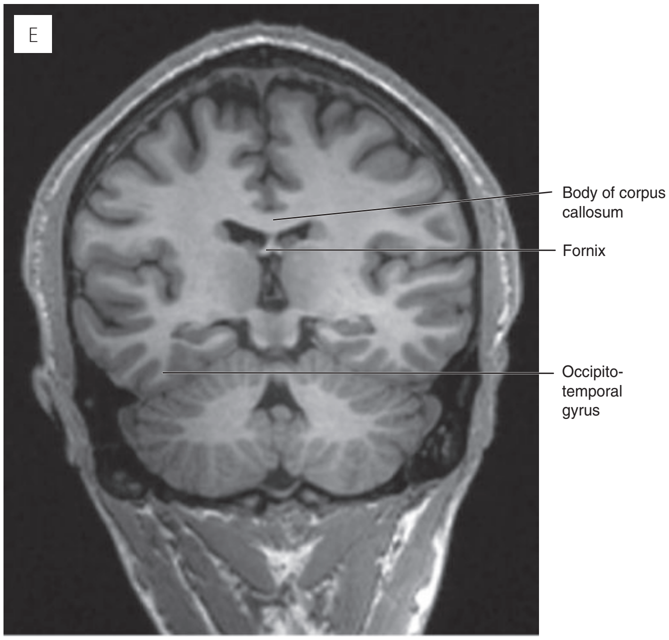


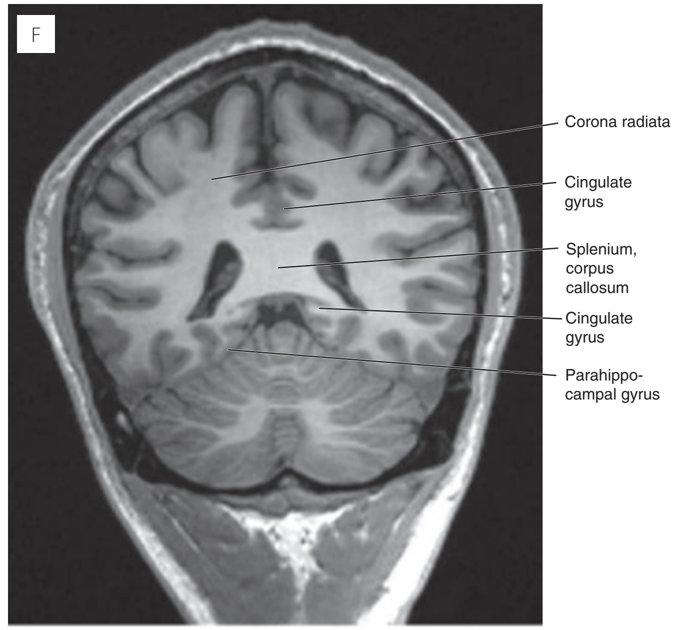


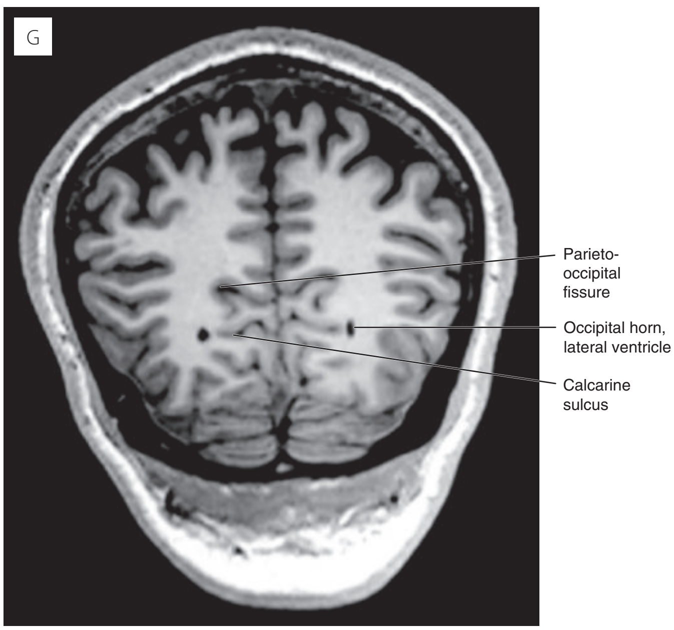


**Fig. 1.50** (*cont.*)

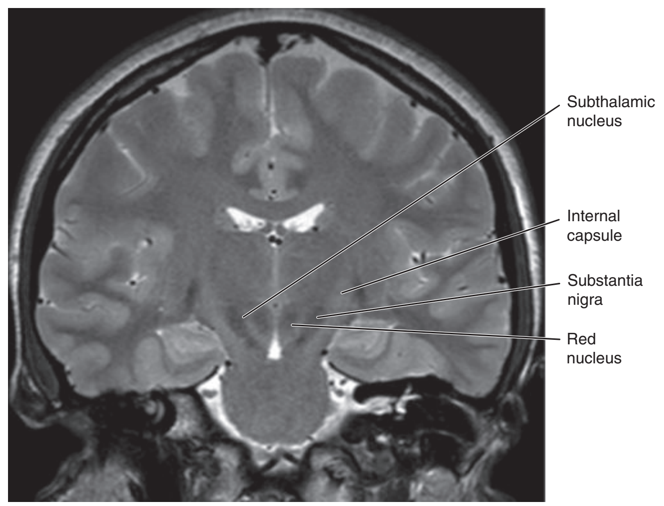


**Fig. 1.51** T2 coronal MRI. Subthalamic nucleus.

becoming part of the paraterminal gyrus in behind the subcallosal area.

The olfactory nerve, like the optic nerve, is really part of the CNS and not strictly a cranial nerve. The olfactory bulb receives tiny fibres from the nasal mucosa through the cribriform plate and projects an axonal bundle, the olfactory tract, that runs posteriorly along the inferior surface of the frontal lobe. It divides into medial and lateral tracts at the olfactory trigone, a point in the basal forebrain just in front of the anterior perforated substance (so-called because it is the point of entry for multiple small striate arteries) (Fig. 1.55).

The mamillary bodies (or nuclei) are part of the hypothalamus and are situated at the ends of the columns of the fornices. They relay impulses from the hippocampal formation and amygdala nuclear complexes to the thalamus (along the mammillothalamic tract (Fig. 1.56)). They are of particular relevance in patients with Wernicke-Korsakoff syndrome, in whom they may be atrophied as a result of chronic thiamine deficiency.

## The cerebral hemispheres

The cerebral cortex is organized into folds called gyri between which there are CSF-filled grooves called sulci. The deeper and more anatomically constant sulci are known as fissures. The lateral (Sylvian) fissure marks the superior margin of the temporal lobe, while the parieto-occipital fissure divides the parietal and occipital lobes. The central sulcus marks the

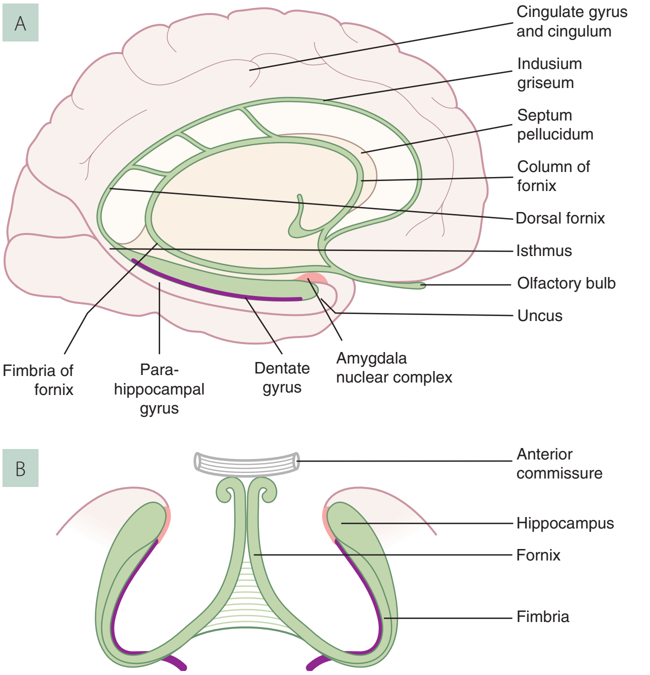


**Fig. 1.52** (A) Medial aspect of cerebral hemisphere showing the limbic system. (B) The hippocampus viewed from above.

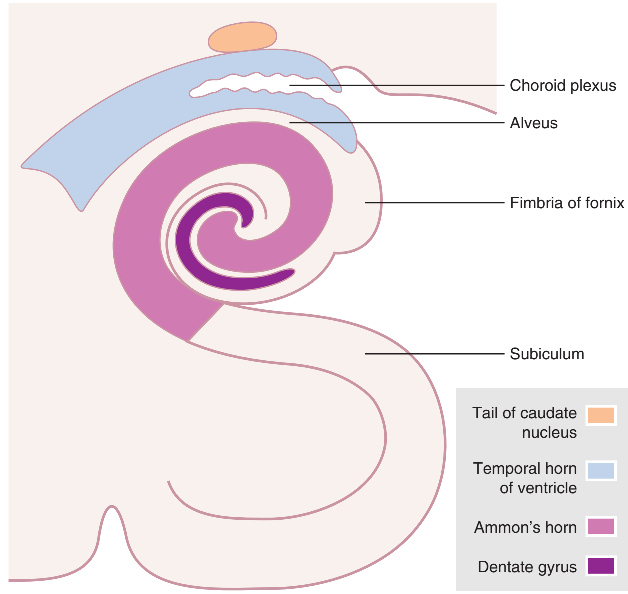


**Fig. 1.53** The limbic lobe.

division between the frontal and parietal lobes. The insula is an area of invaginated cortex lying deep within the Sylvian fissure, covered by the frontal, temporal and parietal opercula (Latin for 'little lids') (Figs. 1.45, 1.48, 1.49, 1.50).

Cortical anatomy is subject to individual variation but the more constant gyri and sulci are illustrated in Fig. 1.57.

The key facts concerning the functional anatomy of specific cortical areas are given here.

## Frontal lobe

- Anterior to central sulcus
- Precentral gyrus contains primary motor cortex
- Lateral surface of precentral gyrus supplies head and face
- Medial surface supplies lower limb
- Upper limb takes up the largest area of cortical representation (situated between lower limb and head/face)
- Premotor cortex lies anterior to precentral gyrus
- Three further frontal lobe gyri: superior, middle, inferior, separated by the superior and inferior frontal sulci.

The dominant hemisphere of the frontal lobe also contains Broca's area (involved with motor aspects of speech). It is situated in the pars opercularis, which lies in the posterior aspect of the inferior frontal gyrus. A V-shaped area of cortex immediately anterior to it is a useful and constant cortical landmark, called the pars triangularis (Fig. 1.58d).

## Parietal lobe

- Posterior to central fissure
- Lies above and in front of occipital lobe (divided by parieto-occipital fissure (Fig. 1.58d))
- Postcentral gyrus contains primary somatosensory cortex
- Inferolateral surface supplies face, lips and tongue
- Superolateral surface supplies upper limb
- Medial aspect supplies lower limb.

The parietal lobe also contains two further important gyri: the supramarginal and angular gyri, which are involved in visuospatial processing (especially in the non-dominant hemisphere). The angular gyrus is found on the lateral surface of the cerebrum at the posterior termination of the Sylvian fissure (Fig. 1.45f). The supramarginal gyrus lies in front of the angular gyrus. The medial surface of the parietal lobe is called the precuneus (Figs. 1.57, 1.58).

## Temporal lobe

- Inferior to lateral (Sylvian) fissure
- Transverse gyrus (of Heschl) contains primary auditory cortex (at the superior surface of the temporal gyrus within the Sylvian fissure (Fig. 1.58d))
- Middle and inferior temporal gyri contain large areas of association cortex
- Medial temporal lobe contains limbic structures (parahippocampal gyrus, uncus).

The temporal lobe also contains Wernicke's area (in the dominant hemisphere), which is involved with the receptive aspects of speech and is situated in the posterior part of the superior temporal gyrus, inferior to the angular gyrus.

## Occipital lobe

- Posterior to parieto-occipital fissure
- Primary visual cortex is situated on medial occipital lobe (calcarine cortex)
- Anterior margin marked by the temporo-occipital incisure.

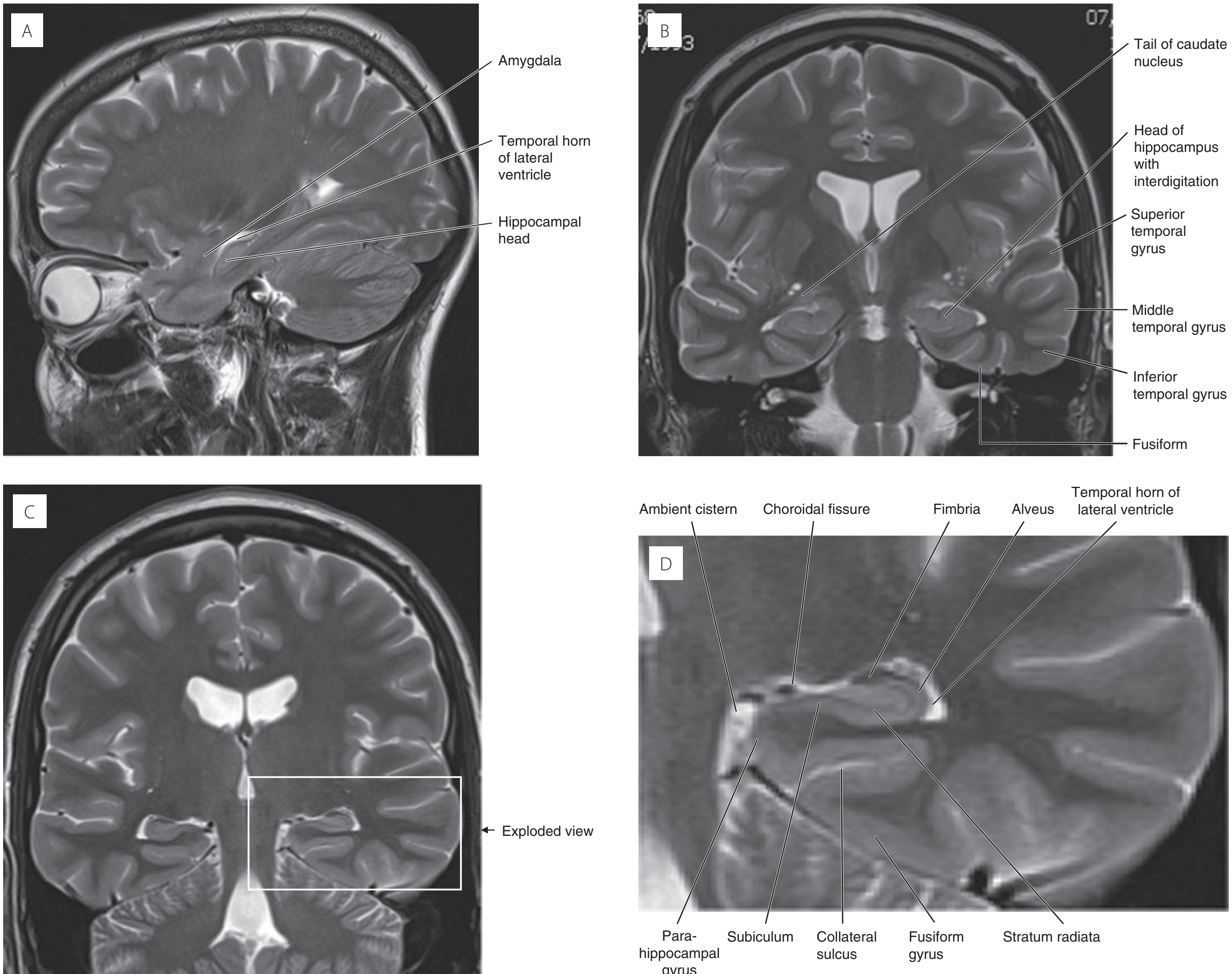


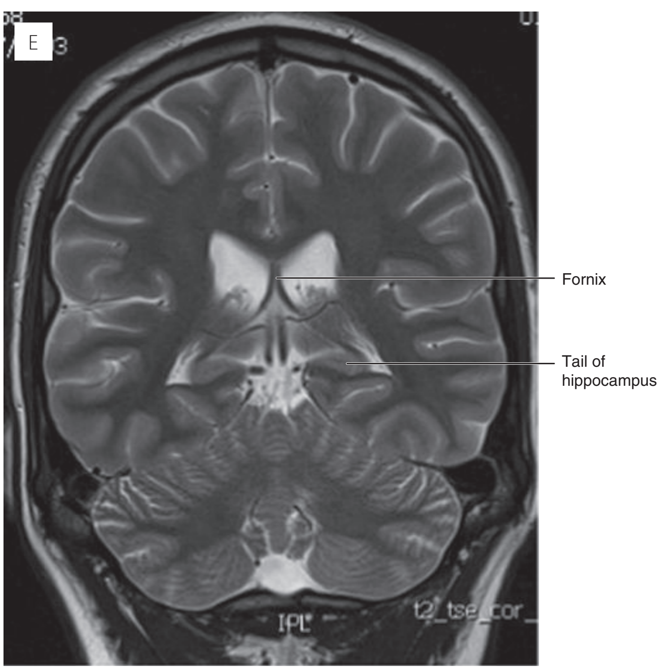


**Fig. 1.54** The hippocampus, (A) T2 parasagittal MRI. T2 coronal MRI (B); the head (C); the body (D); the tail (E).

The medial surface of the occipital lobe is made up of the cuneus (above) and the lingula (below) (Fig. 1.58).

## The central sulcus

The central sulcus is a useful landmark for neuro-radiologists and neurosurgeons alike but identifying it with certainty can present some difficulty on CT and MR images. There are, however, a number of useful tips, which can help determine the position of the central sulcus.

- On axial scans, follow the superior frontal sulcus from anterior to posterior until it meets and forms an angle with the precentral sulcus – the central sulcus is the next one behind (Fig. 1.45k).
- On lateral sagittal images note the Y-shaped sulcus of the pars triangularis at the anterior end of the Sylvian fissure. The next major fissure posterior to the Y is the precentral sulcus (Fig. 1.58d).
- On medial sagittal images follow the cingulate sulcus as it ascends superiorly and posteriorly towards the vertex

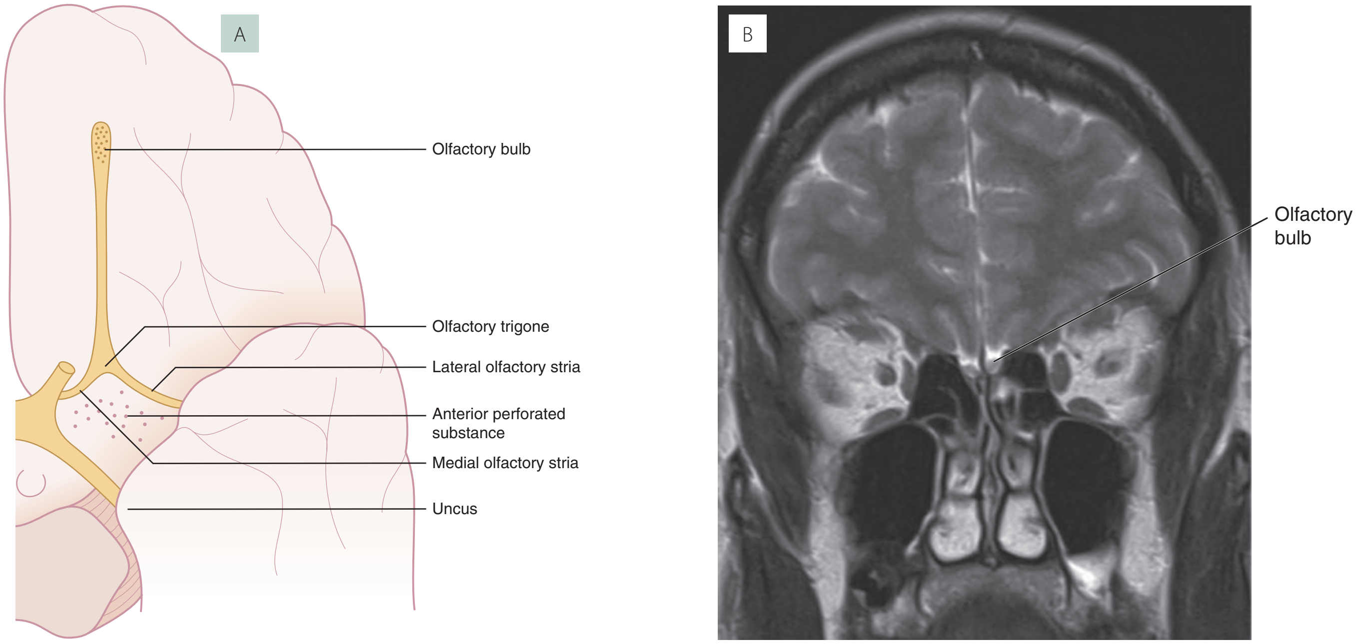


**Fig. 1.55** (A) Line diagram showing the olfactory pathways. (B) T2 coronal MRI. Olfactory bulbs.

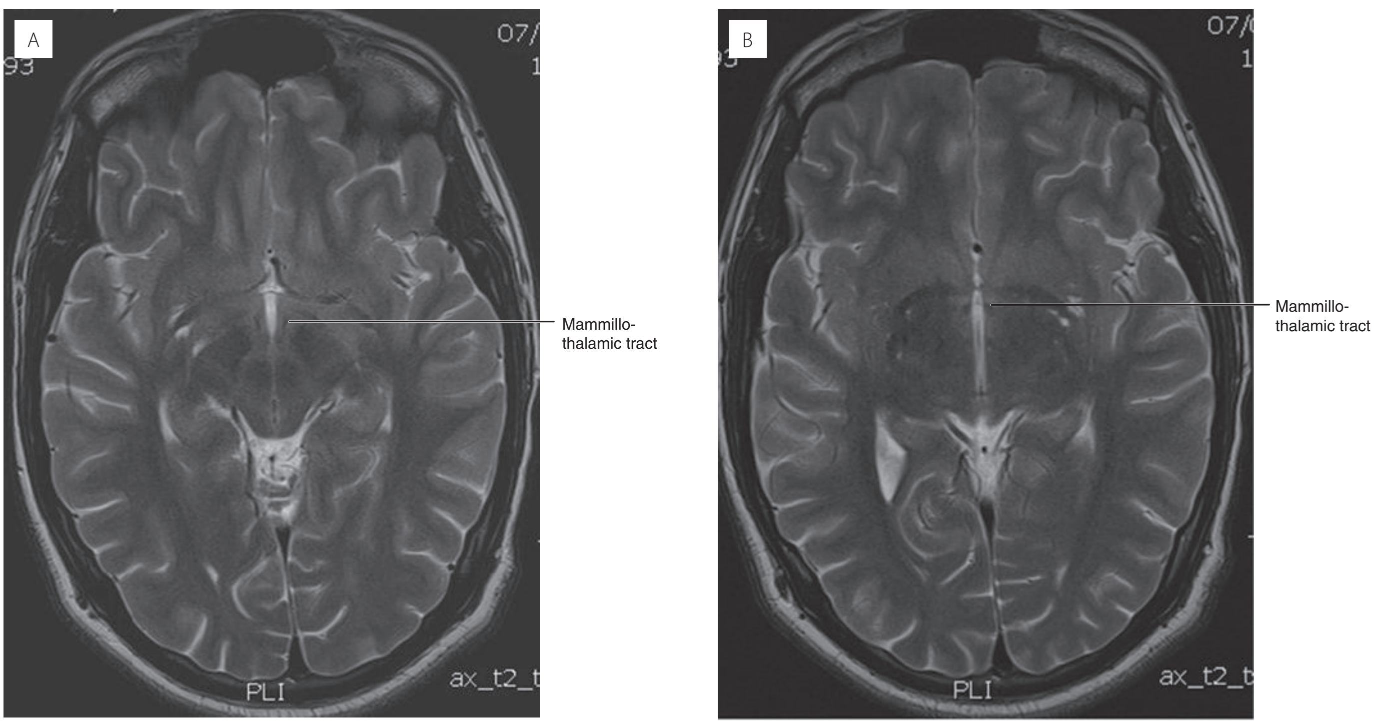


**Fig. 1.56** T2 axial MRI. Mammillothalamic tracts: (B) is superior to (A).

as the pars marginalis (Fig. 1.58a), which on axial images looks like a bracket (Fig. 1.45k). The central sulcus indents the medial part of the paracentral lobule at the vertex on the medial surface of the cerebrum just in front of the pars marginalis.

- The precentral gyrus is usually larger than the postcentral gyrus (and the cortex is slightly thicker).
- The precentral gyrus contains an area at its superior-lateral part, which resembles an upside-down omega (Ω) – an area of cortex that represents the motor-hand area (Fig. 1. 45j).

## White matter tracts

### The internal capsule

The internal capsule is a thick band of projection fibres carrying axons going to and from the cerebral cortex at the level of the basal ganglia and thalamus.

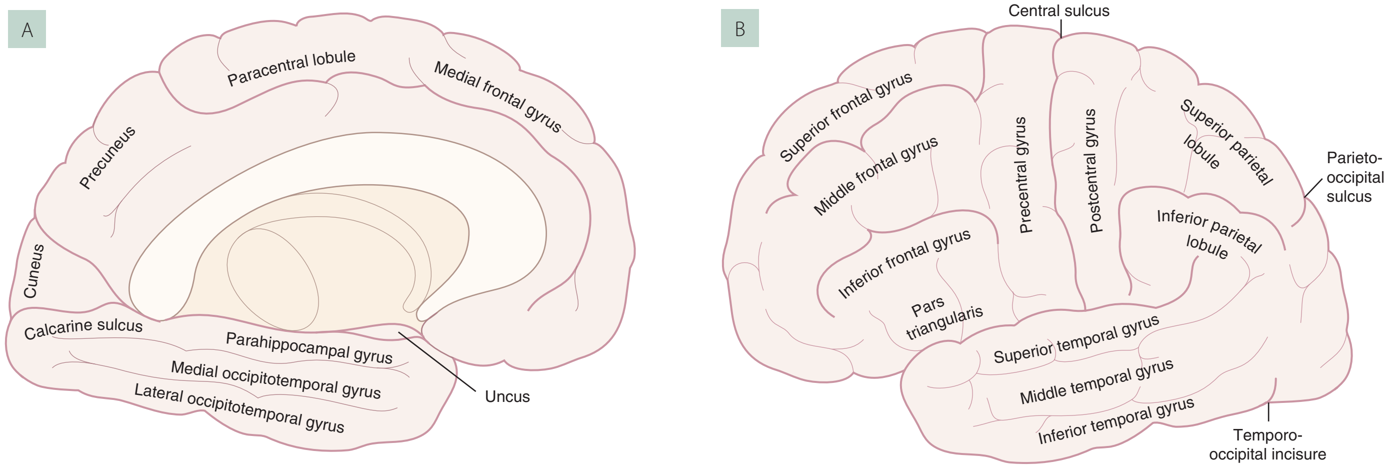


**Fig. 1.57** The cortical gyri: (A) medial and (B) lateral aspects.

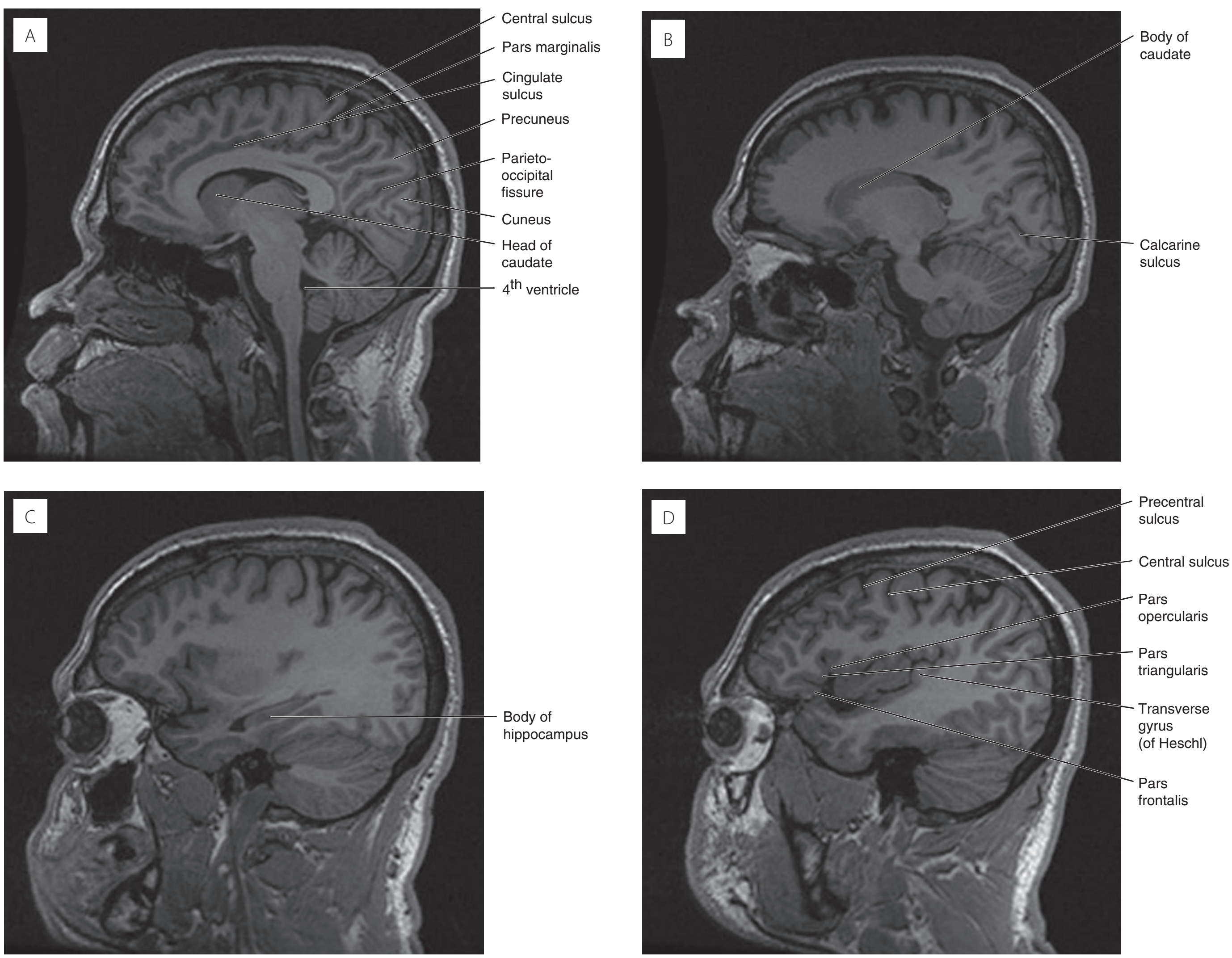


**Fig. 1.58** Sagittal T1-weighted images through the brain: (A)–(D), medial to lateral.

Projection fibres, by definition, pass to or from the more caudal parts of the neuraxis (the term for the brain and spinal cord).

Superiorly the fibres fan out as the corona radiata as they pass the body of the lateral ventricle to continue as the supraventricular white matter tracts, which radiologists refer to as the centrum semiovale (Fig. 1.45i). When viewed axially on CT and MR, the internal capsule resembles a V-shaped tract composed of anterior and posterior limbs, joined by the genu (Fig. 1.45).

Voluntary movement is initiated in the premotor and precentral gyri of the frontal lobe, which send projection fibres to brainstem motor nuclei and spinal cord via the corticospinal and corticobulbar tracts, respectively.

The corticobulbar tracts are at the genu.

In some individuals the corticospinal tracts, in the posterior limb of the internal capsule, show a relatively high T2 signal because of low myelin density. This should not be mistaken for a lesion (Fig. 1.59).

The high density of axons in the internal capsule means that even a small lacunar stroke occurring within it can precipitate profound and extensive neurological deficits. The blood vessels supplying the internal capsule are given below:

- anterior limb – recurrent artery of Heubner (branch of the anterior cerebral artery)
- genu – lenticulostriate arteries (branches of middle cerebral artery)
- posterior limb – anterior choroidal artery (arises from the internal carotid artery).

## The commissural tracts

These link equivalent sites across the cerebral hemispheres.

### Corpus callosum

The corpus callosum is the largest commissure. It forms a C-shaped structure, concave inferiorly. The rostrum is the portion that projects infero-posteriorly from the anterior-most genu. The body curves upwards and posteriorly towards the splenium (Fig. 1.46). The genu fibres curve forward into the frontal lobes, forming forceps minor. Similarly, the fibres of the splenium curve backward into the occipital lobes, as forceps major (Fig. 1.60).

### Anterior commissure

The anterior commissure is a phylogenetically older structure, which comprises a transversely oriented fibre bundle, linking the olfactory tracts and structures within the anterior temporal lobes including the amygdala nuclear complexes. It lies in front of the columns of the fornices, embedded in the anterior wall of the third ventricle (the lamina terminalis) (Figs. 1.45e, 1.50b, 1.61).

### Posterior commissure

The posterior commissure (also known as the epithalamic commissure) runs within the posterior pineal lamina to connect the right and left midbrain. It carries fibres responsible for bilateral pupillary light reflex.

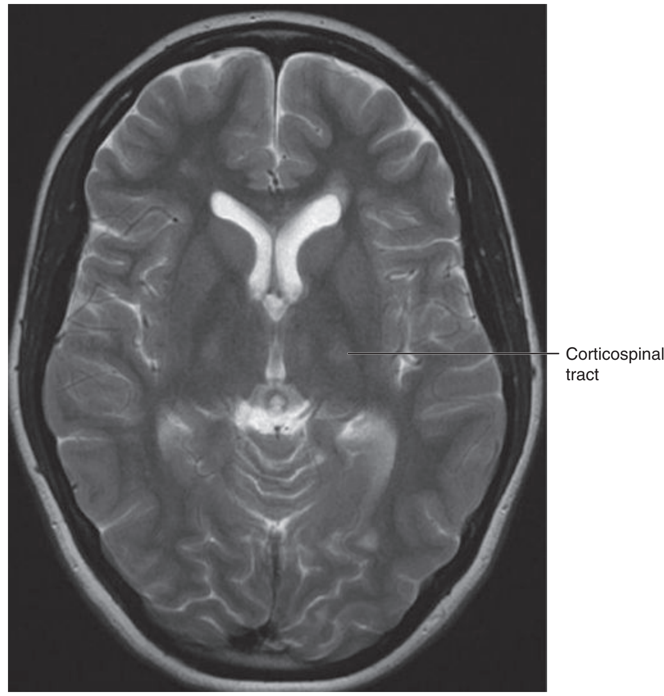


**Fig. 1.59** T2 axial MRI. The corticospinal tracts.

## The ventricular system

The cerebral ventricles are cavities situated deep within the brain. They are lined by ependymal cells and contain the choroid plexus, which produces CSF. There are four ventricles in total: the two paired lateral ventricles and the midline third and fourth ventricles (Fig. 1.62). Each lateral ventricle drains into the third ventricle via the foramen of Monro. The third ventricle communicates with the fourth via the cerebral aqueduct (of Sylvius) (Figs. 1.45c, 1.61).

Each lateral ventricle has a body, atrium and three horns named after the lobe in which they lie: frontal, occipital, temporal. The relations of the frontal horn are the corpus callosum superiorly, the head of the caudate nucleus laterally and

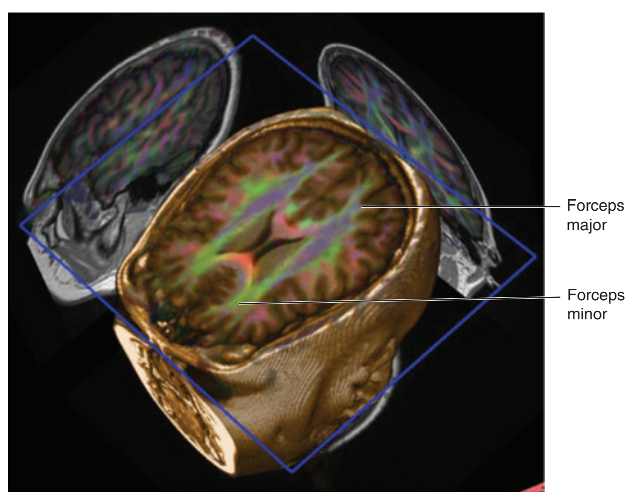


**Fig. 1.60** Diffusion anisotropy (MR) image showing the major white matter tracts. Note that the colour coding denotes vectors. Red: transverse fibres. Blue: vertical fibres. Green: anteroposterior fibres.


**Fig. 1.61** T2W sagittal. The third ventricle. Note that the patient has hydrocephalus.

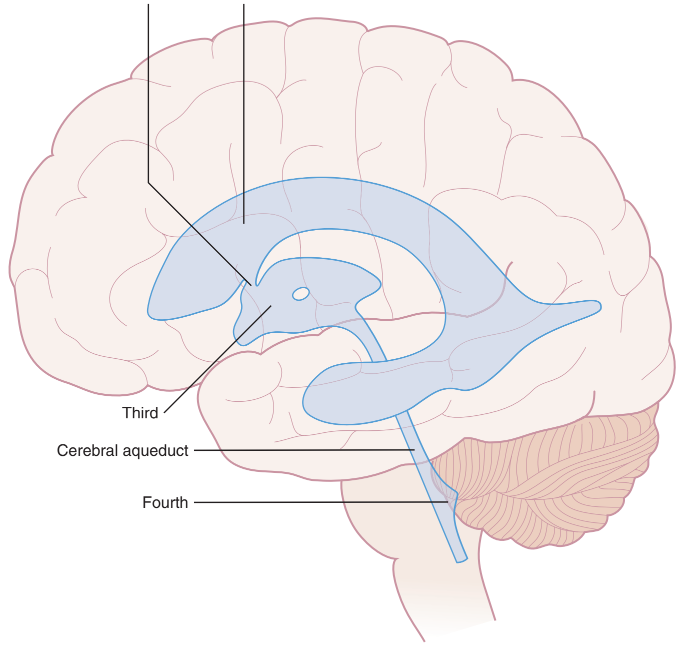


**Fig. 1.62** The cerebral ventricles.

inferiorly and the septum pellucidum medially. The body is formed by the corpus callosum (roof), dorsal part of the thalamus (floor), fornix (medially) and the body and tail of the caudate laterally. The temporal horn (sometimes called the inferior horn) has the tail of the caudate as its roof, the hippocampus medially and inferiorly and the optic radiation and associated white matter tracts medially. The occipital horn is surrounded by the forceps major, a white matter tract of the corpus callosum. The atrium represents the confluence of the three horns and contains the choroid plexus, which is highly vascular and usually calcified on CT (Fig. 1.12d).

The cavum septi pellucidi is a fluid-filled extrapial cavity between the two laminae of the septum pellucidum. It is seen in virtually all neonates and regresses by adulthood. It persists into adulthood in about 10% of people. The cavum vergae is the posterior continuation of the cavum septi pellucidi beneath the splenium and above the fornix.

The cavum closes in posterior to anterior. Therefore in an adult a cavum septi pellucidi can exist in isolation or with a cavum vergae but a cavum vergae cannot persist as the solitary cavum.

The velum interpositum is a cisternal space created by infolding of the tela choroidea beneath the fornix. Inferiorly, it opens into the quadrigeminal cistern. It contains the internal cerebral veins and does not extend anterior to the foramen of Monro, allowing it to be distinguished from the cavum vergae (Fig. 1.45e).

## The third ventricle

The third ventricle is a narrow slit-like vertical cavity between the right and left diencephalon (Figs. 1.45, 1.48, 1.50). Its anterior wall is called the lamina terminalis, which contains the anterior commissure at its superior border. It possesses two recesses anteriorly; the more superior lies above the optic chiasm (the optic or chiasmatic recess) and the more inferior lies behind the infundibulum of the pituitary gland (the infundibular recess) (Fig. 1.61).

Two further recesses are present posteriorly, one above the pineal gland (the suprapineal recess), the other directed into the pineal gland (pineal recess).

## The fourth ventricle

The fourth ventricle is within the dorsal pons and upper medulla. It appears as a diamond-shaped cavity on coronal scans, an inverted U on axial scans and as a triangle on sagittal images.

There are paired lateral apertures (the foramina of Luschka) and a single median aperture (of Magendie), which transmit CSF into the cisterna magna.

These provide routes of spread for disease out of the ventricular system and into the subarachnoid space.

The fourth ventricle is bounded by a tent-shaped roof, made up of the superior medullary velum and inferior medullary velum. The dorsal surface of the pons and medulla form the anterior wall and it is enclosed laterally by the middle cerebellar peduncles (Figs. 1.21, 1.28, 1.46).

Chapter 2

# The orbit and visual pathway

Indran Davagnanam and Jonathan L. Hart

## Plain film

Plain film radiography is no longer used routinely for the evaluation of orbital pathology, but familiarity with normal anatomy remains important when reviewing emergency department trauma radiographs (Fig. 2.1).

## Cross-sectional anatomy

The primary imaging modalities used to examine the orbit and visual pathways in clinical practice are CT and MRI. The divergent, conical anatomy of the orbits and their contents means that a combination of axial, coronal and parasagittal scan planes may be required to delineate anatomical structures optimally.

CT demonstrates orbital anatomy well due to the substantial differences in attenuation of bone, air in adjacent paranasal sinuses, orbital fat and soft tissues. In particular, helical CT with multiplanar reconstructions provides excellent bony anatomical detail. Coronal reformatted images are important for the bony anatomy at the orbital apex, the orbital floor and roof.

MRI is valuable for evaluation of intra-orbital soft-tissue anatomy and is unhindered by artefacts from surrounding bone. Imaging protocols usually include axial and coronal sequences, including thin-section coronal T2-weighted scans with fat suppression. Intravenous gadolinium-enhanced T1-weighted imaging is also combined with fat suppression so that enhancing structures are not obscured by the intrinsic high-T1 signal of normal orbital fat. Acquisition times should be short to minimize the effects of eye movement.

MRI is the preferred technique for demonstration of the intracranial optic nerves, optic chiasm and tracts.

### The orbit

The orbits are pyramidal bony cavities with the apex lying posteriorly and the base anteriorly (Fig. 2.2). The long axes of the orbits are divergent by approximately 45° and the medial walls are roughly parallel. The fragile medial (lamina papyracea) and inferior walls are vulnerable to blowout fractures in blunt trauma (Fig. 2.3). Paranasal sinus pathology may involve the orbits by direct extension.

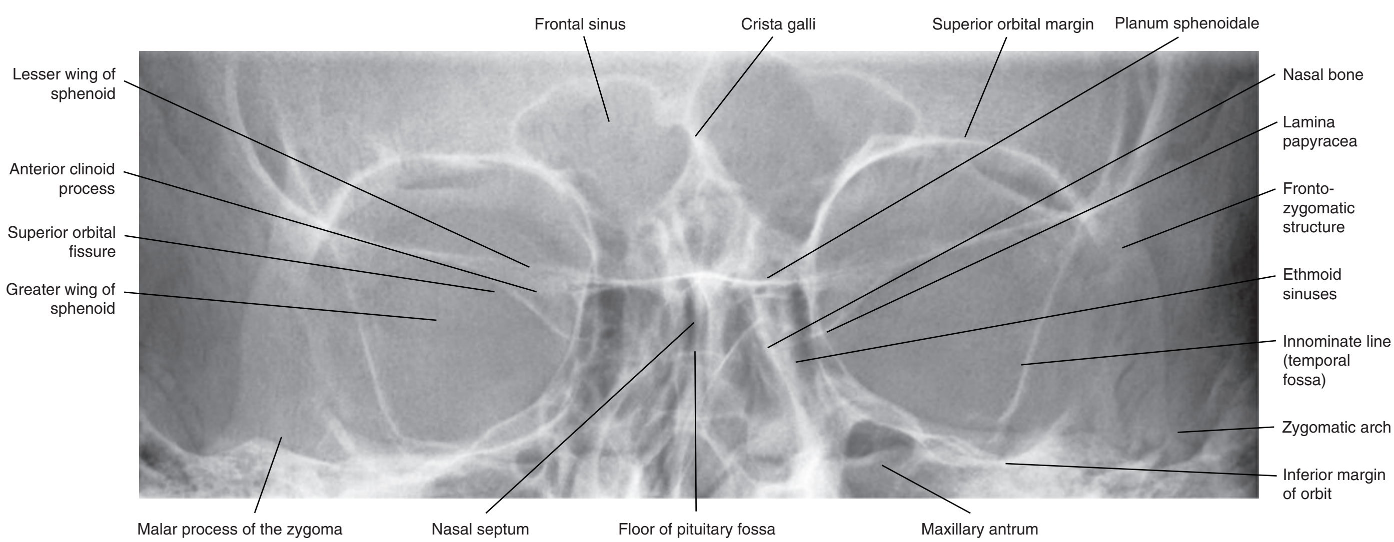


**Fig. 2.1** Occipitofrontal radiograph of the bony orbits.

*Applied Radiological Anatomy, 2nd Edition* ed. Paul Butler, Adam W.M. Mitchell and Jeremiah C. Healy. Published by Cambridge University Press.

### Anatomical relationships

- Superior: anterior cranial fossa and frontal sinus
- Medial: nasal cavity, ethmoid and sphenoid sinus
- Inferior: maxillary sinus
- Posterolateral: temporal fossa and middle cranial fossa

### Osseous anatomy of the orbital walls (Fig. 2.4)

- Roof: frontal bone (predominantly), lesser wing of sphenoid posteriorly
- Medial: (anterior to posterior) frontal process of maxilla, lacrimal bone, ethmoid bone, small sphenoid contribution at apex

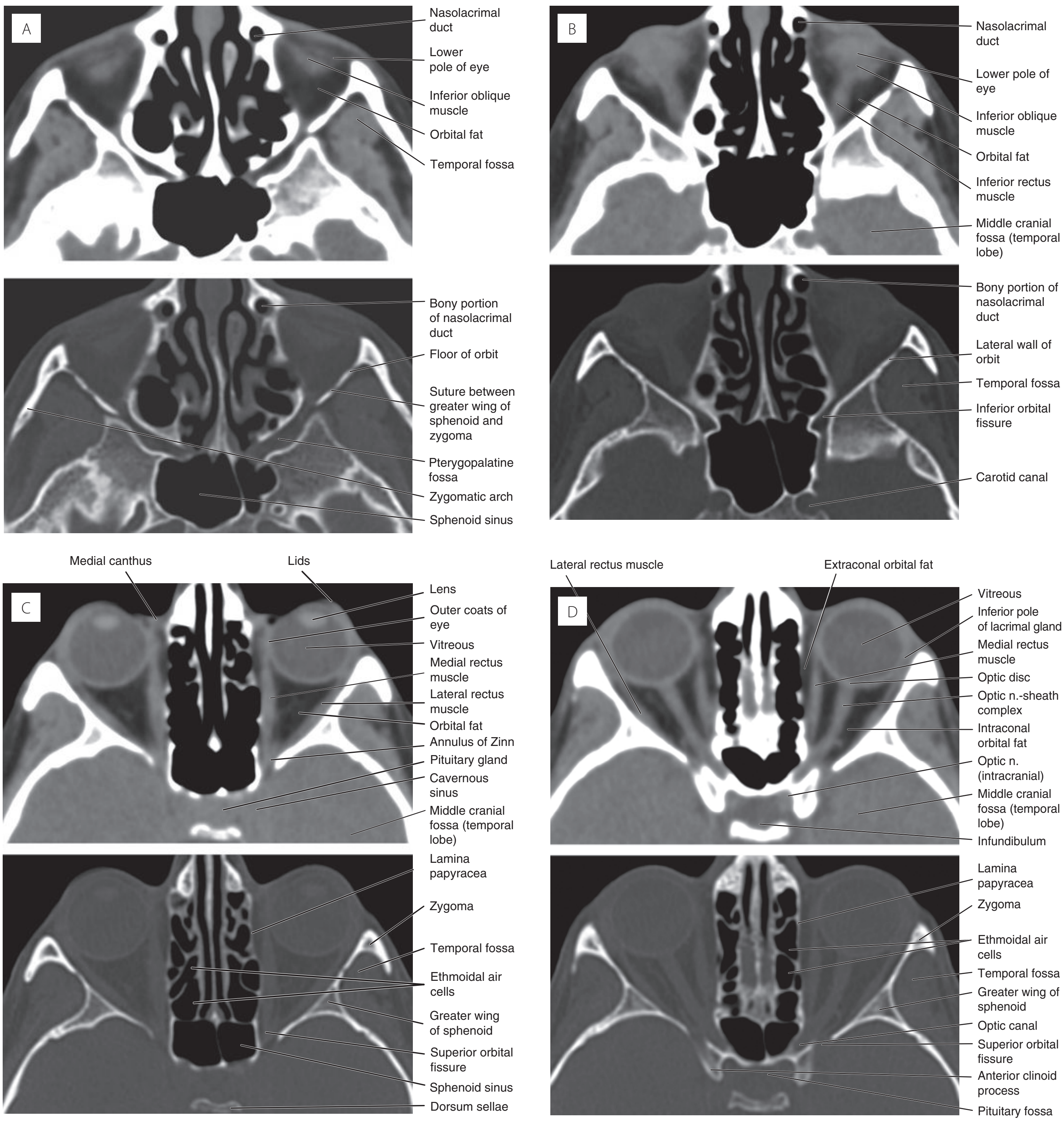


**Fig. 2.2** Paired (soft tissue and bone window settings) axial CT sections through the orbit in a caudal to cranial sequence at the levels of: (A) the pterygopalatine fossa and bony nasolacrimal ducts, (B) the inferior orbital fissure, (C) the superior orbital fissure, (D) the optic canal, (E) the superior rectus muscle, (F) the tendons of superior oblique muscle.

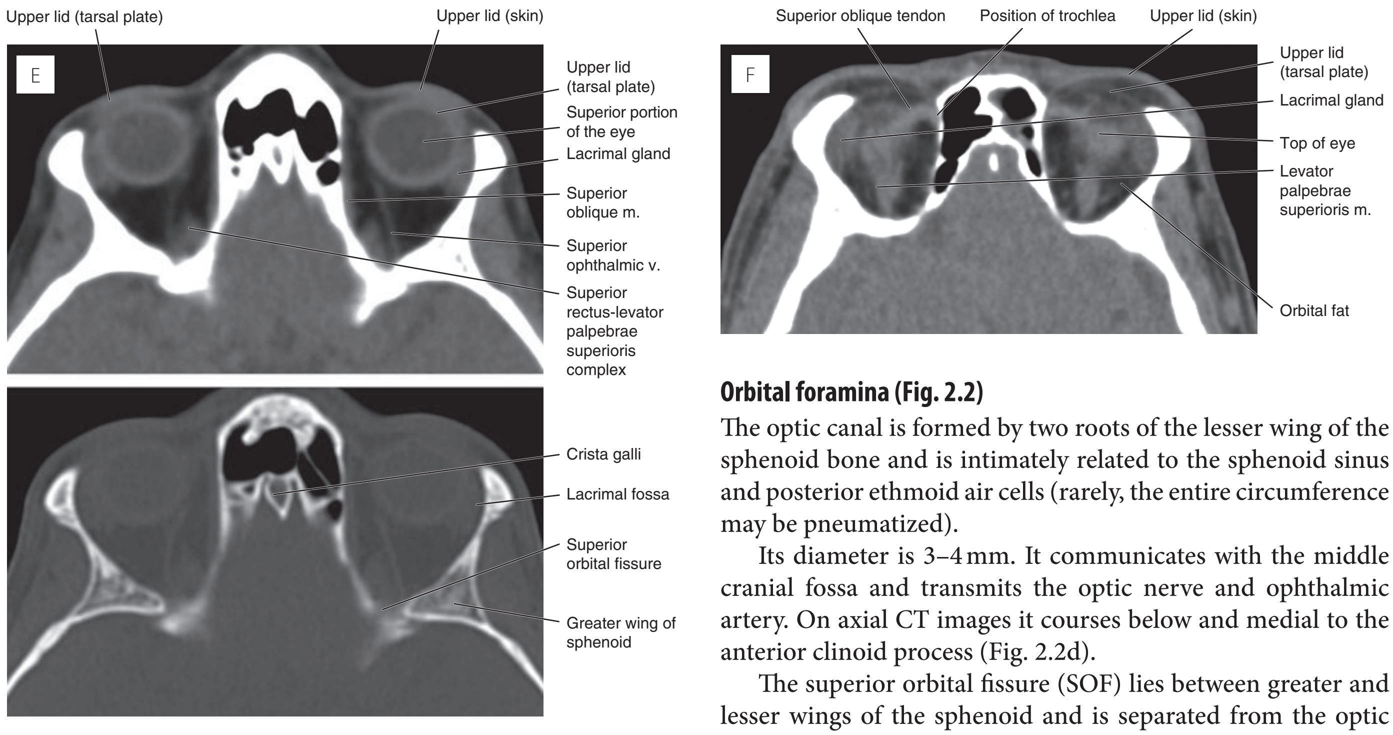


**Fig. 2.2** (*cont.*)

- Floor: (medial to lateral) orbital plate of maxilla and zygomatic bone, orbital process of the palatine bone posteriorly
- Lateral: zygomatic bone and frontal bone

## Orbital foramina (Fig. 2.2)

The optic canal is formed by two roots of the lesser wing of the sphenoid bone and is intimately related to the sphenoid sinus and posterior ethmoid air cells (rarely, the entire circumference may be pneumatized).

Its diameter is 3–4 mm. It communicates with the middle cranial fossa and transmits the optic nerve and ophthalmic artery. On axial CT images it courses below and medial to the anterior clinoid process (Fig. 2.2d).

The superior orbital fissure (SOF) lies between greater and lesser wings of the sphenoid and is separated from the optic canal by the optic strut.

It communicates with the middle cranial fossa and the cavernous sinus lies posteriorly.

The SOF transmits:

- oculomotor (IIIrd cranial) nerve (supplying the superior, medial and inferior recti; inferior oblique and levator palpebrae superioris muscles)

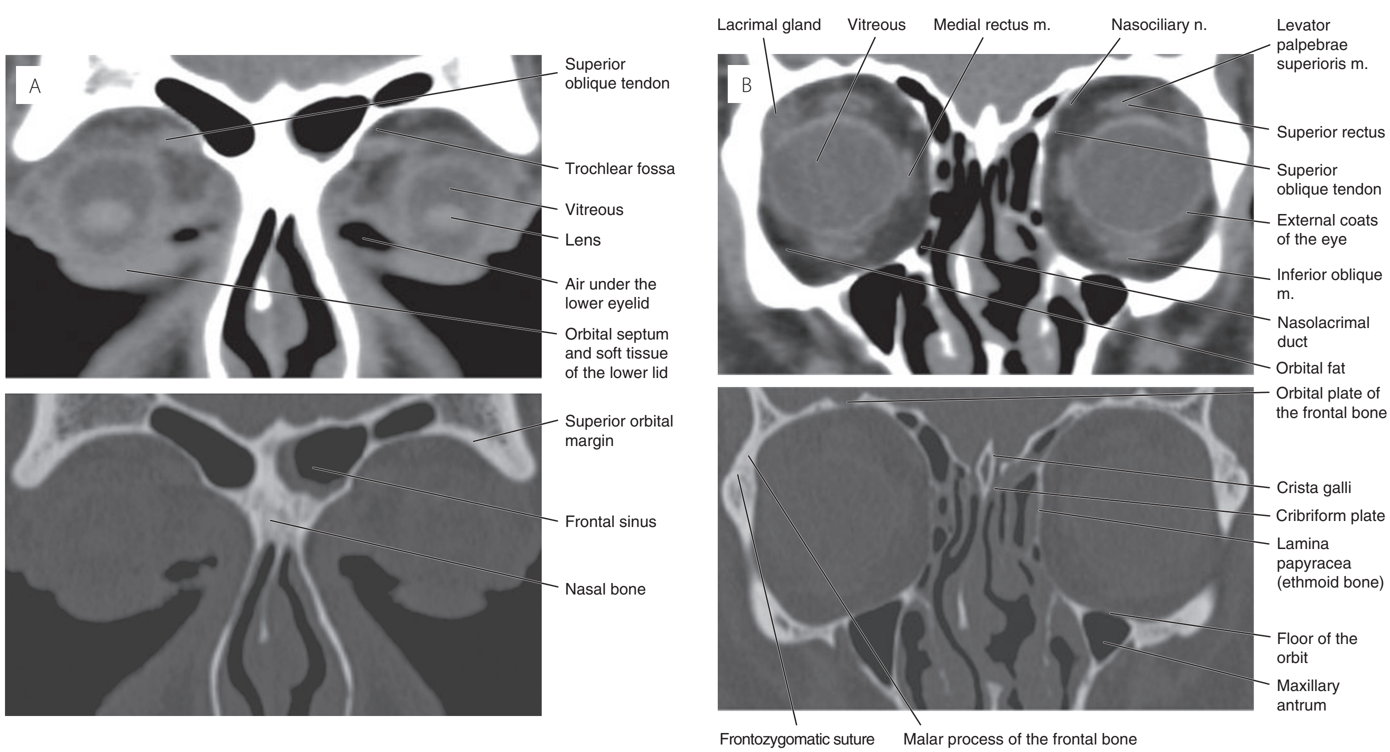


**Fig. 2.3** Coronal reconstructed CT sections of the orbits, from anterior to posterior, imaged on soft-tissue (top panel) and bone (bottom panel) windows at the levels of: (A) the reflected portion of the superior oblique tendon, (B) the mid-globe, (C) the posterior pole of the globe, (D) the extra-ocular muscles, (E) just anterior to the apex of the orbit.

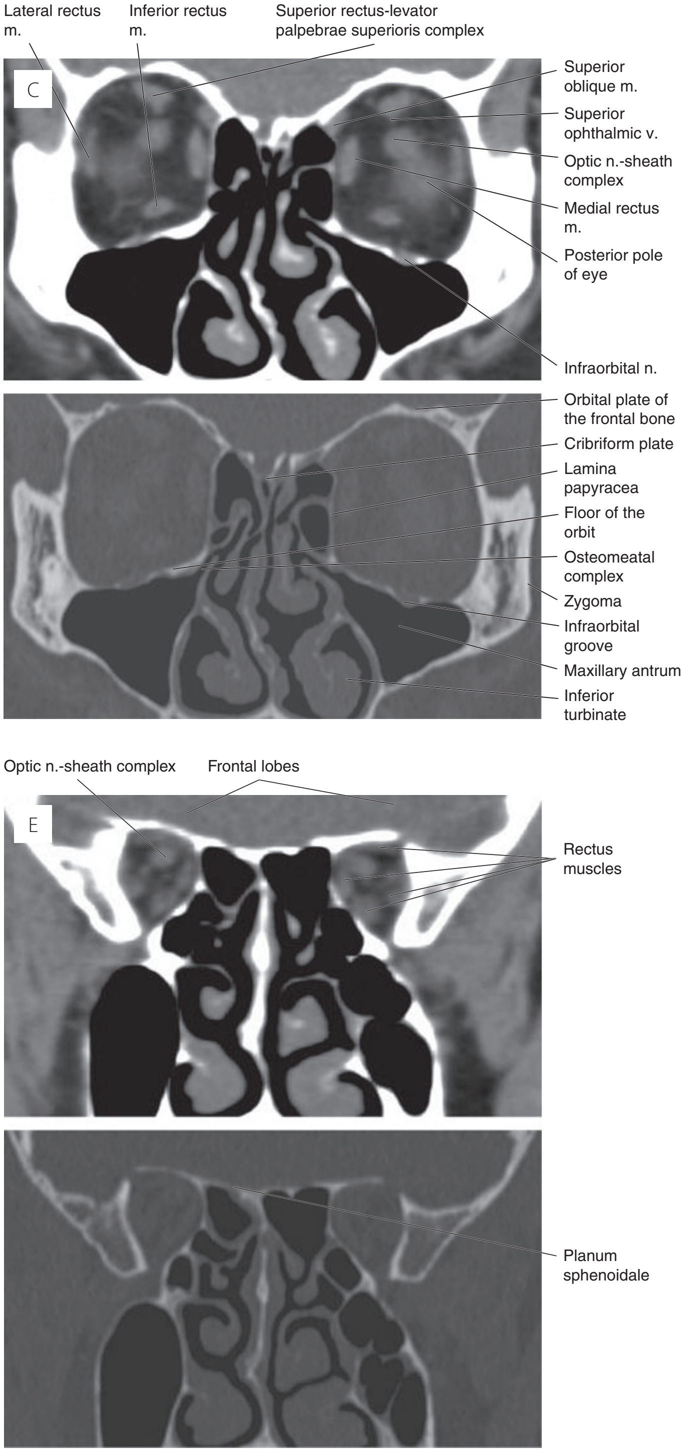


**Fig. 2.3** (*cont.*)

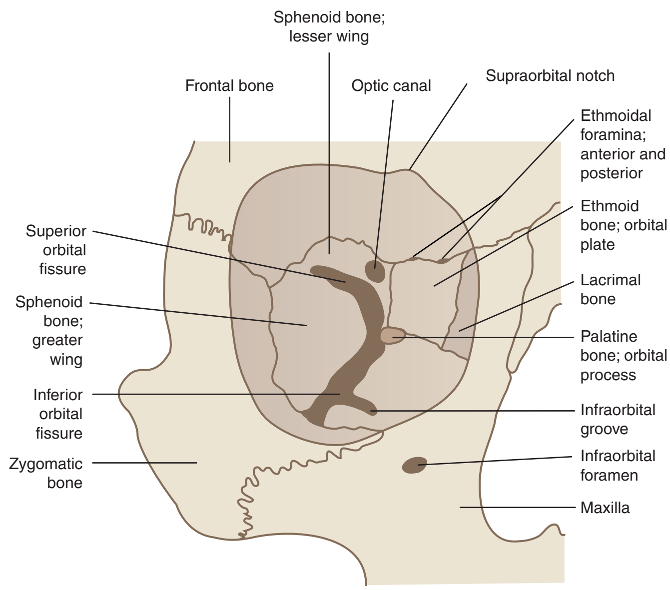


**Fig. 2.4** Bony constituents of the orbit and principal foramina: schematic diagram (frontal view of the right orbit).

- trochlear (IVth cranial) nerve – superior oblique muscle
- abducent (VIth cranial) nerve – lateral rectus muscle
- branches of the ophthalmic (Vi) division of the trigeminal (Vth cranial) nerve
- carotid sympathetic plexus branches
- superior and inferior ophthalmic veins.

A small fat pad in the SOF is an important normal anatomical finding on CT or MRI; effacement may be the only sign of subtle pathology involving the superior orbital fissure.

Small nerves in the orbit, particularly the branches of the ophthalmic division of the trigeminal nerve, the inferior division of the oculomotor nerve and the infraorbital nerve, may be seen on MRI (particularly on coronal sections).

The inferior orbital fissure (IOF) is located in the orbital floor between the greater wing of the sphenoid and orbital plate of the maxilla. It communicates with the pterygopalatine fossa and the masticator space.

The IOF transmits:

- branches of the internal maxillary artery

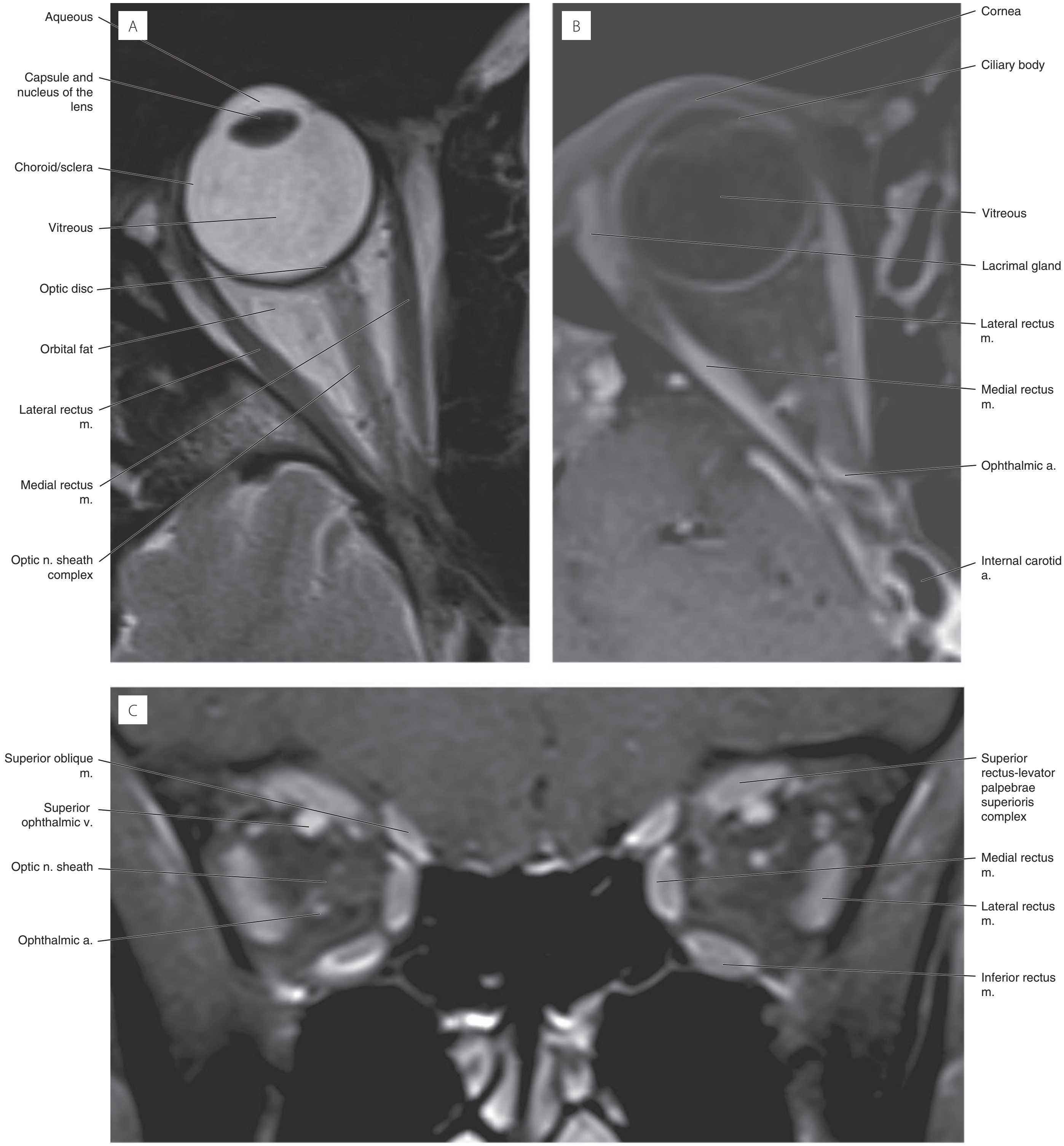


**Fig. 2.5** Spin-echo MRI of the right orbit demonstrating the variation in the normal appearances of the eye depending on the sequence. (A) Axial T2-weighted, (B) axial and (C) coronal T1-weighted post-gadolinium contrast, fat suppressed. Note the normal intense enhancement of the extra-ocular muscles and ciliary body. Contrast enhancement of the meningeal sheath of the optic nerve outlines the nerve itself on the coronal image.

- communications between the inferior ophthalmic vein and the pterygoid venous plexus
- branches of the zygomatic and infraorbital nerves

The supraorbital foramen transmits the supraorbital nerve (Vi).

The infraorbital canal / infraorbital foramen transmits the infraorbital nerve (Vii).

The anterior and posterior ethmoidal foramina transmit the anterior and posterior ethmoidal vessels and nerves (Vi), respectively.

## The orbital compartments

The soft tissue structures of the orbit are surrounded by the orbital fat which fills the cavity. The orbital septum is a fascial

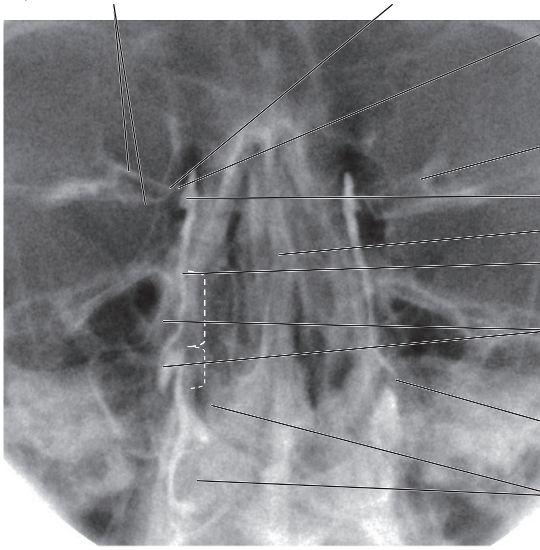


**Fig. 2.6** Dacryocystogram, anteroposterior supine projection.

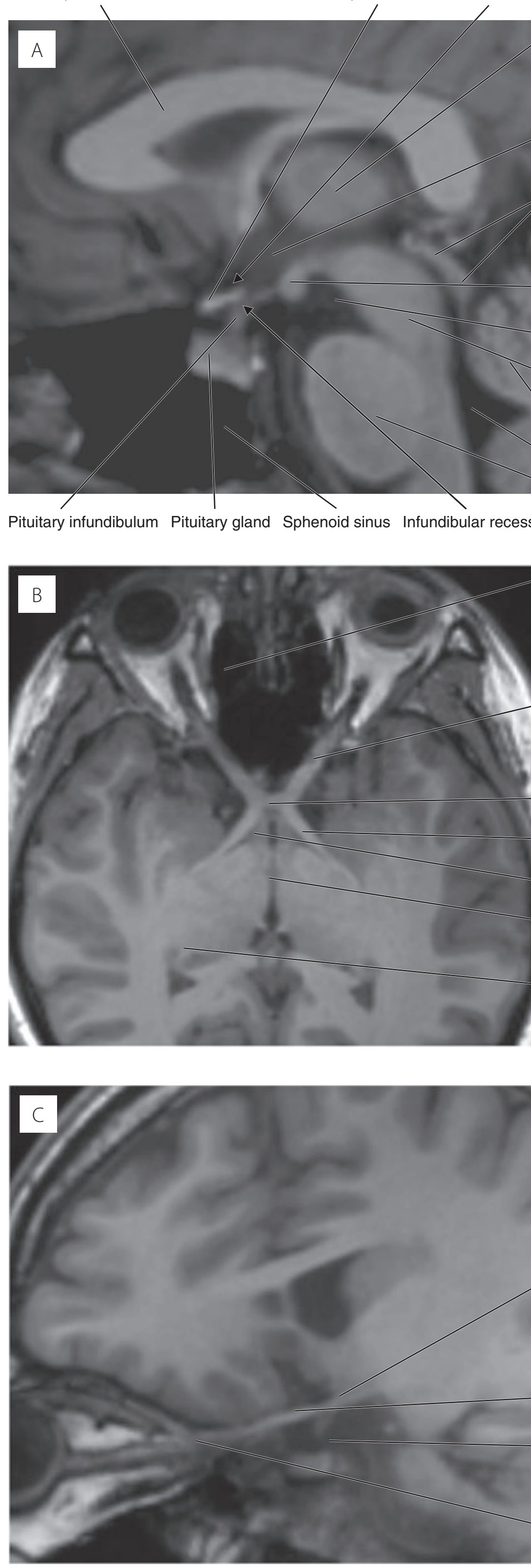


**Fig. 2.7** Sagittal (A), axial (B) and oblique (C) reformatted volume T1-weighted MR images demonstrating the intracanalicular and intracranial segments of the optic nerves and the optic chiasm. There is normal inter-individual variation in the position of the chiasm relative to the pituitary fossa.

layer attached to the orbital margin which separates the extra-orbital pre-septal space from the orbital post-septal space (Fig. 2.2c). Division of the orbital space into intra- and extra-conal compartments is of importance in the differential diagnosis of retro-orbital masses and inflammatory and infiltrative lesions.

The intraconal space is a cone formed by four rectus muscles and fasciae and, importantly, includes the muscles themselves (Fig. 2.5).

## The globe

The lens (due to its low water content) and ciliary bodies are demonstrated as dense structures distinct from the fluid of the anterior chamber and vitreous on CT (Fig. 2.2). The normal aqueous and vitreous humours are of similar attenuation to CSF, although streak artefact from the bone may produce areas of apparent high density.

MRI with surface coils provides superior anatomical detail, but involuntary eye movements inevitably cause some motion artefact (Fig. 2.5). Even with maximal spatial resolution, MRI does not permit differentiation of the three primary layers of the globe (sclera, uvea and retina). However, some ocular diseases are accompanied by detachment and/or effusion, which may permit the different potential spaces between the layers to be visualized. After intravenous gadolinium contrast, the choroid, ciliary body and iris enhance strongly (Fig. 2.5b).

The globe is divided into anterior and posterior segments.

The anterior segment, containing aqueous humour, is anterior to the lens and its supporting circumferential ciliary body, which is attached to the lens by zonule fibres, the contraction of which allows accommodation.

The anterior segment is further divided by the iris into:

- the anterior chamber – the major chamber between cornea and iris
- the posterior chamber – a potential space between iris and lens ligament complex.

The posterior segment (vitreoretinal portion of the eye) contains the vitreous humour. Its three layers comprise (from inside out) retina, uveal tract (choroid, ciliary body and iris) and sclera (the fibrous layer to which the extra-ocular muscles are attached). The optic disc lies slightly medially on the posterior concavity of the globe.

The globe may be evaluated for proptosis on cross-sectional imaging. On an axial section containing the optic lens and optic nerve head, a line is drawn between the bony lateral orbital margins. Normally, one-third of the globe is located behind this interzygomatic reference line.

### The extra-ocular muscles (Figs. 2.2, 2.3, 2.5)

Four fusiform rectus muscles move the eyeball, but the divergent geometry of the orbits is such that the actions of the superior and inferior recti do not occur strictly in the orthogonal planes. The oblique muscles are necessary to assist in direct upward and downward globe movements. The extraconal levator palpebrae superioris elevates the upper eyelid.

The extra-ocular muscles are of normal soft tissue attenuation on CT and signal intensity on MRI. Intravenous gadolinium improves their conspicuity on T1-weighted MRI (when combined with fat saturation sequences) as they enhance strongly due to the lack of blood–tissue barrier. The levator palpebrae superioris is not always identified separately from the superior rectus on standard imaging, and the muscles are sometimes referred to together as the superior muscle complex.

Normal measurements of extra-ocular muscles are described (with maximal diameters of the order of 5 mm), but morphology is at least as important a marker of pathology as muscle size. Measurements also vary with age, sex and interzygomatic distance. The eye position (appreciated from the lens or optic nerve) should be accounted for when assessing relative sizes of the muscles. Divergence of the eyes may be normal in the sleeping patient.

- The rectus muscles arise from a common annular tendon at the orbital apex (Zinn's ligamentous ring). The medial rectus is larger than the opposing lateral rectus muscle.

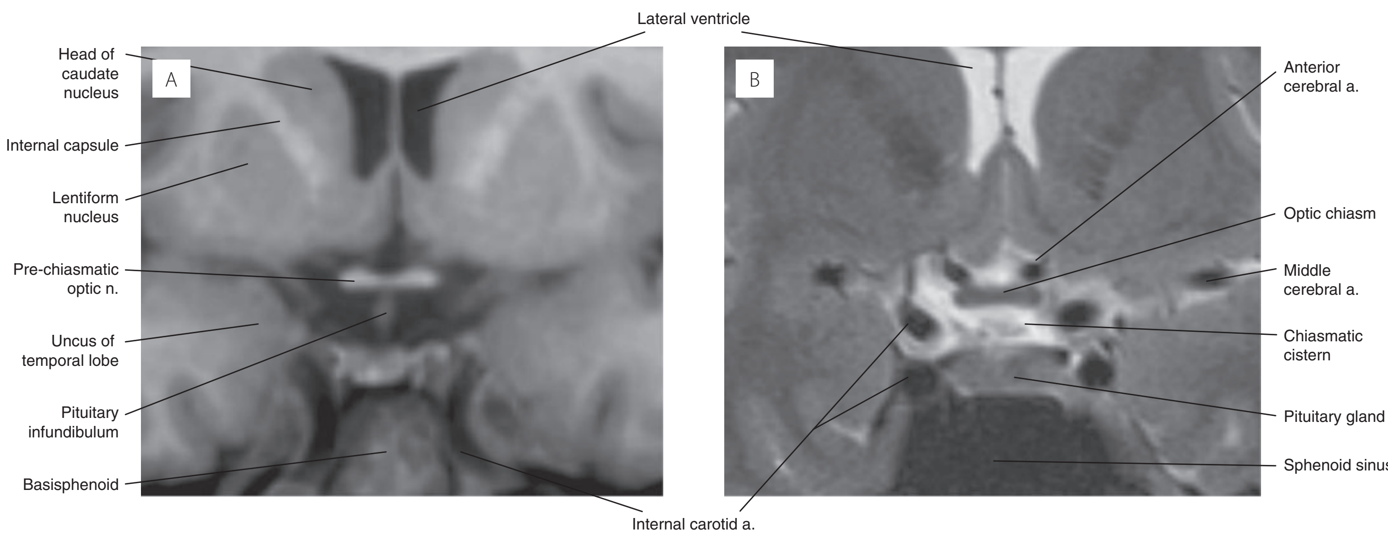


**Fig. 2.8** Coronal MRI. (A) T1-weighted image through the infundibulum of the pituitary gland, demonstrating division of the optic chiasm into the optic tracts; (B) slightly more anterior T2-weighted coronal image through the optic chiasm itself.

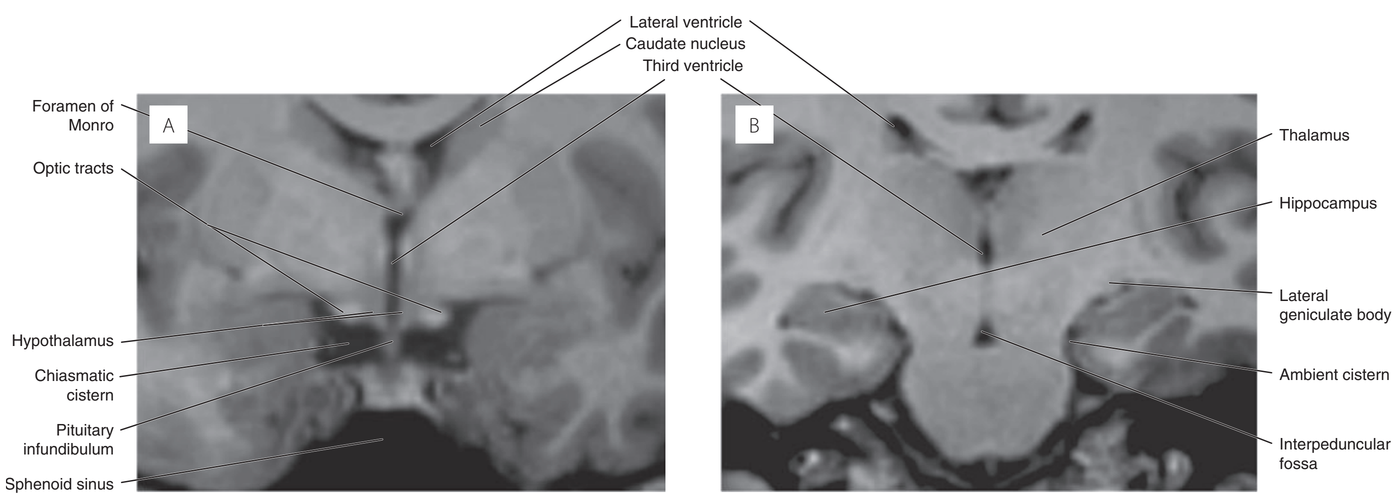


**Fig. 2.9** Retrochiasmal optic pathways: (A) optic tracts, (B) lateral geniculate bodies on coronal reformatted volume T1-weighted inversion recovery MRI.

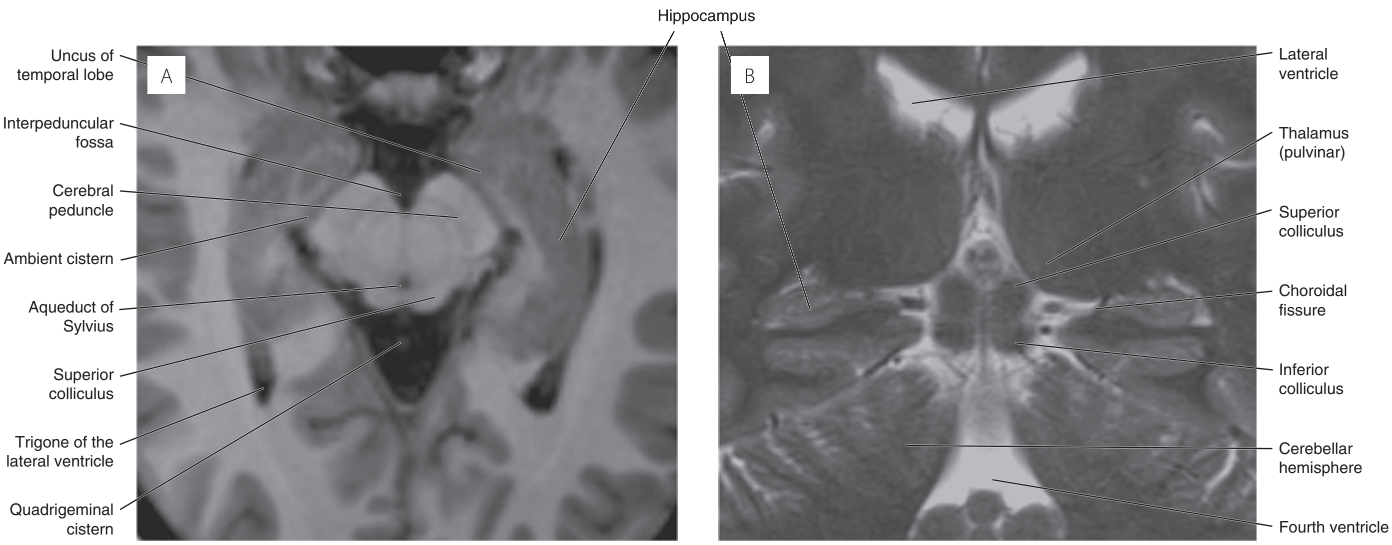


**Fig. 2.10** Superior colliculi. (A) Axial T1-weighted MRI through the midbrain and (B) coronal T2-weighted image through the quadrigeminal plate.

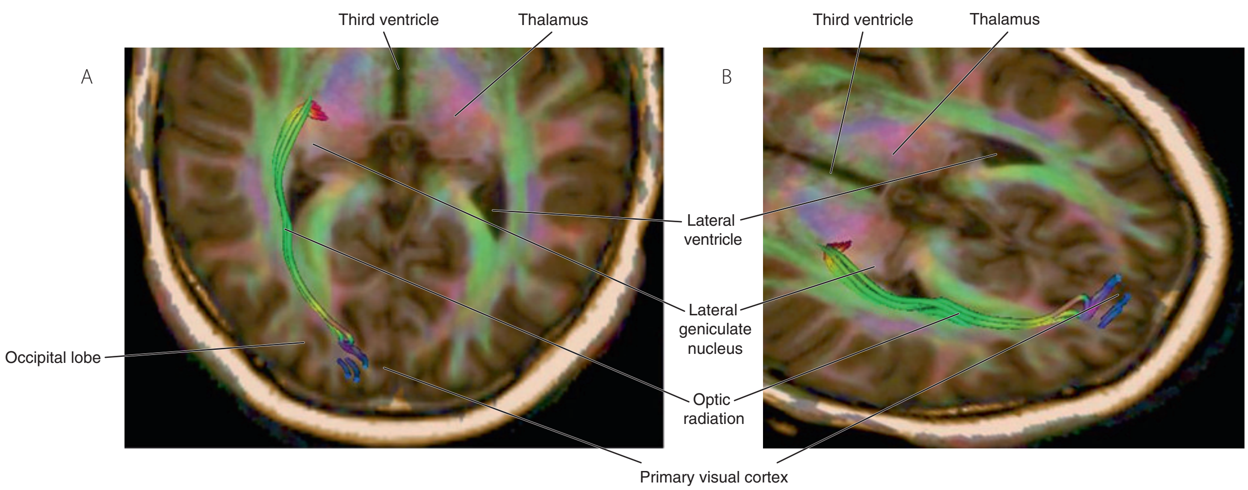


**Fig. 2.11** Retrochiasmal optic pathways: axial diffusion tensor fractional anisotropy maps demonstrating the optic pathways from lateral geniculate nucleus to the primary visual cortex. Images provided by Dr. L Mancini, Department of Neuroimaging Physics, National Hospital for Neurology and Neurosurgery, UK.

- The superior oblique muscle is the longest and thinnest muscle and arises from the body of the sphenoid. Its tendon loops around the trochlea (L. pulley) on the superomedial orbital wall to insert into the posterosuperior sclera. It may not be distinguishable from medial rectus on axial imaging. Calcification of the trochlea may be a normal finding on CT.
- The inferior oblique muscle is relatively short and thick. It arises from the medial orbital floor and inserts into the inferolateral sclera.
- Levator palpebrae superioris arises from the lesser wing of the sphenoid and penetrates the orbital septum to insert into the superior tarsal plate.

## The lacrimal apparatus (Fig. 2.6)

The lacrimal gland and nasolacrimal duct are well demonstrated on cross-sectional imaging, but dacrocystography is required to optimally delineate the lacrimal canaliculi, lacrimal sac and nasolacrimal duct pathway. A number of valves are described along the lacrimal pathway, but these are of little functional importance.

- The lacrimal gland lies in the lacrimal fossa on the lateral orbital roof and is divided into orbital and palpebral lobes by the orbital septum. It drains via multiple ducts into the superior fornix.
- The lacrimal sac lies in the lacrimal groove between the maxilla and lacrimal bone. It is filled via the lacrimal canaliculi.
- The nasolacrimal duct opens into the anterior part of the inferior meatus of the nasal cavity.

## The optic nerve

The optic nerve is an evagination of cerebral white matter and is therefore surrounded by all of the normal meningeal layers. The 'optic nerve-sheath complex' is formed by the optic nerve and the dural and leptomeningeal coverings. The dura blends

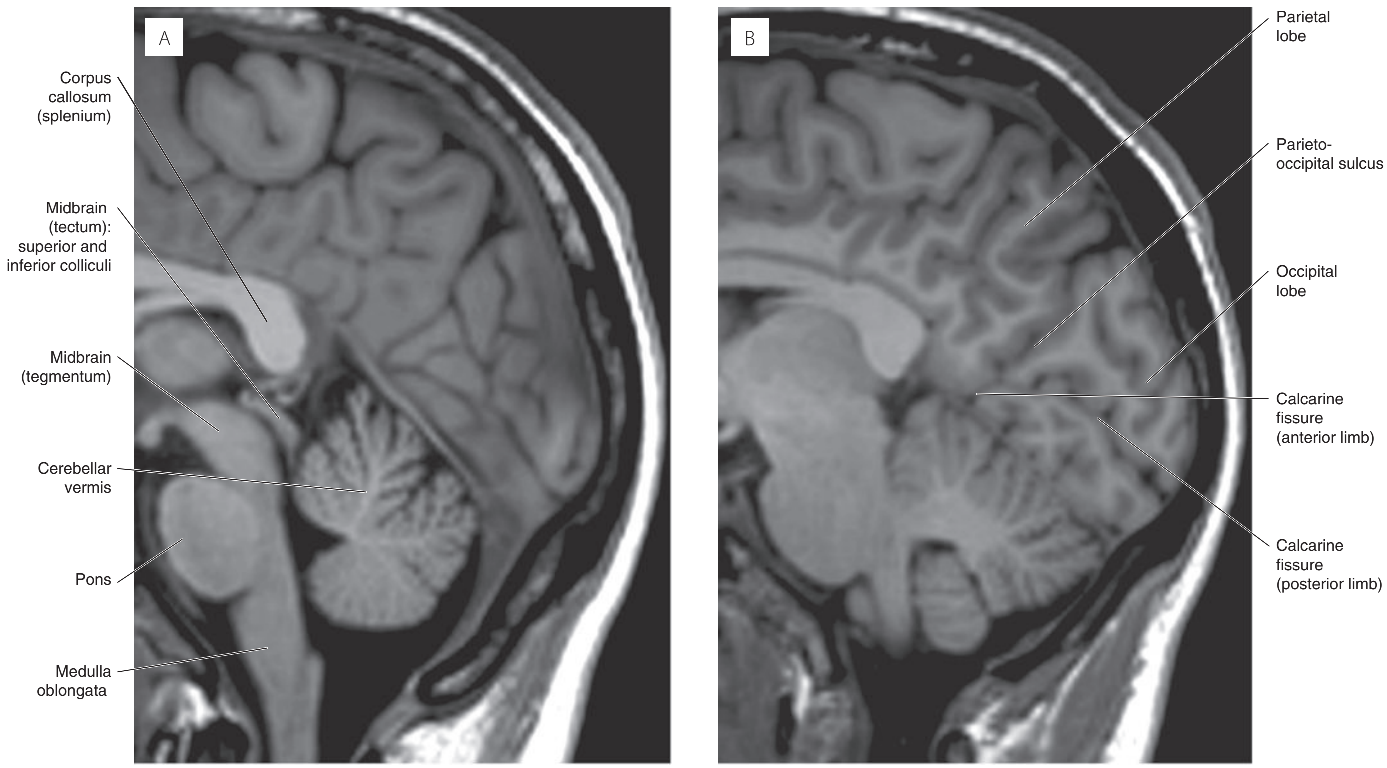


**Fig. 2.12** Visual cortex. (A) Midline sagittal T1-weighted MR image. (B) Similar section 5 mm from the midline demonstrating the calcarine sulcus more clearly.

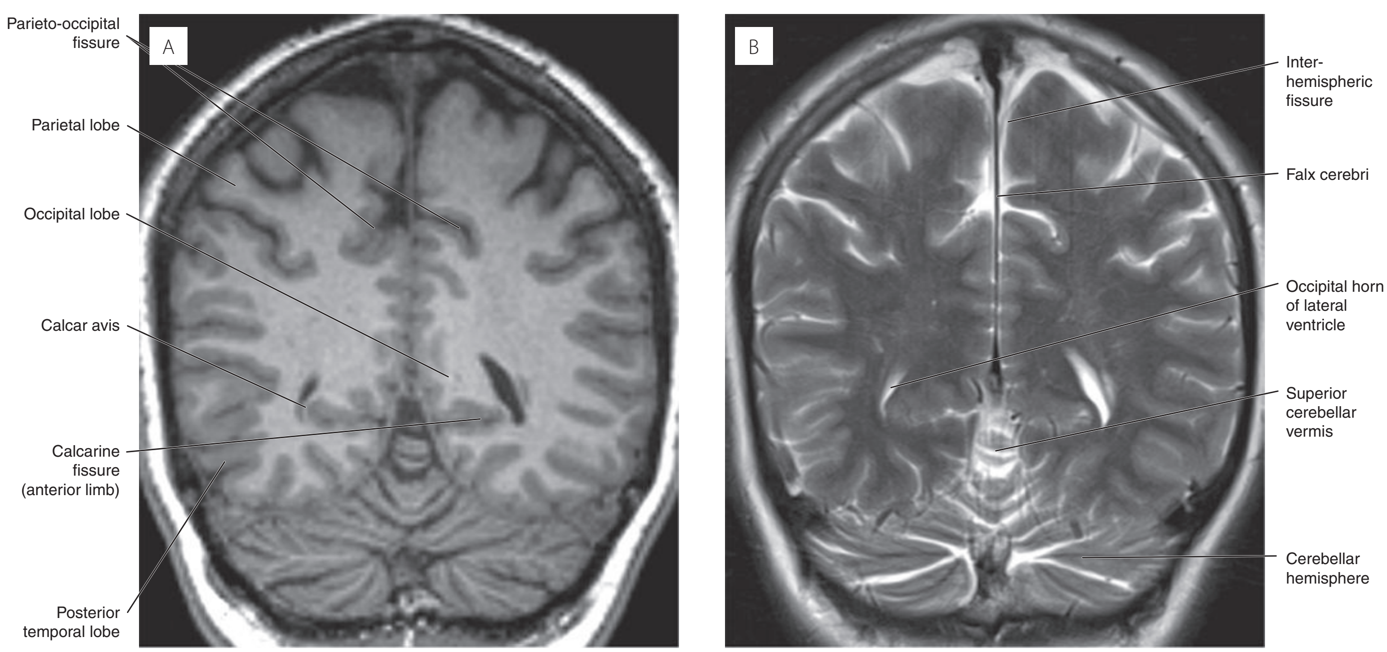


**Fig. 2.13** Calcarine fissure (anterior limb) in the coronal plane. (A) T1-weighted MR image and (B) T2-weighted images through the occipital lobes. The deep fissure and the grey matter lining indents the occipital horns producing the calcar avis.

with the sclera anteriorly and is tightly adherent to the bone of the optic canal posteriorly. Intracranial pressure changes are transmitted to the optic nerve-sheath complex, resulting in papilloedema.

The individual components of the complex are not separated on CT (Fig. 2.2c), but on MRI the optic nerve, the dura and the CSF-containing subarachnoid space can be identified separately, particularly with high-resolution T2-weighted and gadolinium-enhanced T1-weighted images (Fig. 2.5). Unenhanced T1-weighted images do not resolve the components of the normal optic nerve-sheath complex.

The segments of the optic nerve are:

- Intra-ocular: < 1 mm; not normally visible unless pathological (i.e. papilloedema)

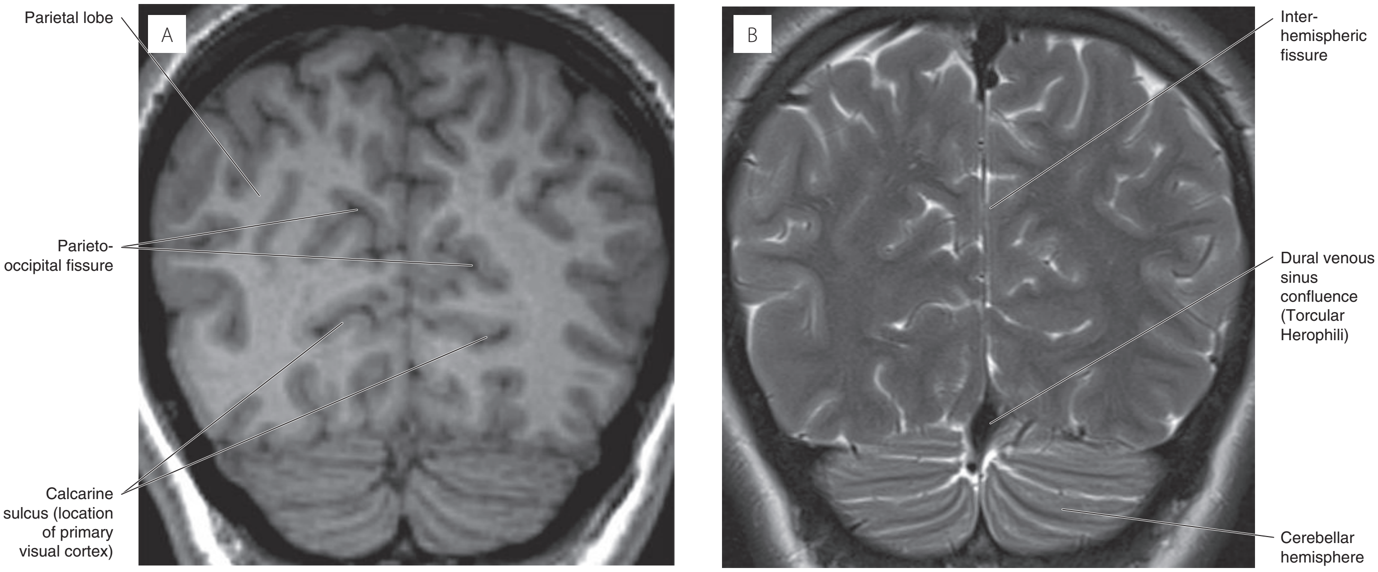


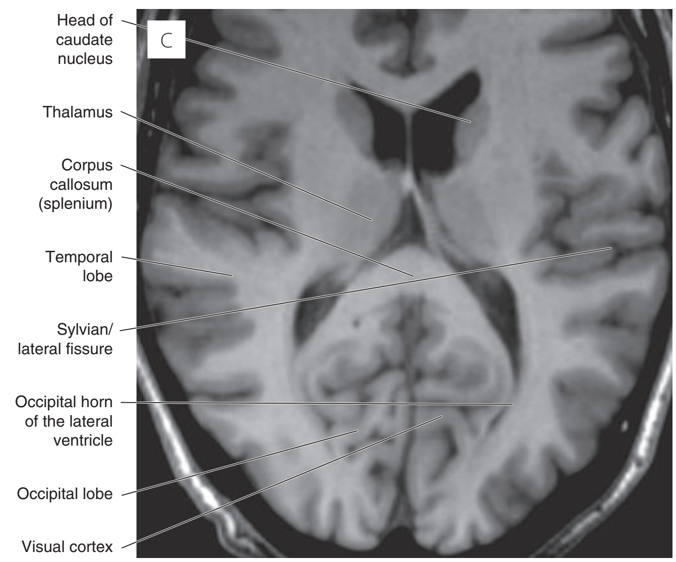


**Fig. 2.14** Coronal (A) T1-weighted MR image and (B) T2-weighted images through the occipital lobes (posterior to those in Fig. 2.13) showing the position of the calcarine fissure (posterior limb) and visual cortex. (C) Axial T1-weighted image in the plane of the calcarine fissure. Note the complex infolding of the cortex lining the calcarine fissure, as compared with the adjacent areas.

- Intra-orbital: a laxity and a sinusoidal course are normal in the neutral position; CSF space is often widest immediately posterior to the optic disc
- Canalicular: CSF around the nerve is normally effaced in the intracanalicular segment
- Intracranial: closely related to the terminal ICA and the A1 segment of the anterior cerebral artery (located superior to the nerve).

## Intracranial visual pathways

### The optic chiasm (Figs. 2.7, 2.8)

The optic chiasm lies in the chiasmatic (or 'suprasellar') cistern, above the pituitary fossa. The pituitary stalk lies posterior to the chiasm.

The position of the chiasm varies with respect to the sella from a more anterior (pre-fixed) location to a posterior (post-fixed) position.

The posterior part of the chiasm contributes to the anterior wall of the third ventricle, with the optic recess above and the infundibular recess below (Fig. 2.7a).

### The optic tracts (Figs. 2.9, 2.10)

The optic tracts run posterolaterally between the crus cerebri and uncus (inferior to the anterior perforated substance). They merge with brain substance as they course posteriorly to the lateral geniculate nucleus (LGN), an elevated region of grey matter on the posterior aspect of the thalamus, lateral to the pulvinar. Fibres from the LGN and visual cortex project to the superior colliculi, which are involved in the control of eye movements (Fig. 2.7a).

### The optic radiation (Fig. 2.11)

Two groups of fibres run to the primary visual cortex.

- The inferior visual field fibres pass directly to the occipital cortex, lateral to the occipital horn of the lateral ventricle. These parallel, compact, myelinated fibres can be identified on axial T2-weighted MRI.
- The superior visual field fibres sweep inferiorly around the temporal horn, forming Meyer's loop. These fibres are not readily apparent on MRI.

### The visual cortex (primary) (Figs. 2.12, 2.13, 2.14)

The visual cortex is located along the superior and inferior margins of the calcarine fissure on the medial aspect of the occipital lobe.

The inferior contralateral visual field lies on the superior aspect of the fissure, the superior contralateral visual field on its inferior aspect.

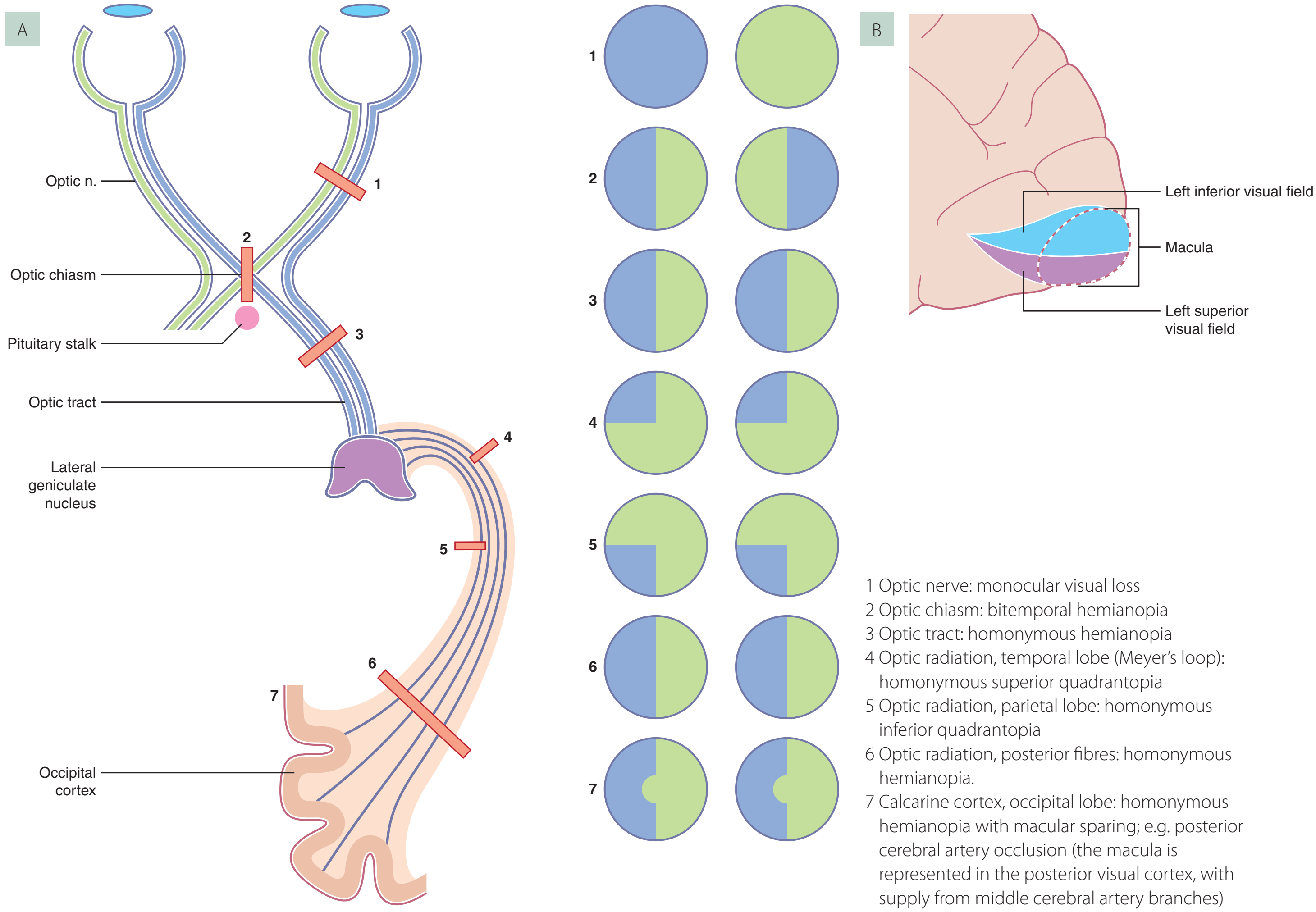


**Fig. 2.15** Lesions of the visual pathway

(A) Diagram showing the effect on the visual field of lesions at various points along the visual pathway

(B) Primary visual cortex along the right calcarine sulcus. A lesion superior to the calcarine sulcus in the right primary visual cortex results in a defect in the left inferior visual field. Note the over-representation of the macula at the posterior aspect of the sulcus (cortical magnification).

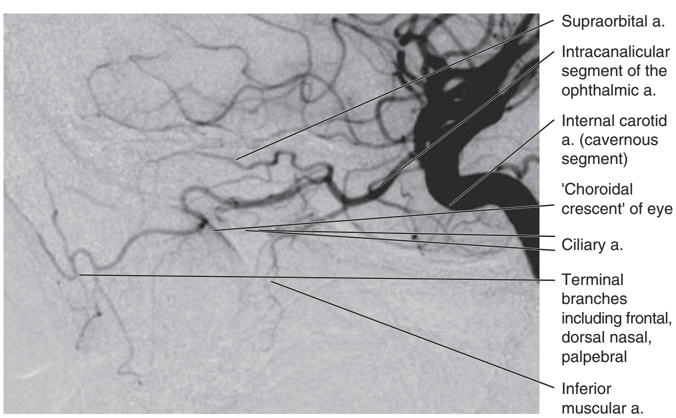


**Fig. 2.16** Selective injection of the internal carotid artery on lateral projection digital subtraction angiography in the arterial phase, centred on the ophthalmic artery.

The cortical representation of the central visual field and fovea is located around and lateral to the occipital pole. The two occupy a disproportionate extent of cortex compared to the peripheral field ('cortical magnification').

Fig. 2.15 shows the visual field defects due to interruption of the visual pathway at various points.

## Vascular anatomy

### The orbit

#### Arterial supply

The ophthalmic artery (Figs. 2.5, 2.16) is the first angiographically visible branch of the intradural internal carotid artery.

It runs through the optic canal in the dural sheath, inferolateral to the nerve at the orbital apex and then crosses (usually superiorly) to the medial aspect of the nerve.

Its major branch, the central retinal artery, pierces the nerve inferomedially, 10 mm posterior to the globe, and runs centrally inside the nerve to the globe.

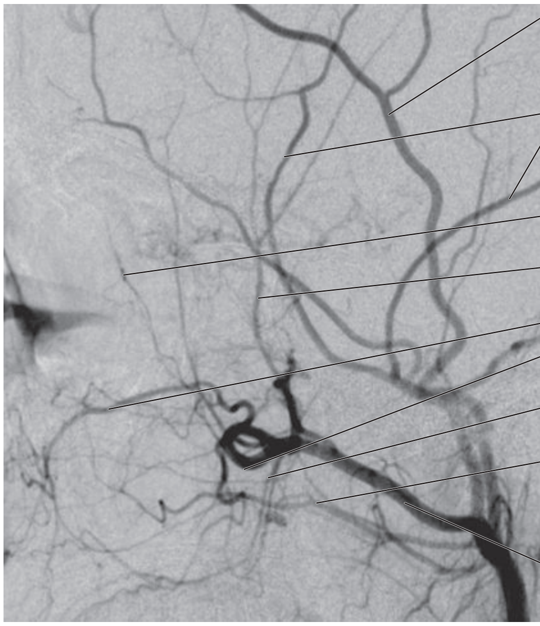


**Fig. 2.17** Selective injection of the external carotid artery on lateral projection digital subtraction angiography in the arterial phase: artefact from eyelid motion shows the position of the anterior margin of the orbit.

Other branches include the long and short posterior ciliary, lacrimal, posterior and anterior ethmoidal, supraorbital and palpebral arteries.

There are extensive anastomoses with the external carotid artery (ECA), notably the middle meningeal and internal maxillary branches, which can put the ophthalmic artery at risk during particulate embolization of lesions supplied by the ECA.

### Venous drainage

The superior ophthalmic vein (SOV) (Figs. 2.2e, 2.5c) is intraconal, coursing inferior to the superior rectus muscle. It provides venous drainage from the face via the angular and supraorbital veins.

The SOV is routinely visualized on CT and MRI. Its diameter is variable (approximately 2 mm is usual) and minor asymmetry is not uncommon.

The inferior ophthalmic vein (IOV) drains into the SOV or directly to the cavernous sinus. It communicates with the pterygoid venous plexus via the IOF and is not consistently demonstrated on cross-sectional imaging.

The central retinal vein drains to the SOV, another orbital vein or directly to the cavernous sinus. There is no functionally significant collateralization within the bulb, hence glaucoma and haemorrhage may occur as a result of its occlusion.

## The visual pathways

### Arterial supply

- Optic chiasm: internal carotid A, anterior cerebral branches
- Optic tract: posterior communicating A and anterior choroidal A
- Lateral geniculate nucleus: anterior choroidal and posterior cerebral A
- Optic radiations: anterior choroidal, middle cerebral and posterior cerebral A
- Visual cortex: posterior cerebral A (with a variable contribution from the middle cerebral A)

Chapter 3

# The petrous temporal bone

Tim Beale and Simon Morley

## Imaging methods

High-resolution computerized tomography (HRCT) and magnetic resonance imaging (MRI) are used in a complementary fashion when assessing the anatomy and pathology of the petrous temporal bone.

## External auditory canal (EAC)

The S-shaped EAC extends from the external auditory meatus (EAM) to the tympanic membrane. The lateral one-third is cartilaginous and the medial two-thirds bony.

The bony EAC is narrowed focally at the isthmus (Fig. 3.1).

The meatus is oval in sagittal cross section and lined closely by skin that attaches directly to the periosteum.

The anatomical relations of the EAC are (Fig. 3.2):

- anteriorly: the mandibular fossa containing the mandibular condyle and temporomandibular joint
- posteriorly: the mastoid process
- inferiorly: the parotid gland and infratemporal fossa
- superiorly: the middle cranial fossa and the temporal lobe.
  The nodal drainage from the EAC is to the intraparotid group.

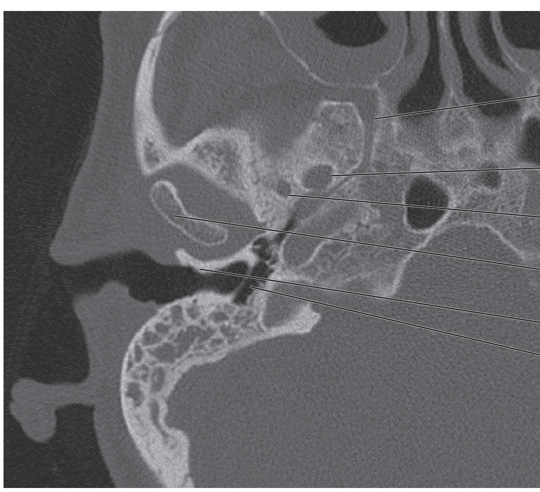


**Fig. 3.1** Axial HRCT. The external auditory canal.

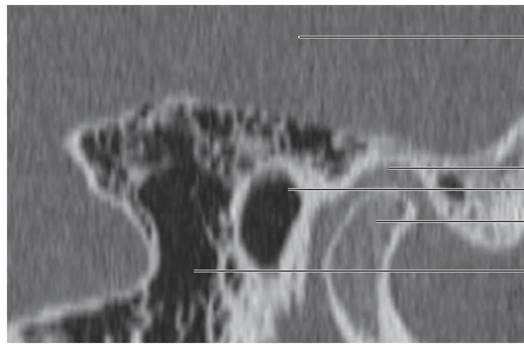


**Fig. 3.2** Sagittal HRCT. Relations of the EAC.

## The tympanic membrane (TM)

The conical tympanic membrane is set at an angle to the floor of the canal and separates the middle ear (mesotympanum) from the external ear (Figs. 3.1, 3.3).

The handle (manubrium) and the lateral (short) process of the malleus are embedded in the TM.

From the malleal prominence the anterior and posterior malleal folds divide the TM into a smaller, thinner pars flaccida above and a larger pars tensa below.

The TM is usually visible in the coronal plane as a thin line on HRCT and is attached superiorly to the scutum (shield) (Figs. 3.3b and 3.6) and peripherally to a bony annulus.

## The middle ear and mastoid

The middle ear (ME) cavity is divided in the coronal plane into hypotympanum, mesotympanum or epitympanum (attic) along the superior and inferior margins of the EAC. The anatomy is complex but well shown by HRCT (Figs. 3.4–3.6).

### Medial wall

There are several important anatomical landmarks along the medial wall of the ME cavity.

The cochlear promontory overlies the basal turn of the cochlea, with the oval window superior and the round window posteroinferior to it.

The cochleariform process is a depression in the anterior aspect of the medial wall marking the point where the tensor

*Applied Radiological Anatomy, 2nd Edition* ed. Paul Butler, Adam W.M. Mitchell and Jeremiah C. Healy. Published by Cambridge University Press.

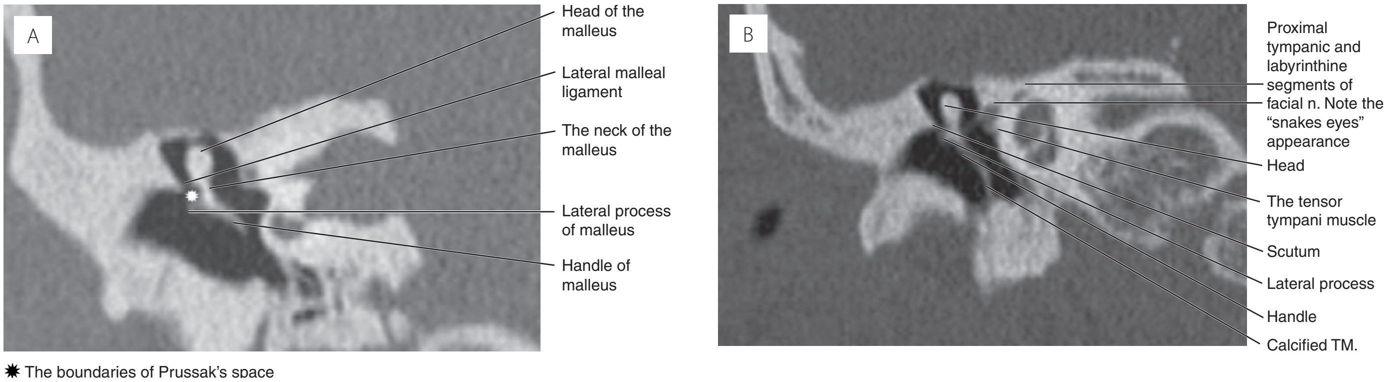


**Fig. 3.3** Coronal HRCT. The malleus.

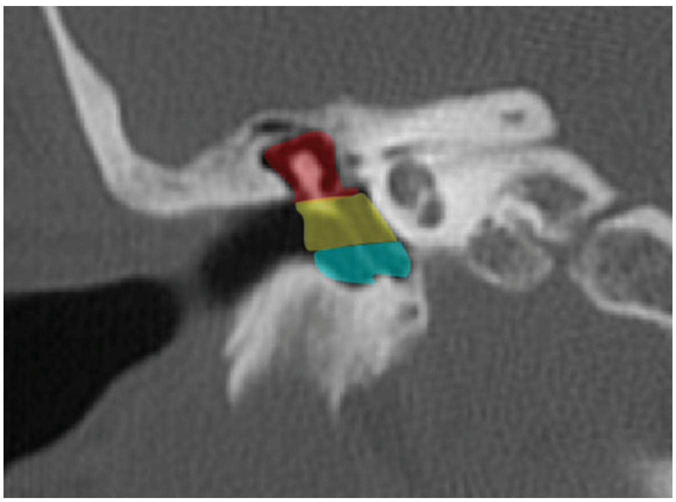

**Fig. 3.4** Coronal HRCT. The compartments of the middle ear (ME) cleft; red, epitympanum (or attic); yellow, mesotympanum; and blue, hypotympanum.

tympani muscle turns laterally to attach to the neck of the malleus (Fig. 3.5d).

More posteriorly the lateral semicircular canal (LSCC) protrudes into the epitympanum, with the tympanic segment of the facial nerve passing just inferior to it and lateral to the oval window (Fig. 3.6b).

## Lateral wall

The lateral wall comprises mainly the scutum and superior to it a thin wall covering the tegmental air cells superior to the medial EAC.

## Posterior wall

The pyramidal eminence separates the sinus tympani medially from the facial recess laterally (Figs. 3.5b and 3.7). The stapedius muscle extends from the pyramidal eminence to attach to the neck of the stapes (Fig. 3.7).

The aditus or passageway extends between the posterior wall of the attic and the antrum (Fig. 3.5e).

## Roof and floor

The tegmen is the thin bony plate covering the roof of the tympanic cavity separating it from the middle cranial fossa (Fig. 3.6).

The floor consists of bone of variable thickness, which overlies the internal carotid canal anteriorly and the jugular bulb posteriorly.

## Aberrant internal carotid artery (ICA)

This is a collateral circulation secondary to failure of development of the first embryonic segment of the ICA. The collateral

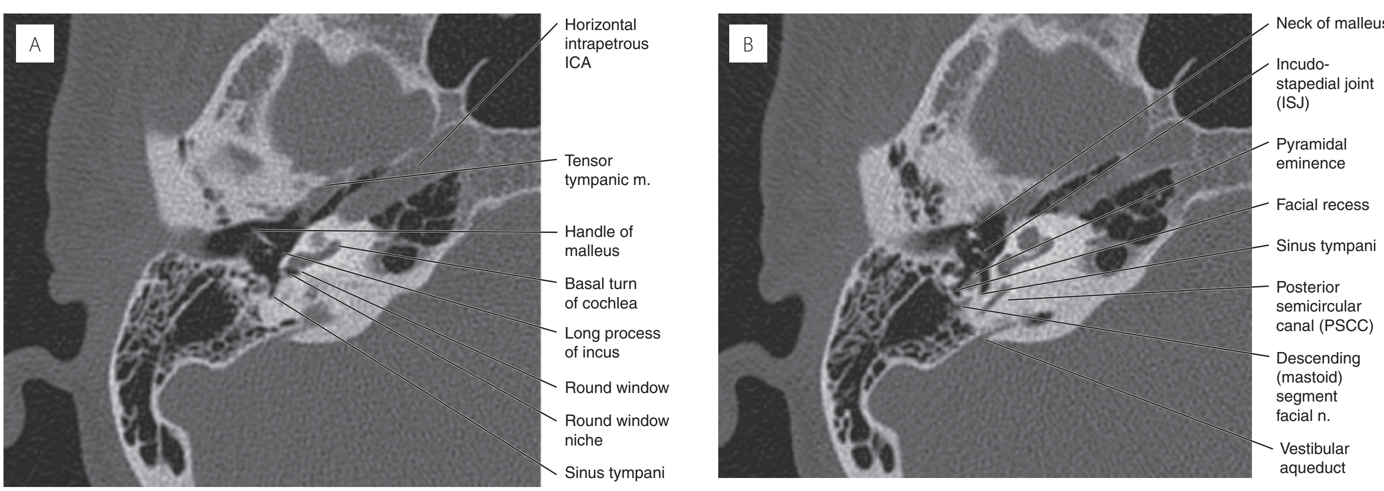


**Fig. 3.5** Axial HRCT middle ear. a–e, inferior to superior.

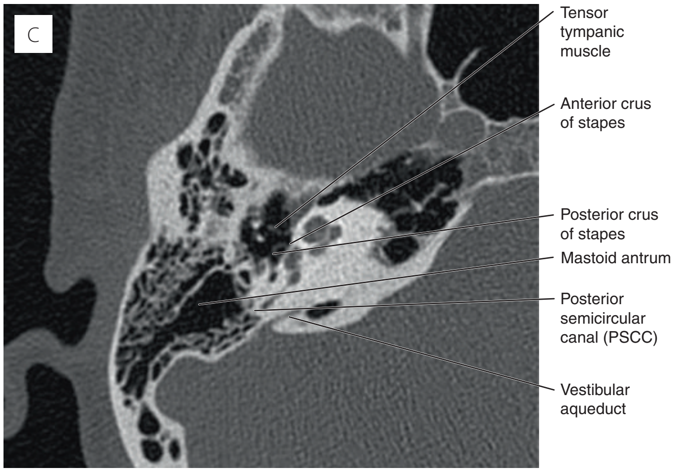


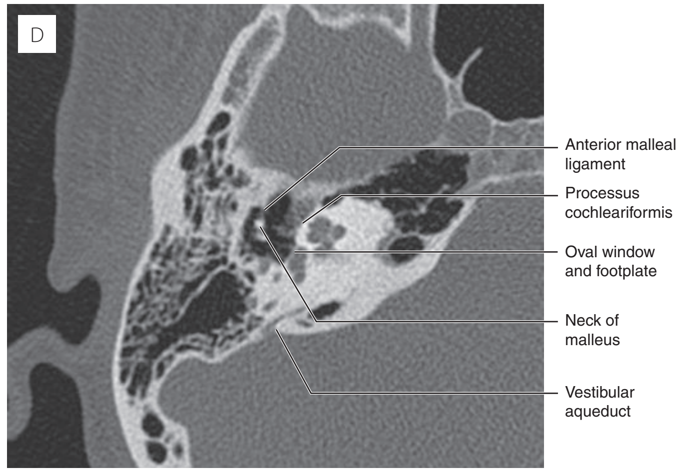


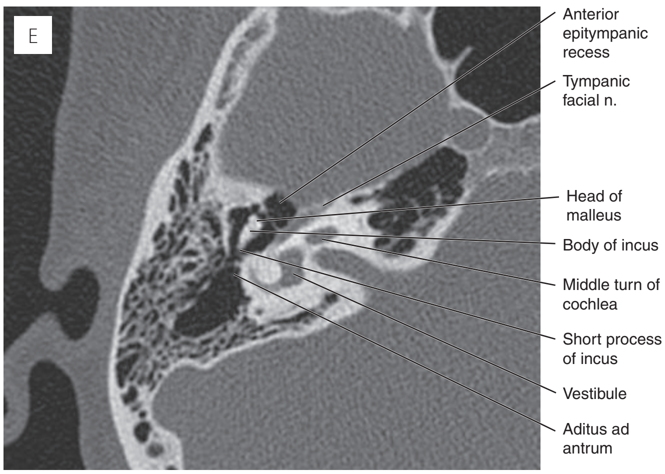


**Fig. 3.5** *(cont.)*

route is via the inferior tympanic artery, which is markedly enlarged, anastomoses with the caroticotympanic branch of the ICA and connects with the horizontal intrapetrous ICA. It does this by coursing over the cochlear promontory and is seen as a retrotympanic vascular mass.

This can be recognized on imaging (Fig. 3.8).

## The auditory ossicles

### Malleus

The malleus is made up of the head, neck, lateral (short) process, anterior process and handle (manubrium). The lateral process and handle of the malleus are embedded in the TM (Fig. 3.3).

The malleus articulates with the larger body of the incus at the synovial diarthrodial malleoincudal joint within the attic and is best visualized on axial (Fig. 3.5e) or sagittal oblique images.

On axial images the malleoincudal joint resembles an ice cream (head of malleus) sitting on a cone (body of incus) and on sagittal reformatted images a molar tooth (Fig. 3.9).

### Incus

The incus consists of a body and short, long and lenticular processes. The short process extends posteriorly within the fossa incudis just inferior to the aditus ad antrum (Fig. 3.5e).

The long and lenticular processes meet at an angle of approximately 90°. This ‘hockey stick’ appearance is best demonstrated in the coronal plane (Figs. 3.6a, 3.8).

The body and short process ‘ice cream cone’ is best seen on axial images (Fig. 3.5e)

The cup-shaped lenticular process of the incus articulates with the head (capitulum) of the stapes at the incudostapedial joint (ISJ), which is again a synovial diarthrodial articulation (Figs. 3.5b, 3.11).

### Stapes

The stapes consists of the head (capitulum) anterior and posterior crura and the tympanic portion of the footplate (Figure 3.5c,d).

These components together are described as the stapes superstructure.

The space between the stapes crura is called the obturator foramen.

### Ossicular ligaments

The superior, lateral and anterior malleal ligaments, supporting the malleus, can be seen on HRCT (Fig. 3.5d). The others cannot.

### Prussak’s space

Prussak’s space is the most common site of origin for acquired cholesteatoma and is located between the lateral mallear ligament superiorly, the lateral (short) process of the malleus inferiorly, the pars flaccida of the TM laterally and the neck of the malleus medially (Fig. 3.3a).

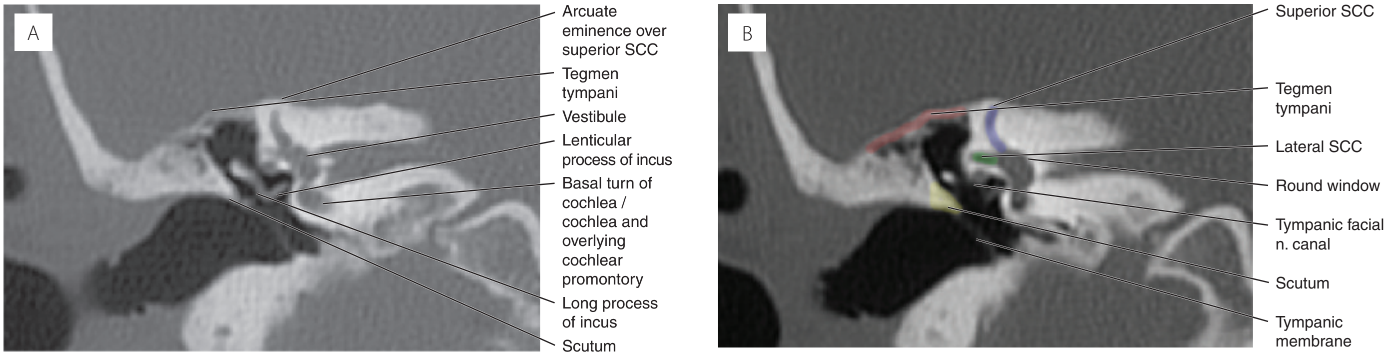


**Fig. 3.6** Coronal HRCT middle ear (A is anterior to B).Tegmen (red), lateral SCC (green), superior SCC (blue) and Scutum (yellow) coloured.

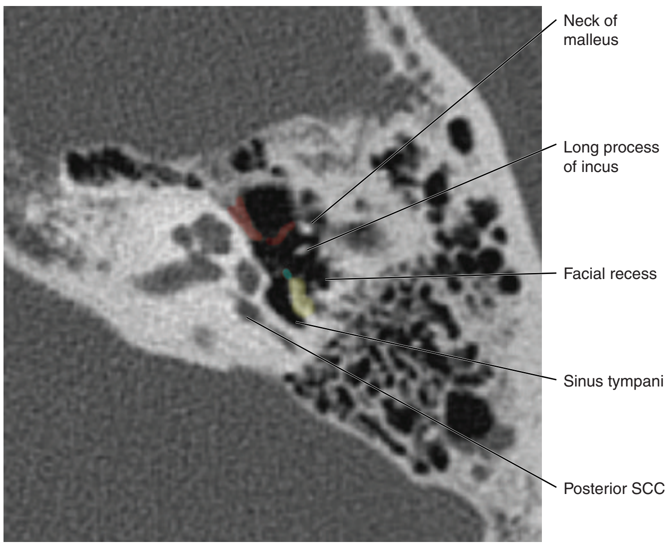


**Fig. 3.7** Axial HRCT middle ear: tensor tympani (red) and stapedius (turquoise) muscles and pyramidal eminence (yellow) coloured.

## The mastoid antrum and petromastoid aircells

There is great variability in the degree of temporal bone pneumatization, which can be very extensive, but which is usually symmetrical.

The mastoid antrum communicates with the epitympanum via the aditus.

The inferior extension of the antrum is called the central mastoid tract and the more peripheral air cells the peripheral mastoid area.

Asymmetrical pneumatization of the petrous apices is a normal anatomical variation (Fig. 3.12). On MRI the T1 high signal from fatty marrow on the non-pneumatized side can be mistaken for pathology.

### Koerner's septum

This is a bony septum of variable thickness and is part of the petrosquamosal suture. It is a surgical landmark and passes through the antrum, where it can be confused with the medial wall of the antrum at surgery (Fig. 3.13).

## The inner ear

This consists of the bony labyrinth demonstrated by HRCT surrounding the membranous (endolymphatic) labyrinth, shown on MRI. The perilymphatic fluid is interposed between the two.

### The cochlea

The cochlea is located anteriorly and converts mechanical energy from movement of the stapes footplate into electrical energy. It consists of 2½ to 2¾ turns with its base at the lateral end of the internal auditory canal (IAC).

The modiolus is the central axis from which a thin bony plate (the spiral lamina) projects and attaches to the outer cochlea wall. In addition there is a thicker plate of bone (the interscalar septum) that separates the individual turns of the

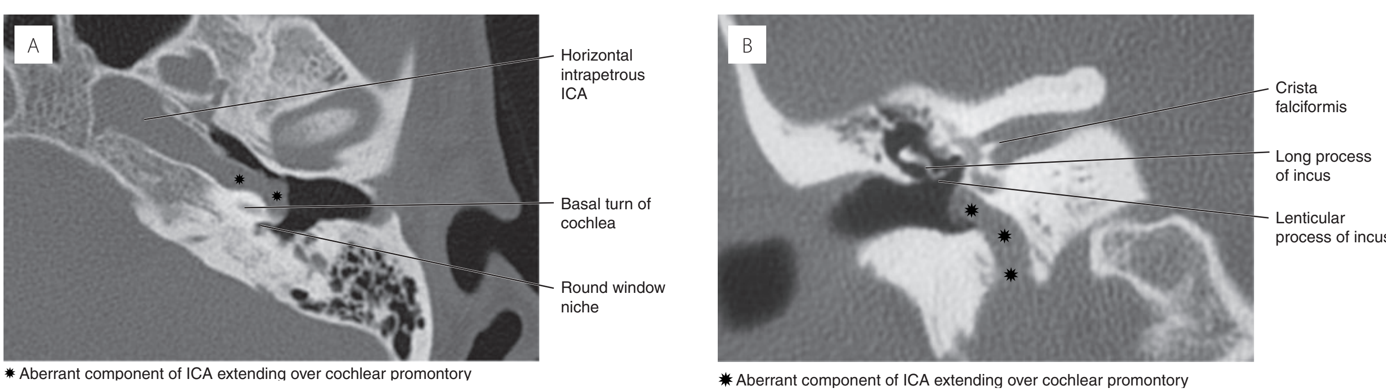


**Fig. 3.8** HRCT middle ear. (A) Axial and (B) coronal.

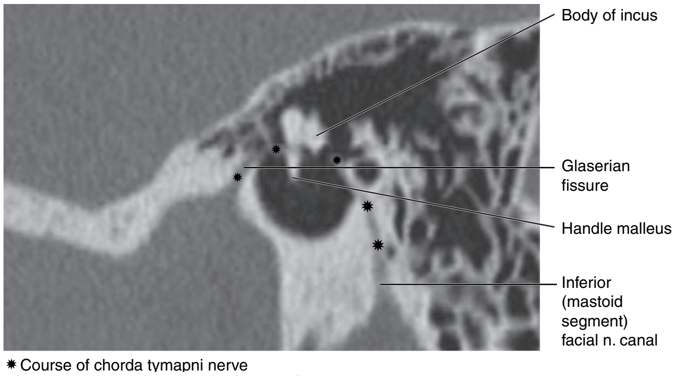


**Fig. 3.9** Sagittal HRCT 'molar tooth' sign.

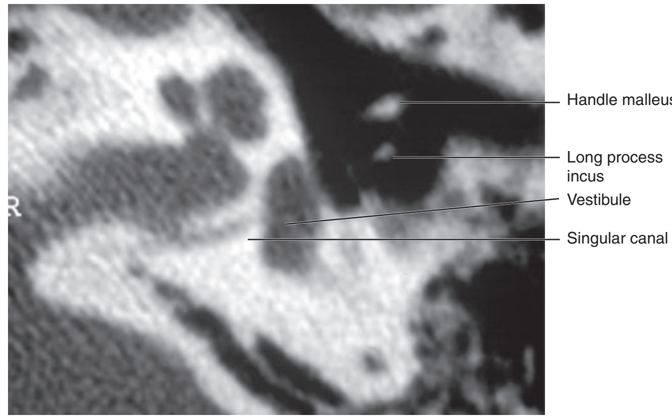


**Fig. 3.10** Axial HRCT magnified. The ossicles.

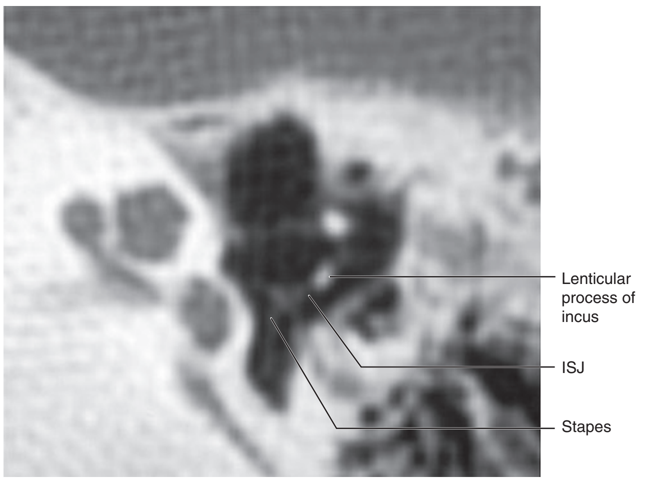


**Fig. 3.11** Axial HRCT magnified. The ossicles: note the alignment of the stapes and lenticular process of incus in a normal ISJ.

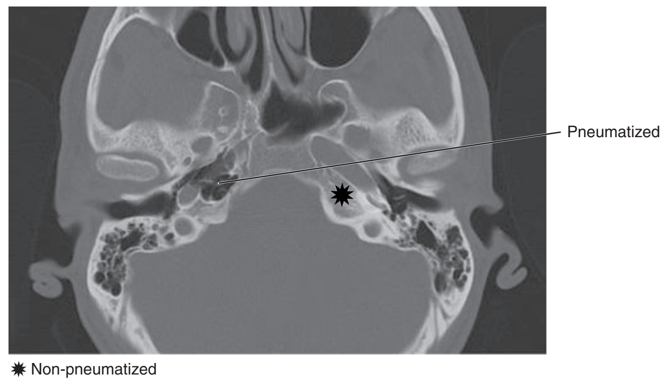


**Fig. 3.12** Axial HRCT. Asymmetrical petrous apex pneumatization.

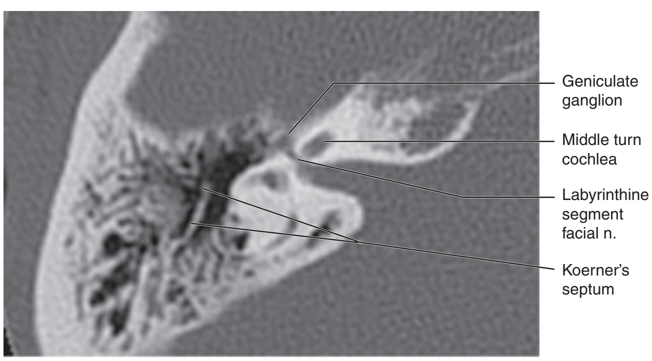


**Fig. 3.13** Axial HRCT. Koerner's septum.

cochlea and also projects out from the modiolus. The modiolus, spiral lamina and interscalar septum are all clearly visible on both HRCT and MRI (Fig. 3.14).

The cochlear nerve passes through the central core of the modiolus.

The scala tympani and vestibuli are the perilymph channels that parallel and surround the endolymph (cochlear duct). As the perilymph of the scala tympani and vestibuli closely resembles CSF, both scala are clearly visualized on T2-weighted MR sequences (Fig. 3.15).The cochlear duct, however, because of its small size cannot yet be clearly differentiated as a separate entity.

## The cochlear aqueduct

This is a narrow channel containing perilymph that connects the scala tympani of the basal turn with the subarachnoid space. It is parallel and inferior to the IAC and best identified from its lateral aspect in the round window region.

## The vestibule

The vestibule (Figs. 3.5e, 3.6, 3.16) contains the saccule (anterior) and the utricle (posterior) which cannot yet be clearly differentiated on routine imaging.

There are five openings in the posterior vestibule (utricle) for the three semicircular canals (the posterior and superior semicircular canals have a common crus).

## The vestibular aqueduct

The vestibular aqueduct arises from the posterosuperior vestibule and is directed posteriorly and inferiorly. It is seen on axial images but multiplanar reformatted images in particular in the parasagittal plane are sometimes required to assess the whole course (Fig. 3.5c).

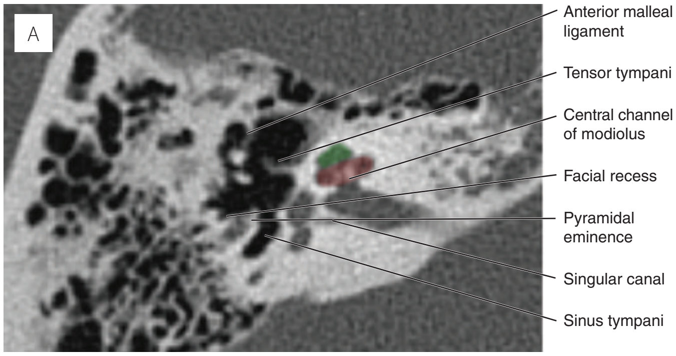


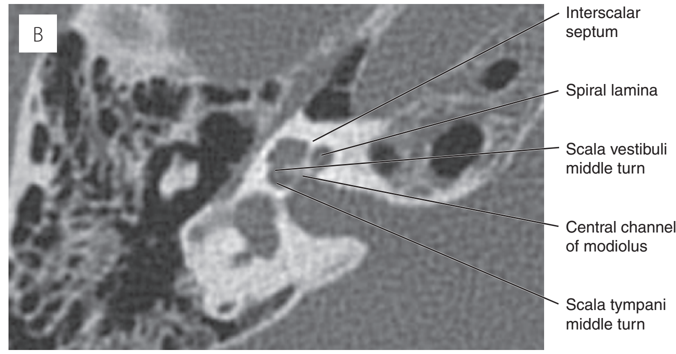


**Fig. 3.14** Axial HRCT (A is inferior to B).

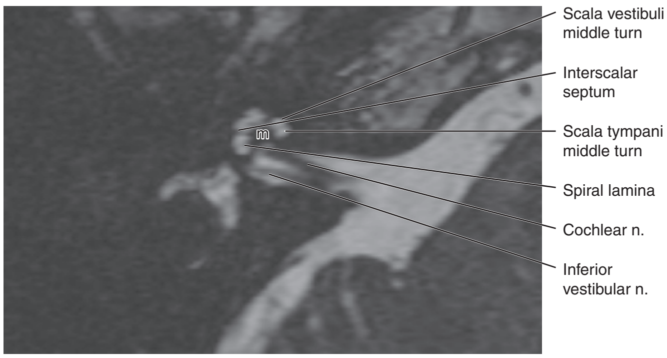


**Fig. 3.15** Axial T2 MRI. Cochlea. m = modiolus.

## The semicircular canals

There are three semicircular canals, the lateral, superior and posterior. Each semicircular canal describes two-thirds of a circle and is orthogonal with the others. The superior semicircular canal (SSCC) is perpendicular to and the posterior semicircular canal (PSCC) parallel to the long axis of the petrous bone (wedge) (Fig. 3.16).

The bony covering of the superior semicircular canal forms the arcuate eminence, a ridge on the superior surface of the petrous bone that can be seen also on skull radiographs (Fig. 3.6a). Passing inferior to the SSCC is the petromastoid canal, which contains the subarcuate artery. It is of variable size, extends from the posterior fossa to the mastoid antrum and can be mistaken for a fracture (Fig. 3.16a).

The bony covering of the lateral semicircular canal (LSCC) is a prominent landmark on the medial wall of the middle ear cleft (Fig. 3.6b).

Commonly the nerve of the PSCC passes initially in a separate canal, the singular canal, which is clearly visible on HRCT prior to joining the inferior vestibular nerve in the IAC (Fig. 3.14a).

## The internal auditory canal

There is individual variation in size and shape of the normal internal auditory canal (IAC) but the right and left IACs are symmetrical.

The IAC:

- is cylindrical in shape and lies in a horizontal plane; it can therefore be clearly seen in both the axial and coronal planes, (Figs. 3.8b, 3.16c)
- is lined with dura and contains cerebrospinal fluid
- transmits the facial (VIIth cranial) and vestibulocochlear nerves (Fig. 3.17).

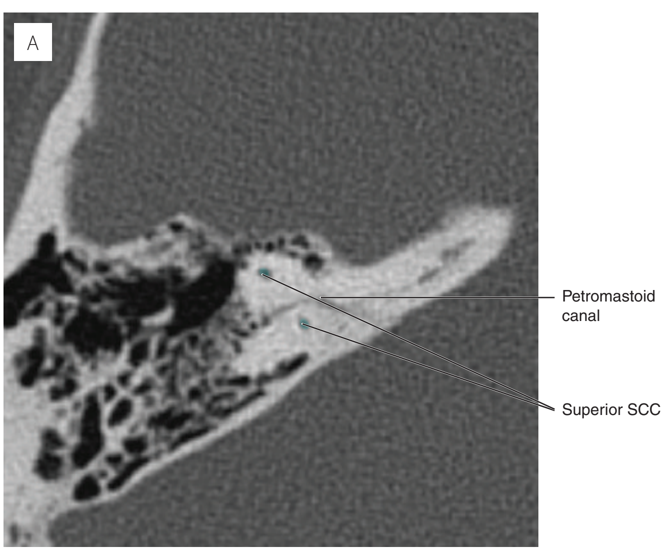


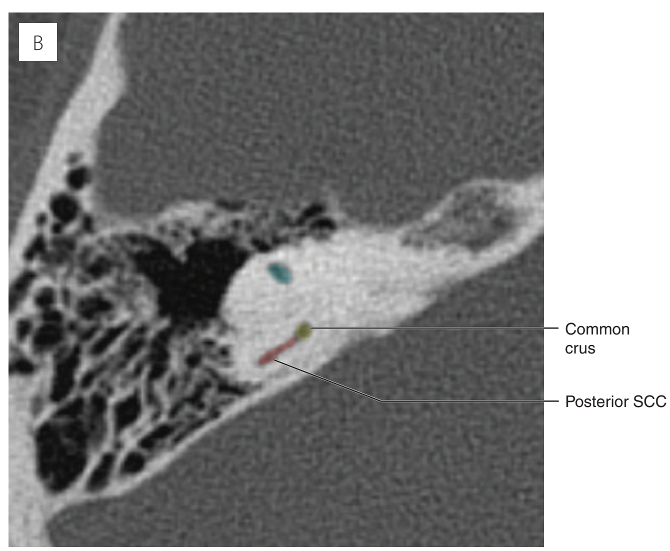


**Fig. 3.16** Axial HRCT. Semicircular canals (SCCs) and vestibule (A–D, superior to inferior): superior SCC (turquoise), posterior SCC (red), lateral SCC (green), common crus (yellow) and vestibule (purple) coloured.

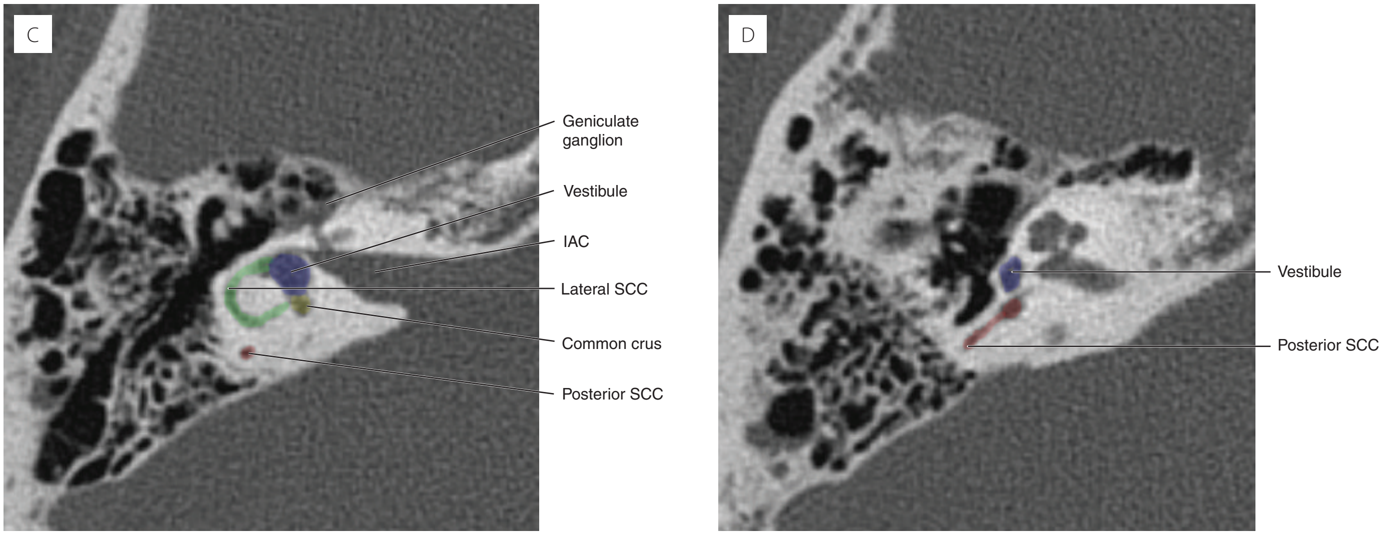


**Fig. 3.16** (*cont.*)

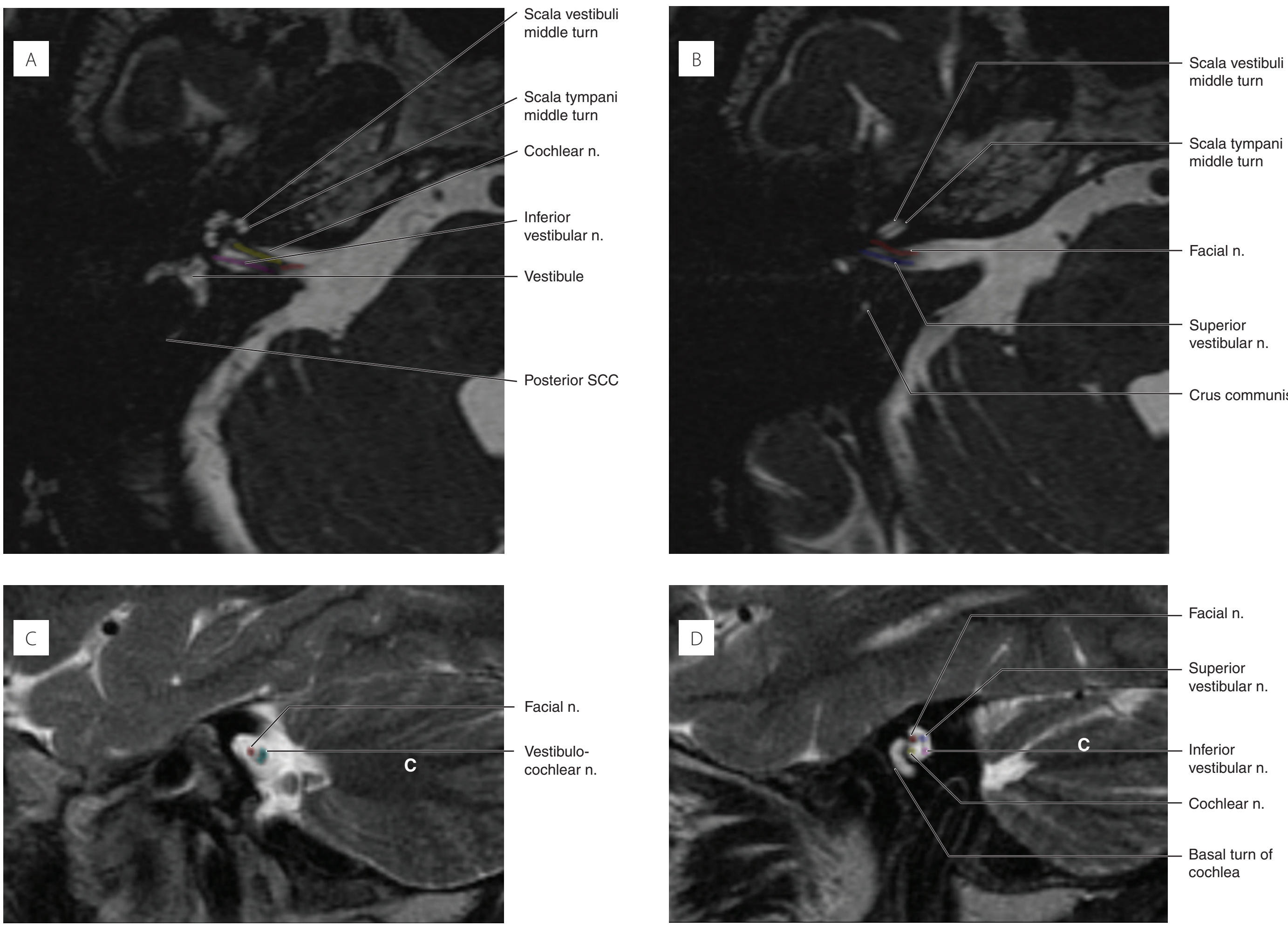


**Fig. 3.17** Axial (A,B) and sagittal oblique (C,D) MRI through IAC. Image C through porus of IAC with facial n. (red) and vestibulocochlear n. (turquoise). Image D through fundus of IAC with superior vestibular n. (purple), inferior vestibular n. (pink) and cochlear n. (yellow).

At the porus acousticus, the medial opening of the IAC, there are usually only two distinct nerves visible (Fig. 3.17c), the larger and more posterior vestibulocochlear (VIIIth cranial) nerve and the smaller, more anterior facial nerve.

At the fundus, the lateral portion of the IAC, the vestibulocochlear (VIIIth cranial) nerve has divided into a separate cochlear nerve anterorinferiorly seen entering the modiolus and the superior and inferior vestibular nerves in the posterosuperior and posteroinferior quadrants, respectively (Fig. 3.17d).

The fundus is divided into halves by the horizontal crista falciformis, a bony bar of variable size that is clearly seen on HRCT (Fig. 3.8b). There is also a vertical crest of bone at the fundus called Bill's bar, which further divides the fundus into quadrants; however, this cannot yet be clearly identified on imaging.

## The facial (VIIth cranial) nerve

The facial (VIIth cranial) nerve consists of a larger motor and smaller sensory root.

### Intracranial course

High-resolution axial T2-weighted MRI demonstrates the nerve as it exits the brainstem at the pontomedullary junction, courses through the cisternal space anterior to the larger VIIIth nerve (Fig. 3.18) and enters the anterosuperior quadrant of the IAC (Fig. 3.17d).

### Intratemporal course

MRI and HRCT are complementary when assessing the intratemporal course of the facial nerve, which is divided into labyrinthine, tympanic and mastoid segments.

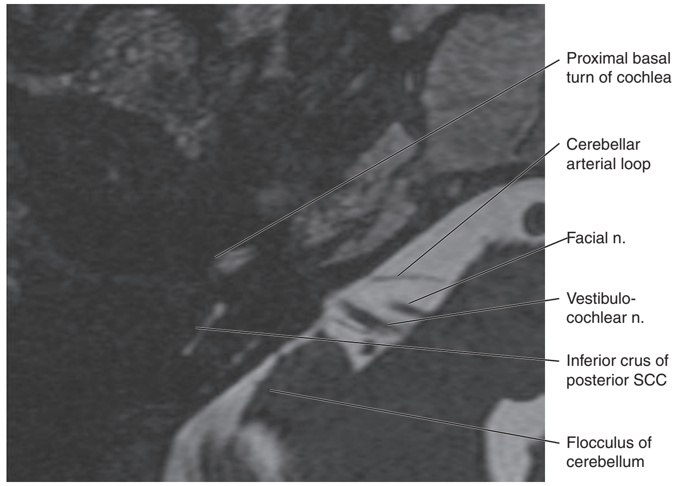


**Fig. 3.18** Axial T2 MRI.

The first (labyrinthine) segment of the facial nerve is the narrowest and shortest segment and extends anterolaterally from the IAC superior to the cochlea, terminating at the geniculate ganglion (Fig. 3.19a). The most proximal branch of the facial nerve is the greater superficial petrosal nerve, which extends anteriorly from the geniculate ganglion in a small groove to supply secretomotor fibres to the lacrimal gland and

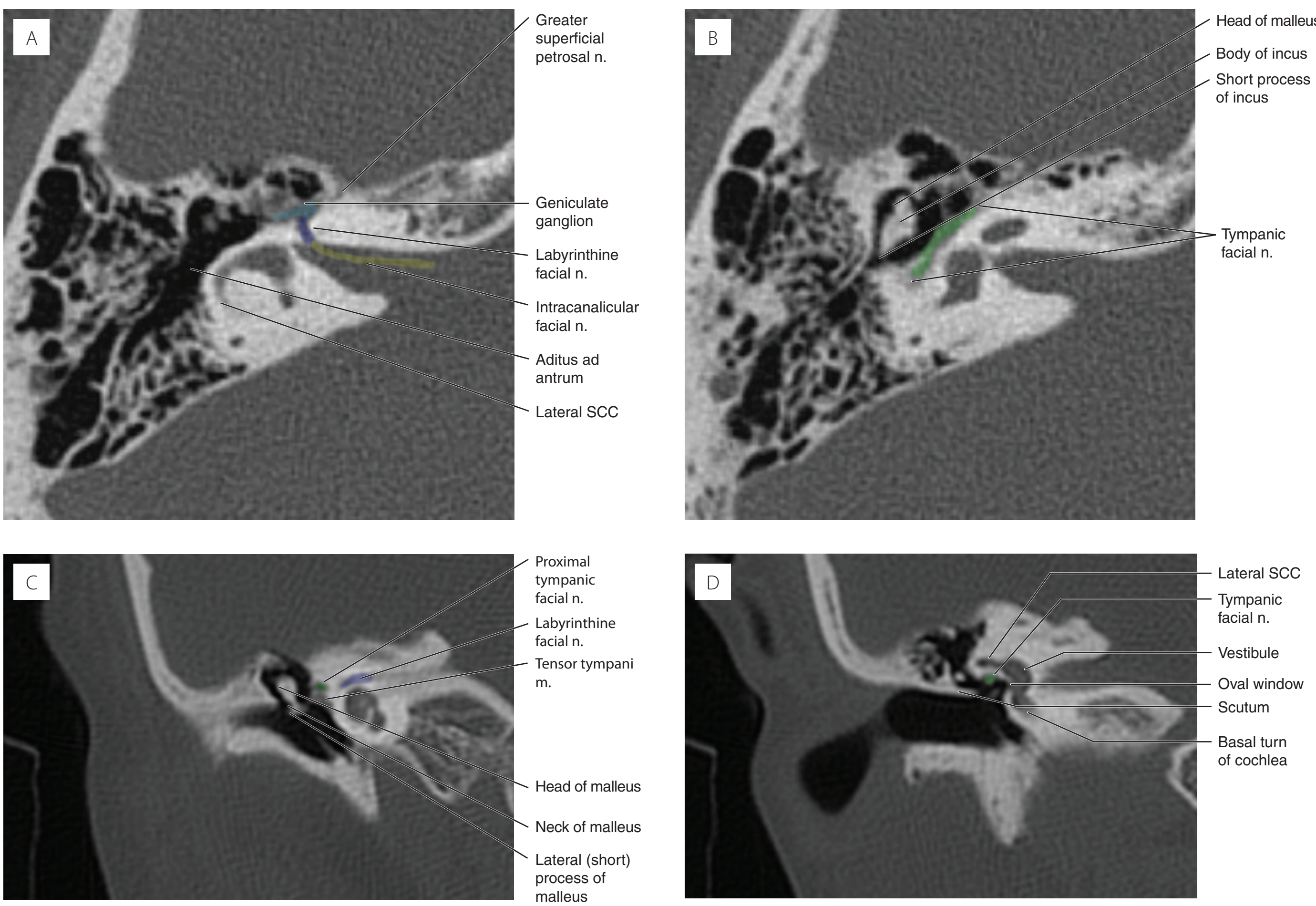


**Fig. 3.19** HRCT. The facial nerve. Axial (A is superior to B); coronal (C is anterior to D), (E) sagittal. Facial nerve: intracanalicular (yellow), labyrinthine (purple), geniculate ganglion (turquoise), tympanic segment (green). In panel E: C, mandibular condyle; E, external auditory canal.

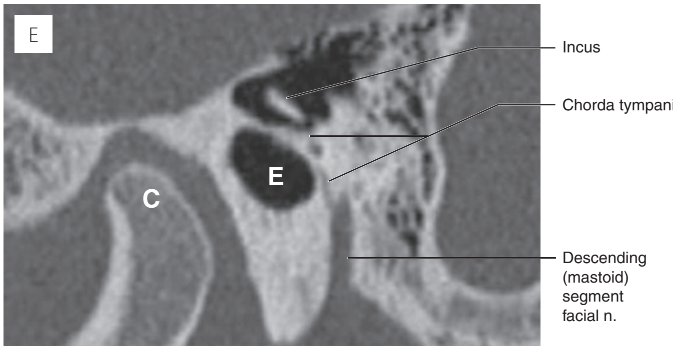


**Fig. 3.19** (*cont.*) C, mandibular condyle, E, external auditory canal.

receive taste fibres from the hard palate. The facial nerve then turns posteriorly at an acute angle at the geniculate ganglion or anterior genu to form the tympanic segment (Fig. 3.19b).

The second or tympanic segment is further subdivided.

The proximal tympanic segment is just superior to the tensor tympani tendon (Fig. 3.19c), the mid-portion immediately inferior to the LSCC (Fig. 3.19d) and the posterior segment inferior to the short process of the incus.

The third or mastoid segment originates at a second, posterior genu where the facial nerve turns inferiorly at an obtuse angle to descend and exit the skull base at the stylomastoid foramen (Fig. 3.19e).

The two main branches of the mastoid segment are the nerve to stapedius and the chorda tympani. The chorda tympani originates just above the stylomastoid foramen and extends anteriorly and superiorly in its own canal to enter the middle ear cleft lateral to the long process of the incus. It carries afferent taste fibres from the anterior two-thirds of the tongue and efferent secretomotor fibres to sublingual, submandibular and minor salivary glands (Figs. 3.9, 3.19e).

The classic 'snakes eyes' appearance of the facial nerve is seen on coronal scans (Fig. 3.3b) when it passes through both the distal labyrinthine and proximal tympanic segments on the same image just posterior to the geniculate ganglion.

Axial scans are best for assessing the labyrinthine segment on both HRCT and MRI. The tympanic segment can be seen on both axial and coronal sequences, although coronal CT best demonstrates the relationship of the nerve to the oval window and stapes and the presence of any dehiscence of the bony canal wall.

Although the posterior genu can be seen in both the axial and coronal planes, sagittal oblique reformatted images are usually best for assessing this region.

The normal facial nerve will enhance with gadolinium to a minor degree at both the geniculate ganglion and proximal tympanic segment due to a perineural capillary-venous plexus.

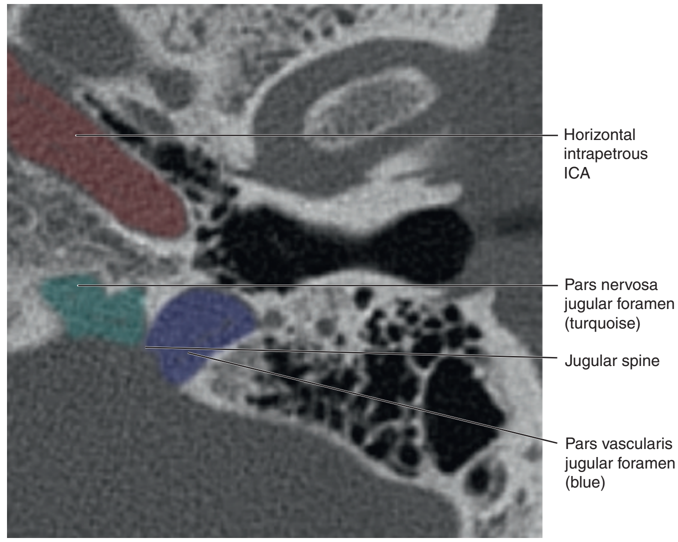


**Fig. 3.20** Axial CT. Jugular foramen.

The intracanalicular, labyrinthine and mastoid segments never normally enhance.

T1-weighted axial scans at the stylomastoid foramen clearly demonstrate the dark dot of the facial nerve surrounded by fat and it is a useful review area when assessing for possible pathology at this site such as possible involvement of the facial nerve by a deep lobe of parotid lesion.

## The jugular foramen

The jugular foramen (Fig. 3.20) connects the sigmoid sinus to the internal jugular vein and is divided into two parts, a smaller anterior pars nervosa, which despite its name contains only the glossopharyngeal (IXth cranial) nerve, and Jacobsen's nerve (the tympanic branch of the IXth nerve), and drains the inferior petrosal sinus and a larger posterior pars vascularis that contains the vagus (Xth cranial), spinal accessory (XIth cranial) and the auricular branch of vagus (Xth cranial) nerve (Arnold's nerve) as well as draining the jugular bulb and sigmoid sinus.

## Jugular bulb

The jugular bulb is the dilatation of the jugular vein within the superior aspect of the jugular foramen. In the coronal plane it is inferior to the vestibule in the posterior hypotympanum and on MRI is in the same plane as the odontoid peg. The jugular foramen is commonly larger on the right side but when normal its cortical margins and the jugular spine are preserved.

A high-riding jugular bulb is defined when the superior aspect of the bulb extends above the floor of the internal auditory canal (IAC).

Chapter 4

# The extracranial head and neck

Tim Beale

## The suprahyoid neck

The suprahyoid neck extends from the skull base to the hyoid bone. It is divided into a number of spaces by the three layers of deep cervical fascia, which act as barriers to the spread of disease (Fig. 4.1).

This method also simplifies the differential diagnosis and has largely replaced the divisions based on various muscular triangles.

The three layers of deep cervical fascia are the superficial (investing) layer, the middle (visceral) layer and the deep (prevertebral) layer.

The superficial layer invests all the deep structures apart from the platysma and superficial nodes and sends slips that envelop the sternocleidomastoid and trapezius muscles and the parotid and masticator spaces.

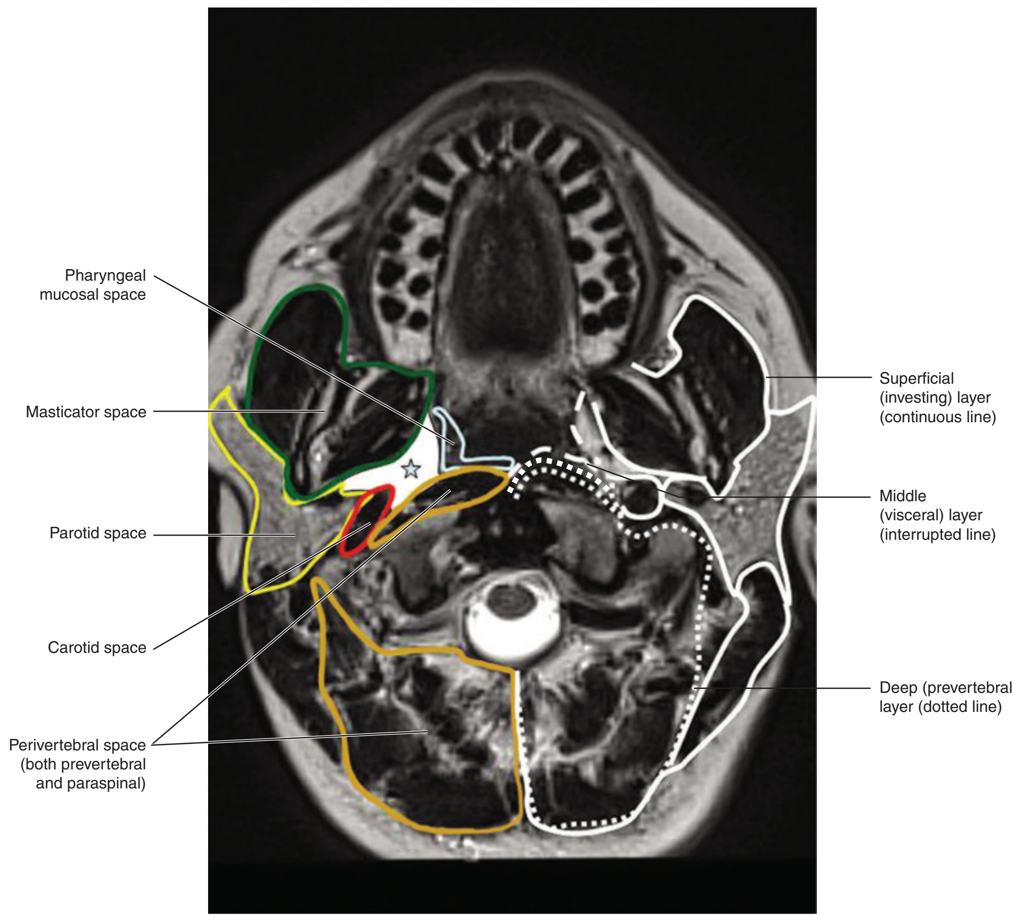


**Fig. 4.1** Axial T2 MRI. The suprahyoid spaces (coloured lines left half of figure) and deep cervical fascia (white lines right half of figure). Note the central location of the parapharyngeal space (white colour and star). The carotid space is made up of all three layers of deep cervical fascia. There are two layers of prevertebral fascia and one layer of visceral fascia anterior to the prevertebral muscle. These form the boundaries of three potential spaces, the prevertebral space, the 'danger' space and the retropharyngeal space (from posterior to anterior). These spaces are not normally visible and all extend inferiorly to approximately T3. The danger space extends further inferiorly and is a conduit for infection into the mediastinum. (Reference Hamsberger. H. *Handbook of Head and Neck imaging* (Masby)).

*Applied Radiological Anatomy, 2nd Edition* ed. Paul Butler, Adam W.M. Mitchell and Jeremiah C. Healy. Published by Cambridge University Press.

The middle layer is more complex. It lies deep to the anterior strap muscles, surrounds the constrictor muscles, oesophagus and thyroid and contributes to the carotid sheath and the anterior aspect of the retropharyngeal space.

The deep layer encircles the vertebrae, paraspinal and prevertebral muscles.

## The parapharyngeal space (PPS)

The PPS is located centrally within the suprahyoid neck and is an inverted pyramid extending from the skull base to its apex at the hyoid bone (Fig. 4.2). Since it contains mainly fat it is easily identified on both CT and MR.

Lesions arising in the parapharyngeal fat space are rare but the direction of its displacement by adjacent pathology yields important clues.

The PPS is sometimes divided further into prestyloid and retrostyloid components. In this chapter we refer to the retrostyloid PPS as the carotid space and the prestyloid PPS as the parapharyngeal space proper (Fig. 4.3).

## The salivary glands

The paired parotid, submandibular and sublingual salivary glands are known as the major salivary glands. Minor salivary glands are also present throughout the whole upper aerodigestive tract and heterotopic salivary tissue has been recorded in the external auditory canal, middle ear, neck and even the mandible.

Ultrasound is usually the first-line imaging modality and for salivary masses can be combined with fine-needle aspiration cytology (FNAC). MRI is often used in a complementary

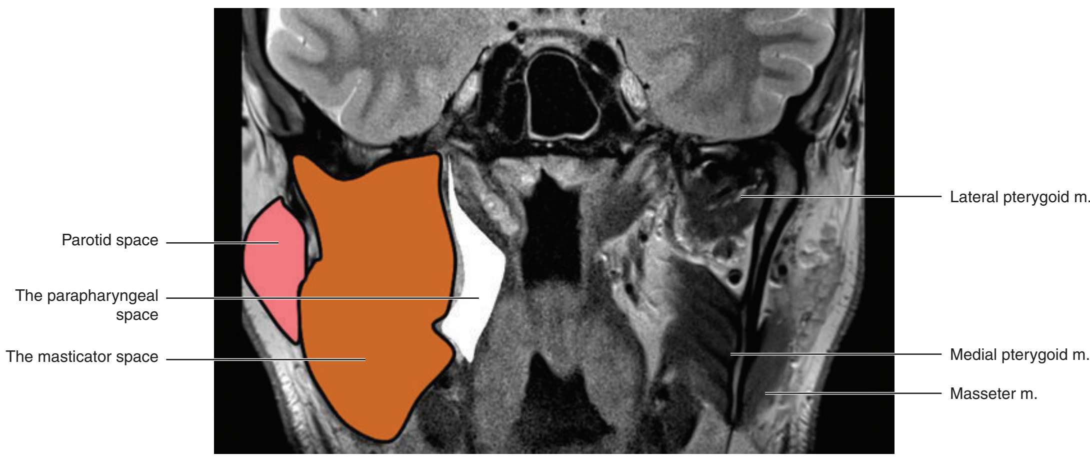


**Fig. 4.2** Coronal T2 MRI. Parapharyngeal space. The parapharyngeal space (PPS) extends from the skull base to the hyoid and opens into the posterior submandibular space (not shown). There is no fascial barrier between the PPS and the posterior submandibular space. The masticator space (MS) and parotid space (PS) are also shown.

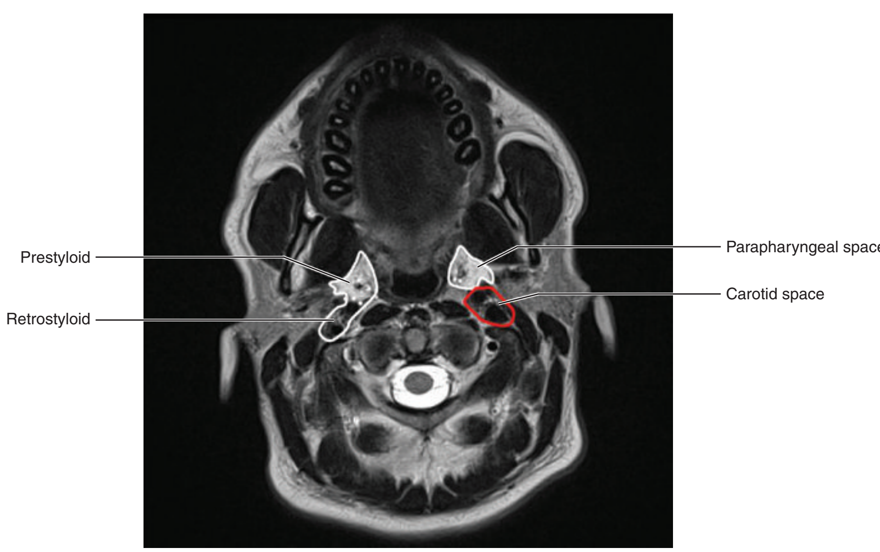


**Fig. 4.3** Axial T2 MRI. The suprahyoid neck. The carotid space is equivalent to the retrostyloid parapharyngeal space and the parapharyngeal proper is equivalent to the prestyloid parapharyngeal space.

fashion to assess the local extent of any lesion, in particular as to whether there is 'deep lobe' involvement or perineural extension. CT may be helpful in the assessment of multiple salivary calculi or acute salivary infection when there is clinical suspicion of an abscess.

MR sialography is increasingly used instead of conventional sialography, with the latter reserved for when radiological intervention such as ductal dilatation (sialoplasty or stone extraction) is being considered.

## The parotid gland

The parotid is the largest of the major salivary glands. Anteriorly it is palpable superficial to the ramus of the mandible and the posterior aspect of the masseter muscle. The posterior relations are the mastoid process and sternocleidomastoid muscle. On its deep aspect it is separated from the carotid sheath by the posterior belly of digastric muscle styloid process and styloid muscles (Fig. 4.4). The parotid extends from the level of the external auditory canal inferiorly to the angle of the mandible.

The gland is encapsulated by the superficial layer of cervical fascia (forming the parotid space) and is described as having superficial and deep 'lobes' separated by the facial nerve. More correctly the parotid is superficial when it is external to the mandible and retromandibular when it is deep to the mandible. The larger superficial component lies on the masseter, with the deeper component extending between the styloid process and posterior ramus of the mandible. Indeed a radiological sign of tumours arising from the deep parotid is widening of the stylomandibular 'notch'.

The facial nerve can be identified in the stylomastoid foramen as it exits the skull base on both CT and MRI because it is surrounded by a 'cuff' of fatty tissue (Fig. 4.5). Its extracranial course follows the lateral aspect of the posterior belly of digastric muscle before entering the posterior parotid, where it divides into five main branches (temporal, zygomatic, buccal, mandibular and cervical) that pass lateral to the retromandibular vein and exit the anterior aspect to supply the muscles of facial expression. The facial nerve can sometimes be visualized within the posterior parotid on MRI before it has divided.

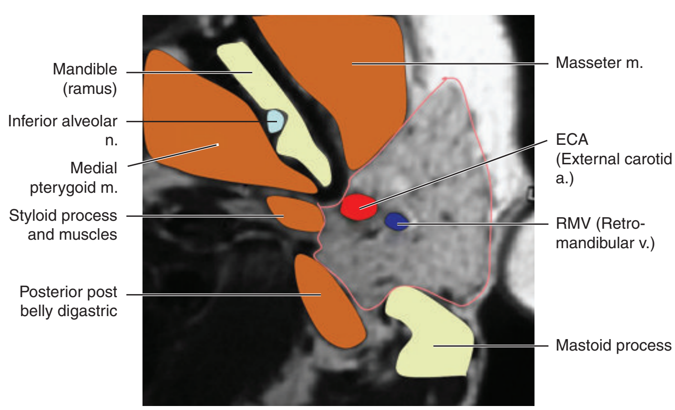


**Fig. 4.4** Axial T1 MRI. The relations of the parotid gland (outlined) to the surrounding structures. ECA = external carotid artery; RMV = retromandibular vein.

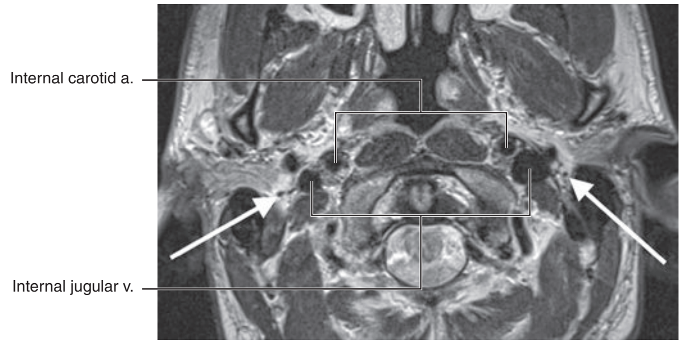


**Fig. 4.5** Axial T2 MRI. At level of stylomastoid foramen. The facial nerve (arrow) shown surrounded by a cuff of fat is easily visible at the stylomastoid foramen. This is a review area when assessing patients with parotid malignancy and/or facial nerve palsy.

One method of mapping the course of the facial nerve is to mark a line between the lateral surface of the posterior belly of digastric muscle and the lateral surface of the ramus of the mandible (Fig. 4.6).

The parotid duct is around 7 cm long and emerges from the anterior parotid superficial to the masseter muscle, then turns 90° to pierce the buccinator muscle to open into the oral cavity at the level of the second upper molar (Figs. 4.6, 4.7). Accessory parotid tissue anterior and separate from the parotid is present in 20% of people and is found along the course of the duct up to the cheek and can be mistaken for a mass.

## The submandibular gland

The submandibular gland has superficial and deep parts that connect around the posterior border of the mylohyoid muscle (Fig. 4.8a,b). The palpable and larger superficial part located between the mandible and external surface of the mylohyoid muscle is the main component of the submandibular space. The smaller deeper part is superior to the mylohyoid muscle and palpable intraorally.

The mandibular branch of the facial nerve is a superficial relation to the gland and therefore the surgical approach is usually made more inferiorly to avoid any damage.

The tortuous facial artery passes from the posterior to the superior aspect of the gland, which it indents, then extends inferiorly onto the deep and inferior aspects of the mandible before passing superiorly on the lateral surface, where it is palpable, and associated with a facial node, to supply the face.

The main duct emerges anteriorly from the gland where it angles sharply around the posterior border of the mylohyoid muscle and it is at this site where approximately a third of calculi are found. It then passes anteriorly between the mylohyoid and hyoglossus muscles along with the lingual vein and nerve and the hypoglossal nerve before opening at the sublingual papilla in the anterior floor of mouth (Figs. 4.8, 4.9). The submandibular gland is separated from the anterior parotid only by the stylomandibular ligament.

Lesions arising from the tail of parotid lesions can therefore mistakenly be thought to arise from the submandibular gland.

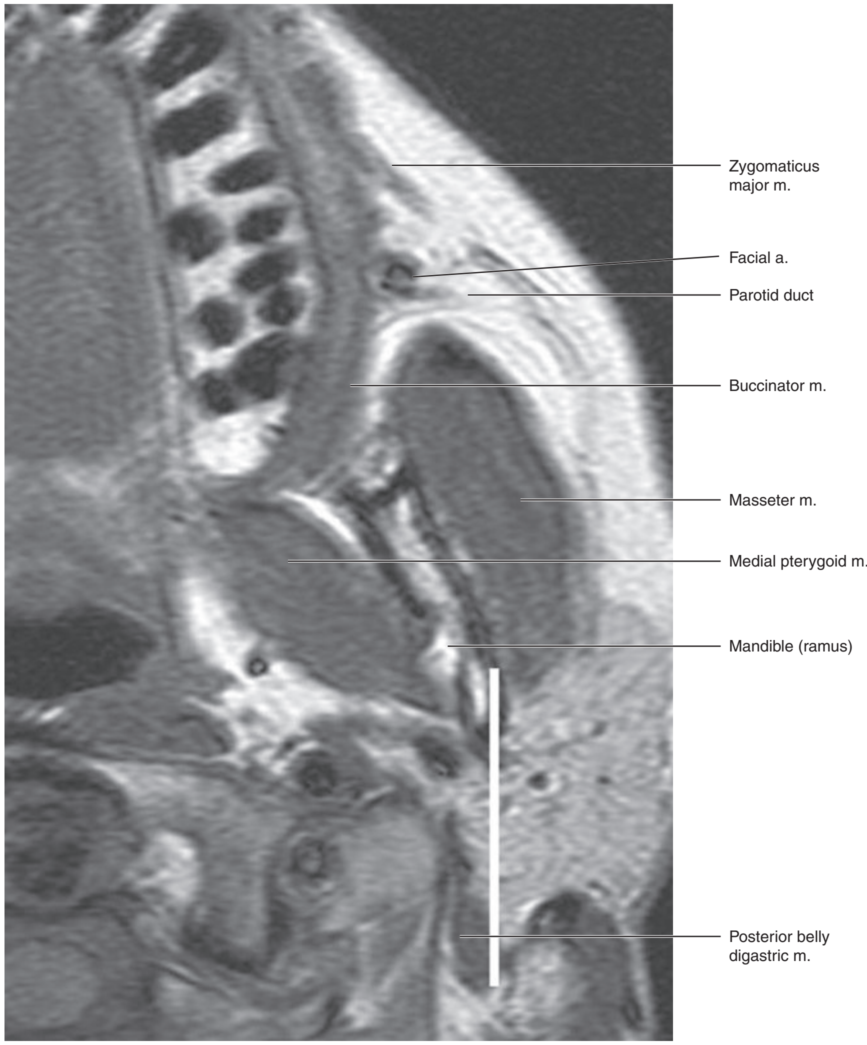


**Fig. 4.6** Axial T1 MRI. Left parotid gland and cheek. The white line between the lateral surface of the posterior belly of digastric muscle and lateral surface of the ramus of the mandible is a method to identify the course of the intraparotid facial nerve. The nerve divides the superficial and deep lobes of the parotid gland.

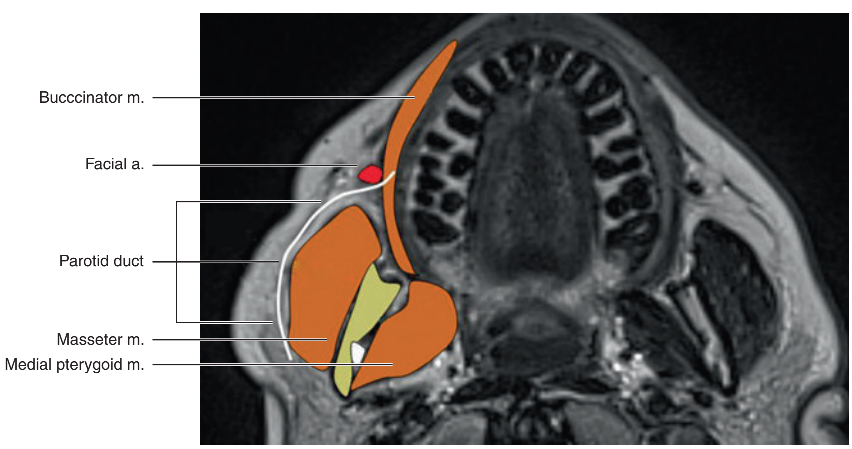


**Fig. 4.7** Axial T2 MRI. The relations of the parotid duct (white line). Note the duct pierces the buccinator muscle to open into the cheek at the level of the upper second molar.

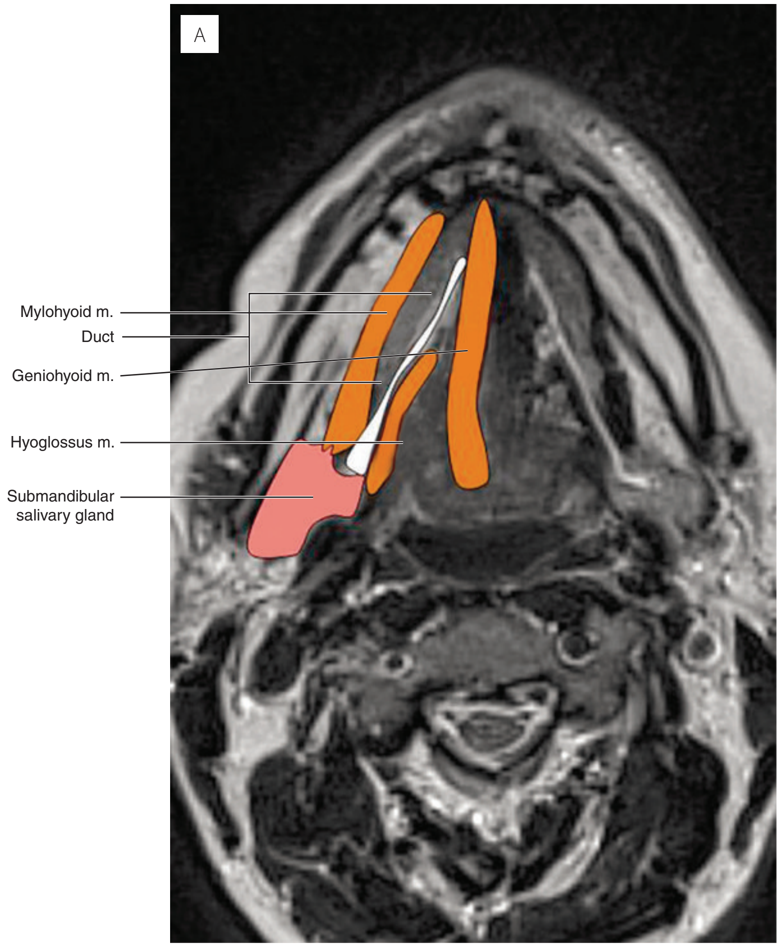


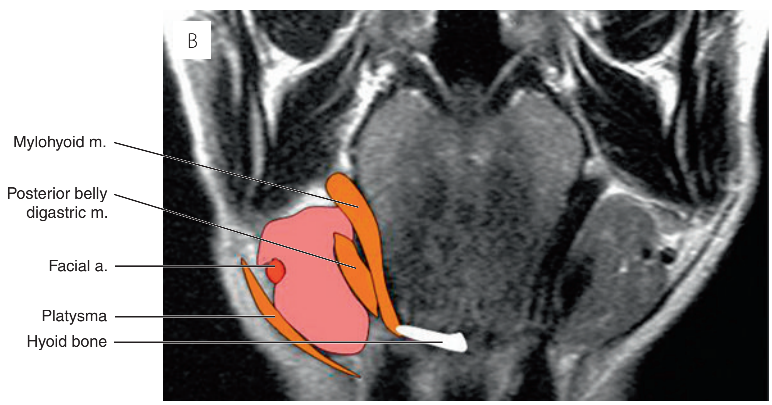


**Fig. 4.8** Axial (A) and coronal (B) T2 MRI. The course and relations of the submandibular duct and submandibular salivary gland (SMG).

## The sublingual gland

The almond-shaped sublingual gland is the smallest of the major salivary glands and lies deep to the anterior floor of mouth mucosa, superior to the mylohoid muscle. It lies on the sublingual groove of the mandible, with the distal submandibular duct separating it from the more medial genioglossus muscle (Fig. 4.10a,b).

## The pharynx

The pharynx is a midline fibromuscular tube extending from the skull base to the lower border of the cricoid cartilage, where it is continuous with the cervical oesophagus. It is divided into the nasopharynx, oropharynx and hypopharynx (Fig. 4.11).

The muscular layer is made up of the three constrictors and the palato- and stylopharyngeus muscles.

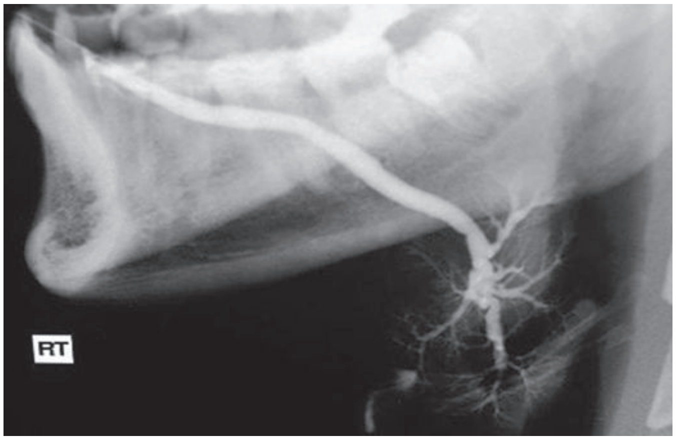


**Fig. 4.9** Right submandibular sialogram. Note mild intraglandular sialectasis.

## Nasopharynx

The nasopharynx acts as a conduit for air and secretions from the nasal cavity.

The anterior limit of the nasopharynx is the nasal choanae; the sloping roof is formed by the central skull base (body of sphenoid and clivus), which slopes down to become the posterior wall overlying the anterior arch of the atlas and the atlanto-axial joint and lateral to this the prevertebral muscles.

The division between the nasopharynx and oropharynx is the hard and soft palate at approximately the C1/2 level. The lateral wall is composed of the cartilaginous Eustachian tube (torus tubarius), with the eustachian tube orifice seen just anterior and the lateral pharyngeal recess or fossa of Rosenmuller just posterior to it. Two muscles that affect the function of the Eustachian tube are the tensor and veli palatini muscles (Fig. 4.12).

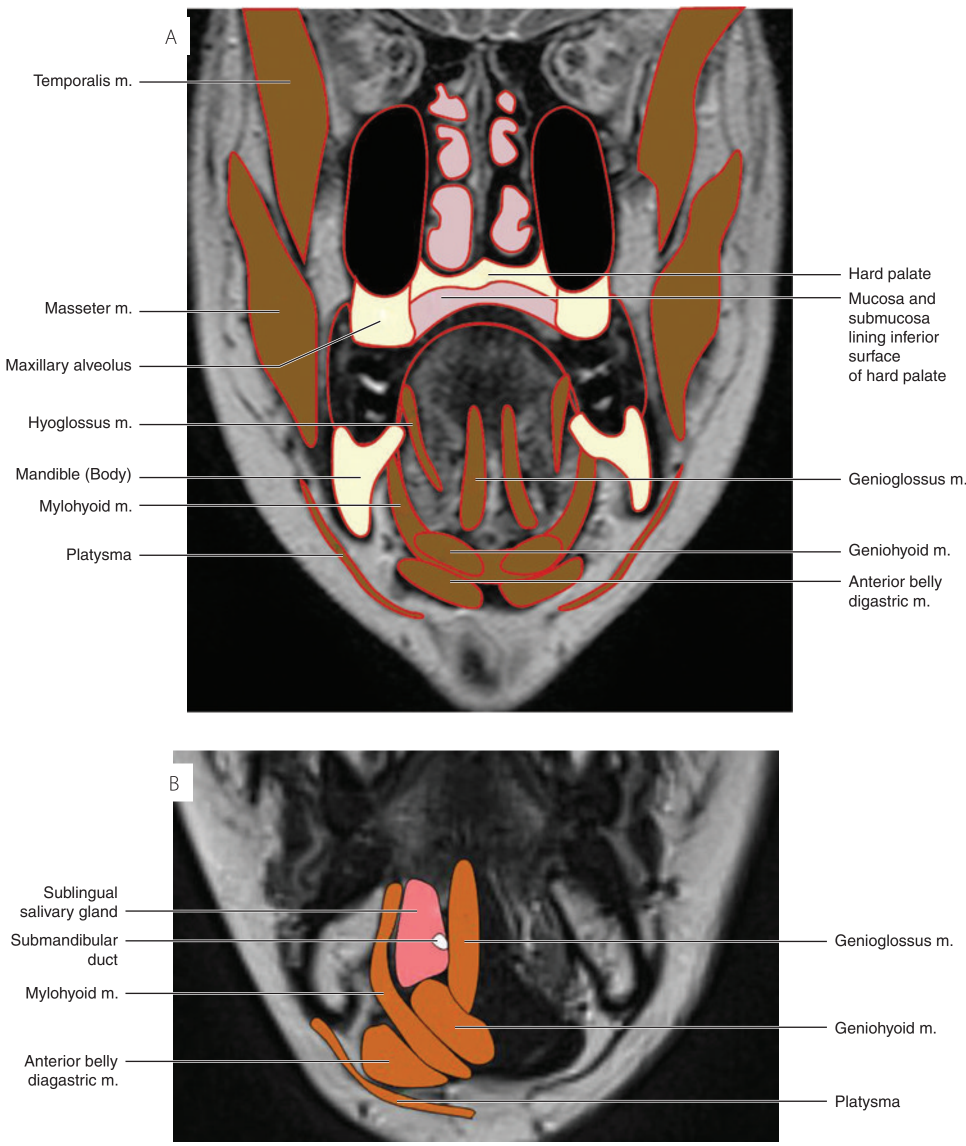


**Fig. 4.10** Coronal images through floor of mouth demonstrating the relation of the sublingual salivary gland to the submandibular duct and adjacent muscles. (A) is posterior to (B).

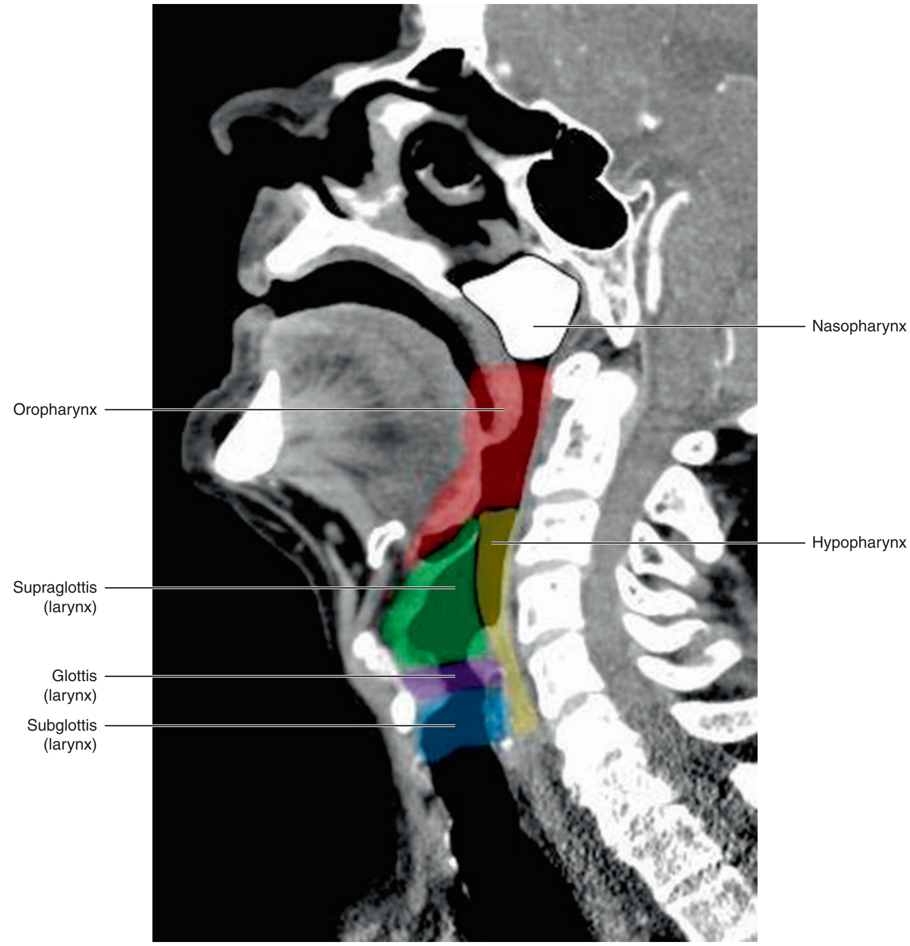


**Fig. 4.11** Sagittal CT. The divisions of the pharynx and larynx.

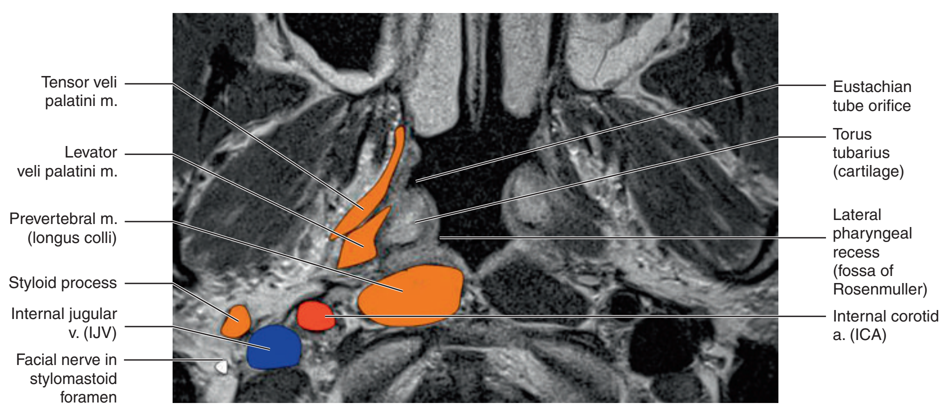


**Fig. 4.12** Axial T2 MRI. The nasopharynx.

The fossa of Rosenmuller is difficult to examine clinically but is the commonest site of origin of nasopharyngeal carcinomas. Nasopharyngeal carcinoma may extend intracranially by eroding the fibrocartilage covering the foramen lacerum and gain access to the intrapetrous internal carotid and cavernous sinus but more commonly tumour extends laterally through the pharyngobasilar fascia into the parapharyngeal and then masticator spaces and from there via the mandibular division of the trigeminal (fifth cranial) nerve (V3) gains access to the middle cranial fossa via the foramen ovale (Fig. 4.13).

## Oropharynx

The oropharynx extends from the inferior surface of the soft palate superiorly to the valleculae inferiorly and includes the tongue base (largely comprising the lingual tonsils), anterior


**Fig. 4.13** Coronal T2 MRI. The nasopharynx.

and posterior tonsillar pillars, faucial tonsils, soft palate and part of the superior and middle constrictors deep to the oropharyngeal mucosa (Figs. 4.11, 4.14). The boundaries of the valleculae are medially the midline glosso-epiglottic fold, anteriorly the tongue base, laterally the pharyngo-epiglottic folds and posteriorly the pharyngeal surface of the suprahyoid epiglottis.

The anterior and posterior tonsillar pillars are both mucosal folds overlying muscles (palatoglossus and palatopharyngeus, respectively) that merge superiorly into the soft palate. The anterior tonsil and anterior tonsillar pillar is the commonest site of oropharyngeal cancer, which may then spread to the glossotonsillar sulcus and tongue base anteriorly and the soft palate superiorly (Fig. 4.15a,b).

## Hypopharynx

The hypopharynx extends from the oropharynx to the cervical oesophagus posterior to the larynx and includes mucosa, minor salivary glands and the inferior constrictor muscle. The latter consists of two parts, the more superior obliquely oriented thyropharyngeus and the horizontal more inferior cricopharyngeus; between the two is a potential weak area through which a pharyngeal pouch may form

The hypopharynx consists of three subsites: laterally the paired pyriform sinuses, in the shape of upturned cones, with the (pyriform) apex inferiorly at the level of the true cords, anteriorly the postcricoid region and posteriorly the posterior hypopharyngeal wall.

The boundaries of the pyriform sinus are laterally the posterior thyroid lamina, posteriorly the lateral aspect of the posterior pharyngeal wall and anteromedially the aryepiglottic fold, which separates it from the larynx (Fig. 4.16). On imaging, the pyriform sinuses are often collapsed but distend when the patient performs a valsalva manoeuvre.

## Larynx

The larynx is divided radiologically into the supraglottis, glottis and subglottis (Fig. 4.11).

The supraglottis extends from the tip of the epiglottis to just superior to the true cords.

The subglottis extends from the inferior surface of the true cords to the inferior aspect of the cricoid cartilage.

The larynx has a cartilaginous skeleton consisting of the cricoid, thyroid and arytenoid cartilages and the covering epiglottis.

The cricoid ring supports the larynx and consists of a cricoid arch and a larger cricoid lamina that faces posteriorly.

The thyroid cartilage protects the larynx and comprises two laminae that meet anteriorly and posterior extensions called

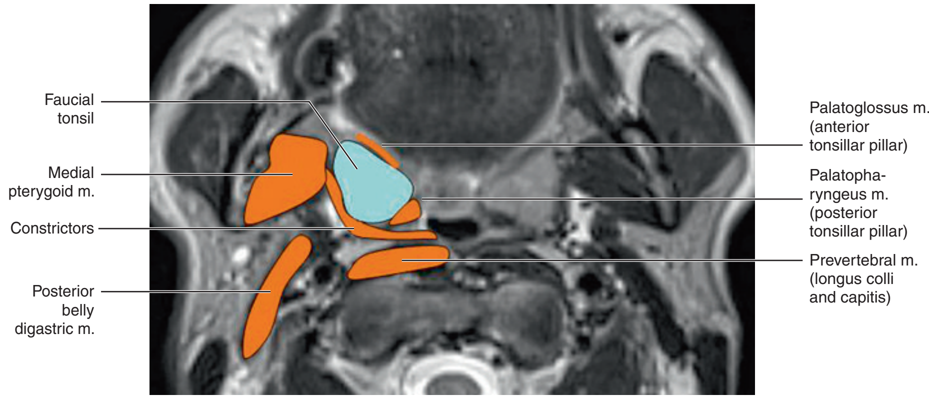


**Fig. 4.14** Axial T2 MRI. The oropharynx.

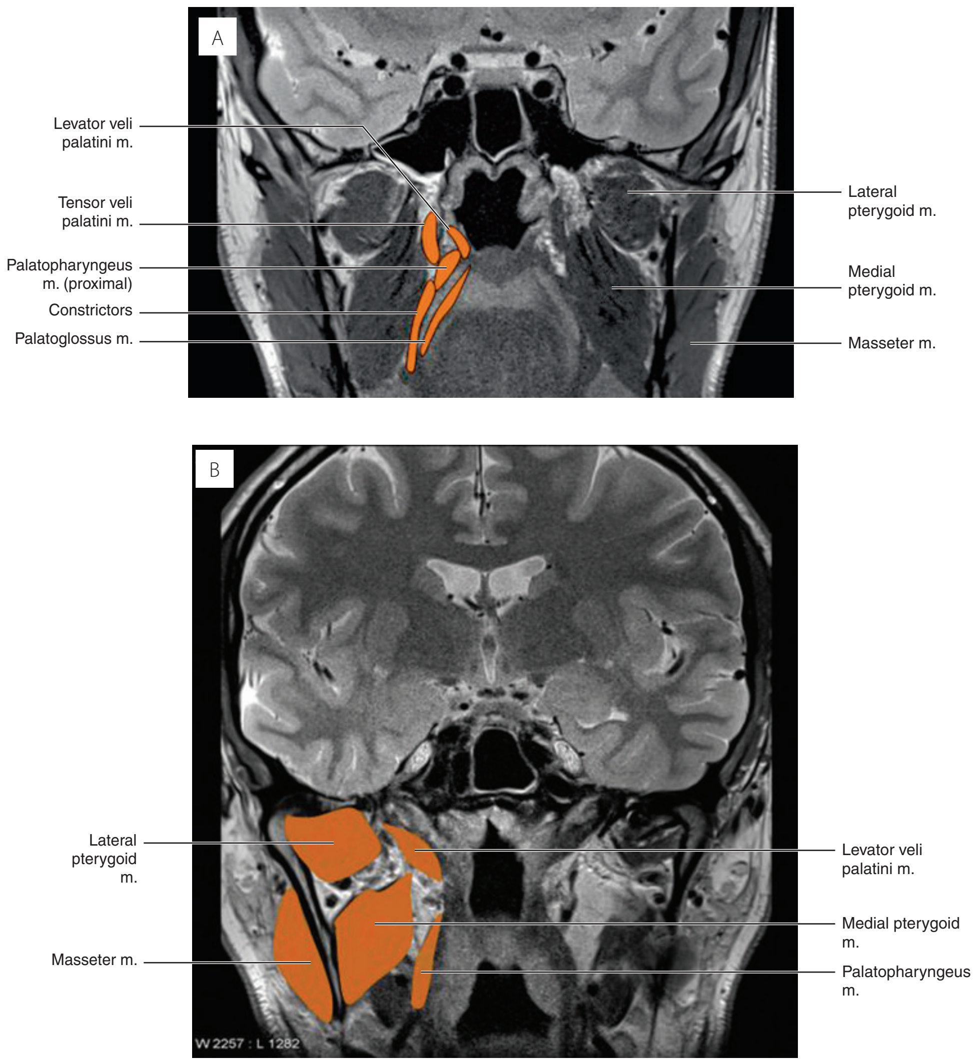


**Fig. 4.15** Coronal T2 MRI. The oropharynx. (A) At the level of the anterior tonsillar pillar (palatoglossus muscle with overlying mucosa). (B) At the level of the posterior tonsillar pillar (palatopharyngeus muscle with overlying mucosa).

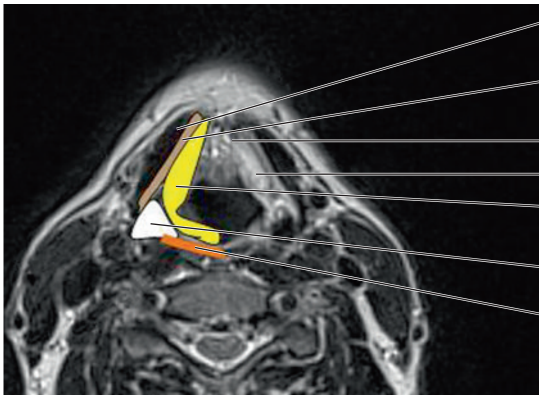


**Fig. 4.16** Axial T2 MRI at the level of the supraglottic larynx and pyriform sinus.

inferior and superior cornua. The inferior cornua articulates with the lateral cricoid at the cricothyroid joint.

The arytenoid cartilages are pyramidal in shape, sit on top of the cricoid lamina and consist of anterior vocal processes to which the posterior vocal cord is attached, a superior process and a larger posterolateral muscular process (Figs. 4.16, 4.17a,b).

The epiglottis protects the larynx and is made of flexible fibrocartilage. On both sides aryepiglottic folds extend from the lateral surface of the epiglottis and attach posteriorly to the superior process of the arytenoid. The inferior margin of the aryepiglottic fold is free and the mucosal surface of the aryepiglottic folds forms the false cords.

The laryngeal ventricle is between the inferior free margin of the false cords and the true cords.

The laryngeal vestibule is the air space within the supraglottic larynx.

The pre-epiglottic and paraglottic fat spaces are two readily identifiable, connected regions within the supraglottic larynx between the mucosa and cartlilage (Fig. 4.16).

## The retropharyngeal space

The retropharyngeal space is a potential space between the middle and deep layers of cervical fascia, extending from the skull base to T4. It provides a potential route of spread of infection to the mediastinum.

Retropharyngeal nodes are seen only in the suprahyoid neck and must be assessed in patients with naso- and oropharyngeal pathology.

## The mandible and masticator space

Each half of the mandible consists of a vertical ascending ramus and a horizontal body, the two joining posteriorly at the mandibular angle, with each body fusing anteriorly at the mental symphysis.

The posterior ramus extends superiorly to become the condylar neck and head and the anterior ramus the coronoid process, the two separated by the sigmoid notch.

The tooth-bearing area or mandibular alveolus opposes the maxillary alveolus above. The mandibular foramen, which contains the inferior alveolar nerve (a branch of the mandibular division of the trigeminal nerve) and the inferior alveolar vessels, opens onto the lingual surface of the ramus and exits anteriorly as the mental branch on the buccal surface at the mental foramen.

The muscles of mastication insert onto the mandible:

- the lateral pterygoid onto the medial mandibular condyle
- the medial pterygoid on the inner surface of the angle
- the temporalis onto the coronoid process and ramus
- the masseter onto the outer surface of the coronoid process ramus and angle (Figs. 4.7, 4.18).

The mandible and surrounding muscles of mastication are invested by the superficial layer of deep cervical fascia to form the masticator space, which contains the mandibular division of the trigeminal nerve (Fig. 4.1a,b). The commonest pathology arising from this space is dental infection. Squamous cell carcinoma arising from the mucosa overlying the mandible may extend proximally along the inferior alveolar nerve and from there via the more proximal mandibular division intracranially (Fig. 4.13).

## Infratemporal fossa

The infratemporal fossa is the area between the pterygopalatine fossa medially and the zygomatic arch laterally and is part of the masticator space and is therefore also called the nasopharyngeal masticator space. It communicates superiorly with the temporal fossa between the zygomatic arch and lateral skull vault, which is thus also known as the suprazygomatic masticator space.

Other muscles that are attached to the mandible are the mylohyoid muscle on the oblique mylohyoid line on the lingual surface of the body, the geniohyoid and genioglossus muscles on the genial tubercles on the inner surface of the mentum and the anterior belly of digastric muscles from fossae either side of the lingual surface of the mentum (Fig. 4.10).

## Teeth

There are two sets of dentition, deciduous and permanent.

The 20 deciduous teeth with the central incisors appear first at approximately 6 months, the remainder appearing up to 3 years of age.

The deciduous teeth are made up of two incisors, one canine and two molars in each quadrant. The first deciduous teeth to be replaced are the incisors, followed by the molars and lastly the canines.

The 32 permanent teeth are made up of two incisors, one canine, two premolars and three molars in each quadrant. The first molar tooth is the first permanent tooth to erupt at about 6 years with the remainder appearing up to 21 years of age (Fig. 4.19).

## Temporomandibular joint (TMJ)

The condyle of the mandible lies within the mandibular (or glenoid) fossa of the temporal bone. Both are covered by a layer of fibrous tissue and separated by a biconcave fibrous disc. The posterior wall of the glenoid fossa is also the anterior wall of the bony external auditory canal. The bony prominence anterior to the glenoid fossa is the articular eminence (or tubercle).

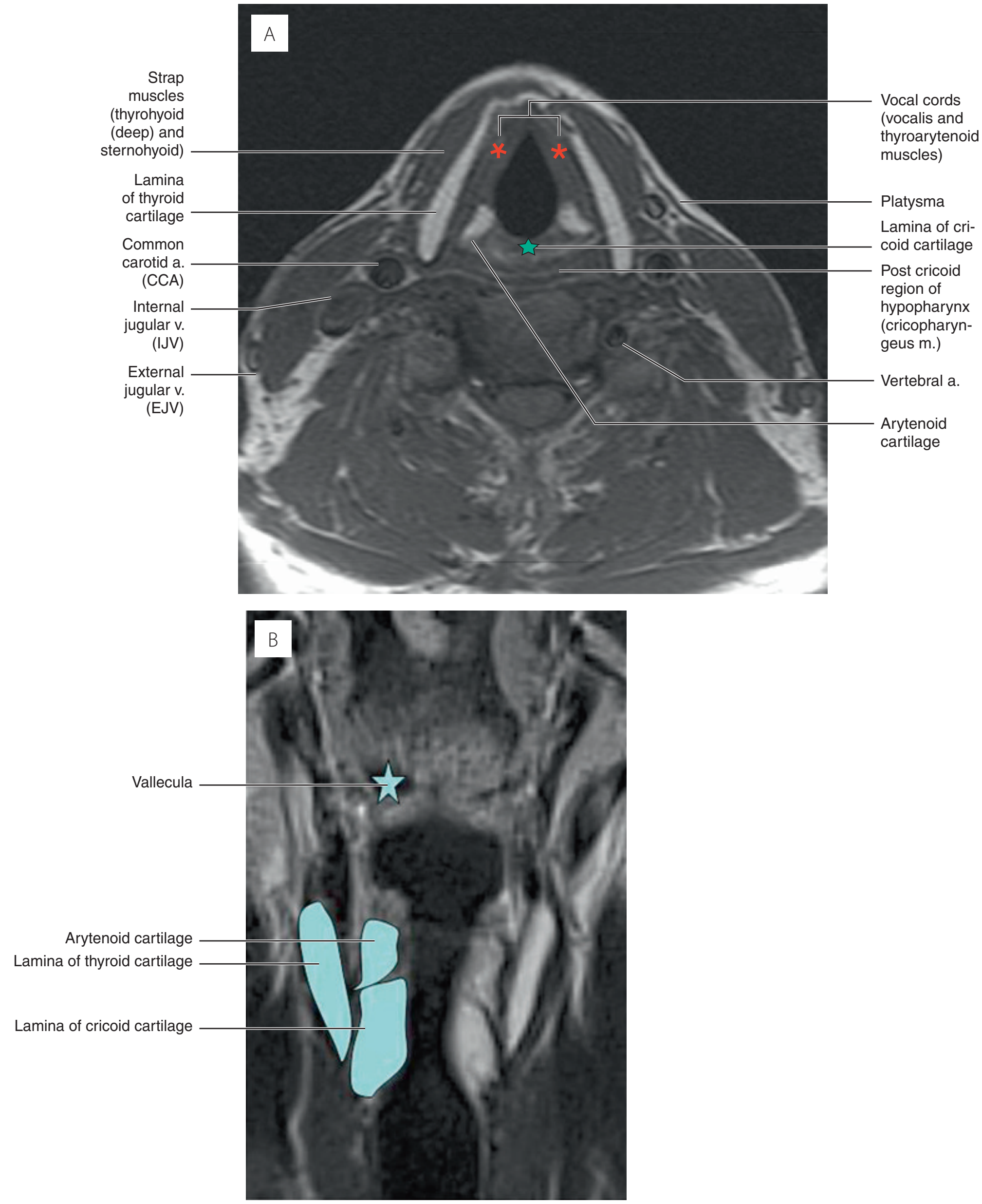


**Fig. 4.17** The larynx. (A) Axial T1 MRI at the level of the vocal cords. (B) Coronal T2 MRI.

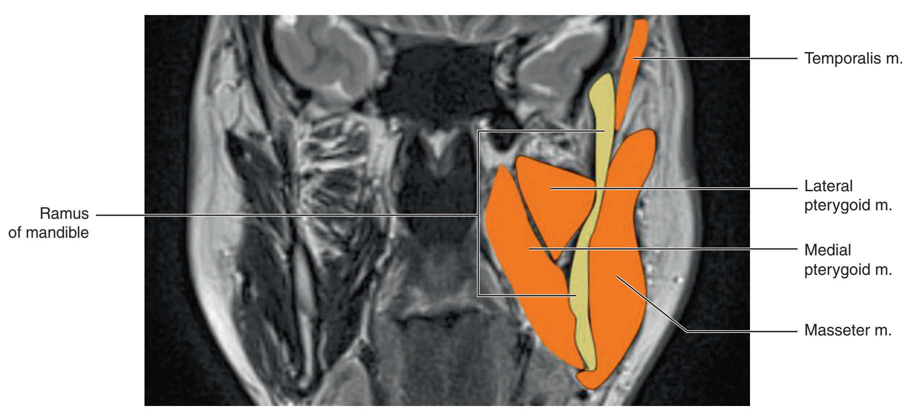


**Fig. 4.18** Coronal T2 MRI. The masticator space and ramus of mandible.

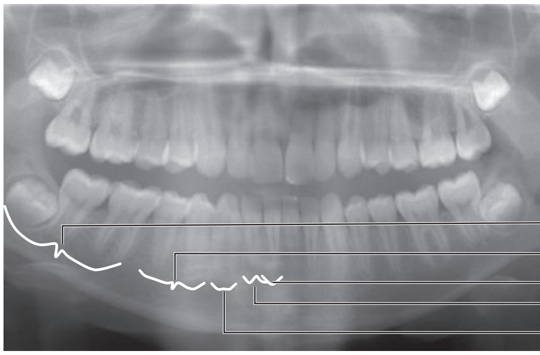


**Fig. 4.19** Orthopantomogram (OPG).

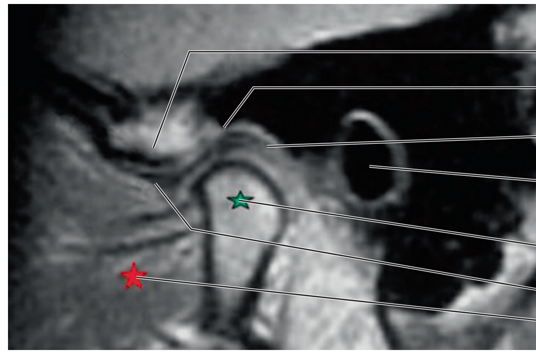


**Fig. 4.20** Sagittal oblique 'proton density' MRI. The temporomandibular joint.

The thicker margins of the disc are called the anterior and posterior bands, with the posterior band located superior to the condyle and the thinner central portion between the condyle and articular eminence (Fig. 4.20). The disc divides the joint into two separate compartments and is attached medially and laterally to both the joint capsule and condyle. The posterior disc attaches to the condyle and temporal bone by retrodiscal soft tissue called the bilaminar zone that allows forward translational movement.

Both rotation and translational movement occur in the TMJ. Rotational movement occurs between the condyle and inferior aspect of the disc whereas translational movement takes place between the glenoid fossa and superior surface of the disc.

MR in the sagittal oblique plane performed in the mouth in closed and open positions and supplemented by a coronal sequence clearly shows the dynamic relationship of the disc to the condyle. CT is useful in trauma or when a biomodel joint replacement is being considered.

## The cervical arteries and venous drainage of the neck

### Arterial supply

In the majority of individuals, the right common carotid artery (CCA) arises from the brachiocephalic artery just posterior to the right sternoclavicular joint, whereas the left CCA arises from the aortic arch. Both carotid arteries are encased within a dense sheath that is composed of all three layers of deep cervical fascia which extends to the skull base (Fig. 4.1).

This sheath of fascia forms the carotid space, which also contains the internal jugular vein (IJV), lateral to the CCA but posterolateral to the internal carotid artery (ICA) (Fig. 4.5).

The carotid space also contains the following cranial nerves, from the skull base to approximately the C1–2 level: the glossopharyngeal, vagus, accessory and hypoglossal nerves (IX–XII). Only the vagus (Xth cranial) nerve continues in the infrahyoid carotid space between the posterior aspect of both CCA and IJV and can be clearly seen on US (Fig. 4.21). A sympathetic plexus and cervical nodes are also found within the carotid space.

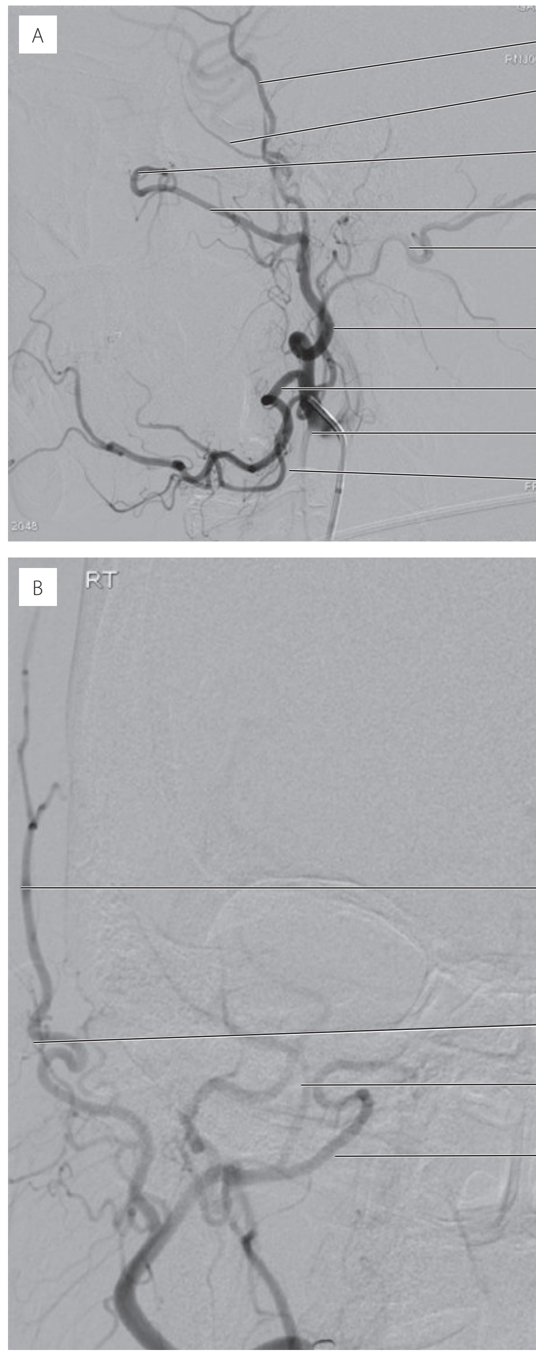


**Fig. 4.21** The external carotid artery and its major branches. (A) Lateral and (B) frontal projections.

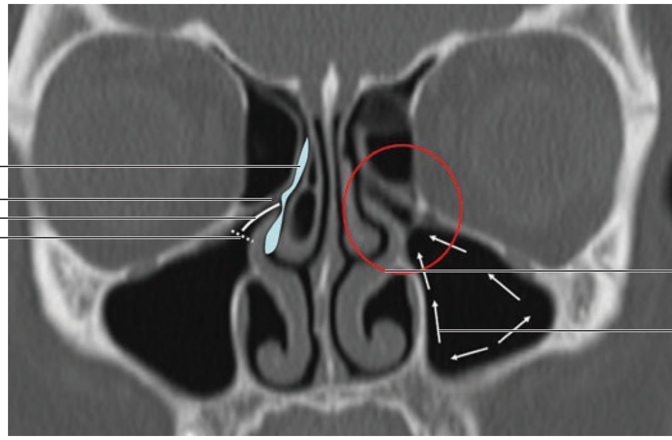


**Fig. 4.22** Coronal CT. The ostiomeatal unit.

The bifurcation of the CCA into internal and external branches (ICA and ECA) occurs at the level of C4 (hyoid bone) and both can be used as a marker of the junction of upper and mid deep cervical nodal levels. The smaller ECA courses anteromedial to the ICA.

The ECA supplies the face, scalp, dura and upper cervical organs (Fig. 4.21a,b). There are many and variable anastomoses between the individual branches of the ECA, and the branches of the ECA and ICA and ECA and vertebral artery.

The vertebral artery is the first branch of the subclavian and passes through the foramina transversarium of the upper six cervical vertebrae. Between the foramina of the atlas and axis it has a posterior convexity (which allows for rotational movement) before entering the skull via the foramen magnum.

## Venous drainage

The internal jugular vein (IJV) emerges from the jugular foramen posterior to the ICA and receives the inferior petrosal sinus just inferior to the skull base. It joins the subclavian vein to form the brachiocephalic at the level of the sternoclavicular joints. It receives a variable number of tributaries in its course.

The internal jugular veins are commonly asymmetrical in size, usually right larger than left (as are therefore the jugular foramen). This asymmetry should not be mistaken as pathological.

The anterior face drains via the facial veins which communicate via the ophthalmic veins with the cavernous sinus. Orbital infection can therefore lead to ophthalmic vein and then cavernous sinus thrombosis.

The cavernous sinus drains externally via the pterygoid venous plexus into the retromandibular vein within the parotid, which is joined by the posterior auricular vein to form the external jugular vein, which in turn drains into the subclavian vein just above the clavicle.

There are variable anterior jugular veins (usually one either side of the midline) that drain just above the sternum into subclavian or external jugular veins.

## The paranasal sinuses and nasal cavity

The anatomy of this region is best assessed by CT acquired axially with multiplanar reformatted images (MFR) in the coronal and sagittal planes.

CT is performed prior to functional endoscopic sinus surgery (FESS) whose aim is to restore the normal drainage pathways. The radiologist must therefore understand the anatomy of the mucociliary drainage pathways, notably the ostiomeatal unit and the sphenoethmoidal recess, and the clinically relevant anatomical variations commonly found in this region.

## The ostiomeatal unit

The ostiomeatal unit (OMU) drains the frontal, anterior ethmoidal and maxillary sinuses.

The OMU is sited in the area of the superomedial maxillary sinus and middle meatus and includes the maxillary sinus ostium, ethmoid infundibulum, hiatus semilunaris, and frontal recess and is best demonstrated on coronal CT. The coordinated action of the cilia clears mucus towards the ostia (Fig. 4.22).

## The frontal sinus and frontal recess

The frontal sinuses are asymmetrical extensions from the anterior ethmoidal air cells between the tables of the frontal bones. They are the last paranasal sinus to aerate and are not fully developed until just after puberty. Aplasia or lack of any extension into the frontal bone is present in between 5 and 8% of people and hypoplasia in 4%.

The frontal sinus drainage pathway is via the frontal recess, which is the shape of an inverted funnel, measures approximately 13 mm long and is formed by the walls of the adjacent air cells, hence the term 'recess' rather than 'duct'.

The frontal recess has an oblique course 50° to the orbitomeatal plane and is therefore best demonstrated on the sagittal reconstructed images (Fig. 4.23).

The usual boundaries of the frontal recess are posteriorly the ethmoidal bulla, anteriorly and inferiorly the agger nasi air cell, medially the olfactory fossa and middle turbinate, laterally the lamina papyracea and superiorly the roof of the anterior ethmoidal air cells (fovea ethmoidalis) (Fig. 4.24).

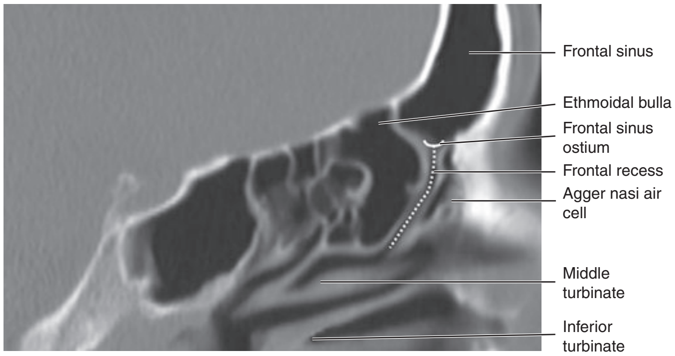


**Fig. 4.23** Sagittal CT. The frontal recess.

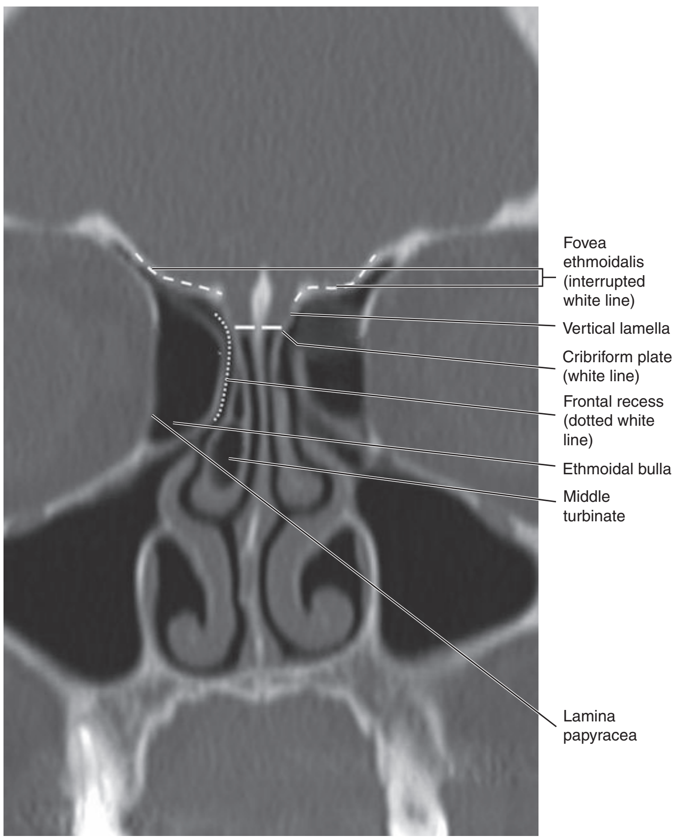


**Fig. 4.24** Coronal CT through frontal recess and anterior cranial fossa (ACF).

The frontal recess anatomy, however, is complex due to the variable accessory air cells that may form part of its boundaries, and drains either into the ethmoid infundibulum or middle meatus depending on the superior attachment of the uncinate process.

These frontal region accessory air cells are as follows.

- The agger nasi air cell (ANC) is the most anterior of the ethmoidal air cells and may vary in size. If large it can displace the frontal recess posteriorly and narrow the ostium.
- The frontoethmoidal air cells are variably classified depending on their number and extent. They are located superior to the ANC and extend into the frontal sinus (Fig. 4.25).
- The frontal bulla cell is an extension of the ethmoidal bulla into the frontal region. The suprabulla air cell is an air cell just superior and anterior to the ethmoidal bulla and the supraorbital air cell usually arises from the anterior ethmoidal air cell and extends into the orbital plate of the frontal bone.

When assessing the frontal sinus and recess region the priority must be first to identify the frontal drainage pathway and to then clearly describe the site of origin, size and relationship of the adjacent air cells forming the frontal recess.

## The maxillary sinus

The maxillary sinus or antrum is the first aerated sinus to form and may be hypoplastic in up to 10% of people. The roof forms the orbital floor in which runs the infraorbital canal and the floor is formed by the maxillary alveolus. The medial wall also forms the lateral wall of the nasal cavity. The main ostium arises in the superior aspect of the medial wall and opens into the ethmoid (maxillary) infundibulum, which is a narrow channel between the uncinate process inferiorly and the lamina papyracea and ethmoidal bulla superiorly. The infundibulum opens into the hiatus semilunaris (Fig. 4.22).

The anatomical variants of the maxillary sinus are sinus septations, accessory sinus ostia and sinus hypoplasia.

The maxillary sinus septum may be fibrous or bony and often extends from the infraorbital canal to the lateral wall. The accessory ostium is seen posterior to the natural ostium and is present in approximately 10% of the population (Fig. 4.26). There may

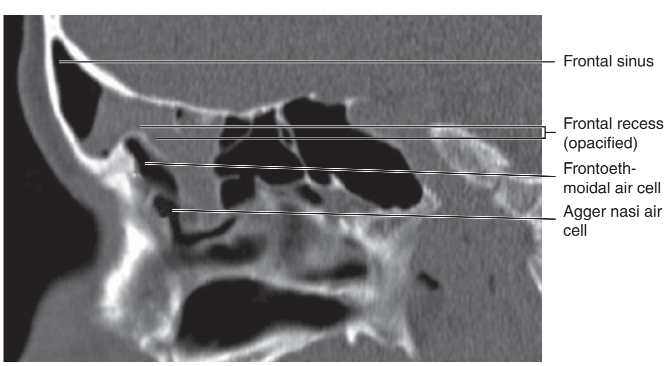


**Fig. 4.25** Sagittal CT. The frontal ethmoidal air cells.

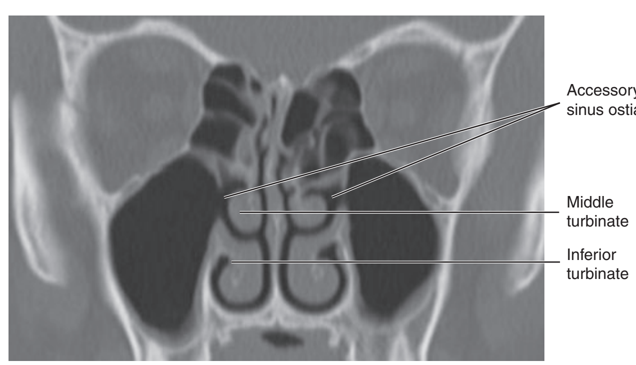


**Fig. 4.26** Coronal CT. Bilateral accessory sinus ostia.

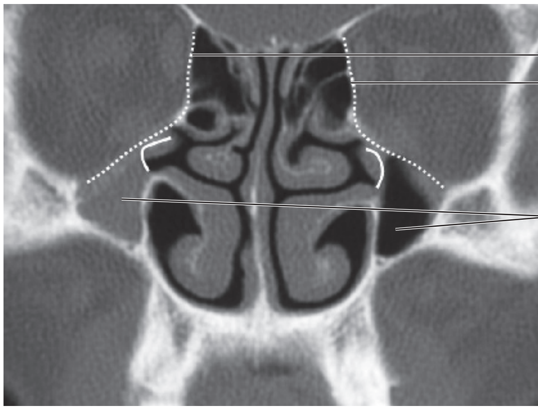


**Fig. 4.27** Coronal CT. Hypoplastic maxillary antra. Note the bilateral atelectatic uncinate processes (continuous white line) with secondary hypoplastic maxillary antra. Dotted white line = medial wall and floor of orbits.

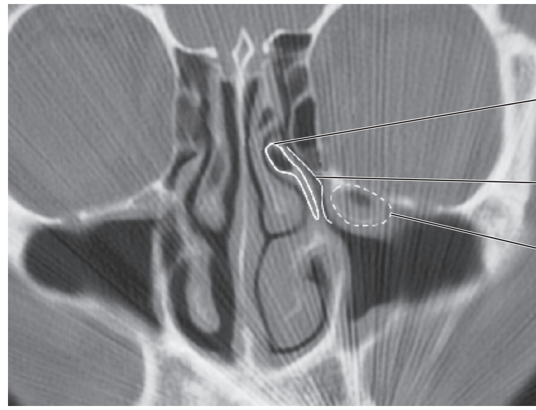


**Fig. 4.28** Coronal CT through outflow of left antrum.


**Fig. 4.29** Axial CT. The relations of the sphenoethmoidal recess (coloured red).

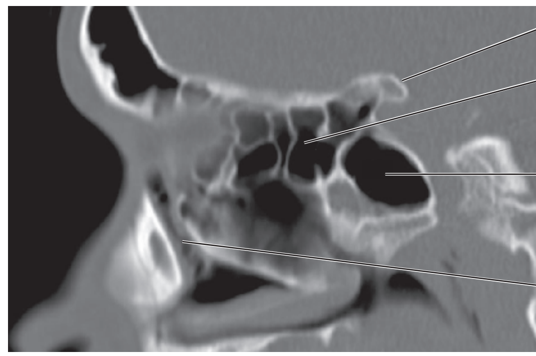


**Fig. 4.30** Sagittal CT. The sphenoethmoidal region.

be circular flow of mucus from the natural ostium inferiorly into the accessory ostium, leading to recurrent sinusitis.

Maxillary sinus hypoplasia may be seen in association with an atelectatic uncinate process (Fig. 4.27) or following surgery, in particular the Caldwell-Luc approach.

Infraorbital (Haller) air cells are centred inferior to the ethmoidal bulla, extend along the orbital floor and may compromise the outflow (Fig. 4.28).

## The sphenoethmoidal region

The sphenoid sinus develops in the body of the sphenoid and drains via a sinus ostium in the medial aspect of the anterior wall into the sphenoethmoidal recess (Fig. 4.29).

The adjacent posterior ethmoidal air cells drain via individual ostia into the superior meatus. The degree of pneumatization of the sphenoid is highly variable and may extend into the greater and lesser wings of the sphenoid and pterygoid processes. This variable pneumatization needs to be carefully assessed prior to endoscopic transsphenoidal surgery.

The posterior ethmoidal air cells may extend above the sphenoid sinus (sphenoethmoidal air cells), displacing the sinus inferiorly (Fig. 4.30). The surgeon needs to be informed of this variable anatomy prior to endoscopic surgery.

There are also a number of important structures, closely related to the sphenoid sinus, which may project into the sinus and which may have a dehiscent bony covering. These are the optic nerve, the maxillary nerve, the vidian canal and the intracavernous segment of the internal carotid artery (Fig. 4.31).

## The nasal cavity

The nasal cavity extends from the palate to the skull base, is divided by the nasal septum and opens posteriorly via the choanae into the nasopharynx and anteriorly via the piriform aperture into the nares or nostrils.

The nasal septum comprises the septal cartilage anteriorly and the perpendicular plate of the ethmoid and the vomer posteriorly (Fig. 4.32). Nasal septal spurs and septal deviation are common.

## Pterygopalatine fossa

The pterygoplatatine fossa (PPF) is an elongated space, wider superiorly and located between the vertical plate of the palatine

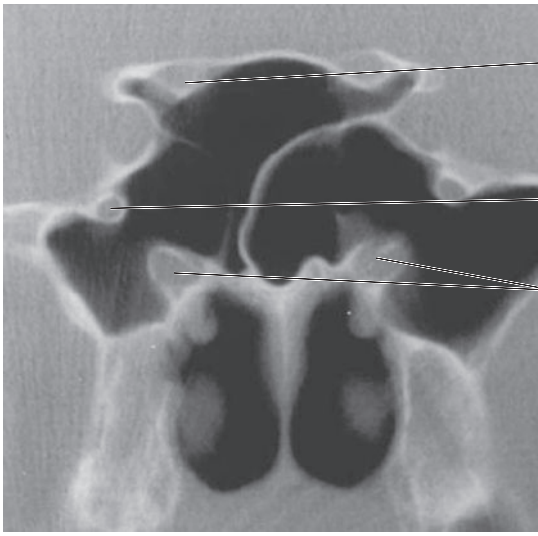


**Fig. 4.31** Coronal CT. The sphenoid sinus. Note the important structures that are intimately associated with the sinus and at risk during endoscopic surgery.

bone (which is fused with the posterior wall of the antrum) anteriorly and the pterygoid process of the sphenoid posteriorly (Fig. 4.33a,b). It is the 'junction box' of the deep neck as it communicates with multiple anatomical sites:

- medially, the nasal cavity via the sphenopalatine foramen
- posteriorly, the middle cranial fossa via the foramen rotundum and the foramen lacerum and facial nerve via the vidian canal
- laterally, the infratemporal fossa (or nasopharyngeal masticator space) via the pterygo-maxillary fissure
- superiorly, the orbit via the inferior orbital fissure
- inferiorly, the palate via the greater and lesser palatine canals.

The PPF is easily visualized on MR and CT as a largely fat-filled space.

It also contains the sphenopalatine ganglion and transmits the maxillary nerve and internal maxillary (Fig. 4.33b).

## The oral cavity

The oral cavity and the oropharynx are separated by a line of structures comprising, superiorly, the junction of soft palate and hard palate, laterally, the anterior tonsillar pillars and inferiorly the vallate papillae on the surface of the tongue. The tongue base is posterior to the vallate papillae and lies within the oropharynx. It consists largely of the lingual tonsils, which form the posterior third of the tongue.

The contents of the oral cavity are the hard palate, maxillary and mandibular alveolar ridges, retromolar trigone, buccal mucosa, floor of mouth and anterior two-thirds of the tongue.

The vestibule is the space between the cheek and lips externally and the teeth and gums internally and contains the superior and inferior gingival sulci.

The hard palate forms the roof of the oral cavity, separating it from the nasal cavity, with the maxillary alveolus and teeth forming the anterior and lateral boundaries of the hard palate. The lateral wall of the oral cavity is the buccal mucosa (cheek)

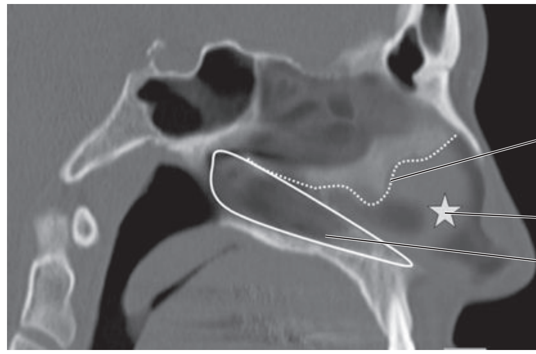


**Fig. 4.32** Sagittal CT through midline of nasal cavity demonstrating the components of the nasal septum.

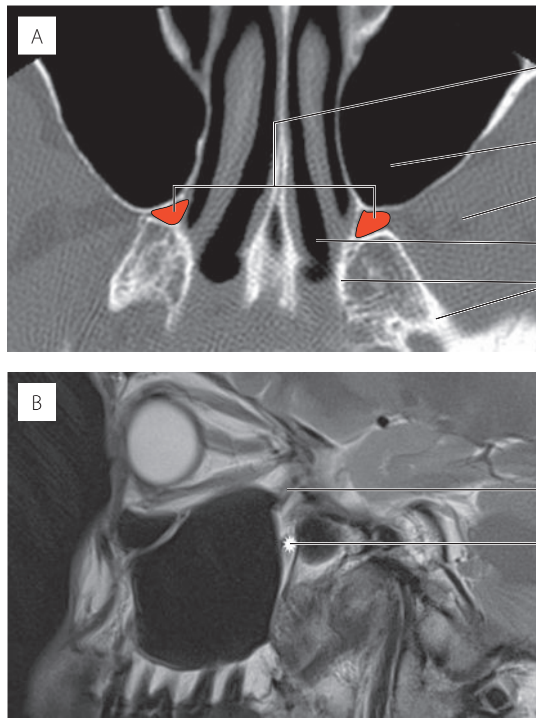


**Fig. 4.33** The pterygopalatine fossa. (A) Axial CT. The pterygopalatine fossa (PPF) outlined red. Note medial relations of nasal cavity and laterally the infratemporal fossa. (B) Sagittal T2 MR. PPF (white star). Note the maxillary antrum anteriorly and the orbital apex superiorly connected by the inferior orbital fissure.

and inferiorly lie the floor of the mouth (mylohyoid muscle), mandibular alveolus and teeth.

## The tongue

The tongue is a muscular organ made up of intrinsic transverse, vertical, inferior and superior fibres visible on ultrasound (Fig. 4.34) and MR.

It is supported by three paired extrinsic muscles. The largest of these is the genioglossus, which arises anteriorly from the genial tubercle on the lingual surface of the anterior mandible and fans out posteriorly into the tongue (Fig. 4.35). The hyoglossus arises from the hyoid and extends superiorly and laterally to blend with the styloglossus muscle, which arises from the styloid process and stylohyoid ligament.

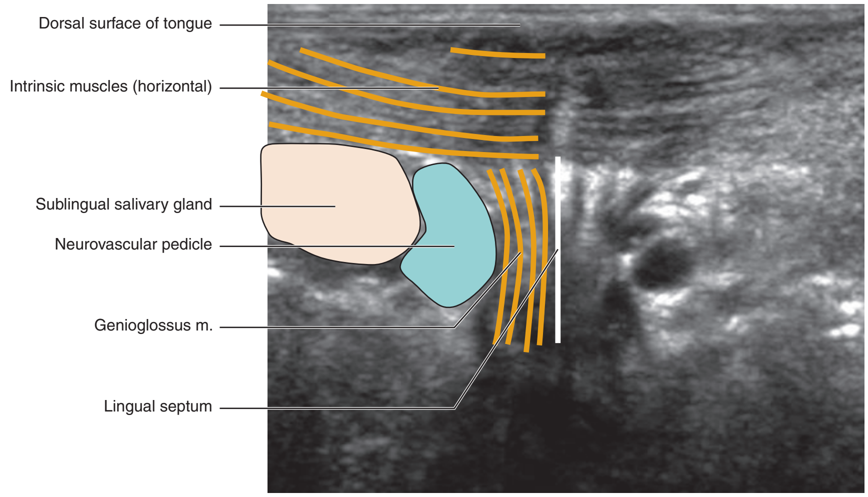


**Fig. 4.34** Coronal ultrasound through the tongue. Note the horizontal intrinsic muscle, the midline lingual septum and the paramedian genioglossus muscles.

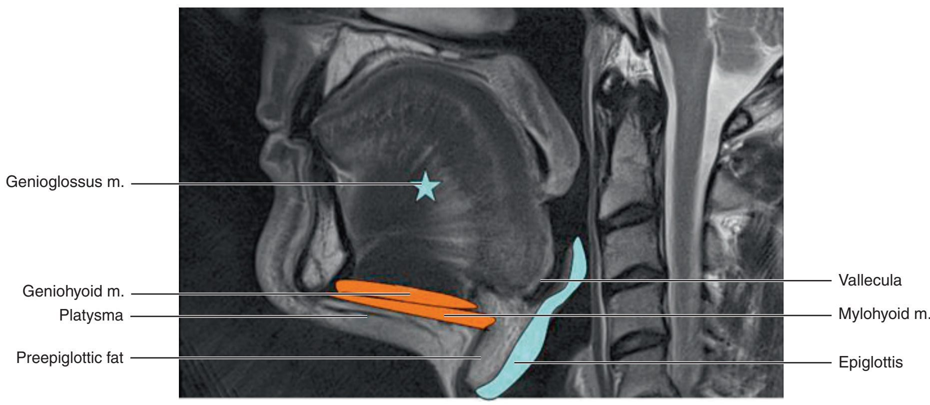


**Fig. 4.35** Sagittal T2 MRI. The tongue.

The hyoglossus muscle is a useful landmark that can be readily visualized on CT and MRI with the lingual artery and glossopharyngeal nerve on its medial aspect and the lingual vein, submandibular duct, lingual and hypoglossal nerves on its lateral aspect.

A midline fibrous septum divides the tongue and is an important radiological landmark when staging oral cancer (Fig. 4.36).

## Sublingual space

The sublingual space is lateral to the genioglossus muscles and separated from the submandibular space by the mylohyoid muscle.

The sublingual space contains the following; anterior hyoglossus muscles, lingual, glossopharyngeal and hypoglossal nerves, lingual artery and vein, sublingual and deep portion of the submandibular salivary glands.

The submandibular duct is within the oral tongue but inferior to the intrinsic tongue muscles.

## Thyroid gland

The thyroid gland consists of two lobes on either side of the trachea separated by an isthmus. It is invested by the mid-layer of deep cervical fascia and due to its superficial location is ideally visualized with ultrasound (Fig. 4.37). A pyramidal lobe may extend superiorly, usually arising from the left side of the isthmus. The strap muscles lie superficial to the gland.

During development the thyroid gland descends from the foramen caecum in the midline of the tongue base on the end of the thyroglossal duct. Rarely descent is incomplete, resulting in a lingual thyroid. More frequently a thyroglossal sinus or cyst may persist, the latter presenting as an anterior cervical swelling.

## Parathyroid glands

There are usually four but occasionally up to six parathyroid glands, which measure approximately 6 × 2 × 2 mm and are most frequently found in the tracheo-oesophageal groove posterior to the mid to inferior lobes of the thyroid. Their position may vary and they can be found within the thyroid gland itself or the mediastinum. The normal parathyroid gland is occasionally visible on ultrasound, which, in conjunction with sestamibi radionuclide imaging, is commonly used to identify overactive glands.

The normal parathyroid glands are not seen routinely on MRI or CT.


**Fig. 4.36** Coronal T2 MRI. The floor of the mouth.

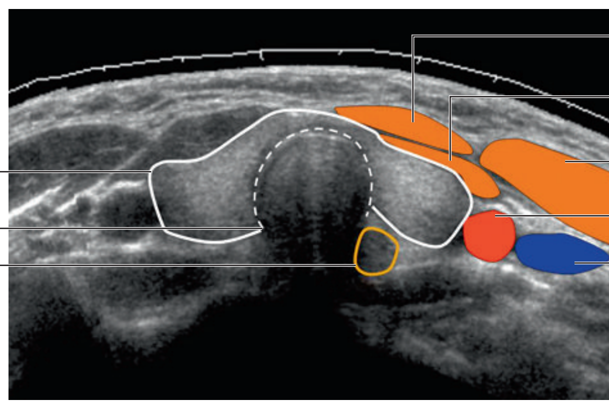


**Fig. 4.37** Panoramic axial ultrasound. The thyroid gland (continuous white line) and the trachea (interrupted white line).

## The cervical lymphatic system

There are approximately 300 lymph nodes within the neck (of the 800 in total throughout the body). A palpable lymph node is a frequent presentation of head and neck malignancy. The location of the node(s) can sometimes point to the likely site of malignancy and their involvement influences prognosis adversely.

The cervical nodes are commonly classified clinically into seven levels, superior to inferior (Fig. 4.38).

Levels 1a and b are submental and submandibular, respectively, and drain the lips, anterior floor of mouth and anterior tongue.

Levels 2 to 4 are synonymous with the upper, mid and lower deep cervical chains and follow the internal jugular vein deep to sternocleidomastoid muscle. The most important node of this chain is the jugulodigastric node in the upper deep cervical region as it is the most frequently involved node in squamous cell carcinomas of the tonsil, lateral tongue base and supraglottic larynx.

Level 5 nodes are those within the posterior triangle, located between the anterior border of the trapezius and posterior border of the sternocleidomastoid muscles. These nodes are also known as the spinal accessory and transverse cervical chains. Level 5 is divided into 5a (above) and 5b (below) relative to the course of the accessory nerve. The most common origin of a malignant 5a node is the naso-pharynx.

Level 6 comprises the anterior cervical nodes, which include the pre- and paratracheal and the less frequently involved prelaryngeal nodes. When a prelaryngeal node is involved in a patient with laryngeal squamous cell carcinoma, subglottic involvement should be sought.

Level 7, the superior mediastinal nodes, should be assessed in cervical oesophageal, thyroid and subglottic laryngeal cancers.

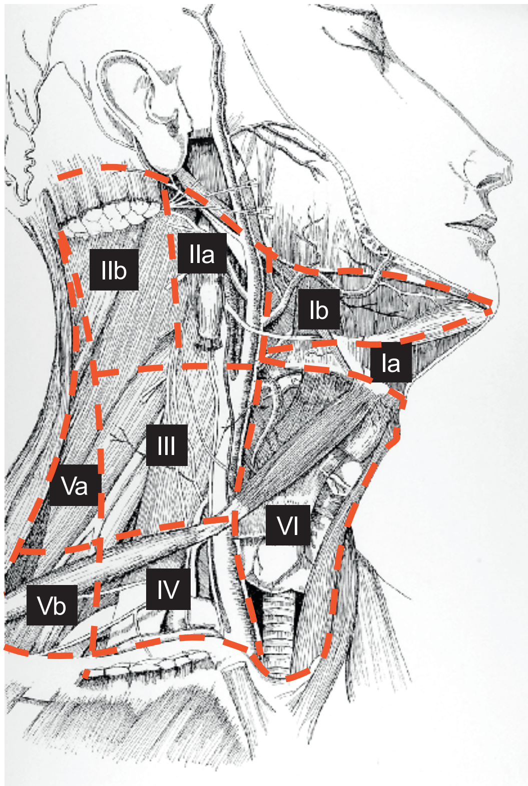


**Fig. 4.38** Illustration of right lateral neck with right submandibular salivary gland and sternocleidomastoid muscle (SCM) removed and internal jugular vein (IJV) tied off. Level Ia: submental. Between anterior bellies of digastric muscles. Level Ib: submandibular. Lateral to anterior belly of digastric muscle around submandibular salivary glands and superior to hyoid bone. Levels II to IV are the deep cervical chain, deep to the SCM muscle surrounding the carotid sheath. Only level II is split into levels IIa and IIb. Level IIa: anterior upper deep cervical including jugulo-digastric node. Anterior, medial and if touching posterior to right IJV above level of hyoid (another land mark is approximately level of carotid bifurcation). Level IIb: posterior upper deep cervical. Posterior to IJV with fat plane between node and IJV and deep to SCM muscle. Level III: mid deep cervical. From hyoid to inferior margin of cricoid cartilage. Level IV: lower deep cervical. From inferior cricoid cartilage to clavicle. Level V: posterior triangle. Between anterior border of trapezius and posterior border of SCM muscles. Separated into upper (Va) from skull base to lower border of cricoid and lower (Vb) lower border cricoid to clavicle. Level VI: anterior neck. From hyoid to manubrium including pre- and paratracheal and prelaryngeal (Delphian) nodes. Level VII: superior mediastinum. Superior aspect of manubrium to inominate vein between carotid arteries (not highlighted on this figure). Note that there are other head and neck nodal groups not included in this classification, including intra- and periparotid, facial and retropharyngeal nodes.

The retropharyngeal and parotid nodes are not included in the above classification. The retropharyngeal node should be assessed in any patient with nasopharyngeal or oropharyngeal malignancy.

The parotid nodes can be around or actually within the gland and drain the adjacent scalp, external auditory canal and pinna and nasopharynx.

The lymph drains ultimately into the thoracic duct on the left, which is frequently visible on CT, and on the right, either directly or via a lymphatic duct, into the junction of subclavian and internal jugular veins.

Chapter 5

# The vertebral column and spinal cord

Asif Saifuddin

## Radiographic anatomy

### Introduction

Radiography remains an important investigation for the assessment of spinal anatomy, with all areas adequately assessed by a combination of anteroposterior (AP) and lateral views. These can be supplemented by:

- AP open mouth view of the odontoid peg and atlanto-axial articulation (Fig. 5.1)
- AP view of the lumbosacral junction with ~25° cranial angulation (Ferguson view) demonstrating the L5/S1 disc space tangentially and the L5 pars en face (Fig. 5.2).

A major advantage of radiography is that it can be obtained in the erect position, allowing accurate assessment of spinal alignment and overall spinal balance in the coronal and sagittal planes.

A major limitation is the inability to assess the soft tissues of the spinal column, which include the intervertebral discs, spinal ligaments, spinal cord and paraspinal musculature:

- these require the additional techniques of CT and MRI.

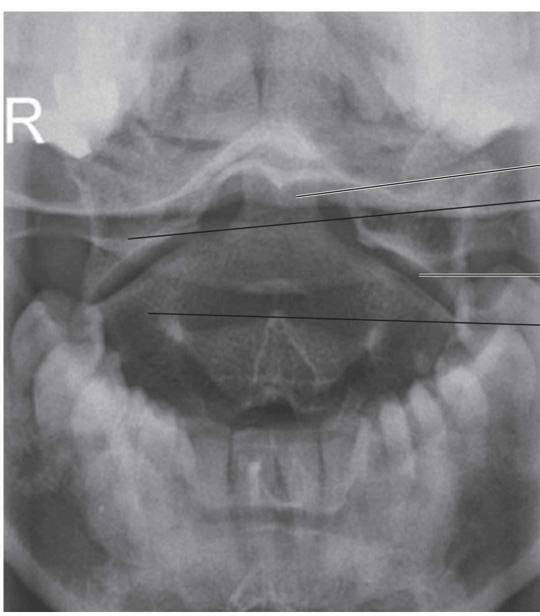


**Fig. 5.1** AP open mouth radiograph of the atlanto-axial joint.

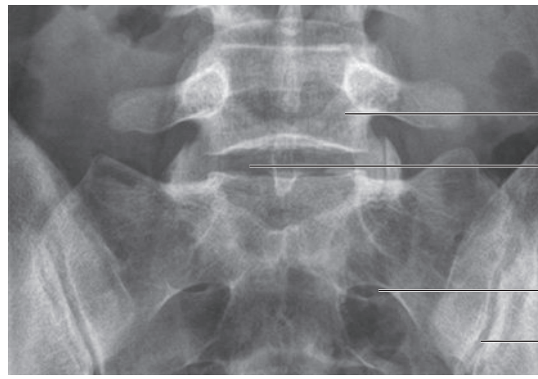


**Fig. 5.2** Ferguson view of the lumbosacral junction.

Therefore, the radiographic anatomy of the spinal column is essentially limited to assessment of the vertebrae, the joints and spinal alignment.

### The vertebral column

The vertebral column commences at the craniocervical junction (C0–C1 articulation) and terminates at the tip of the coccyx.

It comprises seven cervical, 12 thoracic, five lumbar, five sacral and three to five coccygeal vertebrae (Fig. 5.3):

- variation in the numbering of the last lumbar vertebra occurs with lumbosacral transitional junctions, occurring in ~16% of the population and also being termed ‘lumbarization’ or ‘sacralization’
- the lumbosacral transitional vertebra (LSTV) has unilateral or bilateral enlarged transverse processes, which attach to the superior aspect of the sacrum by either a pseudarthrosis or a complete bony ankylosis (Fig. 5.4).

Spinal alignment is assessed in the coronal and sagittal planes:

- in the coronal plane, the C7 spinous process should lie vertically above the mid-sacral line
- in the sagittal plane, the C2 body should lie vertically above L4 and the hips.

Four curvatures are seen in the sagittal plane in adults (Fig. 5.3):

- cervical lordosis; from C1 to T2, ranging from 30 to 40°

*Applied Radiological Anatomy, 2nd Edition* ed. Paul Butler, Adam W.M. Mitchell and Jeremiah C. Healy. Published by Cambridge University Press.


**Fig. 5.3** Sagittal T1W SE MRI showing the spinal curvatures.

- thoracic kyphosis; from T2 to T12, ranging from 20 to 40°
- lumbar lordosis; from L1 to L5, ranging from 20 to 40°
- sacrococcygeal kyphosis (pelvic curvature); from the lumbosacral junction to the tip of the coccyx.

## The cranio-cervical junction

The cranio-cervical junction is composed of the occiput (C0), the atlas (C1) and the axis (C2), forming a bony canal that protects the cervicomedullary junction of the spinal cord.

The occipito-atlantal (C0–C1) articulation comprises two synovial joints formed between the occipital condyles and the lateral masses of the atlas:

- it requires either CT or MRI for optimal evaluation.

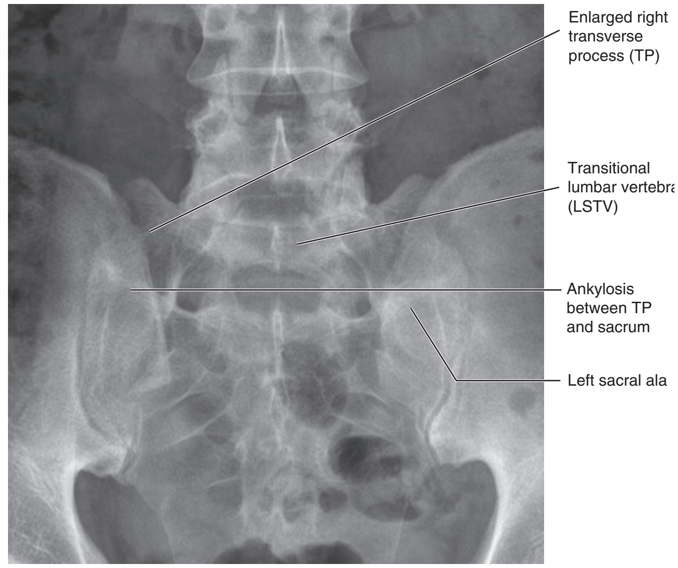


**Fig. 5.4** AP radiograph showing lumbosacral transition.

The atlanto-axial articulation (C1–C2) comprises four synovial joints between the atlas (C1) and the axis (C2):

- the atlas is a bony ring arising from three primary ossification centres, the anterior arch and two neural arches
  - the neural arches fuse by age 3 years to form the posterior arch and fuse with the anterior arch by age 7 years
    - failure of fusion of the anterior and/or posterior arches may result in congenital defects which can mimic fractures
  - the atlas thus comprises an anterior arch, which fuses at the anterior tubercle, the posterior arch and two lateral masses (Figs. 5.1, 5.5)
- the axis is formed from four primary ossification centres, one for each neural arch, one for the body and one for the odontoid process (dens)

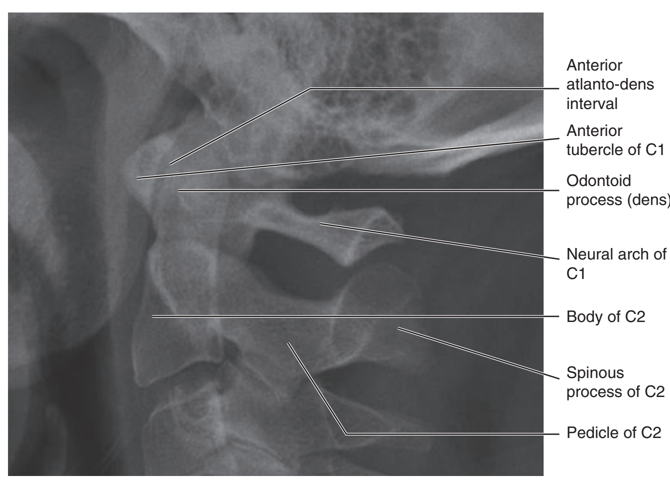


**Fig. 5.5** Coned lateral radiograph of the cranio-cervical junction.

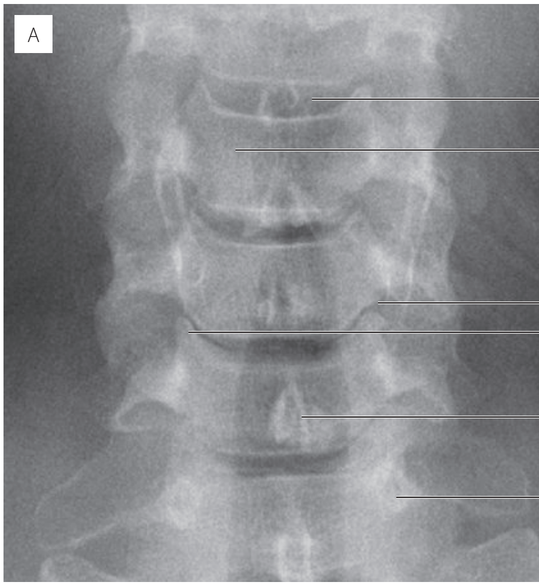


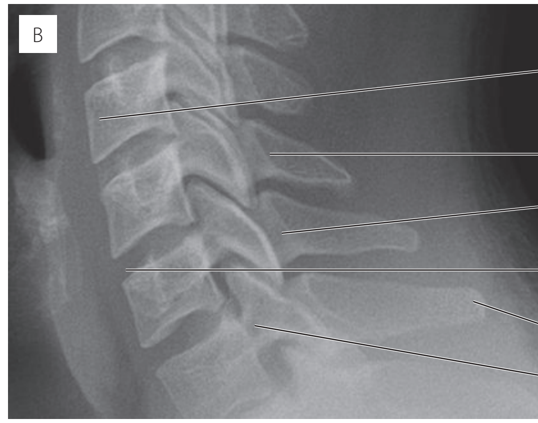


**Fig. 5.6** (A) Coned AP radiograph of the lower cervical spine. (B) Coned lateral radiograph of the lower cervical spine.

  - a secondary ossification centre forms at the tip of the dens, fusing by age 12 years, with failure of fusion resulting in an os odontoideum
  - the odontoid fuses to the C2 body by age 3–6 years and the neural arches fuse posteriorly by 2–3 years and with the body by 3–6 years
  - the axis thus comprises a body, a superiorly protruding dens, two lateral masses and two pedicles which fuse to form a large, commonly bifid spinous process (Figs. 5.1, 5.5)
- the 4 joints of the C1–C2 articulation are:
  - two lateral joints between the lateral masses of C1 and C2 (Fig. 5.1)
  - two median joints, one between the dens and anterior arch of the atlas (Fig. 5.5) and one between the dens and the transverse atlantal ligament, which is not appreciated radiographically
  - the normal anterior atlanto-dens interval is <5 mm in children and <3 mm in adults
  - the normal lateral atlanto-dens interval should show <2–3 mm side-to-side difference.

## Craniometry of the cranio-cervical junction

The normal relationships between the components of the cranio-cervical junction can be assessed by a variety of measurements between landmarks identified on the lateral radiograph.

A number of lines have been described:

- Chamberlains line; runs between the posterior tip of the hard palate and the posterior margin of the foramen magnum
  - the tip of the dens usually lies at or below this line but may extend for 3–6 mm above
- the basion (tip of clivus)–dens interval should be <12 mm.

## The cervical, thoracic and lumbar vertebrae

The sub-axial vertebrae have a relatively uniform anatomical structure, each consisting of a body and neural arch, the latter comprising two pedicles, two laminae, two transverse processes, two superior and inferior articular processes and a spinous process.

Each vertebral body is composed of a shell of outer cortical bone and superior and inferior fibro-cartilaginous end-plates, which enclose a meshwork of internal primary and secondary trabeculae formed of cancellous bone and bone marrow.

The cervical vertebral bodies are relatively small, being greater in the transverse than the AP dimension (Fig. 5.6a,b):

- transverse processes arise from the lateral margins of the body, being optimally assessed with CT
- two uncinate processes point superiorly from the posterolateral aspects of the superior end-plate to articulate with the inferior end-plate of the vertebra above, forming the neurocentral joints (of Luschka) (Fig. 5.6a,b).

The thoracic vertebral bodies (Fig. 5.7a,b) have small facets on their sides for articulation with the rib heads to form the costovertebral joints.

In the immature spine, superior and inferior ring apophyses can be identified on the lateral radiograph (Fig. 5.7b).

The pedicles arise from the posterolateral margins of the vertebral bodies (Figs. 5.7, 5.8).

The laminae are slender plates of bone which extend inferomedially from the pedicles to fuse posteriorly in the mid-line at the base of the spinous process (Figs. 5.7, 5.8).

The transverse processes in the thoracic and lumbar regions arise at the junction of the pedicle and lamina and extend laterally (Fig. 5.8a):

- the thoracic transverse processes articulate with the rib necks at the costotransverse joints.

The superior articular processes extend upwards from the pedicle-lamina junction and articulate with corresponding inferior articular processes arising from the neural arch above to form the facet joint (Fig. 5.9a,b):

- the junction between the superior and inferior articular processes is termed the pars interarticularis (Fig. 5.9a,b).

The spinous processes point inferiorly (Figs. 5.7, 5.8) and are commonly bifid in the cervical region.

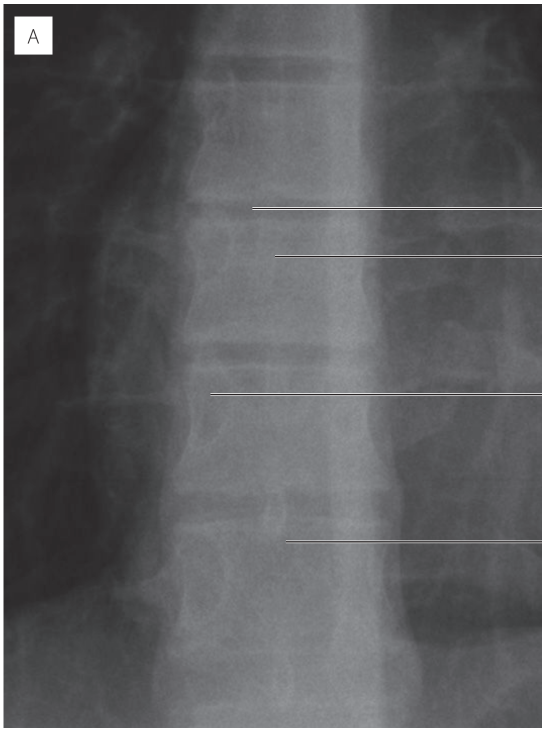


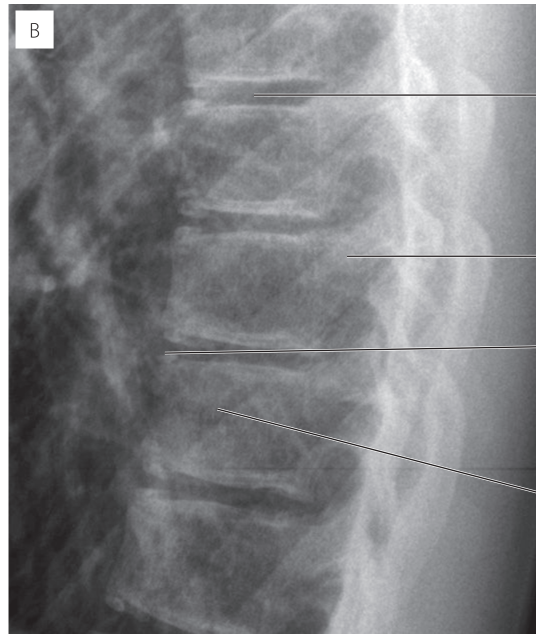


**Fig. 5.7** (A) Coned AP radiograph of the lower cervical spine. (B) Coned lateral radiograph of the lower cervical spine.

Neural arch and facet joint anatomy is optimally demonstrated by MDCT and MRI.

## The spinal canal

The bony spinal canal has the following borders:

- anterior, the posterior vertebral body cortex
- lateral, the pedicles, facet joints and laminae
- posterior, the base of the spinous process, which is represented on lateral radiographs by the spinolaminar line (Fig. 5.6b).

The canal is divided anatomically into the central canal, lateral recess and intervertebral foramen, the anatomy of which is optimally demonstrated by cross-sectional techniques:

- in the cervical region, the AP canal dimension should be approximately equal to or greater than the AP vertebral body dimension
  - the AP canal dimension from C1 to C3 is ~21 mm. and from C4 to C7 is ~18 mm.
- in the lumbar region, the transverse canal dimension, as represented by the interpediculate distance, should progressively increase from L1 to L5
  - the midsagittal diameter is ~18 mm.

The spinal canal contains ligaments, epidural fat, the thecal (dural) sac with its contents of CSF, spinal cord and intradural nerve roots, and the vertebral venous plexus.

## The sacrum and coccyx

The sacrum is a curved triangular bone formed by the fusion of five sacral vertebrae (Fig. 5.10a,b), which extends from the lumbosacral junction to the coccyx and forms the posterior margin of the pelvic cavity:

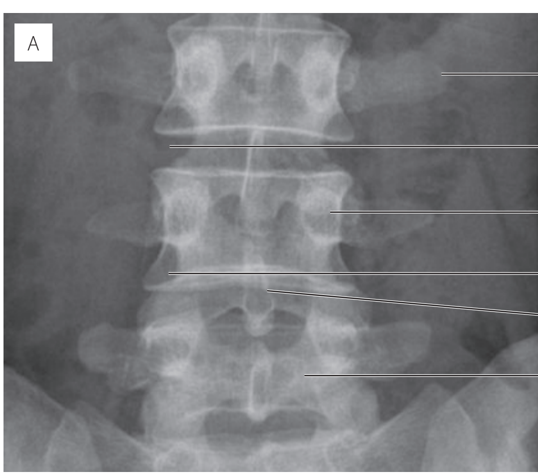


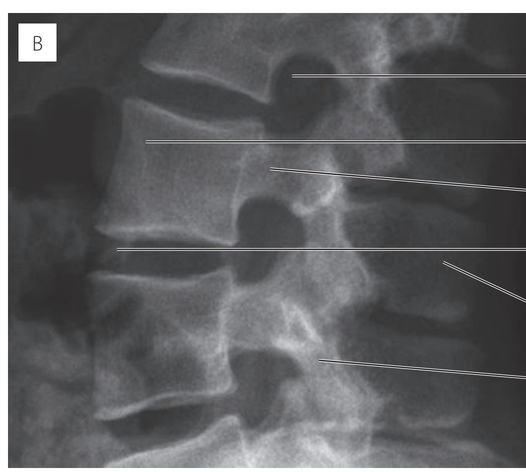


**Fig. 5.8** (A) AP radiograph of the lumbar spine. (B) Coned lateral radiograph of the mid-lumbar spine.

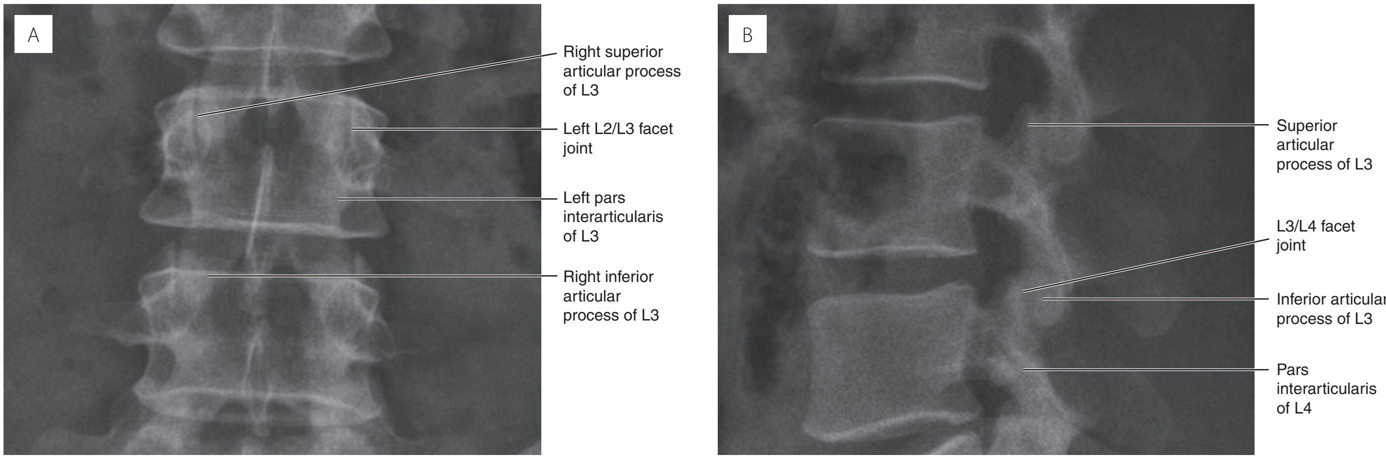


**Fig. 5.9** (A) Coned AP radiograph of the lumbar spine. (B) Coned lateral radiograph of the lumbar spine showing the facet joints.

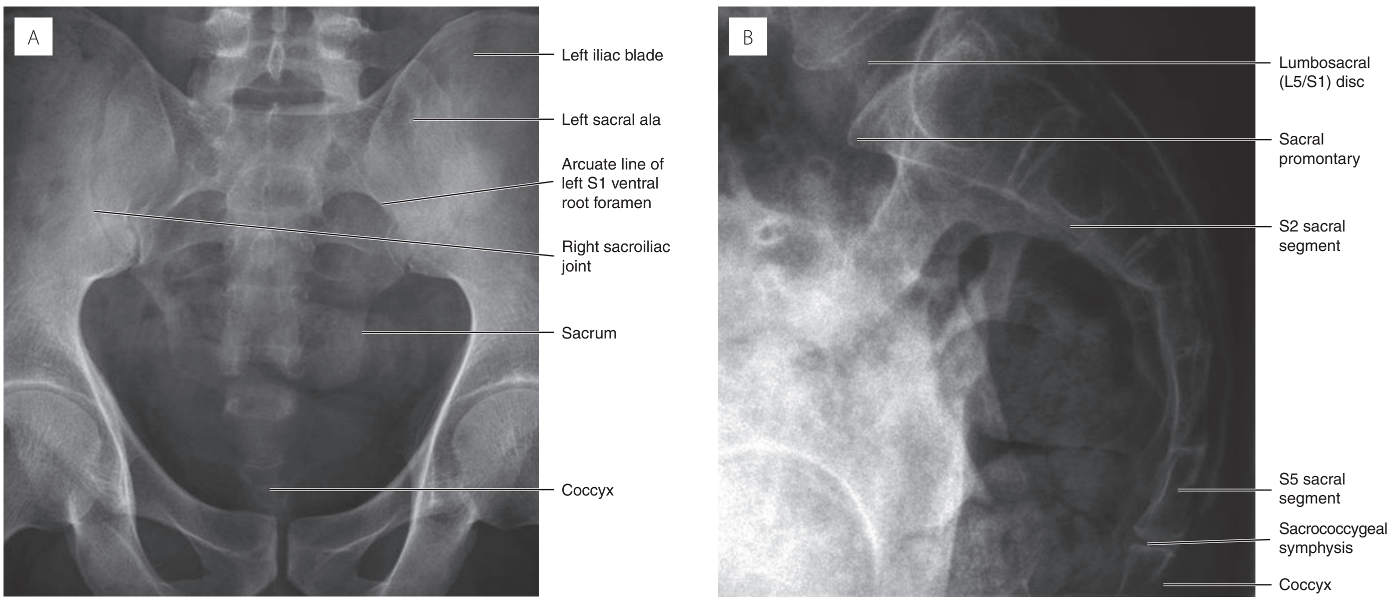


**Fig. 5.10** (A) AP radiograph of the sacrum and coccyx. (B) Lateral radiograph of the sacrum and coccyx.

- the sacral vertebrae may be partially separated by rudimentary fibrocartilaginous discs.

The S1 body protrudes anteriorly as the sacral promontory (Fig. 5.10b), while the lateral masses are flat and are termed the sacral alae (Fig. 5.10a).

The body is perforated by four paired ventral and dorsal sacral foramina, the ventral foramina being evident on the AP radiograph as arcuate lines (Fig. 5.10a):

- these transmit the S1–4 nerve roots.

The sacrum articulates laterally with the iliac blades via the sacroiliac joints (SIJs) (Fig. 5.10a).

The morphology of the sacrum differs between males and females, the female sacrum being shorter, wider and more posteriorly tilted, thus increasing the capacity of the pelvic cavity.

The coccyx is the terminal portion of the vertebral column, being formed by three to five individual vertebrae (Fig. 5.10a,b).

- it is attached to the sacrum by the fibrocartilaginous sacrococcygeal symphysis (Fig. 5.10b), which allows limited movement between the two bones.

## Cross-sectional anatomy

### Computed tomography (CT)

CT optimally demonstrates detail of bony spinal anatomy, particularly of the occipito-atlantal joint (C0–C1), the cervical neural arch, the facet joints and the articulations between the ribs and thoracic vertebrae.

#### The occipito-atlantal (C0–C1) joint

The occipito-atlantal joints are synovial joints formed by the articulations between the occipital condyles and the atlas.

The occipital condyles project from the inferior aspect of the occiput at the anterolateral margins of the foramen magnum and articulate with the concave superior articular surfaces of the lateral masses of C1 (Fig. 5.11a,b).

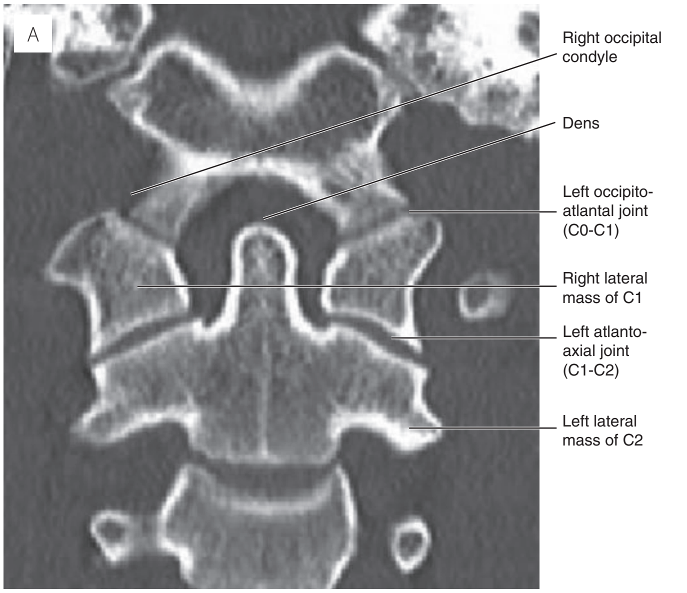


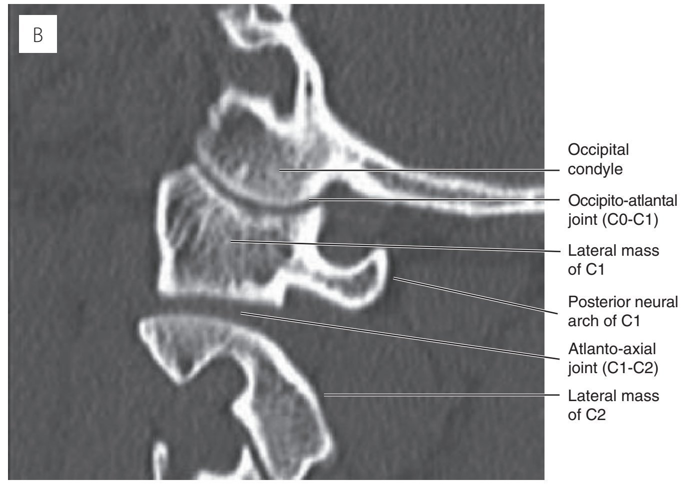


**Fig. 5.11** (A) Coronal MDCT showing the craniocervical junction. (B) Sagittal MDCT showing the craniocervical junction.

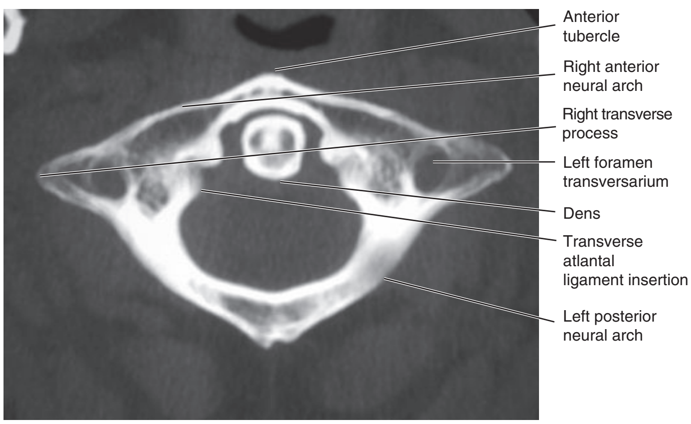


**Fig. 5.12** Axial CT showing the C1 ring.

## The atlas

The atlas has a ring configuration in the axial plane (Fig. 5.12).

The anterior arch forms ~1/5 of the ring and has a central anterior tubercle.

The posterior arch forms ~2/5 of the ring and has a sulcus on each side just posterior to the lateral mass for transmission of the vertebral artery.

The lateral masses are bulky and articulate with C0 and C2:

- from their medial aspects arise two small tubercles for attachment of the transverse atlantal ligament.

The transverse processes arise from the lateral masses and contain the foramen transversarium.

## The cervical neural arch

The transverse processes of the cervical vertebrae arise from the lateral aspects of the vertebral body:

- each transverse process possesses a foramen transversarium (Fig. 5.13), which from C2–C6 transmits the vertebral artery and vein, as well as a plexus of sympathetic nerves.

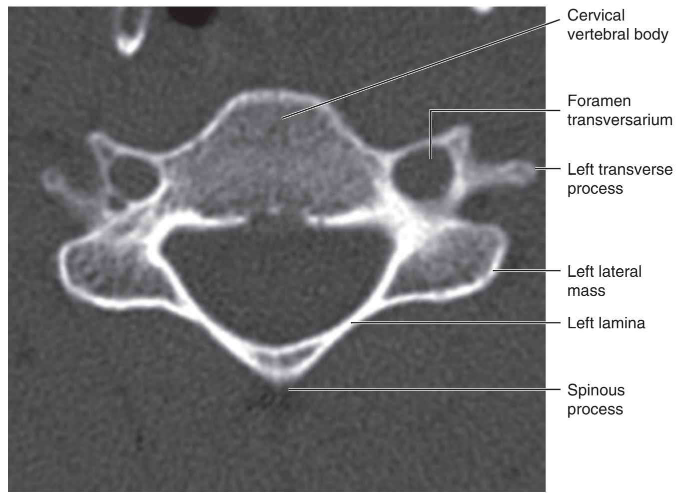


**Fig. 5.13** Axial CT showing the cervical vertebra.

## The facet joint

The facet (zygoapophyseal) joints are paired joints extending from C1/C2 to L5/S1 and are formed by the superior and inferior articular processes:

- the superior articular facet lies anterior to the inferior articular facet
- the articular surfaces are covered by hyaline cartilage and surrounded by a synovium-lined fibrous capsule.

In the cervical region, the articular surface lies in the coronal plane on axial images (Fig. 5.14a) and is angled from anterosuperior to posteroinferior in the sagittal plane (Fig. 5.14b).

In the thoracic region, the articular surface also lies in the coronal plane (Fig. 5.15a,b), apart from the T12/L1 facet, which lies in an oblique plane.

In the lumbar region, the articular surface is curved, with the superior articular process facing posteromedially and the inferior facing anterolaterally (Fig. 5.16a,b):

- facet tropism is a normal variant, occurring most commonly at L4/L5 and L5/S1, referring to asymmetry in the sagittal orientation of the facet joints at the same level.

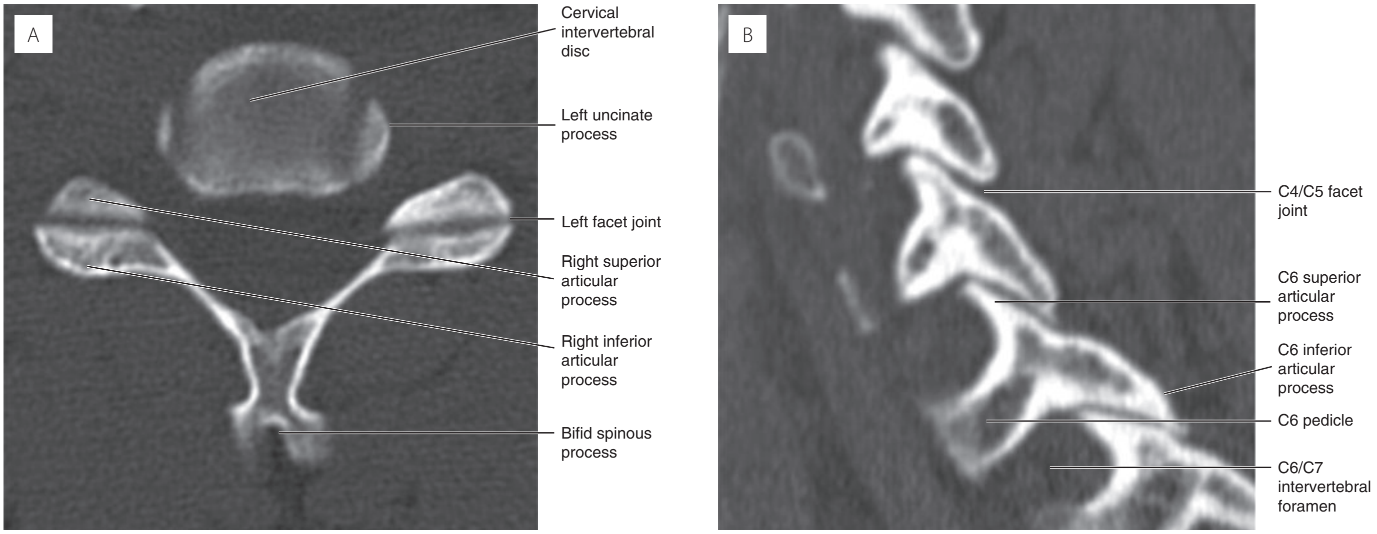


**Fig. 5.14** (A) Axial CT showing the cervical facet anatomy. (B) Sagittal MDCT showing the cervical facet anatomy.

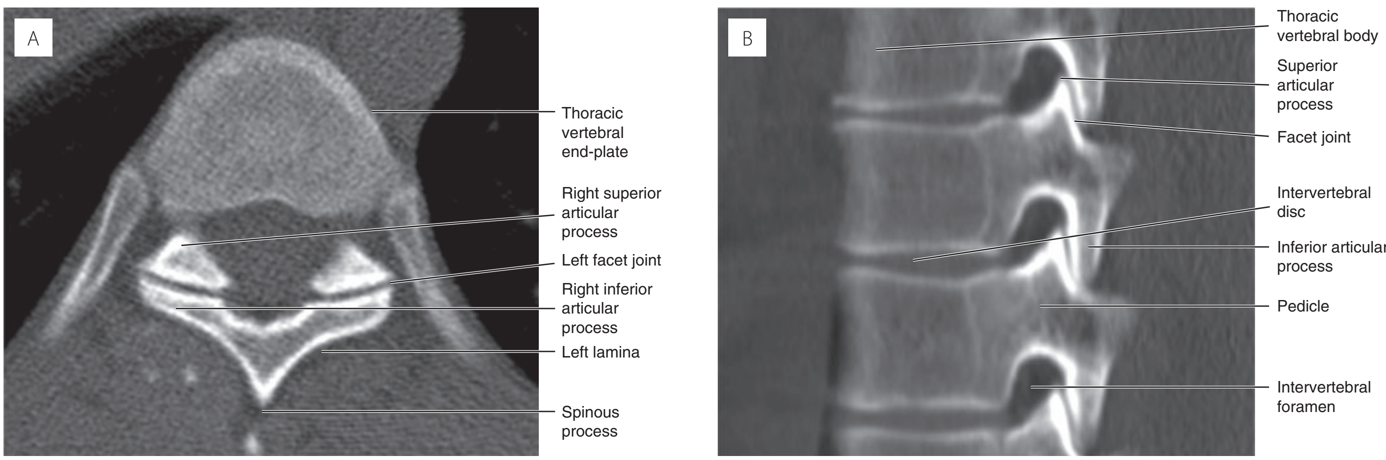


**Fig. 5.15** (A) Axial CT showing the thoracic facet anatomy. (B) Sagittal MDCT showing the thoracic facet anatomy.

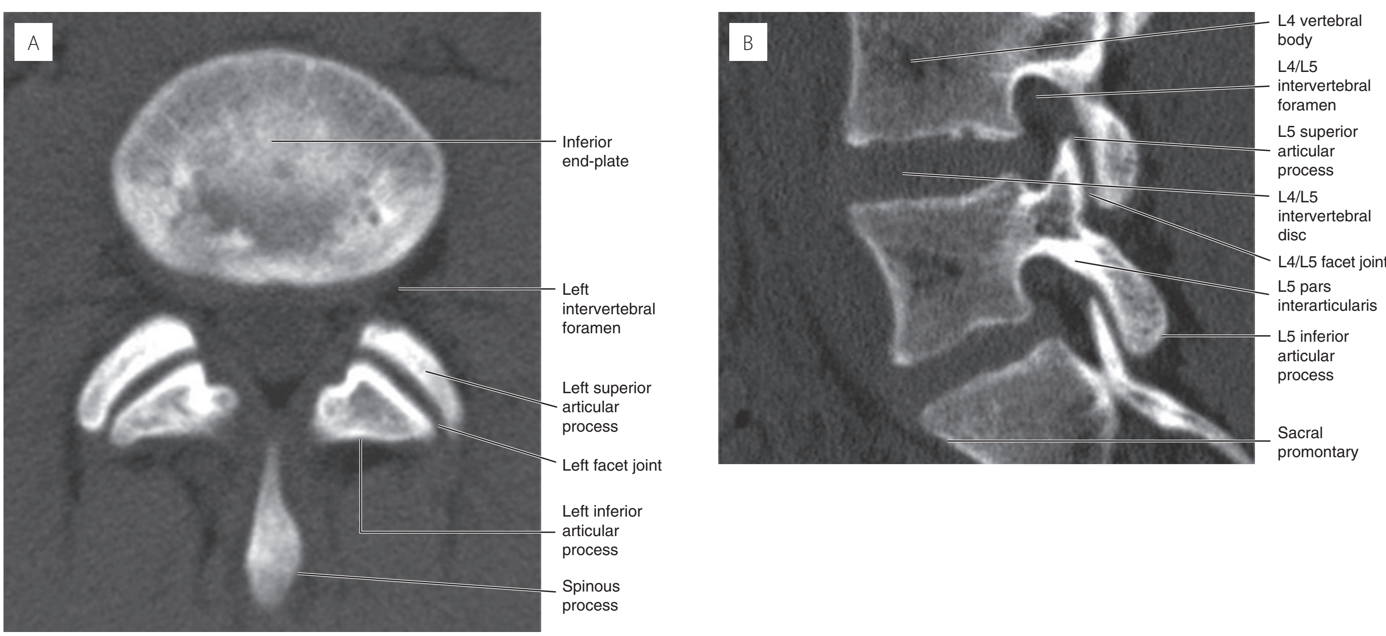


**Fig. 5.16** (A) Axial CT showing the lumbar facet anatomy. (B) Sagittal MDCT showing the lumbar facet anatomy.

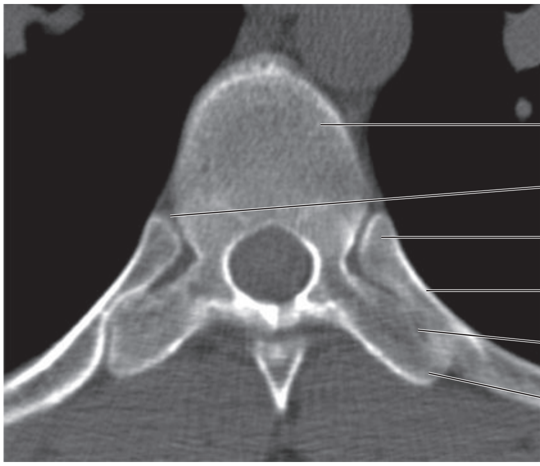


**Fig. 5.17** Axial CT showing the costovertebral and costotransverse joints.

The facet joints are innervated by the medial branch of the dorsal ramus of the mixed spinal nerve:

- each medial branch innervates the facet joint at its level as well as the facet joint below (e.g. the L3 medial branch innervates both the L3/4 and L4/5 facet joints).

### The costovertebral and costotransverse joints

The costovertebral joints are paired synovial joints formed between the rib head and the costal facets of two adjacent thoracic vertebrae, the inferior aspect of the vertebra above and the superior aspect of the vertebra to which the rib corresponds numerically (Fig. 5.17):

- the rib head also articulates with the intervertebral disc
- however, the 1st and 10th–12th ribs only articulate with the corresponding vertebra.

The costotransverse joints are paired synovial joints between facets on the posterior aspect of the rib and the anterior aspect of the transverse process (Fig. 5.17).

## Magnetic resonance imaging (MRI)

MRI is ideally suited to the demonstration of soft tissue anatomy of the spinal column, including the vertebral medullary cavity, the intervertebral discs, the spinal ligaments, the spinal canal and its contents and the paravertebral musculature.

### The vertebral body

The vertebral body contains marrow, the MRI signal intensity (SI) of which is dependent upon the proportion of red (haemopoietic) and yellow (fatty) marrow, this varying with the age:

- in the first month of life, the high proportion of red marrow renders the vertebral body hypointense to the intervertebral disc (IVD)
- marrow conversion occurs during the first to sixth months, with a progressive increase in T1W SI
- in adults, the high proportion of yellow marrow results in the marrow appearing hyperintense to the IVD, particularly in the lumbar region (Fig. 5.18).

Focal variations in marrow SI within the vertebral body are not uncommon:

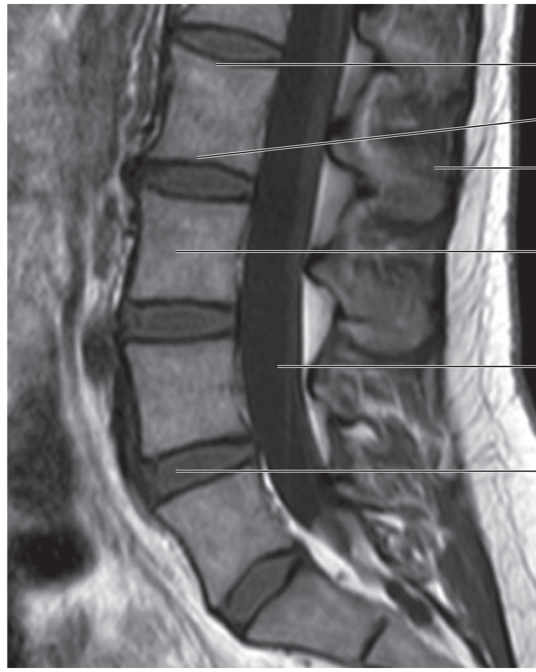


**Fig. 5.18** Sagittal T1W SE MRI of the lumbar spine.

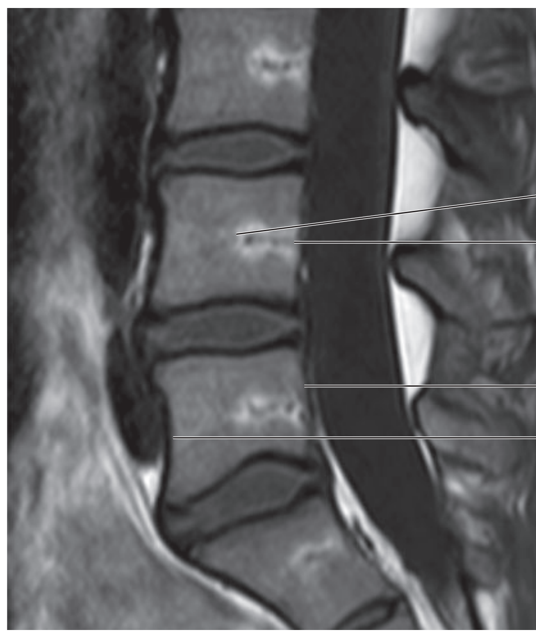


**Fig. 5.19** Sagittal T1W SE MRI of the lumbar spine.

- islands of red marrow or marrow fibrosis appear as areas of reduced T1W and T2W SI
- focal areas of fatty marrow may be seen, particularly around the basivertebral veins (Fig. 5.19)
- in the elderly, the marrow SI may be very heterogeneous.

### The intervertebral discs

The intervertebral discs (IVD) lie between the superior and inferior cartilaginous end-plates of the adjacent vertebrae, being formed of an outer annulus fibrosus (AF) and an inner nucleus pulposus (NP):

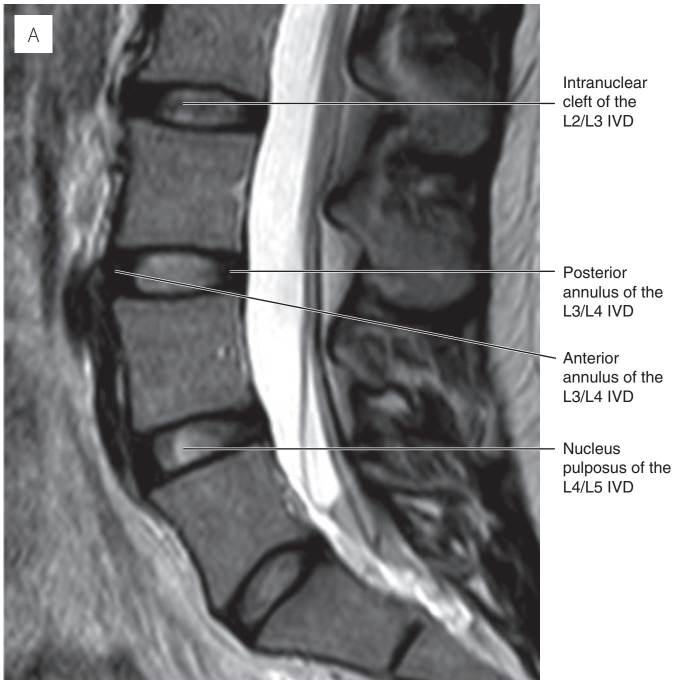


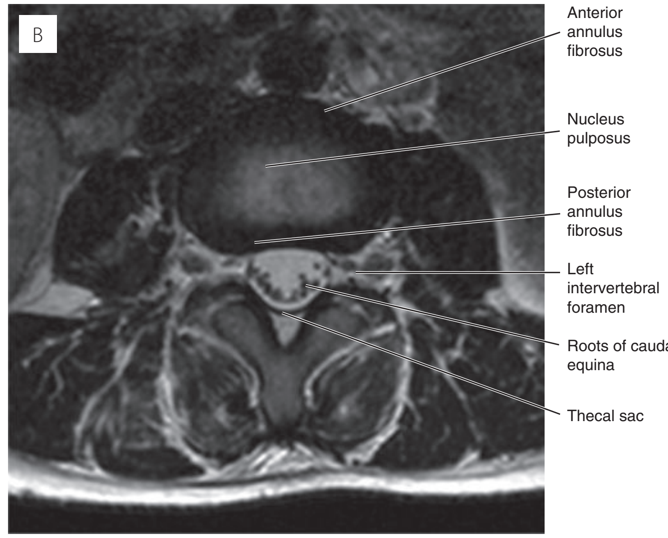


**Fig. 5.20** (A) Sagittal T2W FSE MRI of the lumbar spine. (B) Axial T2W FSE MRI of the lumbar spine.

- the IVD functions to provide motion between individual vertebrae and also allows the effective transfer of load
- the IVD is avascular by age ~25–30 years, the disc receiving nutrition by diffusion through the end-plates
- the NP has no nerve supply, while the outer annulus is supplied by sinuvertebral (recurrent meningeal) nerves
- the discs together account for ~25–30% of spinal column length.

The AF is formed by 15–25 laminae of fibrous connective tissue, which due to its fibrous nature appears black on all MR pulse sequences, particularly T2W images (Fig. 5.20a,b):

- the AF is attached circumferentially to the periphery of the vertebral body via Sharpey's fibres
- the anterior annulus is thicker than the posterior annulus, resulting in the NP lying relatively posteriorly within the IVD (Fig. 5.20a).

The NP consists of a gel-like substance with ~90% of its content being water, rendering it hyperintense on T2W images (Fig. 5.20a,b) and of intermediate SI on T1W images (Fig. 5.18):

- the intranuclear cleft appears as a horizontal band of low SI on sagittal T2W images (Fig. 5.20a), which is a normal finding after the age of 30 years.

### The spinal ligaments

The spinal ligaments are important stabilizers of the vertebral column and, being made of fibrous tissue, appear as thin black stripes on all MRI pulse sequences.

The major ligaments of the cranio-cervical junction include:

- the ligamentum nuchae, which runs from the external occipital protuberance to the posterior arch of the atlas and the cervical spinous processes (Fig. 5.21)
- the tectorial membrane, which connects the clivus to the axis, representing the cephalad extension of the posterior longitudinal ligament (PLL) (Fig. 5.21)
- the transverse atlantal ligament, which connects the posterior dens to the inner margin of the atlas ring (Fig. 5.22)
- the alar ligaments, which run between the lateral margins of the dens and the occipital condyles.

The anterior longitudinal ligament (ALL) and posterior longitudinal ligament (PLL) both arise at the skull base and extend continuously downward, attaching to the front and back of the sacrum:

- the ALL runs anterior to the vertebral bodies and discs, being firmly attached to the anterior annulus (Fig. 5.23)

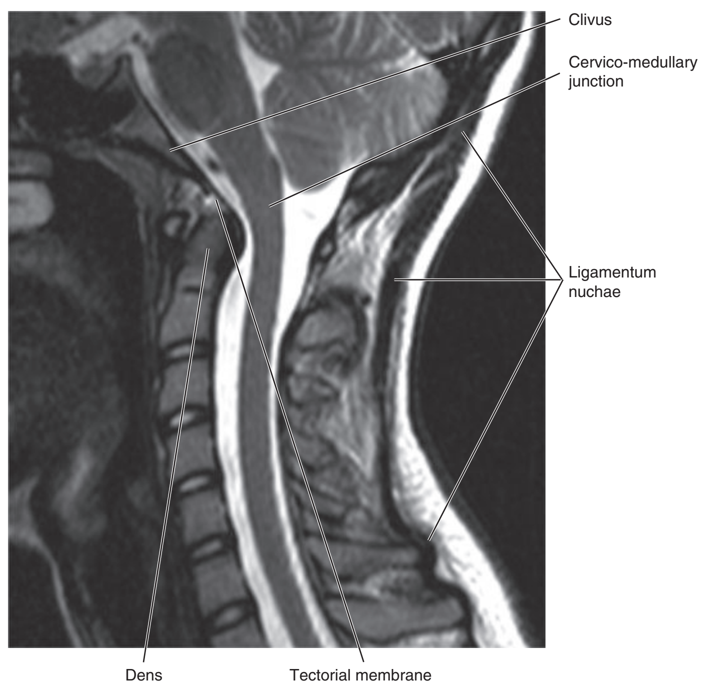


**Fig. 5.21** Sagittal T2W FSE MRI of the cervical spine.

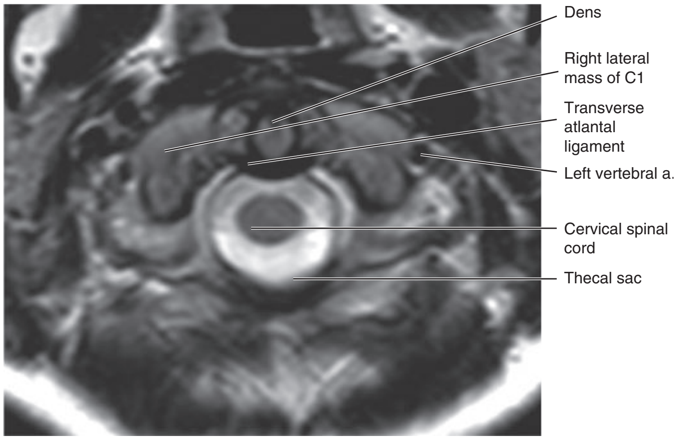


**Fig. 5.22** Axial T2W FSE MRI of the upper cervical spine.

- the PLL runs posterior to the vertebral bodies and discs, being wider at the disc space and being firmly attached to the posterior annulus (Fig. 5.23).

The posterior ligamentous complex (PLC) comprises the ligamentum flavum (LF), interspinous ligament (ISL) and supraspinous ligament (SSL):

- the LF runs between adjacent laminae and the bases of the spinous processes (Fig. 5.24a), running laterally in the lumbar region to cover the anterior aspect of the facet joints (Fig. 5.24b)
- the ISL runs between the adjacent spinous processes and appears relatively hyperintense, since it is bordered on each side by fat (Fig. 5.24a)

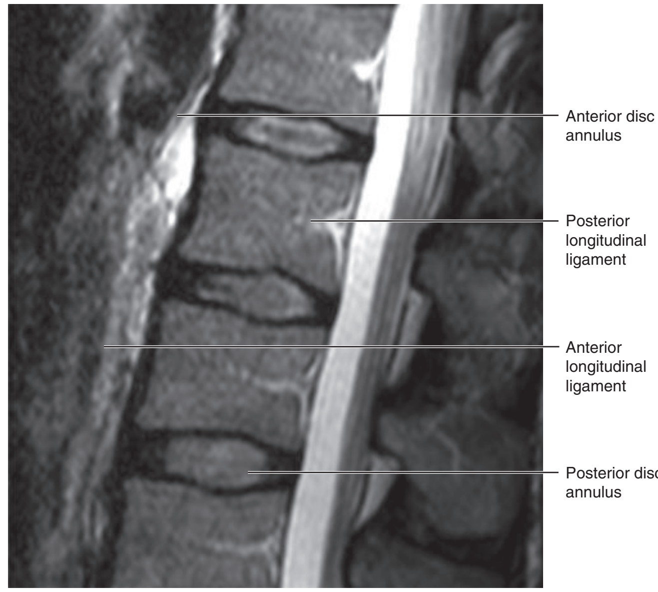


**Fig. 5.23** Sagittal T2W FSE MRI of the lumbar spine.

- the SSL connects the spinous processes of the thoracic and lumbar vertebrae, terminating between L4 and L5 (Fig. 5.24a).

The iliolumbar ligaments arise from the transverse processes of L5 and attach to the posterior iliac crest (Fig. 5.25), helping to stabilize the lumbosacral junction.

## The spinal canal

The spinal canal is divided into the central canal, the lateral recess and the intervertebral foramen (IVF).

The boundaries of the central canal (Fig. 5.26) are:

- anterior: the vertebral body, IVD and PLL
- posterior: the posterior epidural fat pad, LF and base of the spinous process;

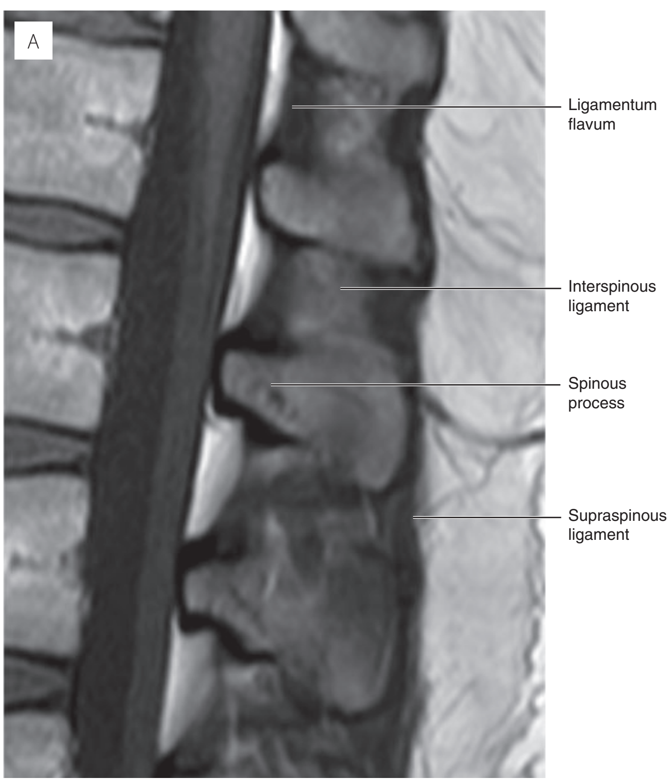


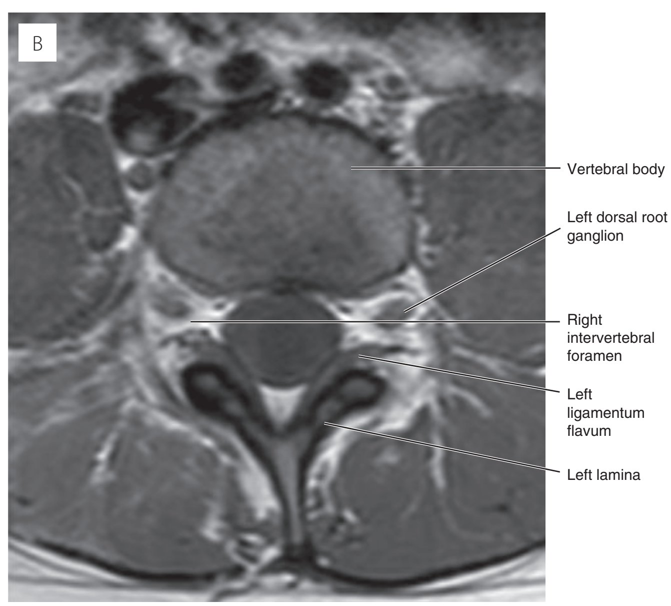


**Fig. 5.24** (A) Sagittal T1W SE MRI of the lumbar spine. (B) Axial T1W SE MRI of the lumbar spine.

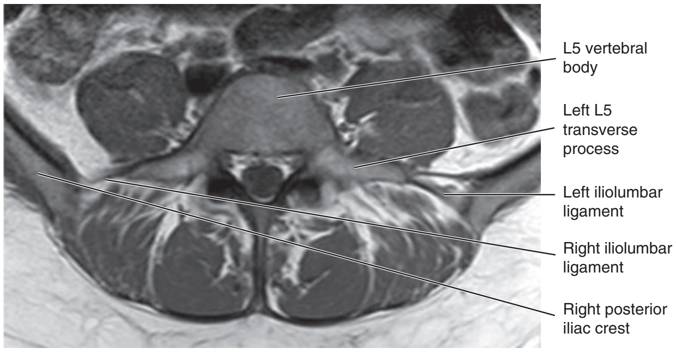


**Fig. 5.25** Axial T1W SE MRI of the lumbosacral junction.

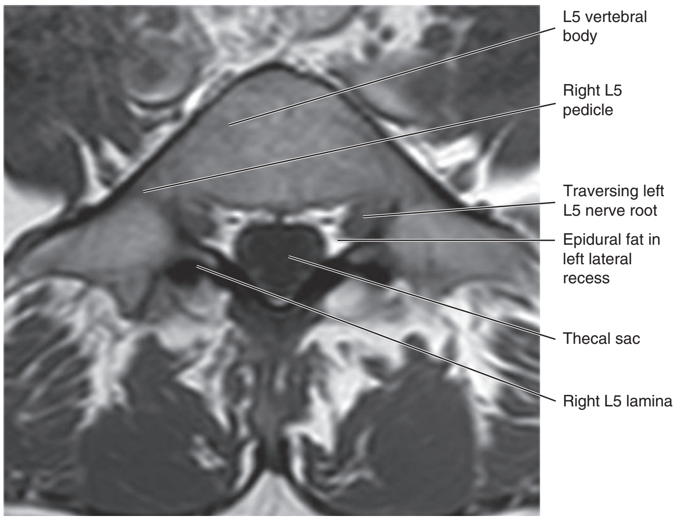


**Fig. 5.27** Axial T1W SE MRI of the lumbar spine.

- it contains the thecal (dural) sac and CSF, the intradural nerve roots and, in the cervical and thoracic region, the spinal cord.

The boundaries of the lateral recess (Fig. 5.27) are:

- anterior: the vertebral body and IVD
- medial: the thecal sac
- lateral: the pedicle, facet joint and IVF
- posterior: the LF and lamina;
- it contains epidural fat, the traversing nerve root and epidural vessels.

The boundaries of the IVF (Figs. 5.14b, 5.15b, 5.16, 5.24b, 5.28) are:

- anterior: the vertebral body and IVD
- posterior: the LF, pars interarticularis and facet joint
- superior and inferior: the pedicles of the adjacent vertebrae;
- it contains epidural fat, the exiting nerve root, radicular vessels and the sinuvertebral nerves.

The sacral canal is bordered anteriorly by the dorsal surface of the sacrum and posteriorly by the laminae, which fuse in the midline to form the median sacral crest:

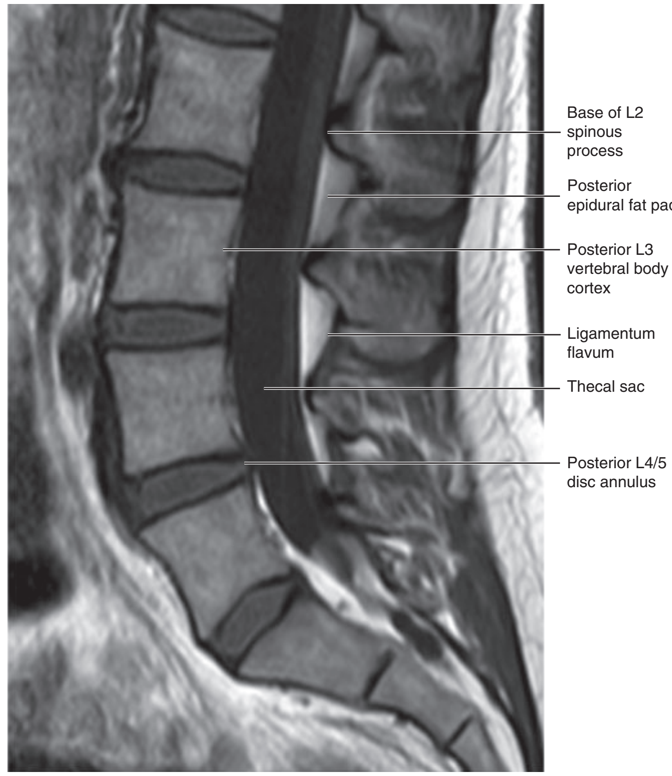


**Fig. 5.26** Sagittal T1W SE MRI of the lumbar spine.

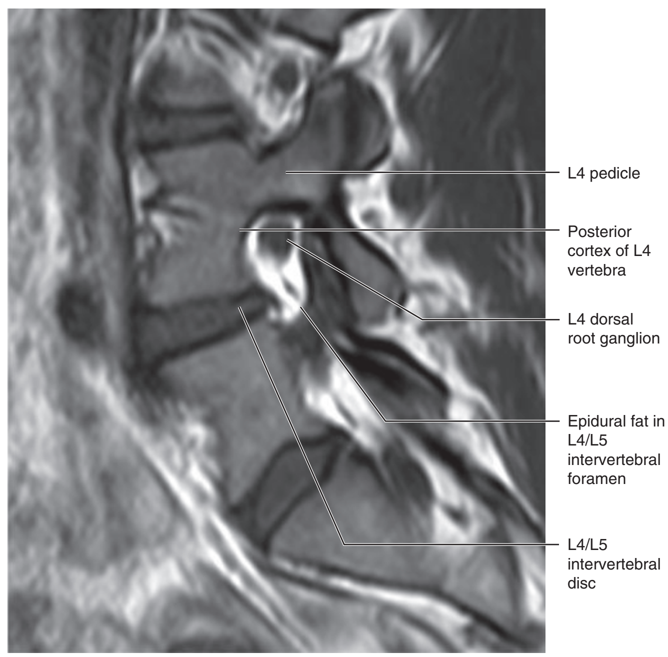


**Fig. 5.28** Sagittal T1W SE MRI of the lumbar spine.

- the upper sacral canal contains the termination of the thecal sac (at ~S2), the sacral roots, the filum terminale and epidural fat (Fig. 5.29a,b)
- at the S5 level, the neural arch is deficient, the opening forming the sacral hiatus (Fig. 5.29a).

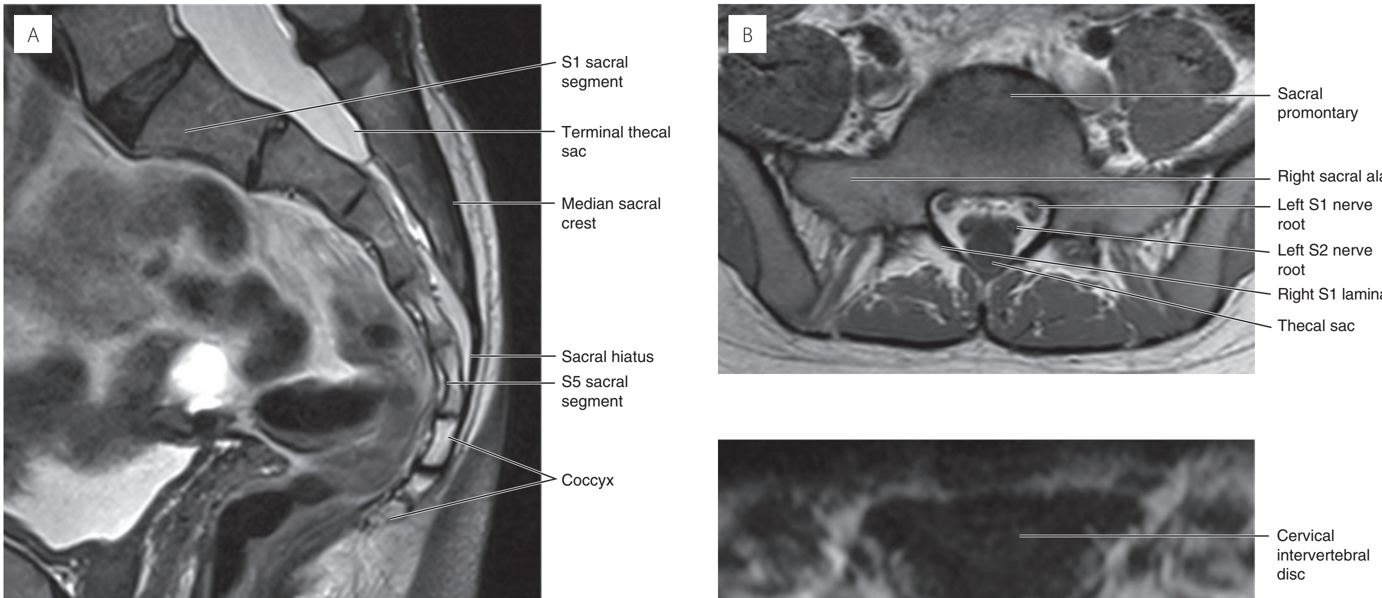


**Fig. 5.29** (A) Sagittal T2W FSE MRI of the sacrum and coccyx. (B) Axial T1W SE MRI of the upper sacrum.

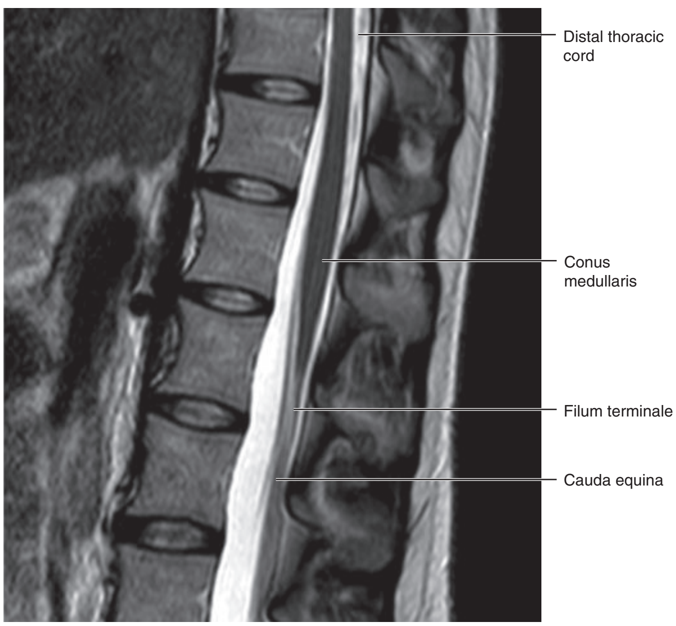


**Fig. 5.30** Sagittal T2W FSE MRI of the thoracolumbar junction.

## The spinal cord and nerves

The spinal cord commences at the cervicomedullary junction within the foramen magnum (Fig. 5.21) and terminates as the conus medullaris at approximately the L1 vertebral level (Fig. 5.30).

It is composed of 31 segments, eight cervical, 12 thoracic, five lumbar, five sacral and one coccygeal, which is mainly vestigial.

The cord is oval in axial section with several grooves identified on its surface:

- the anterior median fissure (Fig. 5.31) contains the anterior spinal artery

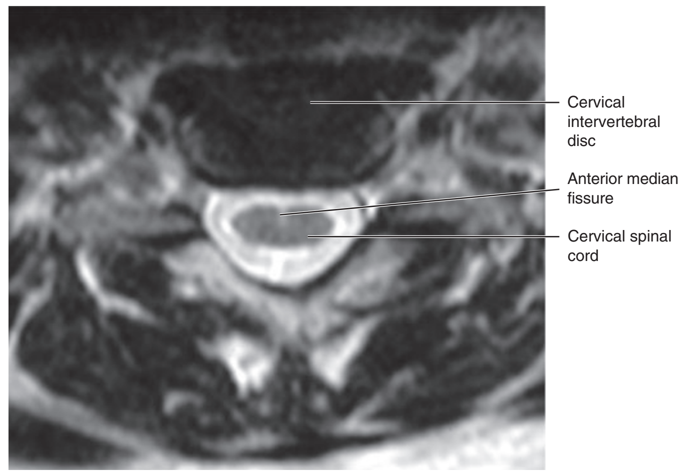


**Fig. 5.31** Axial T2W FSE MRI of the cervical spine.

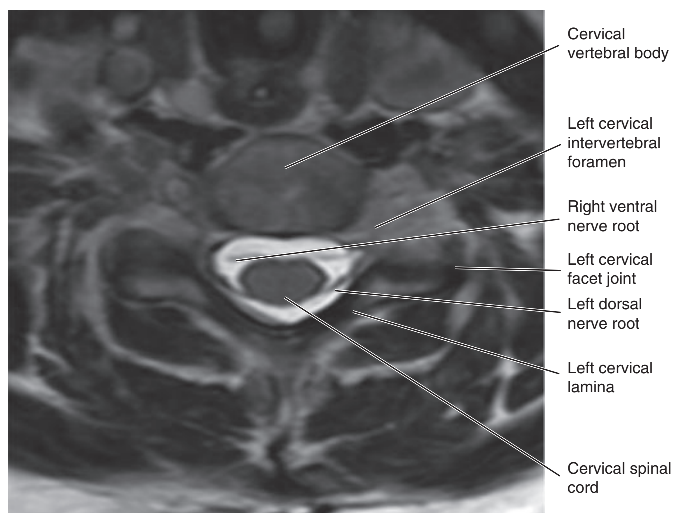


**Fig. 5.32** Axial T2W FSE MRI of the cervical spine.

- the posterior median sulcus is less prominent, while the anterior (ventral) and posterior (dorsal) nerve roots emerge at the anterolateral and posterolateral sulci (Fig. 5.32)
- the outer part of the spinal cord consists of white matter, while the internal part is composed of grey matter (Fig. 5.33)

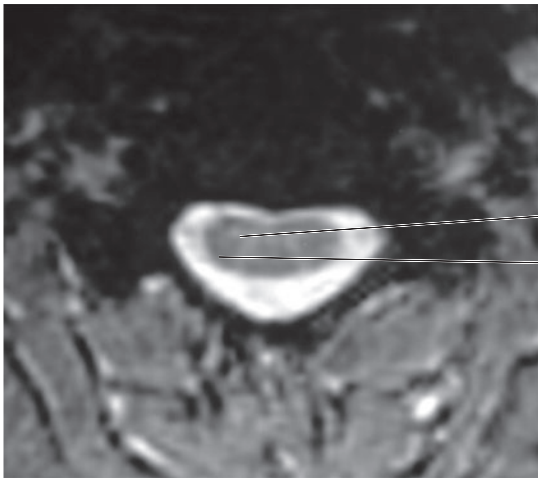


**Fig. 5.33** Axial T2*W GE MRI of the cervical spine.

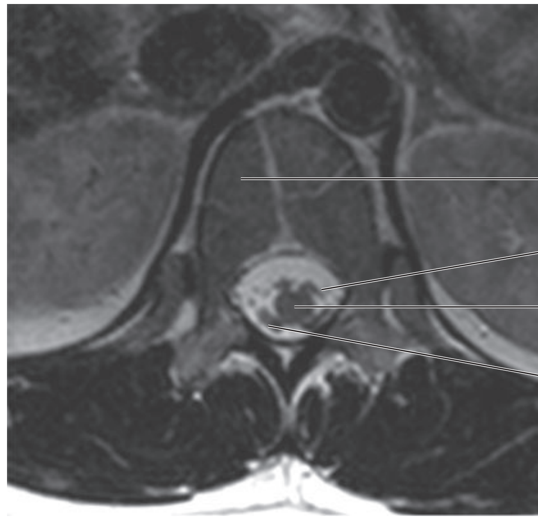


**Fig. 5.34** Axial T2W FSE MRI of the conus medullaris.

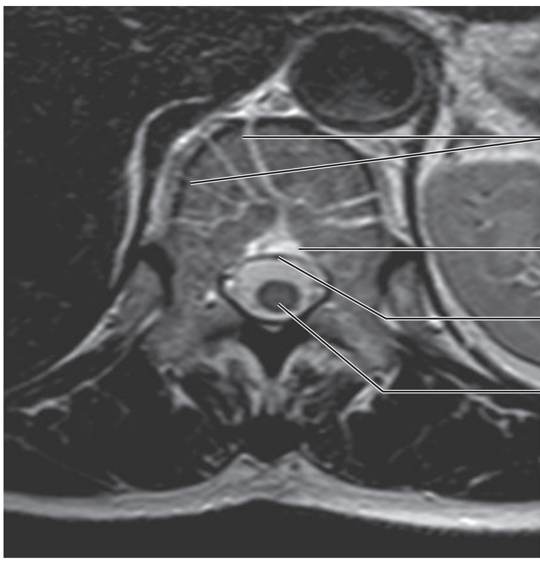


**Fig. 5.35** Axial T2W FSE MRI showing the vertebral veins.

- the midsagittal cord diameter is ~11 mm at C1, 10 mm from C2 to C6 and 7–9 mm below C6, usually occupying ~40% of AP canal diameter.

The blood supply to the cord comprises a complex anastomosis:

- a single anterior spinal artery and paired posterior spinal arteries originate from the vertebral arteries and run the whole length of the cord
- segmental medullary arteries enter the spinal column through the foramina and arise from the vertebral, the posterior intercostal and the lumbar arteries
  - the largest segmental supply is from the artery of Adamkiewicz, which usually arises from a lower left intercostal vessel and supplies the lower two-thirds of the cord.

The pia mater (meningeal covering of the cord) continues caudally through the thecal sac as the filum terminale (Fig. 5.30) and attaches to the coccyx:

- it may normally contain some fat (fatty filum) but should measure <2 mm in transverse dimension.

The cauda equina arises from the conus (Figs. 5.20b, 5.30, 5.34) and represents the intradural lumbar and sacral spinal nerve roots that travel distally prior to exiting at their respective intervertebral foramina.

## The spinal nerves

Each spinal nerve comprises a sensory (dorsal) root, which enters the spinal cord at each level, and a motor (ventral) root, which emerges from the cord at each level (Figs. 5.32, 5.34).

The nerves are numbered according to the level of their emergence from the vertebral canal:

- the C1–7 nerves emerge above their respective pedicles, C8 emerges between C7 and T1, while the remaining nerves emerge below their respective pedicles
- the ventral and dorsal roots combine in the intervertebral foramen to form the dorsal root ganglion (DRG) (Figs. 5.24b, 5.28), from which the mixed spinal nerve arises.

## The spinal venous plexuses

The basivertebral veins are large venous channels within the vertebral bodies that communicate with the internal and external vertebral venous plexuses:

- large vein(s) exit through the posterior cortex of the vertebra (Figs. 5.19, 5.35) and communicate via transverse branches with the anterior internal plexus, which itself communicates with the external vertebral plexus via radicular veins.

## The sacroiliac joints (SIJs)

The SIJs are formed between the sacrum and the iliac blades (Figs. 5.10a, 5.36).

Each joint is divided into a superoposterior ligamentous portion (~1/3) and an anteroinferior synovial portion (~2/3):

- the ligamentous portion is formed by the interosseous sacroiliac ligament

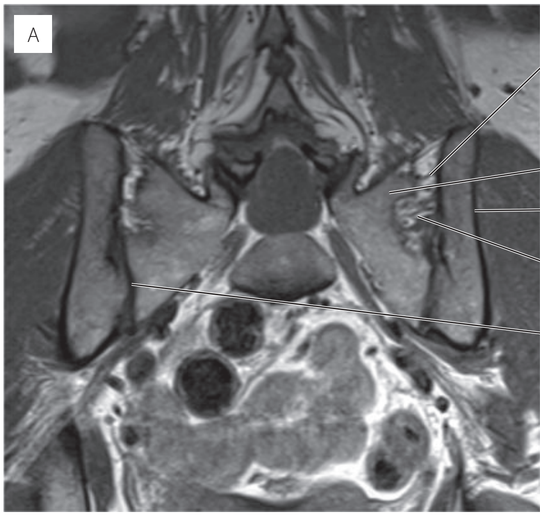


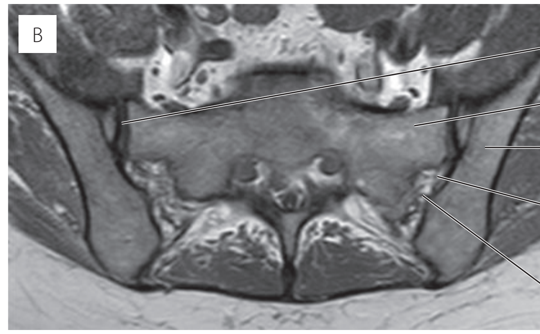


**Fig. 5.36** (A) Coronal T1W SE MRI of the sacroiliac joints. (B) Axial T1W SE MRI of the sacroiliac joints.

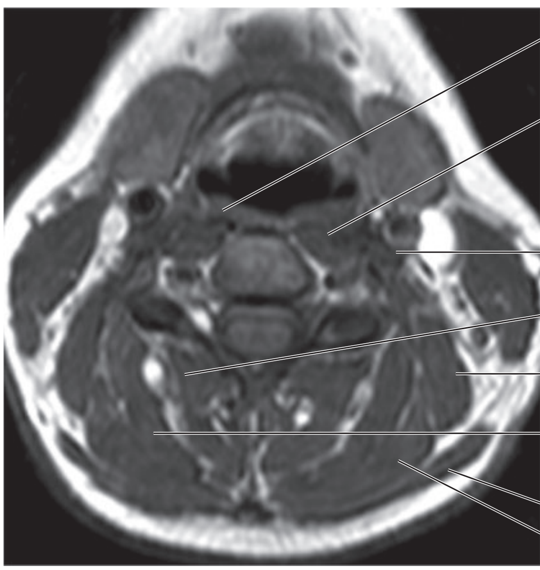


**Fig. 5.37** Axial T1W SE MRI of the cervical muscles.

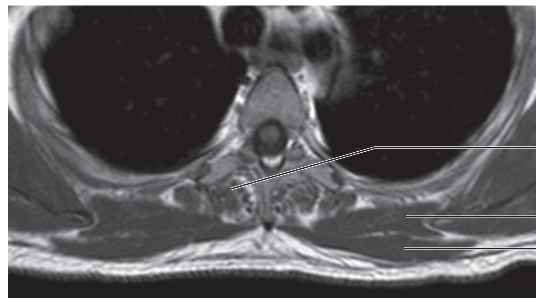


**Fig. 5.38** Axial T1W SE MRI of the thoracic muscles.

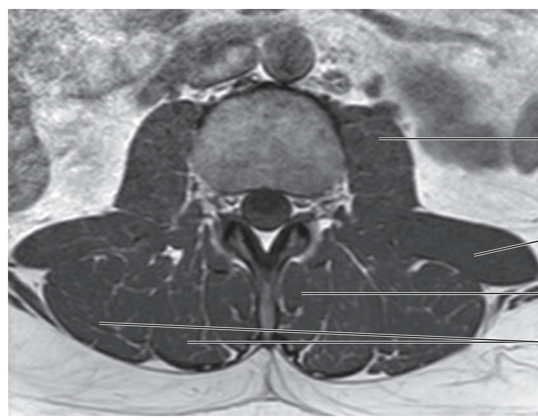


**Fig. 5.39** Axial T1W SE MRI of the lumbar muscles.

- the synovial portion is lined by a combination of hyaline and fibrocartilage, and is further stabilized by the anterior and posterior sacroiliac ligaments.

### The paraspinal musculature

The paraspinal muscles function to provide stability and allow motion between spinal segments.

The cervical paraspinal muscles may be divided into anterior, lateral and posterior groups (Fig. 5.37):

- anterior: longus colli and longus capitis
- lateral: scalenus anterior, medius and posterior
- posterior: levator scapulae, splenius capitis, semispinalis capitis and the cervical portion of erector spinae/multifidus.

The thoracic paraspinal muscles include trapezius, semispinalis thoracis, multifidus and erector spinae (Fig. 5.38).

The thoracolumbar muscles are divided into anterior and posterior (Fig. 5.39):

- anterior: psoas major and occasionally psoas minor
- posterior: multifidus, erector spinae, quadratus lumborum and intertransversarius.

## The brachial plexus

The brachial plexus (BP) represents a network of nerves that originate from ventral rami of the C5–T1 mixed spinal nerves just lateral to the intervertebral foramen:

- it provides motor and sensory innervation to the upper limb.

  The BP is divided into (Fig. 5.40):

- five roots (C5–T1); located between the anterior and middle scalene muscles

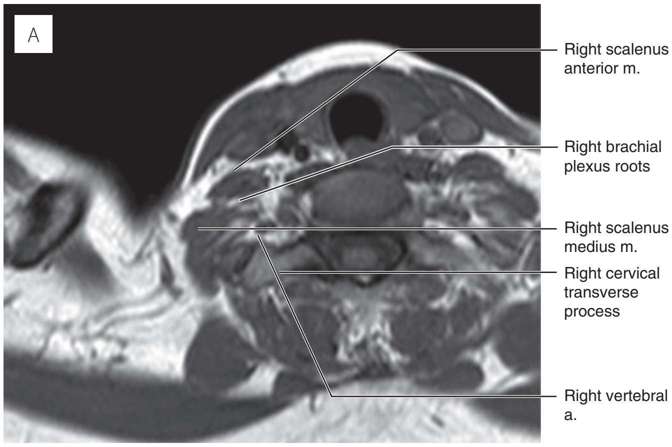


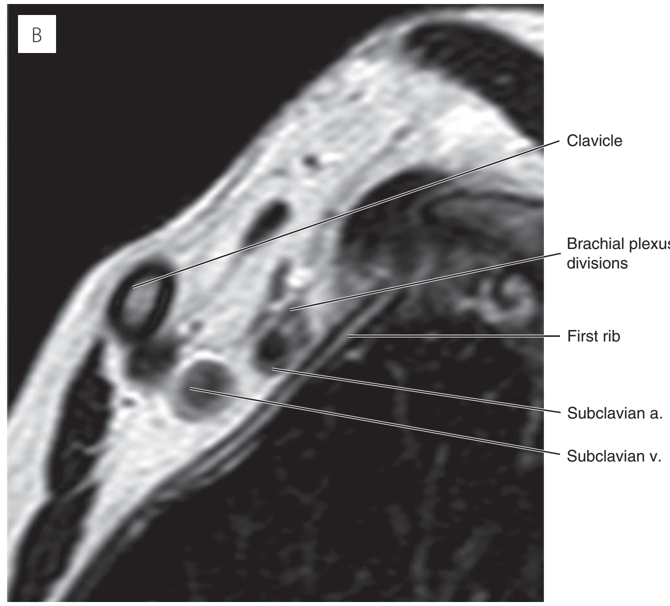


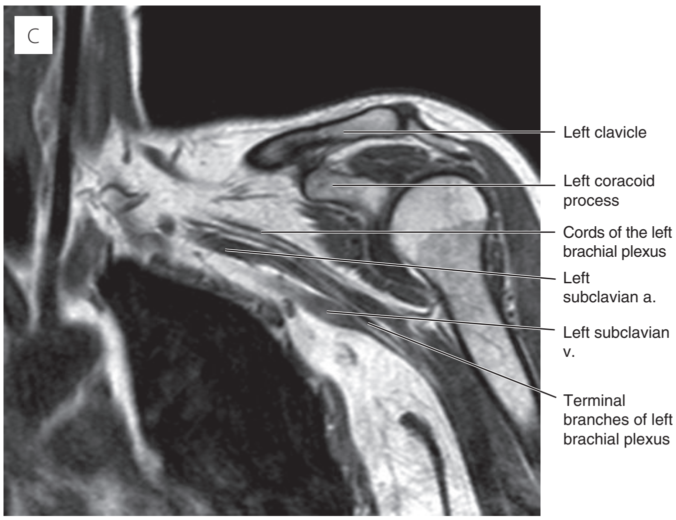


**Fig. 5.40** (A) Axial T1W SE MRI of the supraclavicular right brachial plexus. (B) Sagittal T2W FSE image of the retroclavicular brachial plexus. (C) Coronal T1W SE image of the left infraclavicular brachial plexus.

- three trunks; upper (C5–C6), middle (C7) and lower (C8–T1) originating at the lateral border of the scalene muscles and running in the supraclavicular fossa with the subclavian artery
- six divisions; formed from anterior and posterior bifurcations of each trunk
- three cords; lateral, medial and posterior formed from the divisions and located between the first rib and the coracoid process
- five branches; formed at the lateral border of pectoralis major and being the axillary and radial nerves (posterior cord), the musculocutaneous nerve (lateral cord) and the ulnar and median nerves (medial cord).

The BP may also be classified as supraclavicular (roots and trunks), retroclavicular (divisions) and infraclavicular (cords and terminal branches).

## The lumbosacral plexus

The lumbosacral plexus (LSP) is formed from the ventral rami of the L4–S4 spinal nerves (Fig. 5.41):

- it provides motor and sensory innervation to the lower limb, bladder and bowel.

The L4 and L5 roots combine to form the lumbosacral trunk (LST), which is joined by S1 to form the upper band of the LSP.

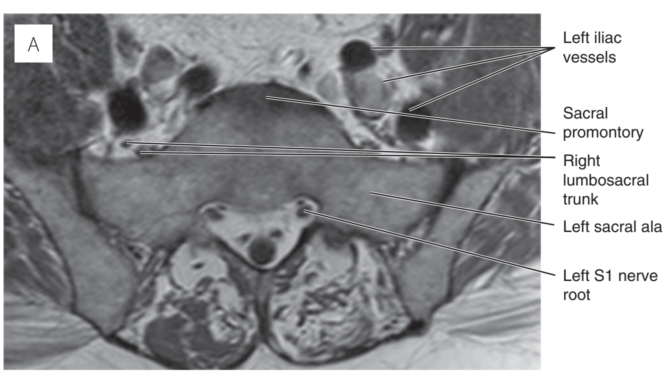


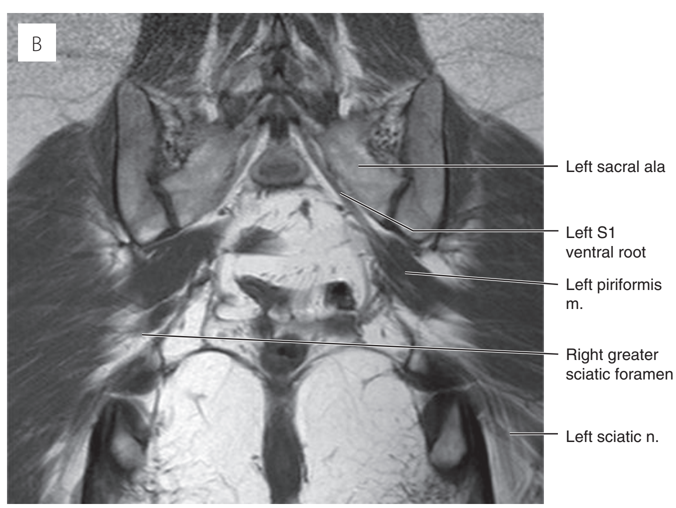


**Fig. 5.41** (A) Axial T1W SE MRI of the lumbosacral trunk. (B) Coronal T1W SE MRI of the left lumbosacral plexus. (C) Axial T1W SE MRI of the right lumbosacral plexus.

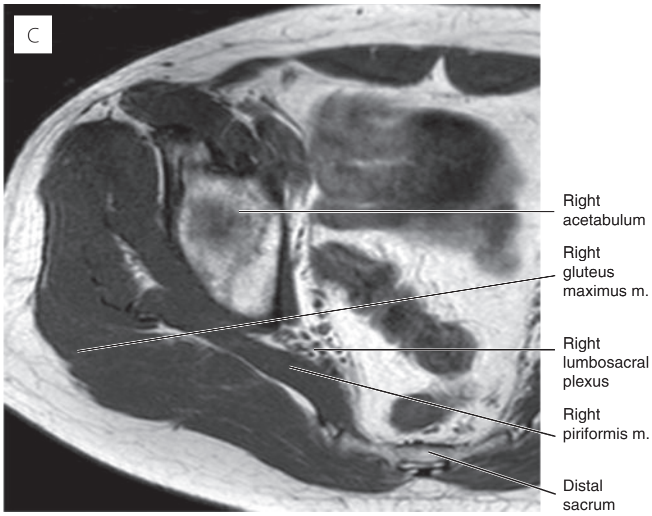


**Fig. 5.41** *(cont.)*

The S2–S4 roots combine to form a smaller lower band.

The LSP splits into anterior and posterior divisions:

- the anterior divisions give rise to the tibial component of the sciatic nerve, the pudendal nerve and the medial part of the posterior femoral cutaneous nerve
- the posterior divisions give rise to the common peroneal component of the sciatic nerve, the gluteal nerves, the lateral part of the posterior femoral cutaneous nerve and nerves to piriformis.

The sciatic nerve exits the pelvic cavity through the greater sciatic foramen.

Chapter 6

# The chest

Sheila Rankin

## Plain radiography

The chest radiograph (CXR) is used for the initial assessment of the lungs, mediastinum and bones.

- Posteroanterior (PA) view – patient upright, on full inspiration with the scapulae moved laterally, so that the lungs are not obscured (Fig. 6.1)
- Lateral view (Fig. 6.2)
- Anteroposterior (AP) view – patient either supine or sitting; on this view there is magnification of the heart and mediastinum and the clavicles obscure the lung apices
- Apical lordotic view – the X-ray beam is angled superiorly 15–20° so the clavicles and first ribs are projected above the lung apices
- Expiration films are used to assess air trapping.

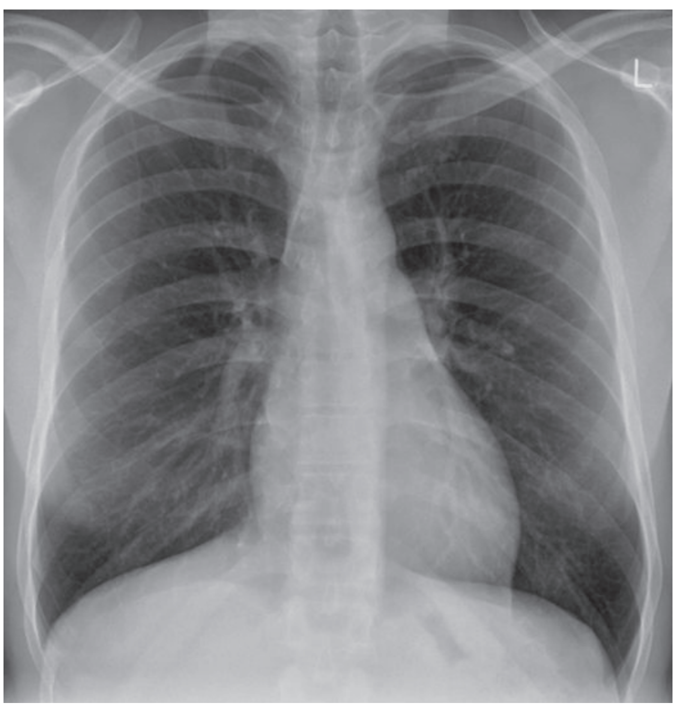


**Fig. 6.1** PA chest X-ray.


**Fig. 6.2** Lateral chest X-ray.

## Cross-sectional imaging

### Computed tomography (CT)

CT provides improved spatial resolution because of lack of overlap of structures. The use of intravenous contrast medium improves the demonstration of vessels.

Multidetector CT produces excellent multi planar reformats and other post-processing can be undertaken (Fig. 6.3).

The data are viewed at different windows and levels for air and soft tissue.

Air-containing structures:

- WW 1500 HU
- WL −600 HU.

Soft tissues and vessels:

- WW 300–500 HU
- WL 30–50 HU.

*Applied Radiological Anatomy, 2nd Edition* ed. Paul Butler, Adam W.M. Mitchell and Jeremiah C. Healy. Published by Cambridge University Press.


Fig. 6.3 Volume rendered CT scan.

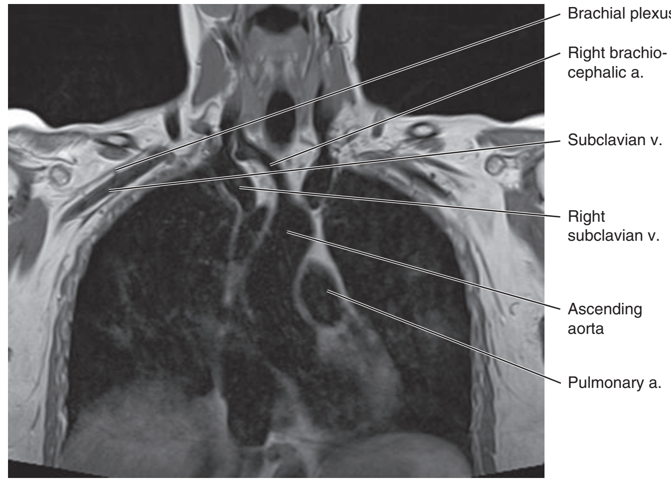

Fig. 6.4 Coronal MRI.

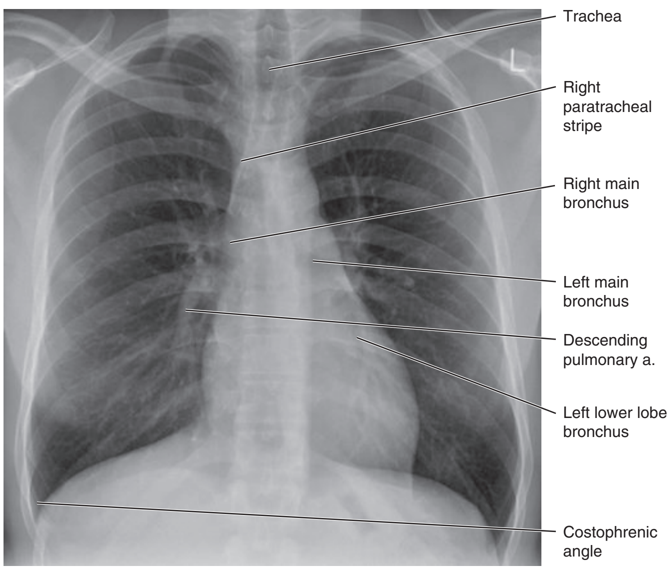

Fig. 6.5 PA chest X-ray.

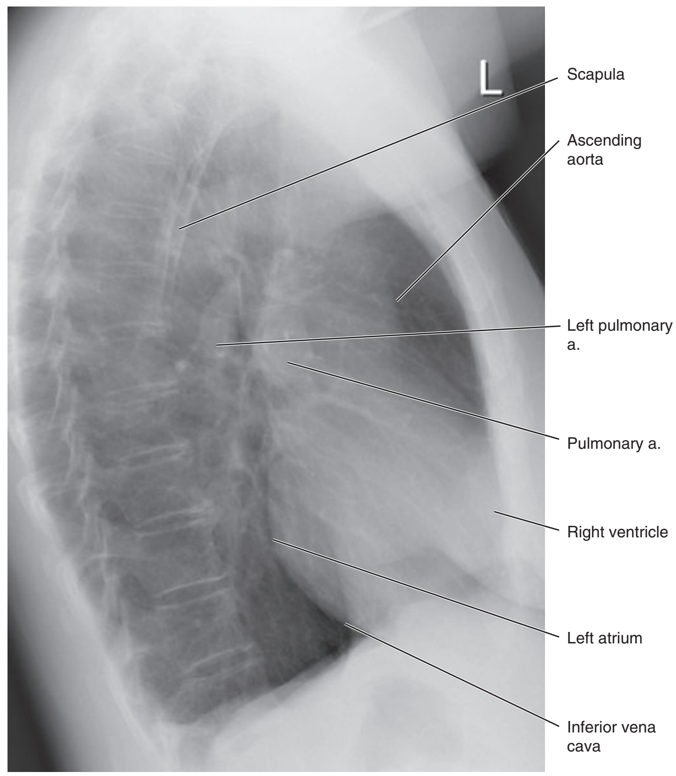

Fig. 6.6 Lateral chest X-ray.

High-resolution CT (HRCT) is used mainly to assess diffuse lung disease. Thin sections minimize partial volume effects and the high-resolution reconstruction algorithm provides edge enhancement.

## MRI

MRI provides excellent contrast resolution and increased soft tissue resolution. It is valuable for assessing the heart, mediastinum, hilar, diaphragm and chest wall (Fig. 6.4).

### Chest

The chest consists of the bony skeleton of the spine and ribs, the chest wall and diaphragm, the mediastinum and great vessels, the airways, lung parenchyma and pulmonary vessels (Figs. 6.5, 6.6).

### Bony thorax

Consists of the thoracic spine, ribs, sternum and clavicle.

### Thoracic spine

Consists of 12 vertebrae:

- body with facets for articulation of the ribs on the lateral aspect
- neural arch surrounding vertebral canal, made up of a pedicle and lamina on each side, a posterior spinous process and bilateral transverse processes, which have a

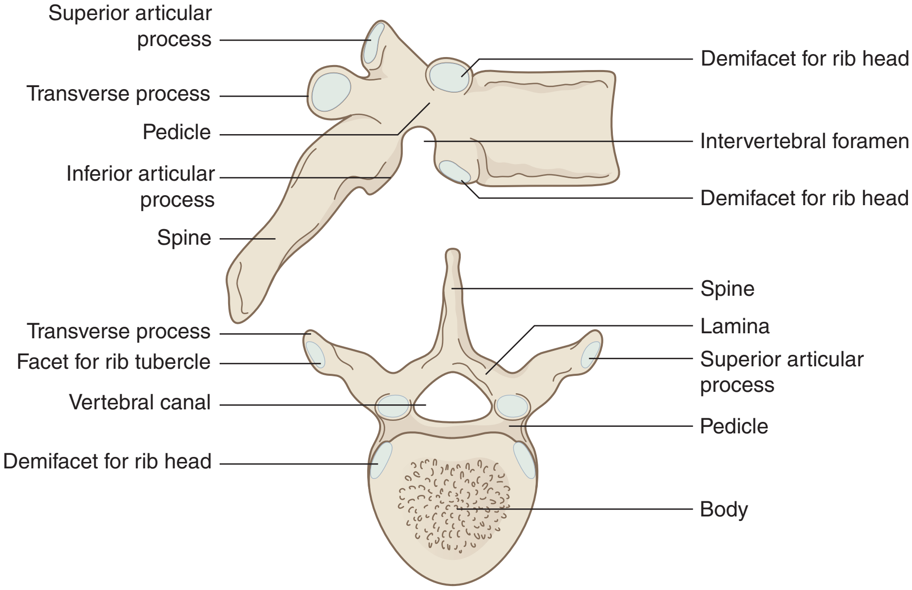


**Fig. 6.7** Thoracic spine (line drawing).

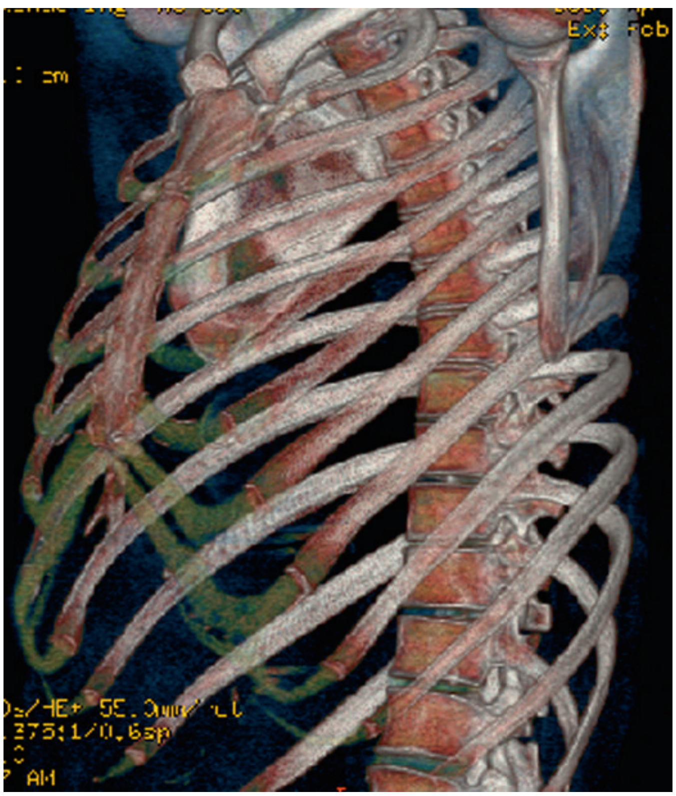

**Fig. 6.8** VR CT demonstrating the ribs.

facet for articulating with the tubercles of the ribs (except T11 and 12). The pedicle forms the intervertebral foramen with its adjacent vertebra and the nerve root pair exit caudad to the corresponding vertebra (Fig. 6.7).

### Ribs

There are twelve pairs of ribs (Fig. 6.8). The first seven are connected to the sternum by costal cartilage, the 8th, 9th and 10th articulate with ribs above and the 11th and 12th are free anteriorly.

Each rib consists of:

- a head with two facets articulating with its corresponding vertebra and the one above
- a neck for attachment of the costo-transverse ligament
- a tubercle with a smooth facet for articulation with the transverse process of its vertebral body and a rough non-articulating process; the 11th and 12th ribs have no tubercle
- a long shaft divided into two parts by the angle, which is the lateral limit of the attachment of the erector spinae muscle.

The first rib is the shortest, with a prominent tubercle for the attachment of the scalenus anterior. The subclavian vein runs anterior to the tubercle and the subclavian artery and lowest trunk of the brachial plexus run in a groove posteriorly (Fig. 6.9).

- a cervical rib occurs in 0.5% of people and is bilateral in 50%. It is attached to C7 and articulates with the first rib.

### Sternum

Consists of:

- manubrium – provides articulation for clavicles 1st and upper part of 2nd ribs
- body – consists of four parts, which fuse by the age of 25 and articulate with 2nd–7th costal cartilages; the junction of the body with the manubrium (angle of Louis) is at T4/5
- xiphoid process – often remains cartilaginous (Fig. 6.10).

### Clavicle

- articulated medially with the manubrium at the sterno-clavicular joint
- articulated laterally with the acromion at the acromio-clavicular joint and also attached to the coracoid process
- subclavian vessels and trunks of brachial plexus pass behind the medial third

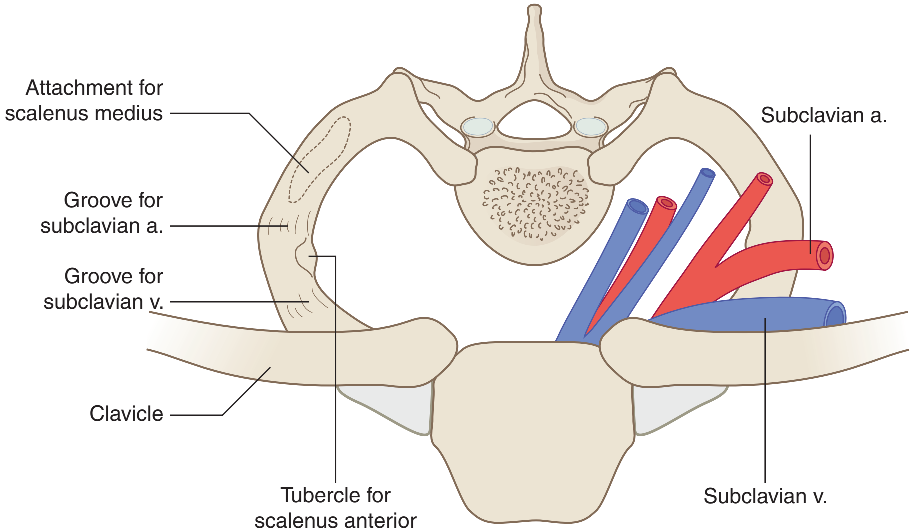


Fig. 6.9 Line drawing of the first ribs.

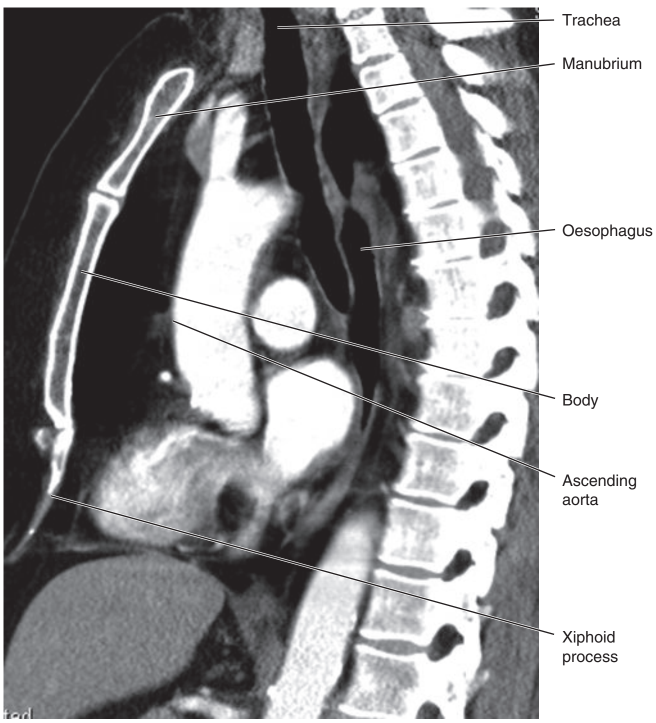


Fig. 6.10 Midline sagittal MPR of thoracic CT.

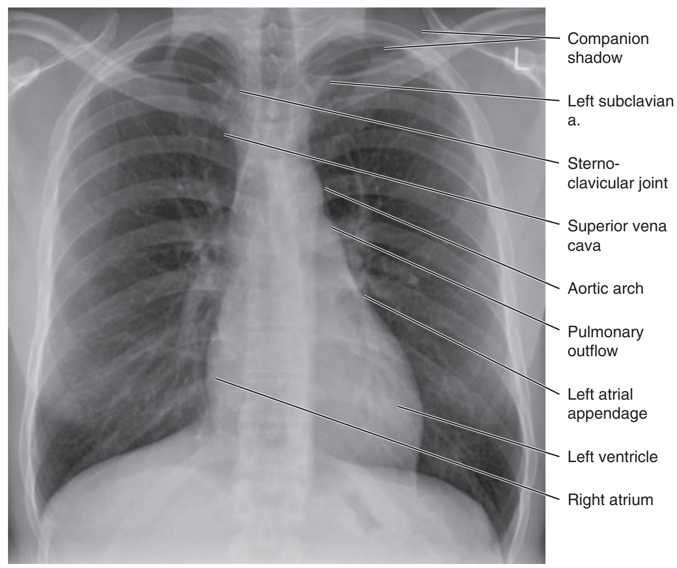


Fig. 6.11 PA chest X-ray.

- on a CXR a soft tissue companion shadow lies above the clavicle (Fig. 6.11).

### Chest wall and diaphragm

The chest wall consists of:

- ribs
- intercostal spaces containing
  - external intercostals
  - internal intercostals
  - innermost intercostals, which is separated from the internal intercostals by
  - neurovascular bundle with the vein lying in a groove on the under surface of the corresponding rib and the artery and nerve lying more inferiorly (Fig. 6.12).
- The posterior intercostal arteries of the lower nine spaces arise from the descending thoracic artery arrow (Fig. 6.13), the first two from the costo-cervical trunk (branch of subclavian artery), the anterior intercostals arise from the internal thoracic artery.
- Intercostal veins drain into azygous and hemiazygous veins, except 1st on right drains into vertebral or brachiocephalic vein and 2nd and 3rd on left form the superior intercostal vein, which crosses the aortic arch to drain into left brachiocephalic vein arrow (Fig. 6.14).

### Diaphragm

Separates the thorax from the abdomen. It consists of

- a peripheral muscular part arising from margins of thoracic outlet
- right crus arises from the front of vertebral bodies of L1–3

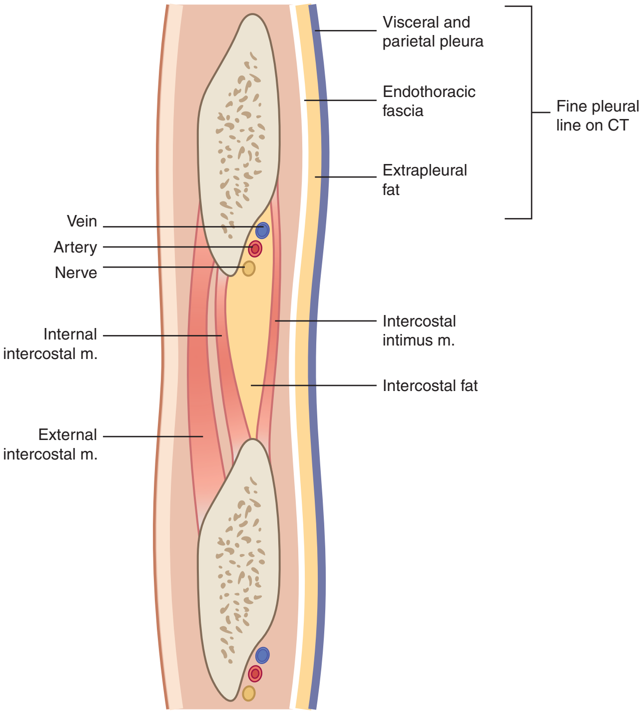


**Fig. 6.12** Line drawing of chest wall.

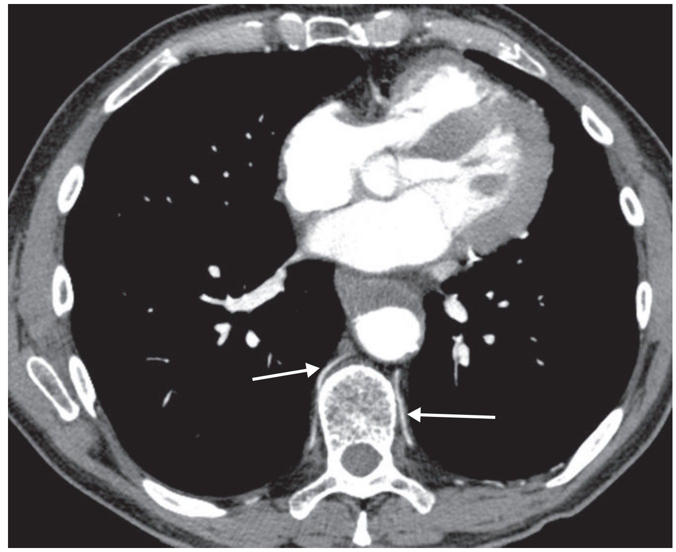

**Fig. 6.13** Axial CT of posterior intercostal arteries (arrows).

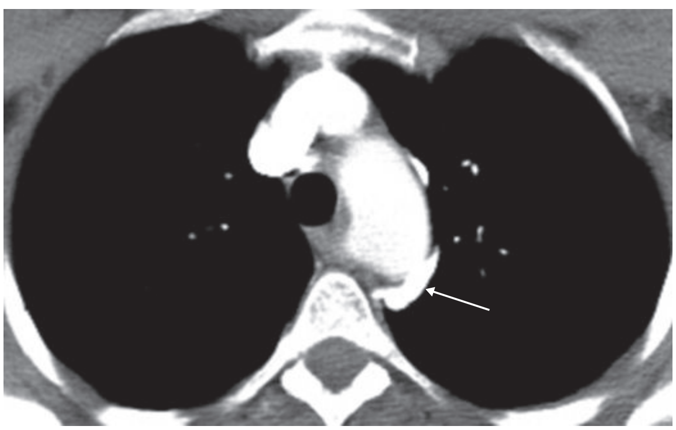

**Fig. 6.14** Axial CT of superior left intercostal vein (arrow).

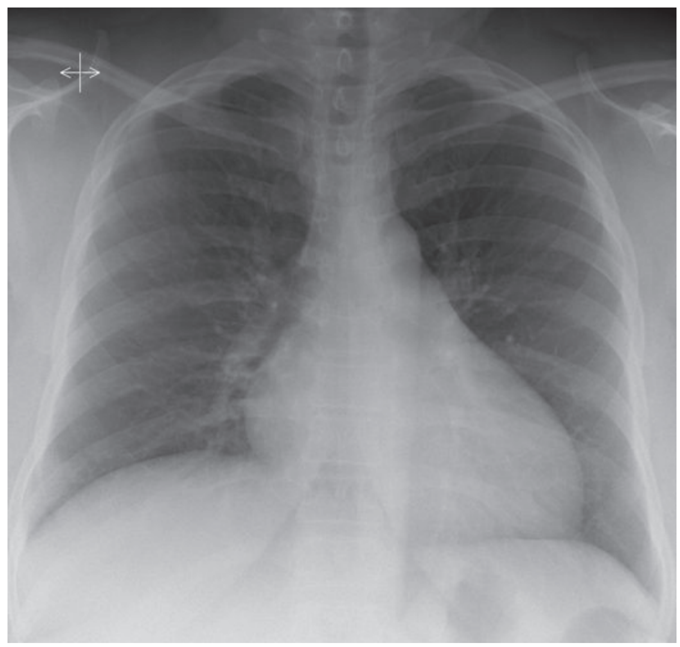

**Fig. 6.15** PA chest, right hemidiaphragm higher than the left.

- left crus from vertebral bodies of L1–2
- arcuate ligament from the fascia of the psoas and quadratus lumborum
- attachments to the lower 6th ribs and sternum
- central tendon, which is partly fused to the pericardium.

There are three main openings:

- aortic – (T12) – transmitting the aorta, thoracic duct and azygous vein
- oesophageal (T10) – oesophagus, left gastric artery and vein and vagus
- vena cava (T8) – inferior vena cava and right phrenic.

The right hemidiaphragm is usually 1–1.5 cm higher than the left, but may be at the same level. On a lateral film the gastric air bubble is below the left hemidiaphragm and the anterior portion is not seen as it is silhouetted by the heart (Figs. 6.15–6.18).

## Airways

The airways consist of the trachea, bronchi, bronchioles and distal small airways.

### Trachea

- 9–12 cm in length. It commences at the level of the cricoid (C6) and bifurcates at the carina (T5), passing from the midline to the right (Figs. 6.5, 6.19)
- The intrathoracic portion measures 6–9 cm
- The transverse diameter is 10–21 mm in women and 13–25 mm in men, the sagittal diameter 10–23 mm in women and 13–27 mm in men
- There are 12–16 incomplete cartilaginous rings. The posterior wall is fibrous tissue. Rings may calcify in older people


**Fig. 6.16** Lateral chest X-ray.

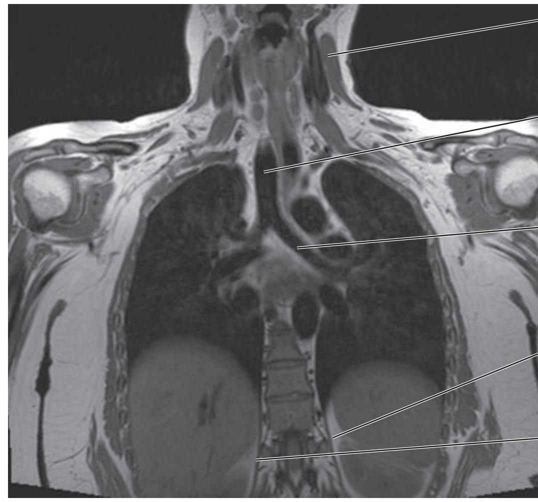


**Fig. 6.17** Coronal MRI.

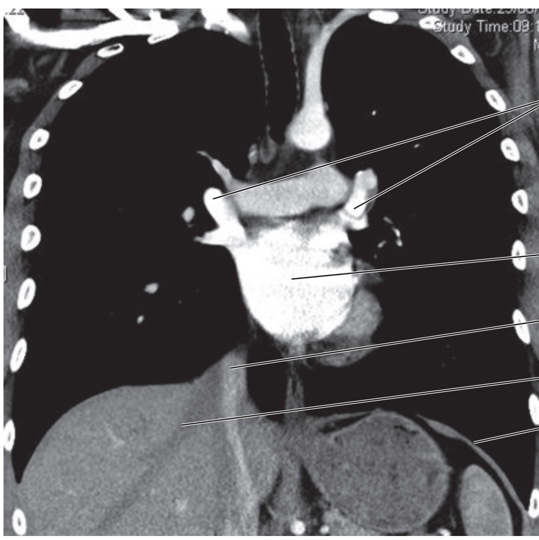


**Fig. 6.18** Coronal MPR CT.

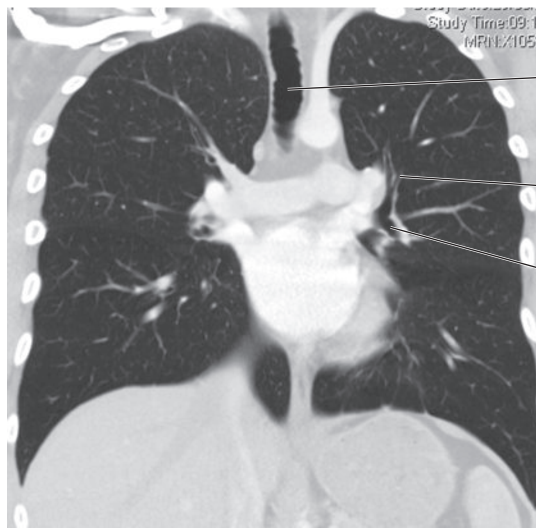


**Fig. 6.19** Coronal MPR CT.

- On CT the membranous posterior wall bows out on inspiration and flattens and bows inwards on expiration
- Extrathoracic trachea diameter varies markedly on forced inspiration and expiration (upto 35%).

### Bronchi

The trachea divides into the main bronchi at the carina.

- Right main bronchus:
  - shorter and more vertically oriented (Fig. 6.20)
  - 2.5 cm long and passes to the root of the lung at T5
  - gives rise to the right upper lobe bronchus and lies inferolateral and posterior to the main pulmonary artery

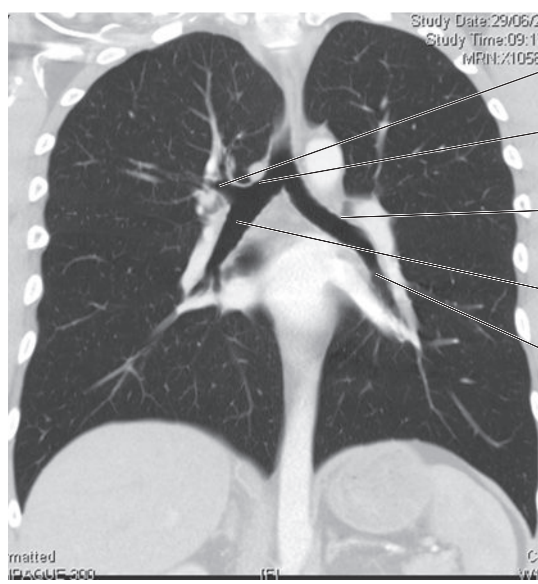


**Fig. 6.20** Coronal MPR CT.

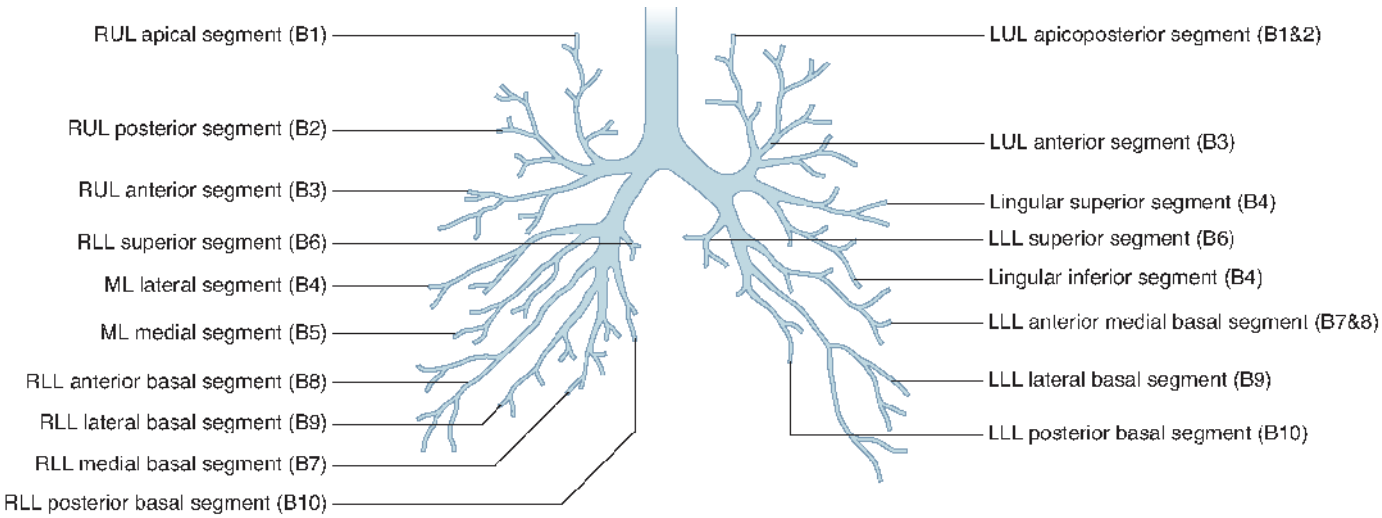


**Fig. 6.21** Line drawing of bronchial tree.

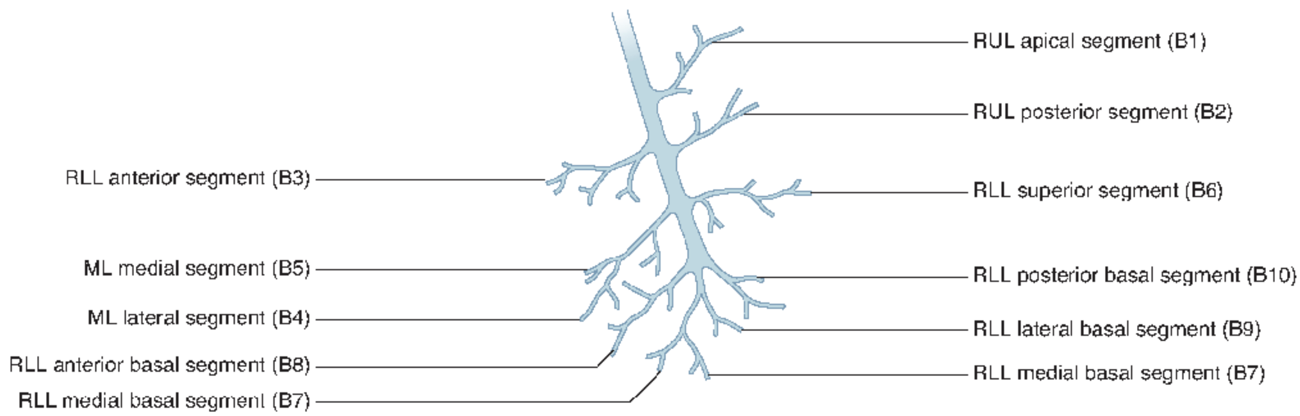


**Fig. 6.22** Line drawing of bronchial tree right lung.

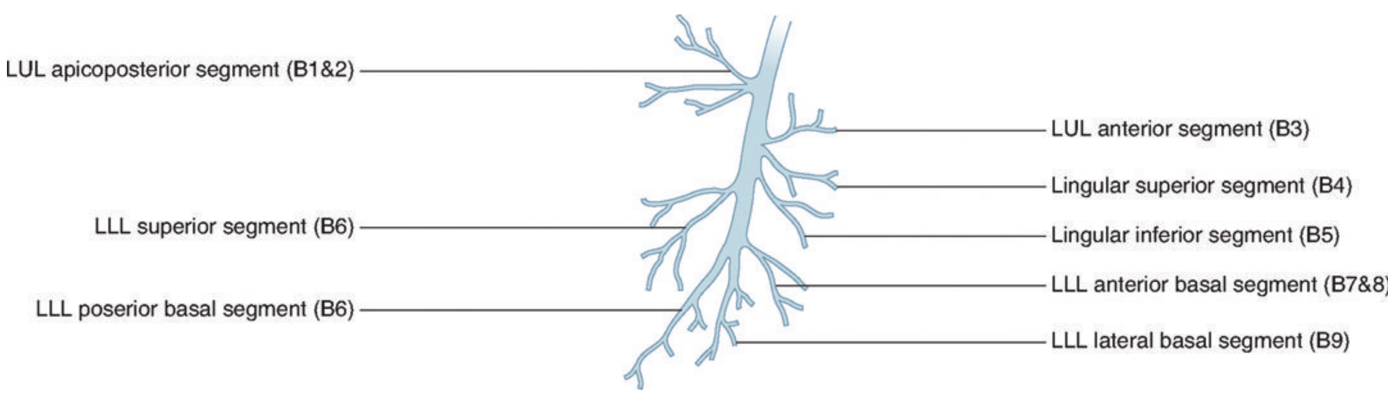


**Fig. 6.23** Line drawing of bronchial tree left lung.

  - posterior wall is <3 mm thick and is in contact with the lung
  - enters the hilum of the lung and continues as the bronchus intermedius, which courses obliquely for 3–4 cm and lies posterior to the right pulmonary artery.
- Left main bronchus:
  - longer and more horizontal (Fig. 6.20)
  - almost 5 cm long and courses below the arch of the aorta
  - enters the hilum at T6 and then courses inferolaterally to the pulmonary artery.
- Accessory tracheal bronchi:
  - pig bronchus – an upper lobe or segmental bronchus arising from the right lateral tracheal wall; occurs in 1–2%
  - accessory cardiac bronchus – a blind-ending bronchus arising from the right main bronchus or bronchus

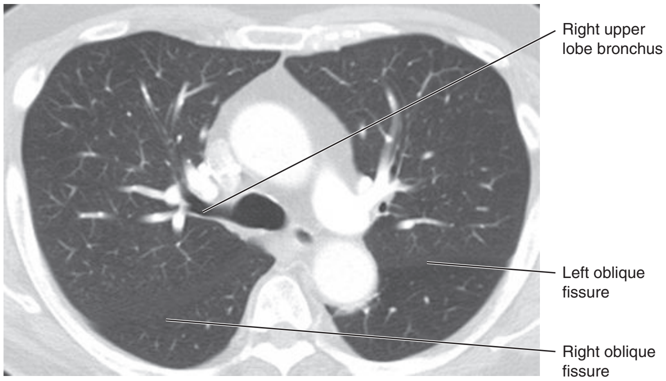


**Fig. 6.24** Axial CT of right upper lobe bronchus.

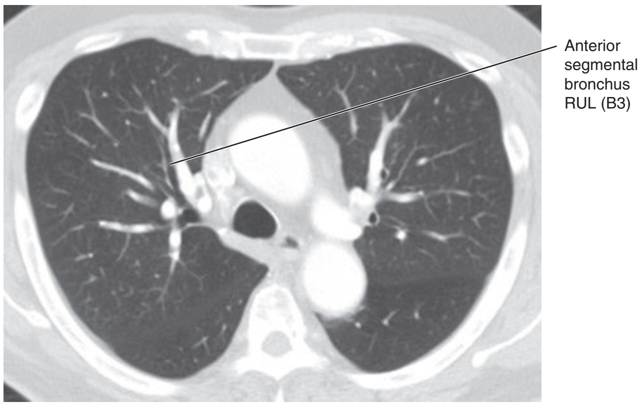


**Fig. 6.26** Axial CT through anterior segmental bronchus RUL (B3) (arrow).

intermedius which courses towards the heart; very rare, occurs in 0.5%.

The lobes of the lung are subdivided into broncho-pulmonary segments, which are supplied by segmental bronchi, arteries and veins. The segmental bronchi are named or numbered (using the Boyden system; 1961) (Figs. 6.21–6.23).

- Right upper lobe bronchus (Fig. 6.24):
  - apical (B1)
  - posterior (B2) (Fig. 6.25)
  - anterior (B3) (Fig. 6.26).
- Right middle lobe bronchus, which courses obliquely anteromedially and caudally and divides into:
  - lateral (B4) – more horizontal
  - medial (B5).

These segmental bronchi are equal in size in 50%, otherwise the medial is larger than the lateral (Fig. 6.27).

- Right lower lobe bronchus (Fig. 6.28):
  - apical (superior) (B6)
  - medial basal (B7)
  - anterior basal (B8)
  - lateral basal (B9)
  - posterior basal (B10).

The apical bronchus arises opposite the right middle lobe bronchus origin (Fig. 6.27).

On CT these are arranged MALP (anticlockwise).

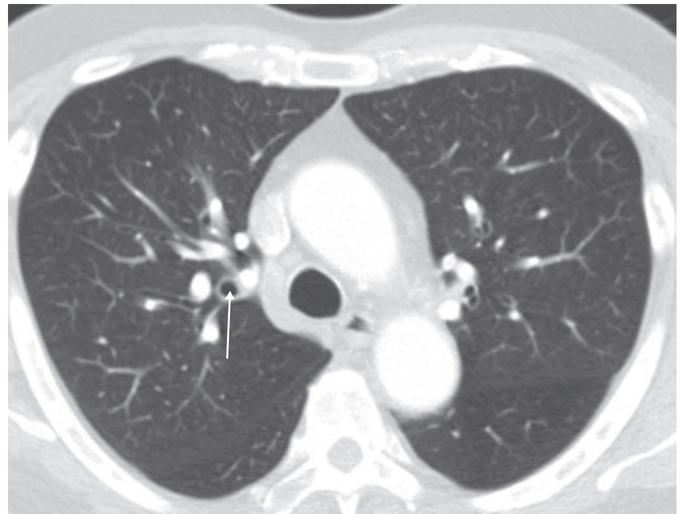

**Fig. 6.25** Axial CT through posterior segmental bronchus RUL (B2) (arrow).

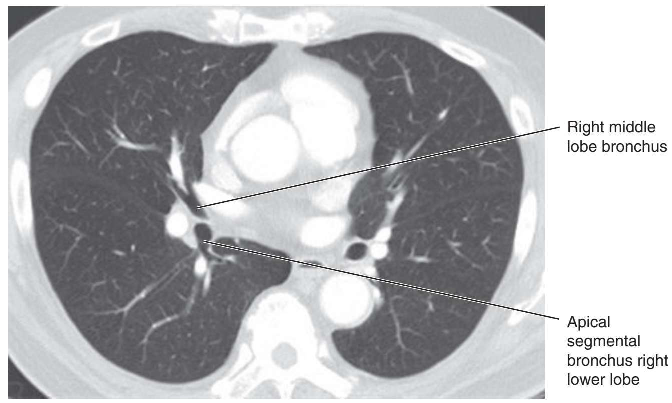


**Fig. 6.27** Axial CT through RML bronchus.

- Left upper lobe bronchus
  - apico-posterior (B1 + B2) (Fig. 6.29)
  - anterior (B3)
  - lingular – superior (B4) (Fig. 6.30)
  - inferior (B5)
- Left lower lobe bronchus
  - apical (superior) (B6) (Fig. 6.31)
  - anteromedial basal (B7 + 8) (Fig. 6.32)
  - lateral basal (B9)
  - posterior basal (B10)

The segmental bronchi divide into smaller airways (6–20 divisions), become bronchioles and divide until the terminal bronchiole and the acinus (Fig. 6.33).

- Acinus
  - 6–10 mm and contains a respiratory bronchiole, alveolar duct, sac and alveoli; not seen on CT
  - up to 24 group to form the secondary pulmonary lobule.
- Secondary pulmonary lobule
  - smallest discrete unit – 1–2.5 cm in diameter, polyhedron shape

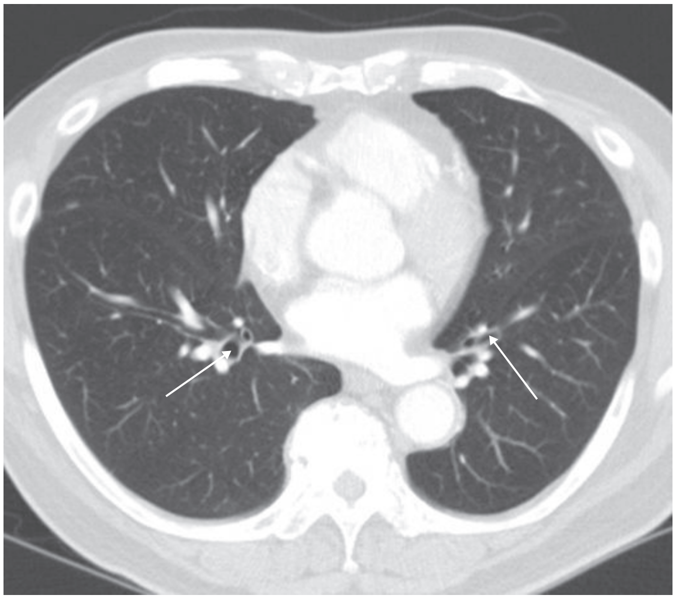

**Fig. 6.28** Axial CT through lower lobe segmental bronchi (arrows).

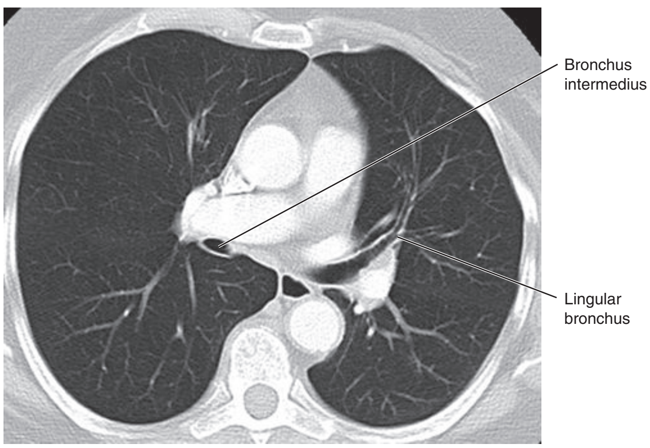


**Fig. 6.30** Axial CT of left upper lobe bronchus, lingular – superior.

- supplied by a lobular bronchiole, artery and vein
- marginated by interlobular septae
- not usually seen on CT; on HRCT can see lobular bronchiole and interlobular septae (Fig. 6.34).

**Lobar anatomy (Fig. 6.35)**

The right lung is larger than the left and has 3 lobes; the left lung has 2 lobes. There are 10 segments in the right lung and 8 in the left and they are named after the bronchi.

- Right upper lobe – three segments:
  - apical
  - posterior – abuts the superior oblique fissure and the posteromedial horizontal fissure
  - anterior – abuts the horizontal fissure, the anterior lateral costal margin and the mid anterior mediastinum.
- Right middle lobe – two segments
  - medial – abuts the right heart border
  - lateral – abuts the oblique fissure and the horizontal fissure.

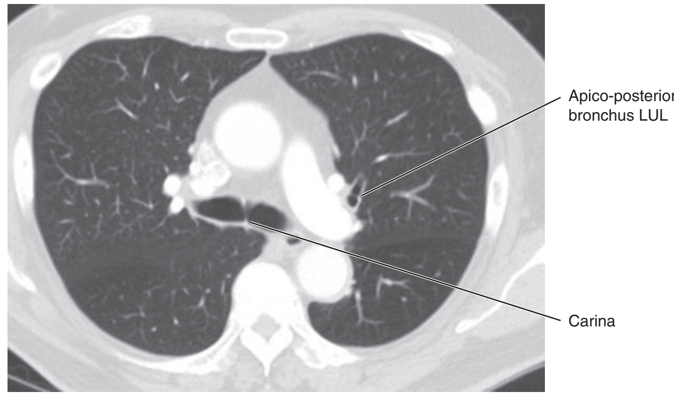


**Fig. 6.29** Axial CT through carina, left upper lobe bronchus.

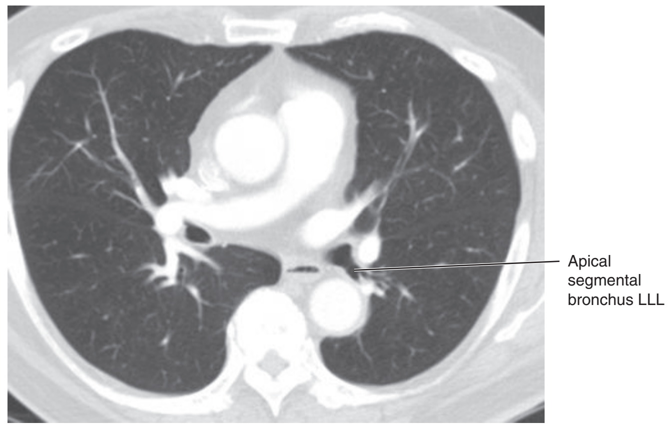


**Fig. 6.31** Axial CT through apical segmental bronchus LLL (B6) (arrow).

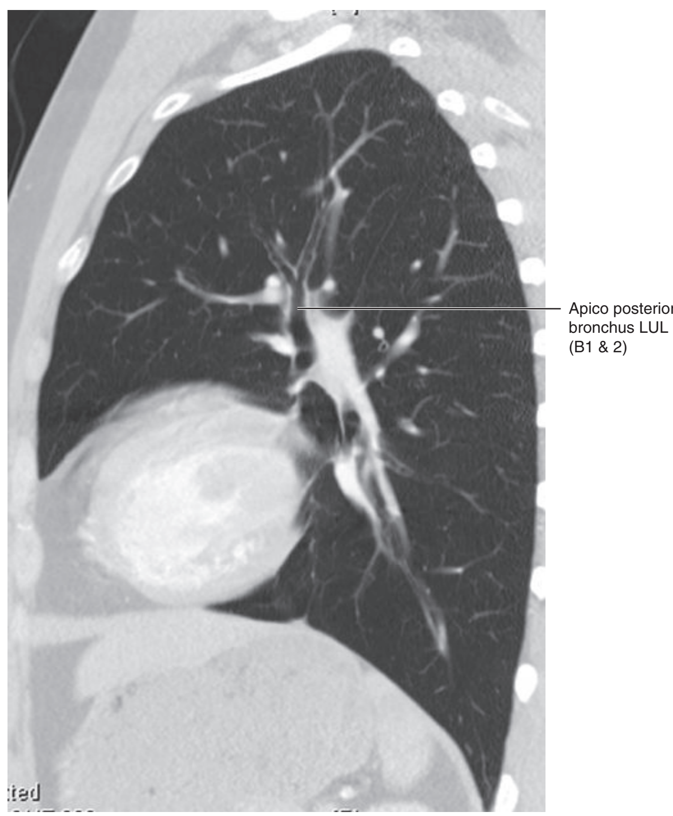


**Fig. 6.32** Sagittal CT of left lower lobe bronchus, anteromedial basal.

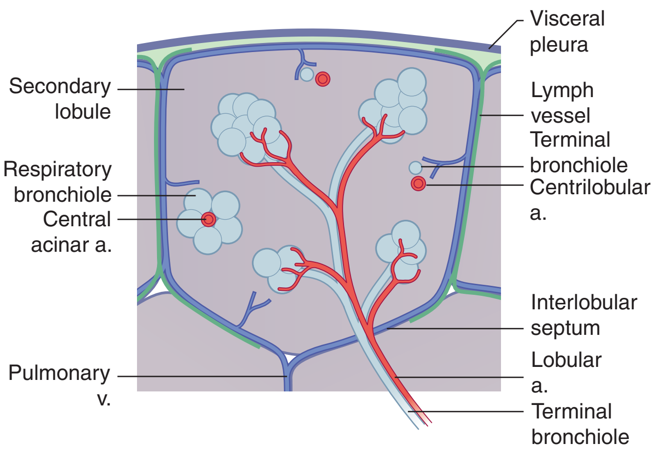


**Fig. 6.33** Line drawing of secondary lobules.

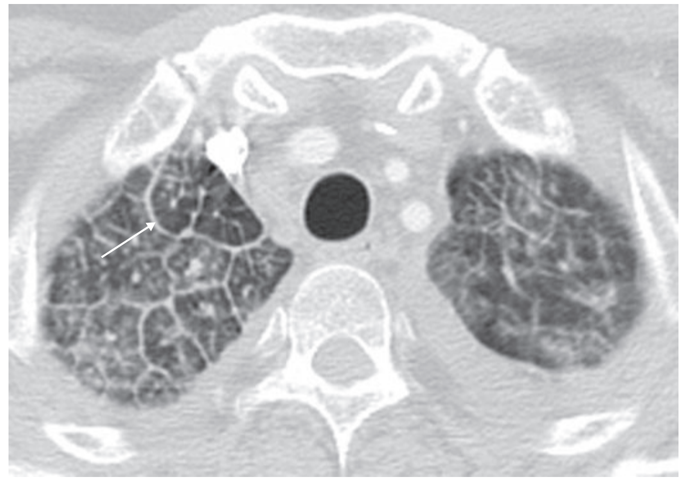

**Fig. 6.34** CT of interlobular septae (arrow).

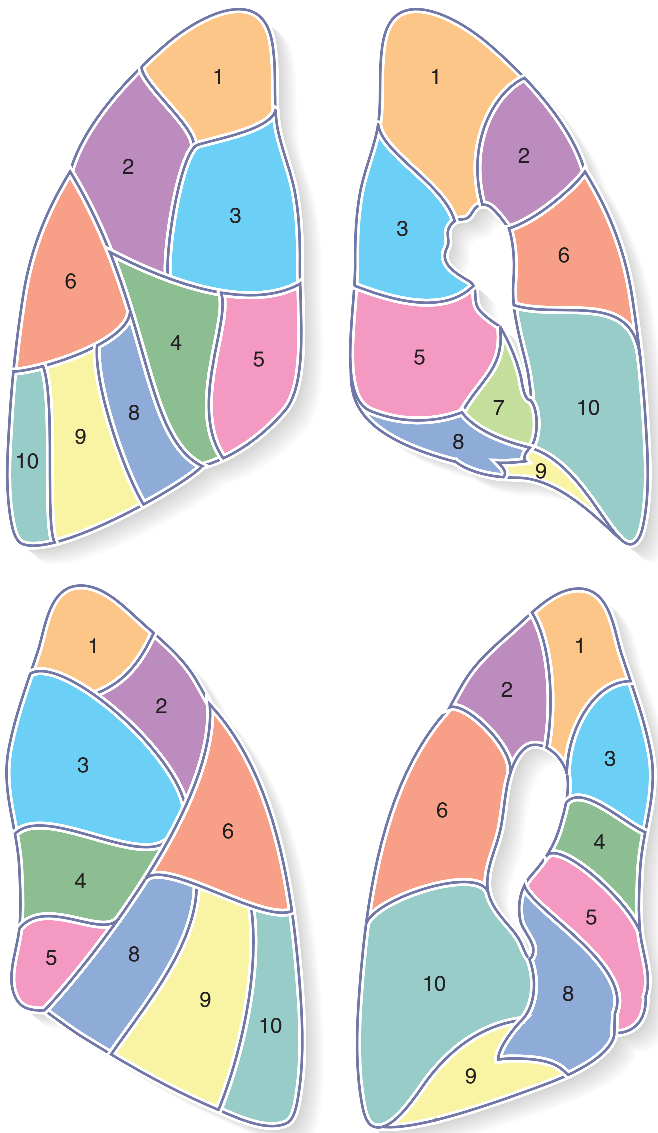


**Fig. 6.35** Line drawing of lobar anatomy.

- Right lower lobe – five segments
  - superior
  - medial basal
  - anterior basal
  - lateral basal
  - posterior basal.

Basal segments abut the right hemidiaphragm.

- Left upper lobe – four segments
  - apico-posterior
  - anterior.

Abuts the superior mediastinum.

- lingula – superior
- inferior.

Abuts the left heart border.

- Left lower lobe – four segments
  - superior
  - anterior basal
  - lateral basal
  - posterior basal.

Abuts the descending aorta (superior and/or posterior basal) and the left hemidiaphragm.

## Pulmonary vessels

### Pulmonary artery

The main pulmonary trunk arises from the right ventricle and divides into a short left pulmonary artery and a longer right pulmonary artery (Fig. 6.36).

The right pulmonary artery runs between the superior vena cava and the right main stem bronchus and divides into

- upper truncus arteriosus which supplies the RUL and lies medial to the bronchus (Figs. 6.37, 6.38)
- descending interlobar artery supplying the RML and RLL and lies lateral to the bronchus.

The left pulmonary artery arches over the left main bronchus and gives rise to

- an ascending branch to the left upper lobe which lies medial to the bronchus – this may arise directly from the main

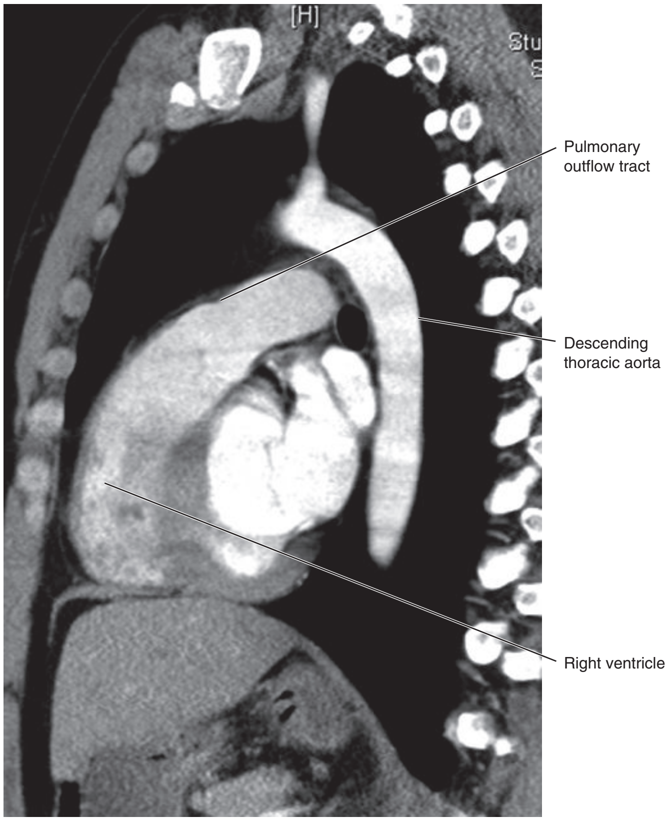


**Fig. 6.36** Sagittal CT of pulmonary artery.

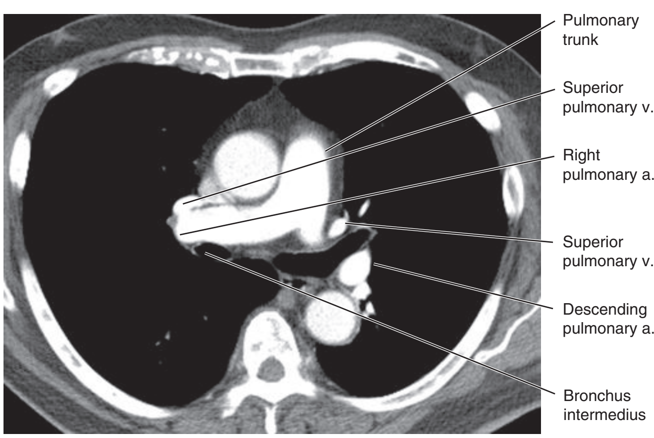


**Fig. 6.38** Axial CT of upper truncus arteriosus.

pulmonary artery or arise from the descending pulmonary artery (Fig. 6.39)

- a descending or interlobar artery to the lingula and left lower lobe lying lateral to the bronchus.

On a CXR:

- the pulmonary trunk is prominent in people less than 25 years old
- the right descending interlobar artery measures up to 15.5 mm in women and 16 mm in men.

On a CT scan:

- the upper limit of normal for the pulmonary trunk is 29 mm, the right pulmonary artery 24 mm, the left pulmonary artery 28 mm and the interlobar arteries up to 16.8 mm.

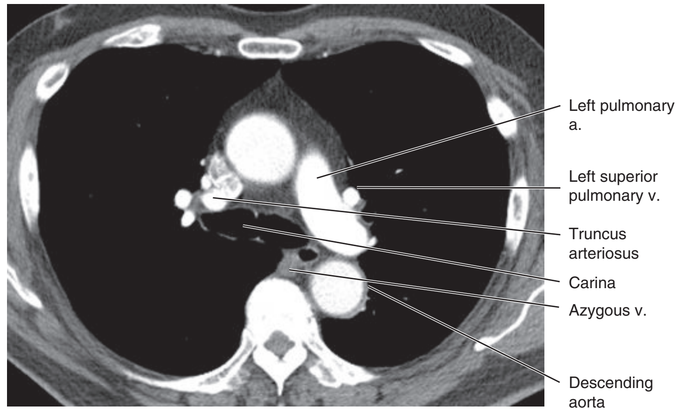


**Fig. 6.37** Axial CT of upper truncus arteriosus.

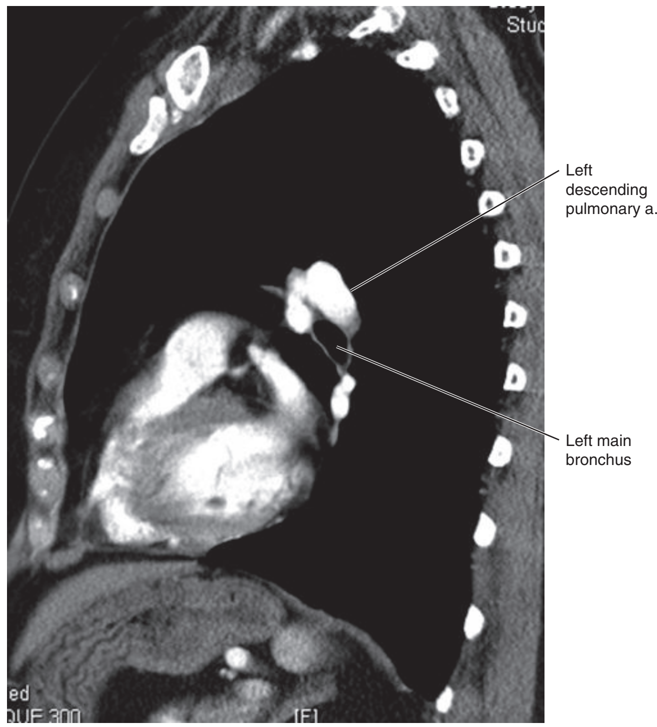


**Fig. 6.39** Sagittal CT of ascending branch.

**Pulmonary veins (Figs. 6.40–6.42, 6.18)**

There are two pairs of veins – superior and inferior veins – on each side in 70% of people.

- Right side

There may be three veins:

  - descending superior and middle lobe veins drain into the superior confluence of the left atrium
  - the inferior vein runs horizontally into the inferior confluence.

- Left side

There are two veins:

- superior pulmonary vein drains the upper lobe including the lingula
- inferior pulmonary vein drains the lower lobe.

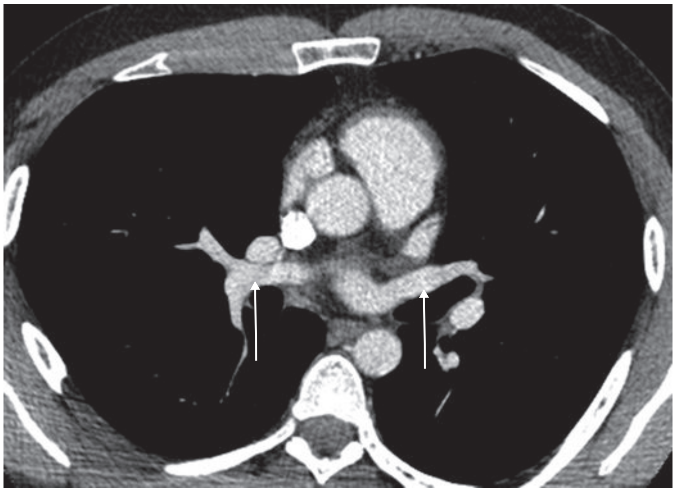

Fig. 6.40 Axial CT through superior pulmonary veins (arrows).

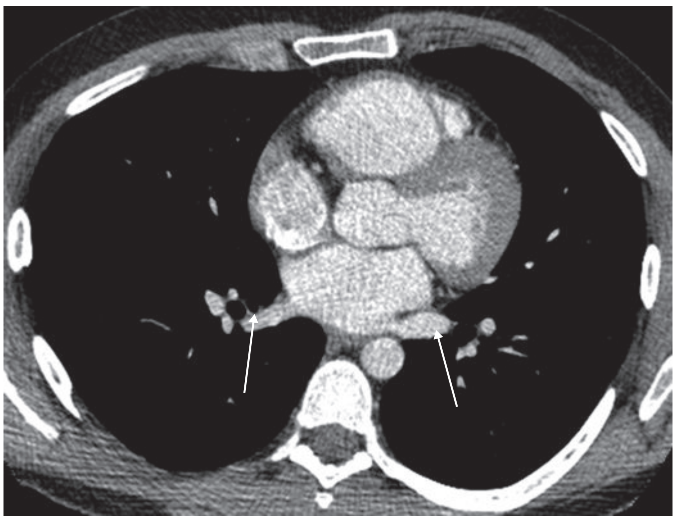

Fig. 6.42 Axial CT through inferior pulmonary veins (arrows).

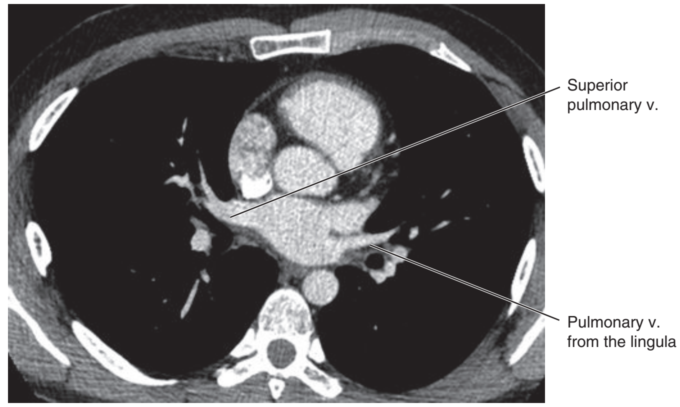


Fig. 6.41 Axial CT.

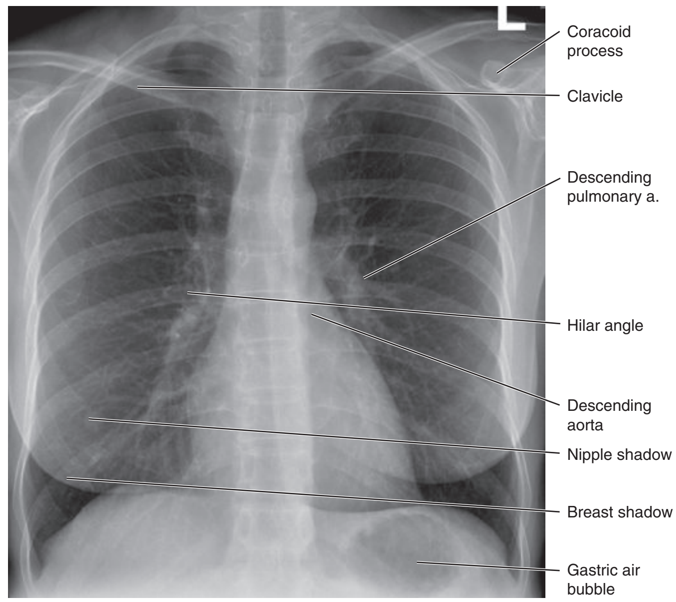


Fig. 6.43 PA chest X-ray.

A common trunk for the superior and inferior veins occurs in 12–25% and is commoner on the left than the right

### Hilum

Well seen on CXR. It consists of the pulmonary artery, pulmonary vein, bronchus and nodes. Inferiorly it extends into the pulmonary ligament.

- Right hilum:
  - right main bronchus lies posteriorly with the right pulmonary artery lying anterior to the bronchus (epiarterial)
  - the superior pulmonary vein lies inferior to the artery and the inferior pulmonary vein lies in the inferior hilum
  - the hilar angle is formed by the superior pulmonary vein crossing the right descending pulmonary artery (Fig. 6.43)
- Left hilum:
  - the left main bronchus lies posteriorly with the pulmonary artery lying superior to the bronchus (hyparterial)
  - the superior pulmonary vein lies anterior to the left main bronchus and the left main pulmonary artery; the inferior pulmonary artery lies in the inferior hilum
  - the left hilum is higher than the right in 97% of people; the height is equal in 3%.

### Pleura

This is a thin continuous membrane consisting of:

- parietal pleura – lines the non-pulmonary surfaces, including the diaphragm and pericardium and mediastinum
- visceral pleura – lines the pulmonary surfaces.

The two layers are continuous in front and behind the root of the lung and attach at the hilum, with the mediastinal pleura extending inferiorly as a double layer below the hilum – the pulmonary ligament.

The two layers cannot be delineated on CT, with the visceral, parietal pleura and pleural fluid combined measuring <0.5 mm. The intercostal strip, which is seen on CT running between the ribs, consists of two layers of pleura, extrapleural

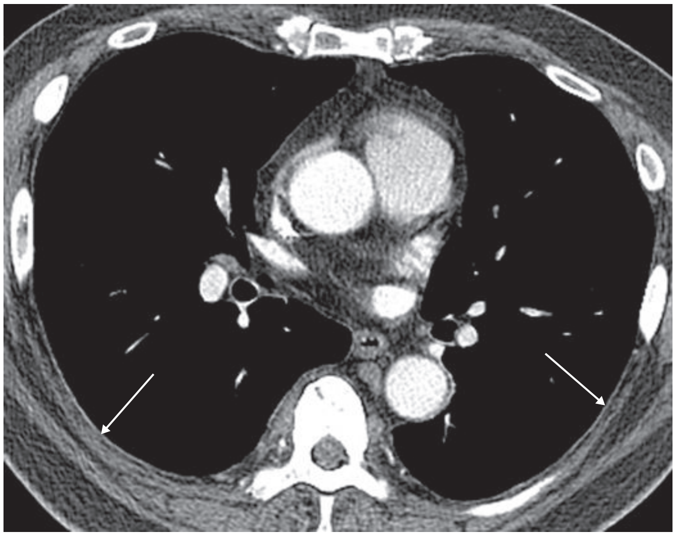

Fig. 6.44 Axial CT of intercostal stripe (arrows).

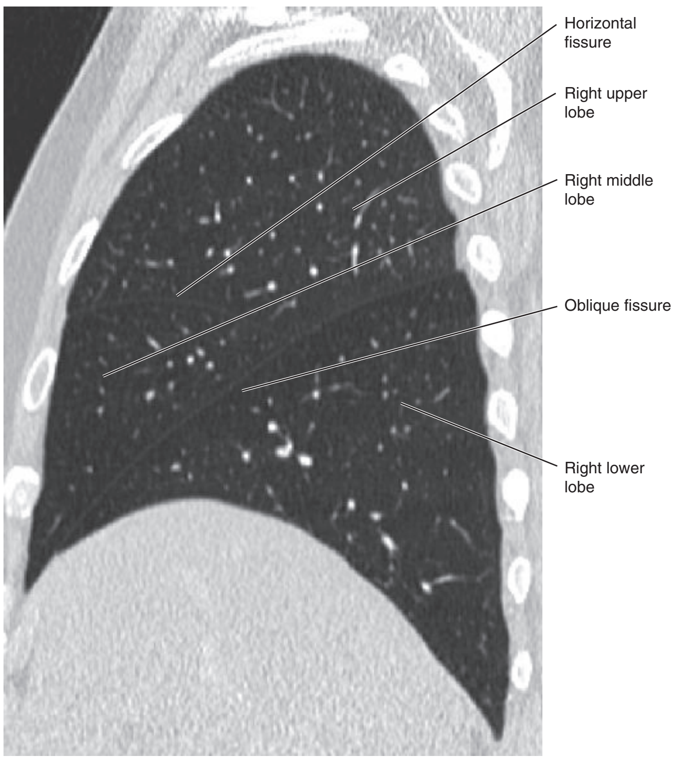


Fig. 6.46 Sagittal CT of oblique fissure.

fat and the extrathoracic fascia and the innermost intercostal muscle (Figs. 6.12, 6.44).

The lobes of the lung are separated by pleural fissures.

Right oblique (major) fissure

- separates the right upper and middle lobe from the right lower lobe
- runs from T5 through the hilum and contacts the diaphragm 3–4 cm posterior to the sternum.

Left oblique fissure

- separates the upper lobe from the lower lobe and follows a similar path, however it arises from T4 in 75% of patients.

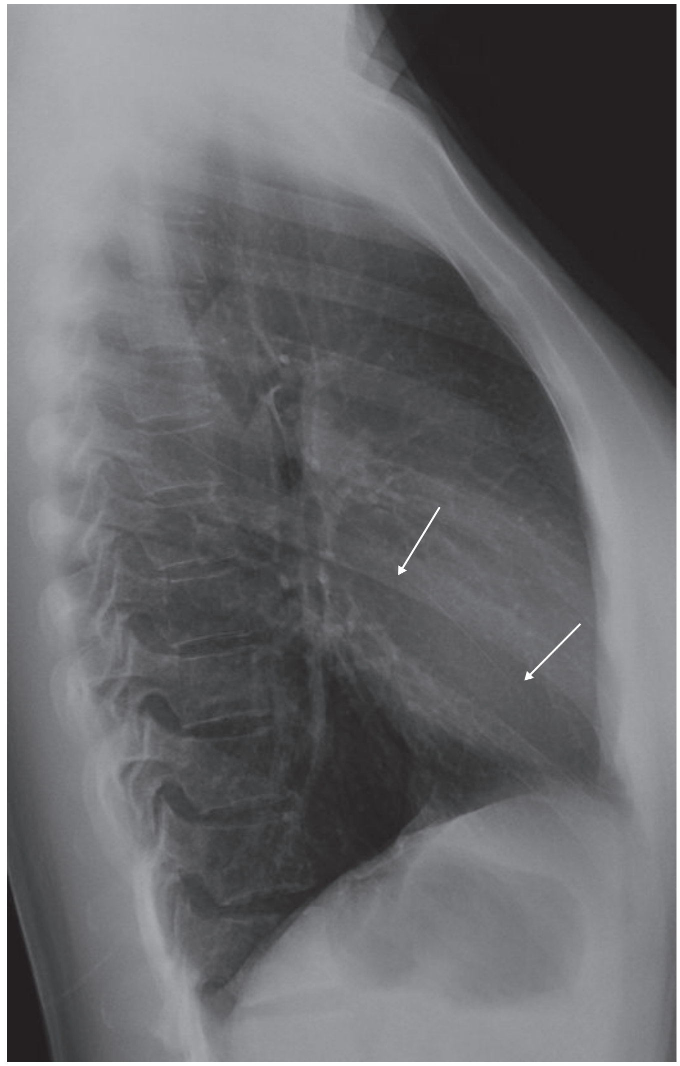

Fig. 6.45 Lateral chest showing oblique fissure (arrows).

The oblique fissure is not seen on a PA CXR, but is seen in a lateral CXR and on CT (Figs. 6.45, 6.46).

Horizontal (minor) fissure

- separates the right upper lobe from the right middle lobe and runs from the chest wall between the 4th and 6th rib to the intralobar artery at the hilum
- is seen in 50–80% of CXRs. On CT it is often seen as an area devoid of vessels, although is seen on high resolution CT (Fig. 6.47).

Azygous fissure

- on the right
- due to an anomalous development of the azygous vein and terminates in a tear-drop opacity
- consists of four layers of pleura; it is variable in size and is supplied by the right apical bronchus or its branches
- seen in 0.5% of CXR with a male:female ratio of 2:1 (Figs. 6.48–6.50).

Incomplete fissures

- fail to reach the hilum

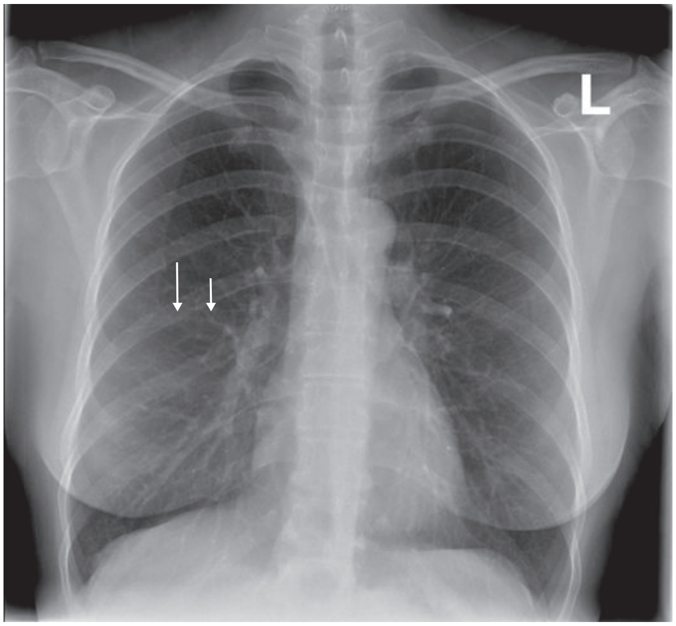


**Fig. 6.47** CXR showing horizontal fissure (arrow).

**Fig. 6.49** Coronal CT showing azygous fissure (arrow).

- are common (right more than left), occurring in up to 73% of oblique fissures and 60–90% of horizontal fissures.

Accessory fissures

- occur in 30–50% of people and are seen in 5–10% of CXR, 16–21% of CT
- fissure separating the left upper lobe from the lingula in 8–18%
- superior accessory – separates the superior segment of the left lower lobe from the basal segments
- inferior accessory separates the medial basal segment from the remainder; this is commoner on the right than the left.

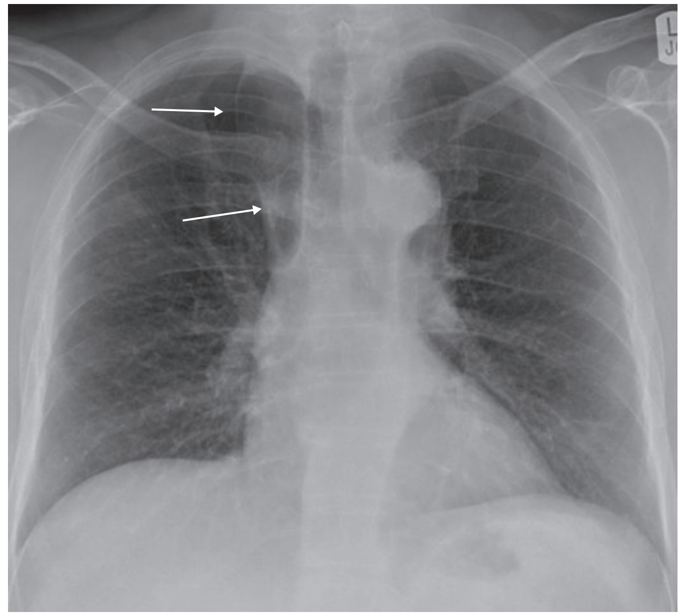

**Fig. 6.48** CXR showing azygous fissure (arrow).

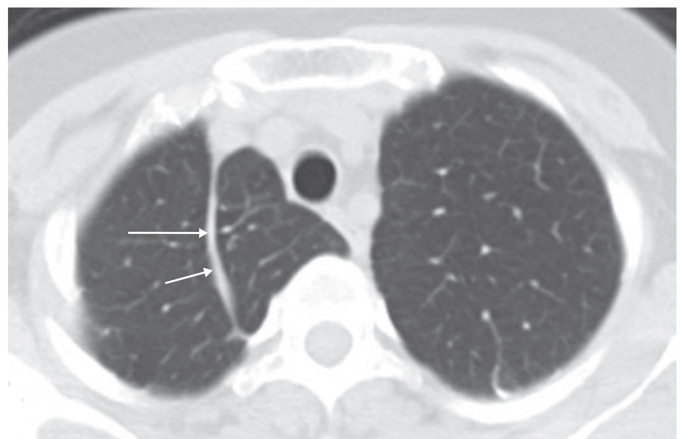

**Fig. 6.50** Axial CT showing azygous fissure (arrow).

## Mediastinum

This extends from the sternum to the thoracic spine and from the thoracic inlet to the diaphragm. For descriptive purposes it can be divided into

- the superior mediastinum which extends from the thoracic inlet to T4/5 and contains the thymus, aortic arch, great vessels, superior vena cava and the trachea
- the inferior mediastinum which lies below this and is divided into the anterior middle and posterior mediastinum.

Radiologically the mediastinum may be divided into

- anterior – lying anterior to the pericardium, ascending aorta and superior vena cava
- middle – contains, heart, great vessels and the hilum andcarina
- posterior – retrocardiac and paravertebral spaces and contains descending aorta, oesophagus, azygous system and spinal column.

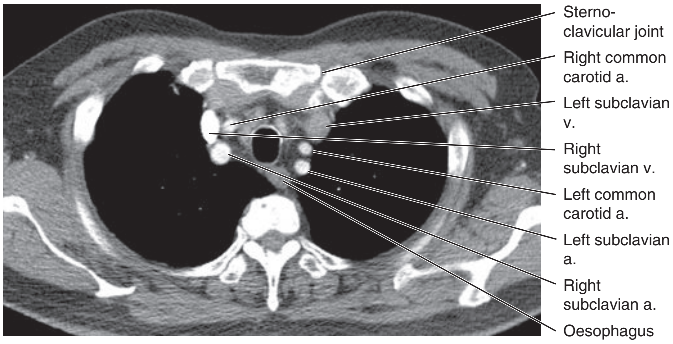


**Fig. 6.51** Axial CT of mediastinum.

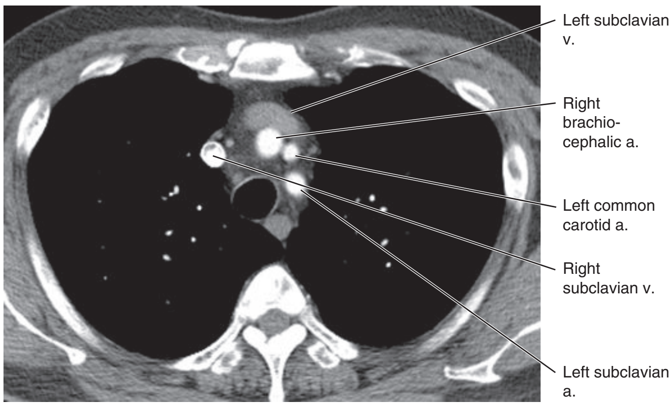


**Fig. 6.53** Axial CT of mediastinum.

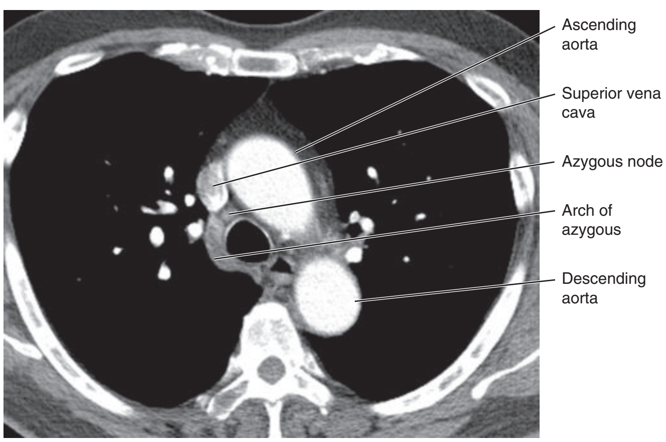


**Fig. 6.55** Axial CT of mediastinum.

On a PA CXR:

- right border – is the SVC, RA and IVC
- left border – the left subclavian artery, aortic arch, pulmonary trunk, left atrial appendage and the left ventricle (Figs. 6.5, 6.11)
- on CT mediastinal structures are well seen (Figs. 6.51–6.61).

### Mediastinal lines

Anterior junction line

- contact of anterior lungs
- lies posterior to the sternum
- consists of four layers of pleura
- runs obliquely from the lower manubrium inferiorly to the left (Fig. 6.62)

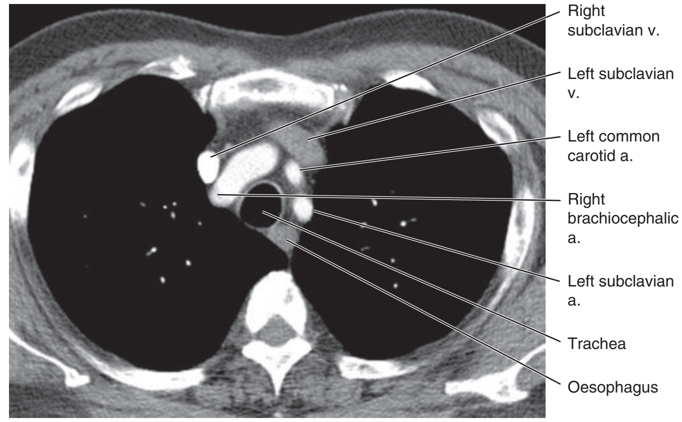


**Fig. 6.52** Axial CT of mediastinum.

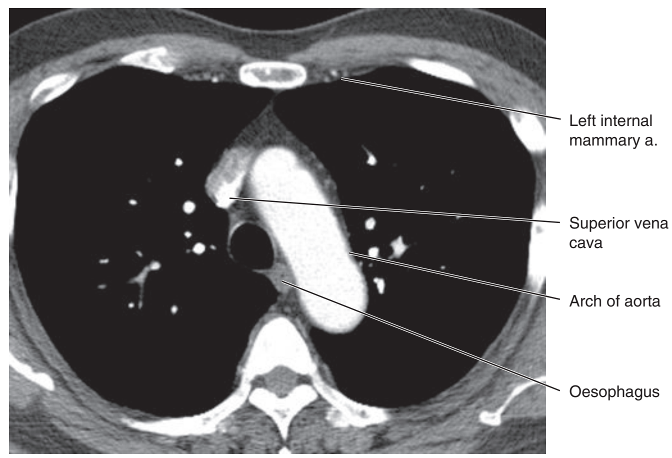


**Fig. 6.54** Axial CT of mediastinum.

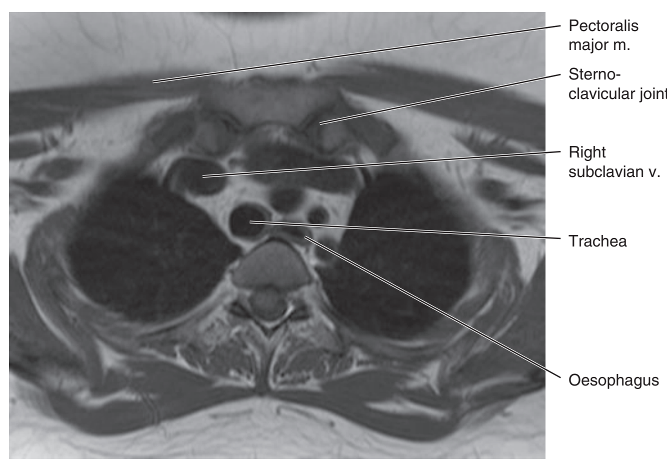


**Fig. 6.56** Axial MRI of mediastinum.

Posterior junction line

- contact of posterior lungs behind the oesophagus and anterior to the spine
- consists of four layers of pleura (Fig. 6.63).

### Thymus

- is related to the anterior great vessels and pericardium
- undergoes age-related changes and fatty replacement

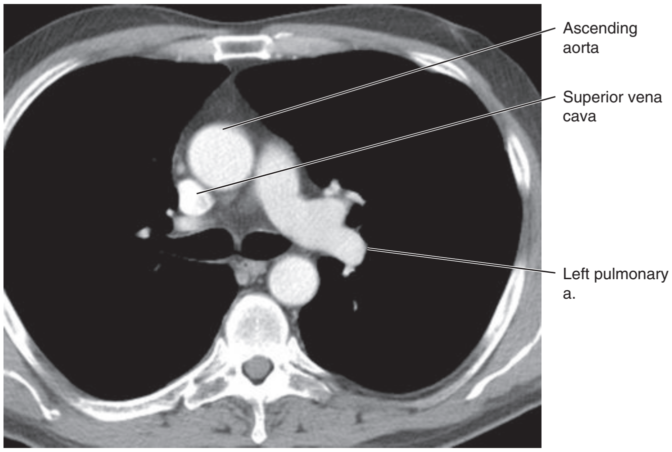


**Fig. 6.57** Axial CT of mediastinum.

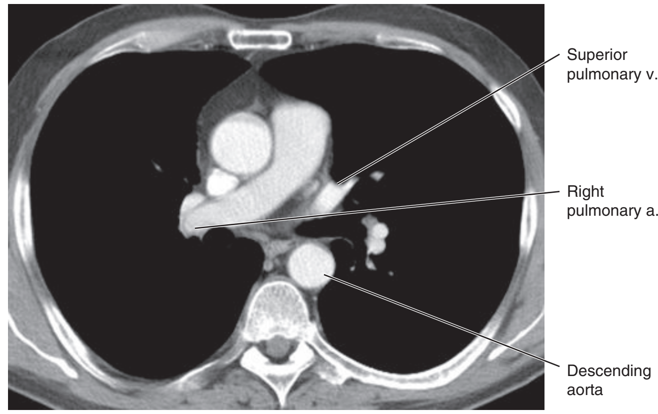


**Fig. 6.58** Axial CT of mediastinum.

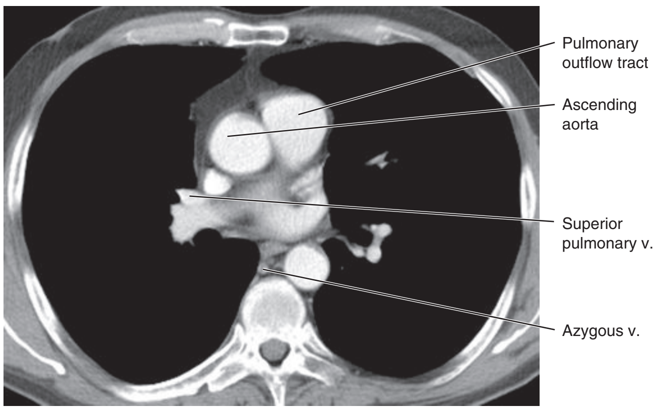


**Fig. 6.59** Axial CT of mediastinum.

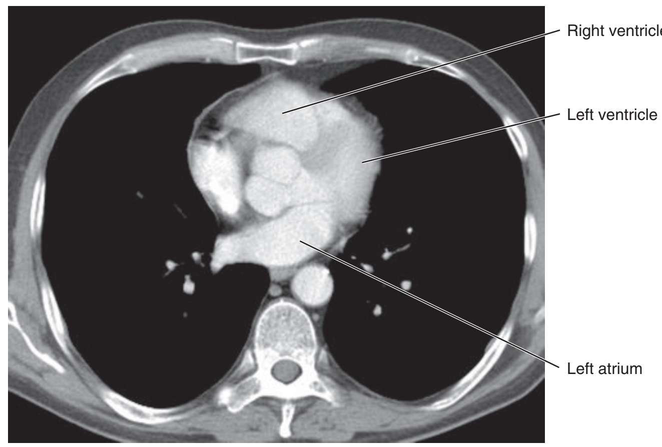


**Fig. 6.60** Axial CT of mediastinum.

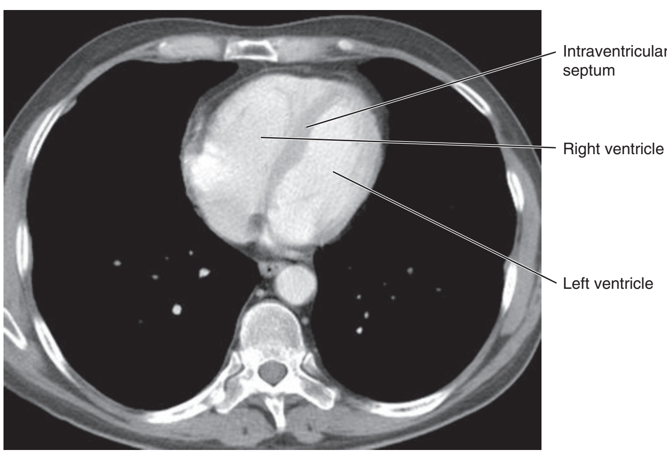


**Fig. 6.61** Axial CT of mediastinum.

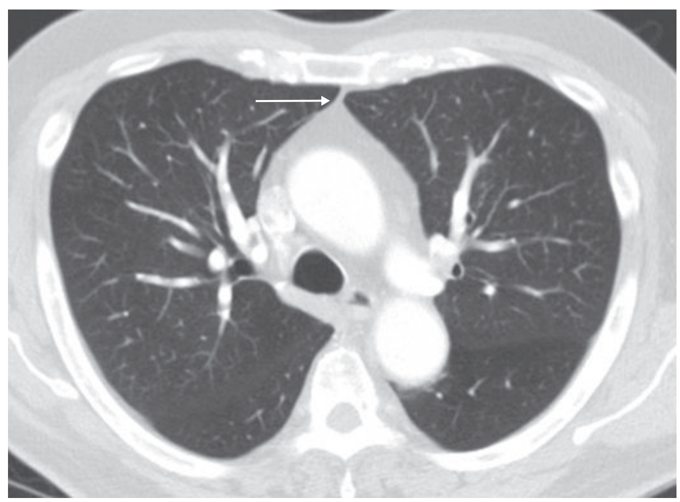

**Fig. 6.62** Axial CT of anterior junction line (arrow).

- is usually arrow-shaped (62%), may have two lobes (32%) or an isolated lobe (6%).

CXR – it may be seen as a 'sail sign' in children (Fig. 6.64). In adults it is not visualized.

CT – it is quadrilateral in children and becomes triangular in late childhood (Fig. 6.65). In children under 5 years the limbs measure 1.4 cm. Aged less than 20 years it measures 1.8 cm and >20 years it measures 1.3 cm. In adults there is fatty replacement (Fig. 6.66).

## Lymph nodes

These are soft tissue masses seen on CT. Normal nodes are less than 1 cm in short-axis diameter and tend to be oval rather than round. The nodal stations commonly used are defined by the AJCC/UICC

Level 1

- highest mediastinal – lie above a horizontal line at the upper left brachiocephalic vein (Fig. 6.67)

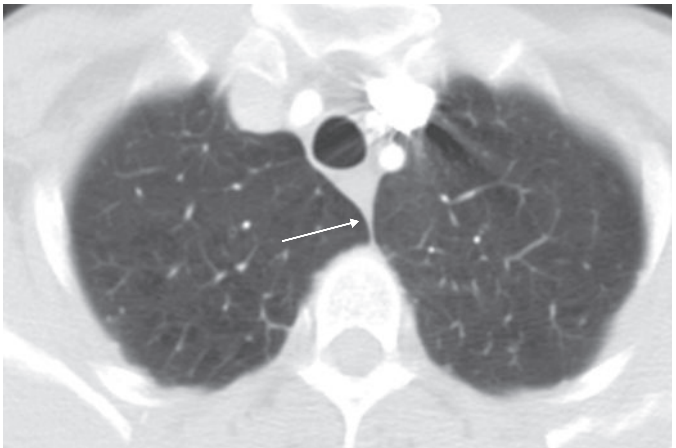

Fig. 6.63 Axial CT of posterior junction line (arrow).

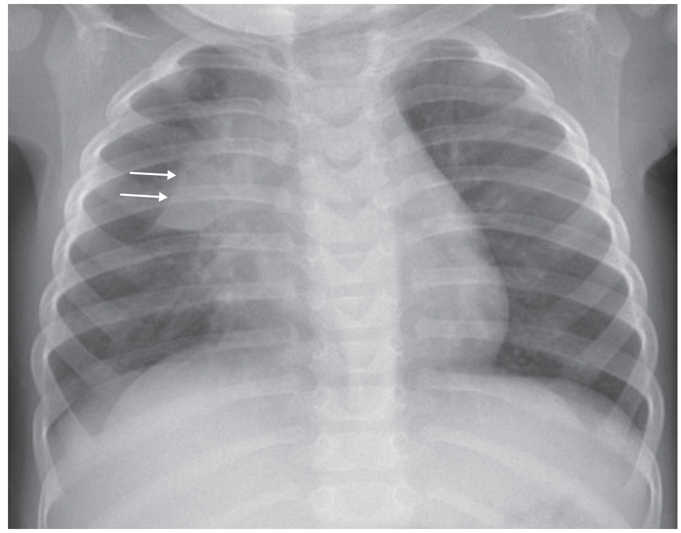

Fig. 6.64 CXR showing thymus (arrow).

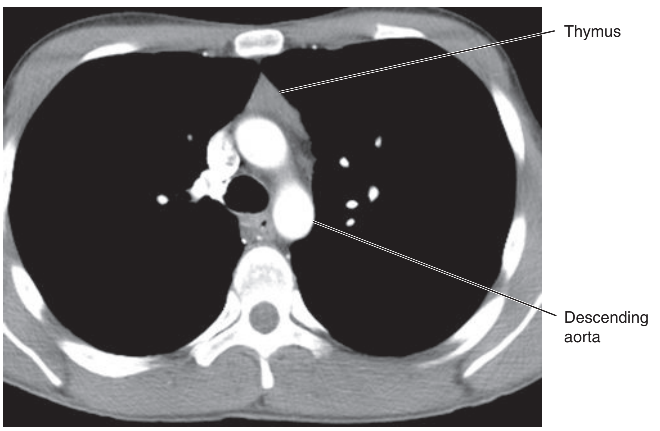


Fig. 6.65 Axial CT of thymus.

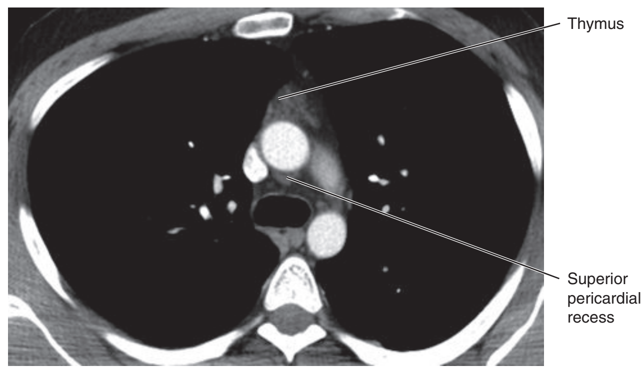


Fig. 6.66 Axial CT of thymus.

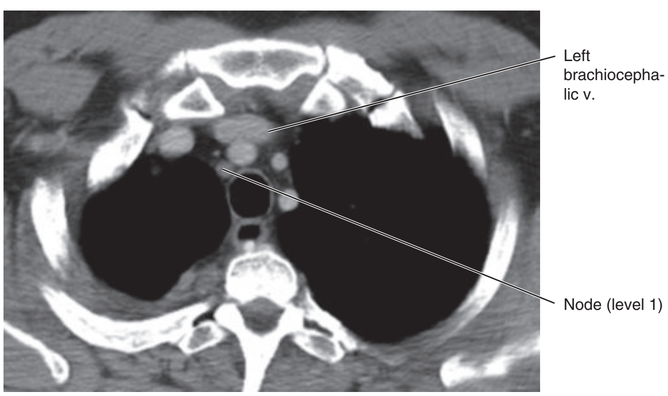


Fig. 6.67 Axial CT, level 1 node.

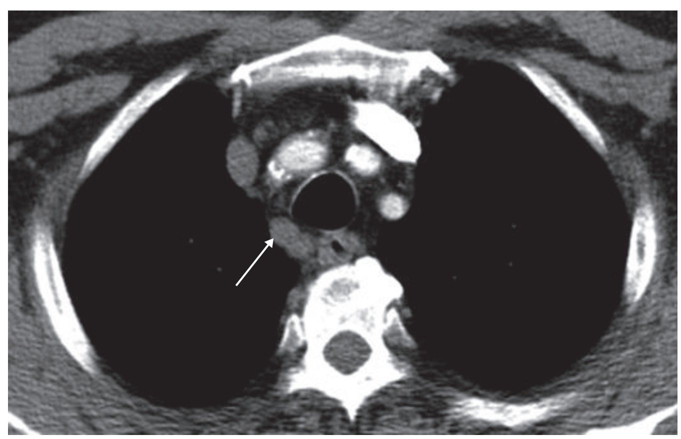

Fig. 6.68 Axial CT, level 3 node (arrow).

Level 2
- upper mediastinal – lie above a line tangential to the upper margin of the arch of the aorta and below level 1

Level 3
- prevascular and retrotracheal (Fig. 6.68)

Level 4
- lower paratracheal – below upper margin of the aortic arch and above the superior aspect of the RMB adjacent to the trachea on the right. On the left between upper margin of the aortic arch and LMB and medial to the ligamentum arteriosus (Figs. 6.69, 6.70)

Level 5
- sub-aortic – lateral to the ligamentum arteriosus, aorta or left pulmonary artery (Figs. 6.71, 6.72)

Level 6
- para-aortic – anterior and lateral to the arch of the

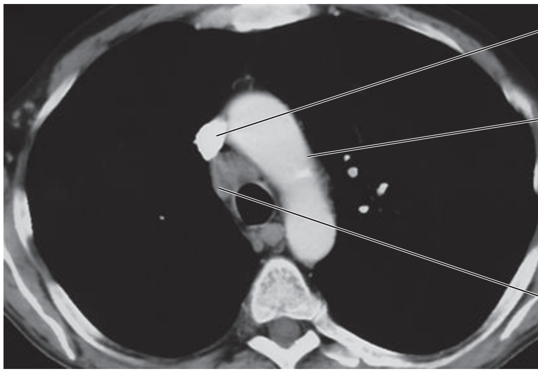


**Fig. 6.69** Axial CT, level 4 node.

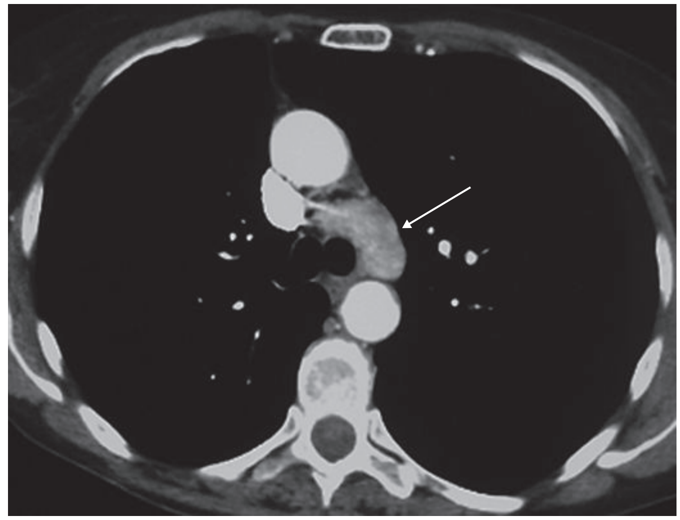

**Fig. 6.70** Axial CT, level 4 node (arrow).

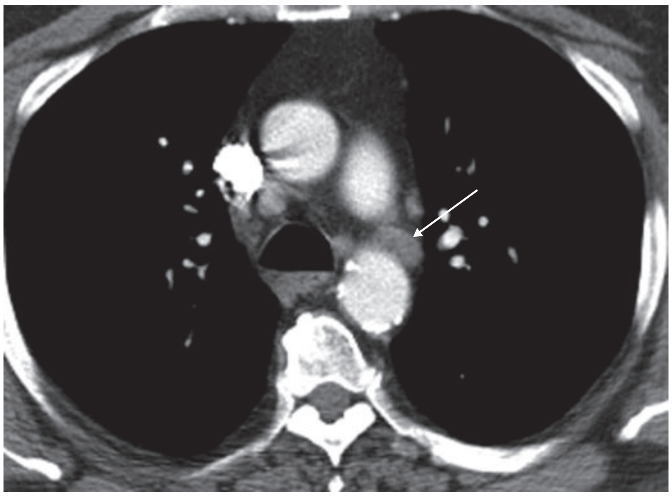

**Fig. 6.71** Axial CT, level 5 node (arrow).

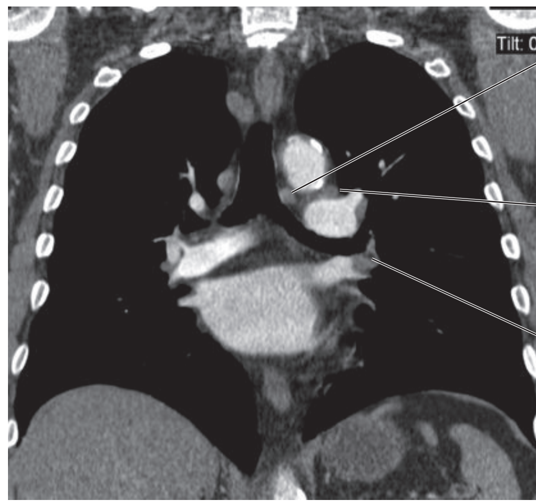


**Fig. 6.72** Axial CT, level 5 node.

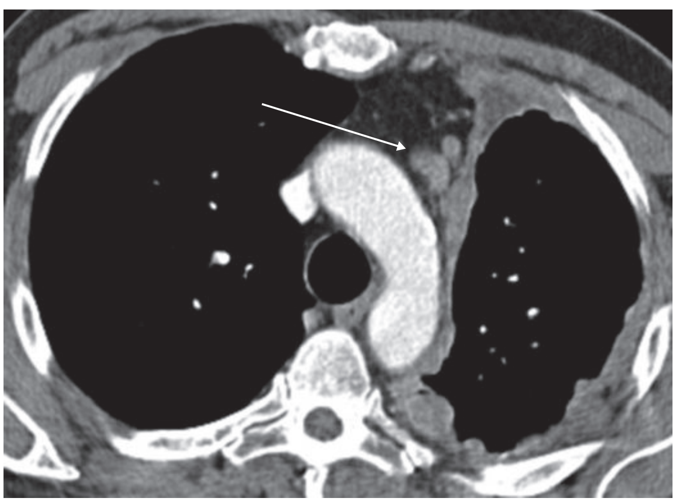

**Fig. 6.73** Axial CT, level 5 node (arrow).

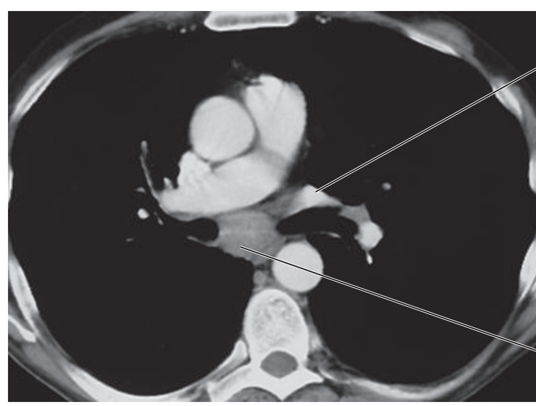


**Fig. 6.74** Axial CT, level 7 node.

aorta or ascending aorta or brachiocephalic artery below the upper aortic arch (Fig. 6.73)

Level 7
- subcarinal (Fig. 6.74)

Level 8
- paraoesophageal

Level 9
- within the pulmonary ligament, along the posterior wall of the lower aspect of the inferior pulmonary vein

Level 10
- hilar.

Chapter 7

# The heart and great vessels

Simon Padley and Narayan Karunanithy

## Embryology

### Heart and pericardium

- The primitive heart forms by the fusion of two parallel tubes to produce a single pulsating tube.
- Grooves then develop along the tube to demarcate the sinus venosus, atrium, ventricle, and bulbus cordis (Fig. 7.1).
- Venous blood, from the umbilical and vitelline (yolk sac) veins drains into the sinus venosus.
- The arterial blood is pumped out through the truncus arteriosus.
- The dorsal and ventral endocardial cushions separate the single atrial cavity from the single ventricle and divide the common atrioventricular opening into a right (tricuspid) and left (mitral) orifice.
- In the fully developed heart the atria and great veins lie posterior to the ventricles and roots of the great arteries.

A detailed account of the division of the single primitive atrium and ventricle is beyond the scope of this book.

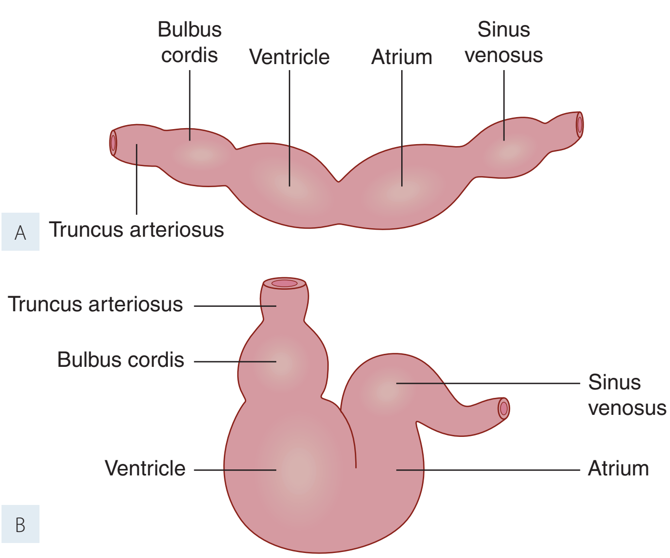


**Fig. 7.1** Development of the fetal heart.

### Aortic arch and derivatives

Six pairs of vascular arches arise from the truncus arteriosus. On either side these arteries join to form the longitudinally placed dorsal aortae. The dorsal aortae fuse distally to form the descending aorta.

- The first, second and fifth arches essentially disappear.
- The third arch becomes the common carotid artery on either side.
- The right fourth arch becomes the brachiocephalic trunk and the right subclavian artery.
- The left fourth arch forms the aortic arch, gives off the left subclavian artery before linking with the descending aorta.
- The proximal parts of the sixth aortic arches persist as the right and left pulmonary arteries. The distal part of the right sixth aortic arch degenerates. The distal part of the left sixth aortic arch retains its connection to the dorsal aorta to form the ductus arteriosus (Fig. 7.2).

## Layers of the heart

There are three layers of the heart.

- Endocardium
  - The innermost, thin, smooth layer of epithelial tissue lines the inner surface of the heart chambers and valves.
- Myocardium
  - The muscular wall of the heart contains elongated circular and spiral fibres to propel blood inferiorly through the atria and superiorly through the ventricles.
- Epicardium
  - This layer is indistinct from the visceral pericardium (see below).
  - The coronary arteries run in the epicardium, giving off perforating vessels that supply the myocardium and endocardium. Hence when perfusion to a segment of heart is compromised, the endocardium and the subendocardial layer of the myocardium are the layers most at risk of ischaemia (Fig. 7.3).

*Applied Radiological Anatomy, 2nd Edition* ed. Paul Butler, Adam W.M. Mitchell and Jeremiah C. Healy. Published by Cambridge University Press.

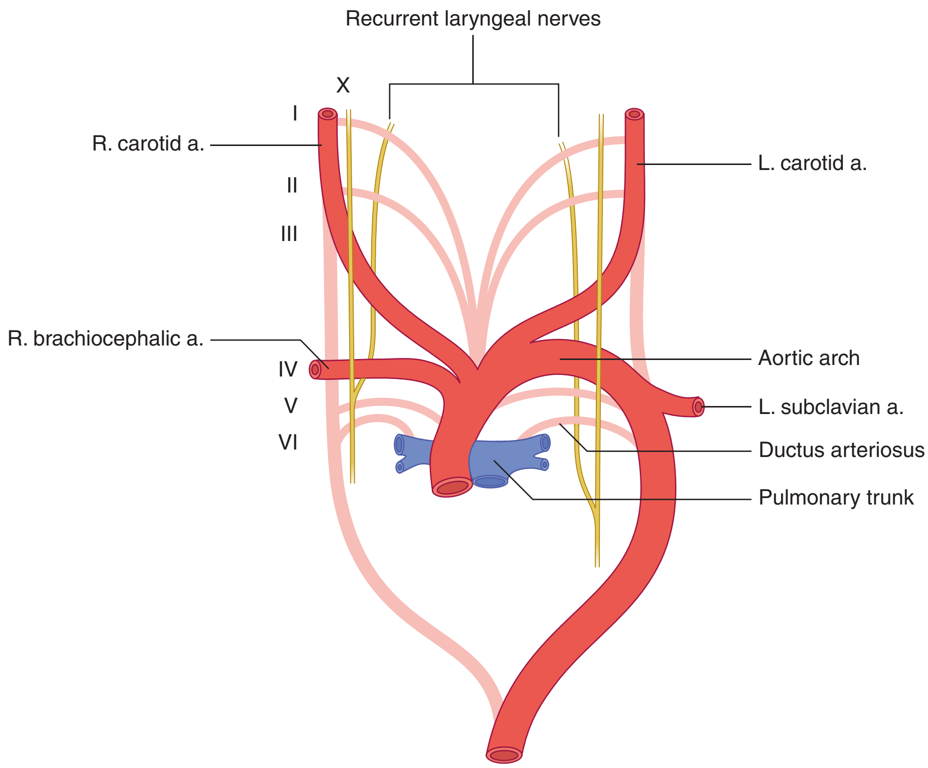


**Fig. 7.2** Development of the aortic arch. The branchial arches that form the components of the aortic arch and great vessels are indicated.

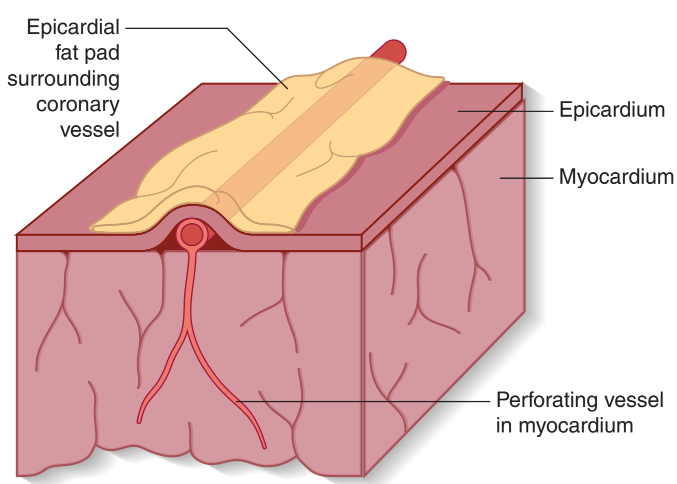


**Fig. 7.3** Schematic view of the myocardial muscle layers showing small perforating vessels arising from the overlying epicardial artery.

## Pericardium

- The pericardium encases the heart, main pulmonary artery, ascending aorta, superior and inferior vena cavae and the pulmonary veins. The pericardium is made up of an outer fibrous and inner serous component.
- The fibrous pericardium helps support the heart within the mediastinum.
- The serous pericardium is composed of the visceral and parietal layers.
- The visceral layer (epicardium) covers the heart and great vessels and is reflected into the parietal layer, which in turn forms the inner lining of the fibrous pericardium.
- The pericardial cavity is the space between the visceral and parietal layers of the serous pericardium and contains 15–50 ml of clear fluid normally.

The normal pericardium is visualized on CT and MR as a thin linear structure (Fig. 7.4).

## Pericardial recesses

The reflections of the pericardium give rise to a number of sinuses and recesses (Fig. 7.5). The fluid-filled recesses and sinuses can be mistaken for enlarged lymph nodes, tumours or cysts.

- Transverse sinus. This lies just above the left atrium and posterior to the great arteries. The recesses formed by the transverse sinus are:
  - Superior aortic recess. This consists of anterior, right (lateral) and posterior portions. The anterior portion is the space between the ascending aorta and main pulmonary artery and is triangular in shape. Fluid here can mimic an aortic dissection. The lateral portion is between the ascending aorta and superior vena cava. The posterior portion lies posterior to the ascending aorta and is also called the superior pericardial recess or superior sinus. Fluid in this portion can be mistaken for lymph nodes.
  - Inferior aortic recess. This is a diverticulum that runs between the lower ascending aorta and the right atrium.
  - Pulmonic recesses. The right and left pulmonic recesses lie inferior to the respective pulmonary arteries. Fluid collections within the pulmonic recesses can mimic the appearance of lymph nodes.

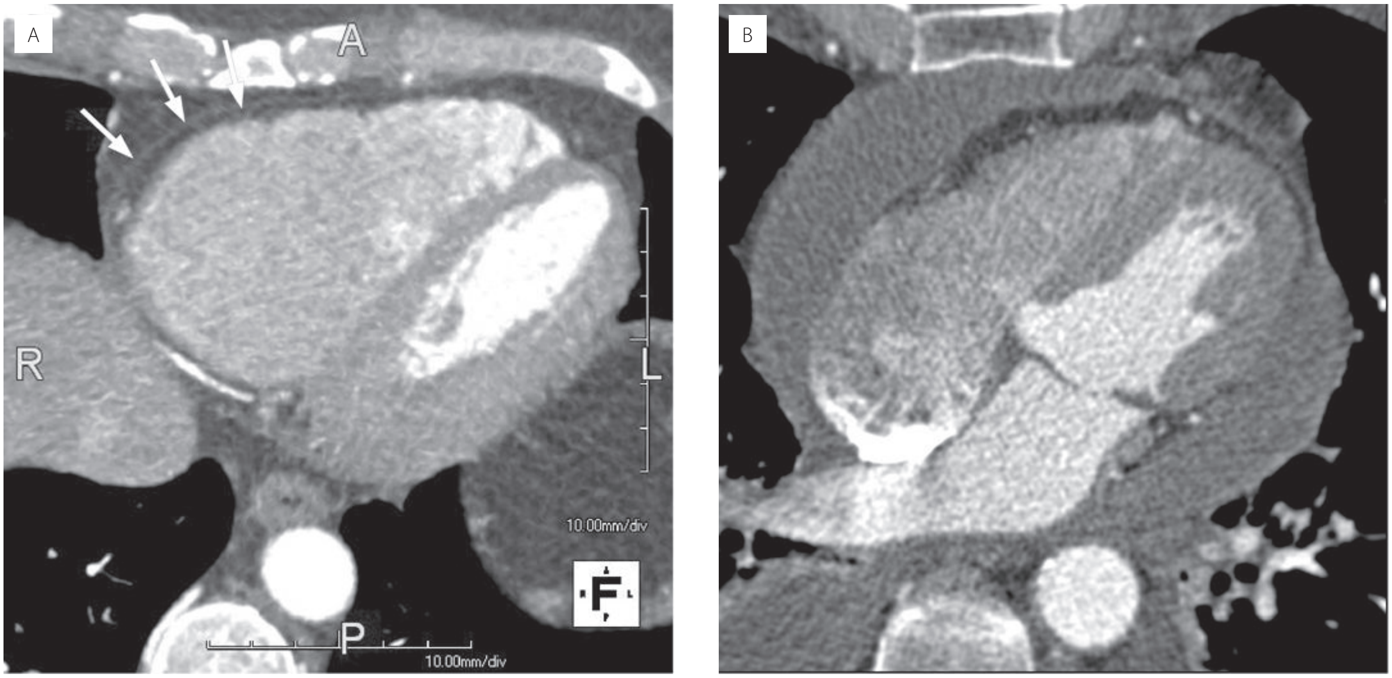


**Fig. 7.4** (A) The pericardium in the normal patient is a thin soft tissue density stripe outlined by fat (arrows). (B) In this patient the pericardial sac is filled with fluid.

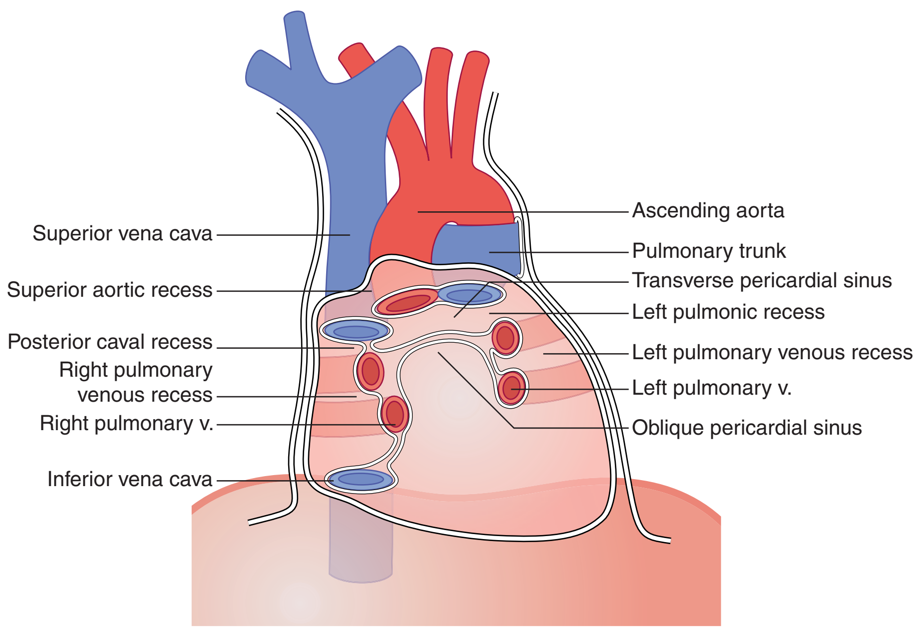


**Fig. 7.5** The sinuses and recesses formed by the pericardium.

- Oblique sinus. Located between the left atrium (anterior) and the oesophagus (posterior). It is separated from the transverse sinus by a reflection of pericardium that runs between the right and left superior pulmonary veins.
  - Posterior pericardial recess. Most cranial reflection of the oblique sinus. Lies posterior to the distal right pulmonary artery and medial to the bronchus intermedius. Fluid in this location can mimic subcarinal lymph node enlargement.

The two recesses formed from the pericardial cavity proper are:

- Pulmonic vein recesses. These are small recesses that lie along the lateral borders of the heart between the superior and inferior pulmonary veins. The left pulmonic vein recess is more frequently identified than the right although the right is usually deeper. Fluid in these recesses can be mistaken for hilar lymph nodes.
- Postcaval recess. Is usually small and lies posterior and to the right of the superior vena cava.

# Heart chambers

## Right atrium

- The superior (SVC) and inferior vena cavae (IVC) enter the right atrium at the superior and inferior extremities of the posterior wall respectively (Fig. 7.6).
- The Eustachian valve is a rudimentary valvular structure at the opening of the IVC that functions to direct oxygenated blood flow towards the foramen ovale in fetal life.
- The opening of the coronary sinus (CS) is located along the posterior wall between the IVC and the tricuspid valve. The Thebesian valve is situated at the opening of the CS.
- The crista terminalis is a vertically oriented ridge between the openings of the SVC and IVC which represents the line of fusion between the anterior trabeculated atrial portion and the posterior smooth-walled sinus venosus portion.

## Right ventricle

- The right ventricle (RV) is the most anterior cardiac chamber. It is relatively thin-walled and more complex in shape than the left ventricle (Fig. 7.7).
- It contains anterior, posterior and medial papillary muscles. The anterior papillary muscle has chordae tendinae that attach to the anterior and posterior cusps of the tricuspid valve, the posterior papillary muscle has chordae tendinae that attach to the posterior and medial (septal) cusps, and the medial papillary muscle has chordae tendinae that attach to the anterior and medial (septal) cusps.
- The moderator band is a ridge of tissue that extends across the right ventricular apex from the anterior papillary muscle to the interventricular septum.

## Left atrium

- The most posterior and cranially situated chamber (Fig. 7.8).
- The left atrioventricular valve is the mitral valve.
- The annulus of the mitral valve is contiguous with the annulus of the aortic valve.

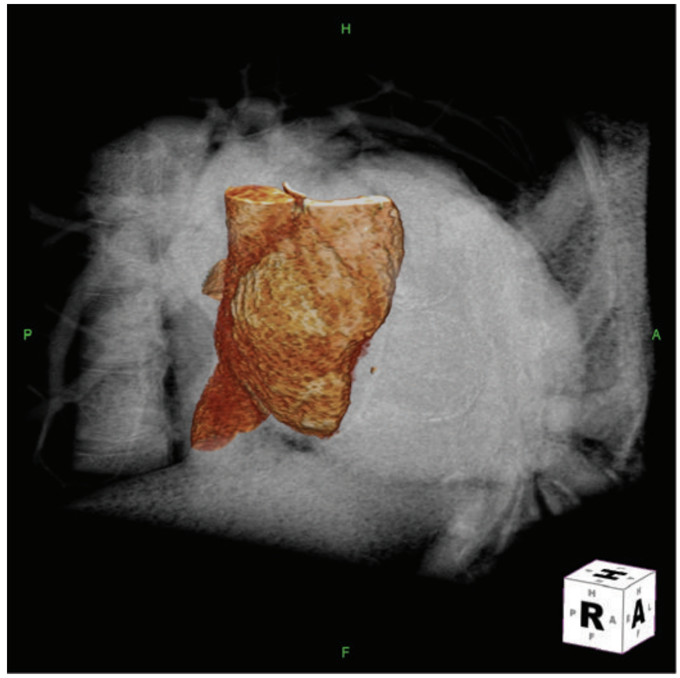


Fig. 7.6 The right atrium is highlighted relative to the other cardiac chambers.

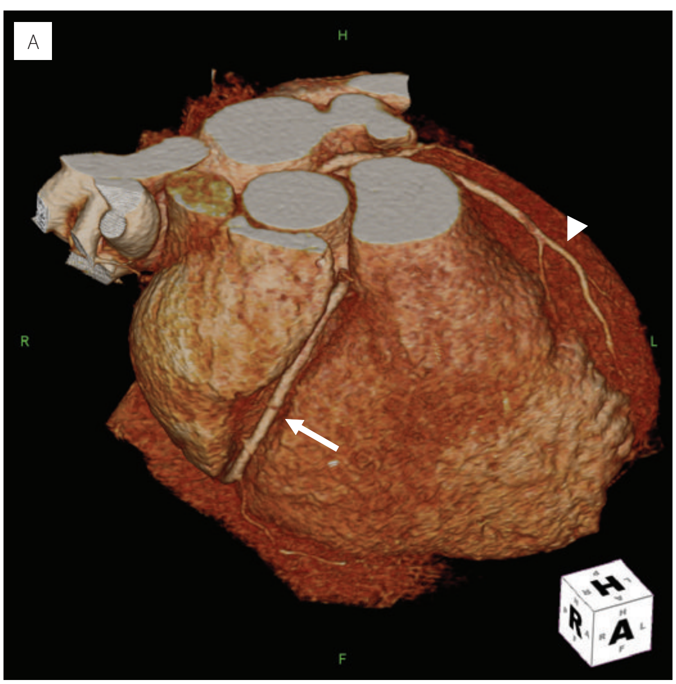


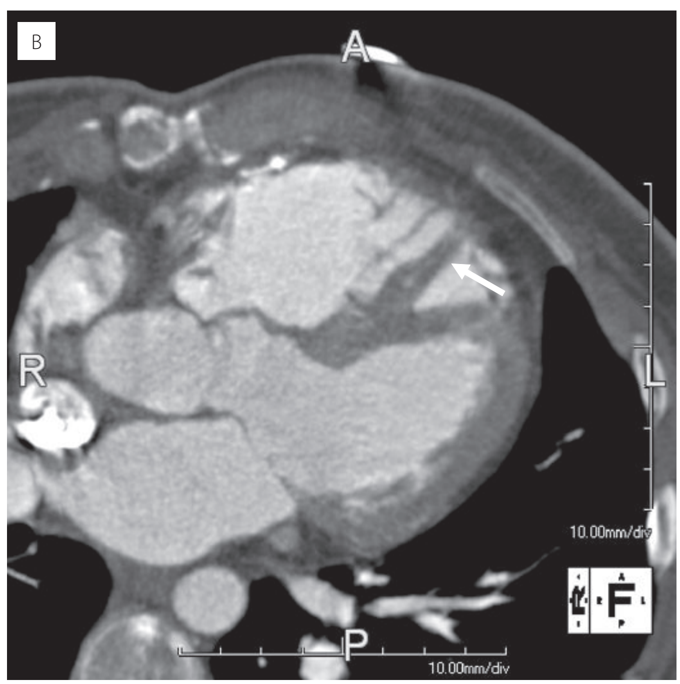


Fig. 7.7 (A) The right ventricle is separated from the right atrium by the right coronary artery (arrow), and separatyed from the left ventricle by the left anterior descending artery (arrowhead), which is a branch of the left coronary artery. (B) An axial view through the cardiac chambers. The right ventricle is the most anterior chamber and in this patient there is a prominent moderator band (arrow).

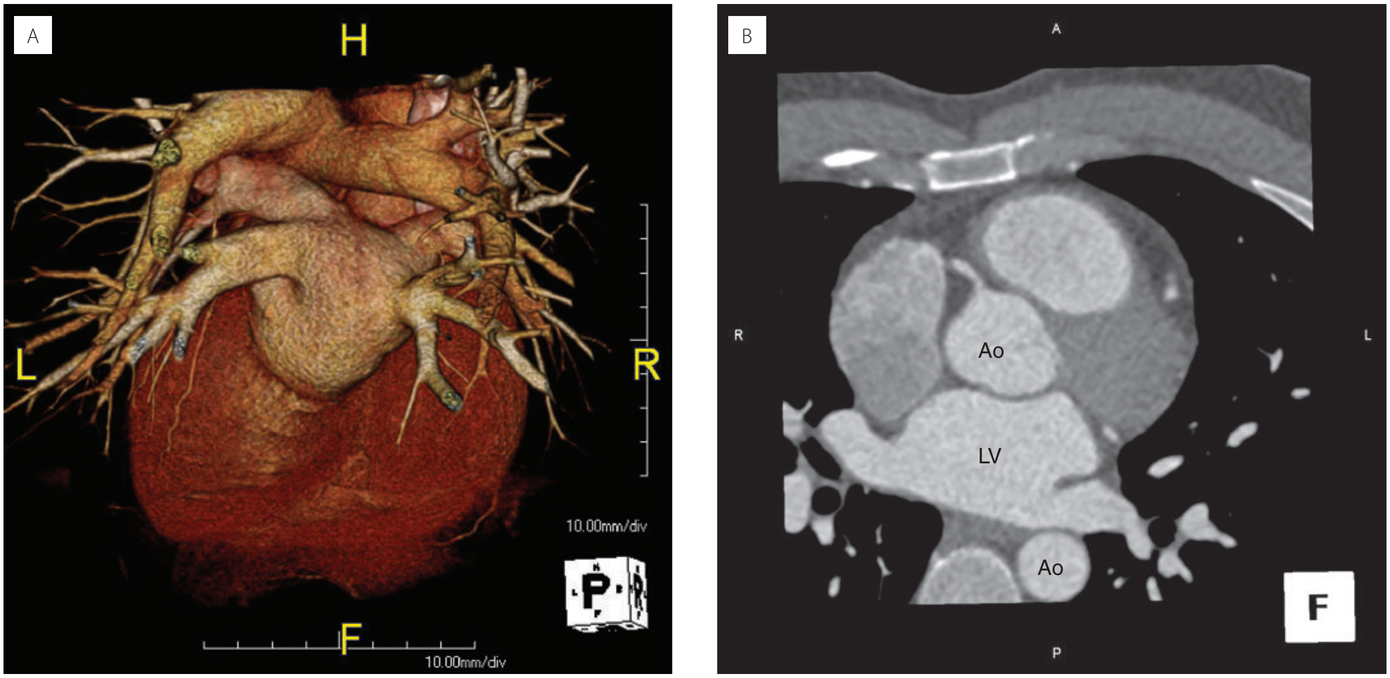


**Fig. 7.8** (A) A posterior view of the heart, derived from a contrast-enhanced CT, demonstrates the left atrium lying below the pulmonary artery branches. There are four veins entering the left atrium. (B) An axial view through the heart demonstrates the most superior of the cardiac chambers, the left atrium (LA). The aorta (Ao) lies in front and behind.

- The chamber has a thin muscular wall and is divided from the right atrium by the inter-atrial septum.
- Typically four pulmonary veins (left and right superior and inferior veins) drain into the LA. Additional pulmonary veins (PV) when present occur more commonly on the right (see below).

## Left ventricle

- The left ventricular myocardium is considerably thicker than the right ventricular myocardium (Fig. 7.9).
- As a result of this and the pressure gradient between the right and left ventricles, the interventricular septum bulges slightly into the right ventricle. Flattening or bulging of the interventricular septum into the left ventricle is an indicator of raised right ventricular pressure.
- The chordae tendinae arising from the anterior and posterior papillary muscles attach to the anterior and posterior mitral valve leaflets.

# The heart in commonly depicted planes

Significant overlap exists in the imaging planes used to depict the cardiac chambers in nuclear medicine, MR imaging and echocardiography. MPR of cardiac CT images can also reproduce these planes. The standard planes include;

- Vertical long axis (left ventricular long axis, apical two chamber) (Fig. 7.10)
  - Parasaggital plane along the long axis of the left ventricle lumen.
  - In addition to depicting the left atrium and left ventricle, useful information regarding the structure and function of the mitral valve can be obtained.
- Horizontal long axis (four chamber) (Fig. 7.11)
  - Provides a horizontal image through all four chambers of the heart. Useful in assessing chamber size and valve position. In particular the area of the left atrium can be measured on this view.
- Left ventricular outflow tract (three chamber, left parasternal) (Fig. 7.12)
  - This is an oblique long-axis view that is used to assess the LA, LV, aortic root, mitral valve and aortic valve.
- Left ventricular short axis (Fig. 7.13)
  - This is an oblique coronal plane perpendicular to the long axis of the LV lumen.
  - The 17-segment standardized myocardial segmentation and nomenclature for tomographic imaging of the heart as recommended by the American Heart Association is derived mainly from this plane (Fig. 7.14).
  - According to this model, the LV is divided into equal thirds. This will generate three circular slices named the basal, mid-cavity and apical slices. When accurate visualization of the whole LV cannot be made to estimate equal thirds (e.g. echocardiography), the anatomical landmarks used to divide the LV into slices are:
    - basal – from the mitral annulus to the tips of the papillary muscles at end-diastole

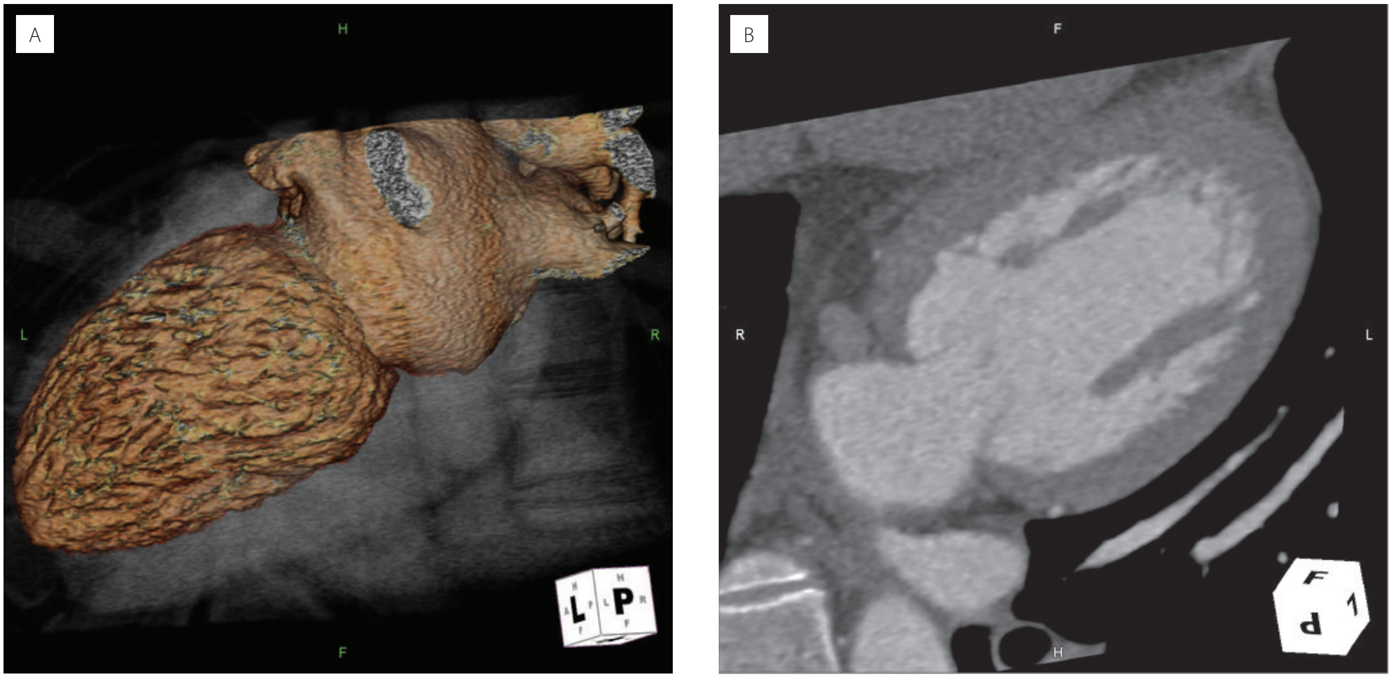


**Fig. 7.9** The left ventricle and the left atrium have been extracted from the cardiac structures to demonstrate that relationship.

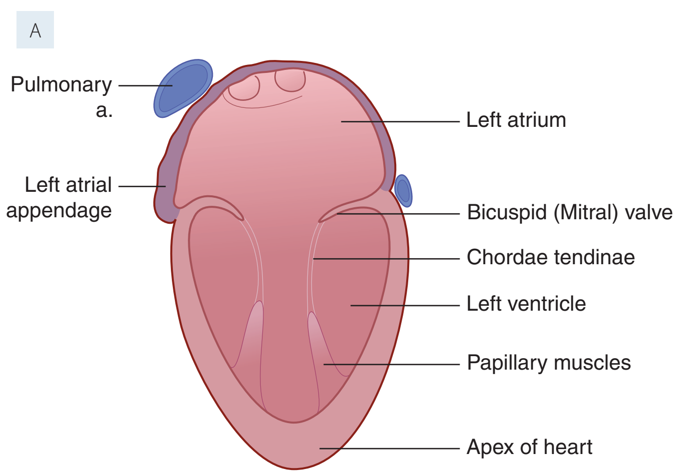


**Fig. 7.10** (A) Vertical long axis view of the left heart chambers. (B) A CT scan demonstrating the equivalent vertical long axis view.

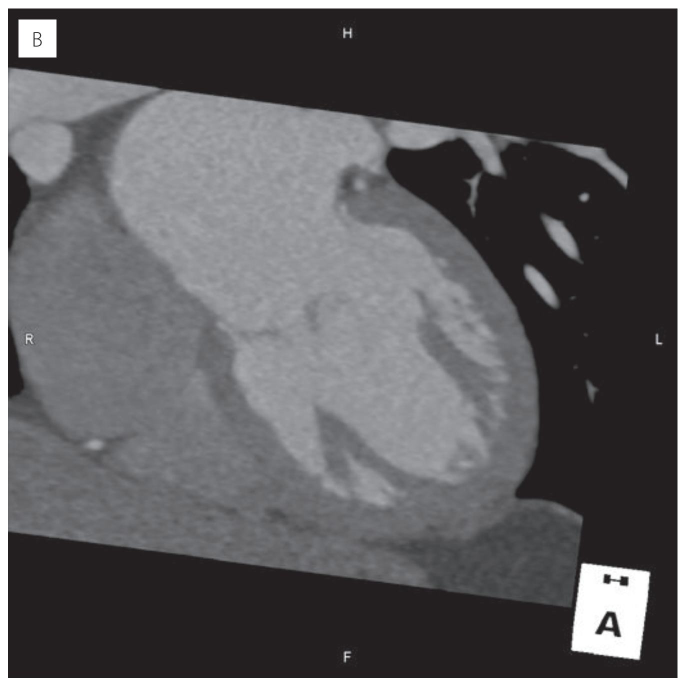


- mid cavity – the region that includes the entire length of the papillary muscles
- apical – the area beyond the papillary muscles to just before the cavity ends.
- The basal and mid-cavity portions are further sub-divided into six segments of 60° each. The apical portion is divided into four segments.
- The true apex is the area of myocardium beyond the end of the left ventricular cavity and is illustrated on the horizontal/vertical long axis images.

## Cardiac valves

Echocardiography is currently the principal imaging modality used for assessment of valve structure and function. However, with advancement in cardiac CT (MDCT) and MR (CMR) technology, comparable data can now be achieved with these modalities. Four-dimensional MDCT provides detailed depiction of leaflet anatomy during late diastole. Valvular calcification is better evaluated and quantified with MDCT. The higher temporal resolution of CMR allows visualization of rapid valve movements. In addition, phase-contrast CMR can be used to quantify flow, allowing estimation of stroke volume and mean velocity across a cardiac valve (Fig. 7.15).

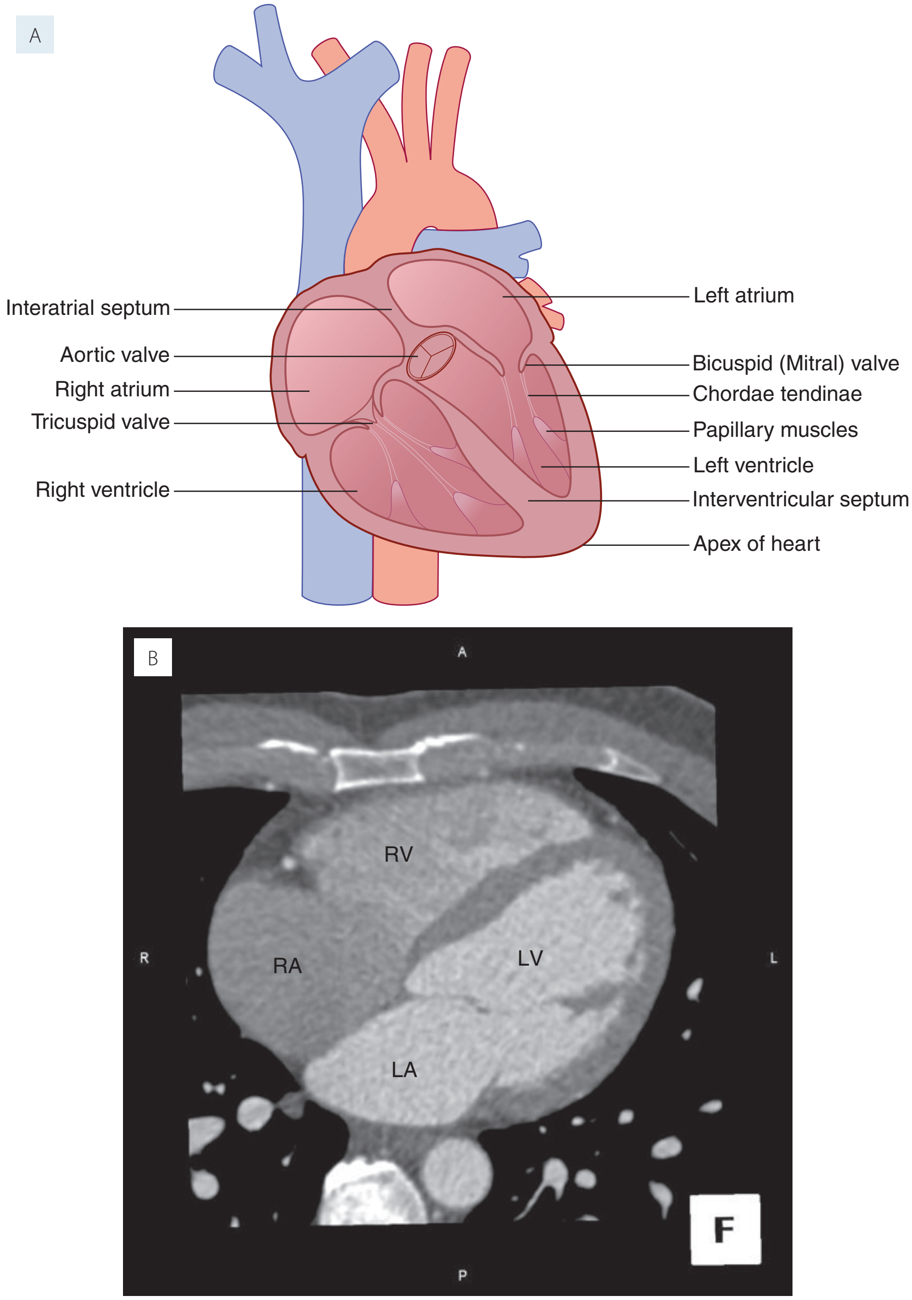


**Fig. 7.11** (A) Four-chamber view. (B) An axial image demonstrating the four chambers of the heart (right ventricle = RV, left ventricle = LV, left atrium = LA, right atrium = RA, arrow = right coronary artery).

## Aortic valve

- The normal aortic valve is a trileaflet structure made up of the right, left and posterior (non-coronary) cusps. The aorta dilates above the cusps to form the coronary sinuses (Fig. 7.16).

## Mitral valve (MV)

- The MV apparatus consists of the mitral valve leaflets, chordae tendinae, papillary muscles and the mitral valve annulus (MVA). The normal mitral valve is a bileaflet structure with an ovoid orifice (Fig. 7.17).
- The anterior leaflet tends to be more mobile and thicker than the posterior leaflet. The leaflets show complex movements during the cardiac cycle.
- Initially, passive opening is followed by rapid, maximal opening with atrial contraction. Then there is partial closure at end-diastole followed by complete closure during ventricular contraction.

## Tricuspid and pulmonary valves

- The normal tricuspid valve is a trileaflet structure with anterior, septal and posterior leaflets. The pulmonary valve is similarly a trileaflet structure.

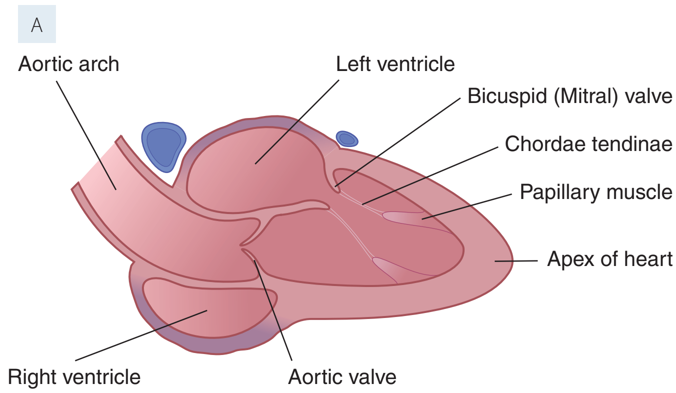


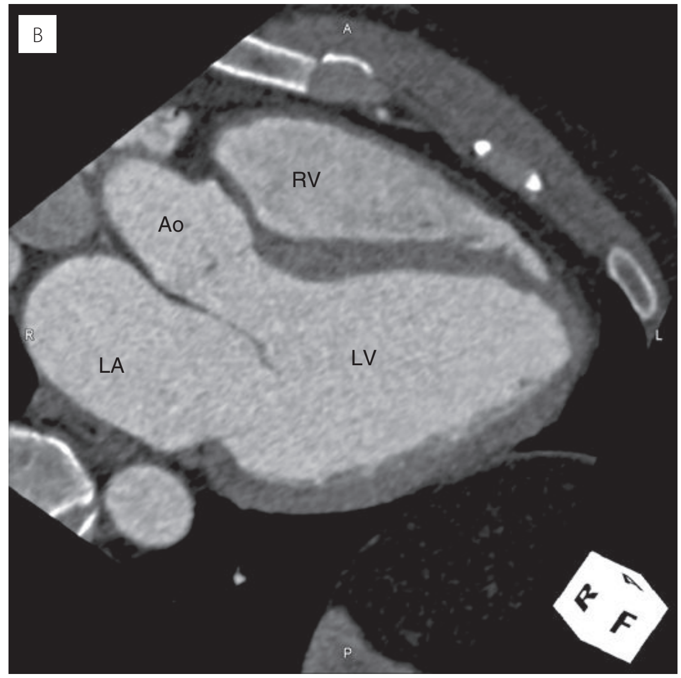


**Fig. 7.12** (A) Left ventricular outflow tract. (B) Equivalent CT of the left ventricular outflow tract view. LA = left atrium, LV = left ventricle, RV = right ventricle, Ao = aorta. Note how the aortic valve and mitral valve are contiguous structures.

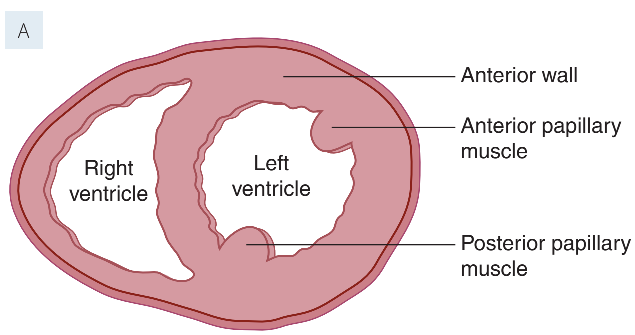


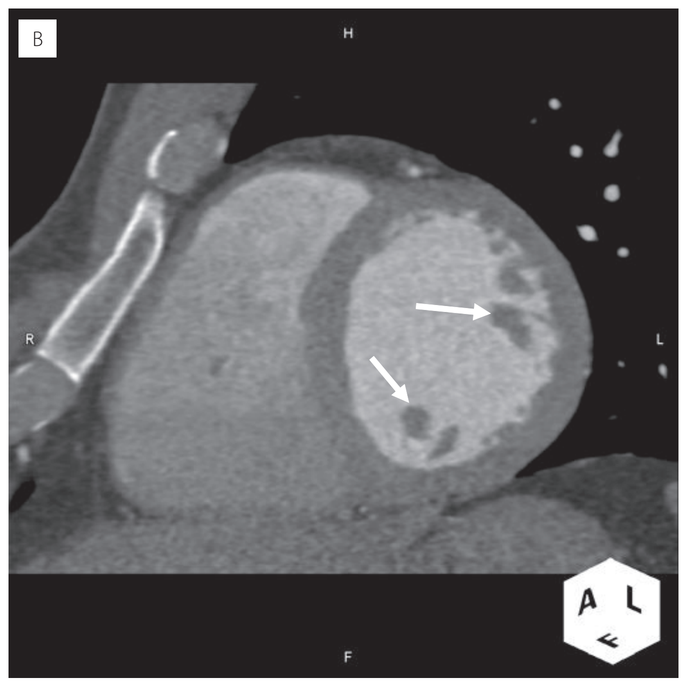


**Fig. 7.13** (A) Left ventricular short axis. (B) Short axis view through the left ventricle. Note the papillary muscles (arrows). The intraventricular septum bulges into the right ventricle.

# Coronary circulation

## Left coronary artery

- The left coronary artery (LCA) normally arises from the left coronary sinus. However, the LCA can arise from the right coronary sinus and follow anomalous courses (Fig. 7.18).
  - The LCA gives rise to the left anterior descending (LAD) and left circumflex (LCx) arteries.
- The LAD courses anterolaterally in the anterior interventricular groove and supplies the majority of the left ventricle. The branches of the LAD are:
  - lateral diagonal branches that supply the LV free wall
  - medial septal branches that supply the interventricular septum.
- The LCx courses in the left atrioventricular groove, giving rise to the obtuse marginal branches.

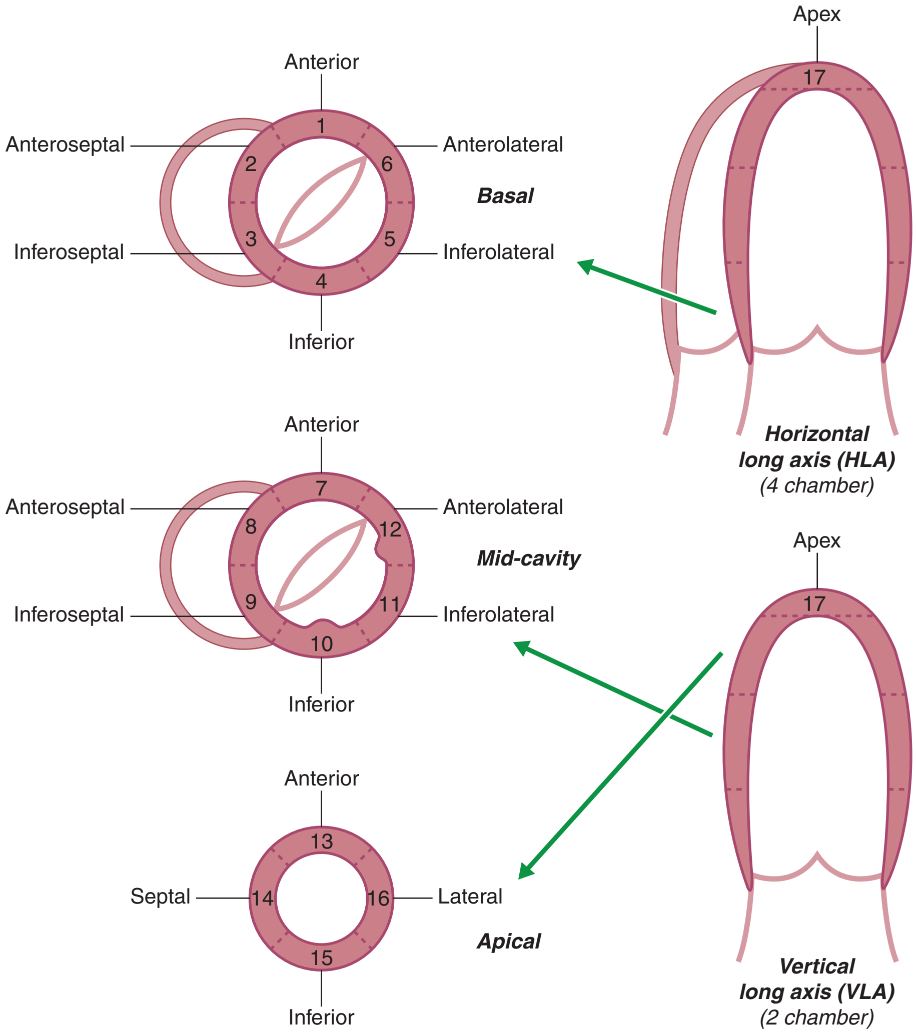


**Fig. 7.14** The 17-segment model used to depict the left ventricle.

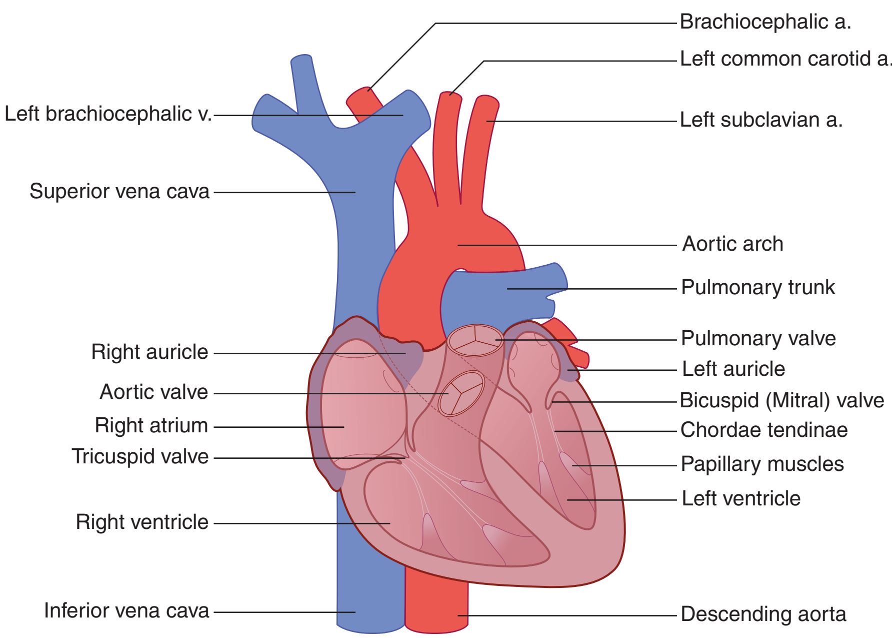


**Fig. 7.15** Depiction of the morphology, orientations and relationship of the cardiac valves.

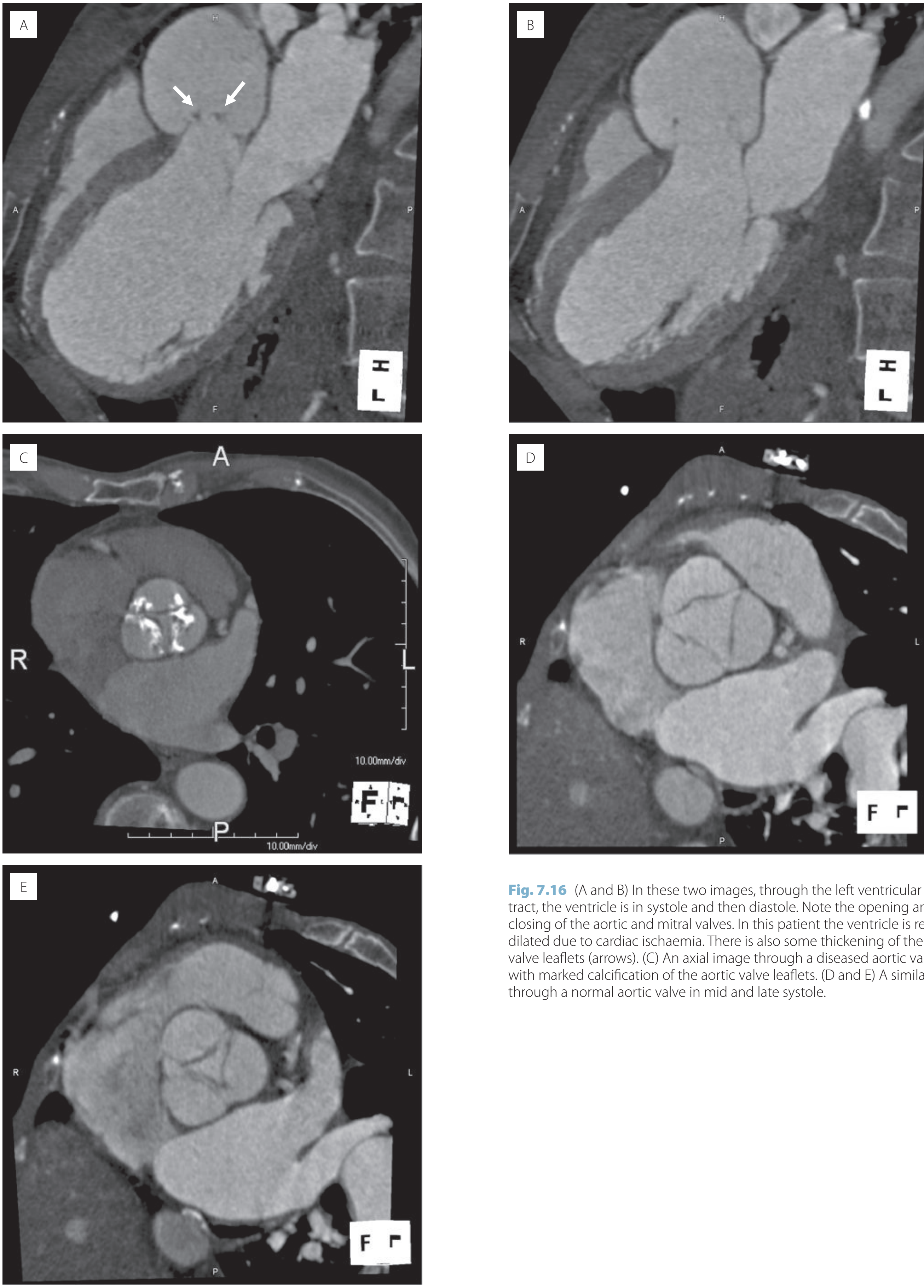


**Fig. 7.16** (A and B) In these two images, through the left ventricular outflow tract, the ventricle is in systole and then diastole. Note the opening and closing of the aortic and mitral valves. In this patient the ventricle is relatively dilated due to cardiac ischaemia. There is also some thickening of the aortic valve leaflets (arrows). (C) An axial image through a diseased aortic valve, with marked calcification of the aortic valve leaflets. (D and E) A similar view through a normal aortic valve in mid and late systole.

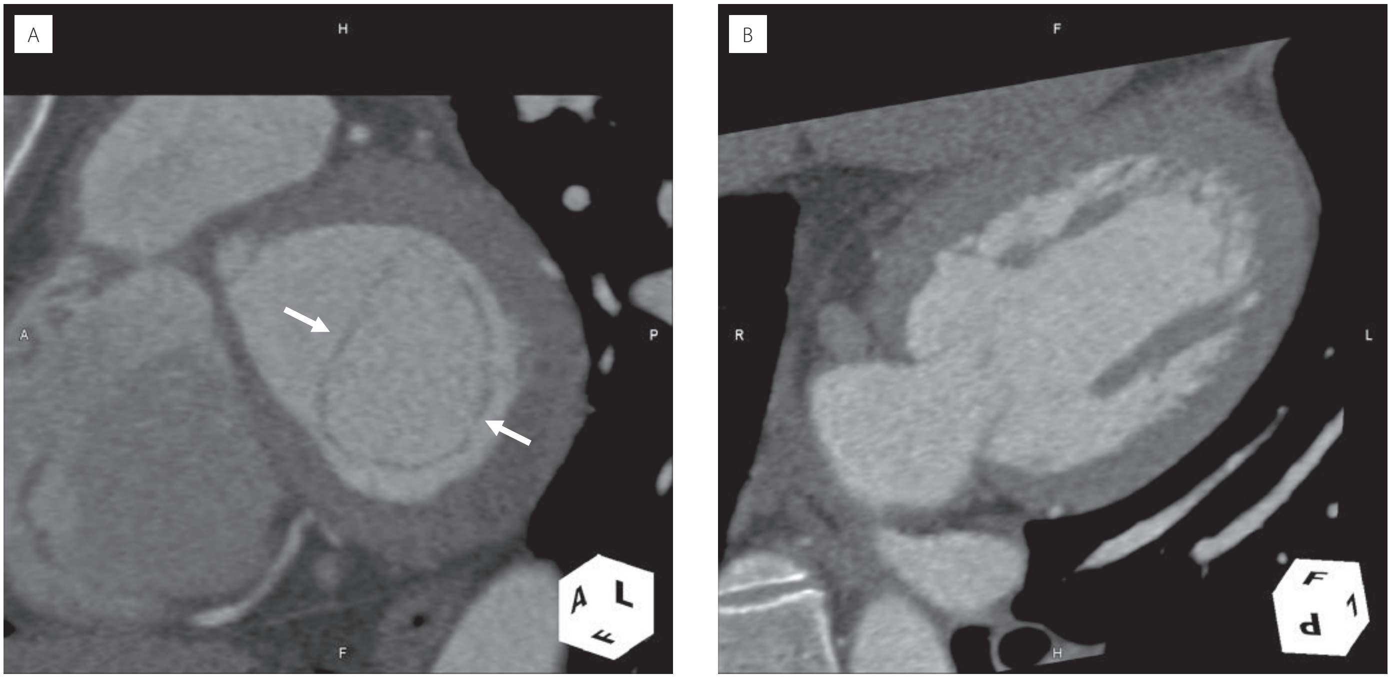


Fig. 7.17 (A) A short axis view through the left ventricle demonstrating the mitral valve leaflets (arrows). (B) Papillary muscles and mitral valve leaflets depicted in the horizontal long axis view.

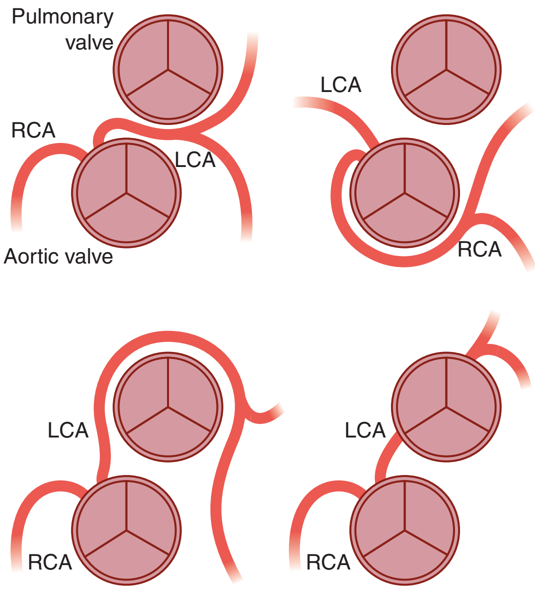


Fig. 7.18 Anomalous courses of the left coronary artery.

- In approximately 15% of patients, a third branch, the ramus intermedius (RI), arises at the division of the LCA, resulting in a trifurcation. The course of the RI is similar to the diagonal branches of the LAD (Fig. 7.19).

## Right coronary artery

- The right coronary artery (RCA) arises from the right sinus of Valsalva and courses in the right atrioventricular groove towards the crux of the heart (Fig. 7.20).
- The conus artery is the first branch of the RCA in approximately 50–60% of patients. In 30–35% of patients the conus artery arises directly from the aorta.
- In 58% of patients the sinoatrial nodal artery arises from the RCA and in the remaining 42% of patients it arises from the LCx. The ventricular branches arising from the RCA are the marginal arteries.
- The RCA terminates in the posterior descending artery in at least 70% of the population, along the inferior aspect of the interventricular septum, and the posterolateral branch to the posterolateral wall of the left ventricle. This indicates a right dominant system – see below (Fig. 7.21).

## Dominance

- The posterior descending artery (PDA) and the posterolateral branch supply the diaphragmatic wall of the left ventricle.
- The coronary artery that gives rise to the PDA and posterolateral branch is referred to as the 'dominant' artery. The RCA is dominant in 70% of cases and the LCA is dominant in 10% of cases (Fig. 7.22). When the LCA is dominant, the PDA and posterolateral branch arise from the LCx artery. In the remaining cases the RCA and LCA are codominant.

## Coronary veins

- The venous anatomy of the heart is variable but the most constant structure is the coronary sinus (CS) (Fig. 7.23).

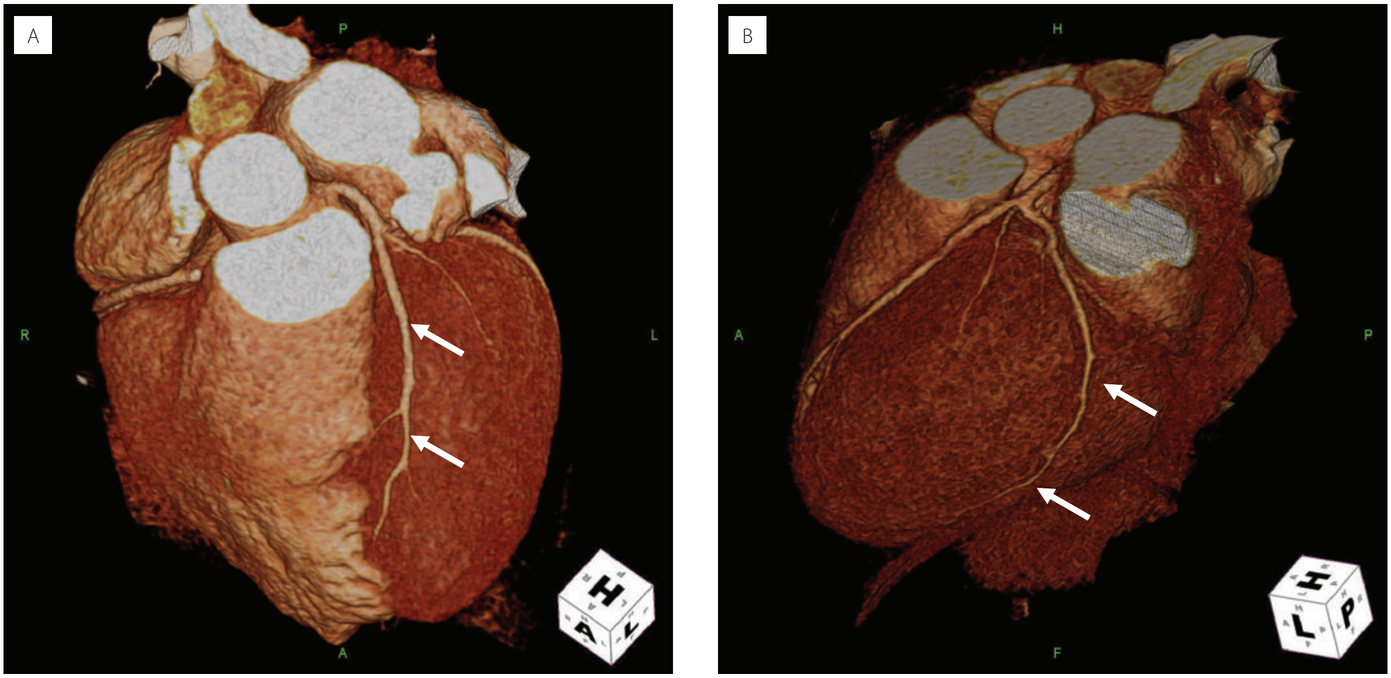


**Fig. 7.19** (A) The coronary arteries are seen over the surface of the cardiac structures. The left anterior descending vessel runs on the superior surface of the intraventricular septum (arrows). (B) The orientation of the heart has been rotated to demonstrate the obtuse marginal branch over the lateral surface of the left ventricle (arrows) giving an early diagonal branch.

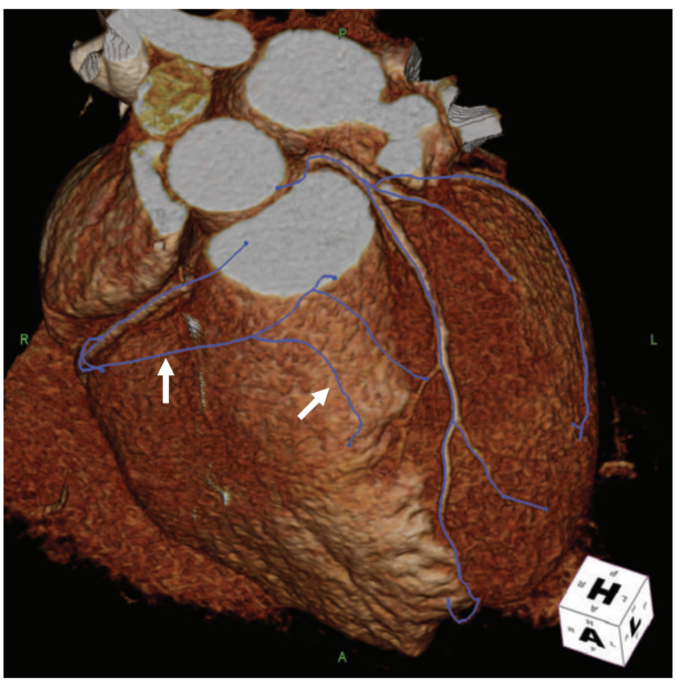


**Fig. 7.20** The course of the right coronary artery is depicted in blue (arrows). This passes in the atrioventricular groove and in this patient provides the posterior descending artery, being a dominant vessel.

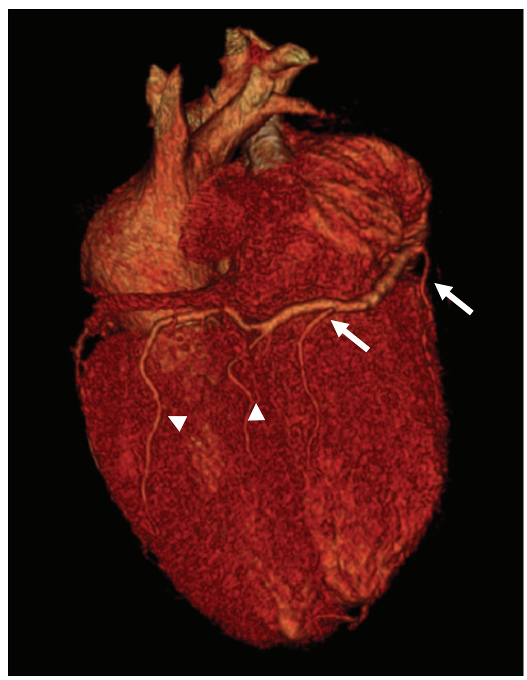

**Fig. 7.21** The heart viewed from below demonstrating a markedly dominant right coronary artery giving rise to the posterior descending and posterolateral vessels (arrowhead) as well as acute marginal vessels (arrows).

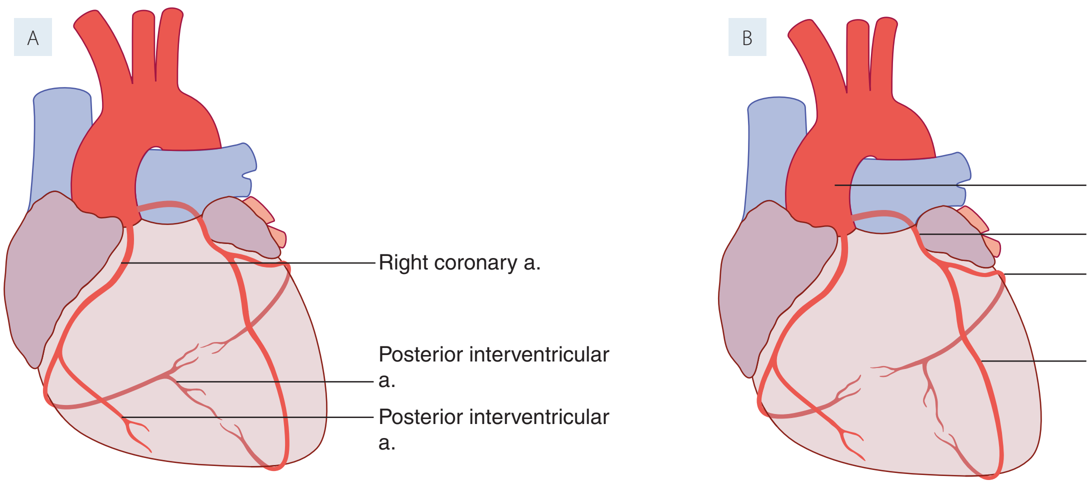


**Fig. 7.22** Variants of coronary dominance. (A) 85% of people have right dominance. (B) Less than 15% have left dominance.

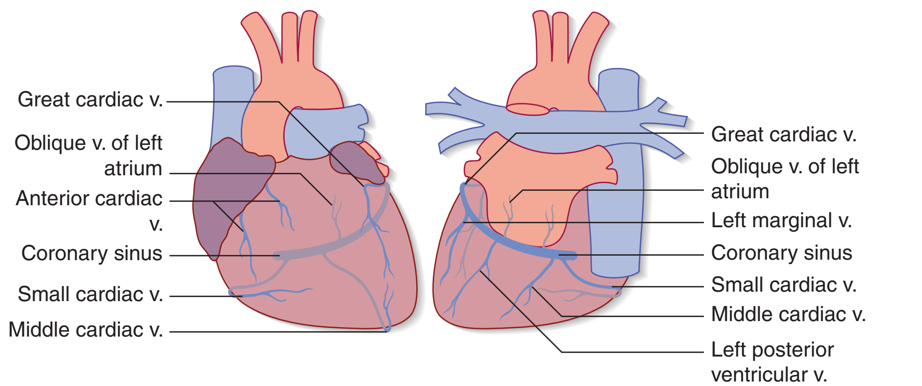


**Fig. 7.23** The anterior and posterior views of the heart depicting the courses of the coronary veins.

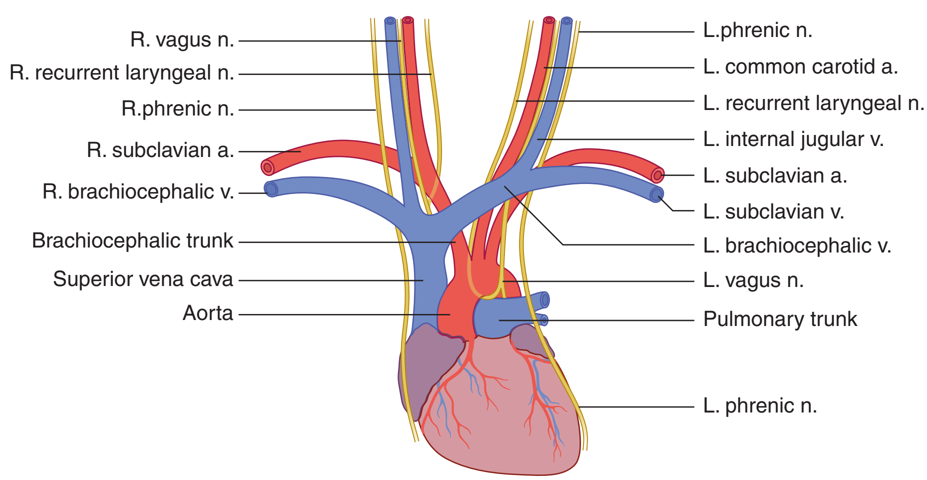


**Fig. 7.24** The inter-relationships of the great vessels within the superior mediastinum.

- The CS runs along the posterior atrioventricular groove before emptying into the right atrium.
- The first branch of the CS is the middle cardiac vein, which courses in the posterior interventricular groove.
- The next branches are the posterior vein of the left ventricle and the left marginal vein.
- The CS then becomes the great cardiac vein, which courses in the left atrioventricular groove with the LCx artery.
- The anterior cardiac veins empty directly into the right atrium.

## Great vessels See Fig. 7.24

### Aorta

In the thorax the aorta is divided into:

- Aortic root
  - The first few centimeters of aorta from its valve to just above the coronary sinuses is the aortic root and this segment is invested within the pericardium (Fig. 7.25).

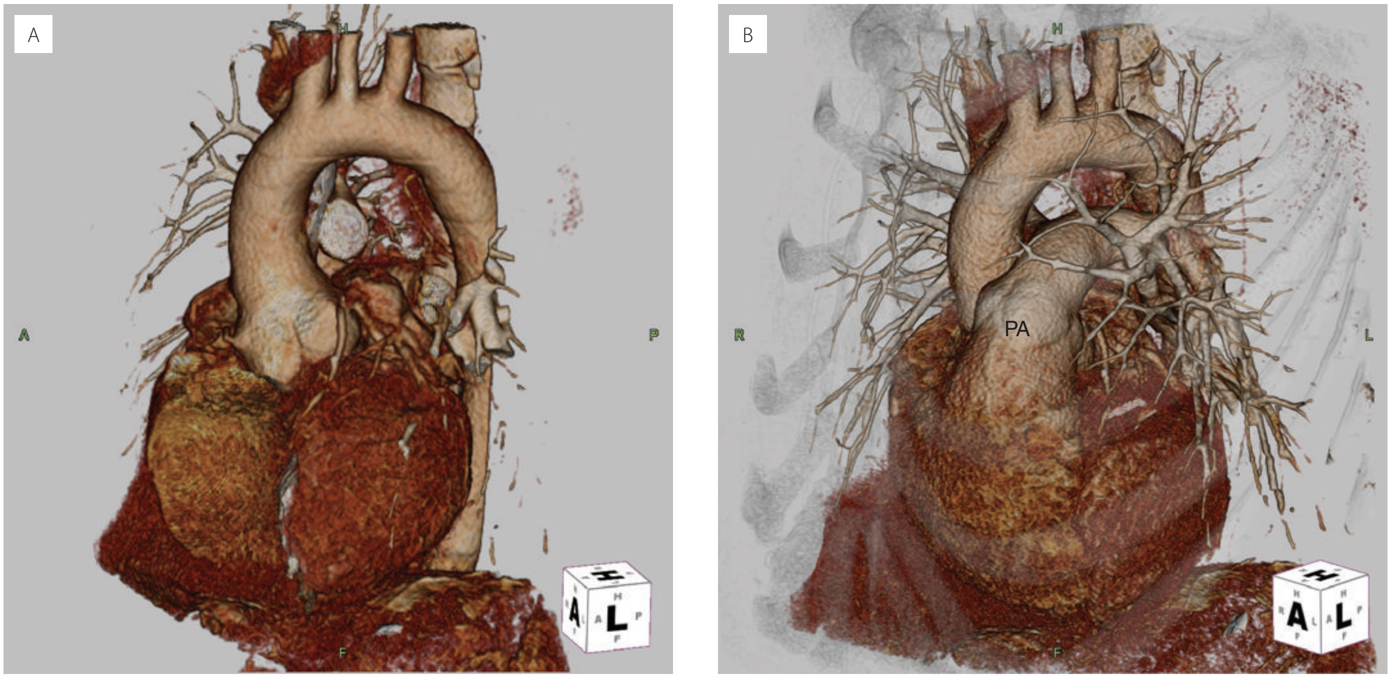


**Fig. 7.25** (A) An image derived from a contrast-enhanced CT scan demonstrating the normal aortic root. (B) The more anterior cardiac structures have been restored into the image in Fig. 7.25A to demonstrate the relationship between the pulmonary outflow tract and the aorta (PA = pulmonary artery).

- Ascending aorta
  - The ascending aorta courses upwards, anteriorly and to the right for a distance of approximately 5 cm, where it becomes the aortic arch (Fig. 7.25).
- Aortic arch
  - The aortic arch runs posteriorly from right to left. At first it lies anterior to the trachea and oesophagus, then over the pulmonary trunk and left main bronchus to a position left of the fourth dorsal vertebral body.
  - Beneath the arch the pulmonary trunk bifurcates and the right pulmonary artery passes to the right under the arch. The left pulmonary artery is attached to the junction of the arch and descending aorta by the ligamentum arteriosum.
  - In 65% the major vessels arising from the arch are:
    - brachiocephalic trunk, which subsequently divides into the right common carotid and right subclavian arteries (Fig. 7.26)
    - left common carotid artery
    - left subclavian artery.
    - variations in origin of the major vessels are common (Fig. 7.27).
- Descending aorta
  - Passes down the posterior mediastinum to the aortic hiatus of the diaphragm at the level of the 12th dorsal vertebral body (T12).

## Bronchial arteries

- The bronchial arteries have variable anatomy in terms of origin, branching pattern and course. The bronchial arteries originate directly from the descending thoracic aorta, most commonly between the T5 and T6 vertebrae. The four typical bronchial artery branching patterns are:
  - two on the left and one on the right that arises as an intercostobronchial trunk (ICBT) (41%)
  - one on the left and one ICBT on the right (21%)
  - two on the left and two on the right, one of which is an ICBT (21%)
  - one on the left and two on the right, one of which is an ICBT (10%) (Fig. 7.28).
- The right ICBT is the most consistently seen vessel at angiography (80% of individuals). The right ICBT usually arises from the right posterolateral aspect of the thoracic aorta and the normal right and left bronchial arteries from the anterolateral aspect of the aorta.
- Right and left bronchial arteries that arise from the aorta as a common trunk are not uncommon at angiography.

## Great veins

- The right and left brachiocephalic veins are located anterior to the arch vessels.
- The right brachiocephalic vein has a vertical course and lies anterior and to the right of the trachea (Fig. 7.29).
- The left brachiocephalic vein follows a more horizontal course (Fig. 7.30).
- The superior vena cava (SVC) is formed by the confluence of the two brachiocephalic veins. The SVC lies to the right of the aortic arch and drains into the right atrium (Fig. 7.29).
- The most common anatomical variant of the SVC is a double SVC. A double SVC can occur as an incidental finding or be associated with cardiac abnormalities such as an atrial septal defect (ASD), Fallot's tetralogy and

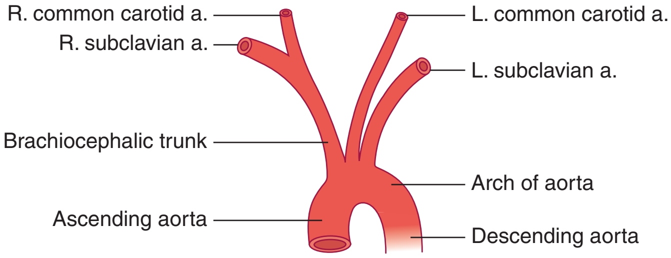


Fig. 7.26 Most common appearance of the aortic arch.

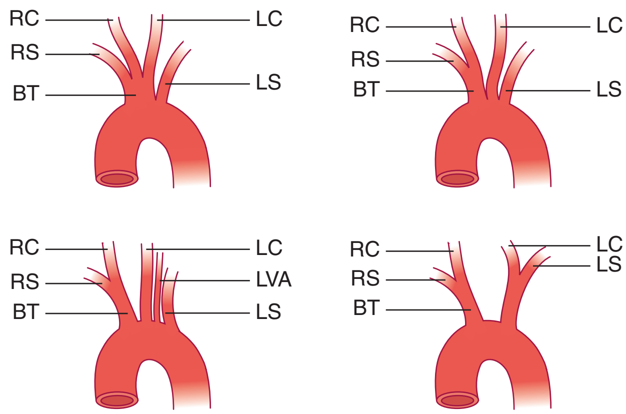


| | | | |
|---|---|---|---|
| **RC** | Right common carotid artery | **LC** | Left common cartoid artery |
| **RS** | Right subclavian artery | **LVA** | Left vertebral artery |
| **BT** | Brachiocephalic trunk | **LS** | Left subclavian artery |

Fig. 7.27 Variations in the appearances of the arch.

coarctation of the aorta. The persistent left SVC represents failure of obliteration of the left anterior cardinal vein present in early embryological development. In 90% of cases the persistent left-sided SVC connects to the right atrium via the coronary sinus (Fig. 7.31). In 10% the left SVC connects to the left atrium, resulting in a right-to-left shunt. The left SVC situated at the angle between the left pulmonary veins and the left atrial appendage can be mistaken for lymphadenopathy on CT.

- A single left-sided SVC is a much rarer variant and may be mistaken for partial anomalous pulmonary venous return.
- The azygos vein passes behind the right crus of the diaphragm to lie in the azygo-oesophageal recess, passing cranially until it arches forward over the tracheobronchial junction on the right to join the posterior surface of the SVC.
- The hemiazygos vein usually drains into the azygos vein at T8 but the hemiazygos–azygos system is quite variable in its course and drainage pattern. The hemiazygos vein may drain directly into the SVC or into the left brachiocephalic vein (Fig. 7.32).

## Pulmonary artery

- The main pulmonary trunk (MPT) is the continuation of the right ventricular outflow tract separated by the pulmonary valve. The MPT bifurcates into right (RPA) and left (LPA) pulmonary arteries (Fig. 7.33).

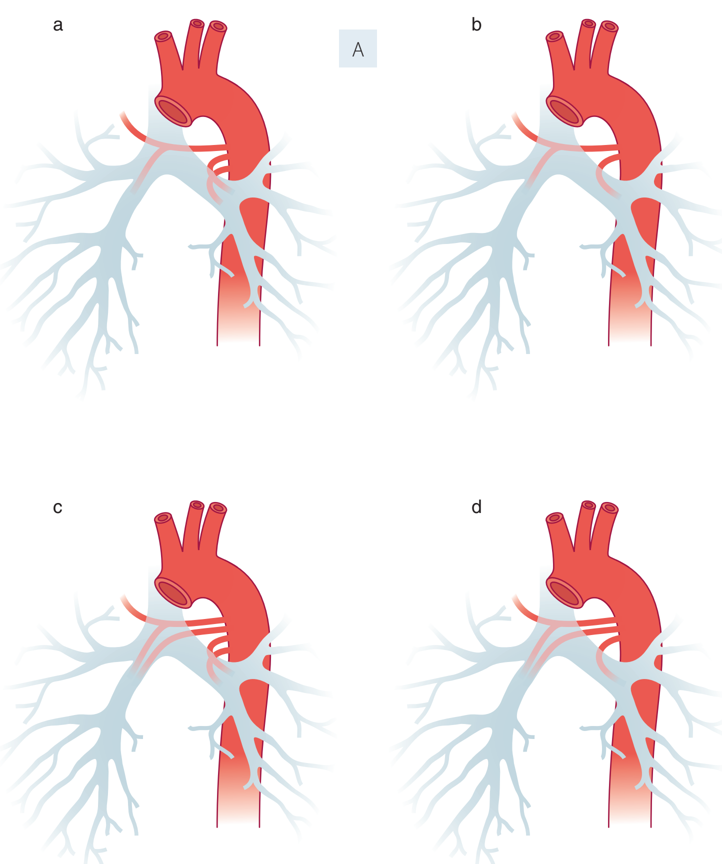


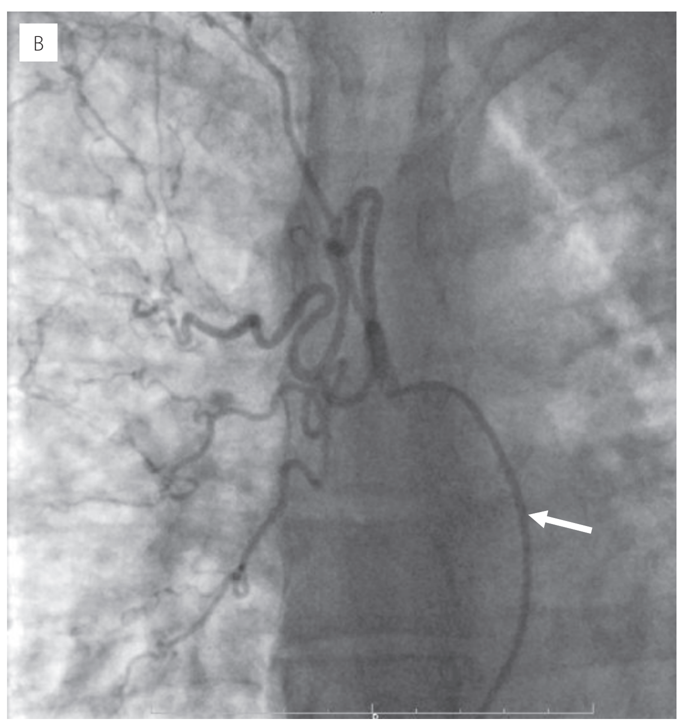


Fig. 7.28 (A) Commonly encountered variations in the bronchial artery origins. (B) This is an image from an angiogram in which a catheter (arrow) has been placed in a separate right bronchial trunk into which contrast has been injected to show the bronchial circulation to the right lung.


**Fig. 7.29** In this patient contrast has been injected into the right antecubital fossa and outlines the right subclavian vein and the superior vena cava.

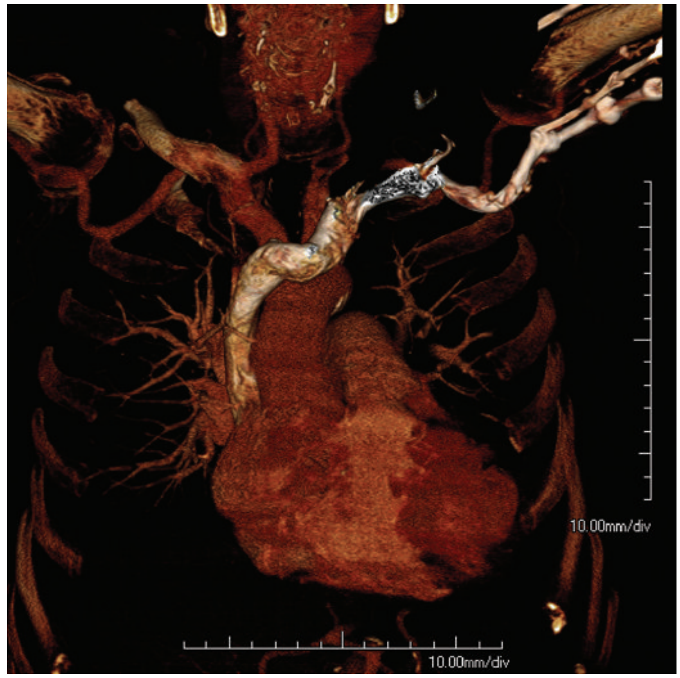


**Fig. 7.30** In this patient contrast has been injected by the left arm and demonstrates the more horizontal and longer course of the left brachiocephalic vein prior to joining the superior vena cava.

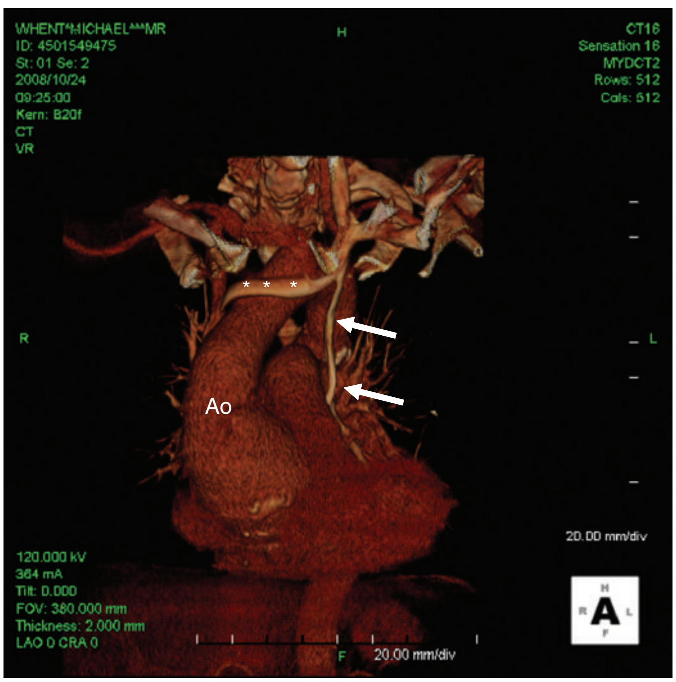


**Fig. 7.31** In this patient there is a persistent left superior vena cava (arrows) which continues to drain inferiorly into the coronary sinus. The left brachiocephalic vein (*) crosses anterior to the aorta (Ao).

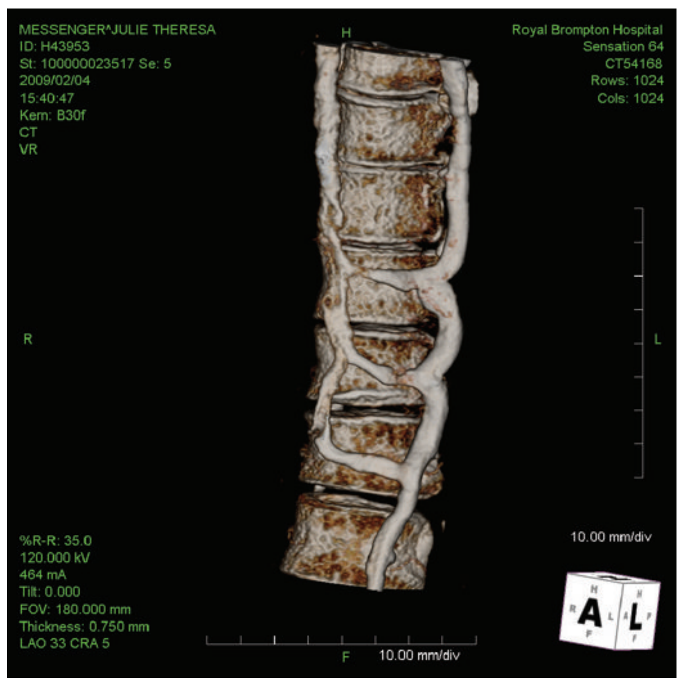


**Fig. 7.32** The hemiazygos and azygos veins join in the mid-lumbar level via communicating vessels that pass anterior to the vertebral bodies.

- The LPA is a direct posterior continuation of the MPT. It courses anteroinferior to posterosuperior over the left main bronchus before dividing into upper and lower lobe trunks.
- The RPA arises almost perpendicular to the MPT and LPA. The RPA then crosses the mediastinum from left to right almost horizontally under the aortic arch before dividing into a smaller upper and a larger lower trunk.
- Anomalous origin of the LPA, which may form a pulmonary sling, can be symptomatic in infancy or adulthood. It could also represent an incidental finding in

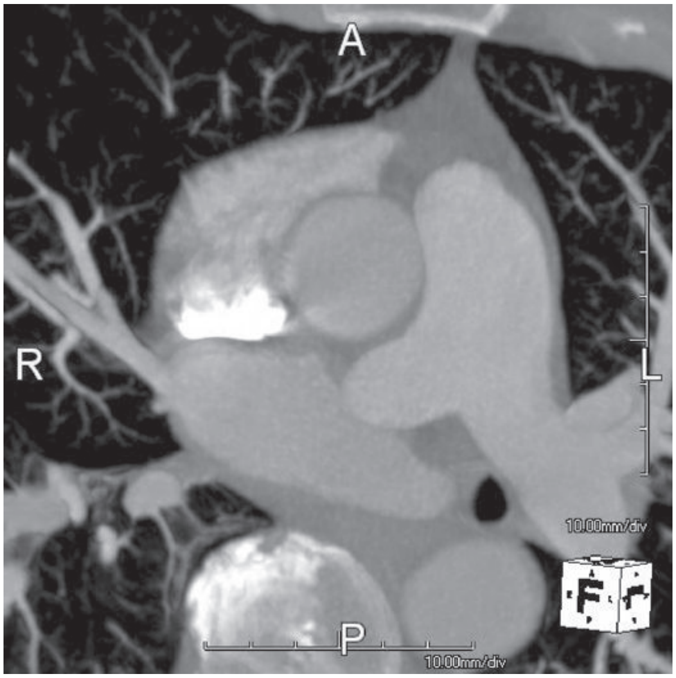


**Fig. 7.33** The pulmonary arteries.

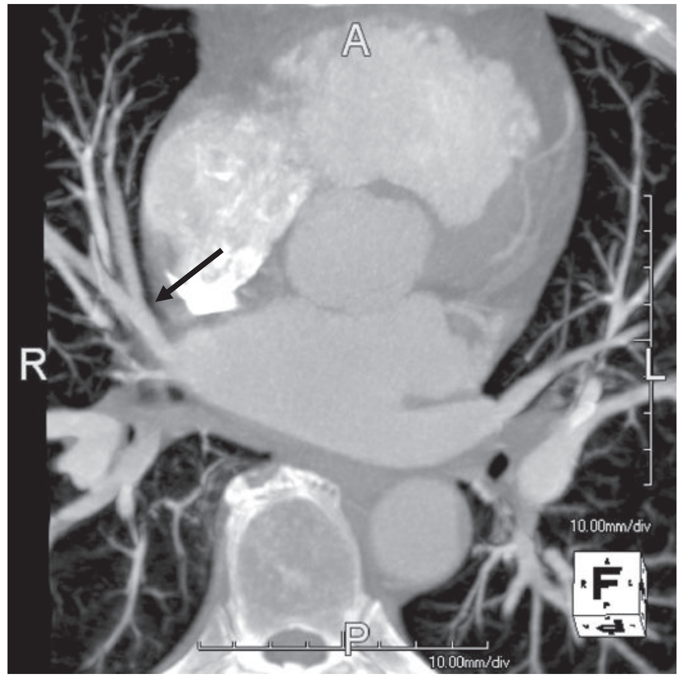


**Fig. 7.34** In this patient there is a separate vein draining the middle lobe into the left atrium (arrow).

an asymptomatic adult. Usually the aberrant LPA arises from the RPA and initially passes lateral to the trachea. It then turns abruptly to the left and passes in between the trachea and oesophagus before reaching the left hilum.

## Pulmonary veins

- Typically four pulmonary veins drain into the left atrium (Fig. 7.8). Normally the upper lobe veins drain the upper and middle lobes on the right and the upper lobe and lingula on the left. The lower lobe veins drain their corresponding lower lobe.
- On the left, it is relatively common to see a common pulmonary vein trunk formed by the confluence of the upper and lower lobe veins. A common right pulmonary vein trunk is relatively uncommon.
  - The site of drainage of the right middle pulmonary vein can be variable (Fig. 7.34). Variants include:
    - directly into the left atrium
    - common ostium with the proximal right superior pulmonary vein
    - right inferior pulmonary vein.

Chapter 8

# The breast

Steven D. Allen

## Introduction

The breast consists mainly of fat and glandular tissue, the latter varying throughout life, in response to female hormones. It approximately overlies the second to sixth ribs and is entirely enveloped in chest wall fascia, which forms septae called Coopers suspensory ligaments. These support the breast, running from the fascia of the pectoralis muscles posteriorly to the skin anteriorly (Fig. 8.1). The internal mammary (thoracic) and lateral thoracic arteries are the main blood supply, supplemented by anterior intercostal and thoracoacromial branches. Venous drainage essentially corresponds to the arteries, with some passage via the azygous system. Lymphatic drainage is of special significance, as spread of primary breast cancer is most commonly disseminated via this route. The majority of lymph passes towards the axilla, where surgically three levels of axillary nodes are denoted in relation to the pectoralis minor muscle (Fig. 8.2). Level 1 nodes are inferolateral, level 2 are posterior and level 3 are superomedial. Part of the medial breast also drains to the internal mammary nodes.

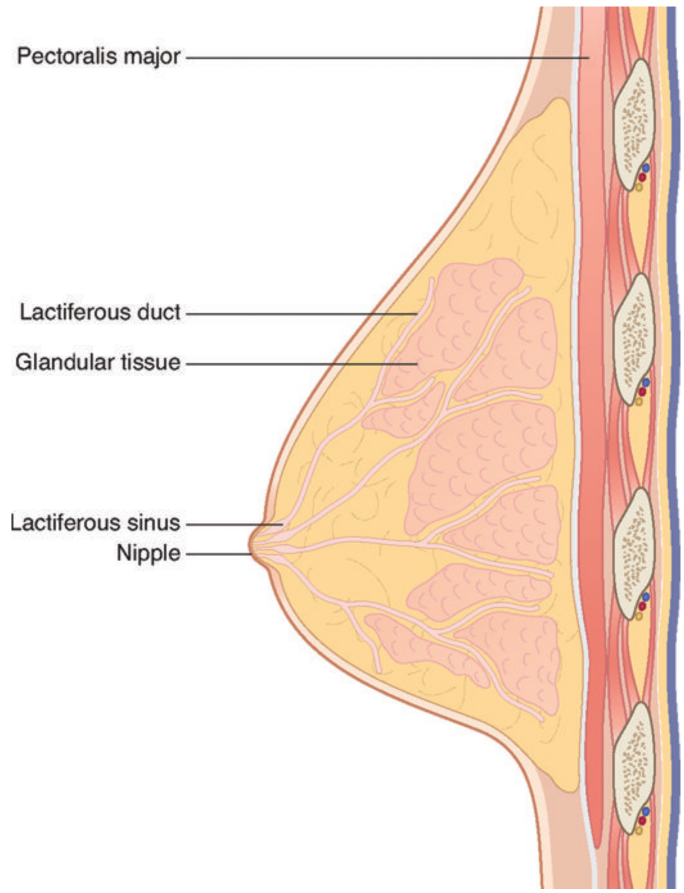


**Fig. 8.1** Line diagram showing anatomical detail in the mediolateral oblique view, as seen on this standard mammographic projection. The breast is seen to consist mainly of fat and glandular tissue, and is entirely enveloped in chest wall fascia, which forms septae called Coopers suspensory ligaments. These support the breast, running from the fascia of the pectoralis muscles posteriorly to the skin anteriorly.

## Embryology/mimics

The breasts develop from an ectodermal milk line running from the axilla to the groin on each side. This thickens and gives rise to 15 to 20 outbuddings which in turn form ducts and then lobes. Several lobules compose each lobe, subdivided by fibrotic and fatty stroma. Each lobule is composed of several acini, the blind saccules that secrete the milk of lactation, as well as their draining ducts. The smallest anatomical unit within the breast is termed the terminal duct lobular unit (TDLU), where the majority of malignant pathologies arise (Fig. 8.3).

Incomplete regression of the milk line can result in an accessory nipple (Fig. 8.4), usually just inferior to the normal nipple, though accessory breast tissue is more common (Fig. 8.5). Congenital absence of breast tissue termed amazia (except nipple) and amastia (all tissue) is rare, though hypoplasia can occur if there is underdevelopment of the chest wall (Poland's syndrome, Fig. 8.6). The normal chest wall can be difficult to distinguish from pathology, if there is a prominent costosternalis muscle (Fig. 8.7). Congenital nipple inversion is much less common than acquired inversion (Fig. 8.8). Breast calcification is very common and can be considered normal where an arterial wall is seen to calcify (Fig. 8.8). Other processes such as plasma cell mastitis, causing often florid benign calcification, should not be confused with sinister pathology (Fig. 8.9). Skin lesions such as sebaceous cysts and moles, particularly if they calcify, can simulate breast pathology

*Applied Radiological Anatomy, 2nd Edition* ed. Paul Butler, Adam W.M. Mitchell and Jeremiah C. Healy. Published by Cambridge University Press.

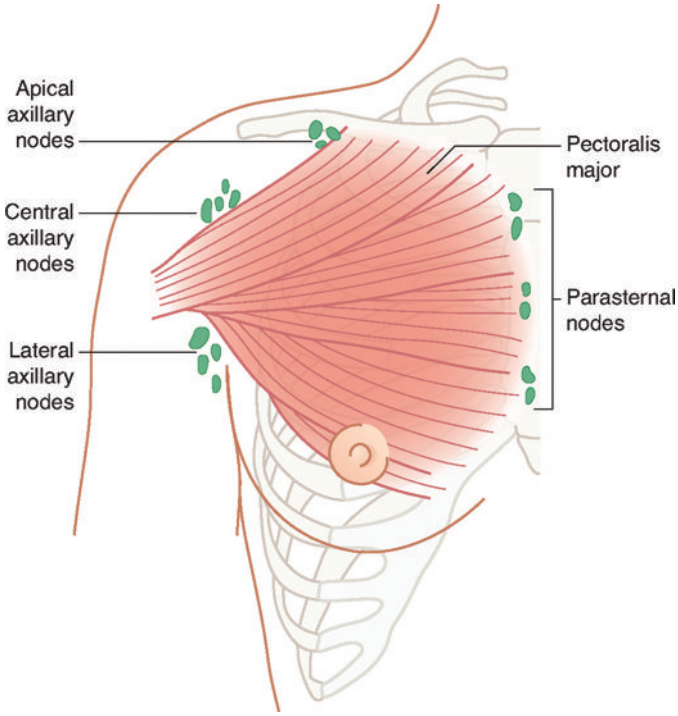


**Fig. 8.2** Line diagram showing the lymphatic drainage of the breast. This is of special significance, as spread of primary breast cancer is most commonly disseminated via this route. The majority of lymph passes towards the axilla, where surgically three levels of axillary nodes are denoted in relation to the pectoralis minor muscle. Level 1 nodes are inferolateral, level 2 are posterior and level 3 are superomedial. Part of the medial breast also drains to the internal mammary nodes.

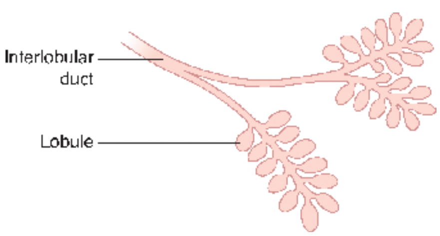


**Fig. 8.3** Line diagram showing the smallest anatomical unit within the breast, which is termed the terminal duct lobular unit (TDLU). This is where the majority of malignant pathologies arise. Several lobules compose each lobe, subdivided by fibrotic and fatty stroma. Each lobule is composed of several acini, the blind saccules that secrete the milk of lactation, as well as their draining ducts.

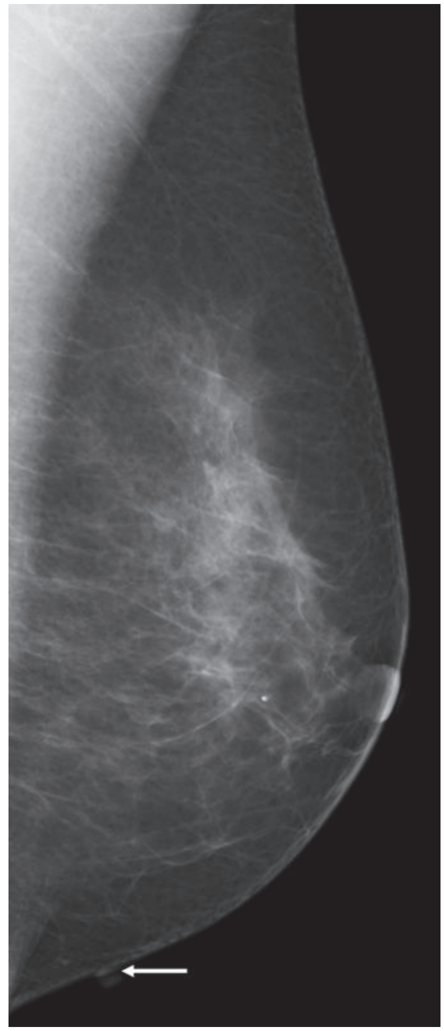

**Fig. 8.4** Left mediolateral oblique mammogram showing a density arising from the skin just beneath the nipple. This is an accessory nipple arising in the primitive milk line.

(Fig. 8.10), though their appearances are usually pathognomic. Many artefacts can mimic or mask pathology and these include specks of deodorant which can appear very much like microcalcification, hair, surgical clips and pacemakers (Figs. 8.11–8.14).

## Mammographic anatomy

Low-energy X-rays exploit the contrast between soft tissue densities to demonstrate the internal architecture of the breast. This technique requires breast compression, with the two standard views remaining the mediolateral oblique and the craniocaudal projections. The former view should show the pectoralis major muscle posteriorly, ideally to nipple level, which itself should be in profile. The supra and inframammary folds should be visible. Skin thickness should be uniform, with focal thickening often representative of pathology. Ducts are usually not identified unless ectatic, calcified and surrounded by fat (Fig. 8.9). Vessels can be traced as linear densities traversing the breast in an undulating fashion, while the suspensory ligaments are more linear and finer. Intramammary nodes are usually in the axillary tail and are small, ovoid or round, and may have a fatty hilum (Fig. 8.15).

Breast density is variable, and is often related to the woman's age. Younger women have denser breasts with anatomical detail difficult to differentiate, but with increasing age fibroglandular tissue is often replaced by more radiolucent fatty tissue, making contrast with lesions more striking (Figs. 8.16–8.18). Women with continued prominent fibroglandular tissue despite advancing age are at an increased risk of breast cancer.

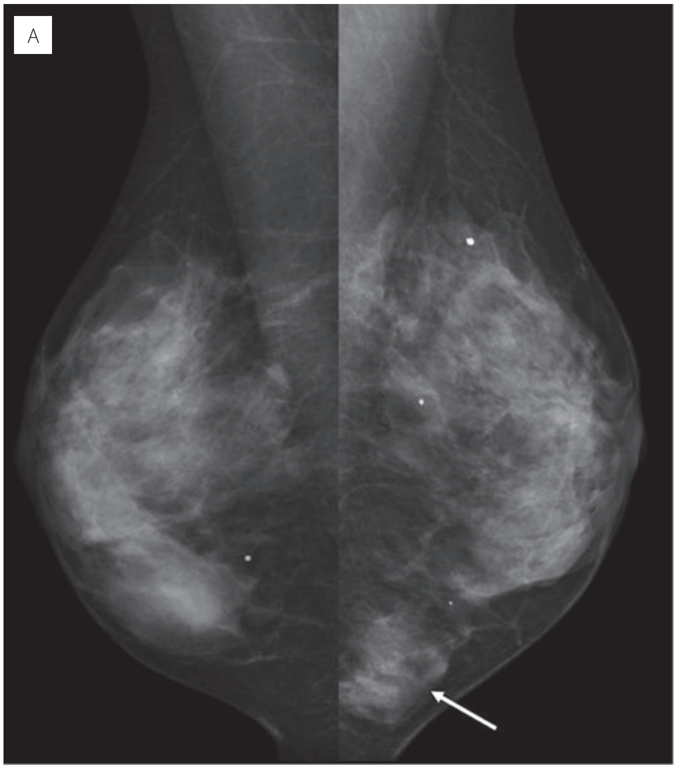


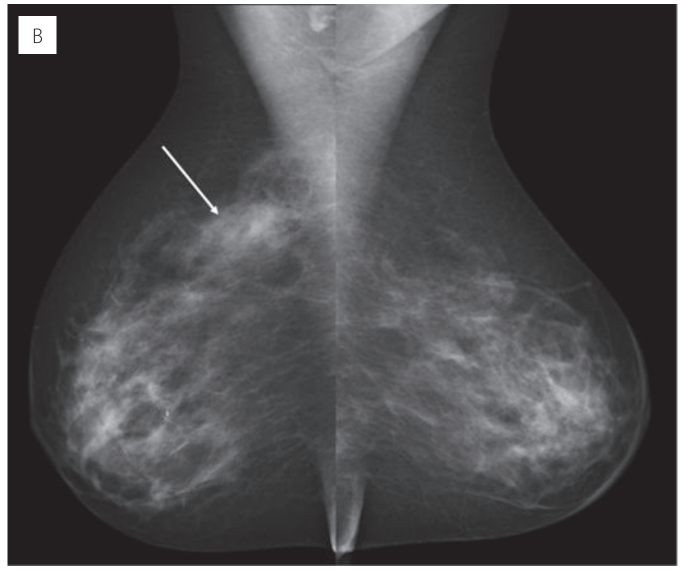


**Fig. 8.5** (A) Mediolateral oblique mammograms showing an asymmetric area of tissue with identical appearances to the main glandular breast tissue (arrow). This is an area of accessory breast tissue, which is more often present superiorly to the main breast plate than at this site. (B) Mediolateral oblique mammograms showing an asymmetric area of tissue with identical appearances to the main glandular breast tissue (arrow). This is an area of accessory breast tissue, which is a normal variant.

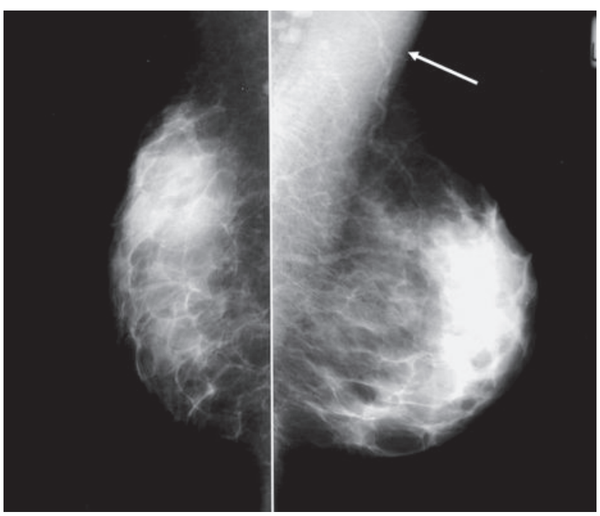

**Fig. 8.6** Mediolateral oblique mammograms showing a normal left pectoralis major muscle (arrow). This is absent on the right side in Poland's syndrome, and can be considered a congenital normal variant. This image is courtesy of Dr Louise Wilkinson.

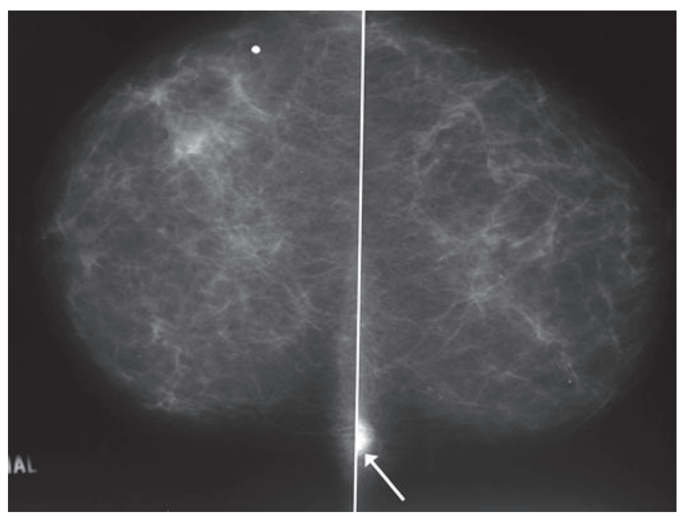

**Fig. 8.7** Craniocaudal mammograms showing a density on the chest wall posteriorly, medially on the left side (arrow). At this site, this density is typical of the chest wall muscle, costosternalis, although distinguishing this from pathology can be difficult.

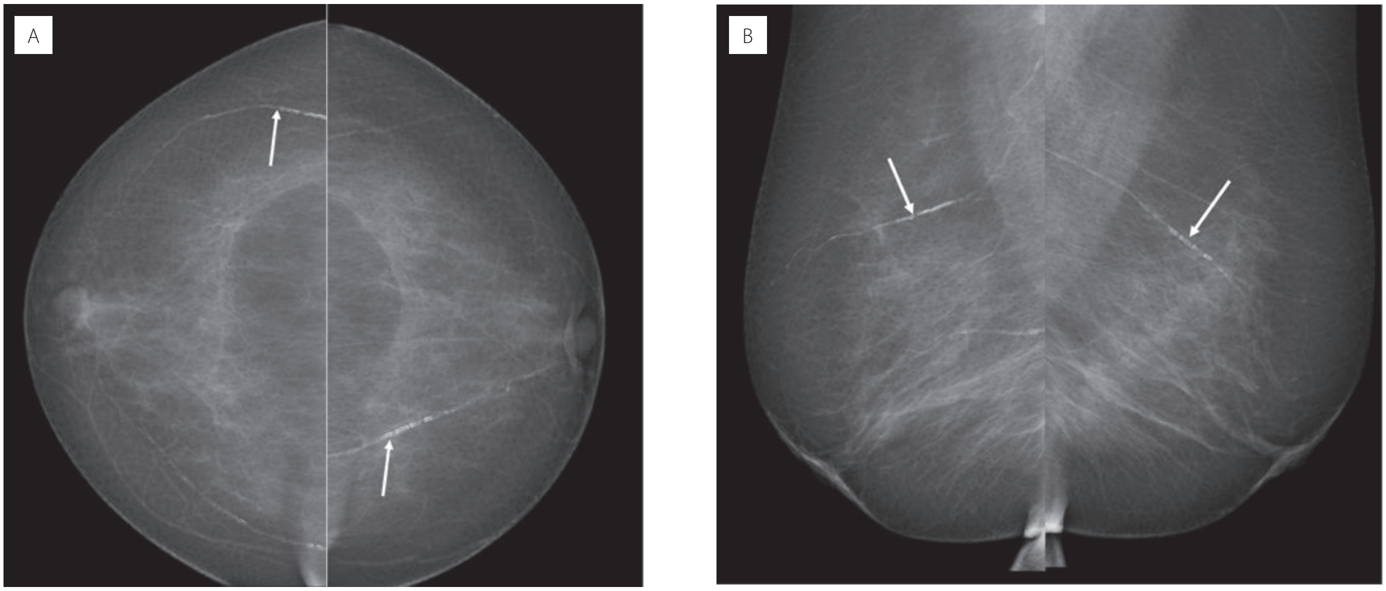


**Fig. 8.8** (A) Craniocaudal mammograms showing the nipples not projected in profile, instead over the retroareolar tissues. These should not be confused with retroareolar lesions. (B) Mediolateral oblique mammograms showing the retroareolar regions to be clear, with the nipples retracted slightly bilaterally. Incidental vascular calcifications are also noted on all films (arrows).

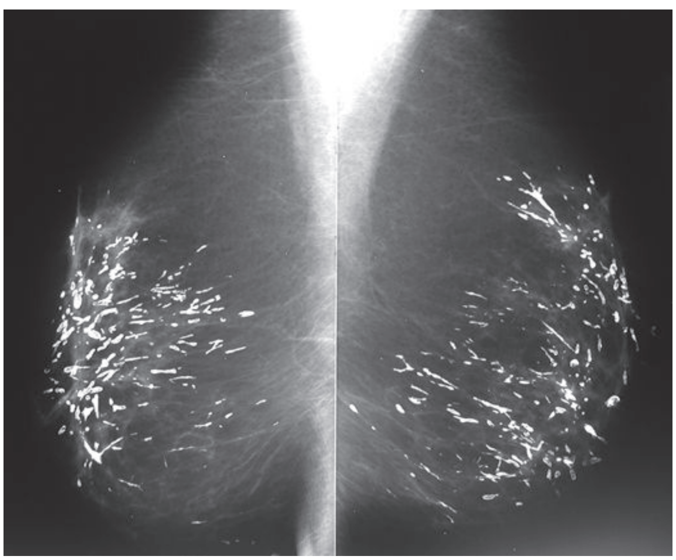

**Fig. 8.9** Mediolateral oblique mammograms showing widespread calcification. This process is ductal, with the anatomical sites of these beautifully denoted. This process is benign and often age-related, as the appearance of these forms is very coarse, and widespread. This image is courtesy of Dr Louise Wilkinson.

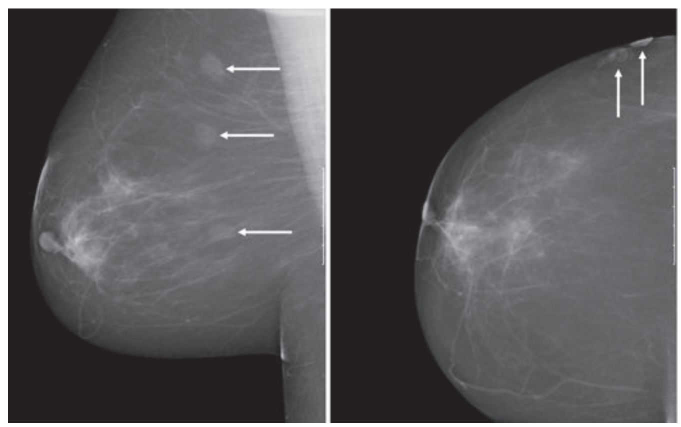

**Fig. 8.10** Right mediolateral oblique and craniocaudal mammograms showing multiple well defined densities. On the latter view these are clearly arising in the skin, representing moles, and should not be confused with true breast pathology.

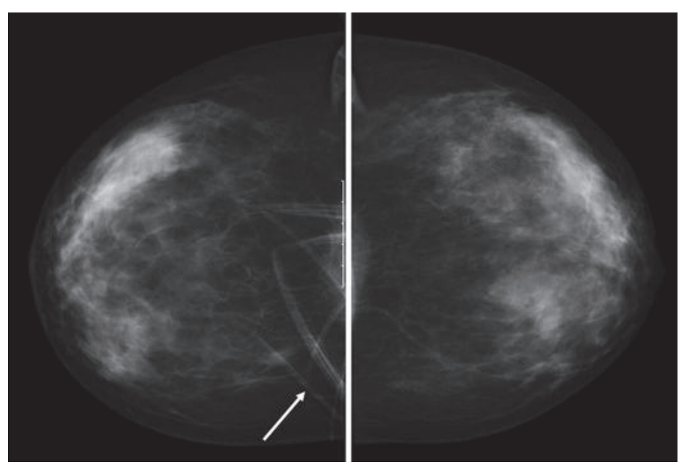

**Fig. 8.11** Craniocaudal mammograms showing linear artefact on the right side posteriorly (arrow). This is representative of hair extensions overlying the breast tissue, and this should not be confused with pathology.

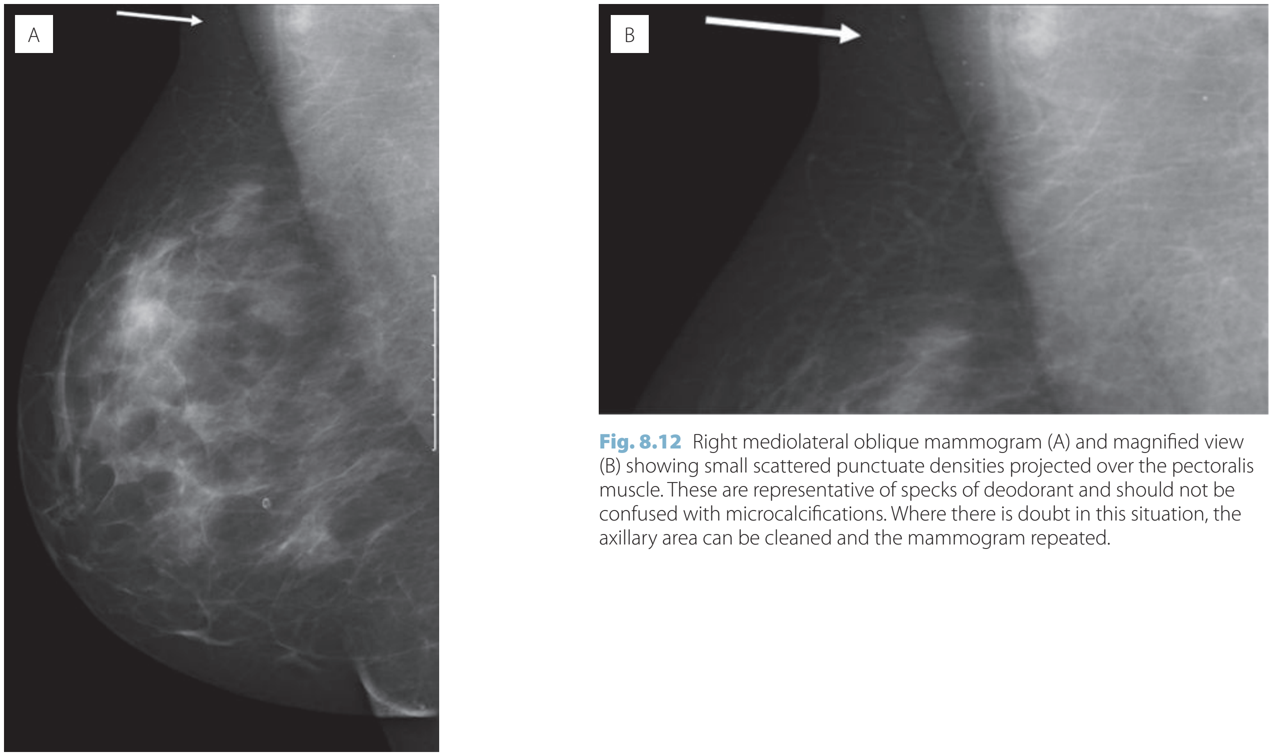


**Fig. 8.12** Right mediolateral oblique mammogram (A) and magnified view (B) showing small scattered punctuate densities projected over the pectoralis muscle. These are representative of specks of deodorant and should not be confused with microcalcifications. Where there is doubt in this situation, the axillary area can be cleaned and the mammogram repeated.

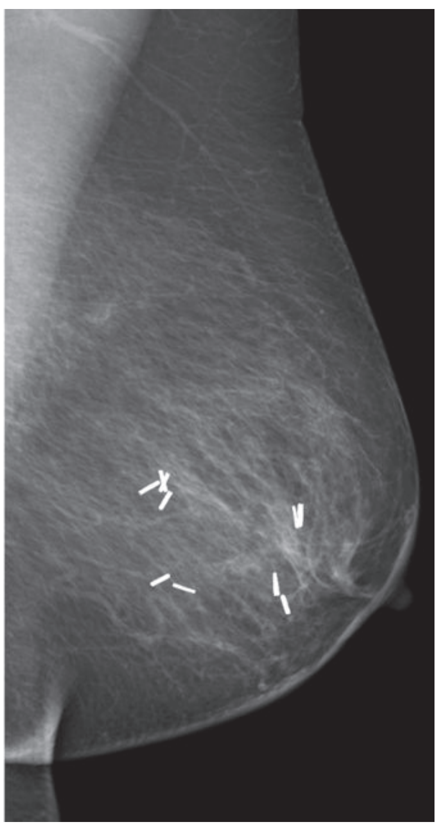

**Fig. 8.13** Left mediolateral oblique mammogram showing a number of metallic densities projected centrally within the breast. These are surgical clips left following an excision of a breast cancer to denote a target for the radiotherapy field. A recent surgical development, they are permanent once placed and will increasingly be present on mammograms in patients who have previously had breast cancer.

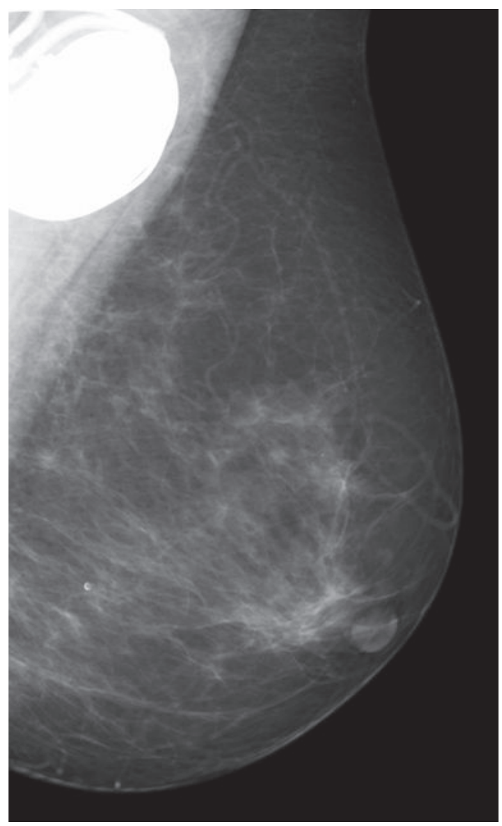

**Fig. 8.14** Left mediolateral oblique mammogram showing a metallic density projected over the pectoralis muscle. This is a pacemaker, and as well as possibly obscuring overlying breast tissue, is usually a contraindication for an MRI scan.

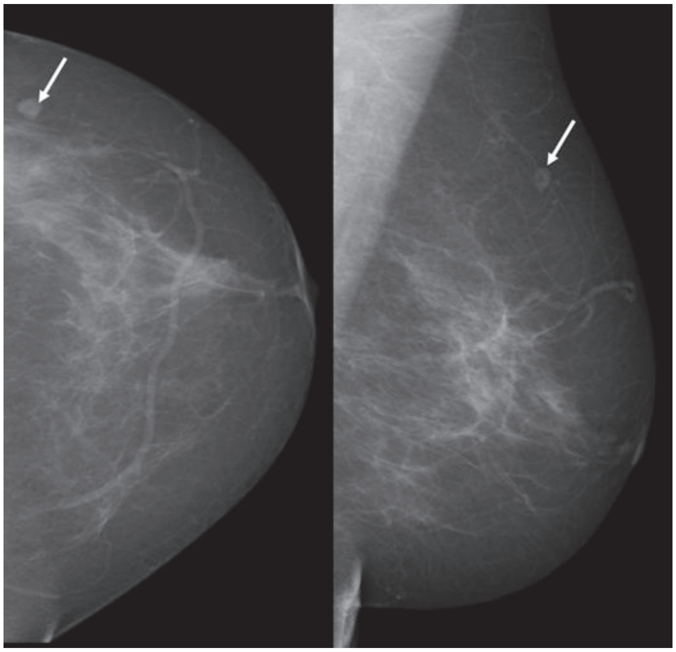

**Fig. 8.15** Left mediolateral oblique and craniocaudal mammograms showing a focal density in the upper outer breast (arrow). The low-density centre of this density and its lobulated outline are typical of a normal intramammary node, and this should not be confused with pathology.

**Fig. 8.16** Mediolateral oblique mammograms showing an involuted background parenchymal pattern. With this breast density pattern, the sensitivity of mammography as a test is excellent, as it is very straightforward to distinguish a lesion from the normal breast tissue.

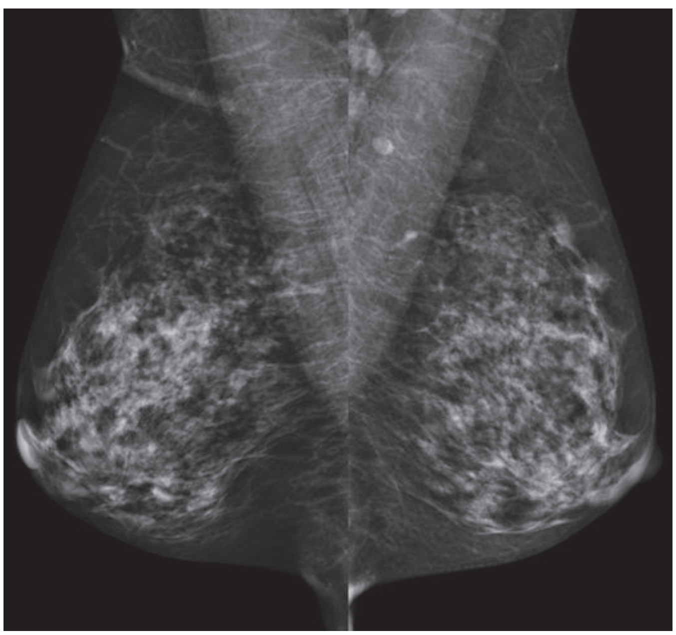

**Fig. 8.17** Mediolateral oblique mammograms showing a nodular background parenchymal pattern. With this breast density pattern, the sensitivity of mammography as a test is reduced, as it is difficult to distinguish a lesion from the normal islands of breast tissue.

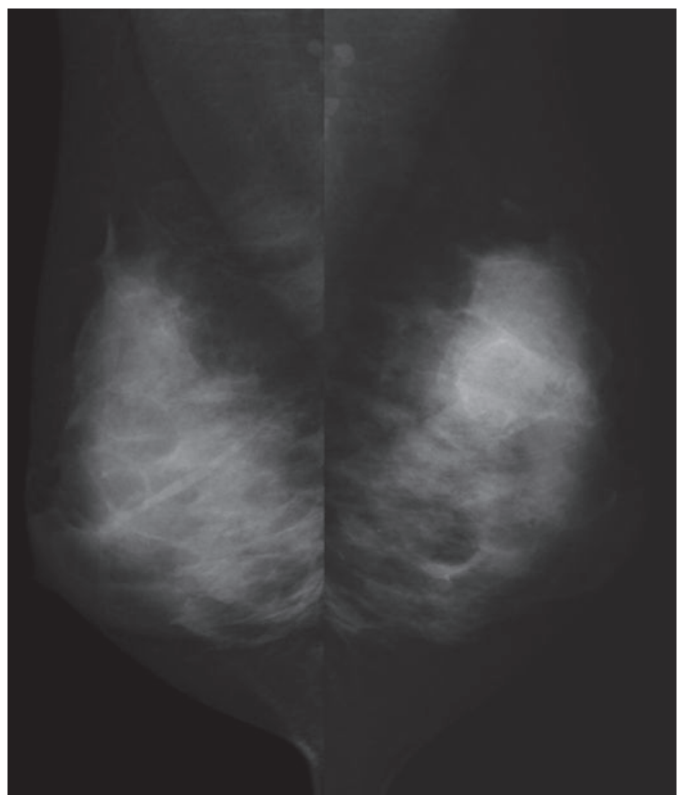

**Fig. 8.18** Mediolateral oblique mammograms showing a fairly uniformly dense background parenchymal pattern. With this breast density pattern, the sensitivity of mammography as a test is substantially reduced, as it is very difficult to distinguish a lesion from the normal breast tissue.

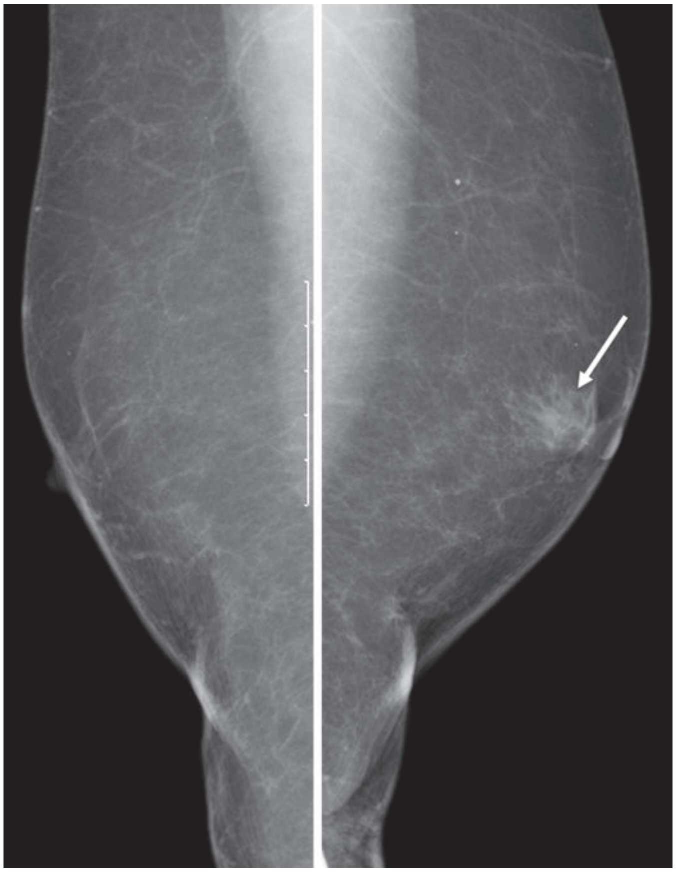

**Fig. 8.19** Mediolateral oblique mammograms in an elderly man. On the left side a small amount of rudimentary breast tissue is present (arrow), though this does not have sinister features to suggest malignant pathology.

Mammography is rarely performed in a man and is usually to differentiate gynaecomastia from breast cancer. In the former, normal fatty tissue is seen with either a rudimentary ductal or glandular pattern in a retroareolar position (Fig. 8.19).

## Ultrasound anatomy

Ultrasound is usually a primary investigation in younger women, otherwise a secondary investigation after a mammogram. A high-frequency probe is used (at least 12 MHz, but increasingly 15 and 18 MHz), and the different anatomical layers of skin, subcutaneous tissue, interlobular fat, fibroglandular tissue and chest wall can be delineated (Figs. 8.20, 8.21). Adipose tissue in fat lobules appears hypoechoic, with ducts tubular and radiating from the nipple. Fibroglandular tissue is usually echogenic, and can cast acoustic shadowing where dense. Deep to the pectoralis muscles, ribs cast acoustic shadowing and the pleura is seen as a linear bright line. Lymph glands are usually ovoid with a prominent echogenic fatty centre.

## MRI anatomy

This is a developing technique but is increasingly used in a number of roles as a second- or third-line investigation. This

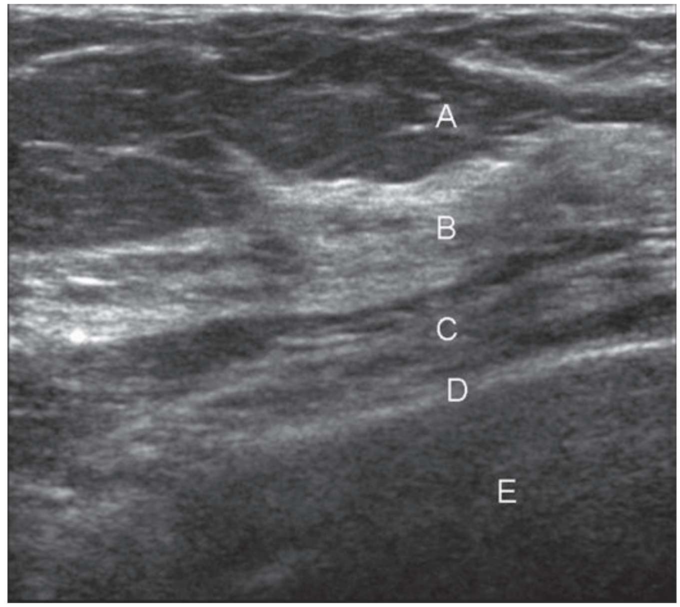


**Fig. 8.20** An ultrasound image of a left breast, with mixed parenchymal and fatty tissue. (A) represents subcutaneous fat, (B) represents undulating glandular tissue, (C) represents pectoralis muscle, (D) represents the pleura, (E) represents the lung.

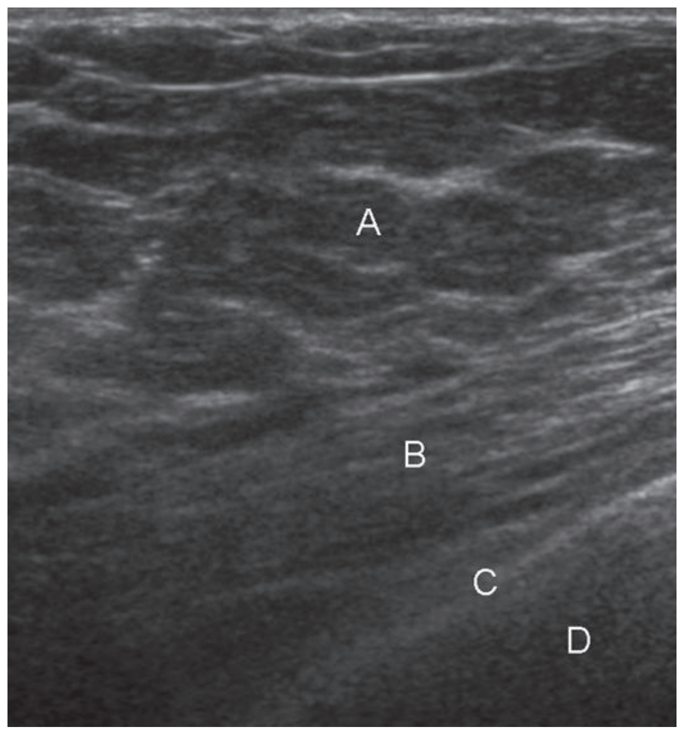


**Fig. 8.21** An ultrasound image of an involuted left breast. (A) represents subcutaneous fat, (B) represents pectoralis muscle, (C) represents the pleura, (D) represents the lung.


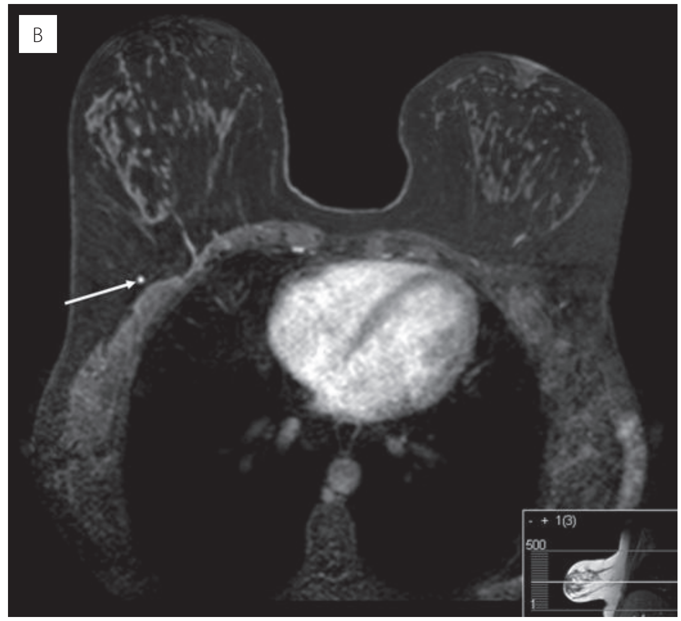


**Fig. 8.22** (A) Unenhanced sagittal image of the left breast in a woman with a moderately involuted parenchymal pattern. More anatomy outside the breast is seen on this modality than on conventional mammography and ultrasound, with a degree of cross-sectional anatomy of the whole thorax available. Views of the upper axilla are often possible with the axillary vessels denoted (arrow). (B) Fat-saturated image post contrast during dynamic contrast administration allows differentiation of breast tissue from pathology by enhancement characteristics of the respective tissues. A small benign axillary lymph node is seen to enhance (arrow).

is performed with the patient prone and the breasts suspended in a receiver coil. As well as the breasts, the axillae, chest wall and variably the mediastinum and spine are demonstrated on certain sequences. It requires administration of intravenous gadolinium, unless the study is to assess for implant rupture. It is ideally performed early in the menstrual cycle such that there is minimal enhancement of background normal breast parenchyma. With its multiplanar capability, and in particular due to the effect of enhancement, excellent differentiation can be made between normal breast parenchyma and pathology even where there is marked background breast density (Fig. 8.22).

Chapter 9

# The anterior abdominal wall and peritoneum

Nishat Bharwani and Rodney H. Reznek

## Radiographic anatomy

### Anterior abdominal wall

Plain film radiography (Fig. 9.1) is not used to evaluate the anterior abdominal wall.

### Peritoneum

Plain radiography (Fig. 9.1) has been superseded by cross-sectional imaging techniques and the peritoneal cavity is visualized only via contrast herniography (Fig. 9.2).

## Cross-sectional anatomy

Cross-sectional imaging techniques optimally assess the anterior abdominal wall and peritoneum.

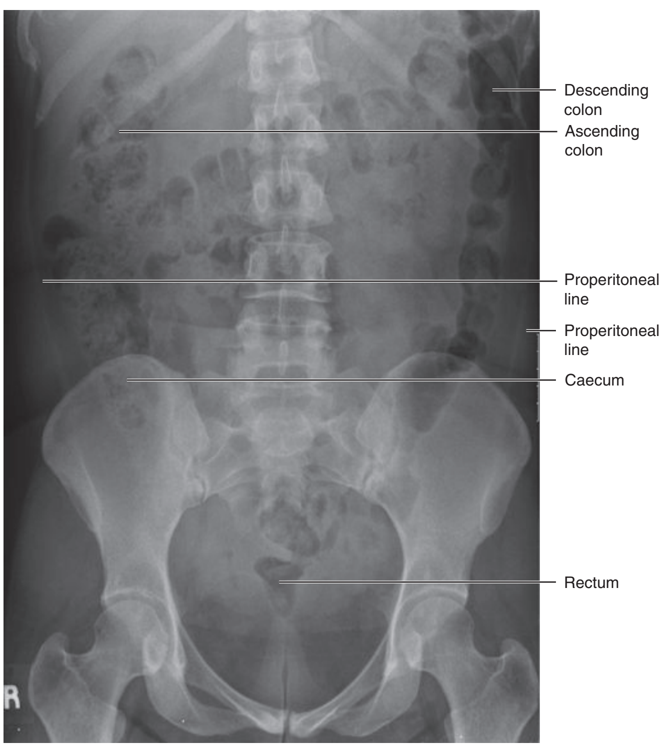


**Fig. 9.1** Plain abdominal radiograph – the anterior abdominal wall and peritoneal cavity cannot be assessed.

### Anterior abdominal wall

#### US

Ultrasound is useful in evaluating focal masses in the anterior abdominal wall but does not demonstrate the anatomical relations as well as computed tomography (CT) or magnetic resonance imaging (MRI).

#### CT/MRI

CT and MRI provide excellent anatomical detail of the anterior abdominal wall in the axial plane.

MRI has superior soft-tissue contrast resolution but images can be degraded by respiratory artefact.

### Peritoneum

#### US

Ultrasound is widely used to detect intraperitoneal collections, but is limited by bowel gas and body habitus.

#### CT/MRI

Contrast-enhanced CT (with or without oral contrast medium) is the method of choice to evaluate the peritoneal spaces, reflections and their contents.

MRI provides good visualization of the peritoneal spaces and reflections; however, bowel peristalsis and respiratory movement can degrade the images.

## Anatomy of the anterior abdominal wall

The anterior abdominal wall extends from the xiphoid and lower six costal cartilages to the anterior aspect of the pelvic bones. It is composed of several layers, including skin, superficial fascia, subcutaneous fat, muscles, transversalis fascia, extraperitoneal fat and peritoneum.

### Superficial fascia

A single fat-containing layer in superior and central anterior abdomen which then divides into two layers inferiorly between which run vessels, nerves and lymphatics.

- Superficial layer (Camper's fascia):
  - thick and contains areolar tissue with variable amounts of fat

*Applied Radiological Anatomy, 2nd Edition* ed. Paul Butler, Adam W.M. Mitchell and Jeremiah C. Healy. Published by Cambridge University Press.


**Fig. 9.2** Single image from a contrast herniogram – contrast medium is instilled into the peritoneal cavity and is seen to outline loops of small bowel in the pelvis. There is no hernia demonstrated on this study.

  - passes over the inguinal ligament
  - continuous with the superficial fascia of the thigh.
- Deep layer (Scarpa's fascia):
  - membranous layer containing elastic fibres
  - connected to the aponeurosis of the external oblique muscle laterally and to the linea alba and symphysis pubis medially
  - continuous with the superficial layer over the trunk superiorly
  - passes over the inguinal ligament inferolaterally to fuse with the underlying fascia of the thigh (fascia Lata)
  - forms the superficial perineal fascia (Colles' fascia) inferomedially by passing over the penis and scrotum in males, and into the labia majora in females.

## Muscles

### Rectus abdominis (Figs. 9.3, 9.4, 9.5, 9.6, 9.8)

- Paired paramedian strap muscles which arise inferiorly from two tendons:
  - lateral (larger) tendon originates on the crest of the pubis and can extend beyond the pubic tubercle to the pecten pubis
  - medial tendon interlaces with the contralateral tendon; continuous with the ligamentous fibres covering the front of the symphysis pubis.
- Attached superiorly by three slips to the 5–7th costal cartilages and occasionally to the costoxiphoid ligaments and xiphoid process.
- Muscle fibres interrupted by three fibrous bands named tendinous intersections
  - –at the level of the umbilicus
  - –at the level of the free edge of the xiphoid process
  - –midway between the above points.
- Enclosed by the rectus sheath (see below).

### External oblique (Figs. 9.3, 9.4, 9.5, 9.6, 9.7, 9.8, 9.9, 9.16)

- Largest and most superficial of the three anterolateral muscles.
- Arises superiorly as slips from the external and inferior borders of the lower eight ribs and interdigitates with the origins of the serratus anterior and latissimus dorsi.
- Posterior fibres pass vertically to insert into the anterior half of the iliac crest.
- Middle fibres pass inferomedially to end in the muscle's aponeurosis, which contributes medially to the rectus sheath and linea alba and is attached inferiorly to the pubic symphysis.
- Inguinal ligament:
  - the thickened free margin of the external oblique aponeurosis between the anterior superior iliac spine and pubic tubercle (extends over 12–14 cm in adults)
  - continuous with the fascia Lata over the thigh
  - lacunar ligament (medial part) of the inguinal ligament forms the medial margin of the femoral ring

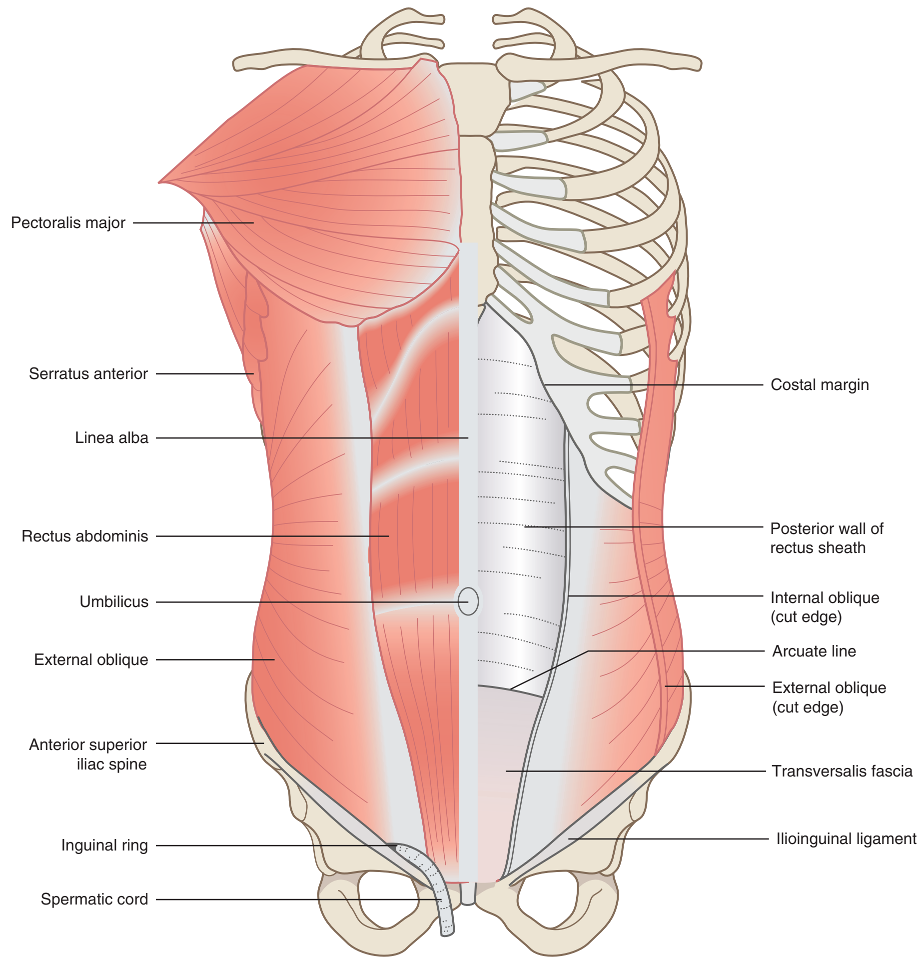


**Fig. 9.3** Anterior abdominal wall (coronal view) – deep dissection. On the right of the image the external oblique muscle is excised, the internal oblique muscle is divided and the rectus abdominis muscle is removed, revealing the posterior wall of the rectus sheath.

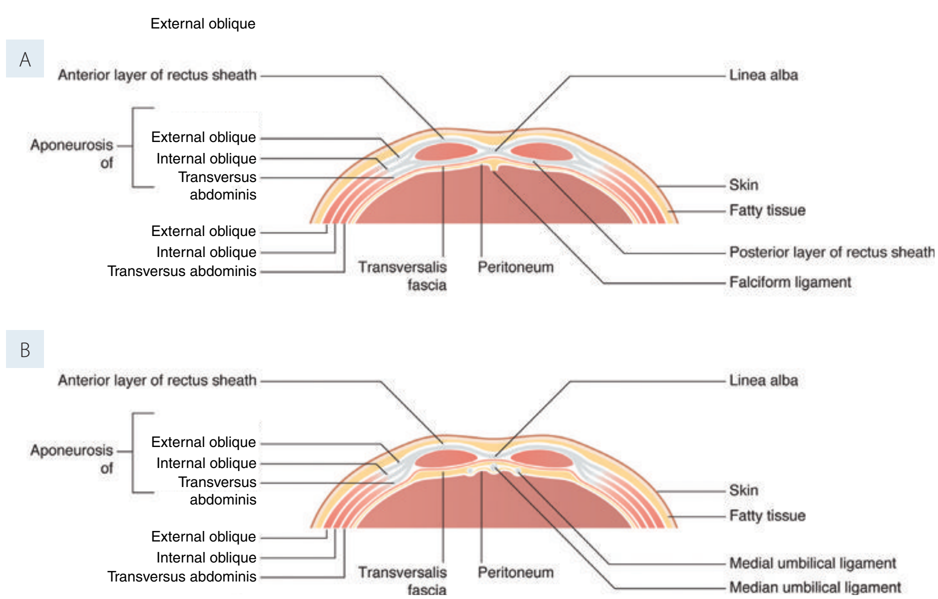


**Fig. 9.4** Rectus sheath (axial sections) A: above the level of the umbilicus the aponeurosis of the internal oblique muscle splits to form anterior and posterior layers of the rectus sheath. At this level the aponeurosis of the external oblique muscle joins the anterior layer of the rectus sheath and the aponeurosis of the transversus abdominis joins the posterior layer. B: below the level of the umbilicus the aponeuroses of all three anterolateral abdominal wall muscles pass in front of the rectus abdominis and the posterior aspect of the muscle is only covered by transversalis fascia.

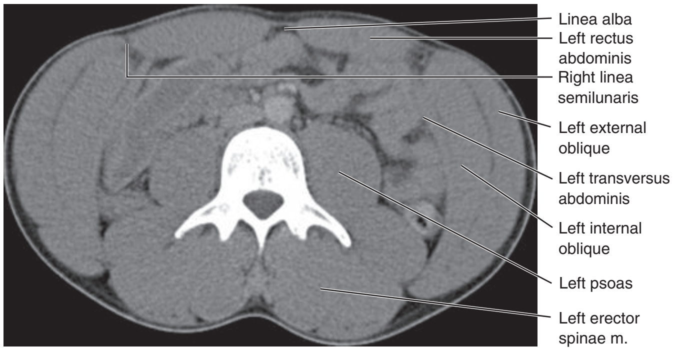


**Fig. 9.5** Axial CT to show the anterolateral abdominal wall musculature above the level of the umbilicus.

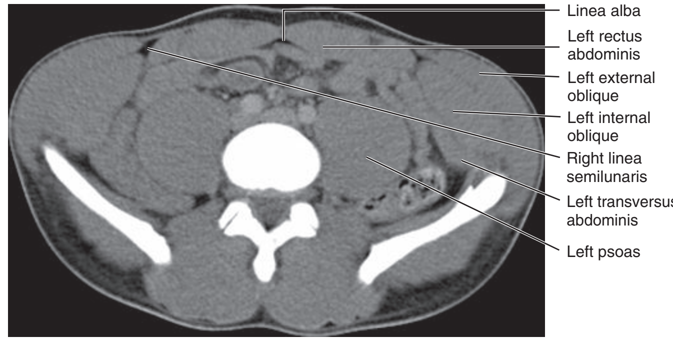


**Fig. 9.6** Axial CT to show the anterolateral abdominal wall musculature below the level of the umbilicus.

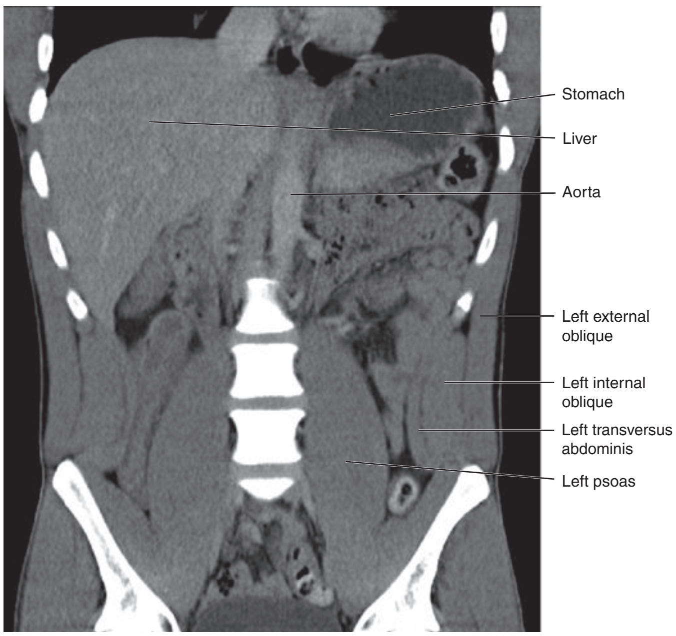


**Fig. 9.7** Coronal CT to show the abdominal wall musculature laterally.

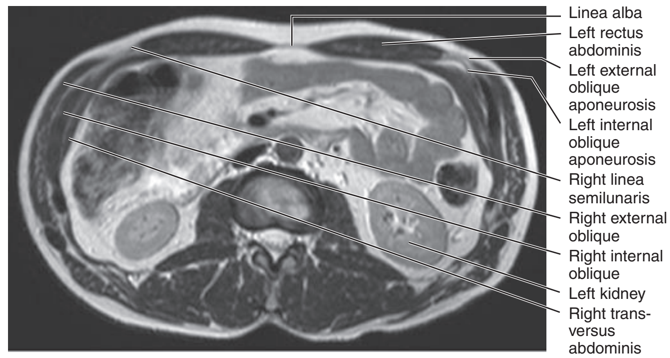


**Fig. 9.8** Axial MRI to show the anterolateral abdominal wall musculature above the level of the umbilicus.

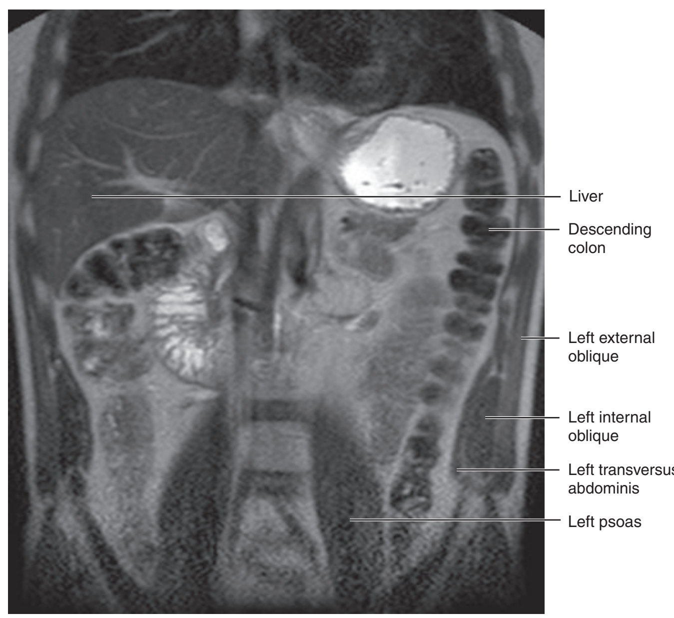


**Fig. 9.9** Coronal MRI to show the abdominal wall musculature laterally.

  - the superficial inguinal ring is a hiatus in the external oblique aponeurosis lying superolaterally to the pubic crest.
  - carries the spermatic cord (males) or round ligament (females) and the ilioinguinal nerve.

### Internal oblique (Figs. 9.3– 9.9 and 9.16)

- Lies deep to the external oblique.
- Arises from:
  - lateral two-thirds of the inguinal ligament
  - anterior two-thirds of the iliac crest
  - thoracolumbar fascia.
- Posterior fibres pass upwards and laterally to the inferior borders of the lower 3/4 ribs, where they are continuous with the intercostal muscles.
- Remaining fibres diverge and end in an aponeurosis attached to the cartilages of the 7th–9th ribs superiorly and passes anterior to the rectus abdominis inferiorly to form the linea alba medially.
- Internal oblique aponeurosis:
  - splits in its upper two-thirds to form part of the anterior and posterior layers of the rectus sheath
  - below the umbilicus the aponeurosis passes anterior to the recti.

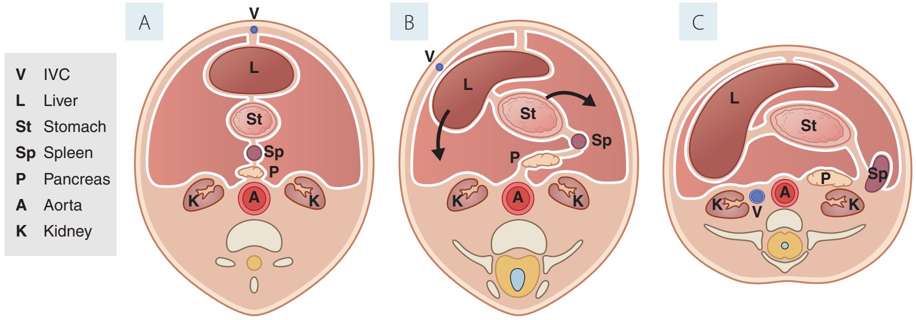


**Fig. 9.10** Embryological development of the peritoneal cavity. (A) Fetus at 5 weeks; (B) fetus at 10 weeks; (C) maturity.

### Transversus abdominis (Figs. 9.3–9.9 and 9.16)

- Innermost of the anterolateral wall muscles.
- Arises from:
  - lateral third of the inguinal ligament
  - inner two-thirds of the iliac crest
  - thoracolumbar fascia between the iliac crest and the 12th rib
  - internal aspects of the lower six costal cartilages (interdigitating with diaphragmatic insertions).
- Aponeurosis:
  - lower fibres travel inferomedially with the internal oblique aponeurosis to insert into the pubis forming the conjoint tendon
  - remaining fibres travel medially to contribute to the linea alba
  - above the umbilicus it passes behind the rectus abdominis and below it passes in front of the muscle.

### Rectus sheath (Fig. 9.4)

- Above the umbilicus:
  - anterior layer: aponeurosis of the external oblique and superficial layer of the internal oblique aponeurosis
  - posterior layer: aponeurosis of the transversus abdominis and deep layer of the internal oblique aponeurosis.
- Below the umbilicus:
  - aponeuroses of all three anterolateral muscles pass in front of the rectus abdominis
  - only covered by transversalis fascia posteriorly.
- Linea alba (Figs. 9.3, 9.4, 9.5, 9.6, 9.8):
  - binds the rectus sheaths medially
  - complex tendinous raphe between the recti formed from the aponeurotic fibres of the anterolateral wall muscles
  - extends from the xiphoid process to the symphysis pubis (superficial fibres) and pubic crest (deep fibres).
- Linea semilunaris (Figs. 9.3, 9.4, 9.5, 9.6, 9.8):
  - binds the rectus sheath laterally
  - formed by the fused aponeuroses of the anterolateral muscles
  - passes from the tip of the ninth costal cartilage to the pubic tubercle.
- Superior and inferior epigastric arteries, associated lymphatics and the distal portions of the thoracoabdominal nerves run within the sheath.
- The inferior epigastric artery demarcates the medial margin of the deep inguinal ring.

## Transversalis fascia (Fig. 9.4)

- Thin areolar membrane lying between the transversus abdominis and the extraperitoneal fat.
- Continuous superiorly with the inferior diaphragmatic fascia and inferiorly with the iliac and pelvic fascia.
- Fuses posteriorly with the thoracolumbar fascia.
- Pierced at the deep inguinal ring by the spermatic cord in males and round ligament in females.

## Extraperitoneal connective tissue

Lies between the peritoneum and inner surface of the transversalis fascia.

# Anatomy of the peritoneum

- In early fetal life (Fig. 9.10) the abdominal cavity divides into two major compartments (the retroperitoneum and the peritoneum).
- The peritoneum is a single serous membrane, lined by flattened mesothelial cells, arbitrarily divided into parietal (lining the abdominal and pelvic walls) and visceral (covering the external surface of most abdominal organs) layers.
- The peritoneal cavity is the potential space between these two layers and is composed of several communicating spaces.
- The main compartment, the greater sac, communicates with the smaller, lesser sac (or omental bursa) via the epiploic foramen (of Winslow) (Fig. 9.11).
- Peritoneal ligaments, mesenteries and omenta are formed by reflections of the parietal peritoneum.

## Peritoneal spaces

The two main peritoneal compartments are separated by the transverse mesocolon, the root of which extends across the infra-ampullary segment of the descending duodenum, the pancreatic head and along the lower edge of the pancreatic body and tail (Fig. 9.11).

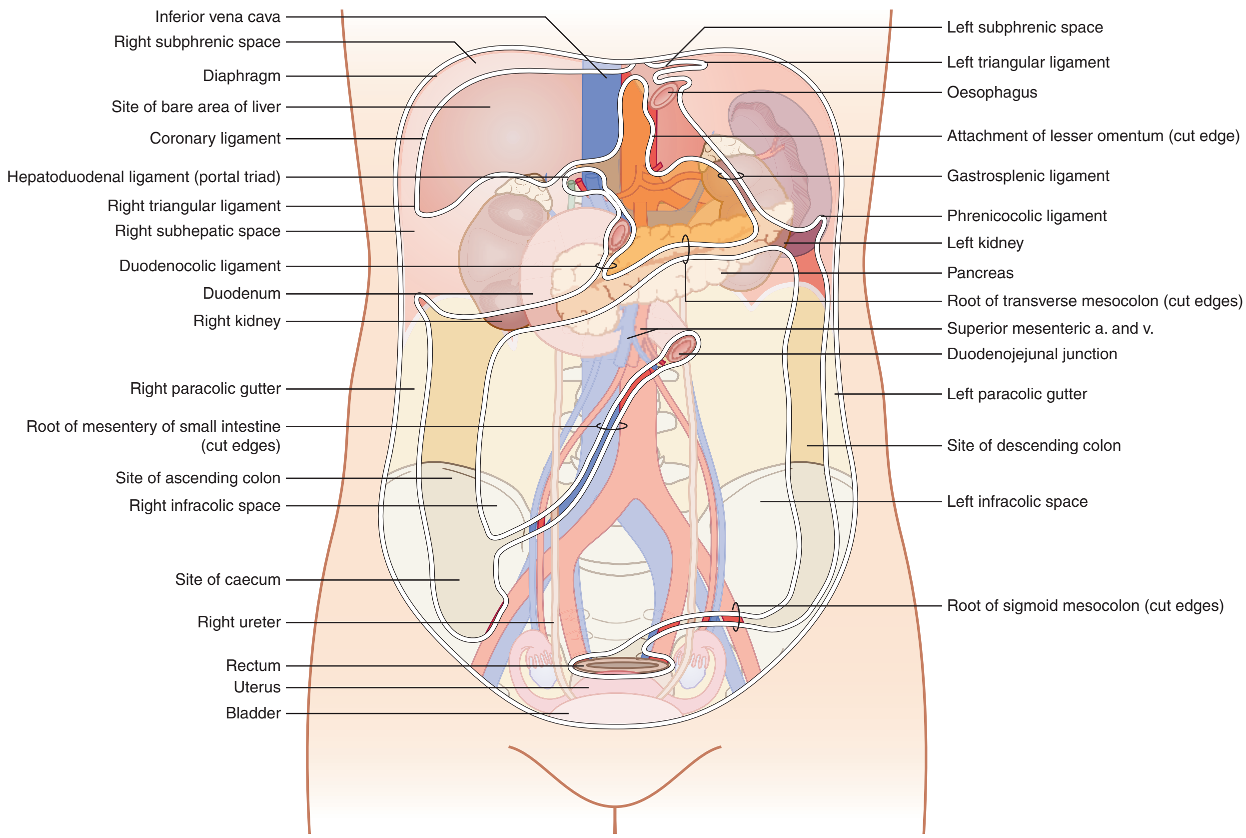


**Fig. 9.11** Coronal view of the peritoneal attachments to the posterior abdominal wall. The positions of the posterior peritoneal spaces are indicated.

## Supramesocolic compartment

Divided arbitrarily into right and left supramesocolic peritoneal spaces, which can be further subdivided into a number of subspaces that are in communication.

## Right supramesocolic space

Three subspaces:

- Right subphrenic space (Figs. 9.11, 9.12a, 9.13, 9.14a,c,d, 9.15a,b,c,d)
    - extends over the diaphragmatic surface of the right lobe of the liver to the right coronary ligament posteroinferiorly and the falciform ligament medially (which separates it from the left subphrenic space).
- Right subhepatic space (Figs. 9.11, 9.12a,b,c, 9.14b, 9.15a)
    - anterior right subhepatic space is limited inferiorly by the transverse colon and its mesentery (Figs. 9.12a, 9.13)
    - posterior right subhepatic space (hepatorenal fossa or Morison's pouch) extends posteriorly to the peritoneum overlying the right kidney (Figs. 9.12a, 9.13, 9.14b,c,d, 9.15d)
    - bounded superiorly by the inferior surface of the right lobe of the liver
    - communicates freely with the right subphrenic space and the right paracolic gutter.
- Lesser sac (Figs. 9.11, 9.12b,c, 9.14b, 9.15c,d)
    - posterior to the lesser omentum, stomach, duodenal bulb and gastrocolic ligament; anterior to the pancreas
    - communicates with the rest of the peritoneal cavity through the epiploic foramen (of Winslow), which lies between the inferior vena cava and the free margin of the hepatoduodenal ligament
    - divided into two recesses by the pancreatogastric fold (peritoneal fold over the left gastric artery):
        - smaller superior recess completely encloses the caudate lobe of the liver and lies posterior to the portal vein at the porta hepatis; superiorly, it extends deep into the fissure for the ligamentum venosum and posteriorly lies adjacent to the right diaphragmatic crus
        - larger inferior recess lies between the stomach and the pancreas; it is bounded inferiorly by the transverse colon and its mesentery, but can extend for a variable distance within the greater omentum; to the left it is bounded by the gastrosplenic and splenorenal ligaments.

## Left supramesocolic space (Figs. 9.11, 9.12)

Four arbitrary subspaces, which are in communication in normal individuals:

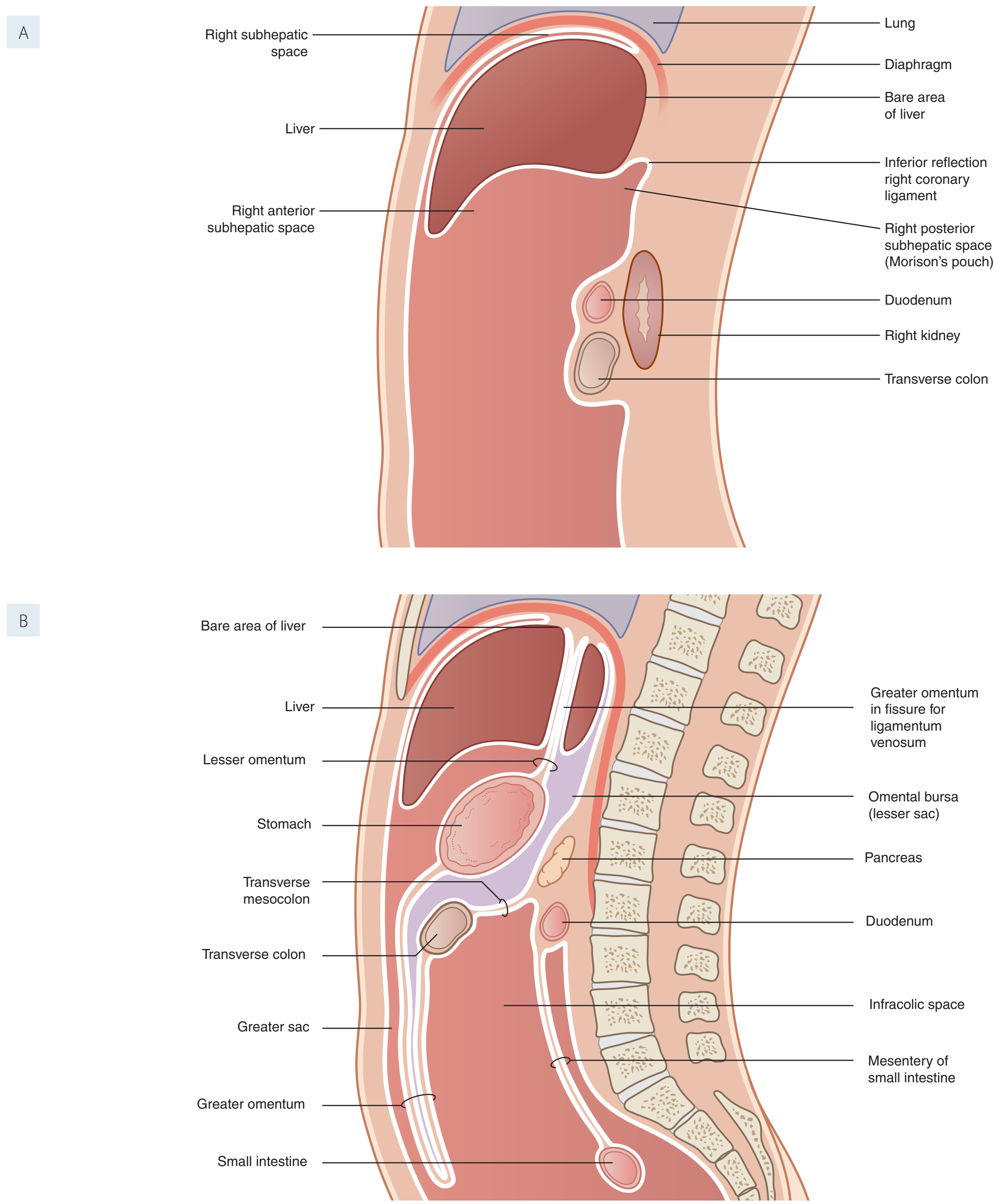


**Fig. 9.12** Sagittal line diagrams through the abdomen. (A) Section through the right lobe of liver and right kidney. (B) Right paramedian section. (C) Median section through the abdomen and pelvis. (D) Left paramedian section. (E) Section through the spleen and left kidney.

- Anterior left perihepatic space (Fig. 9.12d)
  - bounded medially by the falciform ligament, posteriorly by the liver surface and left coronary ligament, and anteriorly by the diaphragm
  - communicates superiorly and to the left with the left anterior subphrenic space, and inferiorly with the greater peritoneal cavity over the surface of the transverse mesocolon.
- Posterior left perihepatic space (gastrohepatic recess) (Figs. 9.12d, 9.14b)
  - surrounds the lateral segment of the left hepatic lobe extending into the fissure for the ligamentum venosum on the right anterior to the main portal vein
  - posteriorly, the lesser omentum separates this space from the superior recess of the lesser sac

C

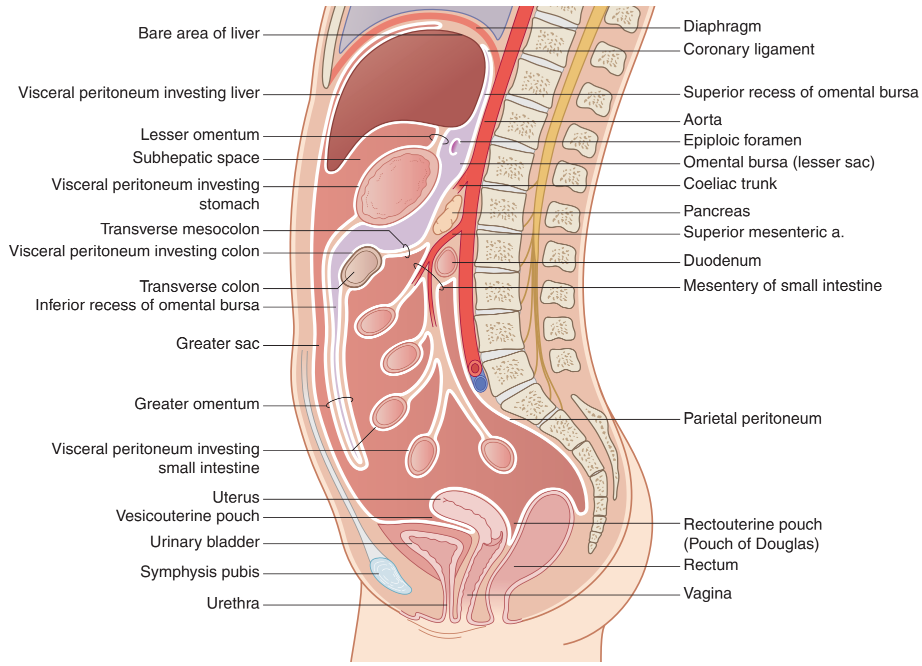


D

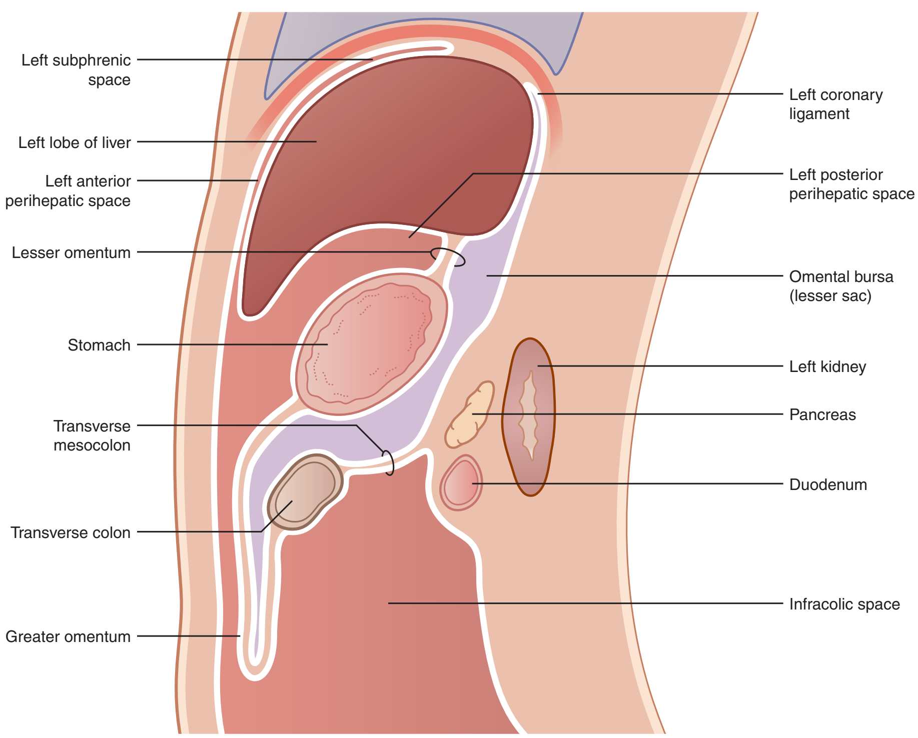


**Fig. 9.12** *(cont.)*

- bounded on the left by the lesser curvature of the stomach
- communicates anteroinferiorly with the anterior left perihepatic space.

- Anterior left subphrenic space (Figs. 9.12d,e, 9.15a,b,c)
  - this lies between the stomach and the left hemidiaphragm
  - communicates on the right with the left anterior perihepatic space, and posteriorly with the posterior subphrenic (perisplenic) space.
- Posterior left subphrenic (perisplenic) space (Figs. 9.12e, 9.14a,b, 9.15d)
  - superior to gastric fundus and spleen
  - covers the superior and inferolateral surfaces of the spleen

E

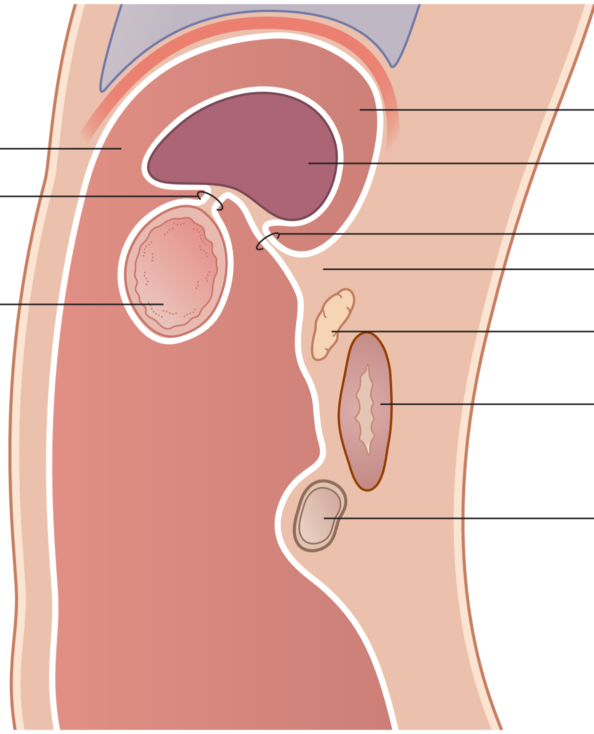


**Fig. 9.12** (*cont.*)


**Fig. 9.13** Sagittal CT taken through the right lobe of liver and right kidney.

- limited inferiorly by the splenorenal and phrenicocolic ligaments, and more superiorly by the gastrosplenic ligament
- partially separated from the rest of the peritoneal cavity by the phrenicocolic ligament which extends from the splenic flexure to the diaphragm.

## Inframesocolic compartment (Fig. 9.12)

Divided into two unequal spaces posteriorly by the root of the small bowel mesentery.

- Right inframesocolic space (Figs. 9.11, 9.13, 9.14d,e,f, 9.15c)
  - bounded by the transverse mesocolon superiorly and to the right, and by the root of the small bowel mesentery inferiorly and to the left.
- Left inframesocolic space (Figs. 9.11, 9.14e,f, 9.15c)
  - larger than on the right
  - in free communication with the pelvis to the right of the midline
  - sigmoid mesocolon forms a partial barrier to the left of the midline.
- Paracolic gutters (Figs. 9.11, 9.14d,e,f, 9.15b,c)
  - peritoneal recesses on the posterior abdominal wall lateral to the ascending and descending colon
  - right paracolic gutter: continuous superiorly with the right subhepatic and subphrenic spaces; larger than the left

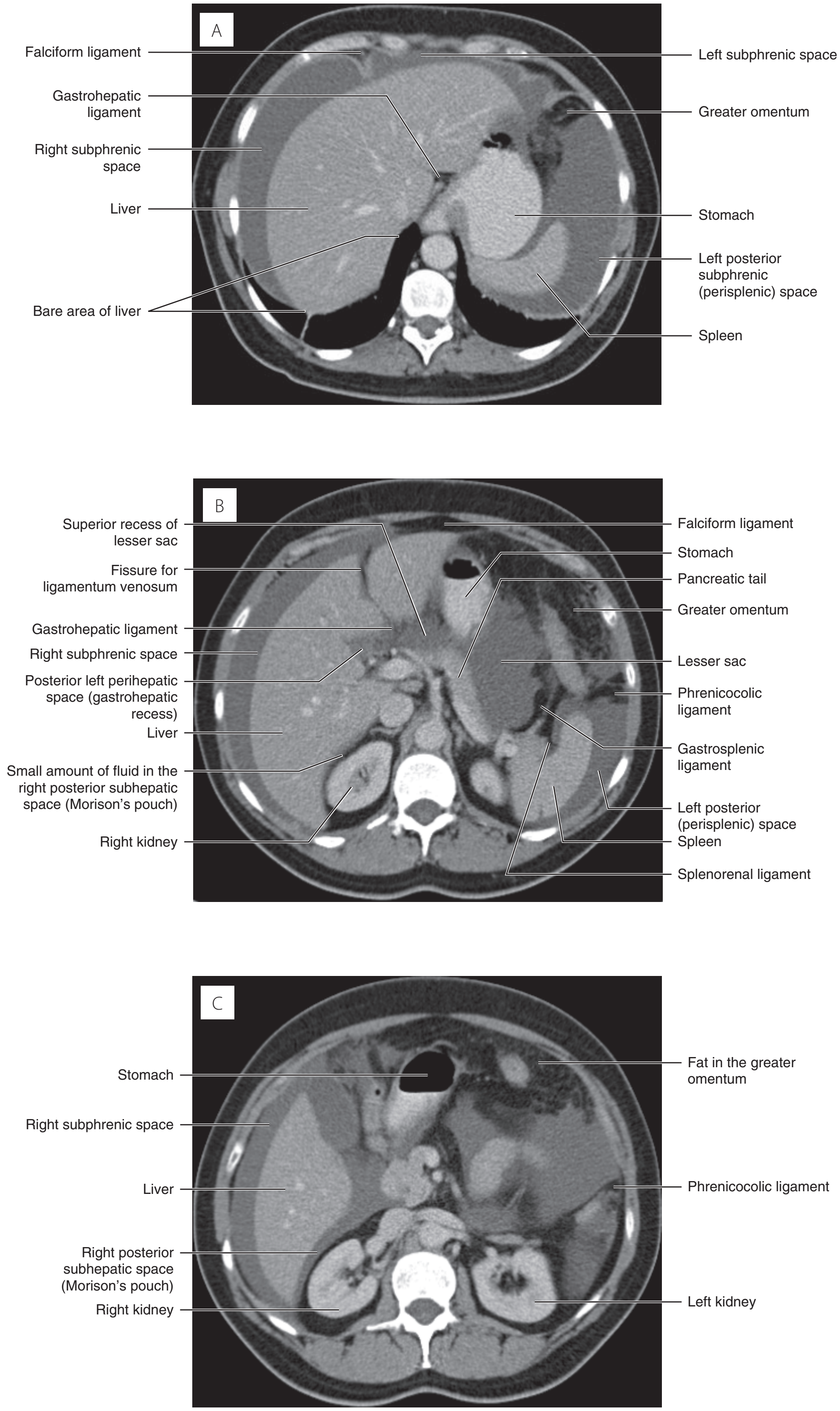


**Fig. 9.14** Axial CT sections in a patient with abdominal and pelvic ascites secondary to an ovarian malignancy. Ascitic fluid distends the potential space of the peritoneal cavity, demonstrating the peritoneal spaces and reflections.

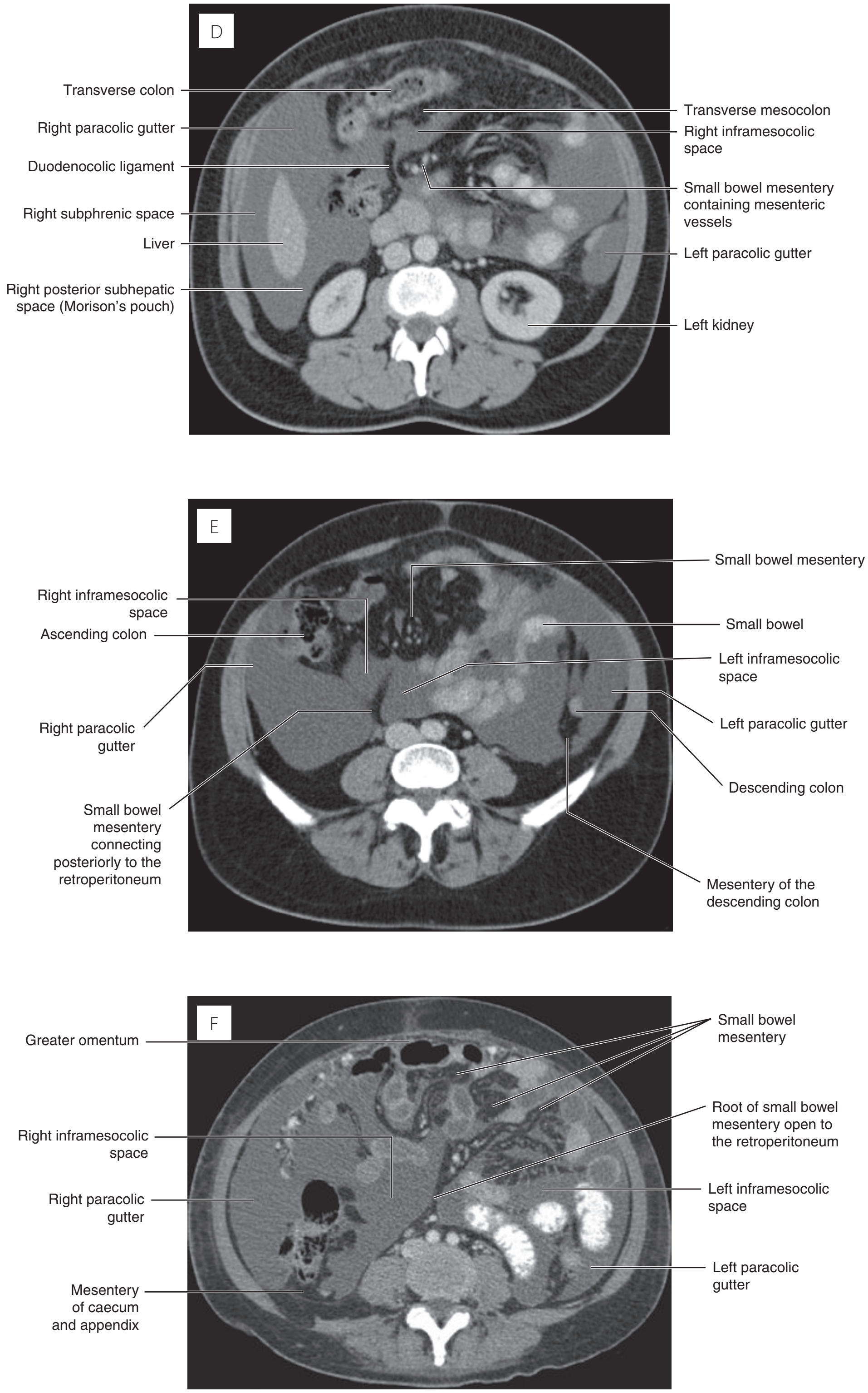
D
Transverse colon
Right paracolic gutter
Duodenocolic ligament
Right subphrenic space
Liver
Right posterior subhepatic space (Morison's pouch)
Transverse mesocolon
Right inframesocolic space
Small bowel mesentery containing mesenteric vessels
Left paracolic gutter
Left kidney
E
Right inframesocolic space
Ascending colon
Right paracolic gutter
Small bowel mesentery connecting posteriorly to the retroperitoneum
Small bowel mesentery
Small bowel
Left inframesocolic space
Left paracolic gutter
Descending colon
Mesentery of the descending colon
F
Greater omentum
Right inframesocolic space
Right paracolic gutter
Mesentery of caecum and appendix
Small bowel mesentery
Root of small bowel mesentery open to the retroperitoneum
Left inframesocolic space
Left paracolic gutter

**Fig. 9.14** *(cont.)*

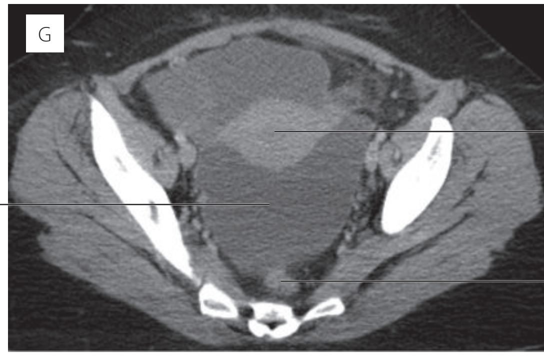


**Fig. 9.14** (*cont.*)

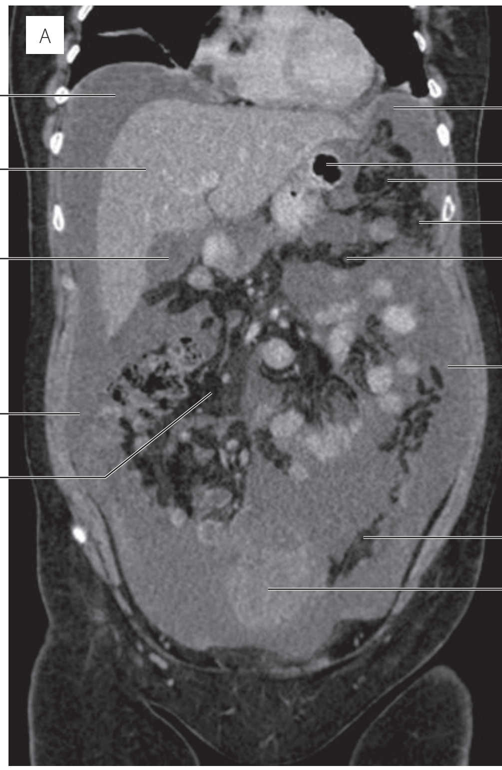


**Fig. 9.15** Coronal CT reformats in a patient with abdominal and pelvic ascites secondary to an ovarian malignancy. Ascitic fluid distends the potential space of the peritoneal cavity, demonstrating the peritoneal spaces and reflections.

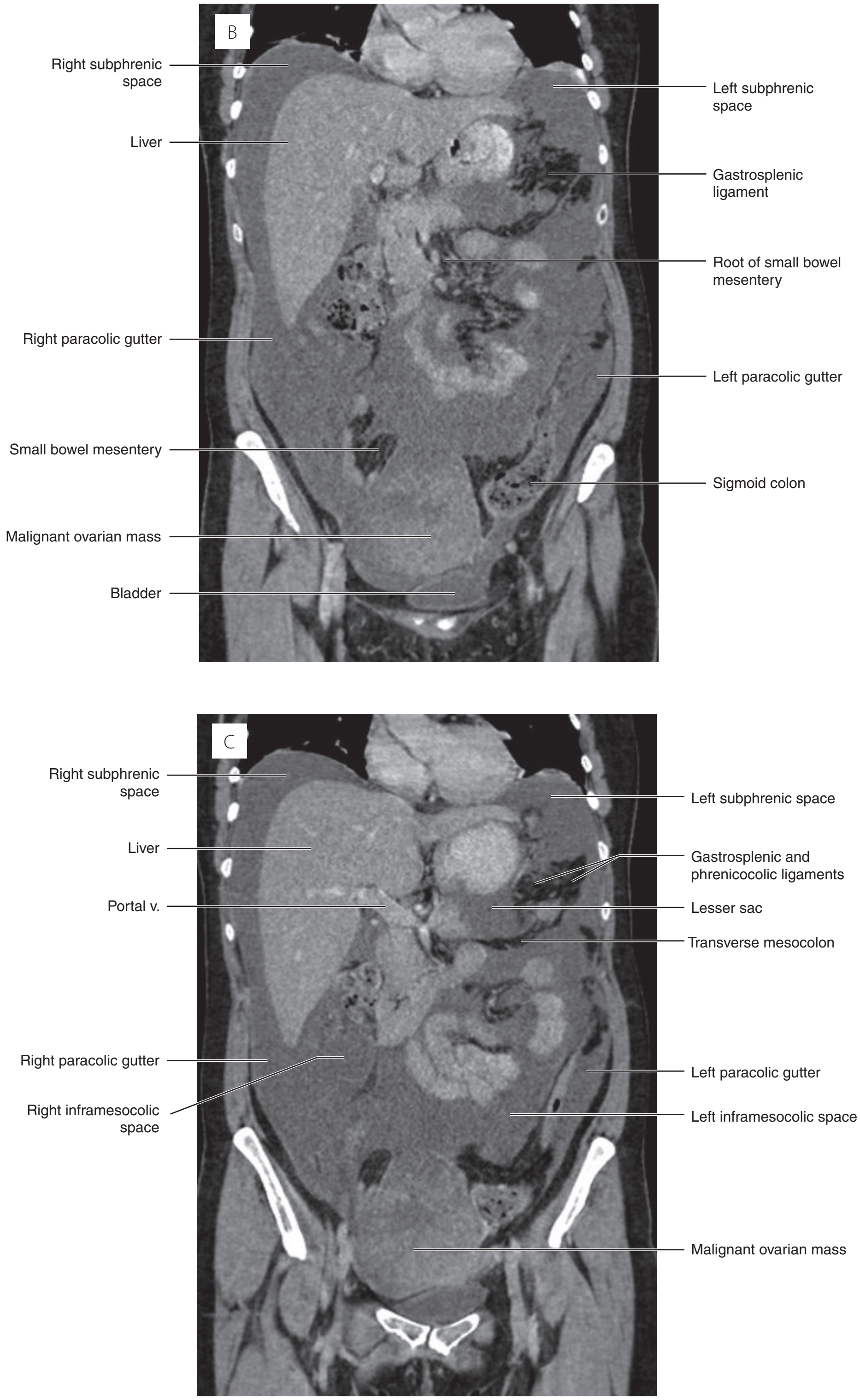
B
Right subphrenic space
Liver
Right paracolic gutter
Small bowel mesentery
Malignant ovarian mass
Bladder
Left subphrenic space
Gastrosplenic ligament
Root of small bowel mesentery
Left paracolic gutter
Sigmoid colon
C
Right subphrenic space
Liver
Portal v.
Right paracolic gutter
Right inframesocolic space
Left subphrenic space
Gastrosplenic and phrenicocolic ligaments
Lesser sac
Transverse mesocolon
Left paracolic gutter
Left inframesocolic space
Malignant ovarian mass

**Fig. 9.15** (*cont.*)

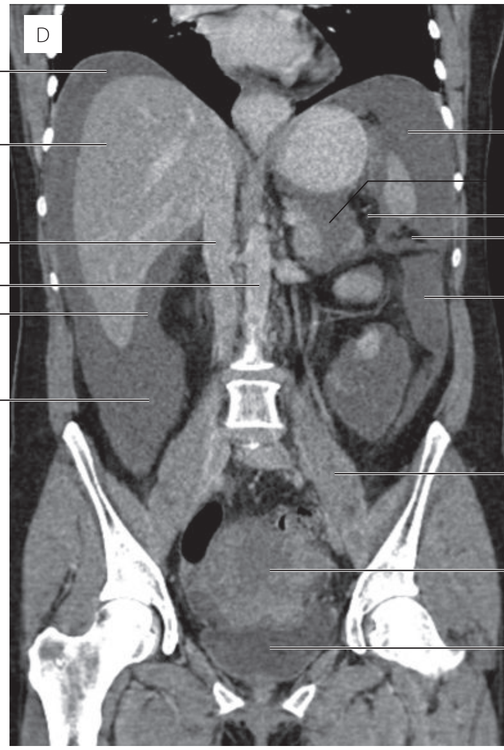


**Fig. 9.15** (*cont.*)

- left paracolic gutter: partially separated from the left subphrenic spaces by the phrenicocolic ligament
- both paracolic spaces are in continuity with the pelvic peritoneal spaces.

## Pelvic peritoneal spaces

- Inferiorly the peritoneum is reflected over the dome of the bladder, the anterior and posterior surface of the uterus and upper posterior vagina in females, and on to the front of the rectum at the junction of its middle and lower thirds.
- The urinary bladder subdivides the pelvis into right and left paravesical spaces.
- In men, there is only one potential space for fluid collection posterior to the bladder, the rectovesical pouch.
- In women there are two potential spaces: posterior to the bladder, the uterovesical pouch (Fig. 9.12c) and, posterior to the uterus, the deeper rectouterine pouch (of Douglas) (Figs. 9.12c, 9.14g).
- The layers of peritoneum on the anterior and posterior surfaces of the uterus are reflected laterally to the pelvic side walls as the broad ligaments, containing the Fallopian tubes.

## Peritoneal reflections (Table 9.1)

The peritoneal reflections in the upper abdomen comprise:

- Eight ligaments:
  - right coronary ligament
  - left coronary ligament
  - gastrosplenic ligament
  - falciform ligament
  - phrenicocolic ligament
  - splenorenal ligament
  - hepatoduodenal ligament
  - duodenocolic ligament.
- Two omenta:
  - lesser omentum (gastrohepatic ligament)
  - greater omentum (gastrocolic ligament).
- Four mesenteries:
  - small bowel mesentery
  - transverse mesocolon
  - sigmoid mesocolon
  - mesoappendix.

The peritoneal reflections carry areolar tissue, vessels, nerves and lymphatics from the retroperitoneum to the

**Table 9.1** Peritoneal reflections: nomenclature

| Term | Definition |
|---|---|
| Peritoneal ligament | Formed by two folds of peritoneum that enclose and support structures within the peritoneal cavity<br>Named according to the structures it joins |
| Omentum | Peritoneal ligament that joins the stomach to another structure |
| Mesentery | Two folds of peritoneum that attach a loop of bowel to the retroperitoneum |

peritoneal organs, forming a natural connection between the retroperitoneum and peritoneum.

These reflections are generally recognizable as fat-containing structures on cross-sectional imaging, either by their typical location and organ relationships or by the landmarks provided by their major constituent vessels.

## Peritoneal ligaments

1. Right coronary ligament (Fig. 9.12a,c)
   - formed by the reflection of the peritoneum from the diaphragm to the posterior surface of the right lobe of the liver
   - the triangular area of liver enclosed by these layers is the bare area devoid of peritoneal covering and is continuous with the anterior pararenal space.
2. Left coronary ligament (left triangular ligament) (Figs. 9.11, 9.12d)
   - flimsy structure formed by apposition of the peritoneal reflections between the left lobe of liver and diaphragm
   - little clinical significance.
3. Gastrosplenic ligament (Figs. 9.11, 9.12e, 9.14b, 9.15a,b,c,d)
   - extends from the greater curve of the stomach to the spleen
   - continuous with the greater omentum
   - contains the left gastroepiploic and short gastric vessels.
4. Falciform ligament (Figs. 9.11, 9.14b)
   - extends from the anterosuperior surface of the liver to the diaphragm and anterior abdominal wall, carrying the ligamentum teres (obliterated left umbilical vein) in its free edge
   - in continuity with the fissure for the ligamentum venosum and coronary ligaments.
5. Phrenicocolic ligament (Figs. 9.11, 9.14b,c, 9.15a,c,d)
   - extends from the splenic flexure to the diaphragm at the level of the eleventh rib
   - continuous with the transverse mesocolon and splenorenal ligament
   - supports the spleen
   - potential barrier to the spread of infected fluid from the pelvis and left paracolic gutter to the left subphrenic space.
6. Splenorenal ligament (Figs. 9.12e, 9.14b)
   - extends from the tip of the pancreatic tail to the splenic hilum, carrying the splenic vessels
   - continuous with the gastrosplenic ligament, forming the left lateral boundary of the lesser sac.
7. Hepatoduodenal ligament (Fig. 9.11)
   - represents the thickened free right edge of the lesser omentum (gastrohepatic ligament)
   - extends from the flexure between the first and second parts of the duodenum to the porta hepatis
   - carries the portal triad (hepatic artery, portal vein and common bile duct)
   - anterior margin of the epiploic foramen (of Winslow).
8. Duodenocolic ligament (Figs. 9.11, 9.14d)
   - extends from the hepatic flexure to the descending duodenum
   - continuous with the transverse mesocolon
   - carries the lymphatic drainage of the right-sided colon to the central superior mesenteric nodes.

## Omenta

1. Greater omentum (gastrocolic ligament) (Figs. 9.12b,c,d, 9.13, 9.14a,b,c,f)
   - largest peritoneal fold consisting of a double sheet folded on itself (i.e. made up of four layers)
   - two layers of peritoneum descend from the greater curve of the stomach and proximal duodenum passing inferiorly, anterior to the small bowel for a variable distance, and then turn superiorly again to insert into the anterosuperior aspect of the transverse colon
   - the left border is continuous with the gastrosplenic ligament
   - the right border extends to the origin of the duodenum
   - contains adipose tissue which is easily identified on CT anterior to the transverse colon superiorly and loops of small bowel inferiorly.
2. Lesser omentum (gastrohepatic ligament) (Figs. 9.12b, c, d, 9.14b)
   - extends from the lesser curvature of the stomach and proximal 2 cm of the duodenum to the liver (attached to the fissures for the porta hepatis and ligamentum venosum)
   - forms the anterior surface of the lesser sac
   - the free edge forms the hepatoduodenal ligament
   - generally wedge-shaped and contains adipose tissue, the gastric artery, the coronary vein, and the left gastric nodal chain
   - identified on cross-sectional imaging by finding the fissure for the ligamentum venosum immediately inferior to the gastro-oesophageal junction.

## Mesenteries

1. Small bowel mesentery (Figs. 9.11, 9.12b,c, 9.14d,e,f, 9.15a,b, 9.16)
   - contains fat, the jejunal and ileal branches of the superior mesenteric arteries and their accompanying veins, nerves and lymphatics
   - suspends 20–25 feet of jejunum and ileum
   - connected to the posterior abdominal wall by an oblique 15 cm root extending from the duodenojejunal flexure to the ileocaecal valve

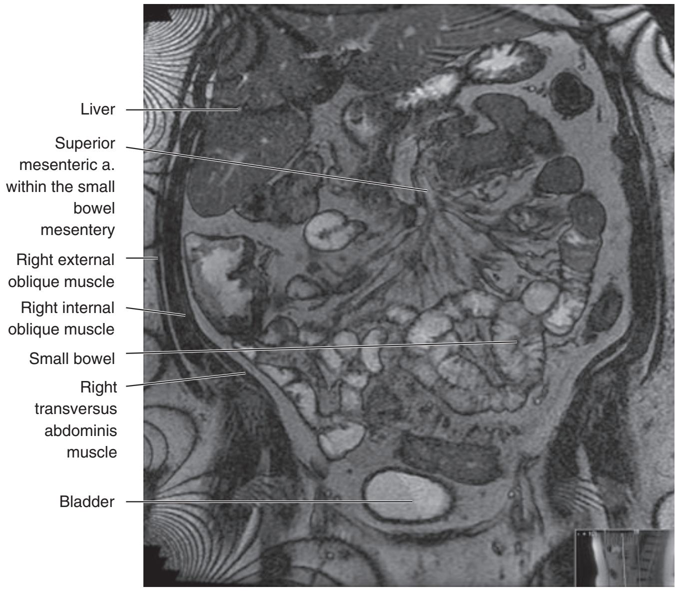


**Fig. 9.16** Coronal MRI image depicting the small bowel mesentery and the lateral abdominal wall musculature.

- the root is a bare area continuous with the left anterior pararenal space superiorly and the right anterior pararenal space inferiorly; it passes in front of the horizontal part of the duodenum (where the superior mesenteric vessels enter the mesentery), abdominal aorta, inferior vena cava, right ureter and right psoas muscle as it travels from left to right.

2. Transverse mesocolon (Figs. 9.11, 9.12b,d, 9.15a,b)
   - connects the transverse colon to the posterior abdominal wall
   - formed by two layers passing from the anterior surface of the head and the anterior border of the body of the pancreas to the posterior surface of the transverse colon, where they separate to surround the bowel
   - the upper layer is adherent to, but separable from, the greater omentum
   - carries the middle colic vessels, autonomic nerves, and lymphatics which supply the transverse colon
   - becomes confluent with the root of the small bowel mesentery near the uncinate process of the pancreas.
3. Sigmoid mesocolon (Figs. 9.11, 9.15a)
   - attaches the sigmoid colon to the pelvic wall in an inverted V, the apex of which lies anterior to the left common iliac artery bifurcation and left ureter; the left limb descends medially to the left psoas muscle; the right limb descends into the pelvis and ends in the midline anterior to S3
   - carries the sigmoid and superior rectal vessels.
4. Mesoappendix (Fig. 9.14f)
   - surrounds the vermiform appendix and attaches to the lower end of the small bowel mesentery close to the ileocaecal junction
   - usually extends to the tip of the appendix and sometimes suspends the caecum.

Chapter 10

# The abdomen and retroperitoneum

Navin Ramachandran and Aslam Sohaib

## Plain film

Plain abdominal radiographs have a very limited role in assessing the anatomy related to the abdominal viscera and the retroperitoneum.

The anatomical structures that can be visualized include:

- liver (Fig. 10.1)
- spleen (especially if enlarged)
- kidneys (Fig. 10.1)
- calcification in the following structures can sometimes be seen: pancreas (Fig. 10.2), spleen, adrenals, aorta, lymph nodes and gallbladder.

## Cross-sectional anatomy

### Liver

- Largest/heaviest solid organ in the body (1.5 kg)
- Anatomical position and relationships: see Figs. 10.3–10.8

**Fig. 10.2** Plain abdominal film of a patient with pancreatic calcification due to chronic pancreatitis.

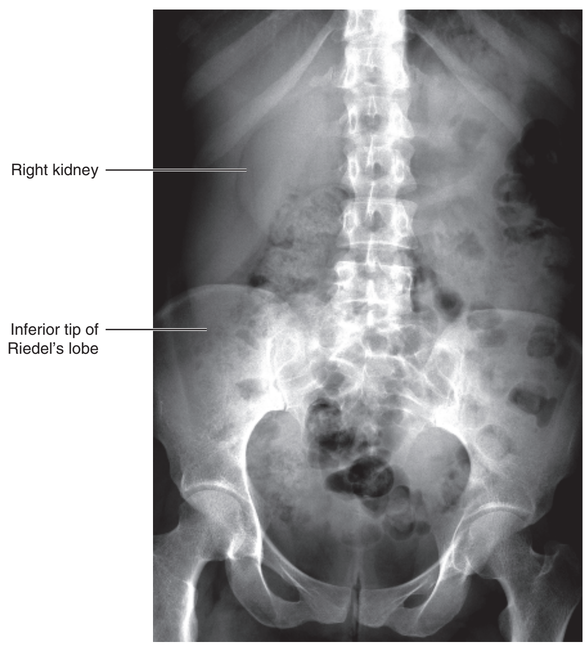


**Fig. 10.1** Plain abdominal X-ray of a Riedel's lobe, an inferior extension of the right hepatic lobe (normal variant).

- Appearance on CT/MRI/US is illustrated in Figs. 10.3–10.8. Table 10.1 shows the signal intensity of abdominal viscera on T1- and T2-weighted images with respect to liver.
- Segmental anatomy of liver (Figs. 10.9–10.12)
  - Previously the liver was divided into right, left, quadrate and caudate lobes.
  - This has been superseded by the Couinaud system of liver segments which reflect function as well as gross anatomy.

**Table 10.1** Signal intensity of abdominal viscera, compared to the liver on T1- and T2-weighted MR images

| Structure | T1-weighted | T2-weighted |
|---|---|---|
| Liver | Equal | Equal |
| Spleen | Lower | Higher |
| Pancreas | Higher (protein content) | Equal / lower |
| Kidney | Lower | Higher |
| Adrenal | Equal / lower | Equal / lower |
| Muscle | Lower | Lower |

*Applied Radiological Anatomy, 2nd Edition* ed. Paul Butler, Adam W.M. Mitchell and Jeremiah C. Healy. Published by Cambridge University Press.

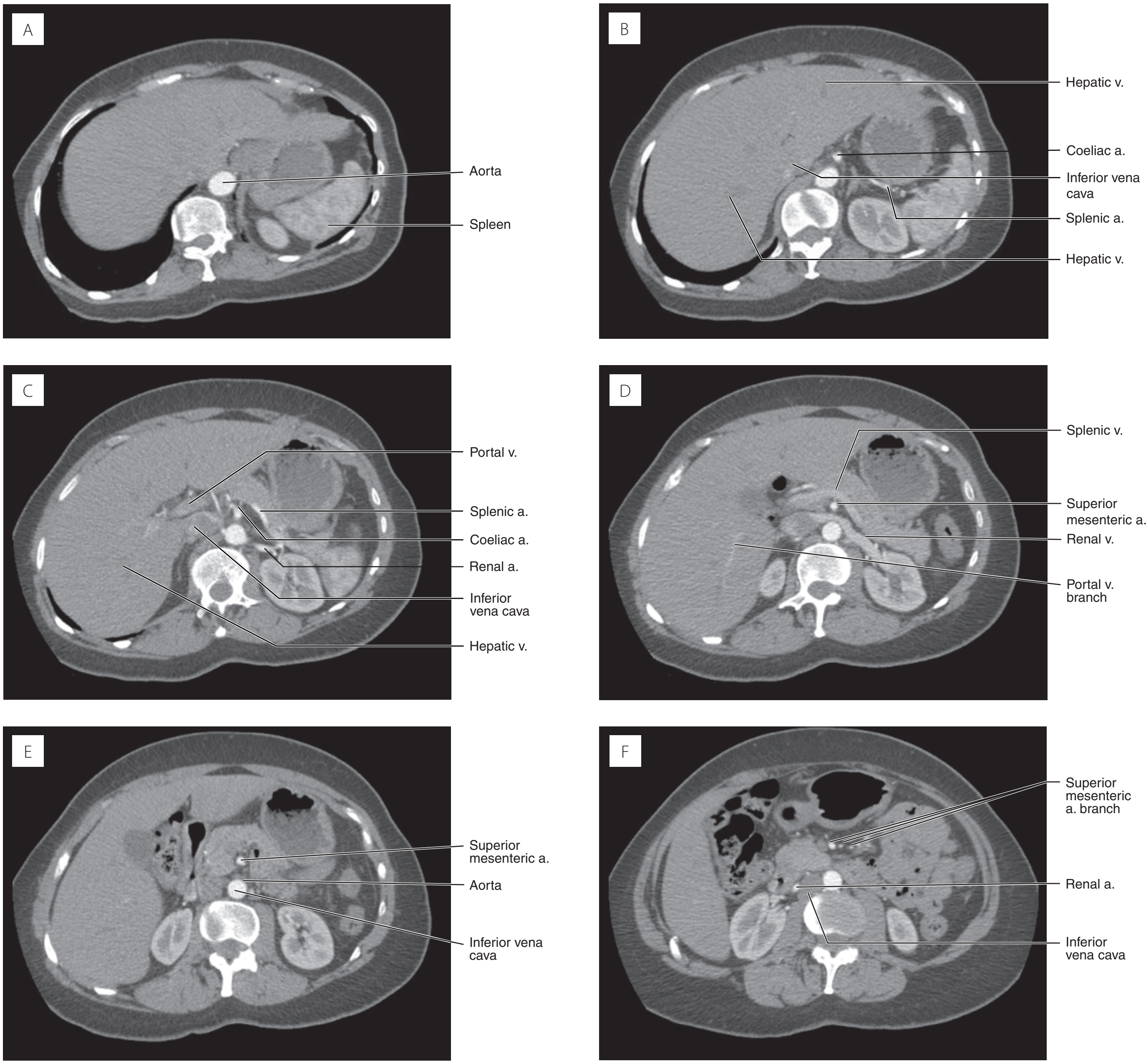


**Fig. 10.3** Arterial phase CT through the upper abdomen. Compare appearances to portal venous scans (Fig. 10.4). Note the inhomogeneous opacification of the spleen, as well as relative underenhancement of the portal venous system and systemic veins.

- nine segments (segments I–III, IVa and IVb, V–VIII)
- caudate lobe = segment I
- portal and hepatic veins used as landmarks to divide the remainder of the liver into eight segments
- the three (left, middle and right) hepatic veins divide the liver into four sections
- the portal veins divide each of these into superior and inferior segments, a total of eight.

· Riedel's lobe (Fig. 10.1), a normal variant, is an inferior extension of the right lobe of the liver (around segment VI). May be mistaken for pathological hepatomegaly. Occurs in 5–10% of females. Rare in males.

• Peritoneal ligaments (Fig. 10.13)

· Falciform ligament = double-fold of peritoneum from umbilicus to liver. Contains ligamentum teres, the remnant of the umbilical vein, which attaches to the left portal vein.

- in the fetus, umbilical vein carries oxygenated blood from the cord via the left portal vein and ductus venosus to the IVC
- umbilical vein can recanalize in portal hypertension.

· Falciform ligament splits into coronary ligament (which becomes the right triangular ligament) and left triangular ligament, between which lies the bare

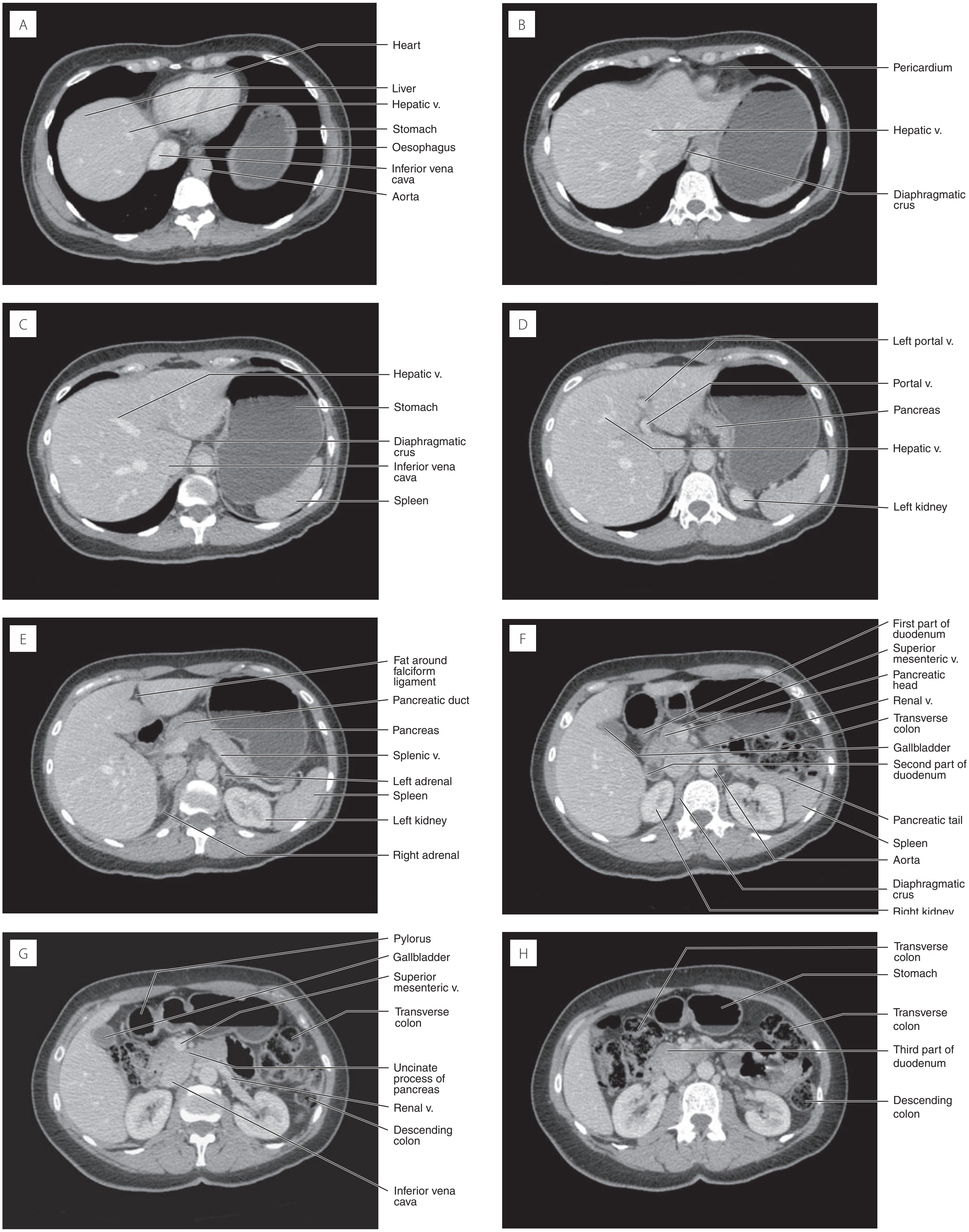


**Fig. 10.4** Portal phase CT through the upper abdomen, axial images. Note the relations of the organs, the relatively higher opacification of the portal and systemic veins compared to the arterial phase scans (Fig. 10.3), and the homogeneous appearance of the spleen.

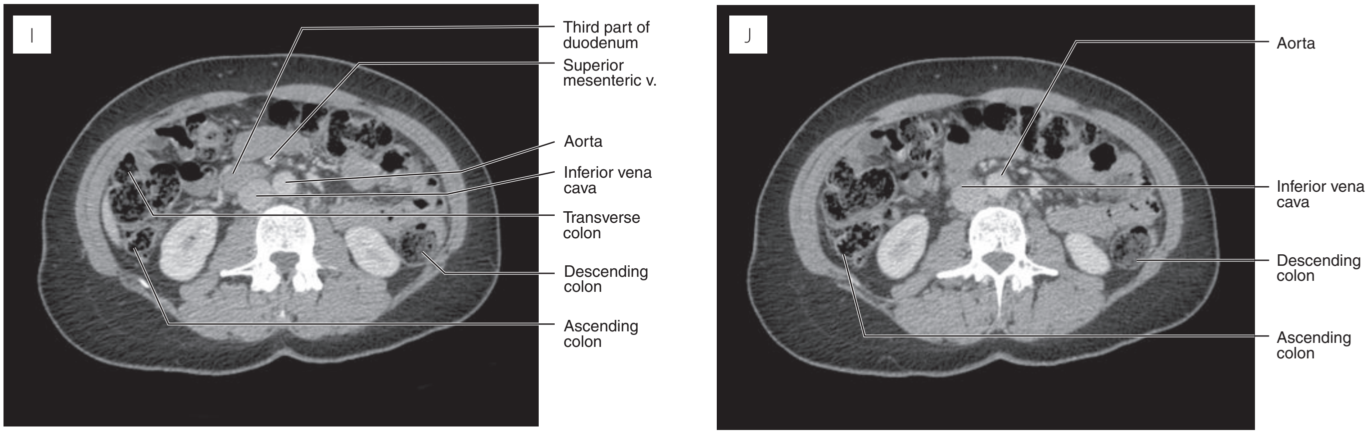


**Fig. 10.4** (*cont.*)

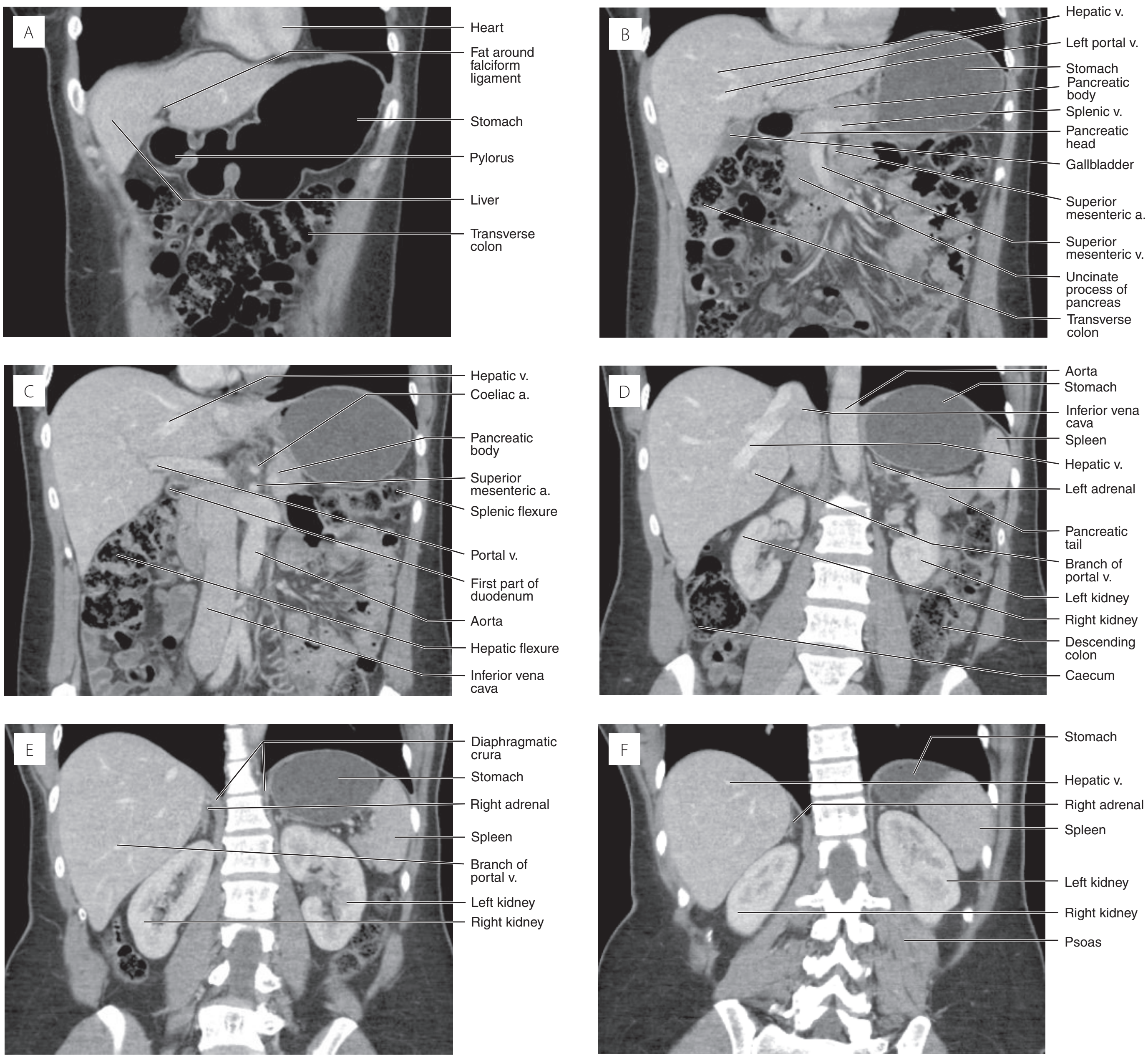


**Fig. 10.5** Portal phase CT through the upper abdomen, coronal images. Note the relations of the organs.

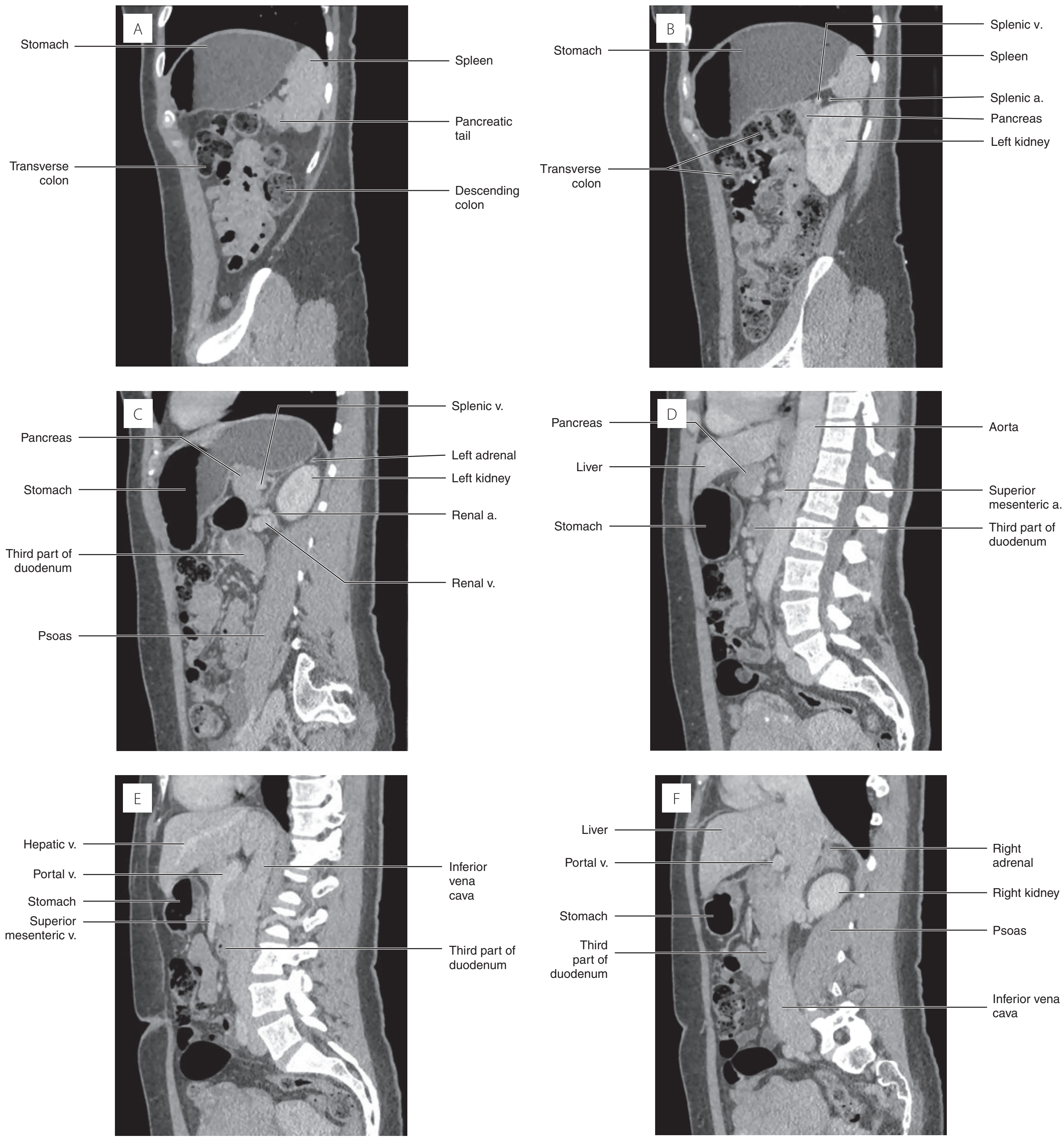


**Fig. 10.6** Portal phase CT through the upper abdomen, sagittal images. Note the relations of the organs.

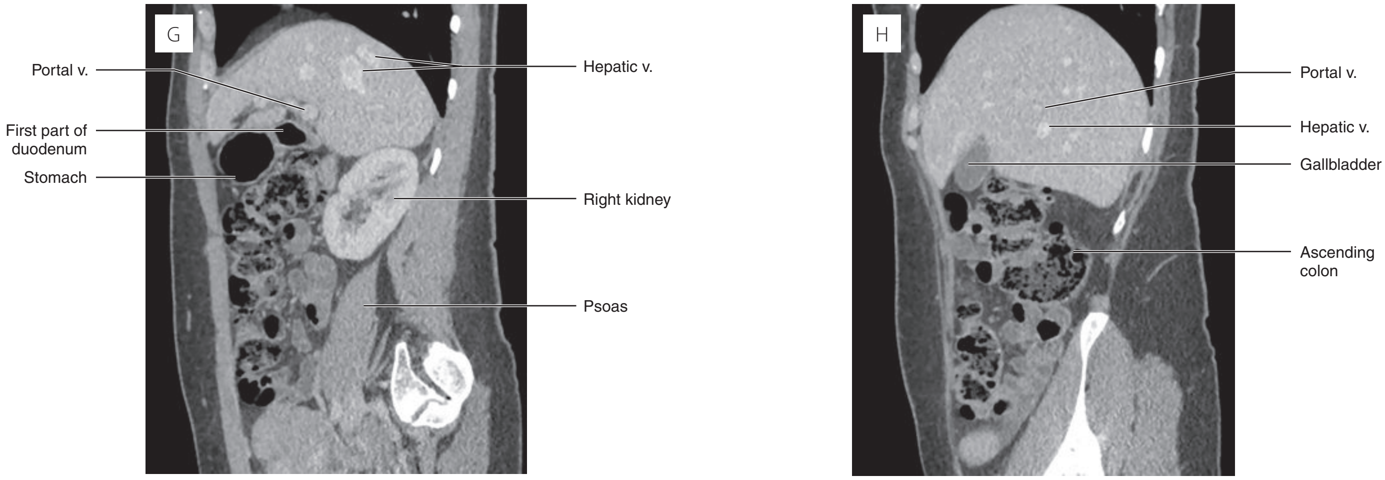


**Fig. 10.6** *(cont.)*

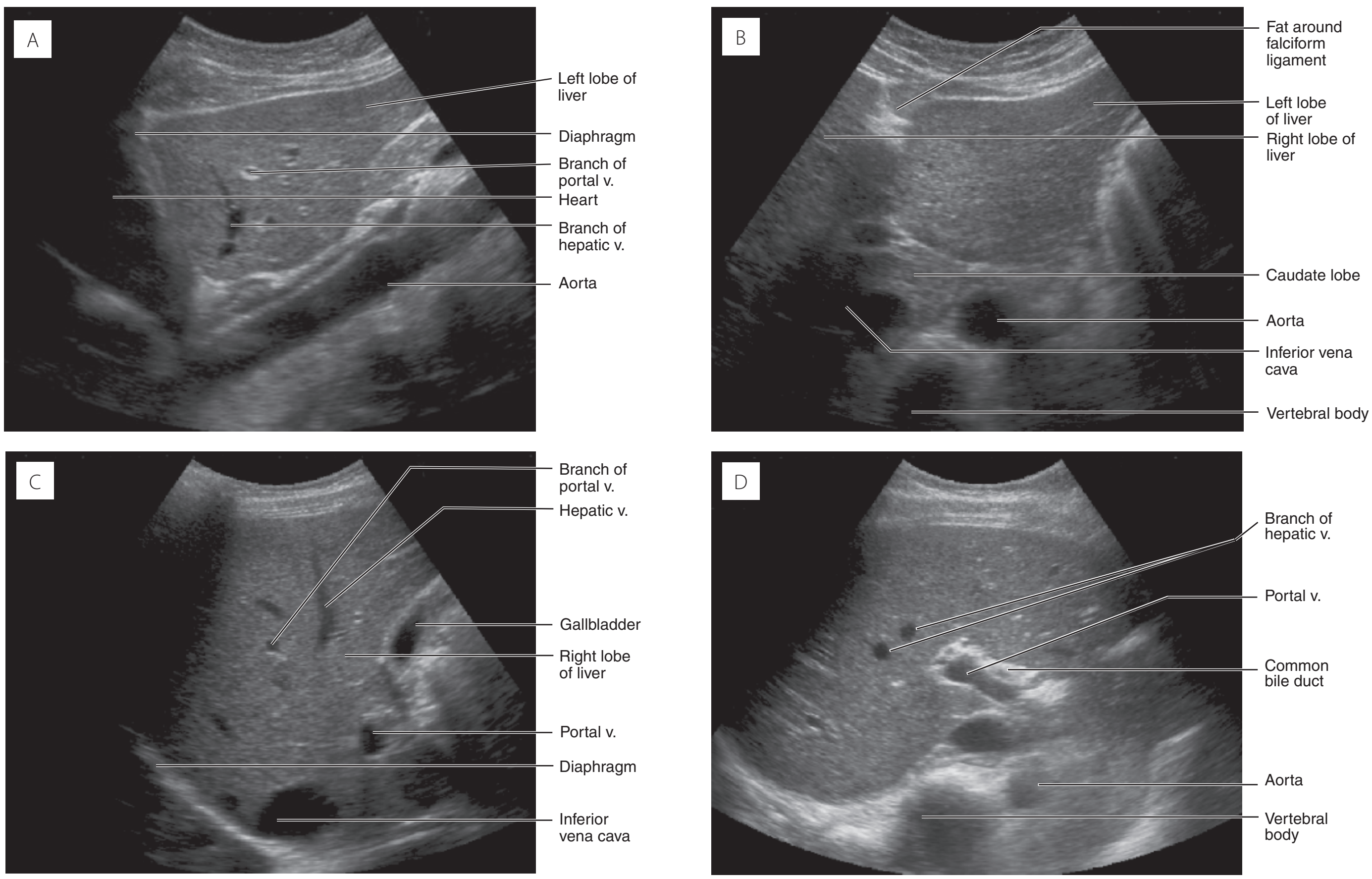


**Figs 10.7** Ultrasound views of the liver derived from recommendations by the American Institute of Ultrasound in Medicine. (A) Longitudinal and (B) transverse views through the left lobe. (C) Longitudinal and (D) transverse views through the right lobe. (E) Transverse image through the caudate lobe. (F) Appearances on the high-frequency linear ultrasound probe. (G) Longitudinal and (H) transverse views comparing the echogenicity of the liver against the right kidney. (I–L) Greyscale and colour Doppler views of the confluence of the hepatic veins and of the main portal vein. (M, N) Transverse images through the liver showing the left and right branches of the portal vein.

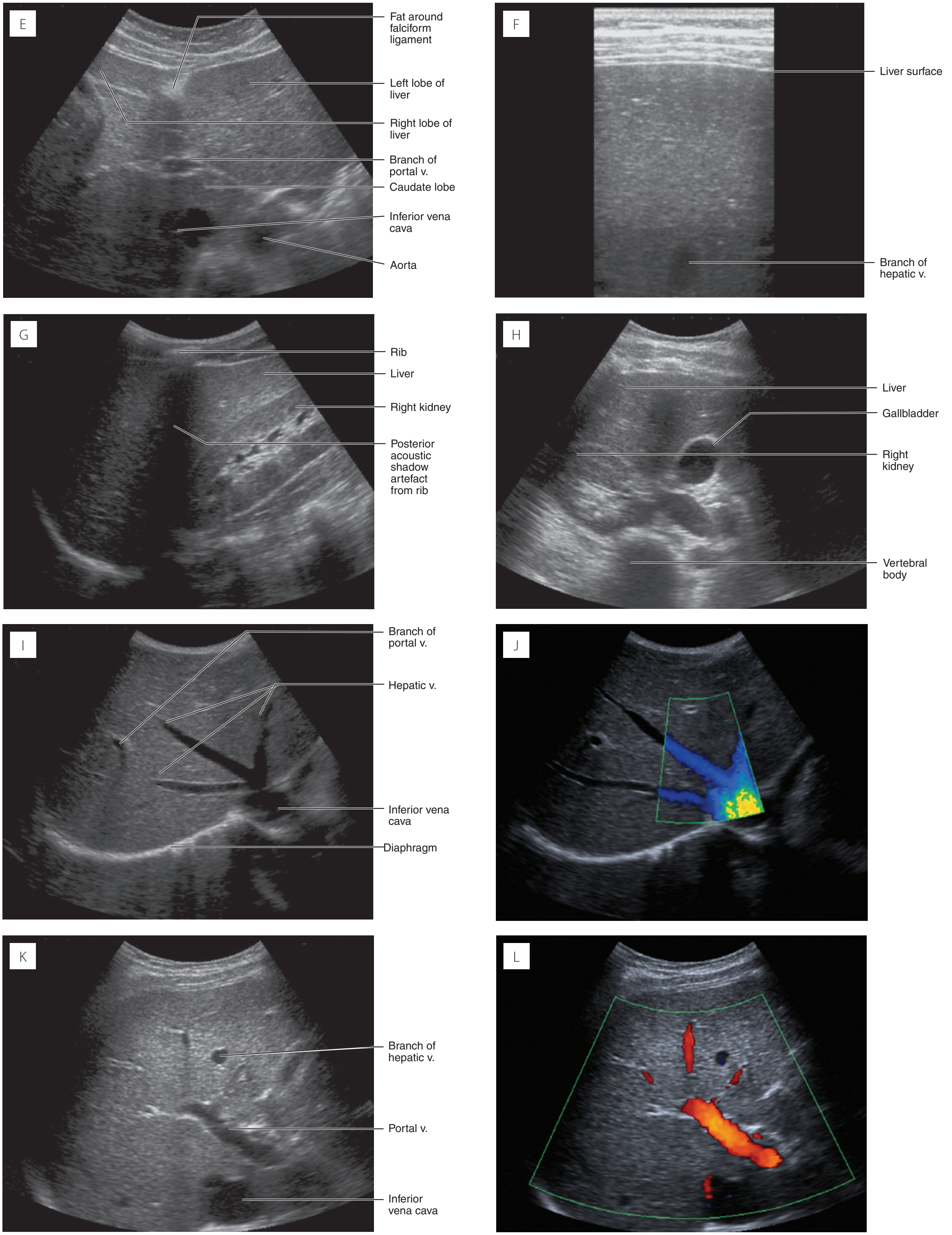
E
Fat around falciform ligament
Left lobe of liver
Right lobe of liver
Branch of portal v.
Caudate lobe
Inferior vena cava
Aorta
F
Liver surface
Branch of hepatic v.
G
Rib
Liver
Right kidney
Posterior acoustic shadow artefact from rib
H
Liver
Gallbladder
Right kidney
Vertebral body
I
Branch of portal v.
Hepatic v.
Inferior vena cava
Diaphragm
J
K
Branch of hepatic v.
Portal v.
Inferior vena cava
L

**Fig. 10.7** *(cont.)*

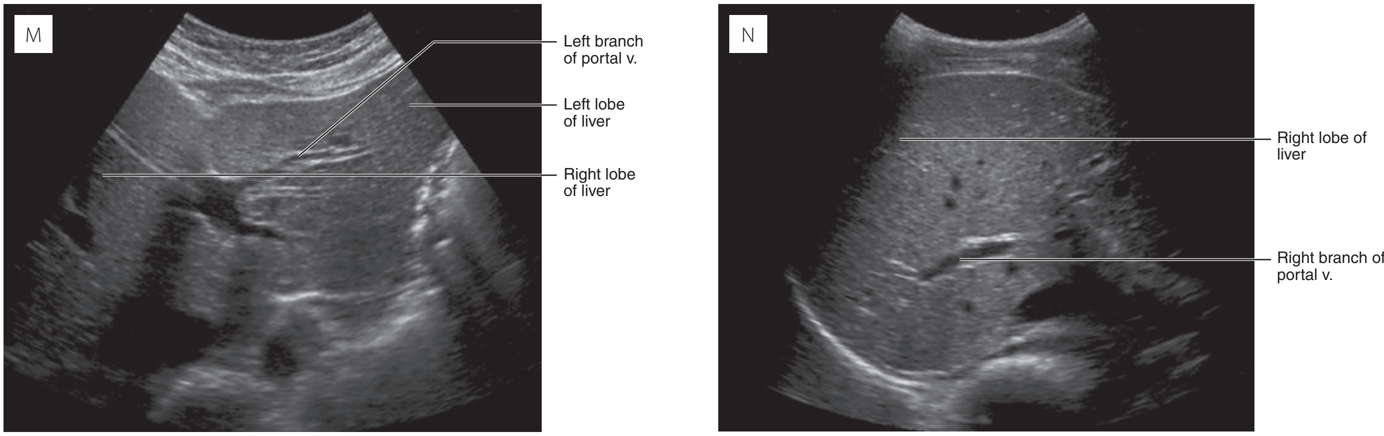


**Fig. 10.7** (*cont.*)

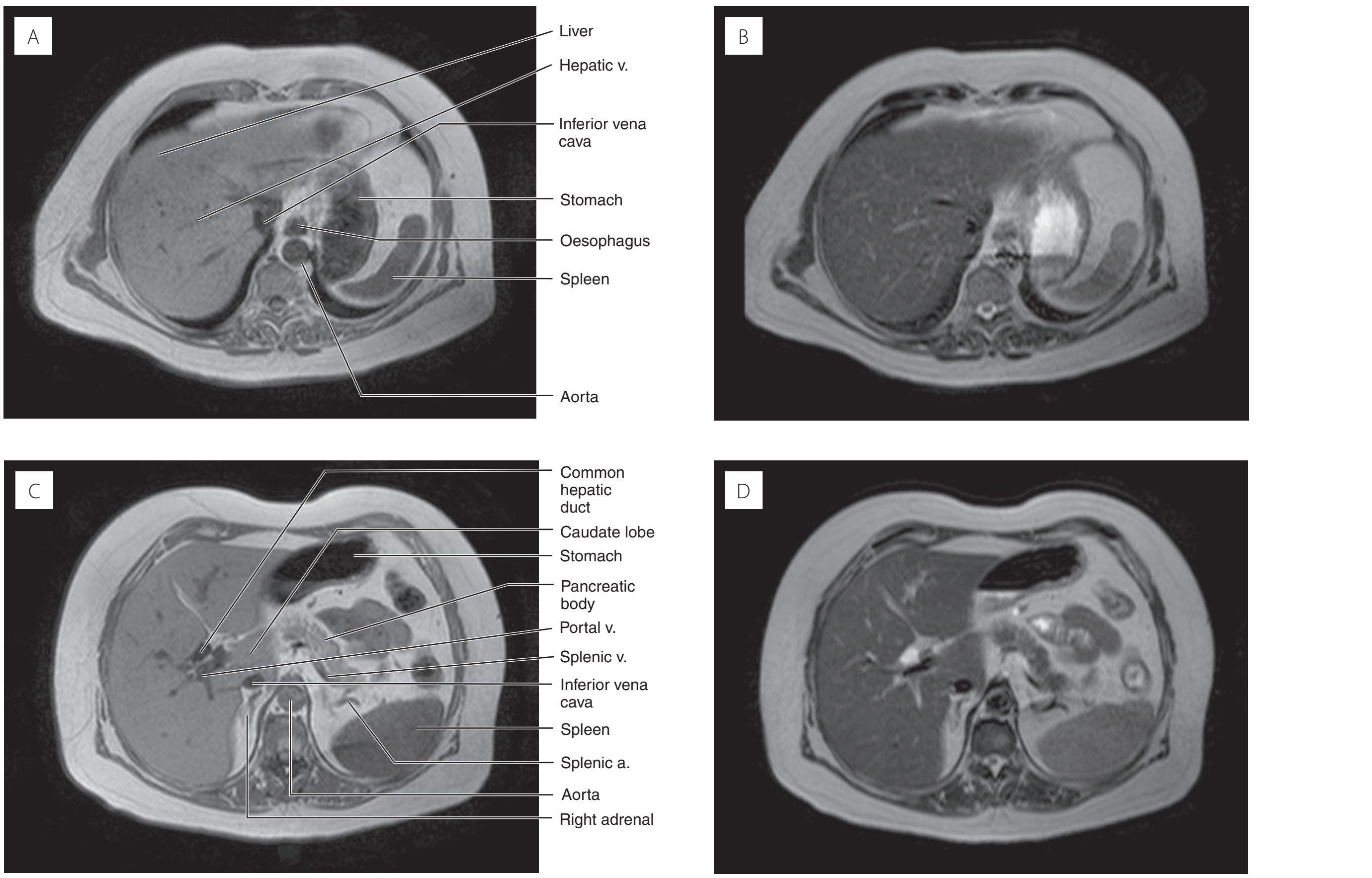


**Fig. 10.8** Paired axial T1- (left) and T2-weighted (right) images through the upper abdomen, demonstrating the differing appearances of organs on the two sequences. Note that appearances are not exactly the same on both sequences due to movement. Labels are provided mainly on the T1-weighted images. The coeliac axis is best seen on the T2-weighted images and therefore only labelled here.

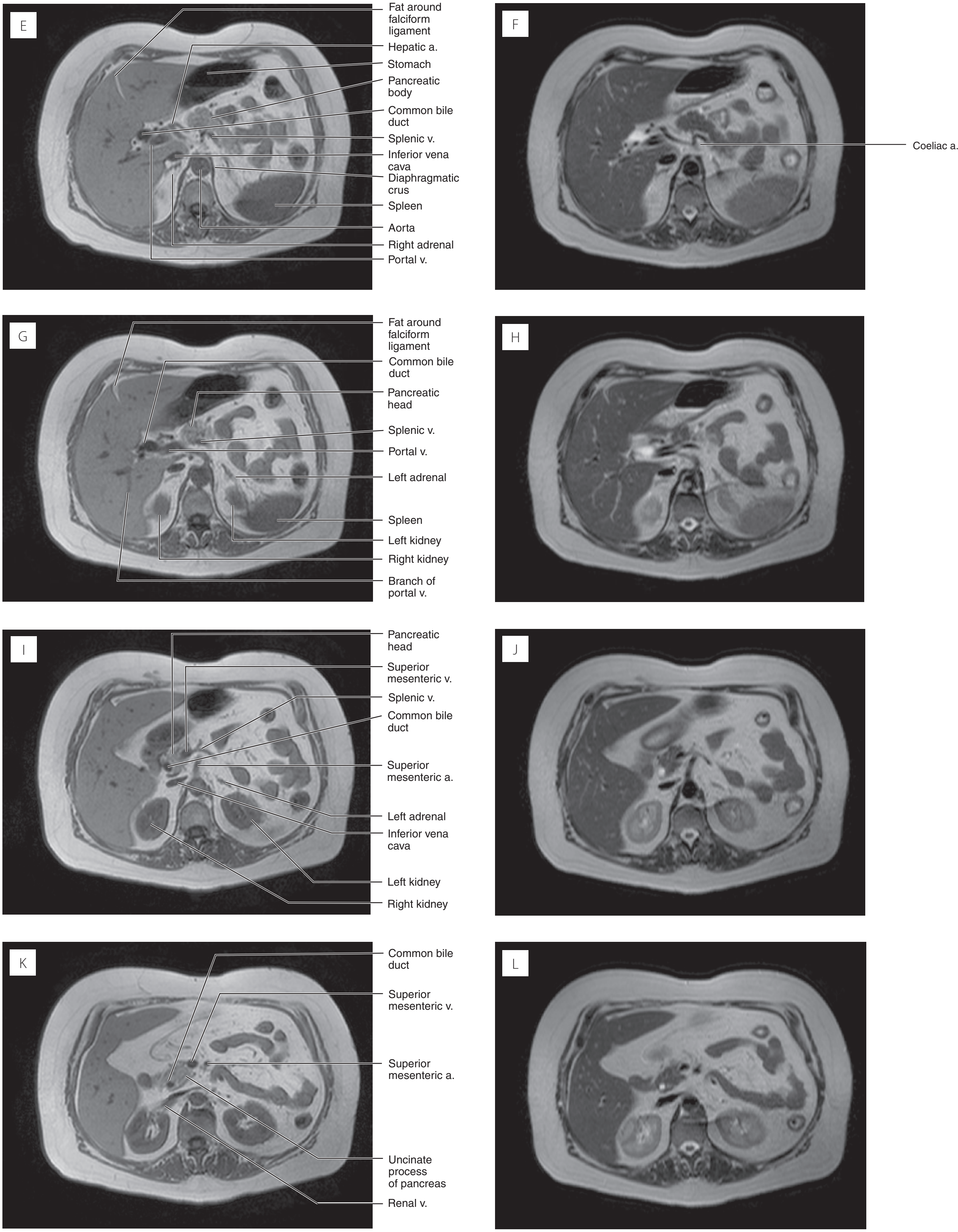
E
Fat around falciform ligament
Hepatic a.
Stomach
Pancreatic body
Common bile duct
Splenic v.
Inferior vena cava
Diaphragmatic crus
Spleen
Aorta
Right adrenal
Portal v.
F
Coeliac a.
G
Fat around falciform ligament
Common bile duct
Pancreatic head
Splenic v.
Portal v.
Left adrenal
Spleen
Left kidney
Right kidney
Branch of portal v.
H
I
Pancreatic head
Superior mesenteric v.
Splenic v.
Common bile duct
Superior mesenteric a.
Left adrenal
Inferior vena cava
Left kidney
Right kidney
J
K
Common bile duct
Superior mesenteric v.
Superior mesenteric a.
Uncinate process of pancreas
Renal v.
L

**Fig. 10.8** *(cont.)*

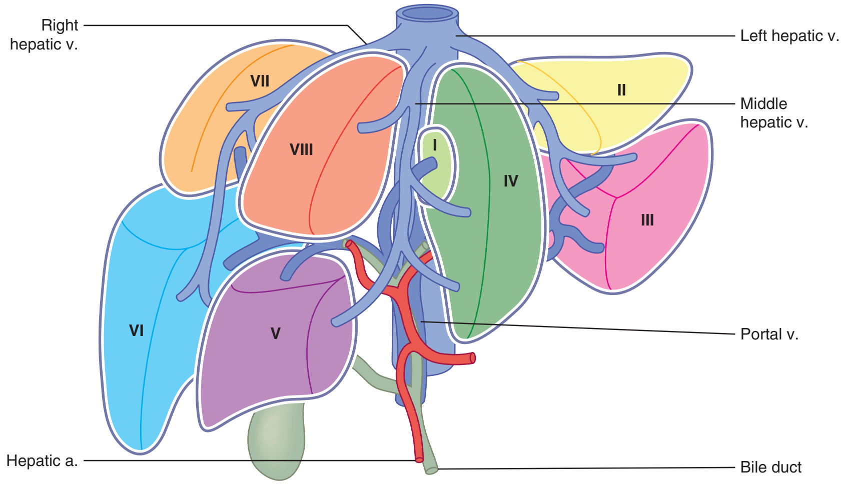


**Fig. 10.9** Segmental liver anatomy.

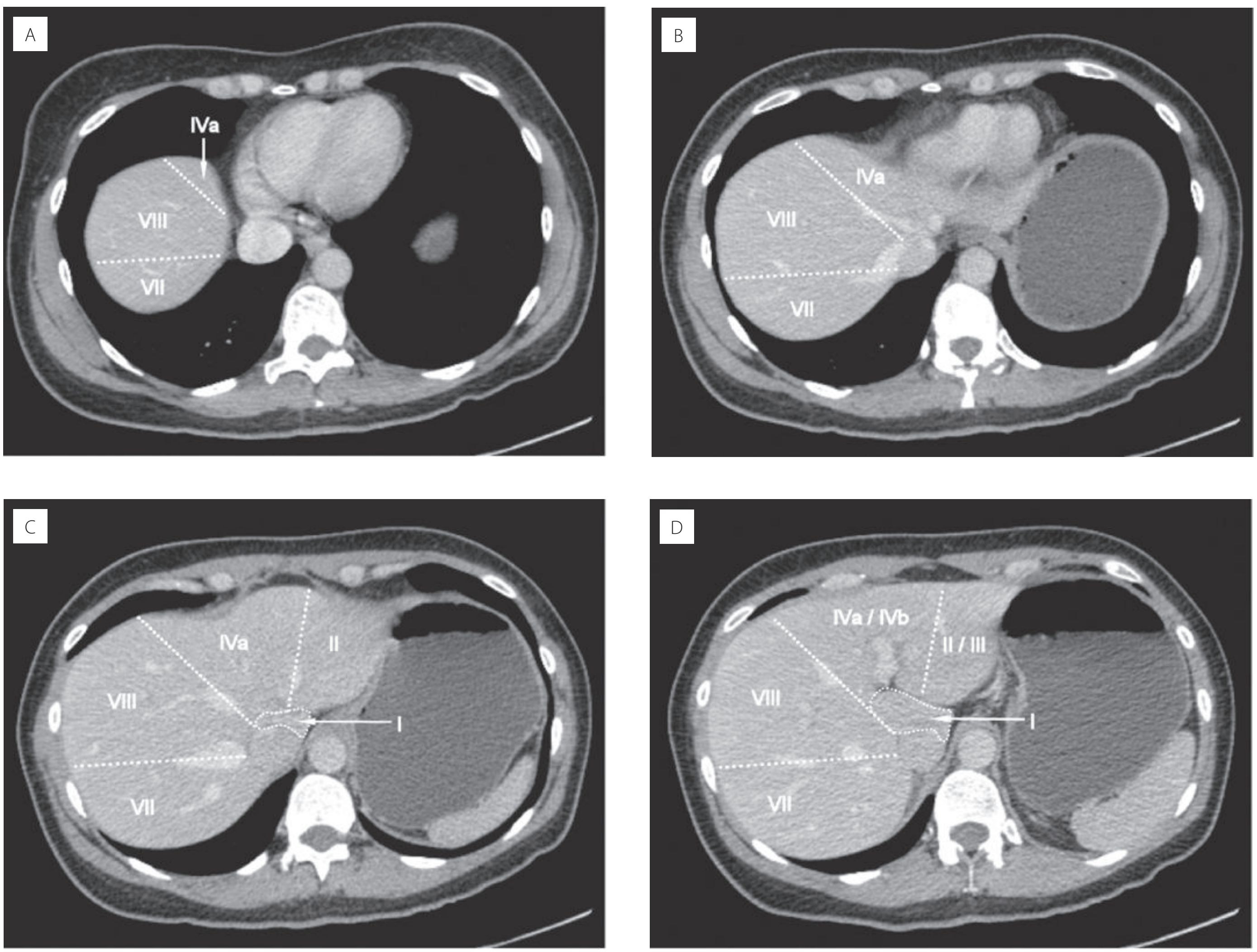


**Fig. 10.10** Segmental anatomy of the liver, axial. Segments labelled.

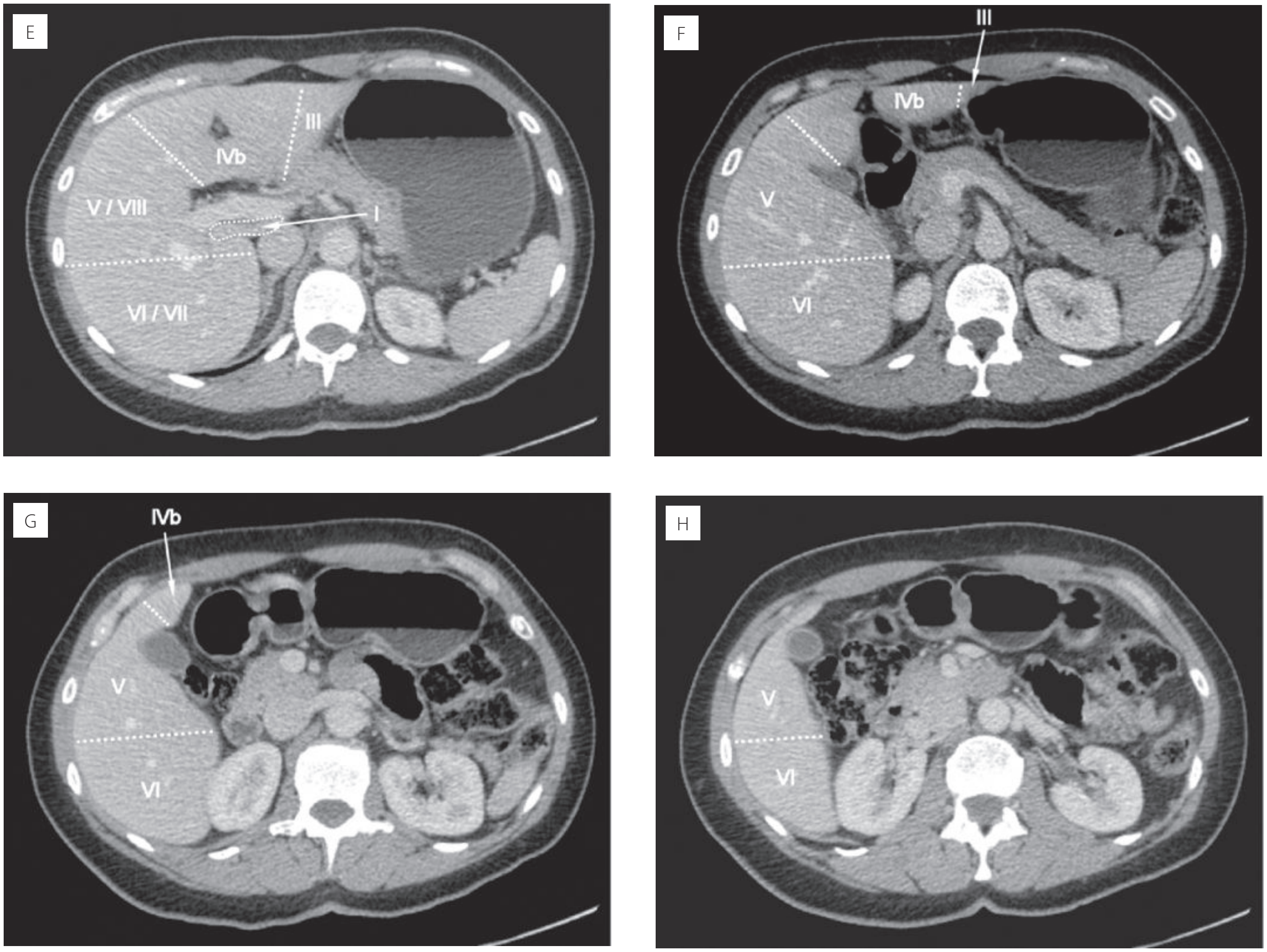


**Fig. 10.10** (*cont.*)

area of the liver. These ligaments attach the liver to the diaphragm.

- Blood supply (Figs. 10.14–10.23)
  - The liver has a dual blood supply: hepatic artery and portal vein.
  - Hepatic artery (Figs. 10.14–10.19)
    - provides 15% of hepatic blood supply
    - branch of coeliac artery
    - common hepatic artery passes over the head of pancreas and gives off right gastric artery, then gives off gastroduodenal artery at the epiploic foramen to become the hepatic artery proper
    - hepatic artery continues in the free edge of the lesser omentum, anterior to the portal vein and to the left of the common bile duct (CBD)
    - divides into left and right branches at the porta hepatis
    - anatomical variants:
      - relatively common
      - in 90%, right hepatic artery passes anterior to portal vein.
- Accessory arteries are present in addition to the normal artery. Replaced arteries are present in the absence of the normal artery (Fig. 10.19).
  - In 18.5% of individuals, hepatic arteries arise from the superior mesenteric artery (SMA): 10% = replaced right hepatic artery; 6% = accessory right hepatic artery; 2.5% = replaced common hepatic artery.
  - 25% of individuals have left hepatic arteries arising from the left gastric artery: 13% = accessory 12% = replaced.
  - Portal vein (Figs. 10.15–10.18, 10.20)
    - provides 85% of blood supply to liver
    - formed by union of the splenic vein and superior mesenteric vein (SMV) posterior to neck of pancreas at L1/L2
    - runs at posterior aspect of free edge of lesser omentum to the porta hepatis; it lies posterior to hepatic artery and CBD

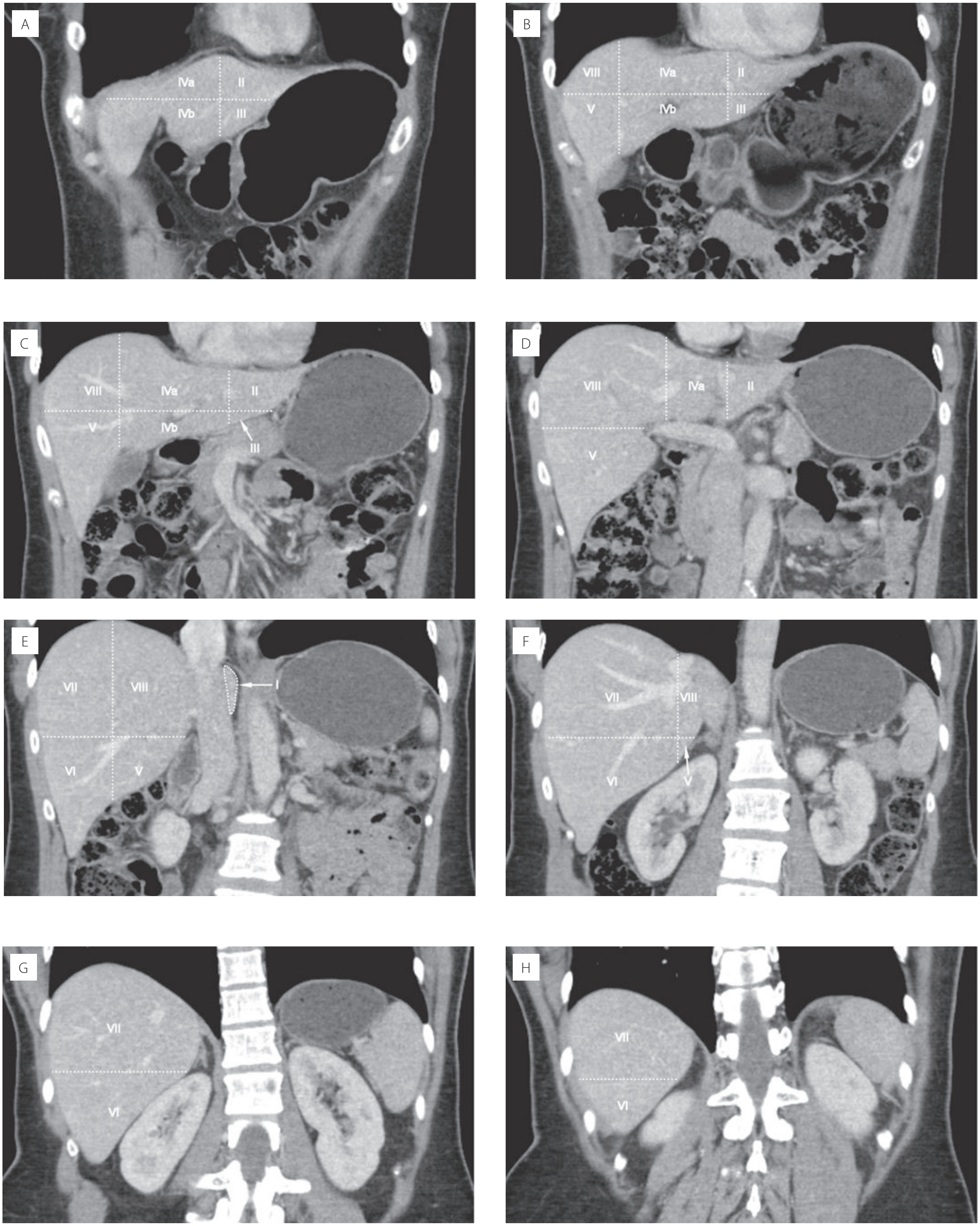


**Fig. 10.11** Segmental anatomy of the liver, coronal. Segments labelled.

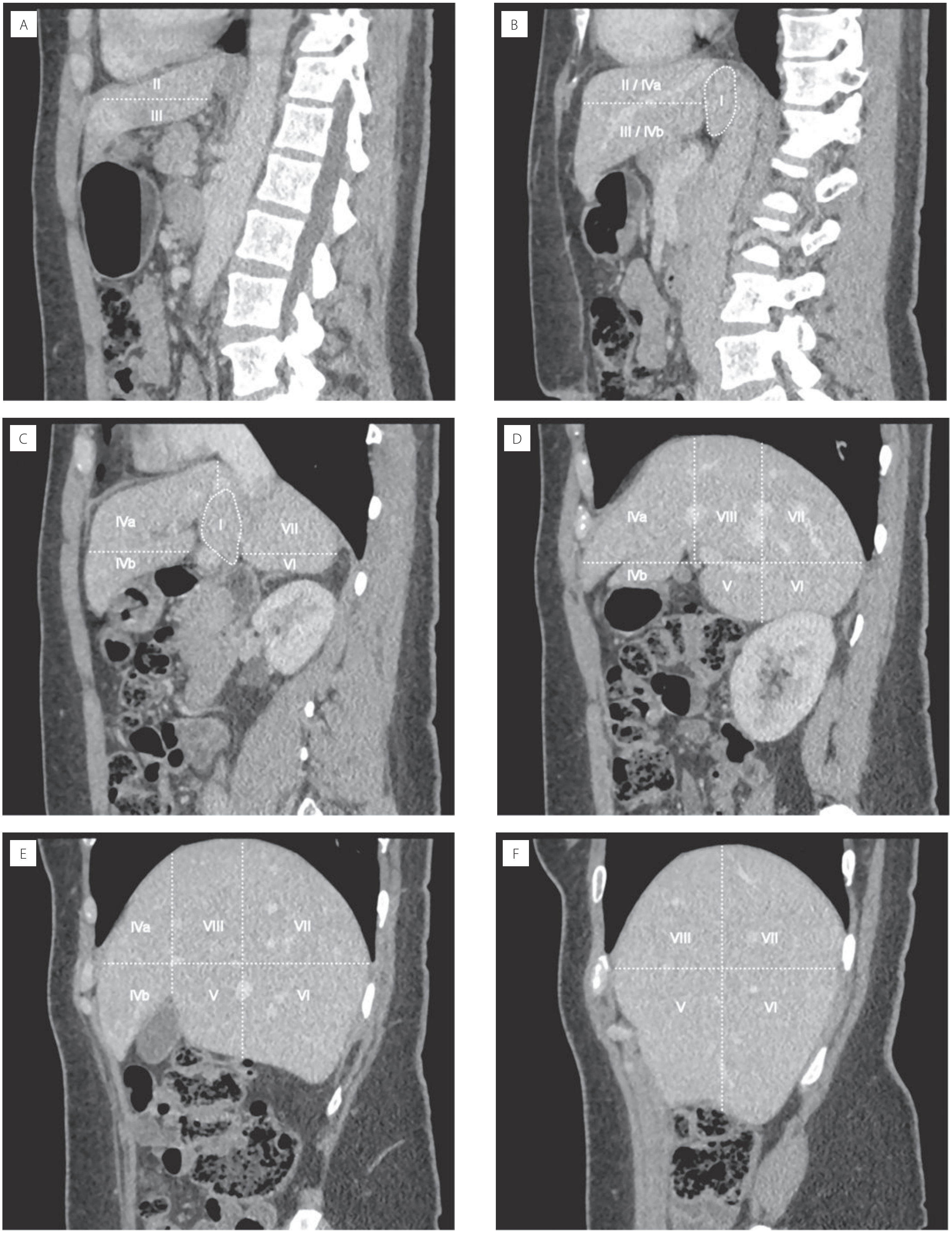


**Fig. 10.12** Segmental anatomy of the liver, sagittal. Segments labelled.

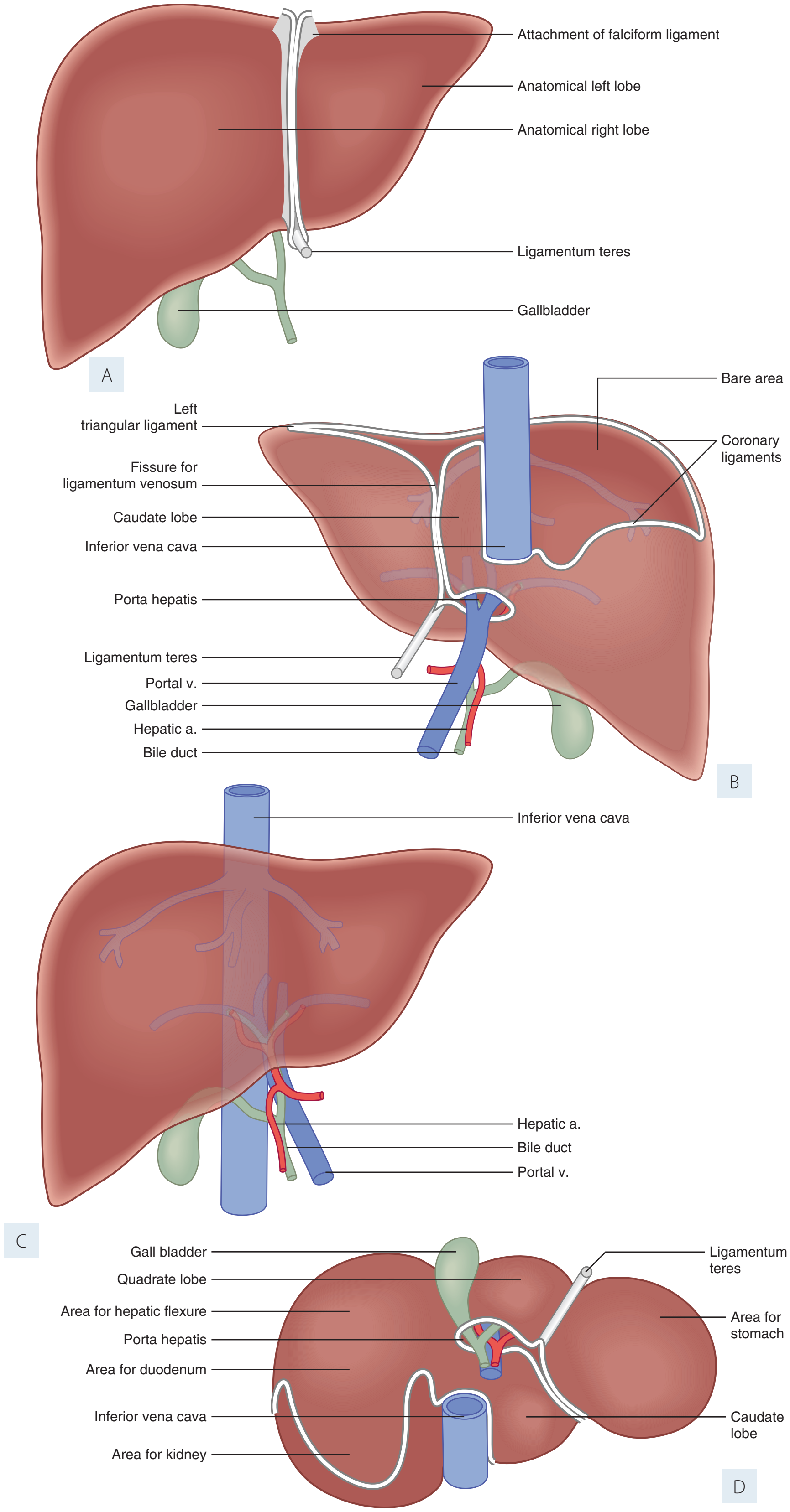


**Fig. 10.13** Peritoneal ligaments. (A) Anterior, (B) posterior, (C) semi-opaque anterior and (D) inferior views of the live.

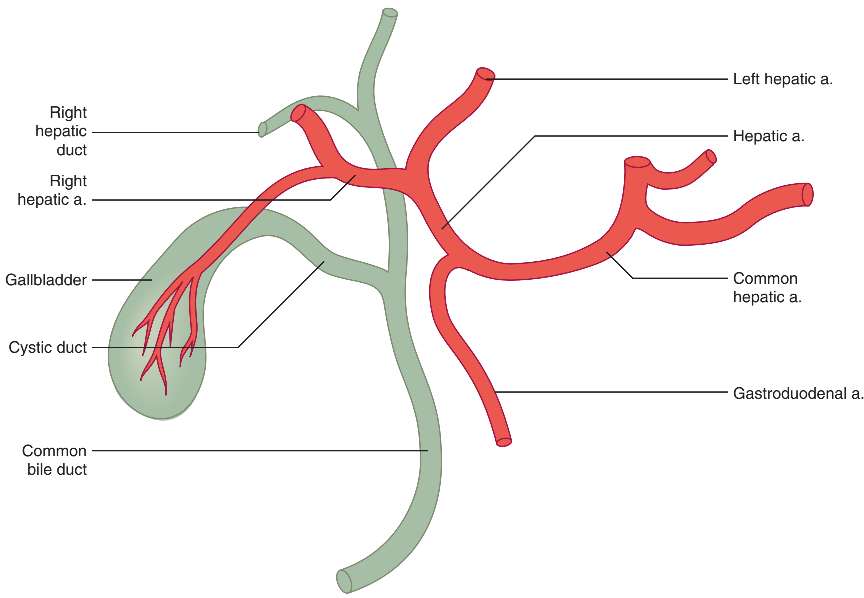


**Fig. 10.14** Relations of the hepatic arterial system.

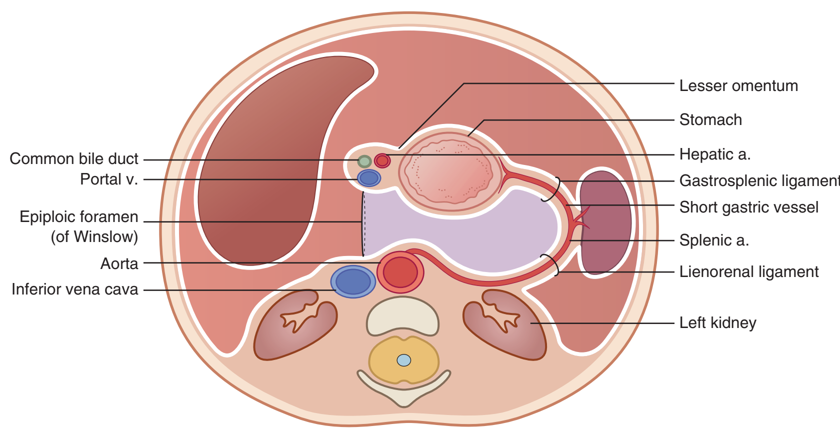


**Fig. 10.15** Hepatic artery in lesser omentum.

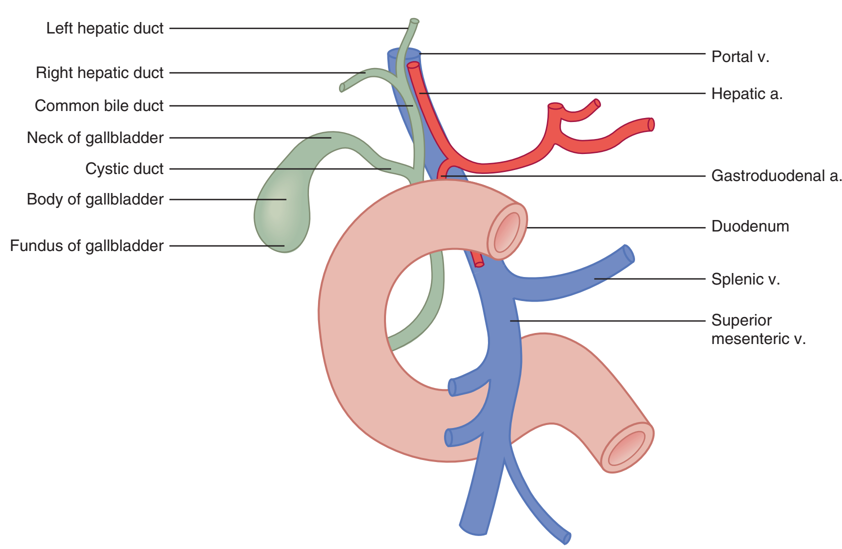


**Fig. 10.16** Relations of portal structures.

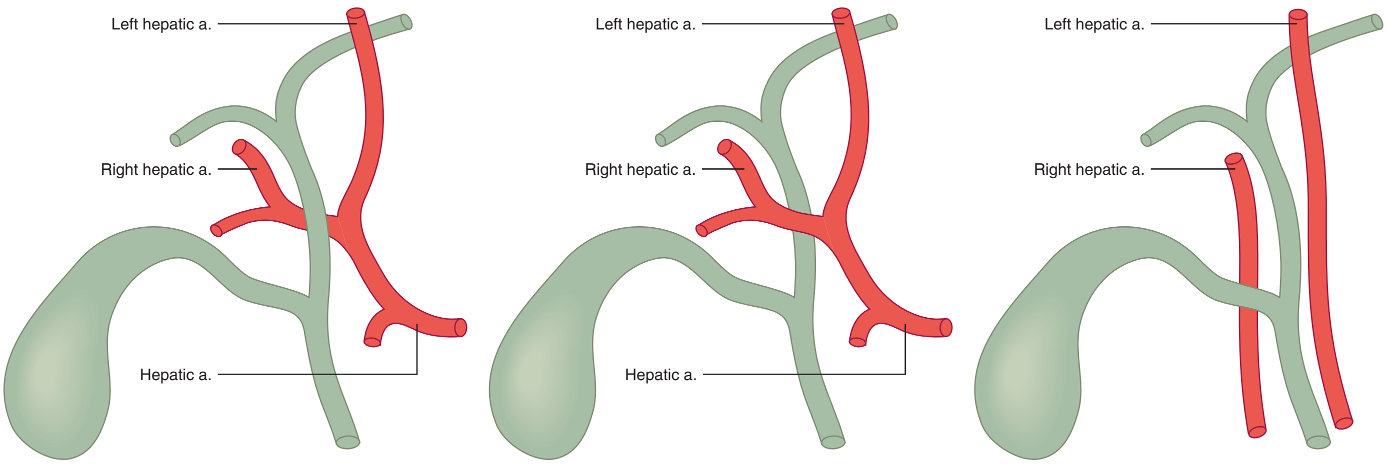


**Fig. 10.17** Relations of the bile ducts and hepatic artery.

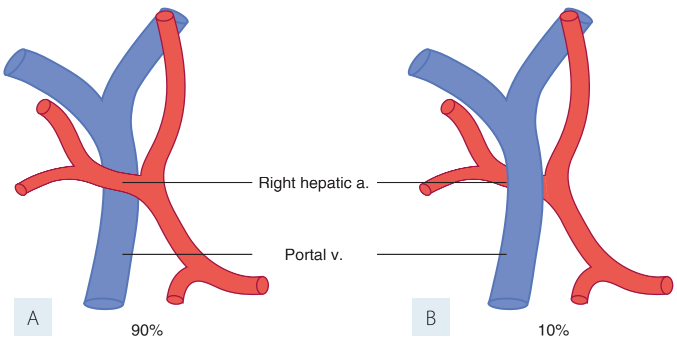


**Fig. 10.18** Variation in relations of hepatic artery and portal vein.

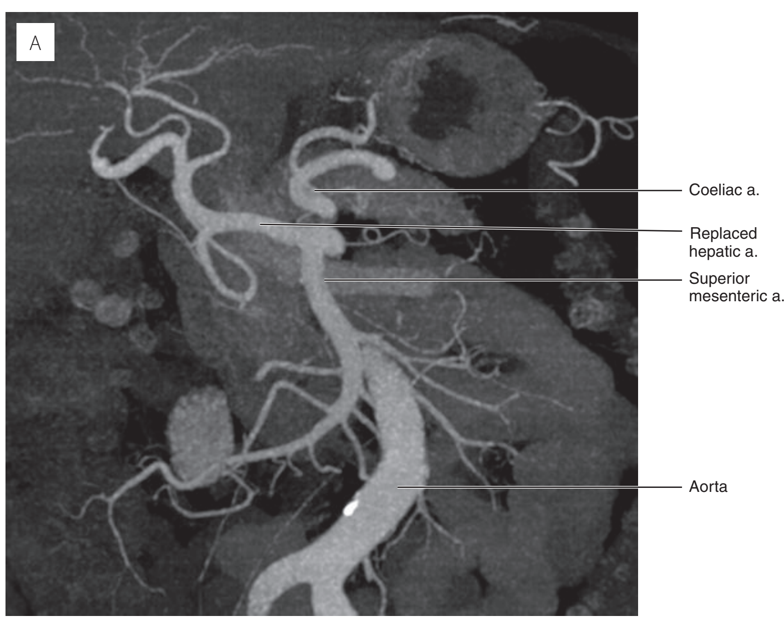


**Fig. 10.19** Normal variations in hepatic arterial tree. Coronal MIP CT images through the upper abdomen in arterial phase enhancement. Normal variant hepatic arteries are seen to arise from the SMA. (A) If no hepatic artery arises from the coeliac axis, this is termed a replaced hepatic artery. (B) If a normal hepatic artery is present from the coeliac axis, this is an accessory hepatic artery.

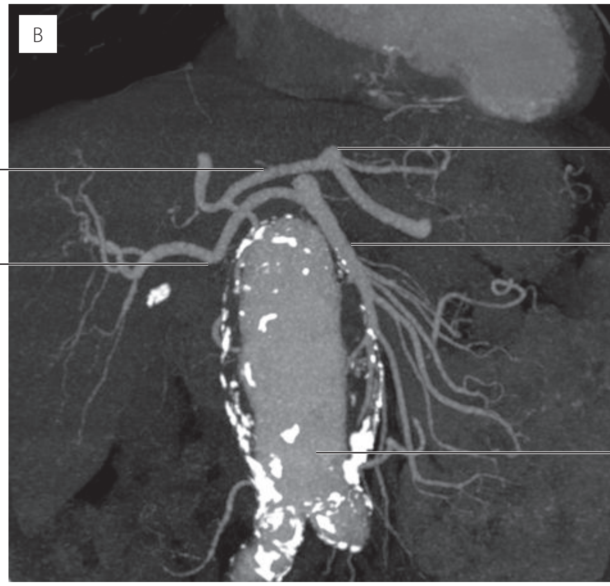


**Fig. 10.19** (*cont.*)

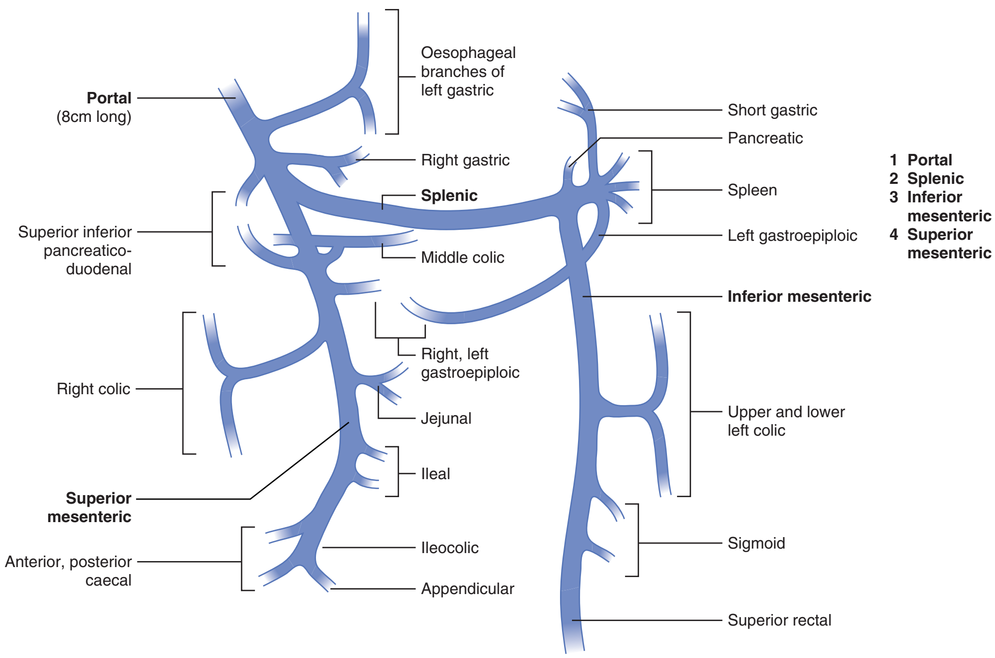


**Fig. 10.20** Portal vein branches.

  - the predominantly portal vein input means that the liver enhances (Figs. 10.3–10.4) poorly in the arterial phase and shows maximal enhancement in the portal venous phase.
- Venous drainage of the majority of the liver is via the hepatic veins:
  - unite to drain into the IVC at T9 close to the diaphragmatic hiatus
  - caudate lobe drains directly into the IVC and may therefore be spared in cases of hepatic vein thrombosis.
- The vasculature (hepatic artery, hepatic vein, portal vein and their branches) can be interrogated, each with their own characteristic traces on spectral Doppler (Fig. 10.21).
- Portosystemic anatomoses (Figs. 10.22–10.23)
  - In portal hypertension tiny collaterals open between the portal and systemic venous system. There are four common sites for these anatomoses to develop:
    - at the gastro-oesophageal junction between the left gastric and the azygos veins
    - at the rectum between the superior rectal veins and the inferior rectal vein

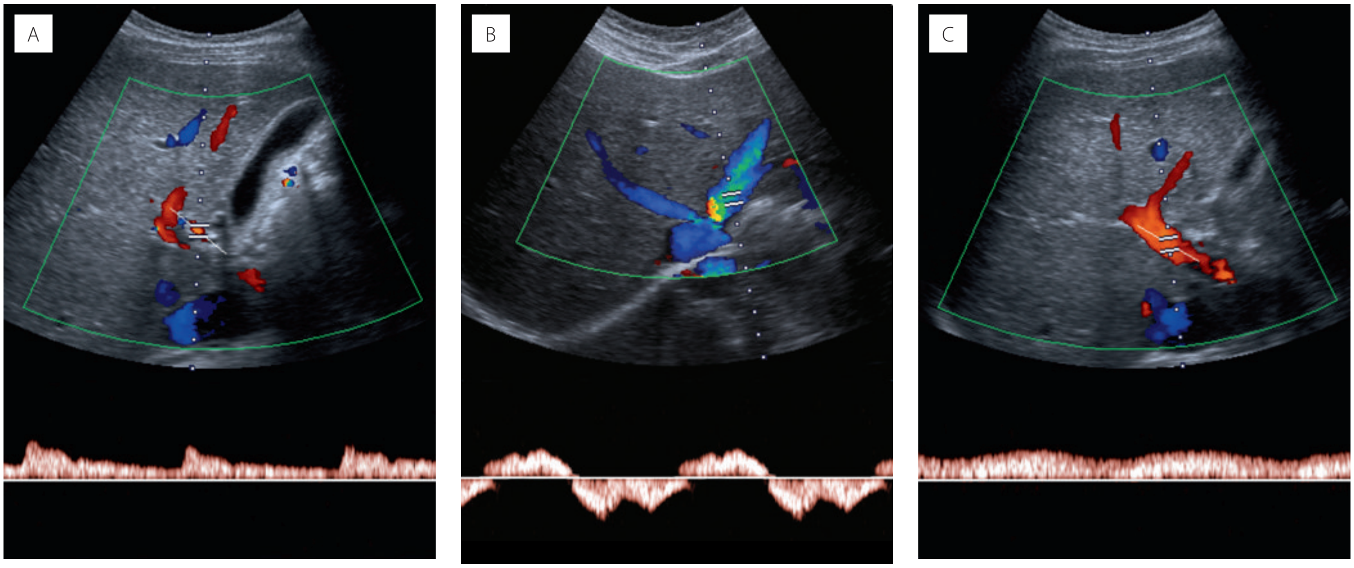


**Fig. 10.21** Typical spectral Doppler traces from (A) hepatic artery, (B) hepatic vein and (C) portal vein.

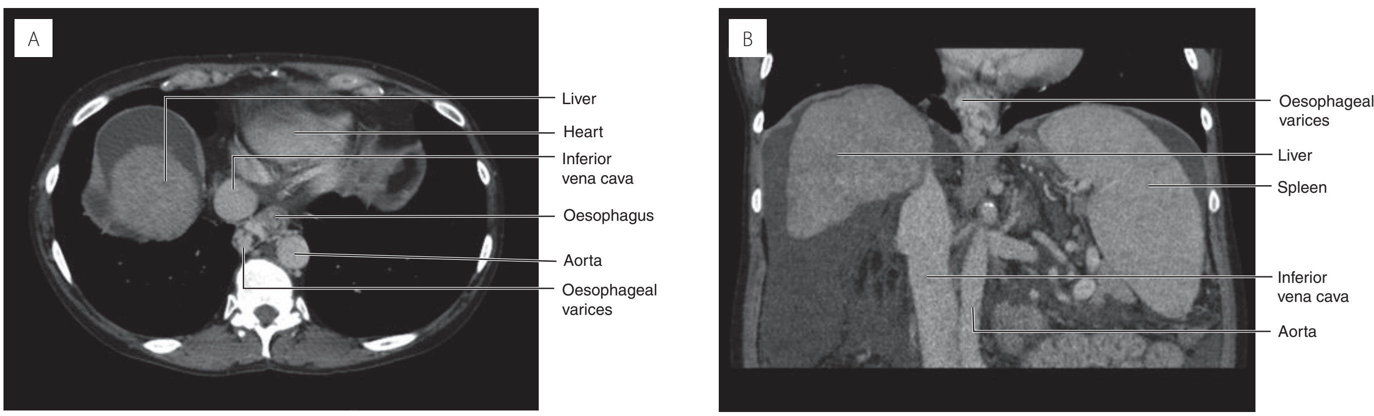


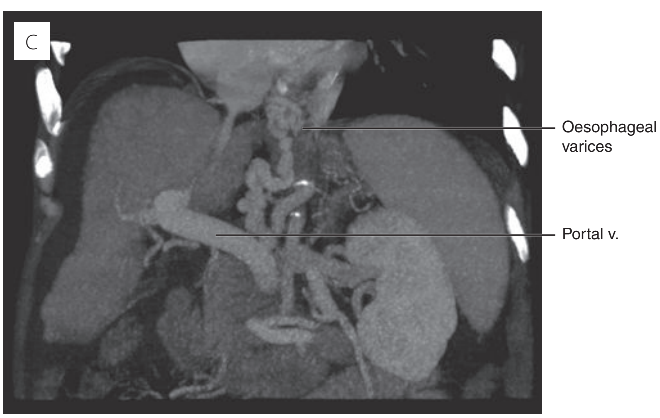


**Fig. 10.22** (A) Axial, (B) coronal and (C) coronal MIP images in a patient with an irregular cirrhotic liver with portal hypertension and splenomegaly with consequent formation of oesophageal varices, i.e. portosystemic anastomosis.

  - at the umbilicus between the umbilical veins and the superficial epigastric veins
  - in the retroperitoneum between the peritoneal veins and the retroperitoneal, renal, lumbar and phrenic veins.

## Gallbladder and biliary tree

- Gallbladder:
  - pear-shaped sac up to 10 cm long and 3 cm diameter
  - hangs down from inferior surface of liver – fundus usually anterior and inferior to the body and neck
    - N. B. Hartmann's pouch = ventral dilatation around gallbladder neck following gallstone impaction at neck; not a feature of normal gallbladder
  - wall thickness < 4 mm
  - cystic duct arises from neck – runs along liver surface to the porta hepatis
  - gallbladder neck and cystic duct have a spiral appearance to folds in the mucosa (spiral valve of Heister; regulates flow of bile); on ultrasound this is highly echogenic and may be mistaken for gallstones
  - covered by peritoneum on fundus and inferior surface; occasionally hangs on its own mesentery.
- Anatomical relationships (Figs. 10.16, 10.24–10.25).
- Blood supply (Fig. 10.14)

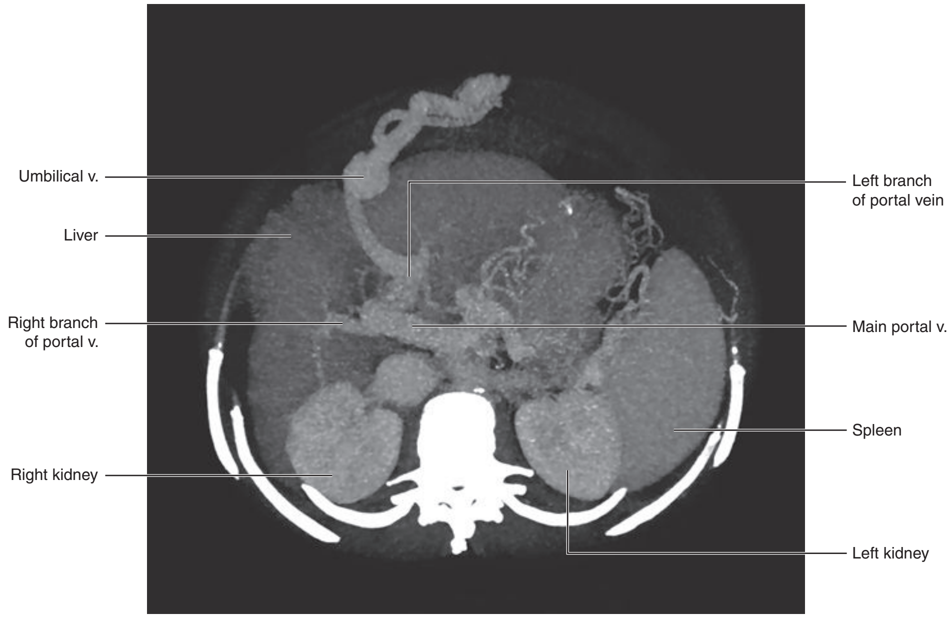


**Fig. 10.23** Axial MIP CT in a patient with portal hypertension. There has been recanalization of the umbilical vein arising from the left portal vein, travelling along the falciform ligament to the umbilicus in the midline.

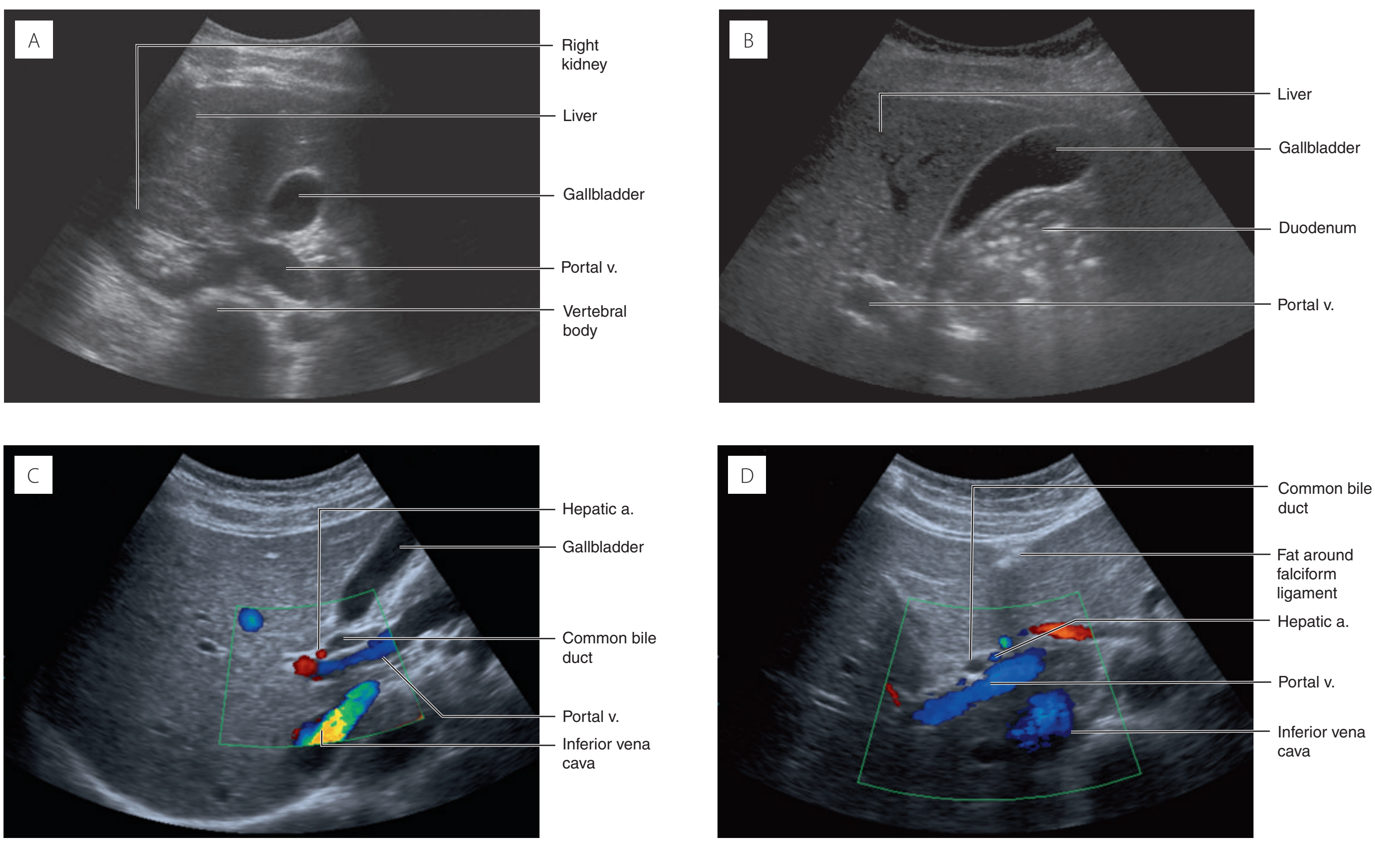


**Fig. 10.24** (A) Transverse and (B) longitudinal ultrasound images through the gallbladder. (C, D) Images of the CBD at the porta hepatis.

- Cystic artery usually from right hepatic artery, in 10% from left hepatic artery and less commonly from common hepatic artery or SMA.
- Cystic veins empty into the liver or the portal vein.

- Biliary tree (Figs. 10.26–10.28):
  - Segmental biliary ducts unite to form left and right hepatic ducts, which unite to form the common hepatic duct (CHD) at the porta hepatis; in two-thirds of individuals, the CHD passes anterior to the right hepatic artery.

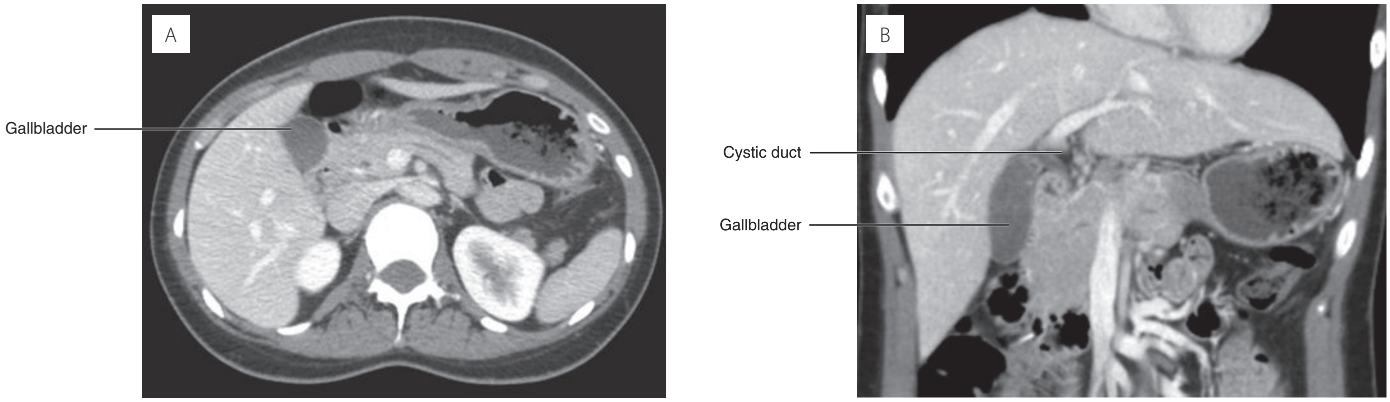


**Fig. 10.25** The appearance of the gallbladder on CT. (A) Axial and (B) coronal CT images.

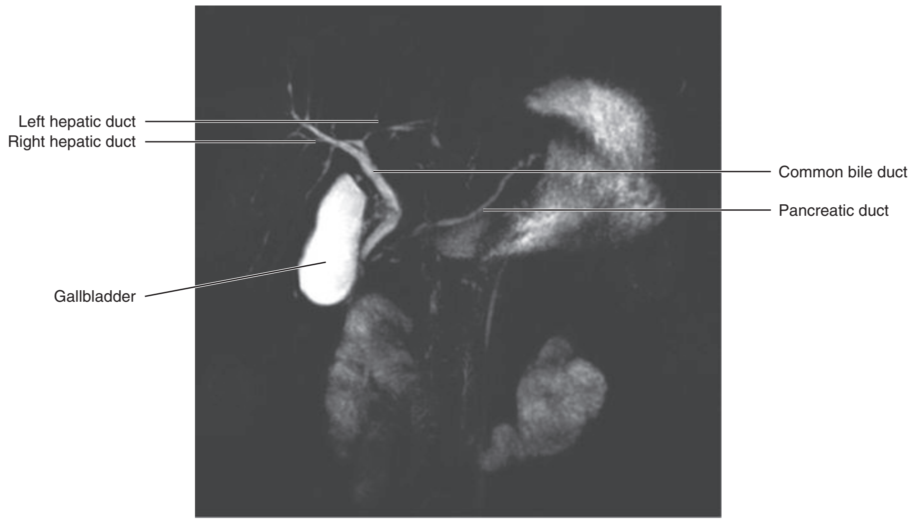


**Fig. 10.26** Normal MRCP. Highly T2-weighted MR sequence which shows fluid within the pancreaticobiliary system.

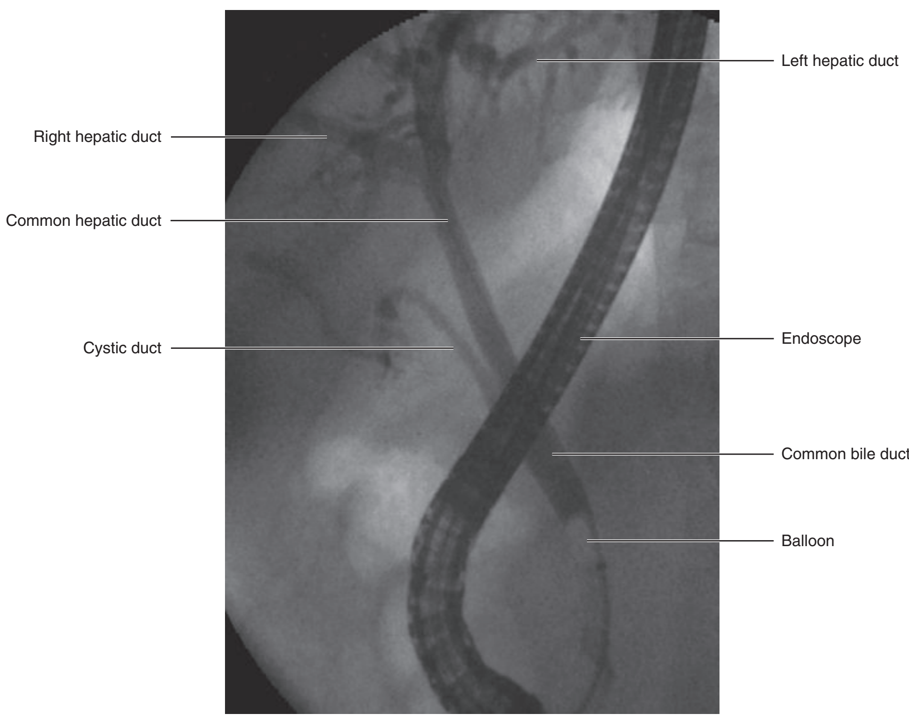


**Fig. 10.27** Normal ERCP. The ampulla of Vater has been catheterized via the side-hole of the endoscope. A balloon is then inflated and contrast instilled to opacify the biliary tree.

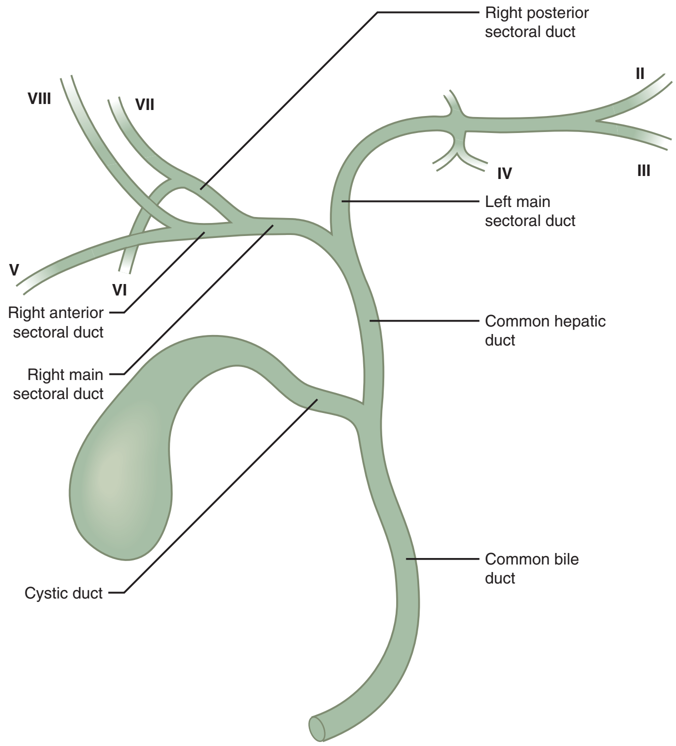


**Fig. 10.28** Segmental biliary drainage of the liver.

- The CHD is joined by the cystic duct at a variable position (usually 3.5 cm) to form the CBD.
- Divisions and relations of the CBD:
  - upper – above the duodenum within the lesser omentum, anterior to the portal vein and to the right of the hepatic artery
  - middle – posterior to the first part of the duodenum with the gastroduodenal artery, sloping away to the right from the portal vein; immediately anterior to the IVC
  - lower – grooves the posterior aspect of the pancreatic head, anterior to the right renal vein; joined by the main pancreatic duct at the ampulla of Vater, opening into the posteromedial wall of the second part of the duodenum.
- Diameter of CBD is variable:
  - up to 5 mm till age of 50 years then 1 mm/decade after that age
  - can be larger in post-cholecystectomy patients (up to 10 mm)
- Anatomical variations very common in intrahepatic ducts (40%), but rarely clinically significant. Variations in extrahepatic ducts less common, but may be associated with intraoperative damage during laparoscopic surgery, if previously not known about. Examples:
  - 5–10% have accessory ducts which may join the remainder of the extrahepatic biliary tree at any point, including the gallbladder
  - non-union of left and right hepatic ducts
  - cystic duct:
    - absence (gallbladder directly connects to hepatic duct)
    - may join anywhere along length of the hepatic duct
  - fistula to respiratory tract
  - variable position of the ampulla, from stomach to third part of duodenum
  - separate openings for CBD and pancreatic duct (close to each other in 40% and far apart in 4%).

## Pancreas

- Long (around 15 cm) epigastric structure extending from duodenal loop to splenic hilum.
  - similar density to liver on CT, but becomes atrophic and fatty with age
- Comprises the head (including uncinate process), neck, body and tail
- Anatomical relationships and position: see Figs. 10.3–10.8 and 10.29–10.30
- Pancreatic duct:
  - begins at tail and runs to head, increasing in size
  - located in the anterior half of the pancreas
  - joins CBD at ampulla of Vater
  - accessory duct of Santorini arises from pancreatic head and drains via the minor papilla into the duodenum, 2 cm proximal to the ampulla of Vater
    - usually communicates with main duct
    - absent in some individuals.
- Blood supply
  - Arterial supply to the pancreatic head is from the superior pancreaticoduodenal artery (from the gastroduodenal artery) and the inferior pancreaticoduodenal artery (from SMA). There are multiple anastomoses between these two vessels.
  - The remainder of the pancreas is supplied from the splenic artery via multiple small direct branches and arteria pancreatica magna. Other arterial supply is from the dorsal pancreatic artery, which arises from the coeliac or proximal splenic artery.
  - Venous drainage from pancreatic head is to SMV and portal veins and to the splenic vein from the rest of the pancreas.
- Anatomical variants (Fig. 10.31)
  - Pancreas divisum: failure of fusion of the ventral and dorsal pancreatic buds. Accessory duct (of Santorini) now drains the body and tail. The main duct (of Wirsung) now drains the head via the ampulla of Vater. Prevalence of 7% in autopsy series.

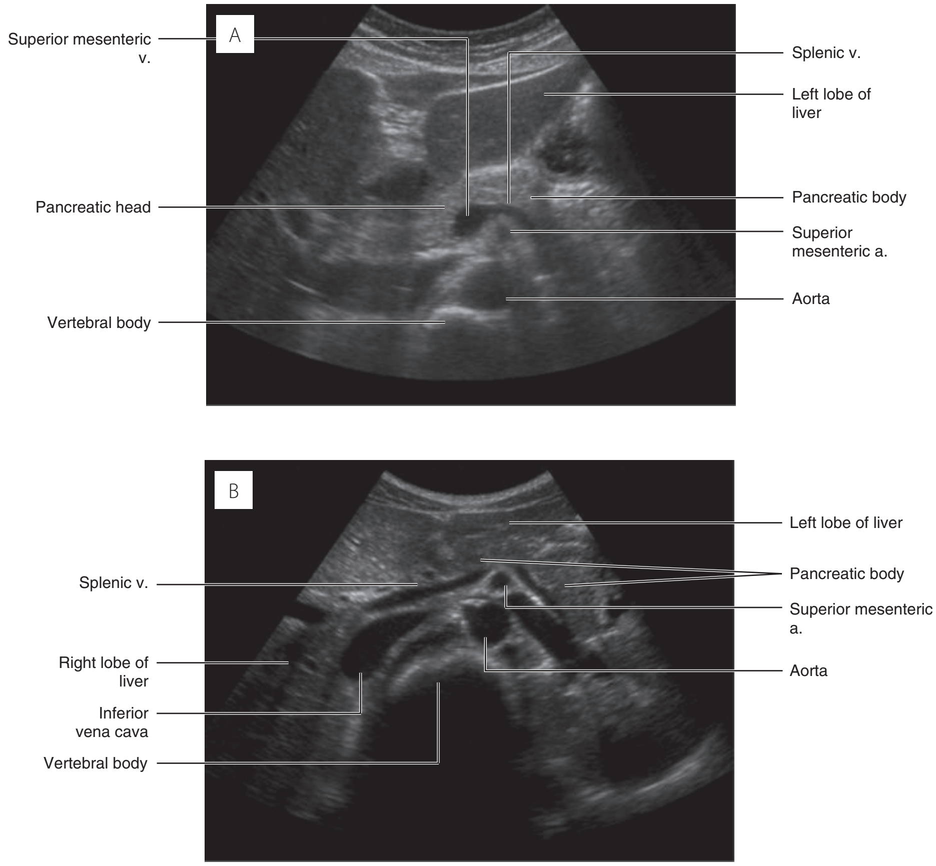


**Figs 10.29** Axial ultrasound images through the pancreas centred on (A) the head and (B) the body. The pancreas may initially be difficult to visualize, but can be identified as it lies immediately anterior to the splenic vein. The pancreas is at least as echogenic as the liver, and is more echogenic with increasing age and body fat.

- Annular pancreas: non-migration of ventral pancreatic bud results in pancreatic tissue encircling second part of duodenum.

## Spleen

- Largest lymphoid mass in the body but also contains haemopoietic tissue.
  - On non-enhanced CT spleen is homogeneous and has an attenuation of 35–55 HU, i.e. 5–10 HU less than that of liver.
  - The spleen normally enhances heterogeneously immediately after injection of a bolus of contrast material on CT and MRI. Only after a minute or more does the splenic parenchyma achieve uniform homogeneous enhancement (Fig. 10.32). This is thought to reflect the variable blood flow within different compartments of the spleen
- The adult spleen measures approximately 12–15 cm length, 4–8 cm in anteroposterior diameter and 3–4 cm in thickness.
- Positioned in the left upper quadrant adjacent to 9th–11th ribs and has a diaphragmatic and visceral surface.
- Anatomical relationships: see Figs. 10.3–10.8 and 10.33.
- Surrounded by peritoneum
  - anteriorly attached to greater curve of stomach by gastrosplenic ligament which contains short gastric and left gastroepiploic vessels
  - posteriorly the lienorenal ligament attaches to the kidney and contains the tail of pancreas and splenic vessels.
- Blood supply
  - Arterial supply from the splenic artery, which divides into 4–6 branches at the hilum. Drainage via the splenic vein, which runs behind the pancreas to join the superior mesenteric vein at the pancreatic neck, forming the portal vein.
- Variants
  - the shape and position of the normal spleen can vary considerably
  - embryologically formed from fusion of multiple small splenunculi
  - accessory or unfused splenunculi seen in 10%.

## Retroperitoneum

- Aorta (Figs. 10.34–10.36)
  - Enters abdomen through aortic hiatus of diaphragm (T12)

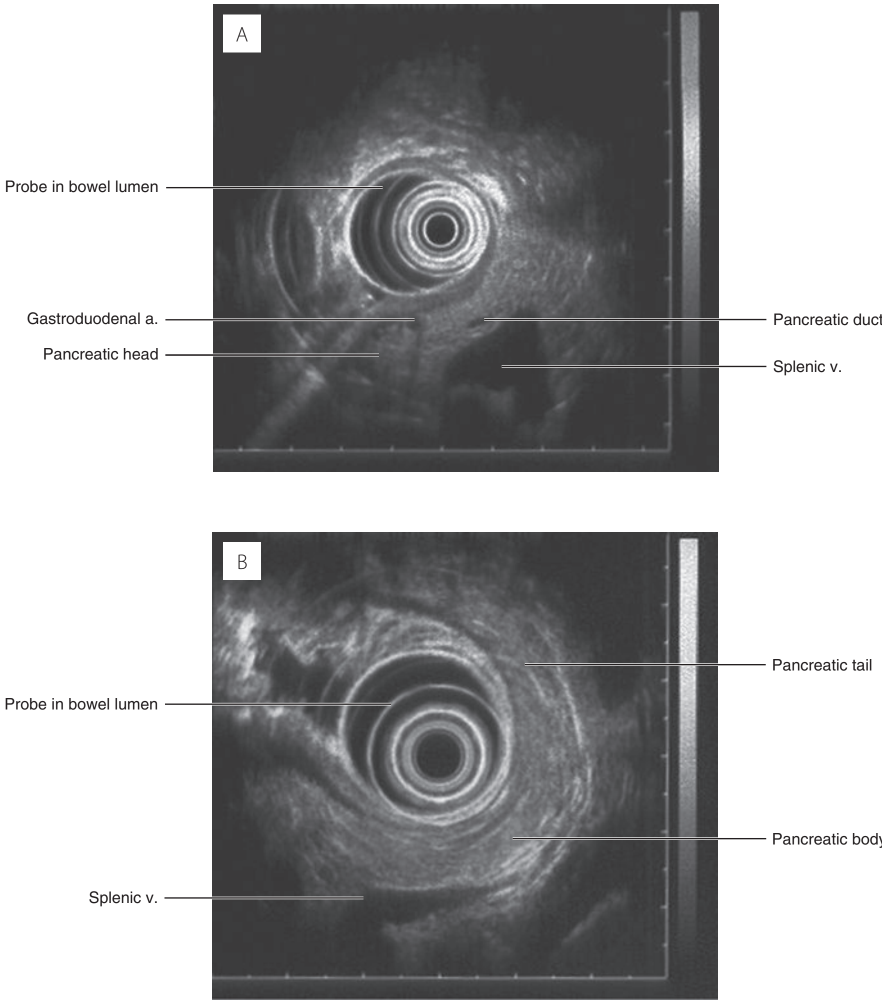


**Fig. 10.30** Endoscopic ultrasound images of the pancreas. (Images courtesy of Dr Z. Amin, University College Hospital, London.)

- Branches:
  - unpaired branches to GI tract:
    - coeliac artery (T12/L1)
    - SMA (L1)
    - IMA (L3)
  - paired arteries to genitourinary tract:
    - middle suprarenal arteries (L1)
    - renal arteries (L2)
    - gonadal arteries (L2)
  - arteries to diaphragm and abdominal wall:
    - pair of inferior phrenic arteries (T12)
    - four pairs of lumbar arteries (L1–4)
    - single median sacral artery (L4)
  - termination branches:
    - common iliac arteries (L4)

- IVC (Figs. 10.37, 10.38)
  - Enters abdomen through caval hiatus of diaphragm (T8)
  - Tributaries:
    - hepatic veins × 3 (T9)
    - genitourinary tract:
      - right suprarenal vein (L1)
      - renal veins (L1); the left suprarenal and gonadal veins drain into the left renal vein
      - right gonadal vein (L2)
    - abdominal wall:
      - inferior phrenic vein (T8)
      - two pairs of lumbar veins (L3–L4)
      - median sacral vein (L5)
    - at origin:
      - common iliac arteries (L5)
- Posterior wall venous system (Fig. 10.39):
  - Venous anastomosis between lumbar, sacral and intercostal veins, IVC, azygos and hemiazygos veins
  - Ascending lumbar vein crosslinks the segmental lumbar branches

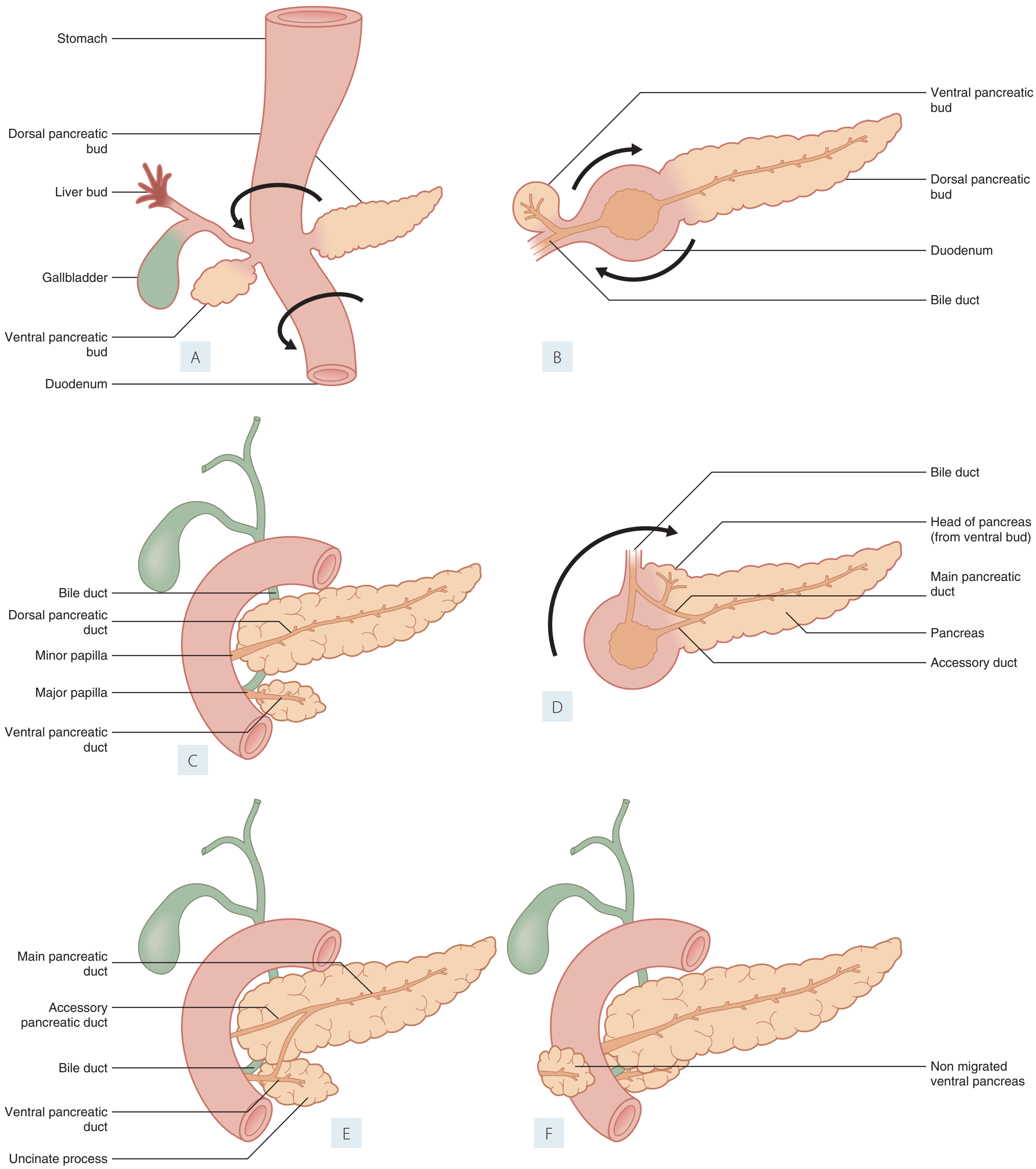


**Fig. 10.31** Stages in development of the pancreas. (A) Frontal view of developing pancreatic buds. (B) Transverse view of (A). (C) AP view after migration of ventral bud into final position. (D) Transverse view of (C). (E) AP view of buds following fusion of ducts. (F) AP view of annular pancreas.

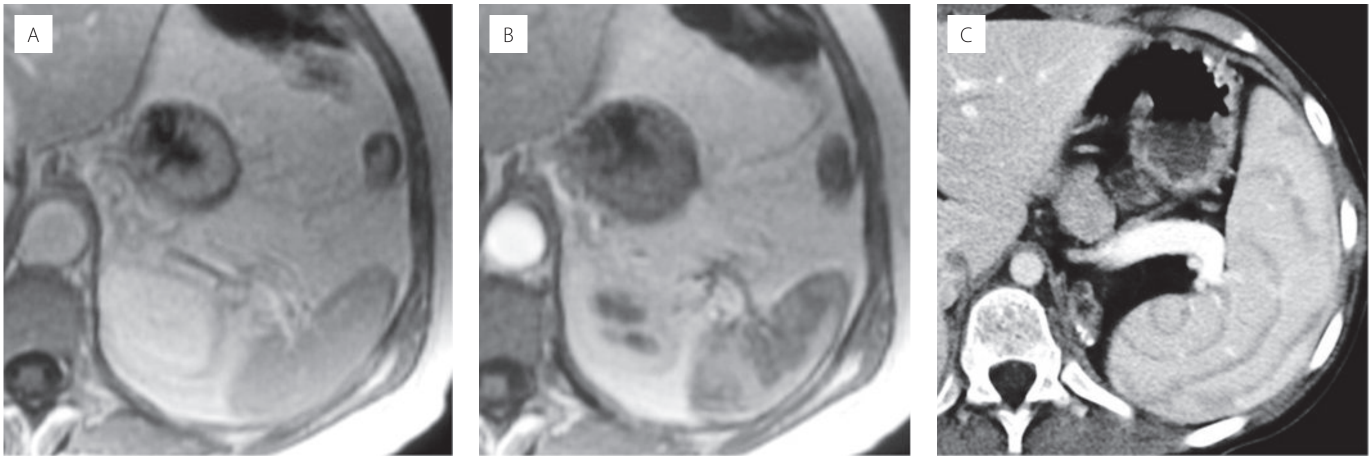


**Fig. 10.32** Examples of different normal patterns of splenic enhancement during arterial phase on CT and MRI. (A) Uniform portal venous enhancement on MRI provided for comparison. (B) Wedge-like segmental arterial phase enhancement on MRI. (C) Ring-like arterial phase enhancement on CT.

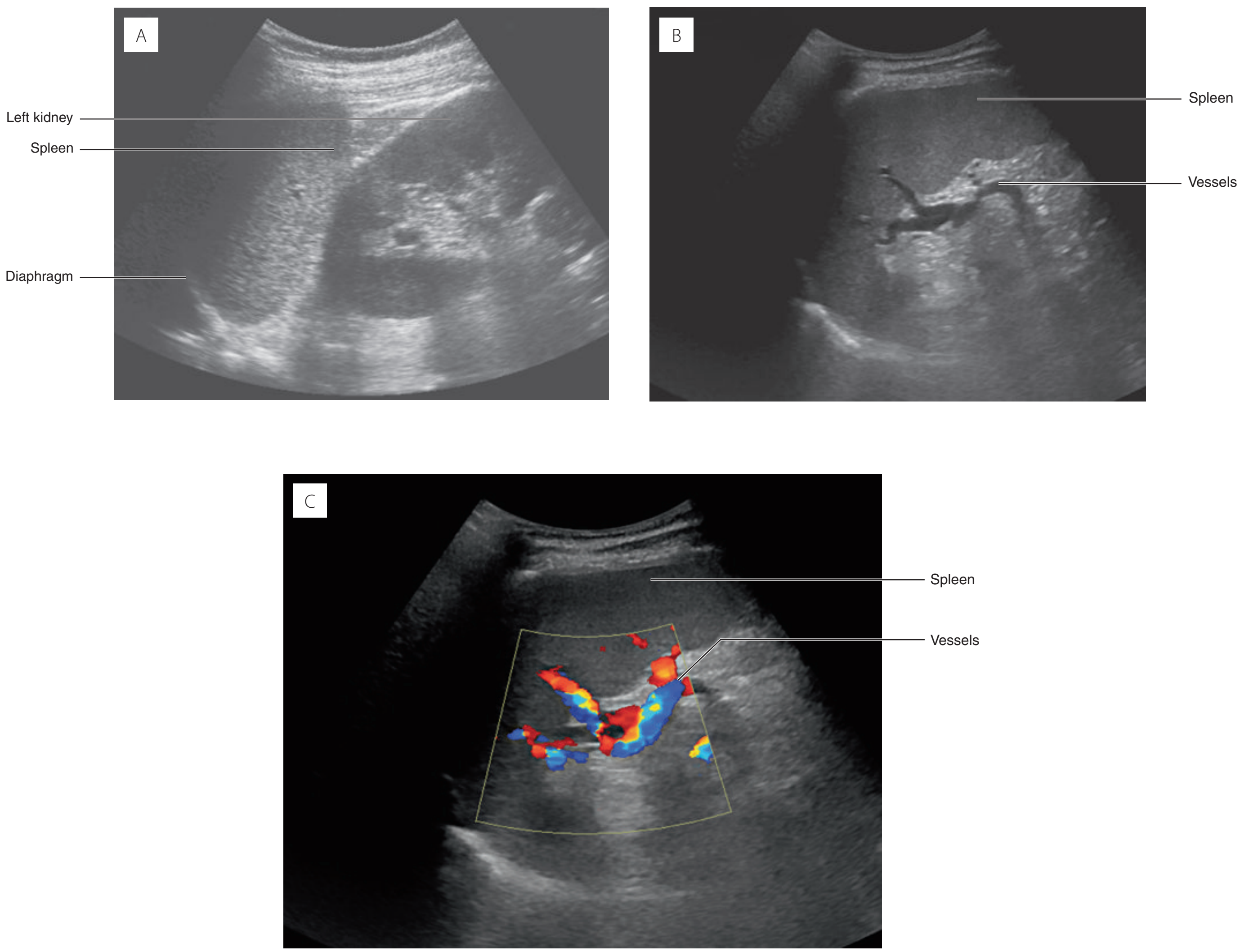


**Fig. 10.33** (A) Longitudinal ultrasound image through the spleen. Note the diaphragm above and the kidney below. The spleen is usually hyperechoic compared to the kidney. (B) Greyscale and (C) colour Doppler images demonstrating vessels entering the splenic hilum.

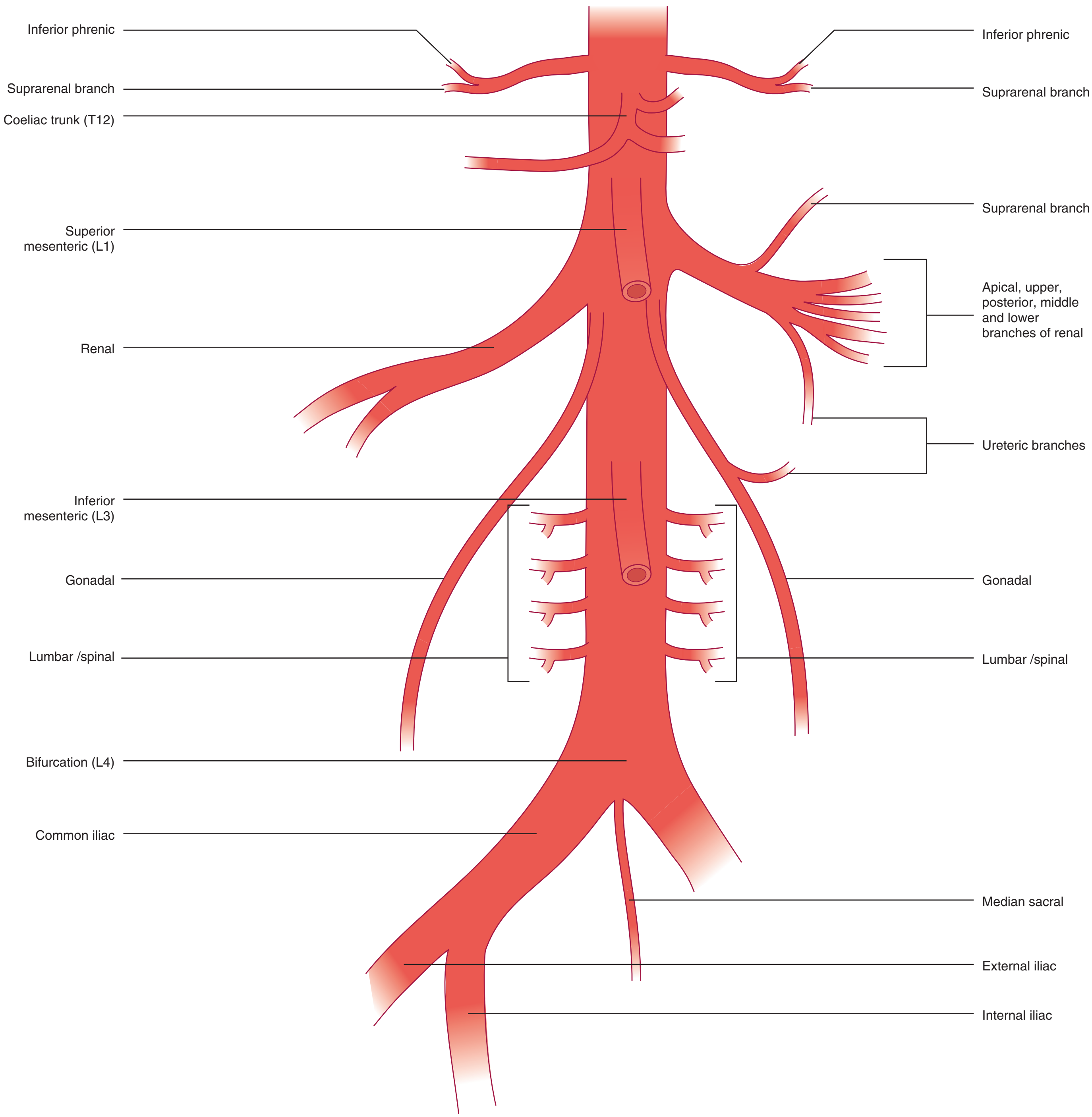


**Fig. 10.34** Branches of the abdominal aorta.

- One median sacral vein and two lateral sacral veins crosslink the segmental sacral branches
- Azygos vein (right) and hemiazygos vein (left) can be continuations of the ascending lumbar veins or subcostal veins, or arise from the renal veins or IVC
  - the hemiazygos vein drains into the azygos at T9
  - the azygos arches over the root of the right lung to drain into the SVC
- If the IVC is blocked or absent, this venous system becomes more prominent, with blood being channelled through it back to the SVC.

- Lymphatic system (Figs. 10.40–10.42):
  - Retroperitoneal nodes are named after adjacent structures
  - All lymph drains into the cisterna chyli, the dilated proximal end of the thoracic duct

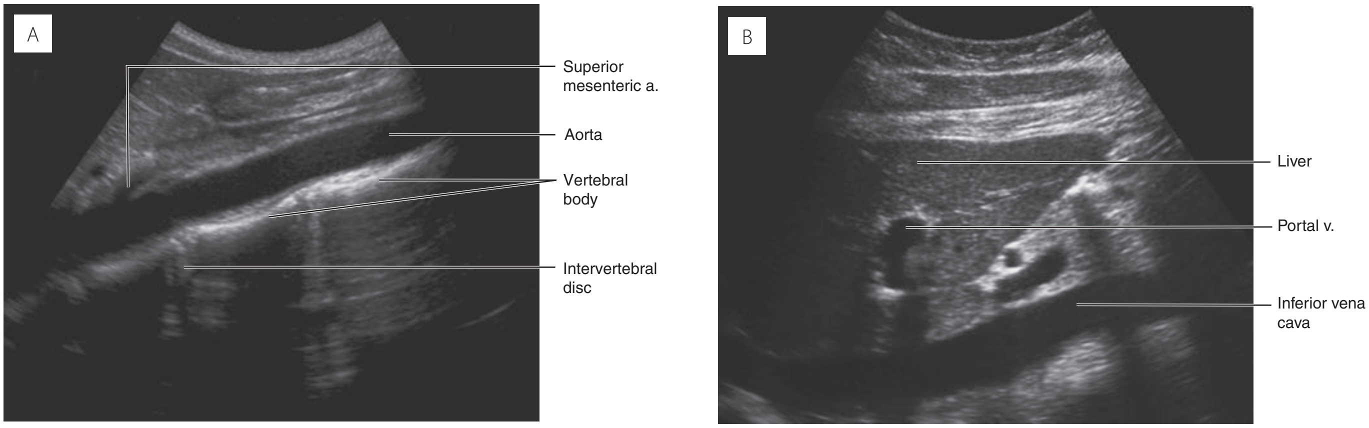


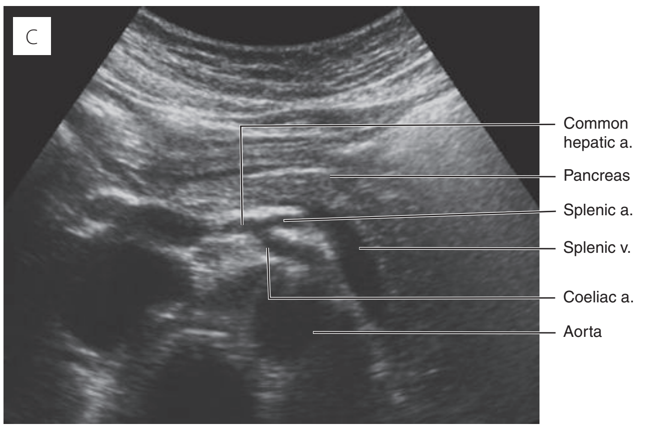


**Fig. 10.35** Ultrasound appearances of the abdominal vessels. Longitudinal images through (A) the aorta showing the SMA and (B) the IVC. (C) Transverse image through the coeliac artery.

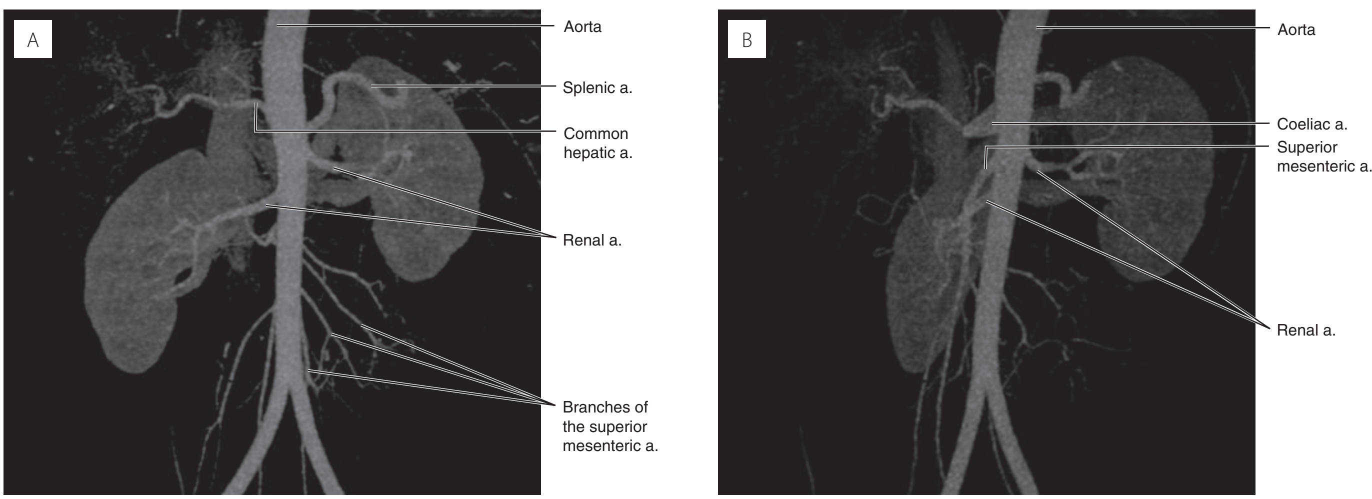


**Fig. 10.36** The aorta and its branches. (A) 3D coronal and (B, C) left/right coronal oblique CT images through the upper abdomen in arterial phase. The origins of the coeliac artery and SMA are obscured on the standard coronal view. (D) Axial MIP CT showing the coeliac axis, and (E) sagittal MIP CT showing the coeliac artery and SMA in arterial phase. (F) Digital subtraction aortogram performed with an arterial catheter in the aorta.

lying between L1/2, the aorta and the right diaphragmatic crus.

## Radionuclide imaging

- Radionuclide imaging techniques predominantly provide functional information of the abdominal viscera with very limited anatomical detail. These techniques are often combined or assessed in conjunction with cross-sectional imaging.
- On FDG-PET imaging the liver shows homogeneous uptake (Fig. 10.43). FDG is transported into cells like glucose and accumulates within the cell in proportion to the rate of glycolysis.
- Tc-labelled aminodiacetic acid (IDA) compounds show biliary excretion through the biliary tree and gallbladder and then into the small bowel.
- Gallium scan – normal accumulation is seen in the liver, bone marrow and variably in the spleen (Fig. 10.43). There

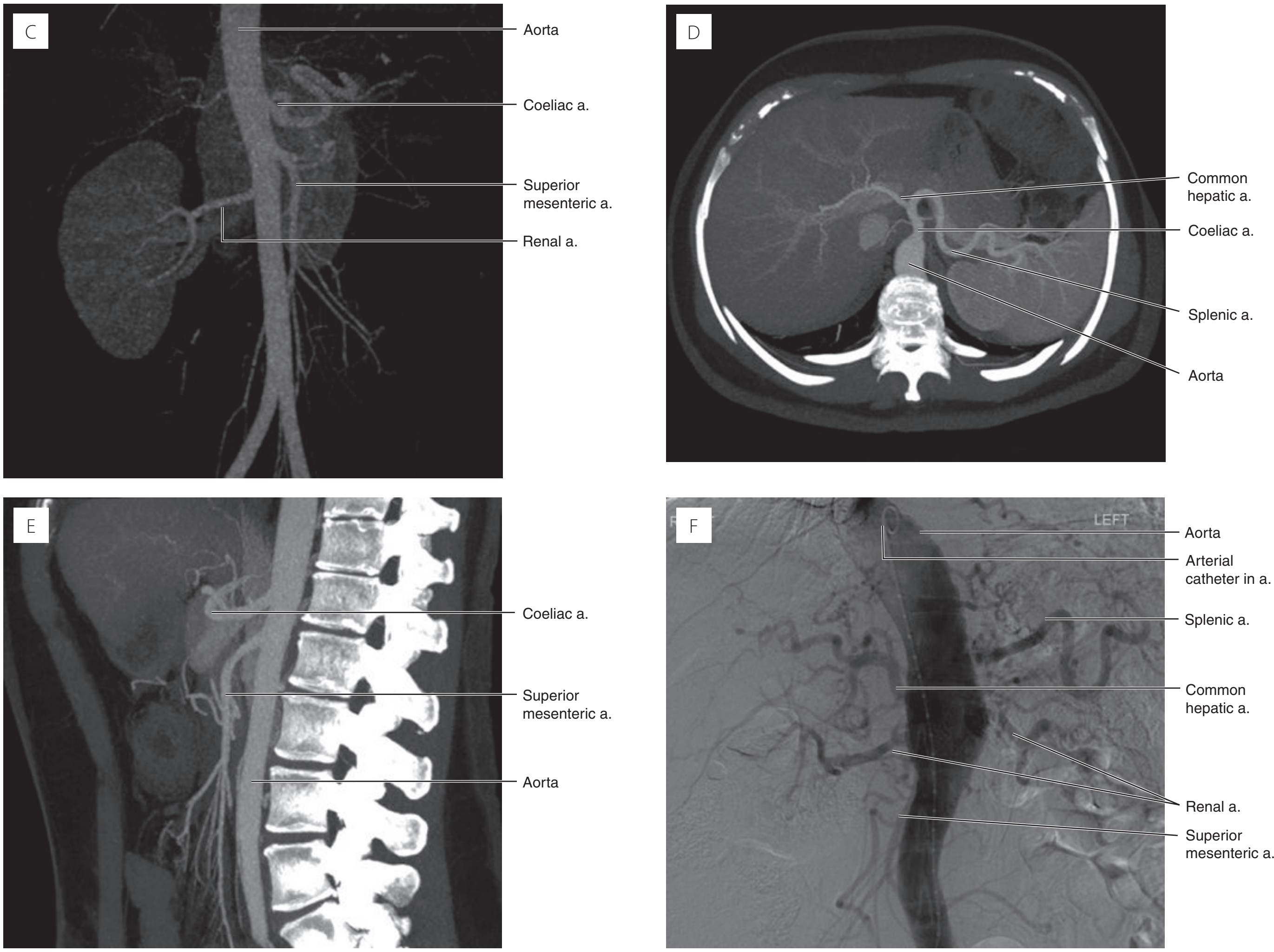


**Fig. 10.36** *(cont.)*

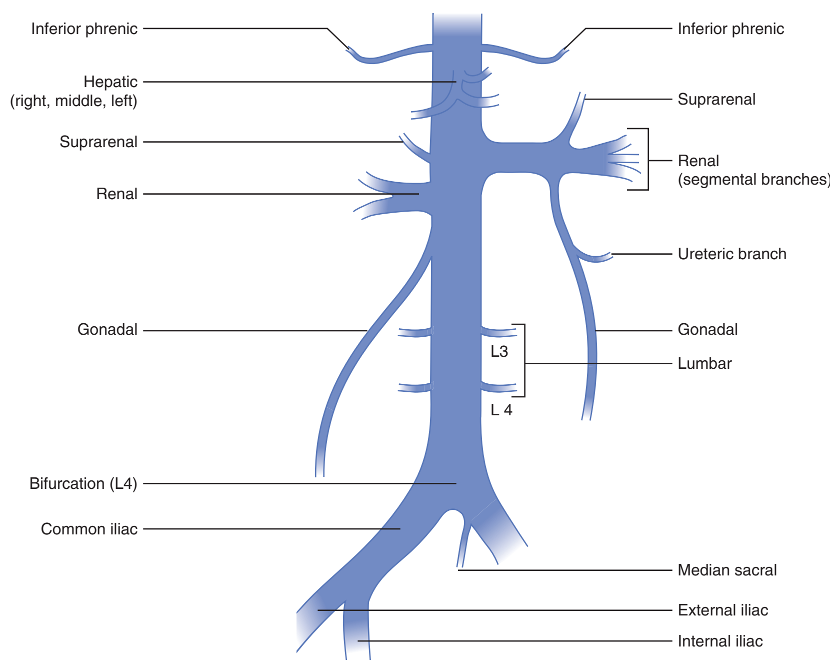


**Fig. 10.37** Branches of the IVC.

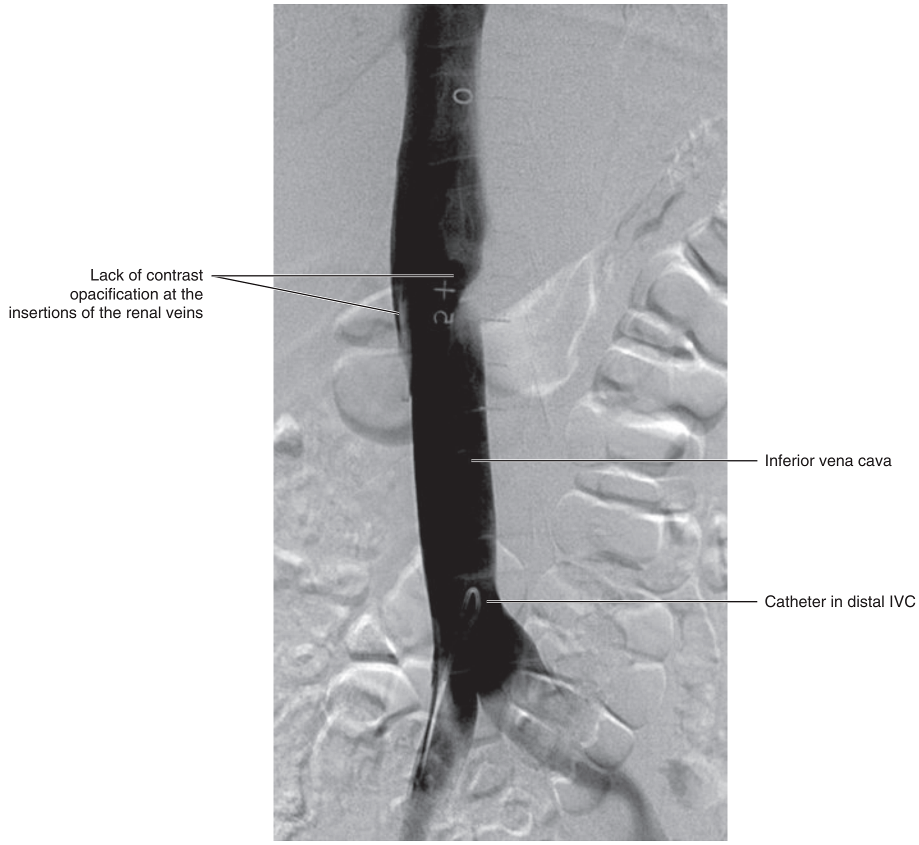


**Fig. 10.38** Normal cavogram. Digital subtraction venogram following contrast injection via a catheter in the distal IVC. Note that the tributary veins of the IVC do not opacify as blood flows in the reverse direction – indeed the insertions of the renal veins are identified by a lack of contrast opacification of the IVC at that level.

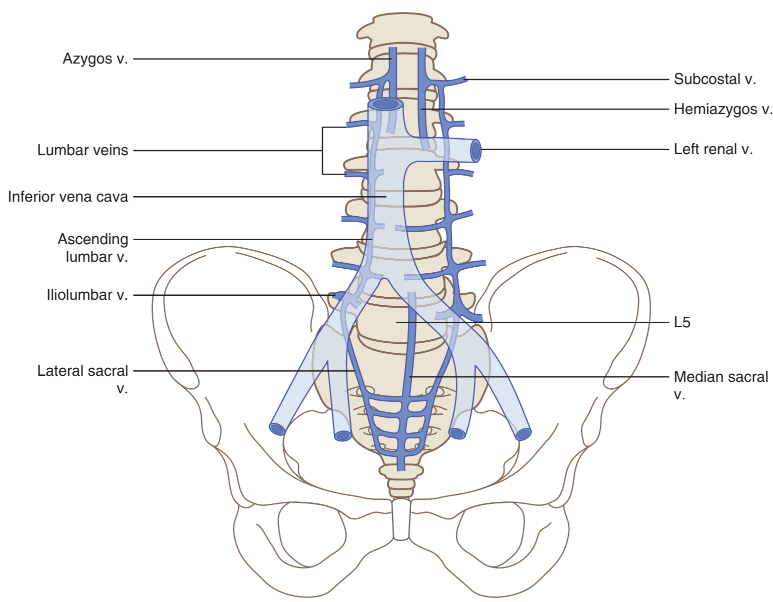


**Fig. 10.39** Posterior wall venous system.

| | |
|---|---|
| 1 | Left para-aortic |
| 2 | Pre-aortic |
| 3 | Retro-aortic |
| 4 | Aortocaval |
| 5 | Right paracaval |
| 6 | Precaval |
| 7 | Retrocaval |
| 8 | Coeliac axis |

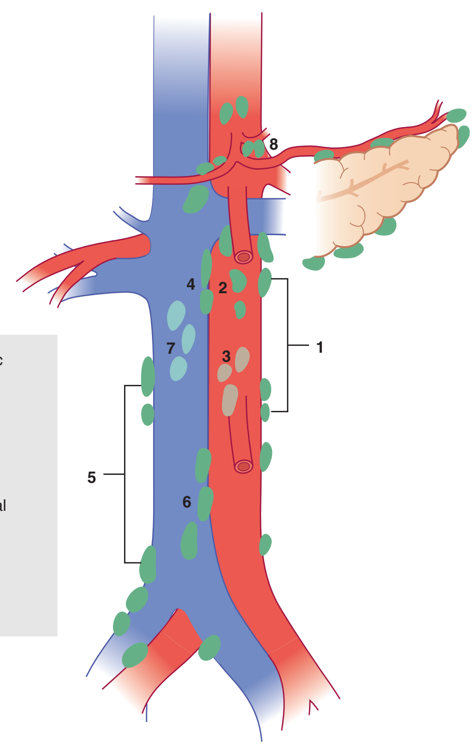


**Fig. 10.40** Abdominal lymph node groups.

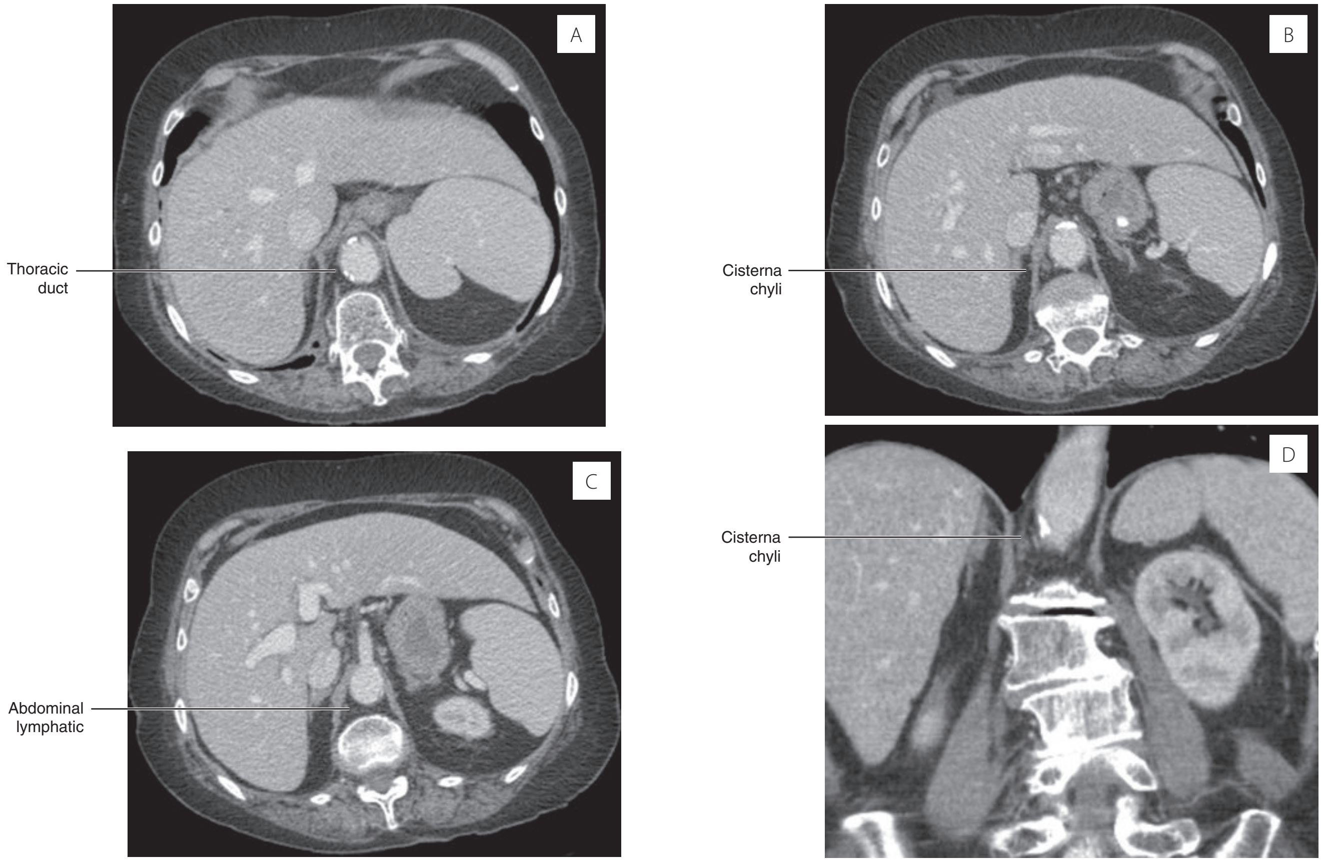


**Fig. 10.41** Cisterna chyli. (A–C) Axial CTs, ordered superior to inferior, showing abdominal lymphatics draining into the cisterna chyli, the dilated proximal end of the thoracic duct lying between the aorta and right diaphragmatic crus. (D) Coronal CT of the same patient.

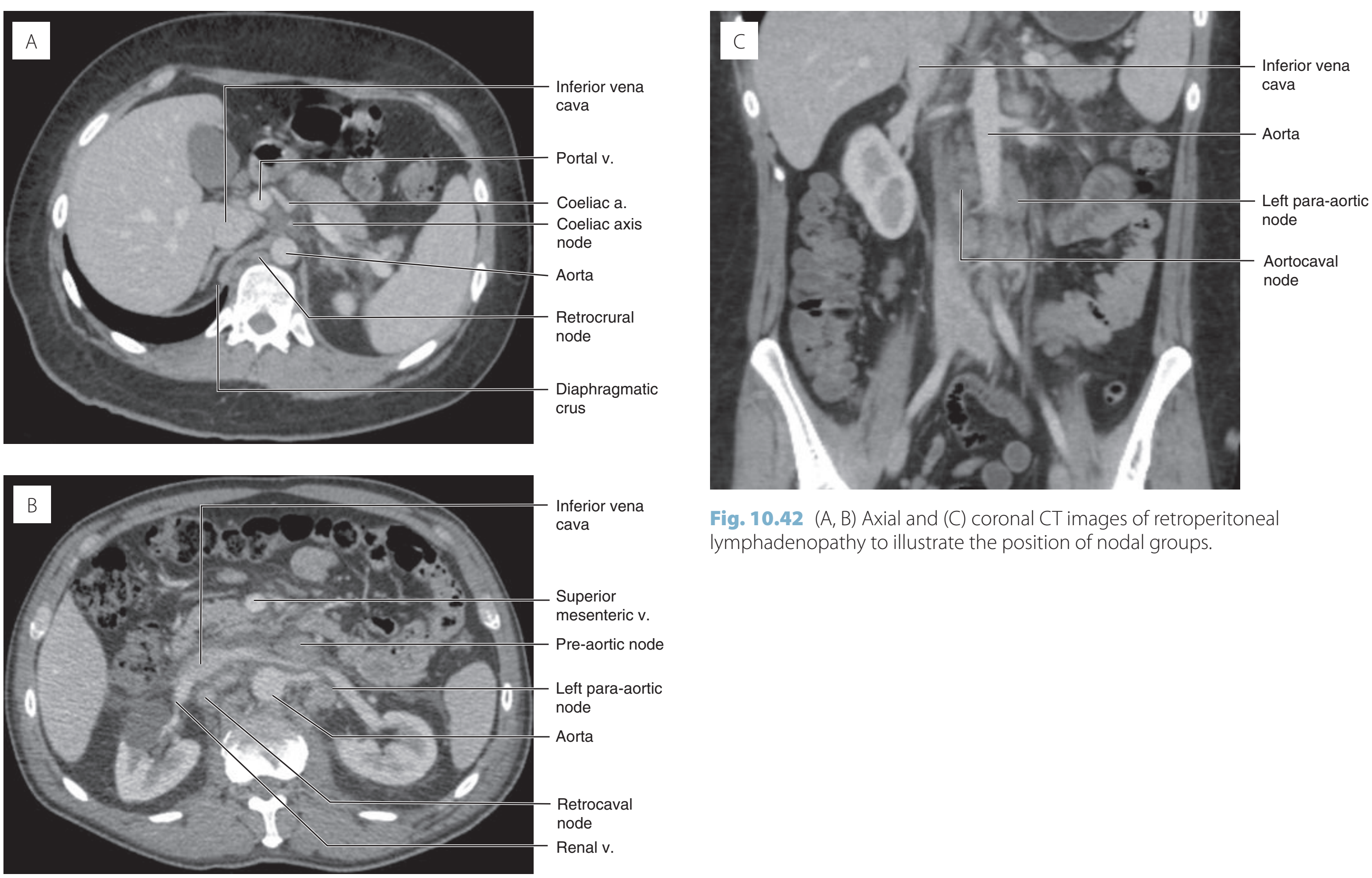


**Fig. 10.42** (A, B) Axial and (C) coronal CT images of retroperitoneal lymphadenopathy to illustrate the position of nodal groups.

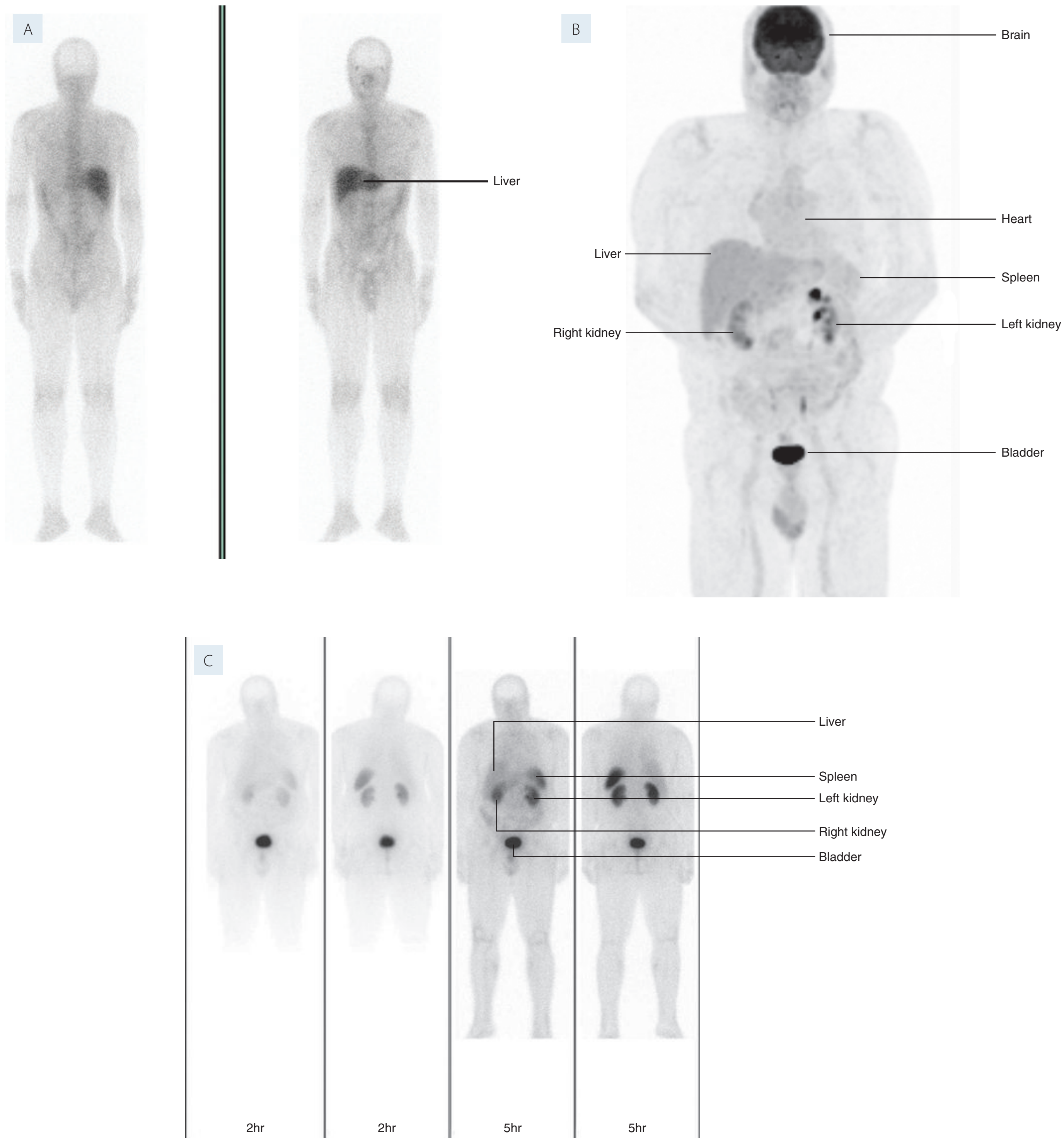


**Fig. 10.43** (Images courtesy of Dr Sue Chau, Royal Marsden Hospital.) Normal activity seen in the abdominal organs on (A) Ga-67, (B) FDG-PET and (C) In-111-octreotide scans.

is significant excretion via the gut and some by the kidneys. Gallium is taken up at inflammatory sites and non-specifically by some tumours.

- Radiolabelled somatostatin receptor analogues (octreotide or lanreotide) bind to somatostatin receptors and are used in imaging neuroendocrine tumours. Normal uptake is in thyroid, liver, spleen, kidneys and reticulo-endothelial system with excretion via the gut and kidneys (Fig. 10.43)
- Denatured labelled red blood cell scans may be used to identify splenic tissue, for example postoperatively.

Chapter 11

# The gastrointestinal tract

Nasir Khan

## Introduction

Cross-sectional imaging plays a major role in the teaching of anatomy, especially in relation to the gastrointestinal (GI) tract. It demonstrates the relations of the GI tract with other abdominal structures and hence allows us to understand local disease processes and the pathways of local and distant spread.

In particular CT and MRI scanning are used to image the small and large bowel in their entirety, whilst ultrasound has taken its place as a more focused tool in the GI tract. It is used transabdominally at high frequencies (10 and 13.5 MHz) to image the pylorus for pyloric stenosis, the appendix, terminal ileum for Crohn's disease and the small/large bowel for intussusception in children. Endoscopic and endocavity ultrasound is used to visualize the proximal GI tract for tumour staging and the anal canal for sphincter tears and fistulae.

Barium studies are still widely used either as a diagnostic tool or, in conjunction with CT or MRI, as a problem-solving tool. Therefore, knowledge of luminal anatomy and its variants remains crucial.

## Embryology and development

The GI tract extends from the mouth to the anus, and originates from the primitive foregut, midgut and hindgut (Fig. 11.1).

### Foregut

- The forgut consists of the pharynx, oesophagus, stomach and the first and second parts of the duodenum. The blood supply of these structures is predominantly derived from the coeliac artery, apart from the mid oesophagus, which derives its arterial supply from the thoracic aorta directly and the proximal third of the oesophagus from the inferior thyroid vessels.
- During development, the pancreas and liver arise from buds of the foregut, in the region of the second part of the duodenum, hence the intimate relationship with the bile ducts, portal and hepatic vessels.

### Midgut

- The midgut consists of the third and fourth part of the duodenum, jejunum, ileum, caecum, appendix, ascending colon and proximal two-thirds of the transverse colon. The blood supply is predominantly from the superior mesenteric artery and its branches.
- At 5 weeks, during in utero development, the midgut herniates into the umbilical cord, returning into the abdominal cavity at 10 weeks. As it returns, it performs a 270° anticlockwise rotation, resulting in the fourth part of the duodenum and jejunum lying to the left of the midline and the proximal colon lying to the right. Failure of this rotation results in the D-J flexure and jejunum remaining on the right and colon on the left, known as malrotation. In this situation the small bowel mesentery is short and prone to twisting (volvulus), leading to potential duodenal obstruction and ischaemia.
- Failure of the midgut to return into the abdomen is known as exompholos, whereby the child is born with small and large bowel herniation through the abdominal wall.

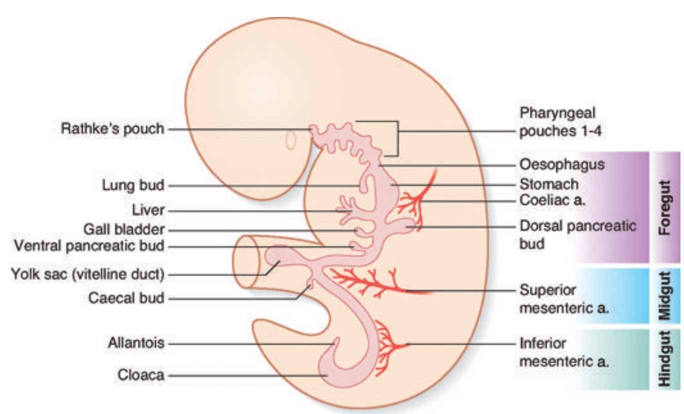


Fig. 11.1 Line diagram shows the primitive GI tract.

*Applied Radiological Anatomy, 2nd Edition* ed. Paul Butler, Adam W.M. Mitchell and Jeremiah C. Healy. Published by Cambridge University Press.

## Hindgut

- The hindgut forms the distal transverse colon, descending colon, sigmoid colon, rectum and anus. The vascular supply is predominantly from the inferior mesenteric artery, except the rectum, which also derives supply from the internal iliac arteries.

## Pharynx

- Muscular tube extending from the base of the skull to the level of C6, where it connects to the cervical oesophagus.
- Three layers: mucosa, fibrous submucosal layer and the muscular layer (made up of three constrictor muscles).
- Food passes over the erect epiglottis, through the piriform fossae and into the cervical oesophagus.

## Cross-sectional anatomy

The naso-, laryngo- and oropharynx are continuous.

- Superiorly – the soft palate.
- Inferiorly – the epiglottis, which protects the larynx during swallowing.
- Anterior surface – formed by the base of the tongue and epiglottis. The laryngopharynx is draped over the posterior aspect of the larynx, creating two posterolateral recesses; the piriform fossae (Fig. 11.2).
- Posteriorly to the oropharynx are the prevertebral muscles.

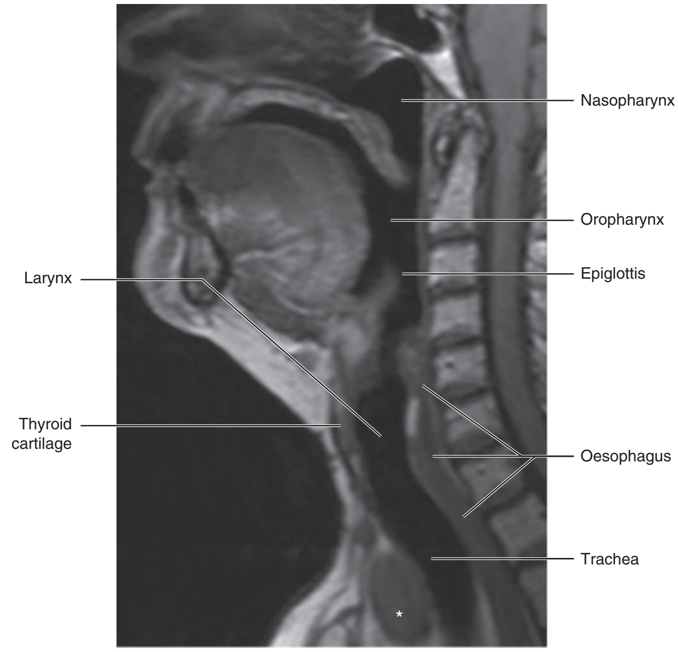


*Incidental enlarged lymph node

**Fig. 11.2** The pharynx and cervical oesophagus on sagittal T1-weighted MRI.

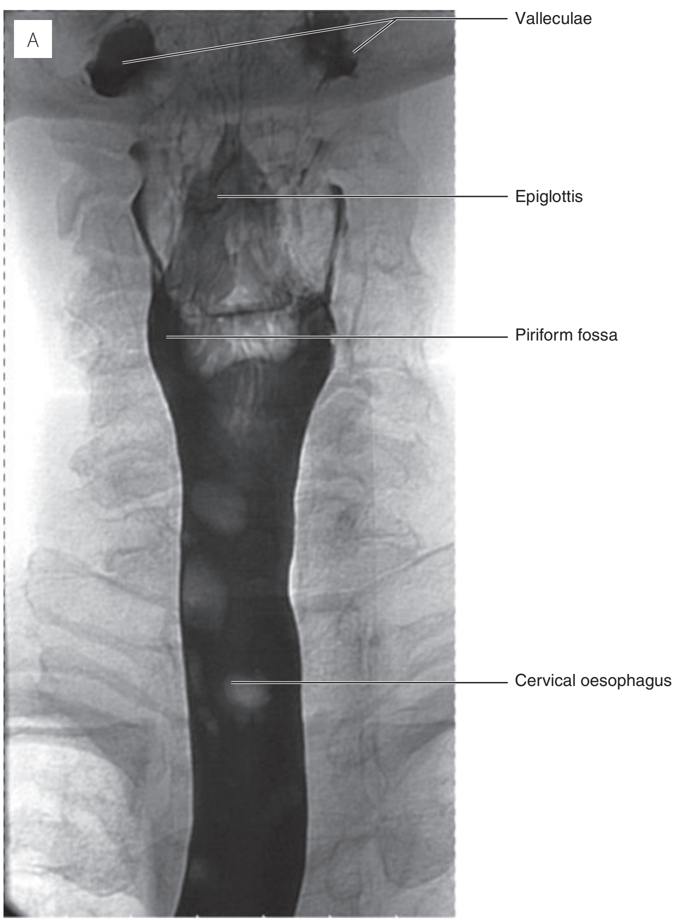


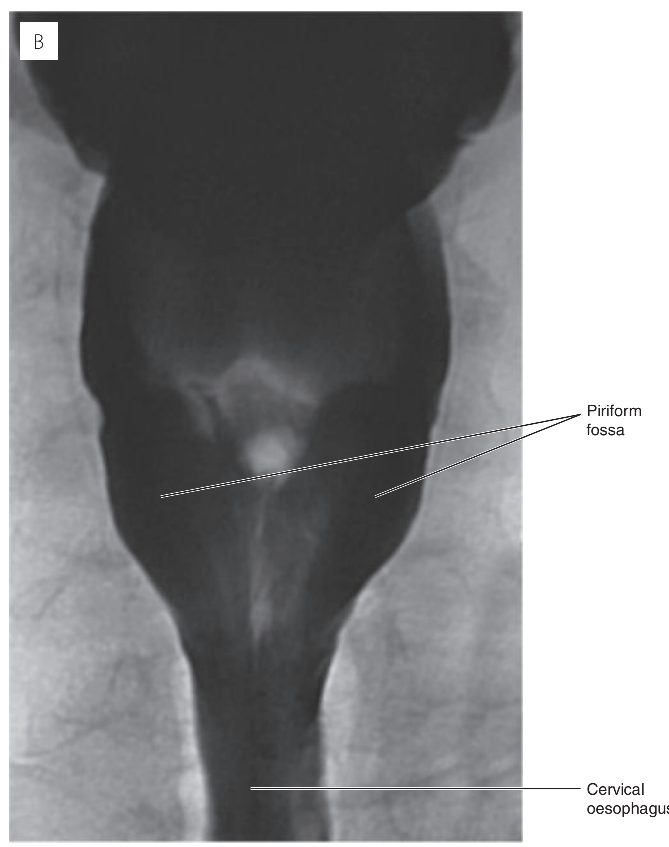


**Fig. 11.3** Barium swallow: AP (A, B) and lateral (C) views of the pharynx and cervical oesophagus.

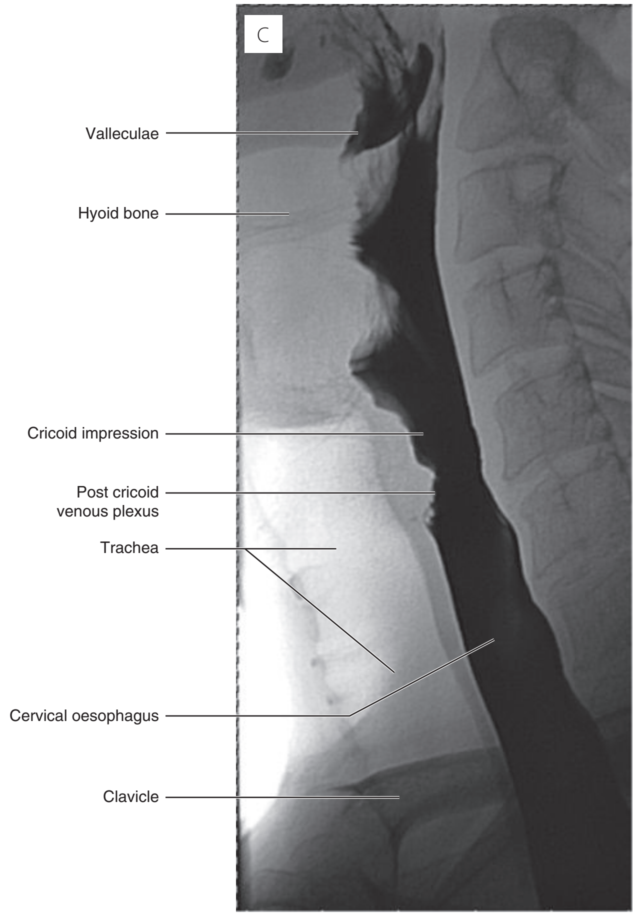


**Fig. 11.3** (*cont.*)

## Plain film and contrast study anatomy

- Plain radiograph has a limited role, with the lateral view mainly used to locate the presence of swallowed foreign bodies.
- Barium swallow, AP view, shows filling of the piriform fossae and valleculae with central filling defects of the base of the tongue and epiglottis (Fig. 11.3A). On the lateral view, the narrow posterior indentation of the cricopharyngeal muscle contraction may be seen at the level of C5/6, which if persistent and severe can cause dysphagia. Anteriorly, a wider but shallow indentation is caused by a submucosal venous plexus (Fig. 11.3C).

# Oesophagus

- Long muscular tube measuring approximately 25 cm.
- Extends from the level of the sixth cervical vertebra, passing through the neck, posterior mediastinum, veering anteriorly low within the thorax before it enters the abdomen, through the diaphragmatic hiatus at T10. Its short course within the abdomen is retroperitoneal and forms the gastro-oesophageal junction as it ends at the cardia of the stomach, at T11.

## Cross-sectional anatomy

### The cervical oesophagus

- Begins at the lower limit of the cricopharyngeus, lying in the midline anterior to the cervical vertebrae, and posterior to the trachea and thyroid gland inferiorly (Fig. 11.4A,B), at which level it moves to the left of the midline (Fig. 11.4C,D) and then enters the thorax, where it will return to the midline at T5.
- Laterally lies the common carotid artery on each side.

### Relations within the chest (Fig. 11.5)

- Anteriorly – as it descends, it passes behind the trachea, left main bronchus, left atrium, left ventricle (upper part).
- Posteriorly – thoracic duct and vertebrae, azygos vein, right posterior intercostal arteries which arise from the descending aorta directly.
- Laterally – on the left, it is in contact with the origin of the left subclavian artery, arch of the aorta, left lung and descending aorta. On the right, the azygos vein lies behind and to the right, crossing it at T4 where it terminates. Above this level, it abuts the right lung.

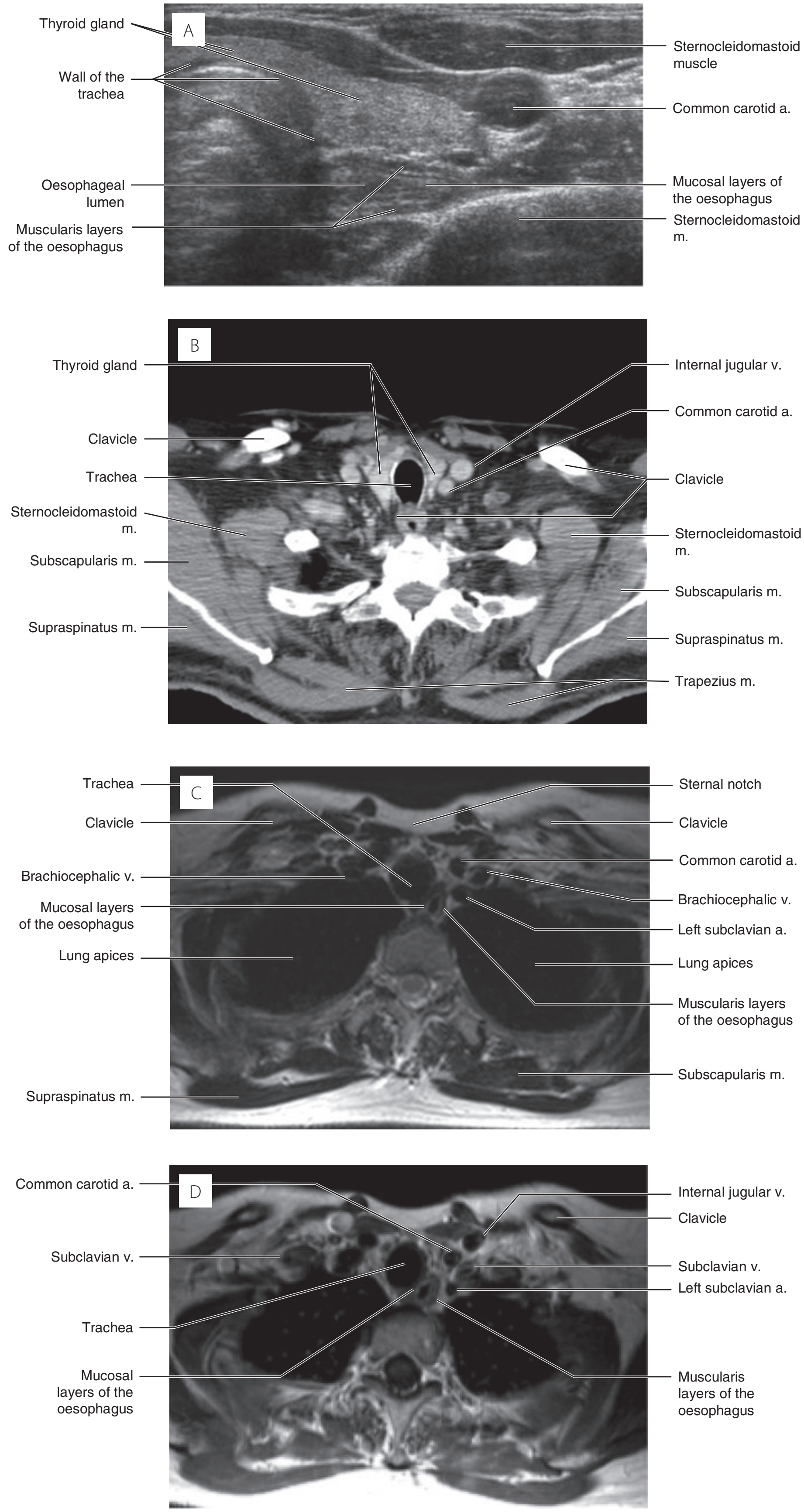


**Fig. 11.4** The cervical oesophagus : (A) ultrasound, and (B) axial CT at the level of the thyroid gland and (C) axial T2 MRI, (D) axial T1 FS MR post gadolinium, at the thoracic inlet. On US and MRI the layers of the oesophagus can be delineated.

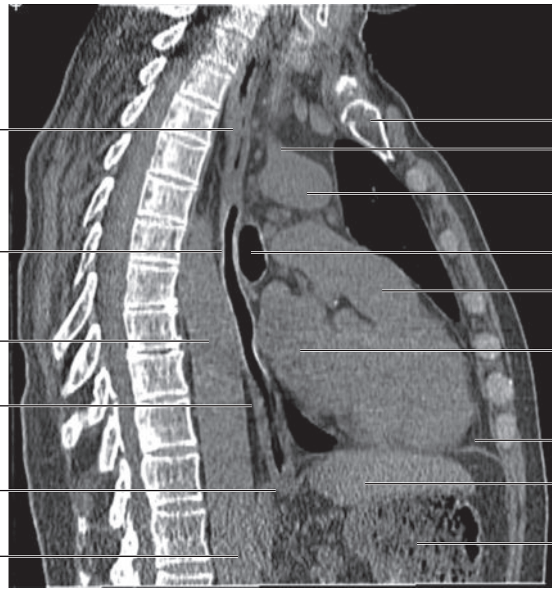


**Fig. 11.5** Multiplanar reformat CT showing the passage of the oesophagus within the chest.

The oesophagus has five layers, as demonstrated on endoscopic ultrasound (Fig. 11.6), the superficial mucosa (hyperechoic), deep mucosa or lamina propria (hypoechoic), submucosa (hyperechoic), muscularis propria (hypoechoic) and the adventitia (hyperechoic). The layers are poorly seen on CT; however, MRI is showing some promise with newer improved sequences (Fig. 11.4C,D).

## Plain film and contrast study anatomy

### Plain chest radiograph

- The oesophagus is difficult to see unless it is dilated and fluid filled.
- Below the level of T4/right hilum, the azygo-oesophageal line may be seen, where the azygos vein and oesophagus abut the right lung.
- Above T4, where the oesophagus abuts the left lung we can see the pleuro-oesophageal line.

### Barium studies

- Show three impressions on the oesophagus – the aortic arch, left main bronchus and the left atrium (Fig. 11.7A).
- Mild fusiform dilatation of the distal oesophagus forms the physiological sphincter.
- Bound superiorly and inferiorly by the A and B (Schatzki's) ring, respectively (Fig. 11.7B). These are minor transient muscular contractions, which if persistent can lead to dysphagia and require endoscopic dilatation.
- Fewer than five folds on the double contrast images. Folds should be thin, measuring less than 3 mm.
- More than five folds suggest stomach herniation.

## Neurovascular and lymphatic anatomy

### Arterial supply and venous drainage

- Upper third – inferior thyroid artery, with drainage into the inferior thyroid vein.
- Middle third – direct oesophageal branches from the descending aorta, with drainage into the azygos vein.
- Distal third – oesophageal branches of the left gastric artery (Fig. 11.13B). Drainage into the oesophageal branch of the left gastric vein which drains into the portal vein.

### Lymphatic drainage

Paraoesophageal lymphatic plexus draining:

- superiorly to the posterior mediastinal lymph nodes and then into the supraclavicular node
- inferiorly to the left gastric /gastrohepatic and coeliac lymph nodes.

This explains the pathway of spread of oesophageal tumours via the lymphatics.

### Nervous system

- Upper oesophagus – branches of the recurrent laryngeal nerve.
- Lower oesophagus – oesophageal plexus, which surrounds the lower oesophagus and is made up of the parasympathetic fibres of the vagus nerve and vasomotor sympathetic fibres from the upper 4–6 thoracic spinal segments.

## Stomach

- Thick J-shaped muscular bag which is fixed at both orifices; the inlet – the cardiac orifice, and outlet – the pylorus.

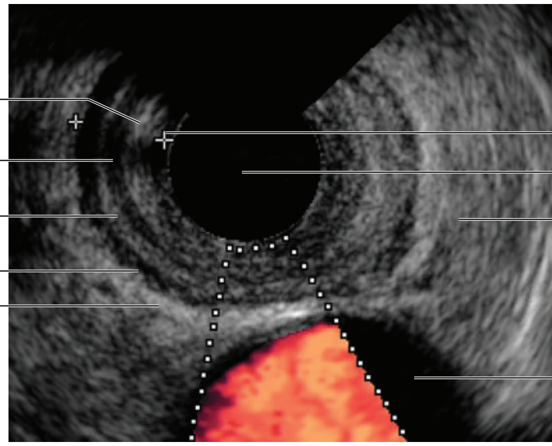


**Fig. 11.6** Oesophagus as seen on endoscopic ultrasound.

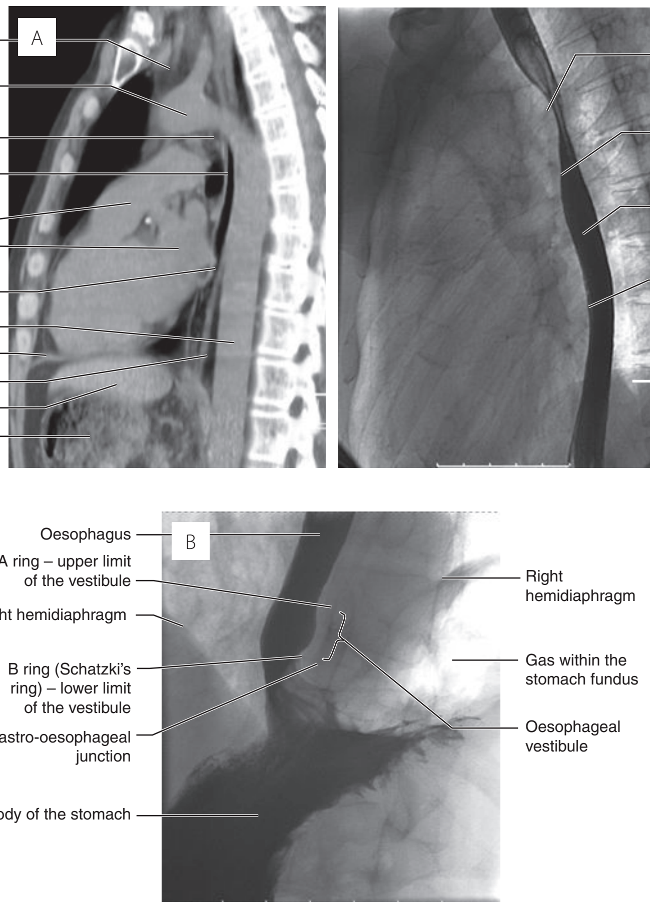


**Fig. 11.7** Barium swallow: oblique view (A) shows the three normal impressions on the oesophagus with sagittal MPR CT correlation; (B) gastro-esophageal junction and vestibule.

- Two surfaces:
  - anterosuperior surface – lesser curve
  - posteroinferior surface – greater curve, which as the stomach fills, expands inferiorly and anteriorly as the majority of the stomach is mobile
  - covered by peritoneum and are divided by the peritoneal attachments of the lesser and greater omentum.
- The maximum volume in adults is 1500 ml and at puberty 1000 ml.

There are three muscle layers; inner oblique, middle circular and outer longitudinal layer. Circular muscle surrounds the body but is especially prominent at the pylorus and the oblique muscle forms a sling around the cardiac orifice to prevent reflux. The longitudinal layer is mostly centred on the lesser and greater curves.

## Plain film and contrast study anatomy

On the plain film, the stomach may not be seen if fluid-filled or empty, otherwise the gastric bubble is seen on the erect X-ray.

Geographically it is divided into (Fig. 11.8):

- fundus – lying above the cardiac orifice adjacent to the left hemidiaphragm
- body – extends from the cardia to the incisura angularis (angulation of the lesser curve)
- antrum – crosses the midline, extending from the incisura to the sulcus intermedius
- pylorus – narrow thickened muscular canal from the sulcus to the pyloric orifice, 1–2 cm in length. It behaves as a physiological and anatomical sphincter and lies at the level of L1, 2.5 cm to the right of the midline.

The gastric rugae are seen on the double-contrast barium meal, and are thick linear elevations or folds of the gastric mucosa, measuring 3–5 mm. These run mostly along the longitudinal axis of the stomach. Within the pylorus these have the appearance of fine lines. In the antrum, small nodular mucosal elevations are seen, called areae gastricae, measuring 2–3 mm.

## Cross-sectional anatomy

The anatomical layers are best seen on endoscopic ultrasound, where there are five layers: mucosa, muscularis mucosa, submucosa, muscularis and serosa (Fig. 11.9).

### Relations (Figs. 11.8, 11.10)

- Anteriorly – left lobe of the liver medially, anterior abdominal wall laterally and left hemidiaphragm superiorly.
- Posteriorly – peritoneum of the lesser sac superiorly and stomach bed inferiorly.

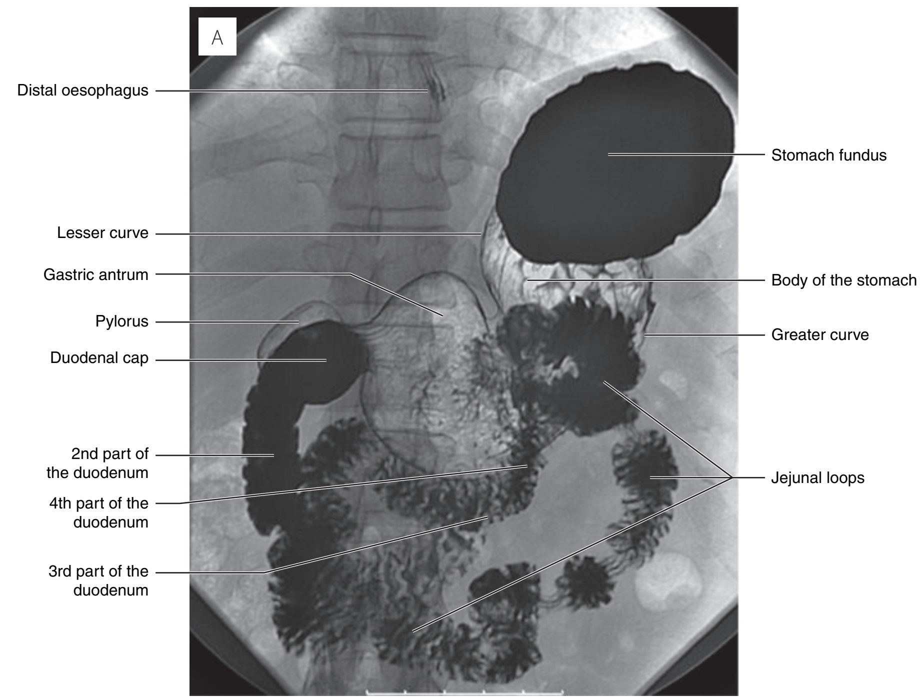


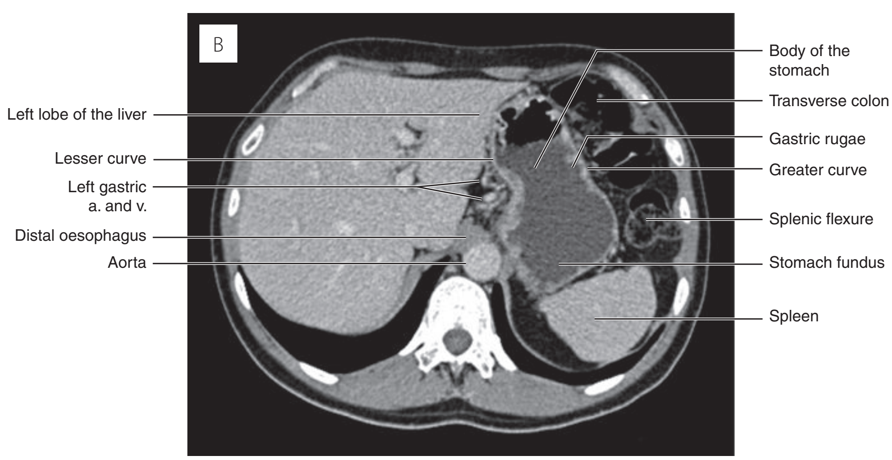


**Fig. 11.8** Barium meal (A), CT (B, C) and MR (D) of the stomach: gastric rugae and areae gastricae demonstrated.

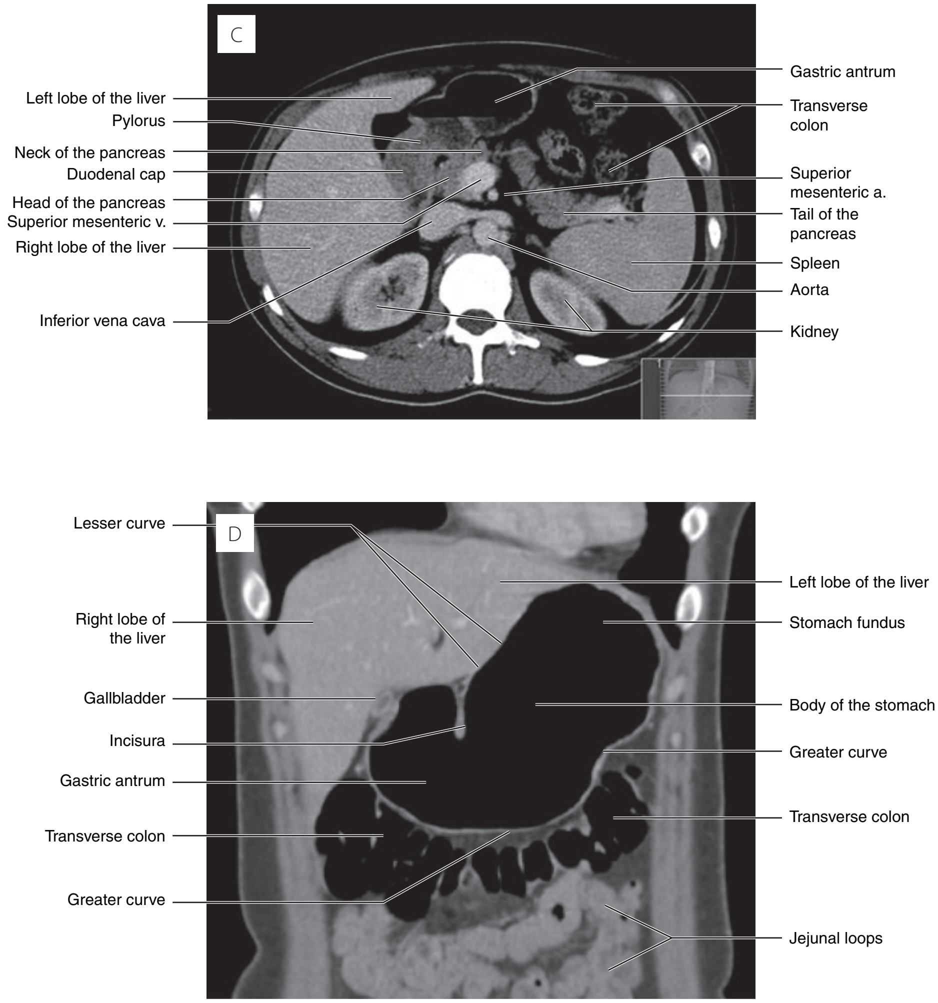


**Fig. 11.8** (*cont.*)

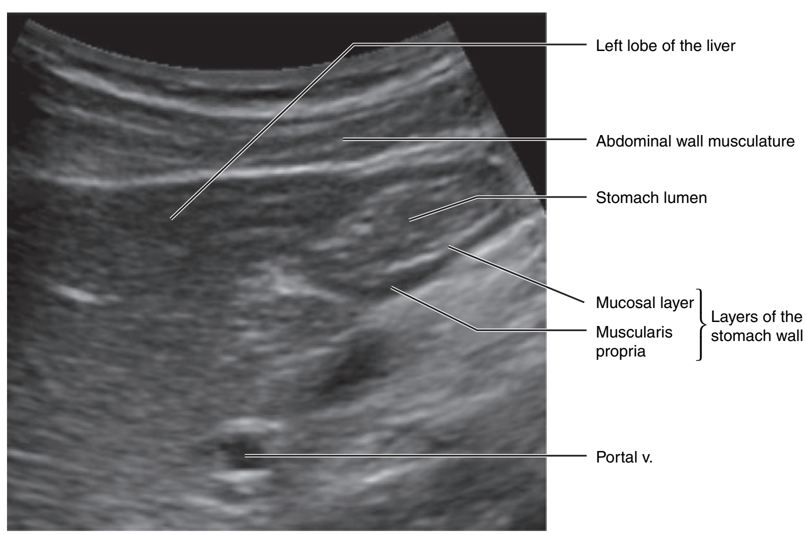


**Fig. 11.9** The stomach as seen on transabdominal ultrasound.

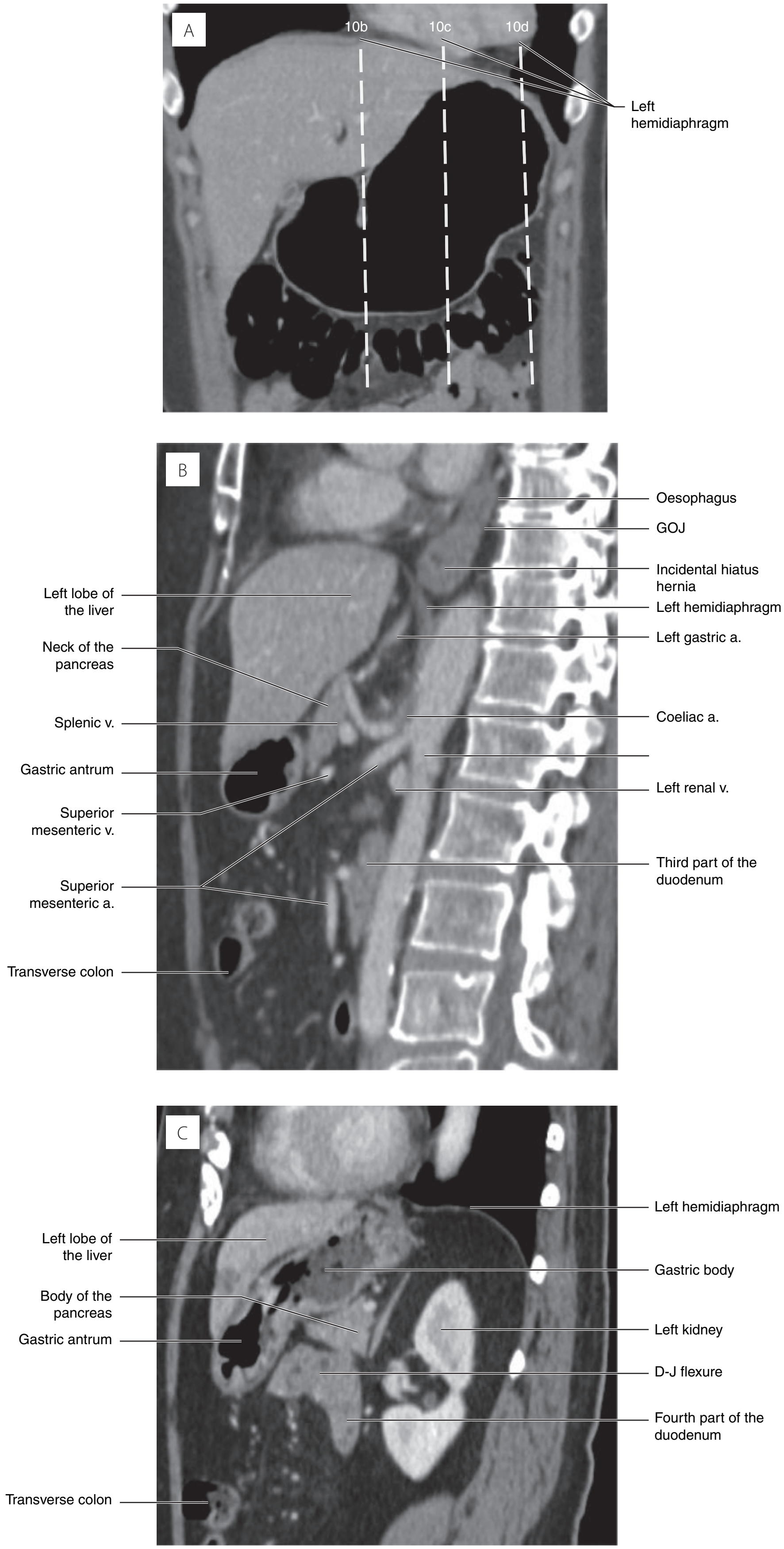


**Fig. 11.10** Multiplanar reformat CT showing the relations of the stomach: (A) coronal image and sagittal images through the (B) gastric antrum, (C) gastric body and (D) gastric fundus.

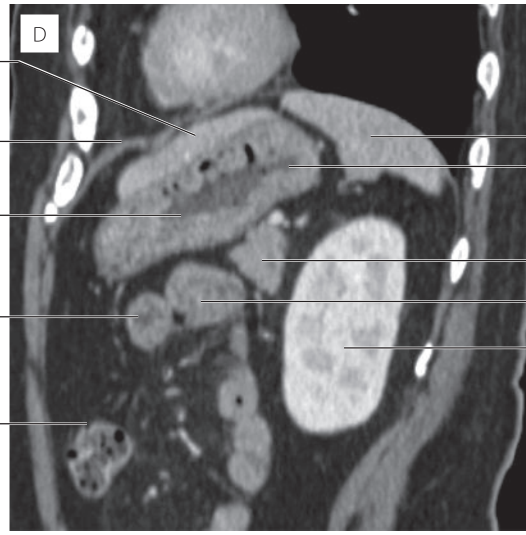


**Fig. 11.10** (*cont.*)

## The stomach bed (Fig. 11.11)

- Laterally – the gastric surfaces of the spleen, left kidney and left adrenal gland.
- Centrally – the full length of the pancreas.
- Medially – the aorta and coeliac axis.
- Inferiorly – transverse mesocolon which attaches the transverse colon to the anterior surface of the pancreas.

Ultrasound is not routinely used because of gas within the stomach; however, the pylorus can be seen and examined in the infant to look for pyloric stenosis (Fig. 11.12). The mucosa is echogenic and muscle layers are echo-poor. Normal limits are a length of < 15 mm and overall wall thickness < 8 mm.

CT is not routinely used in the investigation of the stomach as the stomach appears thick-walled when collapsed, giving the appearance of pseudotumour. It is used to stage gastric tumours or investigate outlet obstruction/extrinsic compression seen on endoscopy. MRI may show promise due to reasonable visualization of the gastric wall.

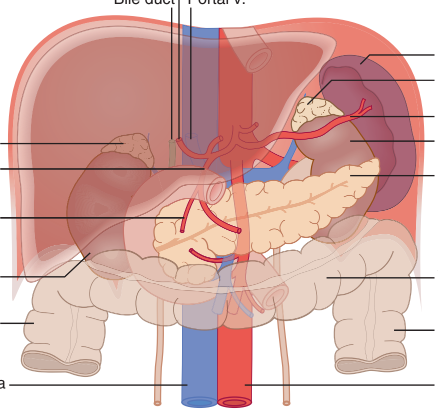


**Fig. 11.11** Line diagram showing the stomach bed.

## Arterial supply (Fig. 11.13)

- Lesser curve and GOJ – left gastric artery arising from the coeliac trunk and right gastric artery, which variably arises from the common hepatic or left hepatic artery.
- Greater curve – right gastroepiploic artery arising from the gastroduodenal artery, a branch of the common hepatic artery, and the left gastroepiploic arising from the splenic artery.
- Fundus – short gastric arteries arising from the splenic artery, also contributes to supply to the greater curve.

## Venous drainage

Same gastric distribution to arteries:

- gastric veins, left and right, drain into the portal vein
- short gastric veins and left gastroepiploic drain to splenic vein
- right gastroepiploic drains to the superior mesenteric artery.

## Lymphatic drainage

All drain to coeliac nodes, via lymph node chains along their respective arteries.

- Lesser curve – left gastric drains to coeliac nodes directly and right gastric to the retroduodenal nodes.
- Fundus and greater curve – short gastric and left gastroepiploic drain to splenic hilar nodes and to the peripancreatic nodes posteriorly. Right gastroepiploic drains via the retroduodenal nodes.

## Nervous system

Parasympathetic supply from left and right vagus nerves.

- Anterior vagal trunk – supplies the lesser curve, cardia and pylorus. Fibres from the left vagus nerve.
- Posterior vagal trunk – supplies the majority of the stomach, i.e. anterior and posterior body. Fibres from the

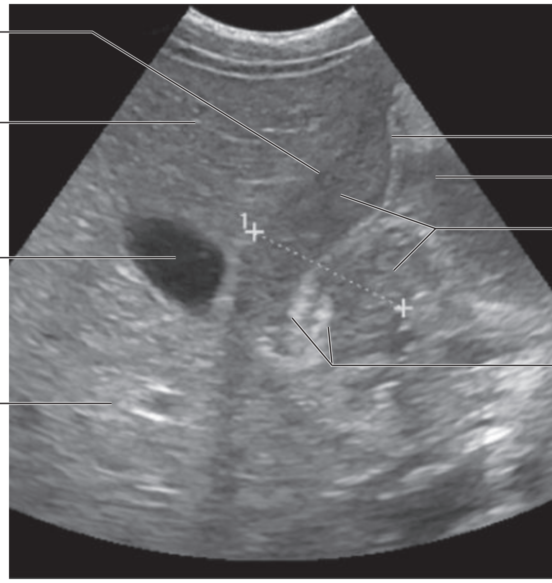


**Fig. 11.12** Ultrasound image showing the normal layers of the pylorus.



**Fig. 11.13** Digital subtraction angiogram of the coeliac artery showing vascular supply to the stomach: (A, B) coeliac artery injection, (C) selective left gastric artery injection with retrograde flow into right gastroepiploic and gastroduodenal artery. (D) Line diagram of the venous drainage of the stomach.

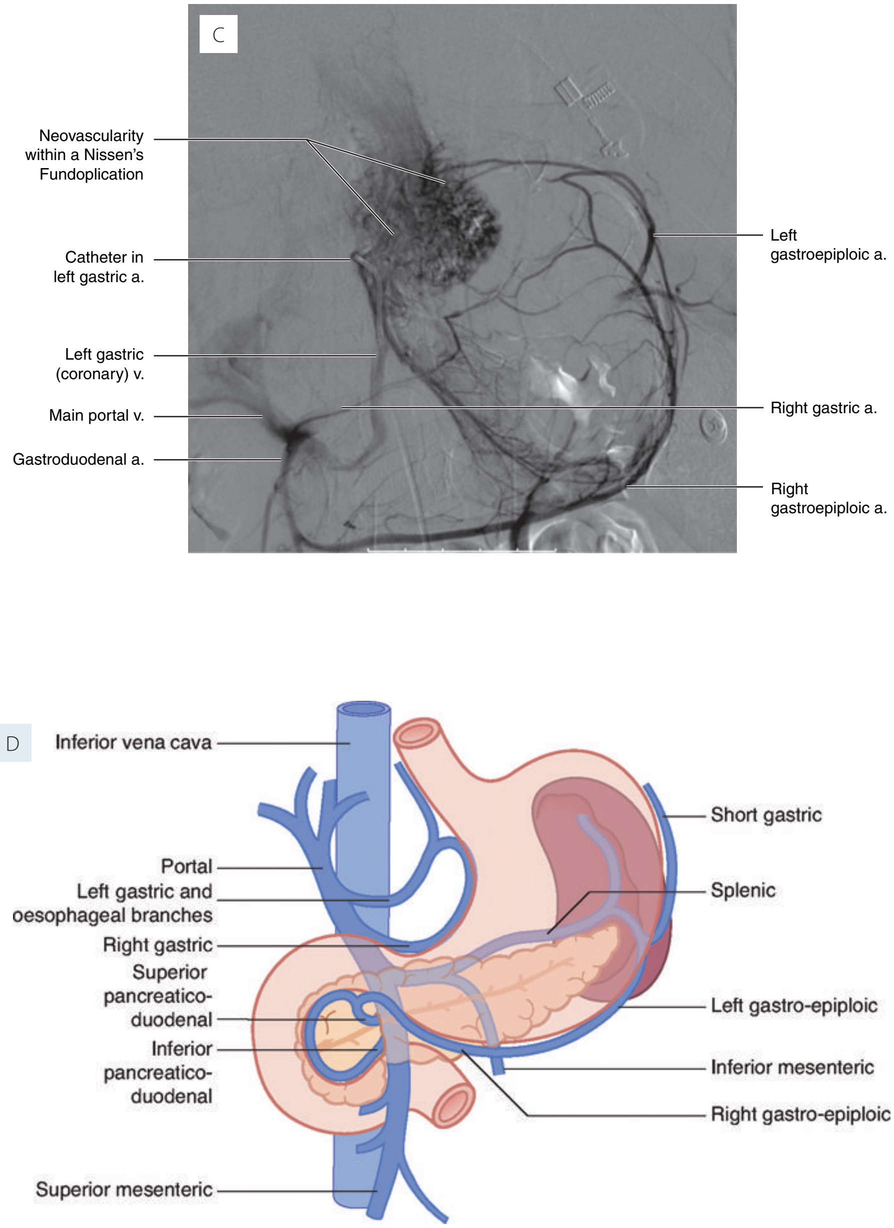


**Fig. 11.13** (*cont.*)

right vagus nerve, which goes on to supply the pancreas, small intestines and proximal large bowel up to the mid transverse colon (boundary of mid and hindgut).

- Sympathetic nerves from the coeliac plexus and splanchnic nerves.

## Duodenum

The duodenum is a 25 cm C-shaped muscular tube, which curves over and around the head and uncinate process of the pancreas; it then lies inferior to the pancreatic body, up to the duodeno-jejunal (D–J) flexure.

The duodenum has four parts, extending from the pylorus to the jejunum (Figs. 11.14, 11.10B,C).

The first 2.5 cm is covered in peritoneum, the remainder is retroperitoneal.

### Cross-sectional anatomy

The first part of the duodenum (duodenal cap) is 5 cm long, lies at the level of L1 and runs superiorly and posteriorly from the pylorus.

#### Relations

- Anteriorly – gallbladder and liver
- Posteriorly - common bile duct, portal vein, gastroduodenal artery, which separate it from the inferior vena cava
- Superiorly – epiploic foramen
- Inferiorly – pancreatic head

The second part of the duodenum is 8 cm long, lies at the level of L2 and runs inferiorly. It has a posteromedial sphincter at its midpoint, called the sphincter of Oddi, into which the CBD and pancreatic duct drain. There may be an accessory opening for pancreatic drainage 2 cm proximally.

## Relations

- Anteriorly – transverse mesocolon crosses its midline. The liver superiorly +/– gallbladder (variable position) and jejunal loops inferiorly
- Posteriorly – right kidney, ureter and adrenal
- Laterally – ascending colon/hepatic flexure, right kidney
- Medially – head of pancreas

The third part of the duodenum is 8 cm long and runs along the inferior margin of the pancreatic body at the level of L3.

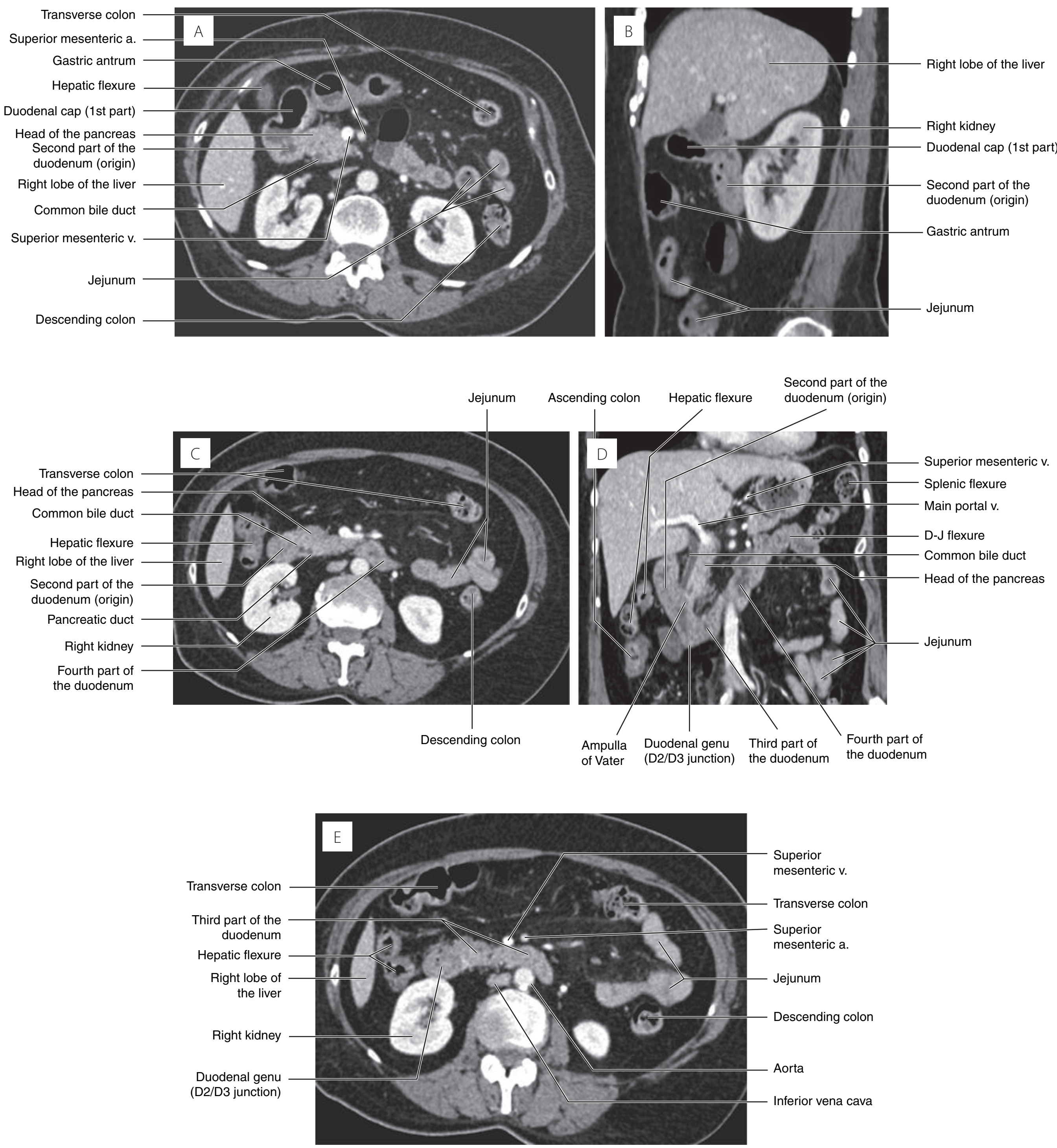


**Fig. 11.14** Axial CT showing the cross-sectional relations of the duodenum: (A) first part, accompanied by a sagittal image (B) showing relation with the gallbladder; (C) second part, with coronal image (D) to show the sphincter of Oddi; (E) third part; (F) fourth part, with an incidental duodenal diverticulum.

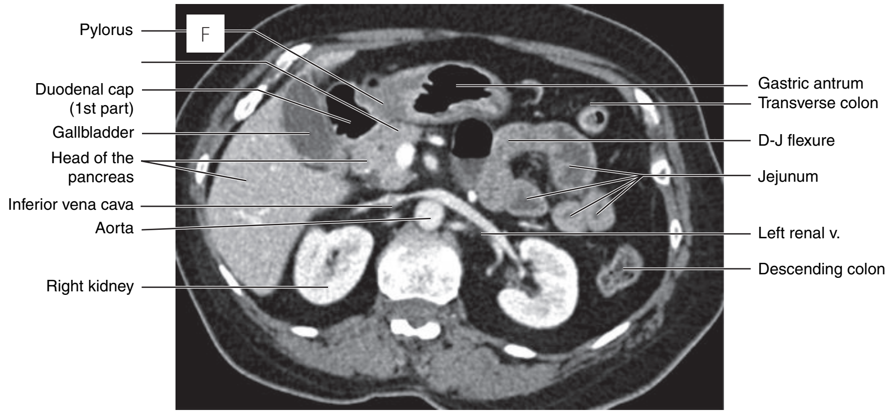


**Fig. 11.14** (*cont.*)

### Relations

- Anteriorly – root of the small bowel mesentery and the superior mesenteric artery and vein
- Posteriorly – right psoas, right ureter, gonadal vessels, aorta and IVC
- Superiorly – head of the pancreas
- Inferiorly – jejunal loops

The fourth part of the duodenum is 4 cm long and lies at the level of L2. It runs superiorly adjacent to the aorta to the D-J flexure, which is fixed by the ligament of Treitz, a peritoneal fold which runs from the root of the small bowel mesentery. This is misplaced in malrotation. There is a further more lateral peritoneal fold which contains the inferior mesenteric vein. Between the two peritoneal folds lies the paraduodenal fossa.

### Relations

- Anteriorly – stomach (superiorly) and jejunal loops (inferiorly)
- Posteriorly – left psoas and lateral border of the aorta

## Plain film and contrast study anatomy

### Barium meal and follow-through

- D1, due to its oblique course, is best seen in the RAO position. Its spiral thin folds are seen, as is the superior indentation of the gallbladder.
- Valvulae conniventes begin in D2 and become significantly more prominent in D4.There is often a posteromedial filling defect with an inferior longitudinal fold, secondary to the ampulla (visible in two-thirds of studies and accessory orifice visible in a quarter of studies).
- D3 can be indented by the SMA/SMV and aorta as the duodenum passes between these structures.

## Neurovascular and lymphatic anatomy

### Arterial supply (Fig. 11.15A,B)

- Right gastric and right gastroepiploic artery supply the first 2.5 cm of the duodenum.
- Superior pancreaticoduodenal branches of the gastroduodenal artery supply distal D1 to mid D2.
- Inferior pancreaticoduodenal arteries of the SMA supply mid D2 to the DJ flexure.

### Venous drainage (Fig. 11.22)

- The first 2.5 cm of duodenum drains to the prepyloric vein which joins the portal vein.
- Remaining duodenum drains along the superior and inferior pancreaticoduodenal veins into the portal vein and SMV, respectively.

### Lymphatic drainage

To local pancreaticoduodenal nodes, these drain:

- distally to the superior mesenteric nodes
- proximally to the pyloric and gastroduodenal nodes, which then drain to the coeliac lymph node group.

### Nervous system

- As for the small bowel – see below.

# Small intestine

The small intestine extends from the D-J flexure (at L2) to the ileocaecal valve (over the right sacroiliac joint). The root of the small bowel is attached to the posterior abdominal wall, between these two points, measuring about 15 cm.

## Meckel's diverticulum

- Embryological remnant of the vitellointestinal duct (occurs in 2% of population).
- Approximately 60 cm proximal to the ileocaecal valve on the antemesenteric border.
- Measures approximately 15 cm and may contain gastric or pancreatic tissue, leading to recurrent haemorrhage (CT scan).
- Apex may be attached to umbilicus directly or via a fibrous band.

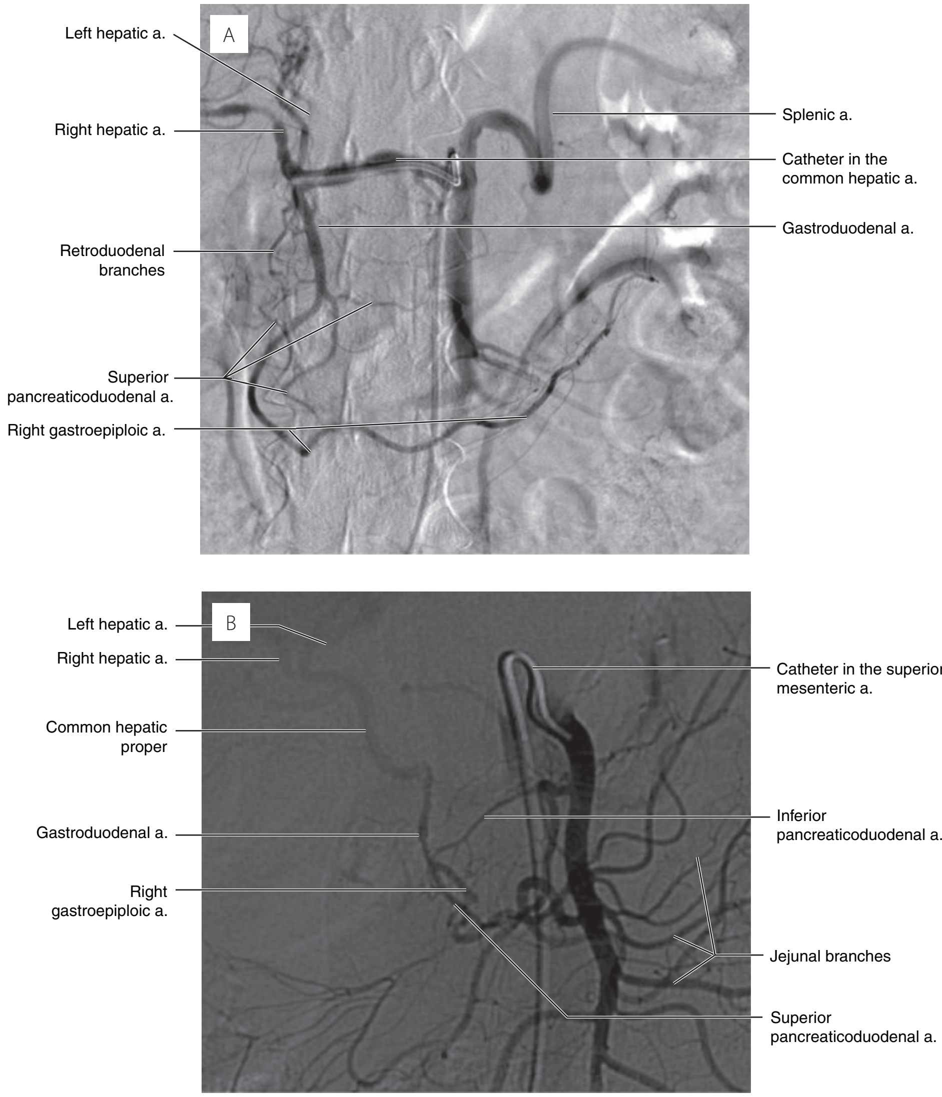


**Fig. 11.15** DSA showing the duodenal arterial supply from the (A) coeliac (selective cannulation of the gastroduodenal artery) and (B) superior mesenteric artery.

## Plain film and contrast study anatomy

### Plain film (Fig. 11.16)

- Air/fluid levels may be seen normally; up to five are allowed on an erect AXR.
- Jejunal loops are situated to the left, and ileal loops in the middle, low and to the right in the abdomen.
- Valvulae seen in small bowel obstruction help differentiate from large bowel obstruction (Fig. 11.17).
- The maximum diameter for jejunum is 3.5 cm and ileum is 2.5 cm.

### Barium follow-through

- Excellent mucosal detail.
- Density of valvulae is high in the jejunum with a gradual reduction in the proximal ileum to relative paucity of folds distally (Fig. 11.18a,b).
- To improve visualization of the terminal ileum, double-contrast views can be obtained by instilling air into the rectum. Air will enter the ileum if the ileocaecal valve is incompetent.

### Small bowel enema

- Excellent double-contrast images of the small bowel.
- Barium is rapidly pumped into the proximal jejunum, via a nasojejunal tube (uncomfortable for patient).
- Maximum diameter – 4 cm jejunum and 3 cm for ileum.

## Cross-sectional anatomy

### Relations

- Anteriorly – anterior abdominal wall
- Posteriorly – transverse colon, which is pushed down by the stomach as it fills. The stomach itself lies posterosuperior to the upper jejunal loops

The terminal ileum can be interrogated on ultrasound, due to fluid content of distal small bowel, especially in Crohn's disease (Fig. 11.19).

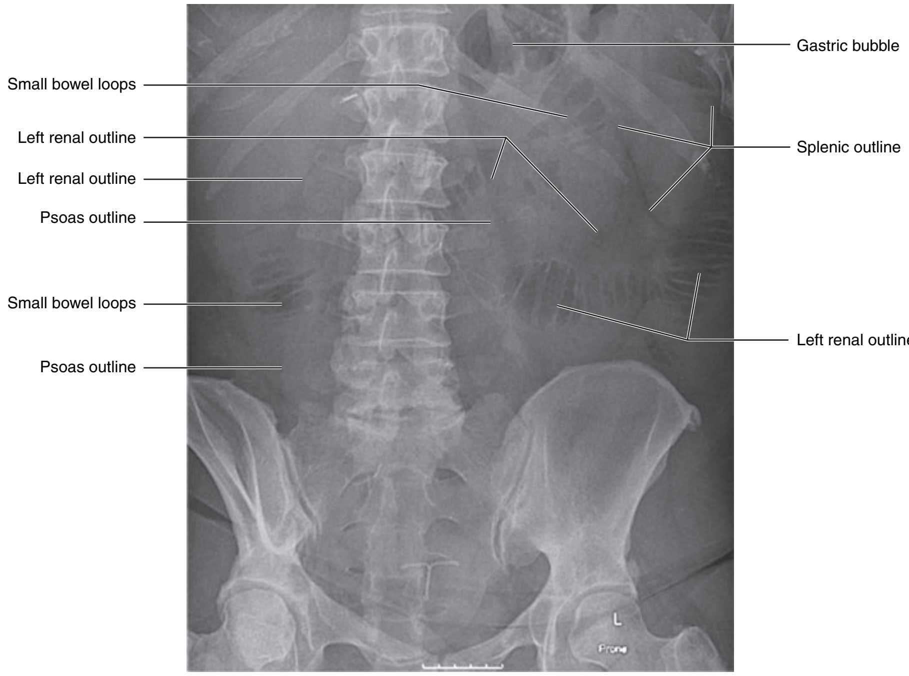


**Fig. 11.16** Plain abdominal X-ray showing the relative absence of bowel gas.


**Fig. 11.17** Plain X-ray after oral contrast ingestion in small bowel obstruction – dilated jejunal loops. The valvulae are clearly visualized, helping differentiation from large bowel.

### CT enterography and MR enterography (Fig. 11.20A,B)

- Relies on adequate distension of small bowel using osmotic non-absorbable oral agents, such as polyethylene glycol, methylcellulose or locust bean gum. Volumen is a new oral agent that may prove useful, especially as it causes little GI upset.
- Distension allows thinning of the bowel wall and separation of folds to detect polyps and focal or diffuse wall thickening.
- MRE is used mostly in the initial diagnosis and follow-up of inflammatory bowel disease; CTE is used for small bowel lesions (often detected on other modalities such as capsule endoscopy).
- CT enteroclysis – oral agent pumped through a nasojejunal tube can give superior distension, especially when looking for small tumours or polyps.

## Neurovascular and lymphatic anatomy

### Arterial supply and venous drainage (Figs. 11.21, 11.22)

- Multiple jejunal and ileal branches of the superior mesenteric artery. The vessels are linked by tiers of arcades, which are single in the jejunum and multiple (up to five) in the ileum. Vessels enter the vasa recta as end arteries.
- The terminal ileum is supplied by small ileal arteries from the SMA and a large ileal branch from the ileocolic artery.
- Jejunum and ileum drain into veins corresponding to the arterial supply into the superior mesenteric vein.

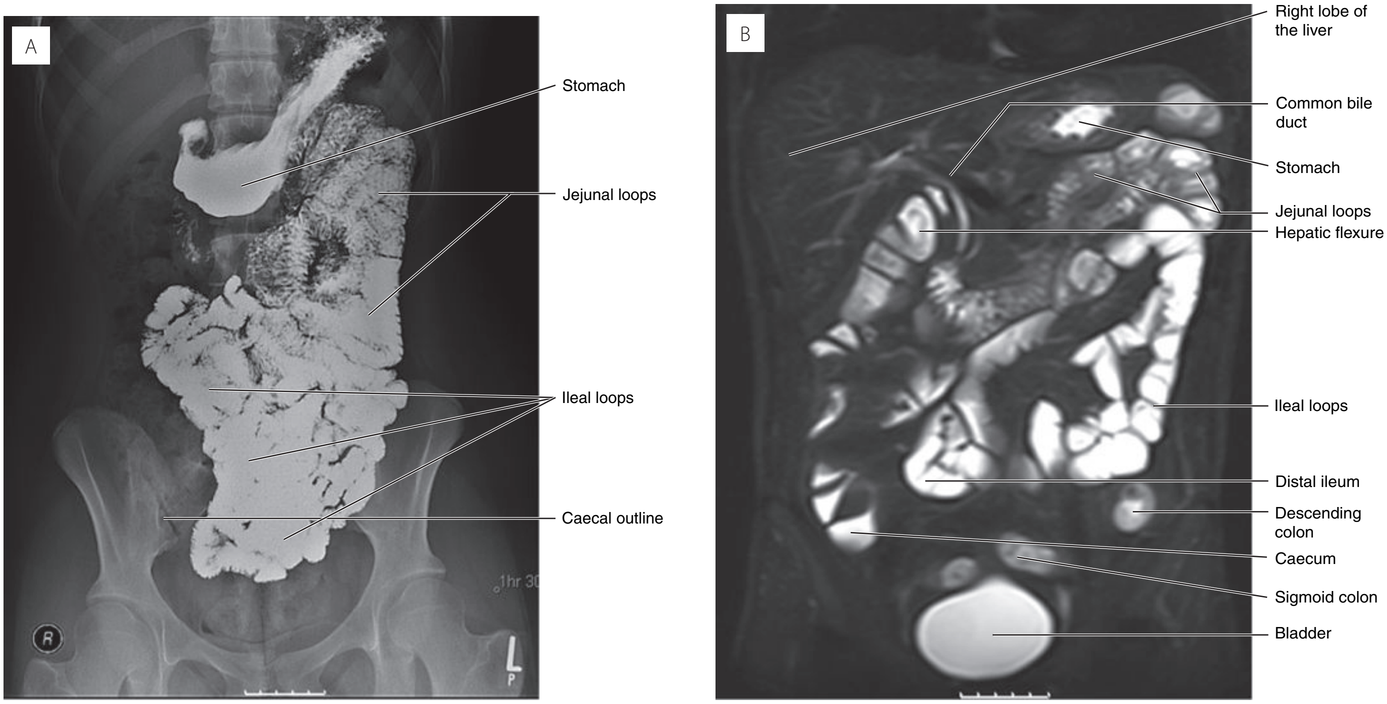


**Fig. 11.18** Small bowel follow-through (A) and small bowel MRI (B) show the position of the jejunal/ileal loops and relative density of folds.

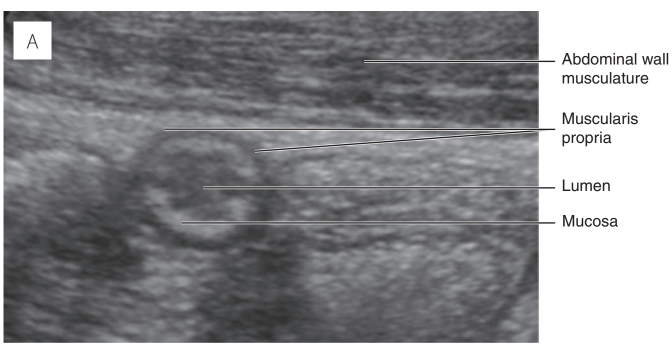


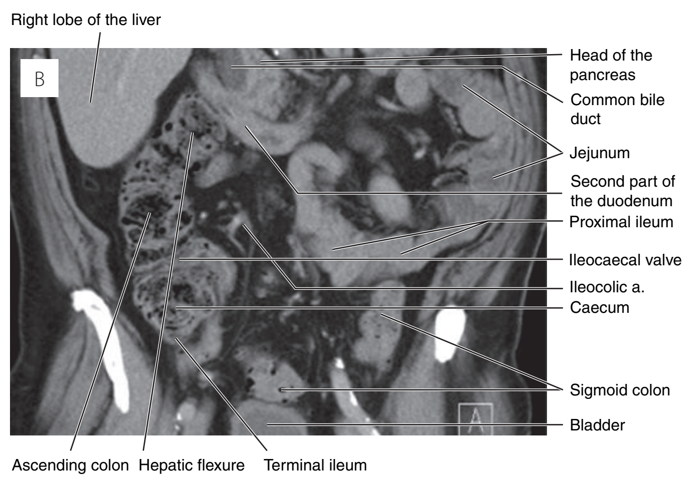


**Fig. 11.19** US (A) and coronal CT (B) showing the terminal ileum.

### Lymphatic drainage

- Mucosal and muscular lymphatics interlink and join to form large lymphatic vessels which travel within the mesentery through waves of lymph nodes, along the arteries.
- All lymphatics eventually drain into the superior mesenteric group of nodes around the SMA origin.

### Nervous system

- Superior mesenteric plexus (around SMA origin) is inferior continuation of the coeliac plexus.
- Presynaptic parasympathetic fibres from right vagus nerve.
- Presynaptic sympathetic fibres from mid thoracic spinal segments – greater and lesser splanchnic nerves.
- Synapse in the superior mesenteric ganglion (anterior to origin of SMA), with postsynaptic axons passing alongside the SMA branches within the mesentery.

## Ileocaecal valve

- Lies on the posteromedial wall of the proximal colon at the junction of the caecum and ascending colon.
- It behaves like a sphincter due to the presence of circular muscle, usually incompetent; hence, the terminal ileum is seen well on barium studies (Fig. 11.23A).
- Seen as a filling defect on barium enema, and as a short mild distal narrowing of the terminal ileum as it passes through the valve (Fig, 11.23A,B).
- On CT, has a fatty low attenuation appearance, mimics a lipoma, although an adjacent lipoma can be missed (Fig. 11.23C).
- Has two horizontal folds or a thickened fold seen well on virtual colonoscopy (Fig. 11.23D).

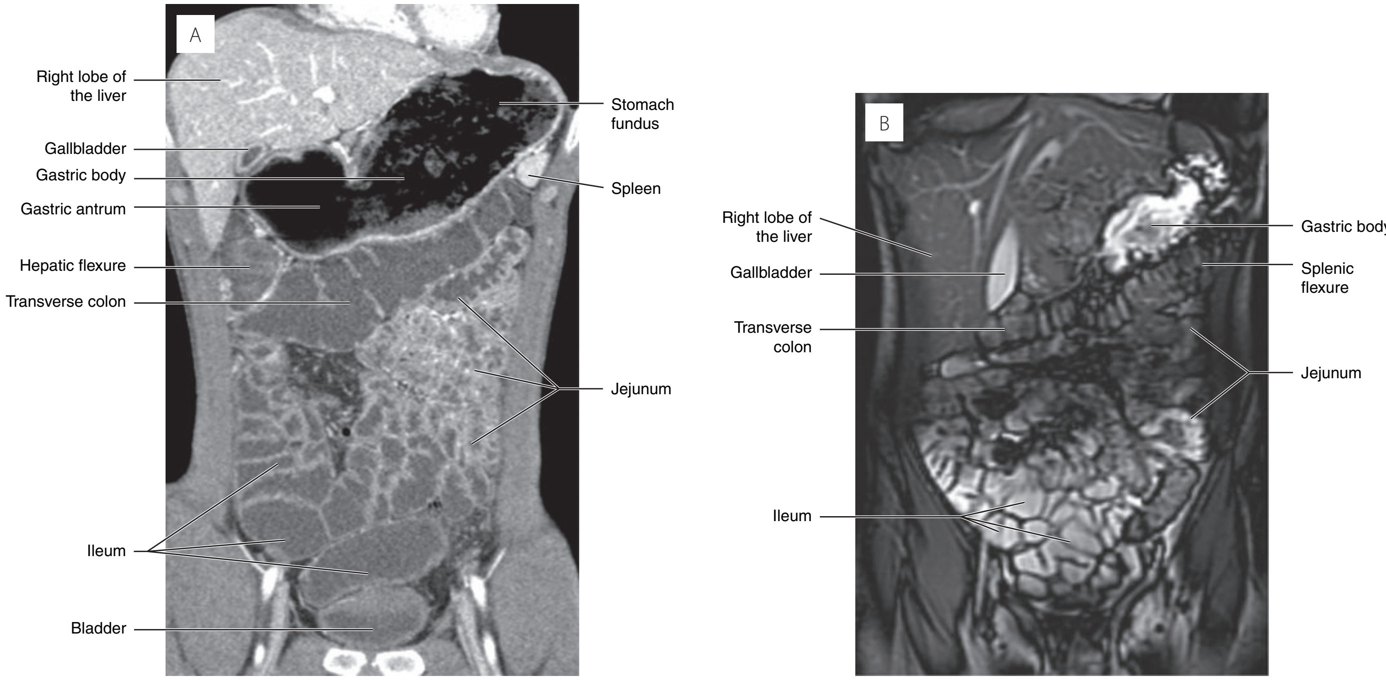


**Fig. 11.20** CT and MR enterography with good bowel preparation: (A) coronal CT MPR and (B) coronal TruFISP MRI sequence.

## Large intestine

The large intestine is a long muscular tube which extends from the caecum to the rectum and measures, approximately, 1.5 m in length.

The colon has three longitudinal muscle layers (taena coli), which converge on the appendix proximally and the rectum distally, both of which have a complete muscular coat. The taena coli are about 30 cm shorter than the colon, producing sacculations and hence the appearance of incomplete rings (haustra).

## Appendix

- Arises from the posteromedial wall of the caecum.
- Has its own, often long, mesentery, within which run vessels and lymphatics.
- Very mobile – retrocaecal in 75% and lying along the right pelvic sidewall in 20%.
- Lumen wide in youth, usually obliterated in old age.
- On plain film, calcification is seen in 10% (appendicolith); 90% of these patients will develop appendicitis in the future.
- Barium enema usually demonstrates the appendix filling with barium.
- On ultrasound, normal appendix is visible in 60% of children and thin adults (Fig. 11.24A).
- Five layers are demonstrated on ultrasound;
  1. Innermost hyperechoic layer – mucosa
  2. Hypoechoic layer – muscularis mucosa
  3. Middle hyperechoic layer – submucosa
  4. Outer hypoechoic layer – muscularis propria
  5. Outermost hyperechoic layer – serosa.
- Appendix is identified in at least 80% of scans performed on multidetector CTs (Figs. 11.23C, 11.24B).

## Cross-sectional anatomy (Fig. 11.28)

### Ultrasound

- Anterior colonic wall and caecal pole are seen; visibility is poor unless colon is markedly thickened and abnormal (Fig. 11.25). Endoscopic ultrasound is excellent for local evaluation of the anorectal wall and sphincters.

### CT

- Shows the colon very well, especially when air is insufflated into the colon, known as virtual CT (Fig. 11.26).
- CT has advantages over barium studies in that it allows assessment of paracolic structures and extent of disease process.

### MRI: assessment of the anorectum

- For cancer staging.
- For fistula formation.
- For function of the rectovaginal septum (weakness can cause rectocoele – anterior bulging of the rectal wall into the posterior wall of the vagina) and pelvic floor for weakness/descent (Fig. 11.27).

## Caecum

- Blind-ending first part of the large intestine, measures up to 6 cm and lies below the ileocaecal valve (Fig. 11.28A).
- Almost entirely covered in peritoneum, except posteriorly, where there is loose connective tissue attaching it to the floor of the right iliac fossa. May have a mesentery, which

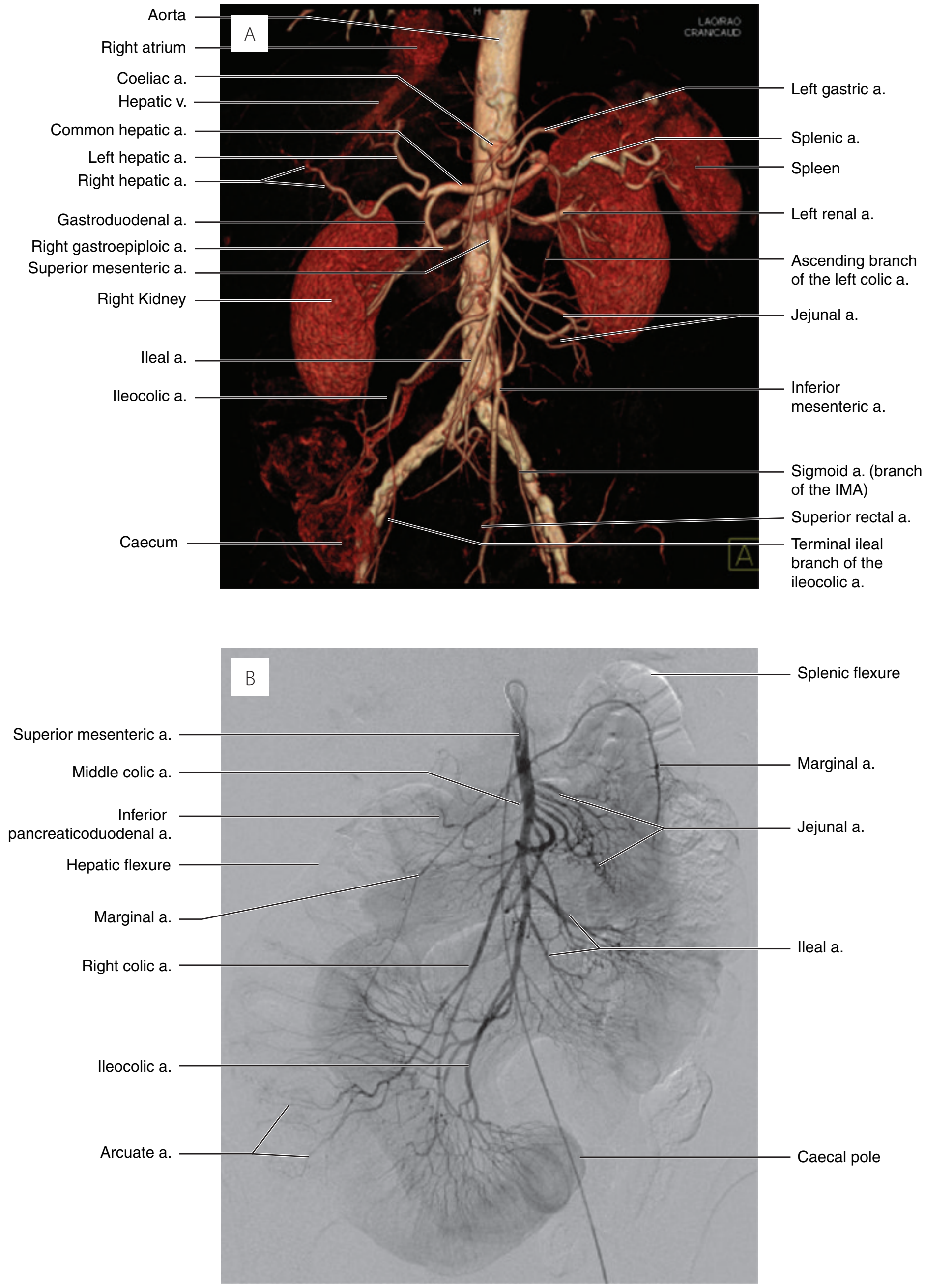


**Fig. 11.21** Mesenteric arterial supply shown on (A) CT angiography with volume rendered reconstructions and (B) digital subtraction angiography.

can rotate when long and lead to volvulus (mesenteroaxial rotation) and form a closed-loop obstruction.

- Posteriorly – psoas, iliacus, lateral cutaneous nerve of the thigh, femoral nerve and often appendix.
- Anteriorly – anterior abdominal wall and ileal loops.
- Medial – terminal ileum.

## Descending colon and ascending colon

Descending (25 cm) and ascending colon (15 cm) are retroperitoneal structures, and are covered by peritoneum on their anterior and lateral surfaces. They are attached to the posterior abdominal wall (Fig. 11.28A).

- Posteriorly – posterior abdominal wall (consisting of: quadrates lumborum, iliacus, lateral cutaneous nerve of the thigh, iliac crest, ilioinguinal iliohypogastric nerves). The distal descending colon lies across the external iliac artery and vein, and also the gonadal vessels.
- Anteriorly – anterior abdominal wall, greater omentum and small bowel loops.
- Laterally – paracolic gutter.
- Medially – right infracolic gutter (AC).

The distal ascending colon curves anteromedially to form the hepatic flexure.

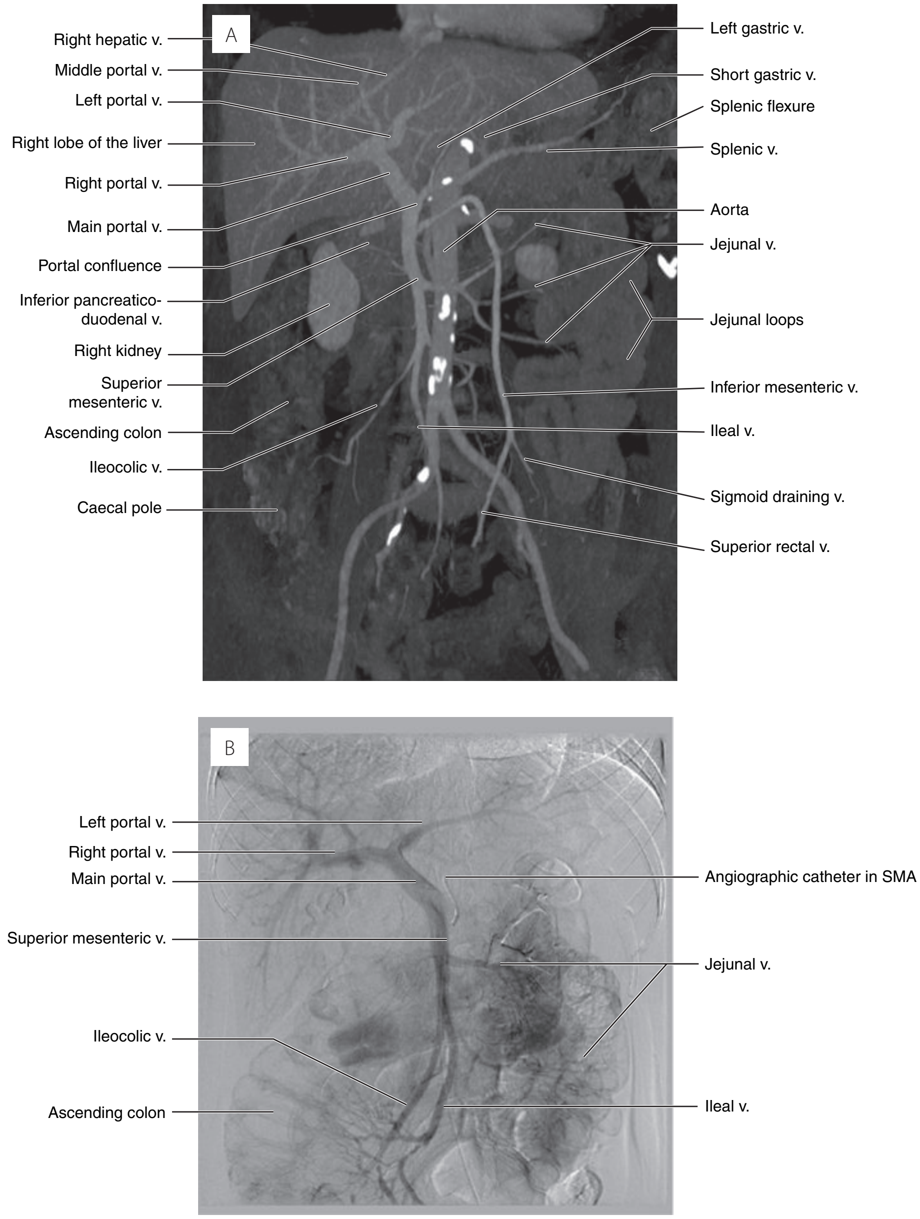


**Fig. 11.22** The mesenteric venous drainage shown on (A) CT venogram and (B) digital subtraction indirect venogram.

## Hepatic flexure

It makes an impression on the inferior surface of the liver and is attached by connective tissue to the anterior pararenal fascia, D2 and head of pancreas (Figs. 11.14A, 11.26A).

- Superiorly – right lobe of the liver (and anterolaterally).
- Posteriorly – right kidney (lower pole).
- Medially – D2 and gallbladder (anteromedially).

## Transverse colon

The transverse colon (45 cm) hangs between the hepatic and splenic flexure and is completely covered in peritoneum, the transverse mesocolon, which is attached to the anterior border of the pancreatic body (lateral attachments of the transverse mesocolon are the lower poles of both kidneys, D2). The transverse colon is also attached to the stomach by the gastrocolic ligament, which is in continuity with the greater omentum, as it hangs down over the transverse colon. It curves posteromedially in its lateral portion under the spleen to form the splenic flexure (Fig. 11.8B,C,D).

- Superiorly – stomach (centrally), gallbladder and liver (medially) and spleen (laterally).
- Below and inferiorly – descending D2, head of pancreas, proximal small bowel mesentery, D-J flexure and small bowel loops.
- Anteriorly – abdominal wall.

## Splenic flexure

Formed by the junction of the transverse colon and descending colon. It is higher than the hepatic flexure. It is attached

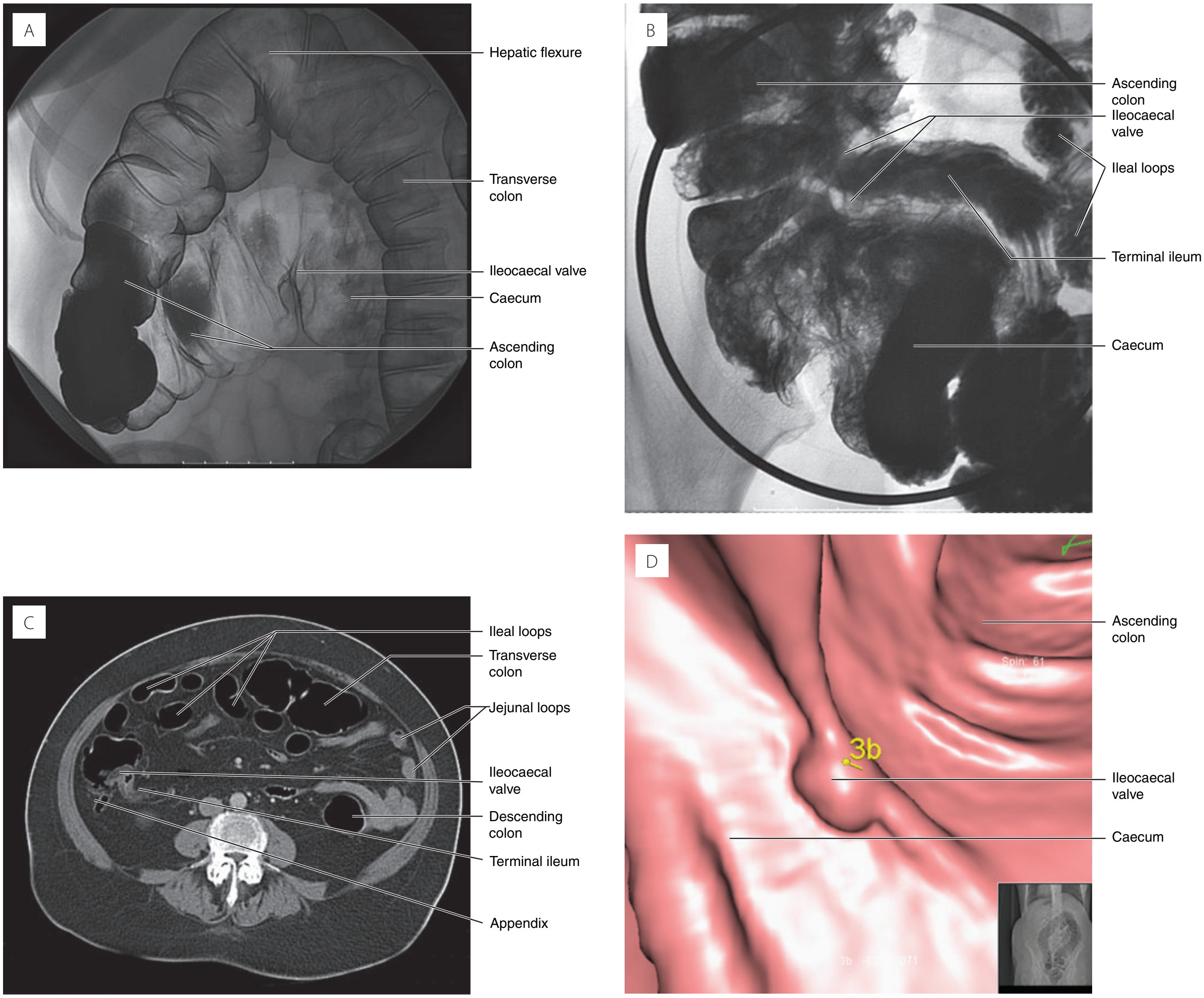


**Fig. 11.23** Ileocaecal valve: (A) on barium follow through – impression of narrowing on the final segment of the terminal ileum; (B) on barium enema seen as a filling defect; (C) on axial CT pneumocolon; (D) on virtual colonoscopy.

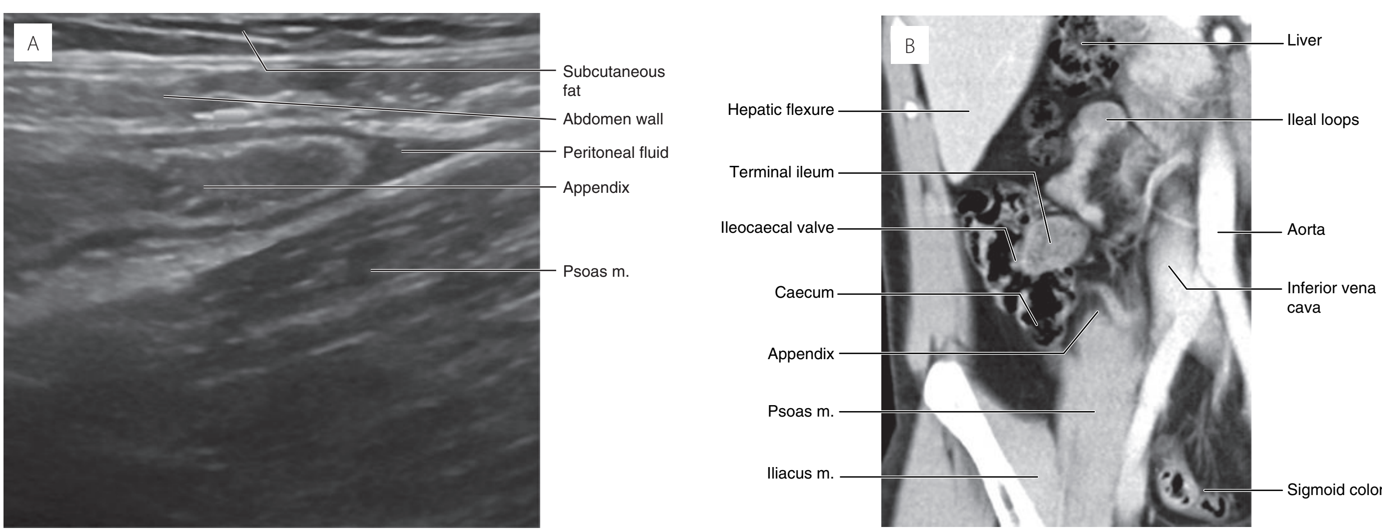


**Fig. 11.24** Images of the appendix on (A) US – slightly thickened; (B) coronal CT of the right iliac fossa.

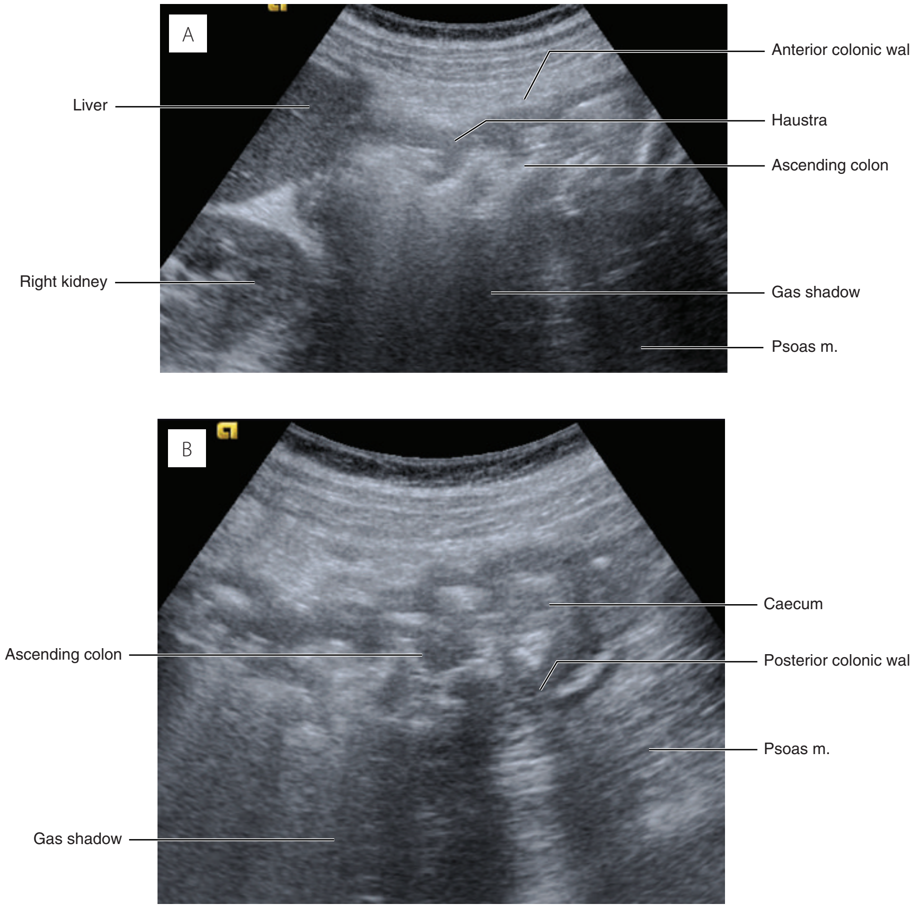


**Fig. 11.25** US of the large bowel: (A) anterior wall and haustra are visible but gas obscures the posterior wall; (B) mild inflammation and intraluminal fluid allows visualization of the whole bowel wall.

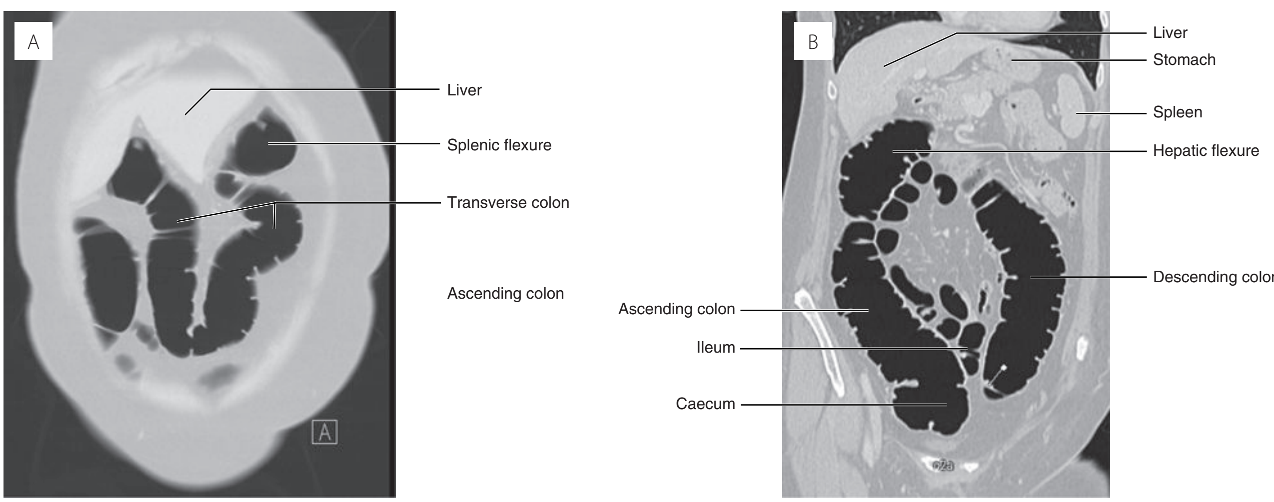


**Fig. 11.26** CT colonography: coronal images (A) and (B) showing the position of the large bowel.

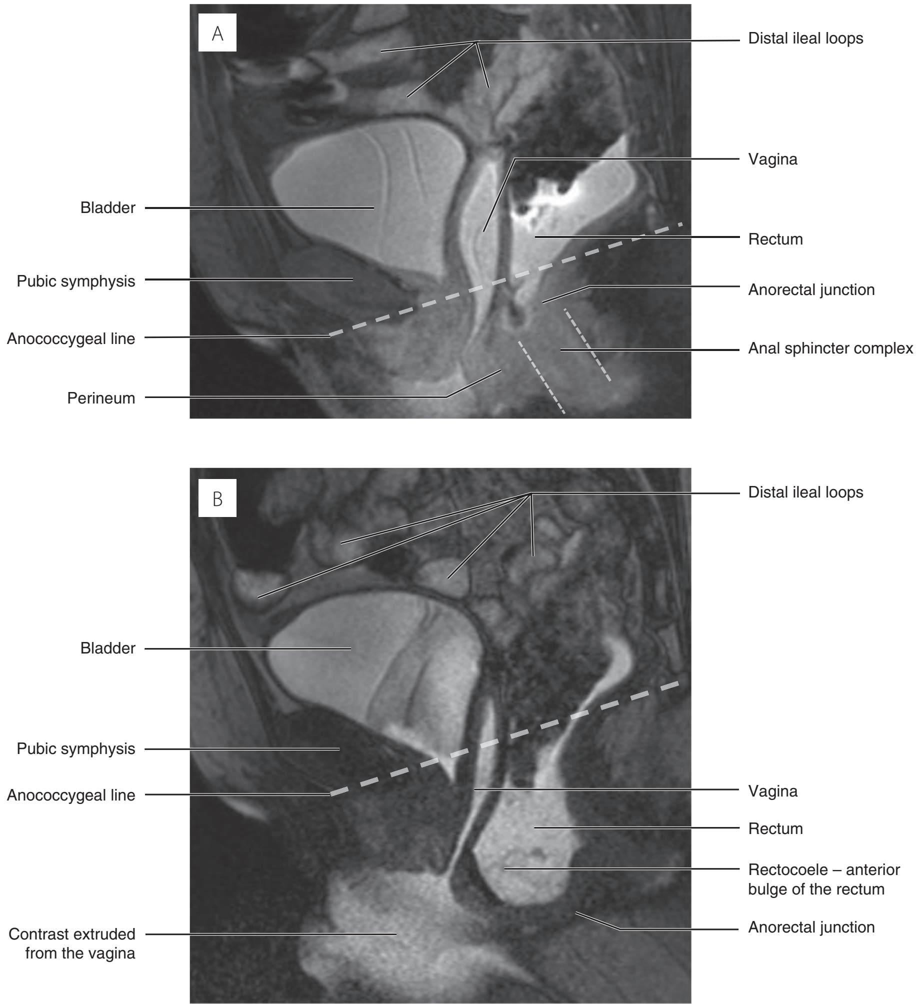


**Fig. 11.27** MR proctogram: (A) normal and (B) abnormal pelvic floor descent

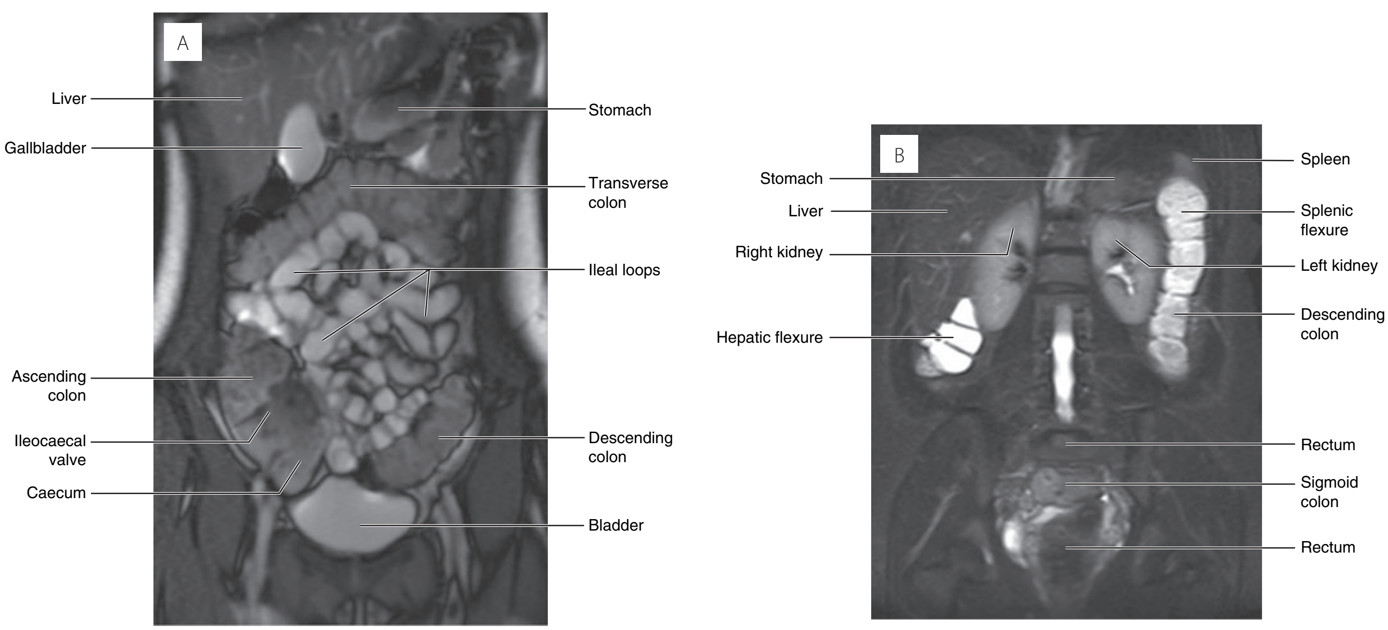


**Fig. 11.28** The large bowel: (A) coronal MRI shows the relations of the ascending/descending colon and caecum; (B) coronal HASTE MR shows the posterior relations of the hepatic and splenic flexures; (C) sagittal CT shows the relations of the descending colon; (D) axial MRI shows the caecum, distal descending colon and sigmoid colon.


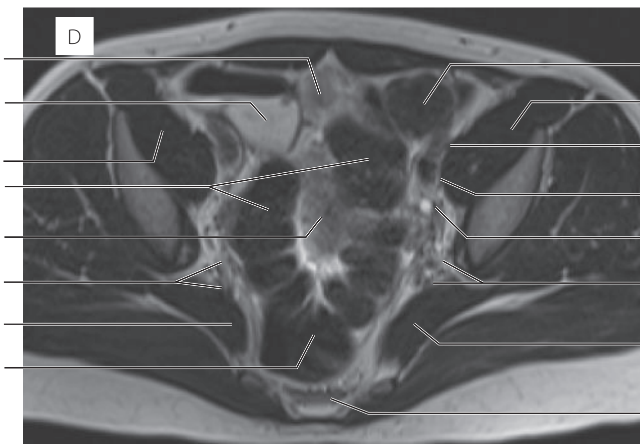


**Fig. 11.28** *(cont.)*

to the left hemidiaphragm by the phrenicocolic ligament (Fig. 11.10D).

- Superiorly – spleen.
- Posteriorly – left kidney.

## Sigmoid colon

The distal descending colon curves medially in the left iliac fossa to join the sigmoid colon. The sigmoid loops up to a variable degree and then down to connect to the rectum at the level of S3. The apex of the sigmoid may be as high as the umbilicus or above depending on how long and redundant the sigmoid is. It is completely covered in peritoneum, the sigmoid mesocolon, the root of which is like an inverted V, with its apex to the left of the midline, its medial limb across the SIJ/sacrum and the lateral limb is just medial to the common iliac vessels.

- Anteriorly – bladder (males), bladder and uterus (females).
- Superiorly and to the right – ileal loops.
- Posteriorly – left internal iliac vessels, ureter, piriformis, sacrum, sacral plexus.
- Laterally to the left – pelvic side wall, ovary or vas deferens (male).

## Rectum

The rectum is, approximately, 15 cm long and lies between the level of the S3 vertebra and the coccyx tip. The lower part of the rectum is slightly dilated to form the rectal ampulla. The rectum is slightly angulated at its midpoint, producing three horizontal shelves, valves of Houston (two left, one right). The upper third of the rectum is draped anteriorly and laterally with peritoneum and the mid third only anteriorly. The lower third is devoid of peritoneum. It is surrounded by the mesorectal fat.

### Relations (Fig. 11.29)

- Anteriorly – bladder and ureters. Vagina / rectovaginal

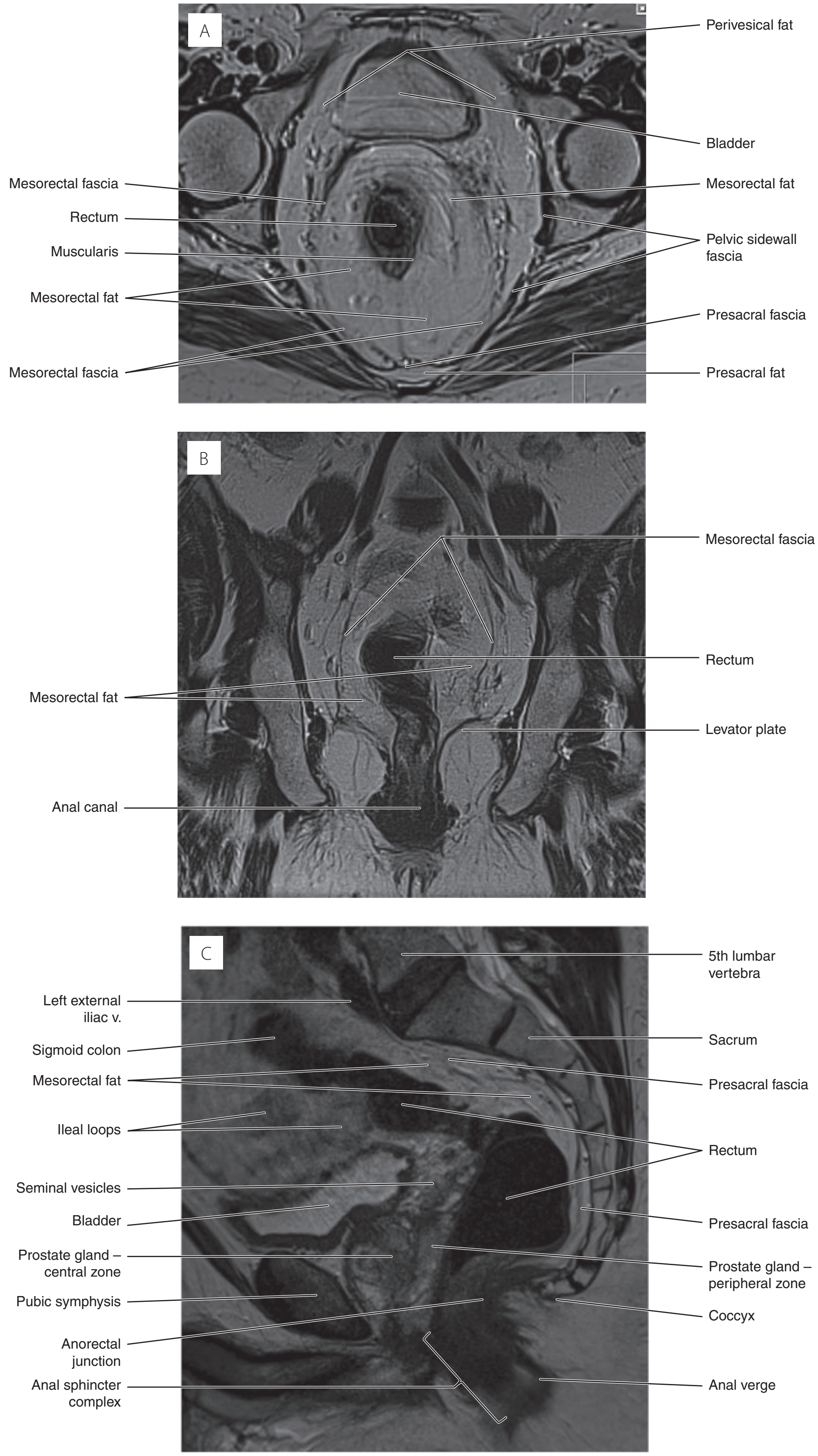


**Fig. 11.29** The rectum, mesorectum and their relations on (A) axial, (B) coronal and (C) sagittal MRI.

septum (muscular layer which separates the two structures) in females and prostate / seminal vesicles in males.

- Posteriorly – presacral fascia, lower three sacral vertebrae, coccyx, median sacral nerves and lower sacral sympathetic chain.
- Laterally – piriformis (inferiorly), sigmoid colon and terminal ileum (related to the upper rectum).

## Mesorectum

- Layer of fat that surrounds the rectum and itself is contained by the mesorectal fascia.
- Important structure in the assessment of rectal cancer respectability and prognosis.
- Contains the superior rectal artery from the IMA, superior rectal vein and its tributaries, lymphatics, lymph nodes and nerve branches of the inferior mesenteric plexus.
- Mesorectal fascia surrounds/contains the mesorectum and separates it from the peritoneum superiorly, extending from the upper rectum to the anorectal junction, where the levators become the puborectalis muscles.

## Plain film and contrast study anatomy

### Plain film

- The colon can be identified as a gas- or faeces-containing structure.

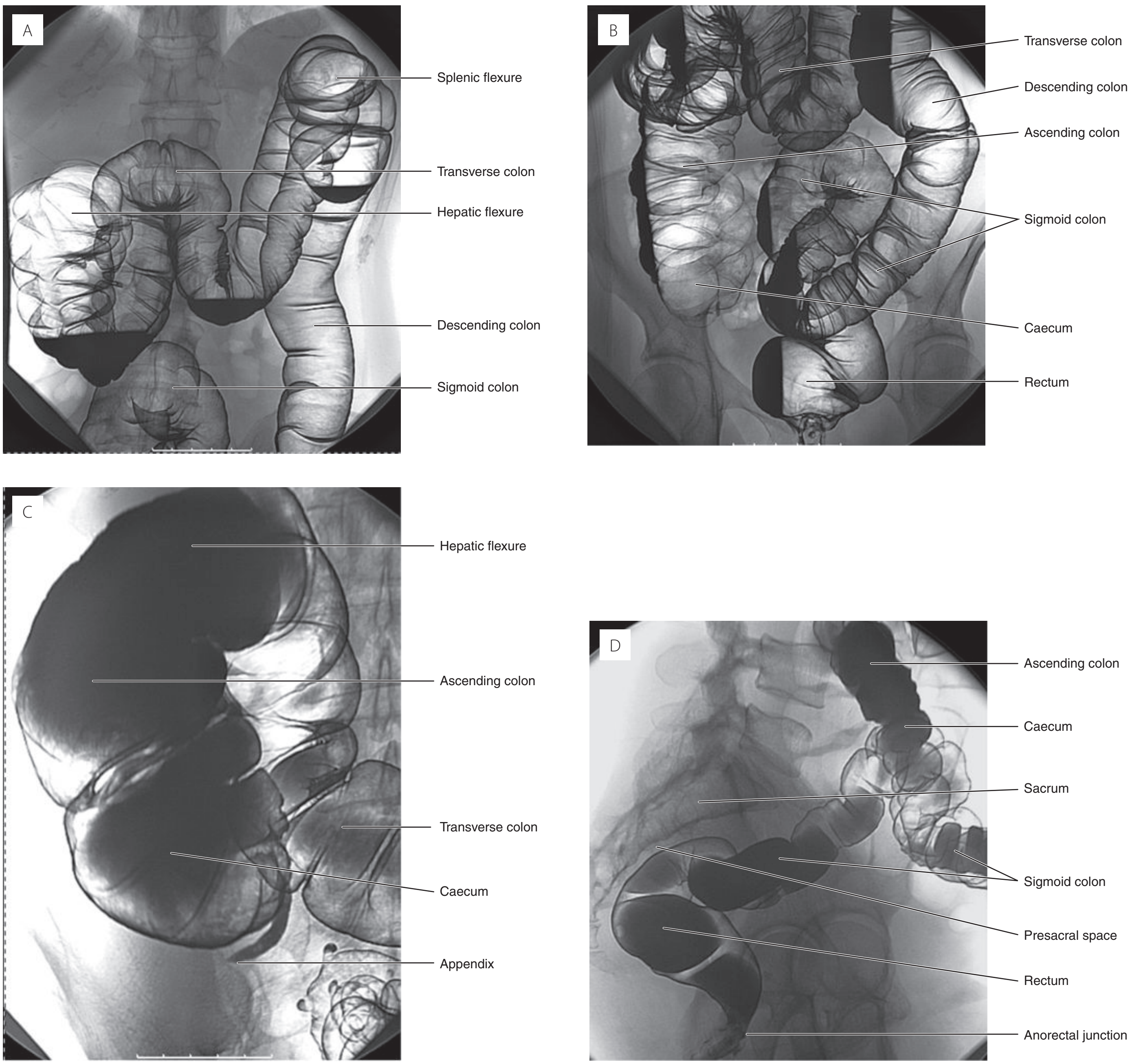


**Fig. 11.30** Barium enema shows (A, B) the colonic haustra and (C) caecum with contrast filling the appendix; (D) the rectum.

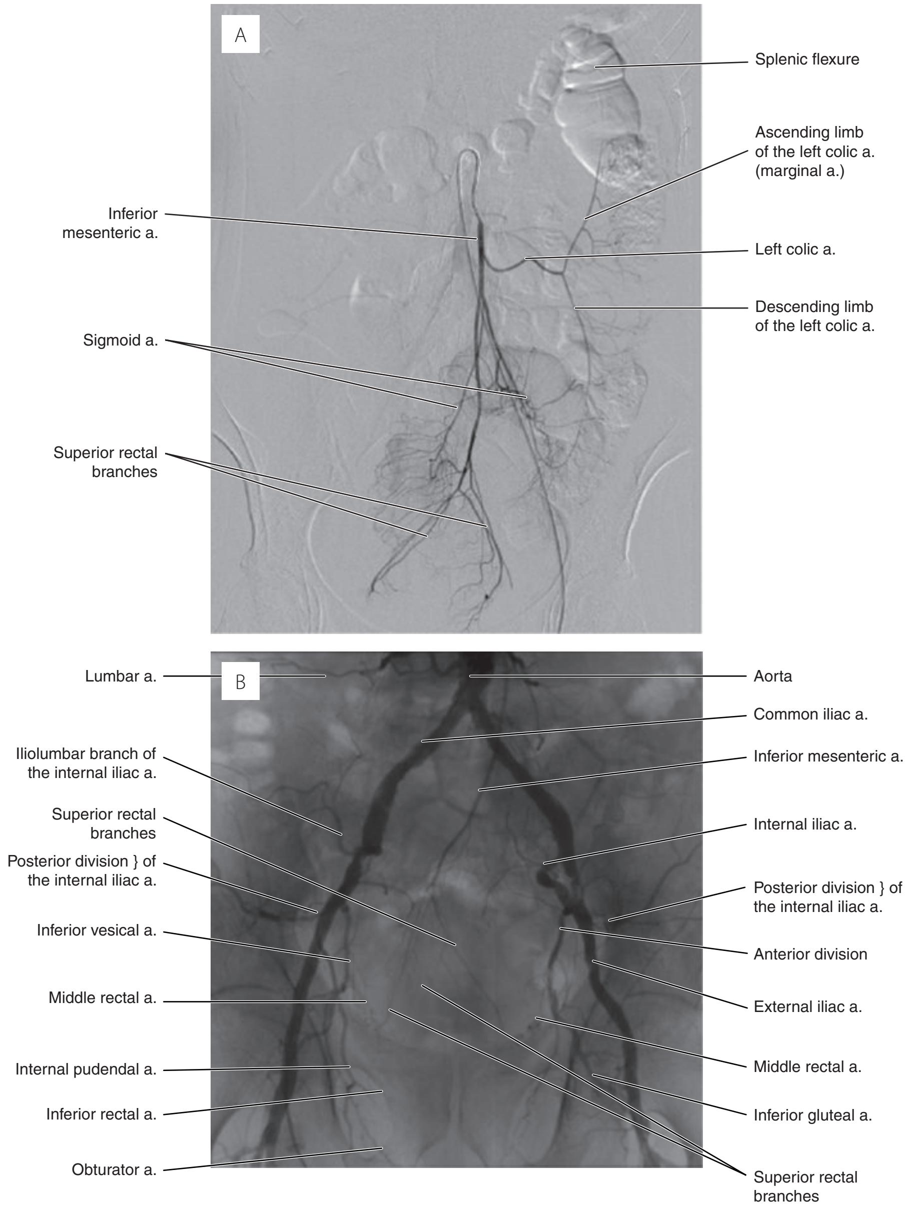


**Fig. 11.31** DSA of (A) the inferior mesenteric artery and (B) the internal iliac artery.

- The large bowel is recognized by the presence of haustra, which become less visible beyond the mid transverse colon (Fig. 11.17). There are no haustra within the rectum.
- The maximum diameter of the colon is 5.5 cm, except the caecum, which is 9 cm.

### Barium enema

- Good double-contrast views obtained from rectum to caecum. Appendix and terminal ileum may also fill. To achieve adequate filling patient needs to be rolled into different positions to allow barium to coat the whole colon (Fig. 11.30).
- Lymphoid follicles (12% of adults) may be seen as small elevations, mainly in the rectum, 1–4 mm.
- There are small fatty peritoneal tags on the free surface of the colon; there are few in the proximal colon and numerous in the sigmoid. Arteries pass through these, producing points of weakness through which the colonic mucosa can protrude and form diverticulae.

## Neurovascular and lymphatic anatomy

### Arterial supply (Figs. 11.21, 11.31)

Superior mesenteric artery supplies from the caecum to the proximal two-thirds of the transverse colon.

- Colic artery (branch of the ileocolic artery) – anterior and posterior caecal branches, appendiceal branch, and ascending colic branch which supplies the proximal ascending colon.
- Right colic artery – distal ascending colon and anastomoses with the right branch of the middle colic artery at the hepatic flexure.

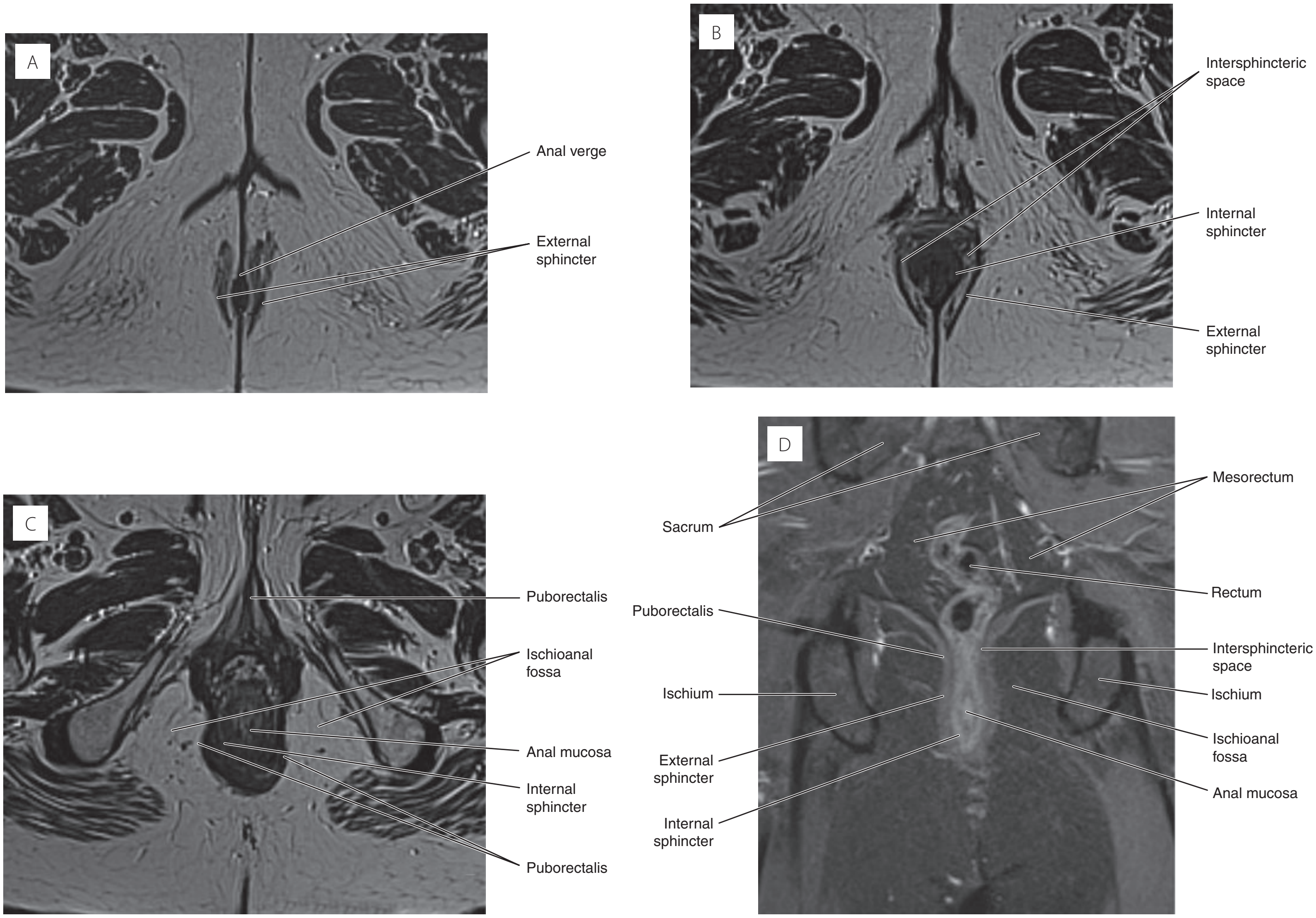


**Fig. 11.32** Anal sphincter complex on MRI: axial T2 images through the (A) lower, (B) mid and (C) upper anal canal. (D) Coronal STIR image through the anal canal.

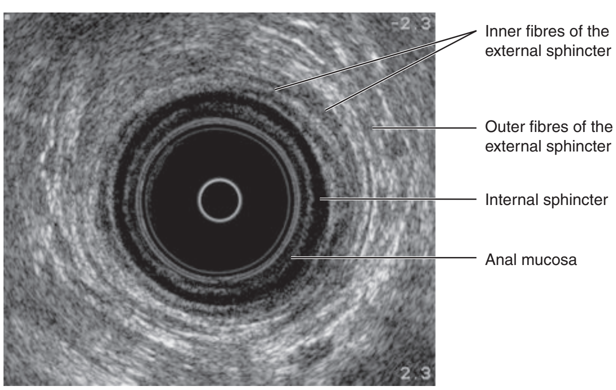


**Fig. 11.33** Axial view of the anal sphincter complex on endoanal ultrasound.

- Middle colic artery – proximal two-thirds of the transverse colon, its right branch anastomoses with the left colic artery, a branch of the IMA.

Inferior mesenteric artery supplies the remaining colon to the middle third of the rectum.

- Ascending branch of the left colic (marginal artery) – distal third of the transverse colon.
- Descending branch of the left colic – proximal descending colon and anastomoses with the marginal artery at the splenic flexure.
- Sigmoid arteries – distal descending colon and sigmoid colon.
- Superior rectal artery – terminal branch of IMA, supplies upper two-thirds of rectum.

Internal iliac artery (anterior division) supplies the mid and lower rectum.

- Middle rectal artery.
- Terminal branch of the internal pudendal artery.

### Venous drainage

Drain according to corresponding arteries.

- Superior mesenteric vein tributaries drain to the portal vein.
- Inferior mesenteric vein tributaries drain to the splenic vein.
- Mid and lower rectum drain to the internal iliac veins via the middle rectal and internal pudendal vein.

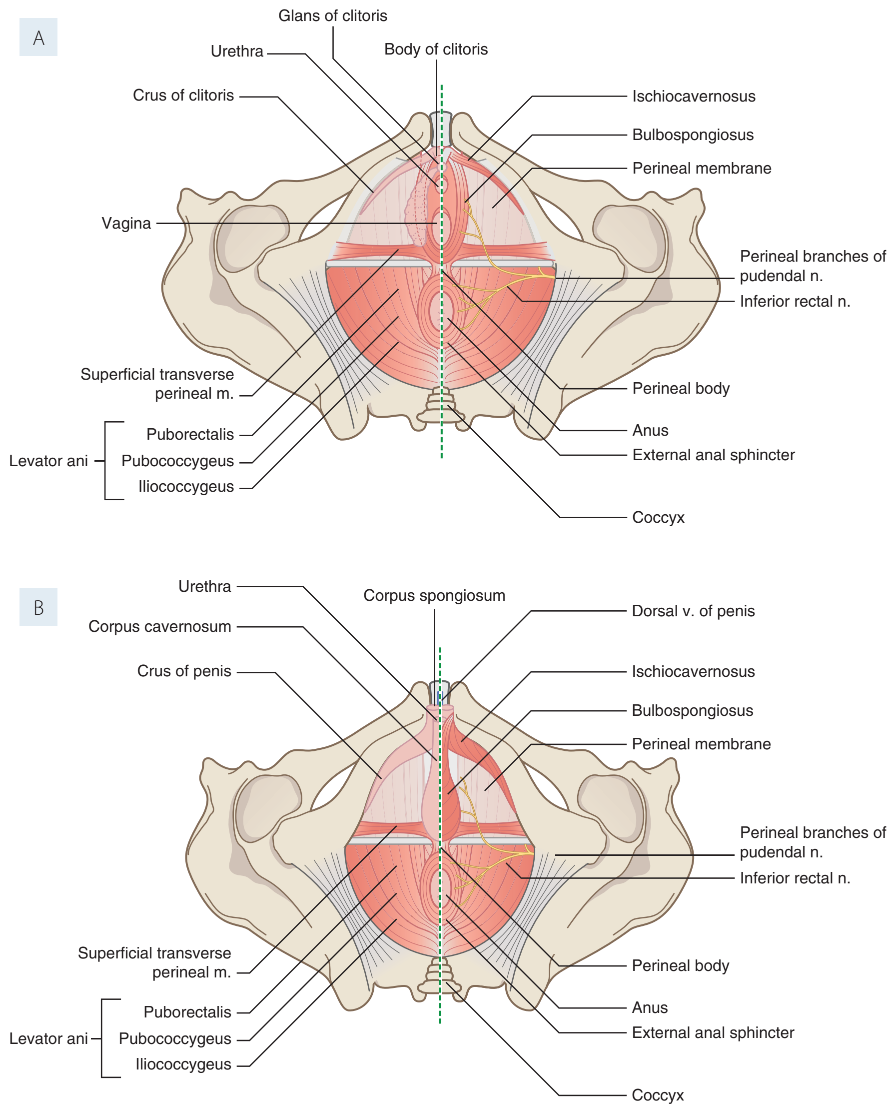


**Fig. 11.34** Line diagram showing the anterior and posterior triangles of the pelvic floor.

### Lymphatic drainage

- Ascending colon and caecum – epiploic nodes (lie along the ascending colon) and via paracolic nodes along the mesenteric arteries to the superior mesenteric group of nodes.
- Appendix – mesoappendiceal nodes and then into paracolic nodes.
- Transverse colon – along the middle and left colic vessels to the superior mesenteric and inferior mesenteric group of nodes respectively. The latter lie around the IMA origin.
- Descending colon – follow the left colic and sigmoid vessels to the inferior mesenteric nodes.
- Rectum – via mesorectal lymph nodes:
  - upper third drains to nodes along the IMV
  - mid and lower rectum drain to internal iliac nodes.

### Nervous system

- Superior mesenteric plexus – caecum to proximal two-thirds of the transverse colon.
- Inferior mesenteric plexus – distal third of the transverse colon to upper rectum.
- Superior and inferior hypogastric plexus – middle and lower rectum.
- Parasympathetic supply from the pelvic splanchnics derived from S2, S3, S4.

## Anal canal

- Terminal part of the GI tract, 2–3 cm to the coccyx tip and 3 cm in length.
- Angled backwards and is 90° to the plane of the rectum (anorectal angle is increased in posterior pelvic floor weakness (Fig. 11.27)).

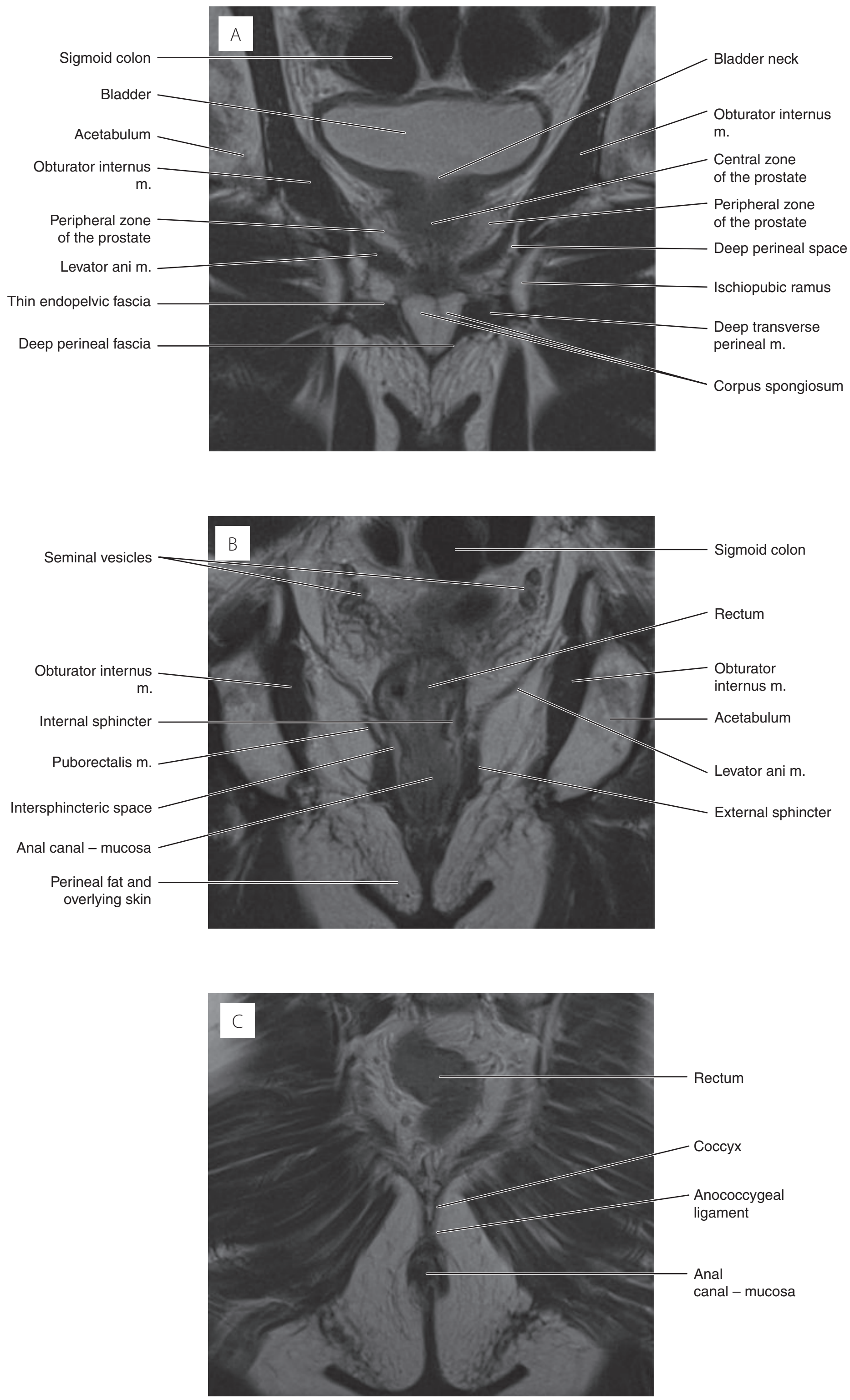


**Fig. 11.35** The pelvic floor on MRI: coronal views through (A) the anterior urogenital triangle, (B) the posterior anal triangle, (C) the posterior wall of the anal canal. Axial views through the (D) anorectal junction and (E) perineum.

- Surface covered in mucosa upper two-thirds, skin lower third. The junction is called the dentate line, the boundary for arteriovenous and lymphatic drainage (important pathway of tumour spread).
- Internal sphincter – under involuntary control (circular smooth muscle), lies in the upper two-thirds of the canal. Normal thickness: 1.5–3.5 mm.
- External sphincter – under voluntary control (circular

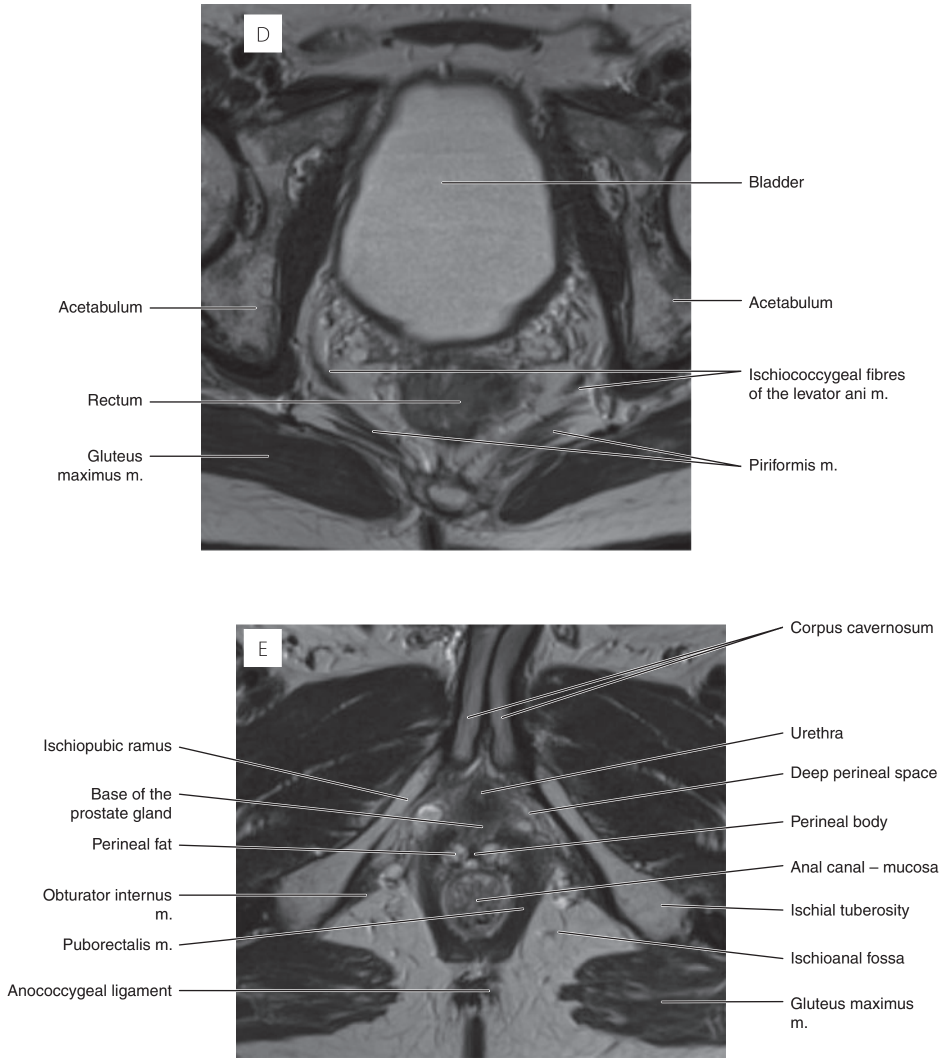


**Fig. 11.35** *(cont.)*

striated muscle), lies in the lower two-thirds of the canal, outside the internal sphincter.

## Cross-sectional anatomy

- MRI excellent for evaluation of the anal canal; fistulae, sphincter tears and tumours. Mostly by use of a body coil rather than endocoil, as the remaining pelvis is not visualized well with the latter (Fig. 11.32).
- Endoanal ultrasound mainly used to evaluate sphincters for tears, post partum or post trauma (Fig. 11.33).

Five layers are seen on T2-weighted MRI / EUS:

- musculus submucosa ani – low signal
- mucosa – high signal (MR), hyperechoic (US)
- internal sphincter – intermediate (MR), hypoechoic (US)
- longitudinal muscle layer – mildly hyperintense (MR), hyperechoic(US)
- external sphincter – three layers, superficial and deep are low signal and subcutaneous layer high signal (MR), intermediate signal (US).

### Arterial supply and venous drainage

Site of important portosystemic anastomoses (Figs. 11.21, 11.31):

- superior rectal artery – upper anal canal
- inferior rectal artery of the pudendal artery and median sacral artery (arises from the aortic bifurcation) – lower anal canal.

Veins follow corresponding arteries. The boundary between the upper and lower anal canal forms an important site for portosystemic collateral formation (varices in cirrhosis).

### Lymphatic drainage

- Upper canal – via mesorectal nodes to IMV or internal iliac nodes
- Lower canal – inguinal lymph nodes.

**Nervous system**

- Internal sphincter – hypogastric plexus
- External sphincter – inferior branch of the internal pudendal nerve.

## Pelvic floor

This is a complex ring of intimately related muscles and fascia, which support the pelvic organs and have a role in sphincter function (Figs. 11.34, 11.35).

Essentially split into:

- superior diaphragm of the levator and coccygeal muscles – support the pelvic organs
- inferior diaphragm (perineum) which is divided by a line between the ischial spines that bisects the perineal body, creating the anterior urogenital triangle and the posterior anal triangle.

### Anterior urogenital triangle

Bound by pubic symphysis, ischial rami laterally and perineal body posteriorly.

- Inferior layer of thick fascia, pierced by the urethra (and vagina in females).
- Superficial perineal pouch – arises inferiorly, and has a fatty and membranous fascia (Colles) which envelops the penis/scrotum or clitoris and is continuous with the fascia (Scarpa's) of the anterior abdominal wall.

The contents of the superficial perineal pouch are described in more detail in the chapters on the male and female pelvis.

### Levator ani

Arises from the pubic bone (pubococcygeus), pelvic fascia of the obturator internus (iliococcygeus) and ischial spines (ischiococcygeus), inserting into the coccyx.

- Anterior fibres form a sling around the vagina/prostate and insert into the perineal body.
- Intermediate fibres form a sling around the anorectal junction and blend with the external sphincter fibres – puborectalis.
- Posterior fibres insert into an anococcygeal body (fibrous raphe), between the anus and the coccyx.

### Posterior anal triangle

- Lies between the ischial tuberosities and the coccyx.
- Anal canal and anococcygeal ligament centrally.
- Ischioanal fossae laterally – lies below the levator plate and bound laterally by the sacrotuberous ligament and gluteus maximus.

**Arterial supply and venous drainage**

- Internal pudendal vessels.

**Nervous system:**

- Pelvic splanchnic nerves derived from second, third and fourth sacral nerve roots.

Chapter 12

# The kidney and adrenal gland

Uday Patel and Hema Verma

## Radiology and renal anatomy

### Plain radiography

- The renal edge may be visible, outlined by the surrounding perirenal fat (see Fig. 12.4). Intrarenal anatomy is never visible. Similarly the bladder may be outlined by the perivesical fat but the non-opacified ureters are also never seen.
- The kidneys are about 3.5 vertebral bodies (11–15 cm) in length (renal size is magnified by 15% on radiographs); however, ptotic kidneys may appear foreshortened, as they flop posteriorly.

## Intravenous urography (IVU)

After opacification by intravenous contrast, the renal parenchyma and outline can be assessed in the early or nephrographic phase, and the collecting system and ureteric anatomy in the urographic phase (see Figs. 12.3a–c, e, g, h, 12.6, 12.7 and 12.9a).

## Cross-sectional anatomy

### Ultrasound

Ultrasound allows multiplanar evaluation of renal anatomy: assessment of size, parenchyma, the pelvicalyceal system, masses and calculi can be readily performed. The liver is

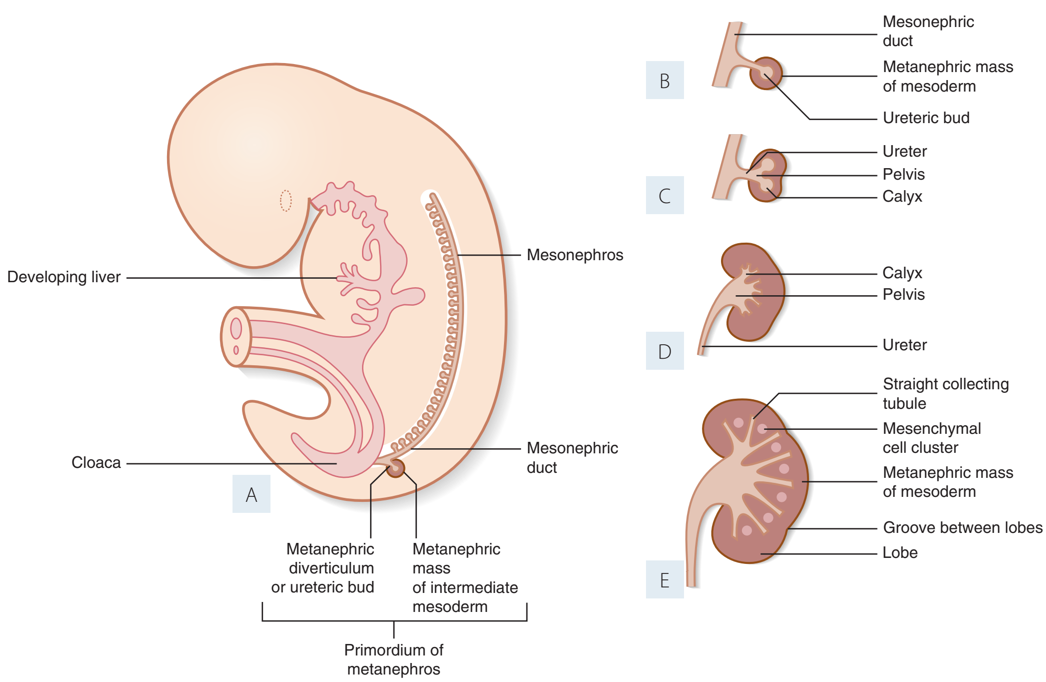


**Fig. 12.1** Line drawing illustrating a 5-week embryo (A) and the primordium of the metanephros. B–E show the consequent stages of development of the metanephric duct (weeks 5–8) into ureter, renal pelvis, calyces and collecting tubules. Fetal lobules (E) exist in the fetus and usually regress during the first year after birth but may persist into adult life.

*Applied Radiological Anatomy, 2nd Edition* ed. Paul Butler, Adam W.M. Mitchell and Jeremiah C. Healy. Published by Cambridge University Press.

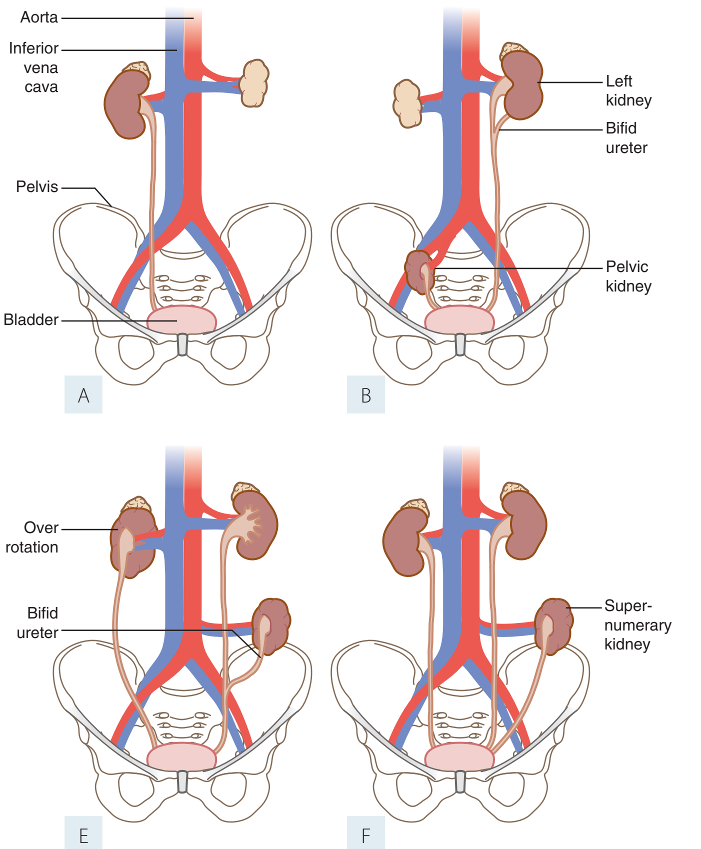


**Fig. 12.2** Diagram A illustrates an absent kidney that results from an absent ureteric bud. Incomplete division of the ureteric bud leads to a bifid ureter (B) and migratory arrest leads to a pelvic kidney (B). Fused kidneys (C) occur due to a kidney crossing over to the contralateral side. A fused pelvic kidney results from lack of migration and ascent of both kidneys (D). Diagram E illustrates a double kidney on the left that is a consequence of complete division of the ureteric bud and on the right, an over-rotated kidney that leads to the renal pelvis facing anterolaterally. Two ureteric buds leads to a supernumery kidney and ureter (F).

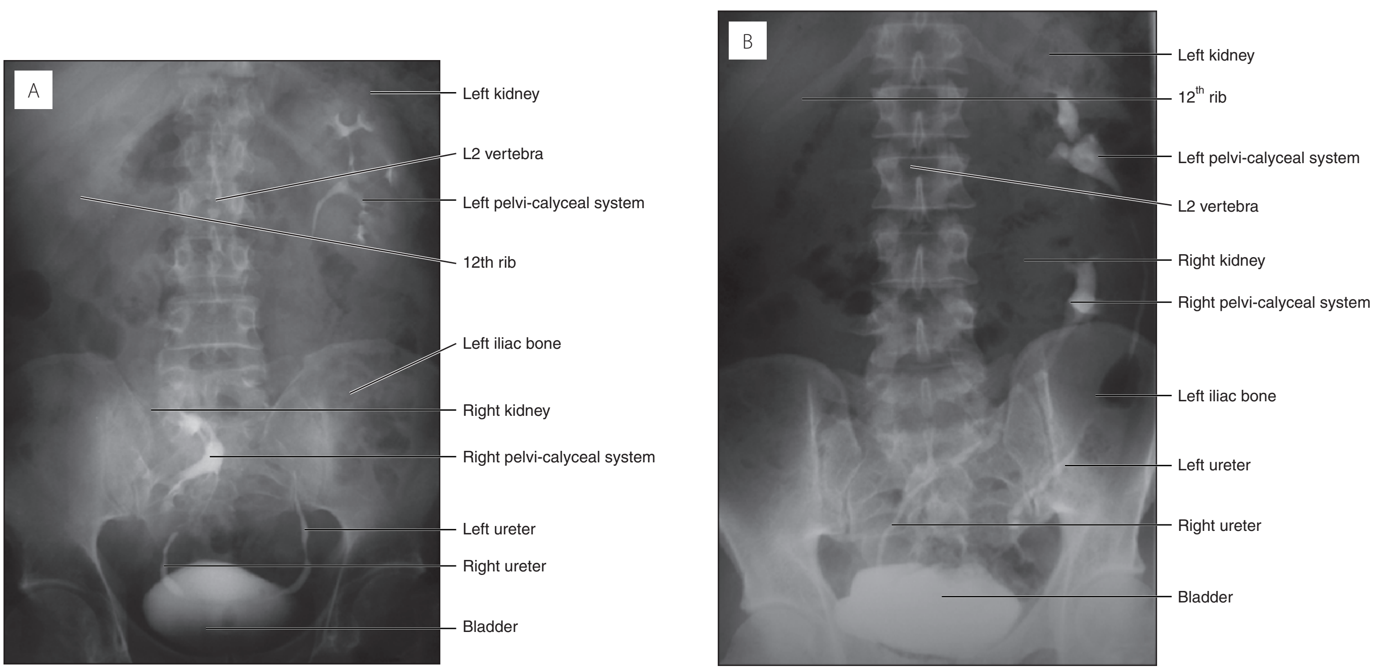


**Fig. 12.3** This montage illustrates several developmental anomalies. (A) Intravenous urogram (IVU) demonstrating a right pelvic kidney that occurs secondary to failure of migration, with an incidence of 1:900 to 1:1200 with no sex predilection. (B) IVU demonstrating left crossed fused ectopia due to fusion of the lower pole of the left kidney with the upper pole of the ectopic right kidney, but note that the ureters are normally sited. These kidneys invariably have an aberrant vascular supply.

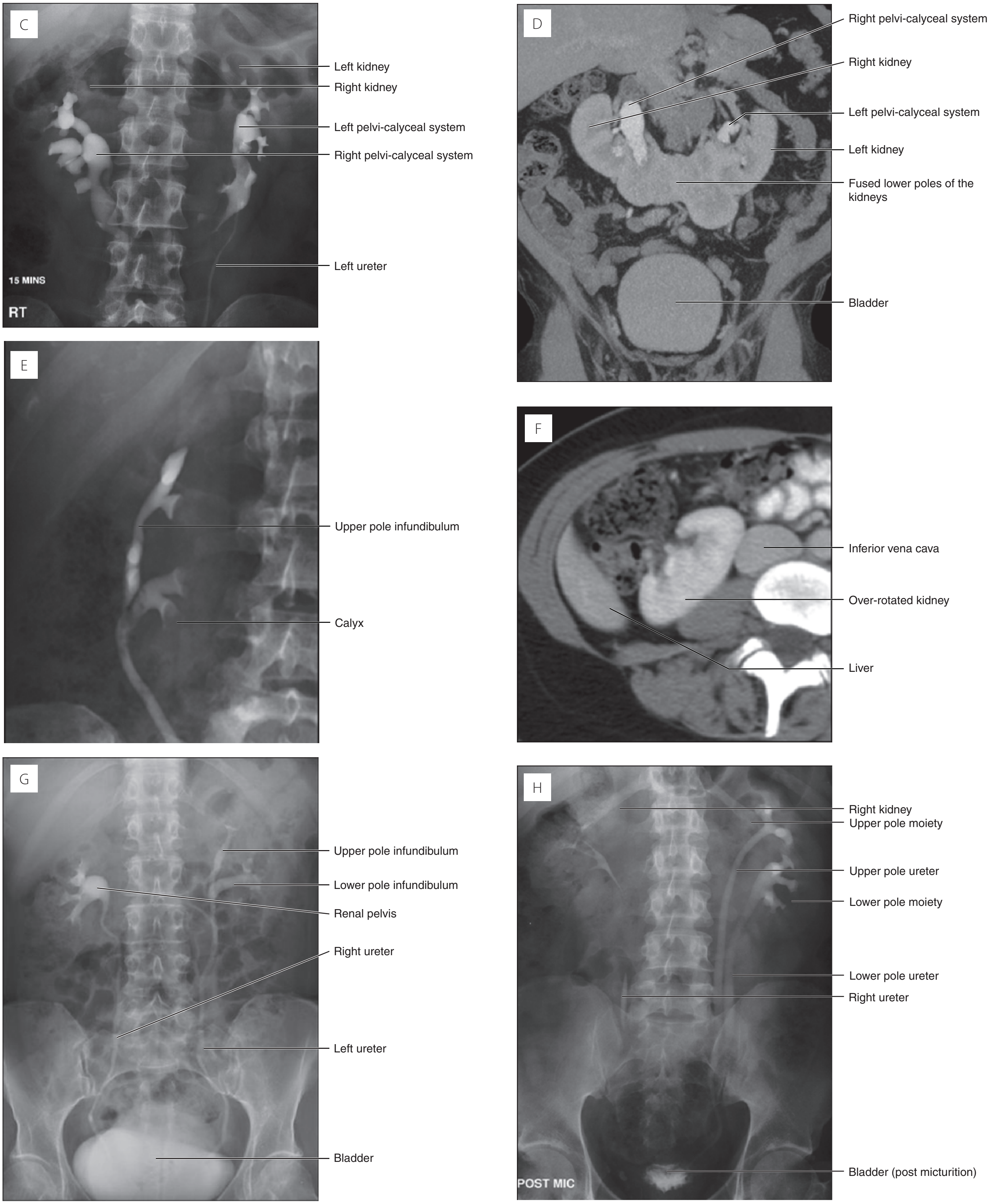


**Fig. 12.3** *(cont.)*
(C, D) IVU (C) and coronal maximum intensity projection (MIP) CT urogram image (D) of a horseshoe kidney. Note the lower poles of the kidney cross the midline and are fused, the hallmark of a horseshoe kidney; the fused tissue may be non-functional fibrous tissue. Horseshoe kidneys are prone to traumatic damage and are the commonest fusion anomaly, associated with Turner's syndrome and trisomy 18. (E, F) IVU (E) and axial CT image post contrast (F) of a right over-rotated kidney. Normally as the kidney ascends during fetal life, the renal pelvis rotates to face anteromedially, but the rotation may go awry, resulting in either under, non-rotated, or as in this case over-rotated pelvis, with the renal pelvis facing anterolaterally, as also demonstrated on the accompanying CT image. (G) IVU illustrating a bifid renal pelvis of the left kidney, which is the mildest version of abnormal ureteric division. (H) IVU illustrating a partial duplex collecting system of the left kidney with fusion of the ureters in the distal third. Complete duplex systems are more common with the ureter of the lower pole moiety inserting normally in the bladder and the upper pole moiety having an ectopic insertion in the bladder, urethra or elsewhere (Weigert-Meyer law).

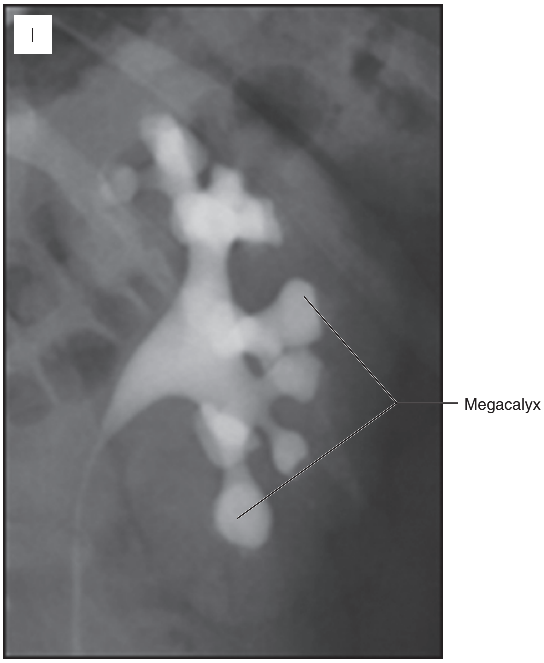


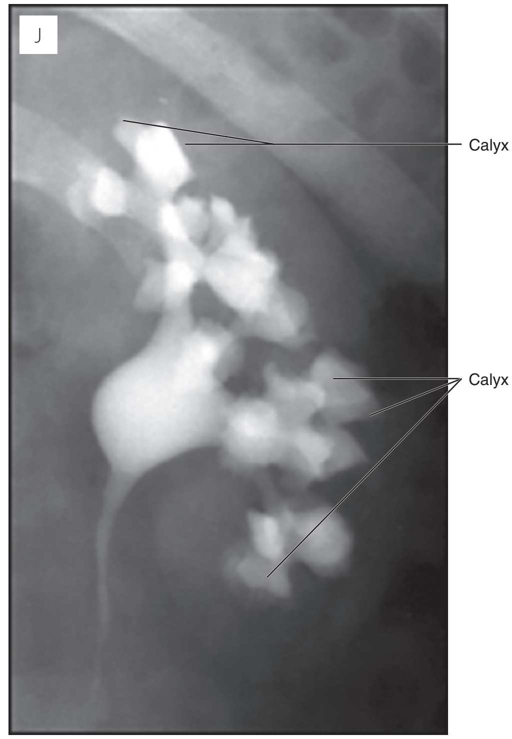


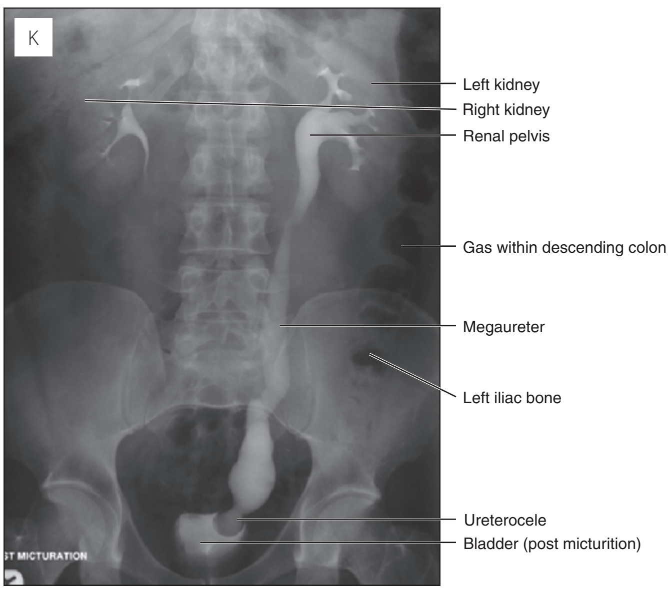


**Fig. 12.3** (*cont.*)

(I) IVU illustrating enlarged flat papillae in megacalycosis and a normal renal pelvis. Megacalycosis may be associated with a megaureter. The presence of a normal renal pelvis allows distinction from hydronephrosis. (J) IVU illustrating multiple (> 20) calyces opening into a normal renal pelvis. This is an example of polycalycosis. Note the similarity between this image and that showing megacalycosis (I). In both cases the calyces are large with flattened papillae, and the only difference is the number of calyces. (K) IVU demonstrating an enlarged left ureter, a megaureter and an associated ureterocoele (dilatation of the intravesical ureter). Ureterocoeles are bilateral in a third of cases and can occur with duplex systems when they are associated with the upper pole moiety. They are often described as having a 'cobra head' appearance.

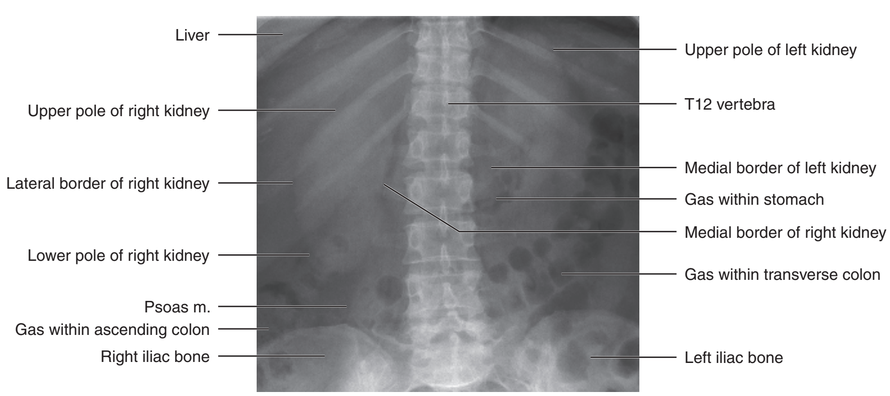


**Fig. 12.4** A coned plain radiograph illustrating the normal renal outline visible due to the surrounding perinephric fat. The left kidney lies superior to the right kidney, and is longer than the right kidney in 80% of cases.

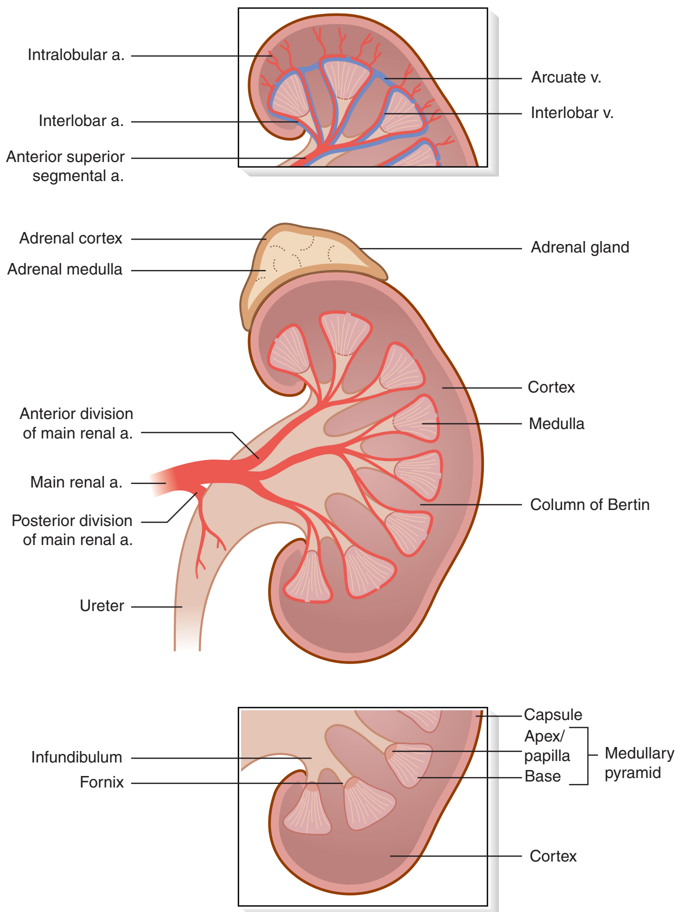


**Fig. 12.5** The divisions of the renal arteries and relations to the collecting system and renal veins are illustrated. The renal pyramid consists of the base and apex; the renal papilla is the indenting tip that contains the open ends of the collecting tubules.

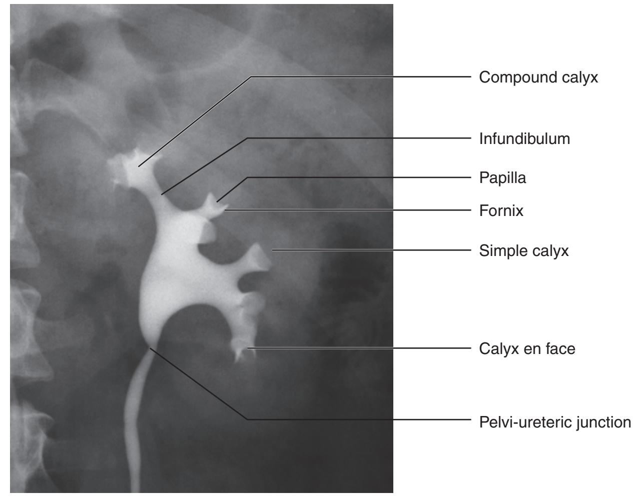


**Fig. 12.6** A coned IVU image of the left kidney illustrating the anatomy of the renal collecting system. This highlights that a compound calyx drains multiple pyramids and that a simple calyx drains only one pyramid.

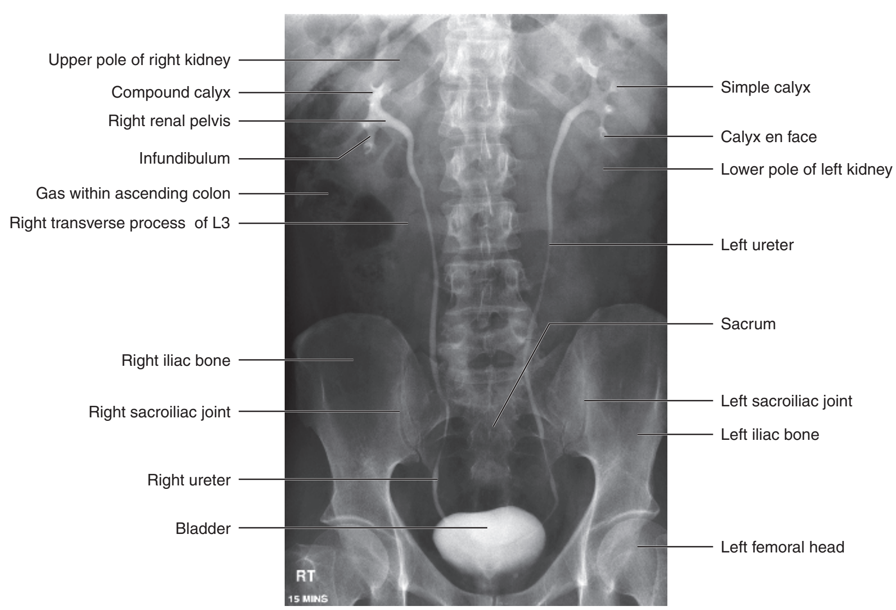


**Fig. 12.7** A full-length IVU image illustrates the entire urinary tract. The ureters may deviate medially in mid-course due to the psoas muscles.

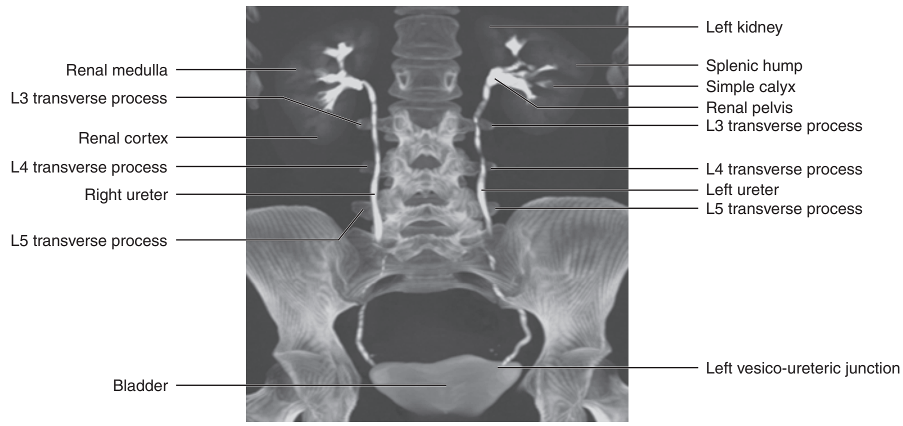


**Fig. 12.8** A coronal MIP of a post contrast CT urogram illustrating the urinary tract. The ureters lie over the tips of the transverse processes of L3–L5 vertebrae and narrow as they cross over the bony pelvic brim and as they insert obliquely into the bladder.

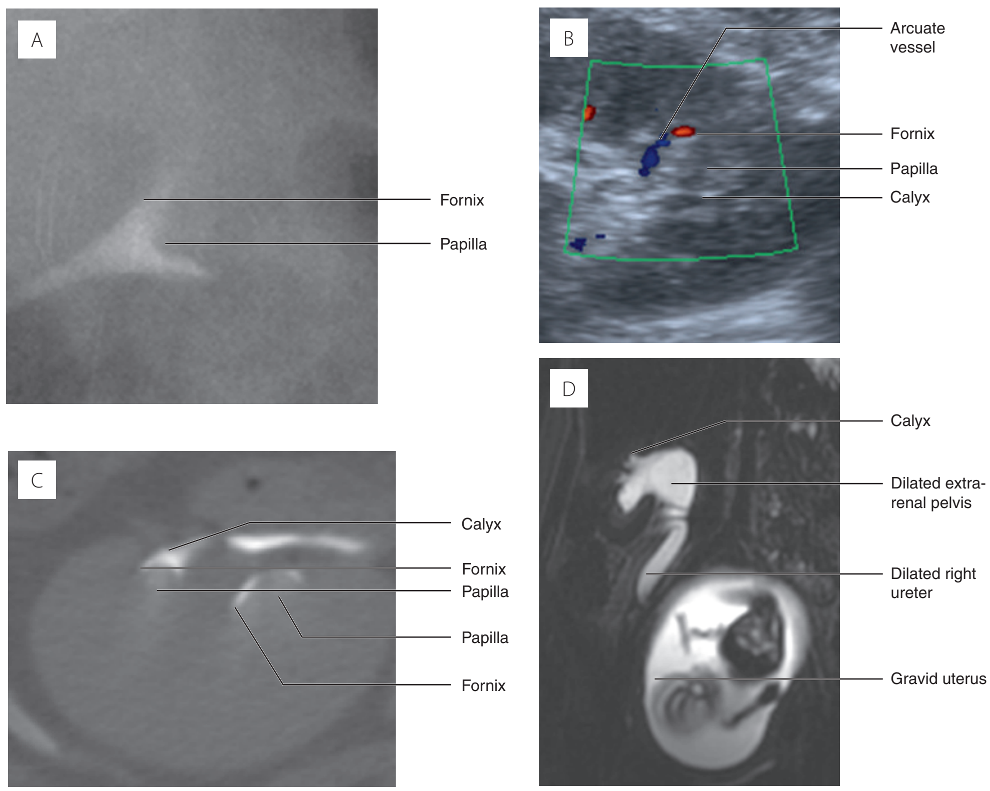


**Fig. 12.9** Four images illustrating the normal calyceal anatomy on an IVU (A), US with colour Doppler (B), post contrast axial CT urogram (C) and heavily T2-weighted MR urogram (D). MR does not optimally demonstrate the pelvi-calyceal system well unless it is dilated as shown in this pregnant patient with hydronephrosis.

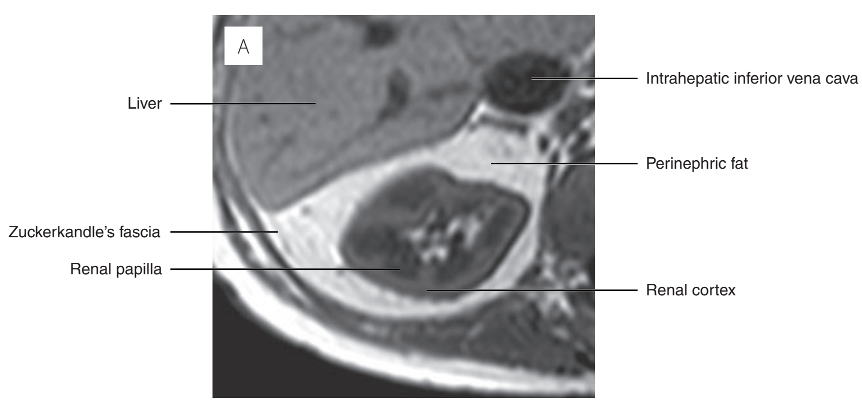


**Fig. 12.10** Axial T1-weighted (A), axial T2-weighted (B) and coronal MR angiogram (C) images illustrate the differences in signal intensity of the renal cortex and medulla on T1- and T2-weighted images. Corticomedullary differentiation is better on T1-weighted images with relatively higher signal intensity of the renal cortex (due to a shorter T1 value) compared to the low signal intensity of the medulla. The cortex and medulla are iso-intense on T2-weighted imaging compared to the low signal returned from the liver.

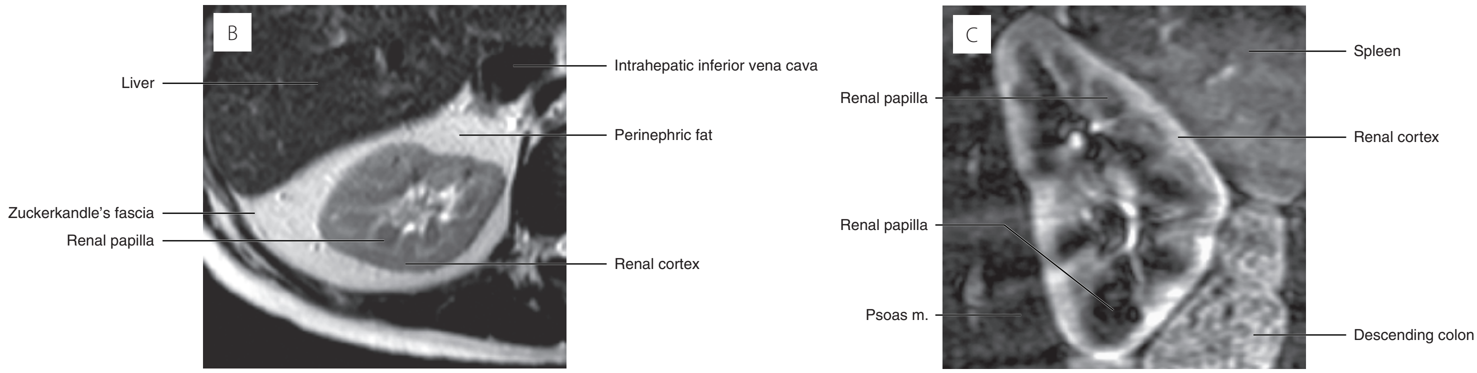


**Fig. 12.10** *(cont.)*

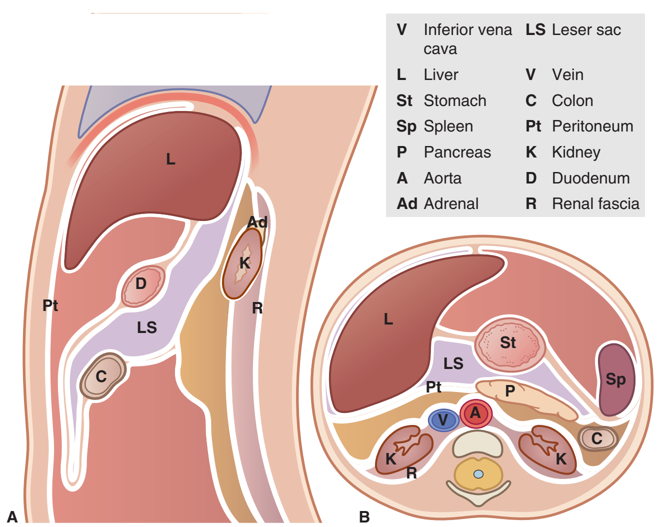


**Fig. 12.11** This illustrates the peritoneal reflection and the perinephric space (green) that surrounds the kidneys (LK – left kidney; RK – right kidney) and adrenal glands (yellow). It is bound by Gerota's fascia anteriorly and Zuckerkandle's fascia posteriorly. The perirenal space is surrounded by the pararenal spaces. The posterior pararenal space (brown) contains only fat; the anterior pararenal space (blue) contains the pancreas (P,) duodenum (D) and descending colon (C). The liver (L), spleen (S) and lesser sac (LS) all lie within the peritoneal space (discussed elsewhere).

used as an acoustic window to assess the right kidney as it lies posteroinferior to the liver. The left kidney requires a more posterior approach as it lies inferomedial to the spleen (see Fig. 12.12).

## CT/MRI

CT/MRI studies are replacing the IVU. Unenhanced CT KUB identifies almost all urinary tract calculi, 'renal phase' enhanced CT and MRI characterizes renal masses and CT urography is a global investigation for haematuria, whilst MR urography is indispensable in pregnancy and childhood. CT/MR angiography is used to evaluate the renal vasculature, but the more distal renal arterial tree is still best visualized with catheter angiography. CT and MRI are complementary investigations but each has its strengths. For instance, CT is better for renal calculi and MRI for the characterization of renal cysts, but anatomical information is more precise on CT as virtual isotropic imaging is feasible (see Figs. 12.8, 12.9, 12.10 and 12.13).

## Nuclear medicine

Nuclear medicine studies can functionally characterize renal disease but with limited structural information.

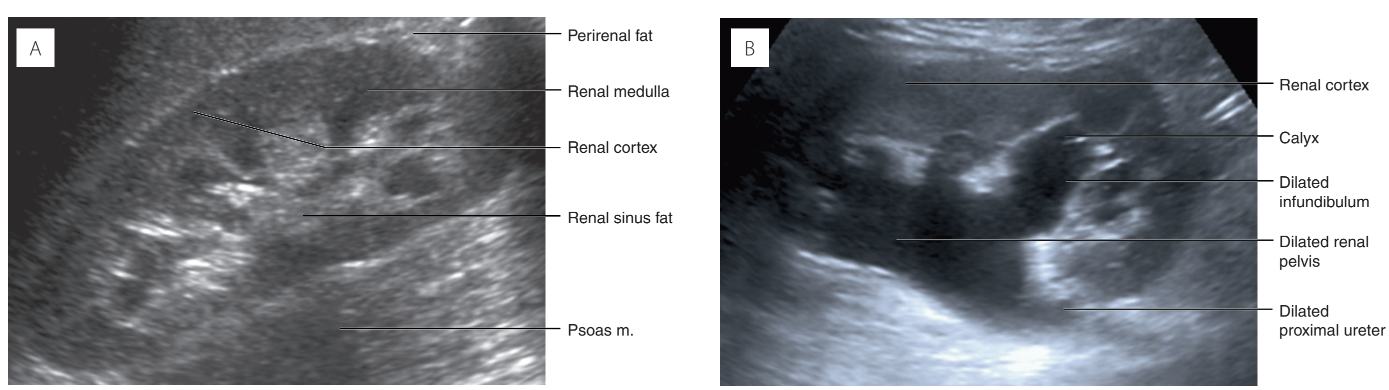


**Fig. 12.12** A longitudinal view ultrasound image through a normal right kidney (A) demonstrates good corticomedullary differentiation but, unlike CT and MR, does not optimally illustrate the perinephric fat. A longitudinal section ultrasound image through a dilated (hydronephrotic) kidney (B) clearly demonstrates the pelvi-calyceal system and proximal ureter. An ultrasound image (C) through a normal kidney illustrates a prominent area of cortex (column of Bertin) due to fusion of the upper and lower pole moieties, also shown on a coronal post contrast CT image (D). An unfused pyramid is illustrated by the dashed lines. An ultrasound image (E) illustrates a triangular-shaped hypoechoic defect in the upper/mid third of the kidney called the inter-renuncular fissure which represents the line of fusion of the upper and lower poles of the fetal kidney; this should not be confused with a scar. A post contrast coronal CT image (F) demonstrates the fissure is continuous with the renal sinus fat.

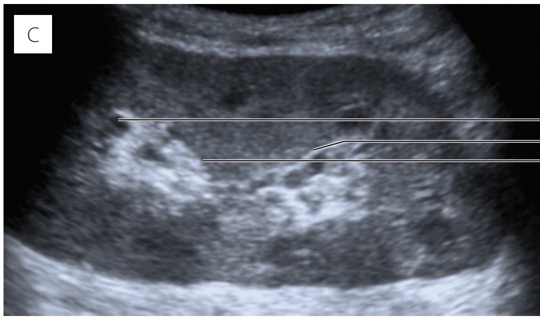


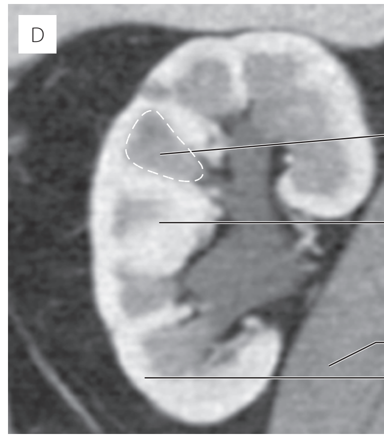


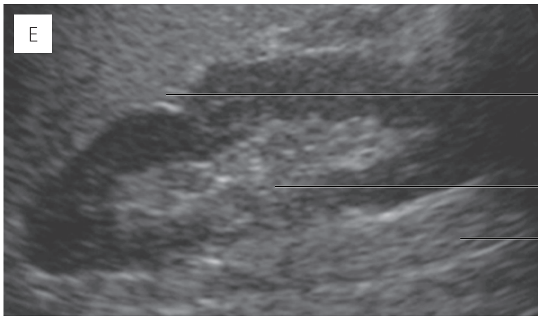


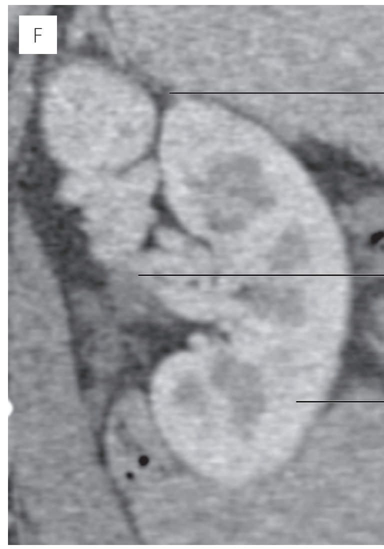


**Fig. 12.12** (*cont.*)

## Embryology of the kidney and ureter

- Develop from the intermediate mesoderm on the dorsal wall of the coelomic cavity, between 5 and 12th weeks.
- Three main components:
  - pronephros
    – involutes completely in the human
  - mesonephros
    - – gives rise to the ureteric (or metanephric) bud, which buds off from the caudal end of the Wolffian duct
    - – ascends and differentiates into:
      - – the collecting system:
        - – ureter
        - – renal pelvis
        - – calyces
  - metanephros
    - – arises from the metanephrogenic blastema, which moulds itself around the developing ureteric bud
    - – ascends and differentiates into:
      - – the nephron or the functional unit of the kidney
        - – glomerulus
        - – Bowman's capsule
        - – collecting tubules.

## Renal ascent and rotation

With development, the kidney migrates superiorly behind the peritoneum, and rotates.

- It migrates superiorly along the posterior abdominal wall and psoas muscles.

**Table 12.1** Summary of the imaging characteristics of the kidneys and ureters

| | Plain films | IVU | US | CT | MRI |
|---|---|---|---|---|---|
| Kidney | Renal outline only seen | Renal parenchyma in nephrographic phase<br>Collecting system in pyelographic phase | Hypoechoic compared to liver parenchyma<br>Collecting system anechoic if distended<br>Echogenic when collapsed | Isodense to liver before contrast<br>Hyperdense to liver post contrast<br>Corticomedullary enhancement at 30–90 s, collecting system visualized > 120 s | Dependent on state of hydration<br>Cortex of higher signal intensity (SI) on T1W (corticomeduallary junction may be seen)<br>High SI to liver on T2W |
| Ureter | Not seen | | Not seen, unless dilated | Isodense before contrast<br>Visualized > 120 s after contrast | Hyperintense on T2W |

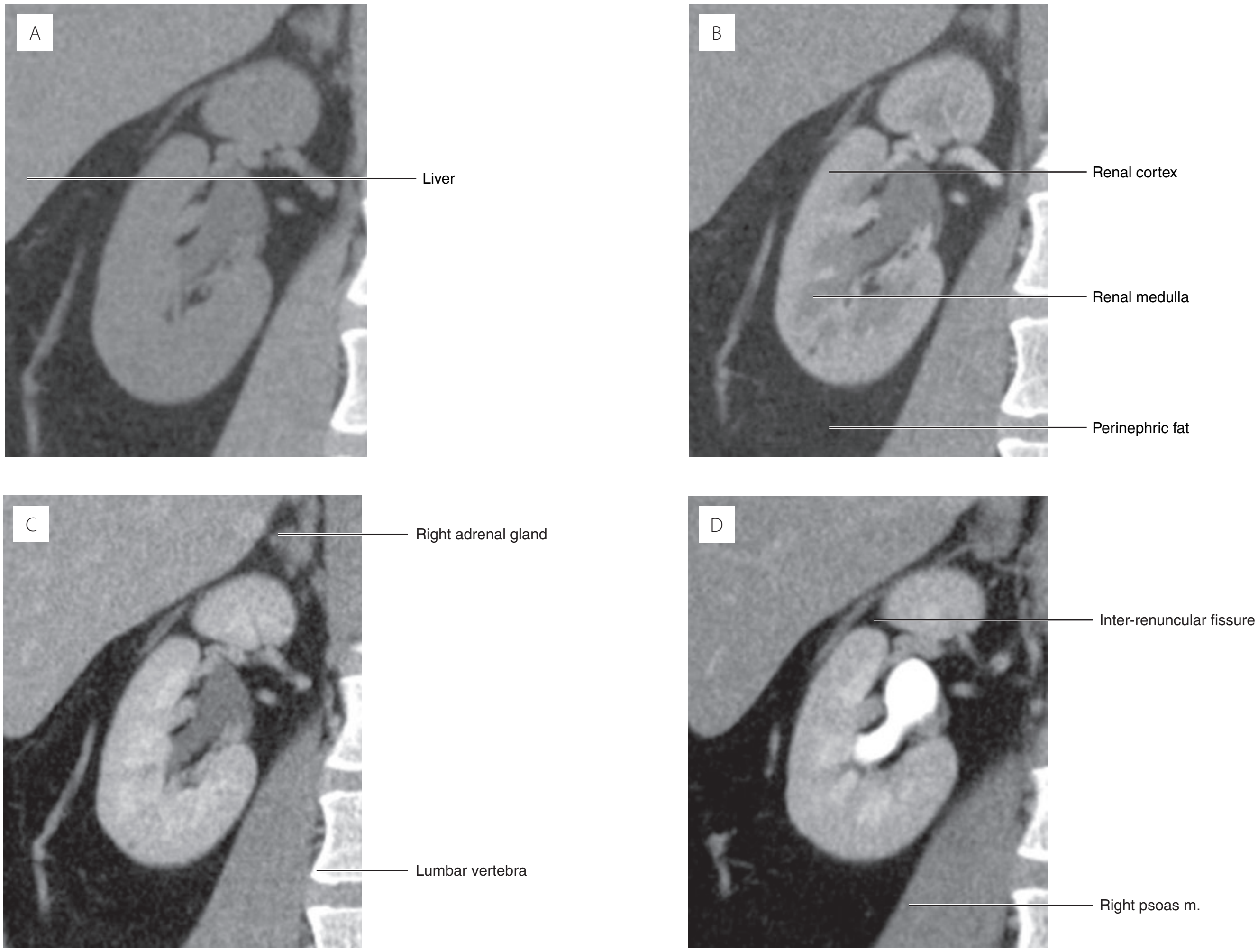


**Fig. 12.13** A series of coronal CT images unenhanced (A) and post contrast in the corticomedullary (B), nephrographic (C) and urographic (D) phases illustrates the differences in corticomedullary differentiation and degrees of opacification of the collecting system.

- As it ascends, the kidney rotates so that its pelvis points anteromedially.
- With ascent, the kidney recruits new arteries superiorly and the lower branches involute. Initially renal arteries are supplied by the iliac arteries and later by the aorta.

Migration (with rotation) explains:

- retroperitoneal position of the kidney and the morphology of the retroperitoneal spaces (see below)
- the frequency of anomalies of:
  - renal ascent and rotation
  - renal arteries and veins.

# Anatomy of the kidney and ureter

## The kidney

### Gross anatomy

The kidney occupies the retroperitoneum between the T12 and L4 vertebral bodies. The right kidney is more inferior, as it is displaced by the liver. This applies in some 75% of cases; in the remainder, the right kidney is higher than the left or at the same height.

- Average length 9–12 cm
- Average breadth 5–7.5 cm; width 2.5 cm
- The left kidney maybe up to 1.5 cm longer than the right kidney in 80% of people
- Weight 125–170 g (males); 115–155 g (females)
- Both kidneys lie obliquely
  - in the coronal plane, the upper pole is medially orientated
  - in the sagittal plane, the upper pole faces more posteriorly
  - in the axial plane, the medial aspect (or the renal pelvis) faces anteromedially.

Most medial is the renal hilum (hilum = a depression or pit on an organ, giving entrance/ exit to vessels and nerves), which from anterior to posterior contains:

- renal vein
- renal artery
- ureter
- lymphatic and sympathetic fibres
- fat (renal sinus fat).

#### Intrarenal anatomy

The kidney is bound by a tough fibro-elastic capsule (which is not visible on imaging) and consists of an outer cortex, with an inner renal medulla composed of up to 12 renal pyramids. Each pyramid originates as an embryologically separate unit. Adjacent pyramids later fuse, but each remains functionally distinct, consisting of a lateral-facing base and a central apex that indents (and drains into) an adjacent calyx. The indenting tip contains the open ends of the collecting tubules, and is known as the renal papilla. Where adjacent pyramids fuse, the cortex can be seen to extend centrally into the medulla as distinct columns (of Bertin).

### The collecting system of the kidney

The functional unit of the kidney (the nephron) is drained by collecting ducts (or ducts of Bellini) that terminate in the papilla to empty urine into the calyx.

- 10–20 collecting ducts empty into each papilla and calyx.
- Typically, each kidney has seven pairs of calyces (seven ventral and seven dorsal calyces), but the number and orientation are highly variable and dependent on the amount of pyramidal fusion.
- Calyces drain into infundibula, which join to form the renal pelvis.
- Calyces are termed either minor/major or simple/compound – minor or simple are small calyces and each drain only a single pyramid. Major or compound calyces are fused adjacent simple calyces, thus larger and drain more than one pyramid. Compound calyces are seen at either pole.
- The infundibula are also variable, but there is usually at least one upper and one lower pole infundibulum (note that sometimes the term major calyx and infundibulum are used synonymously).
- The renal pelvis can also be of variable size in the adult. It is usually intra-renal, but can be extra-renal and hence capacious as it is not constrained by the renal capsule.

**Table 12.2** Relations of the kidney

| | | | |
|---|---|---|---|
| Posterior | | Upper pole | Diaphragm ribs (12th on right, 11th and 12th on left) |
| | | Lower pole | Psoas muscle, quadratus lumborum and transversalis abdominus (medial to lateral) |
| Anterior | | | |
| | Right kidney | Medial | Duodenum, adrenal gland |
| | | Lateral | Right lobe of liver, hepatic flexure and small bowel (superior to inferior) |
| | Left kidney | Medial | Adrenal gland, stomach, pancreas, splenic vessels and jejunum (superior to inferior) |
| | | Lateral | Spleen, splenic flexure |

## The anatomy of the retroperitoneum

The retroperitoneum is divided into three spaces – the perinephric space and the anterior and posterior pararenal spaces. The kidney (and adrenal gland) lies in the most inner perinephric space, suspended by fibrous septa within a fat-containing volume. The boundaries of the perinephric space are tough collagenous renal fascia.

- The perinephric space and renal fascia:
  - Gerota's fascia – anterior
    – continues medially in front of the kidneys and fuses in front of the great vessels with the contralateral anterior renal fascia
  - Zuckerkandle's fascia – posterior
    – passes behind the kidney to merge with the fascia of quadratus lumborum and psoas major, to attach to the vertebral column.
  - The two renal fascia fuse superiorly above the adrenal glands (although sometimes incompletely, such as around the bare area of the liver), and also laterally to form the lateral conal fascia. Inferiorly, it remains variably open.
  - The perinephric boundaries can be likened to an upturned sock. Thus, perirenal urine leaks or haemorrhage do not spread across the midline but can potentially spread down into the pelvis. However, with maldeveloped or malascended kidneys (e.g. a horseshoe kidney), the fascial integrity may be incomplete and contralateral spread may be seen. Fascial integrity may also be disrupted by inflammatory change, malignancy or after surgery.
- The pararenal spaces complete the retroperitoneum. Unlike the perinephric space, they communicate across the midline.
  - The anterior pararenal space contains the duodenum and pancreas (discussed elsewhere).
  - The posterior pararenal space contains fat alone.

## Neurovascular and lymphatic anatomy

### Renal arteries

#### Main renal artery

- Most commonly a single renal artery arising from the abdominal aorta, at L1/2 interspace
- Accessory arteries occur in 20–25% of people. A lower pole artery is the commonest and bilateral in 15%
- Receives up to 30% of cardiac output

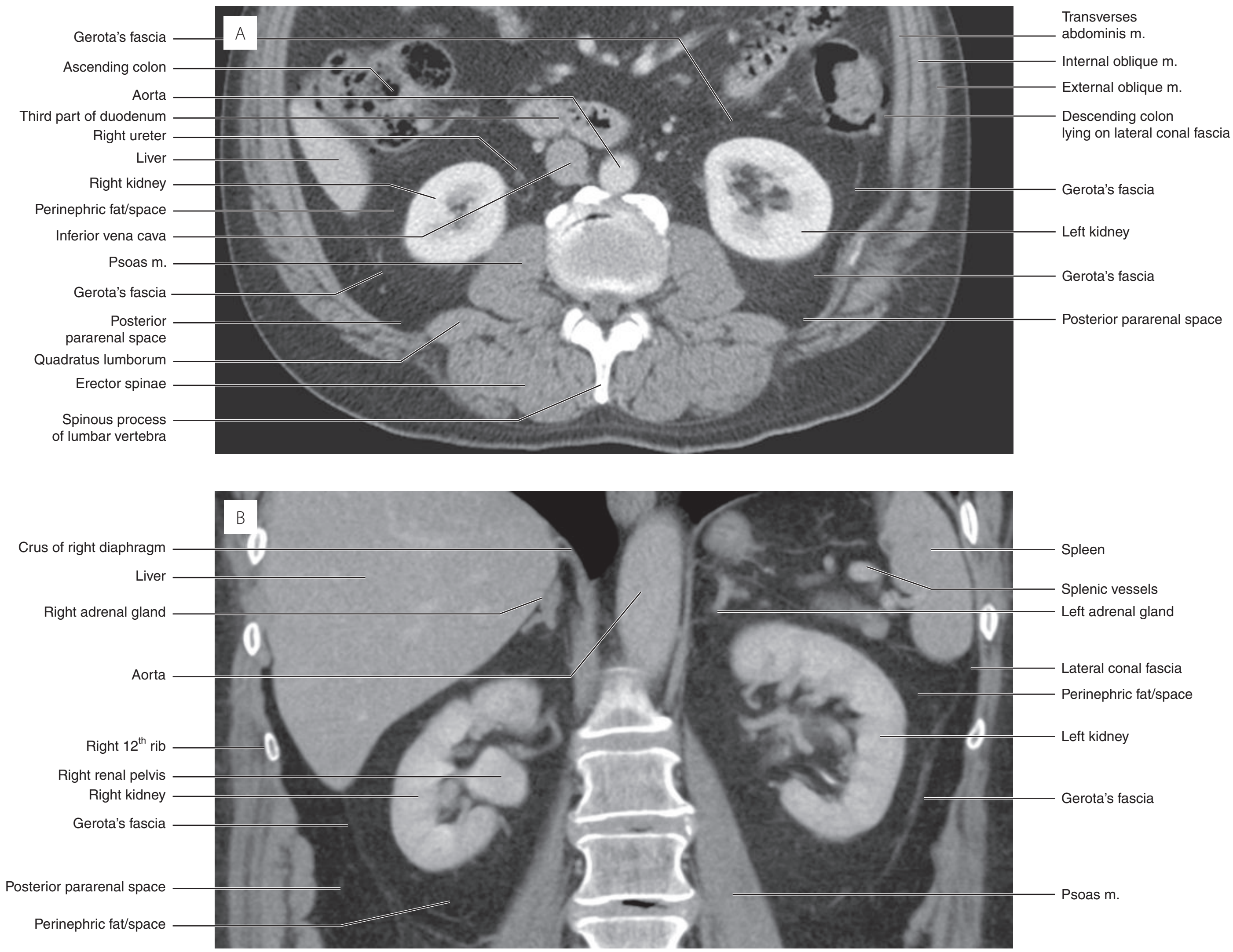


**Fig. 12.14** Portal-venous phase post contrast axial CT (A) and coronal CT urogram (B) images illustrating the perinephric space and surrounding fascial planes. Note that on the coronal image (B), Gerota's fascia is a closed unit superiorly, encasing the adrenal glands and kidneys, but is deficient inferiorly.

- Lies anterior to renal pelvis, posterior to renal vein
- Right renal artery:
  - longer than left
  - downward course and passes posterior to the inferior vena cava
- Left renal artery:
  - arises higher than the right renal artery
  - has a more horizontal orientation.

### Intra-renal arterial anatomy

- The main renal artery divides into segmental arteries near the hilum.
- The first division is classically a posterior segmental branch, supplying the posterior and apical kidney.
- The main renal artery then divides into 4 further segmental branches at the hilum (apical, upper, middle and lower anterior), supplying the anterior surface, lower pole and variable portion of the apex.
- Segmental arteries branch into lobar arteries.
- Lobar arteries divide into interlobar branches (lie between pyramids/lobes)
  - these branch into arcuate arteries that run along the base of the pyramids
  - arcuate arteries branch laterally into the terminal intralobular arteries.

## Renal vein

Renal venules and branch renal veins freely communicate throughout the parenchyma, but finally drain only into the main renal vein.

- The left renal vein is three times longer than the right renal vein:
  - 6–10 cm in length
  - courses anteriorly, between the superior mesenteric artery and aorta
  - enters the medial aspect of inferior vena cava (IVC)
  - three tributaries:

  - left adrenal vein
  - left gonadal vein
  - lumbar veins (variable number).
- The right renal vein is 2–4 cm in length and has no tributaries.
- The commonest normal variant are multiple veins, which occur in 15–30% (commoner on the right).
- Commonest left renal vein anomaly is a circumaortic left renal vein (5–7% of individuals), where the vein bifurcates into anterior and posterior limbs that encircle the aorta.
- The retro-aortic left renal vein (3%) may enter the IVC or have an abnormal caudal course, entering the iliac vein.

## Lymphatic drainage

- Follows the arteries to the para-aortic lymph nodes.

# Anatomy of the ureter

Connects the renal pelvis to the bladder, and is 25–30 cm long.

- Three layered wall:
  - outer adventia
  - middle smooth muscle
  - inner transitional cell epithelium.
- Diameter of approximately 3 mm but has three ‘functionally’ narrow regions:
  - junction of renal pelvis with ureter (the pelviureteric junction)
  - as the ureter crosses bony pelvic brim
  - intravesical ureter where it runs obliquely through the muscular bladder wall (this acts as a reflux-preventing valve).
- Relations (see Figs. 12.7 and 12.8):
  - posterior – psoas muscle, genitofemoral nerve, sacroiliac joint and common iliac vessels, tips of the transverse processes of L2–L5 lumbar vertebrae
  - anterior
    - right – duodenum, gonadal and colic artery
    - left – gonadal and colic artery, sigmoid mesentery.

**Table 12.3** Relations of ureter within the pelvis

| Male | Female |
|---|---|
| Superior and anterior to seminal vesicle | Close to lateral fornix of vagina |
| Inferior to vas deferens | 2.5 cm lateral to cervix |
| | Passes inferior to uterine artery in the broad ligament |
| The ureter deviates laterally at the ischial spines before turning medially, to enter the posterior wall of the bladder | |


**Fig. 12.15** A selective right renal artery angiogram clearly illustrates the main renal artery and branches down to the smaller cortical vessels that are end-arteries. Note the right inferior adrenal artery and a right ureteric artery arising directly from the right renal artery. The remaining ureteric arteries arise from numerous sources.

**Table 12.4** Common normal variants of the kidney and ureter

| Anomaly | Incidence | |
|---|---|---|
| Renal agenesis | 1:1000–1500 | More common on left<br>Other anomalies may be present, e.g. seminal vesicle cyst |
| Pelvic kidney | 1:600 | Failure of migration<br>Receives blood supply from internal iliac artery |
| Horseshoe kidney | 1:1000 | Fusion of lower poles of the kidneys |
| ‘Pancake’ (discoid) kidney | Very rare | Both kidneys are pelvic in location and fused |
| Crossed renal ectopia | 1:1000 | The ectopic kidney has crossed contra-laterally and its upper pole is fused with the lower pole of the normal kidney. However, the ureteric orifices are still normally sited in the bladder. |
| Duplex kidney and ureter | 1: 160<br>M:F = 1:2<br>20% bilateral | If two ureteric buds develop (see above: embryology) then two completely separate ureters with two ureteric orifices are seen – a complete duplex kidney. If a single ureter bifurcates early then a partial duplex kidney results<br>• Commoner in first-degree relatives and 20% bilateral<br>• Affected kidney larger<br>• Ureter draining the upper pole will have an ectopic more caudal insertion into the bladder (Weigert-Meyer rule) but can occasionally insert even more caudally, into the urethra or vagina<br>• Upper pole moiety may obstruct or have a ureterocoele (dilatation of the intramural ureter)<br>• Lower pole moiety tends to reflux due to a less oblique, incompetent course through the bladder wall (has a ‘drooping flower’ configuration on IVU) |

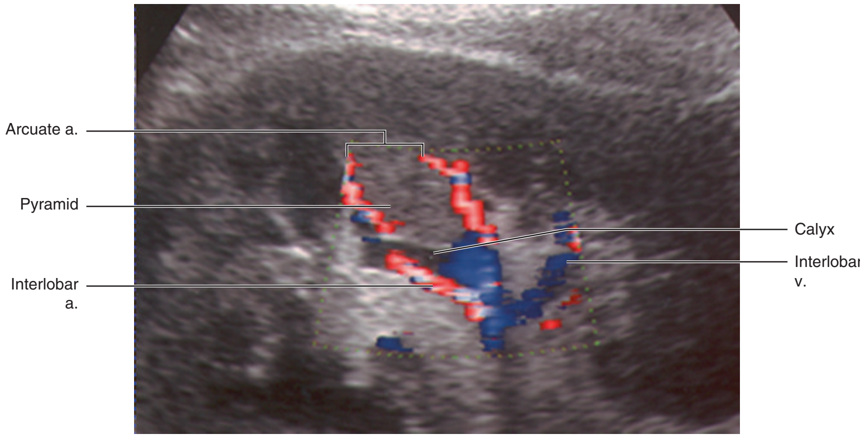


**Fig. 12.16** An ultrasound image with colour Doppler demonstrating that the renal vasculature can be visualized with interlobular vessels associated with a calyx.

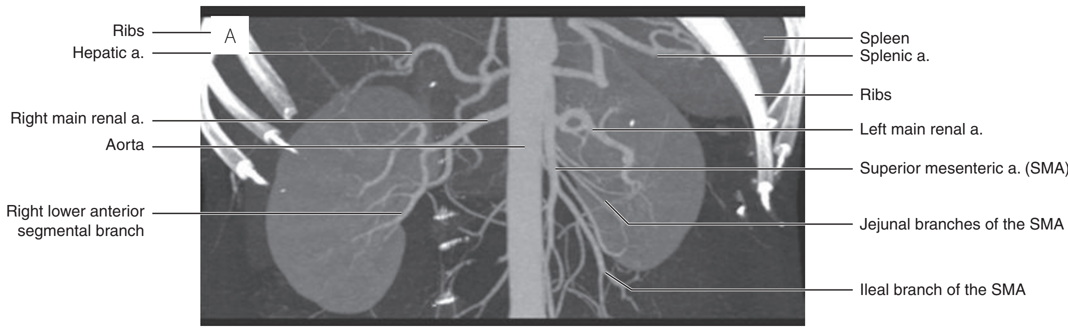


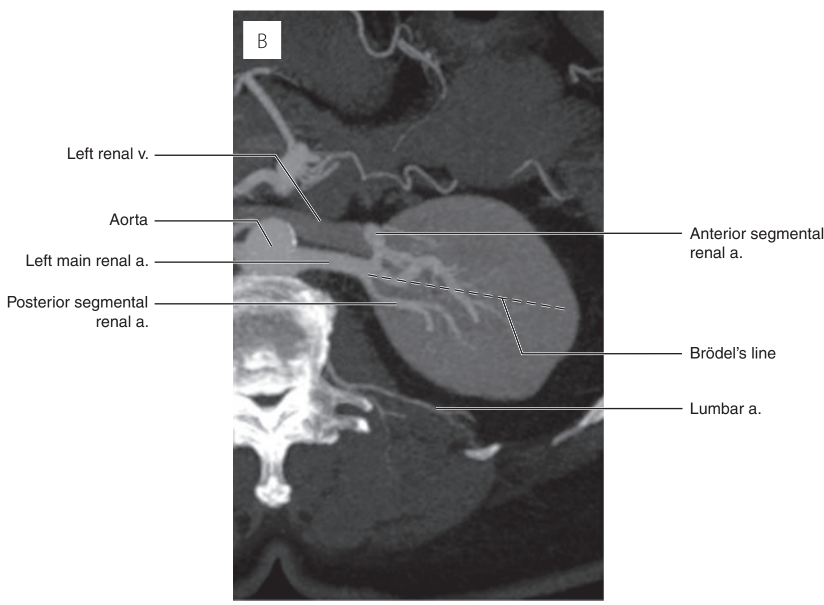


**Fig. 12.17** A coronal CT angiogram MIP (A) illustrates the abdominal and renal vasculature, with multiple branches shown, in contrast to MRA imaging where fewer intrinsic branches are seen (see C). An axial CT angiogram MIP (B) demonstrates the avascular line running between the anterior and posterior renal branches through the longitudinal plane of the kidney – Brödel's line (dashed line). A coronal MRA MIP (C) shows less detailed vascular anatomy than CT but allows clear visualization of the main renal arteries.

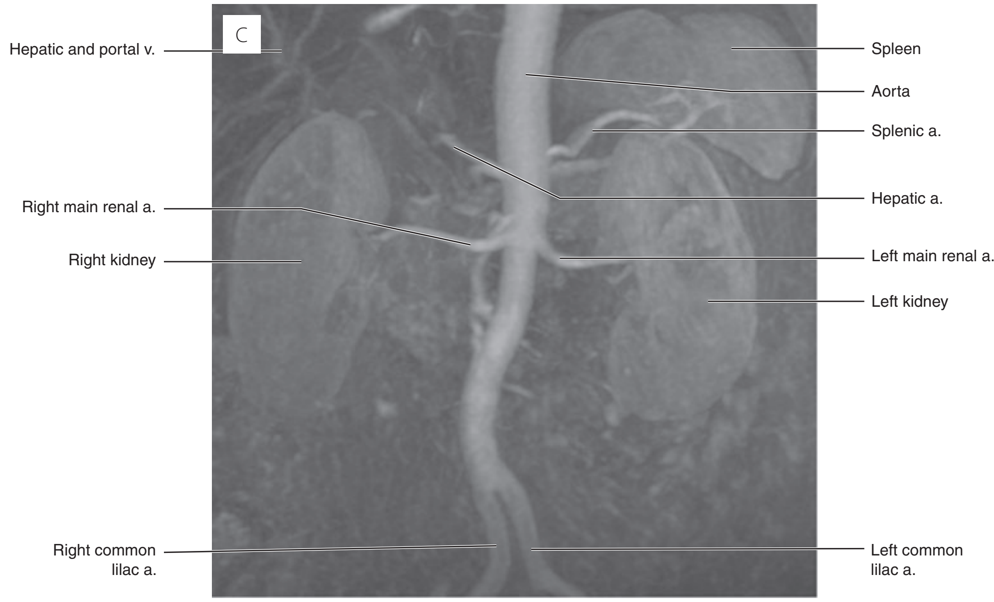


**Fig. 12.17** (*cont.*)

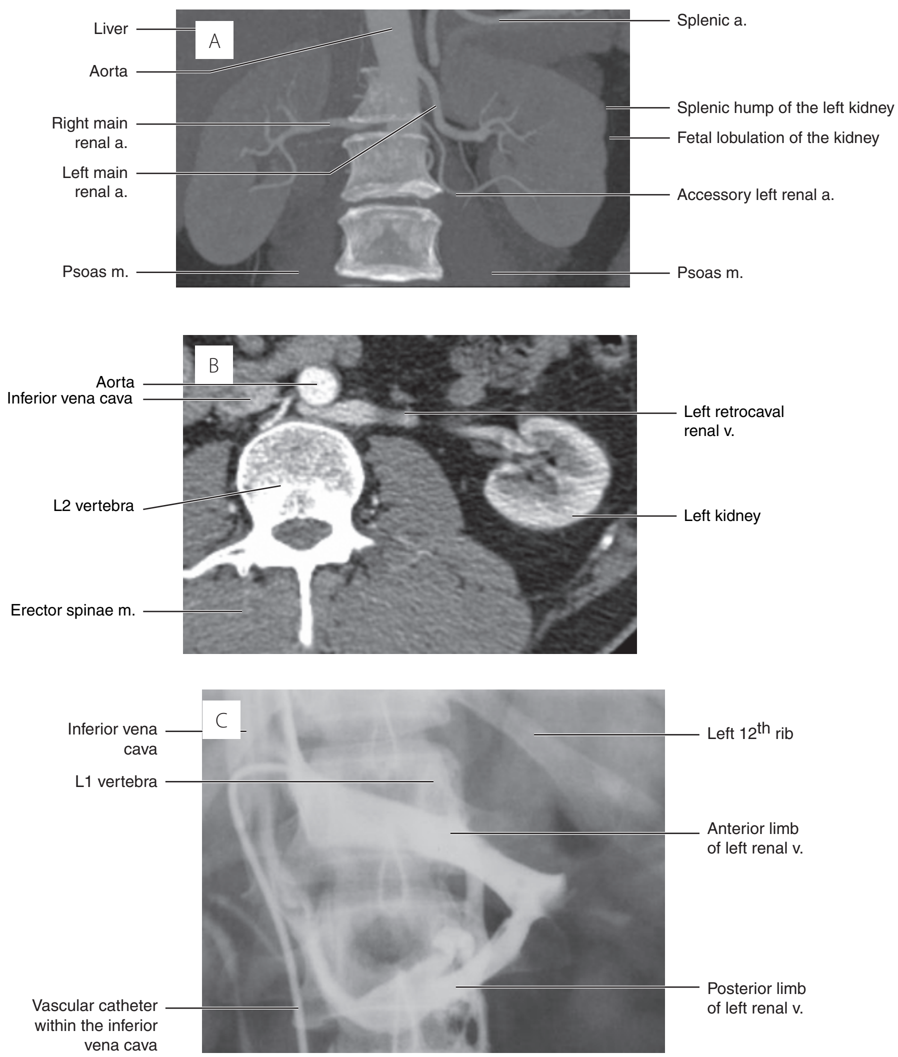


**Fig. 12.18** Montage of commonly encountered vascular anomalies. (A) A coronal CTA MIP illustrating an accessory left renal artery arising from the aorta and a splenic (dromedary) hump of the left kidney. Accessory renal arteries occur in 20–25% of individuals. (B) An axial post contrast (portal venous phase) CT illustrating a retrocaval left renal vein (commonest left renal vein anomaly with an incidence of 5–7%) draining into the inferior vena cava. (C) A renal selective venogram showing the anterior and posterior limbs of a left circumaortic renal vein draining into the IVC, which occurs in 3% of individuals.

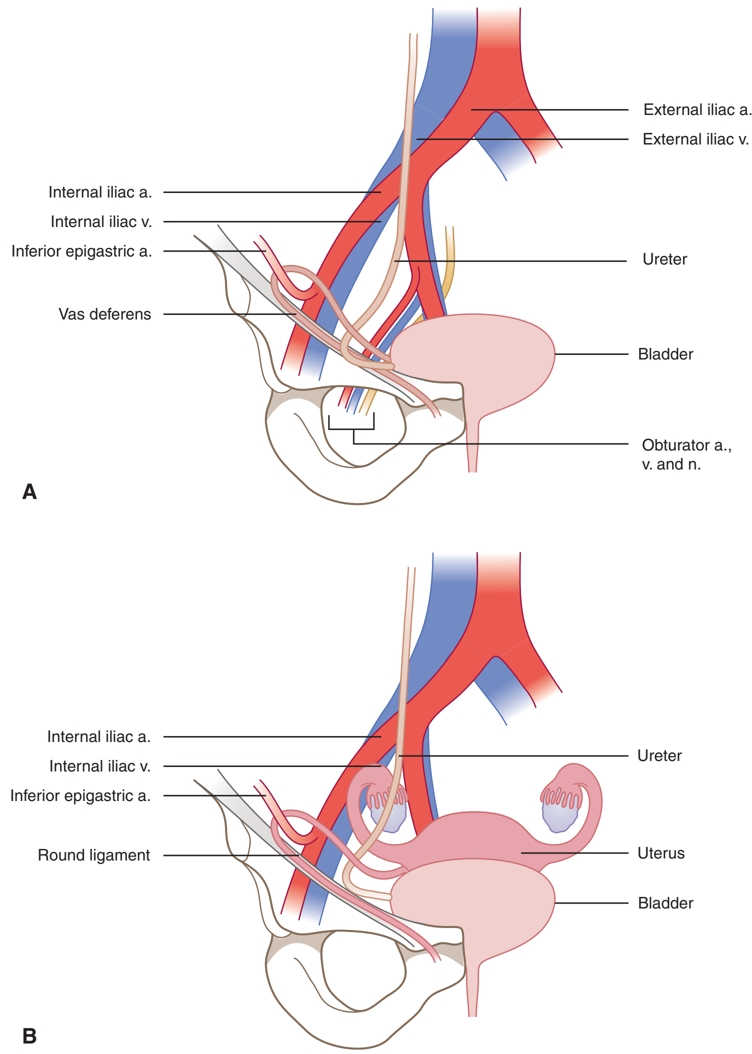


**Fig. 12.19** Diagram A illustrates the relations of the ureter (yellow) in the male pelvis, which lies anterior to the external iliac artery and vein and posterior to the vas deferens. Diagram B illustrates the female pelvis and the ureter (yellow), which lies anterior to the external iliac artery and vein and posterior to the uterine artery and round ligament.

## Neurovascular anatomy

- Arterial supply is highly variable
  - upper ureter – branch from renal artery
  - mid ureter – small medial branches from the aorta
  - lower ureter – small laterally orientated branches from the superior and inferior vesical, middle rectal and uterine arteries.
- Venous drainage is highly variable and not defined.
- Lymphatic drainage
  - abdominal ureter drains to:
    – aorto-caval and common iliac nodes
  - pelvic ureter drains to:
    – internal and external iliac nodes.
- The nervous supply derives from the adjacent renal, aortic and hypogastric autonomic plexuses.
  - Afferent fibres travel with the sympathetic nerves to the spinal cord at T12 – L2.
  - They have an unclear function as the ureteric peristalsis will continue without innervation. Ureteric pain is typically referred loin to groin.

# Anatomy of the adrenal (suprarenal) gland

## Radiology and the adrenal gland

### Plain radiography, ultrasound, CT and MRI

The normal adrenal is never seen on plain films. On ultrasound it is easily seen in neonates (because it is larger) but rarely in adults. It has a thin reflectile core, with a transonic outer portion. On CT and MRI, the adrenals are almost always seen but are clearest in those with sufficient retroperitoneal fat (see Fig. 12.20), as summarized in Table 12.5.

## Nuclear medicine

Various scintigraphic methods and agents are used to provide metabolic information. MIBG (analogue of guanethidine) is used to image medullary disorders (such as phaeochromocytoma) as it is concentrated in sympathoadrenal tissue. Positron

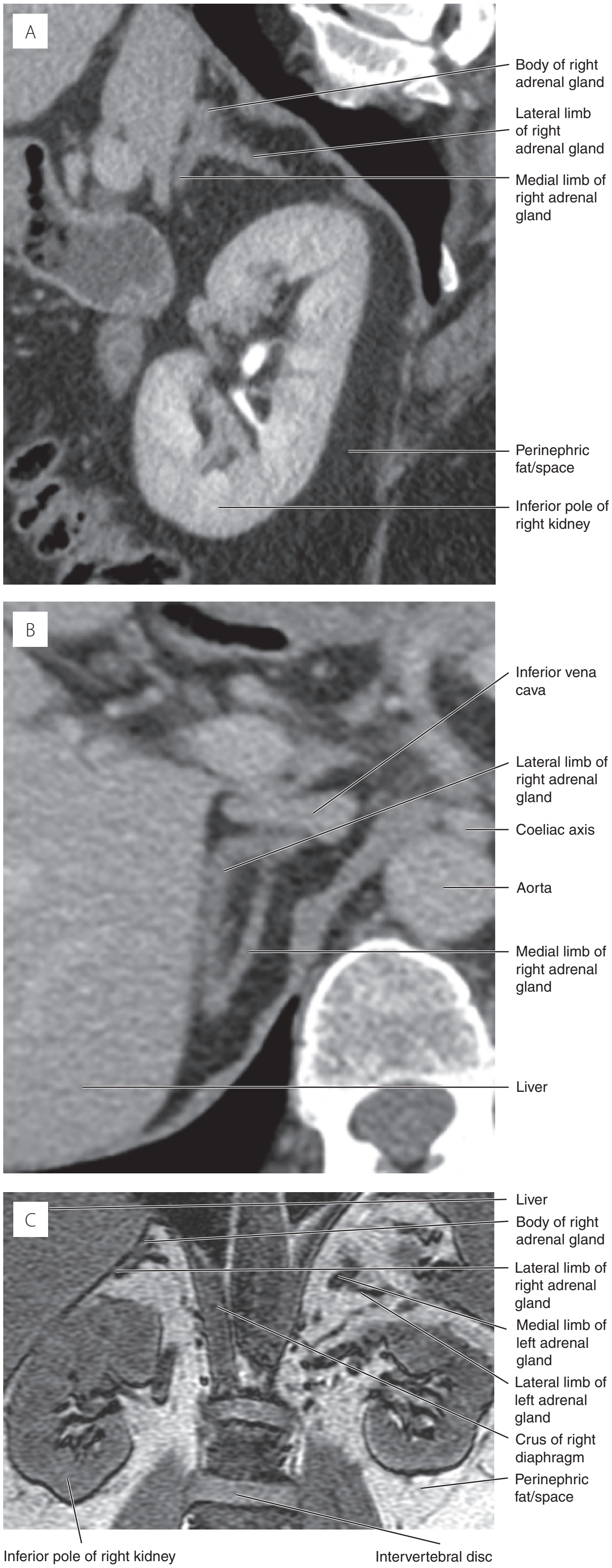


**Fig. 12.20** Sagittal oblique CT image (A), post contrast axial CT (B) and coronal MR T1-weighted out of phase (C) images depicting the differing shapes of the adrenal gland. The right adrenal gland is commonly an inverse Y shape and the left adrenal gland, crescentic or V-shaped.

**Table 12.5** Summary of the imaging characteristics of the adrenals

| Plain films | IVU | US | CT | MRI |
|---|---|---|---|---|
| Not seen | Not seen | Seen in neonates, rarely in adults | Isodense before contrast | Intermediate SI to liver and hypointense to fat on T1W |
| | | Hypoechoic | Enhances poorly | Isointense to liver and hypointense to fat on T2W |
| | | | | Adrenal cortex is hyperintense to the medulla on T1W |

**Table 12.6** Relations of the adrenal gland

| | | |
|---|---|---|
| Right | Anterior | IVC, liver |
| | Posterior | Crus of diaphragm, right kidney |
| Left | Anterior | Lesser sac, stomach, spleen, splenic vein, pancreas |
| | Posterior | Crus of diaphragm, left kidney |
| | Medial | Coeliac ganglion, inferior phrenic and gastric arteries |

emission tomography (PET) with fluorine-18 (F-18) fluorodeoxyglucose (FDG) can be used to differentiate between benign and malignant adrenal lesions depending on the degree of FDG uptake.

## The adrenal gland

Paired retroperitoneal glands, supero-medial to the kidneys within the perinephric space, but outside the renal capsule.

- Develop between weeks 4 and 8 of gestation
- Endocrine organs with an:
  - outer cortex of mesodermal origin
    - three zones – zona glomerulosa, zona fasciculata and zona reticularis, that are fully differentiated by the third year of life
    - lipid-rich and secretes corticosteroids (aldosterone) and androgens
  - inner medulla
    - derived from neural crest cells, that migrate and inter-digitate into the developing renal cortex
    - darker colour
    - related to the sympathetic nervous system and secrete catecholamines
- At birth, the cortex is much larger and later regresses. The adrenal glands are 1/3 the weight of the adjacent kidney at birth, but 1/30 in the adult.
- Adult dimensions:
  - cranio-caudal length 2–4 cm
  - body – right 4–8 mm, left 6–10 mm
  - width of limbs 3–4 mm

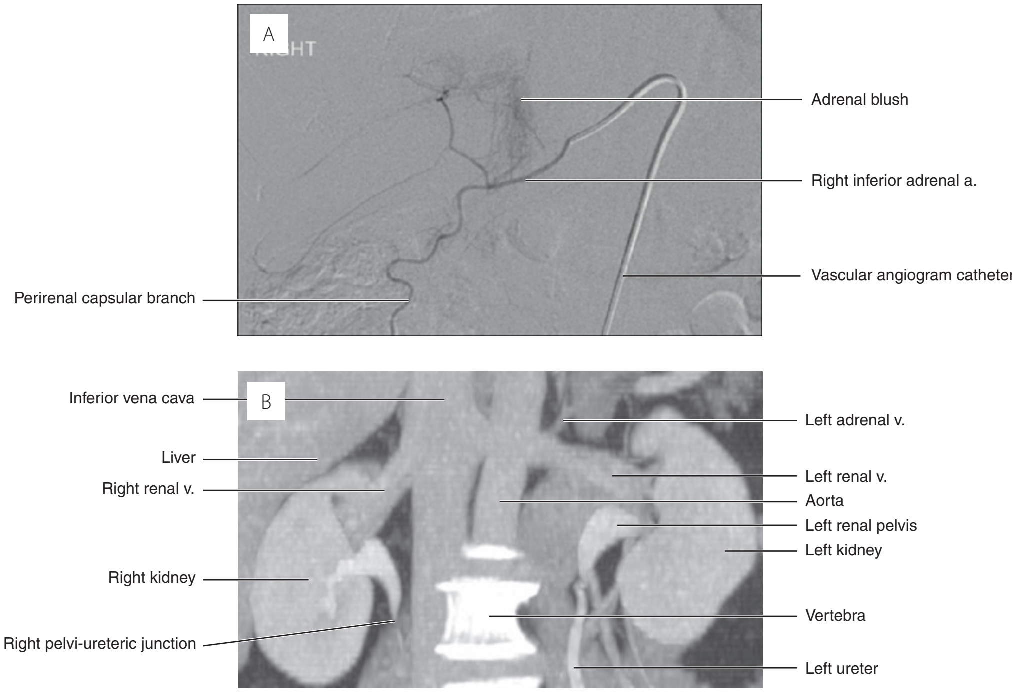


**Fig. 12.21** A selective adrenal angiogram (A) illustrates the right inferior adrenal artery arising directly from the aorta. A CT urogram MIP (B) demonstrates a left adrenal vein draining into the left renal vein.

- Variable shape
  - right gland is linear or inverted 'V' shape
  - left gland is inverted 'Y' or 'V'.

## Neurovascular and lymphatic anatomy

Three arteries on each side:

- superior adrenal artery from the inferior phrenic artery (which is a branch of the abdominal aorta)
- middle adrenal artery arises from the abdominal aorta
- inferior adrenal artery from the renal artery.

A single vein drains each gland.

- The shorter right adrenal vein drains directly into the IVC.
- The longer left adrenal vein empties into the left renal vein and may be joined by the inferior phrenic vein.

Neural anatomy:

- preganglionic sympathetic fibres from the splanchnic nerves
- postganglionic vasomotor fibres are distributed with the arteries supplying the gland to regulate its blood flow.

## Normal variants of the adrenal glands

- Unilateral absent glands are unknown.
- Ectopic adrenal cortical tissue may occur nearby (usually around the coeliac axis) but may also be displaced with the descending gonads during embryological development, and be found in the broad ligament, spermatic cord, testis or epididymis. Ectopic adrenal tissue is present in up to 50% of neonates, but only 1% of adults as it involutes. More distal ectopic adrenal tissue contains cortex alone.

Chapter 13

# The male pelvis

Nevin T. Wijesekera, Michael A. Gonsalves and Uday Patel

## Diagnostic modalities used to image the male pelvis

### Plain radiography and contrast studies (Fig. 13.1)

- Plain radiography is generally not useful to examine the soft tissues of the male pelvis.
- Intravenous urography can normally delineate the ureters and bladder.
- Cystourethrography is used to image the male urethra.

### Cross-sectional imaging

- Soft tissues of the pelvis can be demonstrated using ultrasound, CT and MRI.
- Ultrasound and MRI have the advantage of not using ionizing radiation.

#### Ultrasound

- First-line modality for assessment of the male genitourinary tract.
- Transabdominal ultrasound is used to examine the bladder, typically using a low-frequency curvilinear probe, and requires a full bladder to act as an acoustic window.
- Transrectal ultrasound is used to evaluate the prostate gland, especially to direct prostate biopsy.
- High-frequency linear probes are used to visualize the testes, penis and, less frequently, the urethra.

#### CT

- CT is generally not a first-line imaging test for evaluating male pelvic disorders, as radiation exposure to radiosensitive tissues (especially the testes) should be avoided. However, CT remains the best imaging study for the assessment of pelvic anatomy and pathology in the trauma setting.
- CT has lower contrast resolution than MRI, thus has a relatively limited role in the evaluation of soft tissue structures such as the prostate and penis.

#### MRI

- MRI offers superior contrast resolution and multiplanar imaging capability.
- MRI demonstrates the soft tissues of the male pelvis better than any other imaging modality.
- T1-weighted (T1W) images are the best sequence for defining anatomy, whereas T2-weighted (T2W) images are best for evaluating pathology.

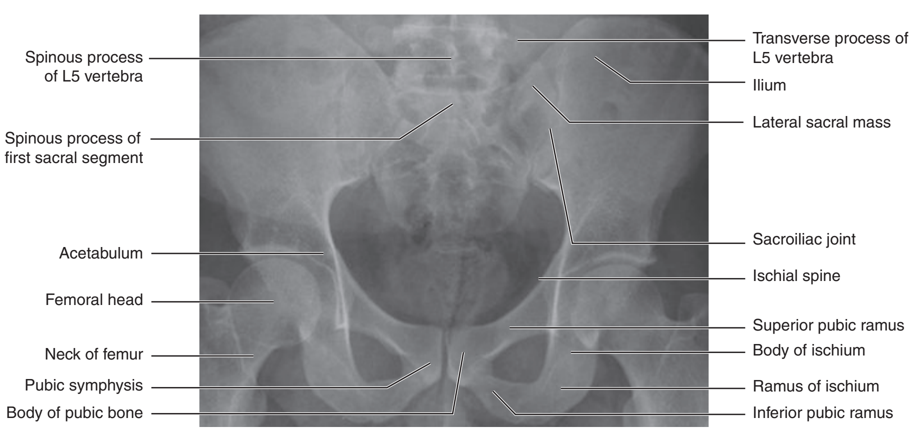


**Fig. 13.1** AP radiograph of male pelvis.

*Applied Radiological Anatomy, 2nd Edition* ed. Paul Butler, Adam W.M. Mitchell and Jeremiah C. Healy. Published by Cambridge University Press.

### Doppler ultrasound / CT and MR angiography / invasive angiography

- Ultrasound (with colour flow and pulsed-wave Doppler techniques), contrast-enhanced CT and MRI are able to assess the pelvic vasculature.
- Invasive pelvic angiography remains the gold standard, particularly for delineating the internal iliac arterial tree.

## Anatomy of the male pelvis

## Pelvic floor and male perineum (Figs. 13.2–13.5; Table 1)

- The pelvic floor supports the pelvis viscera and is composed of a sling of muscles and fascia, pierced anteriorly by the urethra and posteriorly by the rectum.
- The perineum is a region below the pelvic floor, between the anus and scrotum in males.

### Male urogenital triangle

- An imaginary line drawn between the ischial tuberosities divides the perineum into an anterior urogenital triangle and a posterior anal triangle (the latter is the same in both males and females).
- The urogenital triangle is bounded in front by the pubic arch and laterally by the ischial tuberosities. In males, the triangle contains the penis and scrotum.

**Table 13.1** Boundaries of the perineum

| | |
|---|---|
| Anterior | Pubic symphysis |
| Posterior | Coccyx |
| Anterolateral | Ischiopubic rami and ischial tuberosities |
| Posterolateral | Sacrotuberous ligaments (run from the sacrum to the ischial tuberosities) |
| Deep limit | Inferior surface of the pelvic diaphragm |
| Superficial limit | Skin |

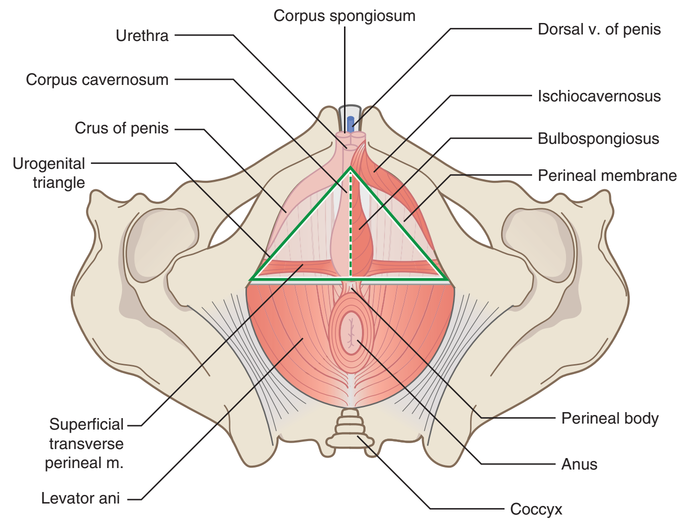


**Fig. 13.2** Root of penis and perineal muscles.

- The urogenital diaphragm is a triangular musculofascial membrane situated in the anterior part of the perineum. The inferior layer of fascia of the urogenital diaphragm is referred to as the perineal membrane.
- The urogenital triangle is divided into two parts by the perineal membrane: the deep perineal pouch above the membrane and the superficial perineal pouch below it.
- Deep perineal pouch:
  - bounded superiorly by the fascia of the pelvic floor and inferiorly by the perineal membrane
  - in males, it contains:
    - (a) deep transverse perineal muscles
    - (b) sphincter urethrae, formed of voluntary muscle
    - (c) paired bulbourethral (or Cowper's) glands, whose ducts open into the bulbous urethra below the perineal membrane.

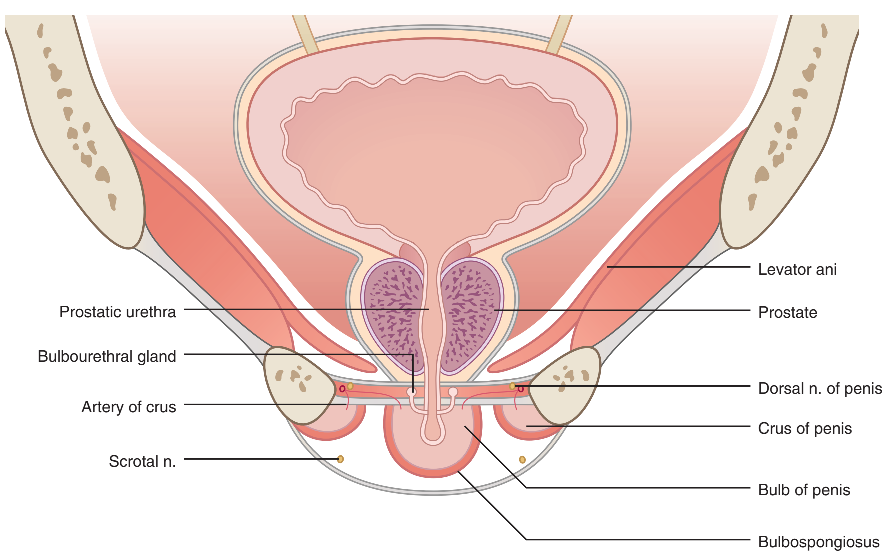


**Fig. 13.3** Coronal section of the male pelvis showing the prostate, the urogenital diaphragm and the superficial perineal pouch.

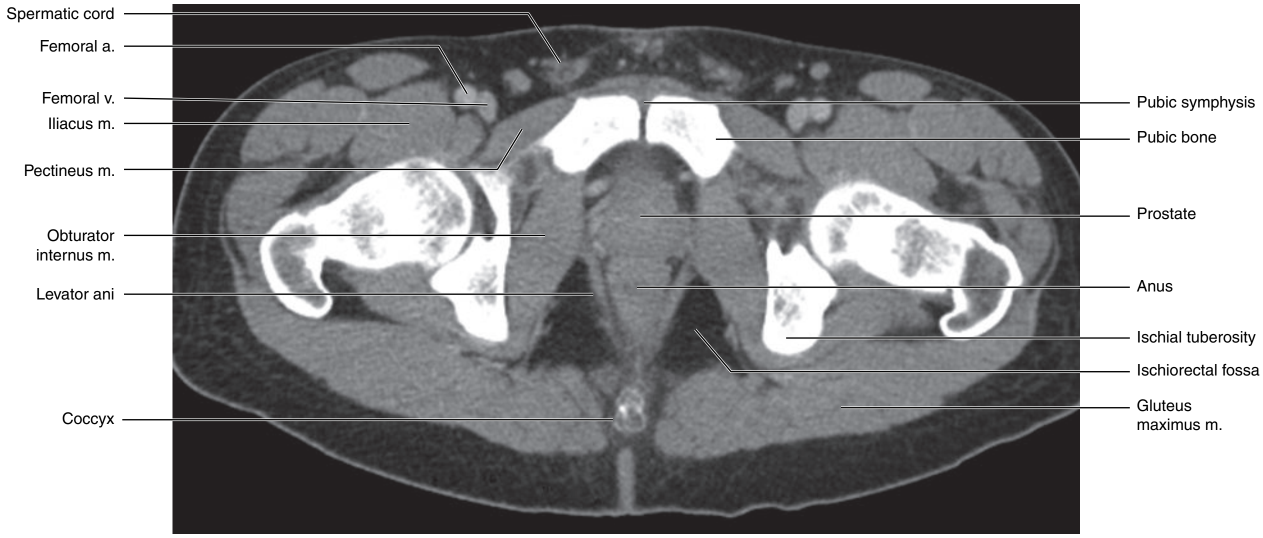


**Fig. 13.4** CT scan of the male pelvis: axial section through the perineum.

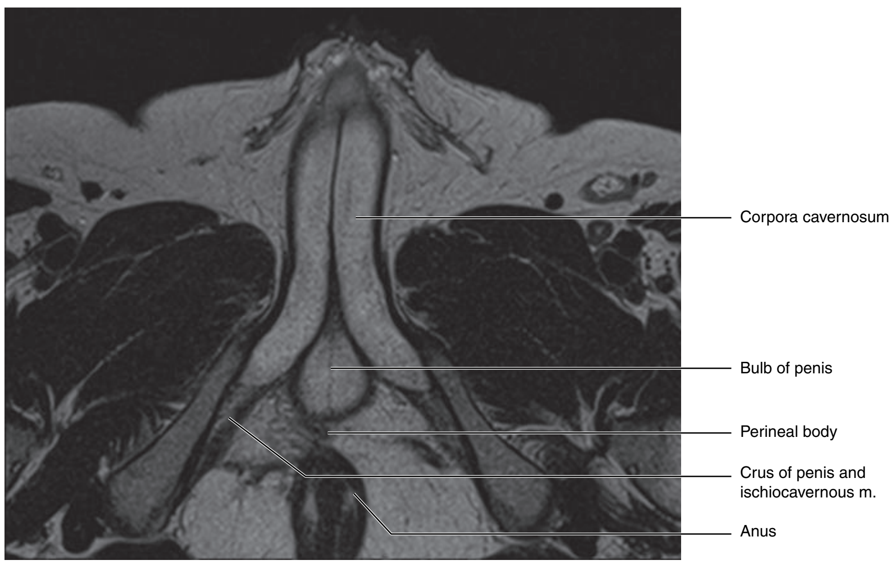


**Fig. 13.5** MR image of the male perineum: axial section through the bulb of the penis.

- Superficial perineal pouch:
  - bounded superiorly by the perineal membrane and inferiorly by the investing fascia of the superficial perineal muscles
  - in males, it contains:
    - (a) bulbospongiosus muscle, which covers the corpus spongiosum and surrounds the urethra, the whole forming the bulb of the penis
    - (b) paired ischiocavernosus muscles, which arise from the ischial ramus and cover the corpora cavernosa of the penis
    - (c) superficial perineal muscles, which run transversely from the perineal body to the ischial rami.
- In the midline, at the junction of the anterior and posterior perineum, lies the fibromuscular perineal body, to which the anal sphincter, bulbospongiosus, transverse perineal and levator ani muscles are attached.

### Imaging of the male pelvic floor

- CT and MRI (Figs. 13.6, 13.7):
  - Both modalities provide excellent visualization of the muscles of the pelvis.
  - MRI is particularly well suited to demonstrate the pelvic floor and viscera.

## Bladder and male urethra

### Bladder (Fig. 13.8; Table 13.2)

- The empty bladder is a three-sided pyramid that has a base, neck, apex, superior surface and two inferolateral surfaces.
- The bladder is anchored inferiorly by condensations of pelvic fascia and, in males, by the prostate.
- The ureters enter the posterolateral angles of the bladder and pass obliquely through the wall for approximately 2 cm before entering the bladder cavity.

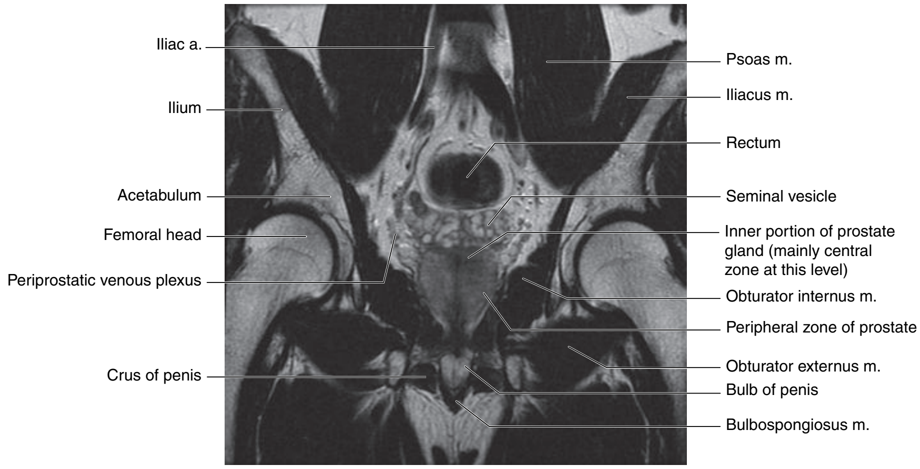


**Fig. 13.6** MR image of the male pelvis: coronal section.

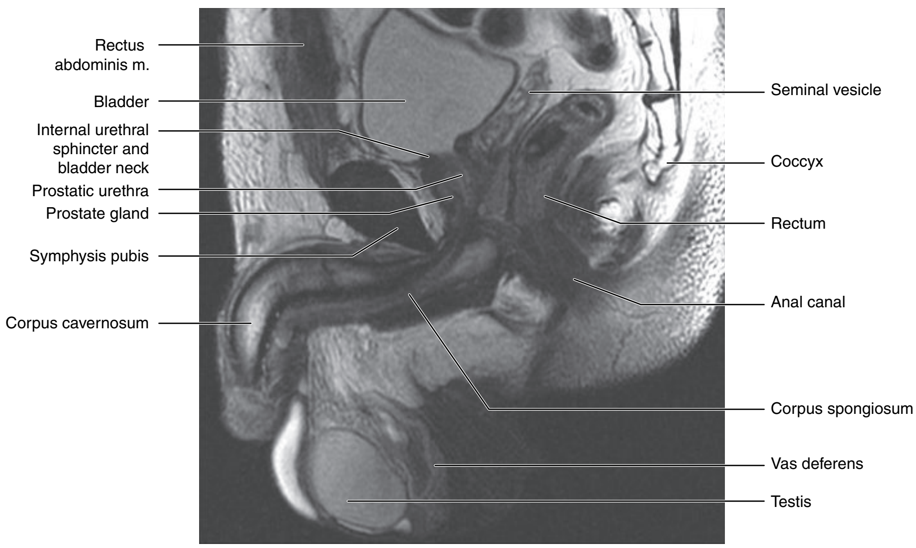


**Fig. 13.7** MR image of the male pelvis: sagittal section.

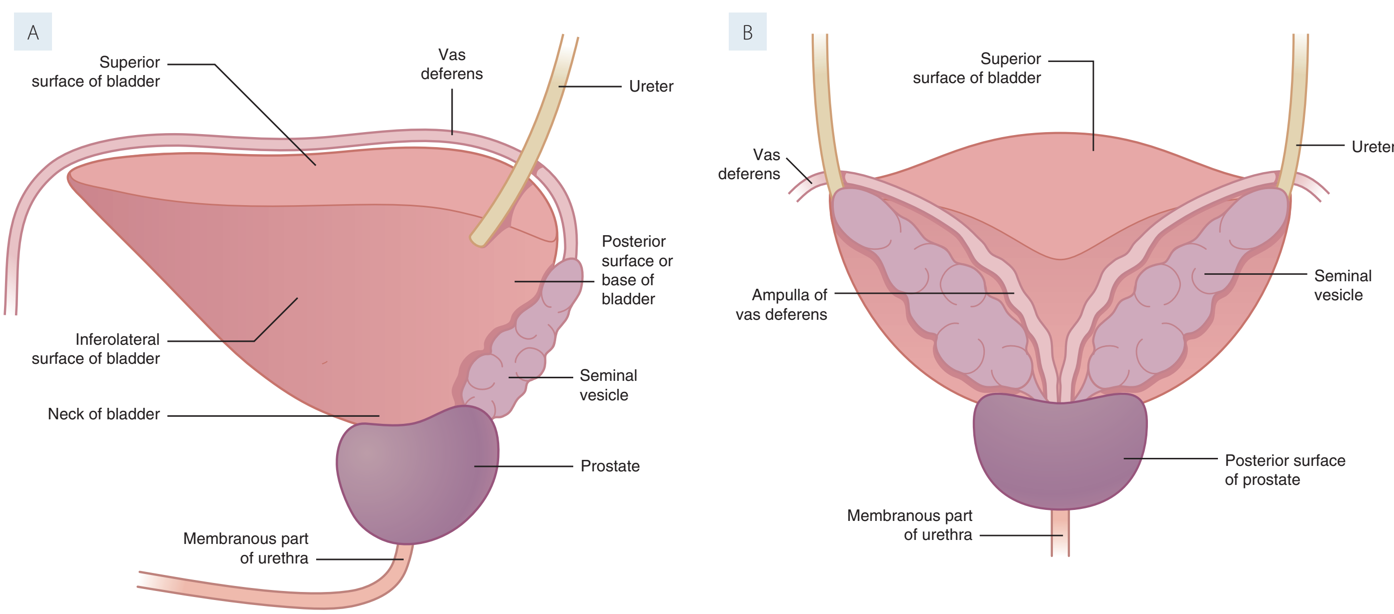


**Fig. 13.8** (A) Lateral view of the bladder, prostate and seminal vesicle. (B) Posterior view of the bladder, prostate, vasa deferentia and seminal vesicles.

**Table 13.2** Relations of the bladder

| Surface | Relations |
|---|---|
| Base | Separated from rectum by rectovesical pouch above and by seminal vesicles and vas deferens below |
| Neck | Base of prostate |
| Apex | Symphysis pubis |
| Superior | Covered by peritoneum |
| Inferolateral | Retropubic fat pad (anteriorly), obturator internus muscle and levator ani (posteriorly) |

- The trigone is a triangular area at the base of the bladder between the two ureteral orifices (superolaterally) and the internal urethral orifice (inferomedially).
- A transverse ridge, known as the interureteric bar, connects the ureteric orifices.
- When the bladder fills, it becomes ovoid and the superior surface rises extraperitoneally into the abdomen.
- The bladder neck gives rise to the urethra, surrounded by the involuntary internal urethral sphincter.
- Internally, the appearance of the bladder wall depends on the state of distention of the organ: it is thick and trabeculated when collapsed, thin and smooth once distended. The area over the trigone always remains smooth.

### Blood supply and lymphatic drainage

- Arterial:
  - superior and inferior vesical arteries, which are branches of the internal iliac arteries.
- Venous:
  - vesical plexus draining into the internal iliac veins.
- Lymphatic drainage:
  - internal iliac then para-aortic lymph nodes.

### Imaging of the bladder

- Plain radiography:
  - on anterioposterior radiographs, the bladder may be seen as a rounded soft tissue mass surrounded by transradiant perivesical fat.
- Contrast studies (Fig. 13.9):
  - the bladder may be filled with contrast, either antegradely during intravenous urography or retrogradely via the urethra (cystography)
  - the full bladder outline is smooth and regular, whereas after micturition corrugations of the bladder wall are seen
  - a prostatic impression may be seen inferiorly.
- Ultrasound (Figs. 13.10, 13.11):
  - best modality to assess the bladder wall, which should not exceed 3–5 mm in thickness, depending on the state of distension
  - ureteric jets may be seen on colour Doppler ultrasound.

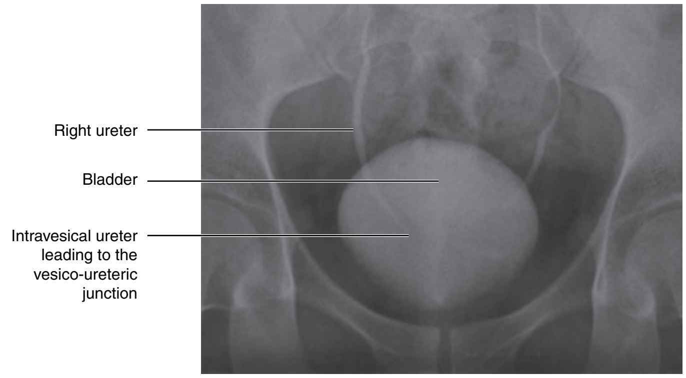


**Fig. 13.9** Intravenous urogram.

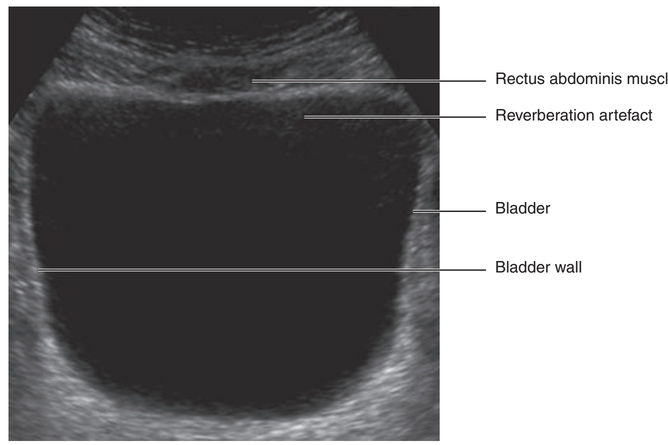


**Fig. 13.10** Ultrasound of bladder.

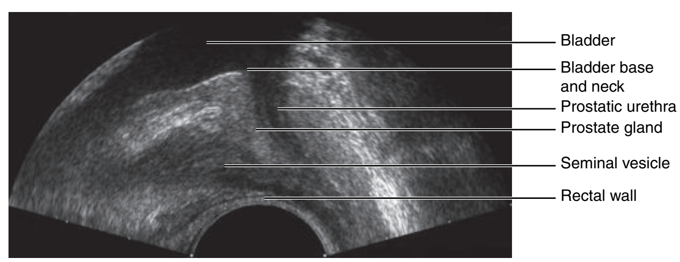


**Fig. 13.11** Longitudinal transrectal ultrasound showing relation of bladder base and neck to the proximal urethra.

- CT and MRI (Figs. 13.12, 13.13):
  - useful to demonstrate the relations of the bladder with surrounding structures
  - MRI is most useful for evaluating the bladder wall.

### Congenital anomalies of the bladder

- Agenesis:
  - a rare anomaly caused by failure of the cloaca to divide into an anterior bladder and a posterior rectum.

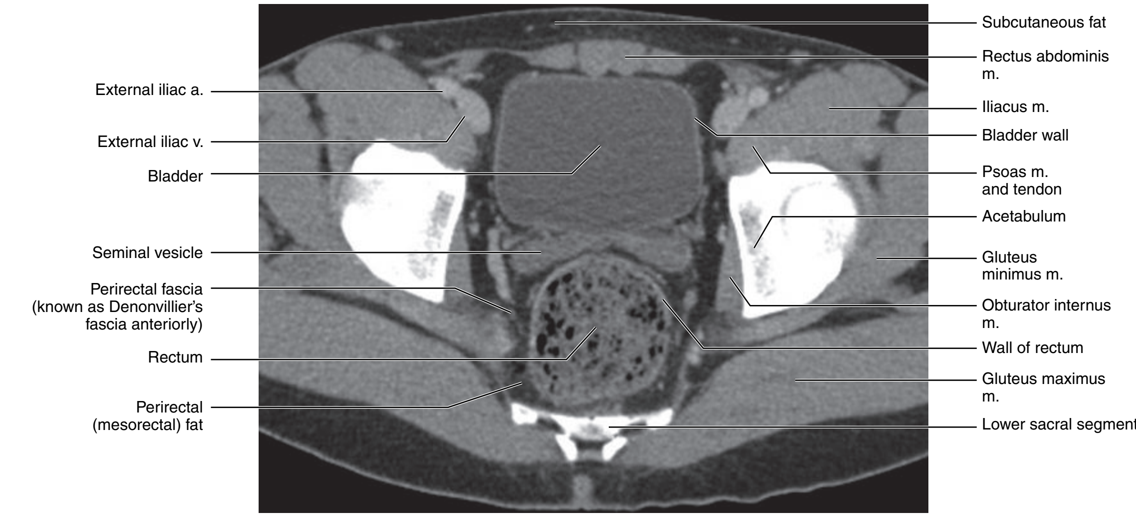


**Fig. 13.12** CT scan of the male pelvis: axial section through the bladder.

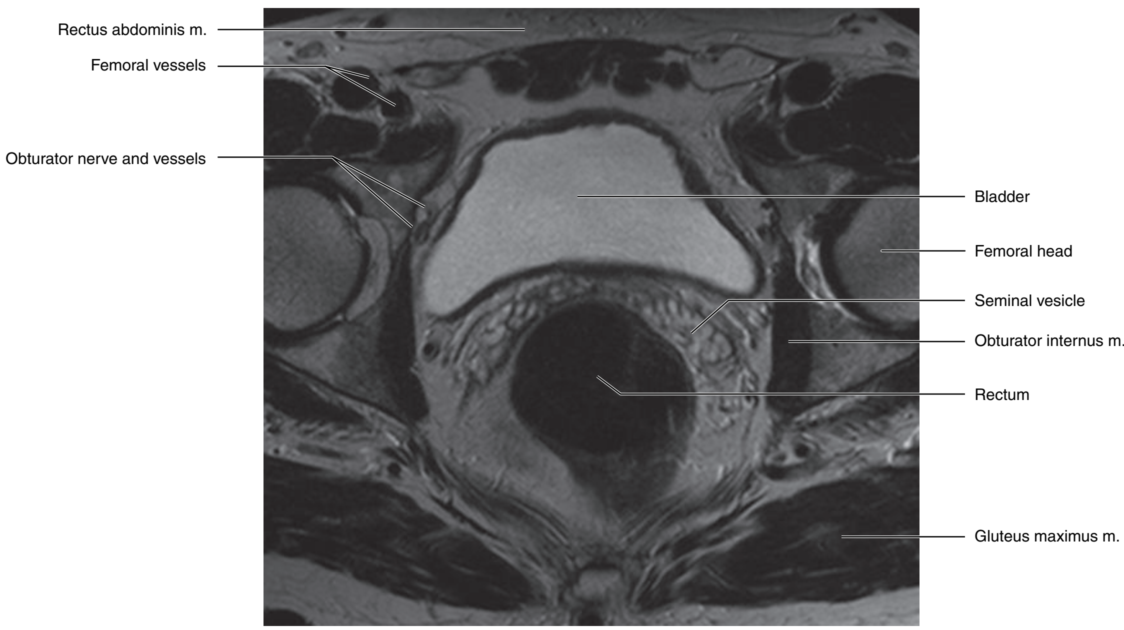


**Fig. 13.13** MR image of the male pelvis: axial section through the bladder.

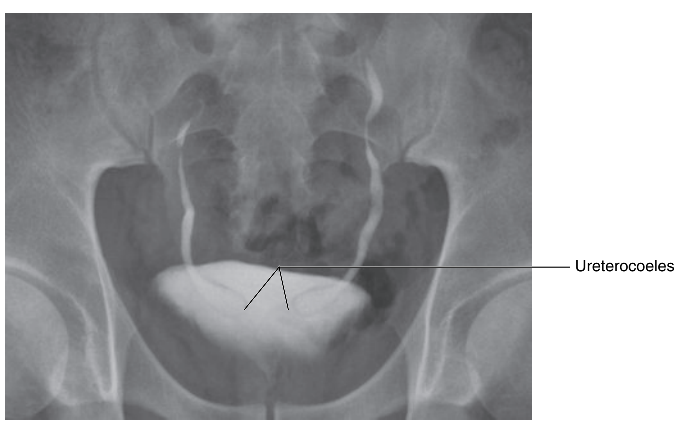


**Fig. 13.14** Intravenous urogram showing bilateral ureterocoeles. Note rounded dilatation of distal ureter (cobra head abnormality) surrounded by thin lucent line.

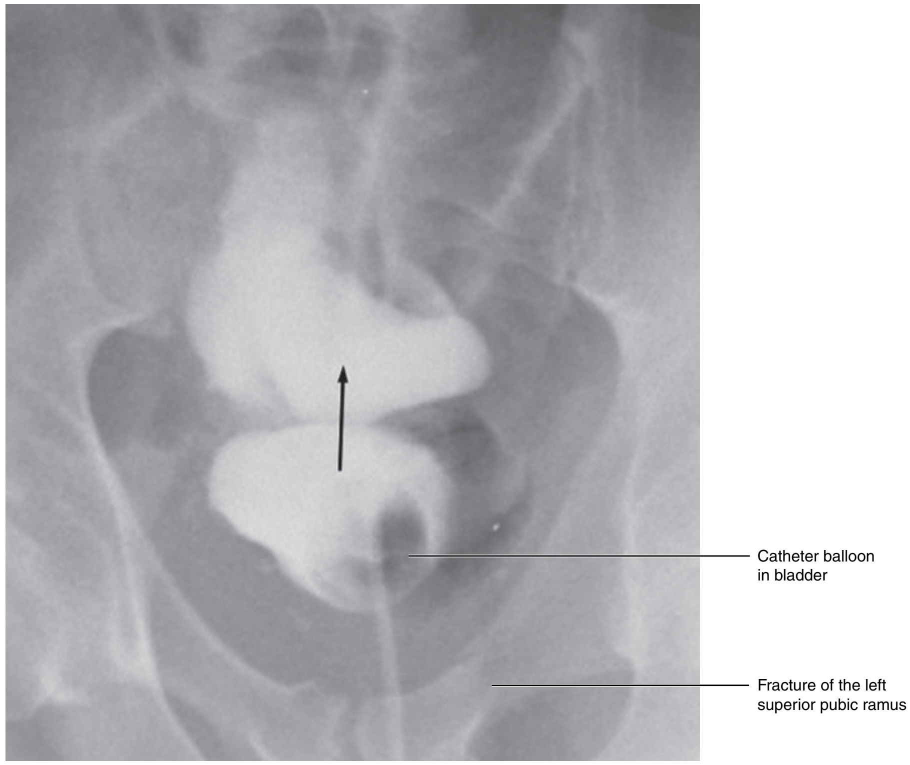


**Fig. 13.15** Cystogram showing intraperitoneal bladder rupture. Note contrast outside the confines of normal bladder and spreading into the peritoneal cavity (arrowed).

- Duplication:
  - complete duplication is an extremely rare anomaly whereby two bladders lie side by side, separated by a peritoneal fold; each bladder has a ureter from the ipsilateral kidney and a separate urethra
  - in partial duplication, the inferior portions of both bladders communicate and drain through a common urethra.
- Septation:
  - division of a single bladder into two portions by a septum in the sagittal or coronal plane.
- Ureterocoele:
  - cystic dilatation of the terminal intravesical ureter (Fig. 13.14).

### Applied anatomy

- Bladder ruptures may occur with pelvic fracture as the bladder neck is relatively fixed to the pelvis.
- Extraperitoneal bladder rupture:
  - occurs in 80%–90% of major bladder injuries
  - usually caused by penetrating trauma
  - cystography may demonstrate a variable path of extravasated contrast material.
- Intraperitoneal bladder rupture (Fig. 13.15):
  - occurs in approximately 10–20% of bladder injuries
  - typically result of a direct blow to the already distended bladder
  - cystography may demonstrate intraperitoneal contrast material around bowel loops, between mesenteric folds, and in the paracolic gutters.

## Male urethra (Fig. 13.16)

- Approximately 18–20 cm long.
- Divided into a posterior part (further divided into prostatic and membraneous urethra) and an anterior portion (further divided into bulbar and penile urethra).
- Prostatic urethra:
  - 3–4 cm long
  - passes through the substance of the prostate
  - a longitudinal midline ridge on the posterior wall, the urethral crest, projects into the lumen
  - on each side of the crest is a shallow depression, the prostatic sinus, into which the prostatic ducts (15–20 in number) open
  - in the middle of the crest, the verumontanum forms a rounded eminence
  - the prostatic utricle, a small recess representing the fused ends of the Müllerian ducts, opens onto the middle of the verumontanum
  - the ejaculatory ducts (the common termination of the seminal vesicles and vasa deferentia) open on either side of the utricle.
- Membraneous urethra:
  - 1.5 cm long

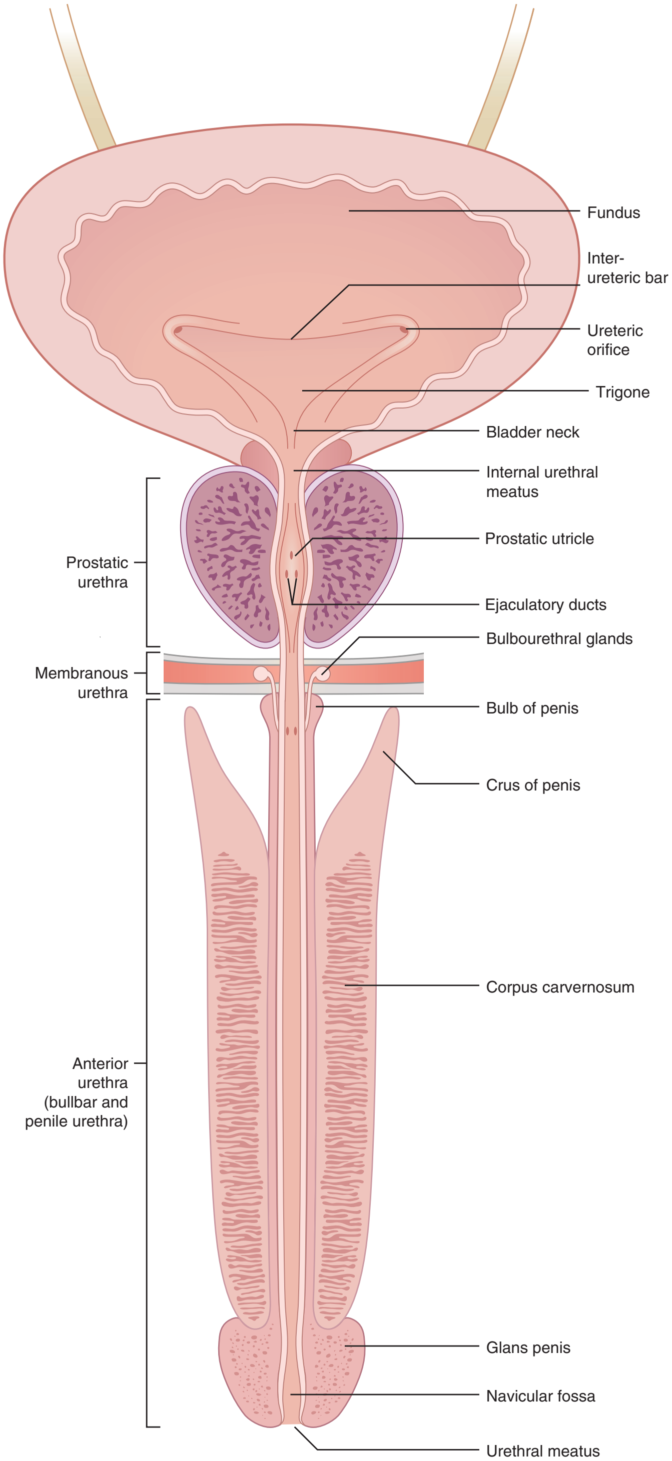


**Fig. 13.16** Male urethra.

- runs through the external urethral sphincter within the urogenital diaphragm
- least distensible part of the urethra

- Bulbar and penile urethra:
  - approximately 15 cm long in the flaccid penis
  - lies within the corpus spongiosum of the penis
  - the bulbar urethra, within the posterior part of the corpus, is the widest part of the urethra
  - bulbourethral (or Cowper's) glands open into the bulbar urethra approximately 2.5 cm below the perineal membrane
  - the penile urethra extends externally, beyond the root of the penis, and is long and relatively narrow when empty
  - at the tip of the glans penis there is a short dilated region, the navicular fossa, the roof of which has a mucosal fold termed the lacuna magna.

### Imaging of the urethra

- Contrast studies (Fig. 13.17):
  - the anterior urethra can be outlined with contrast medium introduced retrogradely
  - demonstration of the posterior urethra may require catheterization of the bladder followed by micturition cystourethrography.

### Congenital anomalies of the urethra

- Posterior urethral valve:
  - an abnormal congenital membrane that is located within the posterior male urethra; this valve is the most common cause of bladder outlet obstruction in male children, and may lead to a variable degree of upper renal tract dilatation.
- Urethral duplication:
  - a rare anomaly with a variable clinical presentation; usually occurs as either a complete or incomplete anomaly.
- Hypospadias:
  - the urethral orifice opens onto the ventral surface of the penis, proximal to the tip of the glans.
- Epispadias:
  - the urethral orifice is located on the dorsal aspect of the penis.
- Urethral meatal stenosis:
  - pinpoint narrowing of the urethral orifice frequently seen in association with hypospadias.
- Congenital urethral stricture:
  - a localized narrowing at the junction of the posterior and anterior urethra.

## Prostate gland, seminal vesicles and ejaculatory ducts

### Prostate gland (Fig. 13.18; Table 13.3)

- A fibromuscular gland shaped like an upside-down pyramid, with approximate dimensions 4 × 3 × 2 cm, which surrounds the prostatic urethra from the bladder base to the urogenital diaphragm.
- The prostate has an outer fibromuscular band, rather than a true capsule.
- The prostate provides about 30% of the volume of seminal fluid.

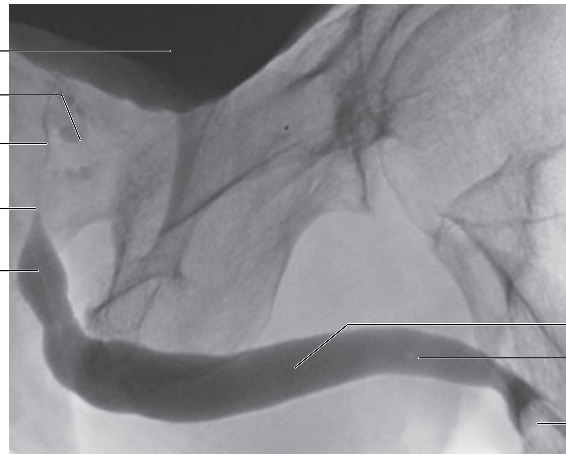


**Fig. 13.17** Retrograde urethrogram in the male.

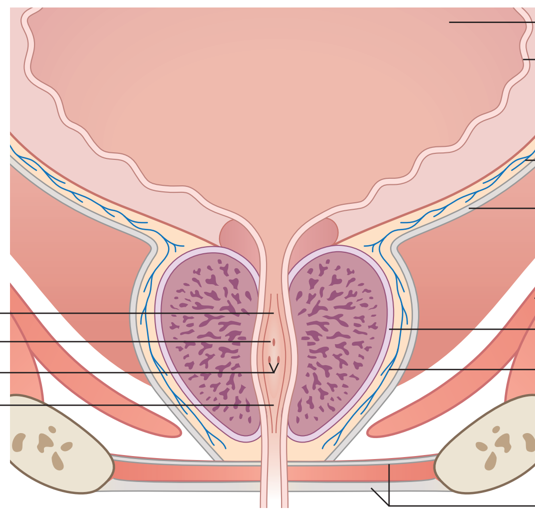


**Fig. 13.18** Prostate gland in coronal section.

**Table 13.3** Relations of the prostate gland

| Surface | Relations |
|---|---|
| Base | Bladder |
| Apex | Urogenital diaphragm |
| Anterior | Separated from pubic symphysis by retropubic fatty space of Retzius |
| Posterior | Rectum |
| Inferolateral | Levator ani and pubic bones |

### Zonal anatomy (Fig. 13.19)

- Three anatomical lobes are recognized after 20 weeks gestation: two lateral lobes and a median lobe.
- In the mature gland, the lobes fuse and the gland is divided into glandular and non-glandular tissue.
- Glandular tissue is subdivided into three zones:
  - central zone or CZ (25% by volume)
    - wedge-shaped and forms base of the prostate
    - surrounds the ejaculatory ducts, posterior to the prostatic urethra
  - transition zone or TZ (5%)
    - lies around the distal part of the prostatic urethra
    - benign prostatic hypertrophy arises from the TZ
  - peripheral zone or PZ (70%)
    - cup-shaped and encloses the central and transition zone
    - prostatic carcinomas arise in the PZ.
- Non-glandular tissue comprises the most anterior fibromuscular stroma.

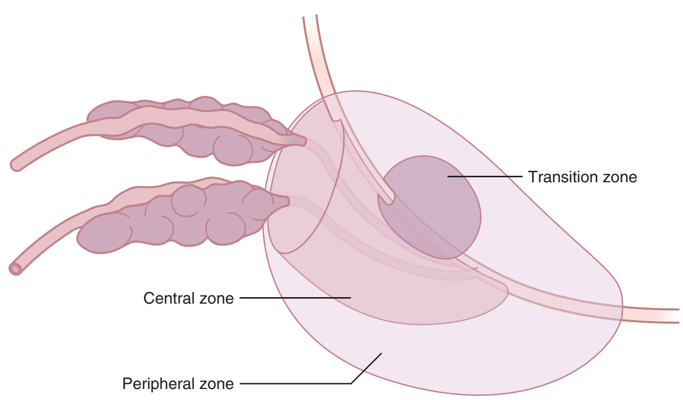


**Fig. 13.19** Anatomical depiction of the zonal anatomy of the prostate gland.

### Blood supply and lymphatic drainage

- Arterial supply:
  - from the inferior vesical, internal pudendal and middle rectal arteries.
- Venous drainage:
  - via the periprostatic plexus to the internal iliac veins and also the vertebral venous plexus (hence the propensity of prostatic carcinoma to spread to the vertebrae).
- Lymphatic drainage:
  - internal iliac and obturator lymph nodes.

### Imaging of the prostate gland

- Ultrasound (Fig. 13.20):
  - The prostate is most frequently imaged by transrectal ultrasound.
  - The peripheral zone is the most reflective, although it may be indistinguishable from the rest of the gland.
  - The urethra is seen as a central anechoic structure, surrounded by a hypoechoic area comprising smooth muscle, periurethral glands and the transition zone.
- CT:
  - The prostate is seen as a soft tissue mass, separated from the obturator internus muscles by a well-defined fat plane.
  - CT cannot delineate the zonal anatomy of the gland.
- MRI (Fig. 13.21):
  - The gland is of homogeneous low signal on T1W sequences.
  - Zonal anatomy is best demonstrated on T2W sequences
    - central and transition zones (sometimes loosely termed the 'central gland') have relatively low T2 signal
    - peripheral zone and seminal vesicles return high T2 signal.
  - MRI is used to stage prostate cancer, with T2W imaging being most useful.

### Congenital anomalies within the prostate gland

- Müllerian duct cyst (Fig. 13.22):
  - A congenital midline prostatic cyst which is developmentally derived from the Müllerian ducts. The cyst is usually large and extends toward the prostate base along the embryological course of the Müllerian duct.

## Seminal vesicles and ejaculatory ducts

- Two lobulated sacs, about 5 cm long, which are adjacent to the base of the bladder, above the prostate.
- Produce about 60% of the volume of seminal fluid.
- The anterior surface contacts the posterior aspect of the bladder.
- The posterior surface is related to Denonvillier's fascia and the rectum.

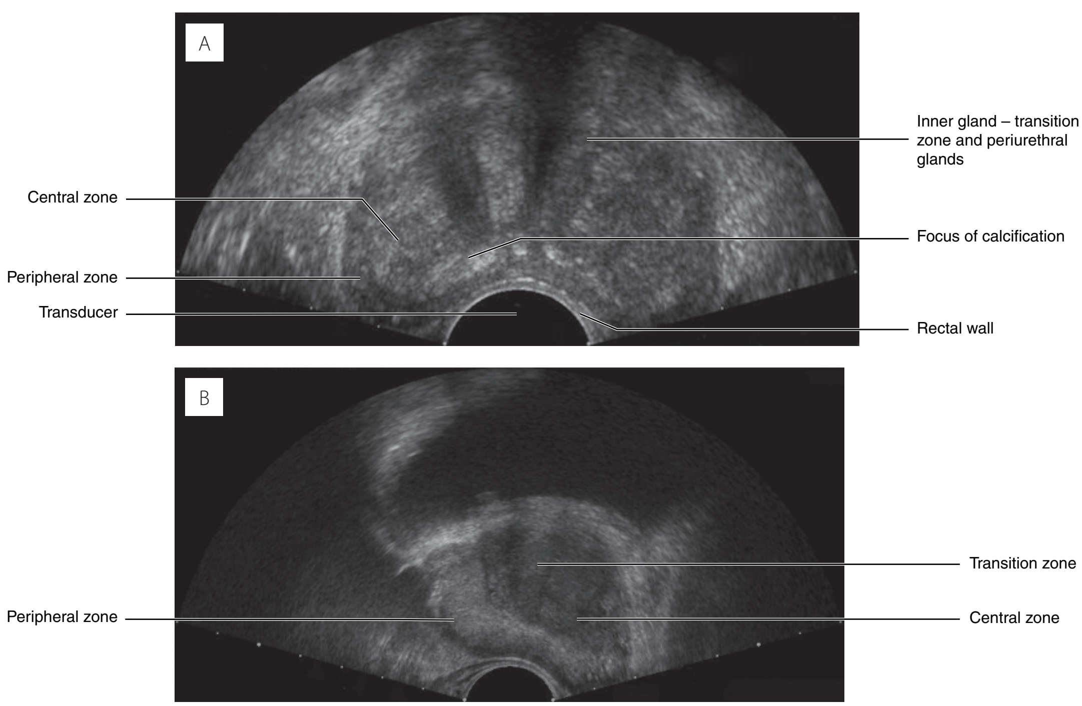


**Fig. 13.20** Transrectal ultrasound of the prostate gland. (A) Transverse image. (B) Longitudinal image.

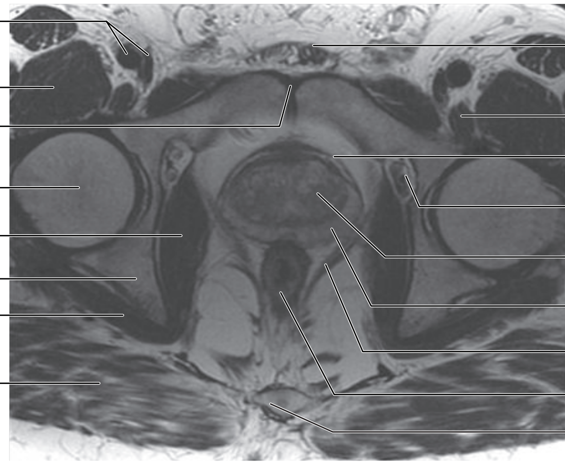


**Fig. 13.21** High-resolution MR image of the male pelvis: axial section through the prostate gland.

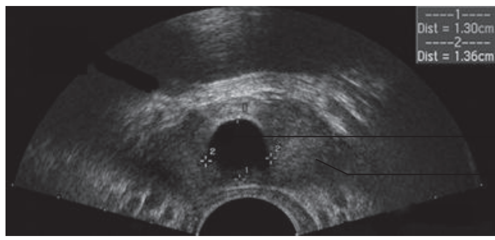


**Fig. 13.22** Transverse transrectal ultrasound of the prostate gland showing a Müllerian duct cyst.

- Inferiorly, each seminal vesicle narrows and fuses with the ipsilateral ampulla of the vas deferens to form an ejaculatory duct, which is about 2 cm long.
- The ejaculatory ducts pierce the prostate gland and run obliquely through it to enter the prostatic urethra.

#### Imaging of the seminal vesicles

- Ultrasound (Figs. 13.23, 13.24):
  - Seminal vesicles are tubular structures containing fluid, located above and lateral to the base of the prostate gland.
  - Ejaculatory ducts are sometimes identified as a triangular hypoechoic 'beak' as they project into the central zone of the prostate gland.
- CT:
  - Seminal vesicles are soft tissue density structures with a characteristic 'bow-tie' appearance, lying in the groove between the bladder base and prostate
  - CT cannot define the internal anatomy of the seminal vesicles.
- MRI:
  - On T1W sequences, the seminal vesicles return low signal in contrast to the surrounding fat.
  - On T2W sequences, the fluid within the seminal vesicles return high signal and the walls may be seen as low signal intensity structures.

## Spermatic cord, scrotum, testes, epididymis and vas deferens

**See Fig. 13.25**

### Spermatic cord

- A tubular structure that suspends the testis in the scrotum, passing from the deep inguinal ring in the abdomen through the inguinal canal, down into the scrotum to the posteromedial border of the testis.
- Contains the first section of the vas deferens, arterial supply, draining veins, lymphatics and nerves.
- Each cord is tightly covered by a fibrous sheath composed of internal spermatic, cremasteric and external spermatic fascial layers (derived from transversalis, internal and external oblique abdominal fasciae respectively).

### Scrotum

- A pouch of skin containing the testes and spermatic cords.
- The subcutaneous tissue contains the dartos muscle, which is a smooth muscle supplied by sympathetic fibres.
- The rugosity of the skin is due to contraction of the dartos.

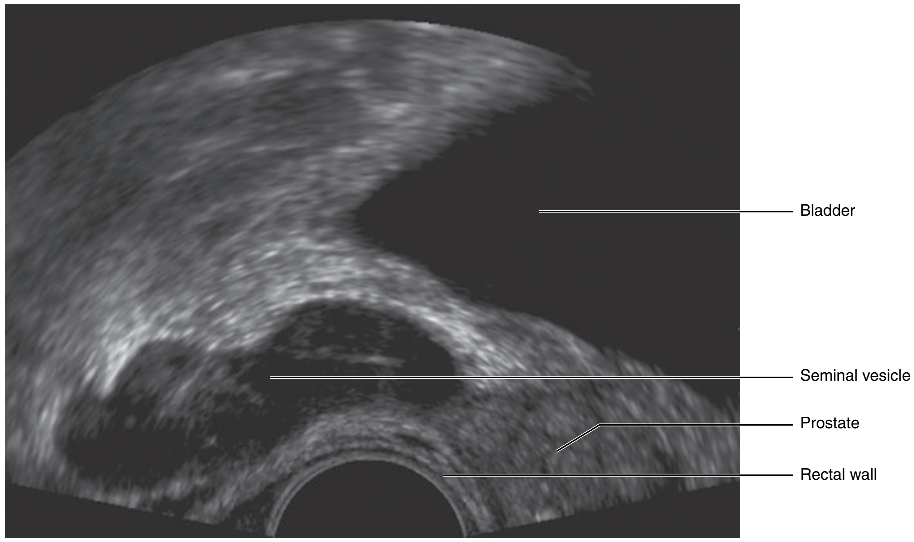


**Fig. 13.23** Longitudinal transrectal ultrasound showing seminal vesicle.

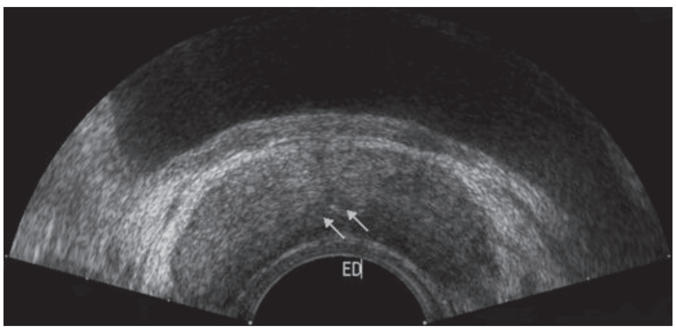


**Fig. 13.24** Transverse transrectal ultrasound showing position of ejaculatory ducts (arrowed).

## Testis (Fig. 13.26)

- Ovoid reproductive and endocrine organs.
- Average testicular dimensions are 5 cm (length), 2.5 cm (breadth), 3 cm (anteroposterior).
- Each testis has an upper pole (usually tilted slightly forwards) and a lower pole.
- The left testis lies lower than the right in 85% of subjects.
- The right and left testes are separated by a fibrous median scrotal septum, which is deficient superiorly.
- Each testis is invested by three coats, which are from outside inwards:
  - the tunica vaginalis, a remnant of the fetal processus vaginalis, which has visceral and parietal layers
  - the tunica albuginea, a thick fibrous capsule, which is thickened posteriorly to form a fibrous septum known as the mediastinum testis; fibrous septa extend from the mediastinum into the testis, dividing it into 200–300 seminiferous tubules
  - the vasculosa contains a plexus of blood vessels and loose connective tissue.
- The seminiferous tubules drain to the rete testis (an anastomosing network of tubules located in the mediastinum testis), from whence 10–15 efferent ductules pierce the tunica, near the upper pole, to enter the head of the epididymis.
- The appendix testis, a remnant of the Müllerian duct, is present in 90% of cases and may be seen as a small sessile projection just below the head of the epididymis

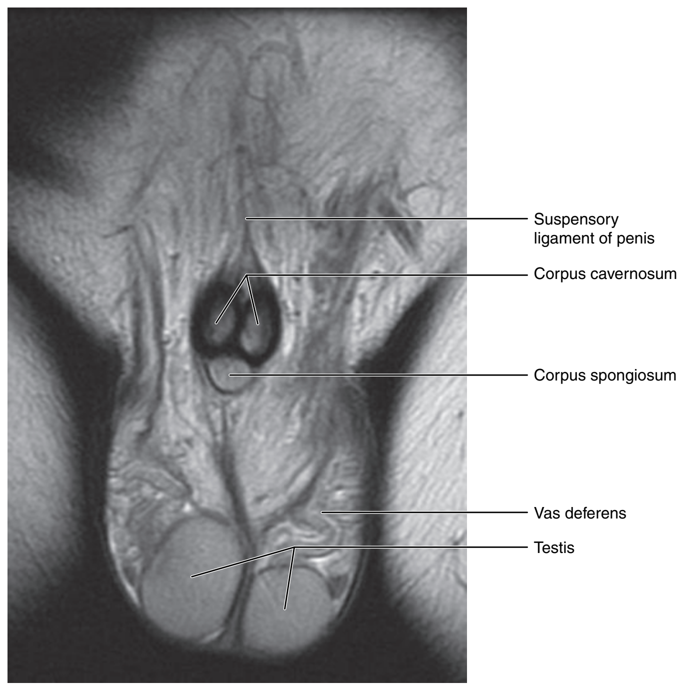


**Fig. 13.25** MR image of the male pelvis: coronal section of the perineum.

### Blood supply and lymphatic drainage

- Arterial supply:
  - The testicular artery arises directly from the aorta at the level of the renal artery.
  - The epididymis and spermatic cord are supplied by branches of the inferior vesical artery and inferior epigastric artery.

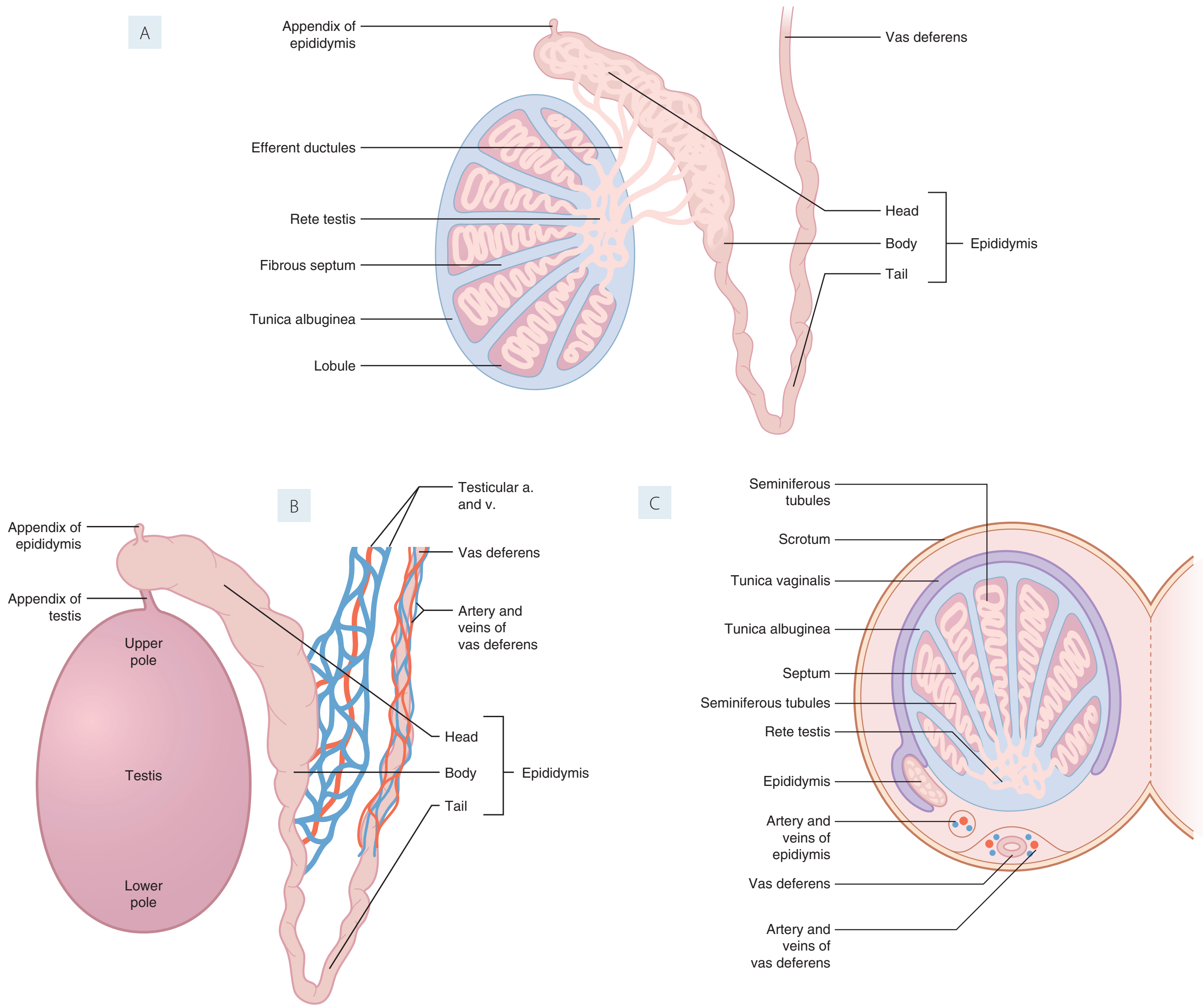


**Fig. 13.26** Testis and epididymis. (A) Internal architecture. (B) Blood supply. (C) Transverse section.

- The scrotum is supplied by the external pudendal branch of the femoral artery.
- Venous drainage:
  - Via the pampiniform plexus of veins above and behind the testis, which anastomose to become one single vein at the upper end of the inguinal ring. The right testicular vein drains into the inferior vena cava and the left into the left renal vein.
- Lymphatic drainage:
  - The testes drain to para-aortic lymph nodes at the level of L1–2.
  - The scrotum drains to the superficial inguinal lymph nodes.

## Imaging of the testis

- Ultrasound (Figs. 13.27–13.30):
  - Oval structure having a homogeneously granular echotexture with uniform medium-level echoes.
  - Vessels coursing through the testis are often identified as hypoechoic linear structures.
  - The mediastinum testis can be identified as an echogenic line posteriorly, parallel to the epididymis.
  - Occasionally the rete testis is prominent as multiple anechoic tubular structures adjacent to the epididymis.
  - The appendix testis may be seen, especially in the presence of a hydrocoele.
- MRI:
  - On T1W sequences, the testis is of homogeneous low signal intensity.
  - On T2W sequences, normal testicular tissue returns high signal intensity.
  - The tunica albuginea, mediastinum testis and fibrous septa are of low signal intensity on T2W sequences.
  - The epididymis is of variable intensity.

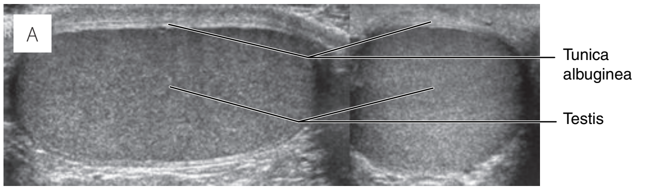


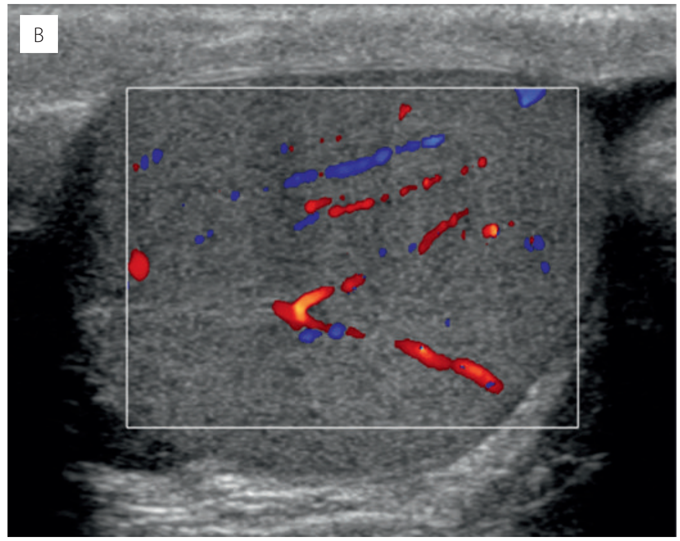


**Fig. 13.27** (A) Ultrasound of the testis: longitudinal (left) and transverse (right) images. (B) Colour Doppler ultrasound showing normal testicular blood flow throughout the gland.

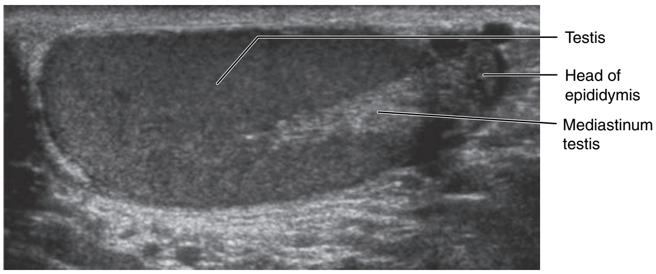


**Fig. 13.28** Ultrasound of testis.

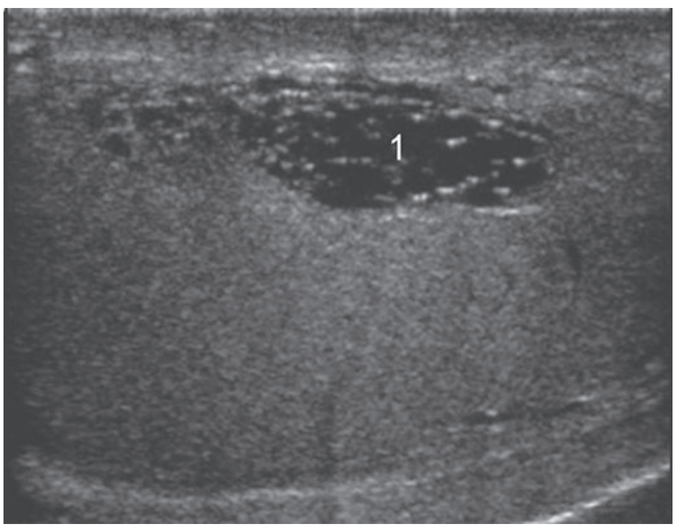


**Fig. 13.29** Ultrasound of the testis showing ectasia of the rete testis – a normal variant.

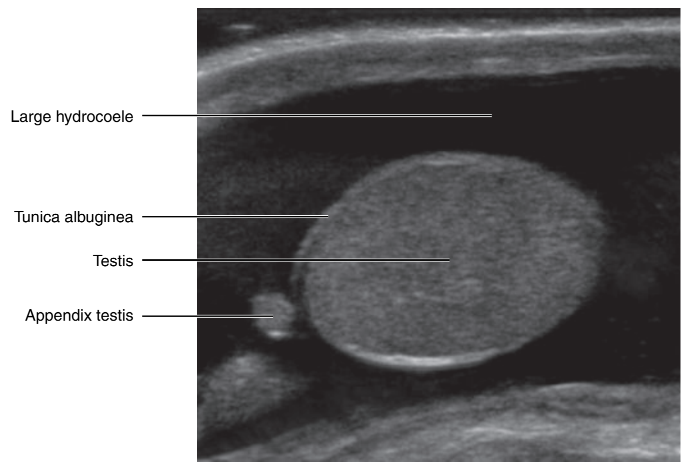


**Fig. 13.30** Ultrasound of the testis.

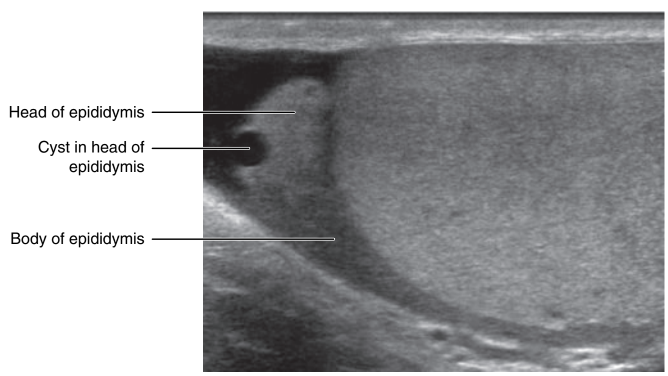


**Fig. 13.31** Ultrasound of the testis.

### Congenital anomalies of the testis

- Congenital hydrocoele:
  - a collection of fluid in the scrotum between layers of the tunica vaginalis; it may be isolated or may communicate with the abdominal cavity through a patent processus vaginalis.
- Cryptorchidism:
  - failure of one or both testes to descend into the scrotum; cryptorchidism affects about 3% of term infants and up to 30% of preterm infants.

## Epididymis (Fig. 13.31)

- A tightly-coiled tube, about 6 m long when unravelled, lying posterior and lateral to the testis.
- Connects the efferent ductules from the rear of each testis to the vas deferens.
- Has a role in the concentration, maturation and storage of sperm.
- Each epididymis has a head at the superior pole and a tail at the inferior pole of the testis.
- The head of the epididymis may have a small sessile projection, known as the appendix of the epididymis.

## Vas deferens

- A muscular tube, about 30–45 cm long, connecting the epididymis to the ejaculatory duct.
- Extends from the tail of the epididymis through the inguinal canal and pelvis to fuse with the duct of the seminal vesicles, to form the ejaculatory duct in the prostate gland.

## Penis (Fig. 13.32)

- The penis consists of an attached root (radix) in the perineum and a free, pendulous body (corpus).
- The body of the penis comprises three cylinders of endothelium-lined erectile tissue which arise from the perineum:
  - paired corpora cavernosa (dorsally)
    - fused in the median plane but diverge posterosuperiorly to form the crura, which attach to the inferior part of the corresponding ischiopubic ramus
    - internally lie numerous smooth muscle-lined interconnected sinusoids
    - within each corpus cavernosum lies a centrally located cavernosal artery
  - corpus spongiosum (ventrally)
    - expanded to form the bulb proximally and the glans penis distally
    - the posterior part of the bulb is penetrated by the bulbar urethra, which then runs in the corpus spongiosum to the external meatus.
- All three corpora are bound together by three surrounding layers of fascia (from deep to superficial):
  - tunica albuginea (a thick fibrous capsule)
  - deep fascia of the penis (Buck's fascia)
  - superficial fascia of the penis.

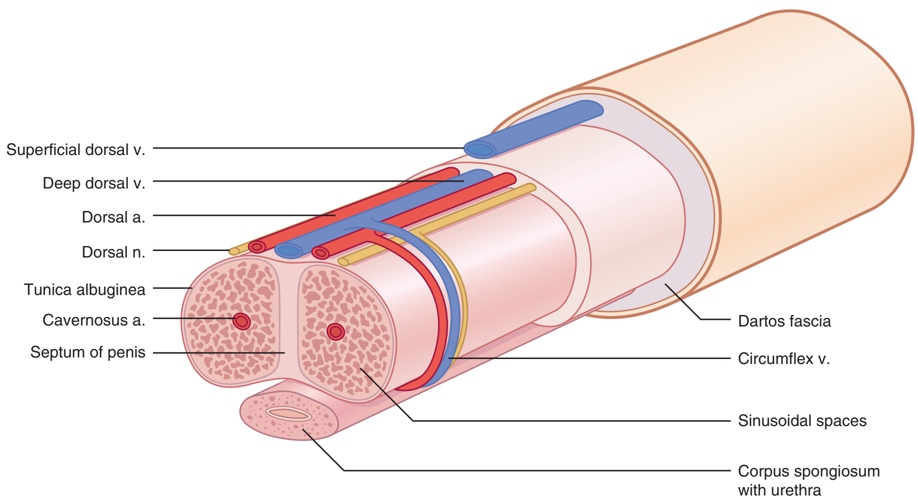


**Fig. 13.32** Cross section of the body of the penis.

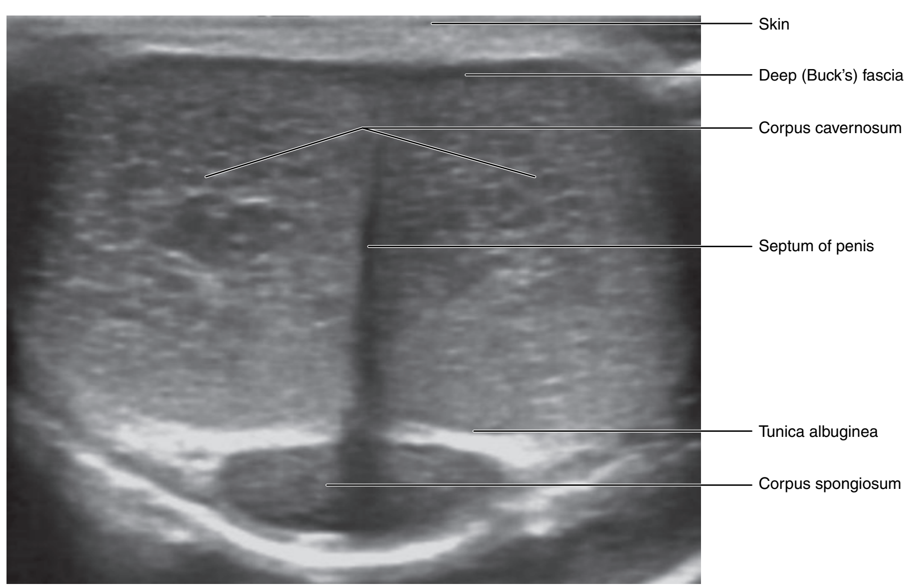


**Fig. 13.33** Ultrasound of the penis.

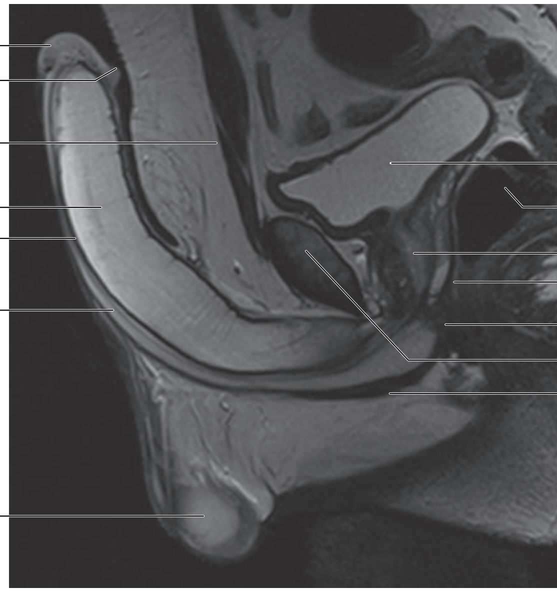


**Fig. 13.34** MR image of the penis: sagittal section through the midline.

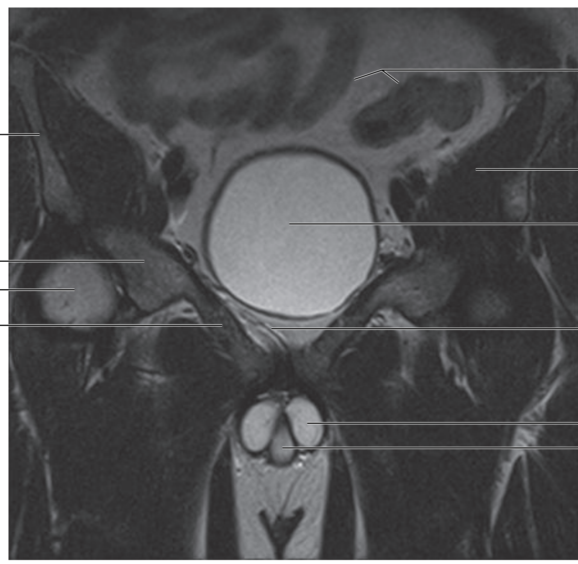


**Fig. 13.35** MR image of the pelvis: coronal section though the root of penis.

## Blood supply and lymphatic drainage

- Arterial supply:
  - originates from internal pudendal arteries; paired deep dorsal arteries chiefly supply the glans and give off the cavernosal arteries and the artery to the bulb.
- Venous drainage:
  - the corpora cavernosa drain mainly via cavernous veins, and via the deep dorsal vein into the internal iliac system; increased arterial flow and sinusoidal distension during sexual arousal compresses the draining veins, resulting in erection.
- Lymphatic drainage:
  - superficial and deep inguinal lymph nodes.

## Imaging of the penis

- Ultrasound (Fig. 13.33):
  - The corpora demonstrate low-level echoes.
  - The urethra appears as a circular echogenic structure, with a central anechoic area, and is best seen when distended.
  - Colour flow Doppler ultrasound allows visualization of the penile arteries, which is important in the assessment of erectile dysfunction.
- MRI (Figs. 13.34, 13.35):
  - Variable appearances depending on the imaging sequence and the state of erection.
  - On T1W sequences, the corpora are indistinguishable and return signal that is lower than fat and higher than

muscle. The tunica albuginea and Buck's fascia are of low signal intensity.
- On T2W sequences, all three corpora have increased signal, in contrast to the fascial layers.
- The corpora are very vascular on contrast-enhanced images.

### Congenital anomalies of the penis

- Chordee:
  - ventral or rotational curvature of the penis, which is most apparent with erection and is caused by fibrous tissue along the usual course of the corpus spongiosum; often associated with hypospadias.
- Other anomalies:
  - less common anomalies include penile agenesis, duplication and lymphoedema; microphallus results from androgen deficiency or insensitivity.

Chapter 14

# The female pelvis

Catriona L. Davies

## Plain radiography/hysterosalpingography/fluoroscopy

This is still the best technique for evaluating the gross bony anatomy of the female pelvis as well as the trabecular bone pattern.

Hysterosalpingography is often used in the investigation of infertility as it allows evaluation of the uterine cavity and fallopian tubes.

Fluoroscopy can also be used to evaluate the other pelvic organs – bladder, urethra and vagina.

However, it is important when imaging women to consider the radiation dose to the pelvic organs. Also the '10 day rule' recommends that non-urgent X-ray examinations that entail pelvic irradiation in the female of child-bearing age should be restricted in order to avoid irradiating the fetus. At a low dose, i.e. 1 mGy, the dose to an embryo/fetus should present no risk of fetal death, malformation, growth retardation or impairment of mental development.

### Effective doses in CT and radiographic examinations

**Table 14.1**

| CT examination | Effective dose (mSv) | Radiographic examination | Effective dose (mSv) |
|---|---|---|---|
| Head | 2 | Skull | 0.07 |
| Chest | 8 | Chest PA | 0.02 |
| Abdomen | 10–20 | Abdomen | 1.0 |
| Pelvis | 10–20 | Pelvis | 0.7 |
| | | Ba swallow | 1.5 |
| | | Ba enema | 7 |
| | | HSG | 1.0 |

## Cross-sectional imaging

Ultrasound is often first line investigation in the evaluation of the female genital tract.

Transbadominal imaging enables visualization of the entire pelvis. It requires a distended bladder to act as an acoustic window. A high-frequency transducer should be used (5.0–7.5 MHz). Both sagittal and transverse planes should be visualized. In 85–90% of patients the uterus and ovaries should be visualized by this method.

Transvaginal imaging using a high-frequency probe is an essential part of pelvic ultrasound examinations, allowing for better resolution of both the uterus and ovaries. Colour and spectral Doppler ultrasound should also be used to distinguish vascular structures from other pathology. This should be performed with an empty bladder in both sagittal and coronal planes.

CT and MRI provide excellent information on the soft tissues of the female pelvis. MRI has the advantage of not utilizing ionizing radiation. It also provides excellent detail of the internal anatomy using either dedicated surface array or endocavitary coils. T1-weighted sequences provide us with the basic anatomy whereas T2 enables pathological evaluation.

#### CTA/MRA/angiography/US/Doppler

US (both colour flow and pulsed-wave Doppler technique) is able to visualize much of the vasculature. Conventional angiography still remains the gold standard, especially in evaluating the internal iliac vasculature, but MRA is being increasingly used in the evaluation of fibroids pre- and post-embolization.

#### CT positron emission tomography (CT PET)

The metabolic information obtained with fluorine 18 fluorodeoxyglucose (FDG) can be combined with the morphological information obtained with CT. It can depict lymph node and distant metastases in the female pelvis.

## True pelvis

### Plain radiographic anatomy

The pelvis is divided into:

- pelvis major (false pelvis)
- pelvis minor (true pelvis)

*Applied Radiological Anatomy, 2nd Edition* ed. Paul Butler, Adam W.M. Mitchell and Jeremiah C. Healy. Published by Cambridge University Press.

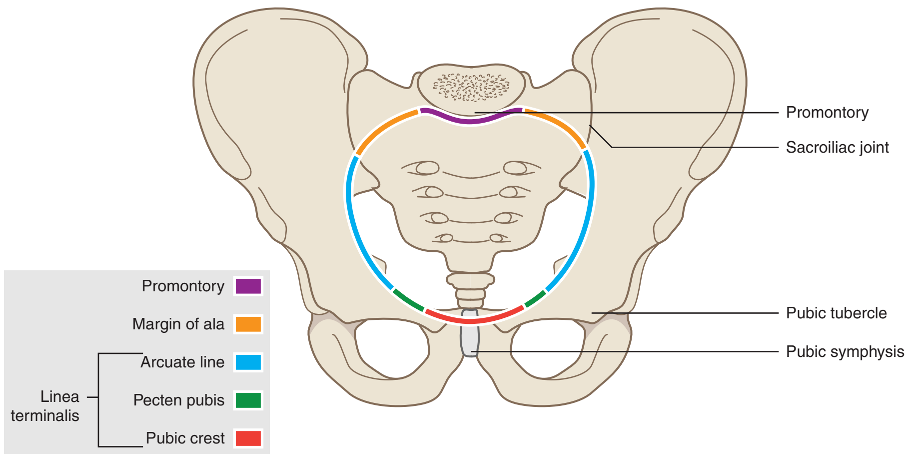


**Fig. 14.1** Female pelvic inlet.

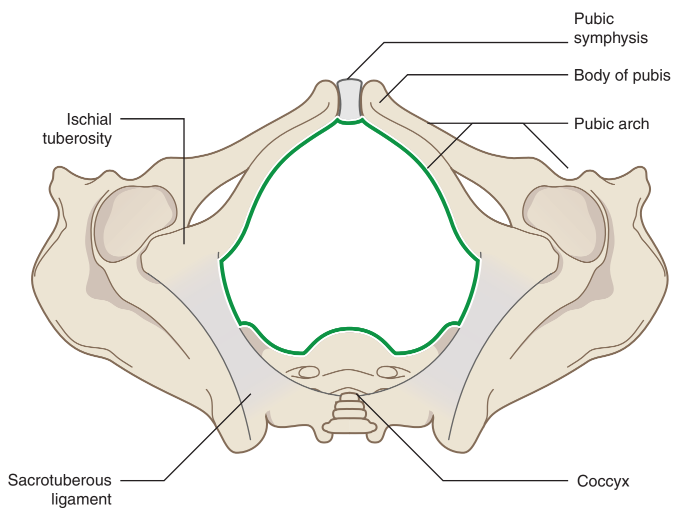


**Fig. 14.2** Female pelvic outlet.

The false pelvis lies above the pelvic brim and is part of the abdominal cavity.

The true pelvis lies below the pelvic brim and contains the pelvic viscera:

Inlet: a plane passing through the promontory of the sacrum, arcuate line of the ilium, the iliopectineal line (oblique ridge on the internal surface of the ilium which continues on the pubis) and posterior surface of the pubic crest (Fig. 14.1).

Outlet: a plane passing through the ischiopubic rami, ischial spines, inferior symphysis pubis, sacrotuberous ligaments and the coccyx (Fig. 14.2).

The bones of the pelvis are the paired innominate bones, the sacrum and the coccyx (Fig. 14.3).

- Innominate

  These articulate with each other anteriorly and with the sacrum posteriorly. They are composed of three parts which fuse at the acetabulum:

  - Ilium
  - Pubic bone
  - Ischium
- Sacrum:
  - five fused vertebrae
  - articulates with lumbar spine superiorly and coccyx inferiorly
  - four pairs of anterior and posterior sacral foraminae which transmit sacral nerves
  - the spinal canal ends posteriorly in the sacral hiatus
  - hiatus is a midline opening that transmits the fifth sacral nerve.
- Coccyx:
  - composed of 3–5 fused vertebrae
  - first segment is often separate.

The female pelvis differs from the male pelvis as follows (Fig. 14.4):

- oval obturator foramen
- wider pubic arch >90°
- wider and shallow pelvis
- oval or rounded inlet, larger outlet
- wide sciatic notch
- less prominent muscle attachments
- small acetabulae
- less curved sacrum.

Four common terms used to describe female pelves:

1. Gynaecoid pelvis (50%):
   - it is the normal female type
   - inlet is slightly transverse oval
   - sacrum is wide with average concavity and inclination
   - side walls are straight with blunt ischial spines
   - sacro-sciatic notch is wide
   - subpubic angle is 90–100°.
2. Anthropoid pelvis (25%):
   - all anteroposterior diameters are long
   - all transverse diameters are short
   - sacrum is long and narrow
   - sacro-sciatic notch is wide
   - subpubic angle is narrow.

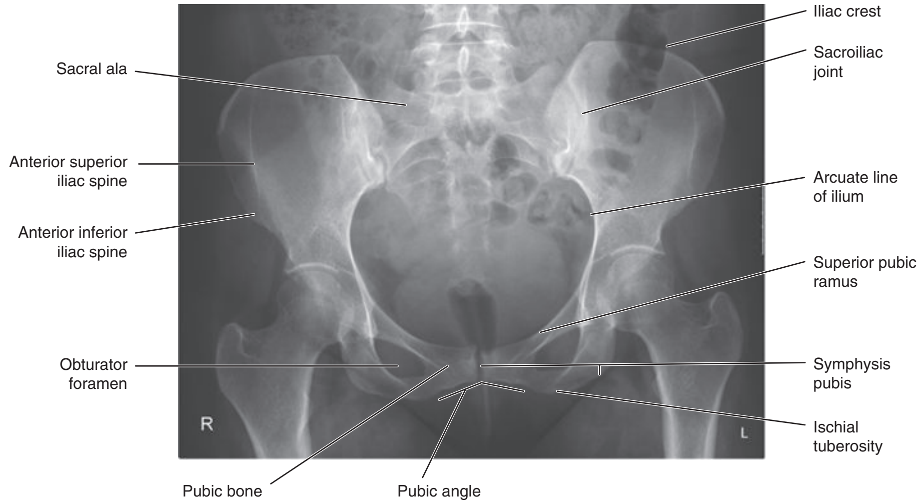


**Fig. 14.3** X-ray of the female pelvis.

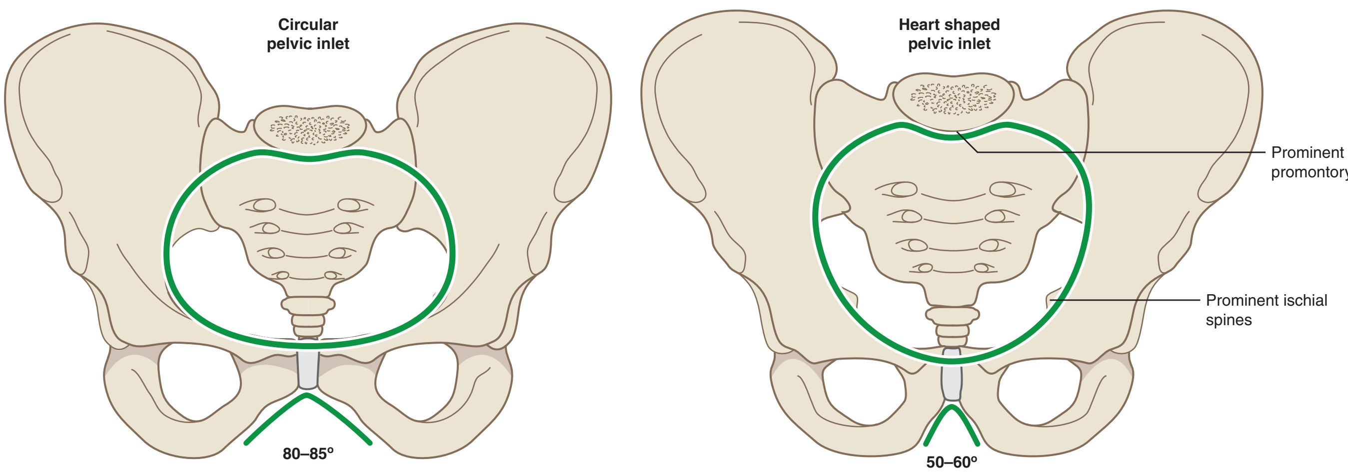


**Fig. 14.4** Structure of the bony pelvis: left, in women; right, in men.

3. Android pelvis (20%):
   - it is a male type
   - inlet is triangular or heart-shaped with anterior narrow apex
   - side walls are converging (funnel pelvis) with projecting ischial spines
   - sacro-sciatic notch is narrow
   - subpubic angle is narrow <90°.
4. Platypelloid pelvis (5%):
   - it is a flat female type
   - all anteroposterior diameters are short
   - all transverse diameters are long
   - sacro-sciatic notch is narrow
   - subpubic angle is wide.

# Cross-sectional anatomy

## Pelvic walls and floor

CT enables excellent visualization of the female pelvic walls and the musculature (Fig. 14.5).

The anterior pelvic wall is formed by:

- continuation of the upper abdominal musculature – external oblique, internal oblique, transversus abdominis, rectus abdominis
- linea alba
- rectus sheath.

The posterior pelvic wall is formed by:

- psoas
- iliacus.

The boundaries of the pelvic floor are;

- anterior: symphysis pubis, bodies of the pubic bones, obturator internus, levator ani
- lateral: ilium, ischium, piriformis, obturator internus, levator ani
- posterior: sacrum, coccyx, piriformis, coccygeus
- inferior: pelvic diaphragm.

MRI is particularly well suited to demonstration of the pelvic floor due to its multiplanar ability.

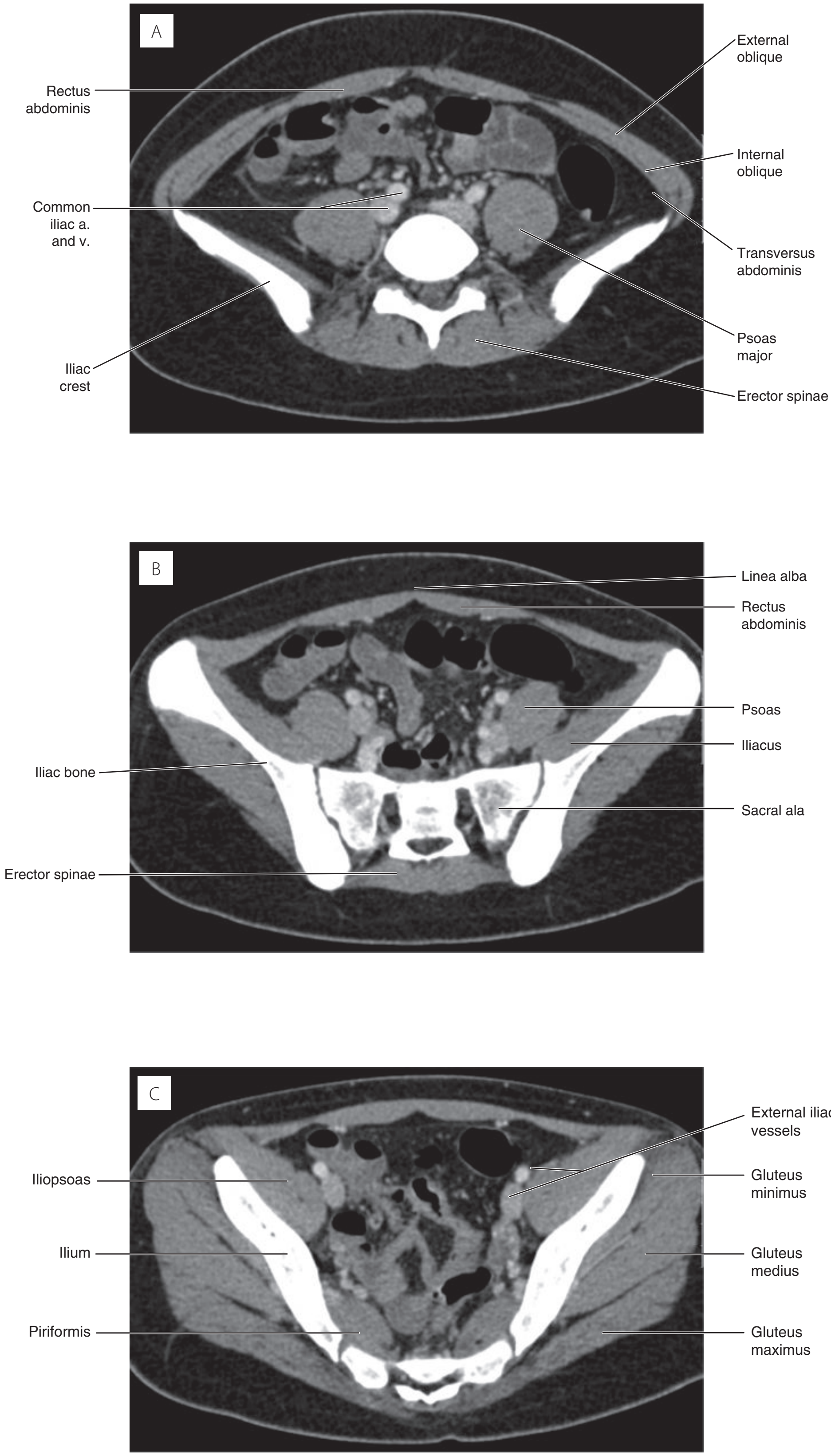


**Fig. 14.5** Axial CT scans through the female pelvis.

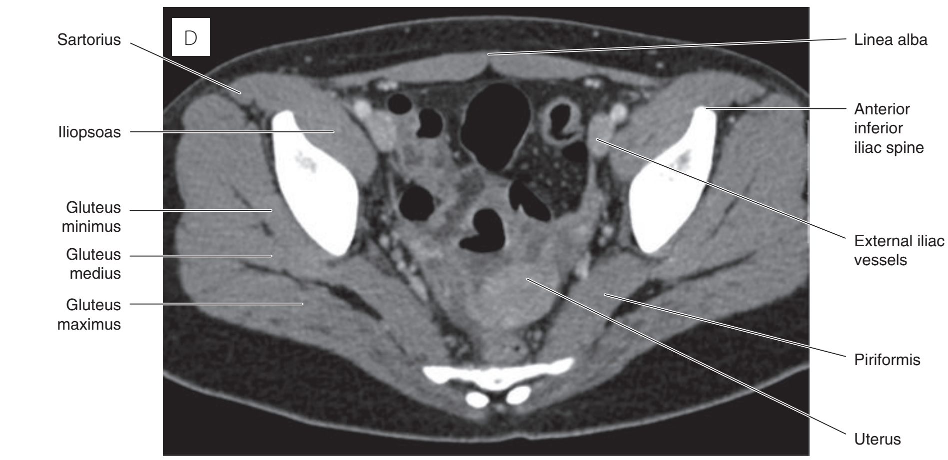
D
Sartorius
Iliopsoas
Gluteus minimus
Gluteus medius
Gluteus maximus
Linea alba
Anterior inferior iliac spine
External iliac vessels
Piriformis
Uterus

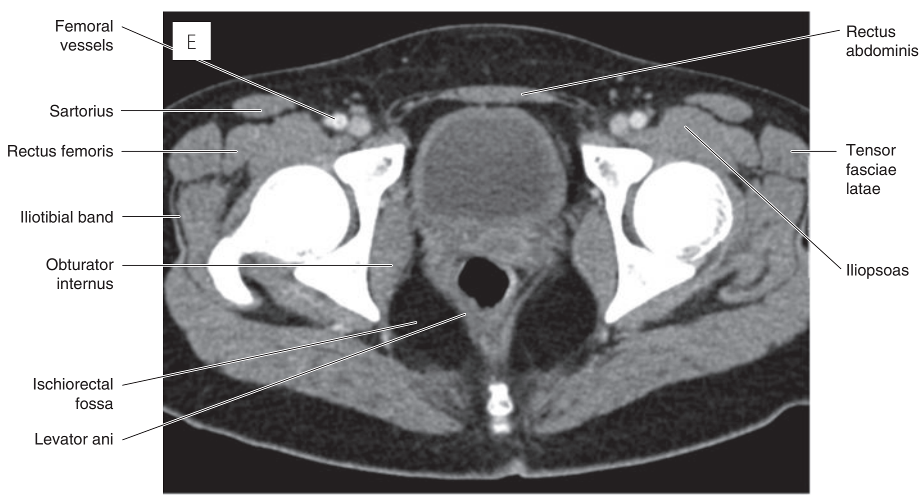
E
Femoral vessels
Sartorius
Rectus femoris
Iliotibial band
Obturator internus
Ischiorectal fossa
Levator ani
Rectus abdominis
Tensor fasciae latae
Iliopsoas


F
Femoral vessels
Rectus femoris
Iliotibial band
Obturator internus
Levator ani
Ischiorectal fossa
Tensor fasciae latae
Gluteus maximus

**Fig. 14.5** *(cont.)*

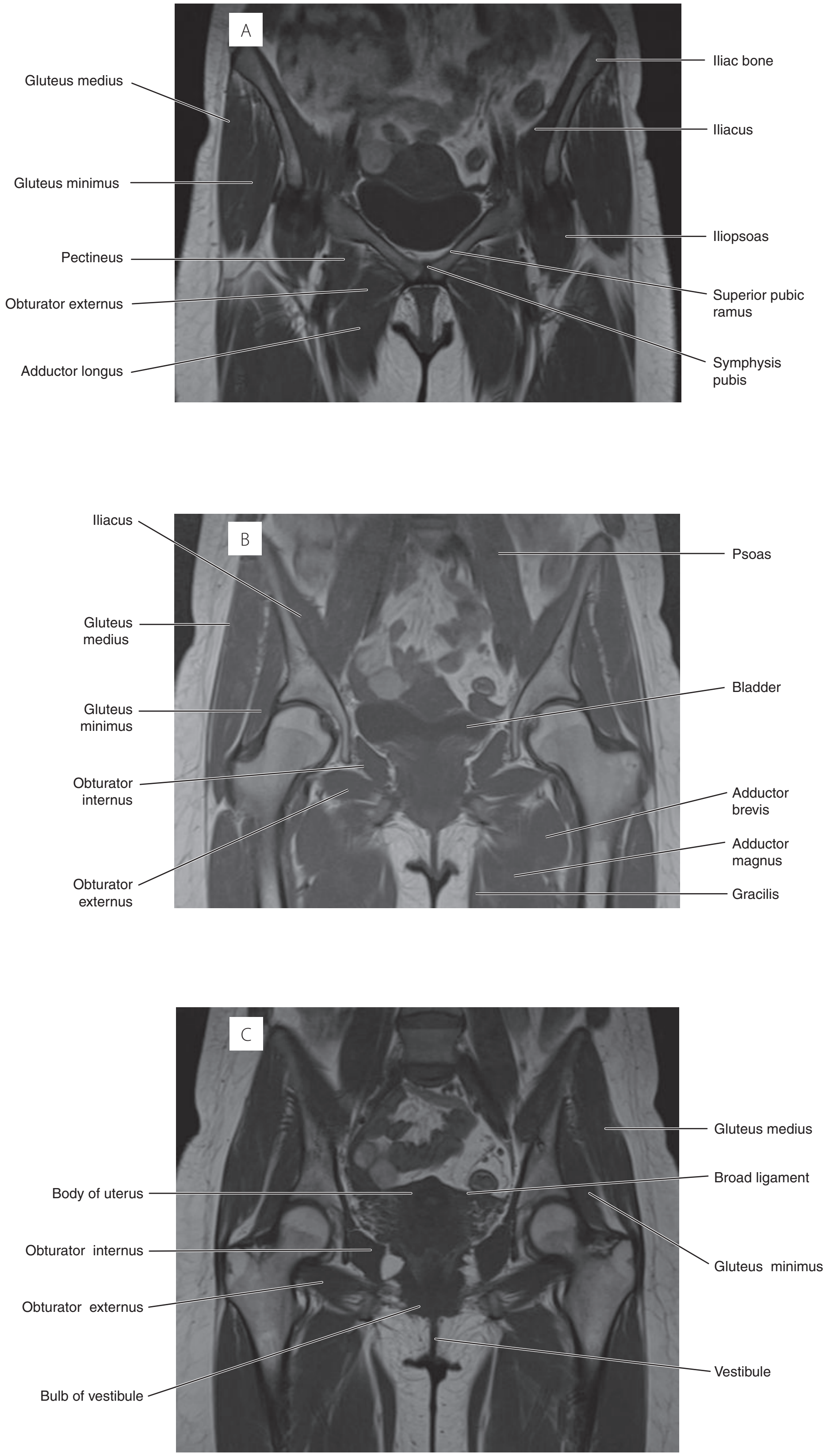


**Fig. 14.6** Coronal T1-weighted MR scans through the female pelvis.


**Fig. 14.6** (*cont.*)

- The pelvic floor is composed of a sling of muscles and fasciae known as the pelvic diaphragm.
- It separates the true pelvis from the perineum.
- This supports the pelvic viscera and is pierced by the rectum, urethra and vagina.
- It closes the pelvic outlet except for a gap between the anterior edges of levator ani. This gap is closed by the urogenital diaphragm.

The muscle groups are clearly visualized using MRI, especially on T1-weighted sequences where the low signal of the muscles contrasts with the high signal of the pelvic fat.

The muscle groups are divided into:

- superior: pelvic diaphragm – levator ani/coccygeus
- inferior: superficial muscles – perineum
  - anteriorly urogenital perineum
  - posteriorly anal perineum.

## Female perineum

- The perineum is the area inferior to the pelvic diaphragm, i.e. below levator ani.
- A line drawn between the ischial tuberosities passing just anterior to the anus divides the perineum into an anterior urogenital triangle and a posterior anal triangle.
- The midpoint of this line is the perineal body or central tendon of the perineum.

The boundaries of the perineum are as follows:

- anteriorly: pubic symphysis
- posteriorly: coccyx
- anterolaterally: ischiopubic rami, ischial tuberosities
- posterolaterally: sacrotuberous ligaments.

The female perineum differs from the male perineum as follows:

- urogenital triangle is pierced by both the urethra and vagina
- urethra is in anterior wall of vagina
- clitoris does not contain part of urethra
- labia majora corresponds to the scrotal sac of the male
- it contains the vestibular bulbs
- the perineal membrane is less well defined
- the perineal body is behind the vagina.

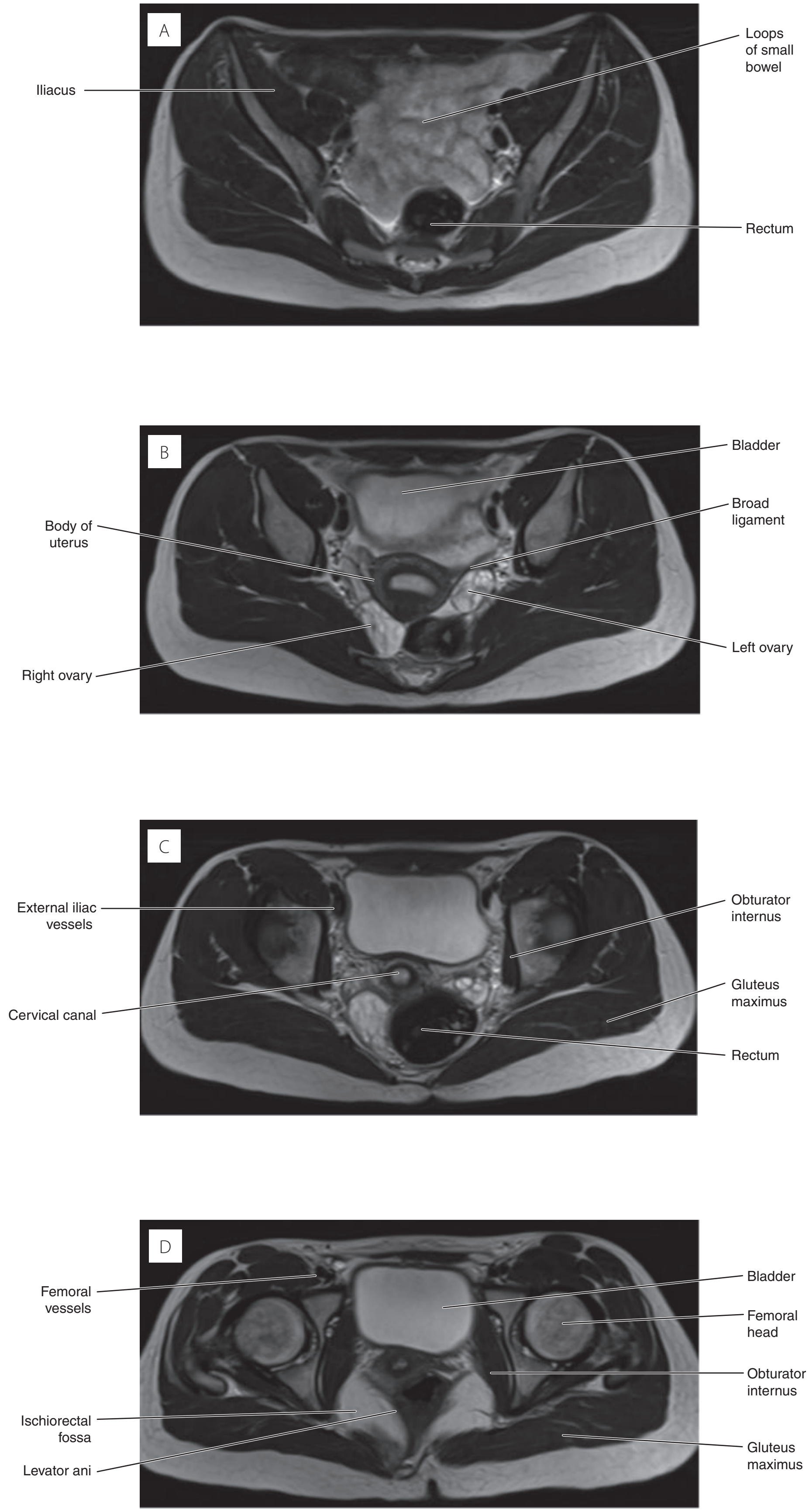


**Fig. 14.7** Axial T2-weighted MR scans through the female pelvis.

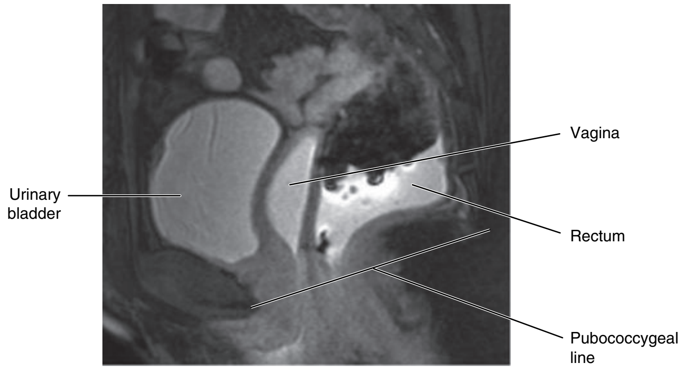


**Fig. 14.8** Proctogram demonstrating pelvic floor anatomy.

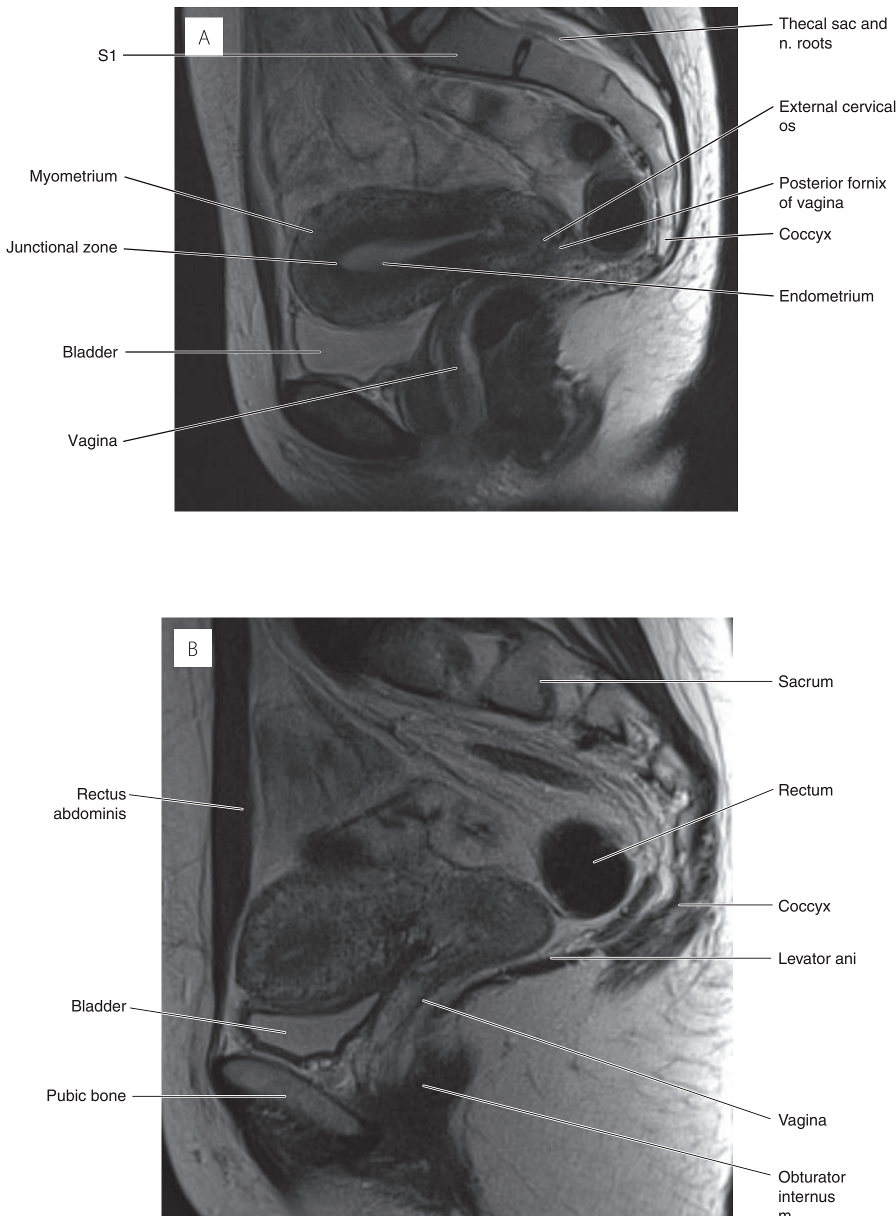


**Fig. 14.9** Sagittal T2 MRI of the female pelvic floor.

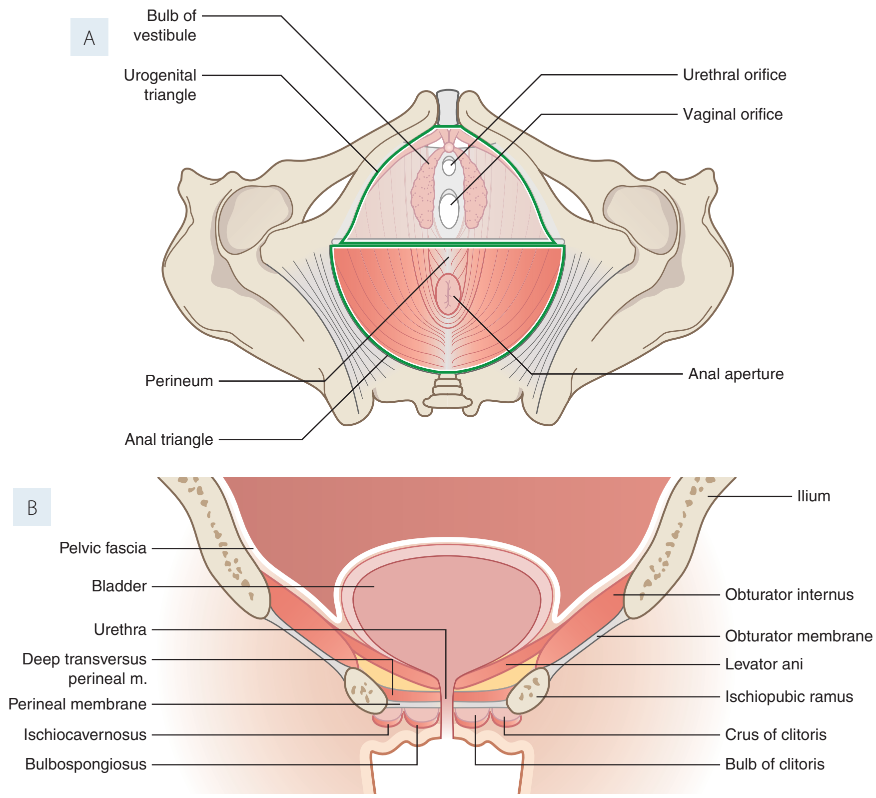


**Fig. 14.10** (A) Axial line diagram of the female perineum. (B) Coronal line diagram of the female perineum.

### Urogenital triangle

- Contains:
  1. mons pubis
  2. labia majora and labia minora
  3. clitoris
  4. vaginal and urethral orifices.
- It is divided into two parts by a perineal membrane.
- This is a triangular membrane which stretches horizontally across the deep perineal pouch.
- It is attached laterally to the ischiopubic rami with its apex attached to the arcuate ligament of the pubis.
- Posteriorly it fuses with the deep part of the perineal body. It is less well defined in the female.
- It is divided into two halves by the vagina and urethra, thus forming a triangle on each side of these structures. The pubo-urethral ligament links the two sides behind the pubic arch.

### Anal triangle

- It is the same in both males and females.
- Contains:
  1. anal canal
  2. anal sphincters
  3. levator ani
  4. ischiorectal fossae on each side.

### Deep perineal space

- Enclosed superficially by the perineal membrane and deeply by a fascial sheath – a condensation of the parietal pelvic fascia.
- Between these two layers lie the deep transverse perinei superficial to the compressor urethrae and sphincter urethrovaginalis.
- The internal pudendal artery enters this pouch on each side and gives off arteries to the clitoris.

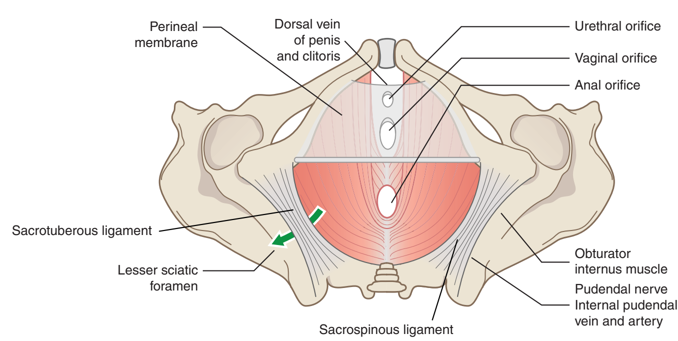


**Fig. 14.11** Areas of communication between the perineum and other regions.

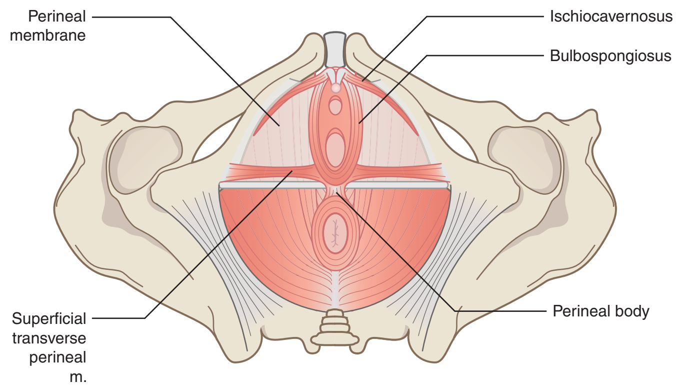


**Fig. 14.12** Muscles of the female perineum.

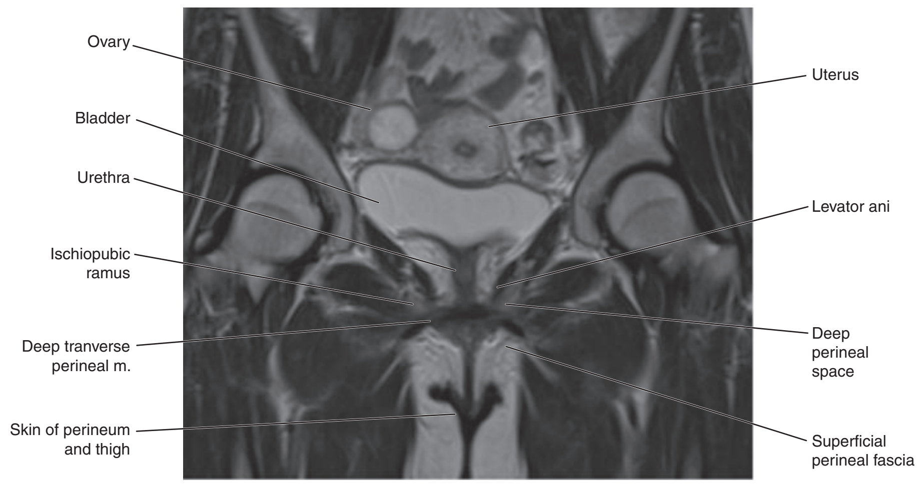


**Fig. 14.13** Muscles and fasciae of the female perineum – coronal T2-weighted MRI.

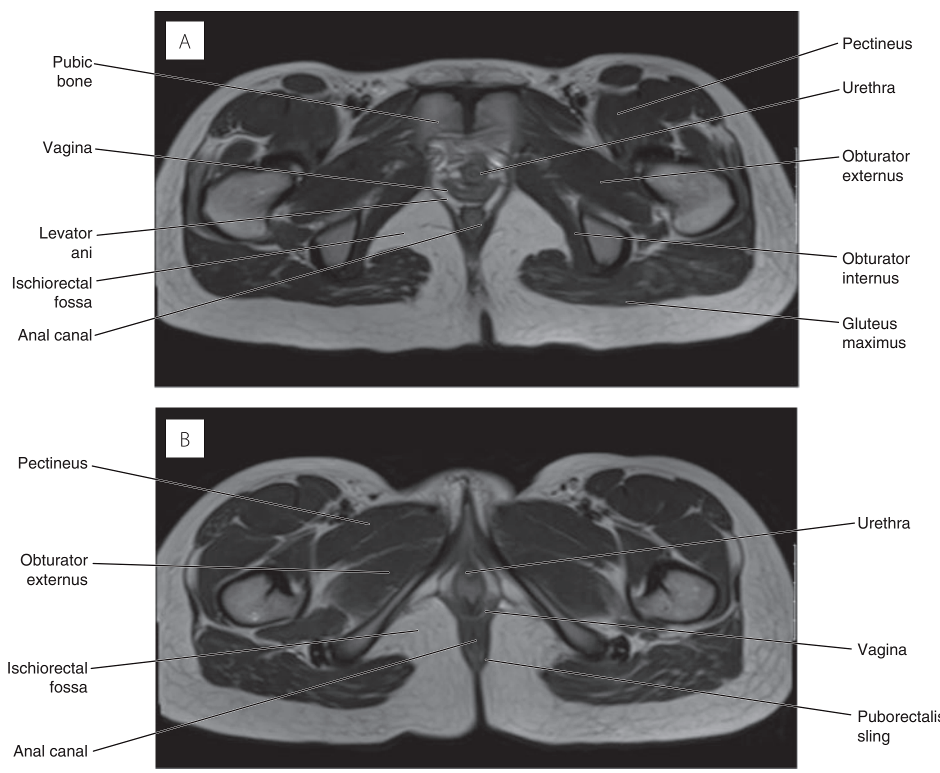


**Fig. 14.14** Axial T2 MRI of the female perineum.

### Superficial perineal space

- Enclosed by fatty and membranous (Colles') fascia.
- Colles' fascia attaches posteriorly to the posterior border of the perineal membrane and laterally to the pubic arch.
- Anteriorly this is continuous with the anterior abdominal wall (Scarpa's) fascia and is continuous over the clitoris.

It contains:

1. greater vestibular or Bartholin's glands at the posterior limit of each bulb
2. bulbospongiosus muscles which cover the bulb of the vestibule and separated in the midline by the vagina and urethra
3. fibromuscular perineal body – small mass of fibrous tissue located at the centre of the perineum – to which the anal sphincter, bulbospongiosus, transverse perineal and levator ani muscles attach
4. root of the clitoris
5. superficial perineal muscles.

## Pelvic ligaments

These ligaments can be divided into true ligaments due to their fibrous structure and the support they provide to the pelvic viscera whilst others are simply folds of peritoneum. CT and MRI allow visualization of several of these ligaments.
Peritoneal folds

- broad ligament
- vesicouterine ligament
- rectovaginal folds.

True ligaments

- round ligaments
- cardinal ligaments/transverse cervical ligaments/ Mackenrodt ligament
- uterosacral ligaments
- ovarian ligament /round ligament of ovary
- suspensory ligament of the ovary/ infundibulopelvic ligament.

### The broad ligament

- Formed by anterior and posterior reflections of peritoneum passing over the fallopian tubes.
- It is a double layered sheet that extends from the sides of the uterus to the lateral walls and floor of the pelvis.
- The upper border is free.
- The lower border is continuous with the peritoneum over the bladder, rectum and pelvic sidewall.
- It holds the uterus in place and contains the fallopian tubes in its free border, connective tissue/ smooth muscle (parametrium), the round ligaments, uterine vessels, lymphatics and laterally the ovarian ligaments.
- Divided into:

1. Upper mesosalpinx - attached above to the fallopian tube, posteroinferiorly to the mesovarium. Superiorly it is attached to the suspensory ligament of the ovary and medially to the ovarian ligament.

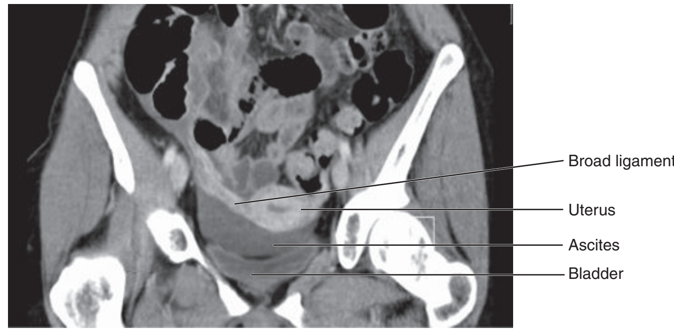


**Fig. 14.15** Coronal CT of the female pelvis showing the broad ligament.

2. Posterior mesovarium – attached to hilum of the ovary
3. Inferior mesometrium – largest part and extends from the pelvic floor to the ovarian ligament and the uterine body.

### Uterovesical and rectovaginal folds

- The anterior/uterovesical fold consists of peritoneum reflected onto the bladder from the uterus forming the vesico-uterine pouch.
- The posterior/rectovaginal fold consists of peritoneum reflected from the posterior vaginal fornix onto the front of the rectum thus creating the pouch of Douglas or recto-uterine pouch.

### Round ligaments

- Flattened bands 10–12 cm in length.
- Originate from the uterine cornu and pass through the inguinal canal into the labia majora.
- The canal of Nuck (processus vaginalis) is a peritoneal diverticulum created where the round ligament enters the inguinal canal.

### Cardinal ligaments

- Condensations of pelvic fascia at the base of the broad ligament.
- Pass to the cervix and upper vagina from the pelvic side walls.

### Uterosacral ligaments

- Extend from the cervix and vagina to the sacrum.
- They form two ridges on either side of the pouch of Douglas, i.e. rectouterine folds

### Ovarian ligaments

1. Suspensory ligament of ovary attaches ovary to pelvic wall and contains ovarian artery and vein
2. Ovarian ligament attaches the inferomedial extremity of the ovary to the lateral angle of the uterus. It lies in the posterior aspect of the broad ligament and is continuous with the medial border of the round ligament.
3. Mesovarium.

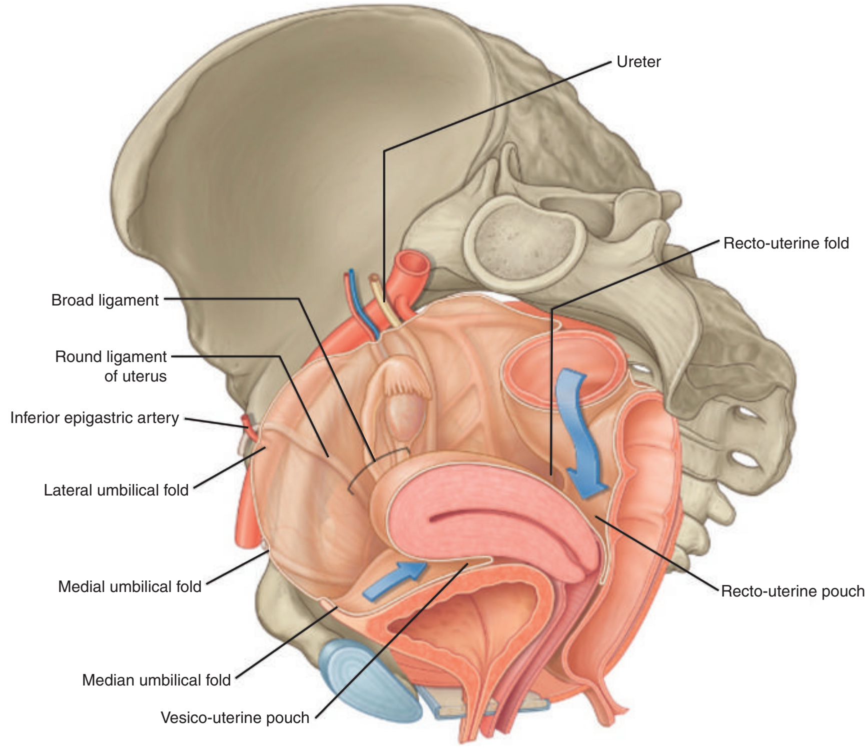


**Fig. 14.16** Peritoneal folds in the female pelvis.

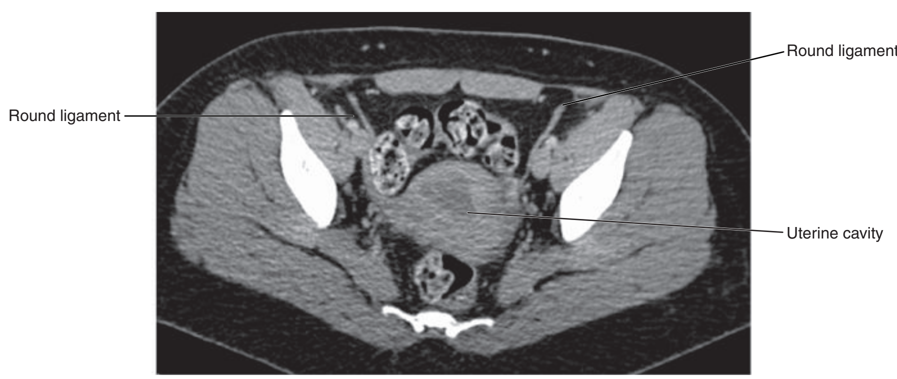


**Fig. 14.17** Axial CT showing the round ligaments.

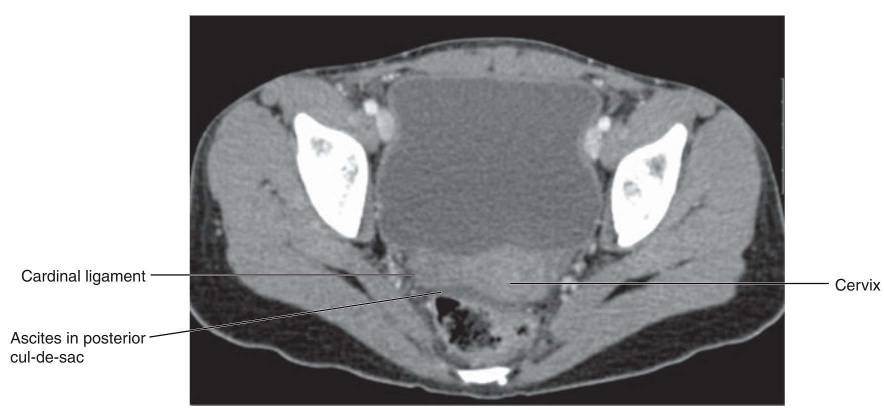


**Fig. 14.18** Axial CT showing the cardinal ligaments.

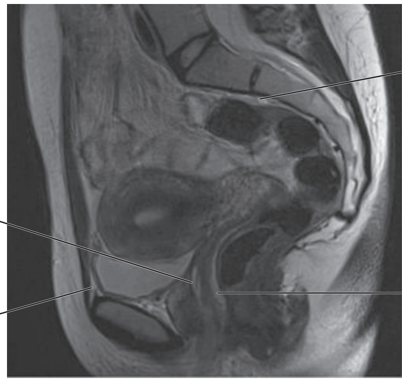


**Fig. 14.19** Sagittal T2 MRI of pelvis showing spaces.

### Pelvic spaces

These spaces contain loose connective tissue but are important surgical dissection planes.

- Vesicovaginal/vesicocervical space – between lower urinary tract and vagina/cervix
- Rectovaginal space – contains fascia which provides support for the rectum
- Paravesicle and pararectal spaces
- Presacral space – between rectum and sacrum/coccyx. Extends as far as aortic bifurcation
- Parametrium – pelvic visceral fascia and contents adjacent to the cervix
- Space of Retzius/ prevesical/ retropubic space – separated from the anterior abdominal wall by transversalis fascia.

# Neurovascular anatomy of the female pelvis

## Pelvic vasculature

- The aorta bifurcates anterior to the fourth lumbar vertebral body at the level of the iliac crests.
- The common iliac arteries enter the pelvis anterior to the common iliac veins on the medial border of the psoas muscles.
- The left common iliac artery is shorter than the right artery.
- The common iliac arteries pass posteriorly to the ureters.
- The common iliac arteries bifurcate at the pelvic brim anterior to the sacroiliac joints into the internal and external iliac arteries.
- At the pelvic inlet the internal iliac arteries pass medially and posteriorly towards the sciatic notch.
- The external iliac arteries run along the medial aspect of the iliopsoas muscle under the inguinal ligament to enter the thigh.
- The internal iliac artery is smaller than the external iliac except in the fetus when it gives rise to the umbilical artery.
- The umbilical artery is the first branch of the internal iliac artery in the fetus and ascends on the deep surface of the anterior abdominal wall to the umbilicus. After birth it persists as the fibrous medial ligament.
- Anterior to the internal iliac artery are the ureter, ovary and fimbriated end of the fallopian tube.
- Posterior are the internal iliac vein, lumbosacral trunk and sacroiliac joints.
- Lateral is the external iliac vein and the obturator nerve.
- Medial is the parietal peritoneum.
- The internal iliac artery divides into anterior and posterior branches at the sciatic foramen.
- The anterior branch continues down to the ischial spine giving off the following branches (visceral):
  - superior vesical artery branch of umbilical artery
  - obturator artery – in 25% may arise from the inferior epigastric artery
  - vaginal artery – corresponds to inferior vesical artery in the male
  - uterine artery
  - middle rectal artery
  - internal pudendal artery
  - inferior gluteal artery.
- The posterior branch divides as follows (muscular):
  - iliolumbar artery
  - lateral sacral arteries
  - superior gluteal artery.
- The external iliac artery is separated from the bowel by the peritoneum.
- It is crossed at its origin by the gonadal vessels, genital branch of the genitofemoral nerve, deep circumflex iliac vein and by the round ligament.
- Posteriorly it is separated from the medial border of psoas by the iliac fascia.
- It gives off two branches just above the inguinal ligament:
  - inferior epigastric artery
  - deep circumflex iliac artery.
- The external and internal iliac veins accompany the arteries. They are medial lower down and then pass posteriorly as they ascend.

## Lymphatics

- Lymph drainage accompanies the vasculature.
- Three chains accompany the external iliac vessels and drain to the common iliac and paraaortic nodes:
  - one anterolateral to artery
  - one posteromedial to the vein
  - middle chain anteriorly to the vessels – contain obturator nodes.
- The internal iliac nodes drain to the common iliac nodes and then to the para-aortic nodes.


**Fig. 14.20** Angiogram demonstrating vascular anatomy of the female pelvis.


**Fig. 14.21** Maximum-intensity projection image obtained from a gadolinium-enhanced MRA of the pelvis.

- Sacral nodes drain to the internal chain.
- Normal lymph nodes are rarely seen on CT. The obturator group is especially important in the assessment of pelvic malignancy. The short axis is <8 mm. Most external iliac and common iliac nodes have a short axis <10 mm.

### CT PET

- Depicts lymph node metastases.
- However, in premenopausal women it is important to remember when interpreting these images that endometrial FDG uptake changes cyclically, increasing during the ovulatory and menstrual phases.
- Equally a corpus luteum cyst can transiently increase ovarian uptake.
- Any postmenopausal uptake is abnormal.

## Important nerves of the pelvis

- The pelvis contains the lumbosacral trunk, sacral and coccygeal plexuses and the pelvic parts of the sympathetic and parasympathetic systems.
- The lumbosacral plexus (L4, 5 and S1–4) lies on the piriformis muscle. Four major nerves arise from it:
  1. sciatic nerve – largest nerve in body and largest branch seen on CT/MR as it passes through greater sciatic foramen into the gluteal region

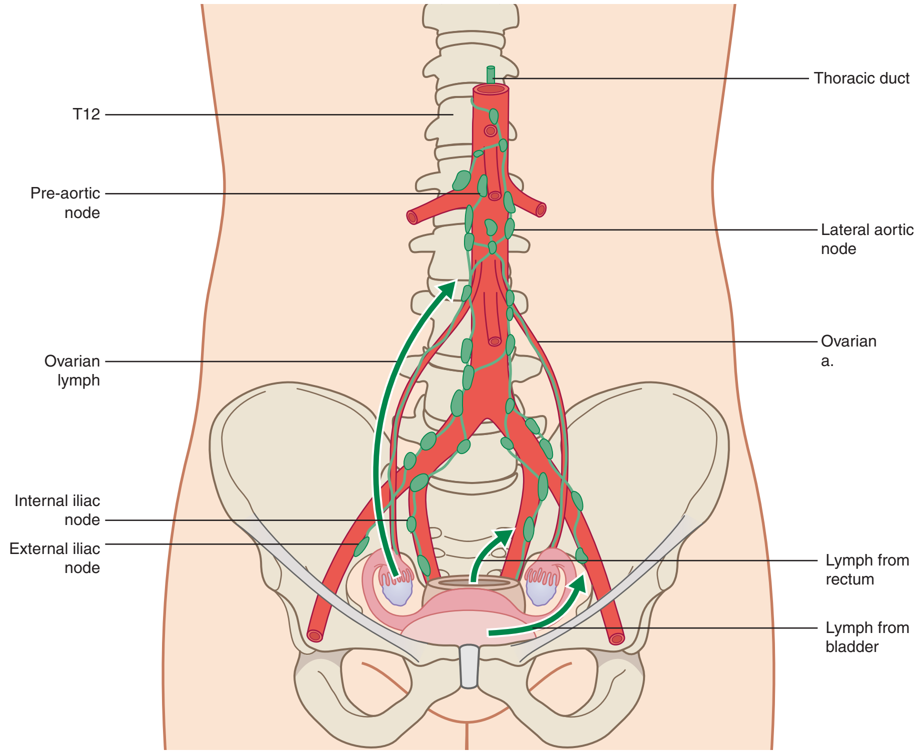


**Fig. 14.22** Pelvic lymphatics.

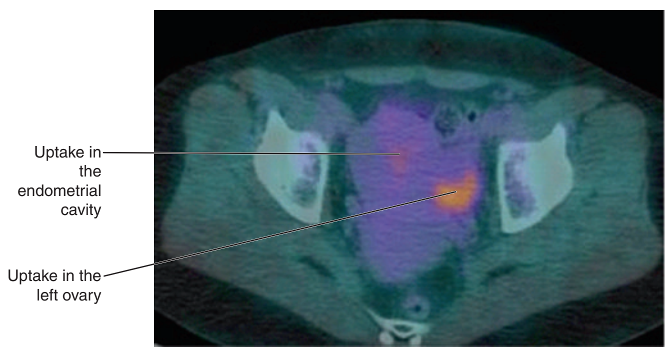


**Fig. 14.23** CT PET showing normal physiological uptake in the endometrium and left ovary.

2. pudendal nerve (S2, 3, 4) – leaves the pelvis between the piriformis and coccygeus muscles; enters the perineum through the lesser sciatic foramen
3. obturator nerve (L2, 3, 4) – descends medial to psoas, runs along lateral pelvic wall, posteromedial to the common iliac vein to enter obturator canal
4. femoral nerve (L2, 3, 4) – descends between the psoas and iliacus muscles before passing under inguinal ligament into the thigh.

## Pelvic viscera

### Bladder and urethra

- In the female pelvis the bladder lies at a lower level as it rests directly on the pelvic fascia above the perineal membrane.
- It is pyramidal in shape with a base, apex, superior and two inferior surfaces. The apex lies behind the symphysis pubis. It is from here that the urachal remnant passes up to the umbilicus, forming the median umbilical ligament. The base is triangular and the ureters enter the posterolateral angles. The inferior angle or neck gives rise to the urethra surrounded by the internal urethral sphincter. The body of the uterus rests on its posterosuperior surface and the cervix and vagina are posterior.
- It is extraperitoneal, with peritoneum being loose over it except posteriorly. Although less fixed than in the male the bladder is attached to the back of the pubis, lateral walls of the pelvis and rectum by condensations of pelvic fascia.
- The distal ureters enter the pelvis anterior to the iliac bifurcation. They run inferoposteriorly anterior to the

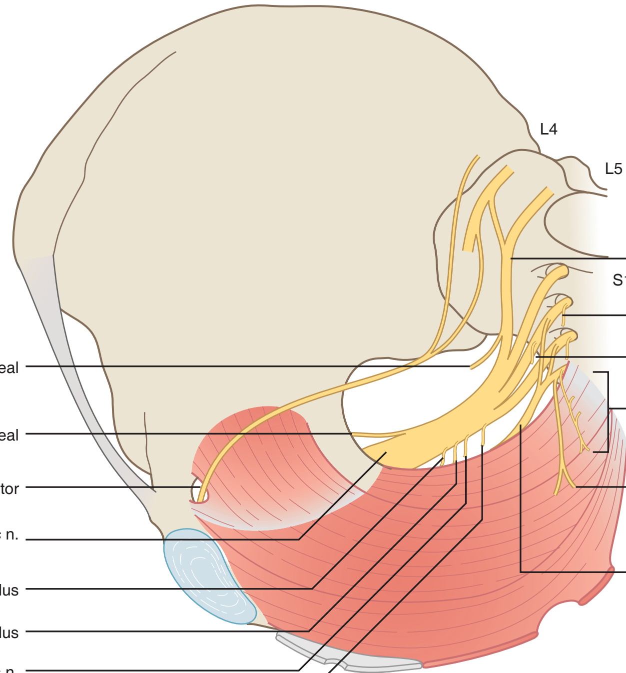


**Fig. 14.24** Sacral and coccygeal plexuses.

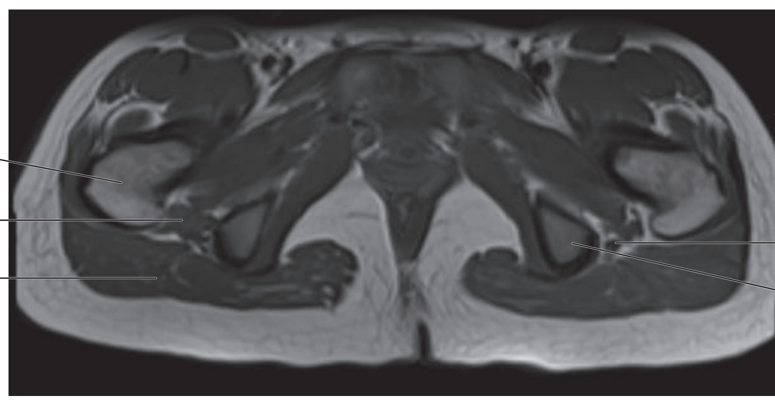


**Fig. 14.25** Axial T1 MRI demonstrating the sciatic nerve.

internal iliac artery and at the level of the ischial spine turn anteromedially to enter the posterolateral bladder. They run just above the lateral fornices of the vagina, lateral to the cervix and inferior to the uterine vessels within the broad ligament. The intramural ureters course for 2 cm before entering the bladder lumen.

- The female urethra is 4 cm long. It extends from the bladder neck to the vestibule, where it opens 2.5 cm behind the clitoris. It crosses the diaphragm anterior to the vagina. The external sphincter is at the diaphragm but less well developed than the involuntary internal sphincter at the bladder neck. Small paraurethral glands open into the vestibule on either side of the urethral orifice. They are equivalent to the male prostate.

#### Vascular supply

- Arterial:
  - bladder – superior and inferior vesical arteries
  - urethra – internal pudendal and vaginal arteries
- Venous
  - bladder – via a venous plexus to the internal iliac vein
  - urethra – internal pudendal and vaginal veins

#### Lymph supply

- Bladder – internal iliac and para-aortic nodes
- Urethra – internal iliac nodes

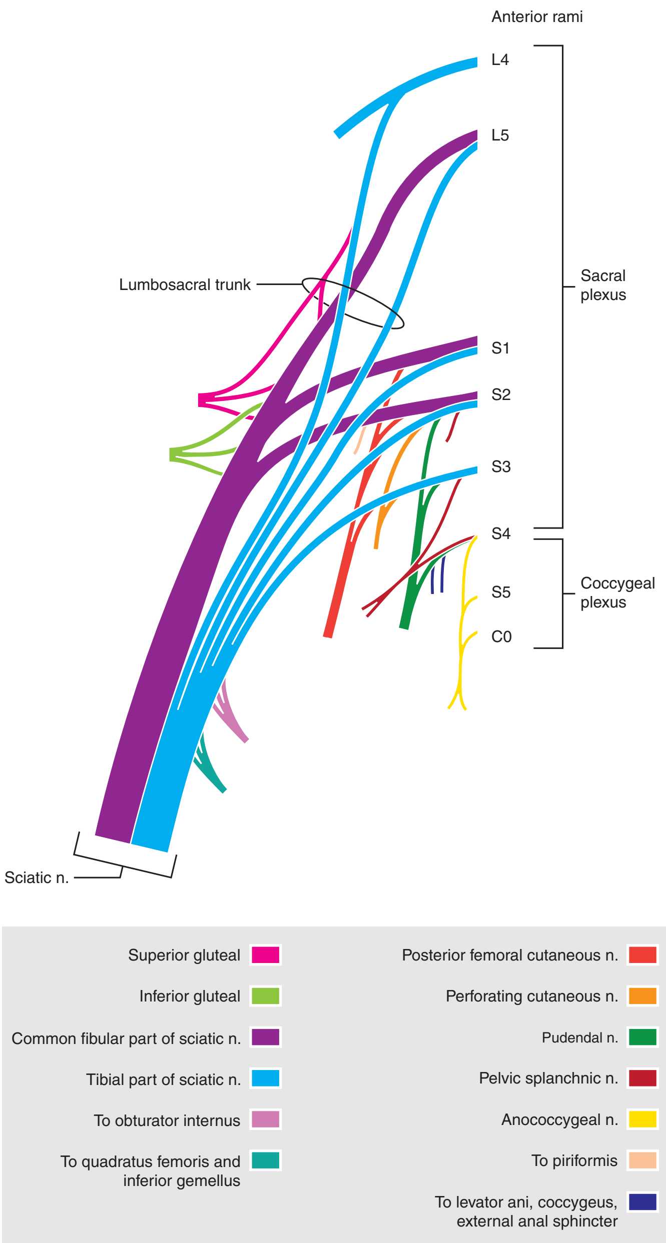


**Fig. 14.26** Components and branches of the sacral and coccygeal plexuses.

#### Nerve supply

- Bladder – vesical nerve plexus which is continuous with the inferior hypogastric plexus
- Urethra – pudendal nerve

#### Internal anatomy

- The bladder wall is trabeculated except at the trigone – the triangular area between the two ureteric orifices and the urethral orifice.

#### Plain radiographic anatomy

Intravenous urogram / cystogram

- Demonstrates the kidneys and bladder.
- The plain film often shows the bladder as a rounded soft tissue mass surrounded by darker perivesical fat.
- An impression on the dome of the bladder in a female after contrast administration is often seen and is due to the fundus of the uterus.

#### Cross-sectional anatomy

Ultrasound is used to assess the bladder wall.

- This should be <4 mm.
- The distal ureters can often be visualized.
- Colour Doppler enables identification of the ureteric jets.

MRI

- On T1-weighted sequences the bladder wall and contents are homogeneous, returning low signal.
- T2-weighted sequences enable good contrast between the high signal urine and the low signal bladder wall.

## Lower genital tract

### Vulva

- The female external organs are known collectively as the vulva: mons pubis, labia majora/minora, vestibule of vagina, clitoris, bulb of vestibule, greater vestibular glands.
- The vestibule is the cavity that lies between the labia minora. It contains the vaginal and urethral orifices and the openings of the greater vestibular glands (Bartholin's).
- The vestibular bulbs correspond to the bulb of the penis and lie on either side of the vestibule into which both the vagina and urethra open. These have erectile tissue and are covered by the bulbospongiosus muscles and then by the skin of the labia minora.

#### Vascular supply

- Arterial: superficial and deep external pudendal branches of the femoral artery and the internal pudendal artery on each side.
- Venous: vulval skin via the external pudendal veins to the long saphenous vein. Clitoral via deep dorsal veins to the internal pudendal vein and the superficial dorsal veins to the external pudendal and long saphenous veins.

#### Lymph supply

- Superficial and deep inguinal nodes.
- Lymph vessels in the perineum and lower part of labia majora drain to the rectal lymphatic plexus.

#### Nerve supply

- Anterior 1/3 labia – ilioinguinal nerve
- Posterior 2/3 labia – perineal nerve
- Lateral aspect – perineal branch of the posterior cutaneous nerve (S2)

### Vagina

- A fibromuscular tube that is approximately 7–9 cm in length and ascends up and back from the vestibule (cleft between labia minora) to surround the cervix at an angle of $>90^0$ to the uterine axis.
- The anterior and posterior walls are in close apposition

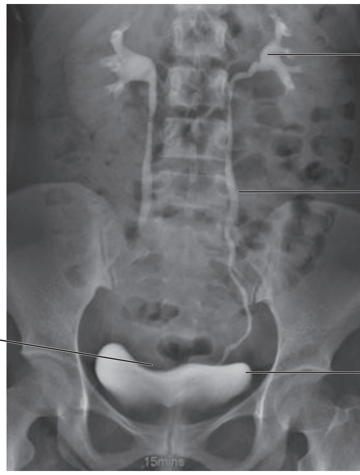


**Fig. 14.27** Female IVU showing bladder with superior indentation from uterus.

to each other except at the superior end where the cervix enters its cavity.

- The posterior wall is 1 cm longer than the anterior wall and is in contact with the external os.
- The recess around the cervix is divided into anterior, lateral and posterior fornices. The posterior fornix is the deepest and related to the rectouterine pouch.
- Inferiorly it pierces the perineal membrane with the urethra.
- The superior aspect of the posterior wall of the vagina is usually covered by peritoneum. The vagina is supported superiorly by the levator ani, transverse cervical, pubocervical and uterosacral ligaments and inferiorly by the perineal membrane and perineal body. The vagina shrinks in length following the menopause and the fornices virtually disappear.

### Relations

- Anterior : cervix, bladder base and urethra
- Posterior:
  - upper – rectouterine pouch of Douglas separating vagina from rectum
  - mid – Denonvillier's fascia separating vagina from ampulla of rectum
  - lower – perineal body separating vagina from anal canal
- Lateral: anterior fibres of levator ani, pelvic fascia and ureters
- Inferior: bulb of vestibule and perineal membrane

### Vascular supply

- Arterial from vaginal, uterine, internal pudendal and middle rectal branches of internal iliac arteries
- Venous from vaginal veins which form a plexus around the vagina that drain to the internal iliac veins

### Lymph supply

- Upper: internal/external iliac nodes
- Middle: internal iliac nodes
- Lower: superficial inguinal nodes

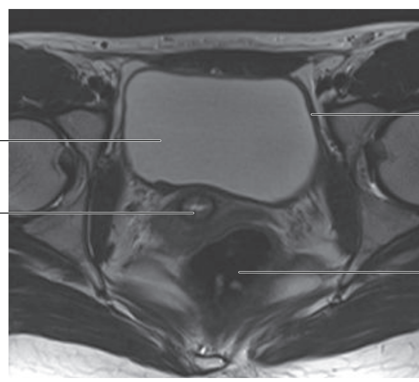


**Fig. 14.28** Axial T2 MRI showing high-signal urine and low-signal bladder wall.

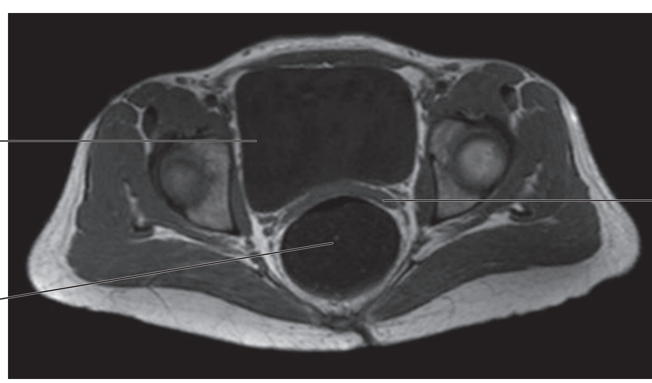


**Fig. 14.29** Axial T1 MRI showing low-signal urine within bladder lumen.

#### Nerve supply

- Upper vagina: pelvic splanchnic nerves
- Lower vagina: pudendal nerve

#### Internal anatomy

- Inner mucosa and external muscular layer composed of inner circular and thicker outer longitudinal muscle.
- There are two longitudinal ridges on its epithelial surface anteriorly and posteriorly. Transverse rugae extend from these. They are divided by sulci of varying depths.

#### Cross-sectional anatomy

Ultrasound

- Seen as a highly echogenic stripe which makes an acute angle with the uterus

MRI

- The internal anatomy can be visualized on the T2 sequences.
- In the early proliferative stage the wall returns low signal and the mucosa and mucus high signal.
- In the secretory stage both the wall and mucus are thickest and of highest signal.
- In the postmenopausal phase the signal intensity of the mucosa decreases and the central mucus becomes thinned.
- Post gadolinium both the wall and submucosa enhance.

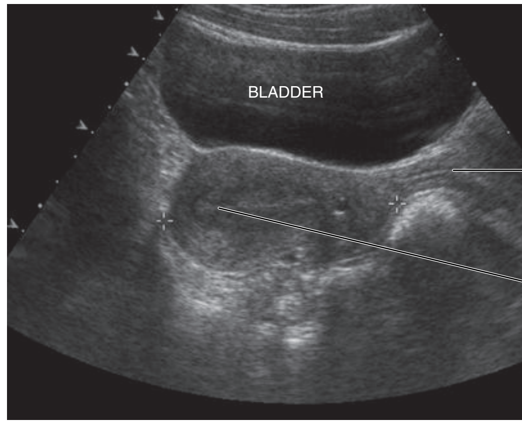


**Fig. 14.30** Transabdominal US showing the echogenic stripe of apposed surfaces of vaginal mucosa.

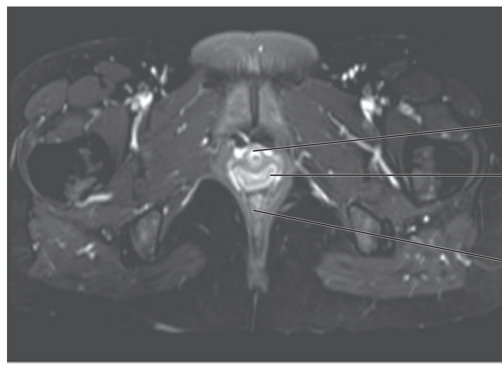


**Fig. 14.31** Axial T1 MRI post gadolinium showing the enhancement pattern of the vaginal wall and submucosa.

### Uterus

- An inverted pear-shaped organ lying between the bladder and rectum.
- Divided into a fundus, body and cervix. The body narrows to a waist called the isthmus, below which lies the cervix.
- The vagina divides the cervix into supravaginal and vaginal parts.
- The fallopian tubes enter each superolateral angle at the cornu of the uterus.
- The cavity of the uterus is triangular in coronal section and flat in anteroposterior plane. It measures 6 cm from the external os to the fundus. The cavity communicates with the cervical canal via the internal os and the cervical canal communicates with the vagina via the external os.
- The cervix is narrower and more cylindrical than the body and measures approximately 2.5 cm.
- The uterus is extraperitoneal – the peritoneum covers the uterus anteriorly and superiorly except for the vaginal part of the cervix. The peritoneum is reflected up over the anteroinferior surface of the uterus forming the vesicouterine pouch before passing off the posterior surface of the uterus and up over the rectum to form the rectouterine pouch of Douglas.

#### Position

- Lies in the true pelvis but its position may change.
- Flexion refers to the axis of the body relative to the cervix.
- Version refers to the axis of the cervix relative to the vagina.
- In the nulliparous female it is often anteverted and anteflexed, i.e. the long axis of the uterus lies horizontally in the sagittal plane.
- In 10–15% of females it is retroverted, i.e. the cervix is directed back and up but still anteflexed.
- If retroflexed the uterus is directed posteriorly to that of the cervix.

#### Relations

- Anterior: uterovesical pouch and superior surface of bladder
- Posterior: pouch of Douglas with large and small bowel within it
- Lateral: broad ligaments and uterine vessels

#### Size and shape

#### Vascular supply

- Arterial: dual blood supply from the uterine artery – a branch of the internal iliac. It passes over the ureter at the level of the internal os. It then courses superiorly along the lateral margin of the uterus in the broad ligament where it anastomoses with the ovarian artery.

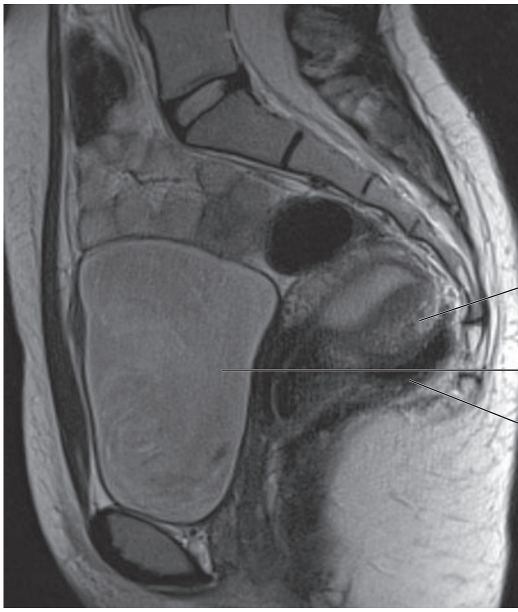


**Fig. 14.32** Sagittal T2 MRI showing a retroverted uterus.

Uterine arteries give rise to the arcuate arteries seen in the outer one-third of the uterus.
- Venous: the uterine vein accompanies the artery and drains into the internal iliac vein.

### Lymph supply

- Fundus: para-aortic nodes
- Body/cervix: internal and external iliac nodes, a few accompany the round ligament through the inguinal canal to the superficial inguinal nodes

### Nerve supply

- Derived from inferior hypogastric plexus especially uterovaginal plexus which lies in the broad ligament
- Parasympathetic fibres are from the pelvic splanchnic nerves

### Internal anatomy

Uterine wall consists of three layers:
- outer serous coat or perimetrium – peritoneum supported by a thin layer of connective tissue
- middle muscular coat or myometrium
- inner mucous layer or endometrium – formed by a layer of connective tissue or stroma. Lined by columnar (non-ciliated) epithelium and tubular glands. Divided into two layers:
  1. stratum functionalis (shed during menstruation)
  2. stratum basalis (permanent and adjacent to myometrium) contains spiral arteries.

Cervix:
- Endocervical canal lined by mucus-secreting columnar epithelium; often seen as folds called plicae palmatae
- Ectocervix lined by stratified squamous epithelium.

**Table 14.2**

| | Length (cm) | AP diam. (cm) | Features | |
|---|---|---|---|---|
| Neonatal | 2.3–4.6 | 0.8–2.1 | Echogenic endometrium/ fluid | Cervix > uterus |
| Prepubertal | 2–3.3 | 0.5–1.0 | Tubular | Cervix 2/3 length of uterus |
| Adult | | | Pear-shaped | Body diameter and length double cervix |
| Nulliparous | 8 | 5 | | |
| Primiparous | +1 | +1 | | |
| Multiparous | +2 | +2 | | |
| Post-menopausal | 3.5–6.5 | 1.2–1.8 | | |

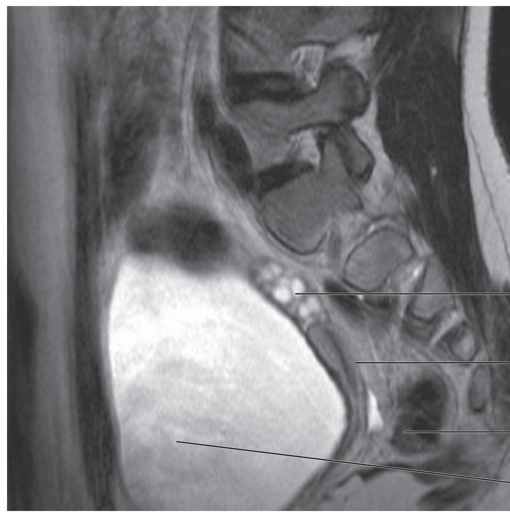


**Fig. 14.33** Sagittal T2 MRI of a child's pelvis.

### Cross-sectional anatomy

Ultrasound

Transabdominal ultrasound enables evaluation of the entire pelvis. Size and position of the uterus can be determined as well as gross pathology.
- Transvaginal US allows detailed evaluation of the internal structure of the uterus.
- The muscular myometrium forms most of the uterine wall.
- It is composed of three layers that can be identified by ultrasound:
  1. inner layer or junctional zone – thin, compact, hypoechoic layer surrounds echogenic endometrium forming a subendometrial halo
  2. intermediate layer – thickest, uniform low to moderate echogenicity
  3. outer layer – less echogenic than intermediate layer, separated from it by arcuate vessels.

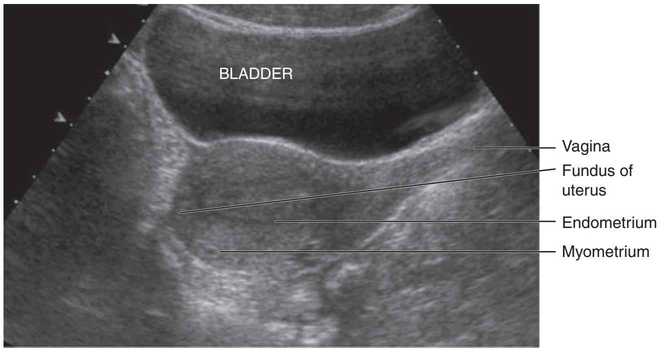


**Fig. 14.34** Transabdominal US showing the uterus in longitudinal section.

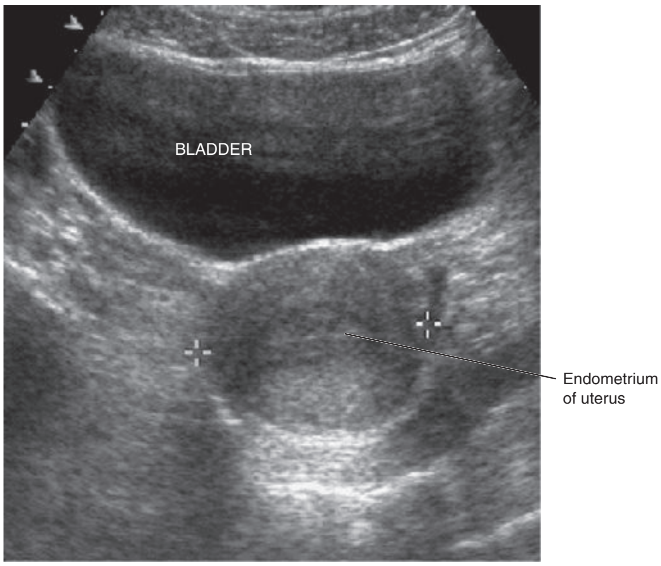


**Fig. 14.35** Transabdominal US showing the uterus in transverse section.

- The arcuate arteries branch into the radial arteries which run in the intermediate layer to the level of the inner layer. These radial arteries then branch into the spiral arteries which supply the functional layer of the endometrium.
- The uterine veins are larger than the arteries and often seen as anechoic areas.
- The Doppler waveform of the uterine arteries shows a high-velocity, high-resistance pattern.
- The endometrium is a mucosal layer which lines the myometrium.
- It is continuous below with the vaginal mucosa through the external os and with the peritoneum above through the os of the fallopian tubes.
- On ultrasound it is a thin echogenic line as a result of specular reflection from the interface between opposing surfaces of the endometrium.
- The endometrium is composed of a superficial functional layer and a deep basal layer.
- The functional layer thickens throughout the menstrual cycle and is shed with menses.
- The basal layer remains intact during the cycle and contains the spiral arteries, which become tortuous and elongate to supply the functional layer as it thickens.

**Early proliferative stage days 0–6; 4–8 mm**

Thin echogenic line as a result of specular reflection from the interface between opposing surfaces of endometrium. Note thin hypoechoic inner layer of myometrium (Fig. 14.37)

**Late proliferative stage days 6–14; 6–10 mm**

Triple layer appearance of endometrium – central echogenic line due to opposed endometrial surfaces surrounded by thicker hypoechoic functional layer, bounded by outer echogenic basal layer (Fig. 14.38)

**Secretory phase days 15–28; 7–14 mm**

The functional layer surrounding the echogenic line has become more hyperechoic due to increased mucus and glycogen within the glands as well as increased number of interfaces caused by the tortuosity of the spiral arteries (Fig. 14.39).

**Post menopausal < 8 mm**

Endometrium becomes atrophic and is seen as a thin echogenic line

3D ultrasound allows multiple views to be reconstructed from a single sweep. The data are displayed in three simultaneous planes. Multiplanar and rendered images can then be rotated and sliced through as with CT or MR. A central localizer point on each image shows the precise location in all three planes.

CT

- Seen as a homogeneous soft tissue mass dorsal to the bladder. May be a central area of low attenuation.
- If a vaginal tampon is used seen as a tubular air-filled structure.
- Post intravenous contrast the uterus enhances and the ureters can be identified laterally to the cervix.
- The broad ligament appears as a thin soft tissue density extending anterolaterally from the uterus to the pelvis sidewalls.

MRI

- Uterus
  - T1 – uniform signal of both the uterus and cervix
  - T2 – three distinct zones:
    - endometrium – high signal

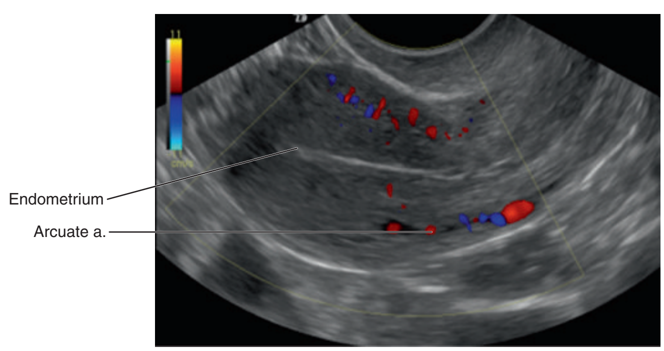


**Fig. 14.36** Normal Doppler flow of the myometrium showing prominent flow in the arcuate arteries.

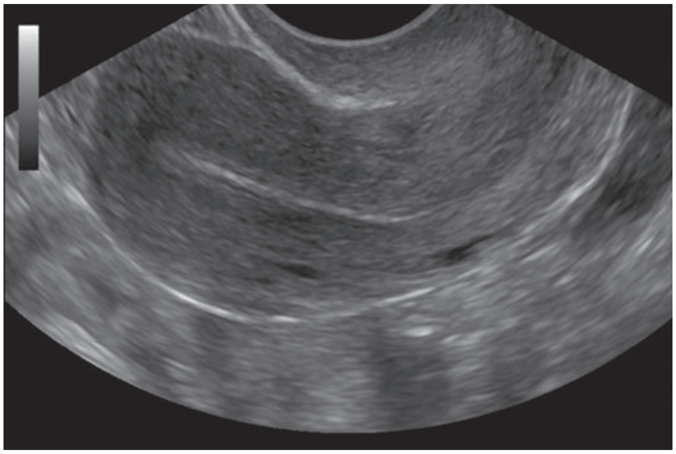

**Fig. 14.37** Transvaginal ultrasound showing normal thin early proliferative endometrium.

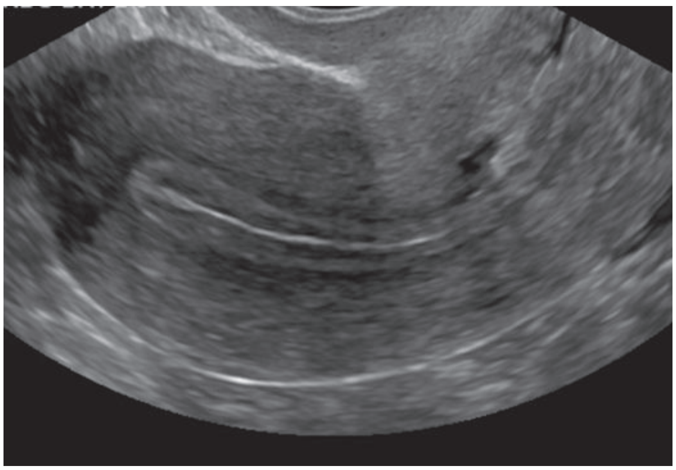

**Fig. 14.38** Transvaginal ultrasound showing normal late proliferative endometrium with triple-layer appearance. Central echogenic line due to opposed endometrial surfaces surrounded by thicker hypoechoic functional layer bounded by outer echogenic basal layer.

- junctional zone – low signal 2–8 mm, thick inner myometrium, low water content
- outer myometrium – intermediate signal

- Post gadolinium
  - pattern of enhancement dependent on menstrual cycle and hormonal status
  - peak enhancement of myometrium at 120 s post injection and decreases over time
  - absence of junctional zone
  - slight enhancement only of endometrium in early phase with marked enhancement on delayed images
- Premenopausal
  - endometrium thickens in secretory phase up to 1 cm
  - myometrial signal increases in secretory phase due to increased water content and vascular flow
  - low signal uterine contractions which may bulge the uterine contour
  - OCP – both endometrium and junctional zone become thin
- Postmenopausal
  - small, indistinct zonal anatomy
  - endometrium <2–3 mm
  - low signal myometrium
  - no cyclical variation
  - similar appearance to postradiation therapy
  - loss of ovarian function
- HRT
  - compares to reproductive age but no cyclical variation

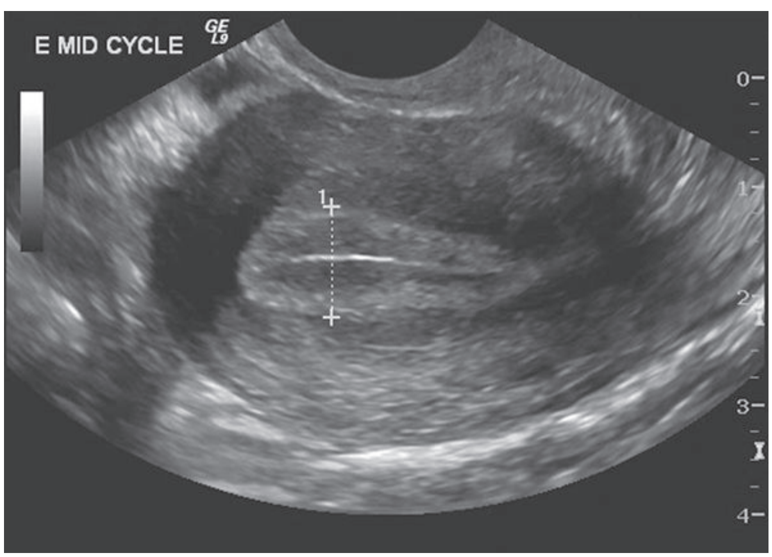


**Fig. 14.39** Transvaginal sagittal ultrasound of the uterus performed during secretory stage of the menstrual cycle showing the appearances of the endometrium at this stage (measured). The central echogenic line is due to the interface of the opposing surfaces of the endometrium. The functional layer of the endometrium surrounding the echogenic line is hyperechoic at this stage.

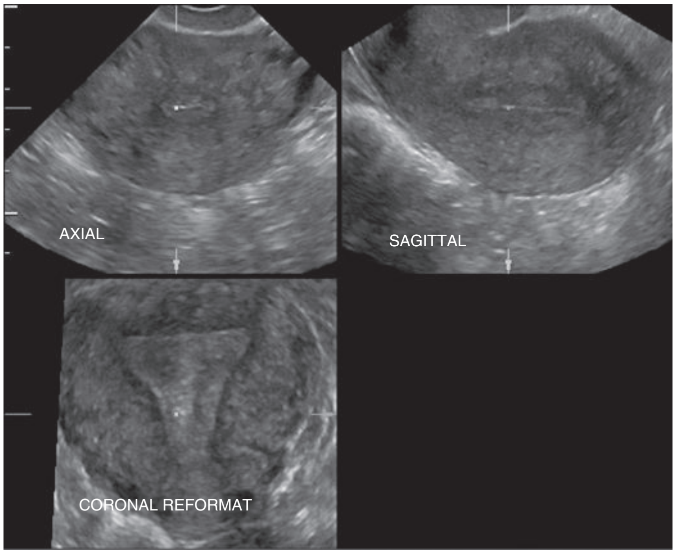


**Fig. 14.40** 3D ultrasound of the uterus and endometrium.

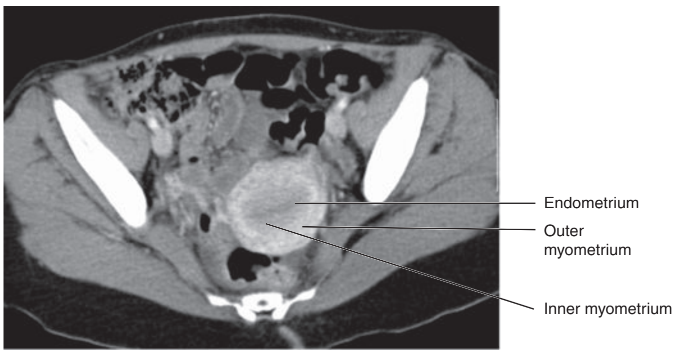


**Fig. 14.42** Axial CT of the female pelvis post intravenous contrast showing uterine enhancement.

- Cervix
  - the appearances do not change with the menstrual cycle or the OCP
  - T2 – three distinct zones:
    - endocervical canal – high signal 3.8–4.5 mm
    - stroma – low signal 3.8–4.2 mm, elastic fibrous tissue, continuous with junctional zone
    - outer layer – intermediate signal, smooth muscle, continuous with the outer myometrium

### Fallopian tubes

These connect the uterus to the peritoneal cavity and are attached to the posterior broad ligament by the mesosalpinx.

- 7–12 cm in length
- They run in the upper free margin of the broad ligament.
- Composed of four segments:
  - intramural/interstitial – pierces the uterine wall; 0.7 mm wide and 1 cm long; narrowest part; opens into cavity via uterine ostium

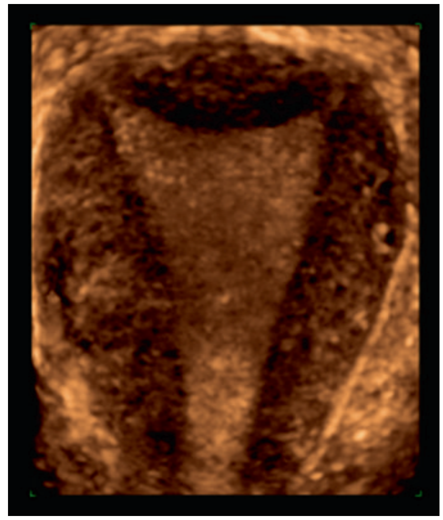

**Fig. 14.41** 3D reformat showing the entire endometrial and fundal contour.

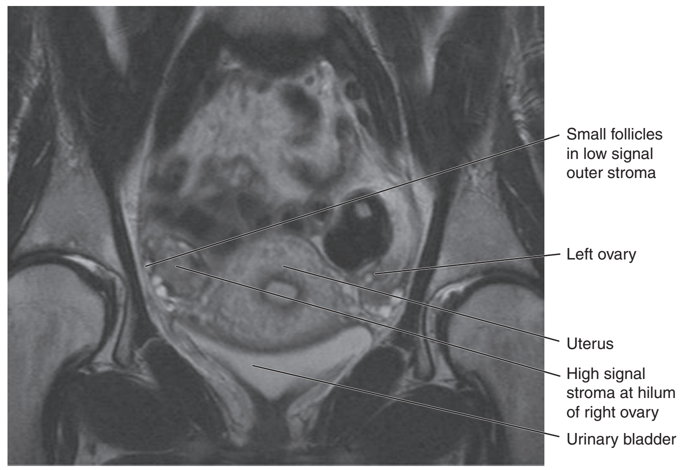


**Fig. 14.43** Coronal T2-weighted image through the female pelvis showing the uterus and both ovaries with the high-signal central stroma and lower outer stroma.

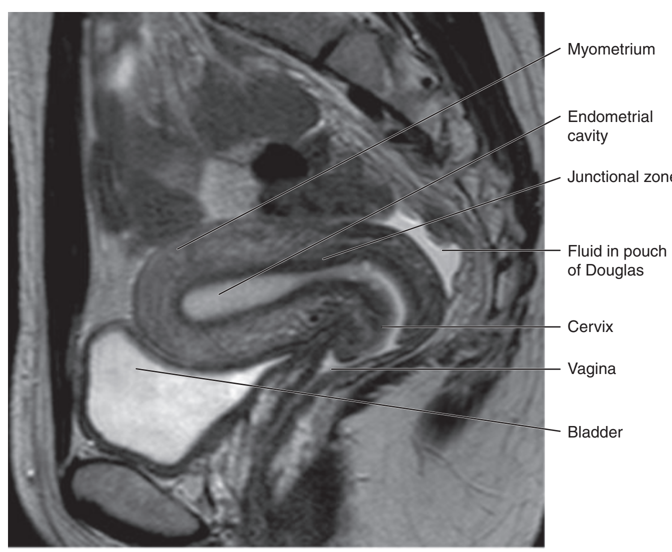


**Fig. 14.44** Sagittal T2-weighted sequence through the female pelvis showing the anatomical relations of the uterus.

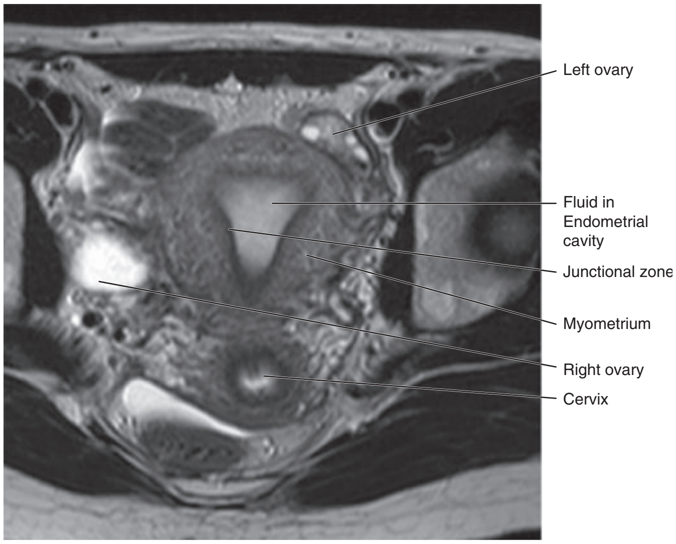


**Fig. 14.45** Axial T2-weighted sequence showing the anteverted uterus and both ovaries containing follicles.

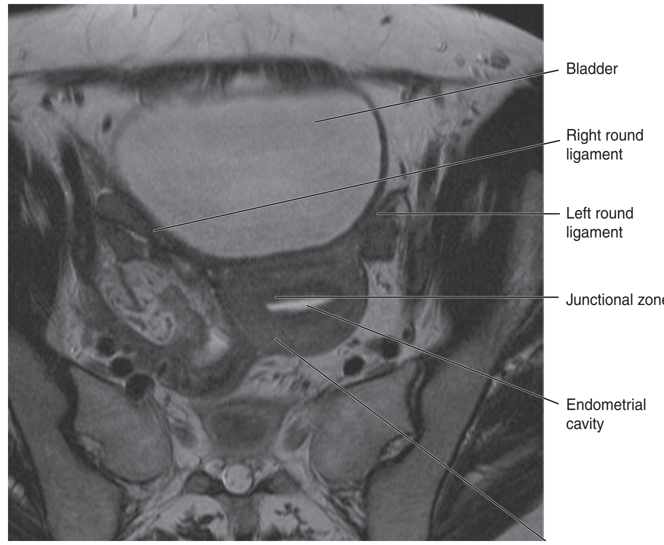


**Fig. 14.46** Axial T2 MRI scan of the female pelvis – small FOV.

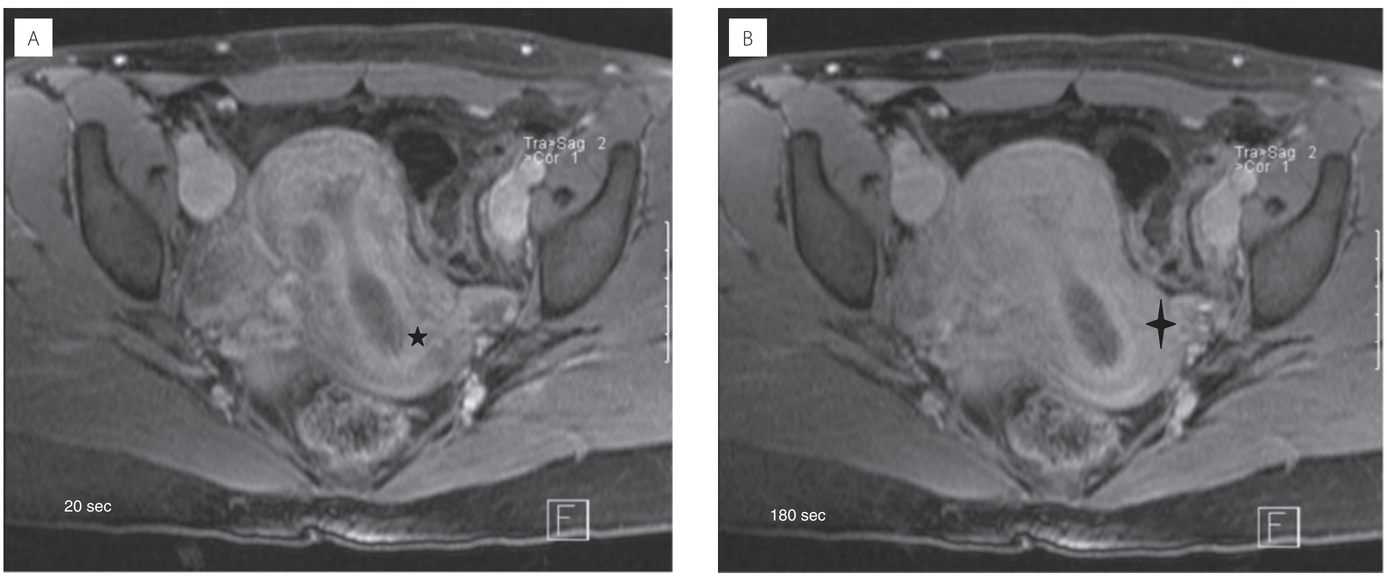


**Fig. 14.47** (A) Dynamic contrast-enhanced axial T1 MRI: showing rapid early subendometrial enhancement at 20 seconds. (B) Dynamic contrast-enhanced axial T1 MRI: showing maximal myometrial enhancement at 180 seconds.

- isthmus – 1–5 mm wide and 3 cm long; long and narrow part lateral to the uterus
- ampulla – 1 cm wide and 5 cm long – dilated tortuous outer part; fertilization usually occurs here
- infundibulum – funnel-shaped lateral part which extends beyond the broad ligament and overhangs the ovary with its fimbriae – one of which is attached to the ovary; its opening into the peritoneal cavity is called the abdominal ostium.

### Vascular supply

- Ovarian and uterine arteries with corresponding venous drainage

### Lymph supply

- Para-aortic nodes

### Nerve supply

- Ovarian and uterine plexuses
- Afferent fibres from the tubes are contained in T11, T12 and L1.

### Plain radiographic anatomy

HSG

- The isthmus and internal os may be seen.
- The uterine cavity is often triangular and smooth-walled leading to the narrowed isthmus and then the wider tortuous ampulla.
- Contrast should spill freely into the peritoneal cavity.

- Longitudinal ridges may be seen on the anterior and posterior walls of the cervical canal.
- In nulliparous females they may have branches running laterally – the plicae palmatae.
- The walls of the uterus may show longitudinal folds and polypoid filling defects may be seen in the secretory phase.

## Ovaries

- Paired reproductive and endocrine organs that lie in the ovarian fossae between the obliterated umbilical artery anteriorly and the internal iliac artery and ureter posteriorly.
- They are attached to the back of the broad ligament by the mesovarium.
- Their anterior borders are attached to the infundibulum of the fallopian tube.
- The suspensory ligament of the ovary is a part of the broad ligament lateral to the mesovarium and running lateral to the pelvic wall. It connects the superior end of the ovary to the lateral pelvic wall.
- Further support is due to the ovarian ligament – a continuation of the round ligament which runs from the medial aspect of the ovary to the cornu of the uterus.

**Table 14.3**

| | Volume 0.523 × length × width × height | Weight | Size | Follicles |
|---|---|---|---|---|
| Neonatal | 2.7 $cm^3$ | | 1.5 × 0.5 × 0.5 cm | Multiple due to influence of maternal hormones |
| 1–8 years | 1.7 $cm^3$ | | | Microcystic ovary – follicles < 2 mm in diameter |
| > 8 years | 4.2 +/− 2.3 $cm^3$ | | | Multicystic ovary > 6 follicles > 4 mm in diameter |
| Adult | 10 +/− 6 $cm^3$ | 2–8 g | 3 × 1.5 × 2 cm Double in size in pregnancy | |
| Postmenopausal | 2–6 $cm^3$ > 8 $cm^3$ abnormal | 1–2 g | 2 × 1.5 × 0.5 cm | |

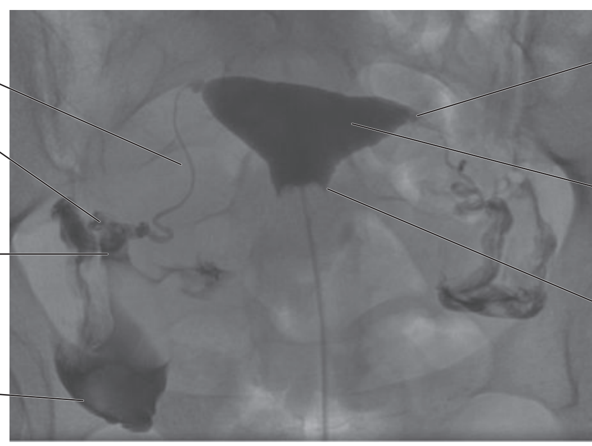


**Fig. 14.48** Hysterosalpingogram.

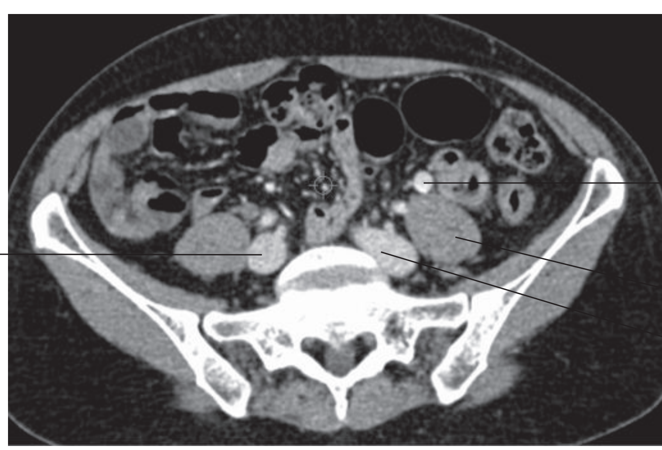


**Fig. 14.49** Axial CT showing a dilated left ovarian vein.

### Position

- Variable, usually lateral or posterolateral to the anteflexed uterus in ovarian fossa – depression on lateral pelvic side wall
- Lateral and superior to the retroflexed uterus
- Free border is directed posterior to the ureter and internal iliac vessels
- Inferior: levator ani
- Lateral: parietal peritoneum separates the ovary from the obturator vessels and nerves
- Medial: uterus and uterine vessels in the broad ligament
- Posterior: ureter/internal iliac artery
- Anterior: obliterated umbilical vein

### Size and shape

- Ellipsoid in shape with their craniocaudal axes parallel to the internal iliac vessels
- Each ovary has a medial and lateral surface, anterior and posterior borders and superior and inferior poles

### Vascular supply

- Arterial: ovarian artery from the aorta at L1/2. Enters the ovarian hilum via the mesovarium.
- Venous: from the pampiniform plexus into the ovarian veins. These drain into the inferior vena cava on the right and the renal vein on the left.

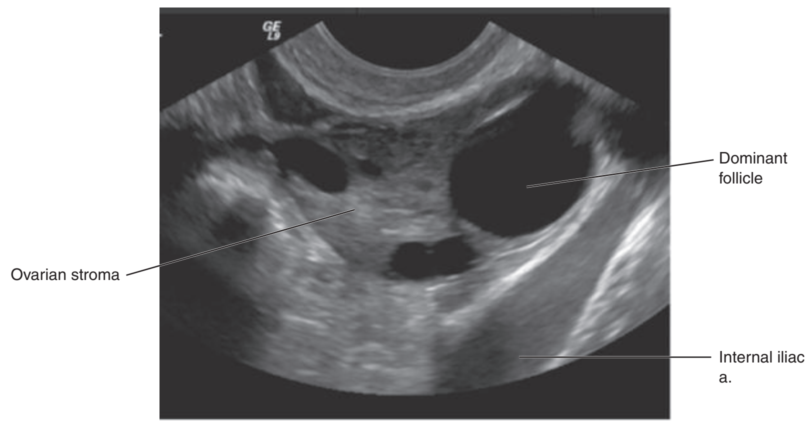


**Fig. 14.50** Transvaginal ultrasound showing a dominant follicle on the left ovary.

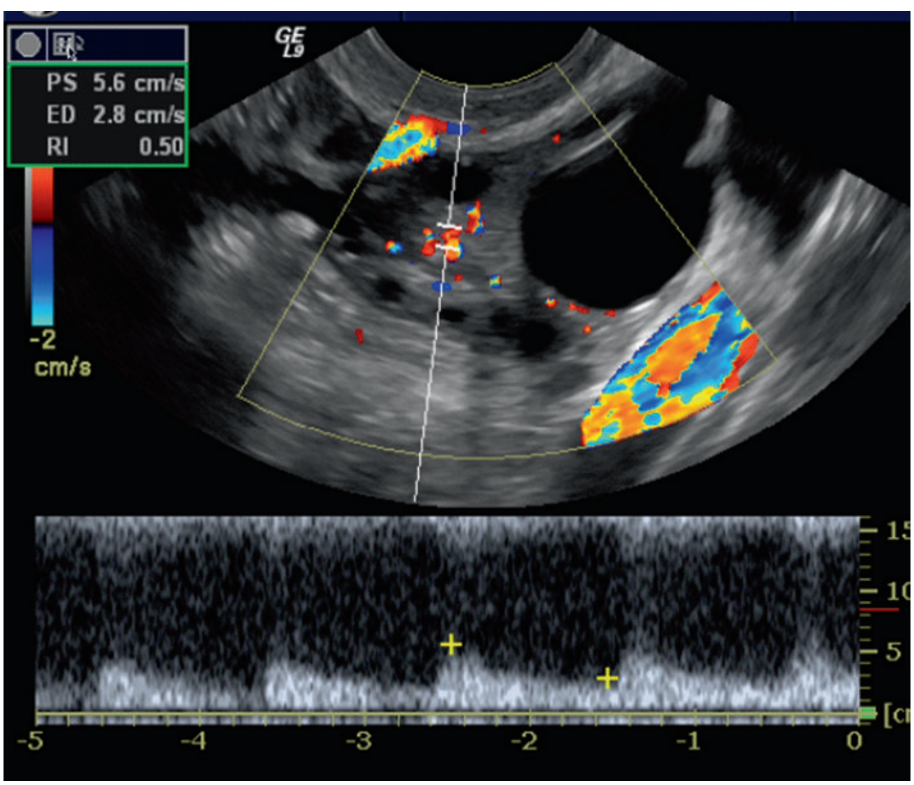


**Fig. 14.51** Transvaginal colour Doppler showing normal arterial flow in an ovary – low-velocity, low-resistance waveform.

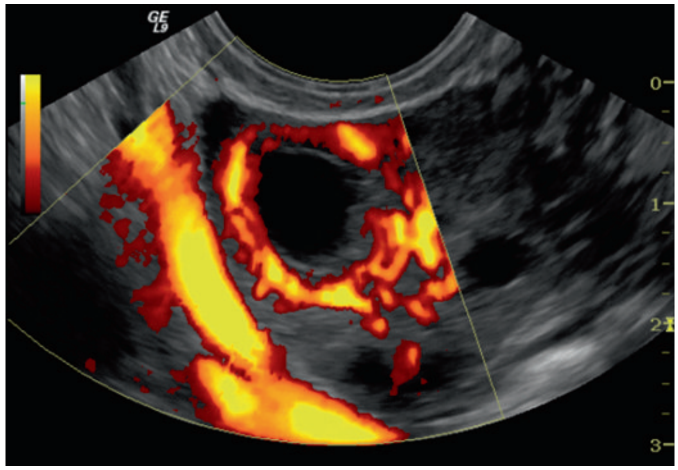


**Fig. 14.52** Transvaginal colour Doppler ultrasound showing increased flow around a corpus luteum cyst – 'ring of fire' appearance.

### Lymph supply

- Along the ovarian vessels to pre-aortic lymph nodes at L1/2.

### Nerve supply

- Ovarian plexus formed from the aortic, renal, superior and inferior hypogastric plexuses.

### Internal anatomy

- The ovary consists of a central vascular medulla and an outer cellular cortex.
- The cortex is composed of reticular fibres and spindle-shaped cells which contain the follicles and corpus lutea.
- The surface is not covered by peritoneum but by a single layer of cuboidal/columnar cells called the germinal epithelium that becomes continuous with the peritoneum at the hilum.
- Beneath the germinal epithelium the connective tissue of the cortex is condensed to form the tunica albuginea – a fibrous outer capsule.
- The medulla is composed of fibrous tissue and vessels.

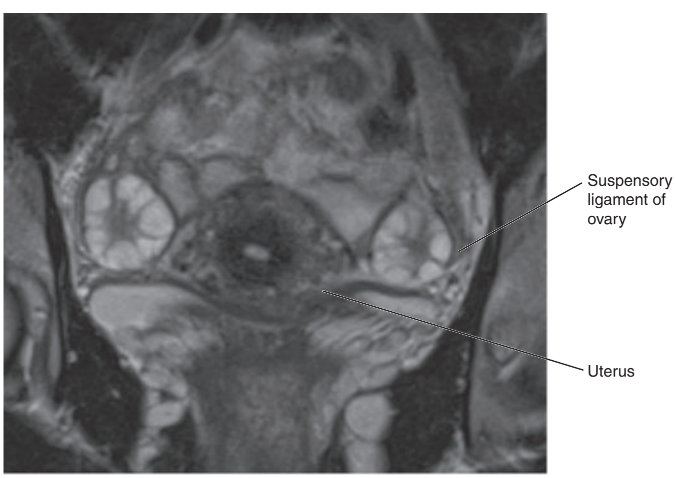


**Fig. 14.53** Coronal T2 MRI showing ovaries.

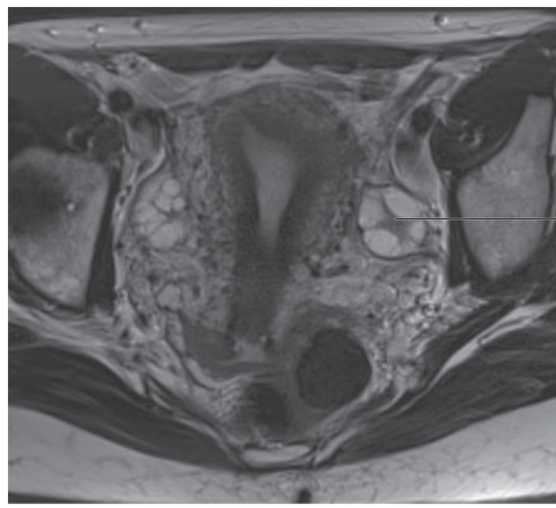


**Fig. 14.54** Axial T2 MRI showing ovaries.

### Cross-sectional anatomy

Ultrasound

- On ultrasound the ovary has a homogeneous echotexture with central echogenic medulla.
- Several small anechoic follicles are seen peripherally in the cortex.
- Echogenic foci are common. These are non-shadowing and can be diffuse. They are caused by a specular reflection from the walls of tiny unresolved cysts.
- Focal calcification may be seen.
- Doppler shows a low-velocity, low-resistance arterial waveform.
- Early proliferative phase – many follicles.
- Pre ovulation – one becomes dominant 2–2.5 cm and others atretic.
- Post ovulation
    - corpus luteum develops
    - variable appearance
    - hypo/isoechoic

**Table 14.4**

| | | | |
|---|---|---|---|
| Arrested development of Müllerian ducts | Agenesis;<br>uterus unicornis unicollis | 1 uterine horn /1 cervix | 10%<br>20% |
| Failure of fusion of Müllerian ducts | Complete:<br>uterus didelphys | 2 vagina / 2 cervices / 2 uterine horns | 5% |
| | Partial:<br>uterus bicornis bicollis | 1 vagina / 2 cervices / 2 uterine horns | 10% |
| | uterus bicornis unicollis | 1 vagina / 1 cervices / 2 uterine horns | |
| | uterus arcuatus | Partial indentation of fundus with normal cavity | |
| Failure of resorption of the median septum | Septate or subseptate uterus – commonest abnormality | Distinguished from above by normal external contour | 55% |

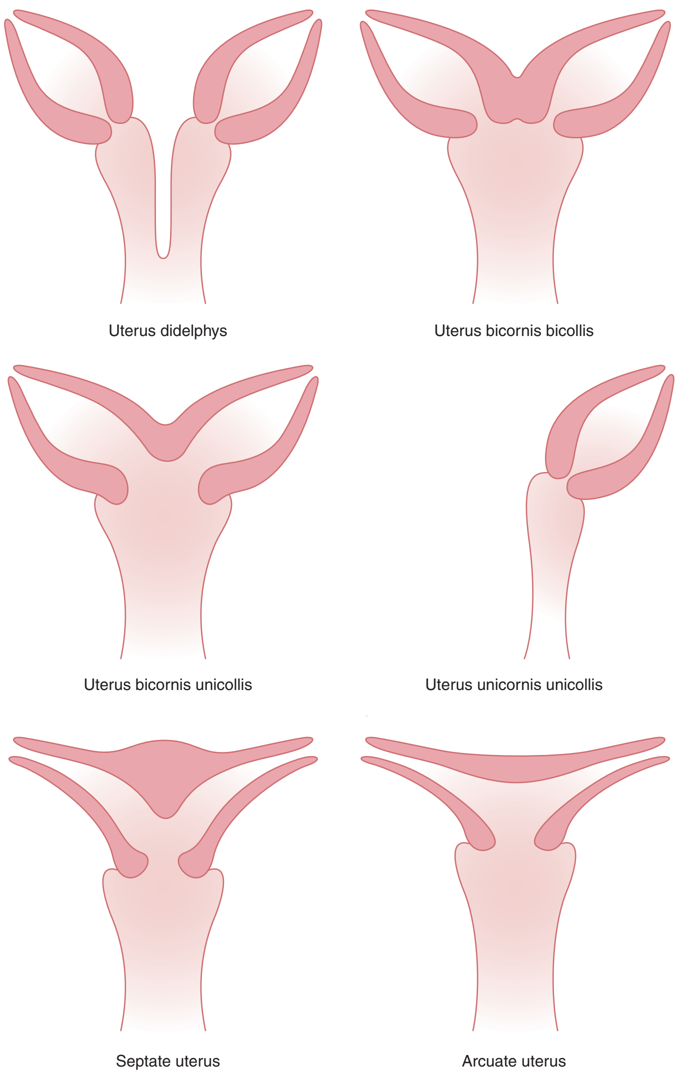


**Fig. 14.55** Line diagrams of congenital anomalies of the uterus.

  - thick echogenic ring
  - haemorrhage common
  - 'ring of fire' on colour Doppler.
- Menstruation – corpus luteum involutes.
- Menopause – ovary atrophies and follicles disappear over subsequent years.

MRI

- T1: uniform intermediate signal with low signal follicles.
- T2: multiple high signal follicles with low signal capsule and medulla slightly higher signal than cortex.
- Postmenopausal ovaries are of homogeneous signal on both T1 and T2.
- Post gadolinium the stroma of the ovary enhances, making the low-signal follicles more prominent.

## Congenital anomalies

- The fused caudal ends of the two Müllerian ducts form the uterus/cervix/upper vagina.
- The unfused ends form the fallopian tubes.
- The median septum formed by the medial walls of the Müllerian ducts resorbs, leaving a single cavity.
- Failure of Müllerian duct development and/or fusion leads to a spectrum of anomalies. Often associated with renal anomalies.

## Imaging during pregnancy

Accurate sagittal and transverse measurements of the mother's pelvic inlet and outlet can help in predicting the likelihood of a vaginal delivery. These measurements include:

- the sagittal inlet (between the promontory and the top of the pubic symphysis)
- the maximum transverse diameter of the inlet
- the bispinous outlet (the distance between ischial spines)
- the sagittal outlet (the distance between the tip of the coccyx and the inferior margin of the pubic symphysis).

The acceptable values for these are 11, 11.5, 9 and 10 cm, respectively.

The above measurements are sometimes made in clinical practice using X-ray or MRI pelvimetry.

Diagnostic imaging may also be required during pregnancy to assess the abdominal or pelvic viscera or the placenta.

Ultrasound remains the initial imaging modality of choice. However, if it is non-diagnostic then further imaging with CT/MRI may be required. CT includes the fetus in the field of view, resulting in an estimated fetal dose of between 12.5 and 35 mSv.

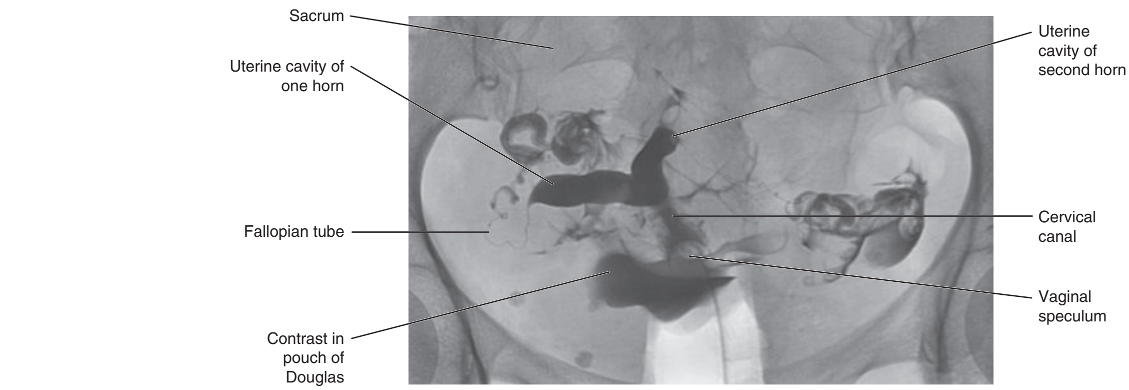


**Fig. 14.56** Hysterosalpingogram showing a uterus bicornis unicollis.

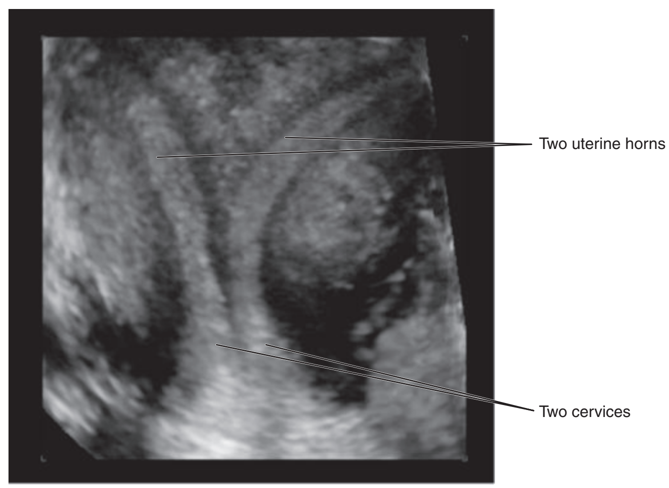


**Fig. 14.57** 3D coronal reformat of a uterus bicornis bicollis.

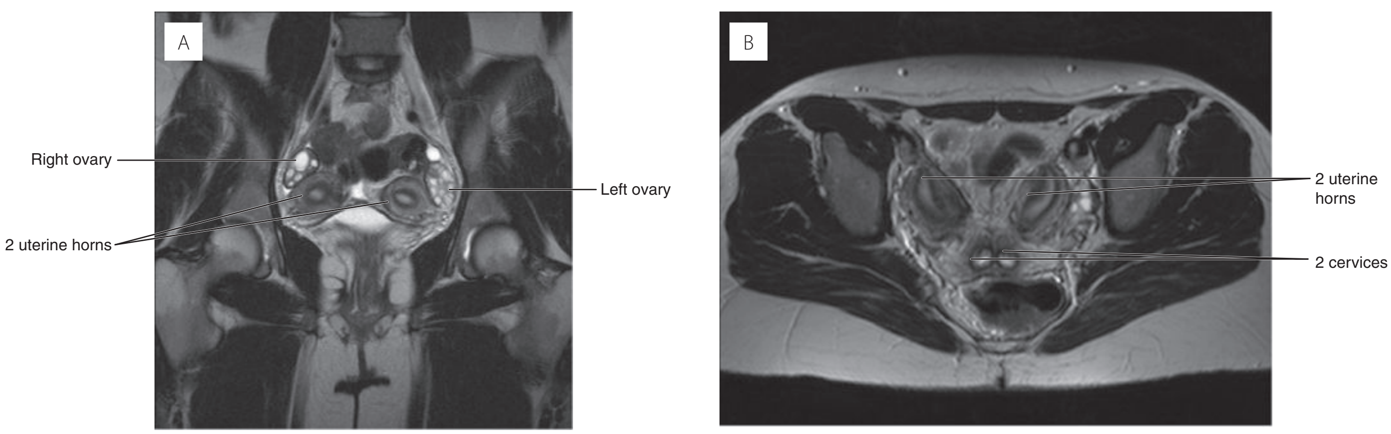


**Fig. 14.58** (A) Coronal MRI showing a uterus didelphys. (B) Axial MRI showing a uterus didelphys.

Therefore MRI which does not utilize ionizing radiation may be beneficial. However, patients should only undergo MR imaging if information cannot be obtained by other non-ionizing means as there are concerns regarding the safety in the setting of pregnancy. In particular imaging in the first trimester is to be avoided as the safety of MR in this period is difficult to establish.

Equally the effects of gadolinium-based agents on the fetus are not fully understood and the use of these agents should be avoided in pregnancy. These agents are also excreted in low concentrations in breast milk and as such it is advisable to interrupt breast feeding for 24–48 hours post administration.

- MRI has an excellent role in evaluating the position of the placenta.
- The point of attachment is determined by the point where the blastocyst becomes embedded. In early pregnancy the

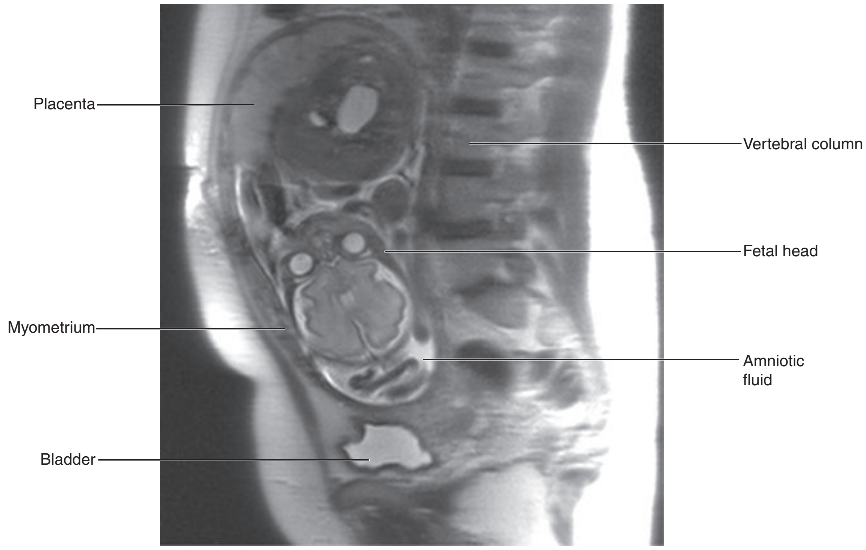


**Fig. 14.59** Sagittal T2-weighted scan showing a normal cephalic presentation.

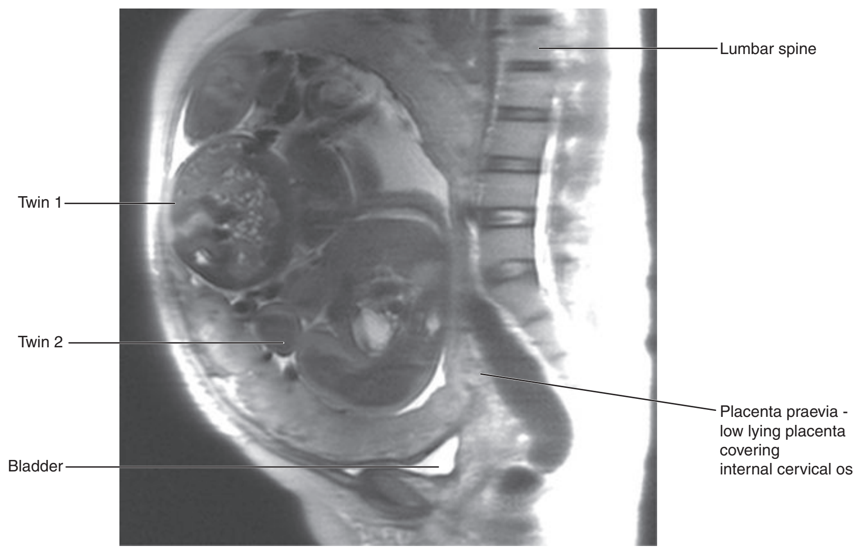


**Fig. 14.60** Sagittal T2-weighted scan of a twin pregnancy with a placenta praevia overlying the internal cervical os.

placenta occupies a large proportion of the uterine cavity and as such will often be situated near the internal os.

- In 1% the placenta remains close to or over the os – placenta praevia.
- Other placental variants include accreta, where the placenta is adhered to the deciduas basalis, increta, where it extends into the myometrium, and percreta, where it passes through the uterine wall.

Chapter 15

# The upper limb

Gajan Rajeswaran and Justin Lee

## Plain radiography/fluoroscopy

Plain radiography demonstrates osseous anatomy and provides some detail of the soft tissue anatomy. Fluoroscopy allows real-time dynamic radiographic assessment of the osseous anatomy and assessment of the joints using fluoroscopic arthrography.

## Cross-sectional imaging

### CT

Multi-slice CT provides more information about the osseous anatomy than plain radiography, showing the trabecular anatomy of the bone in much higher detail. High-resolution 3D reconstructions of the upper limb allow interrogation in any desired plane. Soft tissues including muscles, tendons and joints can also be identified but these are best assessed with ultrasound and MR imaging.

### Sonography

Sonography allows high spatial resolution and dynamic imaging of the soft tissues not obscured by osseous structures. It is particularly optimal for visualization of small and superficial structures (ligaments, tendons) as well as muscle compartments.

### MRI

MR imaging offers high contrast resolution imaging of the musculoskeletal anatomy. Intra-articular structures are best assessed using MR arthrography.

## Shoulder

The upper limb consists of the shoulder, arm, forearm and hand. These regions are connected by the shoulder, elbow and wrist joints overlain by transitional zones, the axilla, antecubital fossa and carpal tunnel, which facilitate the passage of neurovascular structures (Fig. 15.1).

### Plain radiographic anatomy

The bones of the shoulder consist of the clavicle, scapula and proximal humerus.

#### Clavicle

The lateral 1/3 of its inferior surface allows attachment of the coracoclavicular ligament with:

- a bony protuberance, the conoid tubercle
- a lateral roughening, the trapezoid line.

#### Scapula

- The scapula has four main protuberances:
  - coracoid process: anteriorly
  - glenoid fossa: laterally, for articulation with the humeral head
  - spine: posteriorly, dividing the posterior surface into supra- and infra-spinous fossae
  - acromion process: forms the lateral aspect of the spine of the scapula, for articulation with the clavicle.
- The supra- and infraglenoid tubercles provide attachment for the long head of the biceps and triceps brachii muscles respectively.
- Three types of morphological normal variations of the acromion process have been classified by Bigliani, with a fourth type more recently classified by Vanarthos (Fig. 15.2):
  - type 1: flat undersurface
  - type 2: concave undersurface
  - type 3: hooked undersurface
  - type 4: convex undersurface.
- Type 3 and possibly type 2 morphologies predispose to rotator cuff tears as the acromion can impinge on the supraspinatus tendon passing underneath it during dynamic movement (Fig. 15.3).

#### Proximal humerus

- Two bony protuberances, the greater and lesser tubercles, help to define its anatomy. These are separated from:
  - the head by the anatomical neck
  - the diaphysis by the surgical neck
  - each other by the bicipital groove (which allows the passage of the long head of biceps tendon).

*Applied Radiological Anatomy, 2nd Edition* ed. Paul Butler, Adam W.M. Mitchell and Jeremiah C. Healy. Published by Cambridge University Press.

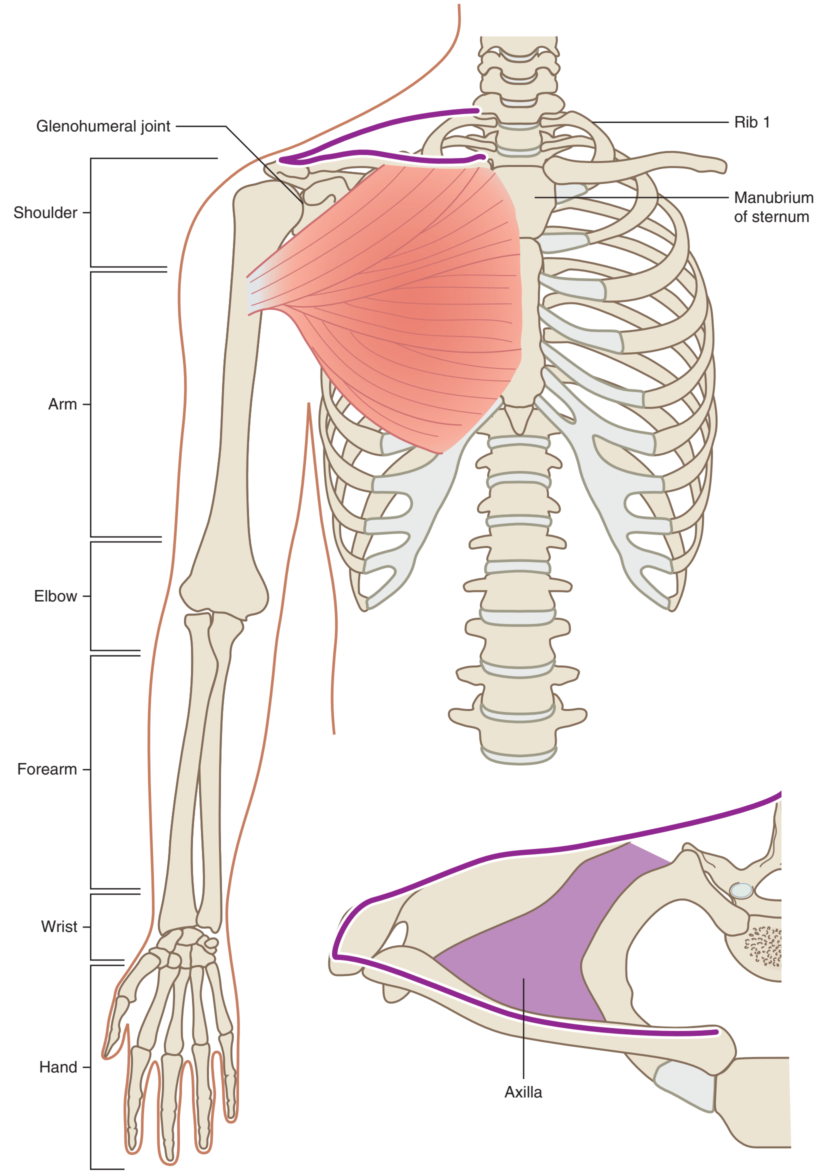


**Fig. 15.1** Diagram of the upper limb.

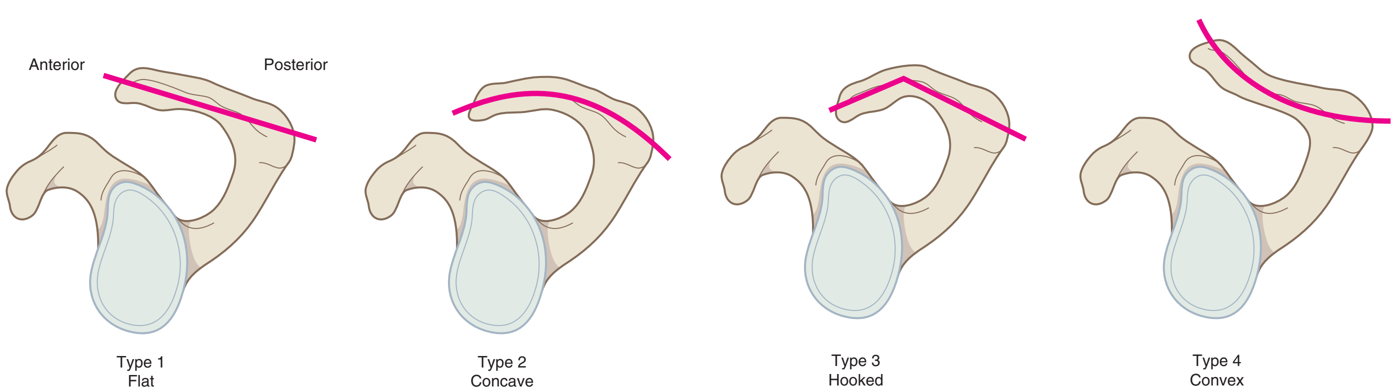


**Fig. 15.2** Classification of acromial morphology.

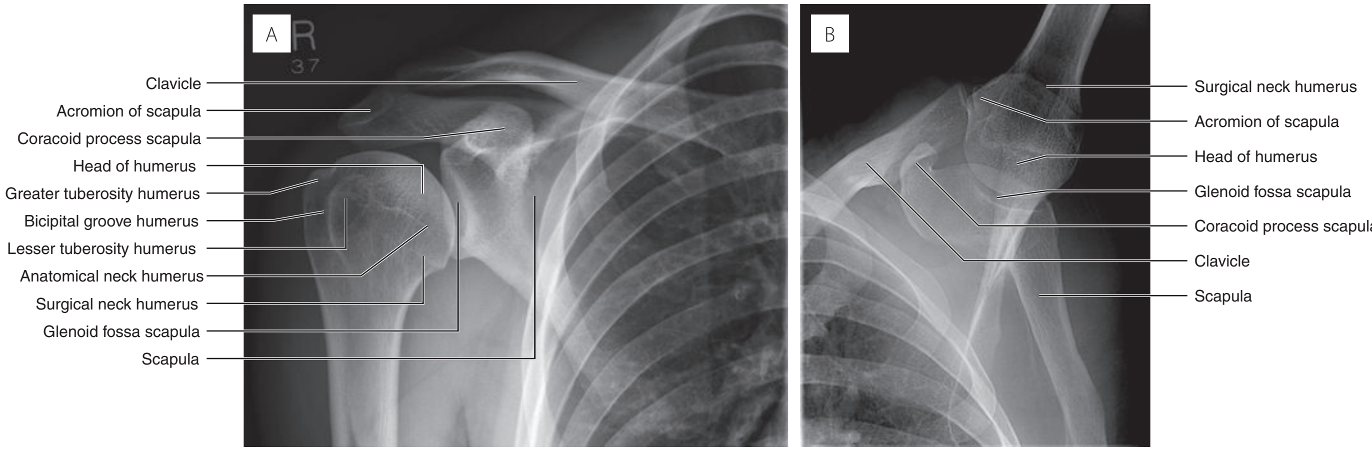


**Fig. 15.3** (A) AP radiograph of the right shoulder and (B) axial radiograph of the right shoulder.

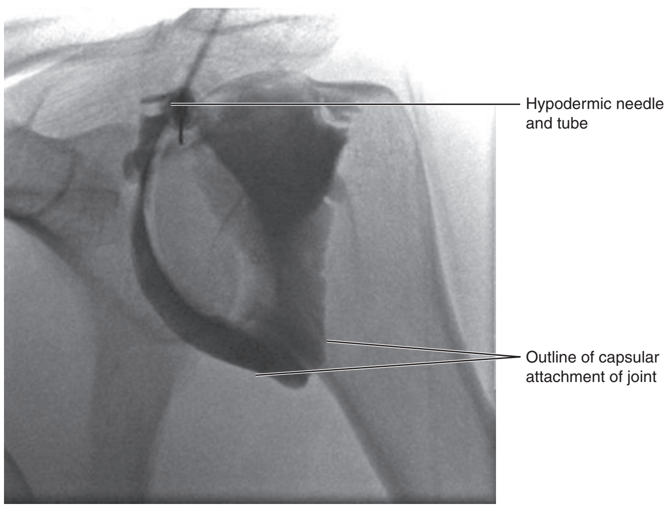


**Fig. 15.4** AP fluoroscopic arthrogram of the left shoulder. Radio-opaque contrast has been injected into the shoulder joint following needle insertion, to outline the joint capsule.

- The axillary nerve and circumflex humeral artery wrap around the surgical neck and are at risk following fracture here.

### Shoulder (glenohumeral) joint (Figs. 15.3 and 15.4)

- Synovial, multiaxial ball-and-socket joint between the hemispherical head of humerus and the shallow glenoid fossa of the scapula.
- Wide range of movement (flexion, extension, abduction, adduction, internal and external rotation and circumduction of the upper limb) but inherent lack of stability.
- On an AP radiograph, the articular surfaces of the humerus and glenoid form parallel arcs.

### Sternoclavicular joint (Fig. 15.5)

- Saddle-shaped, synovial joint.
- Separated into two cavities by intervening disc of fibrocartilage which is attached to the joint capsule.
- Allows horizontal and vertical movement as well as some rotation.

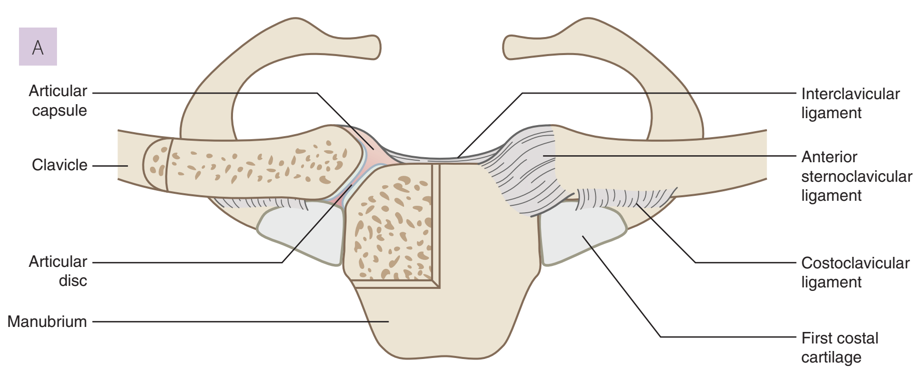


**Fig. 15.5** (A) Illustration of left sternoclavicular joint. (B) Axial fat-saturated proton-density MRI image in a patient with osteoarthritis of the right sternoclavicular joint. The intra-articular disc (white arrow) can be seen as a low-signal linear structure within the joint compartment, highlighted on either side by high-signal joint fluid secondary to the osteoarthritis. Note the cod liver oil capsule (white arrowhead) on the patient's skin, localizing the patient's pain. C = clavicle; S = sternum.

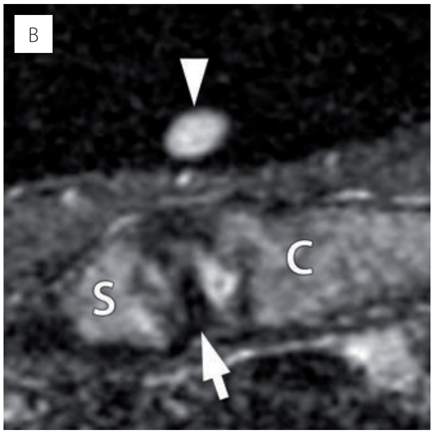


**Fig. 15.5** (*cont.*)

- Enclosed by a joint capsule and strengthened by four ligaments:
  - anterior and posterior sternoclavicular ligaments
  - interclavicular ligament
  - costoclavicular ligament.

### Acromioclavicular joint (Fig. 15.6)

- Synovial plane joint.
- An incomplete disc of fibrocartilage hangs down into the upper part of the joint cavity.
- Allows horizontal and vertical movement as well as some rotation.
- Strengthened by:
  - acromioclavicular ligament: the acromioclavicular distance is 3–8 mm in adults
  - coracoclavicular ligament: the normal coraco-clavicular distance is 10–13 mm and the inferior aspects of the clavicle and acromion normally lie in a straight line.

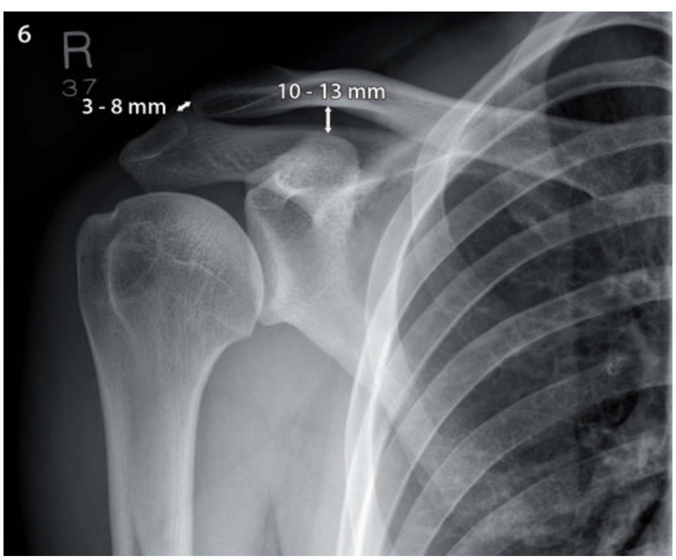


**Fig. 15.6** AP radiograph of right shoulder. Normal acromioclavicular (0.3–0.8 mm) and coracoclavicular (1.0–1.3 mm) distances imply that the acromioclavicular and coracoclavicular ligaments are intact.

### Ossification of the shoulder

- In the fetus, the skeleton consists initially of cartilage, which gradually turns to bone (ossification) during growth.
- Each bone has a primary ossification centre (usually at the centre of the bone) and sometimes one or more secondary ossification centres (usually at the bone ends).
- When the secondary ossification centre does not unite with the main bone an accessory ossicle (normal variant) is formed.
- Accessory ossicles and secondary ossification centres should not be mistaken for fractures.
- The os acromiale is an accessory ossicle occurring in 1–15% of the population. It can result in shoulder impingement by decreasing the space below the coracoacromial arch. There are up to three ossification centres in the acromion: preacromion, mesoacromion and metacromion. Depending on where failure of fusion occurs, this can result in seven types of os acromiale (Figs. 15.7 and 15.8).

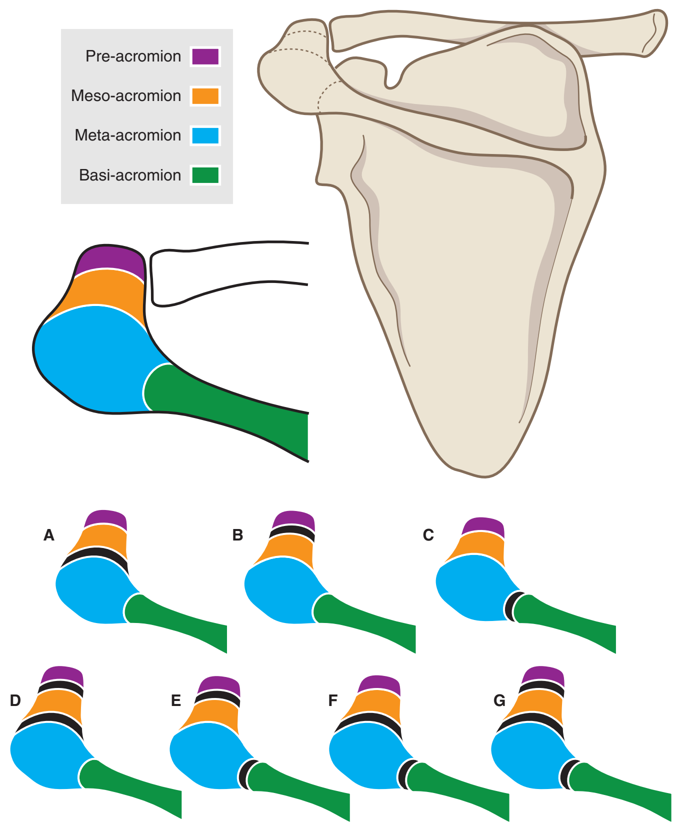


**Fig. 15.7** Ossification of the acromion and types of os acromiale. There are up to three ossification centres of the acromion separate to the basi-acromion: pre-acromion; meso-acromion and meta-acromion. Depending on where failure of fusion (black shaded area) occurs, up to seven types of os acromiale (types A–G) may be formed. The most common is type A, in which there is failure of fusion between the meso- and meta-acromion.

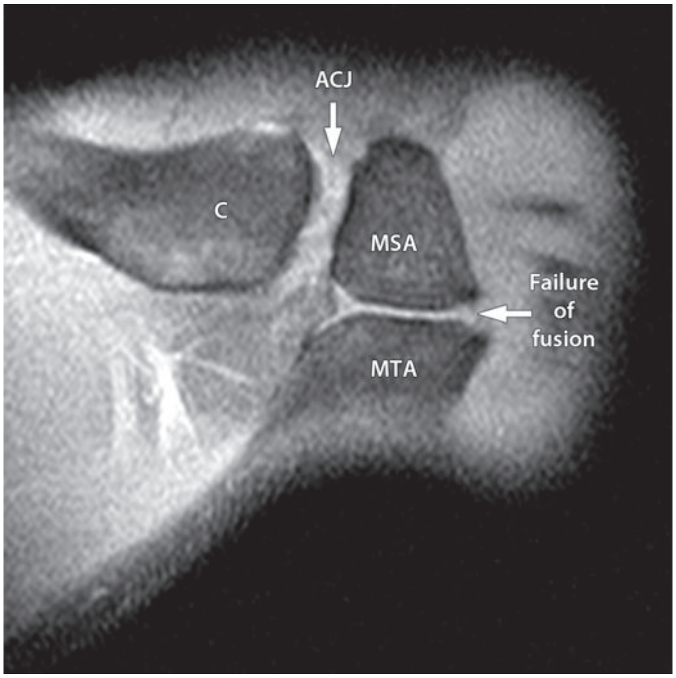


**Fig. 15.8** Axial fat-saturated proton-density MRI image of the shoulder showing a type A os acromiale. There is failure of fusion between the meso-acromion (MSA) and the meta-acromion (MTA). ACJ = acromio-clavicular joint, C = clavicle.

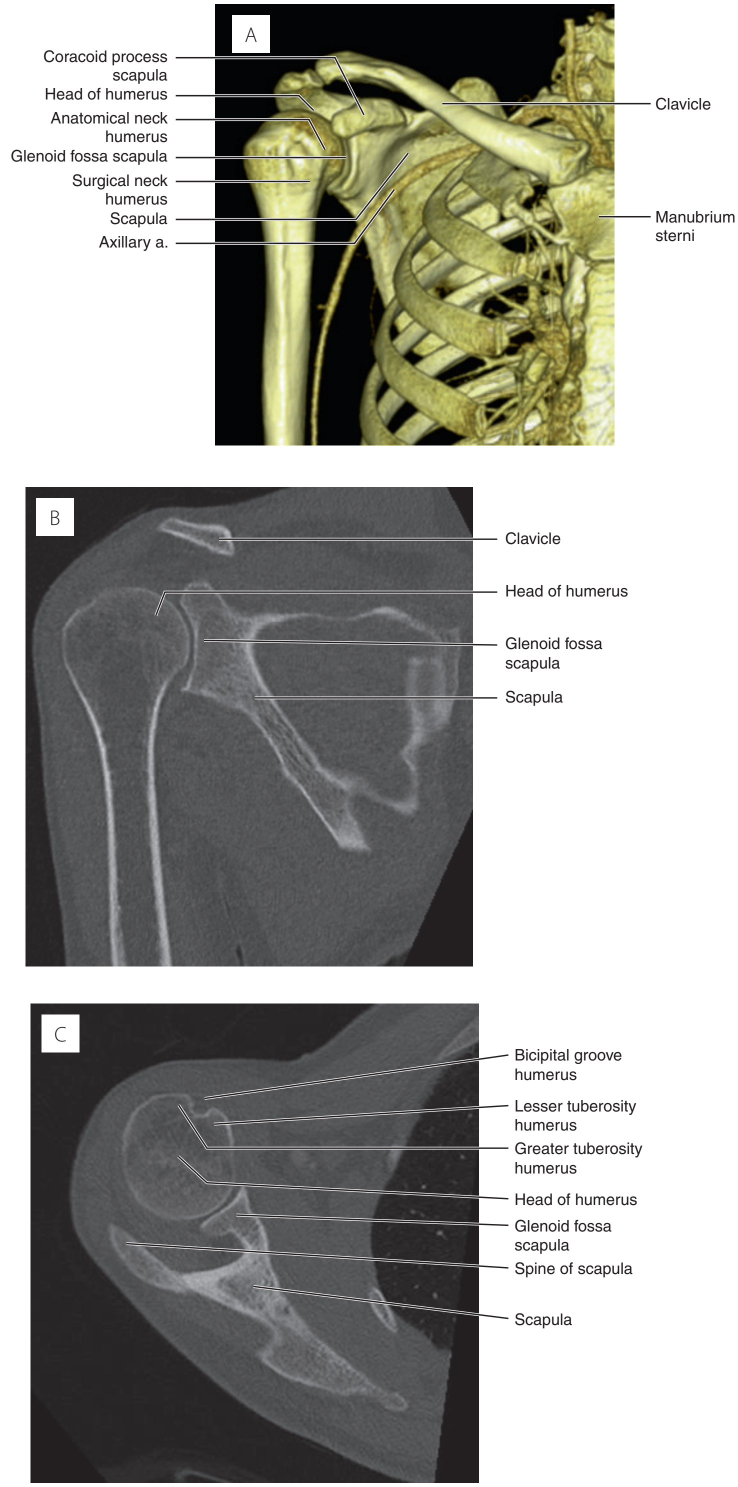


**Fig. 15.9** (A) Coronal CT surface shaded reformat right shoulder, (B) coronal CT right shoulder and (C) axial CT right shoulder.

**Table 15.1** Ossification centres of the scapula

| | Appear | Fuse |
|---|---|---|
| Body | 8th wk gestation | 25 yrs |
| Coracoid (two centres) | 15–18 months | 15 yrs |
| Glenoid | 10–11 yrs | 25 yrs |
| Vertebral border | 14–20 yrs | 25 yrs |
| Acromion (three centres) | 14–20 yrs | 25 yrs |
| Inferior angle | 14–20 yrs | 25 yrs |

**Table 15.2** Ossification centres of proximal humerus

| | Appear | Fuse |
|---|---|---|
| Diaphysis | 8th wk gestation | 20 yrs |
| Head | < 6 months | 20 yrs |
| Greater tubercle | 1–2 yrs | 20 yrs |
| Lesser tubercle | 5 yrs | 20 yrs |

The scapula is ossified from seven or more centres (Tables 15.1 and 15.2).

## Cross-sectional anatomy (Fig. 15.9)

### Shoulder joint capsule

- The fibrous capsule of the joint attaches:
  - medially to the glenoid margin, enclosing the tendon of the long head of the biceps brachii muscle which is intracapsular
  - laterally to the anatomical neck of the humerus except infero-medially, where it is lax, forming the axillary recess, allowing the joint a wide range of movement.
- The anterior joint capsule varies in the way it inserts onto the glenoid:

- Zlatkin categorized this into three types, types 1–3, depending on the proximity of capsular insertion to the glenoid margin
- the further away the insertion from the glenoid margin, the more unstable the joint will be (Figs. 15.10 and 15.11).

### Shoulder joint synovial membrane

- Lines the deep surface of the fibrous capsule, covering the articular cartilage.
- Surrounds the long head of biceps tendon in a synovial sheath which extends distally down into the bicipital groove, to the surgical neck of the humerus.
- Protrudes through the capsule in various areas, forming numerous recesses or bursae:
  - between the superior and middle glenohumeral ligaments, hanging over the superior margin of the subscapularis tendon (the superior subscapularis recess or subscapularis bursa)
  - between the middle and inferior glenohumeral ligaments, deep to the subscapularis tendon (inferior subscapularis recess)
  - between the anterior surface of the subscapularis tendon and the coracoid process (subcoracoid bursa)
  - between teres major and the long head of triceps brachii
  - between the anterior and posterior tendons of the latissimus dorsi muscle
  - between the rotator cuff tendons and the acromion process and deltoid muscle (the subacromial-subdeltoid bursa) (Fig. 15.12).
- All of the recesses/bursae communicate with the joint except for the subacromial-subdeltoid bursa and the subcoracoid bursa, which may communicate with each other.
- Fluid within the subcoracoid bursa can often be confused with fluid in the superior subscapularis recess, that in the

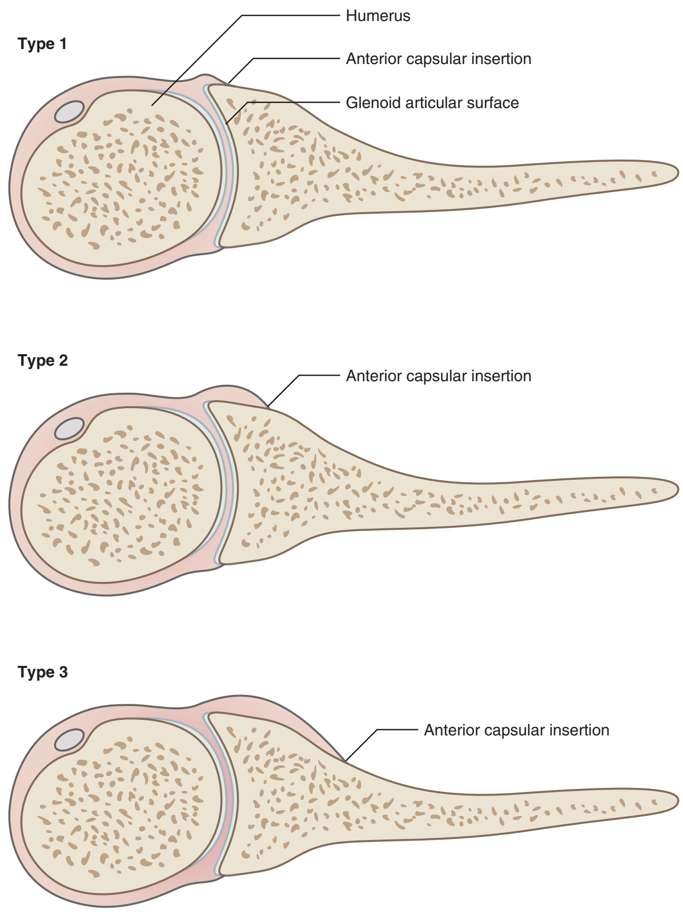


**Fig. 15.10** Classification of shoulder joint anterior capsular insertion. Divided into types 1–3 depending on the proximity of the anterior capsular insertion to the glenoid articular surface. Type 1: onto the labrum/glenoid margin; Type 2: less than 1 cm medial to the glenoid margin; Type 3: greater than 1 cm medial to the glenoid margin.

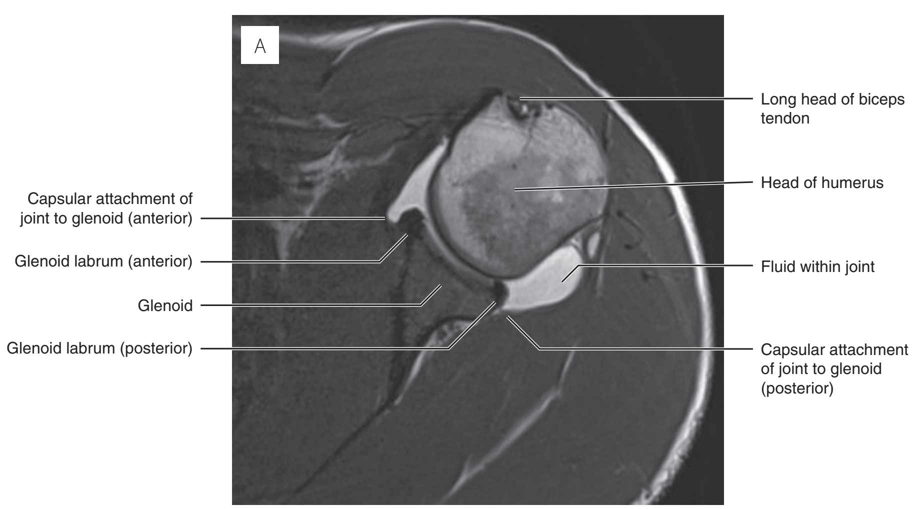


**Fig. 15.11** (A) T1-weighted axial MRI arthrogram, left shoulder (post intra-articular gadolinium injection); (B) fat-saturated T1-weighted coronal MRI arthrogram, left shoulder (post intra-articular gadolinium injection).

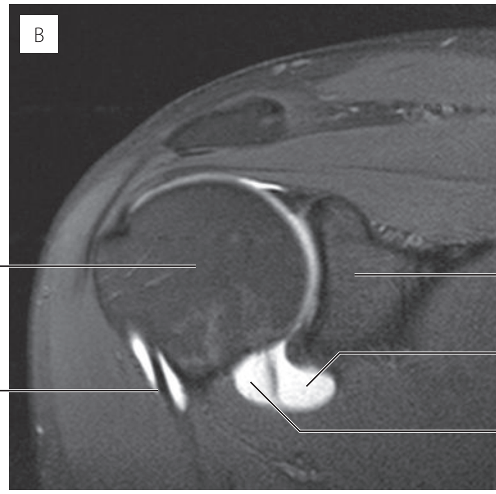


**Fig. 15.11** *(cont.)*

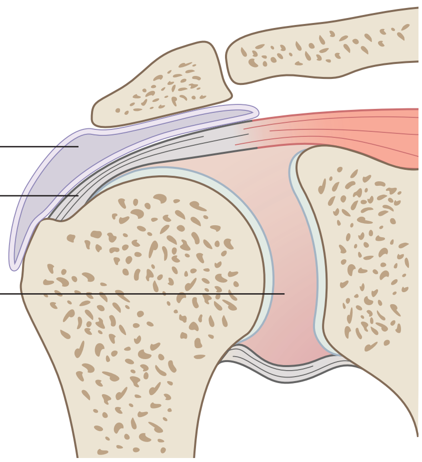


**Fig. 15.12** Illustration of the subacromial-subdeltoid bursa. The subacromial-subdeltoid bursa lies superficial to the rotator cuff tendons and deep to the acromion and deltoid muscle. As a result, on movement of the shoulder (particularly during abduction) it can become easily impinged.

former usually being pathological and that in the latter usually being physiological.

## Glenoid labrum

- Fibrocartilaginous rim around the periphery of the glenoid.
- Deepens the articulating surface of the glenoid.
- Attachment site for long head of the biceps brachii muscle.
- Low signal on all MRI sequences.
- Varying morphology: triangular, round, cleaved, notched, flat (in order of frequency).
- Normal labral variants that can be mistaken for labral tears:
  - Buford complex: congenitally absent anterosuperior labrum associated with a thickened middle glenohumeral ligament
  - sublabral foramen: detachment of the anterosuperior labrum which does not extend posterior to the biceps tendon attachment (Figs. 15.13 and 15.14).

## Shoulder joint ligaments

- The joint is strengthened by static and dynamic stabilizers. The ligaments are static stabilizers, namely:
  - the glenohumeral ligaments (Fig. 15.15):
    - thickenings of the anterior joint capsule
    - three ligaments: superior, middle and inferior
    - when viewed coronally (en face), form a 'Z' shape
    - inferior glenohumeral ligament is most important ligamentous joint stabilizer:
      - split into an anterior and posterior band, with intervening axillary recess
  - the transverse humeral ligament connects the tuberosities and covers the long head of biceps tendon in the bicipital groove and prevents it from dislocating out
  - the coracohumeral ligament
  - the coracoacromial ligament: forms part of the coracoacromial arch (Fig. 15.16).

## Biceps pulley system/rotator interval

- Rotator interval:
  - triangular interspace between the supraspinatus and subscapularis tendons, through which passes the long head of biceps tendon.
- Biceps pulley (Fig. 15.17):
  - complex pulley system that:
    - prevents medial subluxation of the long head of biceps tendon out of the bicipital groove
    - stabilizes the tendon during biceps flexion
  - formed by coracohumeral, superior glenohumeral and transverse humeral ligaments plus the subscapularis tendon.

## Muscles of the shoulder

- These are dynamic stabilizers of the shoulder joint, the most important being the rotator cuff muscles.

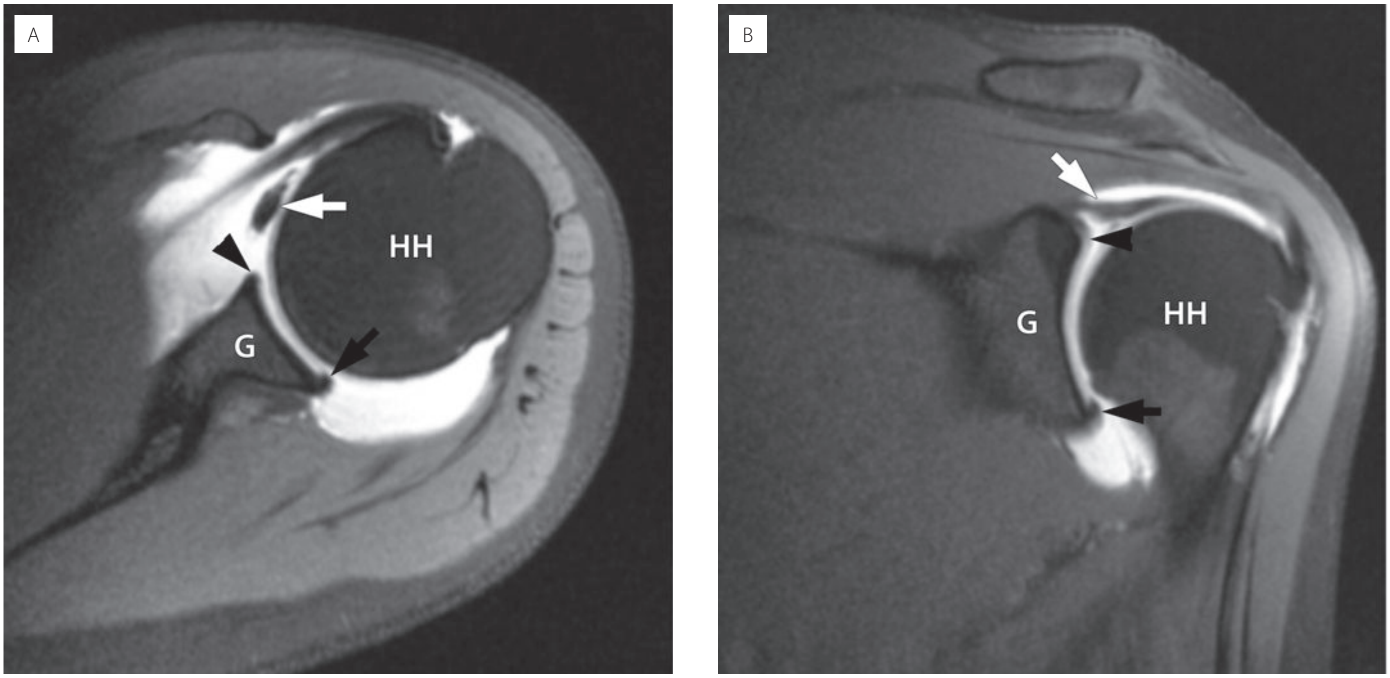


**Fig. 15.13** (A) Fat-saturated T1-weighted axial MRI arthrogram; (B) fat-saturated T1-weighted coronal MRI arthrogram. Left shoulder, post intra-articular gadolinium injection. Buford complex: normal variant anatomy of the glenoid labrum which mimics a labral tear. There is deficiency of the anterosuperior glenoid labrum (black arrowhead) with associated thickening of the middle glenohumeral ligament (white arrow). Note the normal appearance of the glenoid labrum (black arrow). HH = humeral head; G = glenoid of scapula.

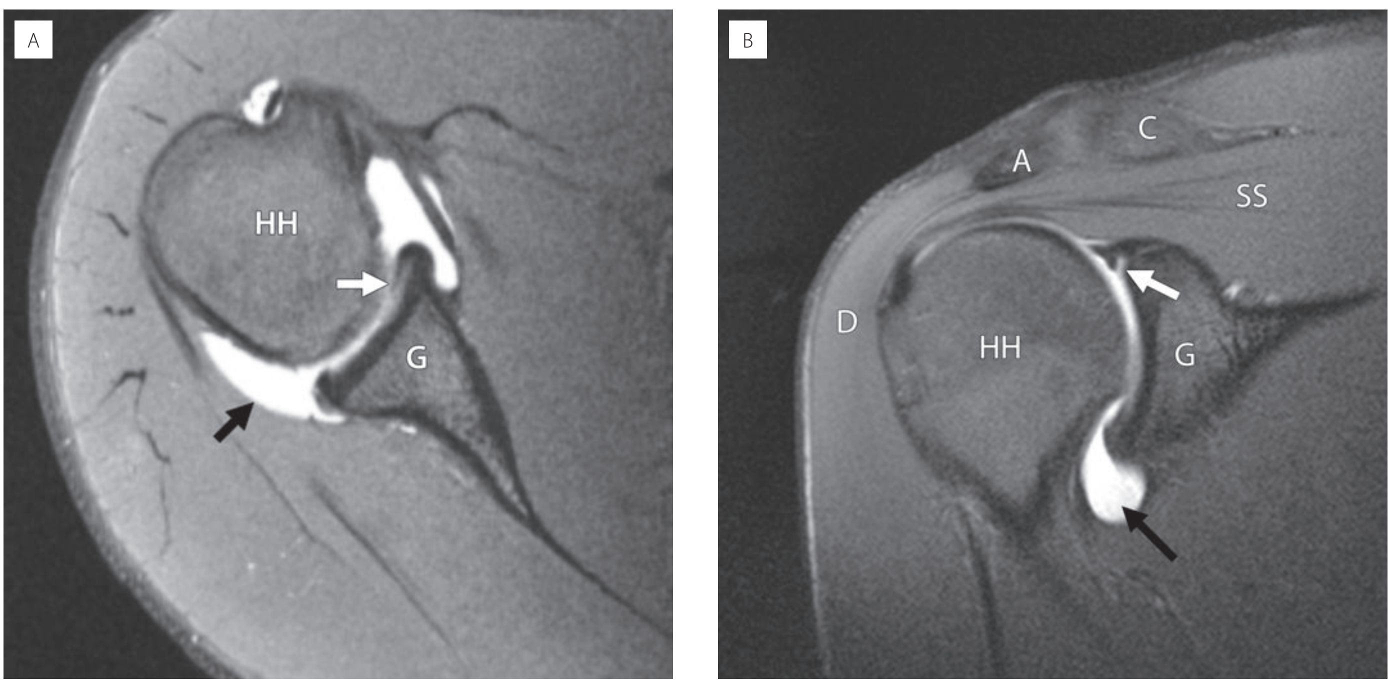


**Fig. 15.14** (A) Fat-saturated T1-weighted axial MRI arthrogram; (B) fat-saturated T1-weighted coronal MRI arthrogram. Right shoulder, post intra-articular gadolinium injection. Sublabral foramen: normal variant anatomy of the glenoid labrum which mimics a labral tear. Contrast has been injected to distend the joint capsule (black arrow). There is separation of the anterosuperior glenoid labrum from the underlying glenoid with contrast seen in between (white arrow). The foramen never extends posterior to the attachment of the long head of the biceps tendon. A = acromion; C = clavicle; D = deltoid muscle; G = glenoid of scapula; HH = humeral head; SS = supraspinatus muscle.

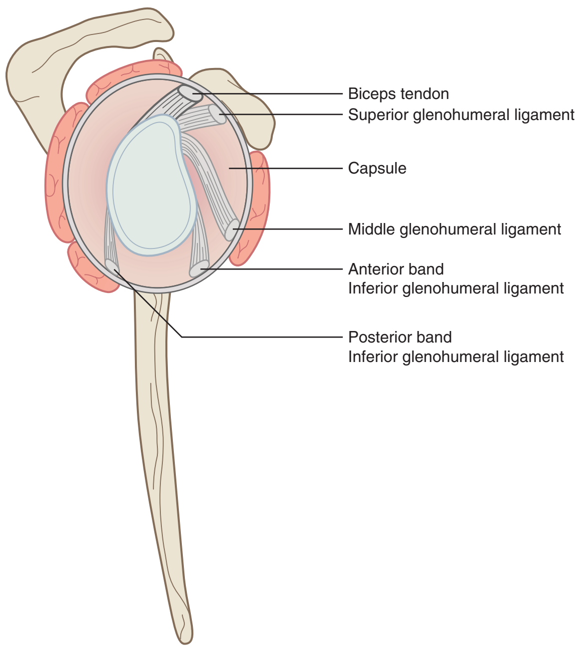


**Fig. 15.15** Glenohumeral ligaments.

- They comprise the supraspinatus, infraspinatus, teres minor and subscapularis (SITS) and are important in providing stability to the shoulder joint, forming a protective 'cuff' around it (Figs. 15.18, 15.19, 15.20 and Tables 15.3–15.5).

### Coracoacromial arch

- Formed (from anterior to posterior) by the coracoid process, coracoacromial ligament and acromion.
- Located within it (from superior to inferior) are the subacromial-subdeltoid bursa, supraspinatus tendon and long head of biceps tendon.
- Anything that decreases the space of the arch can cause shoulder impingement (Fig. 15.20).

# Axilla

## Cross-sectional imaging

The axilla is a pyramidal-shaped potential space through which structures from the neck and chest pass into the upper limb and vice versa.

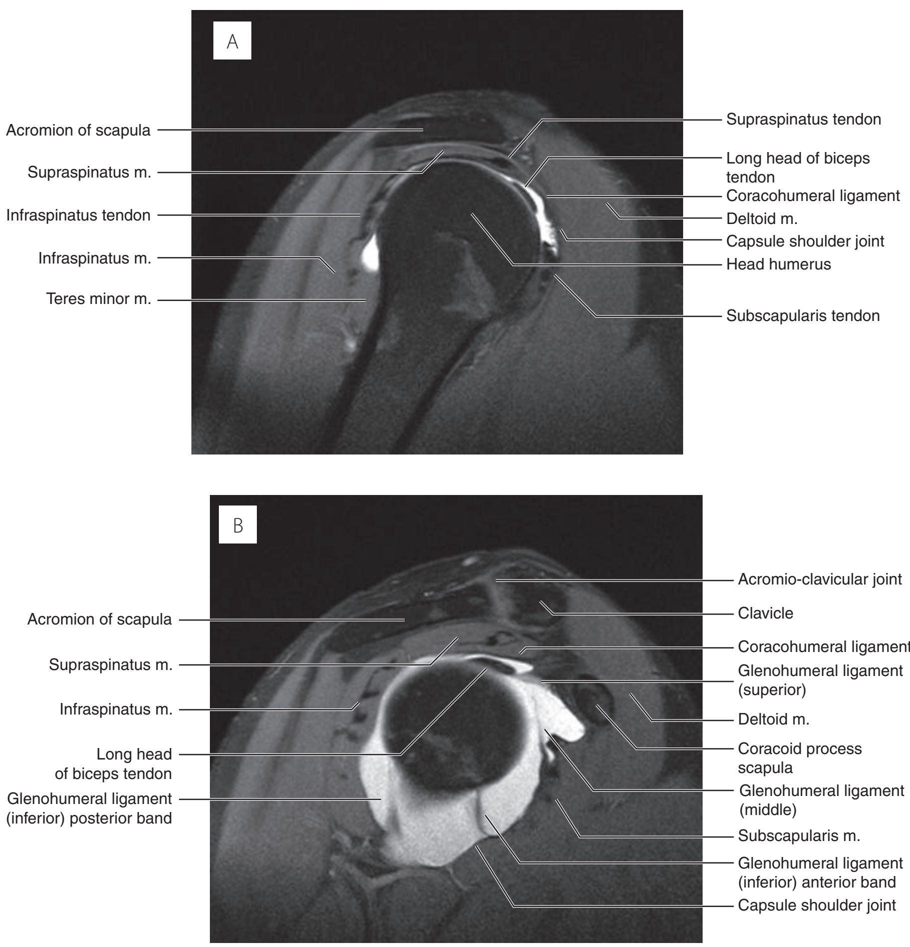


**Fig. 15.16** Sagittal oblique fat-saturated T1-weighted MRI arthrogram, right shoulder (lateral to medial, post intra-articular gadolinium injection).

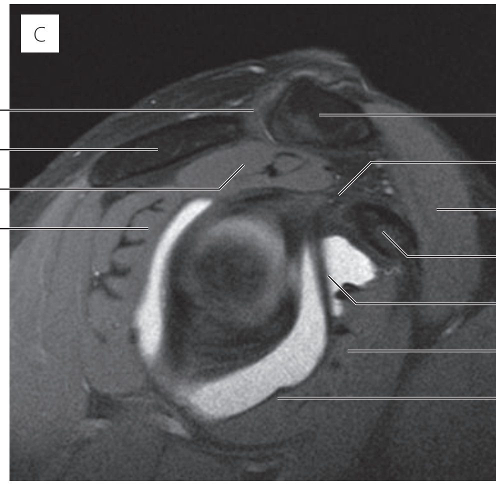


**Fig. 15.16** (*cont.*)

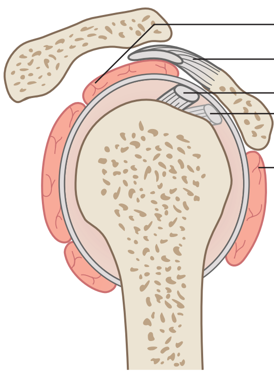


**Fig. 15.17** Biceps pulley system.

The contents of the axilla include the major neurovascular structures (subclavian and axillary artery and vein and the brachial plexus) of the upper limb, lymphatics and the proximal parts of the biceps brachii and coracobrachialis muscles (Figs. 15.21 and 15.22).

## Brachial plexus

Nerve plexus made up of:

- five roots (anterior rami of C5 to T1), which form into
- three trunks (upper, middle and lower), which divide into
- six divisions (anterior and posterior from each trunk), which form into
- three cords (lateral, medial and posterior):
  - the musculocutaneous nerve is the continuation of the lateral cord
  - the ulnar nerve is the continuation of the medial cord
  - the radial and axillary nerves are the continuation of the posterior cord
  - the median nerve is the continuation of a communication between the lateral and medial cords.

The nerve roots pass through the scalene triangle, formed by the anterior and middle scalene muscles, with its apex at the 1st rib.

The roots are in close proximity to the subclavian artery (below the clavicle), which can be used as an anatomical landmark when assessing MRI images (Fig. 15.23).

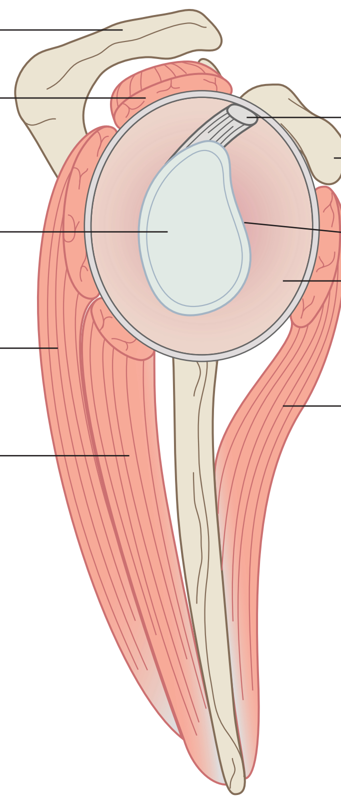


**Fig. 15.18** (A) Illustration of rotator cuff tendons; (B) sagittal T1-weighted MRI image of the left shoulder.

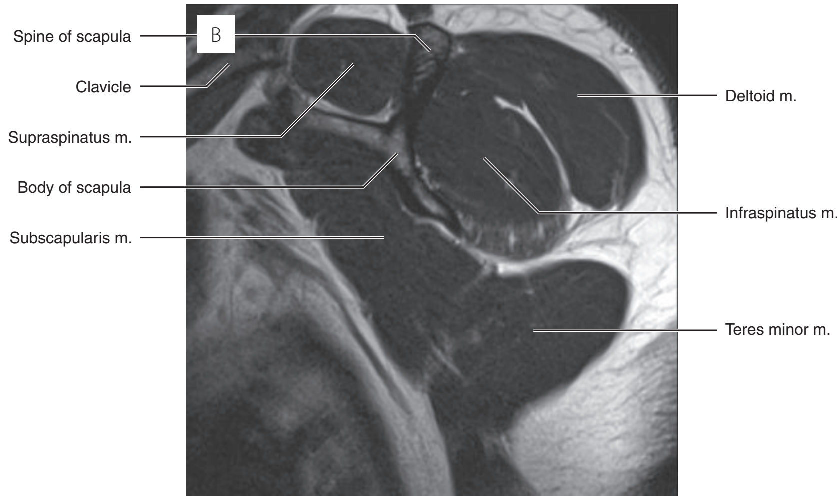


**Fig. 15.18** (*cont.*)

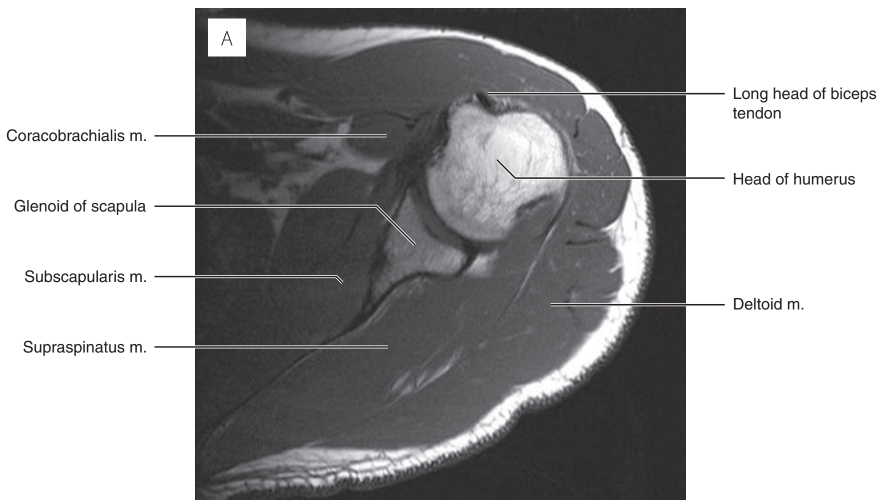


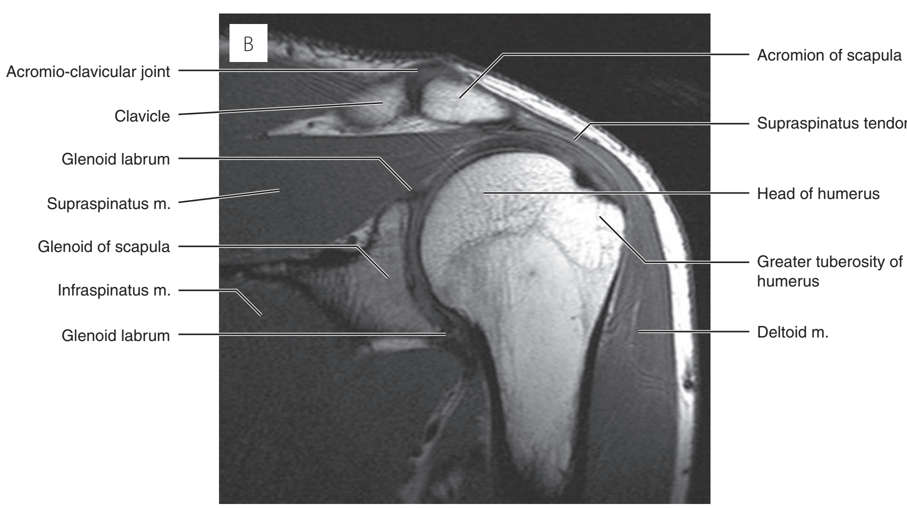


**Fig. 15.19** (A) axial T1 MRI, left shoulder; (B) coronal T1 MRI, left shoulder.

**Table 15.3** Muscles attaching the scapula to the humerus

| Muscle | Origin | Insertion | Action |
|---|---|---|---|
| Deltoid | Lateral 1/3 of clavicle; acromion; spine of scapula | Deltoid tuberosity on lateral humeral diaphysis | Abduction; flexion and internal rotation (anterior fibres); extension and external rotation (posterior fibres) |
| Supraspinatus | Supraspinous fossa of scapula | Greater tuberosity of humerus (upper facet) | Abduction; weak external rotator and flexor |
| Infraspinatus | Infraspinous fossa of scapula | Greater tuberosity of humerus (middle facet) | External rotation; abductor (upper part); adductor (lower part) |
| Teres minor | Upper 2/3 of lateral border of scapula | Greater tuberosity of humerus (lower facet) | External rotation; weak adductor |
| Teres major | Lower 1/3 of lateral border of scapula | Bicipital groove of humerus | Internal rotation and adduction |
| Subscapularis | Subscapular fossa on anterior surface of scapula | Lesser tuberosity of humerus | Internal rotation |

**Table 15.4** Muscles attaching the upper limb to the thoracic wall

| Muscle | Origin | Insertion | Action |
|---|---|---|---|
| Pectoralis major | Clavicle; sternum; 1st six costal cartilages | Lateral lip of bicipital groove and posterior lamina of long head of biceps tendon | Adduction; internal rotation |
| Pectoralis minor | 3rd–5th ribs | Coracoid process of scapula | Depresses shoulder; elevates 3rd–5th ribs if scapula fixed |
| Subclavius | 1st costal cartilage | Clavicle | Depresses clavicle |
| Serratus anterior | 1st eight ribs | Medial border of scapula | Rotates scapula and moves it anteriorly |

# Arm

## Plain radiographic anatomy

### Humerus (Fig. 15.24)

- Deltoid tuberosity: roughened protuberance on the humeral diaphysis for attachment of the deltoid muscle.
- Spiral groove: accommodates the radial nerve.
- Lateral and medial supracondylar ridges: linear elevations on the lateral and medial aspects of the distal humerus that provide attachment for the fascial septa of the arm.

**Table 15.5** Muscles attaching the upper limb to the spine

| Muscle | Origin | Insertion | Action |
|---|---|---|---|
| Trapezius | External occipital protuberance; ligamentum nuchae; spine of C7 and all thoracic vertebrae | Lateral 1/3 of clavicle; acromion and spine of scapula | Acts with other muscles to steady, elevate and rotate the scapula |
| Latissimus dorsi | Spines of lower six thoracic vertebrae, lumbar and sacral vertebrae; iliac crest; lower 3–4 ribs; inferior angle of scapula | Floor of the bicipital groove of humerus | Extends, adducts and internally rotates arm |
| Levator scapulae | Transverse processes of 1st four cervical vertebrae | Medial border of scapula | Elevates medial border of scapula |
| Rhomboid minor | Spines of C7 and T1 vertebrae; lower part of ligamentum nuchae | Medial border of scapula | Elevates medial border of scapula; retracts and fixes scapula |
| Rhomboid major | Spines of C2–C5 vertebrae | Medial border of scapula | Elevates medial border of scapula; retracts and fixes scapula |

## Cross-sectional anatomy

- The arm is encircled by a sheath of deep fascia.
- Lateral and medial intermuscular septae extend from it to the respective supracondylar ridges of the humerus, dividing the arm into separate anterior and posterior fascial compartments.
- Each compartment contains its own muscles and neurovascular supply (Fig. 15.25).

### Anterior (flexor) fascial compartment

- Muscular contents: biceps brachii, coracobrachialis and brachialis muscles
- Blood supply: brachial artery
- Nerve supply: musculocutaneous nerve (Table 15.6 and Fig. 15.26).

### Posterior (extensor) fascial compartment

- Muscular contents: triceps brachii muscle
- Blood supply: profunda brachii and ulnar collateral arteries
- Nerve supply: radial nerve (Table 15.7).

# Elbow

## Plain radiographic anatomy

### Distal humerus

- The distal humeral articular surfaces are the capitellum laterally and the trochlea medially.

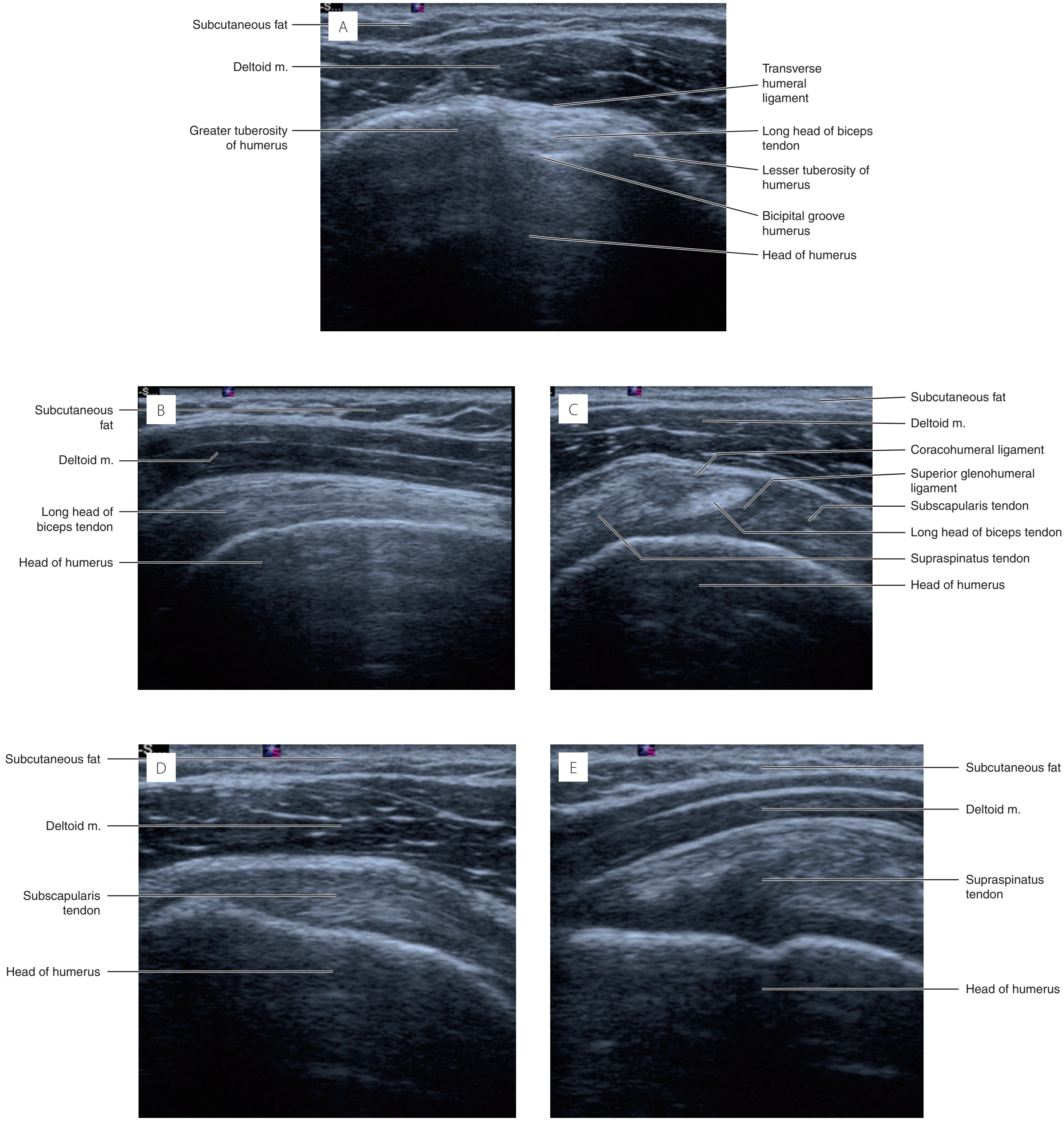


**Fig. 15.20** (A) Axial ultrasound, right long head of biceps tendon; (B) longitudinal ultrasound, right long head of biceps tendon; (C) axial ultrasound, right rotator interval; (D) longitudinal ultrasound, right subscapularis tendon; (E) longitudinal ultrasound, right supraspinatus tendon.

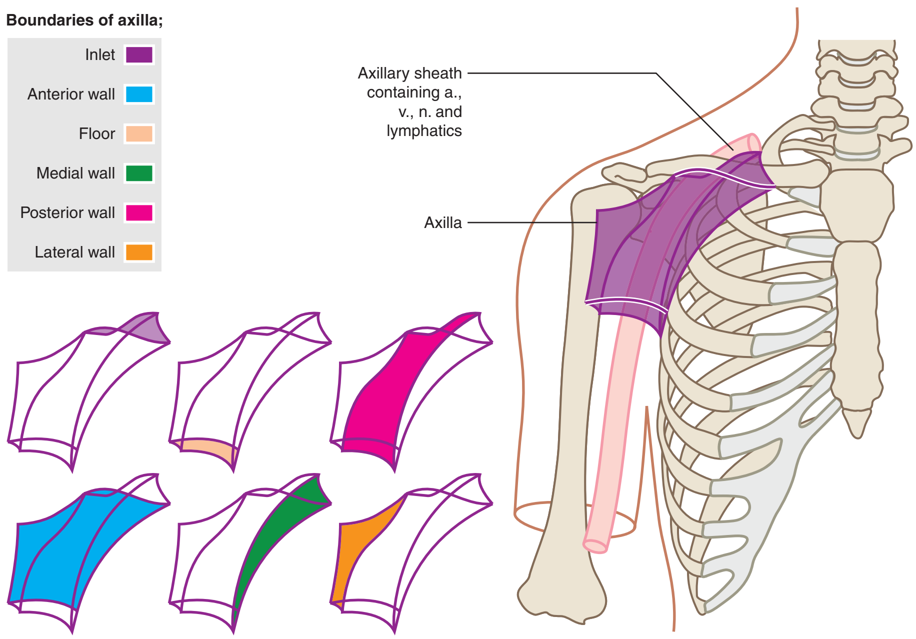


**Fig. 15.21** Line diagrams of the axilla and axilla contents.

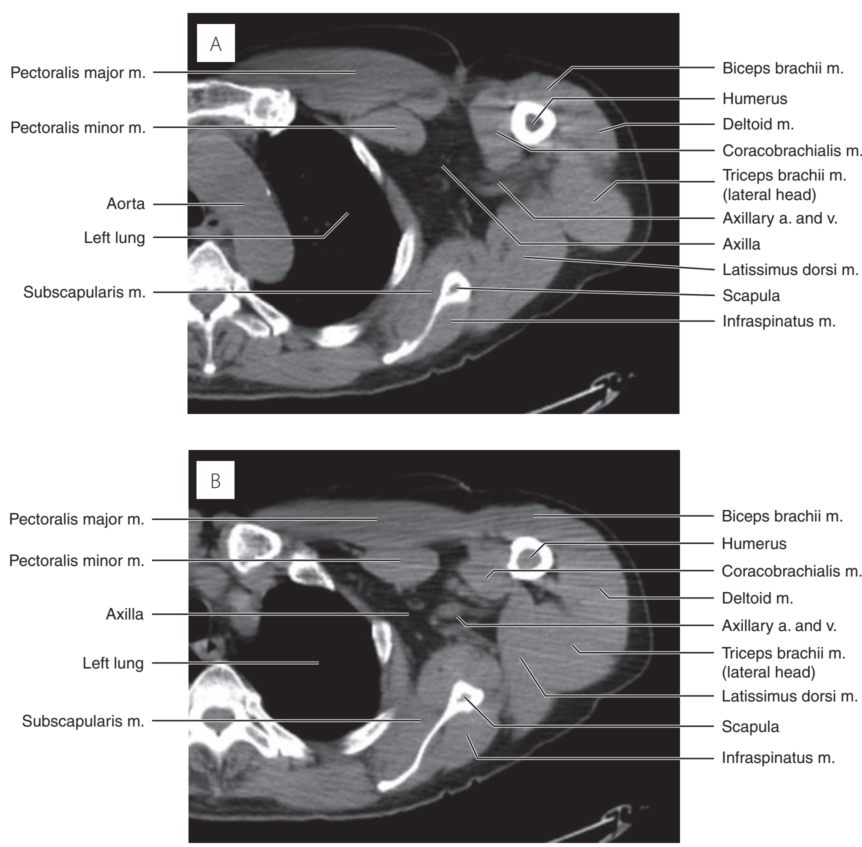


**Fig. 15.22** Axial CT left axilla (superior to inferior).

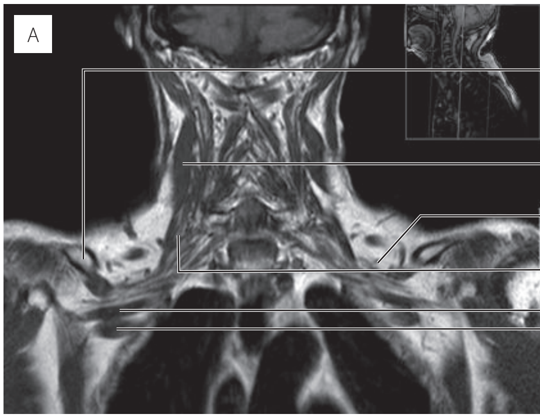


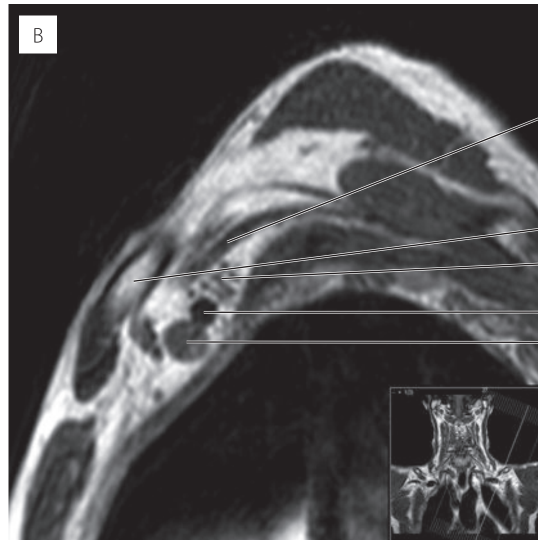


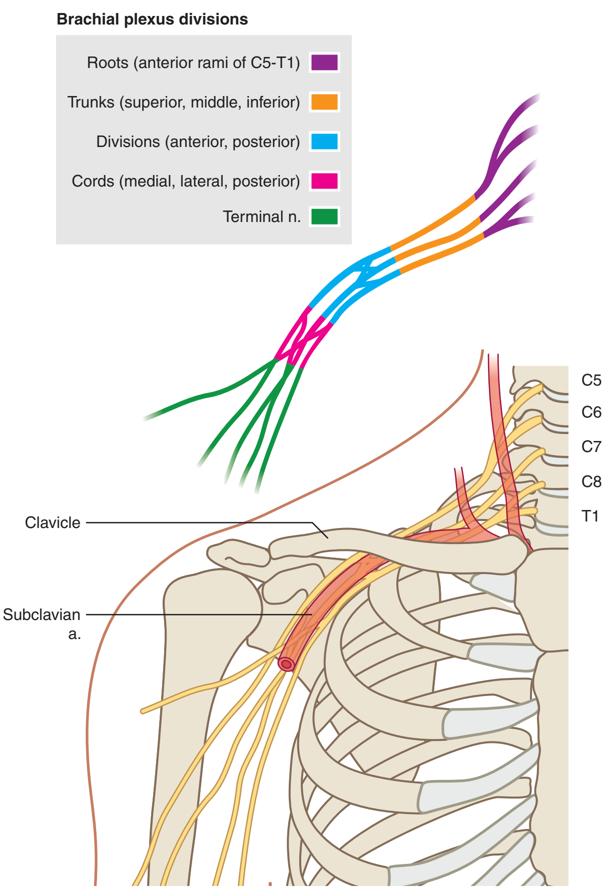


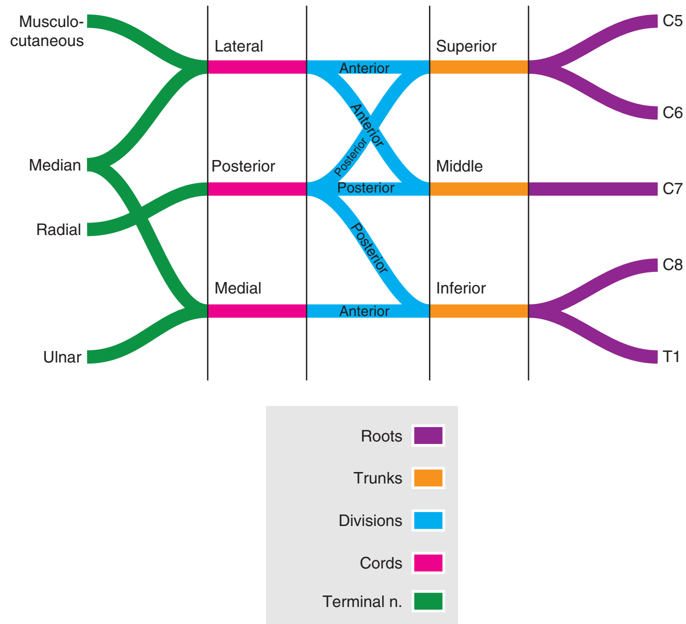


**Fig. 15.23** (A) Coronal T1 MRI, both axillae; (B) sagittal oblique T1 MRI, right axilla.

- Two protuberances, the medial and lateral epicondyles, lie in an extracapsular location (Fig. 15.27).

## Elbow joint

- The elbow joint consists of three articulations all enclosed by a common joint cavity, the radiocapitellar and ulnatrochlear joints (allowing 150° flexion-extension) and proximal radio-ulnar joint (allowing 90° pronation-supination).
- When fully extended, the long axis of the forearm lies laterally at an angle to the long axis of the forearm, termed the carrying angle.
- Fat pads separate the fibrous joint capsule from the synovial membrane:
  - on a normal lateral radiograph, only the anterior fat pad can be seen, closely applied to the anterior

**Table 15.6**

| Muscle | Origin | Insertion | Action |
|---|---|---|---|
| Biceps brachii | Long head: supraglenoid tubercle of scapula<br>Short head: coracoid process of scapula | Radial tuberosity; bicipital aponeurosis of medial forearm | Flexes and supinates forearm; weak arm flexor |
| Coracobrachialis | Tip of coracoid process of scapula | Middle 1/3 of medial border of humerus | Flexes and weakly adducts arm |
| Brachialis | Anterior lower half of humerus | Coronoid process and tuberosity of ulna | Flexes forearm |

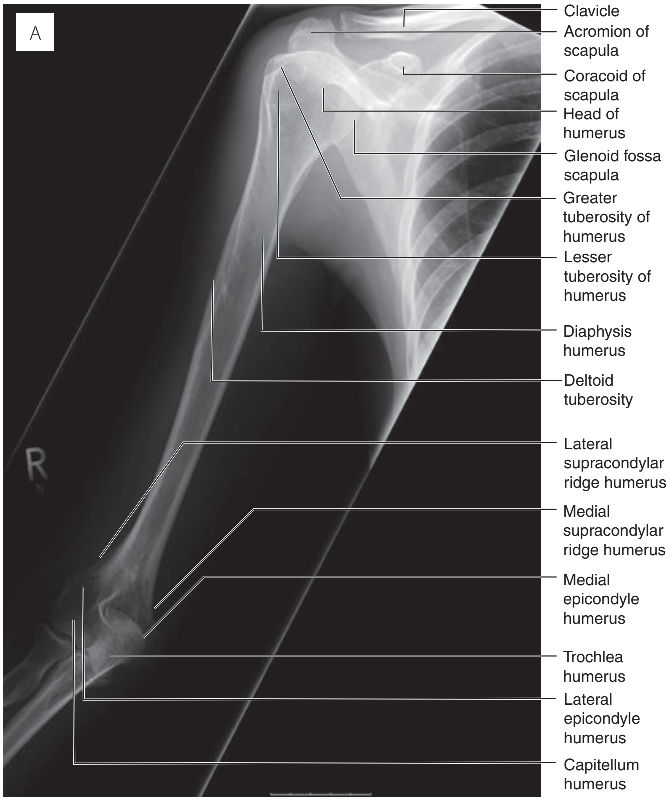


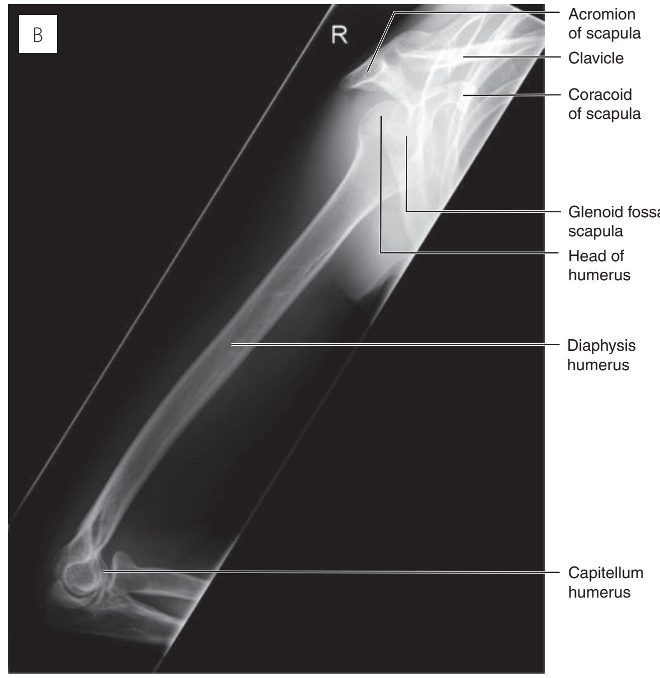


**Fig. 15.24** (A) AP radiograph, right humerus; (B) lateral radiograph, right humerus.

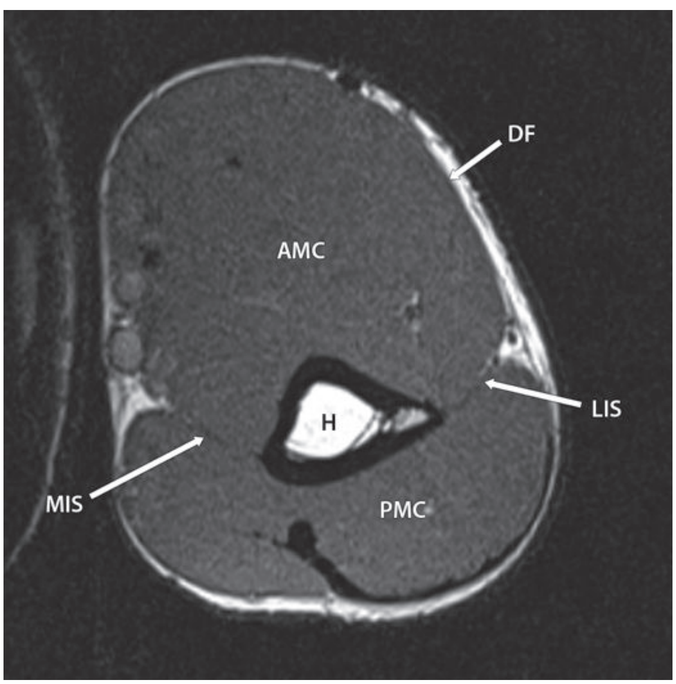


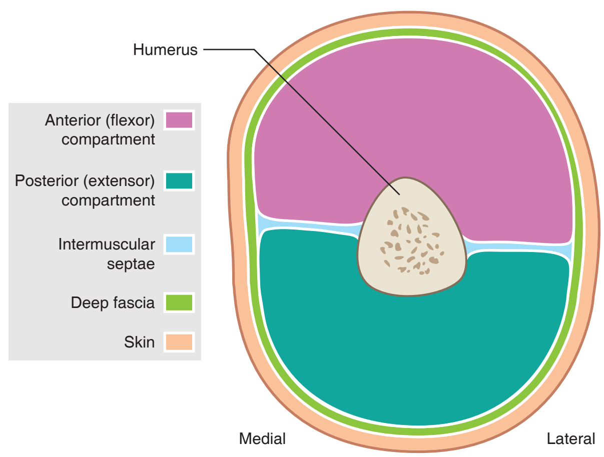


**Fig. 15.25** Axial T1 MRI right arm.

distal humerus as a well defined lucent structure

- an elbow joint effusion will displace the fat pads outwards, making the posterior fat pad visible and the anterior fat pad more prominent (Fig. 15.28).

## Normal lines on the elbow radiograph

- Anterior humeral line:
  - the distal aspect of the humerus is angulated at 40–45° anteriorly relative to the diaphysis
  - as such, approximately 1/3 of the capitellum should lie anterior to a line drawn along the anterior aspect of the humeral diaphysis on a lateral radiograph

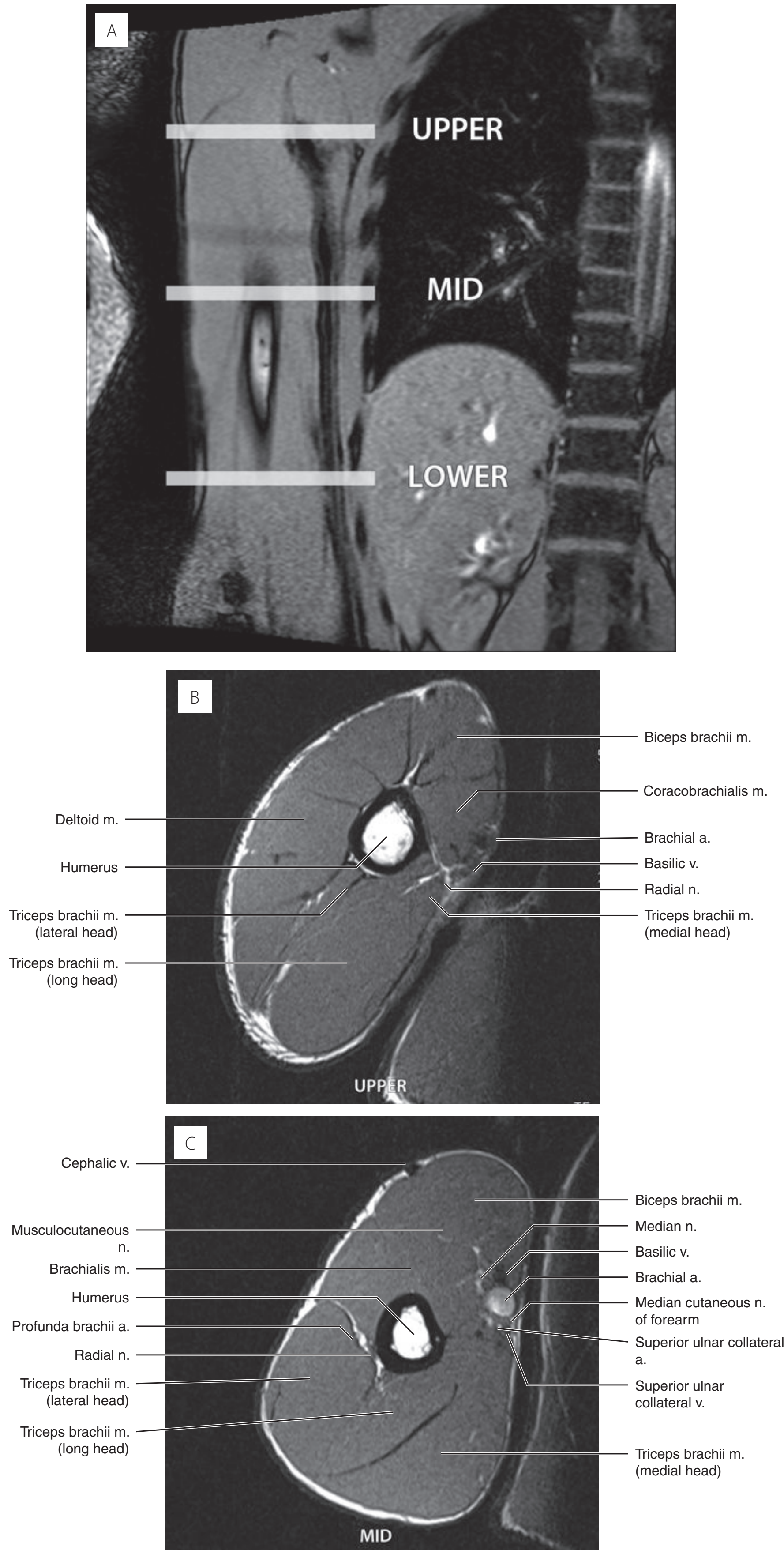


**Fig. 15.26** (A) Scout localizer image of the right arm. The levels that panels (B), (C) and (D) have been taken at are denoted here as UPPER, MID and LOWER. (B) Axial T1 MRI, right arm (upper). (C) Axial T1 MRI, right arm (mid). (D) Axial T1 MRI, right arm (lower). (E) Diagram to show the course of the nerves of the arm in relationship to the muscles.

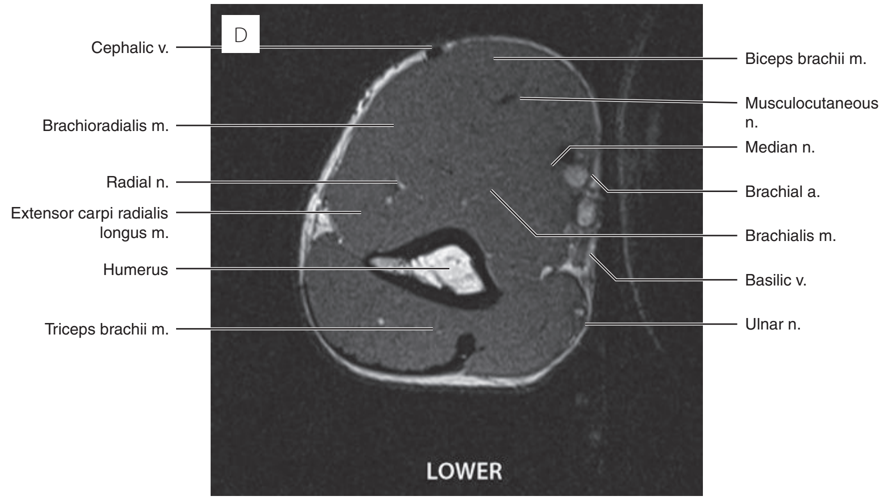


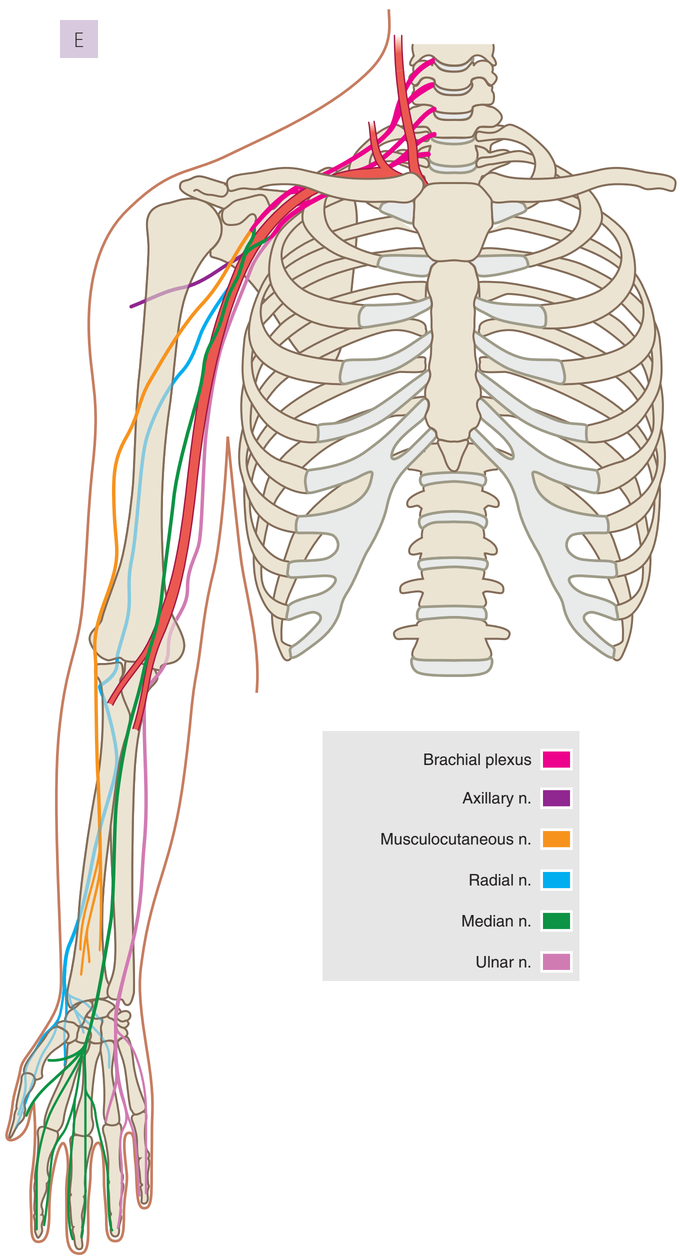


**Fig. 15.26** *(cont.)*

**Table 15.7**

| Muscle | Origin | Insertion | Action |
|---|---|---|---|
| Triceps brachii | Long head: infraglenoid tubercle of scapula<br>Lateral head: upper half of posterior diaphysis of humerus<br>Medial head: lower half of posterior diaphysis of humerus | By a common tendon into posterior part of olecranon process of ulna | Extends forearm |

**Table 15.8** Ossification centres at elbow joint

| | Age at first appearance |
|---|---|
| Capitellum | 1 yr |
| Radial head | 5 yrs |
| Internal (medial) epicondyle | 4–6 yrs |
| Trochlea | 9–10 yrs |
| Olecranon | 9–10 yrs |
| External (lateral) epicondyle | 12 yrs |

- if less than 1/3 of the capitellum lies anterior to the anterior humeral line, it is suggestive of a supracondylar fracture of the humerus.
- Radiocapitellar line:
  - a line drawn along the centre of the radial diaphysis should intersect the capitellum on both the AP and lateral elbow radiograph
  - if this line does not intersect the capitellum, a radial head dislocation is likely (Fig. 15.29).

### Ossification at the elbow

Although exact recall of the dates of ossification is not essential, it is important to remember the order of ossification (CRITOE) as any apparent change in this order usually signifies a fracture (Fig. 15.30and Table 15.8).

## Cross-sectional anatomy

### Elbow joint ligaments (Fig. 15.31)

- The joint capsule is thickened to form the radial (lateral) and ulnar (medial) collateral ligament complexes.
- Radial collateral ligament complex:
  - provides varus stability
  - consists of radial collateral ligament, annular ligament, accessory collateral ligament and lateral ulnar collateral ligament.
- Ulnar collateral ligament complex:
  - provides valgus stability
  - consists of three bundles: anterior (primary valgus restraint), posterior and transverse (Fig. 15.32).

### Median nerve at the elbow

- Located in the anterior cubital fossa, anterior to the brachialis muscle and deep to the bicipital aponeurosis.
- Passes between the heads of the pronator teres muscle as it exits the cubital fossa.
- Gives off the anterior interosseous nerve branch near the bifurcation of the brachial artery.

### Ulnar nerve at the elbow

- Passes superficially through the medial elbow in the cubital tunnel, a fibro-osseous tunnel:
  - curved floor formed by groove between the olecranon process of the ulna and the medial epicondyle of the humerus
  - proximal roof formed by the cubital tunnel retinaculum (CTR), a thickening of fascia that bridges the walls of the bony floor
  - distal roof formed by the arcuate ligament (ligament of Osborne), an aponeurotic sheet connecting the heads of the flexor carpi ulnaris muscle and the distal continuation of the CTR (Fig. 15.33).

### Radial nerve at the elbow

- Lies anterior to the lateral epicondyle of the humerus between the brachialis and brachioradialis muscles.
- Gives off the posterior interosseous (deep motor) branch and a superficial (sensory) branch.
- Posterior interosseous nerve enters the posterior compartment of the forearm between the heads of the supinator muscle.

### Cubital fossa (Fig. 15.34)

- Triangular-shaped potential space in anterior elbow.
- Permits passage of structures from the arm to the forearm.
- Base: imaginary horizontal line connecting the epicondyles of the humerus.
- Apex: point at which the borders of the brachioradialis and pronator teres muscles cross.
- Contents (from lateral to medial):
  - biceps brachii tendon
  - brachial artery, which divides into the radial and ulnar arteries
  - median nerve.

# Forearm

## Plain radiographic anatomy

### Radius and ulna

The radius and ulna are long triangular-shaped bones with anterior, posterior and interosseous borders, the latter of which allow attachment of the interosseous membrane which connects the two bones.

They are joined at the proximal and distal radio-ulnar joints. The proximal radius is formed of the:

- head, for articulation with the capitellum of the humerus and the coronoid process of the ulna at the elbow joint.

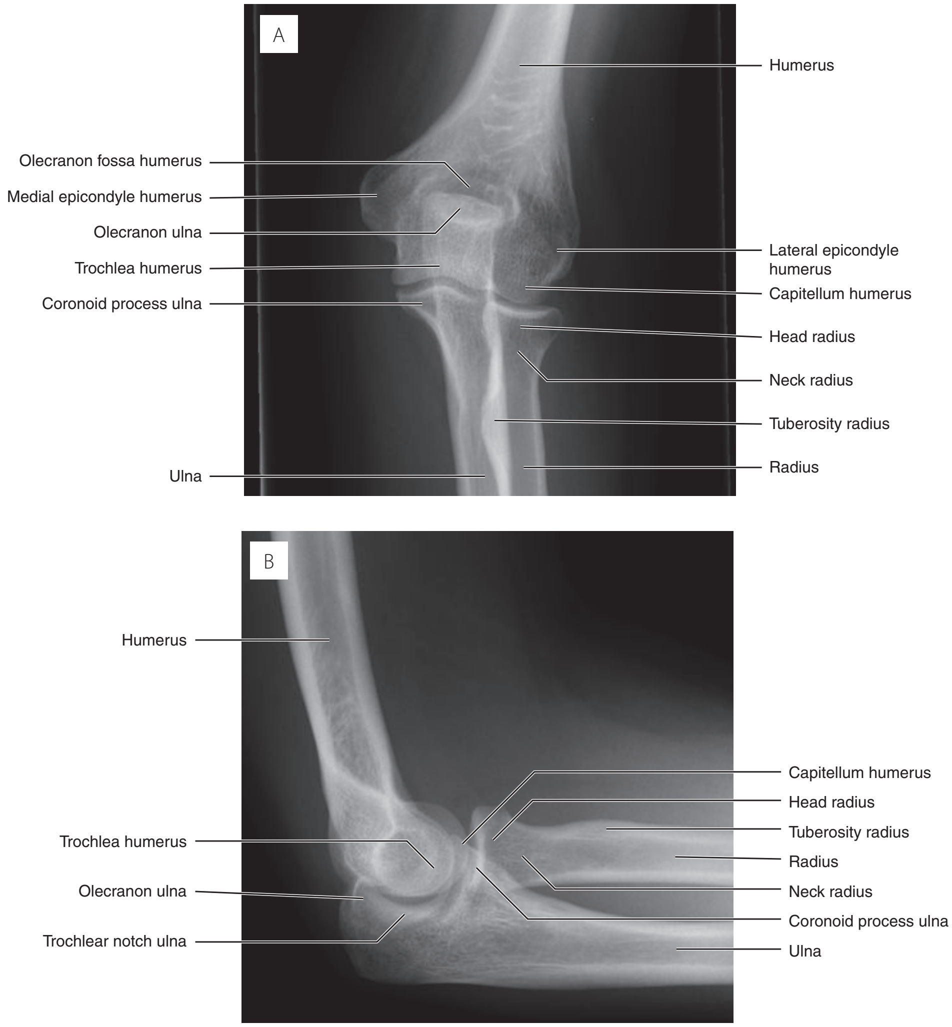


**Fig. 15.27** (A) AP radiograph right elbow; (B) lateral radiograph right elbow.

The distal radius is formed of the:

- broad distal surface, for articulation with the carpal bones at the wrist joint and with the distal ulna at the distal radio-ulnar joint
- styloid process, which provides attachment for the brachioradialis muscle and the radial collateral ligament of the wrist joint.

The proximal ulna is formed of the:

- olecranon process with its trochlear fossa for articulation with the trochlea of the humerus
- coronoid process, a proximal and lateral protuberance that allows articulation with the radial head.

The distal ulna is formed of the:

- head for articulation with the carpal bones at the wrist joint and with the distal radius at the radio-ulnar joint
- styloid process, which provides attachment for the ulnar collateral ligament of the wrist joint.

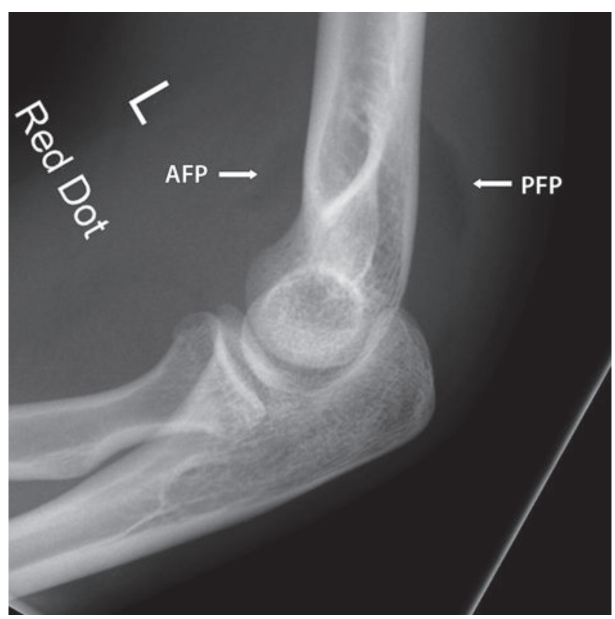


**Fig. 15.28** Lateral radiograph left elbow. The anterior fat pad (AFP) is elevated and the posterior fat pad (PFP) is visible, both of which are abnormal and indicate an underlying joint effusion displacing them outwards.

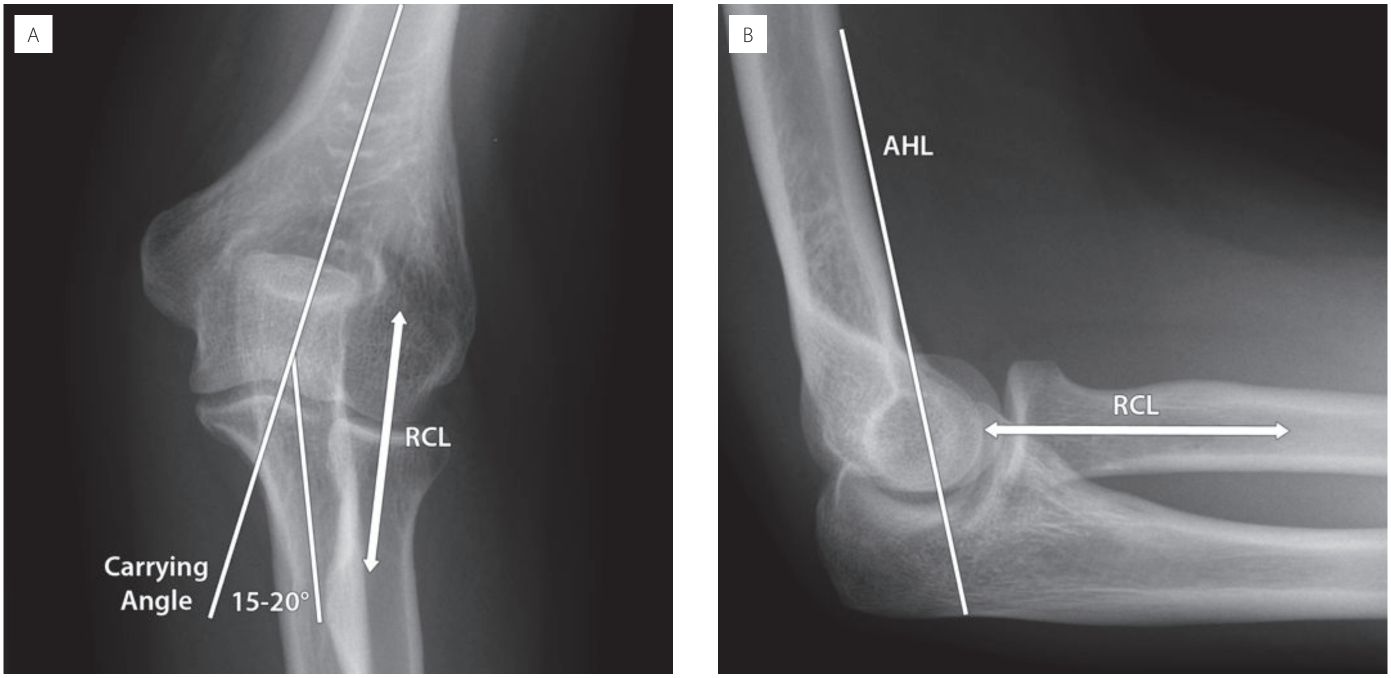


**Fig. 15.29** (A) AP radiograph right elbow; (B) lateral radiograph right elbow. The anterior humeral line (AHL) is a line drawn anterior to the humeral diaphysis. One-third of the capitellum should lie anterior to it. The radiocapitellar line (RCL) should intersect the proximal radial diaphysis and the capitellum. The normal carrying angle of 15–20° is the angle formed between the long axes of the arm and forearm.

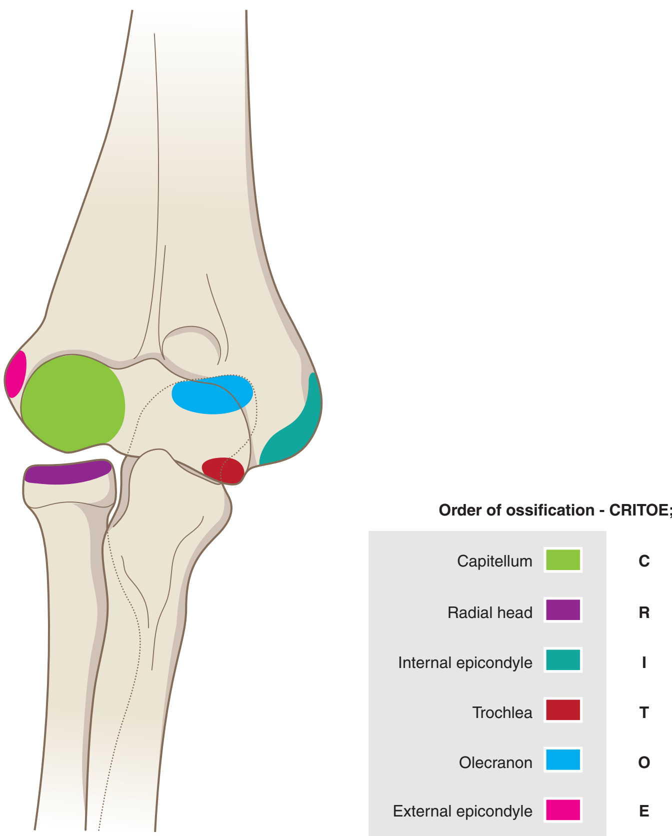


**Fig. 15.30** Diagram to show the normal ossification centres at the elbow. The centres ossify in the following chonological order CRITOE: Capitellum, Radial head, Internal (medial) epicondyle, Trochlea, Olecranon, External (lateral) epicondyle.

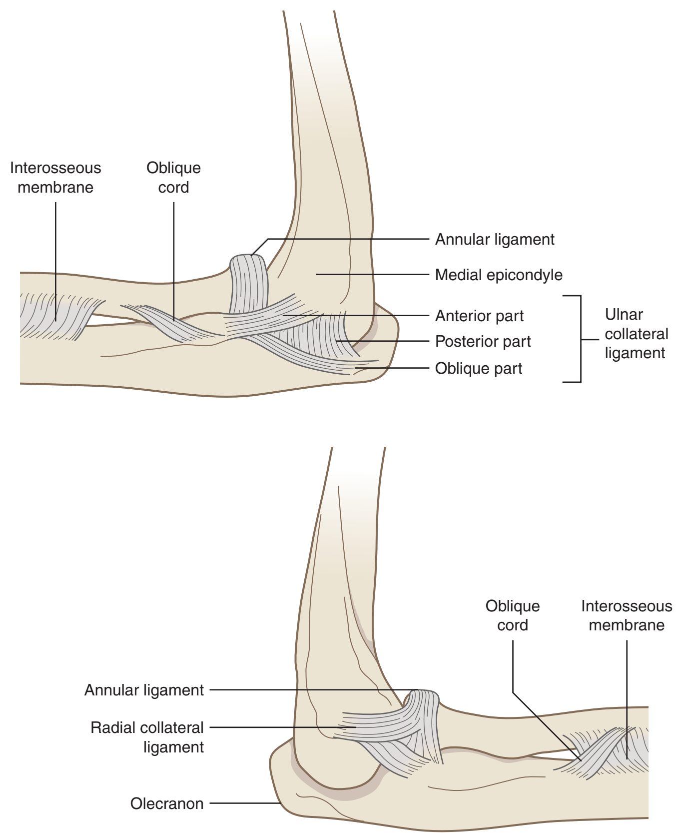


**Fig. 15.31** Diagram showing the intrinsic ligaments of the elbow.

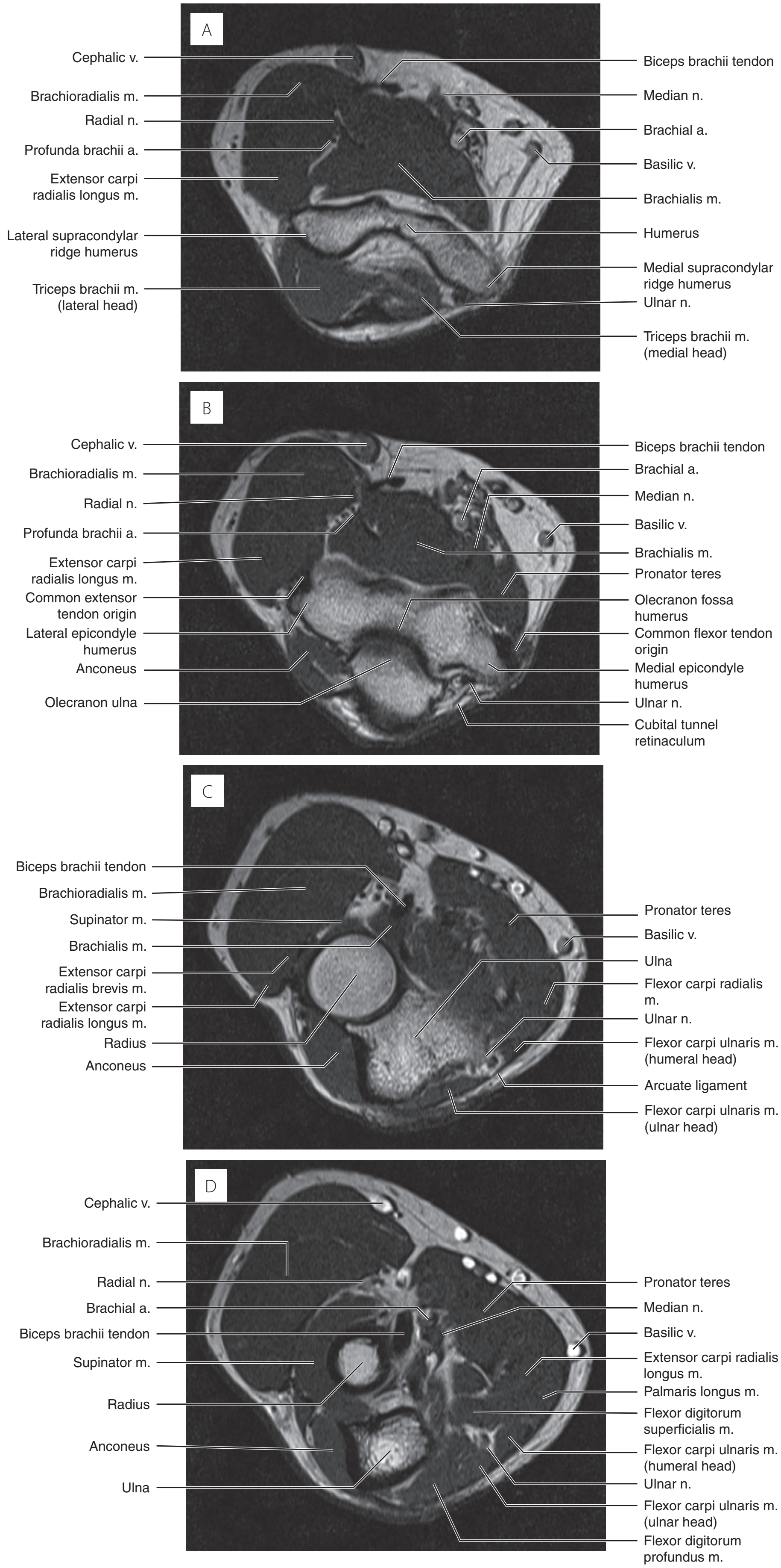


**Fig. 15.32** Axial T1 MRI, right elbow (superior to inferior).

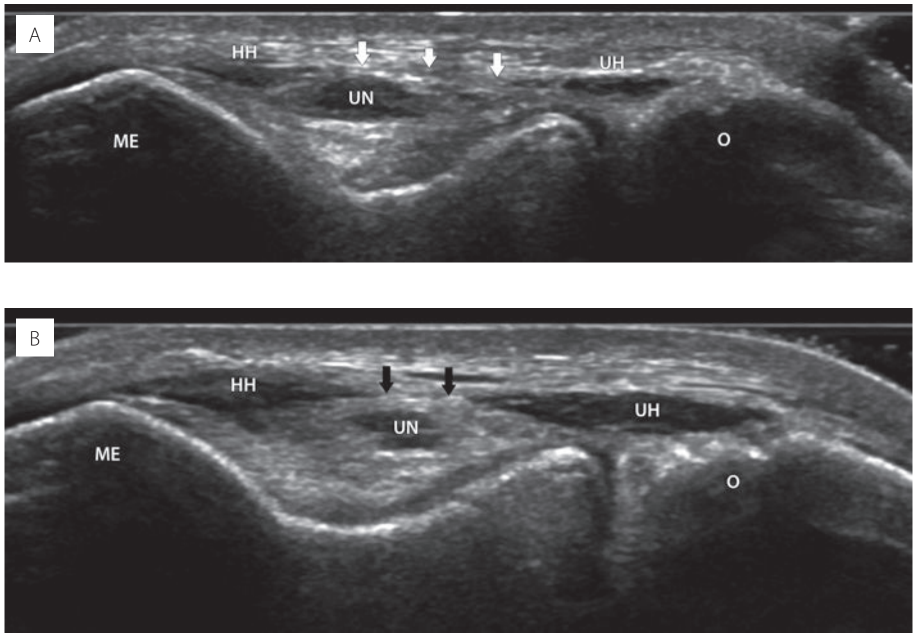


**Fig. 15.33** Transverse ultrasound cubital tunnel, proximal (A) and distal (B). The roof of the cubital tunnel is formed by the cubital tunnel retinaculum (white arrows), a thickening of fascia that continues distally as the arcuate ligament/ligament of Osborne (black arrows), an aponeurotic sheet connecting the humeral head (HH) and ulnar head (UH) of the flexor carpi ulnaris muscle. The floor of the cubital tunnel is formed by the groove between the olecranon process of the ulna (O) and the medial epicondyle of the humerus (ME).

### Ossification in the forearm (Table 15.9 and Fig. 15.35)

**Table 15.9** Ossification centres of the forearm

| | Appear | Fuse |
|---|---|---|
| Radial diaphysis | 8 weeks gestation | |
| Proximal radius | 4–6 yrs | 13–16 yrs |
| Distal radius | 1 yr | 16–18 yrs |
| Ulnar diaphysis | 8 weeks gestation | |
| Proximal ulna | 8–10 yrs | 13–15 yrs |
| Distal ulna | 5–7 yrs | 16–18 yrs |

## Cross-sectional anatomy

- Similarly to the arm, the forearm is encircled by a sheath of deep fascia, attached to the posterior subcutaneous border of the ulna.
- A lateral intermuscular septum passes from the deep fascia to the radius.
- The interosseous membrane passes between the interosseous borders of the radius and ulna, its fibres orientated in an oblique downward and medial fashion:
    - it is taut with the forearm in the mid-prone position
    - it has a round opening in its distal third that allows the passage of blood vessels.
- Together, the deep fascia, lateral intermuscular septum and interosseous membrane divide the forearm into separate anterior and posterior fascial compartments (Fig. 15.36).

### Anterior (flexor) fascial compartment of the forearm

- The muscles of the anterior compartment can be divided into superficial, intermediate and deep layers.
- Blood supply: radial and ulnar arteries.
- Nerve supply: median nerve except for the flexor carpi ulnaris and the medial part of the flexor digitorum profundus which are supplied by the ulnar nerve.
- All four muscles in the superficial layer have a common origin from the medial epicondyle of the humerus, the common flexor origin (Tables 15.10–15.12 and Fig. 15.37).

### Posterior (extensor) fascial compartment of the forearm

- The muscles of the posterior compartment can be divided into superficial and deep layers.
- Blood supply: anterior and posterior interosseous arteries, branches of the common interosseous branch of the ulnar artery.
- Nerve supply: radial nerve.
- All of the muscles in the superficial layer have a common origin from the lateral epicondyle and lateral supracondylar ridge of the humerus, the common extensor origin (Tables 15.13, 15.14).

# Wrist

## Plain radiographic anatomy

### Radiocarpal joint

This is a synovial ellipsoid joint with articulation between the distal radius and the scaphoid, lunate and triquetral carpal bones.

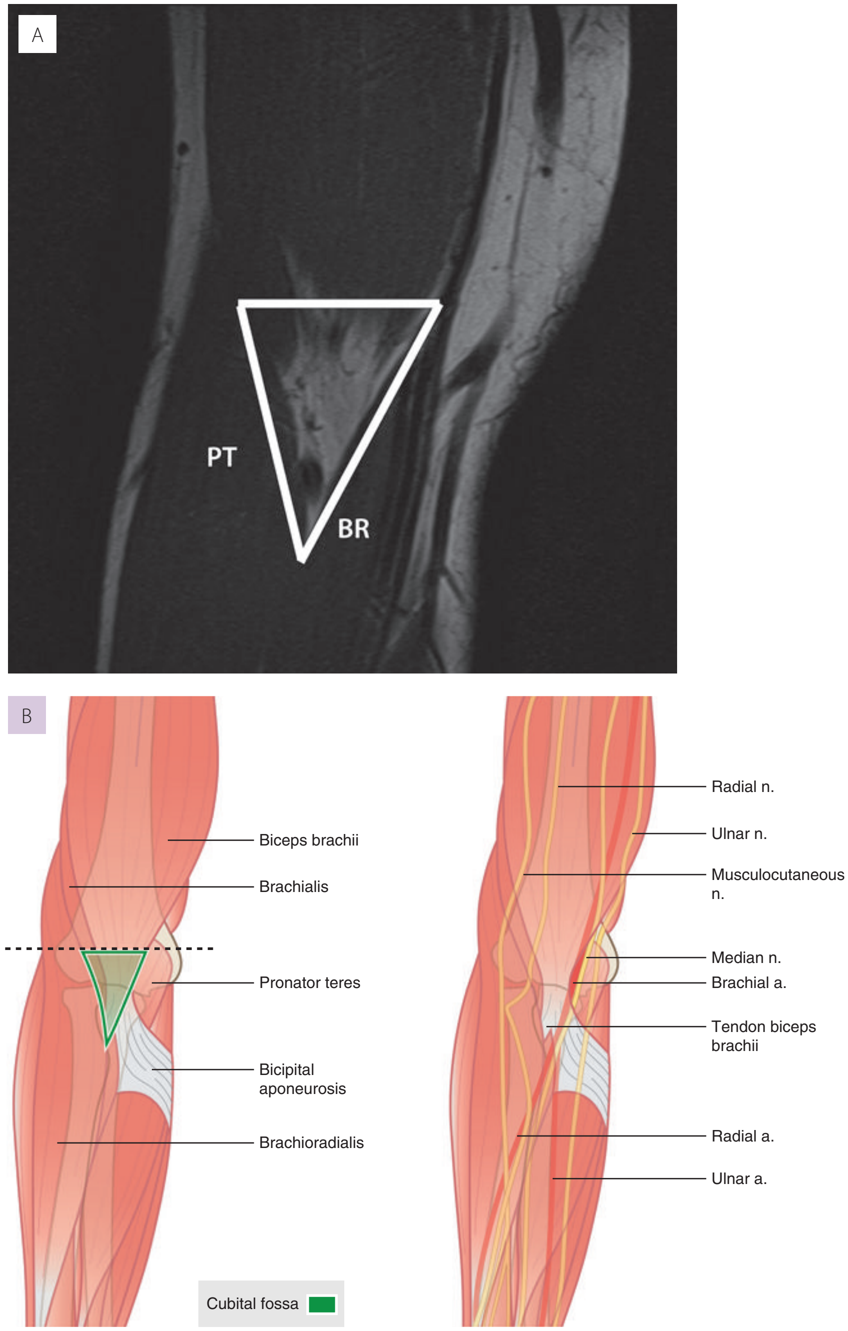


**Fig. 15.34** Coronal T1 MR of right elbow with associated schematic diagram demonstrating the cubital fossa. The cubital fossa is a triangular-shaped potential space. Its base is marked by an imaginary line connecting the humeral epicondyles. Its apex is the point at which the medial borders of the brachioradialis (BR) and pronator teres (PT) muscles cross.

### Important radiographic anatomical features at the wrist

There are important anatomical measurements to evaluate on posteroanterior and lateral radiographs of the wrist that help orthopaedic surgeons plan surgery following trauma.

### Ulnar variance (Fig. 15.38)

- This refers to anatomical variations in the lengths of the radius and ulna.
- On a posteroanterior radiograph of the distal forearm, the radial styloid process usually extends 9–12 mm distal to the articular surface of the ulna.
- Variance refers to the articular surfaces of the radius and ulna at the level of radiolunate articulation and is classified into:
  - neutral ulnar variance: the articular surfaces are at the same level
  - positive ulnar variance: the ulna is distal to the radius
  - negative ulnar variance: the ulna is proximal to the radius.
- False positives or negatives can occur as the wrist position changes and these terms only hold true on a radiograph

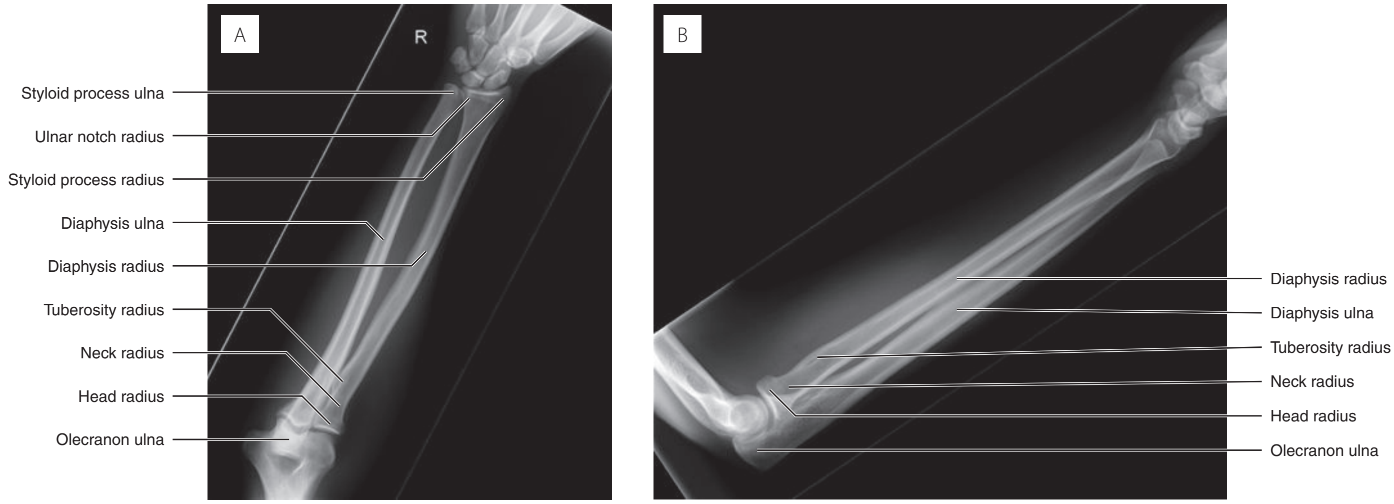


**Fig. 15.35** (A) AP radiograph, forearm; (B) lateral radiograph, forearm.

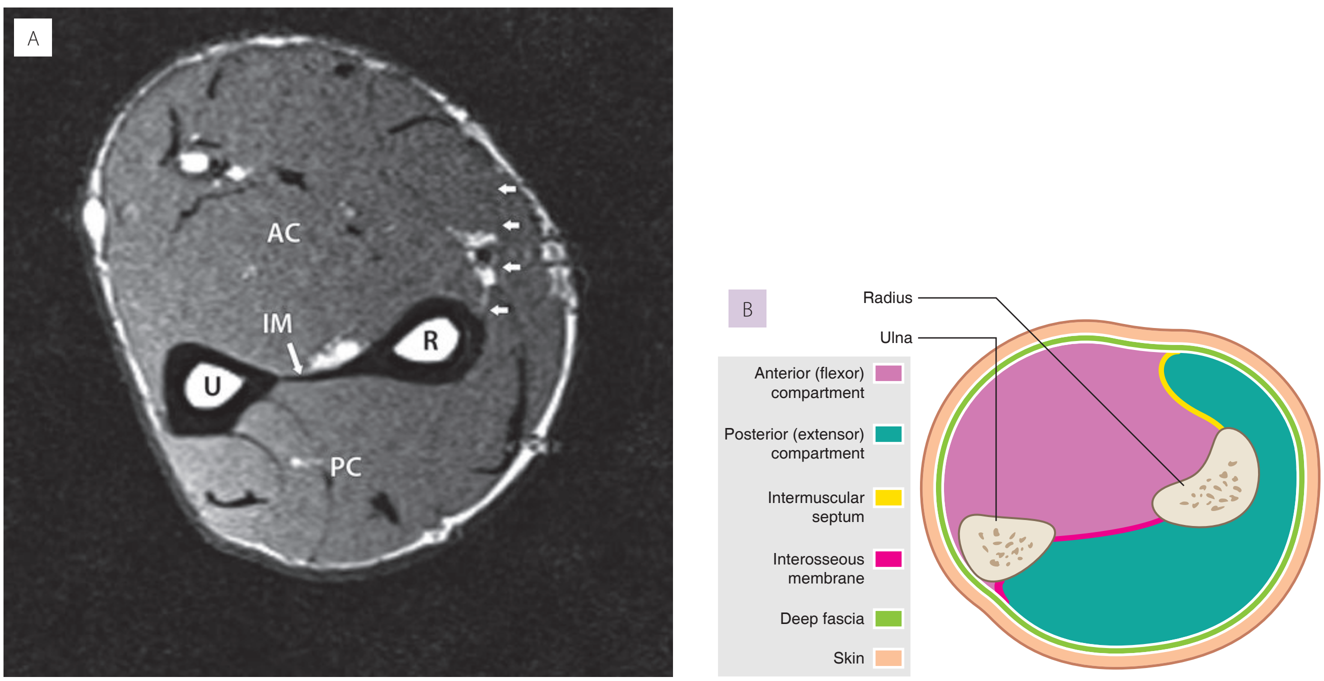


**Fig. 15.36** Axial T1 MR of right forearm with schematic diagram showing the compartments of the forearm. The interosseous membrane (IM) connects the radius (R) and ulna (U). The intermuscular septum (white arrows) connects the deep fascia to the radius. These structures divide the forearm into an anterior (flexor) compartment (AC) and posterior (extensor) compartment (PC).

performed with the wrist flat, the forearm in neutral rotation and flexed to 90° and the shoulder abducted to 90°.

### Ulnar slant of the radius (Fig. 15.39)

- Angle produced by the articular surface of the distal radius on a posteroanterior radiograph.
- Normally 15–25°.

### Palmar inclination (Fig. 15.40)

- Angle of volar tilt of the articulating surface of the distal radius on a lateral radiograph.
- Usually 15–20° (Fig. 15.41).

### Carpus and intercarpal joints (Fig. 15.42)

- The carpus is a set of eight bones formed into two rows (proximal and distal) each with four bones. From lateral to medial:
  - proximal row: scaphoid, lunate, triquetral, and pisiform
  - distal row: trapezium, trapezoid, capitate, and hamate.
- There is mixed opinion as to whether the pisiform is a true carpal bone or a sesamoid bone (see Hand section), as it lies in an anterior plane to the other carpal bones and is contained within the flexor carpi ulnaris tendon.

**Table 15.10** Muscles of the superficial layer of the anterior compartment of the forearm

| Muscle | Origin | Insertion | Action |
|---|---|---|---|
| Pronator teres | Humeral head: medial epicondyle of humerus<br>Ulnar head: coronoid process of ulna | Lateral diaphysis of radius | Pronation and flexion of forearm |
| Flexor carpi radialis | Medial epicondyle of humerus | Bases of index and middle metacarpals | Flexes and abducts wrist |
| Palmaris longus | Medial epicondyle of humerus | Flexor retinaculum and palmar aponeurosis | Flexes wrist |
| Flexor carpi ulnaris | Humeral head: medial epicondyle of humerus<br>Ulnar head: olecranon process and posterior border of ulna | Pisiform; hook of hamate; base of little metacarpal | Flexes and abducts wrist |

**Table 15.11** Muscles of the intermediate layer of the anterior compartment of the forearm

| Muscle | Origin | Insertion | Action |
|---|---|---|---|
| Flexor digitorum superficialis | Humeroulnar head: medial epicondyle of humerus; coronoid process of ulna<br>Radial head: oblique line of diaphysis of radius | By four tendons to the volar aspect of the middle phalanges of the index, middle, ring and little fingers | Flexes proximal interphalangeal joints of fingers; assists in flexing metacarpophalangeal joints and wrist joint |

**Table 15.12** Muscles of the deep layer of the anterior compartment of the forearm

| Muscle | Origin | Insertion | Action |
|---|---|---|---|
| Flexor pollicis longus | Anterior diaphysis of radius | Distal phalanx of thumb | Flexes interphalangeal joint of thumb |
| Flexor digitorum profundus | Anteromedial diaphysis of ulna | By four tendons to the volar aspect of the distal phalanges of the index, middle, ring and little fingers | Flexes distal (and assists with proximal) interphalangeal joints of fingers; assists in flexing wrist joint |
| Pronator quadratus | Distal anterior diaphysis of ulna | Distal anterior diaphysis of radius | Pronates forearm |

**Table 15.13** Muscles of the superficial layer of the posterior compartment of the forearm

| Muscle | Origin | Insertion | Action |
|---|---|---|---|
| Brachioradialis | Lateral supracondylar ridge of humerus | Styloid process of radius | Flexes elbow; rotates arm to mid-prone position |
| Extensor carpi radialis longus | Lateral supracondylar ridge of humerus | Dorsal surface of base of index metacarpal | Extends and abducts wrist |
| Extensor carpi radialis brevis | Lateral epicondyle of humerus | Dorsal surface of base of middle metacarpal | Extends and abducts wrist |
| Extensor digitorum | Lateral epicondyle of humerus | Middle and distal phalanges of index, middle, ring and little fingers | Extends index, middle, ring and little fingers and wrist |
| Extensor digiti minimi | Lateral epicondyle of humerus | Extensor hood of little finger | Extends little finger |
| Extensor carpi ulnaris | Lateral epicondyle of humerus | Base of little metacarpal | Extends and adducts wrist |
| Anconeus | Lateral epicondyle of humerus | Olecranon process of ulna | Extends elbow |

**Table 15.14** Muscles of the deep layer of the posterior compartment of the forearm

| Muscle | Origin | Insertion | Action |
|---|---|---|---|
| Supinator | Lateral epicondyle of humerus; anular ligament; supinator ridge of ulna | Neck and diaphysis of radius | Supinates forearm |
| Abductor pollicis longus | Posterior diaphysis of radius and ulna | Base of thumb metacarpal | Abducts and extends thumb |
| Extensor pollicis brevis | Posterior diaphysis of radius | Base of thumb proximal phalanx | Extends metacarpophalangeal joint of thumb |
| Extensor pollicis longus | Posterior diaphysis of ulna | Base of distal phalanx of thumb | Extends interphalangeal joint of thumb |
| Extensor indicis | Posterior diaphysis of ulna | Extensor hood of index finger | Extends metacarpophalangeal joint of index finger |

- There are multiple intercarpal articulations which share a common synovial cavity strengthened by multiple intercarpal ligaments.
- The intercarpal width should be uniform and not more than 2 mm in adults, except for the scapholunate distance, which should be less than 3 mm.
- On the lateral radiograph, the capitate, lunate and distal radius articulate with each other and should be seen lying one on top of the other in a straight line.

### Carpal stability

- The carpal ring theory has been described by Lichtman to explain carpal stability:

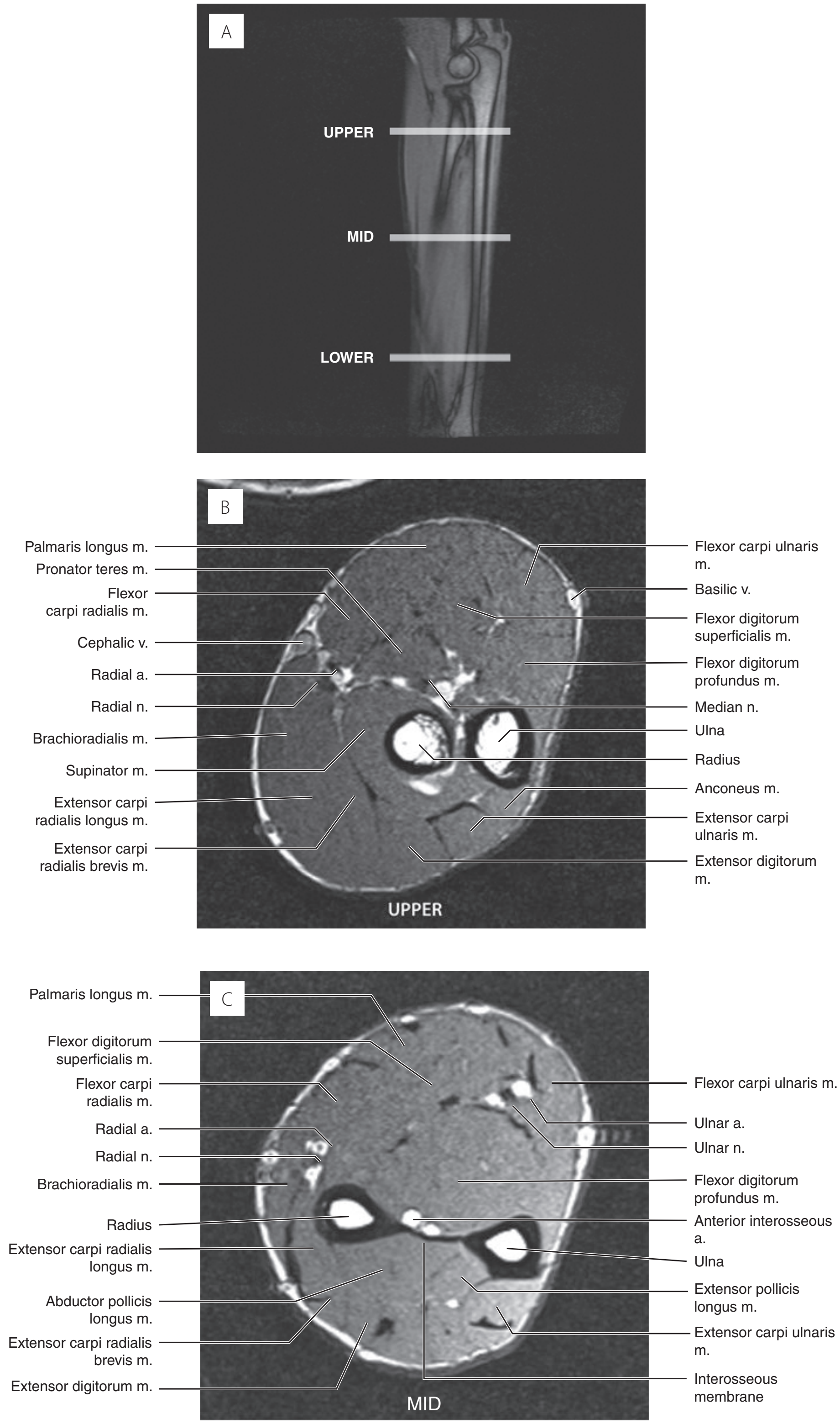


**Fig. 15.37** (A) Scout localizer image of the right forearm. The levels that panels (B), (C) and (D) have been taken at are denoted here as UPPER, MID and LOWER. (B–D) Axial T1 MRI images, right forearm (upper, mid and lower). (E) Diagram to show the superficial, intermediate and deep muscles as well as the blood vessels and nerves within the anterior compartment of the forearm. (F) Diagram to show the superficial and deep muscles as well as the blood vessels and nerves within the posterior compartment of the forearm.

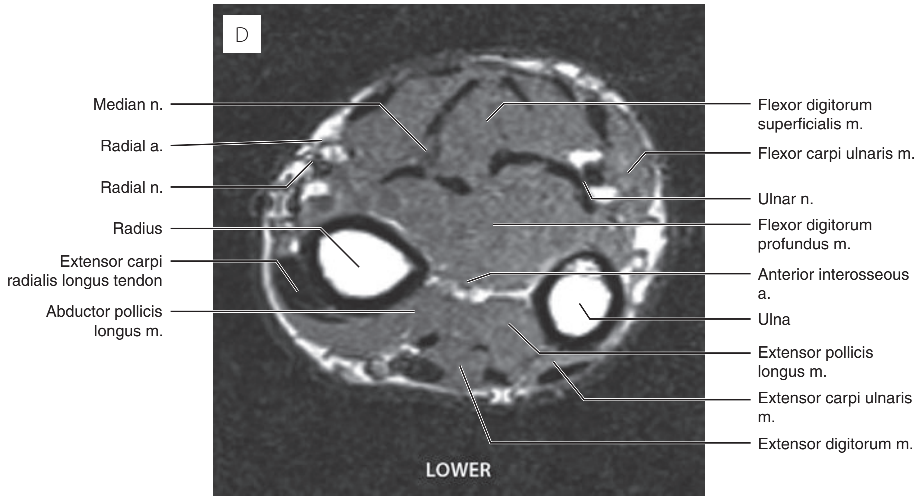


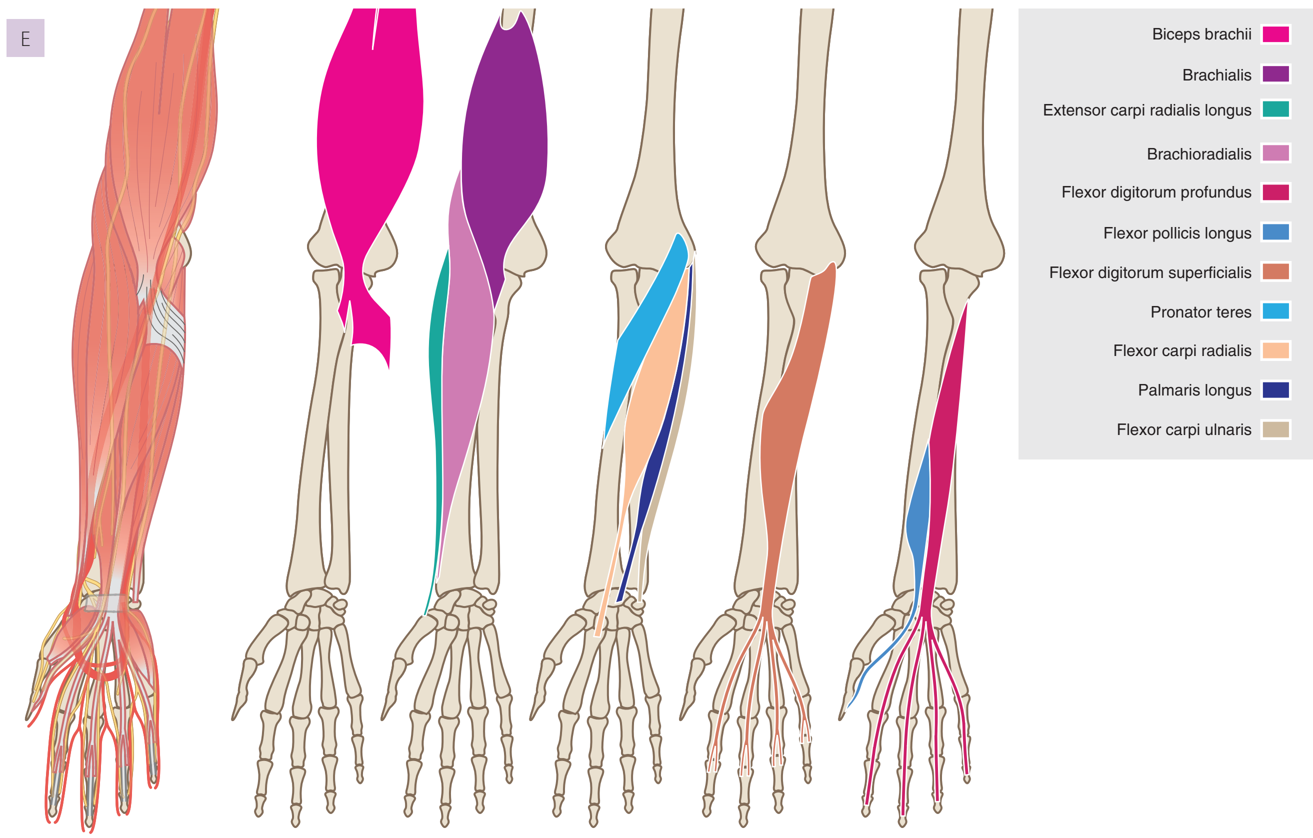


**Fig. 15.37** *(cont.)*

F

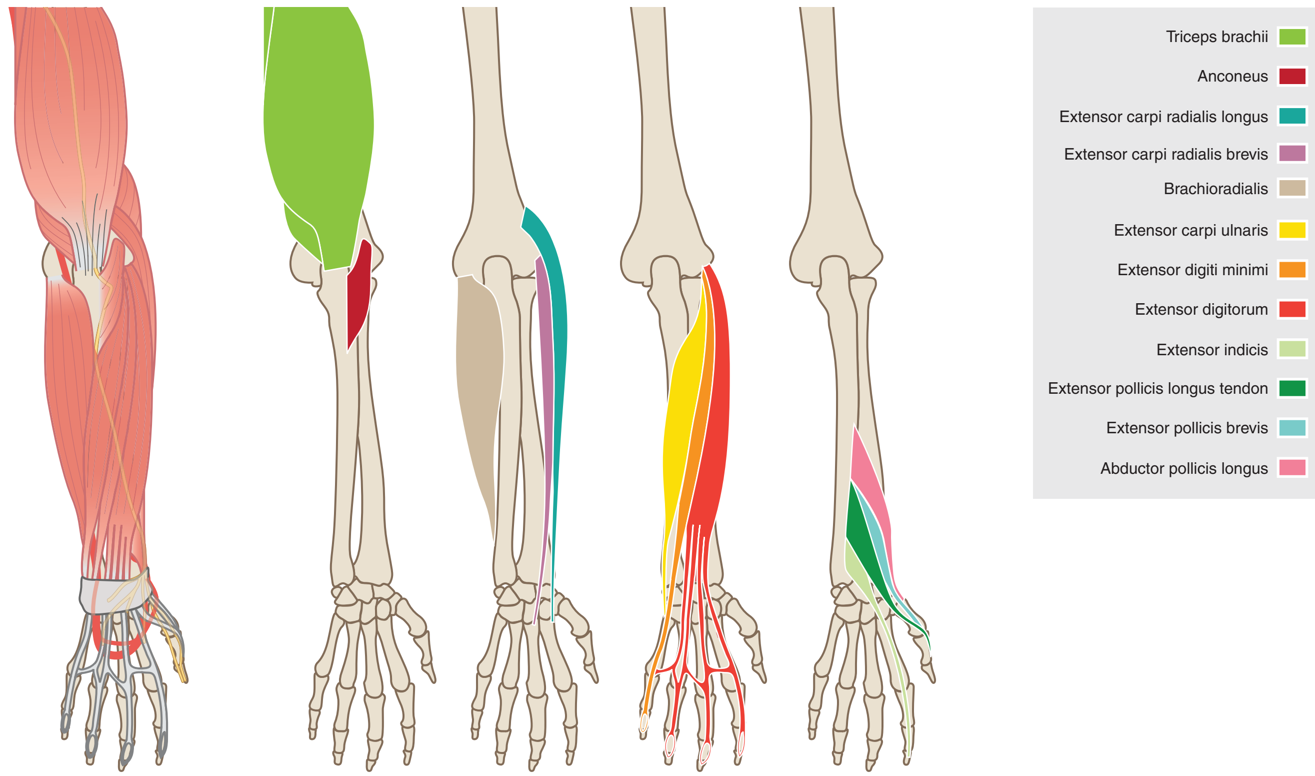


**Fig. 15.37** *(cont.)*

- the proximal carpal row acts as an intercalated segment between the distal radius and ulna and the distal carpal row
- the proximal carpal row moves as a unit stabilized by interosseous ligaments, allowing controlled mobility of the carpus
- in the event of a carpal fracture or interosseous ligament rupture, uncontrolled mobility can occur resulting in instability of the intercalated segment, of which there are two main types:
  - dorsal intercalated segment instability (DISI)
  - volar intercalated segment instability (VISI)
- on the lateral wrist radiograph, stability of the intercalated segment can be assessed by measuring the:
  - scapholunate angle: normally 30–60°
  - capitolunate angle: normally 0–30° (Fig. 15.43).

### Ossification at the wrist (Table 15.15 and Figs. 15.44, 15.45)

**Table 15.15** Ossification centres of the carpus

| | Appear | | Appear |
|---|---|---|---|
| Capitate | 1–3 months | Scaphoid | 4–6 yrs |
| Hamate | 2–4 months | Trapezium | 4–6 yrs |
| Triquetral | 2–3 yrs | Trapezoid | 4–6 yrs |
| Lunate | 2–4 yrs | Pisiform | 8–12 yrs |

## Cross-sectional anatomy

### Wrist joint ligaments (Fig. 15.46)

- Divided into intrinsic (between the carpal bones) and extrinsic (between distal radius and the carpal bones).
- Intrinsic ligaments:
  - scapholunate and lunatotriquetral ligaments are the most important
    - scapholunate ligament (Fig. 15.47): composed of three parts, volar (trapezoid shaped), middle (triangular shaped) and dorsal (band shaped)
    - middle part commonly has perforations that are clinically insignificant.
- Extrinsic ligaments:
  - consist of volar and dorsal ligaments connecting distal radius to carpal bones.

### Triangular fibrocartilage complex (TFCC) (Figs. 15.48, 15.49)

- This complex consists of five structures on the ulnar side of the wrist:
  - triangular fibrocartilage
  - radio-ulnar ligament (dorsal and volar components)
  - ulnar collateral ligament
  - meniscus homologue
  - extensor carpi ulnaris tendon sheath.

- The complex stabilizes the distal radio-ulnar joint and ulnar aspect of the wrist and can be damaged following trauma.

### Carpal tunnel (Figs. 15.50, 15.51)

- Fibro-osseous tunnel that permits the passage of tendons and neurovascular structures from the forearm to the hand.
- Floor: formed by the concavity of the carpal arch.
- Roof: formed by the flexor retinaculum. This is a thickening of fascia that attaches to the scaphoid and trapezium bones on the radial side and to the pisiform and hamate bones on the ulnar side, forming an enclosed tunnel.
- Contents:
  - median nerve
  - four flexor digitorum superficialis tendons
  - four flexor digitorum profunda tendons
  - flexor pollicis longus tendon.
- The flexor retinaculum splits laterally to enclose the flexor carpi radialis tendon in its own compartment.

### Guyon tunnel

- This is a fibro-osseous tunnel that permits the passage of the ulnar nerve as well as the ulnar artery and vein.
- Its floor is formed by the flexor retinaculum and its roof by the palmar carpal ligament.
- It has a proximal radial wall formed by the pisiform and a slightly distal ulnar wall formed by the hook of hamate.

### Extensor compartments of the wrist

- The anatomy of the extensor surface of the wrist is defined by the extensor retinaculum and Lister's tubercle (a dorsal protuberance) of the distal radius.
- The extensor retinaculum is an oblique thickening of fascia that attaches to the distal radius on the radial side and the triquetrum and pisiform on the ulnar side. Its deep attachments to the radius and ulna divide the extensor aspect of the wrist into six compartments, each with a single synovial sheath containing one or more tendons (Table 15.16 and Fig. 15.52).

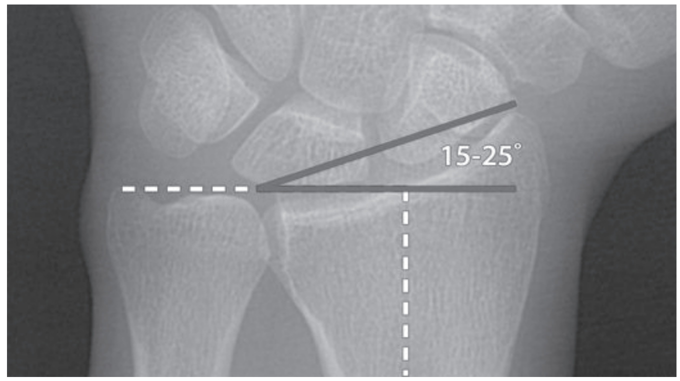


**Fig. 15.39** AP radiograph of the wrist demonstrating ulnar slant of the radius. A horizontal line is drawn perpendicular to the longitudinal axis of the radius at the articulation with the ulna. A second line is drawn joining the radial styloid process and the ulnar aspect of the articular surface of the radius. The ulnar slant is the angle formed between these two lines, normally 15–25°.

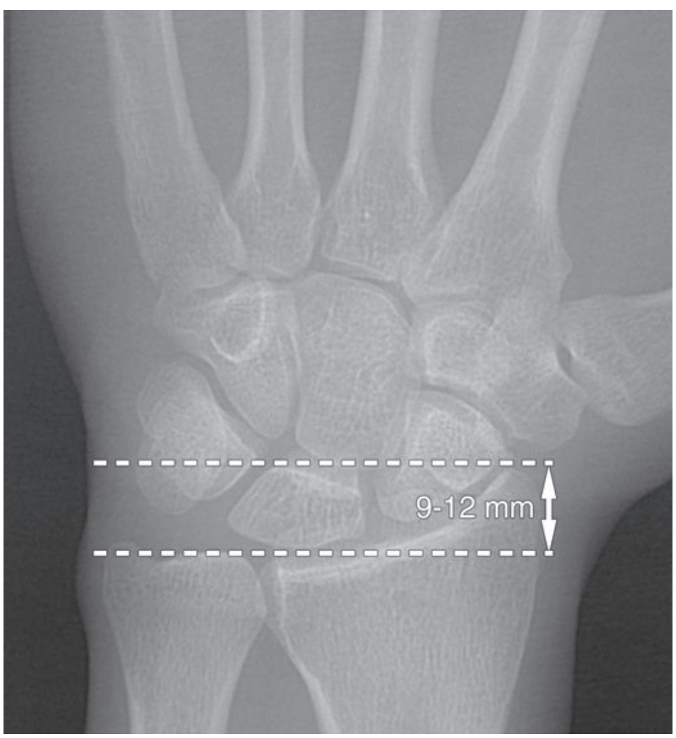


**Fig. 15.38** AP radiograph of the wrist demonstrating neutral ulnar variance. The radial styloid process lies 9–12 mm distal to the ulnar articular surface. The radial and ulnar articular surfaces are at the same level.

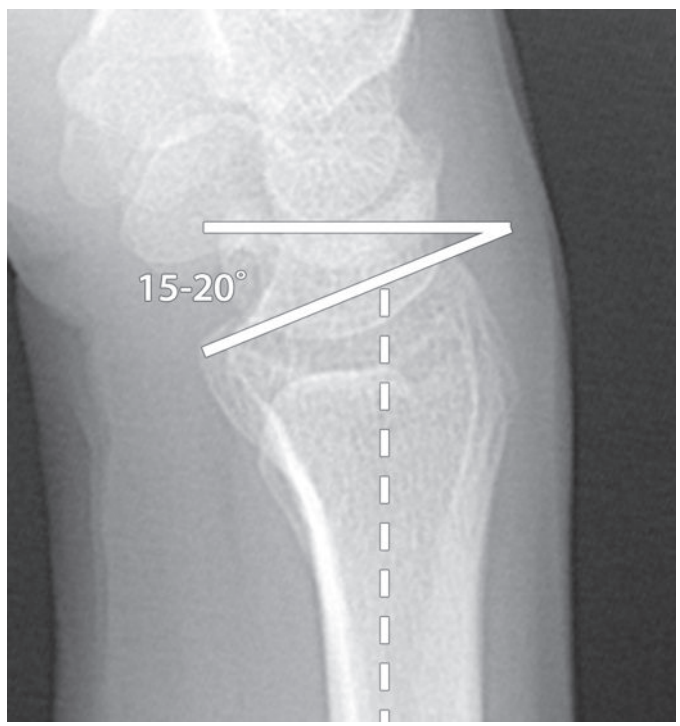


**Fig. 15.40** Lateral radiograph of the wrist demonstrating palmar inclination. A horizontal line is drawn at the level of the radial styloid, perpendicular to the longitudinal axis of the radius. A second line is drawn joining the dorsal and volar aspects of the radial articular surface. The palmar inclination is the angle formed between these two lines, normally 15–20°.

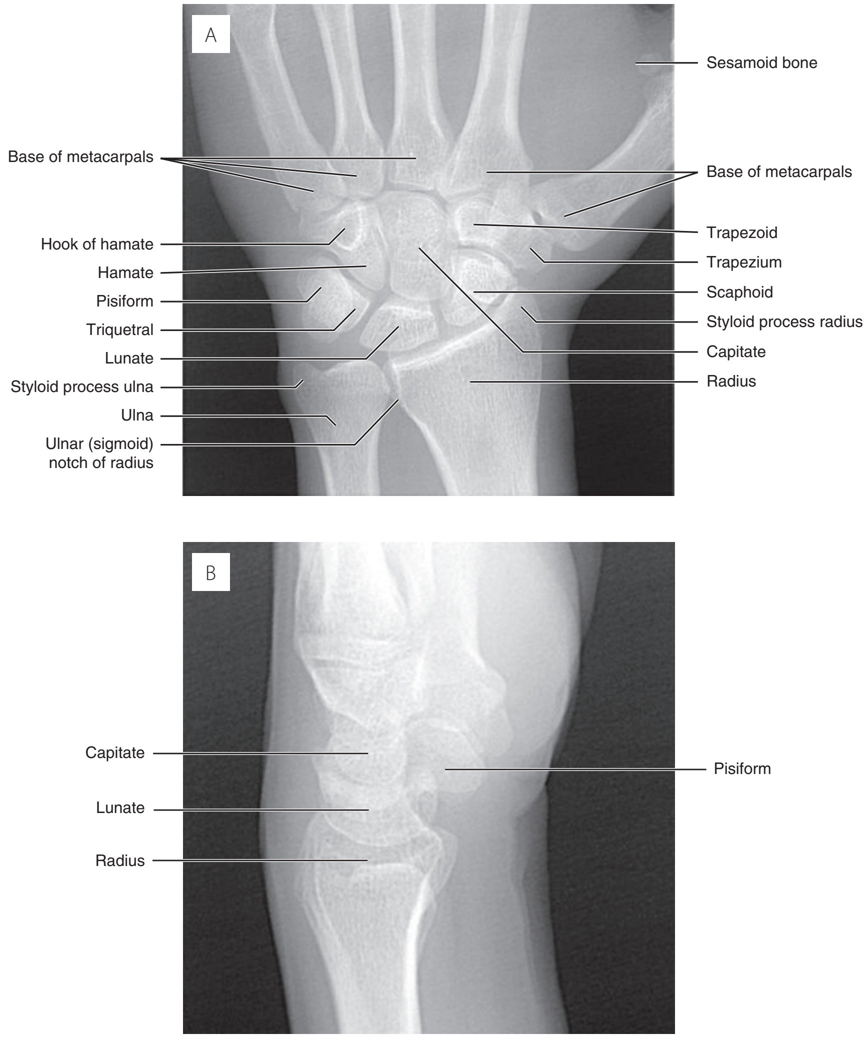


**Fig. 15.41** (A) AP radiograph, right wrist; (B) lateral radiograph, right wrist.

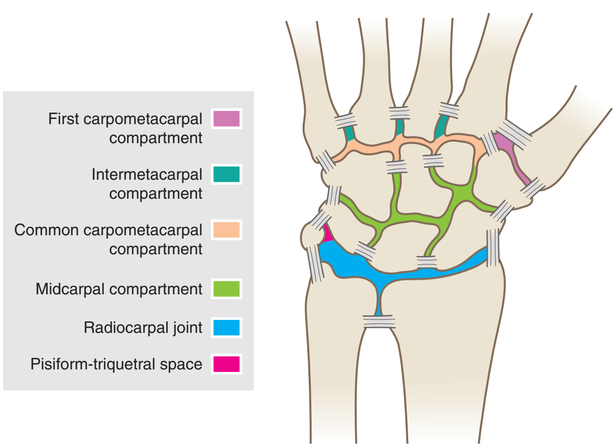


**Fig. 15.42** Diagram to show the carpal joint compartments.

# Hand

## Plain radiographic anatomy (Fig. 15.53)

### Metacarpal bones

To prevent confusion, it is easiest to refer to the digits by name (thumb and index, middle, ring and little fingers) rather than by number.

There are five metacarpal bones, each related to a digit. They consist of a proximal base, a diaphysis, a neck and a distal head.

### Phalangeal bones

- The phalanges are the bones of the digits.
- The thumb has two, the proximal and distal phalanges and the remaining digits have three, the proximal, middle and distal phalanges.
- Each phalanx has a proximal base, a body and a distal head.

### Sesamoid bones

- These are small bones found within tendons that pass over osseous or articular surfaces.
- The majority of the sesamoid bone is contained within the tendon and its free surface is lined with cartilage.

**Table 15.16** Extensor compartments

| Extensor compartment | Location | Contents |
|---|---|---|
| 1 | Radial to the radial styloid | Extensor pollicis brevis and abductor pollicis longus tendons |
| 2 | Ulnar to compartment 1; radial to Lister's tubercle | Extensor carpi radialis brevis and longus tendons |
| 3 | Ulnar to Lister's tubercle | Extensor pollicis longus tendon |
| 4 | Ulnar to compartment 3 | Four extensor digitorum tendons; extensor indicis tendon |
| 5 | Ulnar to compartment 4; dorsal to the radio-ulnar interval | Extensor digiti minimi tendon |
| 6 | Between head and styloid process of ulna | Extensor carpi ulnaris tendon |

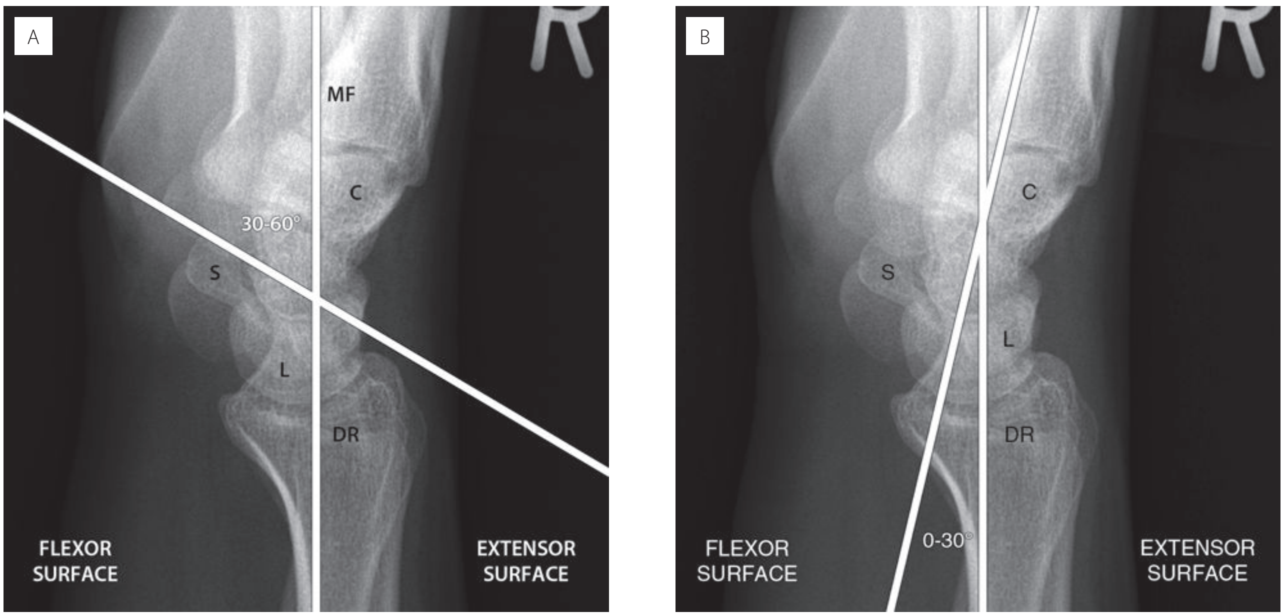


**Fig. 15.43** (A) Lateral radiograph of the right wrist showing the normal scapholunate angle; (B) lateral radiograph of the right wrist showing the normal capitolunate angle. The scapholunate angle is calculated by drawing lines through the longitudinal axes of the scaphoid and lunate – it should normally be between 30 and 60°. The capitolunate angle is calculated by drawing lines through the longitudinal axes of the capitate and lunate – it should normally be between 0 and 30°. C = capitate; DR = distal radius; L = lunate; MF = middle finger metacarpal; S = scaphoid.

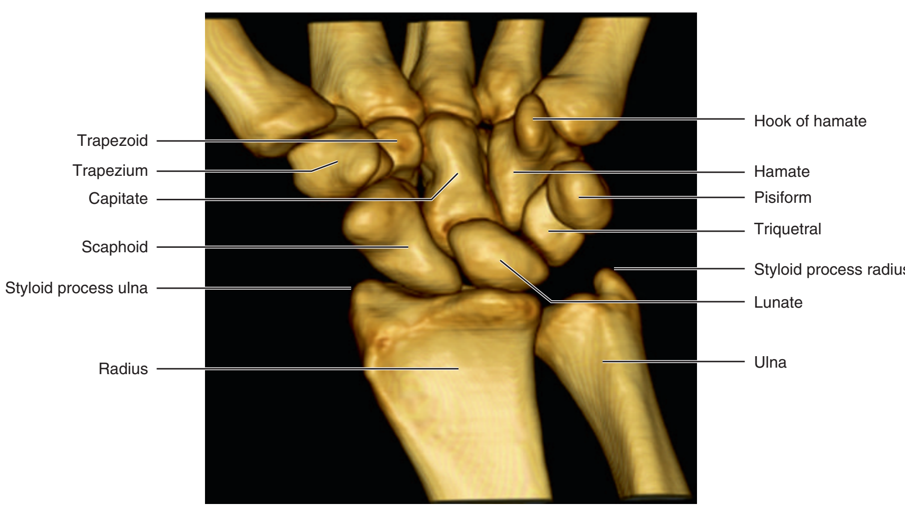


**Fig. 15.44** Surface-shaded reformat CT, right wrist.

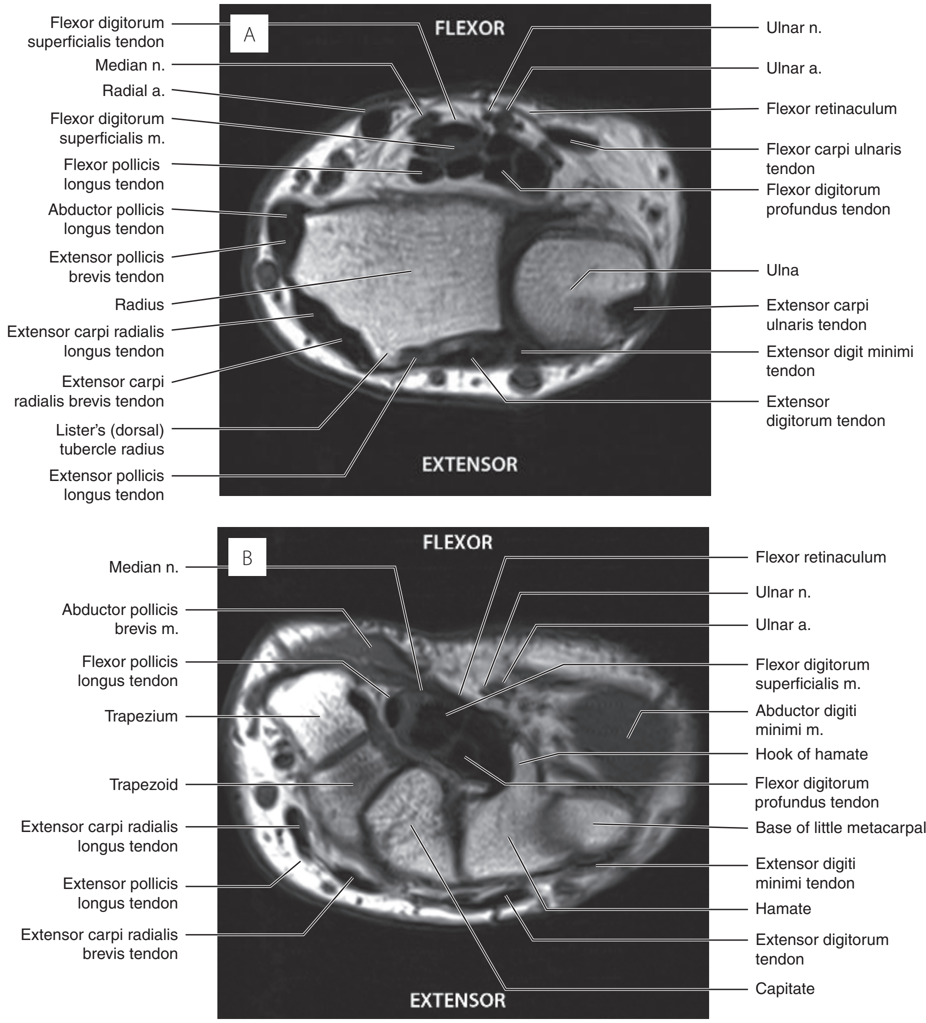


**Fig. 15.45** Axial T1 MRI, right wrist (radio-ulnar joint and carpal tunnel levels).

- In the upper limb, there are up to five sesamoid bones, all contained within the hand or wrist: three are related to the thumb (two at the metacarpophalangeal (MCP) joint and one at the interphalangeal joint) and one each at the MCP joints of the index and little fingers.
- There is mixed opinion as to whether the pisiform is a carpal or a sesamoid bone, as it lies in an anterior plane to the rest of the carpal bones and is contained within the flexor carpi ulnaris tendon.

### Carpometacarpal joints (Fig. 15.54)

- The carpal bones articulate with the metacarpal bones at the five carpometacarpal joints.
- The thumb carpometacarpal joint is the most mobile articulation as it is a synovial saddle joint between the trapezium and the thumb metacarpal.

### Metacarpophalangeal joints

- These are synovial hinge joints between the heads of the metacarpals and the proximal phalanges of the digits.

### Interphalangeal joints

- These are synovial hinge joints that allow flexion and extension.

### Ossification in the hand (Table 15.17)

**Table 15.17** Ossification centres of the hand

| | Appear | Fuse |
|---|---|---|
| Metacarpal diaphysis | 9 weeks gestation | |
| Metacarpal head | 1–2 yrs | 14–19 yrs |
| Phalangeal diaphysis | 8–12 weeks gestation | |
| Phalangeal base | 1–3 yrs | 14–18 yrs |

## Cross-sectional anatomy

### Digital flexor sheath (Figs. 15.55, 15.56)

- Smooth movement of the flexor tendons of the hand is maintained by the digital flexor sheath.
- This consists of an inner synovial (membranous) layer and an outer pulley (retinacular) layer.
- The inner membranous layer is a closed synovial system that bathes the flexor tendons, provides

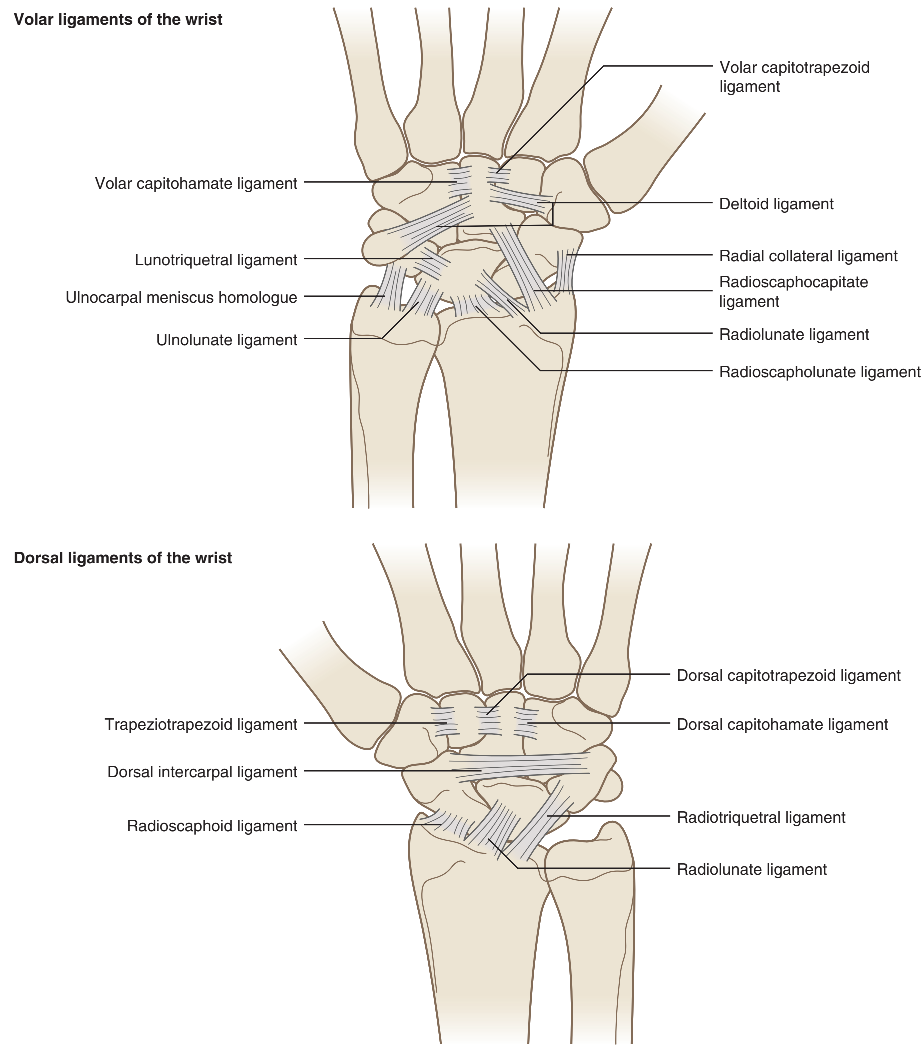


**Fig. 15.46** Diagram to show the wrist joint ligaments.

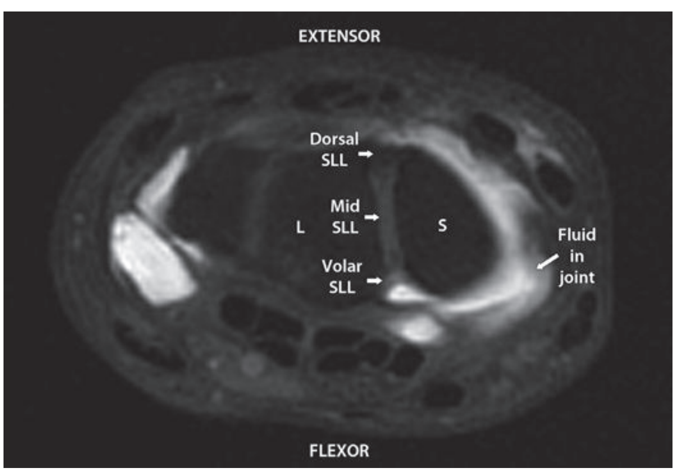


**Fig. 15.47** Axial fat-saturated T1 MRI arthrogram of the right wrist (post intra-articular gadolinium injection) demonstrating the scapholunate ligament. Image demonstrating the dorsal, mid and volar parts of the scapholunate ligament. S = scaphoid; L = lunate; SLL = scapholunate ligament.

nutrition and facilitates smooth movement of the tendons in flexion.

- The outer retinacular layer consists of bands of fibrous tissue that enclose the tendon and synovial sheath and help prevent buckling of these structures during flexion. It consists of the five annular pulleys (A1–A5) and four cruciform pulleys (C1–C4).

### Flexor digitorum tendons (Figs. 15.57, 15.58)

- The flexor digitorum superficialis tendon lies superficial to the profundus tendon in the palm.
- As it courses distally, it divides into two slips to pass laterally and then deep to the profundus tendon and eventually inserts onto the proximal aspect of the middle phalanx.
- The flexor digitorum profundus tendon inserts distally onto the distal phalanx.

### Dorsal extensor hood (Fig. 15.59)

- This is a fibrous expansion on the dorsum of the proximal phalanx of each digit blending with the respective extensor tendon.

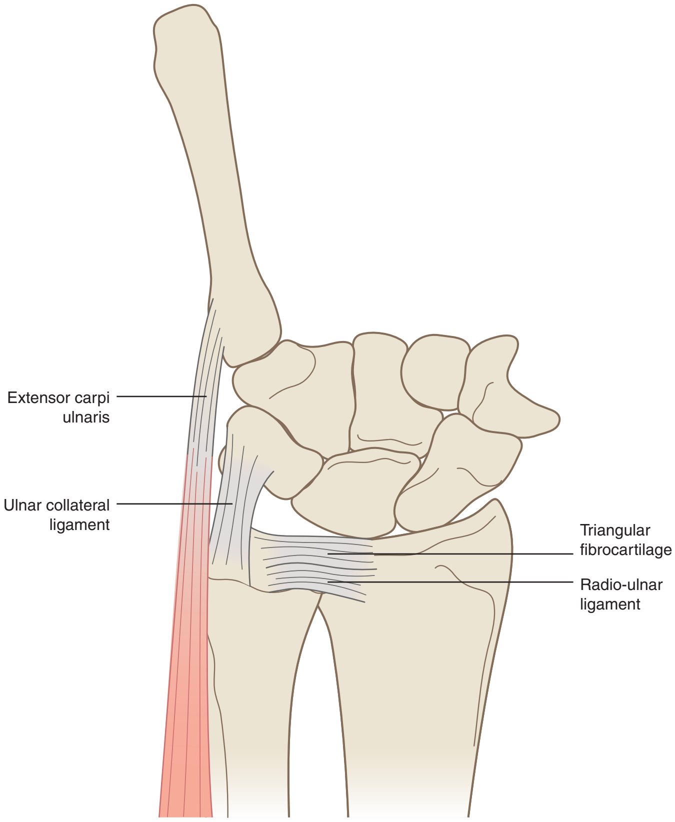


**Fig. 15.48** Diagram to show the components of the triangular fibrocartilage complex (TFCC).

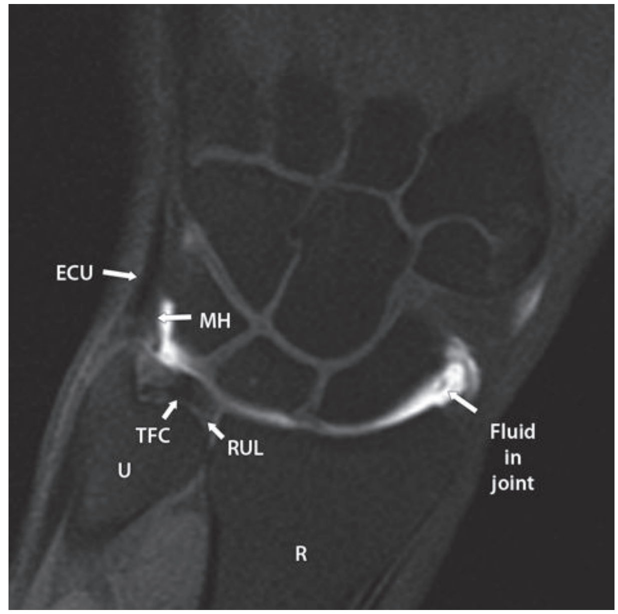


**Fig. 15.49** Coronal fat-saturated T1-weighted MRI arthrogram, right wrist (post intra-articular gadolinium injection). Image demonstrating the components of the triangulo-fibrocartilaginous complex. ECU = extensor carpi ulnaris tendon; MH = meniscus homologue; R = radius; RUL = radio-ulnar ligament; TFC = triangulo-fibrocartilage; U = ulna.

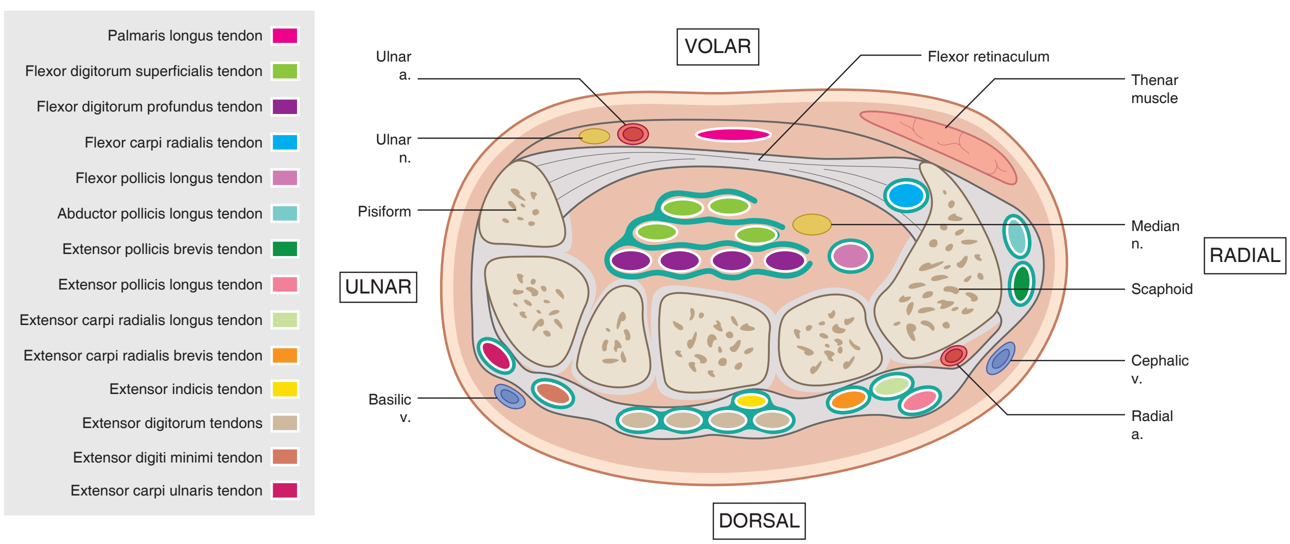


**Fig. 15.50** Diagram to show the carpal and extensor tunnels and their contents.

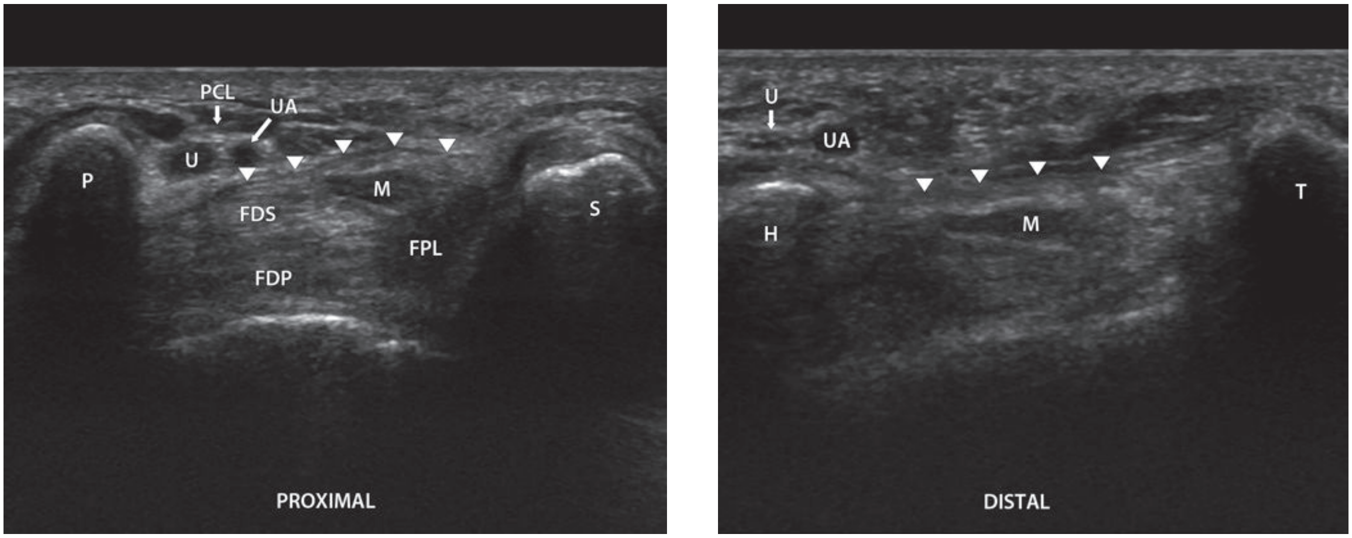


**Fig. 15.51** Transverse ultrasound of the wrist showing the carpal and Guyon tunnels (proximal and distal). The roof of the carpal tunnel is formed by the flexor retinaculum (white arrowheads) and the floor by the carpal bones. The roof of the Guyon tunnel is formed by the palmar carpal ligament. FDP = flexor digitorum profundus tendons; FDS = flexor digitorum superficialis tendons; FPL = flexor pollicis longus tendon; H = hamate; M = median nerve; PCL = palmar carpal ligament; P = pisiform; S = scaphoid; T = trapezium; U = ulnar nerve; UA = ulnar artery.

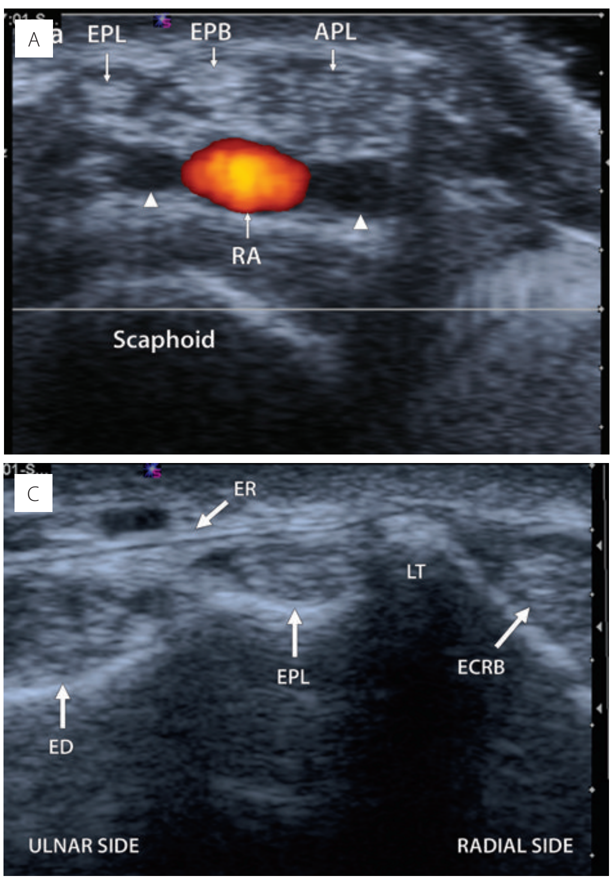


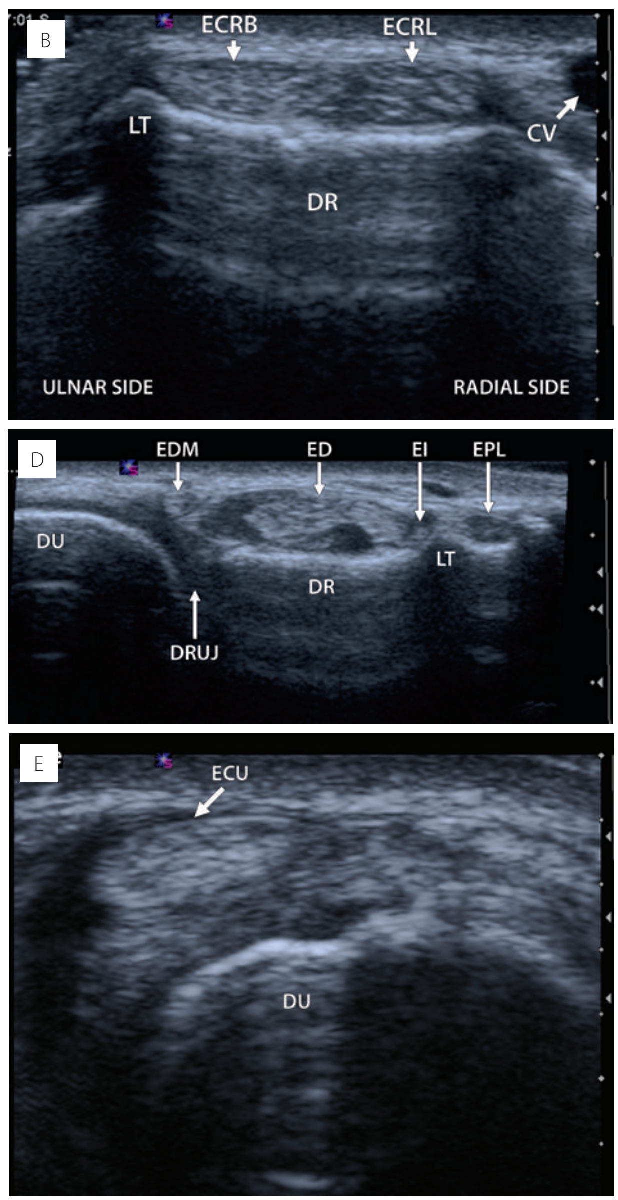


**Fig. 15.52** Transverse ultrasound images demonstrating the extensor compartments of the wrist and their contents. Extensor compartment 1 (A) contains the extensor pollicis brevis (EPB) and abductor pollicis longus (APL) tendons. They lie superficial to the radial artery (RA) and veins (white arrowheads). The extensor pollicis tendon of compartment 3 passes superficially to compartment 1 from the ulnar to the radial side as it courses distally. Extensor compartment 2 (B) contains the extensor carpi radialis brevis (ECRB) and longus (ECRL) tendons. The compartment lies on the radial side of Lister's tubercle of the radius (LT). Extensor compartment 3 (C, D) contains the extensor pollicis longus (EPL) tendon. It lies on the ulnar side of Lister's tubercle of the radius (LT). Extensor compartment 4 (C, D) contains the extensor digitorum (ED) and extensor indicis (EI) tendons. Extensor compartment 5 (D) contains the extensor digiti minimi (EDM) tendon. It lies superficial to the distal radio-ulnar joint (DRUJ). Extensor compartment 6 (E) contains the extensor carpi ulnaris (ECU) tendon. DR = distal radius; DU = distal ulna; CV = cephalic vein; ER = extensor retinaculum.

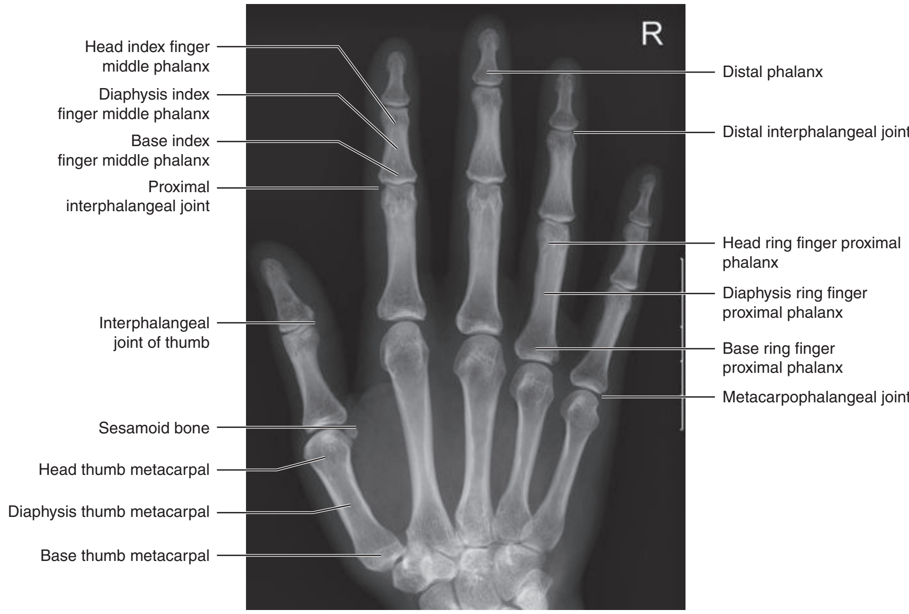


**Fig. 15.53** AP radiograph, hand.

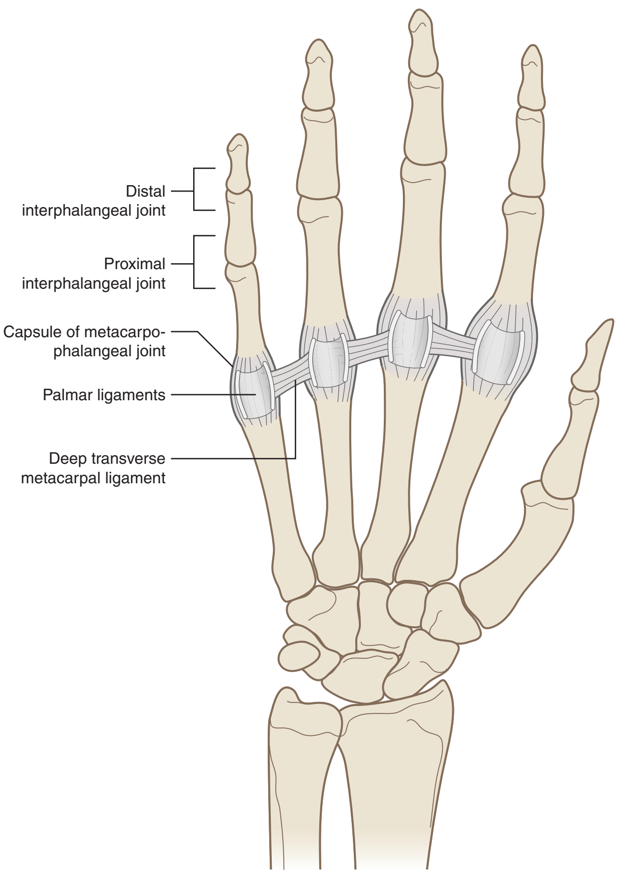


**Fig. 15.54** Diagram to show the carpometacarpal, metacarpophalangeal and interphalangeal joints.

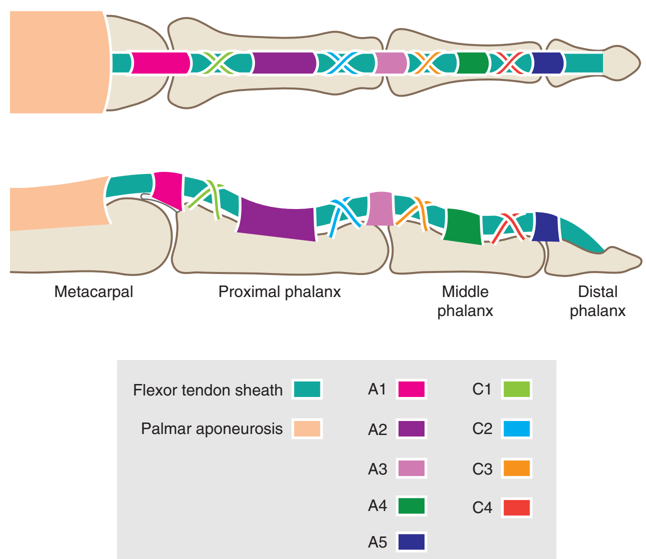


**Fig. 15.55** Diagram to show the layers of the digital flexor sheath.

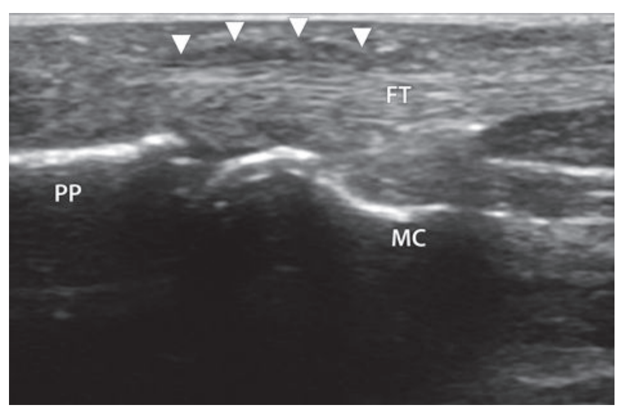


**Fig. 15.56** Longitudinal ultrasound of the digital flexor sheath. The abnormal, thickened A1 pulley is normally < 1.5 mm thick and is easily visible on ultrasound. FT = flexor tendon; MC = metacarpal; PP = proximal phalanx.

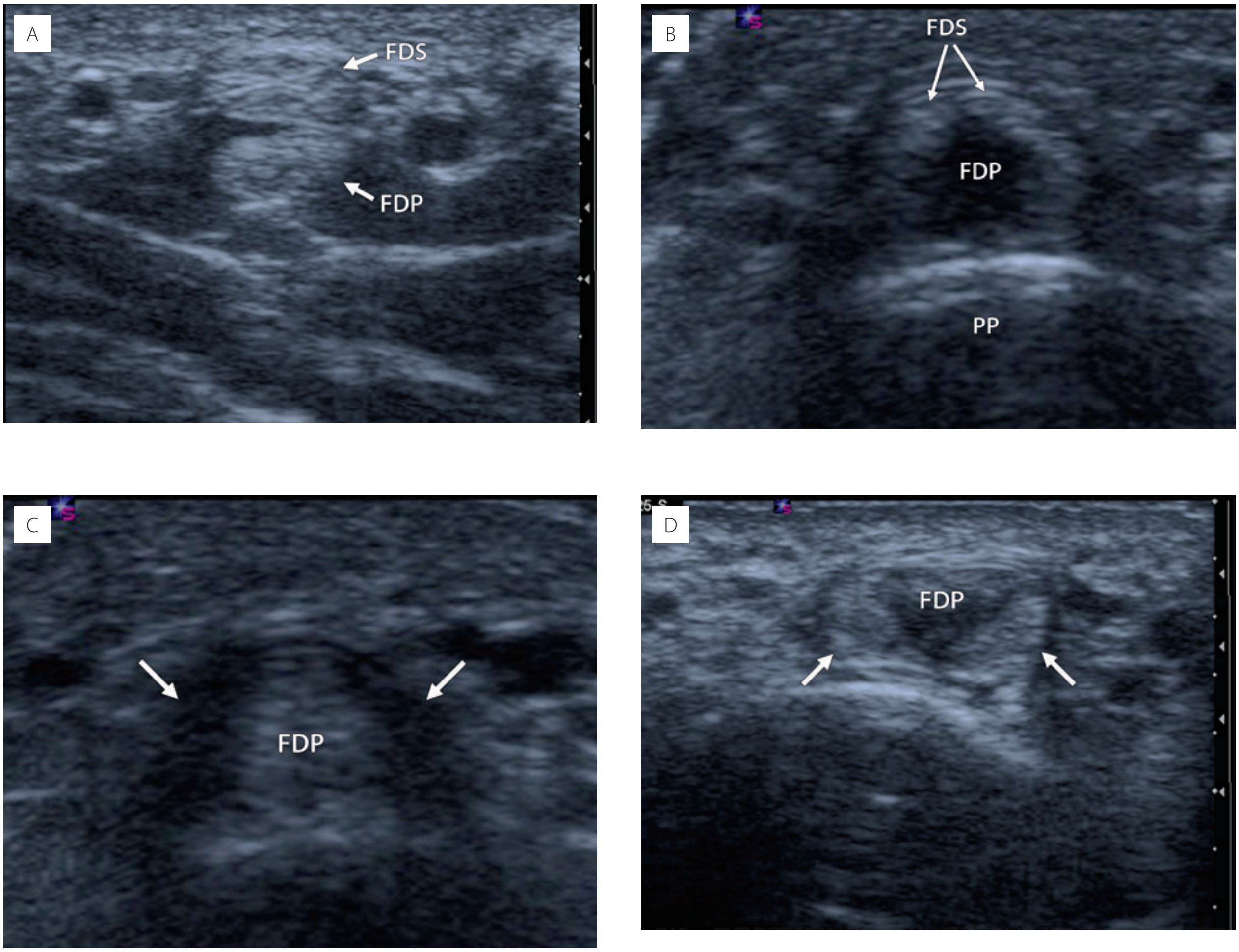


**Fig. 15.57** A–D (proximal to distal): Transverse ultrasound of the flexor digitorum tendons from the palm to the middle phalanx demonstrating the relationship between the flexor digitorum superficialis (FDS) and flexor digitorum profundus (FDP) tendons. At the level of the palm (A) the flexor digitorum superficialis tendon lies superficial to the flexor digitorum profundus tendon. At the level of the proximal third of the proximal phalanx (B) the FDS tendon divides into two slips which pass to the radial and ulnar aspects of the FDP tendon as they course distally (C, white arrows). The FDS slips then reunite deep to the FDP tendon (D, white arrows) and the FDS inserts onto the proximal aspect of the middle phalanx.

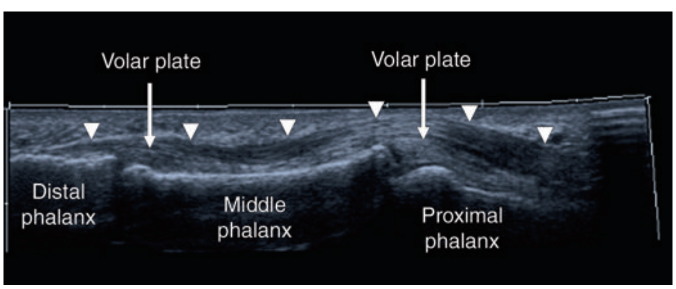


**Fig. 15.58** Extended field of view longitudinal ultrasound showing the flexor digitorum profundus tendon. The flexor digitorum profundus tendon (white arrowheads) lies on the flexor surface of the phalanges and inserts onto the distal phalanx. The volar plates are static stabilizers of the interphalangeal joints.

- It is triangular in shape with its dorsal base wrapped around the extensor aspect of the metacarpophalangeal joint.
- It is attached to the interossei and lumbrical muscles, affording much more precise movement of the fingers, as well as to the deep transverse metacarpal ligaments.
- Each expansion forms a mobile hood that moves distally with flexion of the metacarpophalangeal joint.

### Palmar aponeurosis (Fig. 15.60)

- This is a thickening of the deep fascia of the palm.
- It is attached to the skin distally and is triangular in shape, with its apex attached to the flexor retinaculum or palmaris longus tendon when present.
- It is composed of longitudinal fibres that extend towards the digits and transverse fibres that interconnect the longitudinal fibres.

### Metacarpophalangeal joint of the thumb (Fig. 15.61)

- The metacarpophalangeal joint of the thumb is stabilized by:

- static restraints: ulnar collateral ligament; radial collateral ligament; volar plate; dorsal joint capsule
- dynamic restraints: intrinsic and extrinsic muscles of the thumb.

- The ulnar collateral ligament (UCL) can be injured following a valgus strain to the thumb:
  - normally, the aponeurosis of the adductor pollicis muscle (AA) lies superficial to the UCL
  - in full thickness rupture of the UCL, the AA can dip into the tear and prevent healing, termed a Stener lesion. This usually requires surgical repair.

### Intrinsic muscles of the hand

- The small muscles of the hand all originate in the hand and are involved with precision movement and grip.
- They are all innervated by the ulnar nerve except for the three thenar muscles and the lateral two lumbricals, which are innervated by the median nerve (Table 15.18 and Figs. 15.62, 15.63).

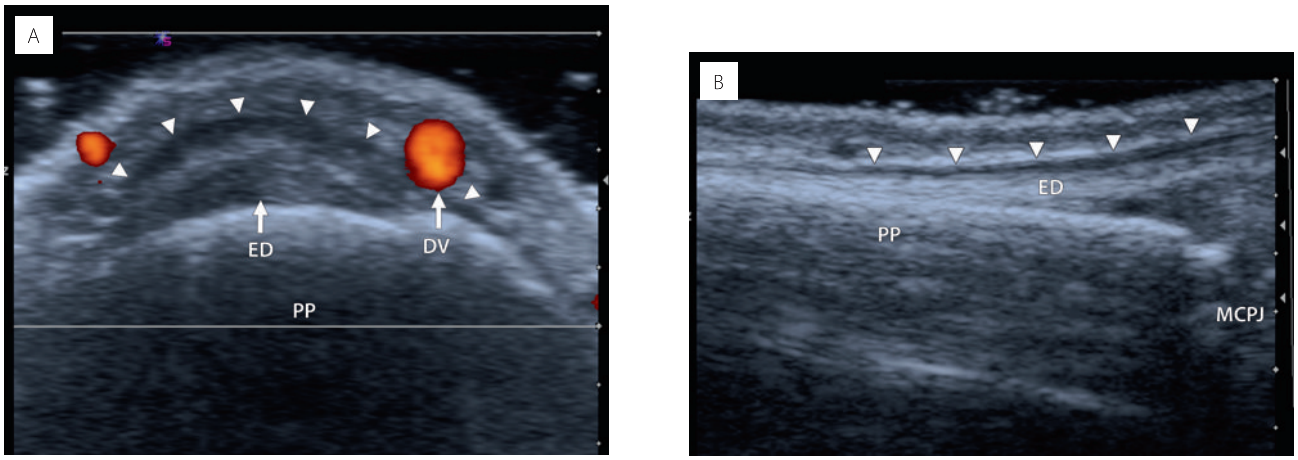


**Fig. 15.59** Transverse and longitudinal ultrasounds of the digital extensor hood. The dorsal extensor hood (white arrowheads) lies on the extensor surface of extensor digitorum tendon (ED), blending with it and attaching to the proximal phalanx (PP) on each side. DV = digital vein; MCPJ = metacarpophalangeal joint.

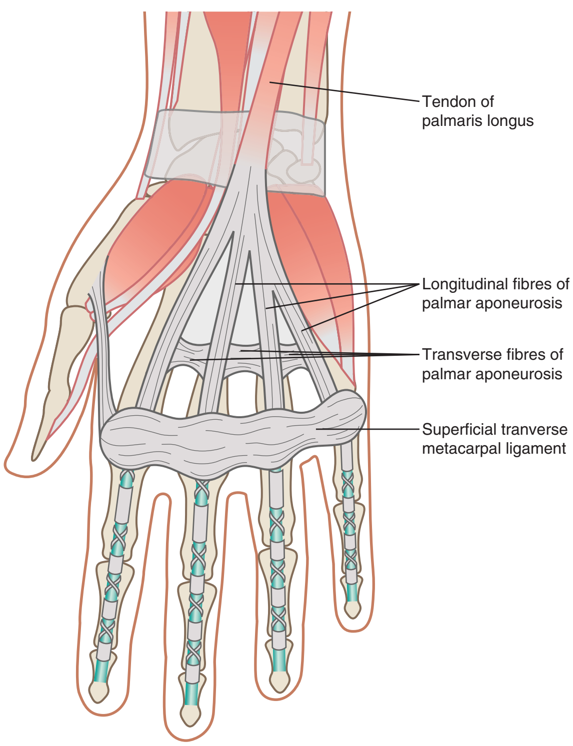


**Fig. 15.60** Diagram demonstrating the palmar aponeurosis.

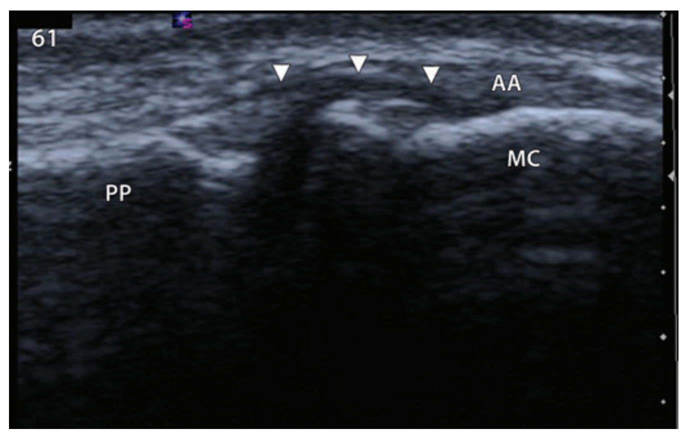


**Fig. 15.61** Longitudinal ultrasound of the ulnar surface of the thumb metacarpophalangeal joint. The ulnar collateral ligament (white arrowheads) is a static restraint on the metacarpophalangeal joint to valgus strain. It attaches to the distal metacarpal (MC) and proximal aspect of the proximal phalanx (PP). It normally lies deep to the adductor pollicis aponeurosis (AA).

**Table 15.18**

| Muscle | Origin | Insertion | Action |
|---|---|---|---|
| Palmaris brevis | Flexor retinaculum; palmar aponeurosis | Skin of palm | Improves grip |
| Lumbricals (four) | Tendons of flexor digitorum profundus | Extensor hoods of index, middle, ring and little fingers | Flexes metacarpophalangeal joints and extends interphalangeal joints of fingers |
| Palmar interossei (four) | Sides of thumb, index, ring and little metacarpals | Extensor hoods and proximal phalanges of thumb, index, ring and little fingers | Adduct fingers towards middle finger |
| Dorsal interossei (four) | Sides of metacarpals | Extensor hoods and proximal phalanges of index, middle and ring fingers | Abduct fingers away from middle finger |
| Adductor pollicis | Oblique head: index and middle metacarpals Transverse head: middle metacarpal | Base of proximal phalanx of thumb | Adduction of thumb |
| **Thenar muscles** | | | |
| Abductor pollicis brevis | Scaphoid; trapezium; flexor retinaculum | Bases of proximal phalanx of thumb | Abduction of thumb |
| Flexor pollicis brevis | Flexor retinaculum | Base of proximal phalanx of thumb | Flexes metacarpophalangeal joint of thumb |
| Opponens pollicis | Flexor retinaculum | Diaphysis of metacarpal of thumb | Medially rotates thumb |
| **Hypothenar muscles** | | | |
| Abductor digiti minimi | Pisiform | Base of proximal phalanx of little finger | Abducts little finger |
| Flexor digiti minimi | Flexor retinaculum | Base of proximal phalanx of little finger | Flexes little finger |
| Opponens digiti minimi | Flexor retinaculum | Metacarpal of little finger | Laterally rotates little finger |

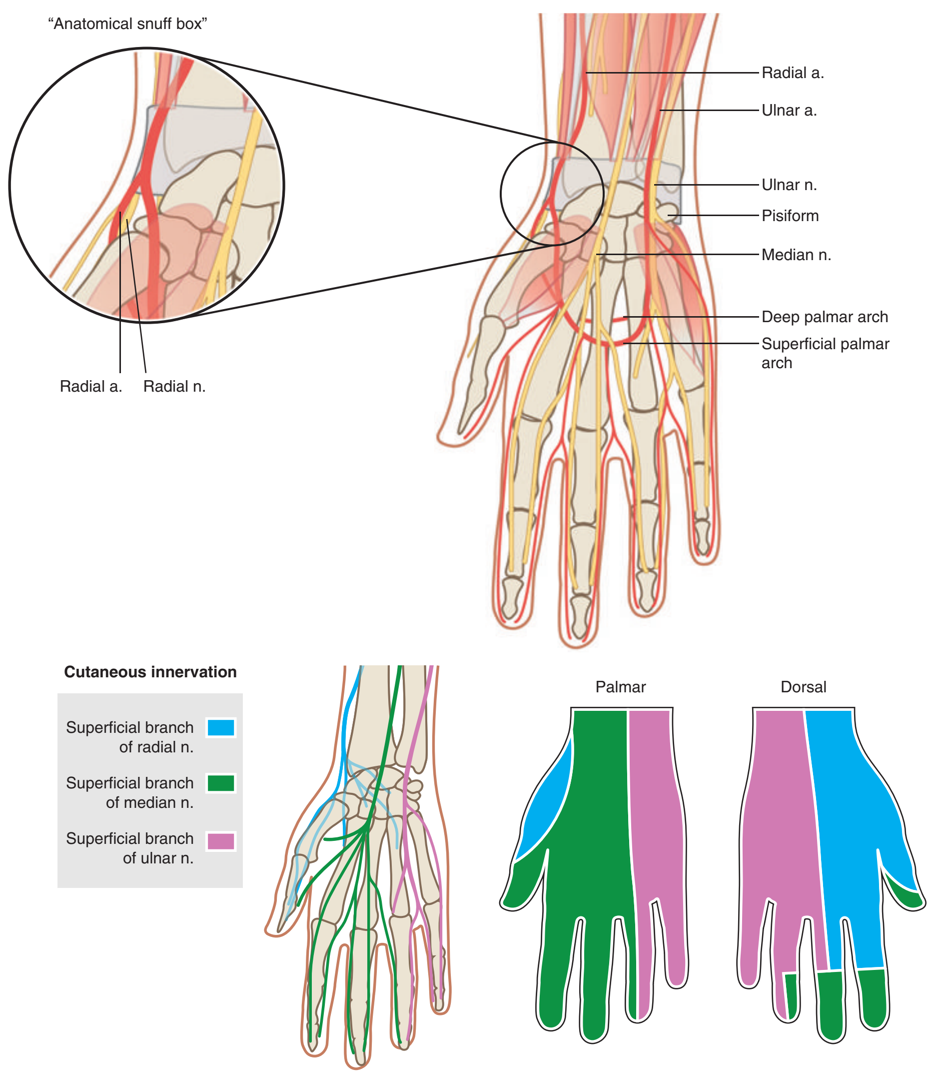


**Fig. 15.62** Diagram to show the neurological and vascular supply of the hand.

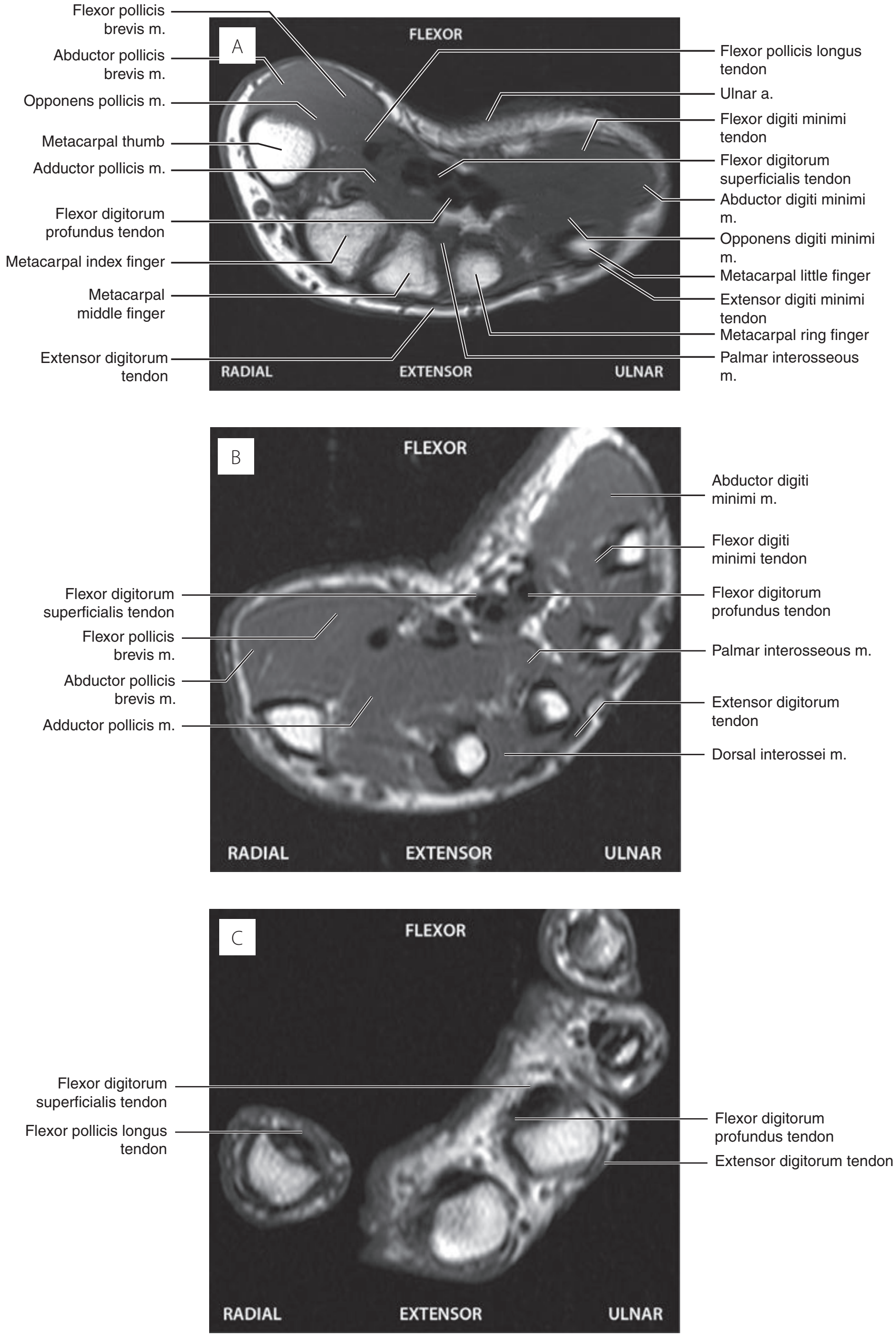


**Fig. 15.63** Axial T1 MRI, right hand (proximal, mid and distal).

Chapter 16

# The lower limb

Gonzalo Ansede, Adam W. M. Mitchell and Jeremiah C. Healy

## Imaging modalities

### Plain radiography

Plain radiography demonstrates osseous anatomy and provides some detail of the soft tissue anatomy.

### Cross-sectional imaging

#### CT

Multi-slice CT allows high-resolution 3D reconstructions of the lower limb that enable exceptional visualization of the bony anatomy. Soft tissues including muscles, tendons and joints can also be identified but these are optimally assessed with sonography and MR imaging.

#### Sonography

Sonography allows high spatial resolution and dynamic imaging of the soft tissues not obscured by osseous structures. It is particularly optimal for visualization of small and superficial structures (ligaments, tendons) as well as muscle compartments and the neonatal/infant hip.

#### MRI

MR imaging offers high contrast resolution imaging of the musculoskeletal anatomy. Intra-articular structures are optimally assessed on MR arthrography.

## The pelvis

### Bone anatomy

#### Adult pelvis

The pelvic bone is composed of three parts; the ilium, ischium and pubis. These meet at the triradiate cartilage, seen as a lucency within the acetabulum in the immature skeleton (Figs. 16.1–16.3).

#### The sacrum

- Triangular bone formed by five fused vertebrae.
- Four pairs of dorsal and ventral foramina for the respective rami of the sacral nerves.
- The base of the sacral body is located superiorly and articulates with the lumbar spine.
- The sacral ala, on either side of the body of the base of the sacrum, are large triangular surfaces, which support the psoas major and the lumbosacral trunk.
- The ear-shaped (auricular) surface articulates with the ilium and occupies the wide superior aspect of the lateral sacral surface.
- The sacral hiatus is a horseshoe-shaped deficiency in the lower end of the dorsal surface communicating with the sacral canal.

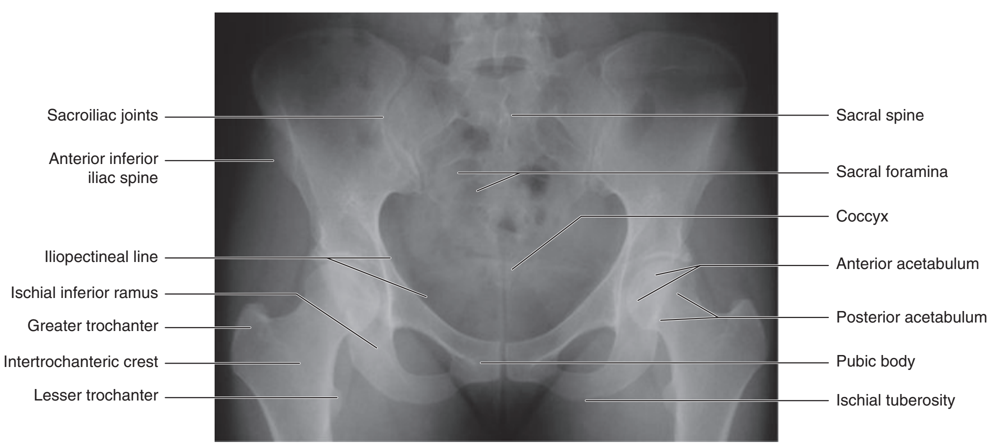


**Fig. 16.1** Pelvis frontal radiograph.

*Applied Radiological Anatomy, 2nd Edition* ed. Paul Butler, Adam W.M. Mitchell and Jeremiah C. Healy. Published by Cambridge University Press.

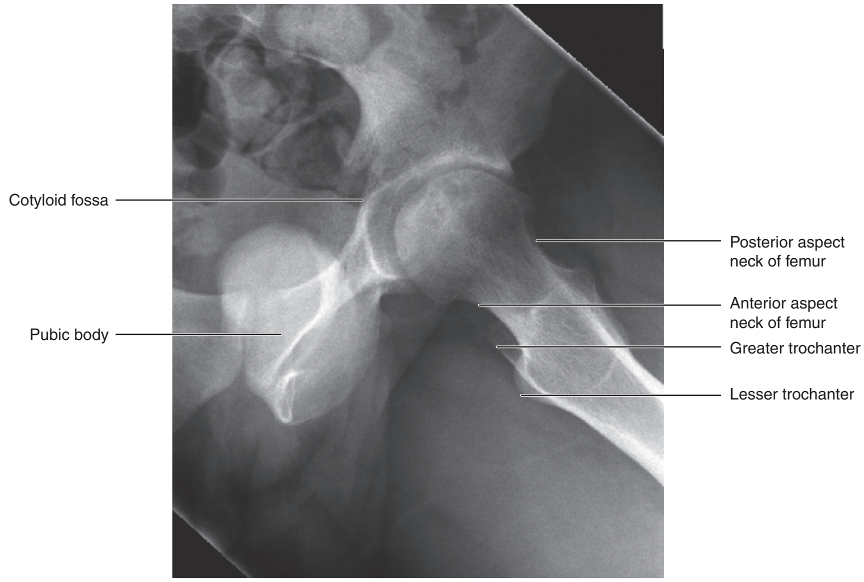


**Fig. 16.2** Hip lateral radiograph.

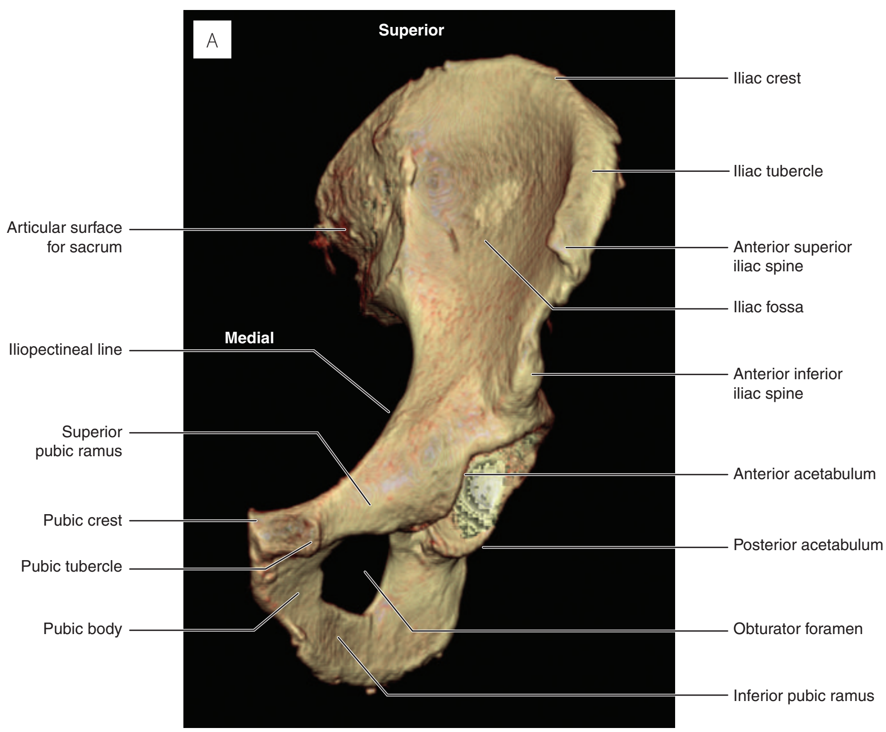


**Fig. 16.3** Surface-shaded CT image of the pelvic bone. Anterior (A), lateral (B) and medial (C) views.

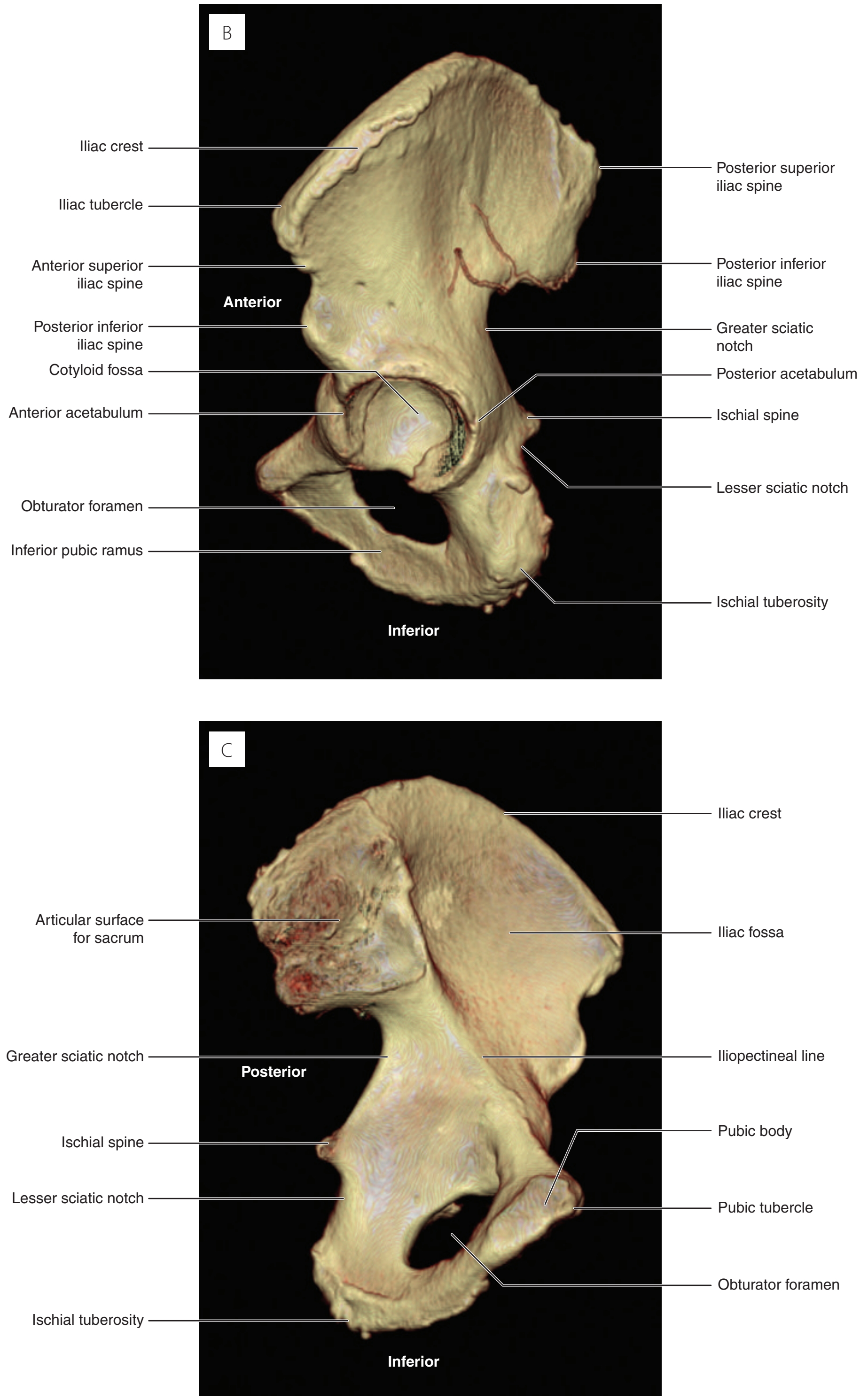


**Fig. 16.3** *(cont.)*

The coccyx, a triangular bone formed by three to five fused vertebrae, articulates with the inferior end of the sacrum

The sacrum and pelvic bones form a bone ring with an intervening pubic symphysis and a pair of sacroiliac joints. Like a Polo mint, the ring cannot be broken in a single location. Two or more sites of the ring must be disturbed when the ring is broken (Fig. 16.4).

## Infant pelvis

The femoral capital epiphyses can be evaluated:

- on sonography from birth until ossification (at 3 to 6 months)
- on plain radiography afterwards (Fig. 16.5).

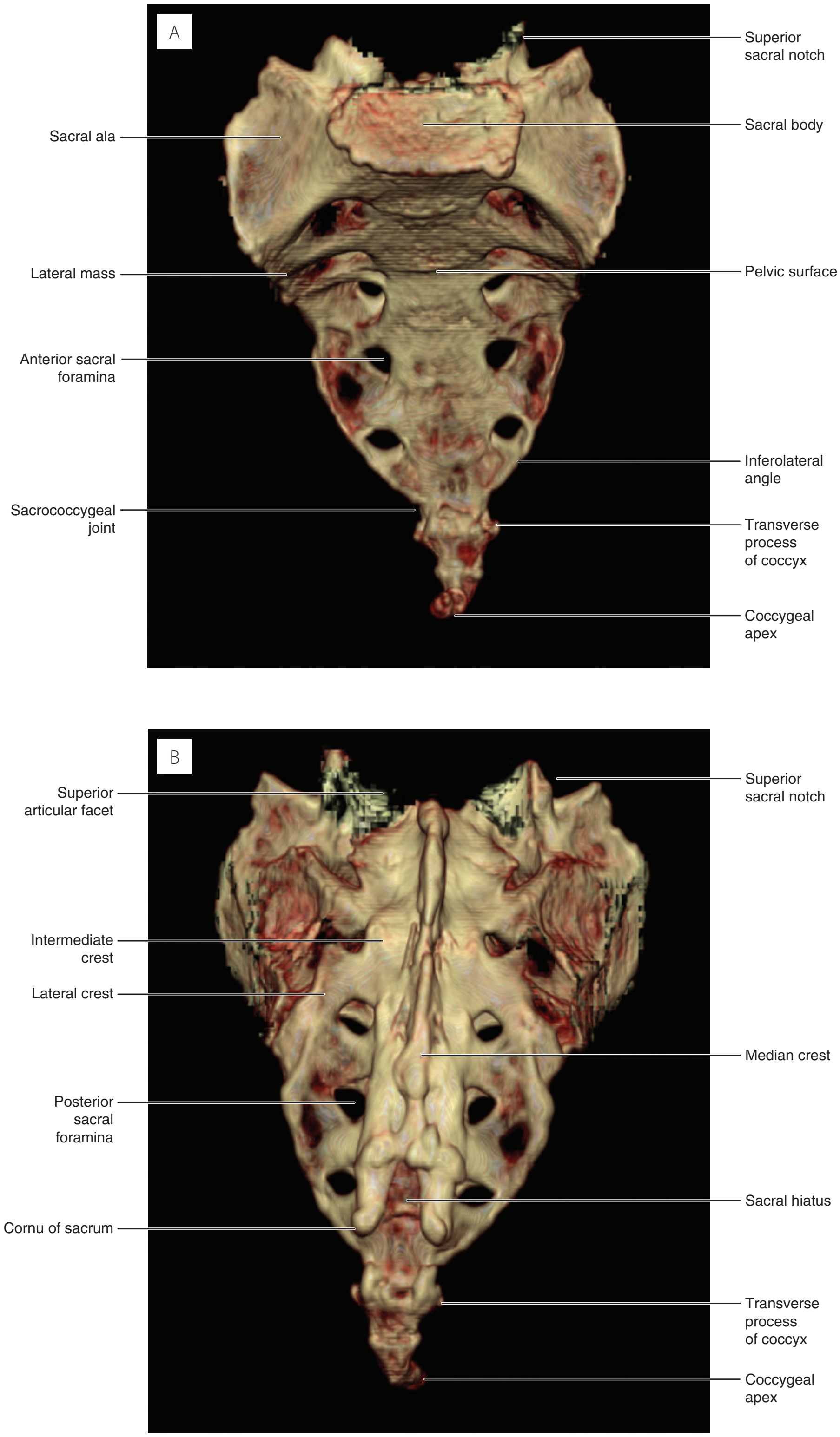


**Fig. 16.4** Surface-shaded CT images of the sacrum. Anterior (A), posterior (B) and lateral (C) views.

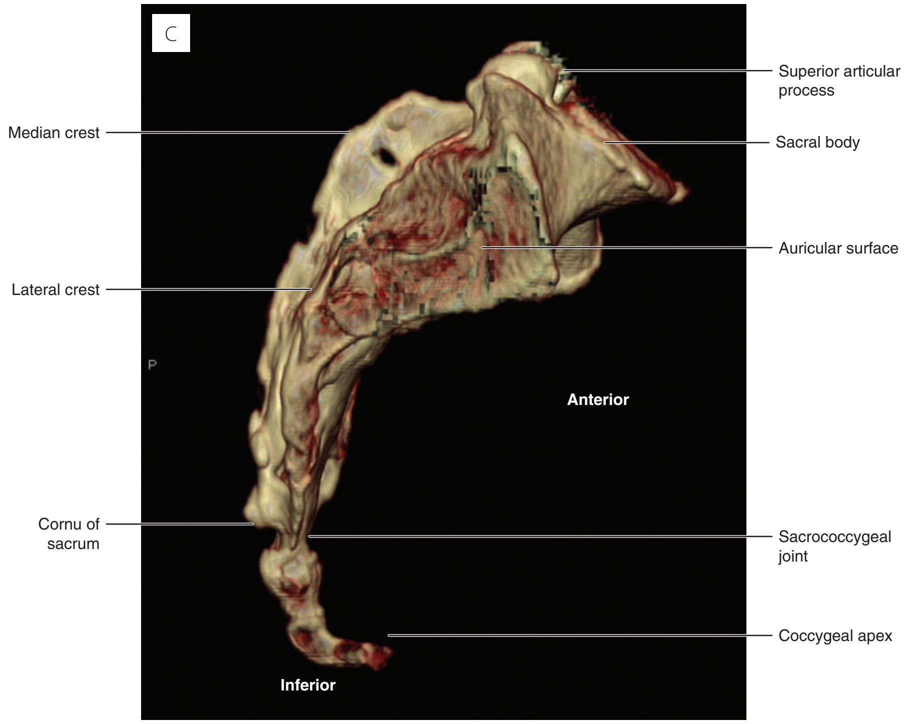


**Fig. 16.4** *(cont.)*

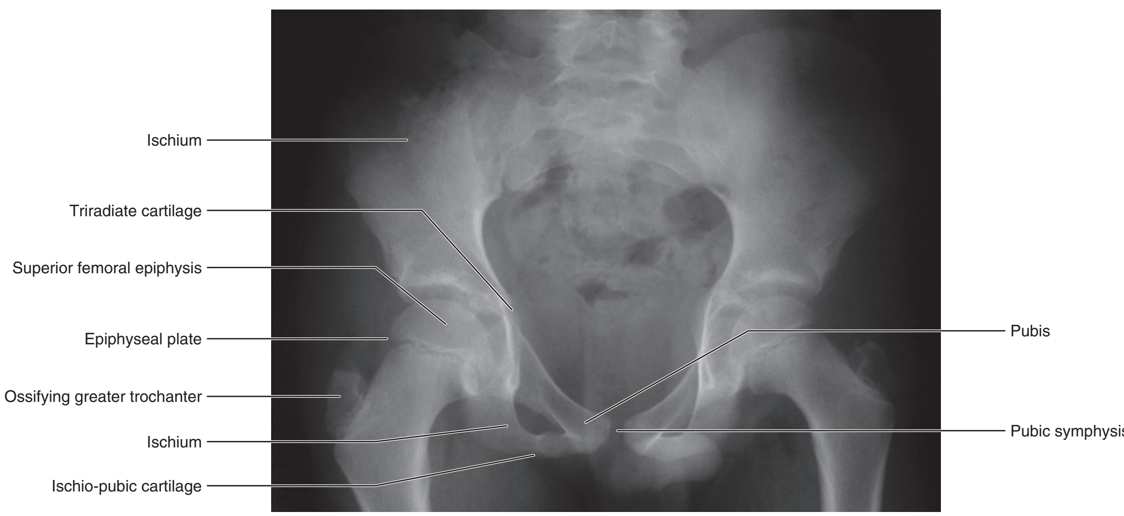


**Fig. 16.5** Immature pelvis frontal radiograph.

## Ossification of the pelvis and sacrum

- Epiphyses are secondary ossification centres at the end of a long bone normally forming part of a joint (Tables 16.1, 16.2).
- Apophyses are secondary ossification centres that do not articulate but may have tendinous insertions
- Secondary ossification centres may appear irregular and fragmented in the normal immature skeleton.

## Pelvis radiographic assessment (Figs. 16.6 and 16.7)

- Shenton's line is an arc formed by the superior border of the obturator foramen and the medial aspect of the femoral neck and should be smooth.
- The iliopectineal line (junction between the ilium and pubis) is a smooth curved line extending superiorly from the superior border of the superior pubic ramus.
- The ilioischial line (junction between the ilium and ischium) is a smooth curve extending superiorly from the superior border of the inferior pubic ramus.
- The acetabular tear drop is formed by the quadrilateral plate of the ilium medially, the inferior part of the acetabular fossa inferiorly and the anterior part of the acetabular fossa laterally. The distance from the acetabular teardrop to the medial aspect of the femoral head should be less than 11 mm and symmetrical (±2 mm).

**Table 16.1** Ossification of the pelvis

| Ossification centre | Appear | Fuse |
|---|---|---|
| Ilium | 8 weeks gestation | 7–8 yrs |
| Ischium | 18–22 weeks gestation | |
| Pubis | 18–22 weeks gestation | |
| Triradiate ligament: two ossification centres. | Puberty | 20–25 yrs |
| Iliac crest | Puberty | 20–25 yrs |
| Capital femoral epiphysis | 3–6 months | 16–20 yrs |

**Table 16.2** Ossification of the sacrum is analogous to the remainder of the spine

| Ossification centre | Appear | Fuse |
|---|---|---|
| Vertebral body centre | 10–20 weeks gestation | Vertebra and both vertebral arches fuse at 8 years |
| Half of vertebral arch | 10–20 weeks gestation | Ipsilateral vertebral arch and costal elements fuse at 5 years |
| Vestigial costal elements | 6–8 months gestation | |

- The outer margin of the anterior acetabular column is a smooth line from the inferior margin of the superior pubic ramus to the upper outer margin of the acetabular roof.
- The outer margin of the posterior acetabular column is a smooth line from the inferior margin of the inferior pubic ramus to the upper outer margin of the acetabular roof. The posterior column extends more laterally than the anterior column.

Assessment of the infant hip for developmental dysplasia of the hip and dislocation can be made with the following:

- Shenton's line.
- The Y line runs along the triradiate cartilages at the unossified acetabular centres between the three pelvis bones.
- Perkin's line is drawn perpendicular to the Y line along the superior corner of the bony acetabulum. The superior capital epiphysis should lie in the inner lower quadrant.
- The acetabular angle (15–35°) between the Y line and a line drawn across the roof of the acetabulum.
- The iliac angle (44–74°) between the Y line and a line drawn along the anterior aspect of the ilium.
- Lines along the femoral shafts meet at the midline in Von Rosen's view (legs abducted 45° and internally rotated) (Fig. 16.8).

## Joints

### Hip joint

Different imaging modalities allow evaluation of the hip joint structures. Intrarticular features are best assessed on MR arthrography

- MR direct arthrography consists of percutaneous administration of a gadolinium solution into a joint, causing distension of the capsule (Fig. 16.10).
- In MR indirect arthrography, intravenous gadolinium progressively accumulates in the joint synovium with a similar athrographic effect although no joint distension is achieved. Imaging is performed after an appropriate delay and lower limb exercises to allow maximal synovial enhancement.

### The hip

- The hip is a synovial ball and socket joint between the femoral head and acetabulum and is best assessed with a dedicated surface coil and on direct MR arthrography.

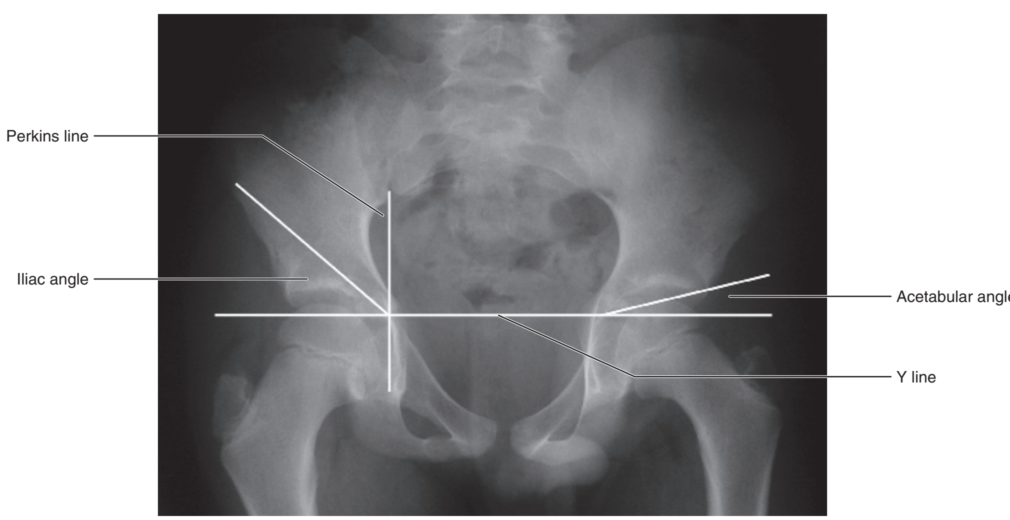


**Fig. 16.6** Pelvis assessment.

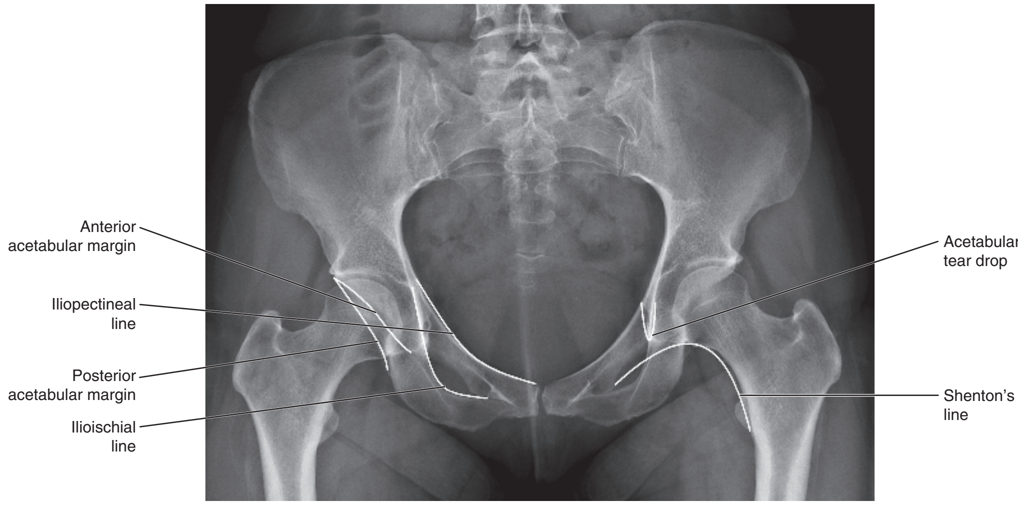


**Fig. 16.7** Lines in pelvis.

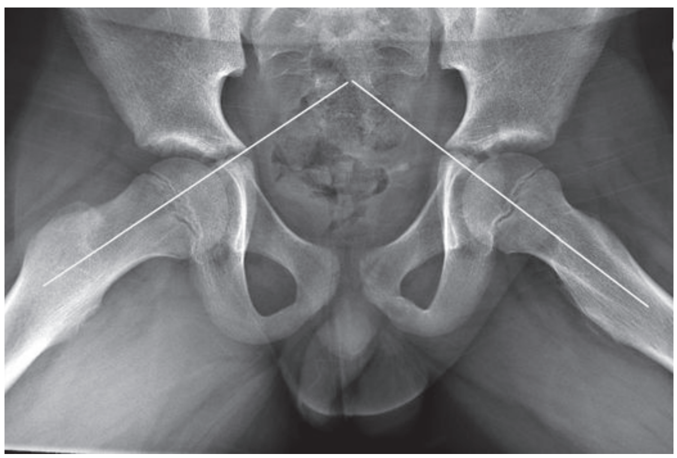

**Fig. 16.8** Von Rosen's view (legs abducted 45° and internally rotated) is used in the evaluation of developmental hip dysplasia. Lines along the femoral shafts should meet at the midline in the normal pelvis.

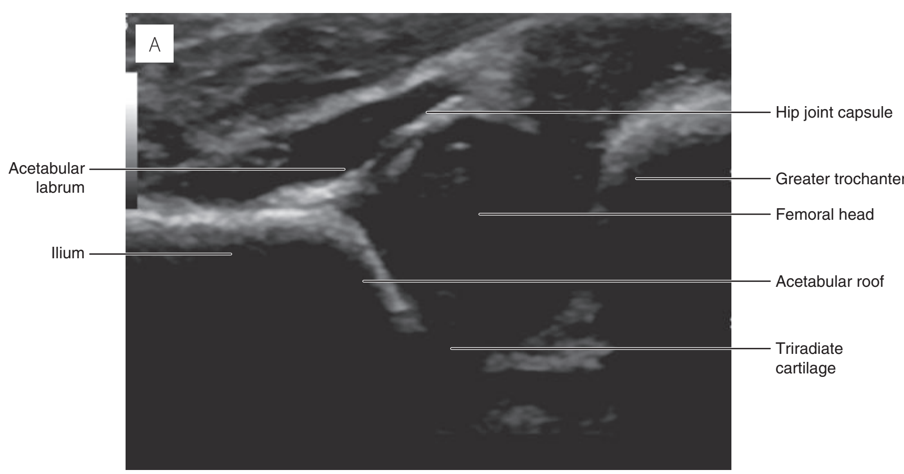


**Fig. 16.9** Neonatal hip sonography. The alpha angle is formed by the acetabular roof and the ilium. The beta angle is formed by the straight lateral edge of the ilium and the end of the acetabular labrum. A mature hip should have an α angle > 60° and β angle < 55°.

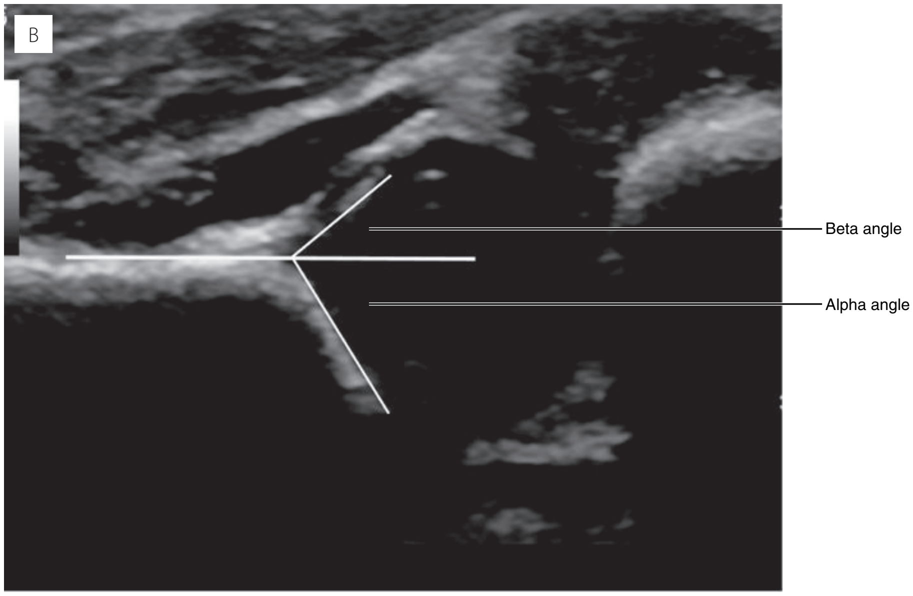


**Fig. 16.9** (*cont.*)

- The articular surface of the acetabulum is an inverted horseshoe with a fat-filled central part (cotyloid fossa) and an inferiorly placed acetabular notch bridged by the transverse acetabular ligament. The articular cartilage is thickest at the weight-bearing superior surface.
- The ligamentum teres attaches to the cartilage deficient fovea capitis and the cotyloid fossa.
- The acetabular fibrocartilaginous labrum deepens the articular cup and is seen, preferably on MR arthrography, as a triangular filling defect attached to the acetabular rim. The labrum is thickest posterosuperiorly and is deficient inferiorly where it is continuous with the tranverse acetabular ligament. The joint capsule originates from the bone surrounding the external aspect of the labrum, forming a well-defined recess, the perilabral recess.
- The capsule is strongest superiorly and anteriorly and attaches to the rim of the acetabulum and transverse acetabular ligament. Distally it attaches to the trochanteric line anteriorly and 1 cm proximal to the intertrochanteric crest posteriorly and is reinforced by three strong ligaments:
  - the iliofemoral ligament is very strong, Y-shaped and runs from the intertrochanteric line (base of the Y) to the anterior inferior iliac spine (apex of the Y)
  - the triangular pubofemoral ligament inferiorly attaches to the iliopubic eminence and superior pubic ramus and blends distally with the capsule and iliofemoral ligament
  - the ischiofemoral ligament posteriorly has broad iliac attachments and inserts into the inner aspect of the greater trochanter.

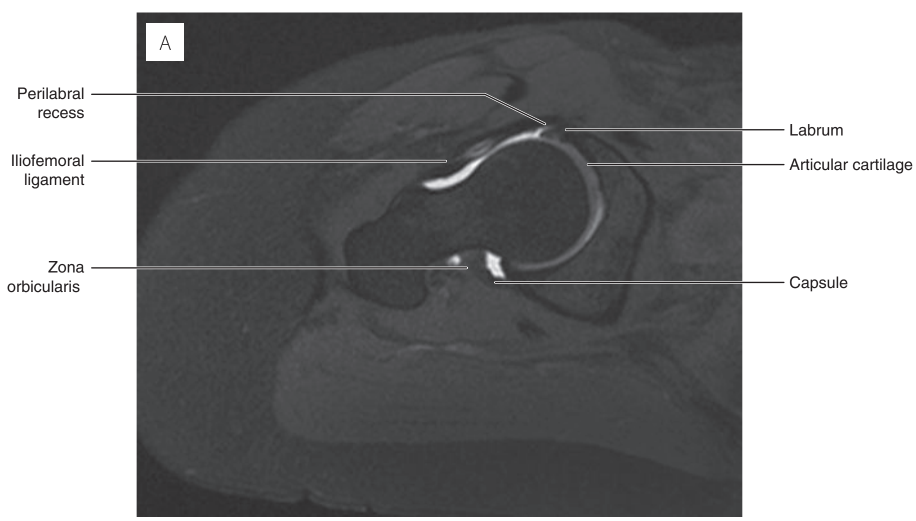


**Fig. 16.10** Hip joint MR arthrogram, axial (A) and coronal (B) images.

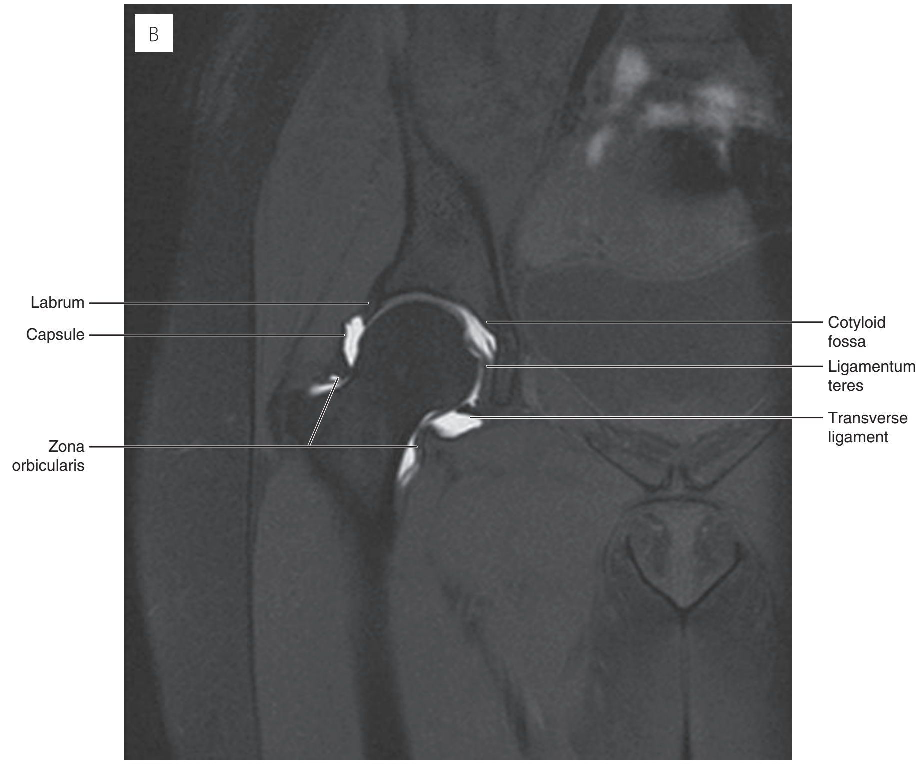


**Fig. 16.10** (*cont.*)

- The synovium covers the internal surface of the capsule, intracapsular femoral neck, labrum, cotyloid fossa and ligamentum teres. It may communicate with the psoas bursa anteriorly through a capsular defect.

### Sacroiliac joints (Fig. 16.11)

- The sacroiliac joints are symmetrical and as they lie in a coronal oblique plane, a dedicated coronal oblique view is required.
- The sacroiliac joints are synovial joints between the flat and irregular surfaces of the sacrum and the ilium. The hyaline cartilage on the anterior part of the sacral and iliac articular surfaces is thinner than that on the posterior part of the sacrum. Fibrous adhesions and gradual fusion across the joint occurs with age, and this may even lead to ossification in old age.

Stability is conferred by the curvatures and irregularities of the articular surfaces and by a number of ligaments.

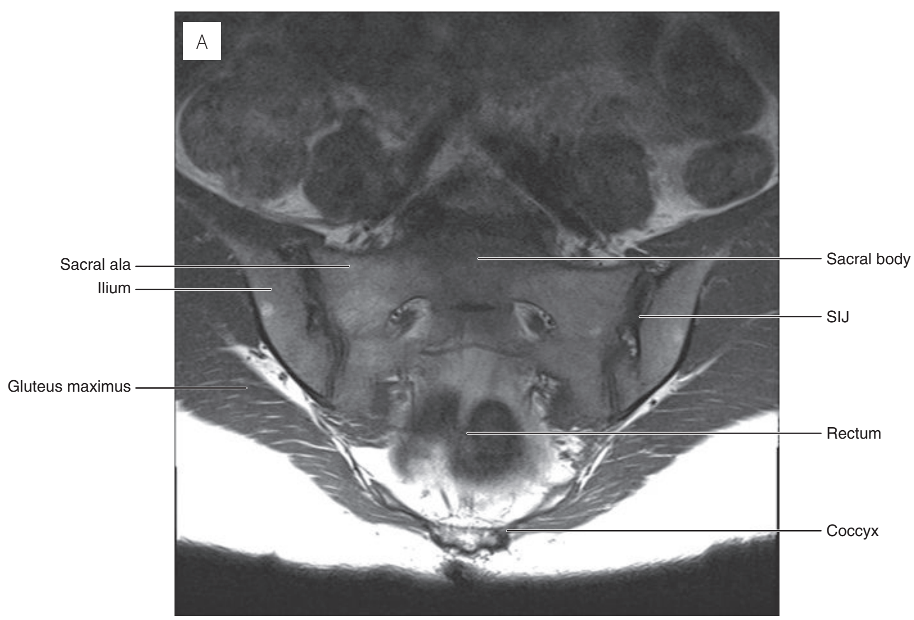


**Fig. 16.11** Sacroiliac joints, axial oblique MR images.

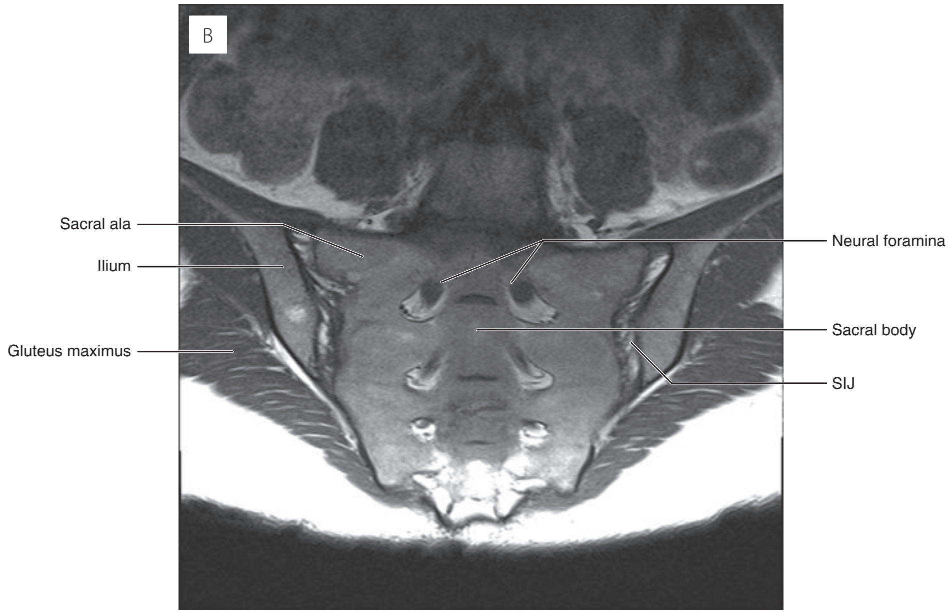


**Fig. 16.11** (*cont.*)

- The dense sacroiliac interosseous ligament, the strongest ligament in the body, lies above and posterior to the joint.
- The sacrotuberous ligament runs from the ischial tuberosity to the side of the sacrum and coccyx, and defines the posterior limit of the lesser sciatic foramen.
- The triangular sacrospinous ligament runs from the ischial spine (apex) to the side of the sacrum and coccyx (base), and separates the greater and lesser sciatic foramina.
- The iliolumbar ligament runs from the transverse process of the fifth lumbar vertebra to the iliac crest.

These ligaments may calcify in old age and allow subtle rotatory movements at the sacroiliac joint particularly during pregnancy.

### Pubic symphysis

- The pubic symphysis is a cartilaginous joint covered by dense ligaments, and contains a fibrocartilaginous disc resembling an intervertebral disc (Figs. 16.12, 16.13). Stability is mainly provided by the interpubic disc and the superior and arcuate ligaments.
- The superior ligament connects the pubic bones above, and reaches the pubic tubercle. The arcuate pubic ligament is a thick arch of fibres connecting the inferior aspect of the pubic bones. It blends with the interpubic disc and extends onto the inferior pubic ramus.
- The anterior pubic ligament strengthens the interpubic disc, and is formed by interlacing collagen fibres which decussate with the external oblique

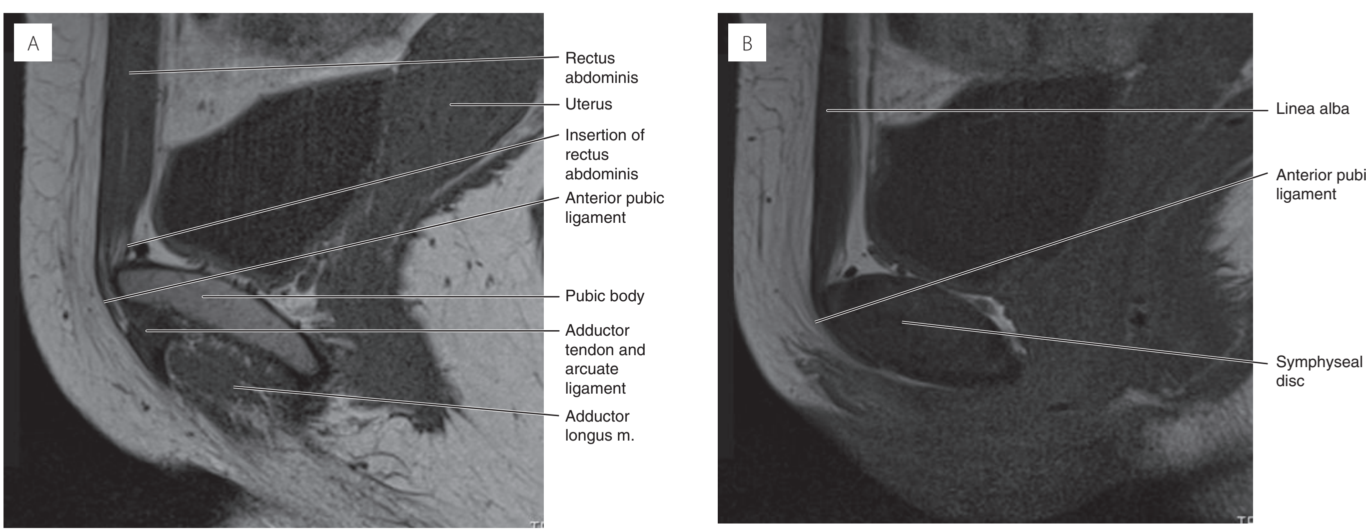


**Fig. 16.12** Sagittal paramedian (a) and midline (b) MR images of the pubic symphysis.

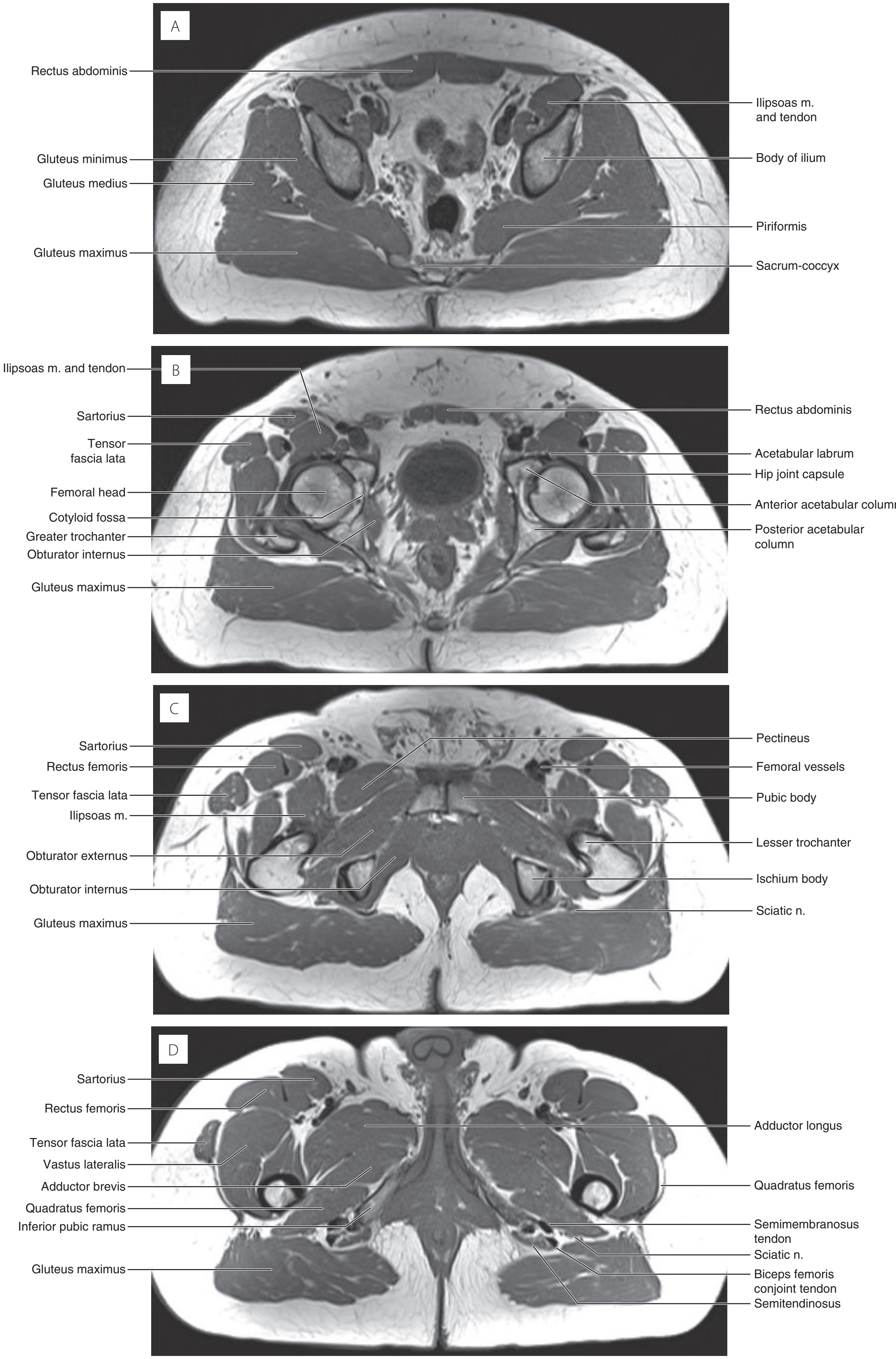


**Fig. 16.13** Pelvis MR axial images. From superior to inferior.

aponeurosis and the medial tendons of the rectus abdominis.

- The proximal insertion of gracilis, adductor longus and adductor brevis on the anterior surface of the pubic body is adjacent to the anterior pubic ligament.

## Muscles of the pelvic girdle

### Glutei

- All glutei muscles (Table 16.3) are hip extensors and abductors and arise from the posterior surfaces of the ilium, sacrum and adjacent deep fascia.
- Gluteus maximus is the largest muscle in the body and is the only muscle covering the greater trochanter, separated by an intervening bursa.
- Medius and minimus attach to the greater trochanter and stabilize the hip when the contralateral limb is raised during walking.

### Hip lateral rotators (Table 16.4 and Figs. 16.14–16.16)

- Piriformis passes posterior to the hip joint and through the greater sciatic foramen.
- The sciatic nerve passes inferior to piriformis to become a posterior relation of the other hip lateral rotators.
- Quadratus femoris inserts into the quadrate tubercle, unlike all other lateral hip rotators which insert into the greater trochanter.
- Obturator internus hooks around the lesser sciatic foramen to attach to the greater trochanter.

**Table 16.3** Gluteal muscles

| Muscle | Origin | Insertion | Action |
|---|---|---|---|
| Gluteus maximus | Lateral sacrum and posterior iliac crest | Gluteal tuberosity (femur) and iliotibial band | Keeps knee extended; hip external rotator |
| Gluteus medius | Outer surface of ilium | Greater trochanter: posterolateral surface | Hip abductor and medial rotator |
| Gluteus minimus | Outer surface of ilium | Greater trochanter: anterior surface | Hip abductor and medial rotator |

- The superior and inferior gemelli merge with obturator internus tendon and lie superior and inferior to it.
- Obturator internus and the gemelli fill the gap between piriformis superiorly and quadratus femoris inferiorly.
- Obturator externus passes inferior to the hip joint and is anterior to the sheet of muscle formed by the remaining lateral rotators.

## Nerves and vessels

### Sciatic nerve

The sciatic nerve (L4, 5, S1, 2, 3) exits the pelvis through the greater sciatic notch below piriformis to lie on the other hip external rotators and is covered by gluteus maximus (Fig. 16.17).

### Greater sciatic foramen

- The greater sciatic foramen is bounded anterolaterally by the greater sciatic notch of the ilium, posteromedially by the sacrotuberous ligament and inferiorly by the sacrospinous ligament and the ischial spine.
- Piriformis muscle passes through it to exit the pelvis and divides into the supra- and infra-piriform foramina transmitting the gluteal nerves and vessels, pudendal nerves and vessels and the sciatic nerve among other structures (Table 16.5).

### Lesser sciatic foramen

The lesser sciatic foramen, bounded by the ischial spine, sacrotuberous and sacrospinous ligaments, communicates the pelvis with the posterior compartment of the thigh and transmits the obturator internus tendon, and the pudendal nerve and vessels (Fig. 16.18).

### Obturator canal

The obturator canal is a passageway through the obturator foramen, formed by a defect of the obturator membrane, allowing passage of the obturator artery, vein and nerve from the pelvis to the adductor compartment of the thigh.

**Table 16.4** Lateral rotator muscles of the hip

| Muscle | Origin | Insertion | Action |
|---|---|---|---|
| Piriformis | Anterior aspect of sacrum | Anterior part of medial surface of greater trochanter | Hip lateral rotator and stabilizer |
| Quadratus femoris | Ischial tuberosity | Quadrate tubercle on posterior aspect of femur | Hip lateral rotator and stabilizer |
| Obturator externus | Outer obturator membrane and surrounding ischium/pubis | Trochanteric fossa on medial aspect of greater trochanter | Hip lateral rotator |
| Obturator internus | Inner obturator membrane and surrounding ischium/pubis | Middle part of medial surface of greater trochanter | Hip lateral rotator |
| Gemellus superior | Ischial spine | | Hip lateral rotator and stabilizer |
| Gemellus inferior | Ischial tuberosity | | Hip lateral rotator and stabilizer |

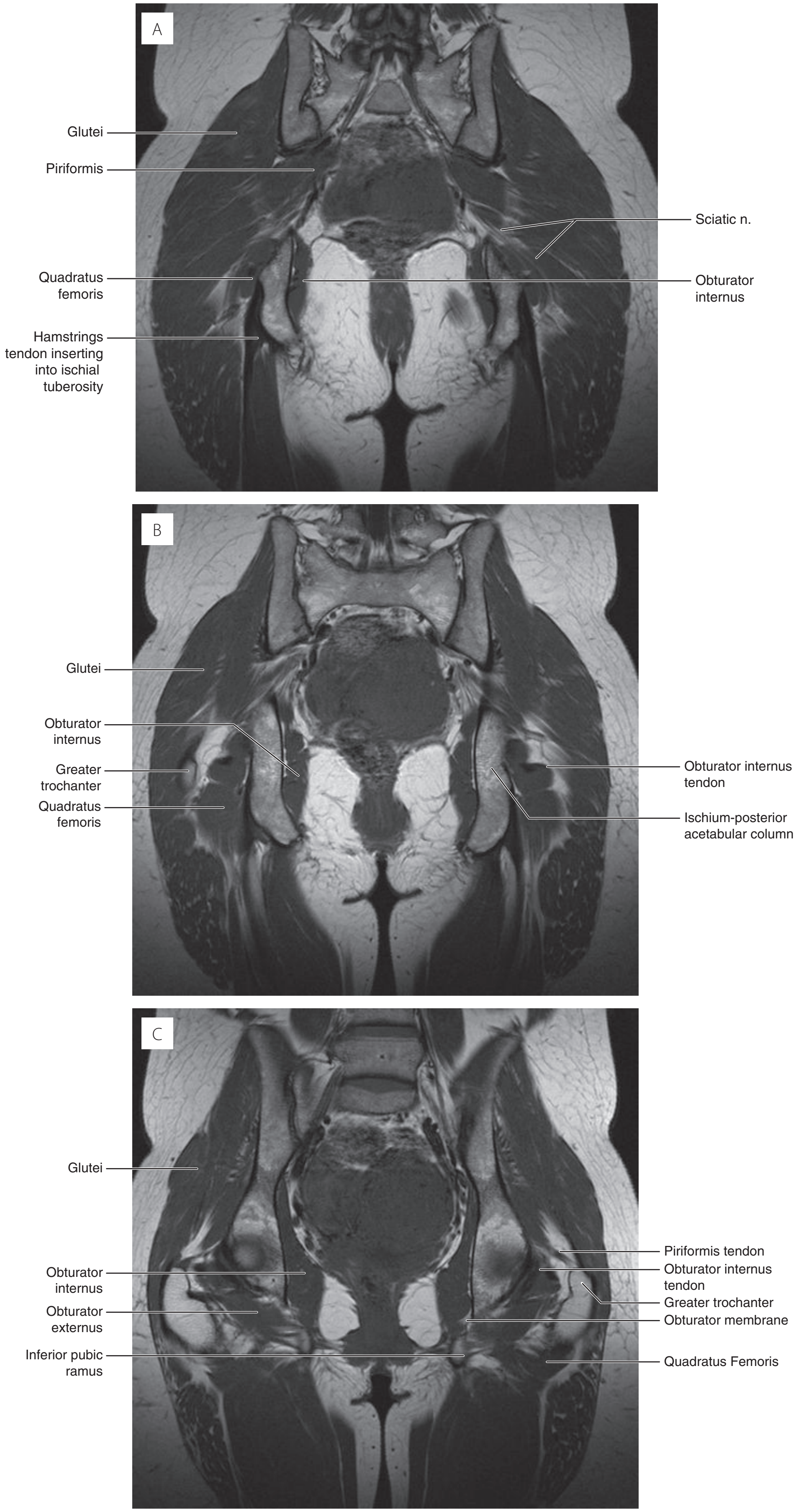


**Fig. 16.14** Hip external rotators MR coronal images. From posterior to anterior.

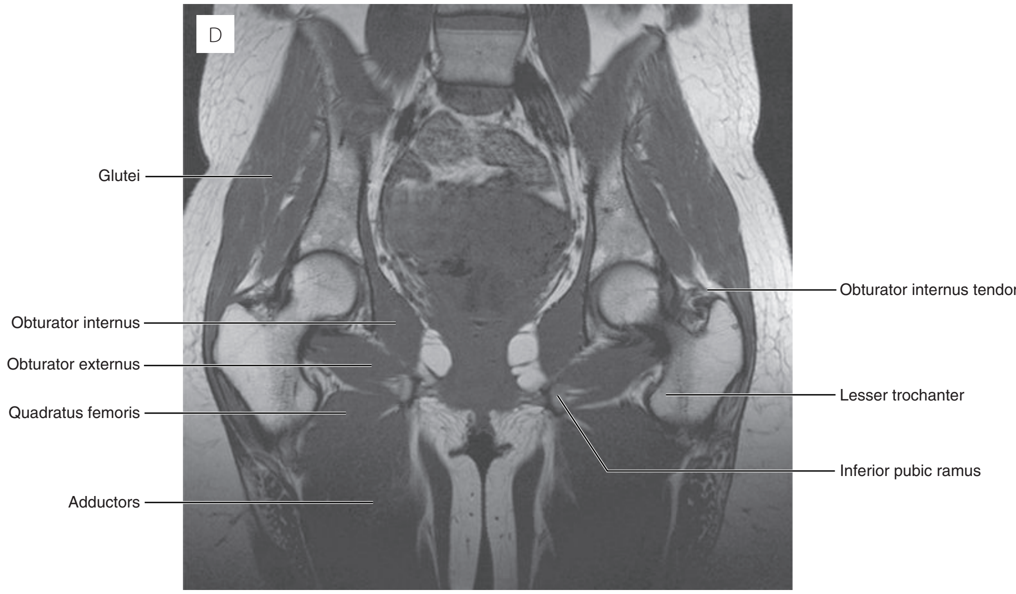


**Fig. 16.14** (*cont.*)

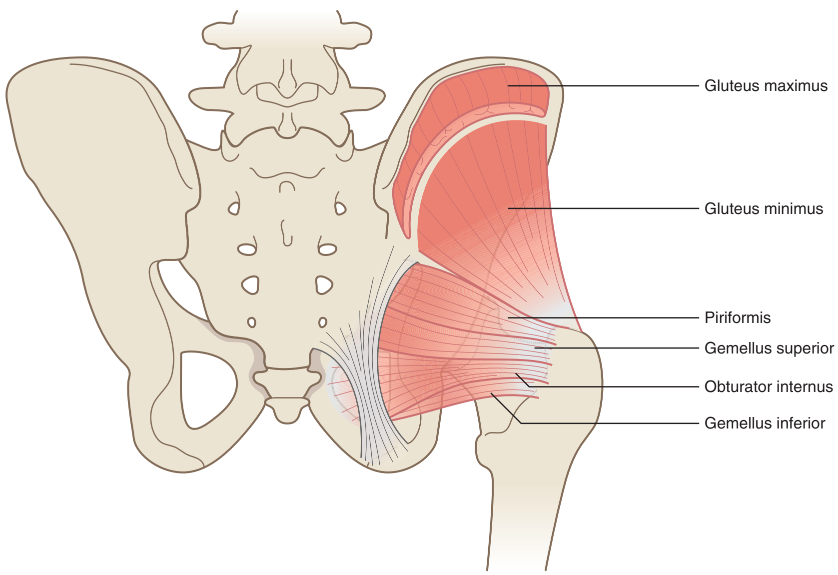


**Fig. 16.15** Hip rotators. Posterior view of the glutei and lateral rotators of the hip. The obturator externus (not shown) lies on a deeper anatomical plane.

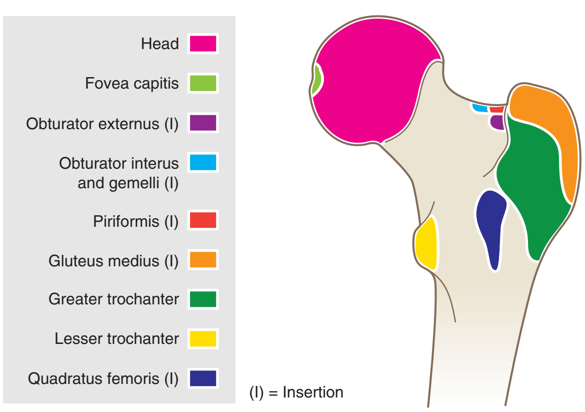


**Fig. 16.16** Insertion of lateral rotators into the greater trochanter.

# The thigh

## Bone anatomy

### Femur

The femur is the longest bone of the body and consists of a head, neck, shaft and expanded lower end (Fig. 16.19).

- The head is more than half a sphere and is directed forwards, medially and upwards and has a central pit or fovea where the ligamentum teres is attached.
- The blood supply to the head is derived from three sources:
  - the principal supply is from a vascular ring in close association to the joint capsule
  - terminal medullary branches from the femoral shaft
  - negligible supply to the central part of the head from the artery of the ligamentum teres.

**Table 16.5** Foramina communicating the pelvis and the thigh

| Foramen | Vessels | Nerves | Other structures |
|---|---|---|---|
| Suprapiriform foramen | Superior gluteal vessels | Superior gluteal nerve | |
| Infrapiriform foramen | Inferior gluteal vessels<br>Internal pudendal vessels | Sciatic nerve<br>Inferior gluteal nerve<br>Pudendal nerve<br>Posterior femoral cutaneous nerve<br>Nerve to obturator internus<br>Nerve to quadratus femoris | |
| Lesser sciatic foramen | Internal pudendal vessels | Pudendal nerve<br>Nerve to the obturator internus | Obturator internus tendon |
| Obturator canal | Obturator vessels | Obturator nerve | |

- The neck is about 5 cm long and makes an angle of 125–135° with the shaft, and is also anteverted by 8°. The degree of anteversion is larger in neonates and reduces progressively with age (Fig. 16.20 and Table 16.6).
- Between the greater and lesser trochanters, there is a rough intertrochanteric line anteriorly and a more rounded intertrochanteric crest posteriorly.
- The shaft of the femur is angled medially (10° in men, 14° in women) so that the medial condyles at the knee are close to each other but the heads are separated by the bony pelvis.
- The distal shaft is angled posteriorly and expanded into medial and lateral condyles separated posteriorly by the intercondylar fossa.
- The medial condyle is larger and the inferior surface of the femur is nearly horizontal despite the shaft obliquity.
- The lateral condyle bears the majority of the patellar articulation and is grooved posterolaterally by popliteus tendon.

**Table 16.6** Anteversion of femoral neck

| Age (years): | 1 | 2 | 3–5 | 6–12 | 13–15 | Up to 20 |
|---|---|---|---|---|---|---|
| Anteversion of femoral head | < 50° | < 30° | 25° | 20° | 17° | 11° |

**Table 16.7** Ossification of the femur

| Ossification centre | Appear | Fuse |
|---|---|---|
| Femoral shaft (1y centre) | 7th week gestation | All fuse at 18–20 years |
| Distal femoral epiphysis (2y centre) | 9th month gestation | |
| Femoral head (2y centre) | 3–6 months age | |
| Greater trochanter (2y centre) | 4 years age | |
| Lesser trochanter (2y centre) | Puberty | |

## Muscles of the thigh

### Anterior compartment

- Hip flexors and knee extensors.
- Psoas major arises from the lumbar spine and twelfth vertebra, descends deep to the inguinal ligament and blends with iliacus, which originates from the internal surface of the ilium, and inserts into the lesser trochanter. Psoas bursa separates psoas tendon from the anterior capsule of the hip joint.
- Tensor fascia lata merges with the thickened lateral deep fascia of the thigh (fascia lata or iliotibial tract) which inserts into the lateral tibial condyle.
- Sartorius is a strap muscle running from the AIIS (Anterior inferior iliac spine) to the medial tibial condyle forming part of the pes anserinus.
- Quadriceps femoris inserts into the superior patellar border.
- Rectus femoris has a distinct intramuscular tendon and arises from the AIIS (straight head) and the superior margin of the acetabulum (reflected head) which may appear irregular.

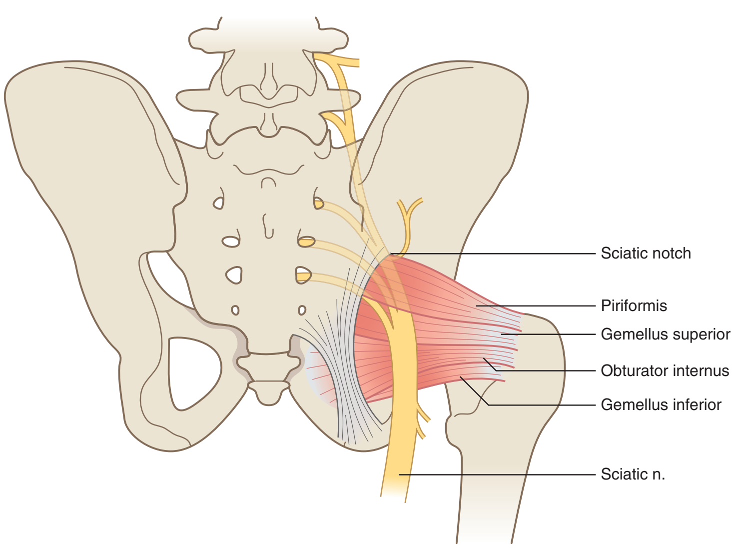


**Fig. 16.17** Sciatic nerve exiting the pelvis.

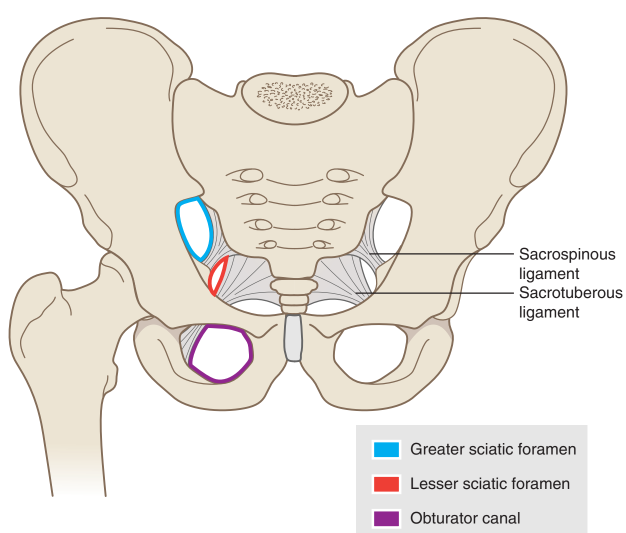


**Fig. 16.18** Foramina communicating the pelvis to the lower limb.

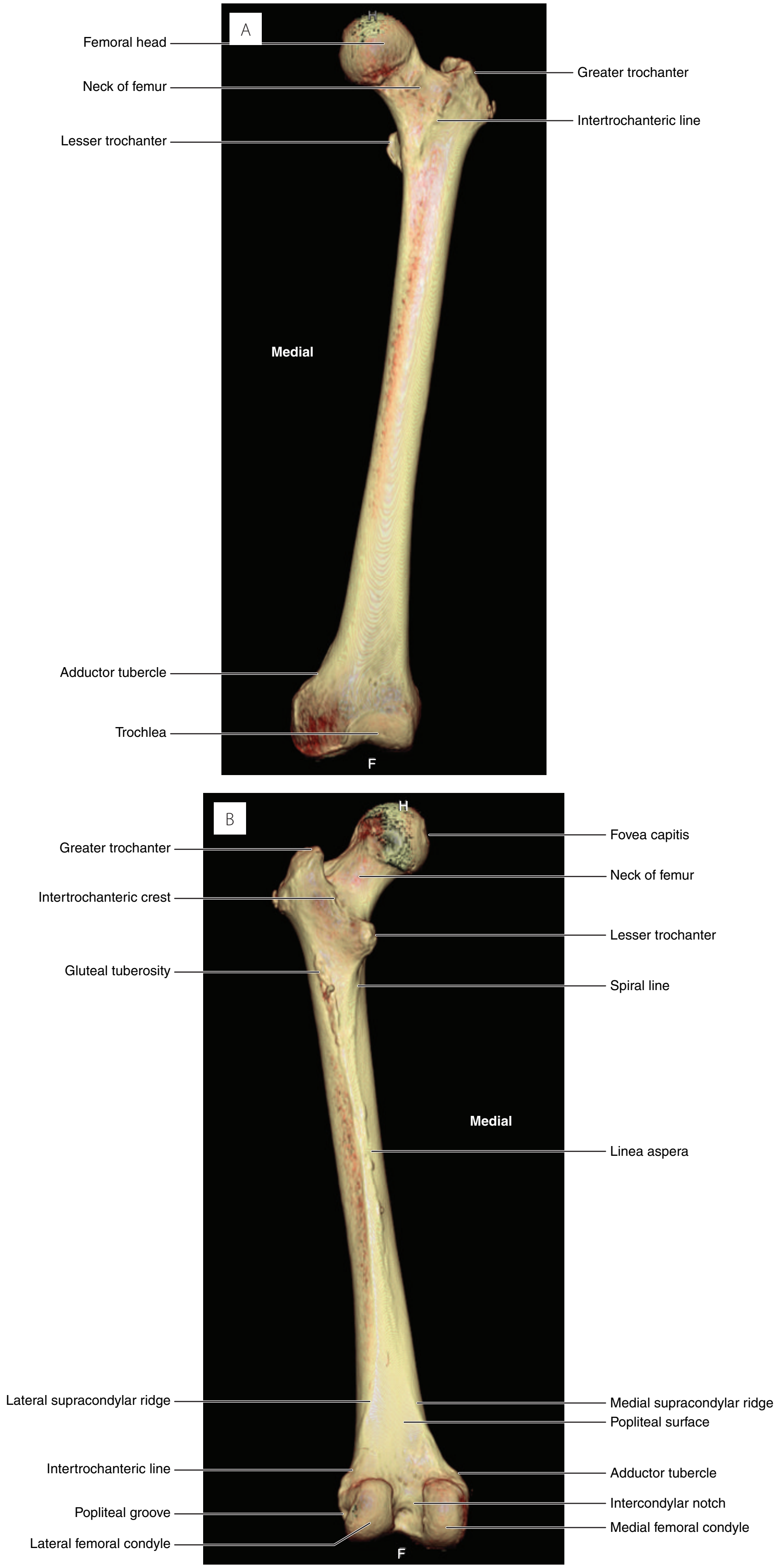


**Fig. 16.19** Surface-shaded CT images of the femur. Anterior (A), posterior (B) views.

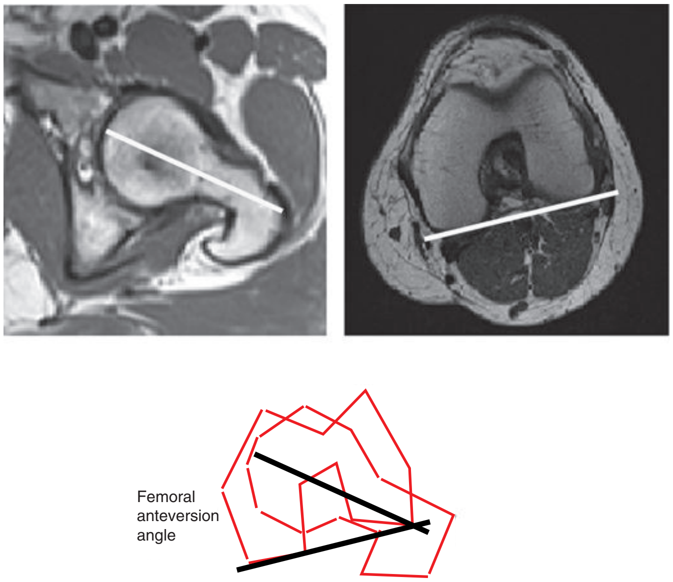


**Fig. 16.20** Anteversion and angulation of the femoral neck.

- Vastus intermedius, lateralis and medialis originate from the femur.
- Vastus medialis has a lower musculotendinous junction than its lateral counterpart and has horizontal fibres inserting into the medial surface of the patella to stabilize it and prevent (lateral) dislocation (Figs. 16.21, 16.22 and Table 16.8).

### The adductor muscles

- The adductors insert along the linea aspera on the posterior surface of the femur.
- Gracilis, a thin strap muscle, acting as knee flexor and medial rotator of the flexed knee, forms part of the pes anserinus.
- Adductor magnus is large with a broad attachment including the adductor tubercle, and has an adductor hiatus, a defect in its distal part allowing passage of the femoral vessels into the popliteal fossa (Figs. 16.21, 16.22 and table 16.9).

### The hamstrings

- Hamstrings have a complex proximal insertion from the ischial tuberosity and flex the knee.
- Semimembranosus forms a membrane-like tendon with complex distal tendinous expansions over the posteromedial aspect of the tibial condyle, popliteus muscle and lateral femoral condyle, via the oblique popliteal ligament.
- Semitendinosus is more posterior and passes over the medial collateral ligament to insert into the pes anserinus aponeurosis.
- Biceps femoris crosses the hip and knee joint and is prone to traumatic muscular tears. Biceps femoris has two proximal attachments, the long and short head; the latter may be absent (Table 16.10 and Figs. 16.23, 16.24).

**Table 16.8** Anterior thigh muscular compartment

| Muscle | Origin | Insertion | Action |
|---|---|---|---|
| Iliopsoas | Inner surface ilium (iliacus)<br>Lumbar transverse processes | Lesser trochanter | Hip |
| Tensor fascia lata | Outer surface of iliac crest | Iliotibial band | Maintains knee extended and abducts hip |
| Sartorius | Ant sup iliac spine | Upper medial aspect prox tibia | Flexes and lat rotates hip; flexes and med rotates knee |
| Rectus femoris | Straight head: ant inf iliac spine<br>Reflected head: ilium above acetabulum | Quads tendon | Hip flexor; knee extensor |
| Vastus medialis | Extensive from medial aspect of femur | Quads tendon and medial aspect of patella | Knee extensor and patella stabilizer |
| Vastus lateralis | Extensive from lateral aspect of femur | Quads tendon | Knee extensor |
| Vastus intermedius | Anterior and lateral aspect of femur | Quads tendon | Knee extensor |

**Table 16.9** Thigh adductors

| Muscle | Origin | Insertion | Action |
|---|---|---|---|
| Adductor magnus | Ischial tuberosity and ischiopubic ramus | Extensive along gluteal line and adductor tubercle | Adducts, extends and med rotates hip |
| Adductor longus | Pubic body | Linea aspera (femur) | Adducts and med rotates hip |
| Adductor brevis | Pubic body and inf ramus | Linea aspera (femur) | Adducts hip |
| Gracilis | Ischiopubic ramus | Medial aspect of upper tibia | Adducts hip; flexes and med rotates knee |
| Pectineus | Pectineal line | Below lesser trochanter | Flexes, adducts and med rotates hip |

### Pes anserinus

- Sartorius, gracilis and semitendinosus insert (from medial to lateral) into the anterolateral aspect of the medial tibial condyle to form an aponeurosis.
- These muscles form a tripod: the apex is the pes anserinus and the tripod base is a triangle formed by the muscles' attachments on the pelvis (Fig. 16.25).
- Pes anserine bursa lies deep to the aponeurosis and may be liable to injury from overuse.

## Nerves and vessels

### Sciatic nerve

The sciatic nerve travels in the hamstring compartment of the thigh. It loses its gluteal cover proximally and is covered by deep fascia until it dives deep to biceps femoris in the midline of the hamstring compartment. It divides into the posterior tibial and common peroneal nerves as it reaches the popliteal fossa.

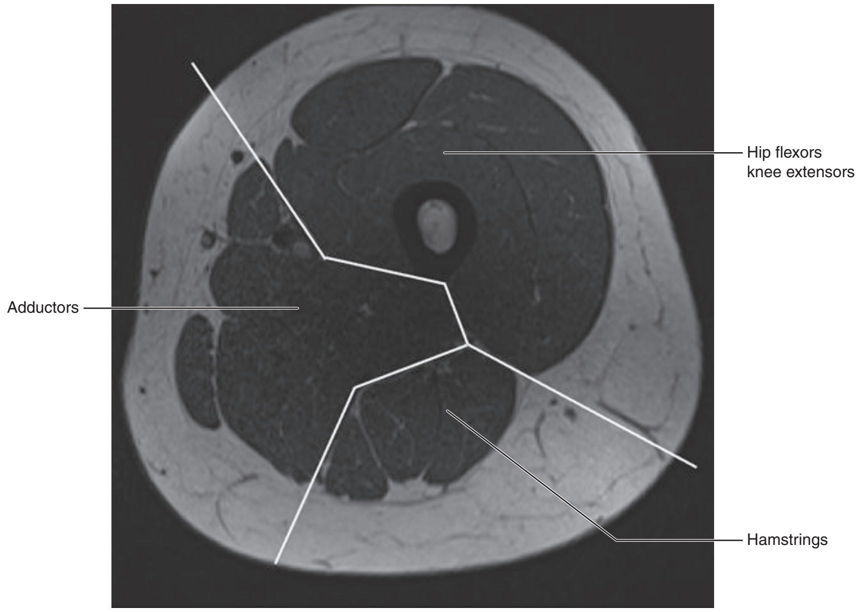


**Fig. 16.21** Muscular compartments of the thigh.

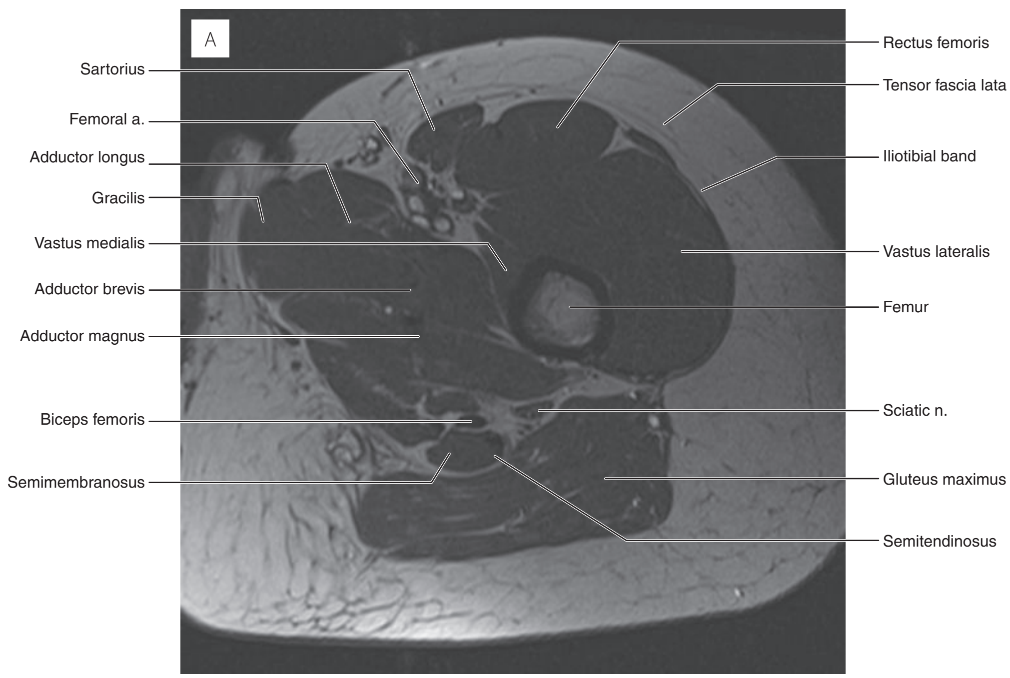


**Fig. 16.22** Thigh axial MR images. From superior to inferior.

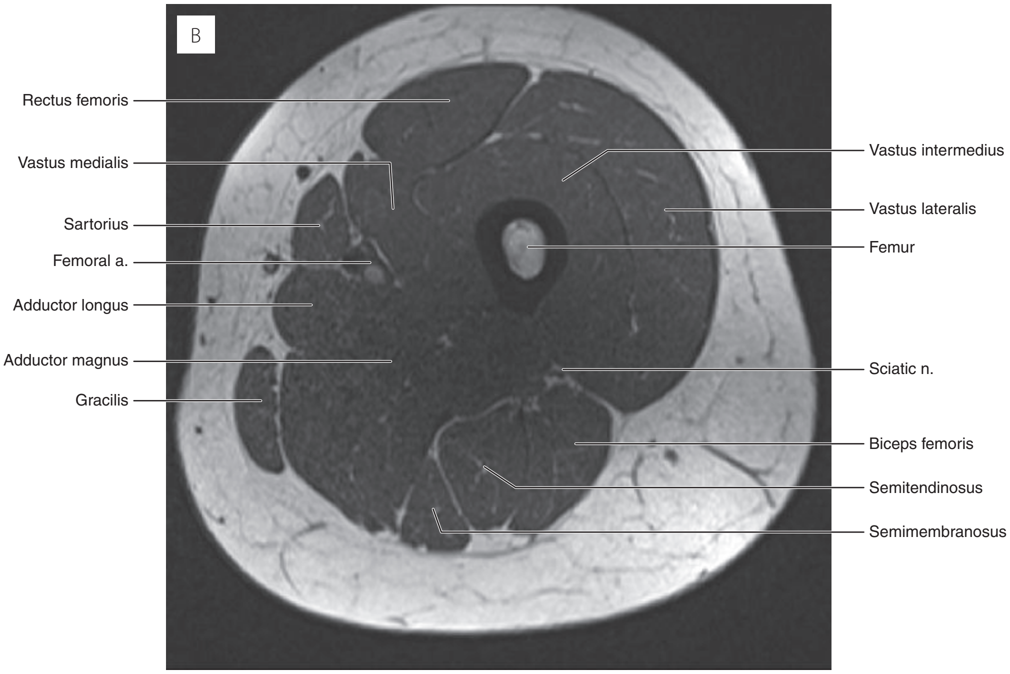


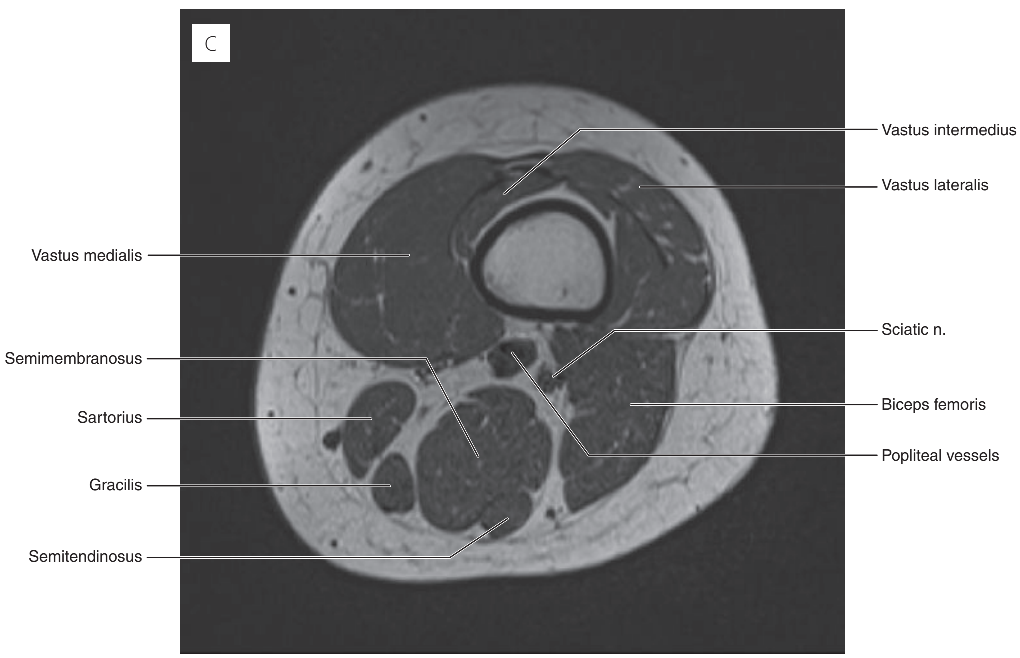


**Fig. 16.22** *(cont.)*

**Table 16.10** Hamstrings

| Muscle | Origin | Insertion | Action |
|---|---|---|---|
| Semimembranosus | Ischial tuberosity (post surface) | Complex over medial tibial condyle, posterior knee capsule and oblique popliteal ligament | Flexes and med rotates knee; extends hip |
| Semitendinosus | Ischial tuberosity (post surface) | Medial aspect of upper tibia | Flexes and med rotates knee; extends hip |
| Biceps femoris | Long head: ischial tuberosity<br>Short head: linea aspera, lat femur | Styloid process of fibular head, MCL and lat tibial condyle | Flexes and lat rotates knee; hip extensor (long head) |

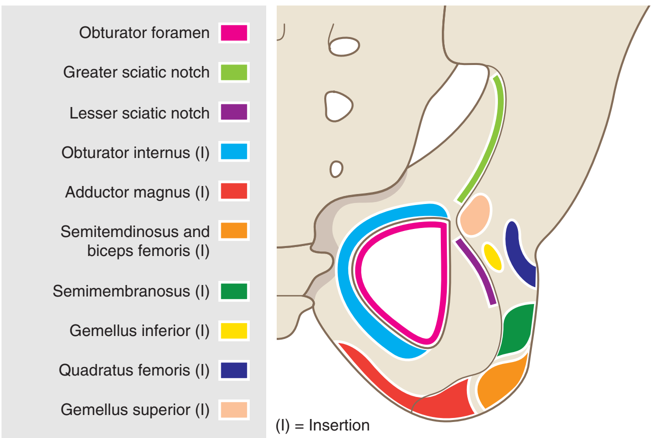


**Fig. 16.23** Hamstring origin. The long head of biceps and semitendinosus have a common origin from a conjoint tendon. Semimembranosus is medial to biceps femoris distally but its proximal attachment on the ischial tuberosity lies superior and lateral to that of the conjoint tendon.

### Femoral nerve and vessels

The femoral nerve (L2, 3, 4), artery, vein and lymphatics (from lateral to medial) pass under the inguinal ligament to run through the femoral triangle over the adductors. The femoral nerve splits within the triangle and the vessels run distally to pass through the adductor hiatus (adductor magnus) to enter the popliteal fossa (Fig. 16.26).

## Knee

### Plain radiography

- The knee joint is formed by the femoral condyles, patella and tibial plateau.
- The joint space of the femoro-tibial compartments and the patello-femoral compartment should range between 3 and 8 mm.

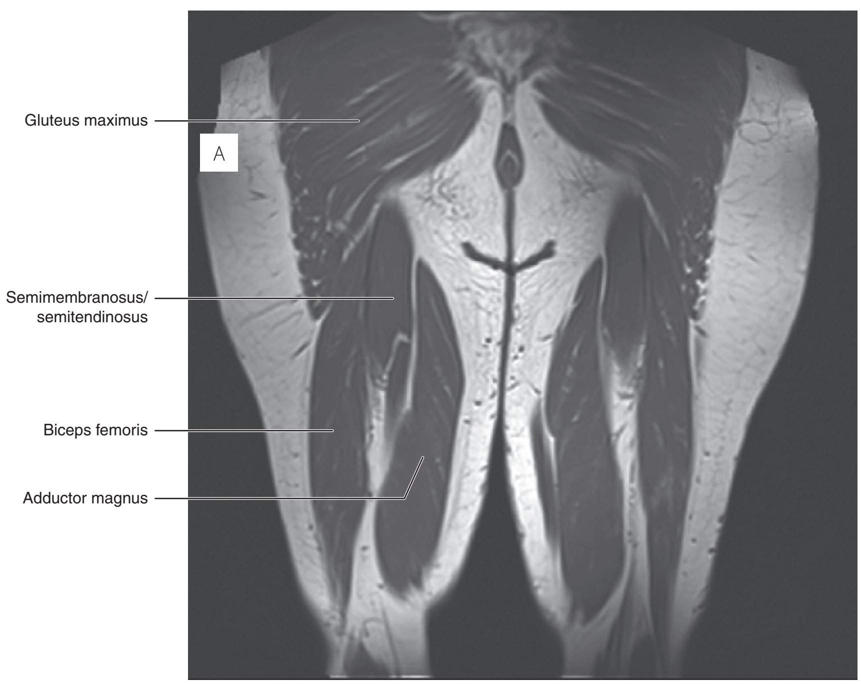


**Fig. 16.24** Thigh coronal MR images. From posterior to anterior.


**Fig. 16.24** (*cont.*)

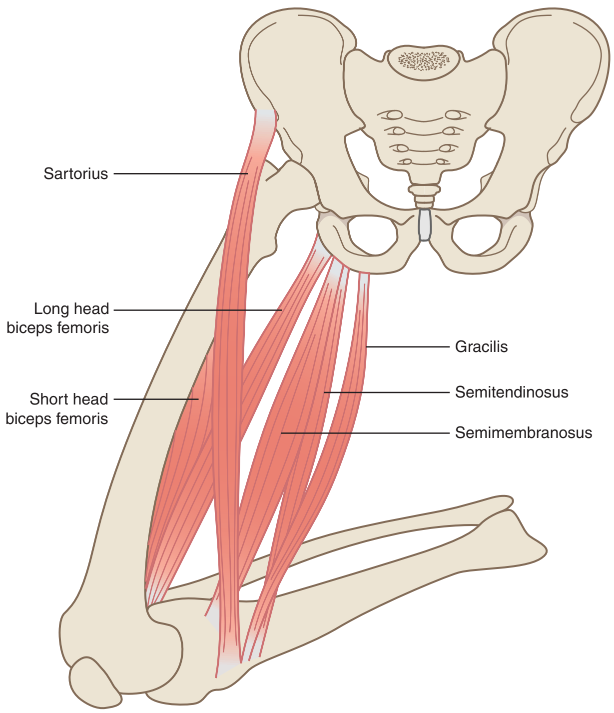


**Fig. 16.25** Diagram of the pes anserine muscles (gracilis, semitendinosus and sartorius) forming an inverse tripod.

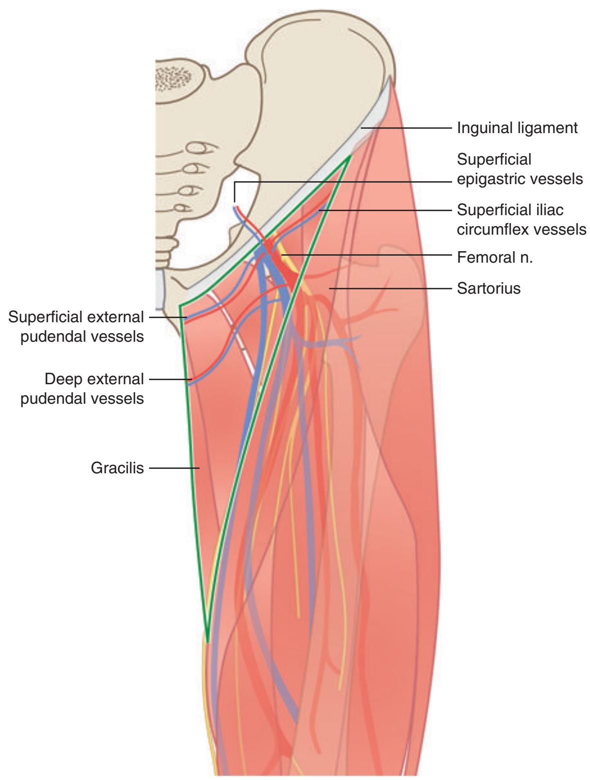


**Fig. 16.26** Femoral triangle.

- The suprapatellar bursa is best seen when distended with joint fluid and is normally less than 5 mm on a lateral view (5–10 mm is borderline and > 10 mm is in keeping with a joint effusion) (Figs. 16.27, 16.28).

### Patella and fabella

- The patella is a flattened sesamoid bone within the quadriceps tendon. It is triangular with an inferior apex lying about 1 cm proximal to the knee joint line in the erect position.
- The retropatellar articular surface is divided into a larger lateral facet and a smaller medial facet for articulation with the corresponding femoral condyles. The anterior surface is irregular owing to the entry of nutrient vessels.
- Several ossification centres appear at 3 years and fuse at puberty (Table 16.11). These may give rise to an irregular appearance of the normal unfused patella. A bipartite (or multipartite) patella is a common variant when the superolateral corner fails to fuse.
- The fabella is a sesamoid bone frequently found in the lateral head of gastrocnemius.

## Knee joint

The knee is a synovial hinge joint and the largest in the body (Fig. 16.30).

### Articular surfaces

- The medial and lateral tibiofemoral compartments, between the corresponding femoral and tibial condyles, have a joint space ranging from 3 to 8 mm.
- The medial tibial articular surface is larger than its lateral rounder counterpart.
- The femoral condyles have a groove at the junction of the patellar and tibial articular areas.
- The patellofemoral compartment is a saddle joint between the femoral trochlea and patella, formed by a large steeper lateral facet, resisting patellar lateral displacement, and two smaller medial facets.
- The patellar articular cartilage varies in thickness.

### Capsule

- The fibrous capsule attaches to the margin of the articular surfaces.
- It is partly deficient superiorly, where the joint cavity communicates with the suprapatellar bursa, and posteriorly, where it may allow communication with the semimembranosus and popliteal bursa.
- The capsule includes the tibial tuberosity and fibular head and is pierced by popliteus tendon posteriorly.
- The capsule blends with and is strengthened by multiple structures:

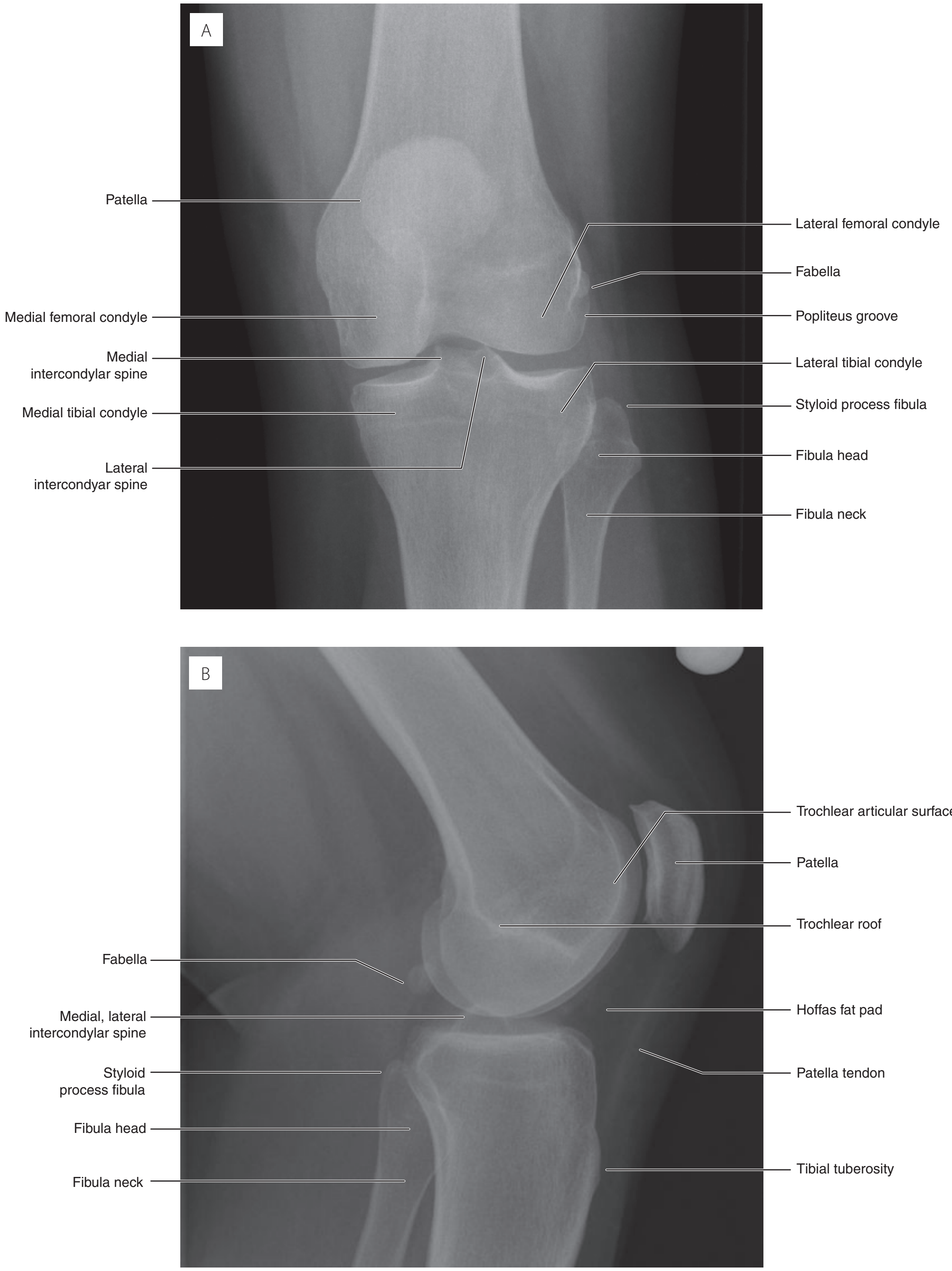


**Fig. 16.27** Knee plain radiography. Frontal (A), lateral (B) and skyline views (C).

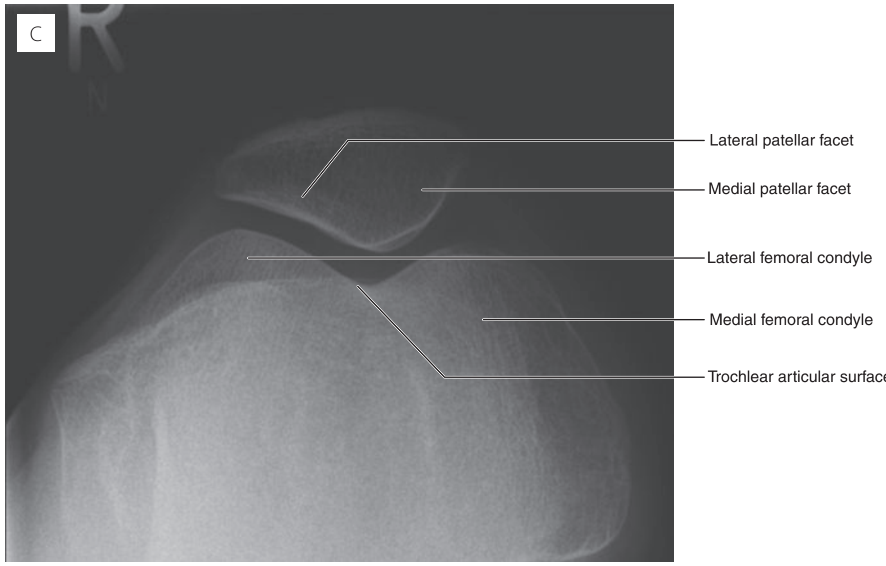


**Fig. 16.27** (*cont.*)

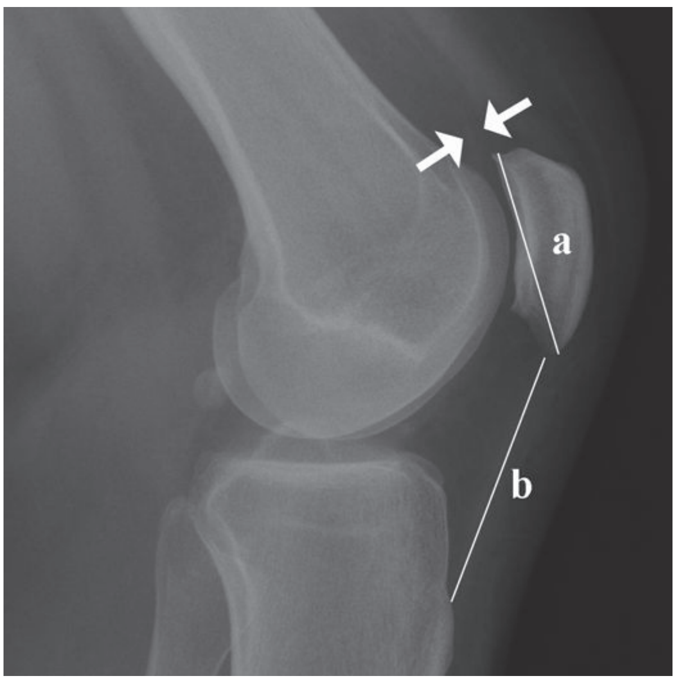


**Fig. 16.28** Knee measurements. Patella measurements are made on a lateral knee radiograph with 30° of flexion. The diagonal length of the patella (a) is approximately equal to the length of the patella tendon (b). Patella alta occurs when b > a and patella baja is seen when b < a. A variation of 20° is within normal limits. Suprapatellar bursa is normal when < 5 mm (between arrows).

**Table 16.11** Ossification of tibia and fibula

| Ossification centres | Appear | Fuse |
|---|---|---|
| Shafts | 7–8 weeks gestation | |
| Proximal tibial epiphysis | Usually present at birth | 16–18 yrs |
| Proximal fibular epiphysis | 3–4 yrs | |
| Lower ends (tib and fib) | 1st year | 15–17 yrs |
| Medial malleolus | Grows from distal tibial epiphysis (7 yrs), although may have separate ossification centre | |
| Tibial tuberosity | Grows from proximal tibial epiphysis (10 yrs), although may have separate ossification centre | |

- the gastrocnemius heads and oblique popliteal ligament posteriorly
- medial collateral ligament and external aspect of medial meniscus
- tendon expansions of vastus lateralis, iliotibial tract and vastus medialis anteriorly, forming the patellar retinacula.

### Synovium

- The synovium lines most of the capsule and extends into the suprapatellar bursa for approximately 10 cm above the superior part of the patella.
- The infrapatellar bursa separates the synovium from the patellar tendon, where two synovial infoldings (the alar folds) fuse into a central fold to insert on to the anterior part of the intercondylar fossa.
- Posteriorly, an anterior synovium reflection from the capsule covers the front and sides of the cruciate ligaments, rendering them intracapsular but extrasynovial.
- The menisci are not covered by synovium.

### Menisci

- The concavity of the tibial articular surfaces is partially covered and accentuated by two semilunar fibrocartilages, or menisci, which distribute weight-bearing stresses through the joint surfaces and improve stability.
- The menisci cross section is triangular.
- Menisci are poorly vascularized with only partial blood supply from the external surface, hence they heal poorly following trauma.
- The medial meniscus is larger, more semicircular and thickest posteriorly.
- The lateral is smaller, thicker and forms a nearly complete ring. The anterior and posterior horns attach to the corresponding intercondylar regions.

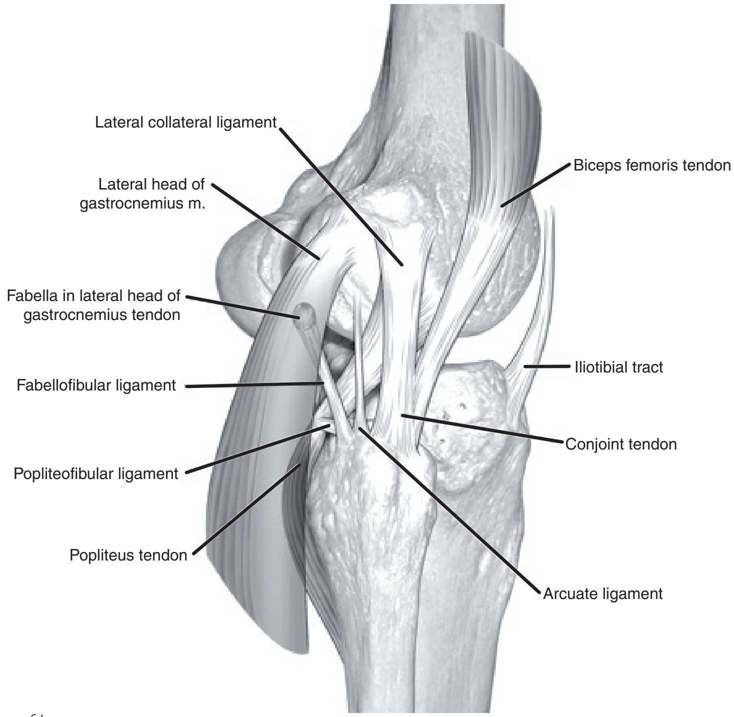


**Fig. 16.29** Posterolateral corner of knee.

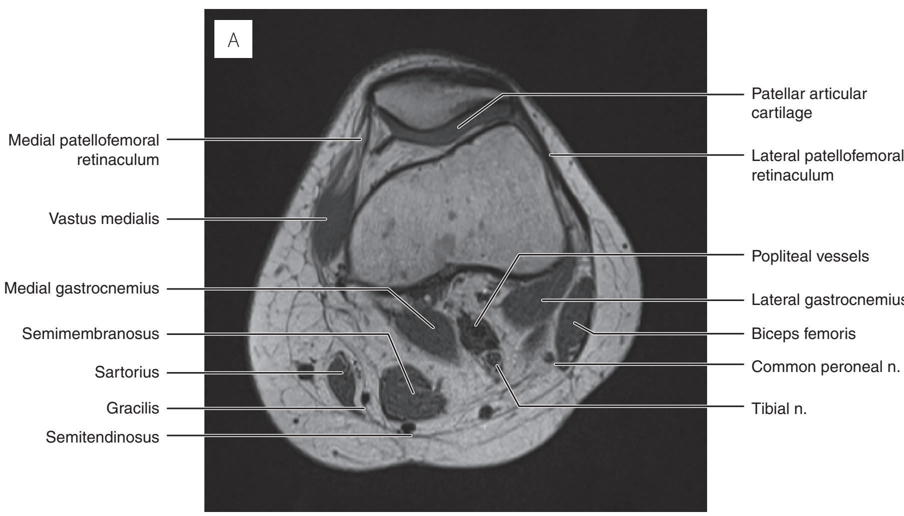


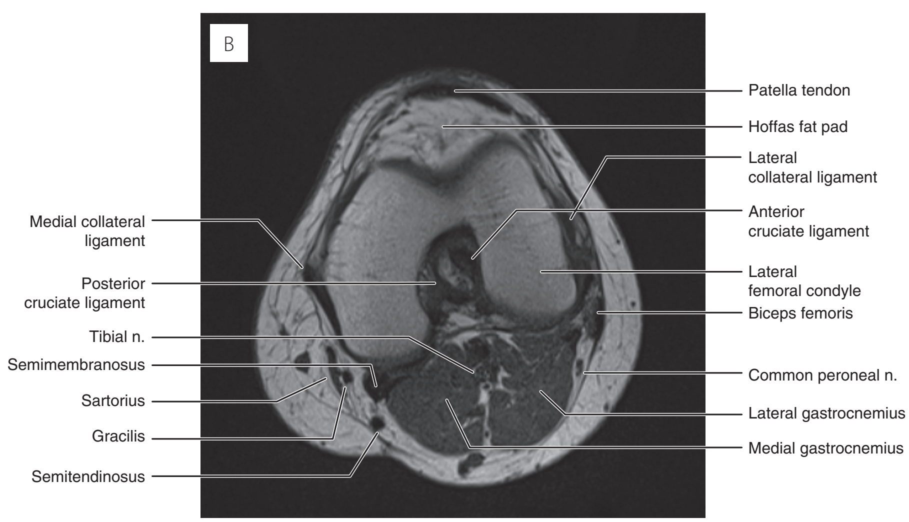


**Fig. 16.30** Knee axial, sagittal and coronal MR images.

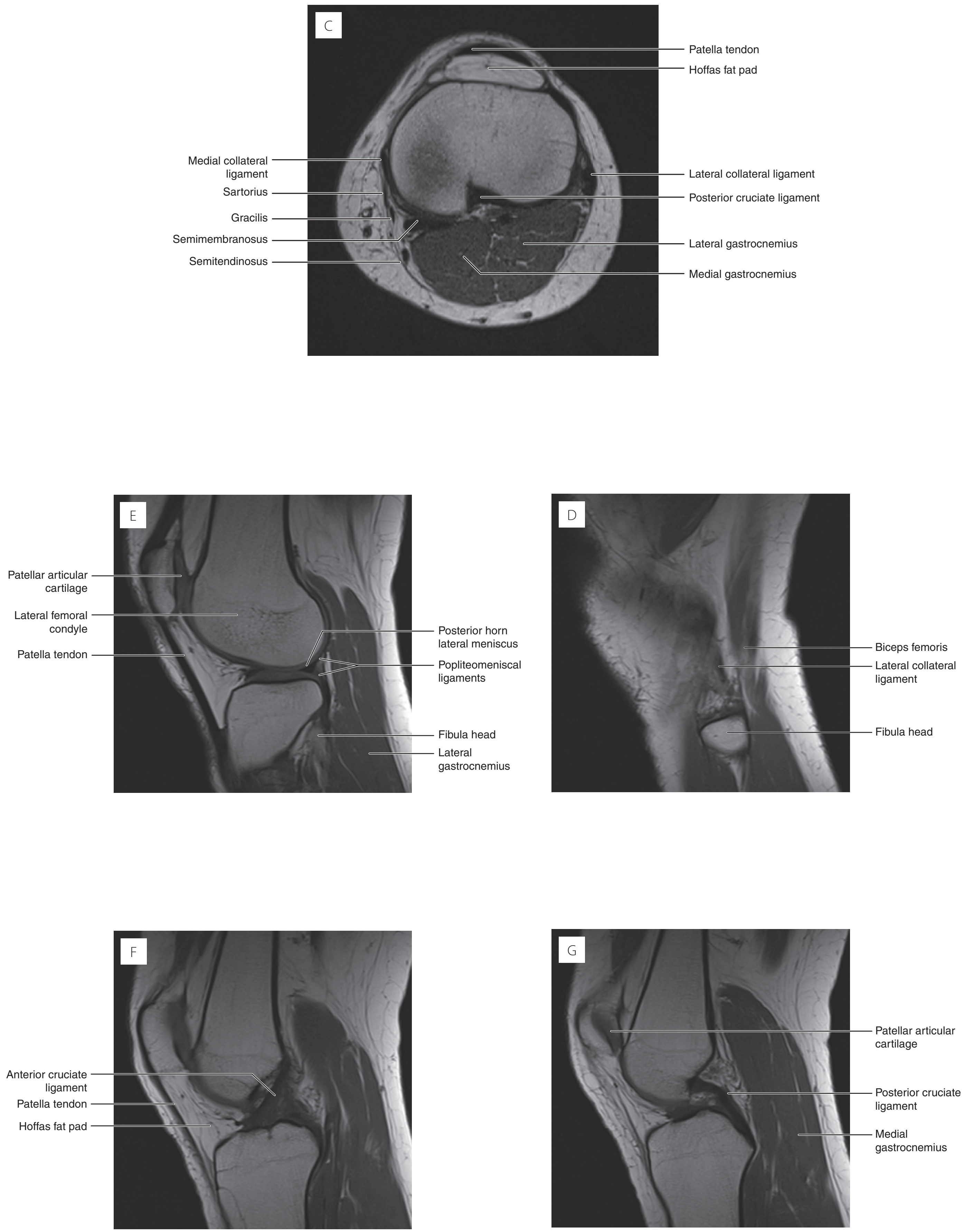


**Fig. 16.30** *(cont.)*

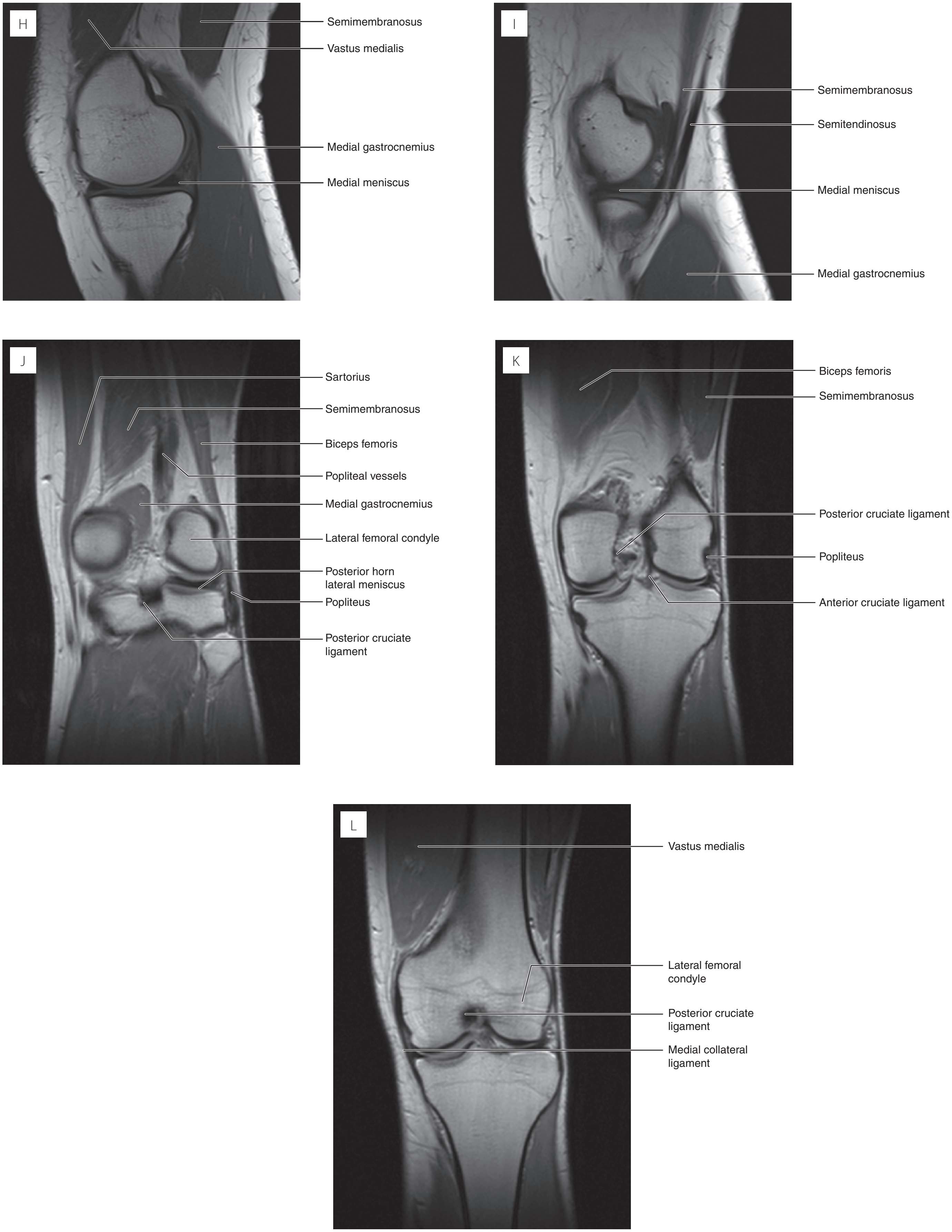


**Fig. 16.30** (*cont.*)

#### Meniscal attachments

- The meniscofemoral ligament, from the posterior horn of the lateral meniscus to the medial femoral condyle, is divided by the posterior cruciate ligament into the ligaments of Humphrey anteriorly and ligament of Wrisberg posteriorly.
- The external aspect of the medial meniscus blends with the capsule and medial collateral ligament (unlike the lateral meniscus).
- Popliteus tendon blends with the lateral meniscus and separates it from the lateral collateral ligament. Popliteus contraction during flexion pulls the posterior horn of the lateral meniscus posteriorly allowing external rotation of the femur to unlock the extended knee.
- Transverse ligament joins the anterior horns of the menisci.

### Cruciate ligaments

- Extrasynovial and intracapsular, and found in the intercondylar region.
- The anterior cruciate ligament (ACL) arises from the medial part of the anterior intercondylar area of the tibia and passes upwards, laterally and posteriorly to attach to the posterior part of the medial aspect of the lateral femoral condyle. On MR images, the anteromedial bundle (AMB) and a more vertical posterolateral bundle (PLB) are clearly defined as they are surrounded by higher-signal connective tissue.
- The AMB is taut in all knee positions, resists posterior femoral translation at 30° flexion, and maintains functional isometry of the knee. The PLB is taut on extension, resisting hyperextension and preventing posterior translation of the femur on the tibia.
- Unlike other tendons and ligaments, the ACL is of heterogeneous signal on MRI.
- The posterior cruciate ligament (PCL) attaches to the posterior intercondylar area of the tibia and passes upwards, medially and anteriorly to attach to the anterior part of the lateral aspect of the medial femoral condyle. The PCL is stronger than the ACL and resists anterior femoral translation on the tibia and, like the ACL, is also formed by two bundles (anterolateral and posteromedial) too tightly bound to be resolved on MR imaging. PCL is intensely hypointense on MR, but its C-shape configuration renders it susceptible to the MR magic angle phenomenon (signal abnormality at 55° to the magnetic (Z) axis) and hence high signal at the apex of the C is commonly seen and of no pathological significance.

### Collateral ligament complexes

- The medial collateral ligament is composed of deep fibres intimately related to the meniscotibial and meniscofemoral ligaments, and to the joint capsule. The superficial fibres form a band from the femoral medial condyle to the medial aspect of the proximal tibia.
- The lateral collateral ligament complex is composed of three layers; an outer layer with the iliotibial band anteriorly and the biceps femoris tendon posteriorly, the cord-like fibular collateral ligament forms the middle layer, and the deep layer is formed by the popliteus tendon.

### Posterolateral corner

Composed of several structures, including:

- popliteus
- popliteofibular ligament
- biceps tendon
- arcuate ligament
- thickening of the lateral knee joint capsule (meniscofemoral and meniscotibial)
- lateral head of gastrocnemius.

#### Popliteus

- Main internal rotator of the tibia allowing unlocking prior to flexion from full extension.
- Arises from the posteromedial aspect of the proximal tibia and its tendon extends superolaterally between the joint capsule and posterior horn of the lateral meniscus, giving rise to a pseudotear appearance of the meniscal posterior horn.
- It runs within and inserts into the popliteal sulcus of the femoral condyle.
- Additional insertions include the lateral meniscus and the styloid process of the fibular head via the popliteofibular ligament, an important stabilizer of the posterolateral corner of the knee.

#### Popliteofibular ligament

- It runs from the lateral aspect of popliteus to the medial surface of styloid process of fibula.
- May be the fibular origin of popliteus.

#### Biceps femoris tendon

- Long head and direct arm of short head insert as conjoint tendon on the lateral basal aspect of the fibular head.
- Anterior arm of short head inserts as conjoint tendon with lateral capsular ligament on the superolateral aspect of the tibia.

#### Arcuate ligament

- The arcuate ligament is a Y-shaped capsular thickening with medial and lateral limbs.
- Medial limb arises from fibular styloid process, lateral to popliteofibular ligament, and blends with posterior knee capsule and oblique popliteal ligament fibres.
- Lateral limb arises just below the fabellofibular ligament and blends with the posterior knee capsule.

#### Fabellofibular ligament

- Runs from the fabella to lateral aspect of the fibular styloid process.

## Extensor mechanism

- Consists of the quadriceps tendon, the patella and the patellar tendon (Fig. 16.31).
- During knee flexion the patella tracks along the femoral trochlea and is restrained from lateral subluxation by the strong and horizontally arranged fibres of the vastus medialis and by a steeper and larger lateral facet on both the femur and patella.
- The lateral pull on the extensor mechanism is secondary to the normal valgus alignment of the knee (normal Q angle = 15°) (Fig. 16.32).
- A tibial tuberosity–trochlear groove (TTTG) distance of less than 20 mm is required for normal patellar tracking on the femoral trochlea during knee flexion-extension (Fig. 16.33).

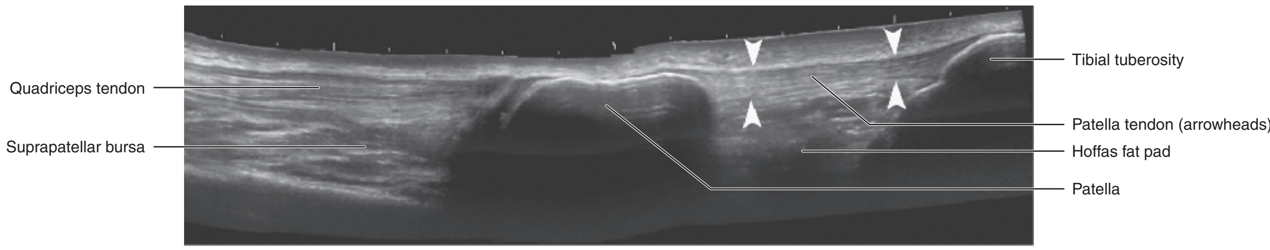


**Fig. 16.31** Extensor mechanism extended filed of view ultrasound.

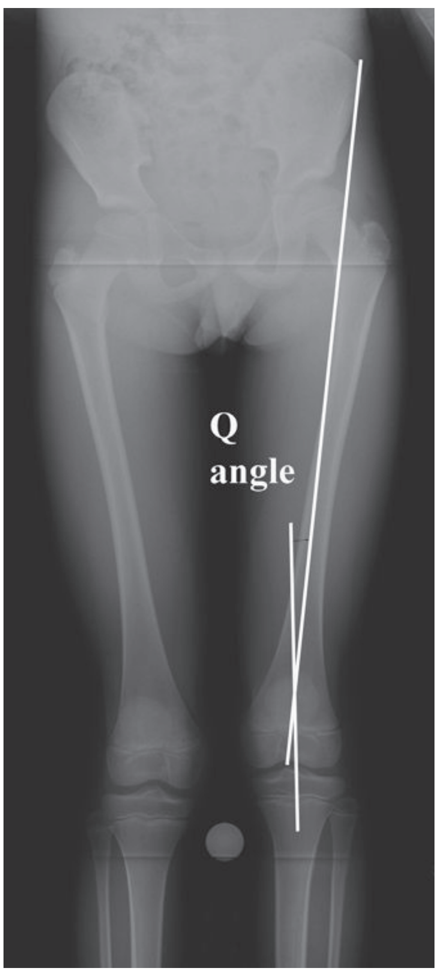


**Fig. 16.32** The Q-angle is formed from a line drawn from the ASIS to the centre of the kneecap, and from the centre of the kneecap to the tibial tubercle. To find the Q-angle, measure that angle, and subtract from 180°.

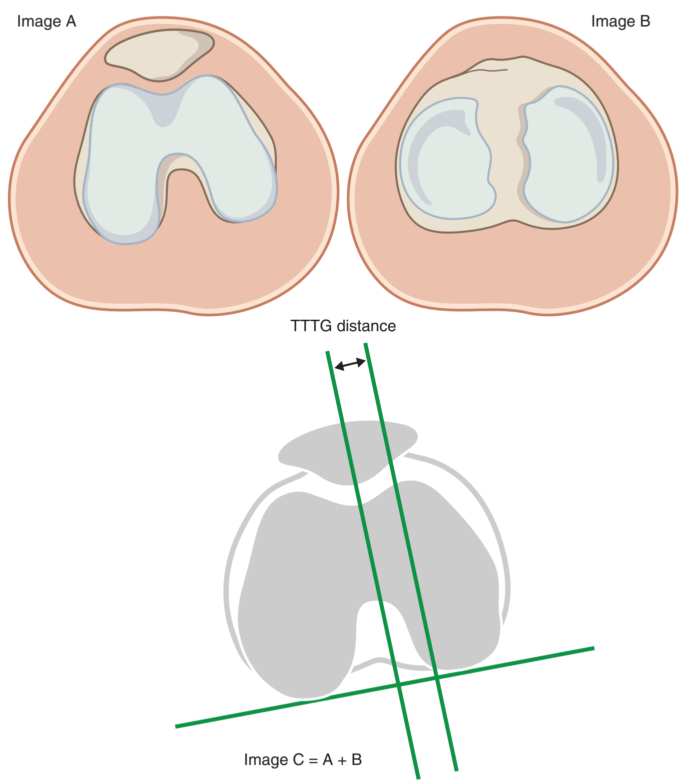


**Fig. 16.33** Tibial tuberosity – trochlear groove (TTTG) distance. Two axial images of the knee, the first through the deepest part of the femoral trochlea (Image A) and the second through the tibial tuberosity (Image B), are superimposed (Image C). Two lines perpendicular to the plane drawn across the posterior aspect of the femoral condyles are drawn. These lines run through the tibial tuberosity and the concavity of the trochlea and the distance between them is the TTTG distance (normal < 20 mm).

## Popliteal fossa

- Rhomboid potential space posterior to the knee. The gastrocnemius heads lie deep to the distal hamstrings.
- Floor: femur, popliteus and posterior knee joint capsule.
- Roof: fascia lata, superficial nerves and short saphenous vein.
- Contents (superficial to deep): tibial nerve, popliteal vein and artery.
- Common peroneal nerve runs along the posterior edge of biceps femoris.
- Short saphenous vein perforates superficial fascia and dives deep to join the popliteal vein.
- Popliteal artery divides into anterior and posterior tibial arteries (Figs. 16.34, 16.35).

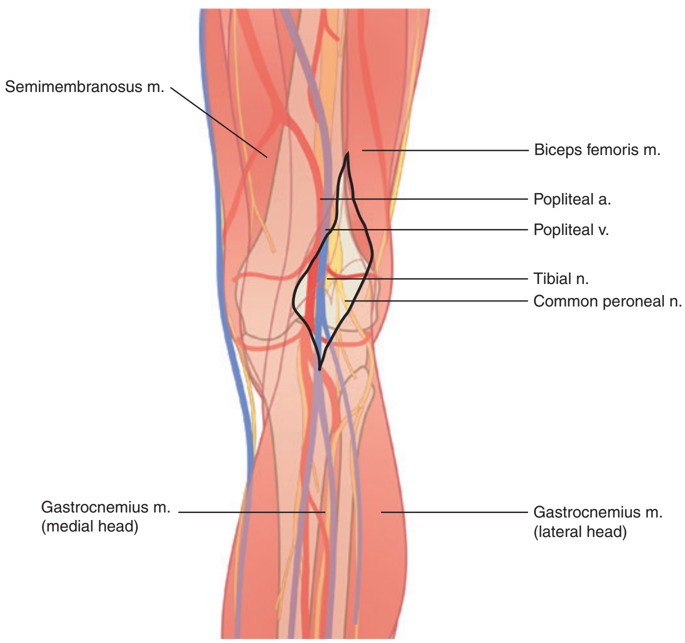


**Fig. 16.34** Diagram of popliteal fossa.

# Leg

## Bone anatomy

### Tibia

- The tibia (Fig. 16.36) is expanded superiorly into a larger medial and smaller lateral condyles.
- The intercondylar area has a raised intercondylar eminence, with medial and lateral tubercles, separating the articular surfaces.
- The tibial tuberosity is a rough prominence onto which the patella tendon inserts and may be fragmented and irregular in the immature skeleton.
- The shaft is triangular in cross section and its anteromedial surface and anterior edge are subcutaneous. The lateral surface gives rise to the interosseous membrane and the posterior surface is crossed by the soleal line, which descends medially, giving rise to the soleus muscle.
- The distal end of the tibia is expanded and wider anteriorly, with a short medial and inferior projection, the medial malleolus.

### Fibula

- The fibula is slender and is mainly a site of attachment for muscles with little weight-bearing action.
- The common peroneal nerve winds around the neck where it is liable to injury.
- The expanded distal end forms the lateral malleolus which is more inferior and posterior than its medial counterpart.

## Muscles of the leg

### Posterior compartment

- Achilles tendon, the largest tendon in the body, is formed by the merger of gastrocnemius and soleus.

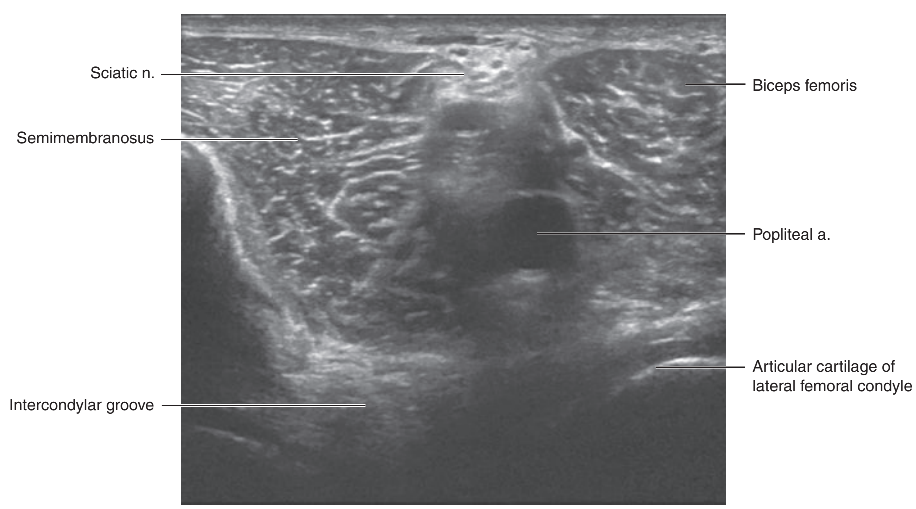


**Fig. 16.35** Popliteal fossa axial sonogram.

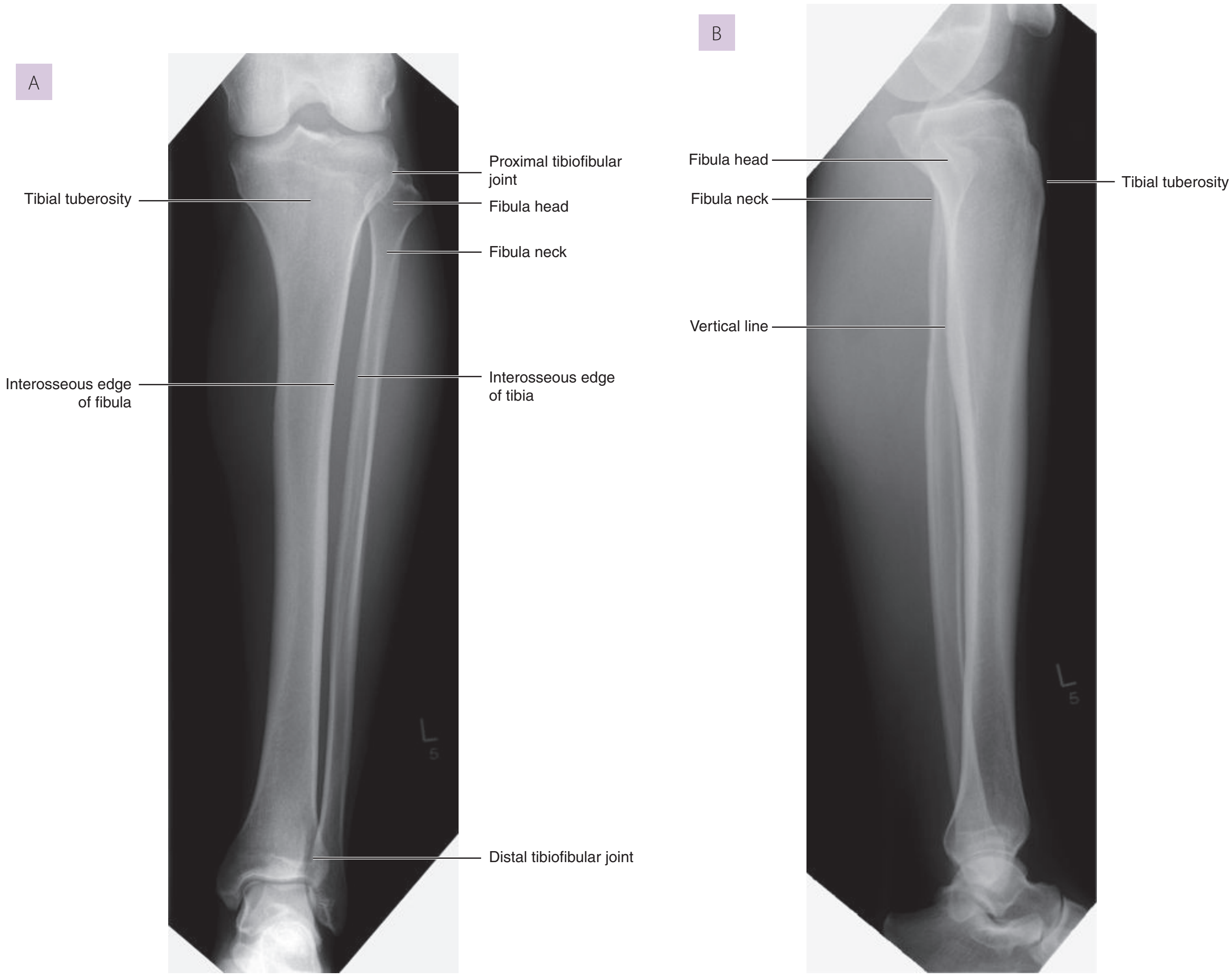


**Fig. 16.36** Tibia and fibula.

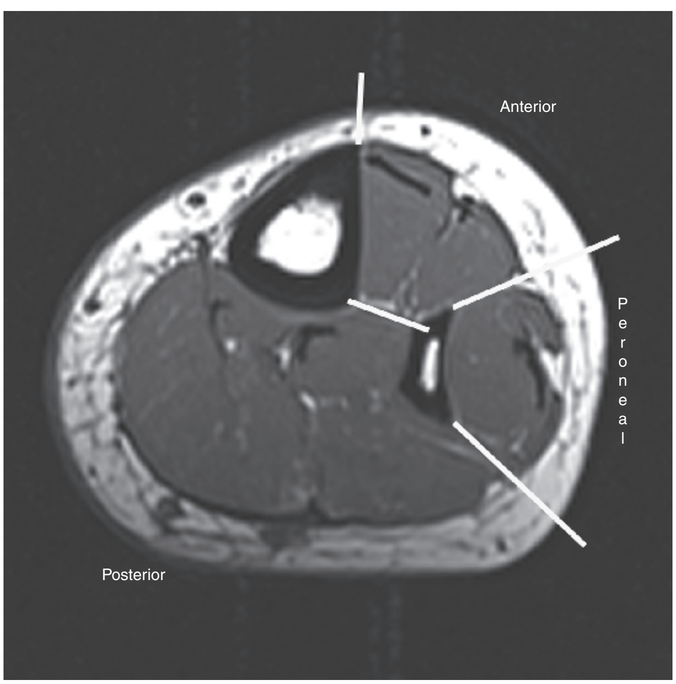


**Fig. 16.37** Muscular compartments of the leg.

- Tibialis posterior is bipennate and deep to the long flexors.
- Plantaris runs between the medial gastrocnemius and soleus, and is absent in up to 10% of individuals (Table 16.12).

### Anterior compartment

- Unyielding walls of the anterior compartment (Table 16.13) render it susceptible to compartment syndrome.

### Peroneal muscles (Table 16.14)

## Tibiofibular joints

- Proximal tibiofibular joint is a synovial plane joint strengthened by ligaments.
- Distal tibiofibular joint is a syndesmosis united by anterior and posterior ligaments and an interosseous ligament.
- Interosseous membrane further stabilizes both joints.

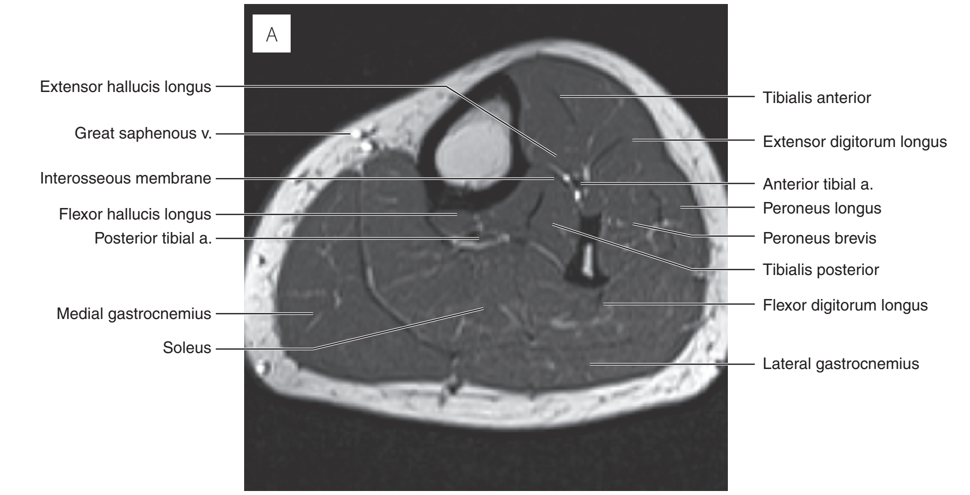


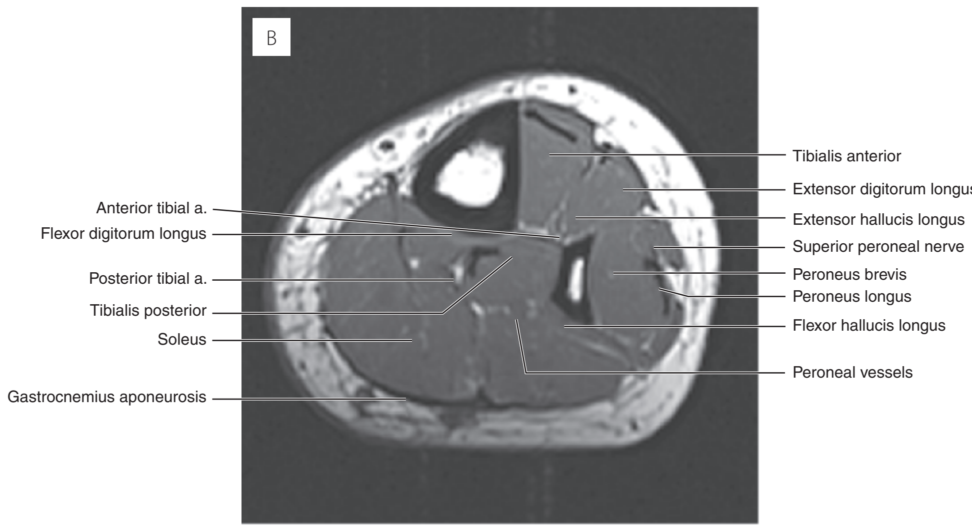


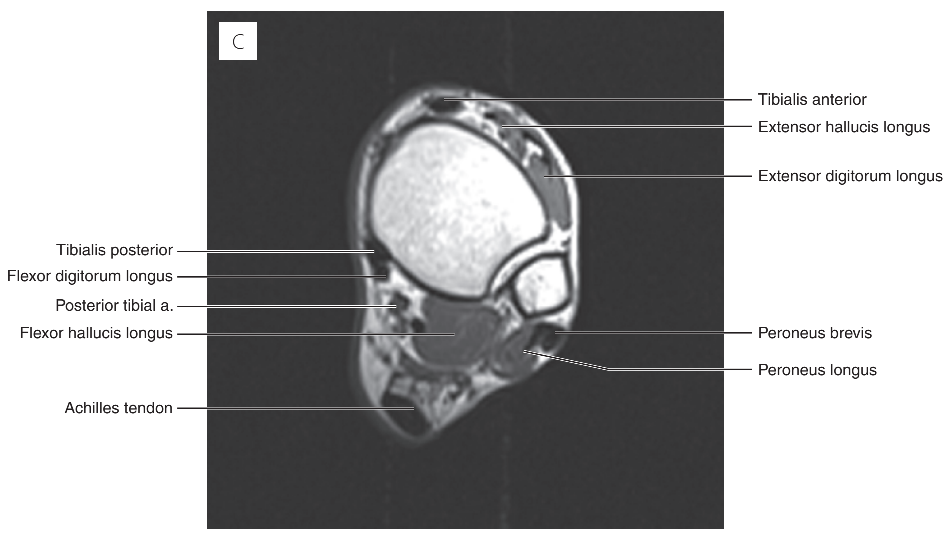


**Fig. 16.38** Leg MR axial images. From superior to inferior.

**Table 16.12** Posterior muscular compartment of the leg

| Muscle | Origin | Insertion | Action |
|---|---|---|---|
| Gastrocnemius | Lat head: post surface of lat fem condyle<br>Med head: above post aspect of med fem condyle | Achilles tendon-calcaneus | |
| Soleus | Soleal line, mid 1/3 of post tibia and upper 1/4 of post fibula | Achilles tendon- calcaneus | Plantar flexes foot |
| Accessory soleus (6% of population) | Distal posterior aspect of the tibia and deep fascia of the normal soleus/flexor tendons | Anteromedial to the Achilles tendon insertion, on calcaneus | |
| Plantaris | Lateral supracondylar ridge above lat head gastrocnemius | Achilles tendon: deep and medial to gastrocnemius | Plantar flexes foot and flexes knee |
| Tibialis posterior | Upper half of tib/fib and interosseous membrane | Navicular tuberosity and spring ligament | Plantar flexes and inverts foot; maintains longitudinal arches |
| Flexor digitorum longus | Post tibial shaft below soleal line | Base of distal phalanges (lat four toes) | Flexes toes, ankle and supports longitudinal plantar arch |
| Flexor hallucis longus | Lower 2/3 fibula and interosseous membrane | Base of distal phalanx of big toe and slips to FDL tendons | Flexes big toe, ankle and supports longitudinal plantar arch |

**Table 16.13** Anterior muscular compartment of the leg

| Muscle | Origin | Insertion | Action |
|---|---|---|---|
| Tibialis anterior | Upper half lat tibia and interosseous memb | Med cuneiform and base of 1st MT | Dorsiflexes and everts the foot; maintains longitudinal plantar arch |
| Extensor hallucis longus | Middle half ant tibia | Base distal phalanx great toe | Extends big toe and supports longitudinal plantar arch |
| Extensor digitorum longus | Upper 2/3 ant fibula and interosseous memb | Extensor hood lat four toes | Extends toes and ankle |
| Peroneus tertius | Lower anterior fibula | Proximal 4th–5th MT | Extends and everts foot |

**Table 16.14** Peroneal muscular compartment of the leg

| Muscle | Origin | Insertion | Action |
|---|---|---|---|
| Peroneus longus | Upper 2/3 fibula and head | Plantar surface of med cuneiform and base of 1st MT | Plantar flexes and everts foot; maintains plantar arches |
| Peroneus brevis | Lower 2/3 fibula | Tuberosity base 5th MT | Dorsiflexes and everts foot; supports lat long plantar arch |
| Peroneus quartus (accessory muscle) | Variable: from the peroneal muscles | Variable: calcaneus, cuboid or peroneal muscles | Postulated to stabilize hindfoot pronation (requirement of bipedal posture) |

# Nerves and vessels

## Tibial nerve and posterior tibial artery

- The tibial nerve is the largest branch of the sciatic nerve and runs with the posterior tibial nerve (Fig. 16.39).
- Proximally, they run deep to soleus, resting on tibialis posterior.
- Distally, they become superficial occasionally covered by FHL.
- Run deep to the flexor retinaculum between FDL and FHL.
- Post tibial artery is medial to tibial nerve from mid leg down to hindfoot.

## Sural nerve

- Branch of tibial nerve.
- Joined by the sural communicating nerve from the common peroneal nerve.
- Superficial to the gastrocnemius heads.
- Runs superficially alongside short saphenous nerve posterior to lateral malleolus.

## Peroneal nerves

- Common peroneal nerve winds around the fibular neck deep to peroneus longus to divide into deep and superficial peroneal nerves.
- Deep peroneal nerve runs with anterior tibial artery within the peroneal compartment on the anterolateral tibial surface.
- Superficial peroneal nerve exits the peroneal compartment to become subcutaneous in the distal third of the leg.

## Peroneal artery

- Peroneal artery arises from the post tibial artery or popliteal trifurcation to run along the medial fibular crest in the post muscular compartment.

## Anterior tibial artery

- Terminal branch of the popliteal artery arising at the inferior edge of the popliteus.

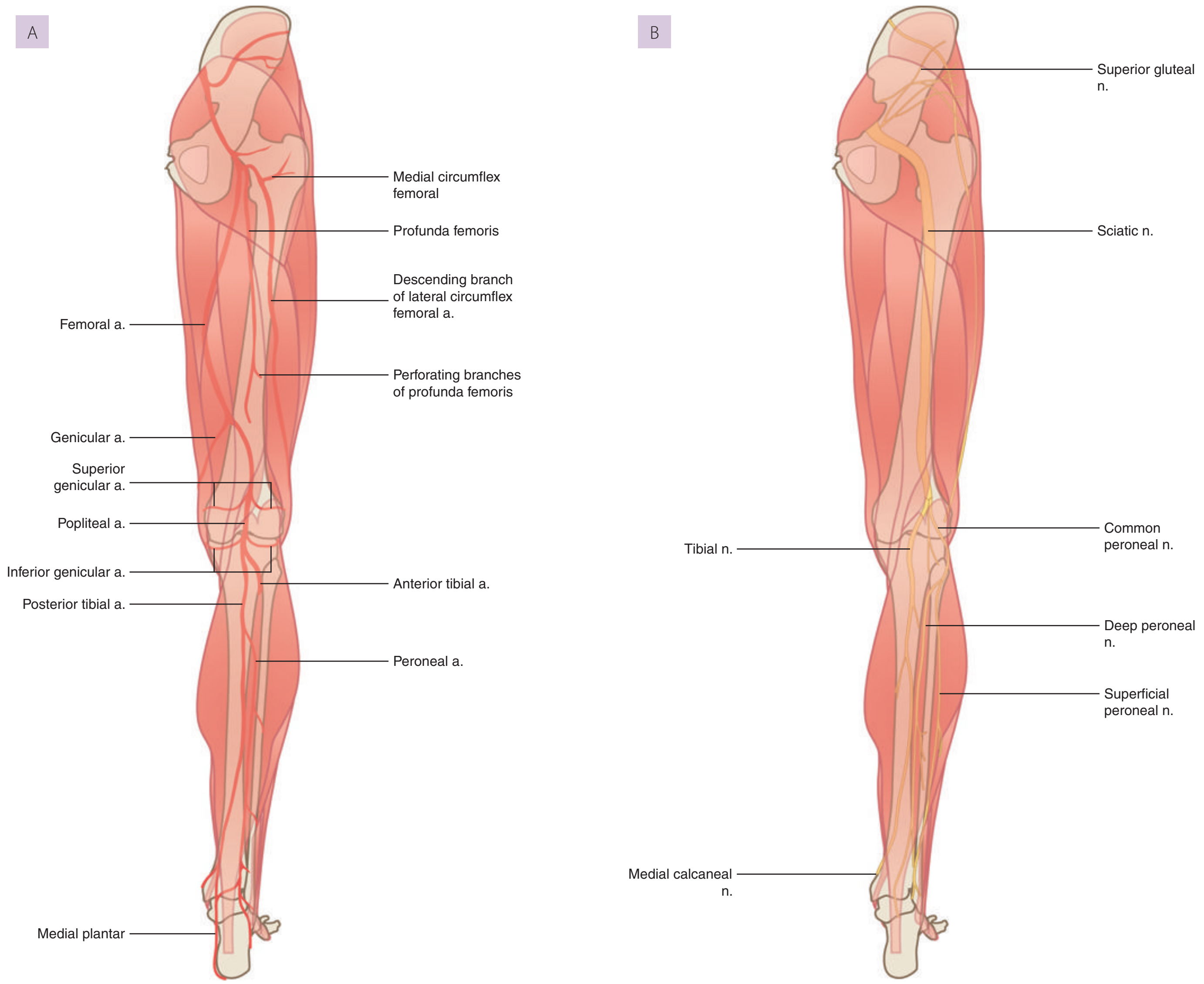


**Fig. 16.39** Vessels and nerves in the leg.

- Crosses over the superior edge of the interosseous membrane to run along its anterior surface.
- Enters the foot deep to the extensor retinaculum midway between the malleoli to become the dorsalis pedis artery lying deep and medial to extensor digitorum longus.

# The ankle and foot

## Bone anatomy

### The ankle

The ankle joint is formed by the talus and the ankle mortise formed by the tibia (inferior articular surface and medial malleolus) and the lateral malleolus (Fig. 16.40). The tibia and talus are wider anteriorly, conferring on the tibiotalar joint increased stability and reduced rotational movement during dorsiflexion.

### Tarsal bones

The tarsus is composed of seven bones arranged in three rows:

- proximal row: talus, calcaneus
- middle row: the navicular
- distal row: three cuneiforms medially and the cuboid laterally.

### Talus

- The talus has no muscle attachments.
- The body lies between the malleoli and has a convex superior articular surface (talar dome) for the tibiotalar joint.
- The posterior process is grooved and may be separate as the os trigonum.
- The neck is grooved inferiorly to form the sinus tarsi.
- The head articulates with the navicular bone.
- The long axis of the talus points along the line of the 1st metatarsal after the age of 5 years.


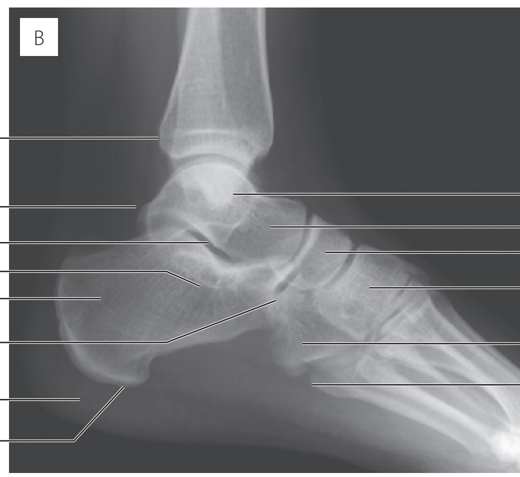


**Fig. 16.40** Plain radiographs of the ankle. Frontal (A) and lateral (B) views.

- The talar inferior surface has three articular facets for the calcaneum and one for the plantar ligament.
  - The larger oval posterior talocalcaneal articular facet is on the plantar aspect of the body and is separated, by the sinus tarsi, from the remainder of the articular facets in the head.
  - The talar head contains the middle and anterior talocalcaneal articular facets and, medially, a facet for the spring ligament. They are continuous with the talonavicular facet on the anterior convex surface of the talar head.

### Calcaneus

- Largest tarsal bone with a shelf-like medial projection, the sustentaculum tali, and a peroneal tubercle on the lateral surface (Figs. 16.41, 16.42).
- Calcaneal long axis points forward and laterally.
- Its superior surface bears three articular facets which correspond with the facets on the talus: the posterior and middle facets are separated by a groove, the sulcus calcanei, which together with the sulcus tarsi form the sinus tarsi. The middle facet lies on the sustentaculum tali and may be continuous with the anterior facet, similar to those in the talus.
- The calcaneal tuberosity is the posterior attachment for the plantar aponeurosis.
- The anterior tubercle is anterior and serves as attachment for the long plantar ligament.
- Heel pad thickness between the tuberosity and the skin is 21 mm in the female and 23 mm in the male.
- The posterior surface is the site of attachment of Achilles tendon.

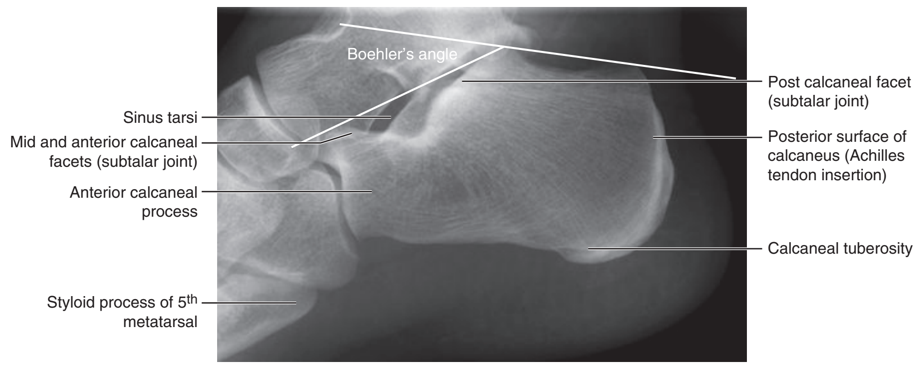


**Fig. 16.41** Calcaneus lateral plain radiograph.

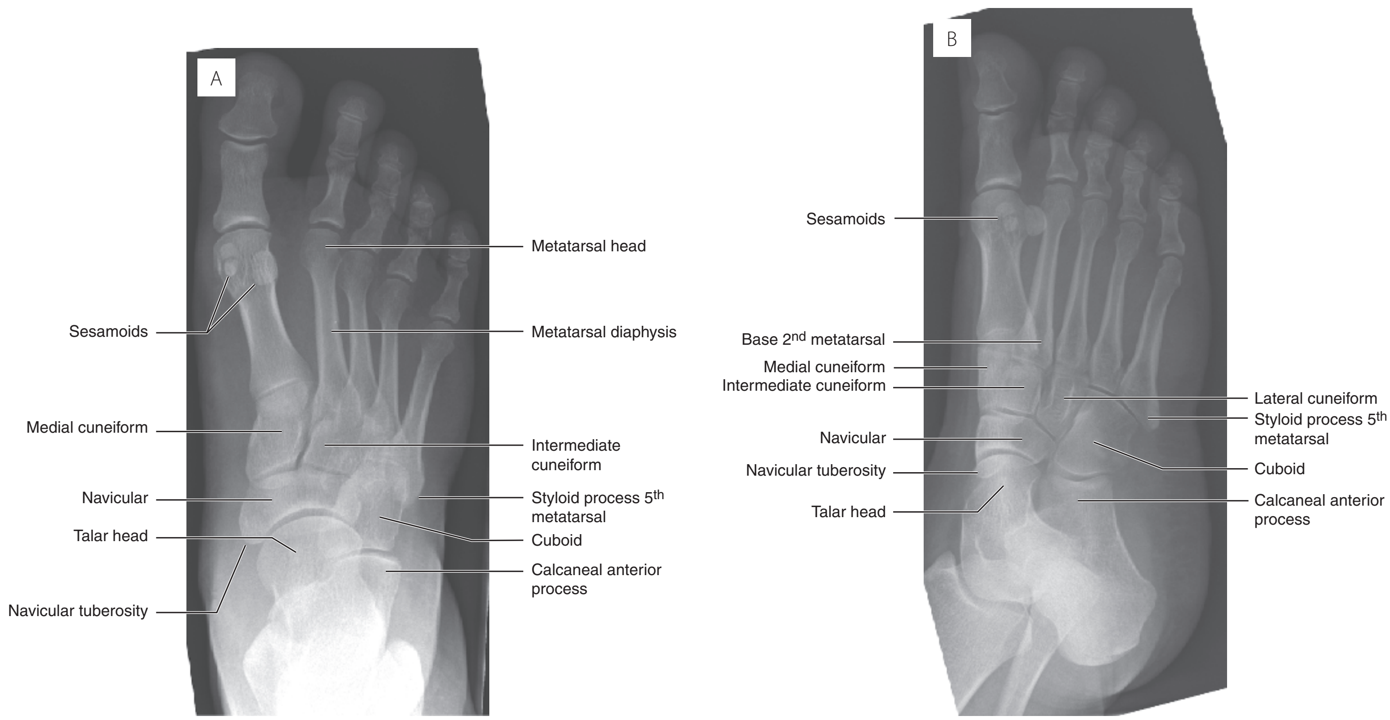


**Fig. 16.42** Foot plain radiographs. Frontal (left) and oblique (right) views.

- Boehler's calcaneal critical angle (30° to 35°) is the angle between two lines drawn from the posterior end of the superior articular surface of the calcaneus: the first posteriorly to the posterosuperior calcaneal corner and the second, anteriorly, to the anterior end of the superior calcaneal surface. If less than 28° it denotes structural damage of the calcaneus.

## Navicular

- The large posterior surface articulates with the talar head.
- Three smaller anterior facets articulate with the cuneiforms.
- Occasionally, a lateral facet articulates with the cuboid.
- The medial tuberosity is part of tibialis anterior tendon insertion.

## Cuneiforms

- The medial, intermediate and lateral cuneiform bones are wedge-shaped and articulate with the first, second and third metatarsal bases, respectively. The collateral surfaces of these bones are therefore aligned across the tarso-metatarsal joints.

## Cuboid

- Grooved laterally and inferiorly by peroneus longus tendon.
- It articulates distally with the 4th and 5th metatarsals, proximally with the calcaneus, and occasionally with the navicular medially.

### Metatarsals and sesamoids

- The metatarsals have a base, for articulation with the tarsal bones, a shaft, a neck and a head for articulation with the proximal phalanges.
- The first metatarsal is thickest and shortest and bears two articular facets on the plantar aspect of the head for a pair of sesamoid bones within the flexor hallucis brevis tendons. The sesamoids may be bipartite when the sum of the two parts is larger than the accompanying unipartite sesamoid bone. This feature is not seen in a fractured sesamoid.
- The base of the fifth metatarsal bears a styloid process for attachment of the peroneus brevis tendon. When ossified separately, the physis is longitudinal to the bone, unlike a fracture, which commonly runs transversely.
- A number of sesamoid bones (bones within a tendon) and accessory ossicles (unfused ossification centres) may be encountered (Fig. 16.43).

### Phalanges

There are two phalanges in the hallux and three in the other toes. The hallux is often adducted (Fig. 16.44).

## Ankle joint

### Articular surfaces

- Lower tibial surface and the inner surface of the medial malleolus.
- Inner surface of the lateral malleolus.
- The trochlear surface of the talus is wider anteriorly, providing more stability during dorsiflexion (standing) (Fig. 16.45).

### Capsule

- Attaches to the articular margins except where it extends to include the talar neck.

### Synovium

- Lines the capsule and extends up between the distal ends of the tibia and fibula.

### Ligaments

- The ankle is strengthened by strong collateral ligaments but it is weak anteriorly and posteriorly.
- Deltoid ligament is complex, formed by different bundles and is triangular:
  - the apex attaches to the medial malleolus tip

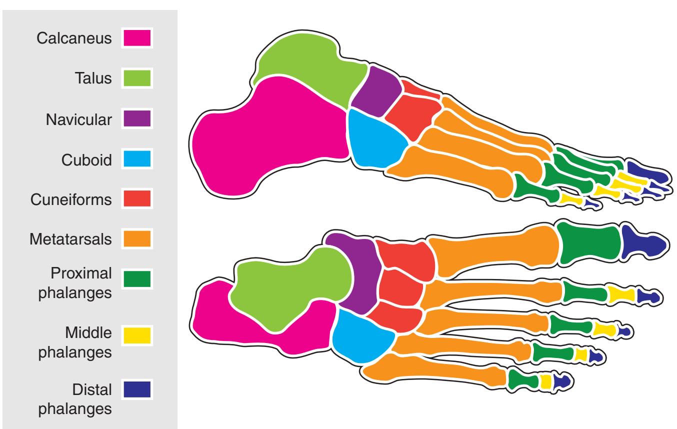


**Fig. 16.43 a** Foot bones, accessory ossicles and sesamoid bones.

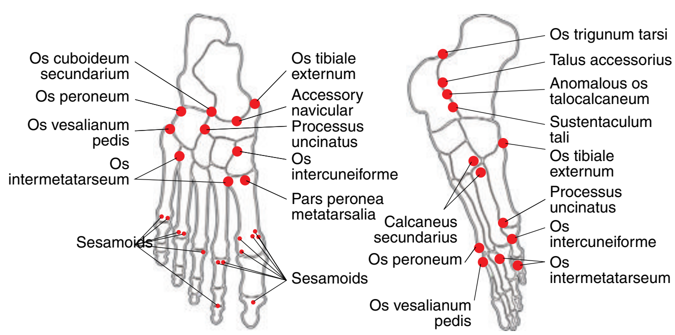


**Fig. 16.43 b** Foot bones, accessory ossicles and sesamoid bones.

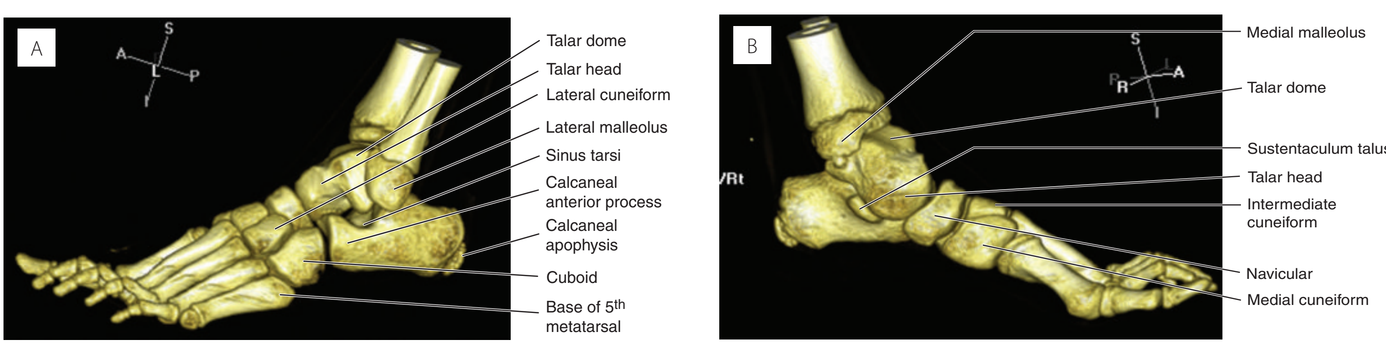


**Fig. 16.44** Surface-shaded 3D CT of the foot.

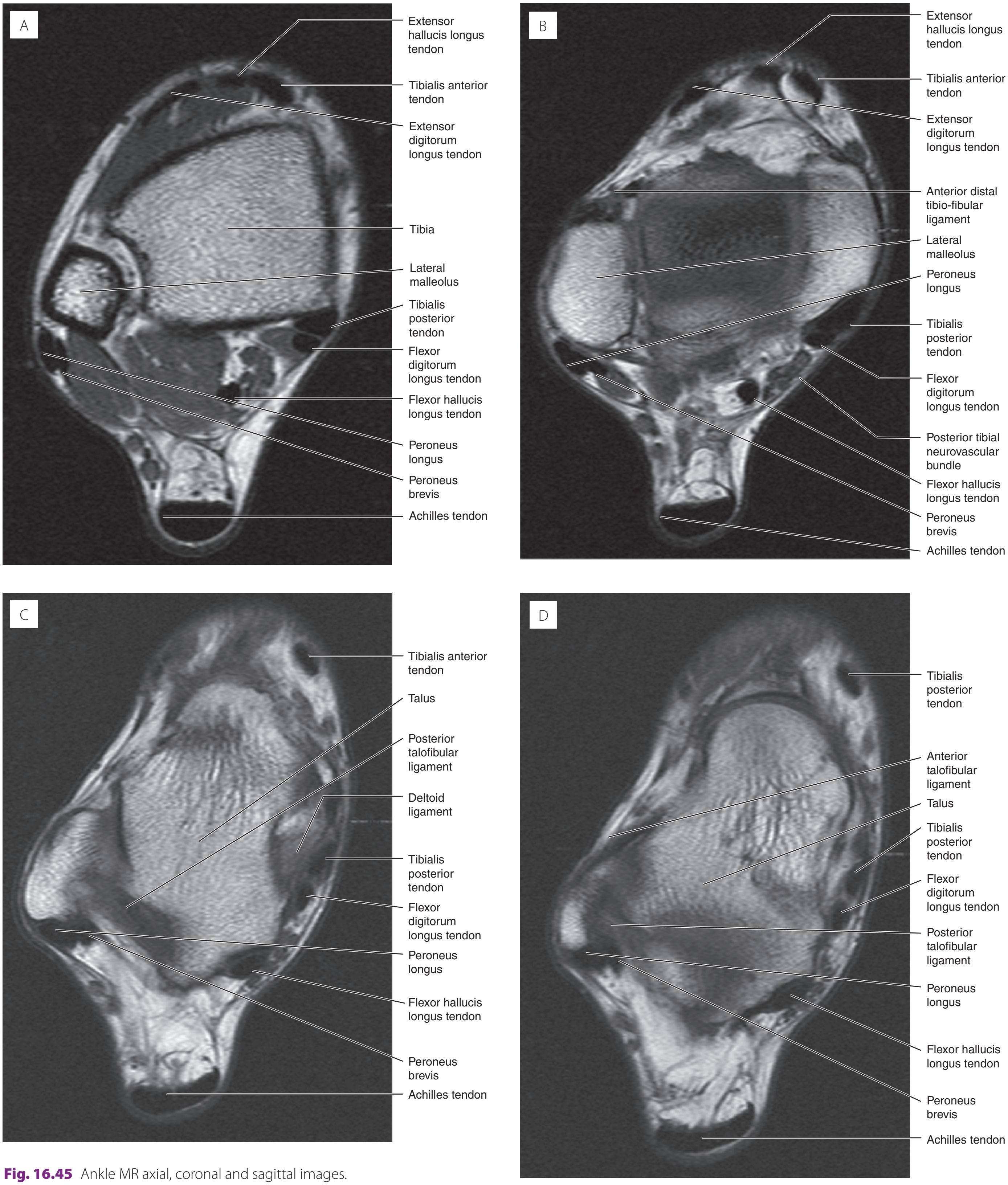


**Fig. 16.45** Ankle MR axial, coronal and sagittal images.

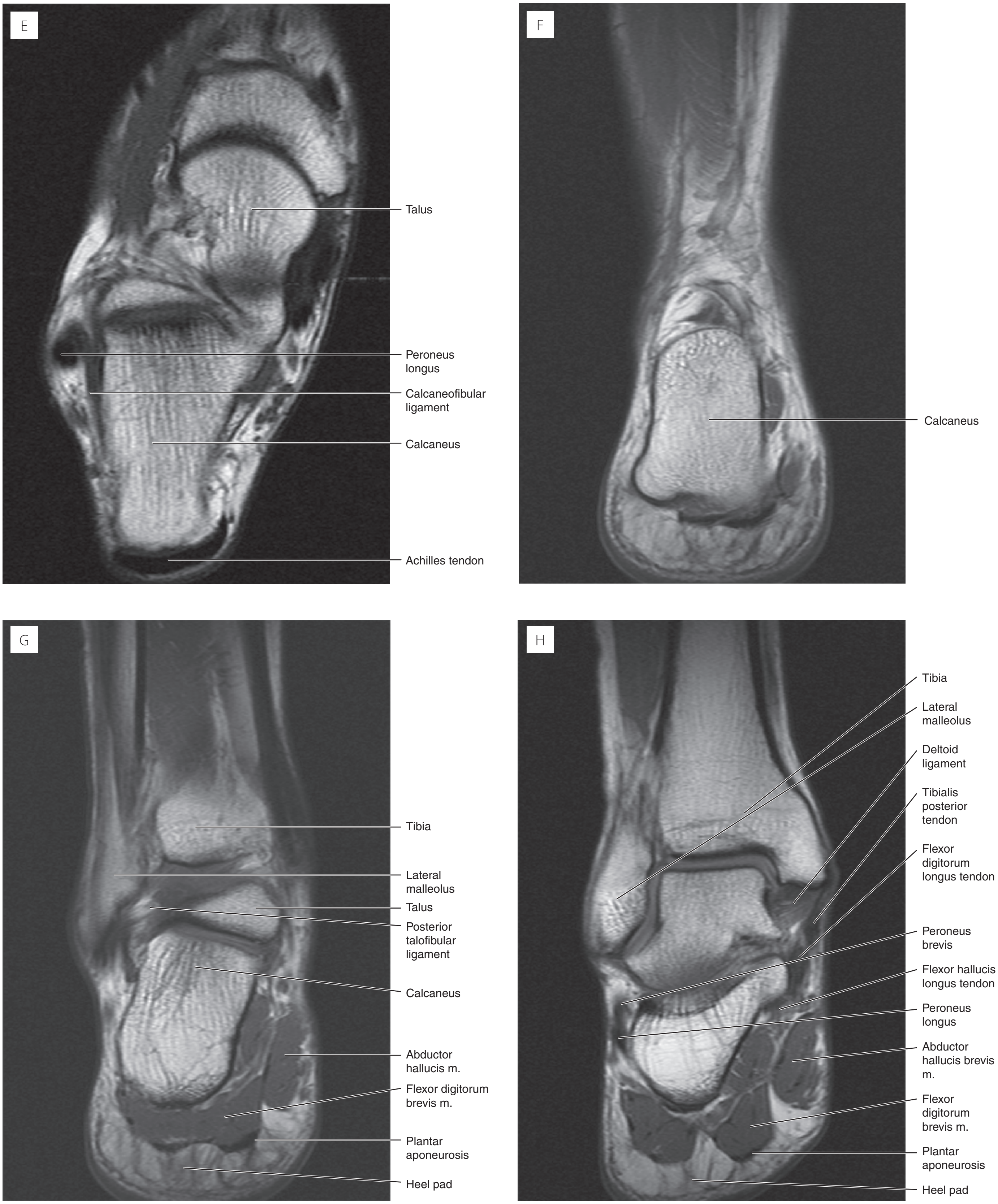


**Fig. 16.45** *(cont.)*

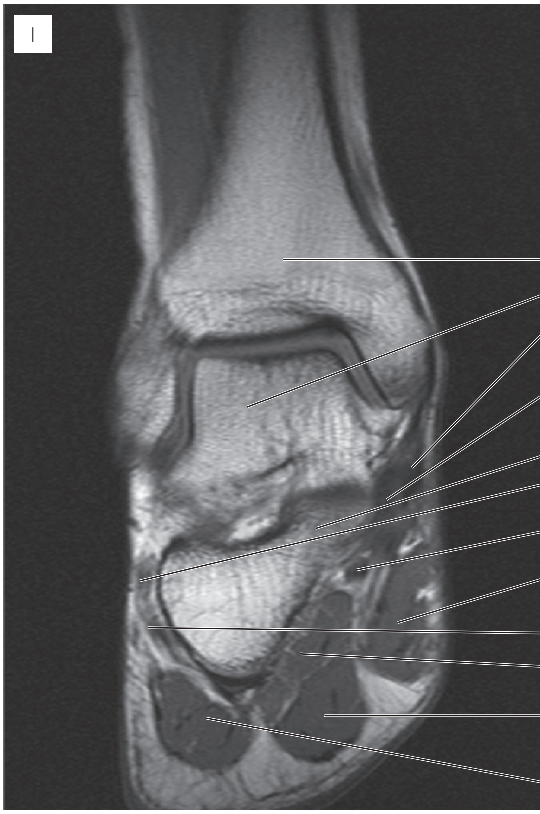


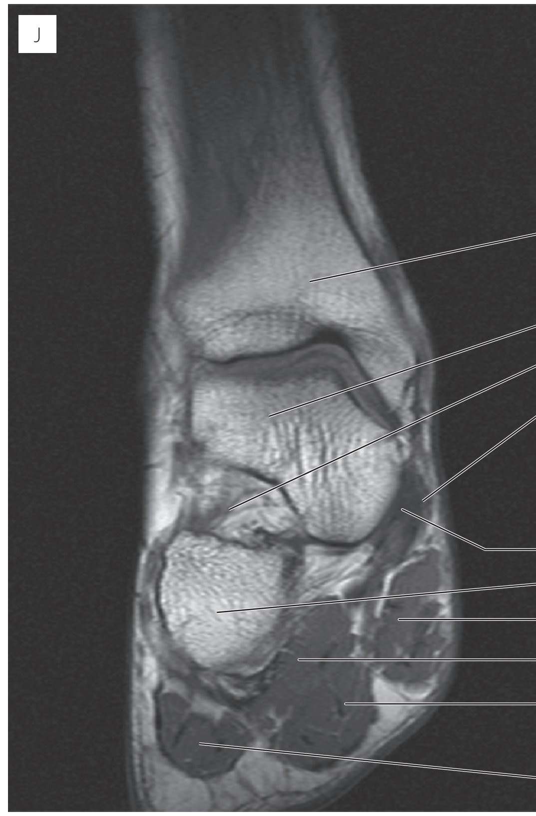


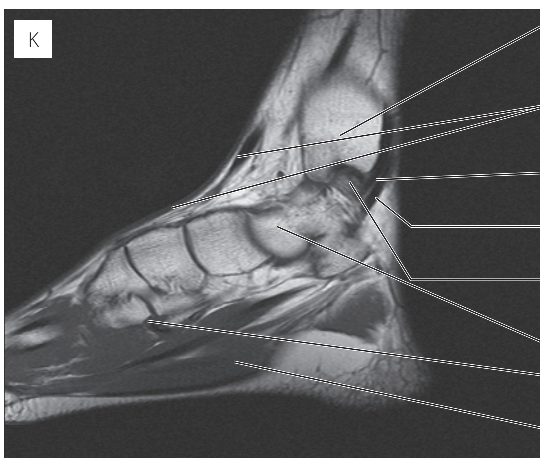


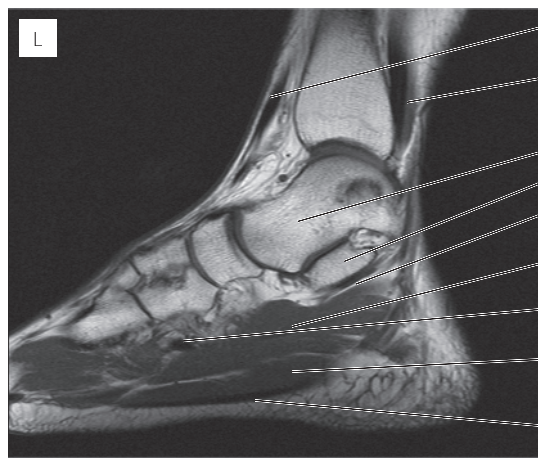


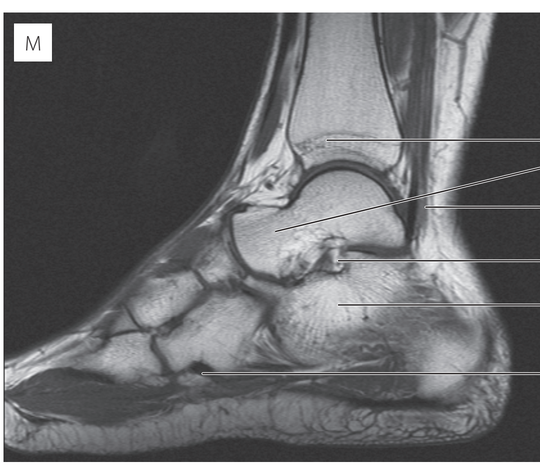


**Fig. 16.45** *(cont.)*

  - the base originates from the medial aspect of the talus (anteriorly and posteriorly), sustentaculum tali and the navicular tuberosity.
- All lateral ligaments originate from the lateral malleolus.
- Anterior talofibular ligament (ATFL) is anteromedial, inserting into the lateral surface of the talar neck.
- Calcaneofibular ligament (CFL) is cord-like and runs from a depression anterior to the fibular apex to a tubercle on the lateral surface of the calcaneus.
- Posterior talofibular ligament (PTFL) passes medially from the malleolar fossa (lateral malleolus) to the posterior talar process.

- The sequence usually followed during traumatic injury of the lateral ligaments is ATFL, CFL and PTFL.

## Retinacula

Thickenings of deep fascia preventing bowstringing of tendons as they cross the tibiotalar joint.

### Extensor retinaculum

- Superior and inferior bands.
- Superior band attaches to the distal end of the anterior aspect of the tibia and fibula.
- Inferior band is Y-shaped: the stem is lateral and attaches to the upper surface of the calcaneus. The medial arms attach to the plantar aponeurosis and the medial malleolus.
- Retinacula bind the following tendons: the tibialis anterior (TA) tendon is larger than the extensor hallucis longus (EHL) and extensor digitorum longus (EDL). They are rarely affected by pathology.
- The TA tendon is the only tendon with a synovial sheath deep to the superior extensor retinaculum (Fig. 16.46).

### Flexor retinacula

- Flexor retinacula roof the tarsal tunnel (Fig. 16.47) and insert into the tip of the medial malleolus and the medial calcaneal process and plantar aponeurosis.
- The tendons travel through independent fibro-osseous tunnels.
- The tibialis posterior (TP) tendon is larger (4–6 mm) than the more posterior flexor digitorum longus (FDL) and flexor hallucis longus (FHL).

### Long flexor tendons

- Distal TP tendon expands as it inserts into the navicular and spring ligament and loses its synovial sheath just proximal to its insertion, where a small volume of tenosynovial fluid is normal.
- FHL grooves the posterior aspect of the calcaneum and talus and lies below the sustentaculum tali.
- FHL and FDL cross at the knot of Henry in the sole of the hindfoot.
- The distal FDL lies superficially between the sesamoid bones of the MTPJ of the big toe.

### Peroneal retinacula

- The superior peroneal retinaculum runs from the posterior edge of the lateral malleolus to the lateral calcaneus (Fig. 16.48).
- The inferior peroneal retinaculum is continuous with the inferior extensor retinaculum and also attaches to the lateral calcaneus.
- A fibrous band from the retinaculum reaches the peroneal tubercle separating the peroneus longus and brevis tendons.

### Peroneal tendons

- The musculotendinous junction of the peroneus brevis (PB) may be low-lying and appear larger than the peroneus longus (PL) tendon.

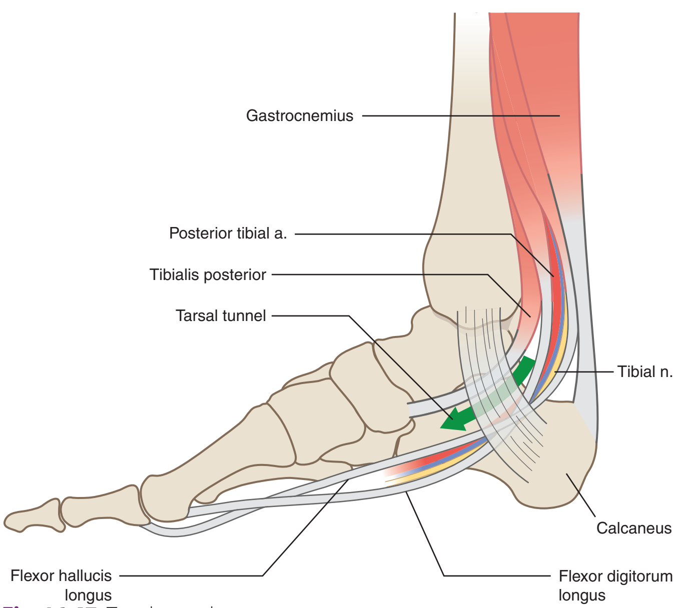

**Fig. 16.47** Tarsal tunnel.

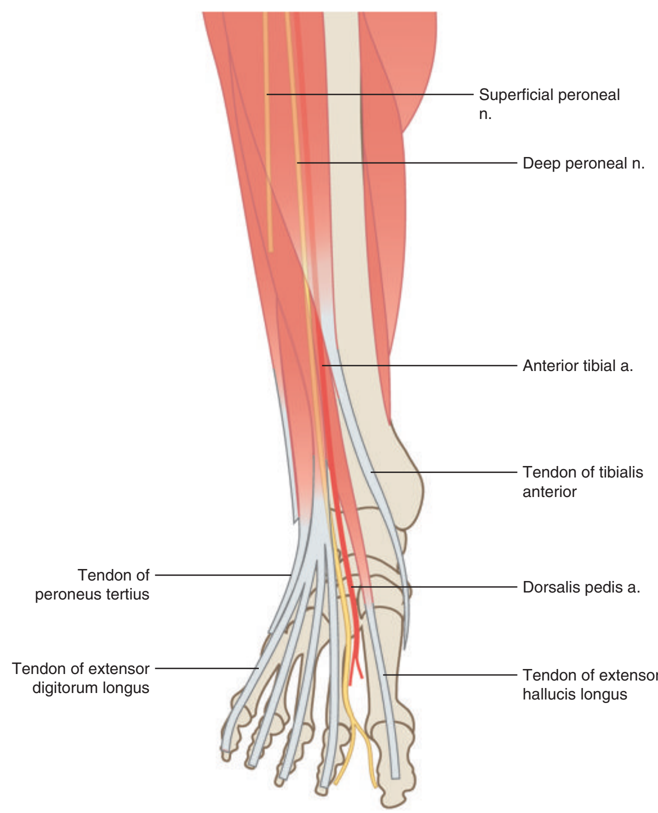

**Fig. 16.46** Extensor retinacula.

- PB is deep to PL as they pass deep to the retinaculum and is liable to attrition, injury and longitudinal splits.
- The PB tendon attaches into the tuberosity of the base of the fifth metatarsal.
- The PL tendon grooves the cuboid, is deep to the long plantar ligament and the complex attachment includes the plantar surface of the medial cuneiform and base of the 1st metatarsal.

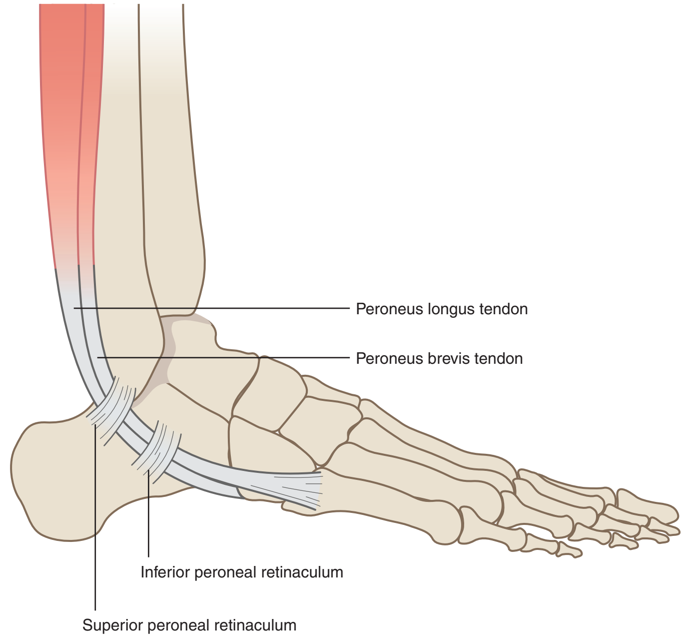


**Fig. 16.48** Peroneal retinaculae.

## Foot joints

### Subtalar joint

- The subtalar joint is a compound, multiaxial joint allowing inversion and eversion of the foot (Fig. 16.49).
- Consists of two parts with their own capsule and synovial cavity:
  - the talocalcaneal joint between the posterior facets
  - the talocalcaneonavicular joint, which has contiguous parts formed between the following:
    - middle talar facet and sustentaculum tali
    - anterior talar facet and spring ligament
    - talar head and navicular bone.
- Stability is provided by the articulating bony contours, the spring ligament and tarsal ligaments:
  - the spring ligament (plantar calcaneonavicular) is a broad thick slinglike structure attaching to the calcaneum and navicular and wraps under the talar head
  - the spring ligament reinforces the talocalcaneonavicular joint, supports the head of the talus and the medial longitudinal arch of the foot.

### Calcaneocuboid joints

The calcaneocuboid joint is stabilized by intertarsal and plantar ligaments.

### Tarsometatarsal joints

The tarsometatarsal joints (TMTJ) allow limited gliding movements and are stabilized by dorsal and plantar ligaments, and interosseous ligaments such as the Lisfranc ligament running from the medial cuneiform to the 2nd metatarsal.

Injuries to the TMTJ or Lisfranc joint, though rare, may be undiagnosed or inadequately treated, resulting in poor long-term outcomes. Plain radiography may reveal loss of the alignment of the cuneiforms and metatarsals

### Metatarsophalangeal joints

The metatarsophalangeal joints (MTPJ) are reinforced by collateral, plantar and deep transverse metatarsal ligaments. The latter two blend into each other and are continuous with the volar plate on imaging.

### Interphalangeal joints

The interphalangeal joints are hinge joints stabilized by collateral and plantar ligaments.

## Dorsum of foot

- The extensor digitorum brevis (EDB) is the only intrinsic dorsal muscle.
- The EDB is deep to the extensor digitorum longus tendons and forms four tendons fusing with the extensor hoods of the medial four toes.
- The extensor hood is a tendinous expansion at the level of the MTPJ and phalanges receiving contributions from the EHL, EDL, EDB, lumbricals and interosseous muscles.

## Sole of the foot

- The plantar aponeurosis is a thickening of the deep fascia attached to the calcaneal tuberosity and fans out anteriorly to insert into bones, ligaments and dermis of the forefoot. The medial part is thickest, reaching 4 mm.
- The long plantar ligament extends from the plantar surface of the calcaneus to the ridge and tuberosity on the plantar aspect of the cuboid and forms a tunnel for PL tendon.
- The wide short plantar ligament is deep to the long plantar ligament and extends from the calcaneal tubercle to the plantar surface of the cuboid.
- Plantar ligaments limit depression of the longitudinal arch.
- The intrinsic muscles of the sole of the foot are organized into four layers (Fig. 16.51 and Table 16.15).

### Intermetatarsal space

The intermetatarsal neurovascular bundle runs between the third and fourth muscular layers and adjacent to the intermetatarsal bursa (diameter up to 3 mm) (Fig. 16.52).

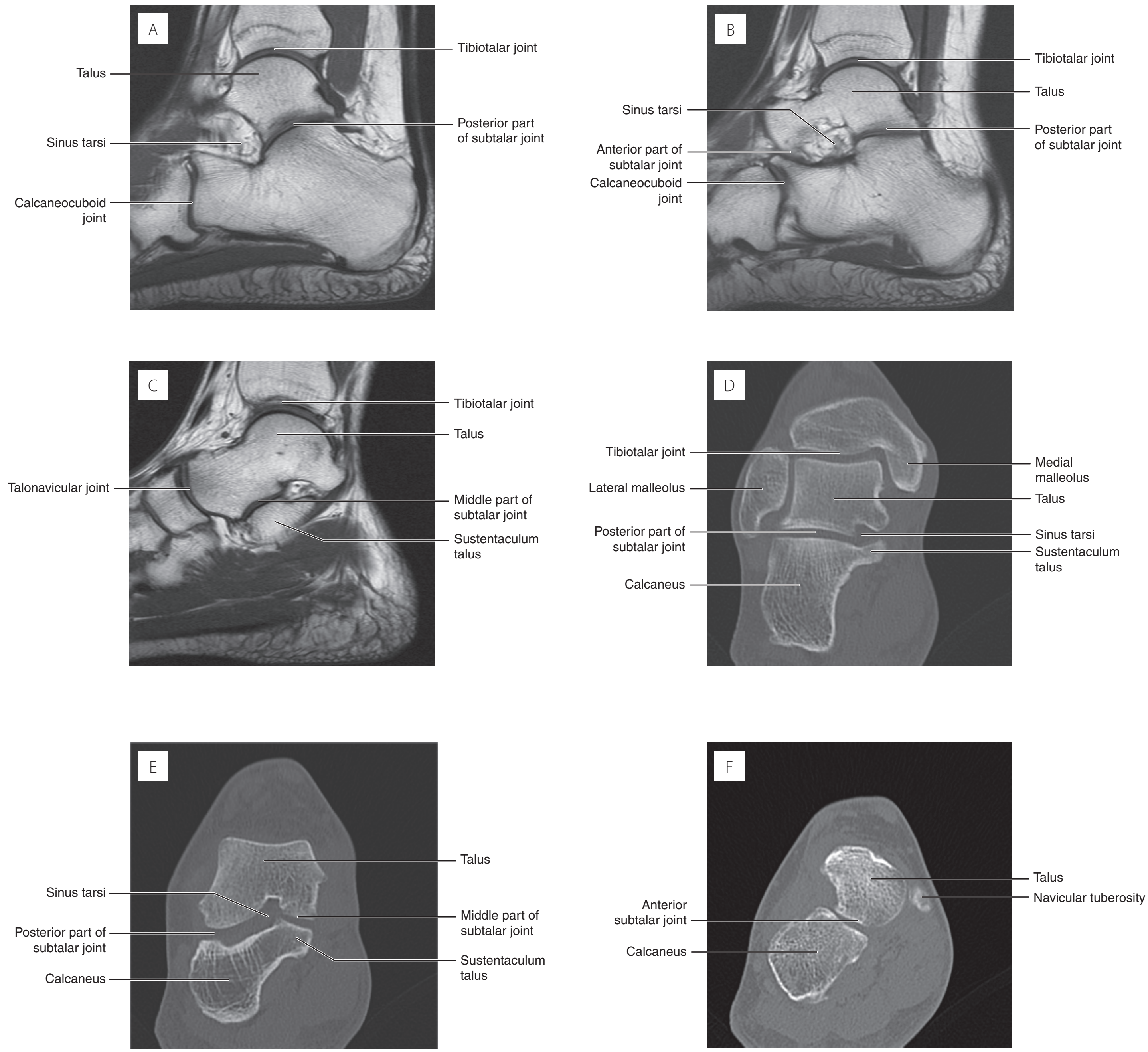


**Fig. 16.49** Subtalar joint: CT coronal (A–C) and MR sagittal (D–F) images.

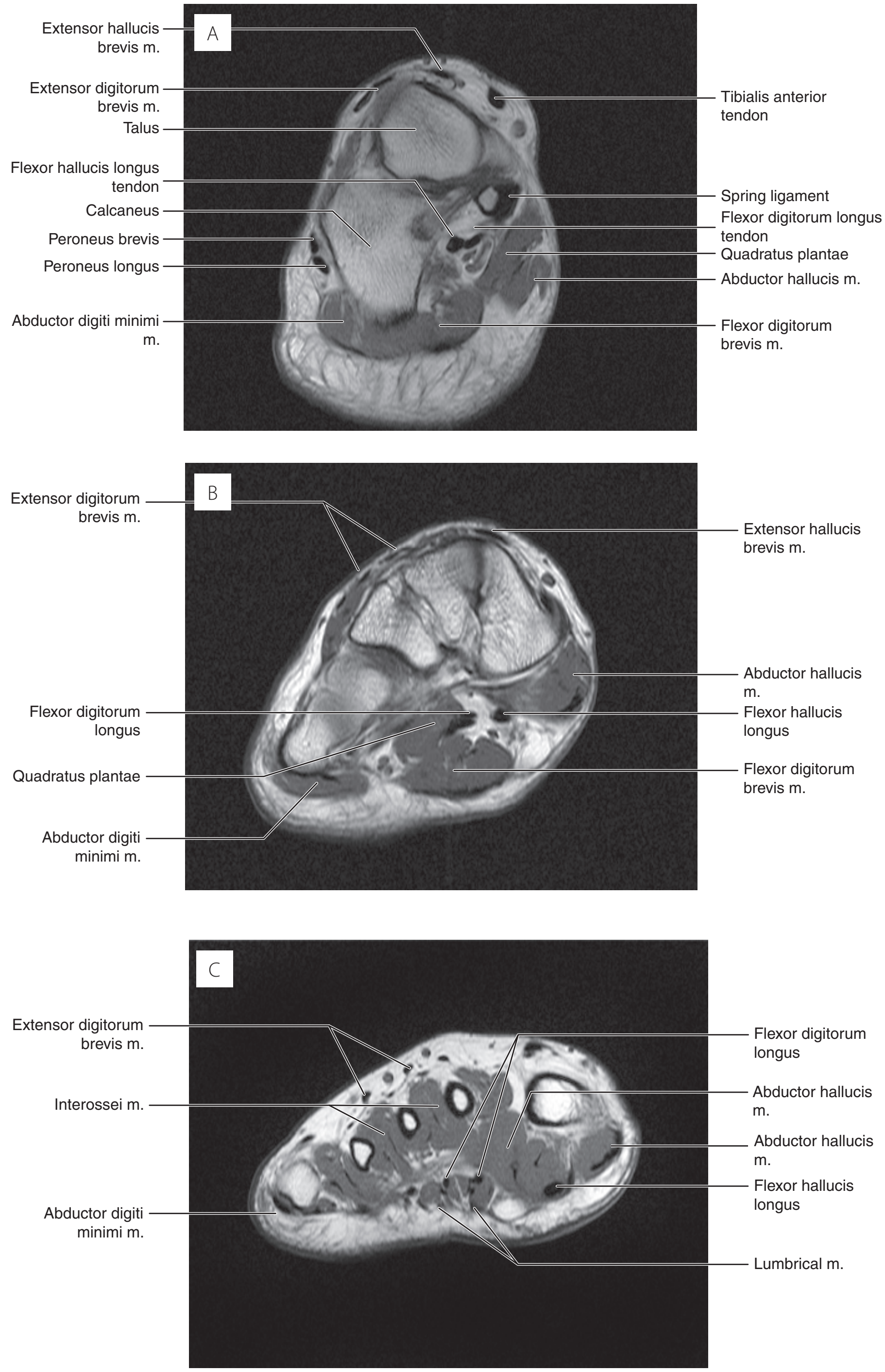


**Fig. 16.50** Foot MR axial and coronal images.

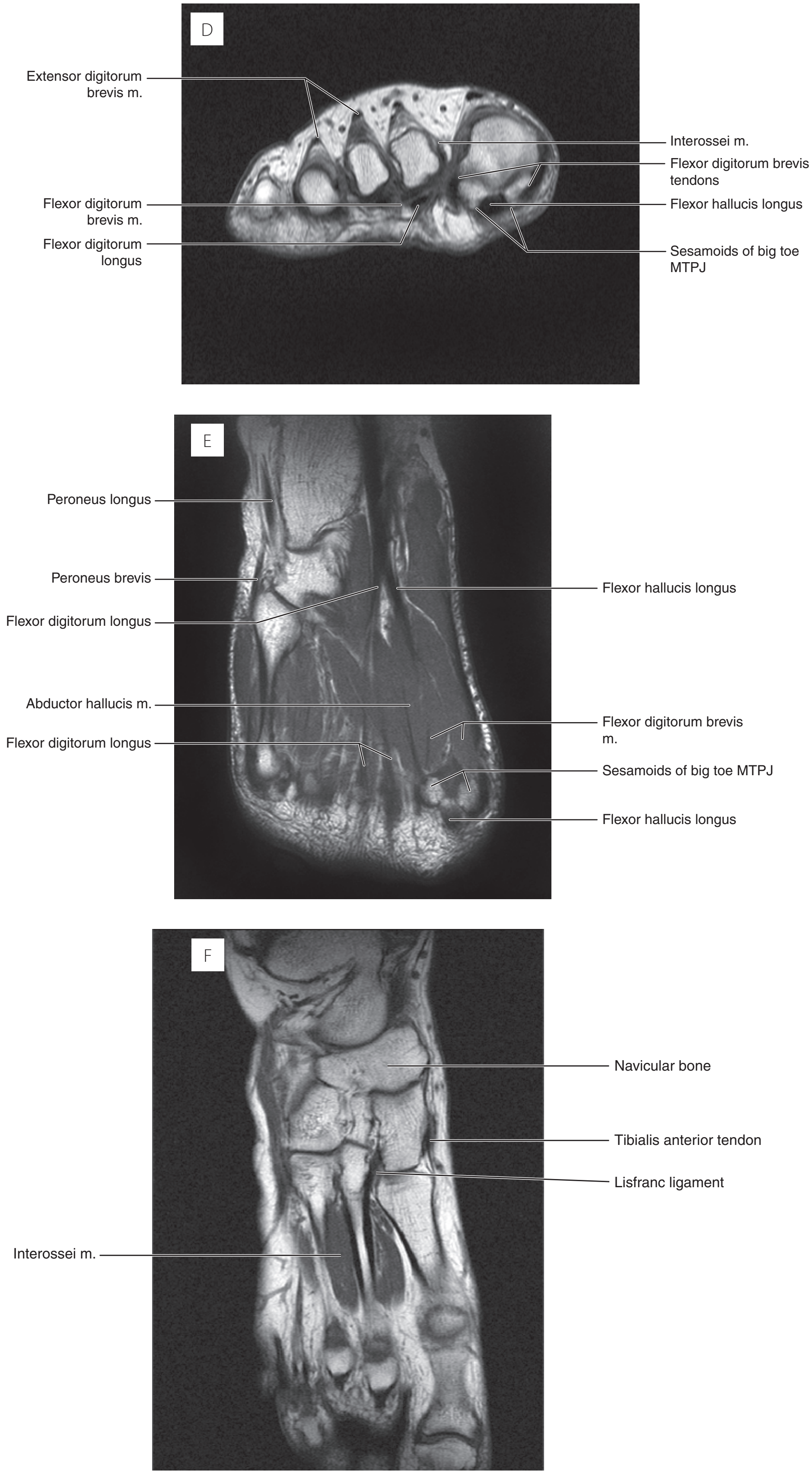


**Fig. 16.50** *(cont.)*

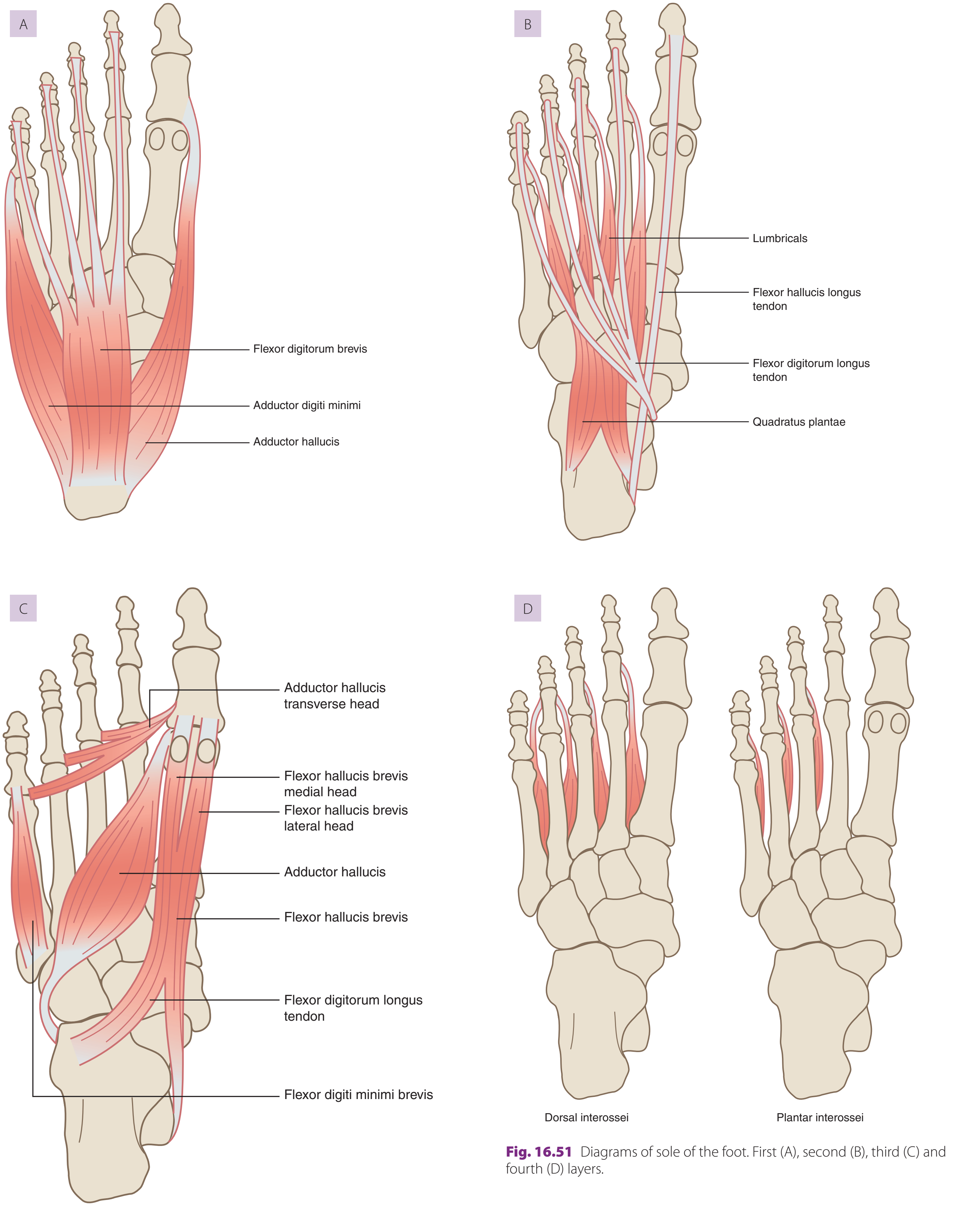


**Fig. 16.51** Diagrams of sole of the foot. First (A), second (B), third (C) and fourth (D) layers.

**Table 16.15** Sole of the foot muscles

| Layer | Muscles | Proximal attachment | Distal attachment | Remarks |
|---|---|---|---|---|
| 1st | Abductor hallucis | Med process of post calcaneal tuberosity | Prox phalanx big toe via med sesamoid | Elastic spring to maintain the plantar arches |
| | Flexor digitorum brevis | | Merges with FDL tendons | |
| | Abductor digiti minimi | Med and lat processes of post calcaneal tuberosity | Lat base of 5th MT and prox phalanx | |
| 2nd | Quadratus plantae | Calcaneus-med and lat surfaces | FDL tendons | Tendon of FHL crosses deep to the FDL tendon at the knot of Henry |
| | Lumbricals | FDL tendons | Extensor hood | |
| | FDL tendons | | | |
| 3rd | Flexor hallucis brevis | Cuboid and cuneiforms | Two tendons to base prox phalanx of big toe via sesamoids | Muscles in the forefoot acting on the great and little toe |
| | Adductor hallucis | Oblique head: base of 2, 3, 4 MTs<br>Transverse head: plantar MT lig | Base of prox phalanx big toe via lat sesamoid | |
| | Flexor digiti minimi | Base 5th MT | Base prox phalanx little toe | |
| 4th | Interossei muscles (dorsal and plantar)<br>TP and PL tendons | Sides of the metatarsals | Extensor hood and proximal phalanges | Resists MTPJ extension and IPJ flexion during gait<br>Toe abduction and adduction<br>Dynamic stabilizers of plantar arches |

## Arches of the foot

- The bones of the foot form longitudinal and transverse arches relative to the ground, which distribute and absorb forces during standing and locomotion.
- These arches rely on ligaments and tendons for stability.
- Dynamic stabilizers: TP (most significant), FHL, ABH and FDB.
- Static stabilizers: spring ligament, deltoid ligament, long plantar ligament and the plantar fascia.
- If the posterior tibial tendon fails, increased forces are transmitted to the static stabilizers of the ankle.

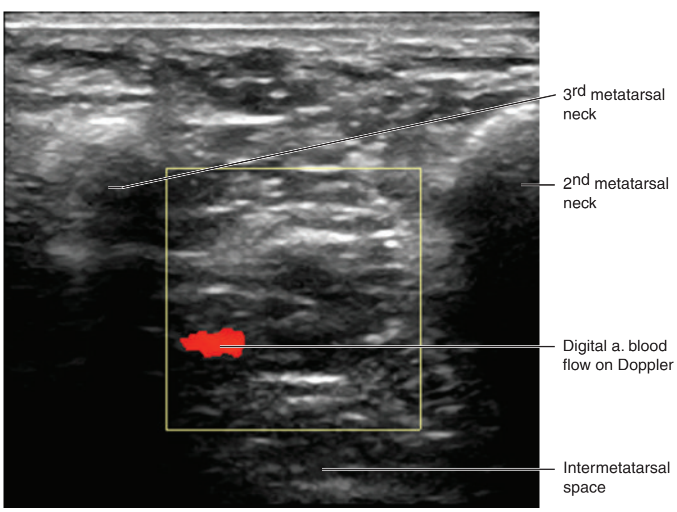


**Fig. 16.52** Sonographic transverse image of the intermetatarsal space.

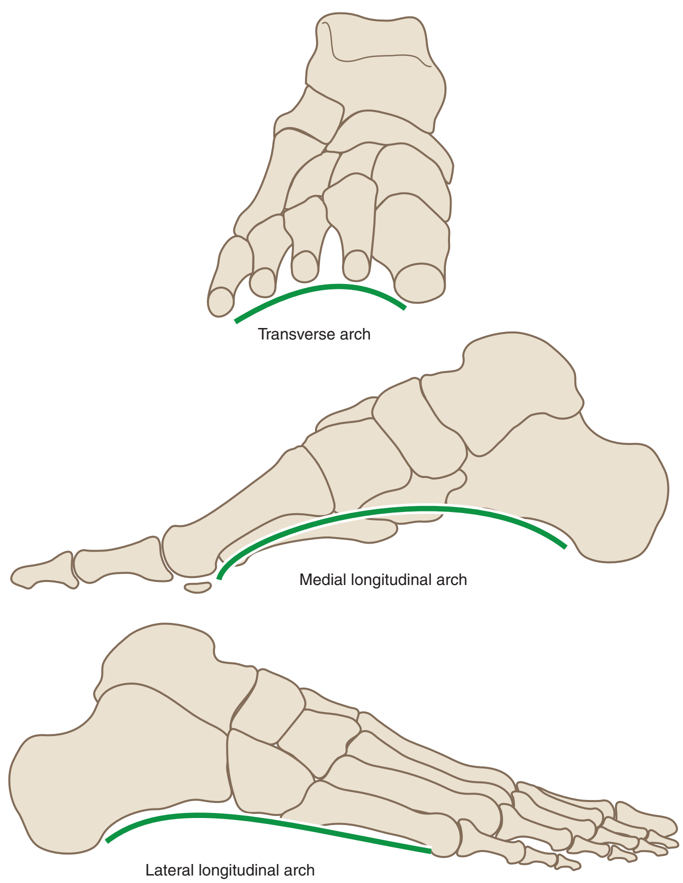


**Fig. 16.53** Diagram of plantar arches.

Chapter 17

# Obstetrical imaging

Ian Suchet

Ultrasound still forms the mainstay of obstetrical imaging. It can be used throughout the entire gestation, resulting in high-resolution real-time two-dimensional (2D) images that can be obtained in any plane. This can be complemented by static three-dimensional (3D) images and motion-enabled four-dimensional (4D) images of the heart and other cardiovascular structures. Ultrasound may be complemented by MRI in the late second or third trimester for evaluating specific fetal or maternal abnormalities.

Indications for obstetric ultrasound are summarized in Table 17.1. The nuchal translucency scan is performed at 11–14 weeks and in the absence of specific indications, the mid-trimester scan should be obtained between 18 and 20 weeks of gestation, when anatomically complex organs such as the heart and brain can be imaged with sufficient clarity to allow detection of malformations.

**Table 17.1** Indications for obstetric ultrasound

| First trimester | Second trimester | Third trimester |
|---|---|---|
| Diagnose an intrauterine pregnancy | Screen for structural fetal anomalies | Evaluation of fetal growth |
| Exclude an ectopic pregnancy | Assess fetal growth | Determine fetal presentation |
| Determine gestational age | Adjunct to amniocentesis or other procedure | Evaluate fetal well-being (biophysical profile score +/– Doppler evaluation) |
| Confirm fetal viability (heart beat) | Placental location | Evaluate cervical insufficiency |
| Determine fetal number and chorionicity in multiple pregnancies | Detect complications in monochorionic pregnancies | Evaluate vaginal bleeding, e.g. suspected placental abruption |
| Detect gross fetal anomalies | Evaluation of suspected fetal demise | Evaluation of suspected fetal demise |
| Evaluate for suspected hydatidiform mole | | Evaluate placental location |
| Nuchal translucency screening – aneuploidy screening | | Evaluate premature rupture of membranes |

## First trimester

The gestational sac can be identified as early as 4 weeks 3 days and can be routinely detected endovaginally after 5 weeks. There is an echogenic rim of tissue surrounding the gestational sac (Fig. 17.1) comprising the:

- decidua basalis (DB) = beneath the implanted embryo; it is here that the placenta subsequently develops
- decidua capsularis (DC) = covers the rest of the chorionic sac
- decidua parietalis (DP) = endometrial reaction which lines the uterine cavity (UC) and is not involved in implantation.

The interface between the deciduas and bright well-vascularized endometrium is called the double decidual reaction and is represented by two concentric rings or crescents around the gestational sac. This implies that this is a true gestational sac associated with an intrauterine pregnancy.

The embryonic pole (CRL) can be distinguished at 5 weeks and 3–4 days (Fig. 17.2). The embryo measures ± 2 mm and grows 1 mm/day. Cardiac activity begins at 5 weeks 2 days, but may not be appreciated until the embryo reaches 5 mm in size (6 weeks 4 days). The amniotic cavity surrounding the embryo is not visualized as a separate structure as it is closely applied to the embryo.

By 6 weeks of gestation (Fig. 17.3) the gestational sac reaches 15.5 mm in diameter, and the embryo has a length of 5–5.5 mm and it can be constantly seen as separate from the yolk sac. The heart has two chambers with active slow pulsations (100–110 bpm).

### Week 7 of gestation (Fig. 17.4)

- Gestational sac = 22 mm in length.
- Embryo = 9–15 mm in length.
- The amniotic cavity expands rapidly and from 9 weeks onwards it begins to occupy most of the gestational sac volume.
- Upper and lower limb buds can be visualized. Lower limbs project 90° off the body.

*Applied Radiological Anatomy, 2nd Edition* ed. Paul Butler, Adam W.M. Mitchell and Jeremiah C. Healy. Published by Cambridge University Press.

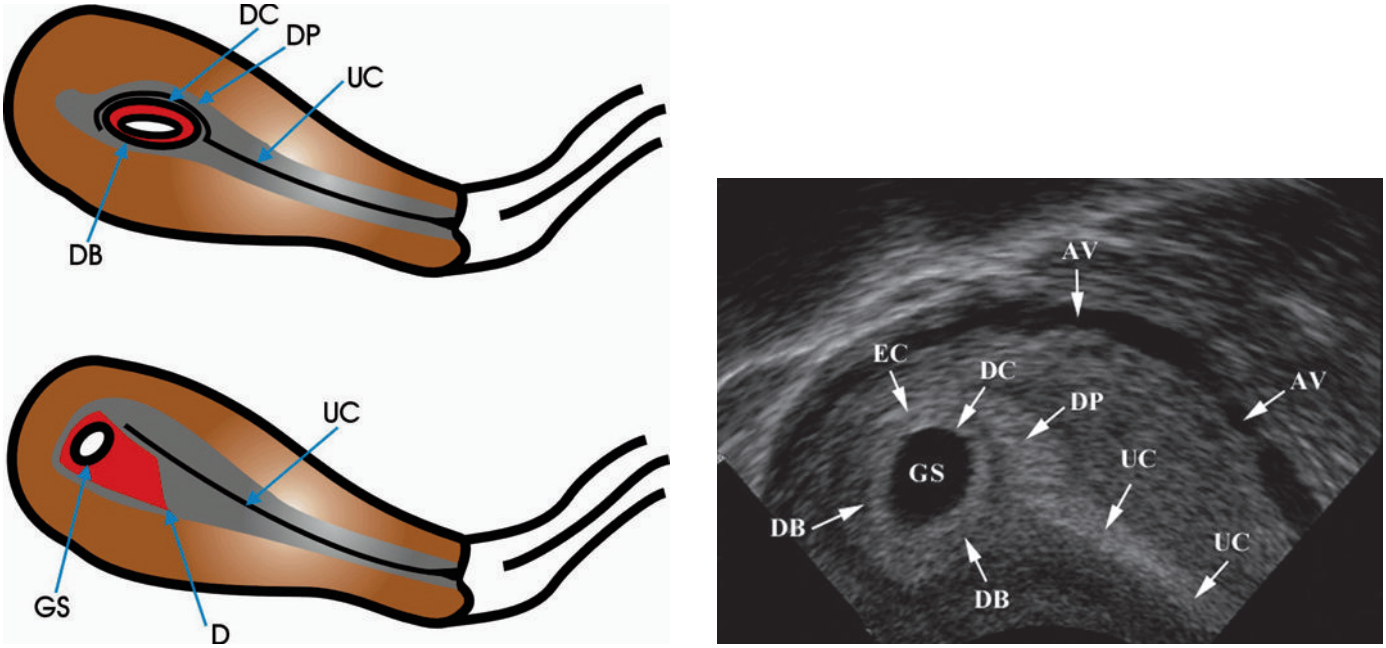


**Fig. 17.1** Transvaginal scan through the uterus at 4 weeks and 4 days. DB = decidua basalis; GS = gestational sac; EC = collapsed endometrial cavity; DC = decidua capsularis; DP = decidua parietalis; UC = uterine (endometrial cavity); AV = arcuate vessels of the uterus.

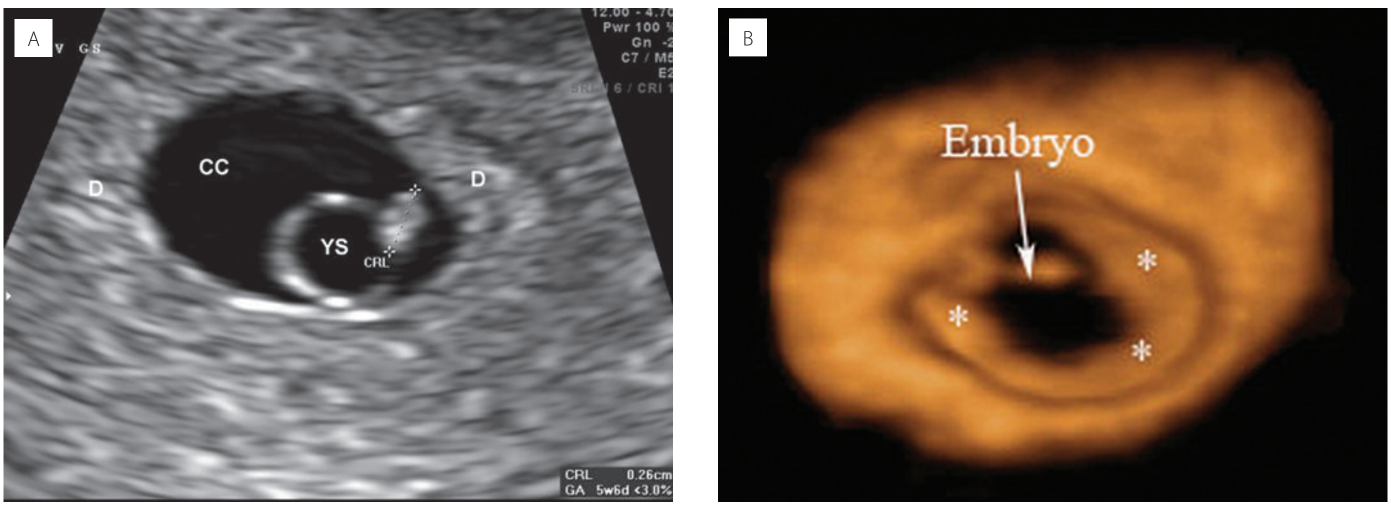


**Fig. 17.2** Two-dimensional (A) and three-dimensional (B) transvaginal scan at 5 weeks of gestation. CRL = crown rump length of embryo; YS = secondary yolk sac; CC = chorionic cavity; D = decidual reaction (*).

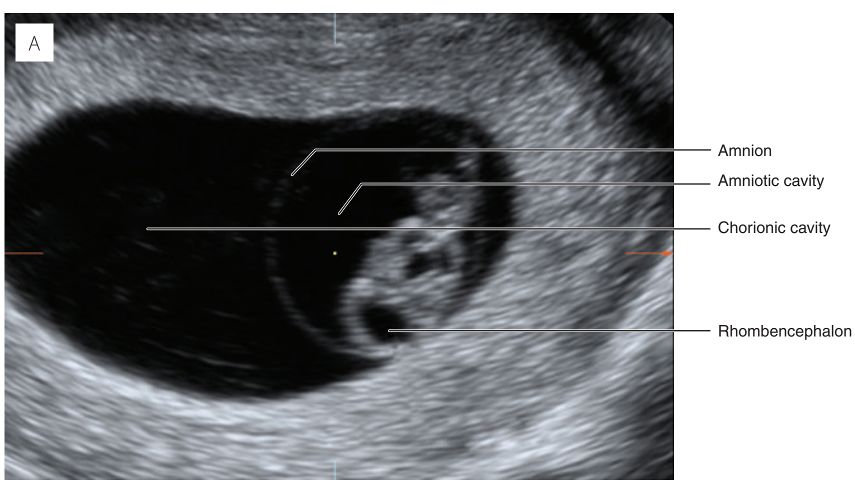


**Fig. 17.3** Two-dimensional (A) and three-dimensional (B) transvaginal scan at 6 weeks of gestation. The amnion and amniotic cavity is first visualized as a separate structure. The more echogenic chorionic cavity surrounds the amniotic cavity. The fluid density structure in the fetal head represents the normal rhombencephalon. The vitelline (allantoic) duct connects the yolk sac to the embryo (between arrowheads) at the umbilicus.

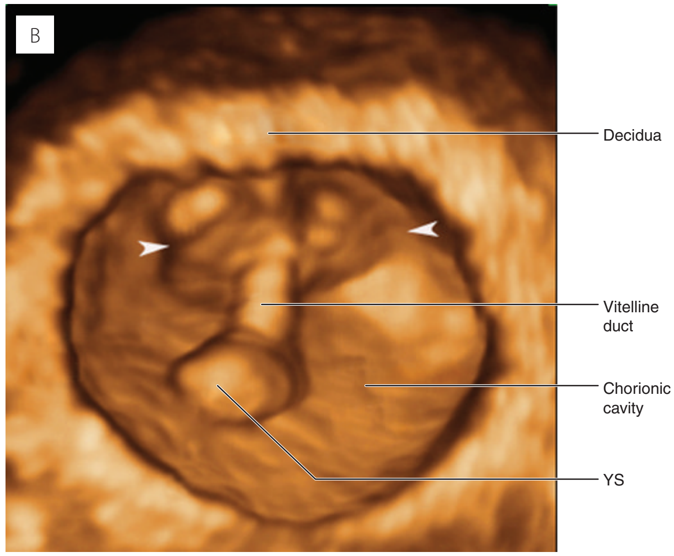


**Fig. 17.3** (*cont.*)

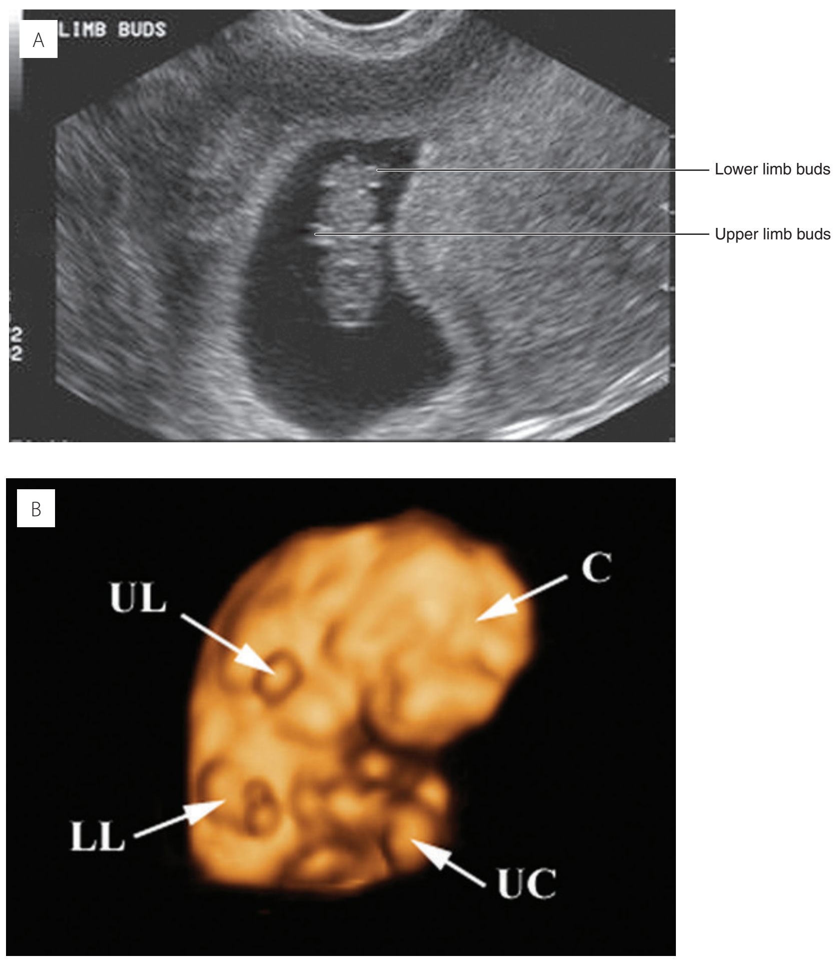


**Fig. 17.4** Two-dimensional (A) and three-dimensional (B) transvaginal scan at 7 weeks of gestation. UL = upper limb; LL = lower limb; C = cranium; UC = umbilical cord.

- Heart
  - ± 2 mm
  - three chambers
  - rate = 112–136 bpm.

## Week 8 of gestation (Fig. 17.5)

- Embryo is ± 30 mm at the end of week 8.
- Head, trunk, limbs and umbilical cord can be appreciated.
- Head size > yolk sac size.
- The developing central nervous system is appreciated by a number of fluid collections.
- Neural tube is imaged as parallel echogenic lines.
- Midgut herniation is present.
- Heart
  - 150–170 bpm (heart rate increases from 6–9 weeks before it starts to decline after week 10).
- Fetal movements (trunk and extremities) are now obvious.

## Weeks 9–12 of gestation (Fig. 17.6)

- The amniotic cavity continues to expand, and ultimately fuses with the chorion.
- The physiological herniation of bowel into the base of the umbilical cord is evident.
- The site of the placenta can now be visualized.
- CRL reaches 40 mm.

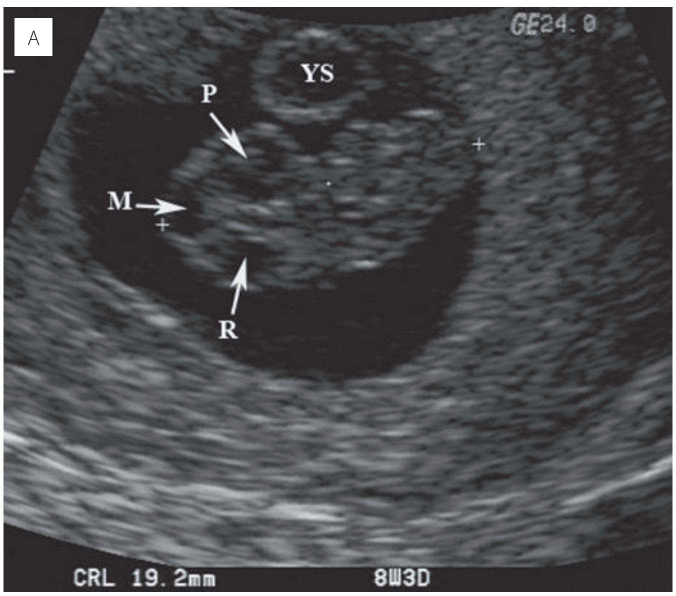


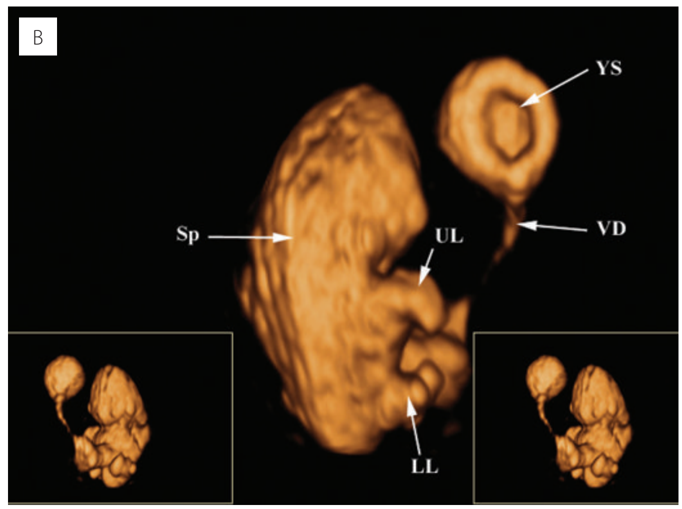


**Fig. 17.5** Two-dimensional (A) and three-dimensional (B) transvaginal scan at 8 weeks of gestation. CRL = between cursors; P = prosencephalon; M = mesencephalon; R = rhombencephalon; Sp = spine; UL = upper limb; LL = lower limb; VD = vitelline duct; YS = secondary yolk sac.

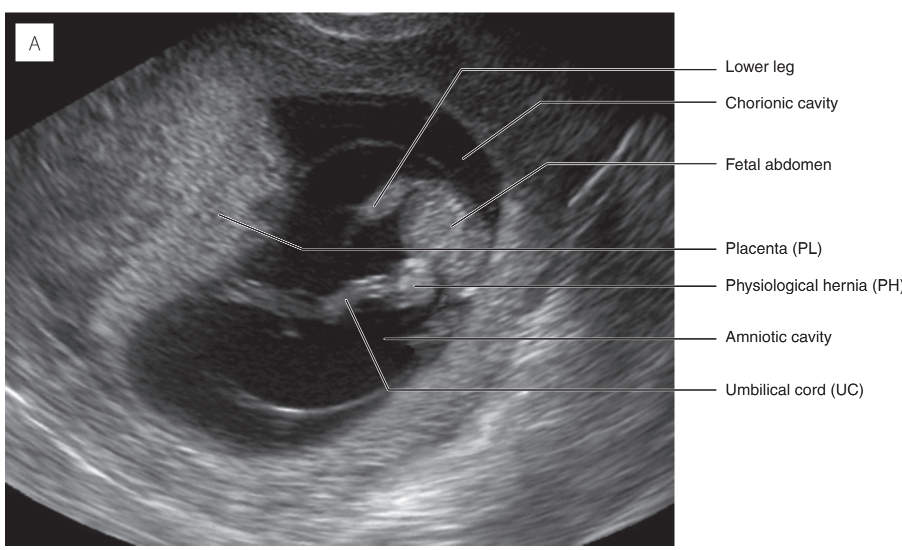


**Fig. 17.6** Two-dimensional (A) and three-dimensional (B) transvaginal scan at 11 weeks of gestation. YS = secondary yolk sac.

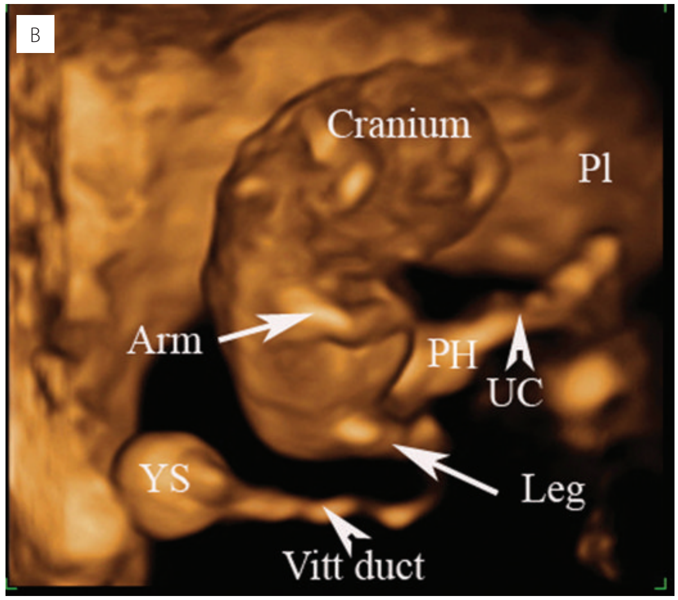


**Fig. 17.6** (*cont.*)

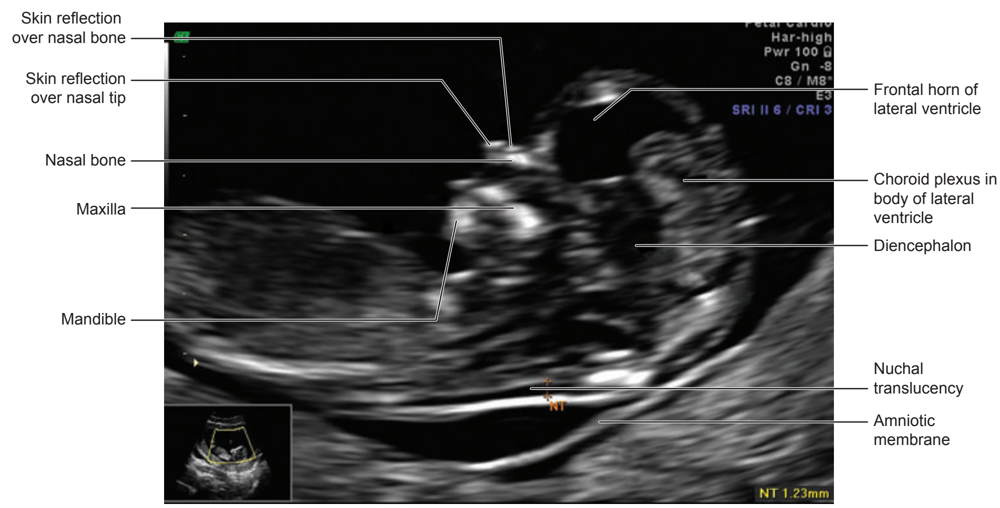


**Fig. 17.7** Nuchal translucency screening at 13 weeks of gestation.

**Table 17.2** Normal ultrasound parameters during the first trimester

| | Ultrasound sign |
|---|---|
| Embryo | Cardiac motion in embryos ≥ 5 mm<br>Fetal heart rate of above 85 beats per minute |
| Yolk sac | Yolk sac < 6 mm; round or spherical; bright echogenic rim and internal anechoic area |
| Amnion | Embryo always visualized when amnion is visible |
| Amniotic fluid | Mean diameter of amniotic cavity is ±10% greater than length of embryo |
| Gestational sac | ≥ 13 mm – yolk sac should be visualized<br>≥ 18 mm – embryo should be visualized<br>Smooth and round on endovaginal scanning |
| Trophoblastic reaction | Regular; double decidual reaction; trophoblastic reaction above 2 mm; no flow in the intervillous space |
| Sac growth | Greater than 0.6 mm/day |
| βhCG correlation | Direct correlation between sac size and βhCG levels |

- The CNS:
  - partition of ventricles and rapid growth
  - lateral ventricle contains the echogenic choroid plexus, which completely fills the ventricle
  - stomach, urinary bladder and kidneys can be occasionally seen.

Nuchal translucency (NT) refers to the normal subcutaneous fluid-filled space between the back of the fetal neck and the overlying skin (Fig. 17.7). In most cases, this area can be measured accurately and reproduced on an ultrasound between 10 and 14 weeks gestation. The combined risk of gestational age of the fetus, maternal age, maternal ethnicity, NT measurement and the presence of a nasal bone in combination with biochemical markers provide an integrated risk of chromosomal aneuploidy (trisomy 21, 13 and 18). The earliest structures seen with consistency are ossification centres in the maxillae, mandible and clavicle.

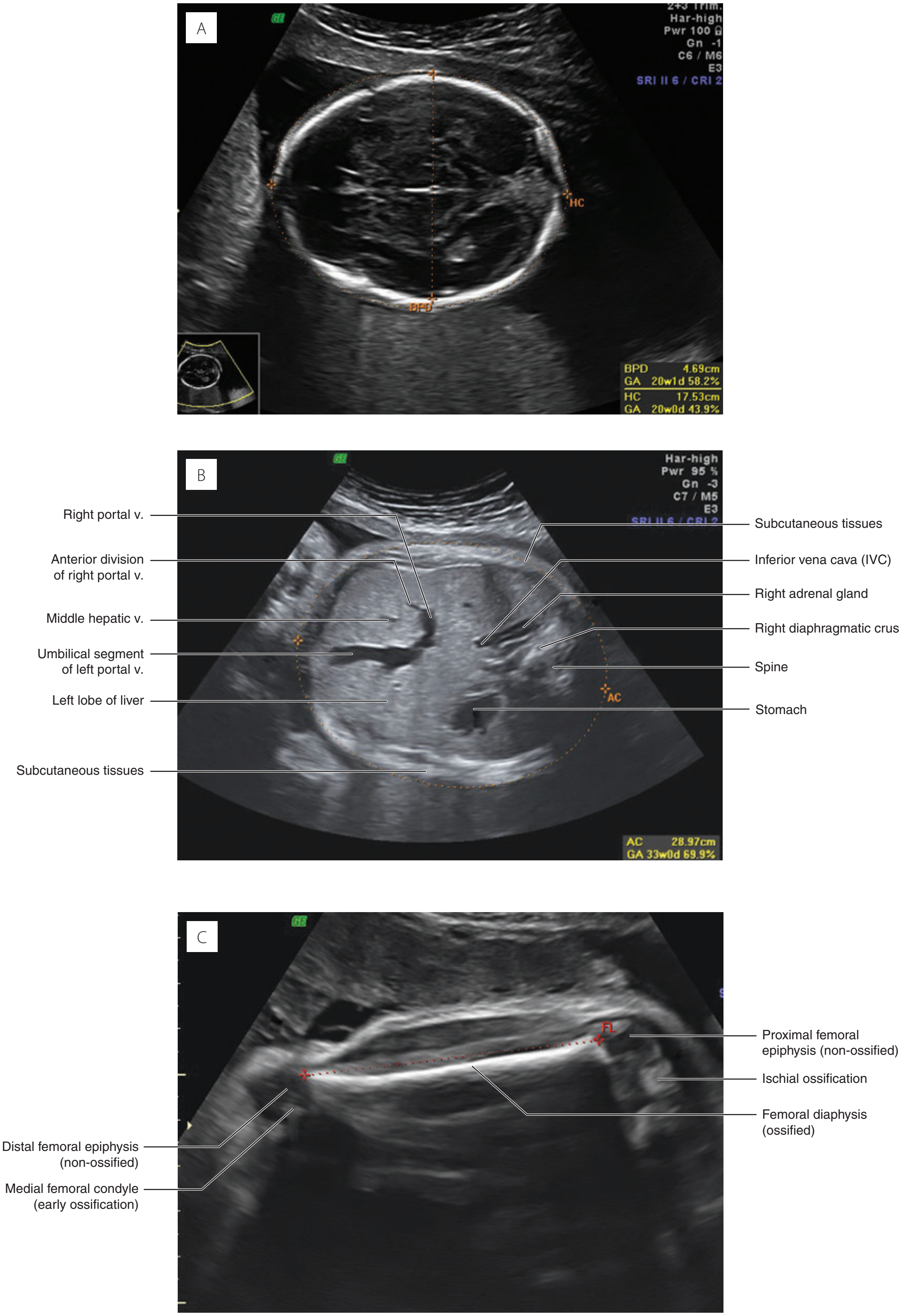


**Fig. 17.8** (A) Biparietal diameter (BPD) and head circumference (HC). The BPD and HC are obtained on an axial plane through the fetal head at a level which includes the midline echo with the cavum septum pellucidum anteriorly and the thalamus more posteriorly. The BPD is measured from the outer surface of the skull table in the near field to the inner margin of the skull in the far field (outer to inner). The HC measurement is obtained by measuring the circumference of the skull table rather than the diameter in the same plane as the BPD. The skull has an ovoid shape with the BPD being 80–90% of the occipitofrontal diameter (OFD). (B) Abdominal circumference (AC). The AC is obtained on a transverse image of the fetal abdomen at a level that demonstrates the umbilical portion of the left portal vein within the liver, as it meets the 'pars transversa' (horizontal portion of the left portal vein). The fluid-filled stomach is present on the left. The measurement includes the subcutaneous tissues. (C) Femur length (FL). The measurement of the femur and other long bones is confined to the ossified diaphysis. The cartilaginous ends, however, should be imaged, thus ensuring that the sonographic plane has passed through the true long axis of the bone.

# Second and third trimesters

## Determination of gestational age

During the first trimester the gestational age is determined by the mean gestational sac diameter or crown–rump length (CRL) (Figs. 17.2A, 17.5A) of the embryo, when it measures between 5 and 75 mm. After this time the CRL is no longer used as the fetus is too large to be measured on a single image, and may vary considerably, depending on fetal flexion or extension.

During the second and third trimesters the gestational age is determined by measuring known body parts. Although tables have been published for a large number of body parts, the head circumference (HC), biparietal diameter (BPD), abdominal circumference (AC) and femur length (FL) are routinely measured (Fig. 17.8).

## Central nervous system (CNS) (Fig. 17.9)

The fetal CNS is evaluated predominantly by transverse axial planes, and occasionally complemented by coronal or parasagittal views.

The fetal head can be delineated from the fetal torso when the embryo reaches a CRL of 10–15 mm. By the 11–12th weeks the intracranial anatomy can be first appreciated. By the end of the first trimester, the thalamus, midbrain, third ventricle and brainstem have achieved an appearance that will remain relatively unchanged other than progressive enlargement until term. The brightly echogenic choroid plexus dominates, and completely fills the lateral ventricles. The frontal horn of the lateral ventricle is devoid of choroid plexus (Fig. 17.7) while the occipital horn has not yet developed and the temporal horn is rudimentary. By 18–20 weeks the fetal CNS is dominated by brightly reflecting (echogenic) structures, including:

- the choroid plexus
- dural reflections such as the falx cerebri and tentorium cerebelli
- the cerebellar vermis
- specular reflections from the wall of the lateral ventricles.

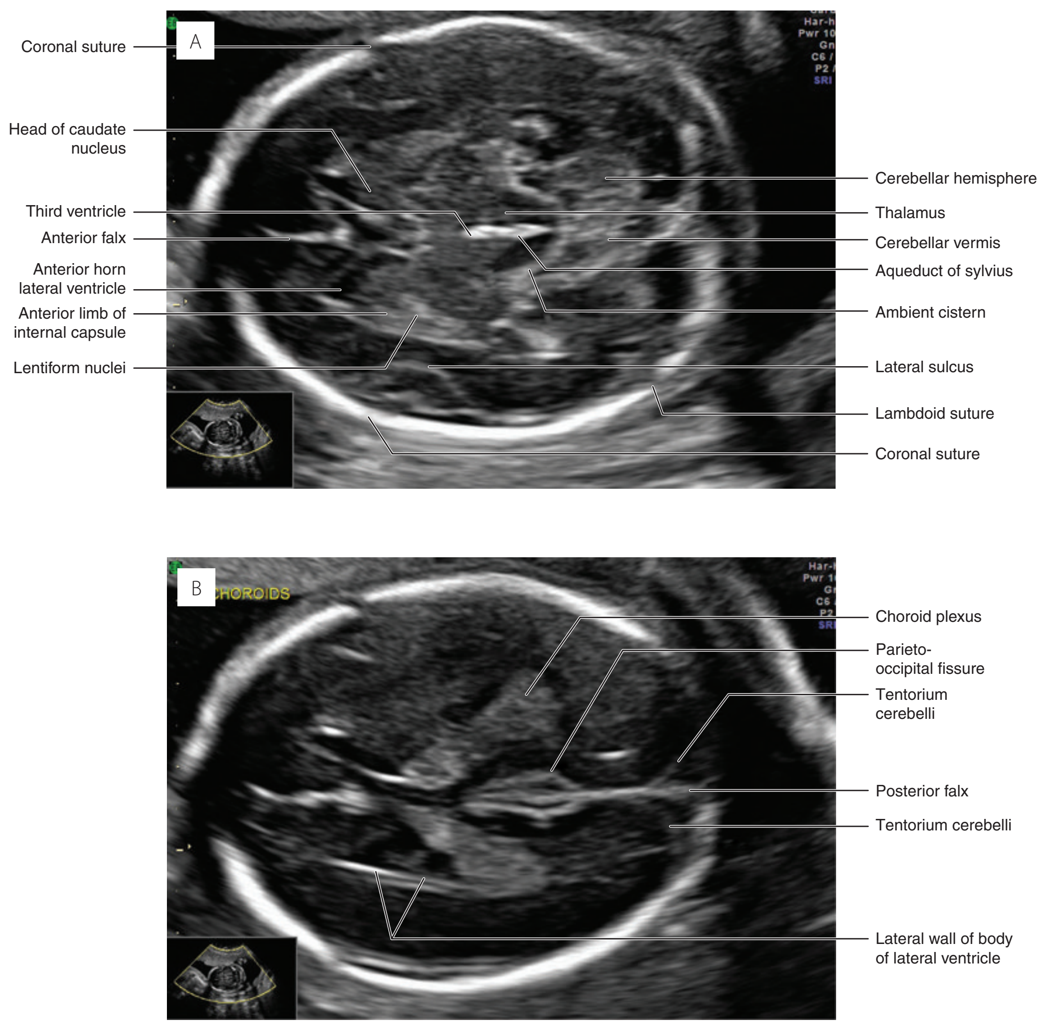


**Fig. 17.9** Axial images through the fetal CNS at 22 weeks at the level of the thalami (A), choroid plexus (B), and lateral ventricles (C).

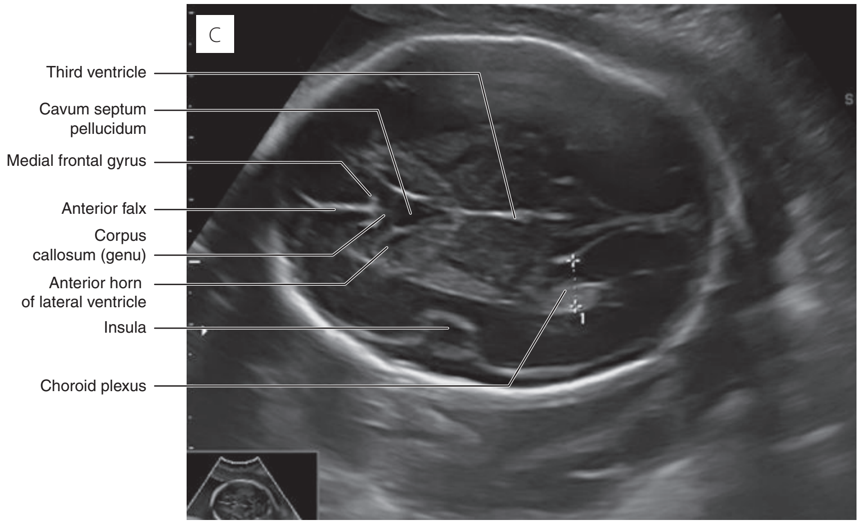


**Fig. 17.9** (*cont.*).

Most of the fetal intracranial structures are visualized by 20 weeks (Fig. 17.9). It is important to evaluate the:

- transverse diameter of the ventricular atrium at the level of the glomus of the choroid plexus (7 mm and an upper limit of 10 mm)
- cavum septi pellucidi (median cleft between the two laminae of the septum pellucidum)
- posterior fossa including the cerebellum and cisterna magna
- development of sulci and gyri; the two most commonly seen are the parieto-occipital fissure (an indentation medial to the interhemispheric cistern) and the lateral fissure (insula and sylvian fossa).

## Nose, face and lips

See Fig. 17.10.

## Chest

The lungs, heart and thoracic cage grow at a constant rate so that the ratio between the heart and thoracic circumference is constant in the second and third trimesters.

In the first trimester it is difficult to differentiate the lung from the liver because of similar echogenicity and the diaphragm is not yet evident. The lung becomes more echogenic than the liver in late second and third trimester and the muscular wall of the diaphragm becomes more visible (Fig. 17.11).

The trachea is normally located posterior and lateral to the junction of the aorta and pulmonary artery/ductus. It is easily visualized as it has a bright echogenic wall and is normally fluid-filled, and therefore sonolucent (Fig. 17.12C), and bifurcates into left and right main stem bronchi and can be visualized inferior to the carina due to the presence of intraluminal fluid.

## Fetal heart

The cardiac chambers and atrioventricular valves (Fig. 17.12) are assessed by the four-chamber view. The heart occupies about one-third of the chest cavity and is located on the left side (apex points left). The left atrium is the most posterior chamber (just anterior to the spine). The left ventricle lies posterolateral and the right ventricle anteromedial. The morphological left ventricle is defined by a smooth ventricular wall, and papillary muscles that attach to the side wall of the ventricle. It is separated from the left atrium by the mitral valve.

The morphological right ventricle has a ventricular wall that is more trabeculated than the left ventricle and has a moderator band at its apex. The papillary muscles attach to the apex of the ventricle. It is separated from the right atrium by the tricuspid valve, which has a septal leaflet that inserts on the interventricular septum and is more apically displaced than the mitral valve (Fig. 17.12A, B).

An axial (transverse) view of the fetal superior mediastinum called the three-vessel view is a simple but crucial view in evaluating the outflow tracts (Fig. 17.12C).

The ascending aorta arises from the morphological left ventricle and the pulmonary artery arises from the morphological right ventricle (Fig. 17.12D). They cross each other at an angle of about 70–90° just distal to their origins. The ascending aorta turns sharply (90°) and continues as the transverse aortic arch which runs parallel to the pulmonary artery–ductus arteriosus.

## Fetal abdomen

Most of the solid organs of the abdomen are well imaged in the second trimester.

The fetal liver occupies most of the upper abdominal cavity (Figs. 17.11 and 17.13). The left lobe is larger than the right lobe and has a uniform low reflectivity. The umbilical vein (Fig. 17.13A) enters the liver anteriorly and runs a 45° oblique course cephalad to join the posterior portal veins and enters the inferior vena cava via the ductus venosus.

Two well-defined fluid collections should always be present within the abdominal cavity (the stomach and urinary bladder) (Fig. 17.13B). Occasionally the gallbladder is seen as an

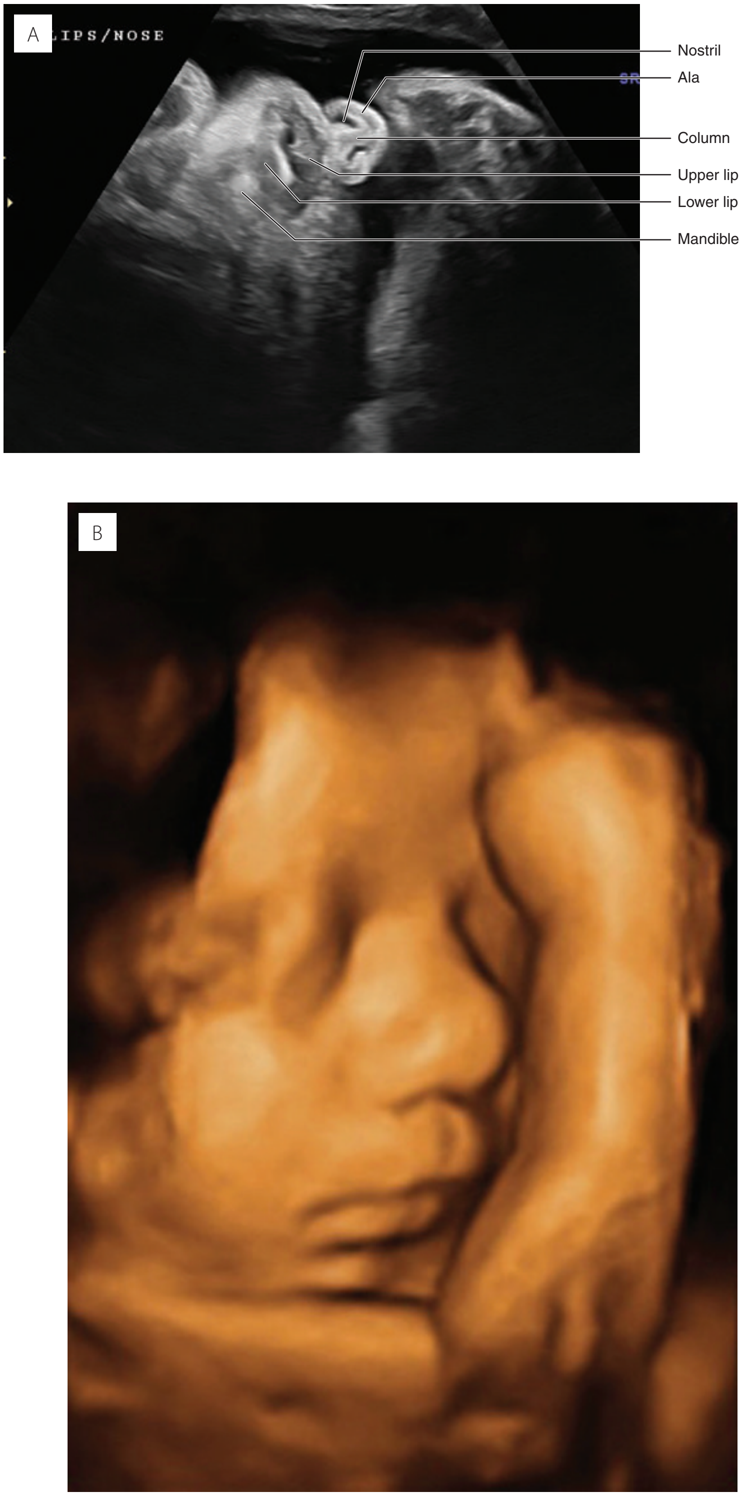


**Fig. 17.10** (A) Coronal image through the fetal nose and lips. (B) 3D surface image of the fetal face.

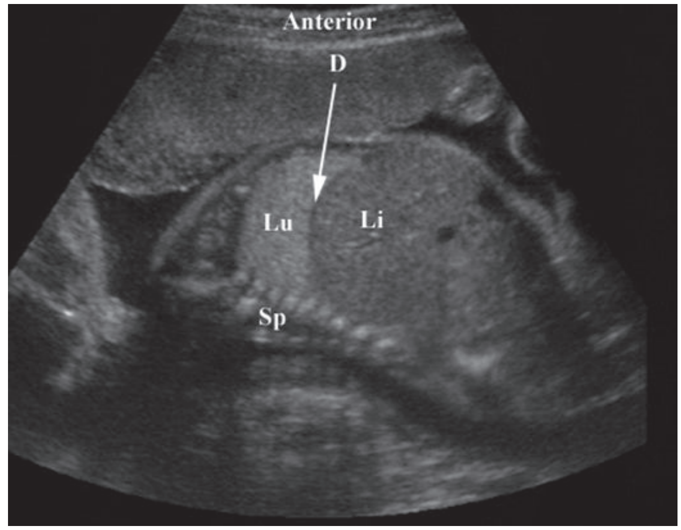


**Fig. 17.11.** Sagittal view through the fetal chest at 30 weeks. The brighter more echogenic lung (Lu) is separated from the darker less echogenic liver (Li) by the hypoechogenic diaphragm (D). The spine (Sp) is seen posteriorly.

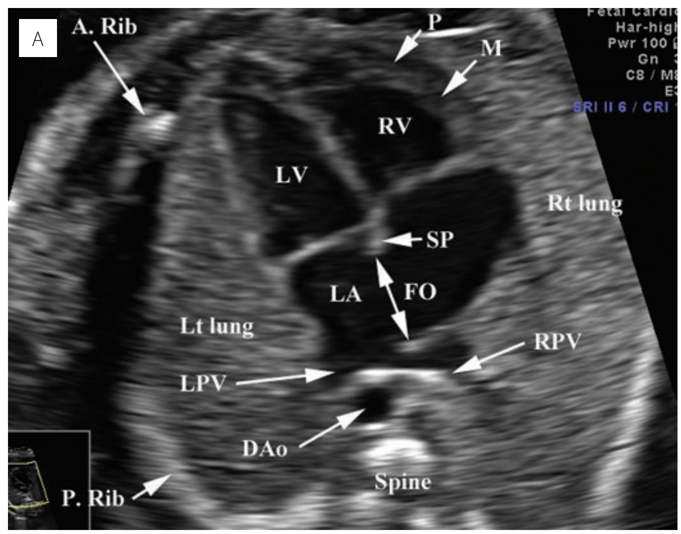


**Fig. 17.12** (A, B) The four-chamber views of the heart at 22 weeks gestation. A. Rib = anterior rib; DA = ductus arteriosus; DAo = descending thoracic aorta; FO = foramen ovale; IVS = interventricular septum; LA = left atrium; LPV = left pulmonary vein; LV = left ventricle; M = myocardium; MB = moderator band; MV = mitral valve; P = pericardium; RPV = right pulmonary vein; RV = right ventricle; SP = septum primum; SS = septum secundum; Tr = trachea; TV = tricuspid valve. (C D) The superior mediastinum at 20 weeks. (C) Three vessels are seen in the superior mediastinum lying side by side with the pulmonary artery (PA) on the left, the ascending aorta (AAo) in the middle and the superior vena cava (SVC) on the right. The pulmonary trunk is slightly larger than the aorta (1.2 to 1 ratio), which in turn is larger than the SVC. The PA arises anterior to the AAo, which in turn is anterior to SVC (PA therefore arises closest to the anterior chest wall). (D) The ascending aorta and main pulmonary artery cross just distal to their origin, and the color flow shows antegrade laminar flow.

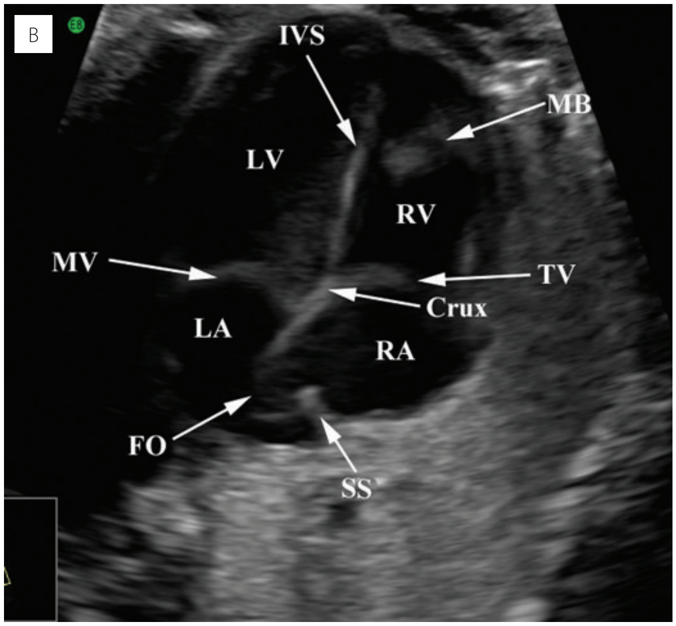


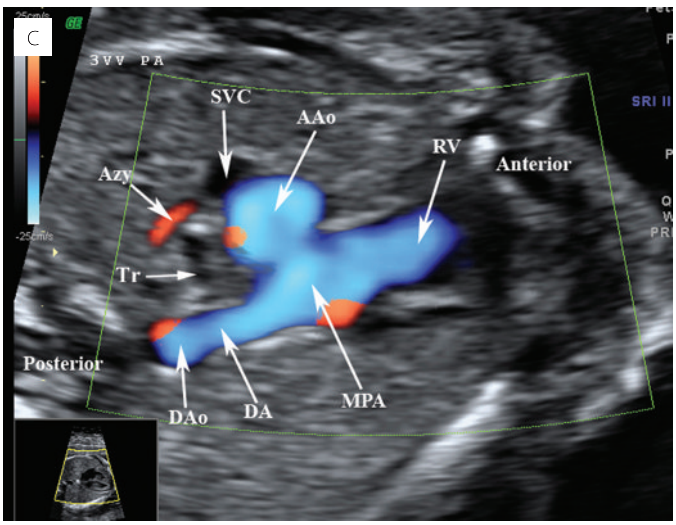


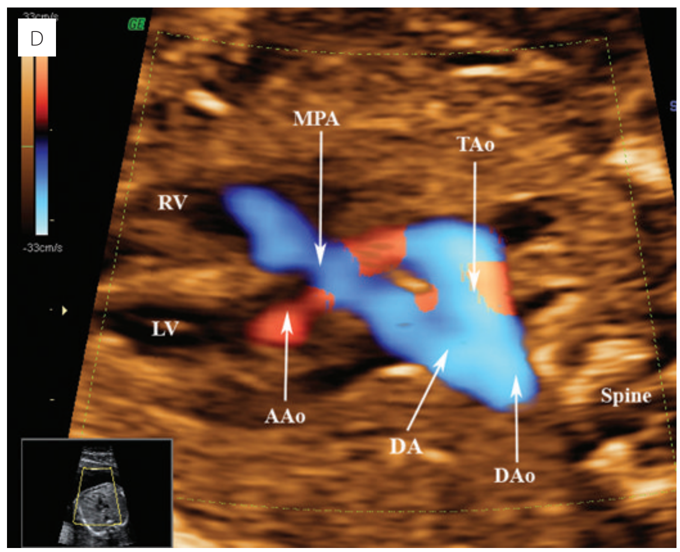


**Fig. 17.12** *(cont.)*

anechoic pear-shaped (cystic) structure at the right inferior border of the liver (Fig. 17.13B).

The fetal stomach should always be visualized as an echo-free cystic structure in the left upper quadrant by 14–16 weeks of gestation. The small intestines and colon are not usually visualized until the third trimester.

The urinary bladder should always be visualized as a round midline, thin-walled anechoic structure in the fetal pelvis (Fig. 17.13D). It can always be localized by the umbilical arteries that course along its lateral margin. Therefore even when completely empty, the position of the umbilical arteries marks the position of the urinary bladder when it lies in its normal location.

The kidneys are visualized on either side of the lumbar spine on transverse views (Fig. 17.13C). They have a homogeneous cortex with medullary pyramids arranged as an echo-poor rosette around the echo-free central renal pelvis. The renal capsule becomes visible at about 20 weeks as a dense thin reflective line that becomes progressively brighter as perinephric fat is deposited. The outline of the kidney becomes increasingly lobulated with advancing gestation (fetal lobulation). The ureters are not visualized unless they are obstructed.

The suprarenal (adrenal) glands are observed in a transverse or sagittal plane just above the kidneys (Fig. 17.8B). They are usually evident by 16–18 weeks of gestation and contain a

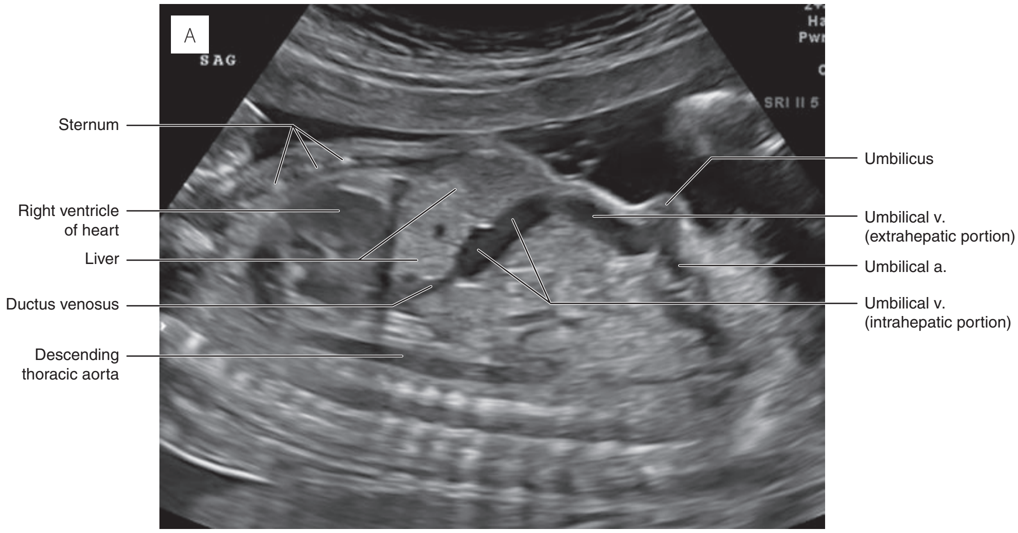


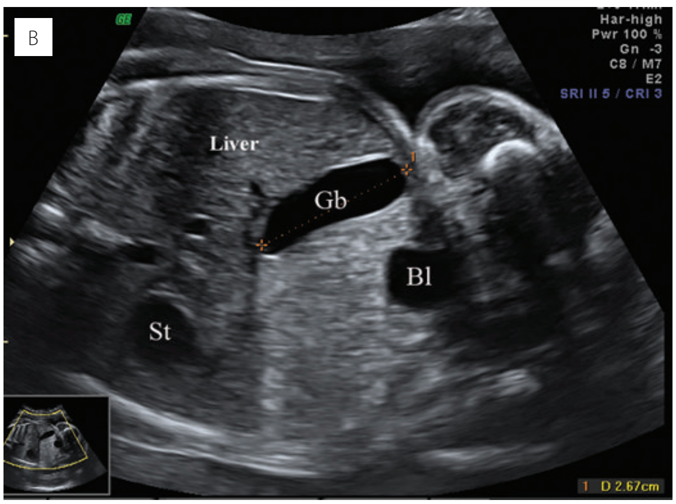


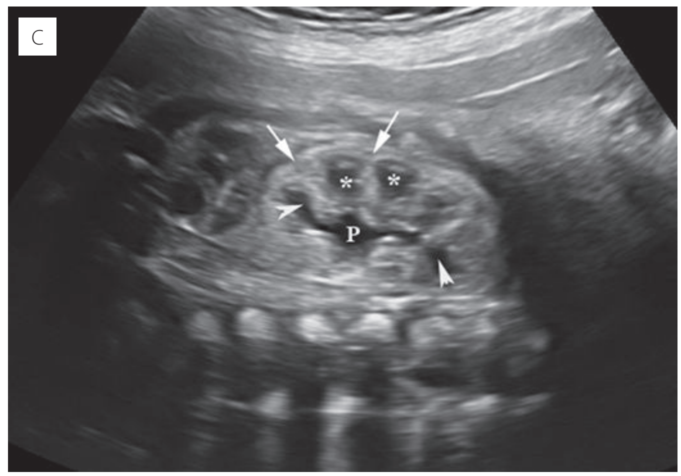


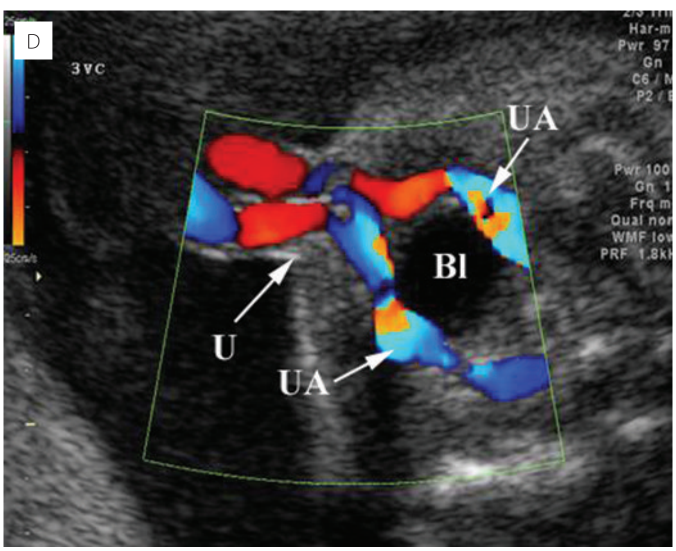


**Fig. 17.13** (A) Sagittal view of the fetal abdomen at 32 weeks. (B) Fluid-containing structures in the fetal abdomen. St = stomach; Gb = gallbladder; Bl = urinary bladder. (C) Sagittal view of a fetal kidney at 32 weeks. P = renal pelvis (fluid-filled); arrowheads = upper and lower pole calyces; arrows = fetal lobulation; * = medullary pyramids. (D) The urinary bladder and umbilical vessels. UA = umbilical artery; Bl = urinary bladder; U = umbilicus.

dense reflective central region (medulla) and a less dense surrounding cortex.

## Umbilical cord and placenta

The umbilical cord contains a single umbilical vein and two umbilical arteries (Fig. 17.14A–C). The larger vein transports oxygenated blood from the placenta to the fetus, while the paired umbilical arteries transport deoxygenated blood from the fetus to the placenta.

Two arteries arise as branches of the internal iliac arteries and course lateral to the urinary bladder toward the umbilical cord (Fig. 17.13D). The intra-abdominal portion of the UV ascends steeply from the cord insertion in the inferior part of the falciform ligament (Fig. 17.13A). The vessel continues in a more horizontal and posterior direction, turning to the right at the confluence with the transverse part of the left portal vein (Fig. 17.8B), which joins the right portal vein (divides into anterior and posterior branches), at the main lobar fissure. Normal coiling of the umbilical cord and the surrounding Wharton's jelly results in a cord that is more resistant to torsion, compression and stretch when compared with a non-coiled cord.

The umbilical cord usually inserts centrally into the placenta (Fig. 17.14D) and into the fetus at the umbilicus. The placenta has a well-defined retroplacental venous plexus and may have numerous echo-free venous lakes within its substance. Its location within the uterus is variable and only significant if there is an accessory lobe or if it covers the internal cervical os.

## Skeletal system (axial and appendicular)

Many of the bones in the appendicular skeleton are cartilaginous; however, ultrasound has the ability to visualize both the ossified and cartilaginous portions of the fetal skeleton.

## Cranium

The ossified portion of the fetal skeleton possesses the highest level of subject contrast and is therefore visualized earlier.

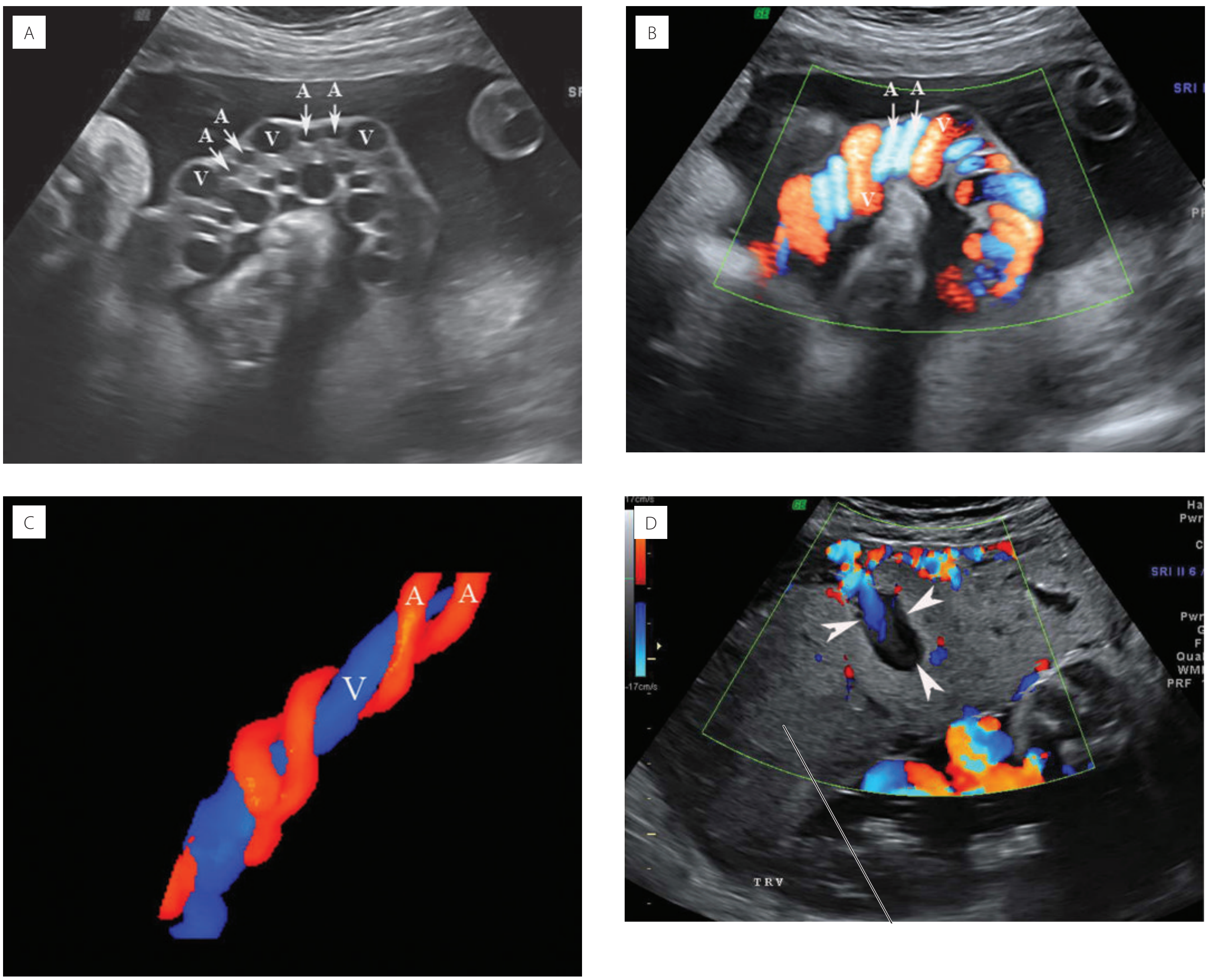


**Fig. 17.14** The umbilical cord and placenta. (A) 2D; (B) colour Doppler; (C) 3D angio mode; (D) placenta. A = umbilical artery; V = umbilical vein; L = retroplacental venous plexus; arrowheads = normal placental venous lake.

Imaging of the sutures and fontanelles with 3D volume imaging gives a more global view of skeletal structures than can be achieved with two-dimensional ultrasound. Calvarial ossification can be imaged from the late first trimester. The sutures and fontanelles represent non-ossified windows for evaluation of intracranial anatomy.

Normal ossification centres appear as areas of increased echogenicity of the bones and may be seen endovaginally from 9 weeks onwards. Osteogenesis starts centrally and spreads peripherally until the whole skeletal element is ossified. Primary cranial ossification completes by week 12 and is always visualized by week 14. The cranial bone, sutures and fontanels are best visualized with three-dimensional (3D) ultrasound (Fig. 17.15).

## Limbs

The distal femoral and proximal tibial epiphyseal centres are evident in the second trimester (Fig. 17.8C), and ossification of the distal femoral epiphysis indicates a gestational age of at least 35 weeks. The patella does not ossify until after birth but can be visualized sonographically while still cartilaginous.

The extremities are first imaged in the late first trimester and visibility increases rapidly (by 15–16 weeks the phalanges can be visualized). Amniotic fluid surrounding the limb enhances visualization.

The proximal humeral epiphyseal centre (Fig. 17.16A) is usually the last of the secondary ossification centres to ossify. 2D ultrasound in a longitudinal plane is the simplest way to visualize a limb.

In the lower leg the lateral bone is the fibula and medial bone is the tibia (Fig. 17.17).

In the forearm, the radius is lateral and the ulna is medial; however, this relationship is more difficult to assess as the radius and ulna may cross during pronation (Fig. 17.16C).

Tibia, fibula, radius and ulna all end at the same level; however, proximally the ulna is longer than the radius and tibia is longer than the fibula.

The hand (Fig. 17.16B,C) is more easily assessed than the foot (Fig. 17.18A) primarily due to size (toes are smaller than the fingers).

Metacarpals (Fig. 17.16b,c) and metatarsals (Fig. 17.18a) are well ossified by 16 weeks, but carpals and tarsal bones (except for tarsal calcaneous and talus) remain cartilaginous throughout pregnancy, and at the wrist appears as a hypoechogenic band spanning the gap from the distal radius and ulna to the proximal metacarpal centres (this band also includes the distal epiphysis of the forearm bone).

The tarsal calcaneous and talus ossify between 20 and 24 weeks, while the remaining tarsals and carpals do not ossify until after birth (Fig. 17.18A,B).

The pelvis, ribs and spine are easily imaged and serve as excellent anatomical landmarks.

In the pelvis, iliac ossification centres are easily observed from the early second trimester onward (ossified by 12 weeks). Ischial ossification is present at 16 weeks (Fig. 17.19), but pubic ossification is not present until 24 weeks.

The spine is evaluated in both longitudinal and transverse axial planes (Figs. 17.20A and 17.21).

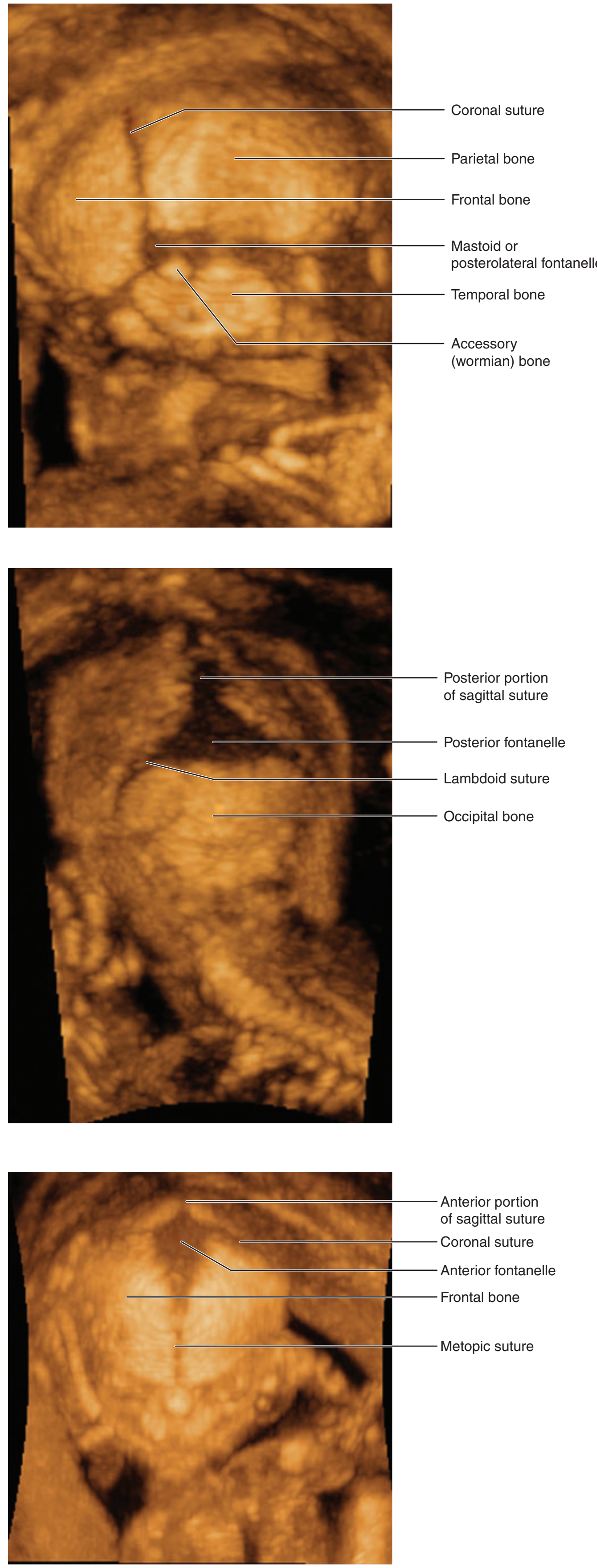


**Fig. 17.15** 3D ultrasound of the fetal cranium at 18 weeks of gestation in maximum-intensity mode.

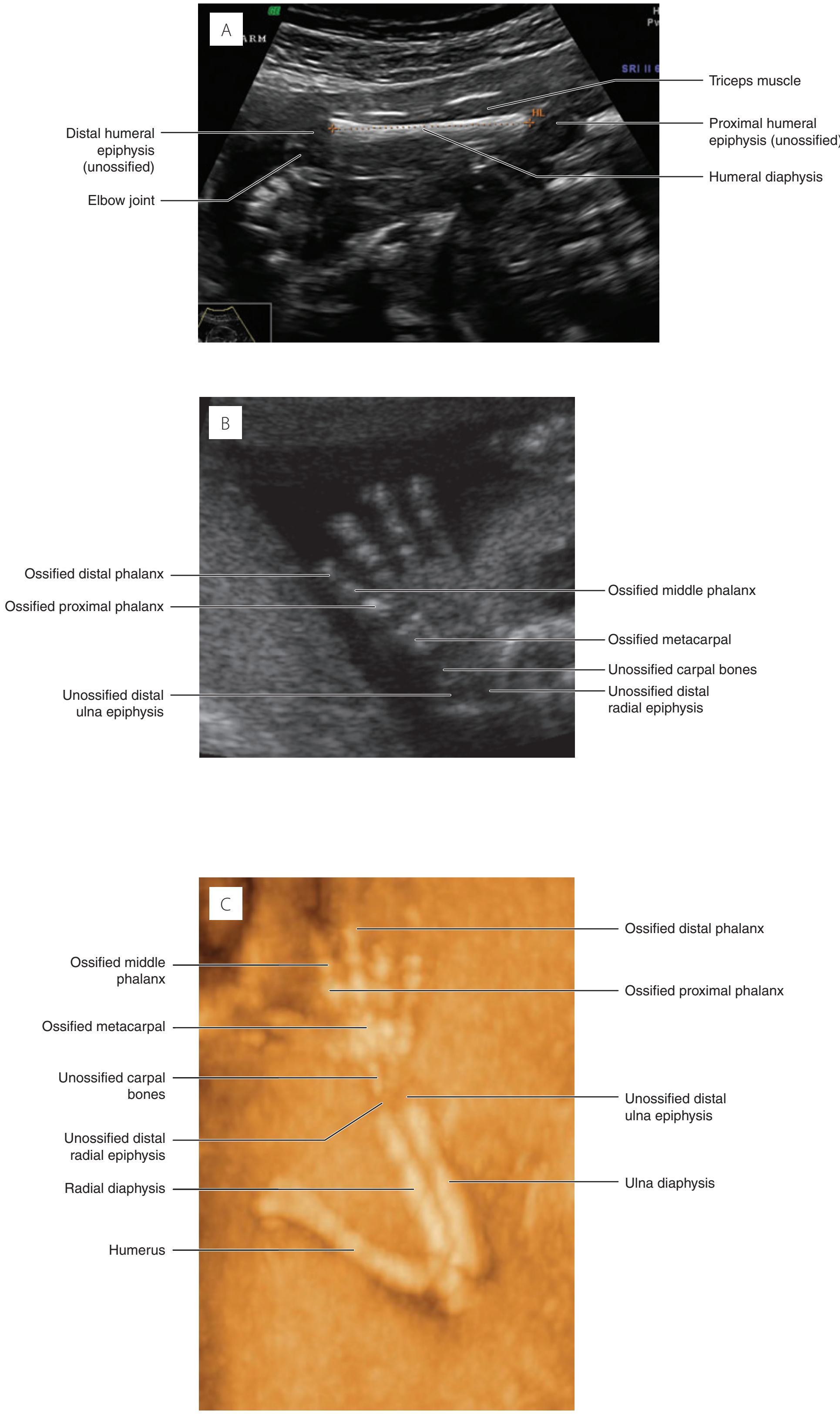


**Fig. 17.16** (A) Upper arm (humerus). (B, C) Forearm and hand. 2D images of the hand (B) and 3D image of the forearm and hand (C).


**Fig. 17.17** Lower leg.

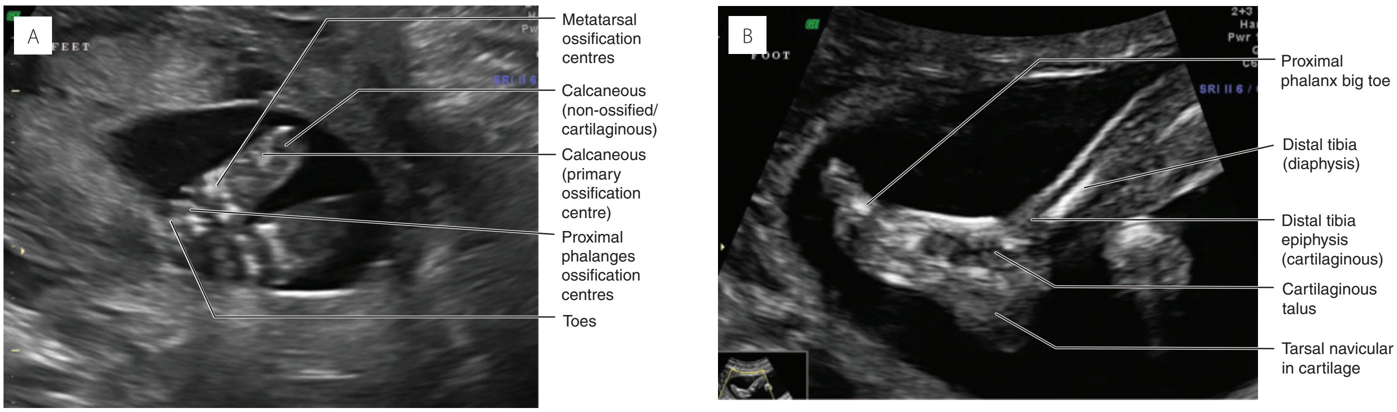


**Fig. 17.18** (A) Foot (transverse view). (B) Sagittal view of foot (24 weeks).

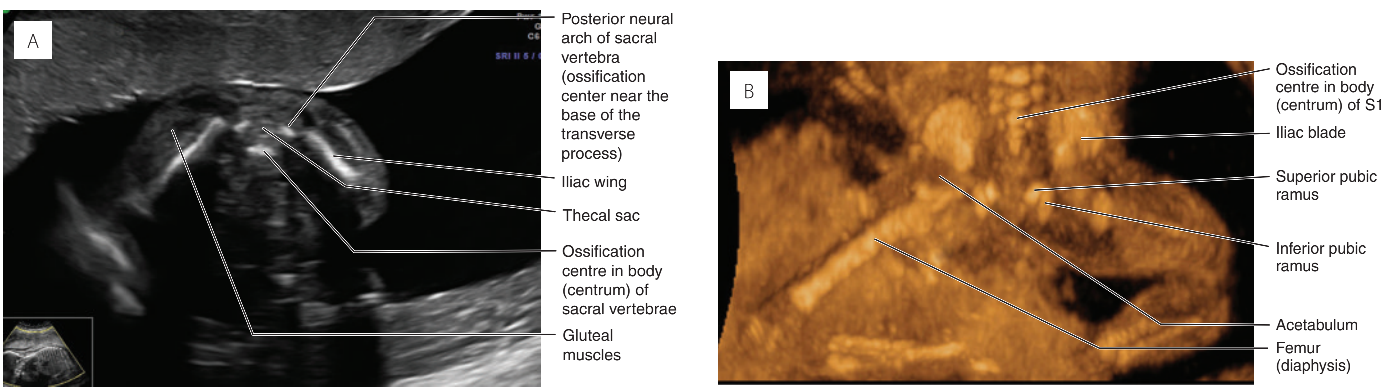


**Fig. 17.19** Fetal pelvis at 26 weeks. (A) 2D transverse view. (B) 3D view in maximum mode.

On longitudinal planes the posterior elements are seen as almost 'parallel' (because they flare in the upper cervical region, diverge slightly in the lumbar region and converge in the sacrum) bands of echoes. The entire spine may not be visualized in a single plane due to normal fetal kyphosis.

Transverse axial planes allow evaluation of the entire spine in a segmental fashion and demonstrate anatomy more easily. Each vertebra contains three primary ossification centres. One centre is in the centra (body) and occurs first in the lower thoracic and upper lumbar spine followed by progressive ossification in both a cephalad and caudal direction.

Ossification of the posterior neural arch appears in a more standard cephalad-caudal direction.

Laminae ossification begins in the cervical spine at 18–19 weeks and ends in the sacral spine around 24 weeks. It is important to confirm that the laminae point centrally and do not flare outwards.

The spinous processes of the posterior neural arch are occasionally seen as they are usually entirely composed of cartilage in utero.

The scapula, clavicles and proximal humerus can be imaged in both two- and three-dimensional images (Fig. 17.20A,B)

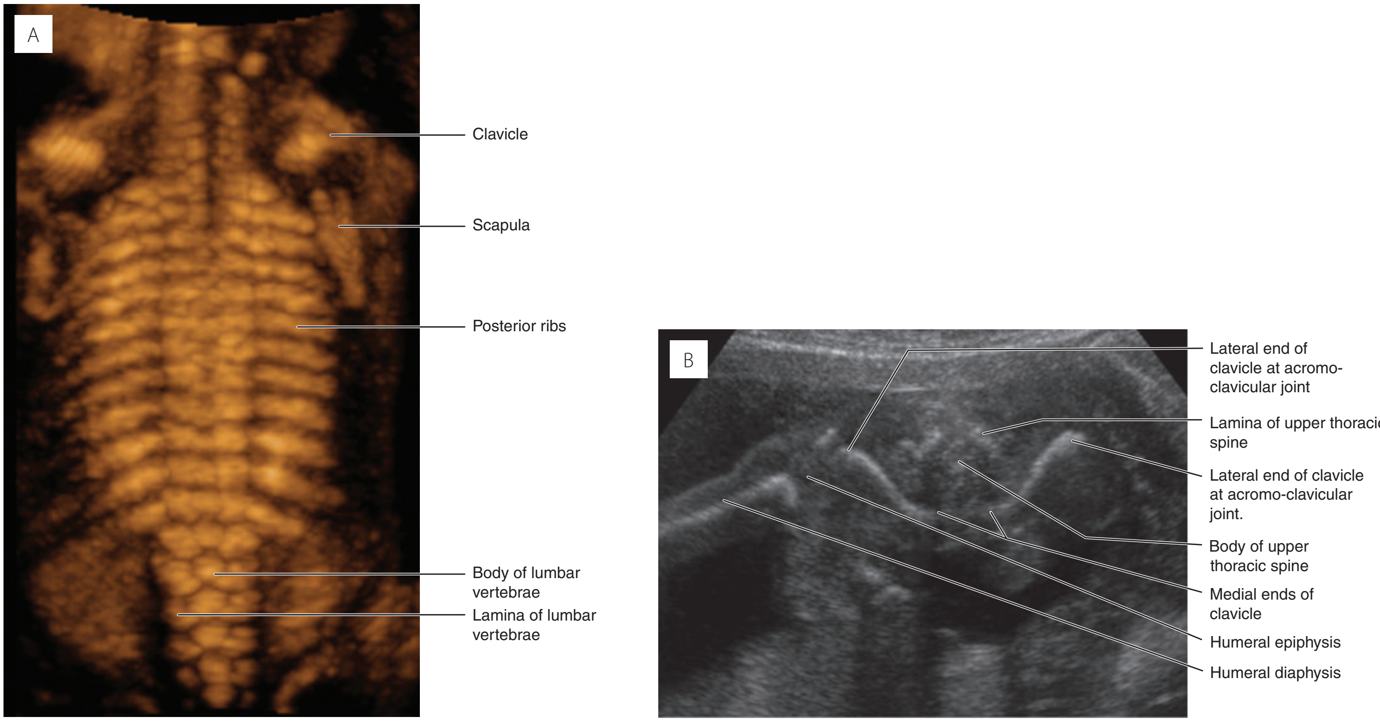


**Fig. 17.20** (A) Ribs, shoulder joint and spine (3D image maximum mode). (B)2D view of the clavicles and shoulder.

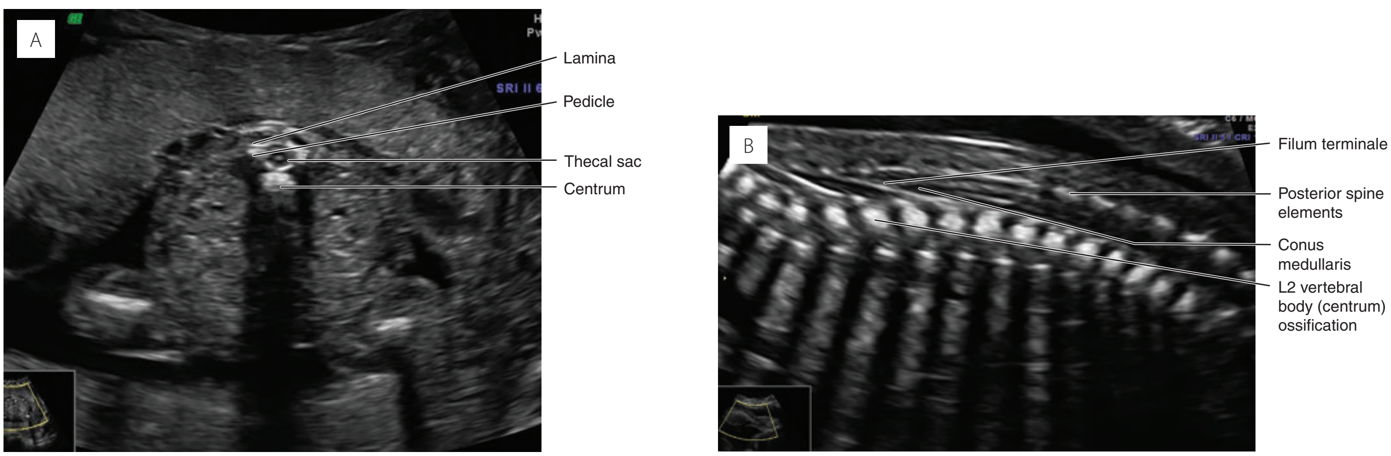


**Fig. 17.21A** Thoracic vertebrae at 32 weeks (transverse view). Spinal canal (longitudinal view).

## Fetal magnetic resonance imaging (MRI)

### See Fig. 17.22

Although ultrasonography remains the primary modality for fetal screening, fetal magnetic resonance imaging (MRI) has become an important tool, providing diagnostic information in selected cases. Initial problems of long scan time and artefacts caused by fetal motion have been overcome by the advent of fast imaging sequences. A complete sequence only needs a few seconds and the use of ultrafast imaging sequences oriented to the fetus has greatly improved diagnostic image quality.

## Indications for fetal MRI

Obstetric ultrasound has a number of areas where appropriate visualization is deficient because of the limitations of the modality itself.

1. Ultrasound is limited by progressive bone ossification. Parts of the cranium, mostly the posterior fossa, can be challenging to visualize in detail.
2. Bone is again a barrier to visualize cleft palate in cases of cleft lip. The hard palate prevents obtaining detail of the soft palate in such cases on ultrasound.
3. Evaluation by ultrasound is also dependent on amniotic fluid volume, fetus position and maternal stature.

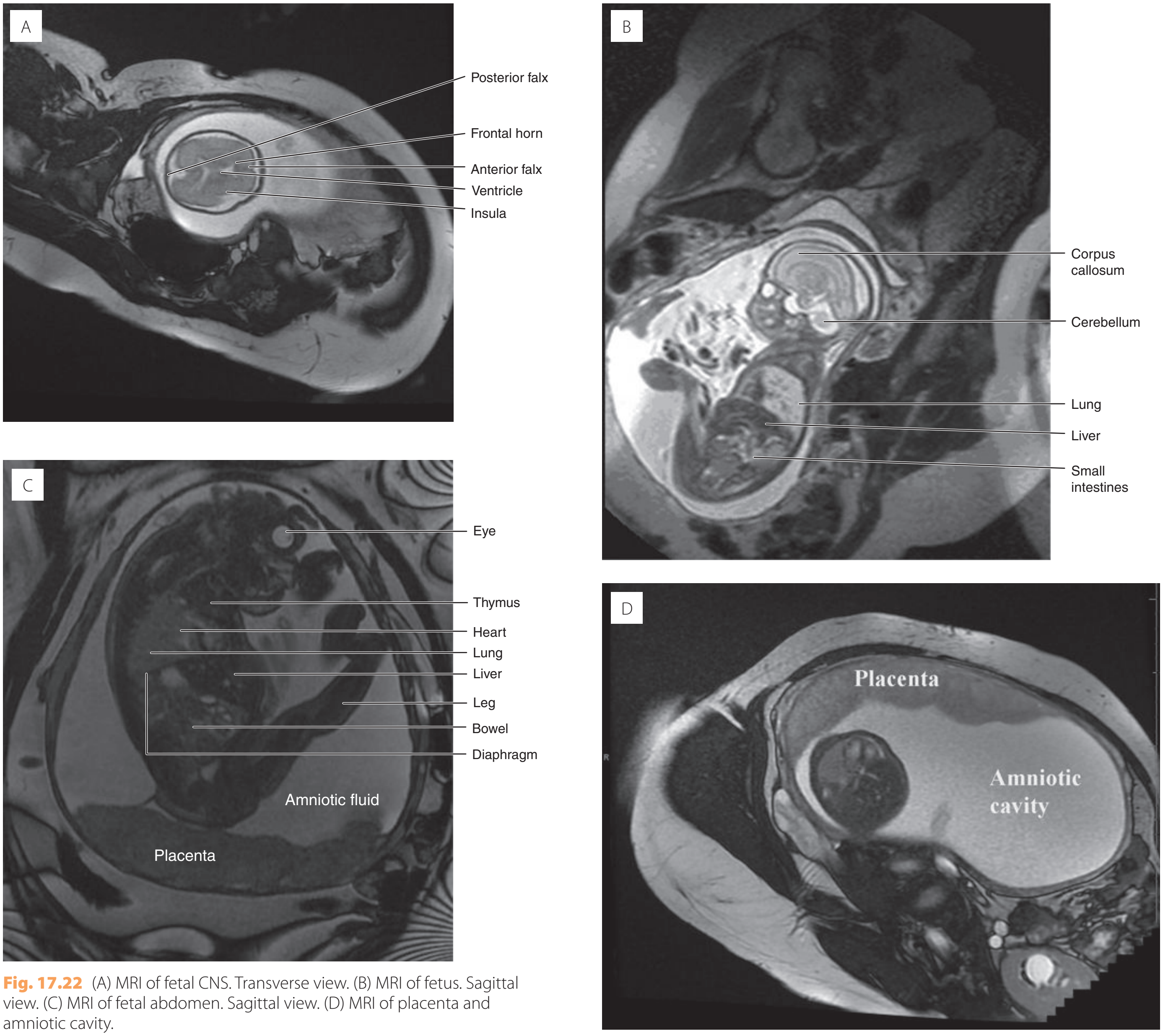


**Fig. 17.22** (A) MRI of fetal CNS. Transverse view. (B) MRI of fetus. Sagittal view. (C) MRI of fetal abdomen. Sagittal view. (D) MRI of placenta and amniotic cavity.

4. Lung abnormalities are also shown to be far better evaluated by MRI. Lung volumes can be estimated in cases of diaphragmatic hernia.
5. When potential airway-compromising abnormalities, such as cystic hygromas or oropharyngeal teratomas, are detected on antenatal ultrasound, MRI allows further detail and higher diagnostic confidence, allowing improved delivery choices and immediate postnatal decision planning.

# Index